Waveguide QED

Yury Holubeu *

December 21, 2025

This note isn't aimed for distribution.

Contents

1 Preface **8**

I Waveguide QED in Nutshell **10**

2 Main formulas **10**
2.1 Basics of wQED . . . 10
2.1.1 Fundamental physics in waveguide QED . . . 10
2.1.2 On coherence functions (??) . . . 10
2.2 Methods for Analyzing Models by Well-known Articles . . . 10
2.3 PP21 Method . . . 10
2.3.1 Parameters and Formalism for Waveguide QED . . . 10
2.3.2 Essence of the PP21 Diagrammatic Method (????) . . . 12
2.3.3 PP21 Diagrammatic Method in Typical Examples (??) . . . 15
2.3.4 Real time wQED in a nutshell(??) . . . 15
2.3.5 Mathematics for PP21 wQED: Main Formulas . . . 15

II My Main Theory **16**

3 Fundamentals of Waveguide QED **16**
3.1 Fundamentals of Waveguide QED . . . 16
3.1.1 Physics of wQED and derivation of the model . . . 16
3.1.2 Hamiltonian, generalized summation convention, and the S matrix . . . 16
3.1.3 Coherence Functions in wQED . . . 18
3.1.4 Origin of special models in scope of wQED (???) . . . 18
3.2 Features of Approaches in wQED . . . 18
3.2.1 Features of PP21 Approach . . . 18

III My Other Theories **19**

4 Fundamentals of Optics and Waveguides **19**
4.1 Other Questions about Waveguide QED . . . 19
4.1.1 Key General Features of wQED . . . 19
4.2 Other Phenomena and Methods of Waveguide QED . . . 19
4.2.1 Purcell Effect . . . 19
4.2.2 On Other Well-Known Phenomena (???) . . . 20

IV Examples and Solved Problems **21**

5 Problems about Derivation of Formalism of wQED **21**
5.1 Problems about mathematical transformations in wQED . . . 21

*https://yuriholubeu.github.io/, yuri.holubev@gmail.com

6 Problems about Special Phenomena of wQED **21**
6.1 Creation of Models of wQED . . . 21
6.2 Single-exitation subspace, Markovian systems . . . 21
6.2.1 Qubit emission . . . 21
6.2.2 Problems for $N = 3$ emission . . . 25
6.2.3 Λ-system . . . 28
6.2.4 V-system . . . 29
6.2.5 Second pair (???) . . . 30
6.3 General dynamics in $\bar{N}_{max} = 1$ systems by K. Piasotski . . . 34
6.3.1 Exact resummation of perturbation theory for the propagator . . . 34
6.3.2 General dynamics in single-excitation subspace . . . 37
6.3.3 Spontaneous emission from the second pair of Bell pairs . . . 38
6.3.4 1 Infinite waveguide . . . 39
6.3.5 2 Semi-infinite waveguide . . . 40
6.3.6 Wave-functions . . . 41
6.3.7 Real time dynamics for $0 < t < \infty$. . . . 42
6.3.8 Long-time limit . . . 44

V Well-known and Important Articles **46**

7 Diagrams for scattering in waveguide QED by Piasotski, Pletyukhov (PP21) **46**
7.1 Introduction . . . 46
7.2 Scattering Theory . . . 47
7.2.1 Hamiltonian, generalized summation convention, and the S -matrix . . . 48
7.2.2 General properties of the scattering matrix in waveguide QED . . . 49
7.2.3 Scattering theory in $N_q = 1$ waveguide QED . . . 50
7.2.4 Generalized cluster decomposition . . . 52
7.2.5 Closed form solution in the Markovian limit . . . 54
7.2.6 Approximation strategies . . . 54
7.2.7 Systems with more than one qubit . . . 55
7.3 Application: a giant acoustic atom . . . 60
7.3.1 Model and conventions . . . 60
7.3.2 Problem formulation . . . 61
7.3.3 Spectral power density . . . 62
7.4 Conclusions and outlook . . . 67
7.5 Appendix . . . 67
7.5.1 Cluster decomposition of three-photon S-matrix . . . 67
7.5.2 Third-order coherence function . . . 72
7.5.3 Diagrammatic representation of the generic three-body transition operator . . . 73
7.5.4 Effect of the non-zero detuning . . . 78
7.6 PP21: Extra Theory about Method and Formalism . . . 80
7.6.1 Scattering theory in waveguide with 1 qubit . . . 80
7.6.2 Generalized cluster decomposition . . . 83
7.6.3 Examples of Diagrams . . . 88
7.6.4 Closed-form solution in the Markovian limit . . . 89
7.6.5 Approximation strategies . . . 90
7.7 Systems with some qubits . . . 91
7.7.1 2-qubit waveguide QED . . . 91
7.7.2 3-qubit waveguide QED . . . 94
7.7.3 Derivation of the Diagrammatic Technique on a Simple Example (!?!?!?) . . . 95
7.7.4 Diagrammatic representation of the generic 3-body transition operator (?????) 95
7.8 Coherence functions . . . 98
7.8.1 Model and conventions (!?!!??!) . . . 98

7.8.2 Problem formulation . . . 99
7.8.3 Spectral power density (???) . . . 101
7.8.4 Second-order coherence . . . 104
7.8.5 Third-order coherence . . . 105
7.8.6 Effect of the non-zero detuning . . . 106
7.8.7 Appendix on 3-order coherence function . . . 107
7.9 Scattering Theory in Waveguide QED . . . 108
7.9.1 3.1 General Definition of the S-Matrix . . . 109
7.9.2 3.2 General Properties of the Scattering Matrix in Waveguide QED . . . 110
7.9.3 3.3 $Q = 1$ Waveguide QED . . . 111
7.9.4 Two Waveguide QED . . . 123
7.9.5 Three Waveguide QED . . . 125
7.10 Giant Acustic Atom Model . . . 128
7.10.1 4.1 Study of Delayed Coherent Quantum Feedback in the Framework of Quantum Acoustics . . . 129
7.10.2 4.2 Model of a Non-locally Coupled Acoustic Atom . . . 130
7.10.3 4.3 Formulation of the Scattering Problem . . . 131
7.10.4 4.4 Single-Phonon Processes: Reflectance and Transmittance . . . 134
7.10.5 4.5 Two-Phonon Processes: Inelastic Spectral Power Density and Second-Order Coherence Function . . . 137
7.10.6 4.6 Three-Phonon Processes: Third-Order Coherence Function . . . 146
7.11 Real-Time Dynamics in Waveguide QED . . . 153
7.11.1 Introduction and Generalities . . . 153
7.11.2 Resummation of the Perturbation Series for the Propagator in $Q = 1$ Waveguide QED . . . 154
7.11.3 General Dynamics in Single Excitation Subspace . . . 156
7.11.4 Spontaneous Emission of a Giant Acoustic Atom . . . 158
7.11.5 Dynamics of Single Excitation States in the System of Two Distant Qubits . . . 160
7.11.6 Spontaneous Emission of a Qubit Into an Array of Coupled Resonators . . . 166
7.12 Conclusions and Outlook . . . 176
7.13 Numerical And Analytical Solutions of Integral Equations . . . 177
7.13.1 A. 1 Single-Photon Effective Vertex . . . 177
7.13.2 A.1.1 Multi-Finger Coupled Qubit . . . 177
7.13.3 A.1.2 Giant Atom. Analytical Solution . . . 178
7.13.4 A. 2 Optimization Scheme for the Numerical Treatment of the Two-Body Effective Vertex Function Integral Equation . . . 180
7.14 Other Features and Questions about PP21 Method . . . 183
7.14.1 Connection of PP21 Method with known QFT and Quantum Optics Theory (????) 183
7.14.2 How Exactly the Experiment "Nonexponential decay of a giant artificial atom" by Andersson et. al. Is Explained by PP21 Method? . . . 183
7.14.3 General properties of the scattering matrix in waveguide QED . . . 183

8 Reliable multiphoton generation in waveguide QED by González-Tudela et al. 184
8.1 Main Theory . . . 184
8.2 Supplemental Material: Reliable multiphoton generation in waveguide QED . . . 189
8.3 Heralding multiple collective atomic excitations in waveguide QED setups using single photon detectors. . . . 189
8.3.1 Atom-waveguide resources . . . 189
8.3.2 Protocol and calculation of probabilities. . . . 190
8.3.3 Fidelities of the protocol. . . . 191
8.4 Heralding single collective excitations using atom-waveguide QED: two-step protocol with exponential scaling. . . . 192
8.4.1 Atom-waveguide resources. . . . 193
8.4.2 Protocol and calculation of probabilities . . . 194

8.5 Heralding single collective excitations using atom-waveguide QED: two-step protocol for polynomial scaling. . . . 196
8.5.1 Atom-waveguide resources for two-step protocol. . . . 197
8.5.2 Protocol and calculation of probabilities 197
8.5.3 Fidelities of the protocol. . . . 200
8.6 Heralding single photon excitations using atom-waveguide QED: single-step protocol for polynomial scaling. . . . 201
8.6.1 Atom waveguide resources. . . . 201
8.6.2 Protocol and calculation of probabilities. . . . 201
8.6.3 Fidelity of the protocol. . . . 203
8.7 Merging protocols for combining collective atomic excitations. . . . 203
8.7.1 Adding excitations one by one. . . . 204
8.7.2 Doubling the number of excitations post-selecting on no detection. . . . 205
8.7.3 Increasing the number of excitations with number resolved detection. . . . 206
8.7.4 Atomic number resolved detection using waveguide QED. . . . 207

9 The giant acoustic atom by Guo et. al. 208
9.1 Introduction . . . 208
9.2 The Model . . . 209
9.3 Single-phonon processes . . . 210
9.3.1 Spontaneous Emission . . . 210
9.3.2 Single-phonon scattering . . . 214
9.4 Two-phonon processes . . . 216
9.4.1 Two-phonon scattering matrix . . . 216
9.4.2 Correction to the transmittance . . . 218
9.4.3 Inelastic power spectrum . . . 219
9.4.4 Production of phonon pairs . . . 221
9.4.5 Second-order coherence correlation functions . . . 222
9.5 Transient dynamics with arbitrary drive strength . . . 224
9.6 Summary and outlook . . . 228
9.7 Single-phonon processes . . . 230
9.7.1 Equations of motion . . . 230
9.7.2 Spontaneous emission . . . 232
9.7.3 Boundary conditions . . . 234
9.7.4 Polynomial decay . . . 235
9.7.5 Reflectance and transmittance . . . 237
9.8 Input-output theory for a giant atom . . . 237
9.9 Computing output-field correlation functions from the cascaded master equation . . . 239

VI Old, Fundamental Theories 240

VII Multiphoton Processes: Main Articles 241

10 Few photon scattering on Bose-Hubbard lattices by Pedersen, Pletyukhov 241
10.0.1 Introduction . . . 241
10.0.2 Model . . . 242
10.0.3 Diagrammatic scattering theory . . . 243
10.0.4 Results . . . 250
10.0.5 Rings . . . 258
10.0.6 Conclusion . . . 259
10.0.7 Appendix: Two photon scattering . . . 260
10.0.8 Appendix: Second-order intensity correlation function . . . 261

11 Diagrammatic Approach to Multiphoton Scattering by See, et al. 261
11.1 Introduction . . . 262
11.2 Model and background of S-matrix . . . 262
11.3 Diagrammatic approach . . . 264
11.4 Paradigmatic examples . . . 266
11.4.1 Two-level system . . . 266
11.4.2 Two collocated atoms . . . 267
11.4.3 Bose-Hubbard model . . . 270
11.5 Conclusion . . . 273
11.6 Cluster decomposition of the S-matrix . . . 274
11.7 Proof . . . 274
11.8 4-point Green's function for two collocated atoms . . . 278

VIII Experiments: Main Articles 279

12 Nonexponential decay of a giant artificial atom by Andersson et. al. 279

IX Bound States with Photons: Main Articles 285

13 Waveguide QED: Many-Body Bound State Effects in Coherent and Fock State Scattering from a Two-Level System by Zheng, Gauthier, Baranger 285
13.1 Introduction . . . 285
13.2 Scattering Eigenstates . . . 286
13.3 Scattering of Fock States . . . 289
13.3.1 Single-Photon Fock State Scattering . . . 290
13.3.2 Two-Photon Fock State Scattering . . . 291
13.3.3 Three-Photon Fock State Scattering . . . 292
13.4 Scattering of coherent-states . . . 293
13.4.1 Correlation . . . 293
13.4.2 Photon Number Distribution . . . 295
13.5 Conclusion . . . 295
13.6 Appendix: Two-photon Scattering Eigenstate . . . 296

14 Bound states and entanglement generation in waveguide quantum electrodynamics by Facchi, Kim, et al. 297
14.1 Introduction . . . 297
14.2 The model . . . 299
14.3 Time evolution and bound state stability . . . 301
14.4 Off-resonant bound states . . . 304
14.5 Extension to generic dispersion relations . . . 305
14.6 Conclusions and outlook . . . 305
14.7 Derivation of the quasi-1D free field Hamiltonian . . . 306
14.8 Interaction Hamiltonian . . . 307
14.9 Energy density . . . 308

X Exact Solutions in wQED: Main Articles 310

XI Other, Non-Typical Theory 311

15 Scattering of massless particles in one-dimensional chiral channel by Pletyukhov, Gritsev **311**
15.1 Introduction . . . 311
15.2 General solution . . . 312
15.2.1 Main result . . . 312
15.2.2 Derivation of the main result . . . 313
15.3 Examples . . . 315
15.3.1 One emitter in the RWA . . . 315
15.3.2 M emitters in the RWA (Dicke case) . . . 315
15.3.3 One emitter beyond the RWA . . . 317
15.3.4 Three-level system, Λ-scheme . . . 317
15.3.5 Three-level system, V-scheme . . . 318
15.3.6 Three-level system, Σ-scheme . . . 319
15.4 A model with several emitters . . . 319
15.4.1 The case of two atoms . . . 319
15.4.2 Calculation of the self-energy and scattering matrices . . . 320
15.4.3 General approach: One-photon scattering . . . 322
15.4.4 Two-photon sector . . . 323
15.5 Coherent light scattering . . . 330
15.6 Conclusions . . . 333

16 Delayed Coherent Quantum Feedback **333**
16.1 Introduction . . . 333
16.2 Model . . . 334
16.2.1 Hamiltonian . . . 334
16.2.2 Scattering problem . . . 335
16.3 Scattering theory approach . . . 336
16.3.1 Scattering matrix . . . 336
16.3.2 Observables . . . 338
16.3.3 Scattering of coherent states in the low-power limit . . . 339
16.4 Matrix product state approach . . . 339
16.4.1 Stroboscopic evolution . . . 340
16.4.2 Matrix product state ansatz . . . 340
16.5 Results . . . 342
16.5.1 First order correlation function: inelastic spectrum . . . 342
16.5.2 Second order correlation function . . . 344
16.5.3 V-level system . . . 345
16.5.4 Finite coherent driving . . . 346
16.6 Conclusion . . . 348
16.7 appendix: Explicit analytic expressions . . . 348
16.7.1 Two-level atom . . . 348
16.7.2 V-level atom . . . 349

17 Input-output theory for waveguide QED with an ensemble of inhomogeneous atoms **350**
17.1 Introduction . . . 351
17.2 Waveguide QED . . . 352
17.2.1 General effective master equation for the inhomogeneous system . . . 352
17.2.2 Input-output theory . . . 354
17.2.3 Dressed basis . . . 354
17.3 $\lambda/2$ separation: Sub- and Superradiance . . . 355
17.3.1 Discussion . . . 355
17.4 Elastic scattering . . . 356
17.4.1 Inelastic scattering . . . 358
17.5 $\lambda/4$ separation: Exchange interaction . . . 359

17.5.1 Discussion . . . 359
17.5.2 Elastic scattering . . . 360
17.5.3 Inelastic scattering . . . 361
17.6 Conclusion . . . 361
17.7 Appendix . . . 362
17.7.1 Derivation of the waveguide QED Hamiltonian with superconducting qubits . . . 362
17.7.2 Master equation for ensemble of inhomogeneous atoms in open 1D space . . . 364
17.7.3 Discussion of the approximations . . . 366
17.7.4 Driving term . . . 368
17.7.5 Evaluation of formula for Omega . . . 369
17.7.6 Input-output theory . . . 370
17.7.7 Relaxation diagonalization . . . 371

XII Typical Theory: Another Explanations 372

18 Few-photon scattering and emission from open quantum systems by Trivedi et. al. 372
18.1 Introduction . . . 372
18.2 Quantum optical systems coupled to waveguides . . . 373
18.2.1 Hamiltonian and input-output formalism . . . 373
18.2.2 Calculating the propagator matrix elements . . . 374
18.2.3 Extension to multiple waveguides . . . 377
18.2.4 Efficient computation of the Green's functions . . . 378
18.3 Scattering matrices . . . 380
18.4 Examples . . . 382
18.4.1 Two-level System . . . 382
18.4.2 Lambda system . . . 385
18.5 Conclusion and outlook . . . 388

XIII Other Experiments 389

XIV Adds 390

A Введение и обзор 390
A.0.1 Другая мотивация . . . 390
A.0.2 Мышление профессионала в КЭД волноводах . . . 390
A.0.3 Literature . . . 391
A.0.4 Обзор . . . 392
A.0.5 Головоломки . . . 394
A.0.6 Короткий исторический обзор . . . 394
A.1 Mathematics for Waveguide QED . . . 395

B Bibliography 396
B.1 From Main Most Useful Articles . . . 396
B.2 From Articles about Main Experiments . . . 408
B.3 From Main Articles about Multiphoton Scattering . . . 410
B.4 From Articles about Other Special Models and Effects . . . 414

1 Preface

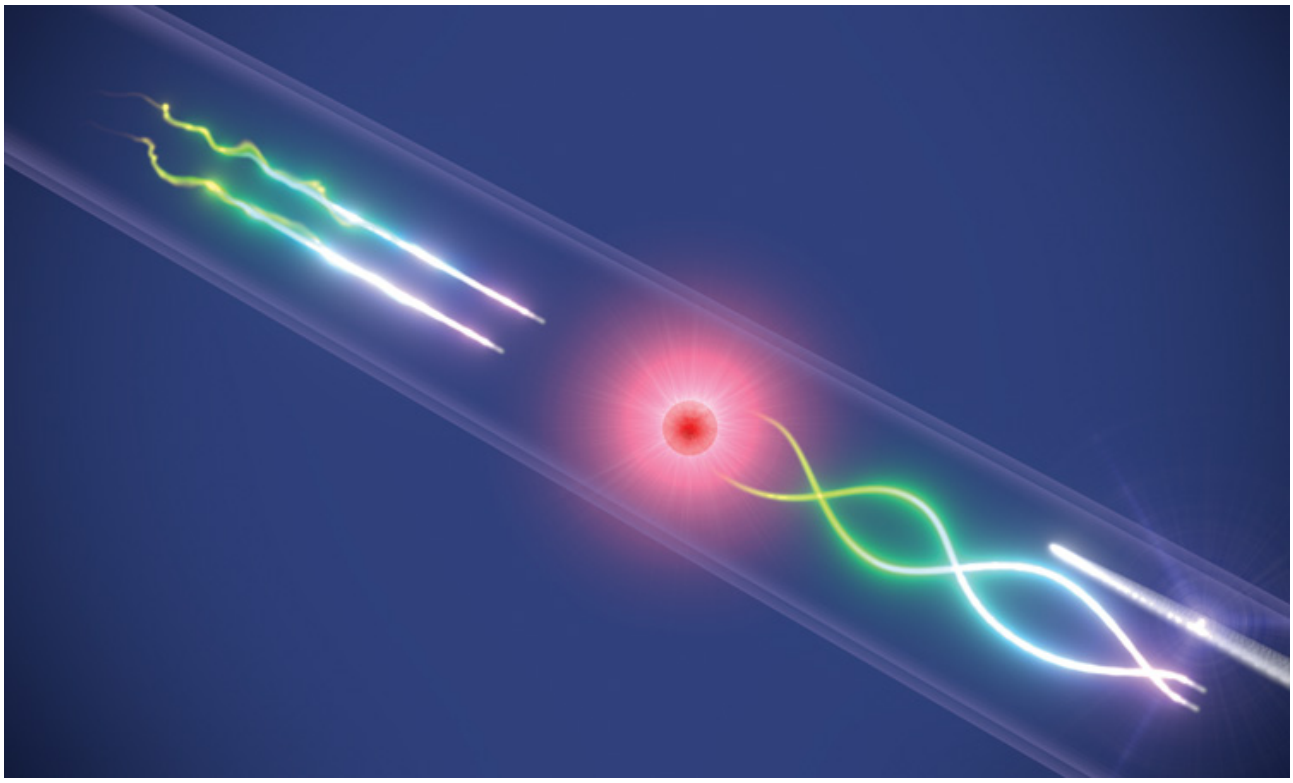

Examples and Solved Problems

Famous Reviews and Important Articles

Old, Fundamental Theories

Multiphoton Processes: Main Articles

Bound States with Photons: Main Articles

Exact Solutions in wQED: Main Articles

Special Effects: Useful, Selected Articles

Main experiments

QED in waveguides is discussed in detail and examples are provided. Mostly this note is made by learning the work of Kiryl Piasotski, but also I used the following literature.

(напишу потом, на самом деле многие этим занимаются, почему - не уверен.)

Фундаментальность фотонных явлений в волноводах

(пока это более всего мотивирует, потому что фундаментально многое можно решить и много уравнений получить. раскрою эту мысль потом.)

(тут примеры от Кирилла, что такие-то взаимодействия атома с светом можно рассматривать в этом формализме)

Множество приложений

Укажем приложения
(потом раскрою)

Удивительные факты

(потом раскрою)

Головоломки для мотивации

(потом раскрою)

Part I
Waveguide QED in Nutshell

2 Main formulas

2.1 Basics of wQED

2.1.1 Fundamental physics in waveguide QED

(пропишу, очень важный раздел!!! пока отдельные дни сидеть на этом нужно.)

2.1.2 On coherence functions (??)

(смысл и формулы, там много всего)

2.2 Methods for Analyzing Models by Well-known Articles

(?????? I'll read them and write here later)

2.3 PP21 Method

2.3.1 Parameters and Formalism for Waveguide QED

Суть модели

$$\mathcal{H} = \mathcal{H}_0 + \mathcal{V},$$

$$\mathcal{H}_0 := \sum_{n=1}^{N_q} \Omega_n \sigma_+^{(n)} \sigma_-^{(n)} + \sum_{\mu=1}^{N_c} \int_{B_\mu} dk \omega_\mu(k) a_\mu^\dagger(k) a_\mu(k); \quad \mathcal{V} = \sum_{\mu=1}^{N_c} \sum_{n=1}^{N_q} \int_{B_\mu} dk \left[g_{\mu,n}(k) a_\mu^\dagger(k) \sigma_-^{(n)} + \text{ h.c. } \right]$$

$$\mathcal{H}_0 := \omega_s a_s^\dagger a_s + \sum_{n=1}^{N_q} \Omega_n \sigma_+^{(n)} \sigma_-^{(n)}, \qquad \text{(count energy)}$$

$$\mathcal{V} := a_s^\dagger v_s + v_s^\dagger a_s \qquad \text{(annihilate and excite)}$$

$$s = (\mu, k) \qquad \text{(multi-index)},$$

the generalized summation convention: If two multiindices are repeated, summation over the channel index μ and integration with respect to the momentum k (over the relevant bandwidth B_μ) is implied.

$$v_s := \sum_{n=1}^{N_q} g_{\mu,n}(k) \sigma_-^{(n)} \qquad \text{(bare interaction vertex)}$$

$$[a_\mu(k), a_{\mu'}^\dagger(k')] = \delta_{\mu,\mu'} \delta(k - k'), \qquad [a_\mu^\dagger(k), a_{\mu'}^\dagger(k')] = [a_\mu(k), a_{\mu'}(k')] = 0.$$

$$\mathcal{S} = 1_{\mathscr{H}} - 2\pi i\delta\left(\epsilon_i - \epsilon_f\right)\mathcal{T}(\epsilon_i), \qquad \mathcal{T}(\epsilon) := \mathcal{V} + \mathcal{V}\mathcal{G}(\epsilon)\mathcal{V} \qquad \text{(T-matrix)}$$

$$\mathcal{G}(\epsilon) := \frac{1}{\epsilon - \mathcal{H} + i\eta} = \sum_{n=0}^{\infty}\left(\mathcal{G}_0(\epsilon)\mathcal{V}\right)^n\mathcal{G}_0(\epsilon) \qquad \text{(“Gr f.”)},$$

$$\mathcal{G}_0(\epsilon) := \frac{1}{\epsilon - \mathcal{H}_0 + i\eta}, \quad \eta \to 0^+ \text{(“Bare Gr f.”)}$$

$$\langle N_p', g|\mathcal{T}^{(1)}|N_p, g\rangle = \sum_{n=0}^{\infty}\langle N_p', g|a_{s_1'}^\dagger v_{s_1'}\left(\mathcal{G}_0\mathcal{V}\mathcal{G}_0\mathcal{V}\right)^n\mathcal{G}_0 v_{s_1}^\dagger a_{s_1}|N_p, g\rangle$$

Типичные преобразования

$$a_s G_0\left(z\right) = G_0\left(\mathcal{H}_0 - \omega_s\right)a_s \qquad \text{for} \qquad G_0(z) := \frac{1}{z - \mathcal{H}_0},$$

По этим правилам и двигаем операторы для обнуления одних и вычисления других.

Следующая модель (????)

The dynamics of the system is generated by

$$\begin{aligned}
\mathcal{H} &= \mathcal{H}_0 + \mathcal{V},\\
\mathcal{H}_0 &= \sum_{\mu=\pm}\int_{-\infty}^{\infty} dx a_\mu^\dagger(x)\left(-\mu i c\partial_x\right)a_\mu(x) + \sum_{n=0}^{N-1}\epsilon_n|n\rangle\langle n|,\\
\mathcal{V} &= \sum_{n=1}^{N-1}\sqrt{c\Gamma_n}\sum_{\mu=\pm}a_\mu^\dagger(0)|n-1\rangle\langle n| + \text{ h.c.}
\end{aligned}$$

(???? про смысл этой модели еще раз!!!) Here signs are $\mu = +$ or $-$, and $\eta = \mp$ for each $\mu = \pm$.

$$a_\mu(x) = \int\frac{dk}{\sqrt{2\pi}}a_{\mu,k}e^{\mu i k x}, \quad a_{\mu,k} := \int\frac{dx}{\sqrt{2\pi}}e^{-\mu i k x}a_\mu(x),$$
$$\left[a_{\mu,k}, a_{\mu',k'}^\dagger\right] = \delta_{\mu,\mu'}\delta\left(k - k'\right), \quad \left[a_{\mu,k}^\dagger, a_{\mu',k'}^\dagger\right] = \left[a_{\mu,k}, a_{\mu',k'}\right] = 0,$$

we find that

$$\mathcal{H}_0 = \sum_{\mu=\pm}\int_{-\infty}^{\infty} dk\cdot ck\cdot a_{\mu,k}^\dagger a_{\mu,k} + \sum_{n=0}^{N-1}\epsilon_n|n\rangle\langle n|,$$
$$\mathcal{V} = \sum_{n=1}^{N-1}\sqrt{\frac{\Gamma_n}{2\pi}}\sum_{\mu=\pm}\int dk a_{\mu,k}^\dagger|n-1\rangle\langle n| + \text{h.c.} \equiv \sum_{n=1}^{N-1}\sqrt{\frac{\Gamma_n}{2\pi}}\sum_{\mu=\pm}\int dk\left(a_{\mu,k}^\dagger|n-1\rangle\langle n| + a_{\mu,k}|n\rangle\langle n-1|\right)$$

(?? такая формула????)

It follows that we have to apply the usual diagrammatic rules with $\omega_s = \omega_{\mu,k} = ck, \mu = \pm$ and

$$v_s = v_{\mu,k} = \sum_{n=1}^{N-1}\sqrt{\frac{\Gamma_n}{2\pi}}|n-1\rangle\langle n|.$$

For example, consider the self-energy diagram

$$\Sigma(z) = v_s^\dagger G_{\text{free}}\left(z-\omega_s\right) v_s =$$
$$= \sum_{\mu=\pm}\int dk \underbrace{\left(\sum_{n''=1}^{N-1}\sqrt{\frac{\Gamma_{n''}}{2\pi}}\left|n''\right\rangle\left\langle n''-1\right|\right)}_{\text{absorption}} \underbrace{\frac{1}{z-\sum\limits_{n=0}^{N-1}\epsilon_n|n\rangle\langle n|-ck}}_{\text{free propagation}} \underbrace{\left(\sum_{n'=1}^{N-1}\sqrt{\frac{\Gamma_{n'}}{2\pi}}\left|n'-1\right\rangle\left\langle n'\right|\right)}_{\text{emission}} =$$
$$= \sum_{n=1}^{N-1}\frac{\Gamma_n}{\pi}\int dk \frac{1}{\omega-\epsilon_{n-1}-ck+i\eta}|n\rangle\langle n| =$$
$$= -i\sum_{n=1}^{N-1}\Gamma_n|n\rangle\langle n|.$$

Here we used that $z=\omega+i\eta, \eta=0^+$ on the Bromwich contour and employed the Sokhotski-Plemelj theorem $\lim_{\eta\to 0^+}\int dx\frac{f(x)}{x\pm i\eta} = P\int dx\frac{f(x)}{x}\mp i\pi f(0)$.

(?? про вывод еще подумаю больше)

Due to the locality of our potential in position space $\propto\delta(x)$, it is possible to show that all of the higher-order diagrams vanish exactly. The dressed propagator is hence

$$G_{\text{dr}}(z) = \sum_{n=1}^{N-1}\frac{|n\rangle\langle n|}{z-\epsilon_n+i\Gamma_n}+\frac{|0\rangle\langle 0|}{z-\epsilon_0}.$$

Free propagater is

$$G_{\text{free}}\left(z-\omega_s\right) = \frac{1}{z-\sum\limits_{n=0}^{N-1}\epsilon_n|n\rangle\langle n|-ck}$$

Note that the ground state of the emitter is the only subradiant (no broadening $\Longrightarrow$ no decay, i.e. there is nowhere to emit a photon from the ground state) subspace. In particular, one expects the spectral density of the photons emitted from such a system to be roughly given by

$$\rho(\omega) = -\frac{1}{\pi}\,\text{Im}\{\text{tr}[G(\omega+i\eta)]\} = \frac{1}{\pi}\sum_{n=1}^{N-1}\frac{\Gamma_n}{\left(\omega-\epsilon_n\right)^2+\Gamma_n^2}+\delta\left(\omega-\epsilon_0\right),$$

which we shall prove in the next problem.

2.3.2 Essence of the PP21 Diagrammatic Method (????)

Суть метода (!??!?)

Our model is as follows:

(???????????/)

Diagrammatic theory of scattering and dynamics of multiphoton states in waveguide QED works like this:

(?????)

The N_p-photon scattering matrices in single-qubit waveguide QED may be conveniently parametrized in terms of effective (N_p-1)-photon vertex functions and the equations satisfied by these vertex functions were established.

(??? тут основные формулы!!!)

Next, certain practical issues related to the direct sum representation of the S matrix, separation of elastic contributions to effective vertices, as well as the generalized cluster decomposition were discussed.

(??? тут основные формулы!!!)

Further, a generalization to the waveguide QED systems with more than a single qubit was given. Specifically, in the case of the two-qubit systems, it was established that the equations governing multiphoton vertex functions remain the same as in the case of a single qubit, up to the inclusion of higher-order vertex corrections.

Moreover, we have shown that once the integral equations governing N_q-photon scattering matrix in N_q waveguide QED, these equations hold for any system of qubits and established the generic equations governing two- and three-photon scattering operators by considering two- and three-photon scattering on two and three qubits, respectively.

Next, the diagrammatic theory of scattering was applied to a problem of scattering of a weakly coherent pulse on the giant acoustic atom. Namely, by expanding a coherent state perturbatively in a coherence parameter up to third order in $|\alpha|$ and studying its scattering on the atom, we were able to establish the first-, second-, and third-order coherence functions of scattered radiation. Moreover, a set of approximation routines was suggested along with the exact method and the two were compared where appropriate. Further, the statistical properties of scattered surface acoustic waves were studied, and the effect of the non-Markovian nature of the setup on statistics was discussed.

Основные формулы и соотношения

$$\mathcal{S} = 1_{\mathscr{H}} - 2\pi i\delta\left(\epsilon_i - \epsilon_f\right)\mathcal{T}(\epsilon_i), \qquad \mathcal{T}(\epsilon) := \mathcal{V} + \mathcal{V}\mathcal{G}(\epsilon)\mathcal{V},$$

$$\mathcal{G}(\epsilon) = \frac{1}{\epsilon - \mathcal{H} + i\eta} = \sum_{n=0}^{\infty}\left(\mathcal{G}_0(\epsilon)\mathcal{V}\right)^n\mathcal{G}_0(\epsilon), \qquad \mathcal{G}_0(\epsilon) = \frac{1}{\epsilon - \mathcal{H}_0 + i\eta}, \quad \eta \to 0^+$$

$$v_{s'}^\dagger a_{s'}\mathcal{G}_0(\epsilon)a_s^\dagger v_s = \Sigma^{(1)}(\epsilon) + \mathcal{R}^{(1)}(\epsilon),$$

$$\Sigma^{(1)}(\epsilon) := v_s^\dagger\mathcal{G}_0(\epsilon - \omega_s)v_s, \qquad \mathcal{R}^{(1)}(\epsilon) := a_{s'}^\dagger\mathcal{R}^{(1)}_{s',s}(\epsilon)a_s,$$
$$\mathcal{R}^{(1)}_{s',s}(\epsilon) := v_s^\dagger\mathcal{G}_0(\epsilon - \omega_{s'} - \omega_s)v_{s'}$$

$$\left(\mathcal{G}^{(1)}\right)^{-1}(\epsilon) = \mathcal{G}_0^{-1}(\epsilon) - \Sigma^{(1)}(\epsilon)$$

$$\mathcal{W}^{(1)} := \mathcal{R}^{(1)}(\epsilon) + \mathcal{R}^{(1)}(\epsilon)\mathcal{G}^{(1)}\mathcal{R}^{(1)}(\epsilon)$$

$$\mathcal{T}^{(1)}(\epsilon) = \sum_{n=1}^{\infty} T^{(1,n)}_{s'_1\ldots s'_n,s_1\ldots s_n}(\epsilon)a_{s'_1}^\dagger\ldots a_{s'_n}^\dagger a_{s_n}\ldots a_{s_1},$$

$$T^{(1,1)}_{s'_1,s_1}(\epsilon) := \langle g|v_{s'_1}G^{(1)}(\epsilon)v_{s_1}^\dagger|g\rangle$$
$$\vdots$$
$$T^{(1,n>1)}_{s_1\ldots\ldots s'_n,s_1\ldots s_n}(\epsilon) := \langle g|v_{s'_1}G^{(1)}\left(\epsilon - \sum_{l=2}^{n}\omega_{s'_l}\right)W^{(1,n-1)}_{s_2\ldots s'_n,s_2\ldots s_n}(\epsilon)G^{(1)}\left(\epsilon - \sum_{l=2}^{n}\omega_{s_l}\right)v_{s_1}^\dagger|g\rangle.$$

$$W^{(1,1,C)}_{s_1,s_1}(\epsilon) = W^{(1,1)}_{s'_1,s_1}(\epsilon) + i\pi v^\dagger_{s_1} v_{s'_1} \delta\left(\epsilon - \omega_{s'_1} - \omega_{s_1}\right).$$

$$W^{(1,n,C)}_{s'_1\ldots s'_n,s_1\ldots s_n}(\epsilon) = W^{(1,n)}_{s'_1\ldots s'_n,s_1\ldots s_n}(\epsilon) - W^{(1,1)}_{s'_1,s_1}\left(\epsilon - \sum_{l=2}^{n}\omega_{s'_n}\right) G^{(1)}\left(\epsilon - \omega_{s_1} - \sum_{l=2}^{n}\omega_{s'_l}\right) W^{(1,n-1)}_{s_2\ldots s'_n,s_2\ldots s_n}(\epsilon - \omega_{s_1}).$$

$$T^{(1,2)}_{s'_1 s_2,s_1 s_2}(\omega_{s_1}+\omega_{s_2}) = -i\pi\delta\left(\omega_{s_1} - \omega_{s'_2}\right) T^{(1,1)}_{s'_1,s_1}(\omega_{s_1}) T^{(1,1)}_{s'_2,s_2}(\omega_{s_2}) + T^{(1,2,C)}_{s_1 s'_2,s_1 s_2}(\omega_{s_1}+\omega_{s_2}),$$

$$\mathcal{S}_2 = \left[\frac{1}{2} S^{(1)}_{s'_1,s_1} S^{(1)}_{s'_2,s_2} - 2\pi i T^{(1,2,C)}_{s'_1 s_2,,1 s_2}(\omega_{s_1}+\omega_{s_2})\delta\left(\omega_{s'_1}+\omega_{s'_2} - \omega_{s_1} - \omega_{s_2}\right)\right] a^\dagger_{s_1} a^\dagger_{s'_2} a_{s_2} a_{s_1}.$$

$$\begin{aligned}\mathcal{S}_3 = \Bigg[&\frac{1}{3!}\delta_{s'_1,s_1}\delta_{s'_2,s_2}\delta_{s'_3,s_3} - 2\pi i \frac{1}{2!}\delta_{s'_2,s_2}\delta_{s'_3,s_3} T^{(1,1)}_{s'_1,s_1}(\omega(k_1))\delta\left(\omega(k'_1) - \omega(k_1)\right) - \\ &- 2\pi i \frac{1}{1!}\delta_{s'_3,s_3} T^{(1,2)}_{s'_1 s'_2,s_1 s_2}(\omega(k_1)+\omega(k_2))\delta\left(\omega(k'_1)+\omega(k'_2) - \omega(k_1) - \omega(k_2)\right) - \\ &- 2\pi i T^{(1,3)}_{s'_1 s'_2 s'_3,s_1 s_2 s_3}(\omega(k_1)+\omega(k_2)+\omega(k_3))\delta\left(\omega(k'_1)+\omega(k'_2)+\omega(k'_3) - \omega(k_1) - \omega(k_2) - \omega(k_3)\right)\Bigg] \cdot \\ &\cdot a^\dagger_{s'_1} a^\dagger_{s'_2} a^\dagger_{s'_3} a_{s_3} a_{s_2} a_{s_1}.\end{aligned}$$

$$\begin{aligned}&T^{(1,3)}_{\mu'_1 k'_1,\mu'_2 k'_2,\mu'_3 k'_3;\mu_1 k_1,\mu_2 k_2,\mu_3 k_3}\left(\omega(k_1)+\omega(k_2)+\omega(k_3)\right) = \\ &= g^*_{\mu_1}(k_1)\, g^*_{\mu_2}(k_2)\, g^*_{\mu_3}(k_3)\, g_{\mu'_1}(k'_1)\, g_{\mu'_2}(k'_2)\, g_{\mu'_3}(k'_3) \cdot \\ &\cdot \tilde{G}^{(1)}(\omega(k_1))\, \tilde{G}^{(1)}(\omega(k'_1))\, F^{(1,2)}(k'_2, k'_3, k_2, k_3, \omega(k_1)+\omega(k_2)+\omega(k_3)),\end{aligned}$$

where $F^{(1,2)}(k'_2, k'_3, k_2, k_3, \omega(k_1)+\omega(k_2)+\omega(k_3))$ is not an entirely connected object defined via

$$F^{(1,2)}(k'_1, k'_2, k_1, k_2, \epsilon) := \frac{1}{g_{\mu'_1}(k'_1)\, g_{\mu'_2}(k'_2)\, g^*_{\mu_1}(k_1)\, g^*_{\mu_2}(k_2)} \left\langle g \left| W^{(1,2)}_{\mu'_1 k'_1 \mu'_2 k'_2,\mu_1 k_1 \mu_2 k_2}(\epsilon) \right| g \right\rangle$$

(???? и зачем мы умножаем и потом делим на одни и те же множители?????)

Separation of elastic contribution (43) translates into the following decomposition:

$$\begin{aligned}&F^{(1,2)}(k'_2, k'_3, k_2, k_3, \omega(k_1)+\omega(k_2)+\omega(k_3)) = \\ &= F^{(1,1)}(k'_2, k_2, \omega(k'_1)+\omega(k'_2))\, \tilde{G}^{(1)}(\omega(k_1)+\omega(k_3)-\omega(k'_3))\, F^{(1,1)}(k'_3, k_3, \omega(k_1)+\omega(k_3)) + \\ &+ \bar{F}^{(2,2)}(k'_2, k'_3, k_2, k_3, \omega(k_1)+\omega(k_2)+\omega(k_3))\end{aligned}$$

In order to understand the difference between the singlequbit and the two-qubit theories, let us have a closer look at the equation defining $\mathcal{W}^{(2)}$:

$$\mathcal{W}^{(2)} = \mathcal{R}^{(1)} + a^\dagger_{s'_1} v_{s'_1} \mathcal{G}_0 v^\dagger_{s_1} a_{s_1} + \mathcal{R}^{(1)}\mathcal{G}^{(1)}\mathcal{W}^{(2)} + a^\dagger_{s'_1} v_{s'_1} \mathcal{G}_0 v^\dagger_{s_1} a_{s_1} \mathcal{G}^{(1)}\mathcal{W}^{(2)}.$$

(!!! оттренирую его, важный очень раздел для систематизации происходящего!!!)

Hierarchies

we arrive at the following hierarchy of integral equations:

$$W^{(1,1)}_{s'_1,s_1}(\epsilon) = R^{(1)}_{s'_1,s_1}(\epsilon) + R^{(1)}_{s'_1,s}(\epsilon) G^{(1)}(\epsilon - \omega_s) W^{(1,1)}_{s,s_1}(\epsilon),$$

$$W^{(1,2)}_{s'_1,s_1}(\epsilon) = \text{напишу потом}$$

Since the lowest term in the expansion of $\mathcal{W}^{(2)}$ is again a single-photon operator

$$\mathcal{W}^{(2)} = \sum_{n=1}^{\infty} a^\dagger_{s'_1} \dots a^\dagger_{s'_n} \mathcal{W}^{(2,n)}_{s'_1 \dots s'_n, s_1 \dots s_n} a_{s_n} \dots a_{s_1}$$

we see that the hierarchy of equations satisfied by the twophoton vertex functions is precisely the same as (29) and (30) with $R^{(1)}$ being replaced by $R^{(2)}$ (see Fig. 4).

Типичный пример для иллюстрации диаграммного метода PP21

Giant acoustic atom as example for PP21

2.3.3 PP21 Diagrammatic Method in Typical Examples (??)

(уже скоро решу, дошел почти до них)

2.3.4 Real time wQED in a nutshell(??)

(тут абзац про то, что вообще меняется в формулах в сравнении с прошлой частью, где нет зависимости от времени?? что-то не полностью понял все еще?)

2.3.5 Mathematics for PP21 wQED: Main Formulas

(expansions, transformations and so on. it will be explained in the appendix)

Integrals for for wQED

- Sometimes use Sokhotski–Plemelj theorem

$$\lim_{\varepsilon \to 0^+} \frac{1}{x \pm i\varepsilon} = \mp i\pi\delta(x) + \mathcal{P}\left(\frac{1}{x}\right)$$

- Sometimes compute resides fast.

Part II
My Main Theory

3 Fundamentals of Waveguide QED

(??? write it???)

3.1 Fundamentals of Waveguide QED

3.1.1 Physics of wQED and derivation of the model

(тут важные всякие обсуждения, что вообще происходит прежде чем начинаются эти модели.)

3.1.2 Hamiltonian, generalized summation convention, and the S matrix

Let us describe in details the model and the formalism.

Setting a model

Let us consider a collection of N_q qubits coupled to a waveguide with N_c radiation channels. The Hamiltonian of such a system assumes the form

$$\mathcal{H} = \mathcal{H}_0 + \mathcal{V},$$

where the free Hamiltonian is:

$$\mathcal{H}_0 := \sum_{n=1}^{N_q} \Omega_n \sigma_+^{(n)} \sigma_-^{(n)} + \sum_{\mu=1}^{N_c} \int_{B_\mu} dk \omega_\mu(k) a_\mu^\dagger(k) a_\mu(k)$$

and dipole light-matter interaction term in Hamiltonian in the rotating wave approximation (RWA):

$$\mathcal{V} = \sum_{\mu=1}^{N_c} \sum_{n=1}^{N_q} \int_{B_\mu} dk \left[g_{\mu,n}(k) a_\mu^\dagger(k) \sigma_-^{(n)} + \text{ h.c. } \right]$$

(?????? вот потом и выведу, как это связано с известным мне взаимодействием????)

(?????? почему именно зона Бриллюэна тут???? додумаю, важный вопрос, пока не понимаю.)

(??? другие мультипольные моменты почему не рассматриваются????)

Or explicitly (?? yes???) $\mathcal{V} = \sum\limits_{\mu=1}^{N_c} \sum\limits_{n=1}^{N_q} \int\limits_{B_\mu} dk \left[g_{\mu,n}(k) a_\mu^\dagger(k) \sigma_-^{(n)} + g_{\mu,n}^*(k) a_\mu(k) \sigma_+^{(n)} \right]$.

(??? все еще вопрос, почему у нас ω в общем случае не ck???)

In the above expression, Ω_n is the transition frequency of the n-th qubit, the dispersion relation $\omega_\mu(k)$ and the bandwidth B_μ characterize the radiation channel μ, while $a_\mu^\dagger(k)$ and $a_\mu(k)$ stand for the creation and annihilation field operators of a photon with momentum k and obey the standard bosonic commutation relations:

$$\left[a_\mu(k), a_{\mu'}^\dagger(k') \right] = \delta_{\mu,\mu'} \delta(k - k'),$$
$$\left[a_\mu^\dagger(k), a_{\mu'}^\dagger(k') \right] = \left[a_\mu(k), a_{\mu'}(k') \right] = 0.$$

And σ-operators act on the Hilbert space of the n-th qubit, $\left\{\sigma_3^{(n)}, \sigma_+^{(n)}, \sigma_-^{(n)}\right\}$, they are defined according to $\sigma_l^{(n)} := 1_{\mathbb{C}^2}^{\otimes(n-1)} \otimes \sigma_l \otimes 1_{\mathbb{C}^2}^{\otimes(N_q-n)}$, with the σ matrices being chosen according to the standard convention $\sigma_3 = \begin{pmatrix} 1 & 0 \\ 0 & -1 \end{pmatrix}$, $\quad \sigma_+ = \sigma_-^\dagger = \begin{pmatrix} 0 & 1 \\ 0 & 0 \end{pmatrix}$.

(Тут Пояснения, почему модель именно такая (!?!??!!?))

(ну там типа взаимодействует свет с кубтом, все такое, я хз, четко не понимаю это)

The RWA

The RWA is justified as long as the characteristic operational frequency ω_0 is such that the condition $\left|g_\mu^2(\omega_0)/\omega_0\right| \ll 1$ is satisfied [73]. (????)

One of the main benefits of this approximation is the conservation of the total number of excitations in the system, i.e., an operator

$$\mathcal{N} := \sum_{n=1}^{N_q} \sigma_+^{(n)} \sigma_-^{(n)} + \sum_{\mu=1}^{N_c} \int_{B_\mu} dk a_\mu^\dagger(k) a_\mu(k)$$

commutes with the full Hamiltonian

$$[\mathcal{N}, \mathcal{H}] = 0.$$

(???? why????)

This property allows us to simultaneously diagonalize $\mathcal{H}$ and $\mathcal{N}$. Moreover, the eigenspaces of the Hamiltonian labeled by the eigenvalues of $\mathcal{N}$ are certainly orthogonal, hence, there exists a direct sum decomposition of the total Hilbert space of the system

$$\mathscr{H} = \bigoplus_{N=0}^{\infty} \mathscr{H}_N$$

where $\mathscr{H}_N$ is the $D(N, N_q) = \sum_{l=0}^{\min(N_q,N)} \frac{N_q!}{l!(N_q-l)!}$ dimensional subspace of all possible states with N excitations. Note that here $D(N, N_q)$ does not stand for the dimension of $\mathscr{H}_N$ in the strict mathematical sense (??? why????). Instead, it is a number of ways to distribute N excitations in a system of N_q qubits [i.e., each single-photon infinite-dimensional vector space adds unity to $D(N, N_q)$]. Analogous direct sum decompositions hold for the Hamiltonian, unitary evolution operator, and the S matrix (to be introduced later). Moreover, such a decomposition considerably simplifies the problem since the calculations may be performed in all of the subspaces separately.

Пояснение, что такое RWA (???????)

(пока этот метод не освоил, приведу примеры или подробнее о нем напишу)

Generalized summation convention for compactness (!!!)

To simplify our further analysis, it is useful to introduce compact notations. Thus, we define a multi-index $s = (\mu, k)$ and the generalized summation convention: If two multiindices are repeated, summation over the channel index μ and integration with respect to the momentum k (over the relevant bandwidth B_μ) is implied. We also introduce the following notation for the bare interaction vertex просто потому что это есть половина каждого члена в потенциале взаимодействия:

$$v_s := \sum_{n=1}^{N_q} g_{\mu,n}(k) \sigma_-^{(n)}.$$

Это очень важная формула, потому что дальше постоянно у нас v_s в формулах!

(добавлю еще пояснения, что типа важно так пользоваться обозначениями, иначе вообще с формулами никуда не уедешь!) Поэтому гамильтониан в изначальной форме мы и не используем, иначе все формулы были бы очень большими.

Using these conventions we rewrite parts the Hamiltonian $\mathcal{H} = \mathcal{H}_0 + \mathcal{V}$ as

$$\mathcal{H}_0 = \omega_s a_s^\dagger a_s + \sum_{n=1}^{N_q} \Omega_n \sigma_+^{(n)} \sigma_-^{(n)},$$
$$\mathcal{V} = a_s^\dagger v_s + v_s^\dagger a_s.$$

The scattering matrix, or the S matrix, is the main object of interest in the present section. It can be generally defined via the so-called transition operator, or the T matrix, in the following way:

$$\mathcal{S} = 1_{\mathscr{H}} - 2\pi i \delta(\epsilon_i - \epsilon_f)\, \mathcal{T}(\epsilon_i),$$
$$\mathcal{T}(\epsilon) := \mathcal{V} + \mathcal{V}\mathcal{G}(\epsilon)\mathcal{V},$$

where the T matrix is put on shell, i.e., $\epsilon = \epsilon_i$, and the energies ϵ_i, ϵ_f, corresponding to initial and final states of the system, obey the energy conservation in the scattering processes, which is mathematically ensured by the delta function. (???? потом додумаю, почему действительно дельта функция не дает нам бесконечности?? также про оператор $1_{\mathscr{H}}$ точнее напишу. все это в квантмехе должно быть написано!)

In $\mathcal{T}(\epsilon)$ we have denoted by $\mathcal{G}(\epsilon)$ the retarded Green's operator defined according to

$$\mathcal{G}(\epsilon) = \frac{1}{\epsilon - \mathcal{H} + i\eta} = \sum_{n=0}^{\infty} (\mathcal{G}_0(\epsilon)\mathcal{V})^n \mathcal{G}_0(\epsilon),$$
$$\mathcal{G}_0(\epsilon) = \frac{1}{\epsilon - \mathcal{H}_0 + i\eta}, \quad \eta \to 0^+$$

3.1.3 Coherence Functions in wQED

(??? write, what is it???s)

3.1.4 Origin of special models in scope of wQED (???)

(типа откуда там взять дисперсии и величины ширин распада?? важное дополнение.)

Origin of V and Λ models

3.2 Features of Approaches in wQED

3.2.1 Features of PP21 Approach

(write my ideas about it. now it is written in their article)

Part III
My Other Theories

4 Fundamentals of Optics and Waveguides

(тут по идее общая подготовительная теория курса квантовой оптики и волноводов, которая подразумевается. Пройду когда-то - напишу)

4.1 Other Questions about Waveguide QED

4.1.1 Key General Features of wQED

(useless, but can pe valuabel for general understanding of the subject)

Сравнение с интегралом по траекториям для осциллирующих функций (?????)

(там похожие графики получаются, так что сравню потом, пока не актуально, большой вопрос, нужно оба метода хорошо понять для этого.)

4.2 Other Phenomena and Methods of Waveguide QED

(мб потом вставлю выше, пока не занимался ими, так что поставил сюда, чтобы не отвлекаться)

4.2.1 Purcell Effect

(it is well-known, but for wQED it is not that relevant, more for quantum optics, it will be discussed much more in that note)

мотивация

некоторые люди изучают его вот.

обзор

(вики)

Эффект Парселла - в квантовой электродинамике увеличение скорости испускания осциллятора в резонаторе по сравнению со скоростью спонтанного излучения в свободное пространство.

Скорость испускания осциллятора в резонаторе умножается на коэффициент Парселла:

$$F_p = \frac{3}{4\pi^2}\left(\frac{\lambda_c}{n}\right)^3 \frac{Q}{V}$$

где $\frac{\lambda_c}{n}$ - длина волны в среде резонатора, Q - его добротность, V -модовый объём. Квантовый эмиттер (атом, ион, квантовая точка и т. д.), помещённый в добротный резонатор малого объёма, меняет направленность и скорость спонтанного излучения.

Эффект зависит от плотности мод в резонаторе. Это свойство используется для эффективного согласования излучения квантовых эммитеров с приёмниками излучения (оптическое волокно, волноводы и т. д.)

Пример изменения коэффициента Парселла можно найти в работе Акимова и др., где показано, что излучение квантовой точки, размещённой вблизи серебряной нанопроволочки почти полностью «засасывается» проволочкой[2].

Статья Парселла, в которой был впервые введён этот коэффициент, является одной из самых коротких (один абзац) и одновременно активно цитируемой в современной физике. По данным ISI Web of Knowledge на 2011 год статья цитировалась почти 1700 раз.

модель

пока не актуально, потом мб буду разбирать.

4.2.2 On Other Well-Known Phenomena (???)

(пока хз. по квантовой оптике нужно подготовиться.)

Part IV
Examples and Solved Problems

5 Problems about Derivation of Formalism of wQED

5.1 Problems about mathematical transformations in wQED

(problem-solution section for all from Piasontski's articles)

6 Problems about Special Phenomena of wQED

6.1 Creation of Models of wQED

(create a model of this or that, see articles, where it is done)

6.2 Single-exitation subspace, Markovian systems

(!?!?! казалось бы, можно было бы многое решить, в том числе через формализм PP21, а я и не решал, и даже пока задачи придумать не готов.)

6.2.1 Qubit emission

For a single qubit we have

$$v_{\mu,k} = \sqrt{\frac{\Gamma_1}{2\pi}} |g\rangle \langle e| , \tag{6.1}$$

such that

$$\Sigma(z) = \Gamma_1 |e\rangle \langle e| \sum_{\mu} \int \frac{dk}{2\pi} \frac{1}{z-k} = -i\Gamma_1 |e\rangle \langle e| . \tag{6.2}$$

Such that

$$|\psi(t)\rangle = \oint_{C_\eta} \frac{dz}{2\pi i} \frac{e^{-izt}}{z - \Delta + i\Gamma_1} |e\rangle |\Omega\rangle \tag{6.3}$$

$$+ \sqrt{\frac{\Gamma_1}{2\pi}} \sum_{\mu=\pm} \oint_{C_\eta} \frac{dz}{2\pi i} \frac{1}{z-k} \frac{e^{-izt}}{z - \Delta + i\Gamma_1} a^\dagger_{\mu,k} |g\rangle |\Omega\rangle \tag{6.4}$$

$$= e^{-i\Delta t} e^{-\Gamma_1 t} |e\rangle |\Omega\rangle + \sqrt{\frac{\Gamma_1}{2\pi}} \sum_{\mu=\pm} \frac{e^{-ikt} - e^{-i\Delta t} e^{-\Gamma_1 t}}{k - \Delta + i\Gamma_1} a^\dagger_{\mu,k} |g\rangle |\Omega\rangle \tag{6.5}$$

it follows that

$$P_e(t) = e^{-2\Gamma t}, \quad P_g(t) = 1 - e^{-2\Gamma t}. \tag{6.6}$$

(тут условие)

Wave functions for $N = 2$ emission case

We assume that the entire system is prepared in the following initial state

$$|\psi_0\rangle = |1\rangle \otimes |\Omega_{\text{phot.}}\rangle,$$

where $|1\rangle$ is the excited state of the qubit and $|\Omega_{\text{phot.}}\rangle$ is the vacuum state of photons. The state of the system at later times $t > 0$ is given by

$$|\psi(t)\rangle = \psi^{(1)}(t)|1\rangle \otimes |\Omega_{\text{phot.}}\rangle + \sum_{\mu=\pm} \int dk \psi_\mu^{(0)}(t,k) a_{\mu,k}^\dagger |0\rangle \otimes |\Omega_{\text{phot.}}\rangle,$$

where

$$\psi^{(1)}(t) = \oint_{C_\eta} \frac{dz}{2\pi i} \langle 1|G(z)|1\rangle e^{-izt},$$
$$\psi_\mu^{(0)}(t,k) = \oint_{C_\eta} \frac{dz}{2\pi i} \langle 0\,|G\left(z-\omega_{\mu,k}\right) v_{\mu,k} G(z)|\,1\rangle\, e^{-izt}.$$

Here C_η is a contour such that it is a counterclockwise semi-circle running $i\eta$ above the real axis (from $\infty + i\eta$ to $-\infty + i\eta$) and closing in the lower-half of the complex plane.

Problem of $N = 2$ emission statement

a) Calculate the wave functions, and measure the following hermitian operator $P_1 = |1\rangle\langle 1|$ (a projector on the excited state), i.e. the probability to find the system in the excited state at time t:

$$\langle \psi(t)\,|P_1|\,\psi(t)\rangle = \left|\psi^{(1)}(t)\right|^2 = ?$$

b) Measure also the photon number operator

$$\mathcal{N} := \sum_{\mu=\pm} \int dk a_{\mu,k}^\dagger a_{\mu,k}$$

to show that

$$\langle\psi(t)|\mathcal{N}|\psi(t)\rangle = \sum_{\mu=\pm} \int dk \left|\psi_\mu^{(0)}(t,k)\right|^2 = 1 - \left|\psi^{(1)}(t)\right|^2.$$

This is a manifestation of the unitarity of quantum theory (all probabilities add to one).

c) Consider now the second moment of the number operator

$$\left\langle \psi(t)\,\left|\mathcal{N}^2\right|\,\psi(t)\right\rangle - ?$$

d) Does the photon number fluctuate? That is:

$$\left\langle \psi(t)\,\left|\mathcal{N}^2\right|\,\psi(t)\right\rangle - \langle\psi(t)|\mathcal{N}|\psi(t)\rangle^2 \neq 0?$$

e) Calculate the momentum space probability distribution of photons at time $t > 0$

$$P_\mu(k,t) = \left\langle \psi(t)\left|a_{\mu,k}^\dagger a_{\mu,k}\right|\psi(t)\right\rangle = \left|\psi_\mu^{(0)}(t,k)\right|^2,$$

what does it approach at times $t \gg 1/\Gamma_1$?

Probability of system in the excited state

Using $G(z) = \sum_{n=1}^{N-1} \frac{|n\rangle\langle n|}{z-\epsilon_n+i\Gamma_n} + \frac{|0\rangle\langle 0|}{z-\epsilon_0}$, we have

$$\langle \psi(t)\,|P_1|\,\psi(t)\rangle = \left|\psi^{(1)}(t)\right|^2 = \left|\oint_{C_\eta} \frac{dz}{2\pi i} \frac{e^{-izt}}{z-\epsilon_n+i\Gamma_n}\right|^2 \overset{\text{res}}{=} \left|e^{-it(\epsilon_1 - i\Gamma_1)}\right|^2 = e^{-2\Gamma_1 t}$$

Photon number

$$\langle\psi(t)|\mathcal{N}|\psi(t)\rangle =$$
$$\left(\langle 1|\otimes\langle\Omega_{\text{phot.}}|\psi^{(1)*}(t)+\langle 0|\otimes\langle\Omega_{\text{phot.}}|\sum_{\mu=\pm}\int dk\psi_\mu^{(0)*}(t,k)a_{\mu,k}\right)\cdot$$
$$\cdot\left(\sum_{\mu=\pm}\int dk a^\dagger_{\mu,k}a_{\mu,k}\right)\cdot$$
$$\cdot\left(\psi^{(1)}(t)|1\rangle\otimes|\Omega_{\text{phot.}}\rangle+\sum_{\mu=\pm}\int dk\psi_\mu^{(0)}(t,k)a^\dagger_{\mu,k}|0\rangle\otimes|\Omega_{\text{phot.}}\rangle\right)=$$
$$=$$
$$=\langle 0|\otimes\langle\Omega_{\text{phot.}}|\sum_{\mu_1,\mu_2,\mu_3=\pm}\int dk_1dk_2dk_3\psi_\mu^{(0)*}(t,k)\psi_\mu^{(0)}(t,k)a_{\mu,k}a^\dagger_{\mu,k}a_{\mu,k}a^\dagger_{\mu,k}|0\rangle\otimes|\Omega_{\text{phot.}}\rangle$$

Тут красное уходит потому что справа у нас вакуум $|\Omega_{\text{phot.}}\rangle$, так что после действия оператора уничтожения в центре у нас получается ноль. Слева красное уходит, потому что справа у нас только состояние с невозбужденной двухуровневой системой. Во всех суммах индекс μ должен быть одинаков, то есть или только (+) одновременно, или только (-) одновременно, потому что иначе левый оператор уничтожения будет уничтожать вакуум и будет ноль. По этой же причине только при одном и том же k для трех интегралов все не нулевое, поэтому остается один интеграл.

Here (пакуль тут індэксы толькі 1 і 2, але верныя папросту потым можна расставіць.)

$$a_{\mu,k}a^\dagger_{\mu,k}a_{\mu,k}a^\dagger_{\mu,k}=$$
$$=(a^\dagger_{\mu,k}a_{\mu,k}+\delta_{\mu,\mu'}\delta(k_1-k_2))(a^\dagger_{\mu,k}a_{\mu,k}+\delta_{\mu,\mu'}\delta(k_1-k_2))=$$
$$=\delta_{\mu,\mu'}\delta(k_1-k_2)\delta_{\mu,\mu'}\delta(k_1-k_2)+\delta_{\mu,\mu'}\delta(k_1-k_2)a^\dagger_{\mu,k}a_{\mu,k}+\delta_{\mu,\mu'}\delta(k_1-k_2)a^\dagger_{\mu,k}a_{\mu,k}+a^\dagger_{\mu,k}a_{\mu,k}a^\dagger_{\mu,k}a_{\mu,k}=$$
$$=\delta_{\mu,\mu'}\delta(k_1-k_2)\cdot\delta_{\mu,\mu'}\delta(k_1-k_2)+a^\dagger_{\mu,k}(\delta_{\mu,\mu'}\delta(k_1-k_2)+a^\dagger_{\mu,k}a_{\mu,k})a_{\mu,k}=$$
$$=\delta_{\mu,\mu'}\delta(k_1-k_2)\cdot\delta_{\mu,\mu'}\delta(k_1-k_2)$$

$$\langle\psi(t)|\mathcal{N}|\psi(t)\rangle =$$
$$=\langle 0|\otimes\langle\Omega_{\text{phot.}}|\sum_{\mu_1,\mu_2,\mu_3=\pm}\int dk_1dk_2dk_3\psi_\mu^{(0)*}(t,k)\psi_\mu^{(0)}(t,k)\delta_{\mu_1,\mu_2}\delta(k_1-k_2)\cdot\delta_{\mu_2,\mu_3}\delta(k_3-k_3)|0\rangle\otimes|\Omega_{\text{phot.}}\rangle=$$
$$=\sum_{\mu=\pm}\int dk\left|\psi_\mu^{(0)}(t,k)\right|^2$$

Left side for N

We set $\omega_{\mu,k}=k, c\equiv 1$. From another side,

$$\psi_\mu^{(0)}(t,k)=\oint_{C_\eta}\frac{dz}{2\pi i}\left\langle 0\left|G\left(z-\omega_{\mu,k}\right)v_{\mu,k}G(z)\right|1\right\rangle e^{-izt}\overset{\text{diagr. rules}}{=}$$
$$=\oint_{C_\eta}\frac{dz}{2\pi i}\left\langle 0\left|\left(\sum_{n=1}^{N-1}\frac{|n\rangle\langle n|}{z-k-\epsilon_n+i\Gamma_n}+\frac{|0\rangle\langle 0|}{z-k-\epsilon_0}\right)\left(\sqrt{\frac{\Gamma}{2\pi}}|0\rangle\langle 1|\right)\left(\sum_{n=1}^{N-1}\frac{|n\rangle\langle n|}{z-\epsilon_n+i\Gamma_n}+\frac{|0\rangle\langle 0|}{z-\epsilon_0}\right)\right|1\right\rangle e^{-izt}=$$
$$=\sqrt{\frac{\Gamma}{2\pi}}\oint_{C_\eta}\frac{dz}{2\pi i}\frac{e^{-izt}}{(z-k-\epsilon_0)(z-\epsilon_1+i\Gamma)}\overset{\text{close count. down, res}}{=}$$
$$=\sqrt{\frac{\Gamma}{2\pi}}\cdot\left(\frac{e^{-i(k+\epsilon_0)t}}{k+\epsilon_0-\epsilon_1+i\Gamma}+\frac{e^{-i(\epsilon_1-i\Gamma)t}}{\epsilon_1-i\Gamma-k-\epsilon_0}\right)$$
$$=\sqrt{\frac{\Gamma}{2\pi}}\cdot\frac{e^{-ikt-i\epsilon_0t}-e^{-i\epsilon_1t-\Gamma t}}{k+\epsilon_0-\epsilon_1+i\Gamma}=$$
$$=\sqrt{\frac{\Gamma}{2\pi}}e^{-i\epsilon_0t}\cdot\frac{e^{-ikt}-e^{-i\Delta\cdot t-\Gamma t}}{k-\Delta+i\Gamma}$$

Here $\Gamma_1 \equiv \Gamma$, $\Delta \equiv \varepsilon_1 - \varepsilon_0$.
Then for $t > 0$

$$\int dk \left|\psi_\mu^{(0)}(t,k)\right|^2 = \frac{\Gamma}{2\pi}\int dk \frac{(e^{ikt} - e^{i\Delta\cdot t-\Gamma t})(e^{-ikt} - e^{-i\Delta\cdot t-\Gamma t})}{(k-\Delta+i\Gamma))k-\Delta-i\Gamma)} =$$
$$= \frac{\Gamma}{2\pi}\int dk \left(\frac{1-e^{-2\Gamma t}}{(k-\Delta+i\Gamma))k-\Delta-i\Gamma)} - \frac{e^{-ikt}e^{i\Delta\cdot t-\Gamma t}}{(k-\Delta+i\Gamma))k-\Delta-i\Gamma)} - \frac{e^{ikt}e^{-i\Delta\cdot t-\Gamma t}}{(k-\Delta+i\Gamma))k-\Delta-i\Gamma)}\right) =$$
$$= \frac{\Gamma}{2\pi}\frac{2\pi i(1+e^{-2\Gamma t})}{2i\Gamma} - \frac{\Gamma}{2\pi}\frac{(-1)2\pi i e^{-i(\Delta-i\Gamma)t}e^{-i\Delta\cdot t-\Gamma t}}{(-1)2i\Gamma} - \frac{\Gamma}{2\pi}\frac{2\pi i e^{i(\Delta+i\Gamma)t}e^{-i\Delta\cdot t-\Gamma t}}{2i\Gamma} =$$
$$= \frac{1+e^{-2\Gamma t}}{2} - \frac{e^{-2\Gamma t}}{2} - \frac{e^{-2\Gamma t}}{2} = \frac{1-e^{-2\Gamma t}}{2}$$

Here first contour could be closed up or down, second we should close down, third - up.

$$\sum_{\mu=\pm}\int dk \left|\psi_\mu^{(0)}(t,k)\right|^2 = 1 - e^{-2\Gamma t}$$

Right side for N

From another side

$$\psi^{(1)}(t) = \oint_{C_\eta} \frac{dz}{2\pi i}\langle 1| \left(\sum_{n=1}^{N-1}\frac{|n\rangle\langle n|}{z-\epsilon_n+i\Gamma_n} + \frac{|0\rangle\langle 0|}{z-\epsilon_0}\right)|1\rangle e^{-izt} =$$
$$= \oint_{C_\eta}\frac{dz}{2\pi i}\frac{1}{z-\epsilon_1+i\Gamma}e^{-izt} =$$
$$= e^{-i(\epsilon_1-i\Gamma)t} = e^{-i\epsilon_1 t-\Gamma t}$$

And

$$\left|\psi^{(1)}(t)\right|^2 = \psi^{(1)*}(t)\psi^{(1)}(t) = e^{-2\Gamma t}$$

We see that left-side equals to the right side, thus

$$\langle\psi(t)|\mathcal{N}|\psi(t)\rangle = \sum_{\mu=\pm}\int dk \left|\psi_\mu^{(0)}(t,k)\right|^2 = 1 - \left|\psi^{(1)}(t)\right|^2.$$

Expression for N^2 and squared dispersion of photos

$$\langle\psi(t)|\mathcal{N}^2|\psi(t)\rangle =$$
$$\left(\langle 1|\otimes\langle\Omega_{\text{phot.}}|\psi^{(1)*}(t) + \langle 0|\otimes\langle\Omega_{\text{phot.}}|\sum_{\mu_1=\pm}\int dk_1\psi_{\mu_1}^{(0)*}(t,k_1)a_{\mu_1,k_1}\right)\cdot$$
$$\cdot\left(\sum_{\mu_2=\pm}\int dk_2 a^\dagger_{\mu_2,k_2}a_{\mu_2,k_2}\right)\left(\sum_{\mu_3=\pm}\int dk_3 a^\dagger_{\mu_3,k_3}a_{\mu_3,k_3}\right)\cdot$$
$$\cdot\left(\psi^{(1)}(t)|1\rangle\otimes|\Omega_{\text{phot.}}\rangle + \sum_{\mu_4=\pm}\int dk_4\psi_{\mu_4}^{(0)}(t,k_4)a^\dagger_{\mu_4,k_4}|0\rangle\otimes|\Omega_{\text{phot.}}\rangle\right) =$$
$$=$$
$$= \langle 0|\otimes\langle\Omega_{\text{phot.}}|\sum_{\mu_1,\mu_2,\mu_3,\mu_4=\pm}\int dk_1\ldots dk_4\psi_\mu^{(0)*}(t,k_1)\psi_\mu^{(0)}(t,k_4)a_{\mu_1,k_1}a^\dagger_{\mu_2,k_2}a_{\mu_2,k_2}a^\dagger_{\mu_3,k_3}a_{\mu_3,k_3}a^\dagger_{\mu_4,k_4}|0\rangle\otimes|\Omega_{\text{phot.}}\rangle$$

Тут

$$
\begin{aligned}
&a_{\mu_1,k_1}a^\dagger_{\mu_2,k_2}a_{\mu_2,k_2}a^\dagger_{\mu_3,k_3}a_{\mu_3,k_3}a^\dagger_{\mu_4,k_4} = \\
&= (a^\dagger_{\mu_2,k_2}a_{\mu_1,k_1} + \delta_{\mu_1,\mu_2}\delta(k_1-k_2))(a^\dagger_{\mu_3,k_3}a_{\mu_2,k_2} + \delta_{\mu_2,\mu_3}\delta(k_2-k_3))(a^\dagger_{\mu_4,k_4}a_{\mu_3,k_3} + \delta_{\mu_3,\mu_4}\delta(k_3-k_4)) = \\
&= \Big(a^\dagger_{\mu_2,k_2}a_{\mu_1,k_1}a^\dagger_{\mu_3,k_3}a_{\mu_2,k_2} + a^\dagger_{\mu_2,k_2}a_{\mu_1,k_1}\delta_{\mu_2,\mu_3}\delta(k_2-k_3) + a^\dagger_{\mu_3,k_3}a_{\mu_2,k_2}\delta_{\mu_1,\mu_2}\delta(k_1-k_2) + \\
&\qquad + \delta_{\mu_1,\mu_2}\delta(k_1-k_2)\delta_{\mu_2,\mu_3}\delta(k_2-k_3)\Big)(a^\dagger_{\mu_4,k_4}a_{\mu_3,k_3} + \delta_{\mu_3,\mu_4}\delta(k_3-k_4)) = \\
&= a^\dagger_{\mu_2,k_2}a_{\mu_1,k_1}a^\dagger_{\mu_3,k_3}a_{\mu_2,k_2}a^\dagger_{\mu_4,k_4}a_{\mu_3,k_3} + a^\dagger_{\mu_2,k_2}a_{\mu_1,k_1}a^\dagger_{\mu_4,k_4}a_{\mu_3,k_3}\delta_{\mu_2,\mu_3}\delta(k_2-k_3) + \\
&\quad + a^\dagger_{\mu_3,k_3}a_{\mu_2,k_2}a^\dagger_{\mu_4,k_4}a_{\mu_3,k_3}\delta_{\mu_1,\mu_1}\delta(k_1-k_2) + a^\dagger_{\mu_4,k_4}a_{\mu_3,k_3}\delta_{\mu_1,\mu_2}\delta(k_1-k_2)\delta_{\mu_2,\mu_3}\delta(k_2-k_3) + \\
&\quad + a^\dagger_{\mu_2,k}a_{\mu_1,k}a^\dagger_{\mu_3,k}a_{\mu_2,k}\delta_{\mu_3,\mu_4}\delta(k_3-k_4) + a^\dagger_{\mu_2,k_2}a_{\mu_1,k_1}\delta_{\mu_2,\mu_3}\delta(k_2-k_3)\delta_{\mu_3,\mu_4}\delta(k_3-k_4) + \\
&\quad + a^\dagger_{\mu_3,k_3}a_{\mu_2,k_2}\delta_{\mu_1,\mu_2}\delta(k_1-k_2)\delta_{\mu_3,\mu_4}\delta(k_3-k_4) + \delta_{\mu_1,\mu_2}\delta(k_1-k_2)\delta_{\mu_2,\mu_3}\delta(k_2-k_3)\delta_{\mu_3,\mu_4}\delta(k_3-k_4) = \\
&= \delta_{\mu_1,\mu_2}\delta(k_1-k_2)\delta_{\mu_2,\mu_3}\delta(k_2-k_3)\delta_{\mu_3,\mu_4}\delta(k_3-k_4),
\end{aligned}
$$

потому что у нас в других слагаемых (кроме оставшегося) справа уже стоит a - оператор уничтожения, так что каждое из этих слагаемых после действия на вакуум даст нуль.

В итоге

$$\langle\psi(t)|\mathcal{N}^2|\psi(t)\rangle = \langle 0|\otimes\langle\Omega_{\text{phot.}}|\sum_{\mu=\pm}\int dk\psi^{(0)*}_\mu(t,k)\psi^{(0)}_\mu(t,k)|0\rangle\otimes|\Omega_{\text{phot.}}\rangle$$

$$\langle\psi(t)|\mathcal{N}^2|\psi(t)\rangle = \langle\psi(t)|\mathcal{N}|\psi(t)\rangle$$

Momentum space probability

$$
\begin{aligned}
P_\mu(k,t) &= \left\langle\psi(t)\left|a^\dagger_{\mu,k}a_{\mu,k}\right|\psi(t)\right\rangle = \left|\psi^{(0)}_\mu(t,k)\right|^2 = \frac{\Gamma}{2\pi}\frac{e^{-ikt}-e^{-i\Delta\cdot t-\Gamma t}}{k-\Delta+i\Gamma}\frac{e^{ikt}-e^{i\Delta\cdot t-\Gamma t}}{k-\Delta-i\Gamma} = \\
&= \frac{\Gamma}{2\pi}\frac{1-e^{-ikt}e^{i\Delta\cdot t-\Gamma t}-e^{-ikt}e^{-i\Delta\cdot t-\Gamma t}+e^{-2\Gamma t}}{(k-\Delta)^2+\Gamma^2} = \\
&= \frac{\Gamma}{2\pi}\frac{1+e^{-2\Gamma t}-2\cos)(k-\Delta)t)e^{-\Gamma t}}{(k-\Delta)^2+\Gamma^2} =
\end{aligned}
$$

(я тут построил графики, но не уверен в них, потому что нужно примерно реальные величины Γ и др. брать.)

При $\Gamma t \gg 1$ экспонента мелкая, так что

$$P_\mu(k,t) \approx \frac{\Gamma}{2\pi}\frac{1}{(k-\Delta)^2+\Gamma^2}.$$

Вывод диаграммного метода на примере этой модели

(то же что в теории, только все в рамках этой модели, очень крутой будет пример)

6.2.2 Problems for $N = 3$ emission

Problem statement

We assume that the entire system is prepared in the following initial state

$$|\psi_0\rangle = |2\rangle\otimes|\Omega\rangle,$$

where $|2\rangle$ is the second excited state of the atom. The state of the system at later times $t > 0$ is given by

$$|\psi(t)\rangle = \psi^{(2)}(t)|2\rangle\otimes|\Omega\rangle + \sum_{\mu=\pm}\int dkdk'\psi^{(1)}_\mu(t,k)a^\dagger_{\mu,k}|1\rangle\otimes|\Omega\rangle + \sum_{\mu,\mu'=\pm}\int dkdk'\psi^{(0)}_{\mu,\mu'}(t,k,k')\,a^\dagger_{\mu,k}a^\dagger_{\mu',k'}|0\rangle\otimes|\Omega\rangle,$$

where

$$
\begin{aligned}
\psi^{(2)}(t) &= \oint_{C_\eta}\frac{dz}{2\pi i}\langle 2|G(z)|2\rangle e^{-izt}, \\
\psi^{(1)}_\mu(t,k) &= \oint_{C_\eta}\frac{dz}{2\pi i}\left\langle 1\left|G\left(z-\omega_{\mu,k}\right)v_{\mu,k}G(z)\right|2\right\rangle e^{-izt}, \\
\psi^{(0)}_{\mu,\mu'}(t,k,k') &= \oint_{C_\eta}\frac{dz}{2\pi i}\left\langle 0\left|G\left(z-\omega_{\mu,k}-\omega_{\mu',k'}\right)v_{\mu',k'}G\left(z-\omega_{\mu,k}\right)v_{\mu,k}G(z)\right|2\right\rangle e^{-izt},
\end{aligned}
$$

Here C_η is the contour that is a counterclockwise semi-circle running $i\eta$ above the real axis (from $\infty + i\eta$ to $-\infty + i\eta$) and closing in the lower-half of the complex plane.

a) Calculate the wave functions, and measure the following hermitian operators $P_n = |n\rangle\langle n|, n = 0, 1, 2$.

b) Measure the photon number operator

$$\mathcal{N} = \sum_{\mu=\pm} \int dk a^\dagger_{\mu,k} a_{\mu,k},$$

c) Consider the second moment of the number operator

$$\left\langle \psi(t) \left| \mathcal{N}^2 \right| \psi(t) \right\rangle - ?$$

Does the photon number fluctuate in this case?

d) Determine the spectrum of the photons

$$P_\mu(k,t) = \left\langle \psi(t) \left| a^\dagger_{\mu,k} a_{\mu,k} \right| \psi(t) \right\rangle,$$

what does it approach at times $t \gg 1/\min\{\Gamma_1, \Gamma_2\}$? As $t \gg 1/\min\{\Gamma_1, \Gamma_2\}$, show that the system finds itself in an entangled two-photon state.

Photon number

$$\langle\psi(t)|\mathcal{N}|\psi(t)\rangle =$$

$$\left(\psi^{(2)*}(t)|2\rangle\otimes|\Omega\rangle + \sum_{\mu_1=\pm}\int dk_1 \psi^{(1)*}_{\mu_1}(t,k_1) a_{\mu_1,k_1}\,\langle 1|\otimes\langle\Omega| + \sum_{\mu_2,\mu_2'=\pm}\int dk_2 dk_2' \psi^{(0)*}_{\mu_2,\mu_2'}(t,k_2,k_2')\, a_{\mu_2,k_2} a_{\mu_2',k_2'}\,\langle 0|\otimes\langle\Omega|\right)\cdot$$

$$\cdot\left(\sum_{\mu_3=\pm}\int dk_3 a^\dagger_{\mu_3,k_3} a_{\mu_3,k_3}\right)\cdot$$

$$\cdot\left(\psi^{(2)}(t)|2\rangle\otimes|\Omega\rangle + \sum_{\mu_4=\pm}\int dk_4 \psi^{(1)}_{\mu_4}(t,k_4) a^\dagger_{\mu_4,k}|1\rangle\otimes|\Omega\rangle + \sum_{\mu_5,\mu_5'=\pm}\int dk_5 dk_5' \psi^{(0)}_{\mu_5,\mu_5'}(t,k_5,k_5')\, a^\dagger_{\mu_5,k_5} a^\dagger_{\mu_5',k_5'}|0\rangle\otimes|\Omega\rangle\right).$$

The same way as before,

$$\langle\psi(t)|\mathcal{N}|\psi(t)\rangle = \sum_{\mu_i=\pm}\int d^4k \psi^{(1)*}_{\mu_1}(t,k)\psi^{(1)}_{\mu_4}(t,k) a_{\mu_1,k_1} a^\dagger_{\mu_3,k_3} a_{\mu_3,k_3} a^\dagger_{\mu_4,k_4} +$$

$$+ \sum_{\mu_j=\pm}\int d^6k \psi^{(0)*}_{\mu_2,\mu_2'}(t,k_2,k_2')\psi^{(0)}_{\mu_5,\mu_5'}(t,k_5,k_5') a_{\mu_2,k_2} a_{\mu_2',k_2'} a^\dagger_{\mu_3,k_3} a_{\mu_3,k_3} a^\dagger_{\mu_5,k_5} a^\dagger_{\mu_5',k_5'}$$

Тут i пробегает такие-то значения, j пробегает такие-то значения, а dk это сокращение от всех k.

Тут первый член - абсолютно то же, что и для двух фотонов, поэтому

$$\sum_{\mu_i=\pm}\int d^4k \psi^{(1)*}_{\mu_1}(t,k)\psi^{(1)}_{\mu_4}(t,k) a_{\mu_1,k_1} a^\dagger_{\mu_3,k_3} a_{\mu_3,k_3} a^\dagger_{\mu_4,k_4} = \sum_{\mu=\pm}\int dk \left|\psi^{(1)}_\mu(t,k)\right|^2$$

Во втором члене имеем следующее. Ниже я сразу буду опускать все, что зануляется.

$$
\begin{aligned}
&a_{\mu_2,k_2}a_{\mu_2',k_2'}a^\dagger_{\mu_3,k_3}a_{\mu_3,k_3}a^\dagger_{\mu_5,k_5}a^\dagger_{\mu_5',k_5'} = a_{\mu_2,k_2}a_{\mu_2',k_2'}a^\dagger_{\mu_3,k_3}(a^\dagger_{\mu_5,k_5}a_{\mu_3,k_3}+\delta_{\mu_3,\mu_5}\delta(k_3-k_5))a^\dagger_{\mu_5',k_5'} = \\
&= a_{\mu_2,k_2}a_{\mu_2',k_2'}a^\dagger_{\mu_3,k_3}a^\dagger_{\mu_5,k_5}a_{\mu_3,k_3}a^\dagger_{\mu_5',k_5'}+\delta_{\mu_3,\mu_5}\delta(k_3-k_5)a_{\mu_2,k_2}a_{\mu_2',k_2'}a^\dagger_{\mu_3,k_3}a^\dagger_{\mu_5',k_5'} = \\
&= a_{\mu_2,k_2}a_{\mu_2',k_2'}a^\dagger_{\mu_3,k_3}a^\dagger_{\mu_5,k_5}(a^\dagger_{\mu_5',k_5'}a_{\mu_3,k_3}+\delta_{\mu_3,\mu_5'}\delta(k_3-k_5'))+ \\
&\qquad\qquad +\delta_{\mu_3,\mu_5}\delta(k_3-k_5)a_{\mu_2,k_2}(a^\dagger_{\mu_3,k_3}a_{\mu_2',k_2'}+\delta_{\mu_3,\mu_2'}\delta(k_3-k_2'))a^\dagger_{\mu_5',k_5'} = \\
&= \delta_{\mu_3,\mu_5'}\delta(k_3-k_5')a_{\mu_2,k_2}(a^\dagger_{\mu_3,k_3}a_{\mu_2',k_2'}+\delta_{\mu_3,\mu_2'}\delta(k_3-k_2'))a^\dagger_{\mu_5,k_5}+ \\
&\quad +\delta_{\mu_3,\mu_5}\delta(k_3-k_5)a_{\mu_2,k_2}a^\dagger_{\mu_3,k_3}a_{\mu_2',k_2'}a^\dagger_{\mu_5',k_5'}+\delta_{\mu_3,\mu_5}\delta(k_3-k_5)\delta_{\mu_3,\mu_2'}\delta(k_3-k_2')a_{\mu_2,k_2}a^\dagger_{\mu_5',k_5'} = \\
&= \delta_{\mu_3,\mu_5'}\delta(k_3-k_5')a_{\mu_2,k_2}a^\dagger_{\mu_3,k_3}a_{\mu_2',k_2'}a^\dagger_{\mu_5,k_5}+\delta_{\mu_3,\mu_5'}\delta(k_3-k_5')\delta_{\mu_3,\mu_2'}\delta(k_3-k_2')a_{\mu_2,k_2}a^\dagger_{\mu_5,k_5}+ \\
&\quad +\delta_{\mu_3,\mu_5}\delta(k_3-k_5)\delta_{\mu_2,\mu_3}\delta(k_2-k_3)\delta_{\mu_2',\mu_5'}\delta(k_2'-k_5')+ \\
&\qquad +\delta_{\mu_3,\mu_5}\delta(k_3-k_5)\delta_{\mu_3,\mu_2'}\delta(k_3-k_2')(a^\dagger_{\mu_5',k_5'}a_{\mu_2,k_2}+\delta_{\mu_2,\mu_5'}\delta(k_2-k_5')) = \\
&= \delta_{\mu_3,\mu_5'}\delta(k_3-k_5')a_{\mu_2,k_2}a^\dagger_{\mu_3,k_3}(a^\dagger_{\mu_5,k_5}a_{\mu_2',k_2'}+\delta_{\mu_5,\mu_2'}\delta(k_5-k_2'))+ \\
&\qquad +\delta_{\mu_3,\mu_5'}\delta(k_3-k_5')\delta_{\mu_3,\mu_2'}\delta(k_3-k_2')(a^\dagger_{\mu_5,k_5}a_{\mu_2,k_2}+\delta_{\mu_5,\mu_2}\delta(k_5-k_2))+ \\
&\quad +\delta_{\mu_3,\mu_5}\delta(k_3-k_5)\delta_{\mu_2,\mu_3}\delta(k_2-k_3)\delta_{\mu_2',\mu_5'}\delta(k_2'-k_5')+\delta_{\mu_3,\mu_5}\delta(k_3-k_5)\delta_{\mu_3,\mu_2'}\delta(k_3-k_2')\delta_{\mu_2,\mu_5'}\delta(k_2-k_5') = \\
&= \delta_{\mu_3,\mu_5'}\delta(k_3-k_5')\delta_{\mu_5,\mu_2'}\delta(k_5-k_2')\delta_{\mu_2,\mu_3}\delta(k_2-k_3)+ \\
&\quad +\delta_{\mu_3,\mu_5'}\delta(k_3-k_5')\delta_{\mu_3,\mu_2'}\delta(k_3-k_2')\delta_{\mu_5,\mu_2}\delta(k_5-k_2)+ \\
&\quad +\delta_{\mu_3,\mu_5}\delta(k_3-k_5)\delta_{\mu_2,\mu_3}\delta(k_2-k_3)\delta_{\mu_2',\mu_5'}\delta(k_2'-k_5')+ \\
&\quad +\delta_{\mu_3,\mu_5}\delta(k_3-k_5)\delta_{\mu_3,\mu_2'}\delta(k_3-k_2')\delta_{\mu_2,\mu_5'}\delta(k_2-k_5')
\end{aligned}
$$

То есть тут у нас есть 5 индексов, и в каждой комбинации дельт у нас 3 каждых равны между собой, а оставшиеся 2 равны между собой, но не равны трем другим.

Thus the second term is

$$
\begin{aligned}
&\sum_{\mu_j=\pm}\int d^6k\psi^{(0)*}_{\mu_2,\mu_2'}(t,k_2,k_2')\psi^{(0)}_{\mu_5,\mu_5'}(t,k_5,k_5')a_{\mu_2,k_2}a_{\mu_2',k_2'}a^\dagger_{\mu_3,k_3}a_{\mu_3,k_3}a^\dagger_{\mu_5,k_5}a^\dagger_{\mu_5',k_5'} = \\
&= \sum_{\mu_3,\mu_5=\pm}\int dk_3dk_5\psi^{(0)*}_{\mu_3,\mu_5}(t,k_3,k_5)\psi^{(0)}_{\mu_5,\mu_3}(t,k_5,k_3)+ \\
&+ \sum_{\mu_3,\mu_2=\pm}\int dk_3dk_2\psi^{(0)*}_{\mu_2,\mu_3}(t,k_2,k_3)\psi^{(0)}_{\mu_2,\mu_3}(t,k_2,k_3)+ \\
&+ \sum_{\mu_3,\mu_2=\pm}\int dk_3dk_2\psi^{(0)*}_{\mu_2,\mu_3}(t,k_2,k_3)\psi^{(0)}_{\mu_3,\mu_2}(t,k_3,k_2)+ \\
&+ \sum_{\mu_3,\mu_5'=\pm}\int dk_3dk_5'\psi^{(0)*}_{\mu_3,\mu_5'}(t,k_3,k_5')\psi^{(0)}_{\mu_3,\mu_5'}(t,k_3,k_5').
\end{aligned}
$$

Теперь сменим обозначения:

$$
\begin{aligned}
&\sum_{\mu_j=\pm}\int d^6k\psi^{(0)*}_{\mu_2,\mu_2'}(t,k_2,k_2')\psi^{(0)}_{\mu_5,\mu_5'}(t,k_5,k_5')a_{\mu_2,k_2}a_{\mu_2',k_2'}a^\dagger_{\mu_3,k_3}a_{\mu_3,k_3}a^\dagger_{\mu_5,k_5}a^\dagger_{\mu_5',k_5'} = \\
&= \sum_{\mu_1,\mu_2=\pm}\int dk_1dk_2\psi^{(0)*}_{\mu_1,\mu_2}(t,k_1,k_2)\psi^{(0)}_{\mu_2,\mu_1}(t,k_2,k_1)+ \\
&+ \sum_{\mu_1,\mu_2=\pm}\int dk_1dk_2\psi^{(0)*}_{\mu_2,\mu_1}(t,k_2,k_1)\psi^{(0)}_{\mu_2,\mu_1}(t,k_2,k_1)+ \\
&+ \sum_{\mu_1,\mu_2=\pm}\int dk_1dk_2\psi^{(0)*}_{\mu_2,\mu_1}(t,k_2,k_1)\psi^{(0)}_{\mu_1,\mu_2}(t,k_1,k_2)+ \\
&+ \sum_{\mu_1,\mu_2=\pm}\int dk_1dk_2'\psi^{(0)*}_{\mu_1,\mu_2}(t,k_1,k_2)\psi^{(0)}_{\mu_1,\mu_2}(t,k_1,k_2) \\
&= \\
&4\sum_{\mu_1,\mu_2=\pm}\int dk_1dk_2'\psi^{(0)*}_{\mu_1,\mu_2}(t,k_1,k_2)\psi^{(0)}_{\mu_1,\mu_2}(t,k_1,k_2).
\end{aligned}
$$

В итоге:

$$\begin{aligned}
&\langle\psi(t)|\mathcal{N}|\psi(t)\rangle = \\
&= \sum_{\mu=\pm}\int dk\left|\psi^{(1)}_{\mu}(t,k)\right|^2 + \\
&+ \sum_{\mu_1,\mu_2=\pm}\int dk_1 dk_2 \psi^{(0)*}_{\mu_1,\mu_2}(t,k_1,k_2)\psi^{(0)}_{\mu_2,\mu_1}(t,k_2,k_1) + \\
&+ \sum_{\mu_1,\mu_2=\pm}\int dk_1 dk_2 \psi^{(0)*}_{\mu_2,\mu_1}(t,k_2,k_1)\psi^{(0)}_{\mu_2,\mu_1}(t,k_2,k_1) + \\
&+ \sum_{\mu_1,\mu_2=\pm}\int dk_1 dk_2 \psi^{(0)*}_{\mu_2,\mu_1}(t,k_2,k_1)\psi^{(0)}_{\mu_1,\mu_2}(t,k_1,k_2) + \\
&+ \sum_{\mu_1,\mu_2=\pm}\int dk_1 dk_2 \psi^{(0)*}_{\mu_1,\mu_2}(t,k_1,k_2')\psi^{(0)}_{\mu_1,\mu_2}(t,k_1,k_2).
\end{aligned}$$

Photon number's second moment

Spectrum of photons

Вывод диаграммного метода на примере этой модели

(то же что в теории, только все в рамках этой модели, очень крутой будет пример)

6.2.3 Λ-system

(тут условие)

Решение

We have

$$v_{\mu,k} = \sqrt{\frac{\Gamma_1}{2\pi}}\,|g_1\rangle\langle e| + \sqrt{\frac{\Gamma_2}{2\pi}}\,|g_2\rangle\langle e|\,, \tag{6.7}$$

with the energies $\epsilon_{0,1} = -\Delta_1$ and $\epsilon_{0,2} = -\Delta_2$ we find

$$\begin{aligned}
\Sigma(z) &= |e\rangle\langle e|\,\frac{\Gamma_1}{2\pi}\sum_{\mu}\int dk \frac{1}{z+\Delta_1-k} + |e\rangle\langle e|\,\frac{\Gamma_2}{2\pi}\sum_{\mu}\int dk\frac{1}{z+\Delta_2-k} && (6.8)\\
&= -i(\Gamma_1+\Gamma_2)\,|e\rangle\langle e|\,. && (6.9)
\end{aligned}$$

The state at times $t > 0$ is given by

$$\begin{aligned}
|\psi(t)\rangle = &\oint_{C_\eta}\frac{dz}{2\pi i}\frac{e^{-izt}}{z+i(\Gamma_1+\Gamma_2)}\,|e\rangle\,|\Omega\rangle && (6.10)\\
&+\sqrt{\frac{\Gamma_2}{2\pi}}\oint_{C_\eta}\frac{dz}{2\pi i}\frac{1}{z-k+\Delta_2}\frac{e^{-izt}}{z+i(\Gamma_1+\Gamma_2)}a^\dagger_{\mu,k}\,|g_2\rangle\,|\Omega\rangle && (6.11)\\
&+\sqrt{\frac{\Gamma_1}{2\pi}}\oint_{C_\eta}\frac{dz}{2\pi i}\frac{1}{z-k+\Delta_1}\frac{e^{-izt}}{z+i(\Gamma_1+\Gamma_2)}a^\dagger_{\mu,k}\,|g_1\rangle\,|\Omega\rangle && (6.12)
\end{aligned}$$

$$\begin{aligned}
=&e^{-(\Gamma_1+\Gamma_2)t}\,|e\rangle\,|\Omega\rangle && (6.13)\\
&+\sqrt{\frac{\Gamma_1}{2\pi}}\frac{\left(e^{-i(k-\Delta_1)t}-e^{-(\Gamma_1+\Gamma_2)t}\right)}{k-\Delta_1+i(\Gamma_1+\Gamma_2)}a^\dagger_{\mu,k}\,|g_1\rangle\,|\Omega\rangle && (6.14)\\
&+\sqrt{\frac{\Gamma_2}{2\pi}}\frac{\left(e^{-i(k-\Delta_2)t}-e^{-(\Gamma_1+\Gamma_2)t}\right)}{k-\Delta_2+i(\Gamma_1+\Gamma_2)}a^\dagger_{\mu,k}\,|g_2\rangle\,|\Omega\rangle\,. && (6.15)
\end{aligned}$$

It follows that

$$P_e(t) = e^{-2(\Gamma_1+\Gamma_2)t}, \tag{6.16}$$

$$P_{g_1}(t) = (1-e^{-2(\Gamma_1+\Gamma_2)t})\frac{\Gamma_1}{\Gamma_1+\Gamma_2}, \quad P_{g_2}(t) = (1-e^{-2(\Gamma_1+\Gamma_2)t})\frac{\Gamma_2}{\Gamma_1+\Gamma_2}. \tag{6.17}$$

The reduced density matrix of the system is given by

$$\rho_\Lambda(t) = P_e(t)\left|e\right\rangle\left\langle e\right| + P_{g_1}(t)\left|g_1\right\rangle\left\langle g_1\right| + P_{g_2}(t)\left|g_2\right\rangle\left\langle g_2\right| \tag{6.18}$$

$$+ f(t)\left|g_1\right\rangle\left\langle g_2\right| + f^*(t)\left|g_2\right\rangle\left\langle g_1\right|, \tag{6.19}$$

where

$$f(t) = \sum_{\mu=\pm}\int dk \psi^{g_1}_{\mu,k}(t)\psi^{g_2\dagger}_{\mu,k}(t) = 2i\sqrt{\Gamma_1\Gamma_2}\frac{\left(e^{i(\Delta_1-\Delta_2)t} - e^{-2(\Gamma_1+\Gamma_2)t}\right)}{\Delta_2-\Delta_1+2i(\Gamma_1+\Gamma_2)} \tag{6.20}$$

The eigenvalues of the reduced density matrix are

$$\lambda_e(t) = P_e(t), \quad \lambda_{g,\pm}(t) = \frac{1}{2}\left(P_{g_1}(t)+P_{g_2}(t)\right)(\pm \frac{1}{2}\sqrt{\left(P_{g_1}(t)-P_{g_2}(t)\right)^2+4|f(t)|^2}, \tag{6.21}$$

yielding the following expression for the entropy

$$S = -\sum_\lambda \lambda(t)\log(\lambda(t)). \tag{6.22}$$

For a symmetric Λ-system $\Delta_1 = \Delta_2$ we find that

$$\lambda_{g,+}(t) = (1-e^{-2(\Gamma_1+\Gamma_2)t}), \quad \lambda_{g,-}(t) = 0. \tag{6.23}$$

Вывод диаграммного метода на примере этой модели

(то же что в теории, только все в рамках этой модели, очень крутой будет пример)

6.2.4 V-system

We consider $v_s = \sqrt{\frac{\Gamma_1}{2\pi}}\left|g\right\rangle\left\langle e_1\right| + \sqrt{\frac{\Gamma_2}{2\pi}}\left|g\right\rangle\left\langle e_2\right|$, with $\epsilon_0 = 0$ and $\epsilon_{1,1} = \Delta_1,\ \epsilon_{1,2} = \Delta_2$. One has

$$\begin{aligned}\Sigma^{(1)} &= -i\left(\sqrt{\Gamma_1}\left|e_1\right\rangle + \sqrt{\Gamma_2}\left|e_2\right\rangle\right)\left(\sqrt{\Gamma_1}\left\langle e_1\right| + \sqrt{\Gamma_2}\left\langle e_2\right|\right) \\ &= -i\begin{pmatrix}\Gamma_1 & \sqrt{\Gamma_1\Gamma_2}\\ \sqrt{\Gamma_1\Gamma_2} & \Gamma_2\end{pmatrix}.\end{aligned} \tag{6.24}$$

With this in our hands, we find

$$[G^{(1)}(z)]^{-1} = \begin{pmatrix}z-\Delta_1+i\Gamma_1 & i\sqrt{\Gamma_1\Gamma_2}\\ i\sqrt{\Gamma_1\Gamma_2} & z-\Delta_2+i\Gamma_2\end{pmatrix}, \tag{6.25}$$

or

$$G^{(1)}(z) = \frac{1}{(z-\Delta_1+i\Gamma_1)(z-\Delta_2+i\Gamma_2)+\Gamma_1\Gamma_2}\begin{pmatrix}z-\Delta_2+i\Gamma_2 & -i\sqrt{\Gamma_1\Gamma_2}\\ -i\sqrt{\Gamma_1\Gamma_2} & z-\Delta_1+i\Gamma_1\end{pmatrix} \tag{6.26}$$

$$= \frac{(z-\Delta_2+i\Gamma_2)\left|e_1\right\rangle\left\langle e_1\right| + (z-\Delta_1+i\Gamma_1)\left|e_2\right\rangle\left\langle e_2\right|}{(z-\Delta_1+i\Gamma_1)(z-\Delta_2+i\Gamma_2)+\Gamma_1\Gamma_2} \tag{6.27}$$

$$- i\sqrt{\Gamma_1\Gamma_2}\frac{\left|e_1\right\rangle\left\langle e_2\right| + \left|e_2\right\rangle\left\langle e_1\right|}{(z-\Delta_1+i\Gamma_1)(z-\Delta_2+i\Gamma_2)+\Gamma_1\Gamma_2}. \tag{6.28}$$

The pole equation

$$(z-\Delta_1+i\Gamma_1)(z-\Delta_2+i\Gamma_2)+\Gamma_1\Gamma_2 = 0 \tag{6.29}$$

admits for the following solutions

$$z_\pm = \frac{1}{2}\left[(\Delta_1+\Delta_2-i\Gamma_1-i\Gamma_2(\pm\sqrt{(\Delta_1+\Delta_2-i\Gamma_1-i\Gamma_2)^2-4((\Delta_1-i\Gamma_1)(\Delta_2-i\Gamma_2)+\Gamma_1\Gamma_2)}\right]. \tag{6.30}$$

We note that in the symmetric situation $\Delta_1=\Delta_2=\Delta$ the system admits for and atom-photon bound state, since

$$z_+=\Delta, \quad z_-=\Delta-i(\Gamma_1+\Gamma_2). \tag{6.31}$$

We suppose that the initial state of the system is given by

$$|\psi_0\rangle = \cos\vartheta\,|e_1\rangle + e^{i\varphi/2}\sin\vartheta\,|e_2\rangle\,. \tag{6.32}$$

The state of the system at later times

$$|\psi(t)\rangle = \psi_{e_1}(t)\,|e_1\rangle\,|\Omega\rangle + \psi_{e_2}(t)\,|e_2\rangle\,|\Omega\rangle + \sum_{\mu=\pm}\int dk\psi^g_{\mu,k}(t)a^\dagger_{\mu,k}\,|g\rangle\,|\Omega\rangle\,, \tag{6.33}$$

where

$$\psi_{e_1}(t) = \oint_{C_\eta}\frac{dz}{2\pi i}e^{-izt}\frac{(z-\Delta_2+i\Gamma_2)\cos\vartheta}{(z-z_+)(z-z_-)} - \oint_{C_\eta}\frac{dz}{2\pi i}e^{-izt}\frac{ie^{i\varphi/2}\sin\vartheta\sqrt{\Gamma_1\Gamma_2}}{(z-z_+)(z-z_-)} \tag{6.34}$$

$$= \left((z_+-\Delta_2+i\Gamma_2)e^{-iz_+t}-(z_--\Delta_2+i\Gamma_2)e^{-iz_-t}\right)\frac{\cos\vartheta}{(z_+-z_-)} \tag{6.35}$$

$$-\left(e^{-iz_+t}-e^{-iz_-t}\right)\frac{ie^{i\varphi/2}\sin\vartheta\sqrt{\Gamma_1\Gamma_2}}{(z_+-z_-)}, \tag{6.36}$$

$$\psi_{e_2}(t) = \oint_{C_\eta}\frac{dz}{2\pi i}e^{-izt}\frac{(z-\Delta_1+i\Gamma_1)e^{i\varphi/2}\sin\vartheta}{(z-z_+)(z-z_-)} - \oint_{C_\eta}\frac{dz}{2\pi i}e^{-izt}\frac{i\sqrt{\Gamma_1\Gamma_2}\cos\vartheta}{(z-z_+)(z-z_-)} \tag{6.37}$$

$$= \left((z_+-\Delta_1+i\Gamma_1)e^{-iz_+t}-(z_--\Delta_1+i\Gamma_1)e^{-iz_-t}\right)\frac{e^{i\varphi/2}\sin\vartheta}{(z_+-z_-)} \tag{6.38}$$

$$-\left(e^{-iz_+t}\frac{i\sqrt{\Gamma_1\Gamma_2}\cos\vartheta}{(z_+-z_-)}+e^{-iz_-t}\frac{i\sqrt{\Gamma_1\Gamma_2}\cos\vartheta}{(z_--z_+)}\right) \tag{6.39}$$

Вывод диаграммного метода на примере этой модели

(то же что в теории, только все в рамках этой модели, очень крутой будет пример)

6.2.5 Second pair (???)

In the following, we consider a problem of two distant emitters. We assume that $\omega_{\mu,k}=k$, and that

$$g^{(n)}_{\mu,k} = \sqrt{\frac{\Gamma_n}{2\pi}}e^{-ic_n\mu kR/2}, \quad c_n=(-1)^{n+1}. \tag{6.40}$$

The Green's function in zero-excitation subspace is simply

$$G^{(0)}(z) = \frac{1}{z+\Delta_+}, \quad \Delta_\pm = \frac{\Delta_1\pm\Delta_2}{2}. \tag{6.41}$$

The Green's function in one-excitation subspace is written as

$$G^{(1)}(z) = \frac{g^{(1)}_1(z)\,|10\rangle\langle 10| + g^{(1)}_2(z)\,|01\rangle\langle 01| + g^{(1)}_1(z)g^{(1)}_2(z)m(z)(\sigma^{(1)}_+\sigma^{(2)}_- + \sigma^{(2)}_+\sigma^{(1)}_-)}{1-g^{(1)}_1(z)g^{(1)}_2(z)m^2(z)}, \tag{6.42}$$

$$m(z) = -i\sqrt{\Gamma_1\Gamma_2}e^{i(z+\Delta_+)R}, \quad g^{(1)}_n(z) = \frac{1}{z-c_n\Delta_-+i\Gamma_n}. \tag{6.43}$$

Let us consider the special case $\Delta_1=\Delta_2=:\Delta$ and $\Gamma_1=\Gamma_2=:\Gamma$. In that case $g_1(z)=g_2(z)=:g(z)$. We obtain

$$G^{(1)}(z) = g^{(1)}(z)\frac{|10\rangle\langle 10| + |01\rangle\langle 01| + g^{(1)}(z)m(z)(\sigma^{(1)}_+\sigma^{(2)}_- + \sigma^{(2)}_+\sigma^{(1)}_-)}{1-(g^{(1)}(z)m(z))^2}. \tag{6.44}$$

We consider the second pair of Bell states

$$|\Phi_\pm\rangle = \frac{|10\rangle \pm |01\rangle}{\sqrt{2}}. \tag{6.45}$$

One has

$$|10\rangle\langle 10| + |01\rangle\langle 01| = |\Phi_+\rangle\langle\Phi_+| + |\Phi_-\rangle\langle\Phi_-|, \tag{6.46}$$
$$\sigma_+^{(1)}\sigma_-^{(2)} + \sigma_+^{(2)}\sigma_-^{(1)} = |\Phi_+\rangle\langle\Phi_+| - |\Phi_-\rangle\langle\Phi_-|. \tag{6.47}$$

It thus follows

$$G^{(1)}(z) = g_+^{(1)}(z)\,|\Phi_+\rangle\langle\Phi_+| + g_-^{(1)}(z)\,|\Phi_-\rangle\langle\Phi_-|, \quad g_\pm^{(1)}(z) = \frac{1}{z + i\Gamma(1 \pm e^{i(z+\Delta)R})}. \tag{6.48}$$

The emission vertex is expressed as

$$v_{\mu,k} = \sqrt{\frac{\Gamma}{2\pi}} \sum_{n=1,2} e^{-ic_n \mu k R/2} \sigma_-^{(n)} = \sqrt{\frac{\Gamma}{\pi}} \cos(kR/2) \frac{(\sigma_-^{(1)} + \sigma_-^{(2)})}{\sqrt{2}} - i\sqrt{\frac{\Gamma}{\pi}} \mu \sin(kR/2) \frac{(\sigma_-^{(1)} - \sigma_-^{(2)})}{\sqrt{2}} \tag{6.49}$$

Using

$$\sigma_-^{(1)} = |00\rangle\langle 10| + |01\rangle\langle 11|, \quad \sigma_-^{(2)} = |00\rangle\langle 01| + |10\rangle\langle 11|, \tag{6.50}$$

we deduce

$$\frac{\sigma_-^{(1)} \pm \sigma_-^{(2)}}{\sqrt{2}} = |00\rangle\langle\Phi_\pm| \pm |\Phi_\pm\rangle\langle 11|. \tag{6.51}$$

It hence follows

$$P^{(0)} v_{\mu,k} P^{(1)} = \sqrt{\frac{\Gamma}{\pi}}\,|00\rangle \left(\cos(kR/2)\,\langle\Phi_+| - i\mu \sin(kR/2)\,\langle\Phi_-|\right). \tag{6.52}$$

Assuming that the state of the system at initial time $t_0 = 0$ is given by

$$|\psi_0\rangle = |\Phi_p\rangle, \tag{6.53}$$

the state at latter times $t > t_0 = 0$ is given by

$$|\psi_0\rangle = \psi_p^{(1)}(t)\,|\Phi_p\rangle + \sum_{\mu=\pm} \int dk \psi_{p,\mu,k}^{(0)}(t) a_{\mu,k}^\dagger\,|\Omega\rangle\,|00\rangle, \tag{6.54}$$

where

$$\psi_p^{(1)}(t) = \oint_{C_\eta} \frac{dz}{2\pi i} g_p^{(1)}(z) e^{-izt}, \quad \psi_{\mu,k}^{(0)}(t) = \oint_{C_\eta} \frac{dz}{2\pi i} g^{(0)}(z-k) \tag{6.55}$$

$$\times \sqrt{\frac{\Gamma}{\pi}} \begin{cases} \cos(kR/2), & p = +, \\ -i\mu \sin(kR/2), & p = - \end{cases} \times g_p^{(1)}(z) \tag{6.56}$$

The Green's function is given by

$$g_p(z) = \frac{1}{z + i\Gamma(1 + pe^{i(z+\Delta)R})}. \tag{6.57}$$

Let us try to find real pole solutions z, this essentially implies

$$z = p\Gamma \sin((z+\Delta)R), \quad \cos((z+\Delta)R) = -p. \tag{6.58}$$

For $\cos((z+\Delta)R) = \pm 1$ we have $\sin((z+\Delta)R) = 0$, leading us to the solution

$$z = 0, \quad \cos(\Delta R) = -p. \tag{6.59}$$

The condition $\cos(\Delta R) = -p$ basically implies destructive interference and leads to the formation of an atom-photon bound state, sitting at zero energy.

The Laplace transform of the Green's function is given by

$$\psi_p^{(1)}(t) = \sum_{n=0}^{\infty} \frac{(-p\Gamma e^{i\Delta R})^n}{n!} \Theta(t-nR)(t-nR)^n e^{-\Gamma(t-nR)}. \tag{6.60}$$

For all Δ such that $\cos(\Delta R) \neq -p$ this series approaches 0. For $\cos(\Delta R) = -p$, on the contrary

$$\psi_p^{(1)}(t) = \sum_{n=0}^{\infty} \frac{1}{n!} \Theta(t-nR)(\Gamma(t-nR))^n e^{-\Gamma(t-nR)} \to \frac{1}{1+\Gamma R}. \tag{6.61}$$

The projection of the survival amplitude on the interval $t \in [nR, (n+1)R]$ is given by

$$\sum_{l=0}^{n} \frac{(pe^{i\Delta R})^l}{l!} \frac{\partial^l}{\partial y^l} e^{-y\Gamma(t-lR)}\Big|_{y=1}. \tag{6.62}$$

The reduced density matrix of qubits is given by

$$\rho_Q^{(p)}(t) = |\psi_p^{(1)}(t)|^2 \left|\Phi^{(p)}\right\rangle \left\langle\Phi^{(p)}\right| + N(t) \left|00\right\rangle \left\langle 00\right|, \tag{6.63}$$

$$N(t) = \sum_{\mu=\pm} \int dk |\psi_{\mu,k}^{(0)}(t)|^2 = 1 - |\psi_p^{(1)}(t)|^2. \tag{6.64}$$

Leading to the following expression for the von Neumann entropy

$$S_{\text{vN}}(t) = -|\psi_p^{(1)}(t)|^2 \log\Big(|\psi_p^{(1)}(t)|^2\Big) - (1-|\psi_p^{(1)}(t)|^2) \log\Big(1-|\psi_p^{(1)}(t)|^2\Big), \tag{6.65}$$

which has the property $S(t=0) = S(t\to\infty) = 0$ unless $\cos(\Delta R) = -p$. When the destructive interference condition is satisfied $\cos(\Delta R) = -p$, the entropy reaches

$$S_{\text{vN}}(t) \to \frac{(1+\Gamma R)^2 \log\left[(1+\Gamma R)^2\right] - \left[(1+\Gamma R)^2 - 1\right] \log\left[(1+\Gamma R)^2 - 1\right]}{(1+\Gamma R)^2}. \tag{6.66}$$

The maximum entropy is achieved at

$$R = \frac{\sqrt{2}-1}{\Gamma}. \tag{6.67}$$

Now let us consider the photonic part of the wave function

$$\psi_{\mu,k}^{(0)}(t) = g_{\mu,k}^{(p)} \oint_{C_\eta} \frac{dz}{2\pi i} \frac{1}{z+\Delta-k} \frac{1}{z+i\Gamma(1+pe^{i(z+\Delta)R})} e^{-izt} \tag{6.68}$$

$$= g_{\mu,k}^{(p)} \sum_{n=0}^{\infty} \Theta(t-nR) \frac{(-i\Gamma p e^{i\Delta R})^n}{(k-\Delta+i\Gamma)^{n+1}} \Big(e^{-i(k-\Delta)(t-nR)} \tag{6.69}$$

$$- e^{-\Gamma(t-nR)} \sum_{m=0}^{n} \frac{((\Gamma - i[k-\Delta])(t-nR))^{n-m}}{(n-m)!} \Big). \tag{6.70}$$

For all Δ such that $\cos(\Delta R) \neq -p$ this series approaches

$$\psi_{\mu,k}^{(0)}(t) \to g_{\mu,k}^{(p)} \frac{1}{k-\Delta+i\Gamma(1+pe^{ikR})} e^{-i(k-\Delta)t}, \quad t\to\infty. \tag{6.71}$$

In the case of atom-photon bound states $\cos(\Delta R) = -p$, photonic wave function approaches

$$\psi_{\mu,k}^{(0)}(t) \to g_{\mu,k}^{(p)} \frac{1}{k-\Delta+i\Gamma(1+pe^{ikR})} e^{-i(k-\Delta)t} - g_{\mu,k}^{(p)} \frac{1}{k-\Delta} \frac{1}{1+\Gamma R}, \quad t\to\infty. \tag{6.72}$$

The first-order coherence is given by

$$C_{\mu,\mu'}^{(1)}(x,x'|t,t') = \left\langle \psi_0 | a_\mu^\dagger(x,t) a_{\mu'}(x',t') | \psi_0 \right| \left| \psi_0 | a_\mu^\dagger(x,t) a_{\mu'}(x',t') | \psi_0 \right\rangle = \psi_\mu^{(0)*}(t,x) e^{i\Delta(t-t')} \psi_{\mu'}^{(0)}(t',x') \tag{6.73}$$

Now we introduce $\tau = t - t'$ and $T = \frac{t+t'}{2}$, so that $t = T + \tau/2,\ t' = T - \tau/2$. One has

$$C^{(1)}_{\mu,\mu'}(x,x'|T,\tau) = \psi^{(0)*}_{\mu}(T+\tau/2,x)\psi^{(0)}_{\mu'}(T-\tau/2,x')e^{i\Delta\tau}$$
$$= \int dk \int dk' \frac{e^{-i\mu kx}}{\sqrt{2\pi}} \frac{e^{i\mu' k' x'}}{\sqrt{2\pi}} \psi^{(0)*}_{\mu,k}(T+\tau/2)\psi^{(0)}_{\mu',k'}(T-\tau/2)e^{i\Delta\tau}. \tag{6.74}$$

The local spectral density at time T may be defined via

$$S^{\text{emission}}_{\mu}(x,T|\nu) = \int \frac{d\tau}{2\pi} e^{-i\nu\tau} C^{(1)}_{\mu,\mu}(x,x|T,\tau), \tag{6.75}$$

implying that the total spectrum of emitted radiation is given by

$$S^{\text{emission}}_{\mu}(T|\nu) = \int \frac{d\tau}{2\pi} e^{-i\nu\tau} \int dx C^{(1)}_{\mu,\mu}(x,x|T,\tau)$$
$$= \int \frac{d\tau}{2\pi} \int dk \psi^{(0)*}_{\mu,k}(T+\tau/2)\psi^{(0)}_{\mu,k}(T-\tau/2)e^{i\Delta\tau}e^{-i\nu\tau}. \tag{6.76}$$

Using

$$\psi^{(0)}_{\mu,k}(t) = i \int\limits_{-\infty}^{\infty} \frac{d\omega}{2\pi} \hat{\psi}^{(0)}_{\mu,k}(\omega) e^{-i\omega t}, \tag{6.77}$$

we obtain

$$S^{\text{emission}}_{\mu}(T|\nu) = \int dk \int \frac{d\omega}{2\pi^2} \hat{\psi}^{(0)*}_{\mu,k}(\nu - \Delta - \omega)\hat{\psi}^{(0)}_{\mu,k}(\nu - \Delta + \omega)e^{-2i\omega T}$$

Now, using

$$\hat{\psi}^{(0)}_{\mu,k}(z) = g^{(p)}_{\mu,k} \frac{1}{z + \Delta - k} \frac{1}{z + i\Gamma(1 + pe^{i(z+\Delta)R})} \tag{6.78}$$

we cast

$$S^{\text{emission}}_{\mu}(T|\nu) = -\frac{\Gamma}{2\pi} \int\limits_{+\infty}^{-\infty} \frac{d\omega}{2\pi i} \frac{1}{\omega + i\eta}$$
$$\times \frac{1 + p\cos(\nu R)e^{i\omega R}}{\omega - (\nu - \Delta) + i\Gamma + i\Gamma p e^{-i\nu R}e^{i\omega R}} \frac{1}{\omega + (\nu - \Delta) + i\Gamma + i\Gamma p e^{i\nu R}e^{i\omega R}} e^{-2i\omega T}. \tag{6.79}$$

Now using the fact that

$$\frac{i\Gamma + i\Gamma p\cos(\nu R)e^{i\omega R}}{\omega - (\nu - \Delta) + i\Gamma + i\Gamma p e^{-i\nu R}e^{i\omega R}} \frac{1}{\omega + (\nu - \Delta) + i\Gamma + i\Gamma p e^{i\nu R}e^{i\omega R}} \tag{6.80}$$
$$= \frac{1}{2}\left(\frac{1}{\omega - (\nu - \Delta) + i\Gamma + i\Gamma p e^{-i\nu R}e^{i\omega R}} + \frac{1}{\omega + (\nu - \Delta) + i\Gamma + i\Gamma p e^{i\nu R}e^{i\omega R}} \right) \tag{6.81}$$
$$- \frac{\omega}{\omega - (\nu - \Delta) + i\Gamma + i\Gamma p e^{-i\nu R}e^{i\omega R}} \frac{1}{\omega + (\nu - \Delta) + i\Gamma + i\Gamma p e^{i\nu R}e^{i\omega R}}, \tag{6.82}$$

we rewrite the emission spectral density as

$$S^{\text{emission}}_{\mu}(T|\nu) = \frac{1}{2\pi i} \int\limits_{+\infty}^{-\infty} \frac{d\omega}{2\pi i} \frac{1}{\omega - (\nu - \Delta) + i\Gamma + i\Gamma p e^{-i\nu R}e^{i\omega R}}$$
$$\times \frac{1}{\omega + (\nu - \Delta) + i\Gamma + i\Gamma p e^{i\nu R}e^{i\omega R}} e^{-2i\omega T} \tag{6.83}$$
$$- \frac{1}{4\pi i} \int\limits_{+\infty}^{-\infty} \frac{d\omega}{2\pi i} \frac{1}{\omega + i\eta} \frac{1}{\omega - (\nu - \Delta) + i\Gamma + i\Gamma p e^{-i\nu R}e^{i\omega R}} e^{-2i\omega T} \tag{6.84}$$
$$- \frac{1}{4\pi i} \int\limits_{+\infty}^{-\infty} \frac{d\omega}{2\pi i} \frac{1}{\omega + i\eta} \frac{1}{\omega + (\nu - \Delta) + i\Gamma + i\Gamma p e^{i\nu R}e^{i\omega R}} e^{-2i\omega T}. \tag{6.85}$$

As the "observation time" T tends to infinity $T\to\infty$, unless $\cos(\Delta R)=-p$, we pick up a pole at $\omega=0$ only, so that the emission power spectrum approaches

$$\begin{aligned}S_{\mu}^{\text{emission}}(T|\nu)=&\frac{1}{4\pi i}\left(\frac{1}{(\nu-\Delta)-i\Gamma-i\Gamma pe^{-i\nu R}}-\frac{1}{(\nu-\Delta)+i\Gamma+i\Gamma pe^{i\nu R}}\right)\\=&\frac{\Gamma}{2\pi}\frac{1+p\cos(\nu R)}{|(\nu-\Delta)+i\Gamma+i\Gamma pe^{i\nu R}|^2}.\end{aligned}\tag{6.86}$$

In the case, the atom-photon bound states are present $\cos(\Delta R)=-p$, we have to account for additional poles

$$\begin{aligned}S_{\mu}^{\text{emission}}(T|\nu)=&\frac{1}{\pi}\frac{\cos(2\bar{\nu}T)}{1+\Gamma R}\frac{-\Gamma(1-\cos(2\bar{\nu}R))}{|2\bar{\nu}+i\Gamma(1-e^{2i\bar{\nu}R})|^2}\\&+\frac{1}{\pi}\frac{\sin(2\bar{\nu}T)}{1+\Gamma R}\left(\frac{1}{2\bar{\nu}}-\frac{2\bar{\nu}+\Gamma\sin(2\bar{\nu}R)}{|2\bar{\nu}+i\Gamma(1-e^{2i\bar{\nu}R})|^2}\right)&(6.87)\\&+\frac{\Gamma}{2\pi}\frac{1-\cos(\bar{\nu}R)}{|\bar{\nu}+i\Gamma-i\Gamma e^{i\bar{\nu}R}|^2}&(6.88)\\&+\frac{1}{2}\delta(\bar{\nu})\frac{\Gamma R}{(1+\Gamma R)^2},\quad\bar{\nu}=\nu-\Delta&(6.89)\end{aligned}$$

6.3 General dynamics in $\bar{N}_{max}=1$ systems by K. Piasotski

6.3.1 Exact resummation of perturbation theory for the propagator

K.Piasotski.1

In this section, we derive the full Green's operator in $\bar{N}_{max}=1$ waveguide QED. Our starting point is the following representation of the Green's operator in terms of the transition operator $\mathcal{T}(z)$:

$$\mathcal{G}(z)=\mathcal{G}^{(0)}(z)+\mathcal{G}^{(0)}(z)\mathcal{T}(z)\mathcal{G}^{(0)}(z),\tag{6.90}$$

where the T-operator satisfies

$$\mathcal{T}(z)=\mathcal{V}+\mathcal{V}\mathcal{G}(z)\mathcal{V}.\tag{6.91}$$

Now we define the following states

$$|N_p,0\rangle=\frac{1}{\sqrt{N_p!}}\psi_{s_1\ldots s_{N_p}}a^{\dagger}_{s_1}\ldots a^{\dagger}_{s_{N_p}}|\Omega\rangle\otimes|g\rangle\,,\tag{6.92}$$

$$|N_p-1,1\rangle=\frac{1}{\sqrt{(N_p-1)!}}\psi_{s_1\ldots s_{N_p-1}}a^{\dagger}_{s_1}\ldots a^{\dagger}_{s_{N_p-1}}|\Omega\rangle\otimes|e\rangle\,,\tag{6.93}$$

where $|\Omega\rangle$ is the vacuum state, $|g\rangle\,,\ |e\rangle$ are used symbolically to indicate some state belonging to either ground or excited manifolds, respectively, and s is the multi-index $s=(k,\mu)$ subject to the generalized summation convention

$$A_sB_s:=\sum_{\mu=1}^{N_c}\int\limits_{B_\mu}dkA_\mu(k)B_\mu(k).\tag{6.94}$$

Above, we defined a family of N_p-photon test-functions

$$\psi_{s_1\ldots s_{N_p}}=\psi_{\mu_1,\ldots,\mu_{N_p}}(k_1,\ldots,k_{N_p}),\quad\psi_{s_1\ldots s_{N_p}}=\psi_{\sigma(s_1)\ldots\sigma(s_{N_p})},\quad\sigma\in S_{N_p},\quad|\psi_{s_1\ldots s_{N_p}}|^2=1,\tag{6.95}$$

on the N_p-photon Hilbert space.

The N-excitation subspace is thus spanned by

$$|N,g\rangle\,,\quad|N-1,e\rangle\,.\tag{6.96}$$

Our final goal is to represent the $\mathcal{T}$-operator in all of the N-subspaces separately. For this, we consider the matrix elements of $\mathcal{T}(z)$ in a pair of the above states, keeping N arbitrary.

The diagonal matrix element $\langle N_p', g|\mathcal{T}(z)|N_p, g\big|N_p', g|\mathcal{T}(z)|N_p, g\rangle$ was determined in our previous work and may be expressed as

$$\langle N_p', g|\mathcal{T}(z)|N_p, g\big|N_p', g|\mathcal{T}(z)|N_p, g\rangle = \Big\langle N_p', g|a^\dagger_{s_1'} v_{s_1'} \mathcal{G}^{(1)}(z) v^\dagger_{s_1} a_{s_1}|N_p, g\Big|N_p', g|a^\dagger_{s_1'} v_{s_1'} \mathcal{G}^{(1)}(z) v^\dagger_{s_1} a_{s_1}|N_p, g\Big\rangle \tag{6.97}$$

$$+ \Big\langle N_p', g|a^\dagger_{s_1'} v_{s_1'} \mathcal{G}^{(1)}(z)\mathcal{W}^{(1)}(z)\mathcal{G}^{(1)}(z) v^\dagger_{s_1} a_{s_1}|N_p, g\Big|N_p', g|a^\dagger_{s_1'} v_{s_1'} \mathcal{G}^{(1)}(z)\mathcal{W}^{(1)}(z)\mathcal{G}^{(1)}(z) v^\dagger_{s_1} a_s \tag{6.98}$$

where

$$\mathcal{W}^{(1)}(z) = \sum_{n=1}^{\infty} a^\dagger_{s_1'} ... a^\dagger_{s_n'} \mathcal{W}^{(1,n)}_{s_1'...s_n', s_1...s_n}(z) a_{s_n} ... a_{s_1}, \quad \mathcal{G}^{(1)}(z) = \mathcal{G}^{(0)}(z) + \mathcal{G}^{(0)}(z)\Sigma^{(1)}(z)\mathcal{G}^{(1)}(z), \tag{6.99}$$

$$\Sigma^{(1)}(z) = v_s^\dagger \mathcal{G}^{(0)}(z - \omega_s) v_s, \quad v_s \equiv v_\mu(k) := \sum_{n=1}^{N_q} g_{\mu,n}(k)\sigma_-^{(n)} \equiv g_\mu(k)\sigma_-. \tag{6.100}$$

Furthermore, $\mathcal{G}^{(0)}(z)$ and $\mathcal{W}^{(1,n)}_{s_1'...s_n', s_1...s_n}(z)$ are the operator-valued functions, dependent on the field operators via the complex frequency z, as $z - \mathcal{H}_0$. The effective vertex functions $\mathcal{W}^{(1,n)}_{s_1'...s_n', s_1...s_n}(z)$ satisfy

$$\begin{aligned}\mathcal{W}^{(1,n)}_{s_1'...s_n', s_1...s_n}(z) =& \mathcal{R}^{(1)}_{s_1', s_1}\left(z - \sum_{l=2}^{n}\omega_{s_n'}\right)\mathcal{G}^{(1)}\left(z - \omega_{s_1} - \sum_{l=2}^{n}\omega_{s_l'}\right)\mathcal{W}^{(1,n-1)}_{s_2'...s_n', s_2...s_n}(z - \omega_{s_1}) \\ &+ \mathcal{R}^{(1)}_{s_1', s}\left(z - \sum_{l=2}^{n}\omega_{s_n'}\right)\mathcal{G}^{(1)}\left(z - \omega_s - \sum_{l=2}^{n}\omega_{s_l'}\right)[\mathcal{W}^{(1,n)}_{ss_2'...s_n', s_1...s_n}(z) + \\ &... + \mathcal{W}^{(1,n)}_{s_2'...s_n' s, s_1...s_n}(z)].\end{aligned} \tag{6.101}$$

We note that in the case N_p (say the highest photon number expected to emerge in the problem) is fixed, the hierarchy of integral equations is closed, meaning that one has to solve only the first $N_p - 1$ equations to completely determine the matrix element. Before further taking the matrix elements of (6.98), we shall first express other matrix elements in the form analogous to (6.98). As we shall see, the entire T-matrix may be *completely specified* with the help of the vertex functions $\mathcal{W}^{(1,n)}_{s_1'...s_n', s_1...s_n}(z)$.

We start with the other "diagonal" matrix element

$$\begin{aligned}\langle (N_p-1)', e\,|\,\mathcal{T}(z)\,|\,N_p - 1, e\rangle &= \Big\langle (N_p-1)', e\,\Big|\, a_{s'} v^\dagger_{s'} \mathcal{G}(z) v_s a^\dagger_s \,\Big|\, N_p - 1, e\Big\rangle \\ &= \sum_{n=0}^{\infty}\Big\langle (N_p-1)', e\,\Big|\, a_{s'} v^\dagger_{s'} (\mathcal{G}_0(z)\mathcal{V})^n \mathcal{G}_0(z) v_s a^\dagger_s \,\Big|\, N_p - 1, e\Big\rangle \\ &= \sum_{n=0}^{\infty}\Big\langle (N_p-1)', e\,\Big|\, a_{s'} v^\dagger_{s'} (\mathcal{G}_0(z)\mathcal{V}\mathcal{G}_0(z)\mathcal{V})^n \mathcal{G}_0(z) v_s a^\dagger_s \,\Big|\, N_p - 1, e\Big\rangle \\ &= \sum_{n=0}^{\infty}\Big\langle (N_p-1)', e\,\Big|\, a_{s'} v^\dagger_{s'} (\mathcal{G}_0(z) v_{s_1'} a^\dagger_{s_1'} \mathcal{G}_0(z) a_{s_1} v^\dagger_{s_1})^n \mathcal{G}_0(z) v_s a^\dagger_s \,\Big|\, N_p - 1, e\Big\rangle,\end{aligned} \tag{6.102}$$

where we made use of the $N_{\max} = 1$ nilpotency condition $v_s v_{s'} = v_s^\dagger v_{s'}^\dagger = 0$ and the fact that due to the RWA, only the terms even in the interaction potential do contribute to the above geometric series. We further have

$$\begin{aligned}&\langle (N_p-1)', e\,|\,\mathcal{T}(z)\,|\,N_p - 1, e\rangle \\ &= \sum_{n=0}^{\infty}\Big\langle (N_p-1)', e\,\Big|\, [\mathcal{G}^{(0)}(z)]^{-1}\mathcal{G}^{(0)}(z) a_{s'} v^\dagger_{s'} (\mathcal{G}^{(0)}(z) v_{s_1'} a^\dagger_{s_1'} \mathcal{G}^{(0)}(z) a_{s_1} v^\dagger_{s_1})^n \mathcal{G}^{(0)}(z) v_s a^\dagger_s \mathcal{G}^{(0)}(z)[\mathcal{G}^{(0)}(z)]^{-1} \,\Big|\, N_p - 1, e\Big\rangle \\ &= \sum_{n=1}^{\infty}\Big\langle (N_p-1)', e\,\Big|\, [\mathcal{G}^{(0)}(z)]^{-1}(\mathcal{G}^{(0)}(z) a_{s_1} v^\dagger_{s_1} \mathcal{G}^{(0)}(z) v_{s_1'} a^\dagger_{s_1'})^n \mathcal{G}^{(0)}(z)[\mathcal{G}^{(0)}(z)]^{-1} \,\Big|\, N_p - 1, e\Big\rangle \\ &= \sum_{n=0}^{\infty}\Big\langle (N_p-1)', e\,\Big|\, [\mathcal{G}^{(0)}(z)]^{-1}(\mathcal{G}^{(0)}(z)[\Sigma^{(1)}(z) + \mathcal{R}^{(1)}(z)])^n \mathcal{G}^{(0)}(z)[\mathcal{G}^{(0)}(z)]^{-1} \,\Big|\, N_p - 1, e\Big\rangle \\ &- \Big\langle (N_p-1)', e\,\Big|\, [\mathcal{G}^{(0)}(z)]^{-1} \,\Big|\, N_p - 1, 1\Big\rangle = \Big\langle (N_p-1)', e\,\Big|\, [\mathcal{G}^{(0)}(z)]^{-1}\mathcal{G}^{(1)}(z)[\mathcal{G}^{(0)}(z)]^{-1} \,\Big|\, N_p - 1, e\Big\rangle \\ &+ \Big\langle (N_p-1)', e\,\Big|\, [\mathcal{G}^{(0)}(z)]^{-1}\mathcal{G}^{(1)}(z)\mathcal{W}^{(1)}(z)\mathcal{G}^{(1)}(z)[\mathcal{G}^{(0)}(z)]^{-1} \,\Big|\, N_p - 1, e\Big\rangle - \Big\langle (N_p-1)', e\,\Big|\, [\mathcal{G}^{(0)}(z)]^{-1} \,\Big|\, N_p - 1, e\Big\rangle.\end{aligned} \tag{6.103}$$

Now, let us consider the off-diagonal matrix elements. As opposed to the diagonal case, the only terms in the Neumann series allowed by RWA are the odd ones

$$\begin{aligned}\langle (N_p-1)', e \,|\, \mathcal{T}(z) \,|\, N_p, g\rangle =& \langle (N_p-1)', e \,|\, \mathcal{V} \,|\, N_p, g\rangle + \langle (N_p-1)', e \,|\, \mathcal{V}\mathcal{G}(z)\mathcal{V} \,|\, N_p, g\rangle = \left\langle (N_p-1)', e \,\middle|\, a_s v_s^\dagger \,\middle|\, N_p, g\right\rangle \\ &+ \sum_{n=0}^{\infty} \left\langle (N_p-1)', e \,\middle|\, a_{s'} v_{s'}^\dagger (\mathcal{G}^{(0)}(z)\mathcal{V}\mathcal{G}^{(0)}(z)\mathcal{V})^n \mathcal{G}^{(0)}(z)\mathcal{V}\mathcal{G}^{(0)}(z) a_s v_s^\dagger \,\middle|\, N_p, g\right\rangle \\ =& \left\langle (N_p-1)', e \,\middle|\, a_s v_s^\dagger \,\middle|\, N_p, g\right\rangle \\ &+ \sum_{n=0}^{\infty} \left\langle (N_p-1)', e \,\middle|\, a_{s'} v_{s'}^\dagger (\mathcal{G}^{(0)}(z) v_{s_1} a_{s_1}^\dagger \mathcal{G}^{(0)}(z) v_{s_1'}^\dagger a_{s_1'})^n \mathcal{G}^{(0)}(z) v_{s''} a_{s''}^\dagger \mathcal{G}^{(0)}(z) a_s v_s^\dagger \,\middle|\, N_p, g\right\rangle \end{aligned} \tag{6.104}$$

$$\begin{aligned}&= \sum_{n=0}^{\infty} \left\langle (N_p-1)', e \,\middle|\, [\mathcal{G}^{(0)}(z)]^{-1} (\mathcal{G}_0(z) a_{s_1} v_{s_1}^\dagger \mathcal{G}^{(0)}(z) v_{s_1'} a_{s_1'}^\dagger)^n \mathcal{G}^{(0)}(z) a_s v_s^\dagger \,\middle|\, N_p, g\right\rangle \\ &= \left\langle (N_p-1)', e \,\middle|\, [\mathcal{G}^{(0)}(z)]^{-1} \mathcal{G}^{(1)}(z) a_s v_s^\dagger \,\middle|\, N_p, g\right\rangle + \left\langle (N_p-1)', e \,\middle|\, [\mathcal{G}^{(0)}(z)]^{-1} \mathcal{G}^{(1)}(z) \mathcal{W}^{(1)}(z) \mathcal{G}^{(1)}(z) a_s v_s^\dagger \,\middle|\, N_p, g\right\rangle . \end{aligned} \tag{6.105}$$

Finally, we consider

$$\begin{aligned}&\left\langle N_p', g \,\middle|\, \mathcal{T}(z) \,\middle|\, N_p - 1, e\right\rangle = \left\langle N_p', g \,\middle|\, a_s^\dagger v_s \,\middle|\, N_p - 1, e\right\rangle + \left\langle N_p', g \,\middle|\, a_s^\dagger v_s \mathcal{G}(z) a_{s'}^\dagger v_{s'} \,\middle|\, N_p - 1, e\right\rangle \\ &= \left\langle N_p', g \,\middle|\, a_s^\dagger v_s \,\middle|\, N_p - 1, e\right\rangle + \sum_{n=0}^{\infty} \left\langle N_p', g \,\middle|\, a_s^\dagger v_s (\mathcal{G}^{(0)}(z)\mathcal{V}\mathcal{G}^{(0)}(z)\mathcal{V})^n \mathcal{G}^{(0)}(z)\mathcal{V}\mathcal{G}^{(0)}(z) a_{s'}^\dagger v_{s'} \,\middle|\, N_p - 1, e\right\rangle \\ &= \left\langle N_p', g \,\middle|\, a_s^\dagger v_s \,\middle|\, N_p - 1, e\right\rangle + \sum_{n=0}^{\infty} \left\langle N_p', g \,\middle|\, a_s^\dagger v_s (\mathcal{G}^{(0)}(z) v_{s_2}^\dagger a_{s_2} \mathcal{G}^{(0)}(z) v_{s_1'} a_{s_1'}^\dagger)^n \mathcal{G}^{(0)}(z) v_{s_1}^\dagger a_{s_1} \mathcal{G}^{(0)}(z) a_{s'}^\dagger v_{s'} \,\middle|\, N_p - 1, e\right\rangle \\ &= \sum_{n=0}^{\infty} \left\langle N_p', g \,\middle|\, a_s^\dagger v_s (\mathcal{G}^{(0)}(z) v_{s_1}^\dagger a_{s_1} \mathcal{G}^{(0)}(z) a_{s_1'}^\dagger v_{s_1'})^n \mathcal{G}^{(0)}(z) [\mathcal{G}^{(0)}(z)]^{-1} \,\middle|\, N_p - 1, e\right\rangle \\ &= \left\langle N_p', g \,\middle|\, a_s^\dagger v_s \mathcal{G}^{(1)}(z) [\mathcal{G}^{(0)}(z)]^{-1} \,\middle|\, N_p - 1, e\right\rangle + \left\langle N_p', g \,\middle|\, a_s^\dagger v_s \mathcal{G}^{(1)}(z) \mathcal{W}^{(1)}(z) \mathcal{G}^{(1)}(z) [\mathcal{G}^{(0)}(z)]^{-1} \,\middle|\, N_p - 1, e\right\rangle . \end{aligned} \tag{6.106}$$

Quite remarkably, we see that all of the non-trivial information about the dynamics may be drawn from the knowledge of $\mathcal{G}^{(1)}(z)$ and $\mathcal{W}^{(1)}(z)$ as it is the case in the theory of scattering. Let us also remark that the above calculation proves that all of the T-matrix elements apart from $\langle N_p, 0|\mathcal{T}(z)|N_p, 0|N_p, 0|\mathcal{T}(z)|N_p, 0\rangle$ vanish when being put on shell, as was claimed in (?).

Now, by making use of the relation between the Green's function and the transition operator, we are ready to write the former as

$$\mathcal{G}(z) = \sum_{\sigma,\sigma'=g,e} \mathcal{G}_{\sigma\sigma'}(z) \tag{6.107}$$

where

$$\mathcal{G}_{ee}(z) = P^{(e)} \Big(\mathcal{G}^{(1)}(z) + \mathcal{G}^{(1)}(z) \mathcal{W}^{(1)}(z) \mathcal{G}^{(1)}(z) \Big) P^{(e)}, \tag{6.108}$$

$$\begin{aligned}\mathcal{G}_{gg}(z) =& P^{(g)} \Big(\mathcal{G}^{(0)}(z) + \mathcal{G}^{(0)}(z) a_{s_1'}^\dagger v_{s_1'} \mathcal{G}^{(1)}(z) v_{s_1}^\dagger a_{s_1} \mathcal{G}^{(0)}(z) \\ &+ \mathcal{G}^{(0)}(z) a_{s_1'}^\dagger v_{s_1'} \mathcal{G}^{(1)}(z) \mathcal{W}^{(1)}(z) \mathcal{G}^{(1)}(z) v_{s_1}^\dagger a_{s_1} \mathcal{G}^{(0)}(z) \Big) P^{(g)}, \end{aligned} \tag{6.109}$$

$$\mathcal{G}_{eg}(z) = P^{(e)} \Big(\mathcal{G}^{(1)}(z) a_s v_s^\dagger \mathcal{G}^{(0)}(z) + \mathcal{G}^{(1)}(z) \mathcal{W}^{(1)}(z) \mathcal{G}^{(1)}(z) a_s v_s^\dagger \mathcal{G}^{(0)}(z) \Big) P^{(g)}, \tag{6.110}$$

$$\mathcal{G}_{ge}(z) = P^{(g)} \Big(\mathcal{G}^{(0)}(z) a_s^\dagger v_s \mathcal{G}^{(1)}(z) + \mathcal{G}^{(0)}(z) a_s^\dagger v_s \mathcal{G}^{(1)}(z) \mathcal{W}^{(1)}(z) \mathcal{G}^{(1)}(z) \Big) P^{(e)}. \tag{6.111}$$

Above, we have defined the projections

$$P^{(\sigma)} = \sum_{j=1}^{S_\sigma} |\sigma, j\rangle \langle \sigma, j| , \tag{6.112}$$

onto the $\sigma = g$ ground and $\sigma = e$ excited states. With the help of the vertex expansion (6.99), we obtain

$$\begin{aligned}\mathcal{G}_{ee}(z) =& P^{(e)}(\mathcal{G}^{(1)}(z) + \mathcal{G}^{(1)}(z)\mathcal{W}^{(1)}(z)\mathcal{G}^{(1)}(z))P^{(e)} \\ =& P^{(e)}(\mathcal{G}^{(1)}(z) + \sum_{n=1}^{\infty} \mathcal{G}^{(1)}(z)a^{\dagger}_{s'_1}...a^{\dagger}_{s'_n}\mathcal{W}^{(1,n)}_{s'_1...s'_n,s_1...s_n}(z)a_{s_n}...a_{s_1}\mathcal{G}^{(1)}(z))P^{(e)} \\ =& P^{(e)}\left(\mathcal{G}^{(1)}(z) + \sum_{n=1}^{\infty} a^{\dagger}_{s'_1}...a^{\dagger}_{s'_n}\mathcal{G}^{(1)}\left(z - \sum_{l'=1}^{n}\omega_{s'_{l'}}\right)\mathcal{W}^{(1,n)}_{s'_1...s'_n,s_1...s_n}(z)\mathcal{G}^{(1)}\left(z - \sum_{l=1}^{n}\omega_{s_l}\right)a_{s_n}...a_{s_1}\right)P^{(e)}.\end{aligned} \tag{6.113}$$

When acting upon the N_p-photon state, only the first N_p terms in the above series survive. Instead, we wish to represent the above operator as the direct sum of N_p-photon operators. For that sake, we need to inset the complements of the identity operator on each n-particle subspace

$$\frac{1}{(N_p - n)!}a^{\dagger}_{s_{n+1}}...a^{\dagger}_{s_{N_p}}a_{s_{N_p}}...a_{s_{n+1}}. \tag{6.114}$$

Choosing $N_p = N - 1$, we obtain

$$\begin{aligned}G^{s'_1...s'_{N-1},s_1...s_{N-1}}_{ee}(z) =& P^{(e)}\Big(\frac{1}{(N-1)!}G^{(1)}\left(z - \sum_{l=1}^{N-1}\omega_s\right)\prod_{p=1}^{N-1}\delta_{s_p,s'_p} \\ &+ \sum_{n=1}^{N-1}\frac{\prod_{p=n+1}^{N-1}\delta_{s_p,s'_p}}{(N-n-1)!}G^{(1)}\left(z - \sum_{l'=1}^{N-1}\omega_{s'_{l'}}\right)W^{(1,n)}_{s'_1...s'_n,s_1...s_n}\left(z - \sum_{l''=n+1}^{N-1}\omega_{s_{l''}}\right)G^{(1)}\left(z - \sum_{l=1}^{N-1}\omega_{s_l}\right)\Big)P^{(e)},\end{aligned} \tag{6.115}$$

such that the corresponding component of the Green's function transforms to

$$\overline{P}_{N-1}P^{(e)}\mathcal{G}(z)P^{(e)}\overline{P}_{N-1} = G^{s'_1...s'_{N-1},s_1...s_{N-1}}_{ee}(z)a^{\dagger}_{s'_1}...a^{\dagger}_{s'_{N-1}}a_{s_{N-1}}...a_{s_1}. \tag{6.116}$$

Above we used ordinary letters G, W instead of calligraphic ones $\mathcal{G}$, $\mathcal{W}$, to signify that these objects are no longer operators on the photon space, but are rather their vacuum projections (e.g. $G^{(1)}(z) = \langle\Omega|\mathcal{G}^{(1)}(z)|\Omega|\Omega|\mathcal{G}^{(1)}(z)|\Omega\rangle$).

Likewise, we represent

$$\overline{P}_N P^{(g)}\mathcal{G}(z)P^{(g)}\overline{P}_N = G^{s'_1...s'_N,s_1...s_N}_{gg}(z)a^{\dagger}_{s'_1}...a^{\dagger}_{s'_N}a_{s_N}...a_{s_1}, \tag{6.117}$$

$$\overline{P}_{N-1}P^{(e)}\mathcal{G}(z)P^{(g)}\overline{P}_N = G^{s'_1...s'_{N-1},s_1...s_N}_{eg}(z)a^{\dagger}_{s'_1}...a^{\dagger}_{s'_{N-1}}a_{s_N}...a_{s_1}, \tag{6.118}$$

$$\overline{P}_N P^{(g)}\mathcal{G}(z)P^{(e)}\overline{P}_{N-1} = G^{s'_1...s'_N,s_1...s_{N-1}}_{ge}(z)a^{\dagger}_{s'_1}...a^{\dagger}_{s'_N}a_{s_{N-1}}...a_{s_1}, \tag{6.119}$$

where the vertices are given by

6.3.2 General dynamics in single-excitation subspace

K.Piasotski.2

In single excitation subspace, an arbitrary quantum system interacts with one photon only, meaning that the resummation theory coincides with that of the single qubit in the single-excitation subspace up to replacement of emission v_s and absorption $v^{\dagger}_s$ vertices. Assuming that $\{|\mathfrak{e}_n\rangle\}_{n=1,...,N_e}$ span the single-excitation subspace of our quantum system, whereas the ground-states into which they are allowed to decay are parametrized as $\{|\mathfrak{g}_m\rangle\}_{m=1,...,N_g}$, we may parametrize the emission vertex as

$$v_s = \sum_{n=1}^{N_e}\sum_{m=1}^{N_g} g_{\mu,n,m}(k)\,|\mathfrak{g}_m\rangle\,\langle\mathfrak{e}_n|\,. \tag{6.120}$$

The self-energy in the single-excitation subspace is given by

$$\Sigma^{(1)}(z) = v^{\dagger}_s G^{(0)}(z - \omega_s)v_s = \sum_{n=1}^{N_e}\sum_{n'=1}^{N_e}|\mathfrak{e}_n\rangle\,\langle\mathfrak{e}_{n'}|\sum_{\mu=1}^{N_c}\sum_{m=1}^{N_g}\int_{B_\mu}dk\frac{g_{\mu,n,m}(k)g^*_{\mu,n',m}(k)}{z - \omega_\mu(k) - \epsilon_{\mathfrak{g}_m}}. \tag{6.121}$$

The renormalized Green's function in the single excitation subspace is given by

$$G^{(1)}(z) = [[P^{(e)}G^{(0)}(z)P^{(e)}]^{-1} - \Sigma^{(1)}(z)]^{-1}. \tag{6.122}$$

The Green's function typically possesses poles and branch cuts on the complex z plane. The contribution of the poles located on the lower half of the complex plane $z = \epsilon + i\Gamma, \quad \Gamma \neq 0$ lead to the exponential decay, whereas the contribution of the branch cut integral typically lead to the long potential tails t^{α} weighted with the appropriate exponential decay $t^{\alpha}e^{-\Gamma t}$. The poles of the Green's function on the real axis, on the other hand, correspond to atom-photon bound states, widely studied in quantum-optical and quantum-electronic applications.

Let us consider the following initial state

$$|\psi_0\rangle = \sum_{n=1}^{N_e} \psi_n^{(e,0)} |\Omega\rangle |\mathfrak{e}_n\rangle + \sum_{m=1}^{N_g}\sum_{\mu=1}^{N_c}\int_{B_\mu} dk \psi_{\mu,m}^{(g,0)}(k) a_{\mu,k}^{\dagger} |\Omega\rangle |\mathfrak{g}_m\rangle . \tag{6.123}$$

Due to the conservation of the total excitation number operator, the state at later times $t > 0$ is given by

$$|\psi(t)\rangle = \sum_{n=1}^{N_e} \psi_n^{(e)}(t) |\Omega\rangle |\mathfrak{e}_n\rangle + \sum_{m=1}^{N_g}\sum_{\mu=1}^{N_c}\int_{B_\mu} dk \psi_{\mu,m}^{(g)}(k,t) a_{\mu,k}^{\dagger} |\Omega\rangle |\mathfrak{g}_m\rangle . \tag{6.124}$$

The occupation probability of the n^{th} excited state is given by

$$P_n(t) = \langle \psi(t) | \mathfrak{e}_n \rangle \langle \mathfrak{e}_n | \psi(t) \rangle = |\psi_n^{(e)}(t)|^2. \tag{6.125}$$

The total number of photons in channel μ is given by

$$N_\mu(t) = \int_{B_\mu} dk \left\langle \psi(t)|a_{\mu,k}^{\dagger}a_{\mu,k}|\psi(t)\right|\psi(t)|a_{\mu,k}^{\dagger}a_{\mu,k}|\psi(t)\right\rangle = \sum_{m=1}^{N_g}\int_{B_\mu} dk |\psi_{\mu,m}^{(g)}(k,t)|^2. \tag{6.126}$$

The integrands, by themselves, define the spectral density of photons in channel μ at time $t > 0$

$$S_\mu^{(1)}(k,t) = \sum_{m=1}^{N_g} |\psi_{\mu,m}^{(g)}(k,t)|^2. \tag{6.127}$$

In order to determine the exact wave functions, we apply the theory developed in Section 6.3.1. In particular,

$$\begin{aligned}\psi_n^{(e)}(t) = &\sum_{n'=1}^{N_e}\oint_{C_\eta}\frac{dz}{2\pi i}\left\langle \mathfrak{e}_n|G^{(1)}(z)|\mathfrak{e}_{n'}\right|\mathfrak{e}_n|G^{(1)}(z)|\mathfrak{e}_{n'}\right\rangle \psi_{n'}^{(e,0)}e^{-izt}\\ &+\sum_{n'=1}^{N_e}\sum_{m=1}^{N_g}\sum_{\mu=1}^{N_c}\int_{B_\mu} dk \oint_{C_\eta}\frac{dz}{2\pi i}\langle \mathfrak{e}_n| G^{(1)}(z) |\mathfrak{e}_{n'}\rangle \frac{g_{\mu,n',m}^{*}(k)\psi_{\mu,m}^{(g,0)}(k)}{z-\omega_\mu(k)-\epsilon_m^{(g)}}e^{-izt},\end{aligned} \tag{6.128}$$

$$\begin{aligned}\psi_{\mu,m}^{(g)}(k,t) = &\sum_{n=1}^{N_e}\sum_{n'=1}^{N_e}\oint_{C_\eta}\frac{dz}{2\pi i}\frac{g_{\mu,n,m}(k)}{z-\omega_\mu(k)-\epsilon_m^{(g)}}\langle \mathfrak{e}_n| G^{(1)}(z) |\mathfrak{e}_{n'}\rangle \psi_{n'}^{(e,0)}e^{-izt}\\ &+G^{(0)}(z-\omega_\mu(k))\psi_{\mu,m}^{(g,0)}(k)\\ &+\sum_{m'=1}^{N_g}\sum_{\mu'=1}^{N_c}\int_{B_{\mu'}} dk' G^{(0)}(z-\omega_{\mu'}(k'))\psi_{\mu',m'}^{(g,0)}(k')\end{aligned} \tag{6.129}$$

6.3.3 Spontaneous emission from the second pair of Bell pairs

K.Piasotski.3

Let us consider a system comprised of a pair of equivalent qubits separated by distance R. We assume the qubits to be coupled to a one-dimensional transmission line supporting two distinct types of excitations corresponding to the chirality degree of freedom $\mu = \pm$. The corresponding Hamiltonian is written as

$$\mathcal{H}_0 = \Delta(\sigma_+^{(1)}\sigma_-^{(1)} + \sigma_+^{(2)}\sigma_-^{(2)}) + \sum_{\mu=\pm}\int_{-\infty}^{\infty} dkck a_{k,\mu}^{\dagger}a_{k,\mu}, \tag{6.130}$$

where Δ is the detuning of qubits, we assumed the excitations of the transmission line to be linearly dispersing $\omega_{\mu,k} = ck$ around the operational frequency, and in the following we set $c = 1$. The interaction between qubits and the transmission line is described via the following bare emission vertex

$$v_s \equiv v_{k,\mu} = \sum_{n=1,2} e^{-i\mu k R_n} \sigma_-^{(n)}, \quad R_n = (-1)^n R/2. \tag{6.131}$$

The position space operators are related to the momentum space ones via

$$a_\mu(x) = \int_{-\infty}^{\infty} dk \frac{e^{i\mu kx}}{\sqrt{2\pi}} a_{k,\mu}, \quad a_{k,\mu} = \int_{-\infty}^{\infty} dx \frac{e^{-i\mu kx}}{\sqrt{2\pi}} a_\mu(x). \tag{6.132}$$

We assume that the system is initially prepared in one of the following two states

$$|\psi(0)\rangle = |\Omega\rangle \otimes |\Phi_\pm\rangle, \quad |\Phi_\pm\rangle = \frac{1}{\sqrt{2}}(|10\rangle \pm |01\rangle). \tag{6.133}$$

(?????????????????? недодумано!)

6.3.4 1 Infinite waveguide

We consider

$$H_0 = \Delta\sigma_+\sigma_- + \sum_{\mu=\pm} \int dkck a_{k,\mu}^\dagger a_{k,\mu} \tag{1}$$

$$V(t) = \sqrt{\frac{\Gamma}{2\pi}} \sum_{\mu=\pm} \int dk e^{-i\mu k(R_0+vt)} a_{\mu,k}^\dagger \sigma_- + \text{h.c.} \tag{2}$$

The equations of motion are

$$i\partial_t \psi^{(1)}(t) = \Delta\psi^{(1)}(t) + \sqrt{\frac{\Gamma}{2\pi}} \sum_{\mu=\pm} \int dk e^{i\mu k(R_0+vt)} \psi_\mu^{(0)}(t,k) \tag{3}$$

$$\psi_\mu^{(0)}(t,k) = -i\sqrt{\frac{\Gamma}{2\pi}} \int_0^t dt' e^{-ick(t-t')} e^{-i\mu k(R_0+vt')} \psi^{(1)}(t') \tag{4}$$

It follows

$$i\partial_t \psi^{(1)}(t) = \Delta\psi^{(1)}(t) - \frac{i\Gamma}{2\pi} \int_0^t dt' \sum_{\mu=\pm} \int dk e^{-i(c-\mu v)k(t-t')} \psi^{(1)}(t') \tag{5}$$

We perform the Laplace transform

$$\hat{\psi}^{(1)}(z) = -i\int_0^\infty dt e^{izt} \psi^{(1)}(t), \quad \psi^{(1)}(t) = \int_{+\infty+i\eta}^{-\infty+i\eta} \frac{dz}{2\pi i} e^{-izt} \hat{\psi}^{(1)}(z) \tag{6}$$

It follows that

$$\psi^{(1)}(z) = \frac{1}{z - \Delta + i\widetilde{\Gamma}}, \quad \widetilde{\Gamma} = \Theta(c-|v|)\frac{\Gamma}{c}\frac{1}{1-v^2/c^2} + \Theta(|v|-c)\frac{\Gamma}{|v|}\frac{1}{1-c^2/v^2}. \tag{7}$$

From this we conclude

$$\psi^{(1)}(t) = \int_{+\infty+i\eta}^{-\infty-i\eta} \frac{dz}{2\pi i} \frac{e^{-izt}}{z - \Delta + i\widetilde{\Gamma}} = e^{-i\Delta t} e^{-\widetilde{\Gamma}t} \tag{8}$$

Using (4) we deduce

$$\psi_\mu^{(0)}(t,k) = -e^{-ickt} e^{-i\mu k R_0} \sqrt{\frac{\Gamma}{2\pi}} \frac{e^{i(c-\mu v)kt} e^{-i\Delta t} e^{-\widetilde{\Gamma}t} - 1}{(c-\mu v)k - \Delta + i\widetilde{\Gamma}}. \tag{9}$$

6.3.5 2 Semi-infinite waveguide

6.32.1 Generalities

We have to solve

$$i\partial_t \psi^{(1)}(t) = \Delta\psi^{(1)}(t) + \int_{-\infty}^{\infty} dk g_k^*(t)\lambda_k(t), \tag{10}$$

$$i\partial_t \lambda_k(t) = ck\lambda_k(t) + g_k(t)\psi^{(1)}(t), \quad g_k(t) = -i\sqrt{\frac{2\Gamma}{\pi}}\sin\left(k\left(R_0 + vt\right)\right), \quad R_0 > 0. \tag{11}$$

From the second equation we deduce

$$\lambda_k(t) = -i\int_0^t dt' e^{-ick\left(t-t'\right)} g_k\left(t'\right)\psi^{(1)}\left(t'\right) \tag{12}$$

It follows

$$\left(i\partial_t - \Delta\right)\psi^{(1)}(t) = -i\int_0^{\infty} dt'\Theta\left(t-t'\right)\int_{-\infty}^{\infty} dk e^{-ick\left(t-t'\right)} g_k^*(t) g_k\left(t'\right)\psi^{(1)}\left(t'\right) \tag{13}$$

We consider

$$K\left(t,t'|k\right) = -i\Theta\left(t-t'\right)e^{-ick\left(t-t'\right)} g_k^*(t) g_k\left(t'\right) \tag{14}$$

One has

$$g_k^*(t) g_k\left(t'\right) = \frac{2\Gamma}{\pi}\sin\left(k\left(R_0+vt\right)\right)\sin\left(k\left(R_0+vt'\right)\right) \tag{15}$$

$$= \frac{\Gamma}{\pi}\left(\cos\left(vk\left(t-t'\right)\right) - \cos\left(k\left[2R_0 + v\left(t+t'\right)\right]\right)\right) \tag{16}$$

It follows that

$$K\left(t,t'\right) = \int dk K\left(t,t'|k\right) = -i\widetilde{\Gamma}\delta\left(t-t'\right) + i\Theta\left(t-t'\right)\frac{\Gamma}{\pi}\int dk e^{-ick\left(t-t'\right)}\cos\left(k\left[2R_0 + v\left(t+t'\right)\right]\right) \tag{17}$$

$$= -i\widetilde{\Gamma}\delta\left(t-t'\right) + \kappa\left(t,t'\right) \tag{18}$$

It follows

$$\left(i\partial_t - \Delta + i\widetilde{\Gamma}\right)\psi^{(1)}(t) = \int_0^{\infty} dt'\kappa\left(t,t'\right)\psi^{(1)}\left(t'\right) \tag{19}$$

We note that

$$\kappa\left(t,t'\right) = i\Theta\left(t-t'\right)\frac{\Gamma}{\pi}\int dk e^{-ick\left(t-t'\right)}\cos\left(k\left[2R_0 + v\left(t+t'\right)\right]\right) \tag{20}$$

$$= i\Theta\left(t-t'\right)\frac{\Gamma}{2\pi}\int dk e^{ik\left([c+v]t' - [c-v]t + 2R_0\right)} + i\Theta\left(t-t'\right)\frac{\Gamma}{2\pi}\int dk e^{-ik\left([c+v]t - [c-v]t' + 2R_0\right)} \tag{21}$$

$$= \frac{i\Gamma\Theta\left(t-t'\right)/c}{|1+\beta|}\delta\left(t' - \frac{1-\beta}{1+\beta}t + \frac{T_0}{1+\beta}\right) + \frac{i\Gamma\Theta\left(t-t'\right)/c}{|1-\beta|}\delta\left(\frac{1+\beta}{1-\beta}t + \frac{T_0}{1-\beta} - t'\right) \tag{22}$$

where $T_0 = 2R_0/c$ is the rest delay time. We distinguish between the subluminal propagation regime: $|\beta| < 1$ and superluminal propagation regime: $|\beta| > 1$.

6.32.2 Subluminal propagation regime

6.32.2.1 Atom receding from the mirror

6.3.6 Wave-functions

We restrict ourselves to the regime $|\beta|<1$. Let us consider the case of the qubit receding from the mirror $0\leq\beta<1$:

$$\kappa_r^I\left(t,t'\right)=\Theta(\beta)\Theta(1-\beta)\kappa\left(t,t'\right)=\frac{i\Gamma\Theta\left(t-t'\right)/c}{1+\beta}\Theta\left(t-T_0/(1-\beta)\right)\delta\left(t'-\frac{1-\beta}{1+\beta}t+\frac{T_0}{1+\beta}\right) \tag{23}$$

In the case of the qubit approaching the mirror $-1<\beta<0$ we have:

$$\begin{aligned}\kappa_a^I\left(t,t'\right)&=\Theta(-\beta)\Theta(\beta+1)\kappa\left(t,t'\right)\\&=\frac{i\Gamma\Theta\left(t-t'\right)/c}{1-|\beta|}\Theta\left(t-T_0/(1+|\beta|)\right)\Theta(T/2|\beta|-t)\delta\left(t'-\frac{(1+|\beta|)t-T_0}{1-|\beta|}\right)\\&+\frac{i\Gamma\Theta\left(t-t'\right)/c}{1+|\beta|}\Theta\left(t-T_0/2|\beta|\right)\delta\left(t'-\frac{(1-|\beta|)t+T_0}{1+|\beta|}\right)\end{aligned} \tag{24}$$

We thus have

$$\begin{aligned}\left(i\partial_t-\Delta+i\widetilde{\Gamma}\right)\psi_{I,r}^{(1)}(t)&=\int_0^\infty dt'\kappa_r^I\left(t,t'\right)\psi_{I,r}^{(1)}\left(t'\right)\\&=\frac{i\Gamma/c}{1+\beta}\Theta\left(t-T_0/(1-\beta)\right)\psi_{I,r}^{(1)}\left(\frac{(1-\beta)t-T_0}{1+\beta}\right)\end{aligned} \tag{25}$$

We Laplace transform the equation ($\theta=(1+\beta)/(1-\beta)$)

$$\begin{aligned}\hat{\psi}_{I,r}^{(1)}(z)&=\frac{1}{z-\Delta+i\widetilde{\Gamma}}+\frac{1}{z-\Delta+i\widetilde{\Gamma}}\frac{ie^{izT_0/(1-\beta)}\Gamma/c}{1-\beta}\hat{\psi}_{I,r}^{(1)}(\theta z)\\&=\frac{1}{z-\Delta+i\widetilde{\Gamma}}+\frac{1}{z-\Delta+i\widetilde{\Gamma}}\frac{ie^{izT_0/(1-\beta)}\Gamma/c}{1-\beta}\frac{1}{\theta z-\Delta+i\widetilde{\Gamma}}\\&+\frac{1}{z-\Delta+i\widetilde{\Gamma}}\frac{ie^{izT_0/(1-\beta)}\Gamma/c}{1-\beta}\frac{1}{\theta z-\Delta+i\widetilde{\Gamma}}\frac{ie^{i\theta zT_0/(1-\beta)}\Gamma/c}{1-\beta}\frac{1}{\theta^2 z-\Delta+i\widetilde{\Gamma}}\\&+\frac{1}{z-\Delta+i\widetilde{\Gamma}}\frac{ie^{izT_0/(1-\beta)}\Gamma/c}{1-\beta}\frac{1}{\theta z-\Delta+i\widetilde{\Gamma}}\frac{ie^{i\theta zT_0/(1-\beta)}\Gamma/c}{1-\beta}\frac{1}{\theta^2 z-\Delta+i\widetilde{\Gamma}}\\&\times\frac{ie^{i\theta^2 zT_0/(1-\beta)}}{1-\beta/c}\frac{1}{\theta^3 z-\Delta+i\widetilde{\Gamma}}+\ldots\\&=\frac{1}{z-\Delta+i\widetilde{\Gamma}}+\frac{1}{z-\Delta+i\widetilde{\Gamma}}\sum_{n=0}^{\infty}\prod_{s=0}^{n}\frac{ie^{iz\theta^s T_0/(1-\beta)}\Gamma/c}{1-\beta}\frac{1}{\theta^{s+1}z-\Delta+i\widetilde{\Gamma}}\\&=\sum_{n=0}^{\infty}\frac{(i\Gamma/c)^n}{(1-\beta)^n}e^{iz\frac{1-\theta^n}{(1-\theta)(1-\beta)}T_0}\frac{1}{\prod_{s'=0}^{n}\left[\theta^{s'}z-(\Delta-i\widetilde{\Gamma})\right]}.\end{aligned} \tag{26}$$

One has

$$\begin{aligned}\hat{\psi}_{I,r}^{(1)}(z)&=\sum_{n=0}^{\infty}\frac{(i\Gamma/c)^n}{(1-\beta)^n}e^{iz\frac{1-\theta^n}{(1-\theta)(1-\beta)}T_0}\frac{1}{\prod_{s'=0}^{n}\left[\theta^{s'}z-(\Delta-i\widetilde{\Gamma})\right]}\\&=\frac{1}{z-(\Delta-i\widetilde{\Gamma})}\left[1+\sum_{n=1}^{\infty}\frac{(-i\Gamma/c)^n}{(1-\beta)^n(\Delta-i\widetilde{\Gamma})^n}e^{iz\frac{1-\theta^n}{(1-\theta)(1-\beta)}T_0}\frac{1}{\prod_{s'=0}^{n-1}\left[1-\frac{\theta z}{\Delta-i\widetilde{\Gamma}}\theta^{s'}\right]}\right] \qquad (27)\\&=\frac{1}{z-(\Delta-i\widetilde{\Gamma})}\left[1+\sum_{n=1}^{\infty}\frac{(-i\Gamma/c)^n}{(1-\beta)^n(\Delta-i\widetilde{\Gamma})^n}e^{iz\frac{1-\theta^n}{(1-\theta)(1-\beta)}T_0}\frac{1}{\left(\frac{\theta z}{\Delta-i\widetilde{\Gamma}};\theta\right)_n}\right] \qquad (28)\end{aligned}$$

We rewrite the original equation in time space as

$$\left(i\partial_t - \Delta + i\widetilde{\Gamma}\right)\psi^{(1)}_{I,r}(t) = \frac{i\Gamma/c}{1+\beta}\Theta\left(t - T_0/(1-\beta)\right)\psi^{(1)}_{I,r}\left(\frac{(1-\beta)t - T_0}{1+\beta}\right) \tag{29}$$

Now we define the Mellin transform

$$\bar{\psi}^{(1)}_{I,r}(s) = \int_0^\infty dt t^{s-1}\psi^{(1)}_{I,r}(t) \tag{30}$$

The inverse Mellin transform is given by

$$\psi^{(1)}_{I,r}(t) = \int_{\epsilon-i\infty}^{\epsilon+i\infty}\frac{ds}{2\pi i}t^{-s}\bar{\psi}^{(1)}_{I,r}(s). \tag{31}$$

Let us also determine the relation between Mellin and Laplace transform. By definition

$$\begin{aligned}\hat{\psi}^{(1)}_{I,r}(z) &= -i\int_0^\infty dt e^{izt}\psi^{(1)}_{I,r}(t) = -i\int_{\epsilon-i\infty}^{\epsilon+i\infty}\frac{ds}{2\pi i}\bar{\psi}^{(1)}_{I,r}(s)\int_0^\infty dt t^{-s}e^{izt} \\ &= -i\Theta(1-\epsilon)\int_{\epsilon-i\infty}^{\epsilon+i\infty}\frac{ds}{2\pi i}(-iz)^{s-1}\Gamma(1-s)\bar{\psi}^{(1)}_{I,r}(s)\end{aligned} \tag{32}$$

On the other hand

$$\begin{aligned}\bar{\psi}^{(1)}_{I,r}(s) &= \int_0^\infty dt t^{s-1}\psi^{(1)}_{I,r}(t) = \int_{+\infty+i\eta}^{-\infty+i\eta}\frac{dz}{2\pi i}\hat{\psi}^{(1)}_{I,r}(z)\int_0^\infty dt t^{s-1}e^{-izt} \\ &= \int_{+\infty+i\eta}^{-\infty+i\eta}\frac{dz}{2\pi i}\hat{\psi}^{(1)}_{I,r}(z)(iz)^{-s}\Gamma(s)\end{aligned} \tag{33}$$

We Mellin transform our equation

$$-i(s-1)\bar{\psi}^{(1)}_{I,r}(s-1) - \left(\Delta - i\widetilde{\Gamma}_\Gamma\right)\bar{\psi}^{(1)}_{I,r}(s) = \frac{(i\Gamma/c)T_0^{s-1}}{(1-\beta)^s}\int_0^\infty d\tau\left(1 - \frac{1+\beta}{T_0}\tau\right)^{s-1}\psi^{(1)}_{I,r}(\tau) \tag{34}$$

$$= \frac{(i\Gamma/c)T_0^{s-1}}{(1-\beta)^s}\sum_{l=0}^\infty\binom{s-1}{l}\frac{(-1)^l(1+\beta)^l}{T_0^l}\bar{\psi}^{(1)}_{I,r}(l+1) \tag{35}$$

6.3.7 Real time dynamics for $0 < t < \infty$.

For a stationary qubit $\beta = 0$ we simply obtain:

$$\hat{\psi}^{(1)}_{I,r}(z) = \frac{1}{z - \Delta + i\Gamma/c}\sum_{n=0}^\infty\left(\frac{i\Gamma e^{izT_0}/c}{z - \Delta + i\Gamma/c}\right)^n = \frac{1}{z - \Delta + i\Gamma\left(1 - e^{izT_0}\right)/c} \tag{36}$$

$$\begin{aligned}\psi^{(1)}_{I,r}(t) &= \int_{+\infty+i\eta}^{-\infty+i\eta}\frac{dz}{2\pi i}e^{-izt}\hat{\psi}^{(1)}_{I,r}(z) \\ &= \sum_{n=0}^\infty\Theta\left(t - nT_0\right)\frac{1}{n!}\left(\Gamma\left(t - nT_0\right)/c\right)^n e^{-i\Delta(t-nT_0)}e^{-\Gamma(t-nT_0)/c}\end{aligned} \tag{37}$$

Let us consider the Laplace transform of the propagator in general case $\beta \in [0, 1)$. One has

$$\begin{aligned}\hat{\psi}^{(1)}_{I,r}(t) =& \sum_{n=0}^{\infty}\frac{(i\Gamma/c)^n}{(1-\beta)^n}\int_{+\infty+i\eta}^{-\infty+i\eta}\frac{dz}{2\pi i}e^{-iz\left[t-\frac{1-\theta^n}{(1-\theta)(1-\beta)}T_0\right]}e\frac{1}{\prod_{s'=0}^{n}\left[\theta^{s'}z-(\Delta-i\widetilde{\Gamma})\right]}\\ =&\sum_{n=0}^{\infty}\frac{(i\Gamma/c)^n}{(1-\beta)^n}\Theta\left(t-\frac{1-\theta^n}{(1-\theta)(1-\beta)}T_0\right)\\ &\times\sum_{l=0}^{n}\lim_{z\to\theta^{-l}(\Delta-i\widetilde{\Gamma})}\frac{\left(z-\theta^{-l}(\Delta-i\widetilde{\Gamma})\right)}{\prod_{s'=0}^{n}\left[\theta^{s'}z-(\Delta-i\widetilde{\Gamma})\right]}e^{-iz\left[t-\frac{1-\theta^n}{(1-\theta)(1-\beta)}T_0\right]}\\ =&\sum_{n=0}^{\infty}\frac{(i\Gamma/c)^n}{(1-\beta)^n(\Delta-i\widetilde{\Gamma})^n}\Theta\left(t-\frac{1-\theta^n}{(1-\theta)(1-\beta)}T_0\right)\\ &\times\sum_{l=0}^{n}\frac{1}{\theta^l\prod_{s'\neq l,s'=0}^{n}\left[\theta^{s'-l}-1\right]}e^{-i\theta^{-l}(\Delta-i\widetilde{\Gamma})\left[t-\frac{1-\theta^n}{(1-\theta)(1-\beta)}T_0\right]}.\end{aligned}\tag{38}$$

One has

$$\prod_{s'\neq l,s'=0}^{n}\left[\theta^{s'-l}-1\right]=\prod_{s'=0}^{l-1}\left[\theta^{s'-l}-1\right]\prod_{s'=l+1}^{n}\left[\theta^{s'-l}-1\right]=(-1)^n\left(\theta^{-l};\theta\right)_l(\theta;\theta)_{n-l}\tag{39}$$

Here we defined the q-Pochhammer symbol

$$(a;q)_j=\prod_{s=0}^{j-1}(1-aq^s)\tag{40}$$

This leads to

$$\begin{aligned}\hat{\psi}^{(1)}_{I,r}(t) =&\sum_{n=0}^{\infty}\frac{(-i\Gamma/c)^n}{(1-\beta)^n(\Delta-i\widetilde{\Gamma})^n}\Theta\left(t-\frac{1-\theta^n}{(1-\theta)(1-\beta)}T_0\right)\\ &\times\sum_{l=0}^{n}\frac{1}{\theta^l\left(\theta^{-l};\theta\right)_l(\theta;\theta)_{n-l}}\exp\left\{-i\frac{\Delta-i\widetilde{\Gamma}}{\theta^l}\left[t-\frac{1-\theta^n}{(1-\theta)(1-\beta)}T_0\right]\right\}\end{aligned}\tag{41}$$

Using the following identity

$$\left(\theta^{-l};\theta\right)_l=(\theta;\theta)_l(-1)^l\theta^{-l}\theta^{-\binom{l}{2}}\tag{42}$$

we rewrite the above series as

$$\begin{aligned}\hat{\psi}^{(1)}_{I,r}(t) =&\sum_{n=0}^{\infty}\frac{(-i\Gamma/c)^n}{(1-\beta)^n(\Delta-i\widetilde{\Gamma})^n}\Theta\left(t-\frac{1-\theta^n}{(1-\theta)(1-\beta)}T_0\right)\\ &\times\sum_{l=0}^{n}\frac{(-1)^l\theta^{l(l-1)/2}}{(\theta;\theta)_l(\theta;\theta)_{n-l}}\exp\left\{-i\frac{\Delta-i\widetilde{\Gamma}}{\theta^l}\left[t-\frac{1-\theta^n}{(1-\theta)(1-\beta)}T_0\right]\right\}\end{aligned}\tag{43}$$

We consider the Mellin transform

$$M(s)=\int_0^{\infty}d\tau\tau^{s-1}\exp\left\{-i\frac{\lambda}{\theta^l}\tau\right\}=\theta^{sl}\int_0^{\infty}d\tau'\tau'^{s-1}e^{-(\widetilde{\Gamma}+i\Delta)\tau'}=\theta^{sl}(\widetilde{\Gamma}+i\Delta)^{-s}\Gamma(s)\tag{44}$$

The inverse transform is

$$\exp\left\{-i\frac{\lambda}{\theta^l}\tau\right\}=\int_{c-i\infty}^{c+i\infty}\frac{ds}{2\pi i}\frac{\Gamma(s)\theta^{sl}}{(\widetilde{\Gamma}+i\Delta)^s}\frac{1}{\tau^s}\tag{45}$$

It follows that

$$\hat{\psi}^{(1)}_{I,r}(t)=\sum_{n=0}^{\infty}\frac{(-i\Gamma/c)^n}{(1-\beta)^n(\Delta-i\widetilde{\Gamma})^n}\Theta\left(t-\frac{1-\theta^n}{(1-\theta)(1-\beta)}T_0\right)$$
$$\times\int_{c-i\infty}^{c+i\infty}\frac{ds}{2\pi i}\frac{\Gamma(\widetilde{\Gamma})}{(\widetilde{\Gamma}+i\Delta)^s}\frac{1}{\left(t-\frac{1-\theta^n}{(1-\theta)(1-\beta)}T_0\right)^s}\sum_{l=0}^{n}\frac{\left(-\theta^s\right)^l\theta^{l(l-1)/2}}{(\theta;\theta)_l(\theta;\theta)_{n-l}} \tag{46}$$

Now we make use of the fact that

$$\sum_{l=0}^{n}\frac{\left(-\theta^s\right)^l\theta^{l(l-1)/2}}{(\theta;\theta)_l(\theta;\theta)_{n-l}}=\frac{(\theta^s;\theta)_n}{(\theta;\theta)_n} \tag{47}$$

we write

$$\hat{\psi}^{(1)}_{I,r}(t)=\int_{c-i\infty}^{c+i\infty}\frac{ds}{2\pi i}\frac{\Gamma(s)}{(\widetilde{\Gamma}+i\Delta)^s}\sum_{n=0}^{\infty}\frac{(-i\Gamma/c)^n}{(1-\beta)^n(\Delta-i\widetilde{\Gamma})^n}\Theta\left(t-\frac{1-\theta^n}{(1-\theta)(1-\beta)}T_0\right)$$
$$\times\frac{1}{\left(t-\frac{1-\theta^n}{(1-\theta)(1-\beta)}T_0\right)^s}\frac{(\theta^s;\theta)_n}{(\theta;\theta)_n}. \tag{48}$$

6.3.8 Long-time limit

Let us consider the $t\gg T_0$ limit. In this limit we may omit all of the Θ-functions. It follows

$$\hat{\psi}^{(1)}_{I,r}(t)\to\sum_{n=0}^{\infty}\frac{(-i\Gamma/c)^n}{(1-\beta)^n(\Delta-i\widetilde{\Gamma})^n}\sum_{l=0}^{n}\frac{(-1)^l\theta^{l(l-1)/2}}{(\theta;\theta)_l(\theta;\theta)_{n-l}}\exp\left\{-i\frac{\Delta-i\widetilde{\Gamma}}{\theta^l}\left[t-\frac{1-\theta^n}{(1-\theta)(1-\beta)}T_0\right]\right\} \tag{49}$$

Now we interchange the order of summations

$$\hat{\psi}^{(1)}_{I,r}(t)\to\sum_{l=0}^{\infty}\frac{(-1)^l\theta^{l(l-1)/2}}{(\theta;\theta)_l}\exp\left\{-i\frac{\Delta-i\widetilde{\Gamma}}{\theta^l}\left[t-\frac{T_0}{(1-\theta)(1-\beta)}\right]\right\}$$
$$\times\sum_{n=l}^{\infty}\frac{(-i\Gamma/c)^n}{(1-\beta)^n(\Delta-i\widetilde{\Gamma})^n}\frac{1}{(\theta;\theta)_{n-l}}\exp\left\{-i(\Delta-i\widetilde{\Gamma})\frac{\theta^{n-l}}{(1-\theta)(1-\beta)}T_0\right\}$$
$$=\sum_{l=0}^{\infty}\frac{(-1)^l\theta^{l(l-1)/2}}{(\theta;\theta)_l}\frac{(-i\Gamma/c)^l}{(1-\beta)^l(\Delta-i\widetilde{\Gamma})^l}\exp\left\{-i\frac{\Delta-i\widetilde{\Gamma}}{\theta^l}\left[t-\frac{T_0}{(1-\theta)(1-\beta)}\right]\right\}$$
$$\times\sum_{m=0}^{\infty}\frac{(-i\Gamma/c)^m}{(1-\beta)^m(\Delta-i\widetilde{\Gamma})^m}\frac{1}{(\theta;\theta)_m}\exp\left\{-i\frac{(\Delta-i\widetilde{\Gamma})\theta^m}{(1-\theta)(1-\beta)}T_0\right\} \tag{50}$$

thus, as $t\to\infty$ the probability amplitude factorizes into two summations. We remind ourselves that in the regime under consideration $0\geq\beta<1$ the renormalized decay rate is given by

$$c\widetilde{\Gamma}=\frac{\Gamma}{1-\beta^2} \tag{51}$$

so that

$$\frac{(-i\Gamma/c)^m}{(1-\beta)^m}=(1+\beta)^m(-i\widetilde{\Gamma})^m \tag{52}$$

Denoting $\lambda=\Delta-i\widetilde{\Gamma}$, we write

$$\hat{\psi}^{(1)}_{I,r}(t)\to\sum_{l=0}^{\infty}\frac{\theta^{l(l-1)/2}}{(\theta;\theta)_l}\left(\frac{i\widetilde{\Gamma}(1+\beta)}{\lambda}\right)^l\exp\left\{-i\frac{\lambda}{\theta^l}\left[t-\frac{T_0}{(1-\theta)(1-\beta)}\right]\right\}$$
$$\times\sum_{m=0}^{\infty}\frac{1}{(\theta;\theta)_m}\left(\frac{-i\widetilde{\Gamma}(1+\beta)}{\lambda}\right)^m\exp\left\{-i\frac{\lambda\theta^m}{(1-\theta)(1-\beta)}T_0\right\} \tag{53}$$

Let us consider the first series.
One has

$$\sum_{m=0}^{\infty} \frac{(-i\Gamma/c)^m}{(1-\beta)^m(\Delta - i\widetilde{\Gamma})^m} \frac{1}{(\theta;\theta)_m} \exp\left\{-i\frac{(\Delta - i\widetilde{\Gamma})\theta^m}{(1-\theta)(1-\beta)}T_0\right\} \tag{54}$$

$$= \sum_{j=0}^{\infty} \frac{1}{j!}\left\{-i\frac{(\Delta - i\widetilde{\Gamma})}{(1-\theta)(1-\beta)}T_0\right\}^j \sum_{m=0}^{\infty} \frac{\left(-i\Gamma\theta^j/c\right)^m}{(1-\beta)^m(\Delta - i\widetilde{\Gamma})^m} \frac{1}{(\theta;\theta)_m} \tag{55}$$

$$= \sum_{j=0}^{\infty} \frac{1}{j!}\left\{-i\frac{(\Delta - i\widetilde{\Gamma})}{(1-\theta)(1-\beta)}T_0\right\}^j \frac{1}{\left(\frac{-i\Gamma\theta^j/c}{(1-\beta)(\Delta - i\widetilde{\Gamma})};\theta\right)_\infty} \tag{56}$$

We use the identity

$$\frac{1}{\left(\frac{-i\Gamma\theta^j/c}{(1-\beta)(\Delta - i\widetilde{\Gamma})};\theta\right)_\infty} = \frac{\left(\frac{-i\Gamma/c}{(1-\beta)(\Delta - i\widetilde{\Gamma})};\theta\right)_j}{\left(\frac{-i\Gamma/c}{(1-\beta)(\Delta - i\widetilde{\Gamma})};\theta\right)_\infty} \tag{57}$$

Part V
Well-known and Important Articles

7 Diagrams for scattering in waveguide QED by Piasotski, Pletyukhov (PP21)

Abstract

We give an exposure to diagrammatic techniques in waveguide QED systems. A particular emphasis is placed on the systems with delayed coherent quantum feedback. Specifically, we show that the N-photon scattering matrices in single-qubit waveguide QED systems, within the rotating wave approximation, admit for a parametrization in terms of $N-1$-photon effective vertex functions and provide a detailed derivation of a closed hierarchy of generalized Bethe-Salpeter equations satisfied by these vertex functions.

(still, have no idea, how is it connected with Bethe-Salpeter equation. a separate question.)

The advantage of this method is that the above mentioned integral equations hold independently of the number of radiation channels, their bandwidth, the dispersion of the modes they are supporting, and the structure of the radiation-qubit coupling interaction, thus enabling one to study multi-photon scattering problems beyond the Born-Markov approximation.

Further, we generalize the diagrammatic techniques to the systems containing more than a single emitter by presenting an exact set of equations governing the generic two and three-photon scattering operators.

The above described theoretical machinery is then showcased on the example of a three-photon scattering on a giant acoustic atom, recently studied experimentally [Nat. Phys. **15**, 1123 (2019)].

(todo: study this article, a job for 2 days.)

7.1 Introduction

Waveguide quantum electrodynamics (QED) is a modern field of research focused on the study of light-matter interactions in one dimension. The confinement of electromagnetic radiation to a single spatial dimension allows one to achieve a significant enhancement of the coupling between atoms and fields, as well as to attain a better matching between the spatial modes of the emitting and absorbing atoms [1, 2]. Apart from the purely academic interest in the study of strong light-matter coupling, a great deal of motivation in this field of research comes from the technological sector, namely from the quantum computing [3, 8, 4, 5, 6, 7]. One of the most prominent examples is the so-called quantum network: A system of quantum processors interconnected by quantum radiation channels propagating quantum information and entanglement between them [9].

Although photons are the excellent carriers of quantum information, capable of high fidelity entanglement and information transfer [10, 11, 12], recent advancement in quantum electronics offers a large variety of alternatives. Most commonly, nowadays, waveguide QED setups are realized in the experiments with superconducting quantum circuits, where superconducting transmission lines act as quantum radiation channels, whereas the Josephson-junction-based superconducting quantum bits play the role of quantum emitters [13, 14, 15]. Other examples include superconducting qubits coupled to propagating phonons (surface acoustic waves) employing the piezoelectric effect [16, 17, 18, 19], and surface plasmons coupled to quantum dots [20].

Theoretically, the atom-field interactions in waveguide QED can often be accurately treated in the so-called Markovian limit $\gamma\tau \ll 1$, where γ and τ stand for the characteristic decay rate and time delay in the system [21]. In the course of the last few decades, a significant number of theoretical approaches allowing one to tackle the waveguide QED problems within this limit was proposed. In particular, the Markovian waveguide QED systems are commonly examined theoretically with help of master equation based-approaches [1, 22, 23, 24, 25, 26, 27]. Indeed, within the framework of the associated input-output formalism [1, 28, 29], Lindblad-type equation approaches allow one to study transmission and reflection characteristics, as well as the photonic correlations for arbitrary initial photon states, including coherent, thermal, and Fock ones. Moreover, at a rather modest expense, a substantial variety of theoretical tools are available for a derivation of master equations: equation

of motion-based methods [1, 22, 23], path integral techniques [30], SLH formalism [31], to mention just a few. Recently master equation-based approach was generalized to capture the effects of temporal modulation of the system parameters [32, 33], such as the light-matter coupling strength and the transition frequencies of quantum emitters.

Another frequenter method of studying waveguide QED systems within Markov approximation is the coordinate space Bethe ansatz [34, 35, 36, 41, 37, 38, 39, 40]. Within this approach, one is able to determine the exact stationary eigenstates of the system's Hamiltonian in a subspace of a given excitation number, which, in turn, enables one to calculate stationary observables as well as photonic correlation functions exactly. Moreover, the Bethe ansatz technique was shown to be applicable to the studies of real-time dynamics of few-photon states [36, 42, 43], systems where the photon-photon bound states occur [44, 41], and systems with delayed coherent feedback [45]. Despite its scalability to the cases of multiple emitters and emitters with complicated level structures, this approach is known to be strongly limited by the number of excitations in the system due to the rapid increase of complexity of the resulting Bethe wavefunctions [46, 36, 34, 47].

Another group of systematic methods of studying the waveguide QED systems in the limit of the negligible delay times is comprised of the field theory-based approaches. For example, in [48, 49, 50], by representing the atomic operators in terms of the slave fermions, the authors were able to employ the path integral representation of the field correlation functions, from which the S-matrix may be established by means of the celebrated Lehmann-Symanzik-Zimmermann reduction formula. Another field theoretical method to be mentioned is the so-called diagrammatic resummation theory developed in [51, 52, 53, 54]. Within the framework of resummation theory, one sums the perturbative series of Feynmann diagrams for the matrix elements of the transition operator to infinite orders, which, in turn, allows one to determine the exact S-matrix, with the help of which all of the stationary observables may be calculated [52].

Although physics behind waveguide QED systems is easily accessible in the Markovian limit using a large variety of theoretical tools, there exists a number of problems forcing one to go beyond this approximation [21, 55, 56, 57, 58]. As it is well known, in the single excitation subspace, all of the dynamical and stationary information about the system may be easily obtained (either analytically or numerically) by means of Bethe ansatz for a system of arbitrary complexity [60, 59, 61, 62]. Primarily, this assertion has to do with the fact that it is relatively easy to conceive a closed system of (delay) differential equations governing the evolution of the system. Even though it is possible to proceed in the same manner in higher excitation subspaces [63], the calculations become much more cumbersome and lack systematicity. In the course of the last decade, a number of theoretical approaches allowing one to overcome these difficulties were put forward. On the numerical side, for example, significant progress in the dynamical simulation of the non-Markovian 1D quantum systems was achieved within the framework of matrix product state ansatz [64, 65, 66, 67]. Despite the complexity associated with the non-Markovian waveguide QED systems, a few analytical methods were also recently suggested. In particular, it is a common practice to generalize the Lindblad-type equation approaches to the non-Markovian realm [30, 68, 69, 70]. Although generalized master equations can only provide exact results in the case of linear scatterers, they allow for systematic approximate treatment of systems with nonlinearities such as qubits.

Another common approach to waveguide QED problems with delayed coherent quantum feedback is based on the diagrammatic resummation theory.

In recent years resummation ideas were successfully applied to solve the two-photon scattering and dynamics in the systems with two distant qubits [71], a single qubit in front of a mirror [21],

a giant acoustic atom [59], and a qubit coupled to a resonator array [72].

(todo: create a section about resummation theory)

In this paper, we present a systematic generalizattion of the diagrammatic approach to scattering of multiphoton states in waveguide QED.

(write better, what and how was generalized?)

Our approach is based on the exact resummation of the perturbation theory for the transition operator which turns out to be possible due to the conservation of excitation number guaranteed by the rotating wave approximation. The advantage of our approach is its insensitivity to the form of light-matter coupling constants, thus, allowing one to potentially examine any kinds of waveguide QED systems, including the systems with delayed coherent quantum feedback. We start by making an exposure of the method by the direct example of 1-qubit waveguide QED. This framework lays down a basis for further calculations, in particular general qubit number two and three-photon scattering theory. We then apply the developed theory to a weakly coherent pulse scattering on a giant acoustic atom, an intrinsically non-Markovian system. In particular, we consider the scattering of a coherent state with small enough coherence parameter $|\alpha| \ll 1$ chosen such that the terms of order $|\alpha|^4$ can be ignored. With the help of the general methods developed in Section 7.2 we compute an exact output state of radiation and study the particle correlations in it with the help of the theory of optical coherence. In particular, we compute the first, second, and third-order coherence functions to the lowest order in $|\alpha|$ and discuss the impact of the non-Markovianity of the scatterer on the observable quantities.

7.2 Scattering Theory

In this section, we first set up the notations used throughout the paper. Next, we introduce the general formalism in the framework of the single-qubit waveguide QED. In particular, we extend the findings of the preceding papers [21, 51, 53, 59] to the realm of non-Markovian models by allowing for arbitrary momentum dependence of waveguide modes and radiation-qubit couplings. This development, in turn, allows one to study

multi-photon scattering problems in systems with non-linear dispersion of the modes supported by the radiation channels, as well as the systems with artificial feedback loops, such as a qubit placed in front of a mirror or a giant acoustic atom, for example.

Further on, we generalize the scattering formalism to the systems with a higher number of qubits, where the quantum feedback loops a naturally present due to the finiteness of time required for a photon to propagate between a given pair of distant emitters. Specifically, we discuss two and three-photon scattering problems on an arbitrary number of emitters, extending the approach of [71].

Alongside this, we discuss several practical issues, such as the separation of elastic contributions to the scattering matrices and the generalized cluster decomposition.

7.2.1 Hamiltonian, generalized summation convention, and the S - matrix

Let us consider a collection of N_q qubits coupled to a waveguide with N_c radiation channels. The Hamiltonian of such a system assumes the following form $\mathcal{H} = \mathcal{H}_0 + \mathcal{V}$, where

$$\mathcal{H}_0 = \sum_{n=1}^{N_q} \Omega_n \sigma_+^{(n)} \sigma_-^{(n)} + \sum_{\mu=1}^{N_c} \int_{B_\mu} dk \omega_\mu(k) a_\mu^\dagger(k) a_\mu(k), \tag{7.1}$$

is the free Hamiltonian, and

$$\mathcal{V} = \sum_{\mu=1}^{N_c} \sum_{n=1}^{N_q} \int_{B_\mu} dk [g_{\mu,n}(k) a_\mu^\dagger(k) \sigma_-^{(n)} + \text{h.c.}] \tag{7.2}$$

is the dipole light-matter interaction in the rotating wave approximation (RWA). In the above expression, Ω_n is the transition frequency of the n^{th} qubit, the dispersion relation $\omega_\mu(k)$ and the bandwidth B_μ characterize the radiation channel μ, while $a_\mu^\dagger(k)$ and $a_\mu(k)$ stand for the creation and annihilation field operators of a photon with momentum k and obey the standard bosonic commutation relations:

$$[a_\mu(k), a_{\mu'}^\dagger(k')] = \delta_{\mu,\mu'} \delta(k - k'), \tag{7.3}$$

$$[a_\mu^\dagger(k), a_{\mu'}^\dagger(k')] = [a_\mu(k), a_{\mu'}(k')] = 0. \tag{7.4}$$

The operators acting on the Hilbert space of the n^{th} qubit, $\{\sigma_3^{(n)}, \sigma_+^{(n)}, \sigma_-^{(n)}\}$, are defined according to $\sigma_l^{(n)} = 1_{\mathbb{C}^2}^{\otimes(n-1)} \otimes \sigma_l \otimes 1_{\mathbb{C}^2}^{\otimes(N_q-n)}$, with the σ-matrices being chosen according to the standard convention

$$\sigma_3 = \begin{pmatrix} 1 & 0 \\ 0 & -1 \end{pmatrix}, \quad \sigma_+ = \sigma_-^\dagger = \begin{pmatrix} 0 & 1 \\ 0 & 0 \end{pmatrix}. \tag{7.5}$$

The RWA is justified as long as the characteristic operational frequency ω_0 is such that the condition $|g_\mu^2(\omega_0)/\omega_0| \ll 1$ is satisfied [73]. One of the main benefits of this approximation is the conservation of the total number of excitations in the system, i.e. an operator $\mathcal{N} = \sum_{n=1}^{N_q} \sigma_+^{(n)} \sigma_-^{(n)} + \sum_{\mu=1}^{N_c} \int_{B_\mu} dk a_\mu^\dagger(k) a_\mu(k)$ commutes with the full Hamiltonian, $[\mathcal{N}, \mathcal{H}] = 0$. This property allows us to simultaneously diagonalize $\mathcal{H}$ and $\mathcal{N}$. Moreover, the eigenspaces of the Hamiltonian labeled by the eigenvalues of $\mathcal{N}$ are certainly orthogonal, hence there exists a direct sum decomposition of the total Hilbert space of the system

$$\mathscr{H} = \bigoplus_{N=0}^{\infty} \mathscr{H}_N, \tag{7.6}$$

where $\mathscr{H}_N$ is the $D(N, N_q) = \sum_{l=0}^{\min(N_q,N)} \frac{N_q!}{l!(N_q-l)!}$ dimensional subspace of all possible states with N excitations. Note that here $D(N, N_q)$ does not stand for the dimension of $\mathscr{H}_N$ in the strict mathematical sense. Instead, it is a number of ways to distribute N excitations in a system of N_q qubits (i.e., each single-photon infinite-dimensional vector space adds unity to $D(N, N_q)$). Analogous direct sum decompositions hold for the Hamiltonian, unitary evolution operator, and the S-matrix (to be introduced later). Moreover, such a decomposition considerably simplifies the problem since the calculations may be performed in all of the subspaces separately.

To simplify our further analysis, it is useful to introduce compact notations. Thus we define a multi-index $s = (\mu, k)$ and the generalized summation convention: if two multi-indices are repeated, summation over the

channel index μ and integration with respect to the momentum k (over the relevant bandwidth B_μ) is implied. We also introduce the following notation for the bare interaction vertex

$$v_s = \sum_{n=1}^{N_q} g_{\mu,n}(k)\sigma_-^{(n)}. \tag{7.7}$$

Using these conventions we rewrite the Hamiltonian as

$$\mathcal{H} = \mathcal{H}_0 + \mathcal{V}, \quad \mathcal{H}_0 = \omega_s a_s^\dagger a_s + \sum_{n=1}^{N_q} \Omega_n \sigma_+^{(n)}\sigma_-^{(n)}, \tag{7.8}$$

$$\mathcal{V} = a_s^\dagger v_s + v_s^\dagger a_s. \tag{7.9}$$

The scattering matrix, or the S-matrix, is the main object of interest in the present section. It can be generally defined via the so-called transition operator, or the T-matrix, in the following way:

$$\mathcal{S} = 1_{\mathscr{H}} - 2\pi i\delta(\epsilon_i - \epsilon_f)\mathcal{T}(\epsilon_i), \tag{7.10}$$

$$\mathcal{T}(\epsilon) = \mathcal{V} + \mathcal{V}\mathcal{G}(\epsilon)\mathcal{V}, \tag{7.11}$$

where the T-matrix is put on-shell, i.e. $\epsilon = \epsilon_i$, and the energies ϵ_i, ϵ_f, corresponding to initial and final states of the system, obey the energy conservation in the scattering processes, which is mathematically ensured by the delta-function. In (7.11) we have denoted by $\mathcal{G}(\epsilon)$ the retarded Green's operator defined according to

$$\mathcal{G}(\epsilon) = \frac{1}{\epsilon - \mathcal{H} + i\eta} = \sum_{n=0}^{\infty}(\mathcal{G}_0(\epsilon)\mathcal{V})^n\mathcal{G}_0(\epsilon), \tag{7.12}$$

$$\mathcal{G}_0(\epsilon) = \frac{1}{\epsilon - \mathcal{H}_0 + i\eta}, \quad \eta \to 0^+. \tag{7.13}$$

7.2.2 General properties of the scattering matrix in waveguide QED

Let us consider the scattering problem for the following initial state $|N_p\rangle \otimes |g\rangle$, where $|N_p\rangle$ is a N_p-photon state, and $|g\rangle = |0\rangle^{\otimes N_q}$ is the ground state of the scatterer. Due to the conservation of excitation-number operator, all of the possible $D(N_p, N_q)$ scattering outcomes must contain N_p excitations. Due to the fact that for any system of qubits the ground state $|g\rangle$ is the only non-decaying (subradiant) subspace, in the long-time limit (a priory assumed in scattering theory) all of the emitters will definitely decay into the continuum, leaving us with the only possibility for the system to end up in the state $|N_p'\rangle \otimes |g\rangle$ (here $|N_p'\rangle$ is again a N_p-photon state, with potentially redistributed momenta) [[74]]. If one wishes to extend the scattering theory to the systems with metastable ground states, such as e.g. a Λ three-level system, one then has to consider calculating more matrix elements of the transition operator [75, 76].

Since the only matrix elements, we are interested in are diagonal in both the photon and qubit space, due to the RWA, the only terms contributing to the perturbation expansion of the T-matrix are those containing an even number of interactions $\mathcal{V}$, thus reducing the number of diagrams by half. Another important feature to be mentioned is the nilpotency of the photon-qubit interaction vertex operator $v_{s_1}^\dagger ... v_{s_{N_q+1}}^\dagger = v_{s_1} ... v_{s_{N_q+1}} = 0$, which along with the property $v_s |g\rangle = \langle g| v_s^\dagger = 0$ and the fact that the number of v's and $v^\dagger$'s has to be equal in each graph contributing to the expansion, significantly reduces the number of non-zero diagrams at each order in perturbation theory. In fact, as we are going to see in this section, all of the diagrams contributing to the series for any fixed N_q may be constructed out of a finite number of "clusters", in turn allowing, in principle for the exact resummation of the perturbation series. One can also organize the calculation differently, namely by fixing N_p and allowing N_q to vary instead. Calculation within this approach is facilitated in its turn by the fact that $a_{s_1} ... a_{s_{N_p+1}} |N_p\rangle = \langle N_p| a_{s_1}^\dagger ... a_{s_{N_p+1}}^\dagger = 0$ and the fact that the number of a's and $a^\dagger$'s in each term of the perturbation series have to be equal. Although, these two approaches are clearly dual due to the structure of interaction potential in RWA. This approach is beneficial when studying few-photon scattering on a large number of qubits. This assertion has to do with the fact that once the solution of N_p photon scattering problem on $N_q = N_p$ the scattering of N_p particles on $N_q > N_p$ follows the same lines. Indeed, since v_s ($v_s^\dagger$) by itself contains the sum of all of the single-qubit lowering (raising) operators and the highest number of qubits that the N_p photon pulse can excite equals to N_p, the normal ordered N_p-photon S-matrix cannot contain projectors on subspaces with higher-excitation number than N_p. Using this fact in the following we are going to derive the generic two and three-photon scattering matrices by considering two and three particle scattering on two and three atoms respectively.

7.2.3 Scattering theory in $N_q = 1$ waveguide QED

In this subsection, we would like to make a detailed exposition of our general method by considering the simplest imaginable scenario of a single qubit coupled to a waveguide. As it was anticipated in Subsection 7.2.2, to solve the N_p-photon scattering problem, we shall determine the following matrix elements of the transition operator

$$\left\langle N_p', g \left| \mathcal{T}^{(1)}(\epsilon) \right| N_p, g \right\rangle = \left\langle N_p', g \left| \mathcal{V}\mathcal{G}(\epsilon)\mathcal{V} \right| N_p, g \right\rangle \tag{7.14}$$

$$= \left\langle N_p', g \left| a_{s_1'}^\dagger v_{s_1'} \mathcal{G}(\epsilon) v_{s_1}^\dagger a_{s_1} \right| N_p, g \right\rangle \tag{7.15}$$

$$= \sum_{n=0}^{\infty} \left\langle N_p', g \left| a_{s_1'}^\dagger v_{s_1'} (\mathcal{G}_0(\epsilon)\mathcal{V})^n \mathcal{G}_0(\epsilon) v_{s_1}^\dagger a_{s_1} \right| N_p, g \right\rangle, \tag{7.16}$$

where the superscript (1) refers to the $N_q = 1$ waveguide QED and we have used the fact that $\left\langle N_p', g \left| \mathcal{V} \right| N_p, g \right\rangle = 0$. Note that in what follows, whenever an argument of an object is omitted, we understand that its argument is ϵ, e.g $\mathcal{G}^{(1)}$ stands for $\mathcal{G}^{(1)}(\epsilon)$, etc, however, when the argument of a given operator or vertex function is of importance, it would be explicitly stated. As it was mentioned above, due to RWA, only even terms contribute to the above geometric series, so that

$$\left\langle N_p', g \left| \mathcal{T}^{(1)} \right| N_p, g \right\rangle$$
$$= \sum_{n=0}^{\infty} \left\langle N_p', g \left| a_{s_1'}^\dagger v_{s_1'} (\mathcal{G}_0\mathcal{V}\mathcal{G}_0\mathcal{V})^n \mathcal{G}_0 v_{s_1}^\dagger a_{s_1} \right| N_p, g \right\rangle. \tag{7.17}$$

Now, let us consider the $\mathcal{V}\mathcal{G}_0\mathcal{V}$ term in the brackets above

$$\begin{aligned} \mathcal{V}\mathcal{G}_0\mathcal{V} =& a_{s'}^\dagger v_{s'} \mathcal{G}_0 a_s^\dagger v_s + a_{s'}^\dagger v_{s'} \mathcal{G}_0 v_s^\dagger a_s \\ &+ v_{s'}^\dagger a_{s'} \mathcal{G}_0 v_s^\dagger a_s + v_{s'}^\dagger a_{s'} \mathcal{G}_0 a_s^\dagger v_s. \end{aligned} \tag{7.18}$$

Clearly, the terms with two vs and two $v^\dagger$s do not contribute (they are in fact zero) by the single-qubit nilpotency condition $v^2 = (v^\dagger)^2 = 0$. Among the "diagonal" terms, the only non-zero contribution comes from the $v^\dagger v$ term since the term $vv^\dagger$ annihilates the state $v^\dagger |g\rangle$ and gives zero whenever it is multiplied with $v^\dagger v$ term. Hence, we arrive at

$$\left\langle N_p', g \left| \mathcal{T}^{(1)} \right| N_p, g \right\rangle$$
$$= \sum_{n=0}^{\infty} \left\langle N_p', g \right| a_{s_1'}^\dagger v_{s_1'} (\mathcal{G}_0 v_{s'}^\dagger a_{s'} \mathcal{G}_0 a_s^\dagger v_s)^n \mathcal{G}_0 v_{s_1}^\dagger a_{s_1} \left| N_p, g \right\rangle. \tag{7.19}$$

Now, by using the commutation relations (7.3) and (7.4), one may easily establish the following intertwining property of bosonic operators [51]

$$a_s f(\mathcal{H}_0) = f(\mathcal{H}_0 - \omega_s) a_s, \tag{7.20}$$

$$f(\mathcal{H}_0) a_s^\dagger = a_s^\dagger f(\mathcal{H}_0 - \omega_s), \tag{7.21}$$

where f is some function admitting for the Maclaurin expansion $f(z) = \sum_{n=0}^{\infty} f_n z^n$. So, we see that

$$\begin{aligned} v_{s'}^\dagger a_{s'} \mathcal{G}_0(\epsilon) a_s^\dagger v_s =& v_s^\dagger \mathcal{G}_0(\epsilon - \omega_s) v_s \\ &+ a_{s'}^\dagger v_s^\dagger \mathcal{G}_0(\epsilon - \omega_{s'} - \omega_s) v_{s'} a_s, \end{aligned} \tag{7.22}$$

where in the last term of (7.22) the contraction of the indices s and s' is not assumed. By defining the self-energy operator $\Sigma^{(1)}$ and the effective potential energy operator $\mathcal{R}^{(1)}$ as

$$\Sigma^{(1)}(\epsilon) = v_s^\dagger \mathcal{G}_0(\epsilon - \omega_s) v_s, \quad \mathcal{R}^{(1)}(\epsilon) = a_{s'}^\dagger \mathcal{R}_{s',s}^{(1)}(\epsilon) a_s, \tag{7.23}$$

$$\mathcal{R}_{s',s}^{(1)}(\epsilon) = v_s^\dagger \mathcal{G}_0(\epsilon - \omega_{s'} - \omega_s) v_{s'}, \tag{7.24}$$

and resumming the perturbative series in (7.19), we conclude that

$$\left\langle N_p', g \left| \mathcal{T}^{(1)} \right| N_p, g \right\rangle$$
$$= \left\langle N_p', g \right| a_{s_1'}^\dagger v_{s_1'} \frac{1}{1 - \mathcal{G}^{(1)}\mathcal{R}^{(1)}} \mathcal{G}^{(1)} v_{s_1}^\dagger a_{s_1} \left| N_p, g \right\rangle, \tag{7.25}$$

where we have introduced the following Green's operator $(\mathcal{G}^{(1)})^{-1}(\epsilon) = \mathcal{G}_0^{-1}(\epsilon) - \Sigma^{(1)}(\epsilon)$. By defining the generating operator:

$$\mathcal{W}^{(1)} = \mathcal{R}^{(1)} + \mathcal{R}^{(1)}\mathcal{G}^{(1)}\mathcal{W}^{(1)}, \tag{7.26}$$

we arrive at the following result:

$$\begin{aligned}&\left\langle N_p', g \left| \mathcal{T}^{(1)} \right| N_p, g \right\rangle \\ &= \left\langle N_p', g \left| a_{s_1'}^\dagger v_{s_1'} \mathcal{G}^{(1)} v_{s_1}^\dagger a_{s_1} \right| N_p, g \right\rangle \\ &+ \left\langle N_p', g \left| a_{s_1'}^\dagger v_{s_1'} \mathcal{G}^{(1)} \mathcal{W}^{(1)} \mathcal{G}^{(1)} v_{s_1}^\dagger a_{s_1} \right| N_p, g \right\rangle .\end{aligned} \tag{7.27}$$

By analyzing the structure of $\mathcal{R}^{(1)}$, we conclude that $\mathcal{W}^{(1)}$ admits for the following series representation:

$$\mathcal{W}^{(1)} = \sum_{n=1}^{\infty} a_{s_1'}^\dagger ... a_{s_n'}^\dagger \mathcal{W}^{(1,n)}_{s_1'...s_n', s_1...s_n} a_{s_n} ... a_{s_1}, \tag{7.28}$$

where $\mathcal{W}^{(1,n)}$'s are the operator-valued functions, which depend only on $\epsilon - \mathcal{H}_0$ and $2n$ multi-indices $\{s_1', ..., s_n', s_1, ..., s_n\}$.

By inserting (7.28) in (7.26) and taking the projections onto the particle subspaces we arrive at the following hierarchy of integral equations:

$$W^{(1,1)}_{s_1',s_1}(\epsilon) = R^{(1)}_{s_1',s_1}(\epsilon) + R^{(1)}_{s_1',s}(\epsilon) G^{(1)}(\epsilon - \omega_s) W^{(1,1)}_{s,s_1}(\epsilon), \tag{7.29}$$

$$\vdots$$

$$\begin{aligned}W^{(1,n)}_{s_1'...s_n', s_1...s_n}(\epsilon) =& R^{(1)}_{s_1',s_1}\left(\epsilon - \sum_{l=2}^{n} \omega_{s_n'}\right) G^{(1)}\left(\epsilon - \omega_{s_1} - \sum_{l=2}^{n} \omega_{s_l'}\right) W^{(1,n-1)}_{s_2'...s_n', s_2...s_n}(\epsilon - \omega_{s_1}) \\ &+ R^{(1)}_{s_1',s}\left(\epsilon - \sum_{l=2}^{n} \omega_{s_n'}\right) G^{(1)}\left(\epsilon - \omega_s - \sum_{l=2}^{n} \omega_{s_l'}\right) \left[W^{(1,n)}_{s s_2'...s_n', s_1...s_n}(\epsilon) + ... + W^{(1,n)}_{s_2'...s_n' s, s_1...s_n}(\epsilon)\right]\end{aligned} \tag{7.30}$$

$$\vdots$$

Here, we have used regular letters W, G, R instead of calligraphic ones to indicate that these objects are not operators but are rather their projections on the photonic vacuum (note that $W^{(1,n)}$s are still acting as operators on the qubit space). The collection of the integral equations above may be conveniently represented diagrammatically, see Figure 7.1. Diagrammatic rules may be formulated as follows. To each dotted line associate the bare propagator $G_0(\epsilon)$. To each wavy line with incoming (outgoing) arrow associate the bare absorption $v^\dagger$ (emission v) vertex. Whenever two wavy lines are contracted together, one has to integrate over all momentum and sum over all channels. When a given wavy line passes over the propagator, its argument has to be shifted by the frequency carried by this line (which is a direct consequence of the intertwining property (7.20)).

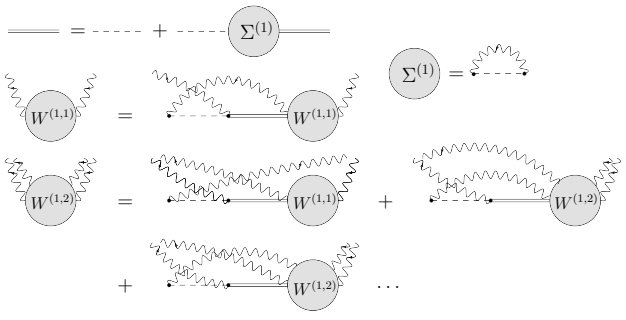

Figure 7.1: Hierarchy of integral equations governing effective multi-photon vertex functions in $N_q = 1$ waveguide QED. Here the $\Sigma^{(1)}$ bubble corresponds to the self-energy in a subspace of a single excitation used to the define the dressed Green's function (represented by a double line) from the bare Green's function (depicted by the dashed line). The $W^{(1,n)}$ bubbles (bubbles with $2n$-amputated legs) represent effective n-photon vertex functions describing effective interaction between n-photons induced by non-linearity. Bare absorption $v^\dagger$ and emission v vertices are represented by black dots with incoming and outgoing photon lines respectively. Diagrammatic rules are as stated in Sec. 7.2.3.

For example, the self-energy diagram in Figure 7.1 is translated as

$$\Sigma^{(1)}(\epsilon) = v_s^\dagger G_0(\epsilon - \omega_s) v_s. \tag{7.31}$$

Now having identified the equations defining the components of $\mathcal{W}^{(1)}$, we may express the transition operator as follows

$$\mathcal{T}^{(1)}(\epsilon) = \sum_{n=1}^{\infty} T^{(1,n)}_{s'_1 \ldots s'_n, s_1 \ldots s_n}(\epsilon) a^\dagger_{s'_1} \ldots a^\dagger_{s'_n} a_{s_n} \ldots a_{s_1}, \tag{7.32}$$

where we have defined the following functions

$$T^{(1,1)}_{s'_1, s_1}(\epsilon) = \left\langle g \middle| v_{s'_1} G^{(1)}(\epsilon) v^\dagger_{s_1} \middle| g \right\rangle, \tag{7.33}$$

$$T^{(1,n>1)}_{s'_1 \ldots s'_n, s_1 \ldots s_n}(\epsilon) = \left\langle g \middle| v_{s'_1} G^{(1)}\left(\epsilon - \sum_{l=2}^{n} \omega_{s'_l}\right) W^{(1,n-1)}_{s'_2 \ldots s'_n, s_2 \ldots s_n}(\epsilon) G^{(1)}\left(\epsilon - \sum_{l=2}^{n} \omega_{s_l}\right) v^\dagger_{s_1} \middle| g \right\rangle. \tag{7.34}$$

Note that we are working with the non-symmetrized forms of operators and perform the symmetrization only when doing actual calculations. Also note that the dependence of $\mathcal{T}^{(1,n)}_{s'_1 \ldots s'_n, s_1 \ldots s_n}$ on $\omega_s a^\dagger_s a_s$ may be omitted taking into account normal ordering, when S-matrix is going to be finally contracted with the initial state, all of the T-matrix components are going to be eventually projected onto the photonic vacuum and energies are going to be put on-shell. Using the above representation of the transition operator we immediately deduce that the scattering operator takes the following form:

$$\mathcal{S} = 1_{\mathscr{H}} - 2\pi i \sum_{n=1}^{\infty} T^{(n)}_{s'_1 \ldots s'_n, s_1 \ldots s_n} \left(\sum_{l=1}^{n} \omega_{s_l}\right) \delta\left(\sum_{l=1}^{n} \omega_{s'_l} - \sum_{l=1}^{n} \omega_{s_l}\right) a^\dagger_{s'_1} \ldots a^\dagger_{s'_n} a_{s_n} \ldots a_{s_1}. \tag{7.35}$$

Practically, when one contracts the S-matrix with the initial N_p-photon state, only first N_p terms in the above series contribute. It is, however, beneficial to represent the S-matrix in terms of the direct sum of N-body operators which act solely in the N-particle subspaces

$$\mathcal{S} = 1_{\mathscr{H}} \oplus \bigoplus_{n=1}^{\infty} \mathcal{S}_n, \tag{7.36}$$

where $\mathcal{S}_n$ may be written as

$$\mathcal{S}_n = S^{(n)}_{s'_1 \ldots s'_n, s_1 \ldots s_n} a^\dagger_{s'_1} \ldots a^\dagger_{s'_n} a_{s_n} \ldots a_{s_1}, \tag{7.37}$$

$$S^{(n)}_{s'_1 \ldots s'_n, s_1 \ldots s_n} = \frac{1}{n!} \prod_{l=1}^{n} \delta_{s'_l, s_l} - 2\pi i \sum_{m=1}^{n} \frac{1}{(n-m)!} T^{(n)}_{s'_1 \ldots s'_m, s_1 \ldots s_m} \left(\sum_{l=1}^{m} \omega_{s_l}\right) \delta\left(\sum_{l=1}^{n} \omega_{s'_l} - \sum_{l=1}^{n} \omega_{s_l}\right) \prod_{r=m+1}^{n} \delta_{s'_r, s_r}. \tag{7.38}$$

Note that the combinatorial prefactors $\frac{1}{(n-m)!}$, $m \in \{0, \ldots, n\}$ and additional δ functions $\delta_{s'_r, s_r}$ are chosen to take into account the excess number of $(n-m)!$ Wick contractions.

7.2.4 Generalized cluster decomposition

In this section, we would like to illustrate how the generalized cluster decomposition in waveguide QED, extensively studied in [[76]-[77]], naturally follows from the results of the previous section.

The cluster decomposition is a way of separating the elastic and inelastic contributions to the S-matrix. The elastic contribution physically corresponds to the scattering channel in which all photons scatter coherently, i.e. conserve their energy individually in the scattering process. On the other hand, the inelastic contribution corresponds to the incoherent scattering. Thereby the photons redistribute their initial energy between one another via effective photon-photon interaction which is mediated by their interaction with nonlinear scatterers (e.g., qubits). In contrast, in the case of a linear scatter (e.g., a cavity mode), the effective photon-photon interaction is not generated, and the n-photon S-matrix simply factors out into the product of n single-particle S-matrices.

The first step towards the cluster decomposition of the multi-photon S-matrices is the realization that the multi-photon vertex functions $W^{(1,n)}$ contain the disconnected components. These, in turn, arise from the projections of $R^{(1)}_{s',s}$ on the ground state of the scatterer thus resulting in the (quasi)elastic contributions

$\propto \delta(\epsilon - ...)$ to $W^{(1,n)}$'s. Not only the separation of these contributions is crucial for the cluster decomposition but is of evident importance for both numerical and analytical treatment of the integral equations (7.29), (7.30). It is the easiest to define the connected parts of the multi-photon vertex functions recursively. First, we observe that

$$\begin{aligned} R^{(1)}_{s',s}(\epsilon) =& v^\dagger_s G_0(\epsilon - \omega_{s'} - \omega_s) v_{s'} && (7.39)\\ =& -i\pi\delta(\epsilon - \omega_{s'} - \omega_s) v^\dagger_s v_{s'} && (7.40)\\ &+ v^\dagger_s P \frac{1}{\epsilon - \omega_{s'} - \omega_s} v_{s'}, && (7.41) \end{aligned}$$

where P stands for the Cauchy principle value. Which helps us to define the connected part of one-particle vertex function as

$$W^{(1,1,C)}_{s'_1,s_1}(\epsilon) = W^{(1,1)}_{s'_1,s_1}(\epsilon) + i\pi\delta(\epsilon - \omega_{s'_1} - \omega_{s_1}) v^\dagger_{s_1} v_{s'_1}. \tag{7.42}$$

By then analyzing the structure of the general equation in the hierarchy (7.30) and bearing in mind the equation satisfied by $W^{(1,1)}_{s'_1,s_1}(\epsilon)$ one may easily deduce the connected part of n-photon effective vertex function may be defined in the following manner

$$W^{(1,n,C)}_{s'_1 \dots s'_n, s_1 \dots s_n}(\epsilon) = W^{(1,n)}_{s'_1 \dots s'_n, s_1 \dots s_n}(\epsilon) - W^{(1,1)}_{s'_1,s_1}\left(\epsilon - \sum_{l=2}^{n} \omega_{s'_n}\right) G^{(1)}\left(\epsilon - \omega_{s_1} - \sum_{l=2}^{n} \omega_{s'_l}\right) W^{(1,n-1)}_{s'_2 \dots s'_n, s_2 \dots s_n}(\epsilon - \omega_{s_1}). \tag{7.43}$$

Now, with the help of the definition (7.42) one may immediately deduce the following decomposition of the two-body transition operator

$$\begin{aligned} & T^{(1,2)}_{s'_1 s'_2, s_1 s_2}(\omega_{s_1} + \omega_{s_2}) \\ & = -i\pi\delta(\omega_{s_1} - \omega_{s'_2}) T^{(1,1)}_{s'_1,s_1}(\omega_{s_1}) T^{(1,1)}_{s'_2,s_2}(\omega_{s_2}) \\ & + T^{(1,2,C)}_{s'_1 s'_2, s_1 s_2}(\omega_{s_1} + \omega_{s_2}), \end{aligned} \tag{7.44}$$

where $T^{(1,2,C)}$ is defined in precisely the same way as $T^{(1,2)}$ but with $W^{(1,1,C)}$ replacing $W^{(1,1)}$. By plugging the representation (7.44) into the definition of the two-photon S-matrix (7.38) we immediately arrive at the following cluster decomposition principle:

$$\begin{aligned} \mathcal{S}_2 = \Bigg[& \frac{1}{2} S^{(1)}_{s'_1,s_1} S^{(1)}_{s'_2,s_2} - 2\pi i T^{(1,2,C)}_{s'_1 s'_2, s_1 s_2}(\omega_{s_1} + \omega_{s_2}) \\ & \times \delta(\omega_{s'_1} + \omega_{s'_2} - \omega_{s_1} - \omega_{s_2}) \Bigg] a^\dagger_{s'_1} a^\dagger_{s'_2} a_{s_2} a_{s_1}. \end{aligned} \tag{7.45}$$

The physical meaning of the above expression is rather clear. The first term, being a product of one-particle S-matrices, describes the coherent scattering of two particles, i.e. a scattering process in which there is no effective interactions between the photons. The second term, on the other hand, is completely connected and describes the incoherent scattering of photons in which the particles redistribute their initial energy by interaction. A slightly more involved, but otherwise completely analogous, calculation may be done in the three-photon sector. As a result, one arrives at the following cluster decomposition of the three-body S-matrix:

$$\begin{aligned} \mathcal{S}_3 = \Bigg[& \frac{1}{6} S^{(1)}_{s'_1,s_1} S^{(1)}_{s'_2,s_2} S^{(1)}_{s'_3,s_3} - 2\pi i T^{(1,2,C)}_{s'_1 s'_2, s_1 s_2}(\omega_{s_1} + \omega_{s_2}) \\ & \times \delta(\omega_{s'_1} + \omega_{s'_2} - \omega_{s_1} - \omega_{s_2}) S^{(1)}_{s'_3,s_3} \\ & - 2\pi i T^{(1,3,C)}_{s'_1 s'_2 s'_3, s_1 s_2 s_3}(\omega_{s_1} + \omega_{s_2} + \omega_{s_3}) \\ & \times \delta(\omega_{s'_1} + \omega_{s'_2} + \omega_{s'_3} - \omega_{s_1} - \omega_{s_2} - \omega_{s_3}) \Bigg] \\ & \times a^\dagger_{s'_1} a^\dagger_{s'_2} a^\dagger_{s'_3} a_{s_3} a_{s_2} a_{s_1}, \end{aligned} \tag{7.46}$$

where the connected part of the three-photon T-matrix may be found in the Appendix 7.5.1.

7.2.5 Closed form solution in the Markovian limit

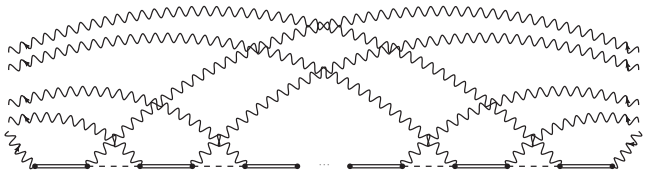

Figure 7.2: Exact diagrammatic representation of the n-particle T-matrix in the Markovian limit. The above diagrams also correspond to the non-crossing approximation discussed in section 7.2.6. As opposed to the exact n-photon T-matrix parameterized by the $n-1$-particle effective vertex function resuming an infinite number of emission and absorption processes in both direct and exchange channels, this approximation replaces the vertex by a sequence of $n-2$ and $n-1$ ($n \geq 2$) alternating excitations and deexcitations of the emitter.

Let us now consider the single-qubit scattering problem in the Markovian limit. Validity of Markovian approximation demands a number of assumptions: linear dispersion relation in all of the channels $\omega_\mu(k) = \omega_{0\mu} + v_\mu k$, broadband limit $B_\mu = \mathbb{R}, \forall \mu \in \{1, ..., N_c\}$ and local couplings (i.e. independent of frequency) $g_\mu(k) = \sqrt{\gamma_\mu/\pi}$. Within the above assumptions, the self-energy diagram reads as $\Sigma^{(1)}(\epsilon) = -i \sum_{\mu=1}^{N_c} \gamma_\mu / v_\mu \, |1\rangle\langle 1|$, which is independent of ϵ (here we have introduced the projector on the qubit's excited state $|1\rangle\langle 1| = \frac{1+\sigma_3}{2}$). By causality, all of the W functions are analytic in momentum (energy) variables in the lower (upper) half of the complex plane. By exploiting this analyticity along with the momentum independence of both coupling constants and self-energy, we can close all of the integration contours in the lower half of the complex momentum plane to render all of the integrals zero, thus promoting the integral equations into algebraic ones. As a result, we recover the solution obtained in [[51]]. Diagrammatically the above solution is equivalent to the so-called non-crossing approximation (which becomes exact in the Markovian limit) and it is represented in Figure 7.2.

7.2.6 Approximation strategies

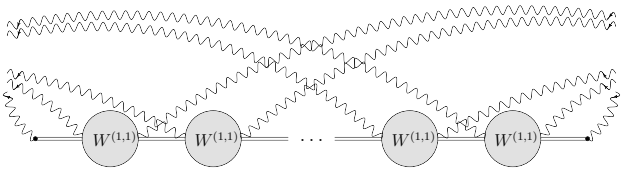

Figure 7.3: Diagrammatic representation of n-particle transition matrix within the weak correlation approximation. Here two-particle bubbles correspond to a single-photon effective vertex functions $W^{(1,1)}$. Opposite to the quasi-Markovian approximation, this approximation resumms exactly all of the single particle processes, ignoring all the connected diagrams corresponding to multiple-particle scattering.

Although it is possible to write an entire hierarchy of exact equations for the multi-photon vertex functions, which in turn parametrize the exact S-matrix, their analytical solution is in general only possible in the Markovian limit. To make some progress in solving the scattering problem, one has to resort to some kind of approximation routine. In this section we propose a couple of physically motivated resummation approaches, allowing one to avoid (or partially avoid) the solution of the exact integral equations.

The most basic approximation, which is accurate in the regime $\gamma\tau \lesssim 1$, where τ is a typical time delay in the system due to photons' propagation between two nearby scatterers, and γ is a typical decay rate of scatterers, is the so called quasi-Markovian approximation. While in the quantum master equation approach it has a long tradition (see, e.g., [22, 23]), it has been recently realised [51, 53] that in the diagrammatic approach it is mathematically equivalent to picking only non-crossing diagrams shown in Fig. 7.2 and thereby fully neglecting vertex corrections. To give a physical explanation of this equivalence, we view photons propagating in the waveguide as an effective reservoir. It is intuitively clear that a fast decay of time correlations between these photons is an essential feature of the Markovian regime (we add here the prefix quasi in order to indicate that the field values at positions of different scatterers can still differ from each other by a phase factor). On the other hand, these time correlations result from correlated virtual processes of emission and absorption of different photons at different scatterers, which are mathematically encoded in the vertex corrections. Thus, the neglect of vertex corrections is equivalent to making the quasi-Markovian approximation. It is also worth noting

that this approximation for a single-photon scattering matrix coincides with its exact expression, since in the absence of other photons the correlations in questions are not generated.

Below we give a step-by-step prescription how to implement the quasi-Markovian approximation in our diagrammatic approach. The exact n-photon transition matrices are represented by a $n-1$-particle effective vertex function in between two dressed Green's functions followed by emission/absorption vertices (see equation (7.34)). In this approximation, the exact multi-photon vertex functions are simply replaced with a sequence of $n-1$ bare and $n-2$ dressed Green's functions interspersed with $2n-2$ emission and absorption vertices. In particular, in the $n=2$ case we get $W^{(1,1)}_{s_1',s_1}(\epsilon) \to v^\dagger_{s_1} G_0(\epsilon-\omega_{s_1'}-\omega_{s_1}) v_{s_1'}$. In the $n=3$ case we obtain $W^{(1,2)}_{s_1's_2',s_1s_2}(\epsilon) \to v^\dagger_{s_1} G_0(\epsilon-\omega_{s_1}-\omega_{s_1'}-\omega_{s_2'}) v_{s_1'} G^{(1)}(\epsilon-\omega_{s_1}-\omega_{s_2'}) v^\dagger_{s_2} G_0(\epsilon-\omega_{s_1}-\omega_{s_2}-\omega_{s_2'}) v_{s_2'}$, and so on. In this approximation, all of the non-trivial momentum dependence of the S-matrix, comes entirely from the frequency dependence of the self-energy diagram. Note that the single-photon T-matrix is completely determined by the dressed propagator $G^{(1)}(\epsilon)$ (see equation (7.33)). This observation explicitly confirms the statement that the quasi-Markovian approximation becomes exact for a single propagating photon.

The second approximation routine, which is more accurate than the quasi-Markovian one for $\gamma\tau \gtrsim 1$, makes a partial account of the vertex corrections. In particular, this approximation is based on the resummation of the full single-photon vertex functions $W^{(1,1)}_{s',s}(\epsilon)$. Diagrammatically, this approximation amounts to the replacement of the dotted lines in Figure 7.2 by the full single-particle bubbles, the resulting n-photon T-matrix is shown in Figure 7.3. This approximation corresponds to resummation of all of the direct interaction diagrams (comping entirely from the single particle sector), completely ignoring the exchange processes (encompassed by the connected parts of many-particle vertices). In order to clarify the matters, let us consider an integral equation governing the two-particle effective vertex shown in Figure 7.1. Using the diagrammatic rules we deduce

$$\begin{aligned}
&W^{(1,2)}_{s_1's_2',s_1,s_2}(\epsilon) \\
&= R^{(1)}_{s_1',s_1}(\epsilon-\omega_{s_2'}) G^{(1)}(\epsilon-\omega_{s_1}-\omega_{s_2'}) W^{(1,1)}_{s_2',s_2}(\epsilon-\omega_1) \\
&+ R^{(1)}_{s_1,s}(\epsilon-\omega_{s_2'}) G^{(1)}(\epsilon-\omega_{s}-\omega_{s_2'}) W^{(1,2)}_{ss_2',s_1s_2} \\
&+ R^{(1)}_{s_1,s}(\epsilon-\omega_{s_2'}) G^{(1)}(\epsilon-\omega_{s}-\omega_{s_2'}) W^{(1,2)}_{s_2's,s_1s_2}.
\end{aligned} \tag{7.47}$$

Note that the last line above corresponds to the exchange interaction between that particles (see also Figure 7.1). If we ignore the the last term completely and take into account the equation satisfied by $W^{(1,1)}$ it is easy to show that

$$\begin{aligned}
&W^{(1,2)}_{s_1's_2',s_1,s_2}(\epsilon) \\
&= W^{(1,1)}_{s_1',s_1}(\epsilon-\omega_{s_2'}) G^{(1)}(\epsilon-\omega_{s_1}-\omega_{s_2'}) W^{(1,1)}_{s_2',s_2}(\epsilon-\omega_1)
\end{aligned} \tag{7.48}$$

is an exact solution of (7.47).

We expect this approximation to get worse as one increases the number of photons in the system since this approximation ignores larger and larger fraction of diagrams with the increase in the number of particles involved in a scattering process. This approximation is beneficial since an integral equation for $W^{(1,1)}$ may be frequently solved analytically by means of the method developed in the supplementary material of [[71]]. Due to the non-trivial momentum dependence of $W^{(1,1)}$, we expect this approximation to be better than a quasi-Markovian one. In what follows we refer to this approximation as to the weak correlation one. Note that as the quasi-Markovian approximation is exact in the single-particle sector, the weak correlation approximation is exact in the two-particle sector, thus in order to test its validity, one has to consider at least a three-photon scattering problem.

7.2.7 Systems with more than one qubit

In this section, we would like to present certain generalizations of the theory developed in Section 7.2.3. Specifically, we would like to demonstrate how the above-presented formalism may be extended to the systems with a larger number of qubits. In particular, we are going to focus our attention on the systems with two and three emitters. By deriving the equations governing two and three-photon scattering matrices in two and three-qubit waveguide QED systems respectively we present the most general two and three-particle equations, holding independently of the number of qubits (see the discussion in Section 7.2.2).

$N_q = 2$ waveguide QED

First, we would like to focus on the case of two emitters coupled to a waveguide since the generalization of the single-qubit results is the most apparent in this case. The starting point in the analysis are equations (7.17) and (7.18). As opposed to the single-emitter case, now, clearly, both diagonal terms $v^\dagger_{s'} a_{s'} \mathcal{G}_0 a^\dagger_s v_s$ and

Figure 7.4: Diagrammatic representation of the replacement required to obtain $R^{(2)}_{s',s}$ from $R^{(1)}_{s',s}$. Note that the extra contribution to the effective potential energy vertex $R^{(2)}$ in two-qubit systems is not single-particle connected, i.e. it is possible to cut the intermediate propagator such that the diagram falls into two distinct pieces. This very fact makes the splitting (7.56)-(7.59) into reducible and irreducible contributions possible.

$a^\dagger_{s'} v_{s'} \mathcal{G}_0 v^\dagger_s a_s$ contribute to the geometric series for the transition operator. Non-diagonal ones still give zero, since they both annihilate the state $v^\dagger |g\rangle$. By resumming the series and introducing the following set of objects

$$\mathcal{R}^{(2)} = a^\dagger_{s'_1} \mathcal{R}^{(2)}_{s'_1,s_1} a_{s_1}, \tag{7.49}$$

$$\mathcal{R}^{(2)}_{s'_1,s_1} = \mathcal{R}^{(1)}_{s'_1,s_1} + v_{s'_1} \mathcal{G}_0 v^\dagger_{s_1}, \tag{7.50}$$

$$\mathcal{W}^{(2)} = \mathcal{R}^{(2)} + \mathcal{R}^{(2)} \mathcal{G}^{(1)} \mathcal{W}^{(2)}, \tag{7.51}$$

we render the matrix elements of the transition operator in the following form

$$\begin{aligned} &\left\langle N'_p, g \middle| \mathcal{T}^{(2)} \middle| N_p, g \right\rangle \\ &= \left\langle N'_p, g \middle| a^\dagger_{s'_1} v_{s'_1} \mathcal{G}^{(1)} v^\dagger_{s_1} a_{s_1} \middle| N_p, g \right\rangle \\ &+ \left\langle N'_p, g \middle| a^\dagger_{s'_1} v_{s'_1} \mathcal{G}^{(1)} \mathcal{W}^{(2)} \mathcal{G}^{(1)} v^\dagger_{s_1} a_{s_1} \middle| N_p, g \right\rangle . \end{aligned} \tag{7.52}$$

Since the lowest term in the expansion of $\mathcal{W}^{(2)}$ is again a single-photon operator

$$\mathcal{W}^{(2)} = \sum_{n=1}^{\infty} a^\dagger_{s'_1} ... a^\dagger_{s'_n} \mathcal{W}^{(2,n)}_{s'_1 ... s'_n, s_1 ... s_n} a_{s_n} ... a_{s_1}, \tag{7.53}$$

we see that the hierarchy of equations satisfied by the two-photon vertex functions is precisely the same as (7.29)-(7.30) with $R^{(1)}$ being replaced by $R^{(2)}$ (see Figure 7.4).

In order to understand the difference between the single-qubit and the two-qubit theories, let us have a closer look at the equation defining $\mathcal{W}^{(2)}$

$$\begin{aligned} \mathcal{W}^{(2)} =& \mathcal{R}^{(1)} + a^\dagger_{s'_1} v_{s'_1} \mathcal{G}_0 v^\dagger_{s_1} a_{s_1} + \mathcal{R}^{(1)} \mathcal{G}^{(1)} \mathcal{W}^{(2)} \\ &+ a^\dagger_{s'_1} v_{s'_1} \mathcal{G}_0 v^\dagger_{s_1} a_{s_1} \mathcal{G}^{(1)} \mathcal{W}^{(2)}. \end{aligned} \tag{7.54}$$

Now let us perform the following separation $\mathcal{W}^{(2)} = \mathcal{W}^{(2,i)} + \mathcal{W}^{(2,r)}$, where the superscripts i and r stand for the irreducible and reducible contributions respectively, and $\mathcal{W}^{(2,i)}$ is chosen to satisfy the following equation (7.26). This leads one to the following equation satisfied by the reducible part

$$\begin{aligned} \mathcal{W}^{(2,r)} =& a^\dagger_{s'_1} v_{s'_1} \mathcal{G}_0 v^\dagger_{s_1} a_{s_1} + \mathcal{R}^{(1)} \mathcal{G}^{(1)} \mathcal{W}^{(2,r)} \\ &+ a^\dagger_{s'_1} v_{s'_1} \mathcal{G}_0 v^\dagger_{s_1} a_{s_1} \mathcal{G}^{(1)} \mathcal{W}^{(2,i)} \\ &+ a^\dagger_{s'_1} v_{s'_1} \mathcal{G}_0 v^\dagger_{s_1} a_{s_1} \mathcal{G}^{(1)} \mathcal{W}^{(2,r)}. \end{aligned} \tag{7.55}$$

The solution of equation (7.55) may then conveniently parametrized as $W^{(2,r)}(\epsilon) = \mathcal{V}^{(2)}(\epsilon) \mathcal{G}^{(2)}(\epsilon) \overline{\mathcal{V}}^{(2)}(\epsilon)$, where

$$\mathcal{G}^{(2)} = \mathcal{G}_0 + \mathcal{G}_0 \Sigma^{(2)} \mathcal{G}^{(2)}, \tag{7.56}$$

$$\Sigma^{(2)} = a_s v^\dagger_s \mathcal{G}^{(1)} v_{s'} a^\dagger_{s'} + a_s v^\dagger_s \mathcal{G}^{(1)} \mathcal{W}^{(2,i)} \mathcal{G}^{(1)} v_{s'} a^\dagger_{s'}, \tag{7.57}$$

$$\overline{\mathcal{V}}^{(2)} = v^\dagger_s a_s + v^\dagger_s a_s \mathcal{G} \mathcal{W}^{(2,i)} =: \sum_{n=1}^{\infty} \overline{V}^{(2,n)}_{s_1 ... s_n} a_{s_1} ... a_{s_n}, \tag{7.58}$$

$$\mathcal{V}^{(2)} = a^\dagger_s v_s + \mathcal{W}^{(2,i)} \mathcal{G} v_s a^\dagger_s =: \sum_{n=1}^{\infty} V^{(2,n)}_{s_1 ... s_n} a^\dagger_{s_1} ... a^\dagger_{s_n}. \tag{7.59}$$

The meaning of the above-defined objects is as follows. $\mathcal{G}^{(2)}(\epsilon)$ may be thought of as a Green's operator in the two-qubit excitation subspace since in practice, it is always projected there. $\Sigma^{(2)}(\epsilon)$ in its turn may be thought of as a self-energy operator in the two-qubit excitation subspace. $\mathcal{V}(\epsilon)$ and $\overline{\mathcal{V}}(\epsilon)$ may be understood as the renormalized absorption and emission vertex operators.

As it was anticipated above, the equations governing a two-photon scattering on a pair of qubits hold in the case of a two-photon scattering for a general N_q system. Bearing this in mind, in Figure 7.5 we present the system of exact integral equations governing the general two-photon scattering problem in waveguide QED (i.e. equations defining $W^{(2,1)}$). These equations were first obtained in [[71]] in relation with the two-photon scattering problem on two distant qubits.

$N_q = 3$ waveguide QED

Let us finally dedicate our attention to three-qubit waveguide QED systems. Due to the enormous increase in the computational complexity, we restrict ourselves to the first non-trivial subspace within such a setup - a three-excitation subspace. As before, the starting point of the analysis is the equation (7.17). No doubt, both of the "diagonal" terms $\sim v^\dagger v$ and $\sim vv^\dagger$ give a non-zero contribution to the transition operator as it was the case in the previous section, however, one can clearly see that now the "off-diagonal" terms (vv, $v^\dagger v^\dagger$) have to be also taken into account. By defining the following operators

$$\mathcal{D}_+ = a^\dagger_{s'} v_{s'} \mathcal{G}_0 a^\dagger_s v_s, \quad \mathcal{D}_- = v^\dagger_{s'} a_{s'} \mathcal{G}_0 v^\dagger_s a_s, \tag{7.60}$$

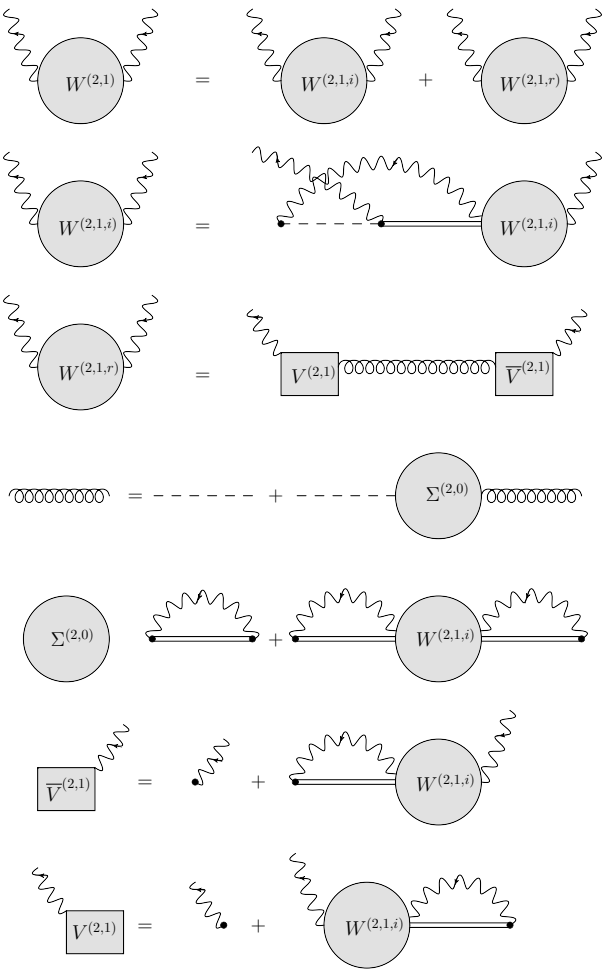

Figure 7.5: Equations corresponding to the general two-photon scattering problem. Equation in the first line describes the splitting of the effective single-particle vertex function $W^{(2,1)}$ in the generic two-photon scattering problem into its reducible $W^{(2,1,r)}$ and irreducible parts $W^{(2,1,i)}$. The irreducible part is generated from the fundamental process of the single-qubit waveguide QED $R^{(1)}$ (as shown in the second line) and thus satisfies the same integral equation as $W^{(1,1)}$. The reducible part, steming from non-single-particle connectedness of the additional contribution to $R^{(2)}$ (see Figure 7.4), is parametrized by the dressed Green's function $G^{(2,0)}$ in two excitation subspace (shown as the curly line) as well as renormalized emission and absorption vertices (indicated by rectangles). As one can see the entire system of equations blows down to the solution of the equation defining the irreducible part of the vertex function, since its knowledge is sufficient to completely determine both the renormalized vertices $V^{(2,1)}$, $\overline{V}^{(2,1)}$ as well as the self energy $\Sigma^{(2,0)}$ in the two excitation subspace.

bearing in mind the rotating wave approximation, and resuming the series (7.17) to incorporate the diagonal terms and again making use of RWA, in the realm of $N_q = 3$ waveguide QED, we obtain

$$\begin{aligned}
&\left\langle N_p', g \middle| \mathcal{T}^{(3)} \middle| N_p, g \right\rangle \\
&= \left\langle N_p', g \middle| a_{s_1'}^\dagger v_{s_1'} \frac{1}{(\mathcal{G}^{(1)})^{-1} - \mathcal{R}^{(3)}} v_{s_1}^\dagger a_{s_1} \middle| N_p, g \right\rangle, \qquad (7.61)\\
&\mathcal{R}^{(3)} = \mathcal{R}^{(2)} + \mathcal{D}, \qquad (7.62)\\
&\mathcal{D} = \mathcal{D}_+ \frac{1}{(\mathcal{G}^{(1)})^{-1} - \mathcal{R}^{(2)}} \mathcal{D}_- \\
&= \mathcal{R}^{(2)} + \mathcal{D}_+ \mathcal{G}^{(1)} \mathcal{D}_- + \mathcal{D}_+ \mathcal{G}^{(1)} \mathcal{W}^{(2)} \mathcal{G}^{(1)} \mathcal{D}_-. \qquad (7.63)
\end{aligned}$$

As usual, we define the $\mathcal{W}^{(3)}$ operator according to

$$\mathcal{W}^{(3)} = \mathcal{D} + \mathcal{D}(\mathcal{G}^{(1)} + \mathcal{G}^{(1)}\mathcal{W}^{(2)}\mathcal{G}^{(1)})\mathcal{W}^{(3)}. \tag{7.64}$$

Which brings the transition operator to the following form

$$\left\langle N'_p, g \middle| \mathcal{T}^{(3)} \middle| N_p, g \right\rangle = \left\langle N'_p, g \middle| \mathcal{T}^{(2)} + a^\dagger_{s'_1} v_{s'_1} \mathcal{G}^{(1)}(1 + \mathcal{W}^{(2)}\mathcal{G}^{(1)})\mathcal{W}^{(3)}(\mathcal{G}^{(1)}\mathcal{W}^{(2)} + 1)\mathcal{G}^{(1)} v^\dagger_{s_1} a_{s_1} \middle| N_p, g \right\rangle. \tag{7.65}$$

Upon the projection, onto the three-photon subspace, we obtain the following elegant set of equations governing the generic (see Section 7.2.2) three-particle T-matrix (see Appendix 7.5.3 for the detailed derivation)

$$\begin{aligned}
T^{(3,3)}_{s'_1 s'_2 s'_3, s_1 s_2 s_3}(\epsilon) =& \left\langle g \middle| v_{s'_1} G^{(1)}(\epsilon - \omega_{s'_2} - \omega_{s'_3})[W^{(2,2)}_{s'_2 s'_3, s_2 s_3}(\epsilon) + V^{(3,2)}_{s'_2 s'_3}(\epsilon) G^{(3,0)}(\epsilon) \overline{V}^{(3,2)}_{s_2 s_3}(\epsilon)] G^{(1)}(\epsilon - \omega_{s_2} - \omega_{s_3}) v^\dagger_{s_1} \middle| g \right\rangle \\
=:& \left\langle g \middle| v_{s'_1} G^{(1)}(\epsilon - \omega_{s'_2} - \omega_{s'_3})[W^{(2,2)}_{s'_2 s'_3, s_2 s_3}(\epsilon) + W^{(3,2)}_{s'_2 s'_3, s_2 s_3}(\epsilon)] G^{(1)}(\epsilon - \omega_{s_2} - \omega_{s_3}) v^\dagger_{s_1} \middle| g \right\rangle, \qquad (7.66) \\
G^{(3,0)}(\epsilon) =& G^{(1)}(\epsilon) + G^{(1)}(\epsilon)\Sigma^{(3,0)}(\epsilon) G^{(3,0)}(\epsilon), \qquad (7.67) \\
\Sigma^{(3,0)}(\epsilon) =& (v^\dagger_s G_0(\epsilon - \omega_s) v^\dagger_{s'} + v^\dagger_{s'} G_0(\epsilon - \omega_{s'}) v^\dagger_s) G^{(1)}(\epsilon - \omega_s - \omega_{s'}) V^{(3,2)}_{ss'}(\epsilon) \qquad (7.68) \\
\equiv& \overline{V}^{(3,2)}_{ss'}(\epsilon) G^{(1)}(\epsilon - \omega_s - \omega_{s'})(v_{s'} G_0(\epsilon - \omega_s) v_s + v_s G_0(\epsilon - \omega_{s'}) v_{s'}), \qquad (7.69)
\end{aligned}$$

$$\begin{aligned}
\overline{V}^{(3,2)}_{s_1 s_2}(\epsilon) =& v^\dagger_{s_1} G^{(2,0)}(\epsilon) \overline{V}^{(2,1)}_{s_2}(\epsilon) + \overline{V}^{(3,2)}_{ss_1}(\epsilon) G^{(1)}(\epsilon - \omega_s) W^{(2,1)}_{s,s_2}(\epsilon), \qquad (7.70) \\
V^{(3,2)}_{s'_1 s'_2}(\epsilon) =& V^{(2,1)}_{s'_1}(\epsilon) G^{(2,0)}(\epsilon) v^\dagger_{s'_2} + W^{(2,1)}_{s'_1, s}(\epsilon) G^{(1)}(\epsilon - \omega_s) V^{(3,2)}_{s'_2 s}(\epsilon). \qquad (7.71)
\end{aligned}$$

Here $G^{(2,0)}(\epsilon)$ is the projection of (7.56) onto the photon vacuum state. As usual, the above equation may be compactly represented diagrammatically as shown in Figure 7.6.

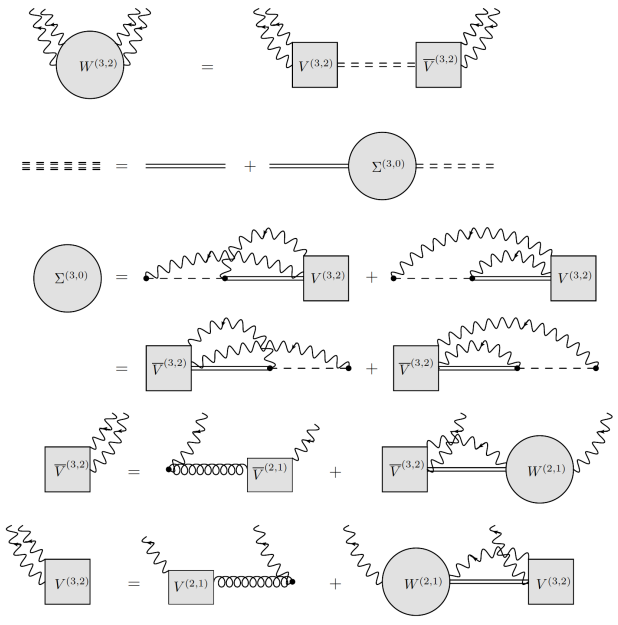

Figure 7.6: Equations corresponding to the general three-photon scattering problem. Here the first line defines the effective two-body vertex function $W^{(3,2)}$ in terms of the dressed Green's function in three excitation subspace shown as a double dashed line as well as effective two-photon absorption/emission vertices depicted by square boxes with a pair of incoming/outgoing amputated photon legs (note that these vertices correspond to the absorption/emission of photon pairs by a system as a whole). As it is shown in the last five lines the effective two-photon emission/absorption vertices as well as the self-energy bubble defining the Green's function in the three-excitation subspace satisfy a closed hierarchy of self-consistent equations, the validity of which is directly proven in Appendix 7.5.3. Curly lines as well as the rectangular boxes with single amputated photon lines are precisely defined in Figure 7.5.

7.3 Application: a giant acoustic atom

In this section, we would like to consider a practical application of the above-developed theory. In order to showcase our method in full glory, we would like to focus on the non-Markovian scattering setup - a giant acoustic atom, extensively studied theoretically and experimentally in [[19], [59], [78, 79, 80, 60, 81]] (see also [[82]] for a detailed review).

7.3.1 Model and conventions

A giant acoustic atom may be defined as a two-level system coupled to an acoustical waveguide, in which the radiation is carried by the surface acoustic waves (SAW), at two distant points $x = \pm R/2$. The Hamiltonian of such a system may be written as $\mathcal{H} = \mathcal{H}_, + \mathcal{V}$

$$\mathcal{H}_0 = \Omega\sigma_+\sigma_- - iv\sum_{\mu=1,2}\int dx c_\mu b^\dagger_\mu(x)\partial_x b_\mu(x), \tag{7.72}$$

$$\mathcal{V} = \sum_{\mu=1,2}(\sqrt{\Gamma_1}b^\dagger_\mu(-R/2) + \sqrt{\Gamma_2}b^\dagger_\mu(R/2))\sigma_- + \text{h.c.} \tag{7.73}$$

Here $b_\mu(x), b^\dagger_\mu(x)$ are the position space field operators of phonons, the index μ distinguishes beetween the right $\mu = 1$ and left $\mu = 2$ mooving fields, and $c_\mu = (-1)^{\mu-1}$. Note that we have made use of the common assumption of the mode dispersion being linear in the vicinity of the relevant energy scale $\sim \Omega$ and the the bandwidth be infinite. Defining the Fourier transformation as

$$b_\mu(x) = \frac{1}{\sqrt{2\pi}}\int dk e^{ic_\mu kx}a_\mu(k), \tag{7.74}$$

we bring the Hamiltonian in to the form (7.1), (7.2):

$$\mathcal{H}_0 = \Omega\sigma_+\sigma_- + v\sum_{\mu=1,2}\int dk k a^\dagger_\mu(k)a_\mu(k), \tag{7.75}$$

$$\mathcal{V} = \sum_{\mu=1,2}\int dk g_\mu(k)a_\mu(k)\sigma_- + \text{h.c.}, \tag{7.76}$$

$$g_\mu(k) = \sqrt{\frac{\Gamma_1}{2\pi}}e^{-ic_\mu kR/2} + \sqrt{\frac{\Gamma_1}{2\pi}}e^{ic_\mu kR/2}. \tag{7.77}$$

In the following subsections we are going to study the scattering of a coherent pulse in the form of a wavepacket centered around the frequency vk_0 (see Section 7.3.2), for that sake it is convenient to perform the following time-dependant gauge transformation:

$$\mathcal{U}(t) = \exp\left(-ivk_0\left[\int dk a^\dagger_\mu(k)a_\mu(k) + \sigma_+\sigma_-\right]t\right). \tag{7.78}$$

The Hamiltonian transforms as $\mathcal{H} \to \tilde{\mathcal{H}} = \mathcal{U}^\dagger(t)\mathcal{H}\mathcal{U}(t) - i\mathcal{U}^\dagger(t)\frac{d\mathcal{U}(t)}{dt} =: \tilde{\mathcal{H}}_0 + \tilde{\mathcal{V}}$, resulting in final form of the Hamiltonian we are going to work with:

$$\tilde{\mathcal{H}}_0 = -\Delta\sigma_+\sigma_- + v\sum_{\mu=1,2}\int dk k\tilde{a}^\dagger_\mu(k)\tilde{a}_\mu(k), \tag{7.79}$$

$$\tilde{\mathcal{V}} = \sum_{\mu=1,2}\int dk\tilde{g}_\mu(k)\tilde{a}_\mu(k)\sigma_- + \text{h.c.}, \tag{7.80}$$

$$\tilde{g}_\mu(k) = \sqrt{\frac{\Gamma_1}{2\pi}}e^{-ic_\mu(k+k_0)R/2} + \sqrt{\frac{\Gamma_1}{2\pi}}e^{ic_\mu(k+k_0)R/2}, \tag{7.81}$$

$$\tilde{a}_\mu(k) = a_\mu(k+k_0), \quad \Delta = \omega_0 - \Omega, \quad \omega_0 = vk_0. \tag{7.82}$$

In the following we adopt the system of units such that $v = 1$, for simplicity we will also assume $\Gamma_1 = \Gamma_2 = \gamma/2$. Furthermore, we shall also drop the tilde symbols out of operators for notational convenience.

7.3.2 Problem formulation

In order to formulate the scattering problem, we define the following wave-packet operators

$$A_\mu^\dagger = \int dk \varphi_L(k) a_\mu^\dagger(k), \tag{7.83}$$

where $\varphi_L(k) = \sqrt{\frac{2}{\pi L}} \frac{\sin(kL/2)}{k}$ is the Fourier transform of the rectangular pulse of length L, with the property $\varphi_L(k) \sim \sqrt{\frac{2\pi}{L}}\delta(k)$, $L \to \infty$ (obviously, it is possible to choose any other nascent δ-function for $\varphi_L(k)$). Note that since we are working in the frame of reference rotating with frequency k_0, peaking of $\varphi_L(k)$ at $k = 0$ corresponds to a pulse centered at $k = k_0$ in the original one. Note that throughout this section we focus on the zero detuning setup $\Delta = 0$, i.e. the initial k_0 is chosen to be equal to Ω. The effect of non-zero detuning of atom from radiation is studied in Appendix 7.5.4. Definition of these wave-packet operators is crucial since the eigenstates of the bare Hamiltonian $\mathcal{H}_0$ are not normalizable. Hence, in order to avoid the ascent of the undefinable quantities such as $\delta(0), (\delta(0))^2, ...$ coming from the elastic clusters of the S-matrix in the calculation of the observables, one has to work with the normalizable states and take the plane-wave limit $L \to \infty$ at the very end. Having defined the Fock creation operators $A_\mu^\dagger$, we can define the coherent state as a displaced vacuum

$$|\alpha\rangle_\mu = e^{-|\alpha|^2/2} e^{\alpha A_\mu^\dagger} |\Omega\rangle = e^{-|\alpha|^2/2} \sum_{n=0}^{\infty} \frac{\alpha^n}{\sqrt{n!}} \left|\Phi_\mu^{(n)}\right\rangle, \tag{7.84}$$

where $\alpha \in \mathbb{C}$ is the so-called coherence parameter, defined such that $|\alpha|^2$ is the average photon number (power), and the normalized n-particle Fock states $\left|\Phi_\mu^{(n)}\right\rangle$ were defined according to

$$\left|\Phi_\mu^{(n)}\right\rangle = \frac{1}{\sqrt{n!}} \left(A_\mu^\dagger\right)^n |\Omega\rangle . \tag{7.85}$$

In what follows, we assume that $|\alpha| \ll 1$ in such a way that the terms of order $|\alpha|^4$ are negligible

$$\begin{aligned} |\alpha\rangle_\mu \approx & e^{-|\alpha|^2/2} \left(|\Omega\rangle + \frac{\alpha}{\sqrt{1!}} \left|\Phi_\mu^{(1)}\right\rangle + \frac{\alpha^2}{\sqrt{2!}} \left|\Phi_\mu^{(2)}\right\rangle \right. \\ & \left. + \frac{\alpha^3}{\sqrt{3!}} \left|\Phi_\mu^{(3)}\right\rangle + \mathcal{O}(|\alpha|^4) \right) \equiv |\alpha\rangle_\mu^{(3)} . \end{aligned} \tag{7.86}$$

The factor $e^{-|\alpha|^2/2}$ has to be retained until various overlaps of states are calculated, to ensure the normalization of both the initial and final states as well as the power conservation (here the normalization is again assumed in the power perturbative regime, that is up to order $\mathcal{O}(|\alpha|^8)$). With this in hands, we formulate the scattering problem as follows. We assume that the initial state of the system is given by $|\psi_i\rangle = |\alpha\rangle_1^{(3)} \otimes |0\rangle$, that is a leftwards-propagating weakly coherent pulse $|\alpha\rangle_1^{(3)}$ is incident on a two-level system which is initially in its ground state $|0\rangle$. According to the theory developed above, the final state of the systems has the following form

$$\begin{aligned} |\psi_f\rangle = & e^{-|\alpha|^2/2} \left(|\Omega\rangle + \frac{\alpha}{\sqrt{1!}} \mathcal{S}_1 \left|\Phi_1^{(1)}\right\rangle \right. \\ & \left. + \frac{\alpha^2}{\sqrt{2!}} \mathcal{S}_2 \left|\Phi_1^{(2)}\right\rangle + \frac{\alpha^3}{\sqrt{3!}} \mathcal{S}_3 \left|\Phi_1^{(3)}\right\rangle \right) \otimes |0\rangle . \end{aligned} \tag{7.87}$$

Inelastic contributions to the n-phonon S-matrices (discussed in Section 7.2.4) introduce a non-trivial momentum redistribution of the incident phonons (note that owing to the linear dispersion relation and our choice of units energy and momentum may be used interchangeably), leading to the non-trivial phonon correlations in the final state. As it is well known, the phononic correlations may be conveniently examined with the help of the so-called coherence functions introduced by Glauber [83] in 1963. Defining the Fourier transform of the field operators according to

$$a_\mu(\tau) = \int dk \frac{e^{ik\tau}}{\sqrt{2\pi}} a(k), \tag{7.88}$$

one constructs the first-order coherence function as

$$\begin{aligned} C_\mu^{(1)}(\tau) = & \left\langle \psi_f | a_\mu^\dagger(\tau) a_\mu(0) | \psi_f | \psi_f | a_\mu^\dagger(\tau) a_\mu(0) | \psi_f \right\rangle \\ = & \left(1 - |\alpha|^2 + \frac{|\alpha|^4}{2} \right) |\alpha|^2 C_\mu^{(1,1)}(\tau) + (1 - |\alpha|^2) \frac{|\alpha|^4}{2} C_\mu^{(1,2)}(\tau) + \frac{|\alpha|^6}{6} C_\mu^{(1,3)}(\tau) + \mathcal{O}(|\alpha|^8), \end{aligned} \tag{7.89}$$

where we have introduced the n-particle Fock state first-order correlation functions as

$$C_{\mu}^{(1,n)}(\tau) = \left\langle \Phi_1^{(n)} \right| (\mathcal{S}_n)^{\dagger} a_{\mu}^{\dagger}(\tau) a_{\mu}(0) \mathcal{S}_n \left| \Phi_1^{(n)} \right\rangle . \tag{7.90}$$

With the help of the first-order coherence function, one may define the spectral power density as the Fourier transform of (7.89):

$$S_{\mu}(k) = \int d\tau \frac{e^{-ik\tau}}{2\pi} C_{\mu}^{(1)}(\tau). \tag{7.91}$$

$S_{\mu}(k)$ is understood as a momentum space distribution of power in the scattered state of radiation, that is to a given mode k (supported by the μ^{th} channel) it associates a certain power $S_{\mu}(k)$. The power conservation condition

$$\sum_{\mu=1,2} \int dk S_{\mu}(k) \to \Phi, \quad \Phi = \frac{|\alpha|^2}{L}, \tag{7.92}$$

is automatically satisfied due to the unitarity of the S-matrix. In a linear system, where the n body S-matrix factorises into the product of single-particle S-matrices, the first order coherence function is a constant, thus leading to the purely elastic power density $S_{\mu}(k) \propto \delta(k)$. Since a qubit is an intrinsically non-linear system, we are going to see that the spectral power density admits for the following decomposition $S(k) = S^{\text{el}}(k) + S^{\text{inel}}(k)$, where $S^{\text{el}}(k) \propto \delta(k)$ is the elastic contribution to the spectral density, and $S^{\text{inel}}(k)$, in turn, is the inelastic part of spectral power density with a non-trivial momentum dependence.

Further, we define the normalized second and third-order coherence functions:

$$C_{\mu,\mu'}^{(2)}(\tau) = \frac{\left\langle \psi_f | a_{\mu}^{\dagger}(0) a_{\mu'}^{\dagger}(\tau) a_{\mu'}(\tau) a_{\mu}(0) | \psi_f \right| \left| \psi_f | a_{\mu}^{\dagger}(0) a_{\mu'}^{\dagger}(\tau) a_{\mu'}(\tau) a_{\mu}(0) | \psi_f \right\rangle}{C_{\mu}^{(1)}(0) C_{\mu'}^{(1)}(0)} = \left(1 - \frac{|\alpha|^2}{2}\right) \frac{1}{2} C_{\mu,\mu'}^{(2,2)}(\tau) + \frac{|\alpha|^2}{6} C_{\mu,\mu}^{(2,3} \tag{7.93}$$

$$C_{\mu,\mu',\mu''}^{(3)}(\tau,\ \tau') = \frac{\left\langle \psi_f | a_{\mu}^{\dagger}(0) a_{\mu'}^{\dagger}(\tau) a_{\mu''}^{\dagger}(\tau') a_{\mu''}(\tau') a_{\mu'}(\tau) a_{\mu}(0) | \psi_f \right| \left| \psi_f | a_{\mu}^{\dagger}(0) a_{\mu'}^{\dagger}(\tau) a_{\mu''}^{\dagger}(\tau') a_{\mu''}(\tau') a_{\mu'}(\tau) a_{\mu}(0) | \psi_f \right\rangle}{C_{\mu}^{(1)}(0) C_{\mu'}^{(1)}(0) C_{\mu''}^{(1)}(0)} = \frac{1}{6} C_{\mu,} \tag{7.94}$$

$$C_{\mu_1,\ldots,\mu_m}^{(m,n)}(\tau_1,..,\tau_{m-1}) = \frac{\left\langle \Phi_1^{(n)} | \mathcal{S}_n^{\dagger} a_{\mu_1}^{\dagger}(0) ... a_{\mu_m}^{\dagger}(\tau_{m-1}) a_{\mu_m}(\tau_{m-1}) ... a_{\mu_1}(0) \mathcal{S}_n | \Phi_1^{(n)} \right| \left| \Phi_1^{(n)} | \mathcal{S}_n^{\dagger} a_{\mu_1}^{\dagger}(0) ... a_{\mu_m}^{\dagger}(\tau_{m-1}) a_{\mu_m}(\tau_{m-1}) ... a_{\mu_1}(0 \right.}{\prod_{l=1}^{m} C_{\mu_l}^{(1)}(0)} \tag{7.95}$$

For pairs of phonons, the normalized second-order coherence function is defined as the arrival probability of the second particle as a function of the delay τ following the detection of the first one, normalized by the individual photon probabilities. Likewise, for particle triples, the normalized third-order coherence function is defined as the arrival probability of the third and second particle as a function of delays τ', τ following the detection of the first one, normalized by the individual phonon probabilities. A perfectly coherent source is characterized by a uniform arrival probability, yielding the correlation functions of all orders equal to unity. Whenever correlation functions exceed unity, particle statistics is said to be super-Poissonian and the particles are said to be bunched together, whereas in the case of correlation functions falling below unity, the statistics of particles is said to be sub-Poissonian and particles are correspondingly said to be anti-bunched.

In the following subsections, we are going to use the ideas developed in Section 7.2.3 in order to compute the above-discussed observables to the lowest order in $|\alpha|$ exactly.

7.3.3 Spectral power density

Let us begin with the analysis of the power spectrum of the SAW scattered by the giant atom. We start by considering the Fock state first-order coherence functions defined via (7.90). In order to establish $C_{\mu}^{(1,1)}(\tau)$ one first has to find the matrix elements of the single-particle S-matrix, which, in turn, demands the knowledge of the dressed propagator in the single-excitation subspace $G^{(1)}(\epsilon)$. The self-energy diagram may be evaluated straightforwardly to yield:

$$\Sigma^{(1)}(\epsilon) = -i\gamma(1 + e^{i(\epsilon + k_0)R})\sigma_+\sigma_-, \tag{7.96}$$

in accordance with reference [[59]]. With this in hands, the single-phonon scattering operator may be easily established with the help of equations (7.33), (7.37) and (7.38):

$$\mathcal{S}_1 = \sum_{\mu',\mu} \int dk dk' S_{\mu' k',\mu k}^{(1)} a_{\mu'}^{\dagger}(k') a_{\mu}(k), \tag{7.97}$$

$$S_{\mu' k',\mu k}^{(1)} = \delta(k - k') S_{\mu',\mu}^{(1)}(k) \sigma_-\sigma_+ \tag{7.98}$$

$$S_{\mu',\mu}^{(1)}(k) = (\delta_{\mu,\mu'} - 2\pi i g_{\mu}^{*}(k) g_{\mu'}(k) \tilde{G}^{(1)}(k)). \tag{7.99}$$

Here the tilde symbol denotes the projection onto the excited state in the qubit space, and $G^{(1)}(\epsilon) = G_0^{-1}(\epsilon) - \Sigma^{(1)}(\epsilon)$ in accordance with the definition in Section 7.2.3. Performing a straightforward calculation, we obtain

$$\begin{aligned} C_\mu^{(1)}(\tau) =& |\alpha|^2 C_\mu^{(1,1)}(\tau) + \mathcal{O}(|\alpha|^4) \\ =& \Phi |S^{(1)}_{\mu 0,10}|^2 + \mathcal{O}(\Phi^2) \qquad (7.100) \\ \Longrightarrow S_\mu(k) =& \Phi |S^{(1)}_{\mu 0,10}|^2 \delta(k) + \mathcal{O}(\Phi^2). \qquad (7.101) \end{aligned}$$

As we can see there exists no inelastic contribution to the spectral density in single-photon sector. In general the phenomenon of resonance fluorescence [[84]], leading to the inelastic power spectrum, is underpinned by the possibility of the two-level system to emit into the modes other than the incident one. This naturally allows the photons incident on the atom to exchange their energy between one another (whilst conserving the total energy) due to the higher order emission and absorption processes, leading to the inelastic power spectrum. In the case of the single-photon however, the particle is ought to conserve its energy individually (as mathematically prescribed by the δ-function in equation (7.98)) leading to the purely elastic spectrum.

In order to obtain the leading order inelastic contribution to the spectral power density, we thus have to consider the contribution of the multi-particle states in the expansion (7.87), so that to allow for the inter-particle interaction. In this case, the information about the inelastic scattering is entirely contained in the connected component of the two-phonon T-matrix (see Section 7.2.4), which captures the nonlinear acoustic effects via the effective single-particle vertex function. Contracting the cluster decomposed S-matrix (7.45) with the two-particle Fock state we arrive at the following result

$$\sum_{\mu,\mu'} \left(\frac{1}{\sqrt{2}} \int dk dk' \varphi(k)\varphi(k') S^{(1)}_{\mu,1}(k) S^{(1)}_{\mu',1}(k') a^\dagger_\mu(k) a^\dagger_{\mu'}(k') - \frac{8\pi^2 i}{L\sqrt{2}} \int dk T^{(2,C)}_{\mu k,\mu' -k,10,10}(0) a^\dagger_\mu(k) a^\dagger_{\mu'}(-k) \right) |\Omega\rangle \otimes |0\rangle \,. \qquad (7.102)$$

Again we would like to emphasize that at this point the plane-wave limit ($L \to \infty$) may only be taken in the term containing the connected component of the S-matrix since in this limit the first part of the state (7.102) is clearly non-normalizable. With the help of the final two-particle state derived above one may easily establish

$$\begin{aligned} C_\mu^{(1,2)}(\tau) =& 16\pi^2 \sum_{\mu'} \mathrm{Im}\{ M_{\mu',\mu}(0) (S^{(1)}_{\mu';1}(0) S^{(1)}_{\mu;1}(0))^* \} \\ &+ 32\pi^3 \sum_{\mu'} \int dk e^{ik\tau} |M_{\mu',\mu}(k)|^2, \qquad (7.103) \end{aligned}$$

where $M_{\mu',\mu}(k)$ is the symmetric part of $T^{(2,C)}_{\mu k,\mu' -k,10,10}(0)$, i.e. $M_{\mu',\mu}(k) = M_{\mu,\mu'}(-k) = (T^{(2,C)}_{\mu' k,\mu -k,10,10}(0) + T^{(2,C)}_{\mu -k,\mu' k,10,10}(0))/2$. Performing the Fourier transform of (7.103) we arrive at the following expressions for the elastic $S^{\mathrm{el}}(k)$ and inelastic $S^{\mathrm{inel}}(k)$ spectral power densities valid to order Φ^3:

$$\begin{aligned} S^{\mathrm{el}}_\mu(k) =& \delta(k) \Bigg(\Phi |S^{(1)}_{\mu;1}(0)|^2 + 16\pi^2 \Phi^2 \\ &\times \sum_{\mu'} \mathrm{Im}\{ M_{\mu',\mu}(0) (S^{(1)}_{\mu';1}(0) S^{(1)}_{\mu;1}(0))^* \} \Bigg), \qquad (7.104) \\ S^{\mathrm{inel}}_\mu(k) =& 32\pi^3 \Phi^2 \sum_{\mu'} |M_{\mu',\mu}(k)|^2. \qquad (7.105) \end{aligned}$$

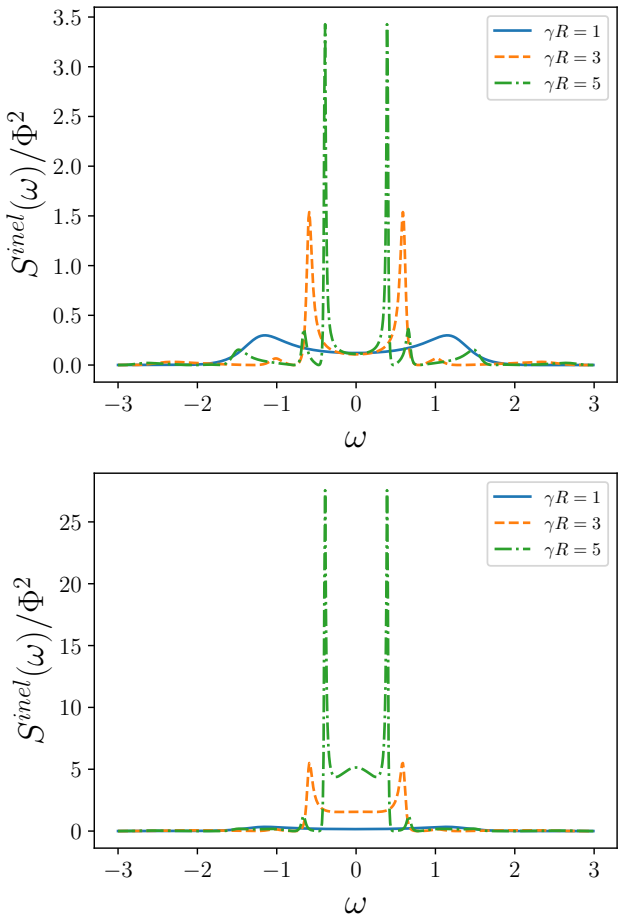

Figure 7.7: Inelastic spectral power density (scaled by Φ^2) of SAW scattered by a giant acoustic atom as a function of frequency $\omega = k$ for a variety of inter-leg separations $\gamma R = 1, 3, 5$. Top panel: exact solution; Bottom panel: quasi-Markovian approximation. Other model parameters: $k_0 R = \pi/4 \mod 2\pi$, and $\Delta = 0$. Here the limit $L \to \infty$ was taken.

The inelastic spectral densities are shown in Figure 7.7 for different inter-leg separations (R = 1, 3, 5). As one can see, the inelastic power spectrum develops a couple of sharp peaks near the origin of momentum space followed by infinitely many smaller side peaks. In order to interpret the nature of these peaks, we adopt the physical picture discussed in [[85, 86, 21]] for an "atom in front of a mirror" system. One can interpret this system as a leaky cavity formed by the two connection points of a giant atom. In this picture these peaks may be thought of as being located at the renormalized excitation frequencies of the effective cavity broadened by the renormalized decay rates. The resulting effect is the formation of sharp, bound-state like peaks in the intensity of the scattered phonons, corresponding to cavity resonances. As the delay γR increases, the peaks get closer to $\omega = 0$, and get sharper, corresponding to a decrease of the effective cavity linewidth $\simeq 1/(\gamma R)$, that is effective cavity resonances approach the resonance of the two-level system, thus making atomic connection points better and better mirrors and hence increasing the quality factor of the effective cavity (quality factor is a common physical measure of both the rate of excitation damping and the rate of energy loss of an oscillator or a cavity)

Additionally, spectral densities based on the approximate solution of the scattering problem in the quasi-Markovian approximation are shown in Figure 7.7. As it was mentioned in the section 7.2.6, quasi-Markovian results show a good agreement with an exact solution in $\gamma R \ll 1$ parameter regime. As the delay time increases $\gamma R \geq 1$, the discrepancy between the approximate and complete solutions becomes dramatic. One can clearly see the tendency of the quasi-Markovian theory to enhance the scattering into the incoming frequency states $\omega = 0$. Indeed, in contrast to the exact solution, taking into account infinitely many excursions of phonons to the qubit, the quasi-Markovian approximation is based on the assumption of a single scattering event after which each phonon immediately leaves the system, thus leading to a more elastic result.

Second-order coherence

Let us now consider the second-order coherence function to the lowest order in Φ - $\mathcal{O}(\Phi^0)$. Performing the relevant Wick contractions we arrive at the following simple expression for the normalized second-order

coherence

$$C^{(2)}_{\mu',\mu}(\tau) = \left| 1 - \frac{4\pi i}{S^{(1)}_{\mu',1}(0) S^{(1)}_{\mu,1}(0)} \int dk e^{ik\tau} M_{\mu',\mu}(k) \right|^2 . \tag{7.106}$$

The independent components of second-order coherence function's components are presented in Figure **??**.

As it was mentioned above, the higher-order coherence functions provide the information about the information about the statistics of radiation scattered by a giant acoustic atom. Since $C^{(2)}_{1,1}(0) > 1$, one can clearly see that the statistics of back-scattered phonons is super-Posissonian, i.e. the particles tend to bunch together. Indeed, this result agrees with the physical expectation that at zero detuning $\Delta = 0$ the power extinction $1 - |S_{11}(0)|^2$ is enhanced even in the presence of pure dephasing[13, 87]. This assertion also explains the anti-bunching of forwardly scattered photons $C^{(2)}_{2,2}(0)$. Another clear feature of the second-order coherence function shown in Figure **??** is presence of long-range quantum correlations of phonons, i.e. the components of $C^{(2)}$ do not decay to unity even for delays significantly exceeding the inter-leg separation $\tau \gg 1$. Note that this correlation effect becomes more and more pronounced with the increase in R, where correlation functions exhibit slightly damped oscillations around unity.

Another interesting feature of the second-order coherence is the presence of the non-differentiable peaks at natural multiples of the inter-leg separation $\tau_n = nR$, $n \in \mathbb{N}$. Physically, this property may again be understood with the help of the simple picture of a leaky cavity formed by the scatterer. Indeed, once a phonon is trapped between the legs of the atom, it may bounce off the cavity's walls back and forth multiple times, leading to the formation of the non-analytical structures present in the second-order coherence. The fact that the non-differentiable peaks are more pronounced at smaller values of n is a direct manifestation of the fact that the quality factor of the effective cavity is not infinite. This property is indeed of interest since the second-order coherence function is an experimentally measurable quantity which makes these sharp peaks a potentially observable effect.

Alongside the exact solution, the results based on the quasi-Markovian approximation are presented in Figure **??** (lower panel). The discrepancy between the two is apparent. Another feature typical of this approximation is the tendency to overestimate the amplitudes of oscillation as was first pointed out in the supplemental material of reference [[71]].

Third-order coherence

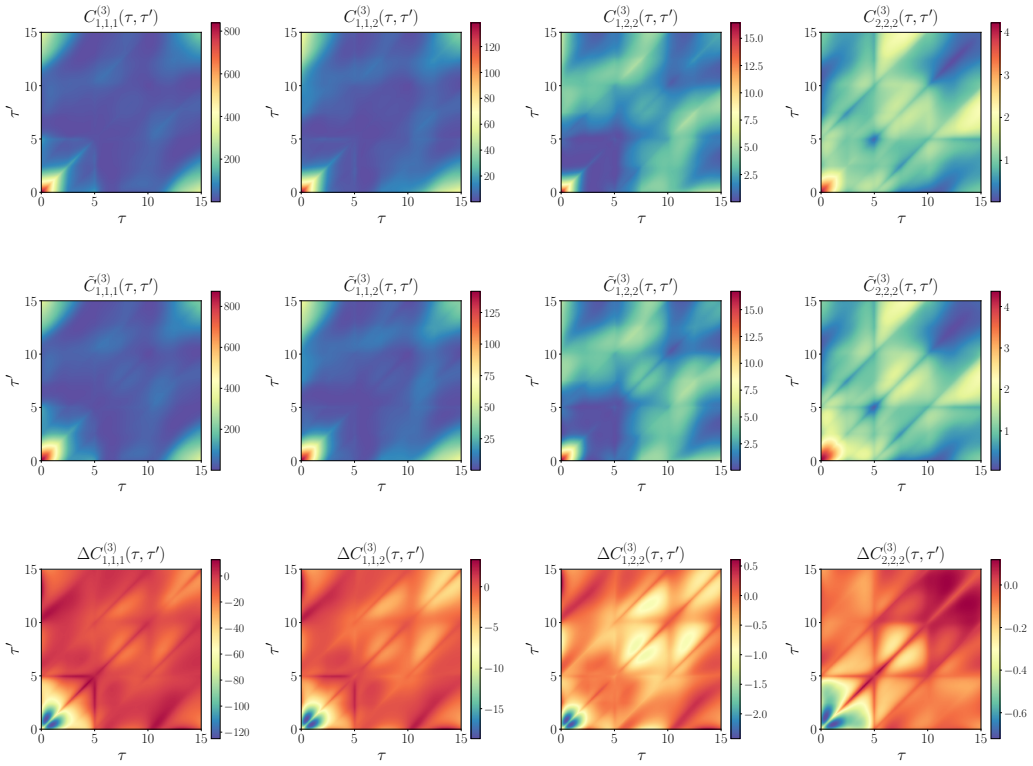

Figure 7.9: Independent components $(\mu,\mu',\mu'') = (1,1,1),\ (1,1,2),\ (1,2,2),\ (2,2,2)$ of the third-order coherence function of phonons scattered by a giant acoustic atom. Top, central, and bottom panels correspond to the exact solution $C^{(3)}_{\mu,\mu',\mu''}(\tau,\tau')$, weak correlation approximation $\tilde{C}^{(3)}_{\mu,\mu',\mu''}(\tau,\tau')$, and their difference $\Delta C^{(3)}_{\mu,\mu',\mu''}(\tau,\tau') = C^{(3)}_{\mu,\mu',\mu''}(\tau,\tau') - \tilde{C}^{(3)}_{\mu,\mu',\mu''}(\tau,\tau')$ respectively. Here $\gamma R = 5$, $k_0 R = \pi/4 \mod 2\pi$, and $\Delta = 0$. Here the limit $L \to \infty$ was taken and by definition $C^{(2)}$ is dimensionless.

Let us finally consider the third-order coherence function. The full expression for the third-order coherence function $C^{(3)}_{\mu,\mu',\mu''}(\tau,\tau')$ in terms of the symmetrized components of two and three-particle transition matrices may be found in Appendix 7.5.2. Although in general, $C^{(3)}_{\mu,\mu',\mu''}$ has 8 independent components in the case of two radiation channels, due to our particular choice of the coupling $\Gamma_1 = \Gamma_2 = \gamma/2$, only four independent components remain:

$$C^{(3)}_{1,1,1}(\tau,\tau'), \quad C^{(3)}_{2,2,2}(\tau,\tau'), \tag{7.107}$$

$$C^{(3)}_{1,1,2}(\tau,\tau') = C^{(3)}_{1,2,1}(\tau,\tau') = C^{(3)}_{2,1,1}(\tau,\tau'), \tag{7.108}$$

$$C^{(3)}_{1,2,2}(\tau,\tau') = C^{(3)}_{2,2,1}(\tau,\tau') = C^{(3)}_{2,1,2}(\tau,\tau'). \tag{7.109}$$

Independent components of $C^{(3)}$ for a system with $R = 5$, $k_0 R = \pi/4 \mod 2\pi$, and $\Delta = 0$ are shown in the top panel of Figure 7.9. First, we note that the individual components of third-order coherence at $\tau,\tau' = 0$ significantly exceed unity, signifying the bunching of phonons. This effect can be attributed to the fact that a single two-level system can only emit and absorb a single quantum of radiation at a time, which, in turn, significantly increases the probability of simultaneous detection of a pair of phonons in the waveguide. Moreover, this effect is more pronounced in those components of the correlation function, describing correlations with phonons in the channel of incident radiation $\mu = 1$. This artifact again has to do with the fact of the enhancement of power extinction by an atom at zero detuning.

Another interesting feature of $C^{(3)}$ to be noticed is the presence of clear peak and downfall structures located on the lines $\tau' - \tau = nR$, $n \in \mathbb{Z}$. Physically $\delta\tau = \tau' - \tau$ corresponds to the average delay time between the second and third phonon detection events upon detection of the first one at zero time. The quantization of $\delta\tau$ in the units of deterministic time delay is the characteristic feature of the system under consideration and may be potentially observed in future experiments via the observation of enhancement/diminution of the conditional probability of arrival of the third particle. In fact, the peak and downfall structures discussed above are non-differentiable, as it was the case with the second-order coherence function, and again this phenomenon may be understood with the help of a simple picture of an effective cavity discussed in Sections 7.3.3 and 7.3.3.

Beside the exact solution $C^{(3)}_{\mu,\mu',\mu''}(\tau,\tau')$, the solution based on the weak-correlation (WC) approximation $\tilde{C}^{(3)}_{\mu,\mu',\mu''}(\tau,\tau')$ as well as the difference between the exact solution and the WC one

$$\Delta C^{(3)}_{\mu,\mu',\mu''} = C^{(3)}_{\mu,\mu',\mu''} - \tilde{C}^{(3)}_{\mu,\mu',\mu''}, \tag{7.110}$$

are shown in Figure 7.9 in central and bottom pannels respectively. As one can anticipate, the WC approximation tends to notably overestimate the amplitude of the third-order coherence function. This effect is especially apparent in the vicinity of $\tau,\tau' = 0$, where the WC approximation significantly overestimates the phononic bunching. Away from the temporal origin, though, the approximation becomes adequate and only slightly deviates from the exact result, as one may infer from the plots in the bottom panel of Figure 7.9. The discrepancy between the exact solution and its WC approximation is not hard to understand. Weak-correlation approximation ignores an infinite diagrammatic channel, consisting of exchange interaction diagrams between the phonons, which are, of course, of importance when one studies the statistical properties of particles.

7.4 Conclusions and outlook

In this paper, the diagrammatic theory of scattering and dynamics of multi-photon states in waveguide QED was developed. In particular, it was shown that the N_p-photon scattering matrices in single-qubit waveguide QED may be conveniently parametrized in terms of effective N_p-1-photon vertex functions and the equations satisfied by these vertex functions were established. Next, certain practical issues related to the direct sum representation of the S-matrix, separation of elastic contributions to effective vertices, as well as the generalized cluster decomposition were discussed. Further, a generalization to the waveguide QED systems with more than a single qubit was given. Specifically, in the case of the two-qubit systems, it was established that the equations governing multi-photon vertex functions remain the same as in the case of a single qubit, up to the inclusion of higher-order vertex corrections. Moreover, we have shown that once the integral equations governing N_q-photon scattering matrix in N_q waveguide QED, these equations hold for any system of qubits and established the generic equations governing 2 and 3 photon scattering operators by considering 2 and 3 photon scattering on two and three qubits respectively.

Next, the diagrammatic theory of scattering was applied to a problem of scattering of a weakly coherent pulse on the giant acoustic atom. Namely, by expanding a coherent state perturbatively in a coherence parameter up to third order in $|\alpha|$ and studying its scattering on the atom, we were able to establish the first, second, and third-order coherence functions of scattered radiation. Moreover, a set of approximation routines was suggested along with the exact method and the two were compared where appropriate. Further, the statistical properties of scattered surface acoustic waves were studied, and the effect of the non-Markovian nature of the setup on statistics was discussed.

In our future work, we are going to present the generalization of the resummation approach enabling one to study real-time dynamics in waveguide QED systems. It would be of further interest to extend the present theory to study scattering in waveguide QED systems containing emitters with more complicated selection rules such as three and four-level systems. Another generalization of the theory presented in this paper of potential future interest is the study of particular 2 and 3-particle scattering problems on systems containing multiple distant qubits. Furthermore, it would be potentially interesting to assess the effects of counter-rotating terms, which were ignored throughout this work, which, however, will require the use of techniques other than the one discussed in this work.

7.5 Appendix

7.5.1 Cluster decomposition of three-photon S-matrix

The starting point of our analysis in this appendix goes back to the definition of the three-body component of the S-matrix entering its direct sum representation (throughout this appendix, for simplicity, it is assumed that $\omega_\mu(k)=\omega(k), \quad B_\mu = B, \quad \forall \mu \in \{1,...,N_c\}$), namely schematically

$$\mathcal{S}_3 = \big[\frac{1}{3!}\delta\delta\delta - 2\pi i T^{(1,1)}\delta(..)\frac{1}{2!}\delta\delta - 2\pi i T^{(1,2)}\delta(..)\delta - 2\pi i T^{(1,3)}\delta(..)\big] a^\dagger a^\dagger a^\dagger aaa.$$

or exactly:

$$\begin{aligned}
\mathcal{S}_3 = \Bigg[& \frac{1}{3!}\delta_{s_1',s_1}\delta_{s_2',s_2}\delta_{s_3',s_3} - 2\pi i T^{(1,1)}_{s_1',s_1}(\omega(k_1))\delta(\omega(k_1')-\omega(k_1))\frac{1}{2!}\delta_{s_2',s_2}\delta_{s_3',s_3} \\
& - 2\pi i T^{(1,2)}_{s_1's_2',s_1s_2}(\omega(k_1)+\omega(k_2))\delta(\omega(k_1')+\omega(k_2')-\omega(k_1)-\omega(k_2))\frac{1}{1!}\delta_{s_3',s_3} \\
& - 2\pi i T^{(1,3)}_{s_1's_2's_3',s_1s_2s_3}(\omega(k_1)+\omega(k_2)+\omega(k_3))\delta(\omega(k_1')+\omega(k_2')+\omega(k_3')-\omega(k_1)-\omega(k_2)-\omega(k_3))\Bigg] \\
& \times a^\dagger_{s_1'} a^\dagger_{s_2'} a^\dagger_{s_3'} a_{s_3} a_{s_2} a_{s_1}.
\end{aligned} \tag{7.111}$$

As before we write

$$T^{(1,2)}_{s_1's_2',s_1s_2}(\omega(k_1)+\omega(k_2)) = -\pi i\delta(\omega(k_1')-\omega(k_1))T^{(1,1)}_{s_1',s_1}(\omega(k_1))T^{(1,1)}_{s_2',s_2}(\omega(k_2)) + T^{(1,2,C)}_{s_1's_2',s_1s_2}(\omega(k_1)+\omega(k_2)). \tag{7.112}$$

Here, as before, the equality symbol is understood in the sense of permutation equivalence and on-shell condition. Now let us start massaging the three-body transition operator. First of all, one has schematically:

$$T^{(1,3)} = g^*g^*g^*ggg\ \tilde{G}^{(1)}\tilde{G}^{(1)}F^{(1,2)}, \tag{7.113}$$

or exactly:

$$\begin{aligned} T^{(1,3)}_{\mu_1'k_1',\mu_2'k_2',\mu_3'k_3';\mu_1k_1,\mu_2k_2,\mu_3k_3}(\omega(k_1)+\omega(k_2)+\omega(k_3)) &= g^*_{\mu_1}(k_1)g^*_{\mu_2}(k_2)g^*_{\mu_3}(k_3)g_{\mu_1'}(k_1')g_{\mu_2'}(k_2')g_{\mu_3'}(k_3') \\ &\times \tilde{G}^{(1)}(\omega(k_1))\tilde{G}^{(1)}(\omega(k_1'))F^{(1,2)}(k_2',k_3',k_2,k_3,\omega(k_1)+\omega(k_2)+\omega(k_3)), \end{aligned} \tag{7.114}$$

where $F^{(1,2)}(k_2',k_3',k_2,k_3,\omega(k_1)+\omega(k_2)+\omega(k_3))$ is not an entirely connected object defined via

$$F^{(1,2)}(k_1',k_2',k_1,k_2,\epsilon) = \frac{1}{g_{\mu_1'}(k_1')g_{\mu_2'}(k_2')g^*_{\mu_1}(k_1)g^*_{\mu_2}(k_2)}\left\langle g\left| W^{(1,2)}_{\mu_1'k_1'\mu_2'k_2',\mu_1k_1\mu_2k_2}(\epsilon)\right| g\right\rangle. \tag{7.115}$$

Separation of elastic contribution (7.43) translates into the following decomposition

$$F^{(1,2)} = F^{(1,1)}\tilde{G}^{(1)}F^{(1,1)} + \overline{F}^{(2,2)}. \tag{7.116}$$

or exactly:

$$\begin{aligned} &F^{(1,2)}(k_2',k_3',k_2,k_3,\omega(k_1)+\omega(k_2)+\omega(k_3)) \\ =&F^{(1,1)}(k_2',k_2,\omega(k_1')+\omega(k_2'))\tilde{G}^{(1)}(\omega(k_1)+\omega(k_3)-\omega(k_3'))F^{(1,1)}(k_3',k_3,\omega(k_1)+\omega(k_3)) \\ &+\overline{F}^{(2,2)}(k_2',k_3',k_2,k_3,\omega(k_1)+\omega(k_2)+\omega(k_3)). \end{aligned} \tag{7.117}$$

Bearing in mind that $\overline{F}^{(2,2)}(k_2',k_3',k_2,k_3,\omega(k_1)+\omega(k_2)+\omega(k_3))$ is an analytic function we decompose the three photon T-matrix as follows

$$\begin{aligned} &T^{(1,3)}_{\mu_1'k_1',\mu_2'k_2',\mu_3'k_3';\mu_1k_1,\mu_2k_2,\mu_3k_3}(\omega(k_1)+\omega(k_2)+\omega(k_3)) \\ =&\overline{T}^{(1,3)}_{\mu_1'k_1',\mu_2'k_2',\mu_3'k_3';\mu_1k_1,\mu_2k_2,\mu_3k_3}(\omega(k_1)+\omega(k_2)+\omega(k_3)) \\ +&\hat{T}^{(1,3)}_{\mu_1'k_1',\mu_2'k_2',\mu_3'k_3';\mu_1k_1,\mu_2k_2,\mu_3k_3}(\omega(k_1)+\omega(k_2)+\omega(k_3)), \end{aligned} \tag{7.118}$$

where we have defined the following objects schematically:

$$\overline{T}^{(1,3)} = g^*g^*g^*ggg\ \tilde{G}\tilde{G}\ \overline{F}^{(1,2)}; \qquad \hat{T}^{(1,3)} = g^*g^*g^*ggg\ \tilde{G}\tilde{G}\ F^{(1,1)}\tilde{G}^{(1)}F^{(1,1)}.$$

and exactly:

$$\begin{aligned} &\overline{T}^{(1,3)}_{\mu_1'k_1',\mu_2'k_2',\mu_3'k_3';\mu_1k_1,\mu_2k_2,\mu_3k_3}(\omega(k_1)+\omega(k_2)+\omega(k_3)) \\ =&g^*_{\mu_1}(k_1)g^*_{\mu_2}(k_2)g^*_{\mu_3}(k_3)g_{\mu_1'}(k_1')g_{\mu_2'}(k_2')g_{\mu_3'}(k_3')\ \tilde{G}(\omega(k_1))\tilde{G}(\omega(k_1'))\ \overline{F}^{(1,2)}(k_2',k_3',k_2,k_3,\omega(k_1)+\omega(k_2)+\omega(k_3)) \end{aligned} \tag{7.119}$$

$$\begin{aligned} &\hat{T}^{(1,3)}_{\mu_1'k_1',\mu_2'k_2',\mu_3'k_3';\mu_1k_1,\mu_2k_2,\mu_3k_3}(\omega(k_1)+\omega(k_2)+\omega(k_3)) \\ =&g^*_{\mu_1}(k_1)g^*_{\mu_2}(k_2)g^*_{\mu_3}(k_3)g_{\mu_1'}(k_1')g_{\mu_2'}(k_2')g_{\mu_3'}(k_3')\ \tilde{G}(\omega(k_1))\tilde{G}(\omega(k_1'))F^{(1,1)}(k_2',k_2,\omega(k_1')+\omega(k_2')) \\ &\tilde{G}^{(1)}(\omega(k_1)+\omega(k_3)-\omega(k_3'))\ F^{(1,1)}(k_3',k_3,\omega(k_1)+\omega(k_3)). \end{aligned} \tag{7.120}$$

In the last equation we have

$$F^{(1,1)}(k_2',k_2,\omega(k_1')+\omega(k_2')) = \hat{G}_0(\omega(k_1')-\omega(k_2)) + \overline{F}^{(1,1)}(k_2',k_2,\omega(k_1')+\omega(k_2')), \tag{7.121}$$

$$F^{(1,1)}(k_3',k_3,\omega(k_1)+\omega(k_3)) = \hat{G}_0(\omega(k_1)-\omega(k_3')) + \overline{F}^{(1,1)}(k_3',k_3,\omega(k_1)+\omega(k_3)). \tag{7.122}$$

The terms in (7.120) containing $\hat{G}_0$ deserve a special attention since they can yield delta-functions determining additional conservation of frequencies.

In particular, the terms with $\hat{G}_0\overline{F}^{(1,1)}$ and $\overline{F}^{(1,1)}\hat{G}_0$ together give

$$
\begin{aligned}
&-2\pi i\delta(\omega(k_3')-\omega(k_3))T^{(1,1)}_{s_3',s_3}(\omega(k_3))\\
&\times\left[T^{(1,2,C)}_{s_1's_2',s_1s_2}(\omega(k_1)+\omega(k_2))-g^*_{\mu_1}(k_1)g^*_{\mu_2}(k_2)g_{\mu_1'}(k_1')g_{\mu_2'}(k_2')\tilde{G}^{(1)}(\omega(k_1))\tilde{G}^{(1)}(\omega(k_1'))P\left(\frac{1}{\omega(k_1)-\omega(k_2')}\right)\right] \qquad (7.123)\\
&+g^*_{\mu_1}(k_1)g^*_{\mu_2}(k_2)g^*_{\mu_3}(k_3)g_{\mu_1'}(k_1')g_{\mu_2'}(k_2')g_{\mu_3'}(k_3')\tilde{G}(\omega(k_1))\tilde{G}(\omega(k_1'))\tilde{G}^{(1)}(\omega(k_1)+\omega(k_3)-\omega(k_3'))\\
&\times\left[P\left(\frac{1}{\omega(k_1')-\omega(k_2)}\right)\overline{F}^{(1,1)}(k_3',k_3,\omega(k_1)+\omega(k_3))+\overline{F}^{(1,1)}(k_2',k_2,\omega(k_1')+\omega(k_2'))P\left(\frac{1}{\omega(k_1)-\omega(k_3')}\right)\right]. \qquad (7.124)
\end{aligned}
$$

The term (7.123) contributes to the $3=2+1$ cluster of the three-photon S-matrix. In turn, the term (7.124) is completely connected and non-singular. This property becomes explicitly visible if we re-express it as

$$
\begin{aligned}
&\frac{g^*_{\mu_1}(k_1)g^*_{\mu_2}(k_2)g^*_{\mu_3}(k_3)g_{\mu_1'}(k_1')g_{\mu_2'}(k_2')g_{\mu_3'}(k_3')}{\omega(k_1')-\omega(k_1)}\\
&\times\Big[\tilde{G}^{(1)}(\omega(k_1'))\tilde{G}^{(1)}(\omega(k_3))\tilde{G}^{(1)}(\omega(k_3')+\omega(k_1')-\omega(k_1))\overline{F}^{(1,1)}(k_2',k_2,\omega(k_1')+\omega(k_2')+\omega(k_3')-\omega(k_1))\\
&-\tilde{G}^{(1)}(\omega(k_1))\tilde{G}^{(1)}(\omega(k_1)+\omega(k_3)-\omega(k_1'))\tilde{G}^{(1)}(\omega(k_3'))\overline{F}^{(1,1)}(k_2',k_2,\omega(k_2')+\omega(k_3'))\Big]. \qquad (7.125)
\end{aligned}
$$

This representation makes it obvious that in the limit $k_1'\to k_1$ this function is finite.

Now, let us consider the contribution to (7.120) containing $\hat{G}_0\hat{G}_0$. It amounts to

$$
\begin{aligned}
&g^*_{\mu_1}(k_1)g^*_{\mu_2}(k_2)g^*_{\mu_3}(k_3)g_{\mu_1'}(k_1')g_{\mu_2'}(k_2')g_{\mu_3'}(k_3')\\
&\quad\times\tilde{G}(\omega(k_1))\tilde{G}(\omega(k_3'))\tilde{G}^{(1)}(\omega(k_2)+\omega(k_1)-\omega(k_1'))\\
&\quad\times\hat{G}_0(\omega(k_3')-\omega(k_3))\hat{G}_0(\omega(k_1)-\omega(k_1'))\\
&=(-i\pi)^2T^{(1,1)}_{s_1',s_1}(\omega(k_1))T^{(1,1)}_{s_2',s_2}(\omega(k_2))T^{(1,1)}_{s_3',s_3}(\omega(k_3))\\
&\quad\times\delta(\omega(k_1')-\omega(k_1))\delta(\omega(k_2')-\omega(k_2)) \qquad (7.126)\\
&-2\pi i g^*_{\mu_1}(k_1)g^*_{\mu_2}(k_2)g_{\mu_1'}(k_1')g_{\mu_2'}(k_2')\tilde{G}^{(1)}(\omega(k_1))\\
&\quad\times\tilde{G}^{(1)}(\omega(k_1'))T^{(1,1)}_{s_3',s_3}(\omega(k_3))\delta(\omega(k_3')-\omega(k_3)) \qquad (7.127)\\
&+g^*_{\mu_1}(k_1)g^*_{\mu_2}(k_2)g^*_{\mu_3}(k_3)g_{\mu_1'}(k_1')g_{\mu_2'}(k_2')g_{\mu_3'}(k_3')\\
&\quad\times\tilde{G}(\omega(k_3'))\tilde{G}(\omega(k_1))\tilde{G}^{(1)}(\omega(k_2)+\omega(k_1)-\omega(k_1'))\\
&\quad\times P\left(\frac{1}{\omega(k_3')-\omega(k_3)}\right)P\left(\frac{1}{\omega(k_1)-\omega(k_1')}\right). \qquad (7.128)
\end{aligned}
$$

The term (7.126) contributes to the $3=1+1+1$ cluster. The term (7.127) contributes to the $3=2+1$ cluster.

The term (7.128) requires a special consideration. Rewriting schematically

$$
\begin{aligned}
\tilde{G}^{(1)}\tilde{G}^{(1)}\tilde{G}^{(1)}\ P\left(\frac{1}{\omega-\omega}\right)P\left(\frac{1}{\omega-\omega}\right)=&\tilde{G}^{(1)}\tilde{G}^{(1)}P\left(\frac{1}{\omega-\omega}\right)\frac{\tilde{G}^{(1)}-\tilde{G}^{(1)}}{\omega-\omega}+\\
&+\underbrace{\tilde{G}^{(1)}\tilde{G}^{(1)}\tilde{G}^{(1)}\ P\left(\frac{1}{\omega-\omega}\right)P\left(\frac{1}{\omega-\omega}\right)}_{=\tilde{G}^{(1)}\tilde{G}^{(1)}\ \frac{\tilde{G}^{(1)}-\tilde{G}^{(1)}}{\omega-\omega}\ P\left(\frac{1}{\omega-\omega}\right)+\tilde{G}^{(1)}\tilde{G}^{(1)}\tilde{G}^{(1)}\ P\left(\frac{1}{\omega-\omega}\right)\ P\left(\frac{1}{\omega-\omega}\right)}
\end{aligned}
$$

oe exactly:

$$\begin{aligned}
&\tilde{G}^{(1)}(\omega(k_3'))\tilde{G}^{(1)}(\omega(k_2)+\omega(k_1)-\omega(k_1'))\tilde{G}^{(1)}(\omega(k_1))\ P\left(\frac{1}{\omega(k_3')-\omega(k_3)}\right)P\left(\frac{1}{\omega(k_1)-\omega(k_1')}\right)\\
=&\tilde{G}^{(1)}(\omega(k_3'))\tilde{G}^{(1)}(\omega(k_1))P\left(\frac{1}{\omega(k_3')-\omega(k_3)}\right)\ \frac{\tilde{G}^{(1)}(\omega(k_2)+\omega(k_1)-\omega(k_1'))-\tilde{G}^{(1)}(\omega(k_2))}{\omega(k_1)-\omega(k_1')}\\
+&\tilde{G}^{(1)}(\omega(k_3'))\tilde{G}^{(1)}(\omega(k_2))\tilde{G}^{(1)}(\omega(k_1))\ \ P\left(\frac{1}{\omega(k_3')-\omega(k_3)}\right)P\left(\frac{1}{\omega(k_1)-\omega(k_1')}\right)\\
=&\tilde{G}^{(1)}(\omega(k_3'))\tilde{G}^{(1)}(\omega(k_1))P\left(\frac{1}{\omega(k_3')-\omega(k_3)}\right)\frac{\tilde{G}^{(1)}(\omega(k_2)+\omega(k_1)-\omega(k_1'))-\tilde{G}^{(1)}(\omega(k_2))}{\omega(k_1)-\omega(k_1')} \qquad (7.129)\\
+&\tilde{G}^{(1)}(\omega(k_2))\tilde{G}^{(1)}(\omega(k_1))\ \frac{\tilde{G}^{(1)}(\omega(k_3'))-\tilde{G}^{(1)}(\omega(k_3))}{\omega(k_3')-\omega(k_3)}\ P\left(\frac{1}{\omega(k_1)-\omega(k_1')}\right) \qquad (7.130)\\
+&\tilde{G}^{(1)}(\omega(k_3))\tilde{G}^{(1)}(\omega(k_2))\tilde{G}^{(1)}(\omega(k_1))\ P\left(\frac{1}{\omega(k_3')-\omega(k_3)}\right)\ P\left(\frac{1}{\omega(k_1)-\omega(k_1')}\right), \qquad (7.131)
\end{aligned}$$

we observe that the terms (7.129) and (7.130) terms give together a non-singular contribution. In fact, schematically:

$$\begin{aligned}
&\tilde{G}^{(1)}\tilde{G}^{(1)}P\left(\frac{1}{\omega-\omega}\right)\frac{\tilde{G}^{(1)}-\tilde{G}^{(1)}}{\omega-\omega}+\tilde{G}^{(1)}\tilde{G}^{(1)}\frac{\tilde{G}^{(1)}-\tilde{G}^{(1)}}{\omega-\omega}P\left(\frac{1}{\omega-\omega}\right)\\
&=\tilde{G}^{(1)}\tilde{G}^{(1)}\tilde{G}^{(1)}\tilde{G}^{(1)}\tilde{G}^{(1)}\frac{(\tilde{G}^{(1)})^{-1}-(\tilde{G}^{(1)})^{-1}}{\omega-\omega}\frac{(\tilde{G}^{(1)})^{-1}-(\tilde{G}^{(1)})^{-1}}{\omega-\omega}\\
&+\tilde{G}^{(1)}\tilde{G}^{(1)}\tilde{G}^{(1)}\frac{1}{\omega-\omega}\left(\tilde{G}^{(1)}\frac{(\tilde{G}^{(1)})^{-1}-(\tilde{G}^{(1)})^{-1}}{\omega+\omega-\omega-\omega}-\tilde{G}^{(1)}\frac{(\tilde{G}^{(1)})^{-1}-(\tilde{G}^{(1)})^{-1}}{\omega-\omega}\right).
\end{aligned}$$

or exactly:

$$\begin{aligned}
&\tilde{G}^{(1)}(\omega(k_3'))\tilde{G}^{(1)}(\omega(k_1))\ P\left(\frac{1}{\omega(k_3')-\omega(k_3)}\right)\ \frac{\tilde{G}^{(1)}(\omega(k_2)+\omega(k_1)-\omega(k_1'))-\tilde{G}^{(1)}(\omega(k_2))}{\omega(k_1)-\omega(k_1')}\\
+&\tilde{G}^{(1)}(\omega(k_2))\tilde{G}^{(1)}(\omega(k_1))\frac{\tilde{G}^{(1)}(\omega(k_3'))-\tilde{G}^{(1)}(\omega(k_3))}{\omega(k_3')-\omega(k_3)}\ P\left(\frac{1}{\omega(k_1)-\omega(k_1')}\right)\\
&=\tilde{G}^{(1)}(\omega(k_3'))\tilde{G}^{(1)}(\omega(k_1))\tilde{G}^{(1)}(\omega(k_2))\tilde{G}^{(1)}(\omega(k_2')+\omega(k_3')-\omega(k_3))\tilde{G}^{(1)}(\omega(k_2'))\\
&\times\frac{(\tilde{G}^{(1)})^{-1}(\omega(k_2'))-(\tilde{G}^{(1)})^{-1}(\omega(k_2')+\omega(k_3')-\omega(k_3))}{\omega(k_3')-\omega(k_3)}\\
&\qquad\qquad\frac{(\tilde{G}^{(1)})^{-1}(\omega(k_2))-(\tilde{G}^{(1)})^{-1}(\omega(k_2)+\omega(k_1)-\omega(k_1'))}{\omega(k_1)-\omega(k_1')}+\\
&+\tilde{G}^{(1)}(\omega(k_2))\tilde{G}^{(1)}(\omega(k_3))\tilde{G}^{(1)}(\omega(k_3'))\frac{1}{\omega(k_1')-\omega(k_1)}\\
&\times\left(\tilde{G}^{(1)}(\omega(k_1'))\frac{(\tilde{G}^{(1)})^{-1}(\omega(k_3))-(\tilde{G}^{(1)})^{-1}(\omega(k_1')+\omega(k_3')-\omega(k_1))}{\omega(k_1')+\omega(k_3')-\omega(k_1)-\omega(k_3)}\right.\\
&\qquad\left.-\tilde{G}^{(1)}(\omega(k_1))\frac{(\tilde{G}^{(1)})^{-1}(\omega(k_3))-(\tilde{G}^{(1)})^{-1}(\omega(k_3'))}{\omega(k_3')-\omega(k_3)}\right).
\end{aligned}$$

In contrast, the term (7.131) is singular and contributes to the $3=1+1+1$ cluster of the scattering matrix. To show this, we first fully symmetrize

$$\begin{aligned}
&\tilde{G}^{(1)}\tilde{G}^{(1)}\tilde{G}^{(1)}P\left(\frac{1}{\omega-\omega}\right)P\left(\frac{1}{\omega-\omega}\right)\to\\
&\frac{1}{3}\tilde{G}^{(1)}\tilde{G}^{(1)}\tilde{G}^{(1)}\left[P\left(\frac{1}{\omega-\omega}\right)P\left(\frac{1}{\omega-\omega}\right)+P\left(\frac{1}{\omega-\omega}\right)P\left(\frac{1}{\omega-\omega}\right)+P\left(\frac{1}{\omega-\omega}\right)P\left(\frac{1}{\omega-\omega}\right)\right].
\end{aligned}$$

or exactly:

$$\tilde{G}^{(1)}(\omega(k_3))\tilde{G}^{(1)}(\omega(k_2))\tilde{G}^{(1)}(\omega(k_1))P\left(\frac{1}{\omega(k'_3)-\omega(k_3)}\right)P\left(\frac{1}{\omega(k_1)-\omega(k'_1)}\right) \tag{7.132}$$

$$\rightarrow$$

$$\frac{1}{3}\tilde{G}^{(1)}(\omega(k_3))\tilde{G}^{(1)}(\omega(k_2))\tilde{G}^{(1)}(\omega(k_1))$$

$$\times\left[P\left(\frac{1}{\omega(k'_3)-\omega(k_3)}\right)P\left(\frac{1}{\omega(k_1)-\omega(k'_1)}\right)+P\left(\frac{1}{\omega(k'_2)-\omega(k_2)}\right)P\left(\frac{1}{\omega(k_3)-\omega(k'_3)}\right)+\right.$$

$$\left.+P\left(\frac{1}{\omega(k'_1)-\omega(k_1)}\right)P\left(\frac{1}{\omega(k_2)-\omega(k'_2)}\right)\right].$$

Owing to the Poincare-Bertrand distributional identity

$$P\left(\frac{1}{x}\right)P\left(\frac{1}{y}\right)=P\left(\frac{1}{y-x}\right)\left[P\left(\frac{1}{x}\right)-P\left(\frac{1}{y}\right)\right]+\pi^2\delta(x)\delta(y), \tag{7.133}$$

we establish the identity

$$P\left(\frac{1}{\omega(k'_3)-\omega(k_3)}\right)P\left(\frac{1}{\omega(k_1)-\omega(k'_1)}\right)+P\left(\frac{1}{\omega(k'_2)-\omega(k_2)}\right)P\left(\frac{1}{\omega(k_3)-\omega(k'_3)}\right)+$$

$$+P\left(\frac{1}{\omega(k'_1)-\omega(k_1)}\right)P\left(\frac{1}{\omega(k_2)-\omega(k'_2)}\right)=\pi^2\delta(\omega(k'_3)-\omega(k_3))\delta(\omega(k'_1)-\omega(k_1)), \tag{7.134}$$

leading us to the result

$$\frac{\pi^2}{3}\tilde{G}^{(1)}(\omega(k_3))\tilde{G}^{(1)}(\omega(k_2))\tilde{G}^{(1)}(\omega(k_1))\delta(\omega(k'_3)-\omega(k_3))\delta(\omega(k'_1)-\omega(k_1)) \tag{7.135}$$

in (7.132).

Combining all of the above results, we arrive at the following decomposition of the three-photon T-matrix schematically

$$T^{(1,3)}=\frac{(-2\pi i)^2}{6}T^{(1)}T^{(1)}T^{(1)}\delta(..)-2\pi iT^{(1,2,C)}T^{(1)}\delta(..)+T^{(1,3,C)},$$

or exactly:

$$T^{(1,3)}_{s'_1s'_2s'_3,s_1s_2s_3}(\omega(k_1)+\omega(k_2)+\omega(k_3))$$

$$=\frac{(-2\pi i)^2}{6}T^{(1)}_{s'_1,s_1}(\omega(k_1))T^{(1)}_{s'_2,s_2}(\omega(k_2))T^{(1)}_{s'_3,s_3}(\omega(k_3))\delta(\omega(k'_1)-\omega(k_1))\delta(\omega(k'_2)-\omega(k_2))$$

$$-2\pi iT^{(1,2,C)}_{s'_1s'_2,s_1s_2}(\omega(k_1)+\omega(k_2))T^{(1)}_{s'_3,s_3}(\omega(k_3))\delta(\omega(k'_3)-\omega(k_3))+T^{(1,3,C)}_{s'_1s'_2s'_3,s_1s_2s_3}(\omega(k_1)+\omega(k_2)+\omega(k_3)), \tag{7.136}$$

with the three-body connected part schematically

$$T^{(1,3,C)}=g^*g^*g^*ggg\left\{\tilde{G}^{(1)}\tilde{G}^{(1)}\tilde{G}^{(1)}\tilde{G}^{(1)}\tilde{G}^{(1)}\frac{(\tilde{G}^{(1)})^{-1}-(\tilde{G}^{(1)})^{-1}}{\omega-\omega}\frac{(\tilde{G}^{(1)})^{-1}-(\tilde{G}^{(1)})^{-1}}{\omega-\omega}\right.$$

$$+\frac{1}{\omega-\omega}\left[\tilde{G}^{(1)}\tilde{G}^{(1)}\tilde{G}^{(1)}\left(\tilde{G}^{(1)}\frac{(\tilde{G}^{(1)})^{-1}-(\tilde{G}^{(1)})^{-1}}{\omega+\omega-\omega-\omega}-\tilde{G}^{(1)}\frac{(\tilde{G}^{(1)})^{-1}-(\tilde{G}^{(1)})^{-1}}{\omega-\omega}\right)+\tilde{G}^{(1)}\tilde{G}^{(1)}\tilde{G}^{(1)}\overline{F}^{(1,1)}-\right.$$

$$\left.\left.-\tilde{G}^{(1)}\tilde{G}^{(1)}\tilde{G}^{(1)}\overline{F}^{(1,1)}\right]+\tilde{G}\tilde{G}\overline{F}^{(1,1)}\tilde{G}^{(1)}\overline{F}^{(1,1)}\right\}+\overline{T}^{(1,3)}.$$

or exactly:

$$
\begin{aligned}
&T^{(1,3,C)}_{s_1's_2's_3',s_1s_2s_3}(\omega(k_1)+\omega(k_2)+\omega(k_3)) = g^*_{\mu_1}(k_1)g^*_{\mu_2}(k_2)g^*_{\mu_3}(k_3)g_{\mu_1'}(k_1')g_{\mu_2'}(k_2')g_{\mu_3'}(k_3')\\
&\times\Bigg\{\tilde{G}^{(1)}(\omega(k_3'))\tilde{G}^{(1)}(\omega(k_1))\tilde{G}^{(1)}(\omega(k_2))\tilde{G}^{(1)}(\omega(k_2')+\omega(k_3')-\omega(k_3))\tilde{G}^{(1)}(\omega(k_2'))\\
&\quad\times\frac{(\tilde{G}^{(1)})^{-1}(\omega(k_{2'}))-(\tilde{G}^{(1)})^{-1}(\omega(k_2')+\omega(k_3')-\omega(k_3))}{\omega(k_3')-\omega(k_3)}\frac{(\tilde{G}^{(1)})^{-1}(\omega(k_2))-(\tilde{G}^{(1)})^{-1}(\omega(k_2)+\omega(k_1)-\omega(k_1'))}{\omega(k_1)-\omega(k_1')}\\
&\quad+\frac{1}{\omega(k_1')-\omega(k_1)}\Bigg[\tilde{G}^{(1)}(\omega(k_2))\tilde{G}^{(1)}(\omega(k_3))\tilde{G}^{(1)}(\omega(k_3'))\\
&\qquad\times\Bigg(\tilde{G}^{(1)}(\omega(k_1'))\frac{(\tilde{G}^{(1)})^{-1}(\omega(k_3))-(\tilde{G}^{(1)})^{-1}(\omega(k_1')+\omega(k_3')-\omega(k_1))}{\omega(k_1')+\omega(k_3')-\omega(k_1)-\omega(k_3)}\\
&\qquad\quad-\tilde{G}^{(1)}(\omega(k_1))\frac{(\tilde{G}^{(1)})^{-1}(\omega(k_3))-(\tilde{G}^{(1)})^{-1}(\omega(k_3'))}{\omega(k_3')-\omega(k_3)}\Bigg)\\
&\qquad+\tilde{G}^{(1)}(\omega(k_1'))\tilde{G}^{(1)}(\omega(k_3))\tilde{G}^{(1)}(\omega(k_3')+\omega(k_1')-\omega(k_1))\overline{F}^{(1,1)}(k_2',k_2,\omega(k_1')+\omega(k_2')+\omega(k_3')-\omega(k_1))\\
&\qquad-\tilde{G}^{(1)}(\omega(k_1))\tilde{G}^{(1)}(\omega(k_3'))\tilde{G}^{(1)}(\omega(k_1)+\omega(k_3)-\omega(k_1'))\overline{F}^{(1,1)}(k_2',k_2,\omega(k_2')+\omega(k_3'))\Bigg]\\
&\quad+\tilde{G}(\omega(k_1))\tilde{G}(\omega(k_1'))\overline{F}^{(1,1)}(k_2',k_2,\omega(k_1')+\omega(k_2'))\tilde{G}^{(1)}(\omega(k_1)+\omega(k_3)-\omega(k_3'))\overline{F}^{(1,1)}(k_3',k_3,\omega(k_1)+\omega(k_3))\Bigg\}\\
&+\overline{T}^{(1,3)}_{s_1's_2's_3',s_1s_2s_3}(\omega(k_1)+\omega(k_2)+\omega(k_3)).
\end{aligned}
\tag{7.137}
$$

Plugging everything into the definition of the three-photon S-matrix we finally obtain

$$
\begin{aligned}
\mathcal{S}_3 = &\Bigg[\frac{1}{3!}S^{(1)}_{s_1',s_1}S^{(1)}_{s_2',s_2}S^{(1)}_{s_3',s_3}-2\pi i T^{(1,2,C)}_{s_1's_2',s_1s_2}(\omega(k_1)+\omega(k_2))S^{(1)}_{s_3',s_3}\delta(\omega(k_1')+\omega(k_2')-\omega(k_1)-\omega(k_2)\\
&-2\pi i T^{(1,3,C)}_{s_1's_2's_3',s_1s_2s_3}(\omega(k_1)+\omega(k_2)+\omega(k_3))\delta(\omega(k_1')+\omega(k_2')+\omega(k_3')-\omega(k_1)-\omega(k_2)-\omega(k_3))\Bigg]a^\dagger_{s_1'}a^\dagger_{s_2'}a^\dagger_{s_3'}a_{s_3}a_{s_2}a_{s_1}.
\end{aligned}
\tag{7.138}
$$

7.5.2 Third-order coherence function

In this appendix we present the formula for the third order coherence function of phonons in the giant atom model. Using the formula (7.138) with $\omega(k)=k$ along with the notations introduced in the Section 7.3, we obtain the following result upon contraction with the three-phonon Fock state

$$
\begin{aligned}
\mathcal{S}_3\left|\Phi^{(3)}_1\right\rangle = \frac{1}{\sqrt{6}}\sum_{\{\mu_i'\}}\Bigg(&\int_{k_1k_2k_3}\varphi(k_1)\varphi(k_2)\varphi(k_3)S^{(1)}_{\mu_1',1}(k_1)S^{(1)}_{\mu_2',1}(k_2)S^{(1)}_{\mu_3',1}(k_3)a^\dagger_{\mu_1'}(k_1)a^\dagger_{\mu_2'}(k_2)a^\dagger_{\mu_3'}(k_3)\left|\Omega\right\rangle\\
&-12\pi i\int_{k_1'k_2'k_1k_2k_3}\varphi(k_1)\varphi(k_2)\varphi(k_3)T^{(2,C)}_{\mu_1'k_1',\mu_2'k_2',\mu_1k_1,\mu_2k_2}(k_1+k_2)\delta(k_1'+k_2'-k_1-k_2)S^{(1)}_{\mu_3';1}(k_3)\\
&\times a^\dagger_{\mu_1'}(k_1')a^\dagger_{\mu_2'}(k_2')a^\dagger_{\mu_3'}(k_3)\left|\Omega\right\rangle\\
&-12\pi i\left(\frac{2\pi}{L}\right)^{3/2}\int_{k_1'k_2'k_3'}Q(k_1',k_2',k_3')\delta(k_1'+k_2'+k_3')a^\dagger_{\mu_1'}(k_1')a^\dagger_{\mu_2'}(k_2')a^\dagger_{\mu_3'}(k_3')\left|\Omega\right\rangle\Bigg),
\end{aligned}
\tag{7.139}
$$

where we have introduced the following symmetrized version of the connected three-phonon transition operator

$$
\begin{aligned}
Q(k_1',k_2',k_3') = \frac{1}{6}\Big[&T^{(3,C)}_{\mu_1'k_1',\mu_2'k_2',\mu_3'k_3',10,10,10}(0)+T^{(3,C)}_{\mu_1'k_1',\mu_3'k_3',\mu_2'k_2',10,10,10}(0)+T^{(3,C)}_{\mu_3'k_3',\mu_2'k_2',\mu_1'k_1',10,10,10}(0)\\
&+T^{(3,C)}_{\mu_3'k_3',\mu_1'k_1',\mu_2'k_2',10,10,10}(0)+T^{(3,C)}_{\mu_2'k_2',\mu_1'k_1',\mu_3'k_3',10,10,10}(0)+T^{(3,C)}_{\mu_2'k_2',\mu_3'k_3',\mu_1'k_1',10,10,10}(0)\Big].
\end{aligned}
\tag{7.140}
$$

Here we have suppressed the dependence of $Q(k_1', k_2', k_3')$ on $\{\mu'\}$ since in the giant atom model the coupling constants are independent of the channel index. Now we consider

$$a_{\mu''}(\tau_3)a_{\mu'}(\tau_2)a_{\mu}(\tau_1)\mathcal{S}_3\left|\Phi_1^{(3)}\right\rangle = \frac{\sqrt{6}}{L^{3/2}}S^{(1)}_{\mu'',1}(0)S^{(1)}_{\mu',1}(0)S^{(1)}_{\mu,1}(0)\Bigg(1-4\pi i\Bigg[\frac{I^{(1)}_{\mu'',\mu'}(\tau_3-\tau_2)}{S^{(1)}_{\mu'',1}(0)S^{(1)}_{\mu',1}(0)} + \frac{I^{(1)}_{\mu,\mu'}(\tau_2-\tau_1)}{S^{(1)}_{\mu,1}(0)S^{(1)}_{\mu',1}(0)} + \frac{I^{(1)}_{\mu'',\mu}(\tau_3-\tau_1)}{S^{(1)}_{\mu'',1}(0)S^{(1)}_{\mu,1}(0)}\Bigg] - 12\pi i\frac{I^{(2)}(\tau_3-\tau_1,\tau_2-\tau_1)}{S^{(1)}_{\mu'',1}(0)S^{(1)}_{\mu',1}(0)S^{(1)}_{\mu,1}(0)}\Bigg), \quad (7.141)$$

where the following functions were defined

$$I^{(1)}_{\mu',\mu}(t_1) = \int_k e^{ikt_1}M_{\mu',\mu}(k), \quad (7.142)$$

$$I^{(2)}(t_2,t_1) = \int_{k,q} e^{iqt_2}e^{ikt_1}Q(-k-q,k,q), \quad (7.143)$$

where $M_{\mu,\mu'}(k) = (T^{(2,C)}_{\mu' k,\mu-k,10,10}(0) + T^{(2,C)}_{\mu-k,\mu' k,10,10}(0))/2$, as before. By introducing the following variables $\tau' = \tau_3 - \tau_1$, $\tau = \tau_2 - \tau_1$, we can immediately write down the normalized third order coherence function to the lowest order in φ as

$$C^{(3)}_{\mu'',\mu',\mu}(t',t) = \left|1-4\pi i\left[\frac{I^{(1)}_{\mu'',\mu'}(t'-t)}{S^{(1)}_{\mu'',1}(0)S^{(1)}_{\mu',1}(0)} + \frac{I^{(1)}_{\mu,\mu'}(t)}{S^{(1)}_{\mu,1}(0)S^{(1)}_{\mu',1}(0)} + \frac{I^{(1)}_{\mu'',\mu}(t')}{S^{(1)}_{\mu'',1}(0)S^{(1)}_{\mu;1}(0)}\right] - 12\pi i\frac{I^{(2)}(t',t)}{S^{(1)}_{\mu'',1}(0)S^{(1)}_{\mu',1}(0)S^{(1)}_{\mu,1}(0)}\right|^2. \quad (7.144)$$

7.5.3 Diagrammatic representation of the generic three-body transition operator

In this Appendix we start our analysis with equation (7.64). Taking matrix elements of (7.64) in the three-particle subspace we arrive at the following integral equation

$$\begin{aligned}
W^{(3,2)}_{s_1's_2',s_1s_2}(\epsilon) =& D^{(2)}_{s_1's_2',s_1s_2}(\epsilon)\\
&+[D^{(2)}_{s_1's_2',\bar{s}_2'\bar{s}_1'}(\epsilon) + D^{(2)}_{s_1's_2',\bar{s}_1'\bar{s}_2'}(\epsilon)]G^{(1)}(\epsilon-\omega_{\bar{s}_1'}-\omega_{\bar{s}_2'})W^{(3,2)}_{\bar{s}_1'\bar{s}_2',s_1s_2}(\epsilon)\\
&+D^{(2)}_{s_1's_2',\bar{s}_1'\bar{s}_2}(\epsilon)G^{(1)}(\epsilon-\omega_{\bar{s}_1'}-\omega_{\bar{s}_2})W^{(2,1)}_{\bar{s}_2,\bar{s}_2'}(\epsilon)G^{(1)}(\epsilon-\omega_{\bar{s}_1'}-\omega_{\bar{s}_2'})W^{(3,2)}_{\bar{s}_1'\bar{s}_2',s_1s_2}(\epsilon)\\
&+D^{(2)}_{s_1's_2',\bar{s}_1\bar{s}_1'}(\epsilon)G^{(1)}(\epsilon-\omega_{\bar{s}_1}-\omega_{\bar{s}_1'})W^{(2,1)}_{\bar{s}_1,\bar{s}_2'}(\epsilon)G^{(1)}(\epsilon-\omega_{\bar{s}_1'}-\omega_{\bar{s}_2'})W^{(3,2)}_{\bar{s}_1'\bar{s}_2',s_1s_2}(\epsilon)\\
&+D^{(2)}_{s_1's_2',\bar{s}_1\bar{s}_2'}(\epsilon)G^{(1)}(\epsilon-\omega_{\bar{s}_1}-\omega_{\bar{s}_2'})W^{(2,1)}_{\bar{s}_1,\bar{s}_1'}(\epsilon)G^{(1)}(\epsilon-\omega_{\bar{s}_1'}-\omega_{\bar{s}_2'})W^{(3,2)}_{\bar{s}_1'\bar{s}_2',s_1s_2}(\epsilon)\\
&+D^{(2)}_{s_1's_2',\bar{s}_2'\bar{s}_2}(\epsilon)G^{(1)}(\epsilon-\omega_{\bar{s}_2'}-\omega_{\bar{s}_2})W^{(2,1)}_{\bar{s}_2,\bar{s}_1'}(\epsilon)G^{(1)}(\epsilon-\omega_{\bar{s}_1'}-\omega_{\bar{s}_2'})W^{(3,2)}_{\bar{s}_1'\bar{s}_2',s_1s_2}(\epsilon)\\
&+D^{(2)}_{s_1's_2',\bar{s}_1\bar{s}_2}(\epsilon)G^{(1)}(\epsilon-\omega_{\bar{s}_1}-\omega_{\bar{s}_2})W^{(2,2)}_{\bar{s}_2\bar{s}_1,\bar{s}_2'\bar{s}_1'}(\epsilon)G^{(1)}(\epsilon-\omega_{\bar{s}_1'}-\omega_{\bar{s}_2'})W^{(3,2)}_{\bar{s}_1'\bar{s}_2',s_1s_2}(\epsilon)\\
&+D^{(2)}_{s_1's_2',\bar{s}_1\bar{s}_2}(\epsilon)G^{(1)}(\epsilon-\omega_{\bar{s}_1}-\omega_{\bar{s}_2})W^{(2,2)}_{\bar{s}_1\bar{s}_2,\bar{s}_2'\bar{s}_1'}(\epsilon)G^{(1)}(\epsilon-\omega_{\bar{s}_1'}-\omega_{\bar{s}_2'})W^{(3,2)}_{\bar{s}_1'\bar{s}_2',s_1s_2}(\epsilon)\\
&+D^{(2)}_{s_1's_2',\bar{s}_1\bar{s}_2}(\epsilon)G^{(1)}(\epsilon-\omega_{\bar{s}_1}-\omega_{\bar{s}_2})W^{(2,2)}_{\bar{s}_1\bar{s}_2,\bar{s}_1'\bar{s}_2'}(\epsilon)G^{(1)}(\epsilon-\omega_{\bar{s}_1'}-\omega_{\bar{s}_2'})W^{(3,2)}_{\bar{s}_1'\bar{s}_2',s_1s_2}(\epsilon)\\
&+D^{(2)}_{s_1's_2',\bar{s}_1\bar{s}_2}(\epsilon)G^{(1)}(\epsilon-\omega_{\bar{s}_1}-\omega_{\bar{s}_2})W^{(2,2)}_{\bar{s}_2'\bar{s}_1,\bar{s}_1'\bar{s}_2'}(\epsilon)G^{(1)}(\epsilon-\omega_{\bar{s}_1'}-\omega_{\bar{s}_2'})W^{(3,2)}_{\bar{s}_1'\bar{s}_2',s_1s_2}(\epsilon), \quad (7.145)
\end{aligned}$$

where the projection of $\mathcal{D}$ onto the 2-particle subspace is given by

$$\begin{aligned}
&D^{(2)}_{s_1's_2',s_1s_2}(\epsilon)\\
&= v_{s_1'}G_0(\epsilon-\omega_{s_2'})v_{s_2'}G^{(1)}(\epsilon)v^\dagger_{s_2}G_0(\epsilon-\omega_{s_2})v^\dagger_{s_1}. \quad (7.146)
\end{aligned}$$

Baring this in mind we make the following ansatz

$$\begin{aligned}
&W^{(3,2)}_{s_1's_2',s_1s_2}(\epsilon)\\
&= v_{s_1'}G_0(\epsilon-\omega_{s_2'})v_{s_2'}G^{(3,0)}(\epsilon)v^\dagger_{s_2}G_0(\epsilon-\omega_{s_2})v^\dagger_{s_1}. \quad (7.147)
\end{aligned}$$

This, in turn, leads to the following Dyson equation

$$G^{(3,0)}(\epsilon) = G^{(1)}(\epsilon) + G^{(1)}(\epsilon)\Sigma^{(3,0)}(\epsilon)G^{(3,0)}(\epsilon), \tag{7.148}$$

where the self-energy in the three-excitation subspace is given by

$$\begin{aligned}
\Sigma^{(3,0)}(\epsilon) =&[v^\dagger_{s'_1}G_0(\epsilon-\omega_{s'_1})v^\dagger_{s'_2} + v^\dagger_{s'_2}G_0(\epsilon-\omega_{s'_2})v^\dagger_{s'_1}]G^{(1)}(\epsilon-\omega_{s'_1}-\omega_{s'_2})v_{s'_1}G_0(\epsilon-\omega_{s'_2})v_{s'_2}\\
&+v^\dagger_{s_2}G_0(\epsilon-\omega_{s_2})v^\dagger_{s'_1}G^{(1)}(\epsilon-\omega_{s'_1}-\omega_{s_2})W^{(2,1)}_{s_2,s'_2}(\epsilon)G^{(1)}(\epsilon-\omega_{s'_1}-\omega_{s'_2})v_{s'_1}G_0(\epsilon-\omega_{s'_2})v_{s'_2}\\
&+v^\dagger_{s'_1}G_0(\epsilon-\omega_{s'_1})v^\dagger_{s_1}G^{(1)}(\epsilon-\omega_{s_1}-\omega_{s'_1})W^{(2,1)}_{s_1,s'_2}(\epsilon)G^{(1)}(\epsilon-\omega_{s'_1}-\omega_{s'_2})v_{s'_1}G_0(\epsilon-\omega_{s'_2})v_{s'_2}\\
&+v^\dagger_{s'_2}G_0(\epsilon-\omega_{s'_2})v^\dagger_{s_1}G^{(1)}(\epsilon-\omega_{s_1}-\omega_{s'_2})W^{(2,1)}_{s_1,s'_1}(\epsilon)G^{(1)}(\epsilon-\omega_{s'_1}-\omega_{s'_2})v_{s'_1}G_0(\epsilon-\omega_{s'_2})v_{s'_2}\\
&+v^\dagger_{s_2}G_0(\epsilon-\omega_{s_2})v^\dagger_{s'_2}G^{(1)}(\epsilon-\omega_{s'_2}-\omega_{s_2})W^{(2,1)}_{s_2,s'_1}(\epsilon)G^{(1)}(\epsilon-\omega_{s'_1}-\omega_{s'_2})v_{s'_1}G_0(\epsilon-\omega_{s'_2})v_{s'_2}\\
&+v^\dagger_{s_2}G_0(\epsilon-\omega_{s_2})v^\dagger_{s_1}G^{(1)}(\epsilon-\omega_{s_1}-\omega_{s_2})W^{(2,2)}_{s_2s_1,s'_2s'_1}(\epsilon)G^{(1)}(\epsilon-\omega_{s'_1}-\omega_{s'_2})v_{s'_1}G_0(\epsilon-\omega_{s'_2})v_{s'_2}\\
&+v^\dagger_{s_2}G_0(\epsilon-\omega_{s_2})v^\dagger_{s_1}G^{(1)}(\epsilon-\omega_{s_1}-\omega_{s_2})W^{(2,2)}_{s_1s_2,s'_2s'_1}(\epsilon)G^{(1)}(\epsilon-\omega_{s'_1}-\omega_{s'_2})v_{s'_1}G_0(\epsilon-\omega_{s'_2})v_{s'_2}\\
&+v^\dagger_{s_2}G_0(\epsilon-\omega_{s_2})v^\dagger_{s_1}G^{(1)}(\epsilon-\omega_{s_1}-\omega_{s_2})W^{(2,2)}_{s_1s_2,s'_1s'_2}(\epsilon)G^{(1)}(\epsilon-\omega_{s'_1}-\omega_{s'_2})v_{s'_1}G_0(\epsilon-\omega_{s'_2})v_{s'_2}\\
&+v^\dagger_{s_2}G_0(\epsilon-\omega_{s_2})v^\dagger_{s_1}G^{(1)}(\epsilon-\omega_{s_1}-\omega_{s_2})W^{(2,2)}_{s_2s_1,s'_1s'_2}(\epsilon)G^{(1)}(\epsilon-\omega_{s'_1}-\omega_{s'_2})v_{s'_1}G_0(\epsilon-\omega_{s'_2})v_{s'_2}.
\end{aligned} \tag{7.149}$$

Let us now consider the expression (7.65) for the transition operator. Concentrating on the three-photon subspace we obtain

$$T^{(3,3)}_{s'_1s'_2s'_3,s_1s_2s_3}(\epsilon) = \left\langle g \,\middle|\, v_{s'_1}G^{(1)}(\epsilon-\omega_{s'_2}-\omega_{s'_3})[W^{(2,2)}_{s'_2s'_3,s_2s_3}(\epsilon) + V^{(3,2)}_{s'_2s'_3}(\epsilon)G^{(3,0)}(\epsilon)\overline{V}^{(3,2)}_{s_2s_3}(\epsilon)]G^{(1)}(\epsilon-\omega_{s_2}-\omega_{s_3})v^\dagger_{s_1} \,\middle|\, g\right\rangle, \tag{7.150}$$

$$\begin{aligned}
V^{(3,2)}_{s'_1s'_2} =&v_{s'_1}G_0(\epsilon)v_{s'_2} + W^{(2,1)}_{s'_1,s}(\epsilon)G^{(1)}(\epsilon-\omega_s)v_sG_0(\epsilon)v_{s'_2} + W^{(2,1)}_{s'_1,s}(\epsilon)G^{(1)}(\epsilon-\omega_s)v_{s'_2}G_0(\epsilon-\omega_s)v_s\\
&+W^{(2,2)}_{s'_1s'_2,\bar{s}'_1\bar{s}'_2}(\epsilon)G^{(1)}(\epsilon-\omega_{\bar{s}'_1}-\omega_{\bar{s}'_2})v_{\bar{s}'_1}G_0(\epsilon-\omega_{\bar{s}'_2})v_{\bar{s}'_2}\\
&+W^{(2,2)}_{s'_1s'_2,\bar{s}'_2\bar{s}'_1}(\epsilon)G^{(1)}(\epsilon-\omega_{\bar{s}'_1}-\omega_{\bar{s}'_2})v_{\bar{s}'_1}G_0(\epsilon-\omega_{\bar{s}'_2})v_{\bar{s}'_2},
\end{aligned} \tag{7.151}$$

$$\begin{aligned}
\overline{V}^{(3,2)}_{s_1s_2} =&v_{s_1}G_0(\epsilon)v_{s_2} + v^\dagger_{s_1}G_0(\epsilon)v^\dagger_{s'}G^{(1)}(\epsilon-\omega_{s'})W^{(2,1)}_{s',s_2}(\epsilon) + v^\dagger_{s'}G_0(\epsilon-\omega_{s'})v^\dagger_{s_1}G^{(1)}(\epsilon-\omega_{s'})W^{(2,1)}_{s',s_2}(\epsilon)\\
&+v^\dagger_{\bar{s}_2}G_0(\epsilon-\omega_{\bar{s}_2})v^\dagger_{\bar{s}_1}G^{(1)}(\epsilon-\omega_{\bar{s}_1}-\omega_{\bar{s}_2})W^{(2,2)}_{\bar{s}_1\bar{s}_2,s_1s_2}(\epsilon)\\
&+v^\dagger_{\bar{s}_2}G_0(\epsilon-\omega_{\bar{s}_2})v^\dagger_{\bar{s}_1}G^{(1)}(\epsilon-\omega_{\bar{s}_1}-\omega_{\bar{s}_2})W^{(2,2)}_{\bar{s}_2\bar{s}_1,s_1s_2}(\epsilon).
\end{aligned} \tag{7.152}$$

Now, our goal is to rewrite the renormalized two-particle emission $V_{s'_1s'_2}$ and absorption $\overline{V}_{s_1s_2}$ vertices, as well as the self-energy in three-excitation subspace $\Sigma^{(3,3)}$ in terms of full Green's and vertex functions, as it is presented in the main text.

First, we note the following identity

$$\begin{aligned}
&v_{s'_1}G_0(\epsilon)v_{s'_2} + W^{(2,1)}_{s'_1,s}(\epsilon)G^{(1)}(\epsilon-\omega_s)v_sG_0(\epsilon)v_{s'_2} = v_{s'_1}G_0(\epsilon)v_{s'_2} + W^{(2,1,i)}_{s'_1,s}(\epsilon)G^{(1)}(\epsilon-\omega_s)v_sG_0(\epsilon)v_{s'_2}\\
&+V^{(2,1)}_{s'_1}(\epsilon)G^{(2,0)}(\epsilon)\overline{V}^{(2,1)}_s(\epsilon)G^{(1)}(\epsilon-\omega_s)v_sG_0(\epsilon)v_{s'_2} = v_{s'_1}G_0(\epsilon)v_{s'_2} + W^{(2,1,i)}_{s'_1,s}G^{(1)}(\epsilon-\omega_s)v_sG_0(\epsilon)v_{s'_2}\\
&+V^{(2,1)}_{s'_1}(\epsilon)G^{(2,0)}(\epsilon)\Sigma^{(2,0)}G_0(\epsilon)v_{s'_2} = v_{s'_1}G_0(\epsilon)v_{s'_2} + W^{(2,1,i)}_{s'_1,s}(\epsilon)G^{(1)}(\epsilon-\omega_s)v_sG_0(\epsilon)v_{s'_2}\\
&+V^{(2,1)}_{s'_1}(\epsilon)[G^{(2,0)}(\epsilon) - G_0(\epsilon)]v_{s'_2} = V^{(2,1)}_{s'_1}(\epsilon)G^{(2,0)}(\epsilon)v_{s'_2}.
\end{aligned} \tag{7.153}$$

Analogously

$$\begin{aligned}
&v^\dagger_{s_1}G_0(\epsilon)v^\dagger_{s_2} + v^\dagger_{s_1}G_0(\epsilon)v^\dagger_{s'}G^{(1)}(\epsilon-\omega_{s'})W^{(2,1)}_{s',s_2}(\epsilon)\\
&= v^\dagger_{s_1}G^{(2,0)}(\epsilon)\overline{V}^{(2,1)}_{s_2}(\epsilon).
\end{aligned} \tag{7.154}$$

Analysing the structure of equations satisfied by $W^{(2,1)}$ and $W^{(2,2)}$ one easily concludes that

$$\begin{aligned}
W^{(2,2)}_{s'_1s'_2,s_1s_2}(\epsilon) =& W^{(2,1)}_{s'_1,s_1}(\epsilon)G^{(1)}(\epsilon)W^{(2,1)}_{s'_2,s_2}(\epsilon)\\
&+ W^{(2,1)}_{s'_1,s}(\epsilon)G^{(1)}(\epsilon-\omega_s)W^{(2,2)}_{s'_2s,s_1s_2}(\epsilon),
\end{aligned} \tag{7.155}$$

$$W^{(2,2)}_{s_1's_2',s_1s_2}(\epsilon) = W^{(2,1)}_{s_1',s_1}(\epsilon)G^{(1)}(\epsilon)W^{(2,1)}_{s_2',s_2}(\epsilon) + W^{(2,2)}_{s_1's_2',ss_1}(\epsilon)G^{(1)}(\epsilon-\omega_s)W^{(2,1)}_{s,s_2}(\epsilon). \tag{7.156}$$

Multiplying (7.155) and (7.156) by $G^{(1)}(\epsilon)v_{s_2}G_0(\epsilon)v_{s_1}$ from the right and by $v^\dagger_{s_2'}G_0(\epsilon)v^\dagger_{s_1'}G^{(1)}(\epsilon)$ from the left respectively and contracting the relevant indices, we obtain

$$W^{(2,2)}_{s_1's_2',s_1s_2}(\epsilon)G^{(1)}(\epsilon-\omega_{s_1}-\omega_{s_2})v_{s_2}G_0(\epsilon-\omega_{s_2})v_{s_1} = W^{(2,1)}_{s_1',s_1}(\epsilon)G^{(1)}(\epsilon-\omega_{s_1})[V^{(2,1)}_{s_2'}(\epsilon)G^{(2,0)}(\epsilon-\omega_{s_1})v_{s_1} - v_{s_2'}G_0(\epsilon-\omega_{s_1})v_{s_1}] + W^{(2,1)}_{s_1',s}(\epsilon)G^{(1)}(\epsilon-\omega_s)W^{(2,2)}_{s_2's,s_1s_2}(\epsilon)G^{(1)}(\epsilon-\omega_{s_1}-\omega_{s_2})v_{s_2}G_0(\epsilon-\omega_{s_1})v_{s_1}, \tag{7.157}$$

$$v^\dagger_{s_2'}G_0(\epsilon-\omega_{s_2'})v^\dagger_{s_1'}G^{(1)}(\epsilon-\omega_{s_1'}-\omega_{s_2'})W^{(2,2)}_{s_1's_2',s_1s_2}(\epsilon) = [v^\dagger_{s_2'}G^{(2,0)}(\epsilon-\omega_{s_2'})\overline{V}^{(2,1)}_{s_1}(\epsilon) - v^\dagger_{s_2'}G_0(\epsilon-\omega_{s_2'})v^\dagger_{s_1}] \times G^{(1)}(\epsilon-\omega_{s_2'})W^{(2,1)}_{s_2',s_2} + v^\dagger_{s_2'}G_0(\epsilon-\omega_{s_2'})v^\dagger_{s_1'}G^{(1)}(\epsilon-\omega_{s_1'}-\omega_{s_2'})W^{(2,2)}_{s_1's_2',ss_1}G^{(1)}(\epsilon-\omega_s)W^{(2,1)}_{s,s_2}(\epsilon). \tag{7.158}$$

Now, defining the following objects

$$K^{(d)}_{s_1's_2'}(\epsilon) = W^{(2,2)}_{s_1's_2',s_1s_2}(\epsilon)G^{(1)}(\epsilon-\omega_{s_2}-\omega_{s_1})v_{s_2}G_0(\epsilon-\omega_{s_1})v_{s_1} + W^{(2,1)}_{s_1',s_1}(\epsilon)G^{(1)}(\epsilon-\omega_{s_1})v_{s_2'}G_0(\epsilon-\omega_{s_1})v_{s_1}, \tag{7.159}$$

$$\overline{K}^{(d)}_{s_1s_2}(\epsilon) = v^\dagger_{s_2'}G_0(\epsilon-\omega_{s_2'})v^\dagger_{s_1'}G^{(1)}(\epsilon-\omega_{s_1'}-\omega_{s_2'})W^{(2,2)}_{s_1's_2',s_1s_2}(\epsilon) + v^\dagger_{s_2'}G_0(\epsilon-\omega_{s_2'})v^\dagger_{s_1}G^{(1)}(\epsilon-\omega_{s_2'})W^{(2,1)}_{s_2',s_2}(\epsilon), \tag{7.160}$$

we establish the following equations

$$K^{(d)}_{s_1's_2'}(\epsilon) = W^{(2,1)}_{s_1',s_1}(\epsilon)G^{(1)}(\epsilon-\omega_{s_1})V^{(2,1)}_{s_2'}(\epsilon-\omega_{s_1})G^{(2,0)}(\epsilon-\omega_{s_1})v_{s_1} + W^{(2,1)}_{s_1',s}(\epsilon)G^{(1)}(\epsilon-\omega_s)[K^{(d)}_{s_2's}(\epsilon) - W^{(2,1)}_{s_2',s_1}(\epsilon-\omega_s)G^{(1)}(\epsilon-\omega_{s_1}-\omega_s)v_sG_0(\epsilon-\omega_{s_1})v_{s_1}], \tag{7.161}$$

$$\overline{K}^{(d)}_{s_1s_2}(\epsilon) = v^\dagger_{s_2'}G^{(2,0)}(\epsilon-\omega_{s_2'})\overline{V}^{(2,1)}_{s_1}(\epsilon-\omega_{s_2'})G^{(1)}(\epsilon-\omega_{s_2'})W^{(1,0)}_{s_2',s_2}(\epsilon) + [\overline{K}^{(d)}_{ss_1}(\epsilon) - v^\dagger_{s_2'}G_0(\epsilon-\omega_{s_2'})v^\dagger_sG^{(1)}(\epsilon-\omega_{s_2'}-\omega_s)W^{(2,1)}_{s_2',s_1}(\epsilon-\omega_s)]G^{(1)}(\epsilon-\omega_s)W^{(2,1)}_{s,s_2}(\epsilon). \tag{7.162}$$

Analogously multiplying (7.155) and (7.156) by $G^{(1)}(\epsilon)v_{s_1}G_0(\epsilon)v_{s_2}$ from the right and by $v^\dagger_{s_1'}G_0(\epsilon)v^\dagger_{s_2'}G^{(1)}(\epsilon)$ from the left respectively, contracting the $s_{1,2}$ indices, and defining

$$K^{(e)}_{s_1's_2'}(\epsilon) = W^{(2,2)}_{s_1's_2',s_1s_2}(\epsilon)G^{(1)}(\epsilon-\omega_{s_1}-\omega_{s_2})v_{s_1}G_0(\epsilon-\omega_{s_2})v_{s_2}, \tag{7.163}$$

$$\overline{K}^{(e)}_{s_1s_2}(\epsilon) = v^\dagger_{s_1'}G_0(\epsilon-\omega_{s_1'})v^\dagger_{s_2'}G^{(1)}(\epsilon-\omega_{s_1'}-\omega_{s_2'})W^{(2,2)}_{s_1's_2',s_1s_2}(\epsilon), \tag{7.164}$$

we deduce

$$K^{(e)}_{s_1's_2'}(\epsilon) = W^{(2,1)}_{s_1',s_1}(\epsilon)G^{(1)}(\epsilon-\omega_{s_1})W^{(2,1)}_{s_2',s_2}(\epsilon-\omega_{s_1})G^{(1)}(\epsilon-\omega_{s_1}-\omega_{s_2})v_{s_1}G_0(\epsilon-\omega_{s_2})v_{s_2} + W^{(2,1)}_{s_1',s}(\epsilon)G^{(1)}(\epsilon-\omega_s)K^{(e)}_{s_2's}(\epsilon), \tag{7.165}$$

$$\overline{K}^{(e)}_{s_1s_2}(\epsilon) = v^\dagger_{s_1'}G_0(\epsilon-\omega_{s_1'})v^\dagger_{s_2'}G^{(1)}(\epsilon-\omega_{s_1'}-\omega_{s_2'})W^{(2,1)}_{s_1',s_1}(\epsilon-\omega_{s_2'})G^{(1)}(\epsilon-\omega_{s_2'})W^{(2,1)}_{s_2',s_2}(\epsilon) + \overline{K}^{(e)}_{ss_1}(\epsilon)G^{(1)}(\epsilon-\omega_s)W^{(2,1)}_{s,s_2}(\epsilon). \tag{7.166}$$

Further we define

$$K_{s_1' s_2'}(\epsilon) = K^{(d)}_{s_1' s_2'}(\epsilon) + K^{(e)}_{s_1' s_2'}(\epsilon), \tag{7.167}$$

$$\overline{K}_{s_1 s_2}(\epsilon) = \overline{K}^{(d)}_{s_1 s_2}(\epsilon) + \overline{K}^{(e)}_{s_1 s_2}(\epsilon). \tag{7.168}$$

With these definitions it is easy to show that the two-particle emission/absorption vertices are given by

$$V^{(3,2)}_{s_1' s_2'}(\epsilon) = V^{(2,1)}_{s_1'}(\epsilon) G^{(2,0)}(\epsilon) V^{(2,1)}_{s_2'}(\epsilon) + \tilde{K}_{s_1' s_2'}(\epsilon), \tag{7.169}$$

$$\overline{V}^{(3,2)}_{s_1 s_2}(\epsilon) = \overline{V}^{(2,1)}_{s_1}(\epsilon) G^{(2,0)}(\epsilon) \overline{V}^{(2,1)}_{s_2}(\epsilon) + \tilde{\overline{K}}_{s_1 s_2}(\epsilon), \tag{7.170}$$

where

$$\begin{aligned} \tilde{K}_{s_1' s_2'}(\epsilon) &= K_{s_1' s_2'}(\epsilon) \\ &- V^{(2,1)}_{s_1'}(\epsilon) G^{(2,0)}(\epsilon) W^{(2,1,i)}_{s_2', s_1}(\epsilon) G^{(1)}(\epsilon - \omega_{s_1}) v_{s_1}, \end{aligned} \tag{7.171}$$

$$\begin{aligned} \tilde{\overline{K}}_{s_1 s_2}(\epsilon) &= \overline{K}_{s_1 s_2}(\epsilon) \\ &- v^{\dagger}_{s_2'} G^{(1)}(\epsilon - \omega_{s_2'}) W^{(2,1,i)}_{s_2', s_1}(\epsilon) G^{(2,0)}(\epsilon) \overline{V}^{(2,1)}_{s_2}(\epsilon), \end{aligned} \tag{7.172}$$

obey the following integral equations

$$\begin{aligned} \tilde{K}_{s_1' s_2'}(\epsilon) =& W^{(2,1)}_{s_1', s}(\epsilon) G^{(1)}(\epsilon - \omega_s) V^{(2,1)}_{s_2'}(\epsilon - \omega_s) G^{(2,0)}(\epsilon - \omega_s) V^{(2,1)}_{s}(\epsilon) - V^{(2,1)}_{s_1'}(\epsilon) G^{(2,0)}(\epsilon) W^{(2,1,i)}_{s_2', s}(\epsilon) G^{(1)}(\epsilon - \omega_s) v_s \\ &+ W^{(2,1)}_{s_1, s}(\epsilon) G^{(1)}(\epsilon - \omega_s) \tilde{K}_{s_2' s}(\epsilon), \end{aligned} \tag{7.173}$$

$$\begin{aligned} \tilde{\overline{K}}_{s_1 s_2}(\epsilon) =& \overline{V}^{(2,1)}_{s}(\epsilon) G^{(2,0)}(\epsilon - \omega_s) V^{(2,1)}_{s_1}(\epsilon - \omega_s) G^{(1)}(\epsilon - \omega_s) W^{(2,1)}_{s, s_2}(\epsilon) - v^{\dagger}_{s} G^{(1)}(\epsilon - \omega_s) W^{(2,1,i)}_{s, s_1}(\epsilon) G^{(2,0)}(\epsilon) \overline{V}^{(2,1)}_{s_2}(\epsilon) \\ &+ \tilde{\overline{K}}_{s s_1}(\epsilon) G^{(1)}(\epsilon - \omega_s) W^{(2,1)}_{s, s_2}(\epsilon). \end{aligned} \tag{7.174}$$

Using equations (7.169), (7.170) together with (7.173), (7.174), we finally arrive at the following equations

$$\begin{aligned} V^{(3,2)}_{s_1' s_2'}(\epsilon) &= V^{(2,1)}_{s_1'}(\epsilon) G^{(2,0)}(\epsilon) v_{s_2'} \\ &+ W^{(2,1)}_{s_1', s}(\epsilon) G^{(1)}(\epsilon - \omega_s) V^{(3,2)}_{s_2' s}(\epsilon), \end{aligned} \tag{7.175}$$

$$\begin{aligned} \overline{V}^{(3,2)}_{s_1 s_2}(\epsilon) &= v_{s_1} G^{(2,1)}(\epsilon) \overline{V}_{s_2}(\epsilon) \\ &+ \overline{V}^{(3,2)}_{s s_1}(\epsilon) G^{(1)}(\epsilon - \omega_s) W^{(2,1)}_{s, s_2}(\epsilon), \end{aligned} \tag{7.176}$$

which are precisely the equations (7.70) and (7.71) stated in the main text.

Now, we turn our attention to the self-energy bubble. Let us show that equations (7.68) and (7.69) hold

via direct substitution. One has

$$
\begin{aligned}
\Sigma^{(3,0)}(\epsilon) &= (v^\dagger_{s'_1} G_0(\epsilon-\omega_{s'_1}) v^\dagger_{s'_2} + v^\dagger_{s'_2} G_0(\epsilon-\omega_{s'_2}) v^\dagger_{s'_1}) G^{(1)}(\epsilon-\omega_{s'_1}-\omega_{s'_2}) V^{(3,2)}_{s'_1 s'_2}(\epsilon) \\
&= v^\dagger_{s'_2}[G^{(2,0)}(\epsilon-\omega_{s'_2}) - G_0(\epsilon-\omega_{s'_2})] v_{s'_2} - v^\dagger_{s'_1} G_0(\epsilon-\omega_{s'_1}) v^\dagger_s G^{(1)}(\epsilon-\omega_{s'_1}-\omega_s) v_{s'_1} G_0(\epsilon-\omega_s) v_s \\
&+ v^\dagger_{s'_1} G_0(\epsilon-\omega_{s'_1}) v^\dagger_{s'_2} G^{(1)}(\epsilon-\omega_{s'_1}-\omega_{s'_2}) V^{(2,1)}_{s'_1}(\epsilon-\omega_{s'_2}) G^{(2,0)}(\epsilon-\omega_{s'_2}) v_{s'_2} \\
&+ v^\dagger_{s'_1} G^{(2,0)}(\epsilon-\omega_{s'_1}) \overline{V}^{(2,1)}_{s}(\epsilon-\omega_{s'_1}) G^{(1)}(\epsilon-\omega_s-\omega_{s'_1}) v_{s'_1} G_0(\epsilon-\omega_s) v_s \\
&+ v^\dagger_{s'_2} G_0(\epsilon-\omega_{s'_2}) v^\dagger_{s'_1} G^{(1)}(\epsilon-\omega_{s'_1}-\omega_{s'_2}) W^{(2,1)}_{s'_2,s}(\epsilon-\omega_{s'_1}) G^{(1)}(\epsilon-\omega_{s'_1}-\omega_s) v_{s'_1} G_0(\epsilon-\omega_s) v_s \\
&+ v^\dagger_{s'_1} G_0(\epsilon-\omega_{s'_1}) v^\dagger_{s'_2} G^{(1)}(\epsilon-\omega_{s'_1}-\omega_{s'_2}) W^{(2,2)}_{s'_1 s'_2, s' s}(\epsilon) G^{(1)}(\epsilon-\omega_{s'}-\omega_s) v_{s'} G_0(\epsilon-\omega_s) v_s \\
&+ v^\dagger_{s'_1} G_0(\epsilon-\omega_{s'_1}) v^\dagger_{s'_2} G^{(1)}(\epsilon-\omega_{s'_1}-\omega_{s'_2}) W^{(2,2)}_{s'_1 s'_2, s s'}(\epsilon) G^{(1)}(\epsilon-\omega_{s'}-\omega_s) v_{s'} G_0(\epsilon-\omega_s) v_s \\
&+ v^\dagger_{s'_2} G_0(\epsilon-\omega_{s'_2}) v^\dagger_{s'_1} G^{(1)}(\epsilon-\omega_{s'_1}-\omega_{s'_2}) W^{(2,2)}_{s'_1 s'_2, s' s}(\epsilon) G^{(1)}(\epsilon-\omega_{s'}-\omega_s) v_{s'} G_0(\epsilon-\omega_s) v_s \\
&+ v^\dagger_{s'_2} G_0(\epsilon-\omega_{s'_2}) v^\dagger_{s'_1} G^{(1)}(\epsilon-\omega_{s'_1}-\omega_{s'_2}) W^{(2,2)}_{s'_1 s'_2, s s'}(\epsilon) G^{(1)}(\epsilon-\omega_{s'}-\omega_s) v_{s'} G_0(\epsilon-\omega_s) v_s, \qquad (7.177) \\
\Sigma^{(3,0)}(\epsilon) &= \overline{V}^{(3,2)}_{s_1 s_2} G^{(1)}(\epsilon-\omega_{s_1}-\omega_{s_2}) (v_{s_1} G_0(\epsilon-\omega_{s_2}) v_{s_2} + v_{s_2} G_0(\epsilon-\omega_{s_1}) v_{s_1}) \\
&= v^\dagger_{s_2}[G^{(2,0)}(\epsilon-\omega_{s_2}) - G_0(\epsilon-\omega_{s_2})] v_{s_2} - v^\dagger_{s'} G_0(\epsilon-\omega_{s'}) v^\dagger_{s_1} G^{(1)}(\epsilon-\omega_{s_1}-\omega_{s'}) v_{s'} G_0(\epsilon-\omega_{s_1}) v_{s_1} \\
&+ v^\dagger_{s'} G_0(\epsilon-\omega_{s'}) v^\dagger_{s_1} G^{(1)}(\epsilon-\omega_{s_1}-\omega_{s'}) V^{(2,1)}_{s'}(\epsilon-\omega_{s_1}) G^{(2,0)}(\epsilon-\omega_{s_1}) v_{s_1} \\
&+ v^\dagger_{s_2} G^{(2,0)}(\epsilon-\omega_{s_2}) \overline{V}^{(2,1)}_{s_1}(\epsilon-\omega_{s_2}) G^{(1)}(\epsilon-\omega_{s_1}-\omega_{s_2}) v_{s_2} G_0(\epsilon-\omega_{s_1}) v_{s_1} \\
&+ v^\dagger_{s'} G_0(\epsilon-\omega_{s'}) v^\dagger_{s_1} G^{(1)}(\epsilon-\omega_{s'}-\omega_{s_1}) W^{(2,1)}_{s',s_2}(\epsilon-\omega_{s_1}) G^{(1)}(\epsilon-\omega_{s_1}-\omega_{s_2}) v_{s_1} G_0(\epsilon-\omega_{s_2}) v_{s_2} \\
&+ v^\dagger_{s'} G_0(\epsilon-\omega_{s'}) v^\dagger_s G^{(1)}(\epsilon-\omega_s-\omega_{s'}) W^{(2,2)}_{ss',s_1 s_2}(\epsilon) G^{(1)}(\epsilon-\omega_{s_1}-\omega_{s_2}) v_{s_1} G_0(\epsilon-\omega_{s_2}) v_{s_2} \\
&+ v^\dagger_{s'} G_0(\epsilon-\omega_{s'}) v^\dagger_s G^{(1)}(\epsilon-\omega_s-\omega_{s'}) W^{(2,2)}_{s's,s_1 s_2}(\epsilon) G^{(1)}(\epsilon-\omega_{s_1}-\omega_{s_2}) v_{s_1} G_0(\epsilon-\omega_{s_2}) v_{s_2} \\
&+ v^\dagger_{s'} G_0(\epsilon-\omega_{s'}) v^\dagger_s G^{(1)}(\epsilon-\omega_s-\omega_{s'}) W^{(2,2)}_{ss',s_1 s_2}(\epsilon) G^{(1)}(\epsilon-\omega_{s_1}-\omega_{s_2}) v_{s_2} G_0(\epsilon-\omega_{s_1}) v_{s_1} \\
&+ v^\dagger_{s'} G_0(\epsilon-\omega_{s'}) v^\dagger_s G^{(1)}(\epsilon-\omega_s-\omega_{s'}) W^{(2,2)}_{s's,s_1 s_2}(\epsilon) G^{(1)}(\epsilon-\omega_{s_1}-\omega_{s_2}) v_{s_2} G_0(\epsilon-\omega_{s_1}) v_{s_1}. \qquad (7.178)
\end{aligned}
$$

This, together with identities (7.153) and (7.154) justifies the proposed representation of the self-energy.

7.5.4 Effect of the non-zero detuning

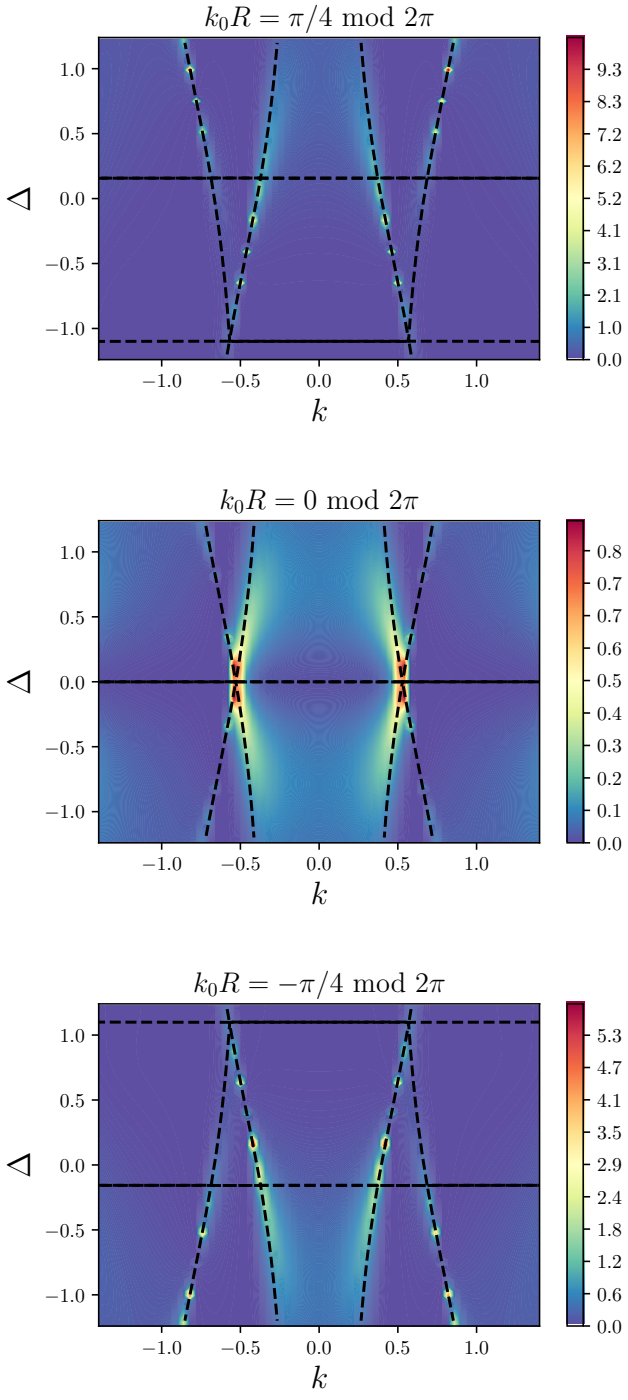

Figure 7.10: Spectral power density (scaled by $1/\Phi^2$) for of the giant atom model as a function of Δ, k for various values of k_0R and $\gamma R = 5$. Here the dashed black lines indicate the pole position of the dressed Green's function in the single excitation subspace.

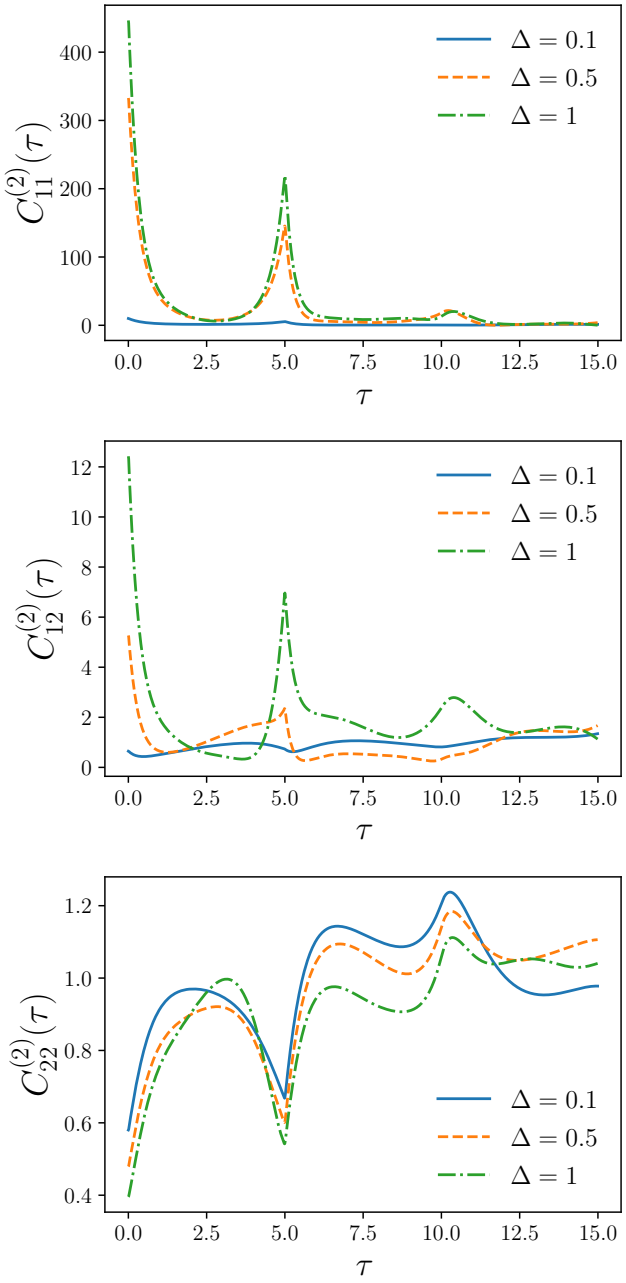

Figure 7.11: Second order coherence function for the system with $k_0R = 3\pi/11,\ \gamma R = 5,\ \Delta = 0.1,\ 0.5,\ 1.0$ (as before, the the second order coherence function is dimensionless).

In this appendix we analyse the effect on non-zero detuning of the atom from radiation on the observable quantities. In particular, we focus on the spectral power density and the second order coherence function. As it was discussed in Section 7.3.3, the sharp bound-state-like peaks in the line-shape of spectral density may be understood with a simple physical picture of an effective cavity. When one increases (or decreases) the detuning from zero value, one effectively changes the modes supported by the cavity and thus one expects the position of the peaks to be shifted. The precise location of the resonances in the spectral density as function of Δ and k for various values of k_0R is shown in Figure 7.10. As we can see, for non-zero dephasing $k_0R \neq 0$ the spectrum is not a symmetric function of Δ. For negative dephasing we find that emission into the zero modes is enhanced for a negatively detuned atom $\Delta < 0$, whereas the picture is opposite for positive k_0R. In general, we can clearly resolve a pair of sharp peaks which eventually merge together at certain values of parameters (e.g. $k_0R = \Delta = 0$). It is interesting to note that the location of this peaks is almost entirely determined by the poles of the dressed propagator in the single-excitation subspace $(G^{(1)}(k))^{-1} = k + \Delta + i\gamma(1 + e^{i(k+k_0)R}) = 0$. This equation is solved by

$$k = \pm i\frac{R\gamma - iR\Delta - W_n(-\gamma R e^{i(k_0-\Delta-i\gamma)R})}{R}, \tag{7.179}$$

where $W_n(z)$ is the n^{th} branch of the Lambert W-function, also known as the product logarithm. The real part of (7.179) with $n = 0, \pm 1$ is plotted as black dashed lines in Figure 7.10. The vertical lines in Figure

7.10 represent the discontinuous jumps of the Lambert function across the branch cut. As one may notice, the formula (7.179) is indeed in perfect agreement with numerical results.

Let us now consider the second order coherence function at non-zero detuning. Second order coherence for the system with $k_0R = 3\pi/11$, $\gamma R = 5$, $\Delta = 0.1,\ 0.5,\ 1.0$ is shown in Figure 7.11. We note that the presence of detuning does not affect the general trend of strong photon bunching in the first channel and their corresponding anti-bunching in the second one, as was discussed in Section 7.3.3. Neither the detuning affects the presence of non-differentiable peaks occurring at integer multiplies of delay time R.

7.6 PP21: Extra Theory about Method and Formalism

7.6.1 Scattering theory in waveguide with 1 qubit

In this section, we would like to make a detailed exposition of our general method by considering the simplest imaginable scenario of a single qubit coupled to a waveguide.

Идея разложения S-матрицы в диаграммы (????)

(???? почему такие разложения работают??? или всегда как-то можно разложить аналогично? пока не очень понимаю это.)

Разложение S-матрицы в диаграммы

In our formalism to solve the N_p-photon scattering problem, we shall determine the following matrix elements of the transition operator:

$$\begin{aligned}\langle N_p', g|\mathcal{T}^{(1)}(\epsilon)|N_p, g\rangle &= \langle N_p', g|\mathcal{V}\mathcal{G}(\epsilon)\mathcal{V}|N_p, g\rangle \\ &= \langle N_p', g|a^\dagger_{s_1'} v_{s_1'}\mathcal{G}(\epsilon)v^\dagger_{s_1} a_{s_1}|N_p, g\rangle \\ &= \sum_{n=0}^{\infty}\langle N_p', g|a^\dagger_{s_1'} v_{s_1'}\left(\mathcal{G}_0(\epsilon)\mathcal{V}\right)^n\cdot\mathcal{G}_0(\epsilon)v^\dagger_{s_1} a_{s_1}|N_p, g\rangle\end{aligned}$$

where the superscript (1) refers to the $N_q = 1$ waveguide QED and we have used the fact that $\langle N_p', g|\mathcal{V}|N_p, g\rangle = 0$. (??? еще раз отслежу, где это????)

Note that in what follows, whenever an argument of an object is omitted, we understand that its argument is ϵ, e.g., $\mathcal{G}^{(1)}$ stands for $\mathcal{G}^{(1)}(\epsilon)$, etc., however, when the argument of a given operator or vertex function is of importance, it would be explicitly stated (?? и когда это так? просто пишем или опускаем, все).

As it was mentioned above, due to RWA, only even terms (??? потом еще раз подумаю, почему????) contribute to the above geometric series, so that

$$\langle N_p', g|\mathcal{T}^{(1)}|N_p, g\rangle = \sum_{n=0}^{\infty}\langle N_p', g|a^\dagger_{s_1'} v_{s_1'}\left(\mathcal{G}_0\mathcal{V}\mathcal{G}_0\mathcal{V}\right)^n\mathcal{G}_0 v^\dagger_{s_1} a_{s_1}|N_p, g\rangle$$

Now, let us consider the $\mathcal{G}_0\mathcal{V}\mathcal{G}_0$ term in the brackets above:

$$\mathcal{V}\mathcal{G}_0\mathcal{V} = a^\dagger_{s'}v_{s'}\mathcal{G}_0 a^\dagger_s v_s + a^\dagger_{s'}v_{s'}\mathcal{G}_0 v^\dagger_s a_s + v^\dagger_{s'}a_{s'}\mathcal{G}_0 v^\dagger_s a_s + v^\dagger_{s'}a_{s'}\mathcal{G}_0 a^\dagger_s v_s.$$

Here the terms with two v's and two $v^\dagger$'s do not contribute (they are in fact zero) by the single-qubit nilpotency condition $v^2 = \left(v^\dagger\right)^2 = 0$. Among the "diagonal" terms, the only nonzero contribution comes from the $v^\dagger v$ term since the term $vv^\dagger$ annihilates the state $v^\dagger|g\rangle$ and gives zero whenever it is multiplied with $v^\dagger v$ term.

(???? я что-то про крос диаг член не понял, почему он обнуляет??? нужно про g додумать это!!)

So we have:

$$\langle N_p', g|\mathcal{T}^{(1)}|N_p, g\rangle = \sum_{n=0}^{\infty}\langle N_p', g|a^\dagger_{s_1'} v_{s_1'}\left(\mathcal{G}_0 v^\dagger_{s'}a_{s'}\mathcal{G}_0 a^\dagger_s v_s\right)^n\mathcal{G}_0 v^\dagger_{s_1} a_{s_1}|N_p, g\rangle.$$

With our Hamiltonian we can interchange order with photon operators by the rule:

$$\begin{aligned}&a_s f\left(\mathcal{H}_0\right) = f\left(\mathcal{H}_0+\omega_s\right)a_s \qquad \leftrightarrow \qquad a_s G_0\left(z\right) = G_0\left(\mathcal{H}_0-\omega_s\right)a_s \text{ for } G_0(z) := \frac{1}{z-\mathcal{H}_0}, \\ &f\left(\mathcal{H}_0\right)a^\dagger_s = a^\dagger_s f\left(\mathcal{H}_0-\omega_s\right),\end{aligned}$$

where f is some function admitting for the Maclaurin expansion $f(\mathcal{H}_0) = \sum_{n=0}^{\infty} f_n \mathcal{H}_0^n$. Proof is done by looking at n-th term of $\mathcal{H}_0$ without the qubit part, and knowing that

$$a_s \mathcal{H}_0 = [a_S, \mathcal{H}_0] + \mathcal{H}_0 a_s = \omega_{s2}[a_s, a_{s2}^\dagger a_{s2}] + \mathcal{H}_0 a_s \qquad [A, BC] = [A, B]C + B[A, C]$$
$$= \omega_{s2}\delta_{s,s2} a_s + \mathcal{H}_0 a_s = \omega_s a_s + \mathcal{H}_0 a_s = (\mathcal{H}_0 + \omega_s) a_s.$$

that

$$a_s \mathcal{H}_0^n = a_s \mathcal{H}_0 \mathcal{H}_0^{n-1} = (\mathcal{H}_0 + \omega_s)\, a_s \mathcal{H}_0 = (\mathcal{H}_0 + \omega_s)^n\, a_s$$

So

$$a_s f(\mathcal{H}_0) = \sum_{n=0}^{\infty} a_s \mathcal{H}_0^n f_n = \sum_{n=0}^{\infty} f_n (\mathcal{H}_0 + \omega_s)^n$$

For $G_0(z) = \frac{1}{z - \mathcal{H}_0}$ we have

$$f(\mathcal{H}_0 + \omega_s) = \frac{1}{z - (\mathcal{H}_0 + \omega_s)} = \frac{1}{(z - \omega_s) - H_0} \equiv G_0(z - \omega_s)$$

Also (??? докажу это позже)

$$f(\mathcal{H}_0)\, a_s^\dagger = a_s^\dagger f(\mathcal{H}_0 - \omega_s),$$

We see that

$$v_{s'}^\dagger a_{s'} \mathcal{G}_0(\epsilon) a_s^\dagger v_s = v_s^\dagger \mathcal{G}_0(\epsilon - \omega_s)\, v_s + a_{s'}^\dagger v_s^\dagger \mathcal{G}_0(\epsilon - \omega_{s'} - \omega_s)\, v_{s'} a_s,$$

where in the last term here the contraction of the indices s and s' is not assumed.

Let's define the "self-energy operator" $\Sigma^{(1)}$ and the "effective potential energy operator" $\mathcal{R}^{(1)}$ to write

$$v_{s'}^\dagger a_{s'} \mathcal{G}_0(\epsilon) a_s^\dagger v_s = \Sigma^{(1)}(\epsilon) + \mathcal{R}^{(1)}(\epsilon),$$

So they will be defined as:

$$\Sigma^{(1)}(\epsilon) := v_s^\dagger \mathcal{G}_0(\epsilon - \omega_s) v_s, \qquad \mathcal{R}^{(1)}(\epsilon) := a_{s'}^\dagger \mathcal{R}^{(1)}_{s',s}(\epsilon) a_s,$$
$$\mathcal{R}^{(1)}_{s',s}(\epsilon) := v_s^\dagger \mathcal{G}_0(\epsilon - \omega_{s'} - \omega_s) v_{s'}$$

so we have:

$$\langle N_p', g | \mathcal{T}^{(1)} | N_p, g \rangle = \langle N_p', g | a_{s_1'}^\dagger v_{s_1'} \frac{1}{1 - \mathcal{G}^{(1)} \mathcal{R}^{(1)}(\epsilon)} \mathcal{G}^{(1)} v_{s_1}^\dagger a_{s_1} | N_p, g \rangle,$$
$$\left(\mathcal{G}^{(1)}\right)^{-1}(\epsilon) := \mathcal{G}_0^{-1}(\epsilon) - \Sigma^{(1)}(\epsilon).$$

(??? тоже еще раз проделаю этот вывод!)

By defining the generating operator

$$\mathcal{W}^{(1)} := \mathcal{R}^{(1)}(\epsilon) + \mathcal{R}^{(1)}(\epsilon) \mathcal{G}^{(1)} \mathcal{R}^{(1)}(\epsilon)$$

we arrive at the following result: (????? додумаю, как мы второй член дальше получили???? ряды что ли какие-то тут суммируются???? мб иначе W определено должно быть?)

$$\langle N_p', g | \mathcal{T}^{(1)} | N_p, g \rangle = \langle N_p', g | a_{s_1'}^\dagger v_{s_1'} \mathcal{G}^{(1)} v_{s_1}^\dagger a_{s_1} | N_p, g \rangle + \langle N_p', g | a_{s_1'}^\dagger v_{s_1'} \mathcal{G}^{(1)} \mathcal{W}^{(1)} \mathcal{G}^{(1)} v_{s_1}^\dagger a_{s_1} | N_p, g \rangle.$$

By analyzing the structure of $\mathcal{R}^{(1)}$, we conclude that $\mathcal{W}^{(1)}$ admits for the following series representation (???? почем???)

$$\mathcal{W}^{(1)} = \sum_{n=1}^{\infty} a_{s_1'}^\dagger \dots a_{s_n'}^\dagger W^{(1,n)}_{s_1' \dots s_n', s_1 \dots s_n} a_{s_n} \dots a_{s_1},$$

where $\mathcal{W}^{(1,n)}$'s are the operator-valued functions (??? можно написать лучше, что за объект????), which depend only on $\epsilon - \mathcal{H}_0$ and $2n$ multi-indices $\{s_1', \dots, s_n', s_1, \dots, s_n\}$. Here and below, we have will use regular letters W, G, R instead of calligraphic ones to indicate that these objects are not operators but are rather their projections on the photonic vacuum (note that $W^{(1,n)}$'s are still acting as operators on the qubit space).

By inserting decomposition of $\mathcal{W}^{(1)}$ into the definition of $\mathcal{W}^{(1)}$ and taking the projections onto the particle subspaces (??? вот тут я не совсем понял, что за проекции??? мб догадаюсь, если подумаю???) we arrive at the following hierarchy of integral equations:

$$W^{(1,1)}_{s_1', s_1}(\epsilon) = R^{(1)}_{s_1', s_1}(\epsilon) + R^{(1)}_{s_1', s}(\epsilon) G^{(1)}(\epsilon - \omega_s) W^{(1,1)}_{s, s_1}(\epsilon),$$

$$W^{(1,2)}_{s'_1,s_1}(\epsilon) = \text{напишу потом}$$

$$\vdots$$

$$W^{(1,n)}_{s'_1,\ldots,s_1\ldots s_n}(\epsilon) = R^{(1)}_{s'_1,s_1}\left(\epsilon - \sum_{l=2}^{n}\omega_{s'_l}\right) G^{(1)}\left(\epsilon - \omega_{s_1} - \sum_{l=2}^{n}\omega_{s'_l}\right) W^{(1,n-1)}_{s'_2\ldots s'_n,s_2\ldots s_n}(\epsilon-\omega_{s_1}) +$$
$$+ R^{(1)}_{s'_1,s}\left(\epsilon - \sum_{l=2}^{n}\omega_{s'_l}\right) G^{(1)}\left(\epsilon - \omega_{s} - \sum_{l=2}^{n}\omega_{s'_l}\right) \left[W^{(1,n)}_{ss'_2\ldots s'_n,s_1\ldots s_n}(\epsilon) + \cdots + W^{(1,n)}_{s'_2\ldots s'_n s,s_1\ldots s_n}(\epsilon)\right].$$

(???? ну тут вообще место подумать!!! пока не полностью понимаю эту формулу, буду перевыводить ее сам еще раз)

Diagrammatic representation

The collection of the integral equations for $W^{(1,n)}_{s'_1,\ldots,s_1\ldots s_n}(\epsilon)$ may be conveniently represented diagrammatically. The objects will be as follows.

The $\Sigma^{(1)}$ bubble corresponds to the self-energy in a subspace of a single excitation used to define the dressed Green's function (represented by a double line) from the bare Green's function (depicted by the dashed line).

The $W^{(1,n)}$ bubbles (bubbles with $2n$-amputated legs) represent effective n-photon vertex functions describing effective interaction between n photons induced by nonlinearity. Bare absorption $v^\dagger$ and emission v vertices are represented by black dots with incoming and outgoing photon lines, respectively.

(see Fig. 1).

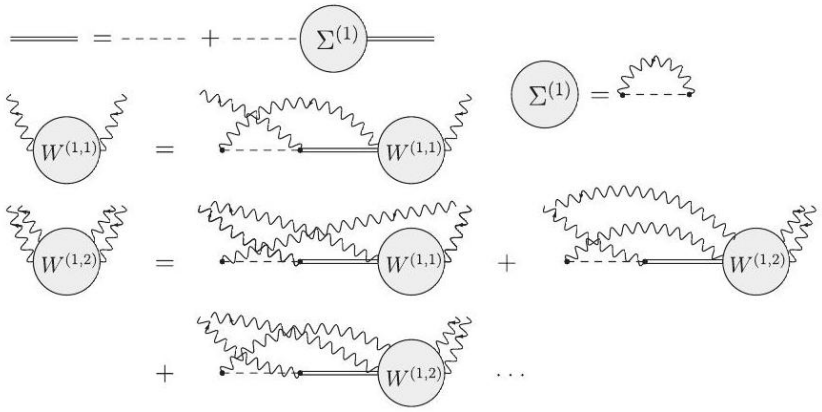

Figure 7.12: FIG. 1. Hierarchy of integral equations governing effective multiphoton vertex functions in $N_q = 1$ waveguide QED.

Diagrammatic rules may be formulated as follows:

1) To each dotted line associate the bare propagator $G_0(\epsilon)$.

2) To each wavy line with incoming (outgoing) arrow associate the bare absorption $v^\dagger$ (emission v) vertex.

3) Whenever two wavy lines are contracted together, one has to integrate over all momentum and sum over all channels.

4) When a given wavy line passes over the propagator, its argument has to be shifted by the frequency carried by this line [which is a direct consequence of the intertwining property (20)].

For example, for the self-energy diagram we have:

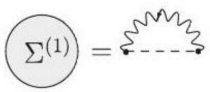

$$\rightarrow \qquad \Sigma^{(1)}(\epsilon) = v_s^\dagger G_0(\epsilon-\omega_s)v_s.$$

(???? окей, скоро про это подумаю.)

T-matrix again

Now having identified the equations defining the components of $\mathcal{W}^{(1)}$, we may express the transition operator as follows:

$$\mathcal{T}^{(1)}(\epsilon) = \sum_{n=1}^{\infty} T^{(1,n)}_{s'_1\dots s'_n,s_1\dots s_n}(\epsilon) a^\dagger_{s'_1}\dots a^\dagger_{s'_n} a_{s_n}\dots a_{s_1},$$

where we have defined the following functions:

$$T^{(1,1)}_{s'_1,s_1}(\epsilon) := \langle g|v_{s'_1} G^{(1)}(\epsilon) v^\dagger_{s_1}|g\rangle$$

$$\vdots$$

$$T^{(1,n>1)}_{s_1\dots\dots s'_n,s_1\dots s_n}(\epsilon) := \langle g|v_{s'_1} G^{(1)}\left(\epsilon - \sum_{l=2}^{n}\omega_{s'_l}\right) W^{(1,n-1)}_{s_2\dots s'_n,s_2\dots s_n}(\epsilon) G^{(1)}\left(\epsilon - \sum_{l=2}^{n}\omega_{s_l}\right) v^\dagger_{s_1}|g\rangle.$$

Note that we are working with the nonsymmetrized forms of operators and perform the symmetrization only when doing actual calculations. Also note that the dependence of $\mathcal{T}^{(1,n)}_{s'_1\dots s'_n,s_1\dots s_n}$ on $\omega_s a^\dagger_s a_s$ may be omitted taking into account normal ordering, when S matrix is going to be finally contracted with the initial state (???? где конкретно????), all of the T matrix components are going to be eventually projected onto the photonic vacuum and energies are going to be put on shell. Using the above representation of the transition operator we immediately deduce that the scattering operator takes the following form:

$$\mathcal{S} = 1_{\mathscr{H}} - 2\pi i \sum_{n=1}^{\infty} T^{(n)}_{s'_1\dots s'_n,s_1\dots s_n}\left(\sum_{l=1}^{n}\omega_{s_l}\right)\delta\left(\sum_{l=1}^{n}\omega_{s'_l} - \sum_{l=1}^{n}\omega_{s_l}\right) a^\dagger_{s'_1}\dots a^\dagger_{s'_n} a_{s_n}\dots a_{s_1}.$$

Practically, when one contracts the S matrix with the initial N_p-photon state, only the first N_p terms in the above series contribute (??? тоже пока не понял, а почему?). It is, however, beneficial to represent the S matrix in terms of the direct sum of N-body operators which act solely in the N-particle subspaces

$$\mathcal{S} = 1_{\mathscr{H}} \oplus \bigoplus_{n=1}^{\infty} \mathcal{S}_n$$

where $\mathcal{S}_n$ may be written as

$$\mathcal{S}_n = S^{(n)}_{s'_1\dots s'_n,s_1\dots s_n} a^\dagger_{s'_1}\dots a^\dagger_{s'_n} a_{s_n}\dots a_{s_1},$$

$$S^{(n)}_{s_1\dots s'_n,s_1\dots s_n} = \frac{1}{n!}\prod_{l=1}^{n}\delta_{s'_l,s_l} - 2\pi i \sum_{m=1}^{n}\frac{1}{(n-m)!} T^{(n)}_{s'_1\dots s'_m,s_1\dots s_m}\left(\sum_{l=1}^{n}\omega_{s_l}\right)\delta\left(\sum_{l=1}^{n}\omega_{s'_l} - \sum_{l=1}^{n}\omega_{s_l}\right)\prod_{r=m+1}^{n}\delta_{s'_r,s_r}.$$

Note that the combinatorial prefactors $\frac{1}{(n-m)!}, m \in \{0,\dots,n\}$, and additional δ functions $\delta_{s'_r,s_r}$ are chosen to take into account the excess number of $(n-m)!$ Wick contractions. (??? тоже пока не очень понял, что за эти свертки???)

7.6.2 Generalized cluster decomposition

Let's illustrate how the generalized cluster decomposition in waveguide QED, extensively studied in [76, 77] (??? напишу про это тоже, что там такое вообще изучалось??), naturally follows from the results of the previous section.

(????? тут я пока ничего не понимаю, просто дальше продолжается та же теория)

Theory

The cluster decomposition is a way of separating the elastic and inelastic contributions to the S matrix. The elastic contribution physically corresponds to the scattering channel in which all photons scatter coherently, i.e., conserve their energy individually in the scattering process. On the other hand, the inelastic contribution corresponds to the incoherent scattering. Thereby the photons redistribute their initial energy between one another via effective photon-photon interaction which is mediated by their interaction with nonlinear scatterers (e.g., qubits). In contrast, in the case of a linear scatter (e.g., a cavity mode), the effective photon-photon interaction is not generated, and the n-photon S matrix simply factors out into the product of n single-particle S matrices.

The first step towards the cluster decomposition of the multiphoton S matrices is the realization that the multiphoton vertex functions $W^{(1,n)}$ contain the disconnected components. These, in turn, arise from the projections of $R^{(1)}_{s',s}$ on the ground state of the scatterer thus resulting in the (quasi)elastic contributions $\propto \delta(\epsilon - \ldots)$ to $W^{(1,n)}$'s. Not only the separation of these contributions is crucial for the cluster decomposition but is of evident importance for both numerical and analytical treatment of the integral equations (29) and (30). It is the easiest to define the connected parts of the multiphoton vertex functions recursively.

First, we observe that

$$R^{(1)}_{s',s}(\epsilon) = v^\dagger_s G_0(\epsilon - \omega_{s'} - \omega_s) v_{s'} = -i\pi\delta\left(\epsilon - \omega_{s'} - \omega_s\right) v^\dagger_s v_{s'} + v^\dagger_s P \frac{1}{\epsilon - \omega_{s'} - \omega_s} v_{s'},$$

where P stands for the Cauchy principal value, which helps us to define the connected part of one-particle vertex function as

$$W^{(1,1,C)}_{s_1,s_1}(\epsilon) = W^{(1,1)}_{s'_1,s_1}(\epsilon) + i\pi v^\dagger_{s_1} v_{s'_1} \delta\left(\epsilon - \omega_{s'_1} - \omega_{s_1}\right).$$

By then analyzing the structure of the general equation in the hierarchy (30) and bearing in mind the equation satisfied by $W^{(1,1)}_{s_1,s_1}(\epsilon)$ one may easily deduce the connected part of n-photon effective vertex function may be defined in the following manner:

$$W^{(1,n,C)}_{s'_1\ldots s'_n,s_1\ldots s_n}(\epsilon) = W^{(1,n)}_{s'_1\ldots s'_n,s_1\ldots s_n}(\epsilon) - W^{(1,1)}_{s'_1,s_1}\left(\epsilon - \sum_{l=2}^{n}\omega_{s'_n}\right) G^{(1)}\left(\epsilon - \omega_{s_1} - \sum_{l=2}^{n}\omega_{s'_l}\right) W^{(1,n-1)}_{s_2\ldots s'_n,s_2\ldots s_n}(\epsilon - \omega_{s_1}).$$

Now, with the help of the definition of components of T one may immediately deduce (???? сделаю это, пока не очевидно это) the following decomposition of the two-body transition operator:

$$T^{(1,2)}_{s'_1 s_2,s_1 s_2}(\omega_{s_1} + \omega_{s_2}) = -i\pi\delta\left(\omega_{s_1} - \omega_{s'_2}\right) T^{(1,1)}_{s'_1,s_1}(\omega_{s_1}) T^{(1,1)}_{s'_2,s_2}(\omega_{s_2}) + T^{(1,2)}_{s_1 s'_2,s_1 s_2}(\omega_{s_1} + \omega_{s_2}),$$

where $T^{(1,2,C)}$ is defined in precisely the same way as $T^{(1,2)}$ but with $W^{(1,1,C)}$ replacing $W^{(1,1)}$.

By plugging the representation (44) into the definition of the two-photon S matrix (38) we immediately arrive at the following cluster decomposition principle:

$$\mathcal{S}_2 = \left[\frac{1}{2} S^{(1)}_{s'_1,s_1} S^{(1)}_{s'_2,s_2} - 2\pi i T^{(1,2,C)}_{s'_1 s_2,,1 s_2}(\omega_{s_1} + \omega_{s_2})\delta\left(\omega_{s'_1} + \omega_{s'_2} - \omega_{s_1} - \omega_{s_2}\right)\right] a^\dagger_{s_1} a^\dagger_{s'_2} a_{s_2} a_{s_1}.$$

The physical meaning of the this expression is rather clear. The first term, being a product of one-particle S matrices, describes the coherent scattering of two particles, i.e., a scattering process in which there are no effective interactions between the photons. The second term, on the other hand, is completely connected and describes the incoherent scattering of photons in which the particles redistribute their initial energy by interaction. (???? тут возможно важная формула, подумаю про нее потом!!!)

A slightly more involved, but otherwise completely analogous, calculation may be done in the threephoton sector. As a result, one arrives at the following cluster decomposition of the three-body S matrix:

$$\mathcal{S}_3 = \left[\frac{1}{6} S^{(1)}_{s'_1,s_1} S^{(1)}_{s'_2,s_2} S^{(1)}_{s'_3,s_3} - 2\pi i T^{(1,2,C)} S_{s'_3,s_3}{}^{(1)} - 2\pi i T^{(1,3,C)}\right] \quad \text{(essentially)},$$

or exactly:

$$\mathcal{S}_3 = \left[\frac{1}{6} S^{(1)}_{s'_1,s_1} S^{(1)}_{s'_2,s_2} S^{(1)}_{s'_3,s_3} - 2\pi i T^{(1,2,C)}_{s'_1 s_2,s_1 s_2}(\omega_{s_1} + \omega_{s_2})\delta\left(\omega_{s'_1} + \omega_{s'_2} - \omega_{s_1} - \omega_{s_2}\right) S^{(1)}_{s'_3,s_3} - \right.$$
$$\left. - 2\pi i T^{(1,3,C)}_{s'_1 s_2 s'_3,s_1 s_2 s_3}(\omega_{s_1} + \omega_{s_2} + \omega_{s_3})\delta\left(\omega_{s'_1} + \omega_{s'_2} + \omega_{s'_3} - \omega_{s_1} - \omega_{s_2} - \omega_{s_3}\right)\right] \cdot$$
$$\cdot a^\dagger_{s'_1} a^\dagger_{s'_2} a^\dagger_{s'_3} a_{s_3} a_{s_2} a_{s_1},$$

where the connected part of the three-photon T matrix may be found by (??? which is done below).

Смысл этой формулы в том, что (!??!?!?!?!? напишу, как ее понимать, это же в 1 части!!!)

Cluster decomposition of three-photon S-matrix (!!!)

(!!!!!! многие формулы тут напишу в формате А=Б+С+Д, где А=... Б=..., иначе ничего не понятно, на страницу такое никогда не поместится!)

Let us start with definition of the three-body component of the S matrix entering its direct sum representation (???? напишу конкретно формулы для этого!?!??!) [throughout this Appendix, for simplicity it is assumed that $\omega_\mu(k) = \omega(k)$, $B_\mu = B, \forall \mu \in \{1, \ldots, N_c\}$], namely schematically:

or exactly:

$$\mathcal{S}_3 = \Big[\frac{1}{3!}\delta_{s_1',s_1}\delta_{s_2',s_2}\delta_{s_3',s_3} - 2\pi i\frac{1}{2!}\delta_{s_2',s_2}\delta_{s_3',s_3}T^{(1,1)}_{s_1',s_1}(\omega(k_1))\delta\left(\omega(k_1')-\omega(k_1)\right) -$$
$$- 2\pi i\frac{1}{1!}\delta_{s_3',s_3}T^{(1,2)}_{s_1's_2',s_1s_2}(\omega(k_1)+\omega(k_2))\delta\left(\omega(k_1')+\omega(k_2')-\omega(k_1)-\omega(k_2)\right)-$$
$$-2\pi i T^{(1,3)}_{s_1's_2's_3',s_1s_2s_3}(\omega(k_1)+\omega(k_2)+\omega(k_3))\delta\left(\omega(k_1')+\omega(k_2')+\omega(k_3')-\omega(k_1)-\omega(k_2)-\omega(k_3)\right)\Big]\cdot$$
$$\cdot\, a^\dagger_{s_1'}a^\dagger_{s_2'}a^\dagger_{s_3'}a_{s_3}a_{s_2}a_{s_1}.$$

As before we write (??? видимо, это важная формула, которую в 1ю часть нужно добавить!! пока не знаком с такими разложениями.)

$$T^{(1,2)}_{s_1's_2',s_1s_2}(\omega(k_1)+\omega(k_2)) = -\pi i\delta\left(\omega(k_1')-\omega(k_1)\right)T^{(1,1)}_{s_1',s_1}(\omega(k_1))T^{(1,1)}_{s_2',s_2}(\omega(k_2)) + T^{(1,2,C)}_{s_1's_2',s_1s_2}(\omega(k_1)+\omega(k_2)).$$

Here, as before, the equality symbol is understood in the sense of permutation equivalence and on-shell condition.

Now let us start massaging the three-body transition operator. First of all, one has

$$T^{(1,3)}_{\mu_1'k_1',\mu_2'k_2',\mu_3'k_3';\mu_1k_1,\mu_2k_2,\mu_3k_3}(\omega(k_1)+\omega(k_2)+\omega(k_3)) =$$
$$= g^*_{\mu_1}(k_1)\,g^*_{\mu_2}(k_2)\,g^*_{\mu_3}(k_3)\,g_{\mu_1'}(k_1')\,g_{\mu_2'}(k_2')\,g_{\mu_3'}(k_3')\cdot$$
$$\cdot\tilde{G}^{(1)}(\omega(k_1))\,\tilde{G}^{(1)}(\omega(k_1'))\,F^{(1,2)}(k_2',k_3',k_2,k_3,\omega(k_1)+\omega(k_2)+\omega(k_3)),$$

where $F^{(1,2)}(k_2',k_3',k_2,k_3,\omega(k_1)+\omega(k_2)+\omega(k_3))$ is not an entirely connected object defined via

$$F^{(1,2)}(k_1',k_2',k_1,k_2,\epsilon) := \frac{1}{g_{\mu_1'}(k_1')\,g_{\mu_2'}(k_2')\,g^*_{\mu_1}(k_1)\,g^*_{\mu_2}(k_2)}\left\langle g\left|W^{(1,2)}_{\mu_1'k_1'\mu_2'k_2',\mu_1k_1\mu_2k_2}(\epsilon)\right|g\right\rangle$$

(???? и зачем мы умножаем и потом делим на одни и те же множители?????)

Separation of elastic contribution (43) translates into the following decomposition:

$$F^{(1,2)}(k_2',k_3',k_2,k_3,\omega(k_1)+\omega(k_2)+\omega(k_3)) =$$
$$= F^{(1,1)}(k_2',k_2,\omega(k_1')+\omega(k_2'))\,\tilde{G}^{(1)}(\omega(k_1)+\omega(k_3)-\omega(k_3'))\,F^{(1,1)}(k_3',k_3,\omega(k_1)+\omega(k_3)) +$$
$$+\bar{F}^{(2,2)}(k_2',k_3',k_2,k_3,\omega(k_1)+\omega(k_2)+\omega(k_3))$$

Bearing in mind that $\bar{F}^{(2,2)}(k_2',k_3',k_2,k_3,\omega(k_1)+\omega(k_2)+\omega(k_3))$ is an analytic function we decompose the three-photon T matrix as follows:

$$T^{(1,3)}_{\mu_1'k_1',\mu_2'k_2',\mu_3'k_3';\mu_1k_1,\mu_2k_2,\mu_3k_3}(\omega(k_1)+\omega(k_2)+\omega(k_3)) =$$
$$= \bar{T}^{(1,3)}_{\mu_1'k_1',\mu_2'k_2',\mu_3'k_3';\mu_1k_1,\mu_2k_2,\mu_3k_3}(\omega(k_1)+\omega(k_2)+\omega(k_3)) +$$
$$+\hat{T}_{\mu_1'k_1',\mu_2'k_2',\mu_3'k_3';\mu_1k_1,\mu_2k_2,\mu_3k_3}(\omega(k_1)+\omega(k_2)+\omega(k_3))$$

where we have defined the following objects:

$$\bar{T}^{(1,3}_{\mu_1'k_1',\mu_2'k_2',\mu_3'k_3';\mu_1k_1,\mu_2k_2,\mu_3k_3}(\omega(k_1)+\omega(k_2)+\omega(k_3)) :=$$
$$= g^*_{\mu_1}(k_1)\,g^*_{\mu_2}(k_2)\,g^*_{\mu_3}(k_3)\,g_{\mu_1'}(k_1')\,g_{\mu_2'}(k_2')\,g_{\mu_3'}(k_3')\cdot$$
$$\cdot\tilde{G}(\omega(k_1))\,\tilde{G}(\omega(k_1'))\,\bar{F}^{(1,2)}(k_2',k_3',k_2,k_3,\omega(k_1)+\omega(k_2)+\omega(k_3))$$

and

$$\hat{T}^{(1,3}_{\mu_1'k_1',\mu_2'k_2',\mu_3'k_3';\mu_1k_1,\mu_2k_2,\mu_3k_3}(\omega(k_1)+\omega(k_2)+\omega(k_3)) :=$$
$$= g^*_{\mu_1}(k_1)\,g^*_{\mu_2}(k_2)\,g^*_{\mu_3}(k_3)\,g_{\mu_1'}(k_1')\,g_{\mu_2'}(k_2')\,g_{\mu_3'}(k_3')\cdot$$
$$\cdot\tilde{G}(\omega(k_1))\,\tilde{G}(\omega(k_1'))\,F^{(1,1)}(k_2',k_2,\omega(k_1')+\omega(k_2'))\,\tilde{G}^{(1)}(\omega(k_1)+\omega(k_3)-\omega(k_3'))\,F^{(1,1)}(k_3',k_3,\omega(k_1)+\omega(k_3))$$

In the last equation we have

$$F^{(1,1)}(k_2',k_2,\omega(k_1')+\omega(k_2')) = \hat{G}_0(\omega(k_1')-\omega(k_2)) + \bar{F}^{(1,1)}(k_2',k_2,\omega(k_1')+\omega(k_2'))$$
$$F^{(1,1)}(k_3',k_3,\omega(k_1)+\omega(k_3)) = \hat{G}_0(\omega(k_1)-\omega(k_3')) + \bar{F}^{(1,1)}(k_3',k_3,\omega(k_1)+\omega(k_3))$$

The terms in (A8) containing $\hat{G}_0$ deserve a special attention since they can yield delta functions determining additional conservation of frequencies. (??????)

In particular, the terms with $\hat{G}_0\bar{F}^{(1,1)}$ and $\bar{F}^{(1,1)}\hat{G}_0$ together give

$$-2\pi i\delta\left(\omega(k_3')-\omega(k_3)\right)T^{(1,1)}_{s_3',s_3}(\omega(k_3))$$
$$\left[T^{(1,2,C)}_{s_1's_2',s_1s_2}(\omega(k_1)+\omega(k_2)) - g^*_{\mu_1}(k_1)\,g^*_{\mu_2}(k_2)\,g_{\mu_1'}(k_1')\,g_{\mu_2'}(k_2')\,\tilde{G}^{(1)}(\omega(k_1))\,\tilde{G}^{(1)}(\omega(k_1'))\,P\left(\frac{1}{\omega(k_1)-\omega(k_2')}\right)\right]+$$
$$+$$
$$+g^*_{\mu_1}(k_1)\,g^*_{\mu_2}(k_2)\,g^*_{\mu_3}(k_3)\,g_{\mu_1'}(k_1')\,g_{\mu_2'}(k_2')\,g_{\mu_3'}(k_3')\,\tilde{G}(\omega(k_1))\,\tilde{G}(\omega(k_1'))\,\tilde{G}^{(1)}(\omega(k_1)+\omega(k_3)-\omega(k_3'))$$
$$\left[P\left(\frac{1}{\omega(k_1')-\omega(k_2)}\right)\bar{F}^{(1,1)}(k_3',k_3,\omega(k_1)+\omega(k_3)) + \bar{F}^{(1,1)}(k_2',k_2,\omega(k_1')+\omega(k_2'))\,P\left(\frac{1}{\omega(k_1)-\omega(k_3')}\right)\right].$$

(???? почему $2\pi i$ у нас только в 1м члене????)

The term (A11) contributes to the $3=2+1$ cluster of the three-photon S matrix.

The term (A12) is completely connected and nonsingular. This property becomes explicitly visible if we reexpress it as

$$\frac{g^*_{\mu_1}(k_1)\,g^*_{\mu_2}(k_2)\,g^*_{\mu_3}(k_3)\,g_{\mu_1'}(k_1')\,g_{\mu_2'}(k_2')\,g_{\mu_3'}(k_3')}{\omega(k_1')-\omega(k_1)}\cdot$$
$$\cdot\Big[\tilde{G}^{(1)}(\omega(k_1'))\,\tilde{G}^{(1)}(\omega(k_3))\,\tilde{G}^{(1)}(\omega(k_3')+\omega(k_1')-\omega(k_1))\,\bar{F}^{(1,1)}(k_2',k_2,\omega(k_1')+\omega(k_2')+\omega(k_3')-\omega(k_1)) -$$
$$-\tilde{G}^{(1)}(\omega(k_1))\,\tilde{G}^{(1)}(\omega(k_1)+\omega(k_3)-\omega(k_1'))\,\tilde{G}^{(1)}(\omega(k_3'))\,\bar{F}^{(1,1)}(k_2',k_2,\omega(k_2')+\omega(k_3'))\Big].$$

This representation makes it obvious that in the limit $k_1'\to k_1$ this function is finite.

Now, let us consider the contribution to (A8) containing $\hat{G}_0\hat{G}_0$. It amounts to

$$g^*_{\mu_1}(k_1)\,g^*_{\mu_2}(k_2)\,g^*_{\mu_3}(k_3)\,g_{\mu_1'}(k_1')\,g_{\mu_2'}(k_2')\,g_{\mu_3'}(k_3')$$
$$\tilde{G}(\omega(k_1))\,\tilde{G}(\omega(k_3'))\,\tilde{G}^{(1)}(\omega(k_2)+\omega(k_1)-\omega(k_1'))\,\hat{G}_0(\omega(k_3')-\omega(k_3))\,\hat{G}_0(\omega(k_1)-\omega(k_1')) =$$
$$=$$
$$=(-i\pi)^2T^{(1,1)}_{s_1',s_1}(\omega(k_1))\,T^{(1,1)}_{s_2',s_2}(\omega(k_2))\,T^{(1,1)}_{s_3',s_3}(\omega(k_3))\,\delta(\omega(k_1')-\omega(k_1))\,\delta(\omega(k_2')-\omega(k_2)) -$$
$$-2\pi i g^*_{\mu_1}(k_1)\,g^*_{\mu_2}(k_2)\,g_{\mu_1'}(k_1')\,g'_{\mu_2'}(k_2')$$
$$\tilde{G}^{(1)}(\omega(k_1))\,\tilde{G}^{(1)}(\omega(k_1'))\,T^{(1,1)}_{s_3',s_3}(\omega(k_3))\,\delta(\omega(k_3')-\omega(k_3))$$
$$g^*_{\mu_1}(k_1)\,g^*_{\mu_2}(k_2)\,g^*_{\mu_3}(k_3)\,g_{\mu_1'}(k_1')\,g_{\mu_2'}(k_2')\,g_{\mu_3'}(k_3')$$
$$\tilde{G}(\omega(k_3'))\,\tilde{G}(\omega(k_1))\,\tilde{G}^{(1)}(\omega(k_2)+\omega(k_1)-\omega(k_1'))\,P\left(\frac{1}{\omega(k_3')-\omega(k_3)}\right)P\left(\frac{1}{\omega(k_1)-\omega(k_1')}\right).$$

The term (A14) contributes to the $3=1+1+1$ cluster. The term (A15) contributes to the $3=2+1$ cluster. The term (A16) requires a special consideration. Rewriting

$$\tilde{G}^{(1)}(\omega(k_3'))\,\tilde{G}^{(1)}(\omega(k_2)+\omega(k_1)-\omega(k_1'))\,\tilde{G}^{(1)}(\omega(k_1))\,P\left(\frac{1}{\omega(k_3')-\omega(k_3)}\right)P\left(\frac{1}{\omega(k_1)-\omega(k_1')}\right)$$
$$=\tilde{G}^{(1)}(\omega(k_3'))\,\tilde{G}^{(1)}(\omega(k_1))\,P\left(\frac{\tilde{G}^{(1)}(\omega(k_2)+\omega(k_1)-\omega(k_1'))-\tilde{G}^{(1)}(\omega(k_2))}{\omega(k_3')-\omega(k_3)}\right)\frac{1}{\omega(k_1)-\omega(k_1')}$$
$$+\tilde{G}^{(1)}(\omega(k_3'))\,\tilde{G}^{(1)}(\omega(k_2))\,\tilde{G}^{(1)}(\omega(k_1))\,P\left(\frac{1}{\omega(k_3')-\omega(k_3)}\right)P\left(\frac{\tilde{G}^{(1)}(\omega(k_2)+\omega(k_1)-\omega(k_1'))-\tilde{G}^{(1)}(\omega(k_2))}{\omega(k_1)-\omega(k_1')}\right)$$
$$=\tilde{G}^{(1)}(\omega(k_3'))\,\tilde{G}^{(1)}(\omega(k_1))\,P\left(\frac{1}{\omega(k_3')-\omega(k_3)}\right)\frac{\tilde{G}^{(1)}_1(\omega(k_3'))-\tilde{G}^{(1)}(\omega(k_3))}{\omega(k_1')}P\left(\frac{1}{\omega(k_1)-\omega(k_1')}\right)$$
$$+\tilde{G}^{(1)}(\omega(k_2))\,\tilde{G}^{(1)}(\omega(k_1))\,\frac{1}{1}\Big)\,P\left(\frac{1}{\omega(k_1)-\omega(k_1')}\right),$$

we observe that the terms (A17) and (A18) give together a nonsingular contribution. In fact,

$$\tilde{G}^{(1)}(\omega(k_3'))\,\tilde{G}^{(1)}(\omega(k_1))\,P\left(\frac{1}{\omega(k_3')-\omega(k_3)}\right)\frac{\tilde{G}^{(1)}(\omega(k_2)+\omega(k_1)-\omega(k_1'))-\tilde{G}^{(1)}(\omega(k_2))}{\omega(k_1)-\omega(k_1')}$$
$$+\,\tilde{G}^{(1)}(\omega(k_2))\,\tilde{G}^{(1)}(\omega(k_1))\,\frac{\tilde{G}^{(1)}(\omega(k_3'))-\tilde{G}^{(1)}(\omega(k_3))}{\omega(k_3')-\omega(k_3)}P\left(\frac{1}{\omega(k_1)-\omega(k_1')}\right)$$
$$=\tilde{G}^{(1)}(\omega(k_3'))\,\tilde{G}^{(1)}(\omega(k_1))\,\tilde{G}^{(1)}(\omega(k_2))\,\tilde{G}^{(1)}(\omega(k_2')+\omega(k_3')-\omega(k_3))\,\tilde{G}^{(1)}(\omega(k_2'))$$
$$\cdot\frac{\left(\tilde{G}^{(1)}\right)^{-1}(\omega(k_2'))-\left(\tilde{G}^{(1)}\right)^{-1}(\omega(k_2')+\omega(k_3')-\omega(k_3))}{\omega(k_3')-\omega(k_3)}\frac{\left(\tilde{G}^{(1)}\right)^{-1}(\omega(k_2))-\left(\tilde{G}^{(1)}\right)^{-1}(\omega(k_2)+\omega(k_1)-\omega(k_1'))}{\omega(k_1)-\omega(k_1')}$$
$$+\,\tilde{G}^{(1)}(\omega(k_2))\,\tilde{G}^{(1)}(\omega(k_3))\,\tilde{G}^{(1)}(\omega(k_3'))\,\frac{1}{\omega(k_1')-\omega(k_1)}\Big(\tilde{G}^{(1)}(\omega(k_1'))$$
$$\cdot\frac{\left(\tilde{G}^{(1)}\right)^{-1}(\omega(k_3))-\left(\tilde{G}^{(1)}\right)^{-1}(\omega(k_1')+\omega(k_3')-\omega(k_1))}{\omega(k_1')+\omega(k_3')-\omega(k_1)-\omega(k_3)}-\tilde{G}^{(1)}(\omega(k_1))\,\frac{\left(\tilde{G}^{(1)}\right)^{-1}(\omega(k_3))-\left(\tilde{G}^{(1)}\right)^{-1}(\omega(k_3'))}{\omega(k_3')-\omega(k_3)}\Big)$$

In contrast, the term (A19) is singular and contributes to the $3=1+1+1$ cluster of the scattering matrix. To show this, we first fully symmetrize

$$\tilde{G}^{(1)}(\omega(k_3))\,\tilde{G}^{(1)}(\omega(k_2))\,\tilde{G}^{(1)}(\omega(k_1))\,P\left(\frac{1}{\omega(k_3')-\omega(k_3)}\right)P\left(\frac{1}{\omega(k_1)-\omega(k_1')}\right)$$
$$\to$$
$$\to\frac{1}{3}\tilde{G}^{(1)}(\omega(k_3))\,\tilde{G}^{(1)}(\omega(k_2))\,\tilde{G}^{(1)}(\omega(k_1))\left[P\left(\frac{1}{\omega(k_3')-\omega(k_3)}\right)P\left(\frac{1}{\omega(k_1)-\omega(k_1')}\right)\right.$$
$$\left.+P\left(\frac{1}{\omega(k_2')-\omega(k_2)}\right)P\left(\frac{1}{\omega(k_3)-\omega(k_3')}\right)+P\left(\frac{1}{\omega(k_1')-\omega(k_1)}\right)P\left(\frac{1}{\omega(k_2)-\omega(k_2')}\right)\right].$$

Owing to the Poincare-Bertrand distributional identity $P\left(\frac{1}{x}\right)P\left(\frac{1}{y}\right)=P\left(\frac{1}{y-x}\right)\left[P\left(\frac{1}{x}\right)-P\left(\frac{1}{y}\right)\right]+\pi^2\delta(x)\delta(y)$, we establish the identity

$$P\left(\frac{1}{\omega(k_3')-\omega(k_3)}\right)P\left(\frac{1}{\omega(k_1)-\omega(k_1')}\right)+P\left(\frac{1}{\omega(k_2')-\omega(k_2)}\right)P\left(\frac{1}{\omega(k_3)-\omega(k_3')}\right)+$$
$$+P\left(\frac{1}{\omega(k_1')-\omega(k_1)}\right)P\left(\frac{1}{\omega(k_2)-\omega(k_2')}\right)=$$
$$=\pi^2\delta\left(\omega(k_3')-\omega(k_3)\right)\delta\left(\omega(k_1')-\omega(k_1)\right)$$

leading us to the result

$$\frac{\pi^2}{3}\tilde{G}^{(1)}(\omega(k_3))\,\tilde{G}^{(1)}(\omega(k_2))\,\tilde{G}^{(1)}(\omega(k_1))\cdot\delta\left(\omega(k_3')-\omega(k_3)\right)\delta\left(\omega(k_1')-\omega(k_1)\right)$$

in (A21).

(??? мб ниже главная формула, которую в 1 часть и вынесу!)

Combining all of the above results, we arrive at the following decomposition of the three-photon T matrix:

$$T^{(1,3)}_{s_1's_2's_3',s_1s_2s_3}(\omega(k_1)+\omega(k_2)+\omega(k_3))=$$
$$=\frac{(-2\pi i)^2}{6}T^{(1)}_{s_1',s_1}(\omega(k_1))\,T^{(1)}_{s_2',s_2}(\omega(k_2))\,T^{(1)}_{s_3',s_3}(\omega(k_3))\,\delta\left(\omega(k_1')-\omega(k_1)\right)\delta\left(\omega(k_2')-\omega(k_2)\right)$$
$$-2\pi iT^{(1,2,C)}_{s_1's_2',s_1s_2}(\omega(k_1)+\omega(k_2))\,T^{(1)}_{s_3',s_3}(\omega(k_3))\,\delta\left(\omega(k_3')-\omega(k_3)\right)$$
$$+T^{(1,3,C)}_{s_1's_2's_3',s_1s_2s_3}(\omega(k_1)+\omega(k_2)+\omega(k_3))$$

with the three-body connected part

$$T^{(1,3,C)}_{s_1's_2's_3',s_1s_2s_3}(\omega(k_1)+\omega(k_2)+\omega(k_3))=$$
$$=\mathfrak{g}_{(1,3,\,C)}\left\{\mathfrak{A}_{(1,3,\,C)}+\frac{1}{\omega(k_1')-\omega(k_1)}\left[\mathfrak{B}_{(1,3,\,C)}-\mathfrak{C}_{(1,3,\,C)}+\mathfrak{D}_{(1,3,\,C)}-\mathfrak{E}_{(1,3,\,C)}\right]+\mathfrak{F}_{(1,3,\,C)}\right\}+$$
$$+\bar{T}_{s_1's_2's_3',s_1s_2s_3}(\omega(k_1)+\omega(k_2)+\omega(k_3)).$$

Where only here the functions are defined as:

$$\mathfrak{g}_{(1,3,\,C)} := g^*_{\mu_1}(k_1)g^*_{\mu_2}(k_2)g^*_{\mu_3}(k_3)g_{\mu'_1}(k'_1)g_{\mu'_2}(k'_2)g_{\mu'_3}(k'_3);$$

$$\mathfrak{A}_{(1,3,\,C)} := \tilde{G}^{(1)}(\omega(k'_3))\tilde{G}^{(1)}(\omega(k_1))\tilde{G}^{(1)}(\omega(k_2))\tilde{G}^{(1)}(\omega(k'_2)+\omega(k'_3)-\omega(k_3))\tilde{G}^{(1)}(\omega(k'_2))\cdot$$
$$\cdot\frac{(\tilde{G}^{(1)})^{-1}(\omega(k'_2))(\tilde{G}^{(1)})^{-1}(\omega(k'_2)+\omega(k'_3)-\omega(k_3))}{\omega(k'_3)-\omega(k_3)}\cdot$$
$$\cdot\frac{(\tilde{G}^{(1)})^{-1}(\omega(k_2))-(\tilde{G}^{(1)})^{-1}(\omega(k_2)+\omega(k_1)-\omega(k'_1))}{\omega(k_1)-\omega(k'_1)};$$

$$\mathfrak{B}_{(1,3,\,C)} := \tilde{G}^{)1)})\omega)k_2))\tilde{G}^{)1)})\omega)k_3))\tilde{G}^{)1)})\omega)k'_3))\cdot$$
$$\cdot\left(\tilde{G}^{(1)}(\omega(k'_1))\frac{(\tilde{G}^{(1)})^{-1}(\omega(k_3))-(\tilde{G}^{(1)})^{-1}(\omega(k'_1)+\omega(k'_3)-\omega(k_1))}{\omega(k'_1)+\omega(k'_3)-\omega(k_1)-\omega(k_3)}\right);$$

$$\mathfrak{C}_{(1,3,\,C)} := \tilde{G}^{(1)}(\omega(k_1))\frac{(\tilde{G}^{(1)})^{-1}(\omega(k_3))-(\tilde{G}^{(1)})^{-1}(\omega(k'_3))}{\omega(k'_3)-\omega(k_3)};$$

$$\mathfrak{D}_{(1,3,\,C)} := \tilde{G}^{(1)}(\omega(k'_1))\tilde{G}^{(1)}(\omega(k_3))\tilde{G}^{(1)}(\omega(k'_3)+\omega(k'_1)-\omega(k_1))\bar{F}^{(1,1)}(k'_2,k_2,\omega(k'_1)+\omega(k'_2)+\omega(k'_3)-\omega(k_1));$$

$$\mathfrak{E}_{(1,3,\,C)} := \tilde{G}^{(1)}(\omega(k_1))\tilde{G}^{(1)}(\omega(k'_3))\tilde{G}^{(1)}(\omega(k_1)+\omega(k_3)-\omega(k'_1))\bar{F}^{(1,1)}(k'_2,k_2,\omega(k'_2)+\omega(k'_3));$$

$$\mathfrak{F}_{(1,3,\,C)} := \tilde{G}(\omega(k_1))\tilde{G}(\omega(k'_1))\bar{F}^{(1,1)}(k'_2,k_2,\omega(k'_1)+\omega(k'_2))\cdot$$
$$\cdot\,\tilde{G}^{(1)}(\omega(k_1)+\omega(k_3)-\omega(k'_3))\bar{F}^{(1,1)}(k'_3,k_3,\omega(k_1)+\omega(k_3)).$$

Plugging everything into the definition of the three-photon S matrix we finally obtain (???? еще раз, какая там формула основная???? забыл уже??? в 1й части укажу это тоже!)

$$\mathcal{S}_3 = \Bigg[\frac{1}{3!}S^{(1)}_{s'_1,s_1}S^{(1)}_{s'_2,s_2}S^{(1)}_{s'_3,s_3} -$$
$$-2\pi i T^{(1,2,C)}_{s'_1s'_2,s_1s_2}(\omega(k_1)+\omega(k_2))S^{(1)}_{s'_3,s_3}\delta\left(\omega(k'_1)+\omega(k'_2)-\omega(k_1)-\omega(k_2)\right)$$
$$-2\pi i T^{(1,3,C)}_{s'_1s'_2s'_3,s_1s_2s_3}(\omega(k_1)+\omega(k_2)+\omega(k_3))\delta\left(\omega(k'_1)+\omega(k'_2)+\omega(k'_3)-\omega(k_1)-\omega(k_2)-\omega(k_3)\right)\Bigg]$$
$$a^\dagger_{s'_1}a^\dagger_{s'_2}a^\dagger_{s'_3}a_{s_3}a_{s_2}a_{s_1}.$$

7.6.3 Examples of Diagrams

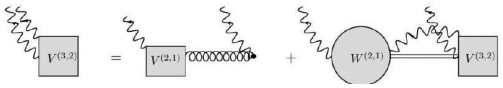

(тут ее формула и смысл)

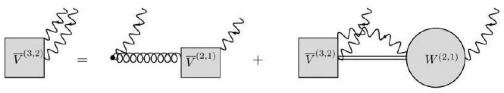

(тут ее формула и смысл)

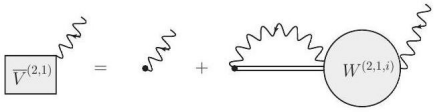

(тут ее формула и смысл)

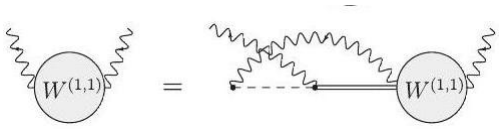

(тут ее формула и смысл)

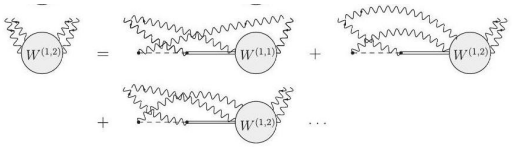

(тут ее формула и смысл)

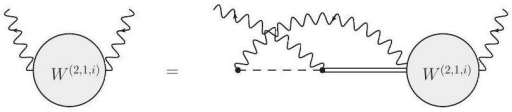

(тут ее формула и смысл)

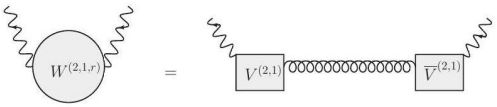

(тут ее формула и смысл)

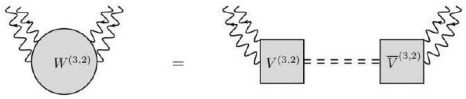

(тут ее формула и смысл)

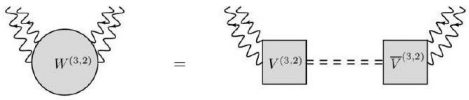

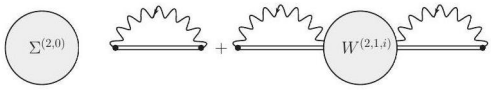

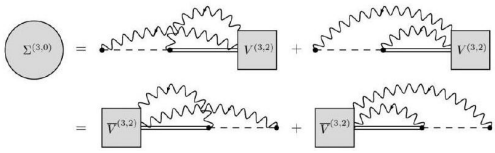

7.6.4 Closed-form solution in the Markovian limit

(??? вообще пока хз.)

Theory

Let us now consider the single-qubit scattering problem in the Markovian limit. Validity of Markovian approximation demands a number of assumptions: Linear dispersion relation in all of the channels $\omega_\mu(k) = \omega_{0\mu} + v_\mu k$, broad-band limit $B_\mu = \mathbb{R}, \forall \mu \in \{1, \ldots, N_c\}$, and local couplings (i.e., independent of frequency) $g_\mu(k) = \sqrt{\gamma_\mu/\pi}$.

Within the above assumptions, the self-energy diagram reads as $\Sigma^{(1)}(\epsilon) = -i \sum_{\mu=1}^{N_c} \gamma_\mu/v_\mu |1\rangle\langle 1|$, which is independent of ϵ (here we have introduced the projector on the qubit's excited state $|1\rangle\langle 1| = \frac{1+\sigma_3}{2}$). By causality, all of the W functions are analytic in momentum (energy) variables in the lower (upper) half of the complex plane. By exploiting this analyticity along with the momentum independence of both coupling constants and self-energy, we can close all of the integration contours in the lower half of the complex momentum plane to render all of the integrals zero, thus promoting the integral equations into algebraic ones. As a result, we recover the solution obtained in [51]. Diagrammatically the above solution is equivalent to the so-called noncrossing approximation (which becomes exact in the Markovian limit) and it is represented in Fig. 2.

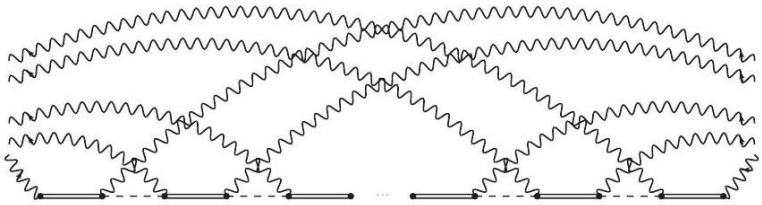

FIG. 2. Exact diagrammatic representation of the n-particle T matrix in the Markovian limit. The above diagrams also correspond to the noncrossing approximation discussed in Sec. II F. As opposed to the exact n-photon T matrix parametrized by the $(n-1)$-particle effective vertex function resuming an infinite number of emission and absorption processes in both direct and exchange channels, this approximation replaces the vertex by a sequence of $n-2$ and $n-1 (n \geqslant 2)$ alternating excitations and deexcitations of the emitter.

Как было бы, если бы не было марковского лимита? (????)

(просто пока не разобрался еще с ним.)

7.6.5 Approximation strategies

Theory

Although it is possible to write an entire hierarchy of exact equations for the multiphoton vertex functions, which in turn parametrize the exact S matrix, their analytical solution is in general only possible in the Markovian limit. To make some progress in solving the scattering problem, one has to resort to some kind of approximation routine. In this section we propose a couple of physically motivated resummation approaches, allowing one to avoid (or partially avoid) the solution of the exact integral equations.

The most basic approximation, which is accurate in the regime $\gamma\tau \lesssim 1$, where τ is a typical time delay in the system due to photons' propagation between two nearby scatterers, and γ is a typical decay rate of scatterers, is the so-called quasi-Markovian approximation. While in the quantum master-equation approach it has a long tradition (see, e.g., [22, 23]), it has been recently realized [51, 53] that in the diagrammatic approach it is mathematically equivalent to picking only noncrossing diagrams shown in Fig. 2 and thereby fully neglecting vertex corrections. To give a physical explanation of this equivalence, we view photons propagating in the waveguide as an effective reservoir. It is intuitively clear that a fast decay of time correlations between these photons is an essential feature of the Markovian regime (we add here the prefix "quasi" in order to indicate that the field values at positions of different scatterers can still differ from each other by a phase factor). On the other hand, these time correlations result from correlated virtual processes of emission and absorption of different photons at different scatterers, which are mathematically encoded in the vertex corrections. Thus, the neglect of vertex corrections is equivalent to making the quasi-Markovian approximation. It is also worth noting that this approximation for a single-photon scattering matrix coincides with its exact expression since in the absence of other photons the correlations in questions are not generated.

Below we give a step-by-step prescription how to implement the quasi-Markovian approximation in our diagrammatic approach. The exact n-photon transition matrices are represented by a $(n-1)$-particle effective vertex function inbetween two dressed Green's functions followed by emission and absorption vertices [see Eq. (34)]. In this approximation, the exact multiphoton vertex functions are simply replaced with a sequence of $n-1$ bare and $n-2$ dressed Green's functions interspersed with $2n-2$ emission and absorption vertices. In particular, in the $n=2$ case we get $W^{(1,1)}_{s_1',s_1}(\epsilon) \to v^\dagger_{s_1} G_0\left(\epsilon - \omega_{s_1'} - \omega_{s_1}\right) v_{s_1'}$. In the $n=3$ case we obtain $W^{(1,2)}_{s_1's_2',s_1s_2}(\epsilon) \to v^\dagger_{s_1} G_0\left(\epsilon - \omega_{s_1} - \omega_{s_1'} - \omega_{s_2'}\right) v_{s_1'} G^{(1)}(\epsilon - \omega_{s_1} - \omega_{s_2'}) v^\dagger_{s_2} G_0\left(\epsilon - \omega_{s_1} - \omega_{s_2} - \omega_{s_2'}\right) v_{s_2'}$, and so on. In this approximation, all of the nontrivial momentum dependence of the S matrix, comes entirely from the frequency

dependence of the self-energy diagram. Note that the single-photon T matrix is completely determined by the dressed propagator $G^{(1)}(\epsilon)$ [see Eq. (33)]. This observation explicitly confirms the statement that the quasi-Markovian approximation becomes exact for a single propagating photon.

The second approximation routine, which is more accurate than the quasi-Markovian one for $\gamma\tau \gtrsim 1$, makes a partial account of the vertex corrections. In particular, this approximation is based on the resummation of the full single-photon vertex functions $W^{(1,1)}_{s',s}(\epsilon)$. Diagrammatically, this approximation amounts to the replacement of the dotted lines in Fig. 2 by the full single-particle bubbles; the resulting n-photon T matrix is shown in Fig. 3.

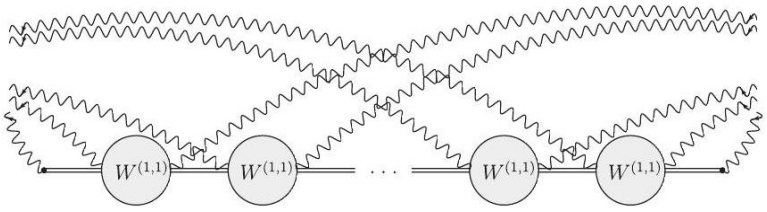

FIG. 3. Diagrammatic representation of n-particle transition matrix within the weak correlation approximation. Here two-particle bubbles correspond to a single-photon effective vertex function $W^{(1,1)}$. Opposite to the quasi-Markovian approximation, this approximation resums exactly all of the single-particle processes, ignoring all the connected diagrams corresponding to multipleparticle scattering.

This approximation corresponds to resummation of all of the direct interaction diagrams (coming entirely from the single-particle sector), completely ignoring the exchange processes (encompassed by the connected parts of many-particle vertices). In order to clarify the matters, let us consider an integral equation governing the two-particle effective vertex shown in Fig. 1. Using the diagrammatic rules we deduce

$$\begin{aligned} W^{(1,2)}_{s_1's_2,s_1,s_2}(\epsilon) = {} & R^{(1)}_{s_1',s_1}\left(\epsilon-\omega_{s_2'}\right) G^{(1)}\left(\epsilon-\omega_{s_1}-\omega_{s_2'}\right) W^{(1,1)}_{s_{s'},s_2}(\epsilon-\omega_1) + \\ & + R^{(1)}_{s_1,s}\left(\epsilon-\omega_{s_2'}\right) G^{(1)}\left(\epsilon-\omega_{s}-\omega_{s_2'}\right) W^{(1,2)}_{ss_2',s_1s_2} + \\ & + R^{(1)}_{s_1,s}\left(\epsilon-\omega_{s_2'}\right) G^{(1)}\left(\epsilon-\omega_{s}-\omega_{s_2'}\right) W^{(1,2)}_{s_2',s_1s_2}. \end{aligned}$$

(потом цвета поставлю, лень уже)

Note that the last line above corresponds to the exchange interaction between that particles (see also Fig. 1). If we ignore the the last term completely and take into account the equation satisfied by $W^{(1,1)}$ it is easy to show that

$$W^{(1,2)}_{s_1's_2',s_1,s_2}(\epsilon) = W^{(1,1)}_{s_1',s_1}\left(\epsilon-\omega_{s_2'}\right) G^{(1)}\left(\epsilon-\omega_{s_1}-\omega_{s_2'}\right) W^{(1,1)}_{s_2',s_2}(\epsilon-\omega_1)$$

is an exact solution of (47).

We expect this approximation to get worse as one increases the number of photons in the system since this approximation ignores a larger and larger fraction of diagrams with the increase in the number of particles involved in a scattering process. This approximation is beneficial since an integral equation for $W^{(1,1)}$ may be frequently solved analytically by means of the method developed in the Supplemental Material of [71]. Due to the nontrivial momentum dependence of $W^{(1,1)}$, we expect this approximation to be better than a quasi-Markovian one. In what follows, we refer to this approximation as to the weak correlation one. Note that as the quasi-Markovian approximation is exact in the single-particle sector, the weak correlation approximation is exact in the two-particle sector, thus in order to test its validity, one has to consider at least a three-photon scattering problem.

7.7 Systems with some qubits

Let's generalize the theory scattering for the systems with a larger number of qubits. In particular, we are going to focus our attention on the systems with two and three emitters. By deriving the equations governing two- and three-photon scattering matrices in twoand three-qubit waveguide QED systems, respectively, we present the most general two- and three-particle equations, holding independently of the number of qubits (see the discussion in Sec. II B).

(!!! ниже приплетены теор части, их в пред часть перенесу!!! ничего нового не должно вводиться!)

7.7.1 2-qubit waveguide QED

(!?! тут теперь у нас везде довечка!!! потом пойму, что конкретно новое изменилось????)

Theory

First, we would like to focus on the case of two emitters coupled to a waveguide since the generalization of the single-qubit results is the most apparent in this case. The starting point in the analysis is Eqs. (17) and (18). As opposed to the single-emitter case, now, clearly, both diagonal terms $v^\dagger_{s'}a_{s'}\mathcal{G}_0 a^\dagger_s v_s$ and $a^\dagger_{s'}v_{s'}\mathcal{G}_0 v^\dagger_s a_s$ contribute to the geometric series for the transition operator. Nondiagonal ones still give zero since they both annihilate the state $v^\dagger|g\rangle$. By resumming the series and introducing the following set of objects

$$\begin{aligned}\mathcal{W}^{(2)} =&\mathcal{R}^{(2)} + \mathcal{R}^{(2)}\mathcal{G}^{(1)}\mathcal{W}^{(2)},\\ \mathcal{R}^{(2)} =& a^\dagger_{s'_1}\mathcal{R}^{(2)}_{s'_1,s_1}a_{s_1},\\ &\mathcal{R}^{(2)}_{s'_1,s_1} = \mathcal{R}^{(1)}_{s'_1,s_1} + v_{s'_1}\mathcal{G}_0 v^\dagger_{s_1},\end{aligned}$$

we render the matrix elements of the transition operator in the form (??? все как и было, только теперь довечки появляются??)

$$\langle N'_p, g|\mathcal{T}^{(2)}|N_p, g\rangle = \langle N'_p, g|a^\dagger_{s'_1}v_{s'_1}\mathcal{G}^{(1)}v^\dagger_{s_1}a_{s_1}|N_p, g\rangle + \langle N'_p, g|a^\dagger_{s'_1}v_{s'_1}\mathcal{G}^{(1)}\mathcal{W}^{(2)}\mathcal{G}^{(1)}v^\dagger_{s_1}a_{s_1}|N_p, g\rangle.$$

Since the lowest term in the expansion of $\mathcal{W}^{(2)}$ is again a single-photon operator

$$\mathcal{W}^{(2)} = \sum_{n=1}^{\infty} a^\dagger_{s'_1}\dots a^\dagger_{s'_n}\mathcal{W}^{(2,n)}_{s'_1\dots s'_n,s_1\dots s_n}a_{s_n}\dots a_{s_1}$$

we see that the hierarchy of equations satisfied by the twophoton vertex functions is precisely the same as (29) and (30) with $R^{(1)}$ being replaced by $R^{(2)}$ (see Fig. 4).

FIG. 4. Diagrammatic representation of the replacement required to obtain $R^{(2)}_{s',s}$ from $R^{(1)}_{s',s}$. Note that the extra contribution to the effective potential energy vertex $R^{(2)}$ in two-qubit systems is not single-particle connected, i.e., it is possible to cut the intermediate propagator such that the diagram falls into two distinct pieces. This very fact makes the splitting (56)-(59) into reducible and irreducible contributions possible.

Отличие рассеяния на одном кубите от рассеяния на двух кубитах

In order to understand the difference between the singlequbit and the two-qubit theories, let us have a closer look at the equation defining $\mathcal{W}^{(2)}$:

$$\mathcal{W}^{(2)} = \mathcal{R}^{(1)} + a^\dagger_{s'_1}v_{s'_1}\mathcal{G}_0 v^\dagger_{s_1}a_{s_1} + \mathcal{R}^{(1)}\mathcal{G}^{(1)}\mathcal{W}^{(2)} + a^\dagger_{s'_1}v_{s'_1}\mathcal{G}_0 v^\dagger_{s_1}a_{s_1}\mathcal{G}^{(1)}\mathcal{W}^{(2)}.$$

Now let us perform the separation $\mathcal{W}^{(2)} = \mathcal{W}^{(2,i)} + \mathcal{W}^{(2,r)}$, where the superscripts i and r stand for the irreducible and reducible contributions, respectively, and $\mathcal{W}^{(2,i)}$ is chosen to satisfy Eq. (26). This leads one to the following equation satisfied by the reducible part:

$$\begin{aligned}\mathcal{W}^{(2,r)} =& a^\dagger_{s'_1}v_{s'_1}\mathcal{G}_0 v^\dagger_{s_1}a_{s_1} + \mathcal{R}^{(1)}\mathcal{G}^{(1)}\mathcal{W}^{(2,r)} +\\ &+ a^\dagger_{s'_1}v_{s'_1}\mathcal{G}_0 v^\dagger_{s_1}a_{s_1}\mathcal{G}^{(1)}\mathcal{W}^{(2,i)} +\\ &+ a^\dagger_{s'_1}v_{s'_1}\mathcal{G}_0 v^\dagger_{s_1}a_{s_1}\mathcal{G}^{(1)}\mathcal{W}^{(2,r)}\end{aligned}$$

The solution of above equation may then conveniently be parametrized as

$$W^{(2,r)}(\epsilon) = \mathcal{V}^{(2)}(\epsilon)\mathcal{G}^{(2)}(\epsilon)\overline{\mathcal{V}}^{(2)}(\epsilon),$$

(???? ПАЧИМУ???) where

$$\begin{aligned}\mathcal{G}^{(2)} &= \mathcal{G}_0 + \mathcal{G}_0\Sigma^{(2)}\mathcal{G}^{(2)},\\ \Sigma^{(2)} &= a_s v^\dagger_s\mathcal{G}^{(1)}v_{s'}a^\dagger_{s'} + a_s v^\dagger_s\mathcal{G}^{(1)}\mathcal{W}^{(2,i)}\mathcal{G}^{(1)}v_{s'}a^\dagger_{s'},\end{aligned}$$

$$\overline{\mathcal{V}}^{(2)} = v_s^\dagger a_s + v_s^\dagger a_s \mathcal{G}\mathcal{W}^{(2,i)} =: \sum_{n=1}^{\infty} \bar{V}^{(2,n)}_{s_1\ldots s_n} a_{s_1}\ldots a_{s_n},$$

$$\mathcal{V}^{(2)} = a_s^\dagger v_s + \mathcal{W}^{(2,i)}\mathcal{G} v_s a_s^\dagger =: \sum_{n=1}^{\infty} V^{(2,n)}_{s_1\ldots s_n} a^\dagger_{s_1}\ldots a^\dagger_{s_n}$$

The meaning of the above-defined objects is as follows. $\mathcal{G}^{(2)}(\epsilon)$ may be thought of as a Green's operator in the two-qubit excitation subspace since in practice, it is always projected there. $\Sigma^{(2)}(\epsilon)$ in its turn may be thought of as a selfenergy operator in the two-qubit excitation subspace. $\mathcal{V}(\epsilon)$ and $\overline{\mathcal{V}}(\epsilon)$ may be understood as the renormalized absorption and emission vertex operators.

As it was anticipated above, the equations governing a two-photon scattering on a pair of qubits hold in the case of a two-photon scattering for a general N_q system. Bearing this in mind, in Fig. 5 we present the system of exact integral equations governing the general two-photon scattering problem in waveguide QED (i.e., equations defining $W^{(2,1)}$). These equations were first obtained in [71] in relation with the two-photon scattering problem on two distant qubits.

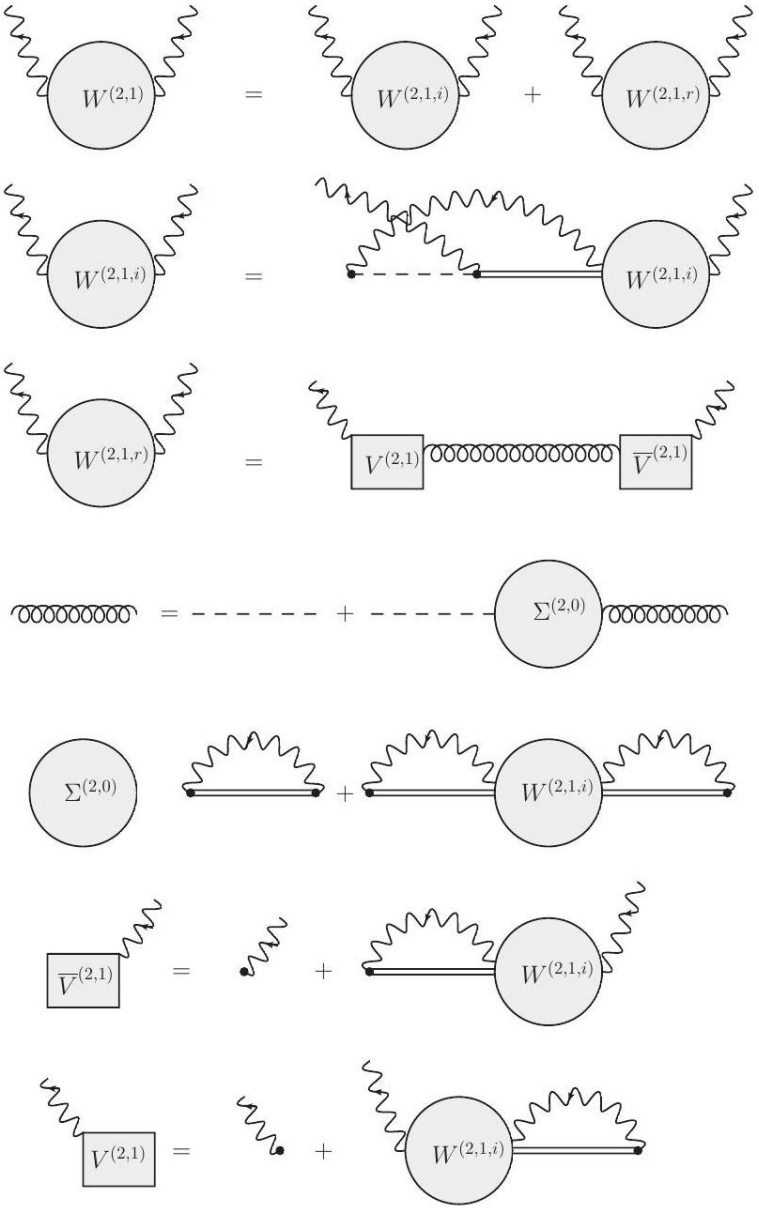

FIG. 5.

Equations corresponding to the general two-photon scattering problem. Equation in the first line describes the splitting of the effective single-particle vertex function $W^{(2,1)}$ in the generic twophoton scattering problem into its reducible $W^{(2,1,r)}$ and irreducible parts $W^{(2,1,i)}$. The irreducible part is generated from the fundamental process of the single-qubit waveguide QED $R^{(1)}$ (as shown in the second line) and thus satisfies the same integral equation as $W^{(1,1)}$. The reducible part, stemming from non-single-particle connectedness of the additional contribution to $R^{(2)}$ (see Fig. 4), is parametrized by the dressed Green's function $G^{(2,0)}$ in two-excitation subspace (shown as the curly line) as well as renormalized emission and absorption vertices (indicated by rectangles). As one can see, the entire system of equations boils down to the solution of the equation defining

the irreducible part of the vertex function since its knowledge is sufficient to completely determine both the renormalized vertices $V^{(2,1)}, \bar{V}^{(2,1)}$ as well as the self-energy $\Sigma^{(2,0)}$ in the two-excitation subspace.

7.7.2 3-qubit waveguide QED

Theory

Let us finally dedicate our attention to three-qubit waveguide QED systems. Due to the enormous increase in the computational complexity, we restrict ourselves to the first nontrivial subspace within such a setup: A three-excitation subspace. As before, the starting point of the analysis is Eq. (17). No doubt, both of the "diagonal" terms $\sim v^\dagger v$ and $\sim vv^\dagger$ give a nonzero contribution to the transition operator as it was the case in the previous section; however, one can clearly see that now the "off-diagonal" terms $\left(vv, v^\dagger v^\dagger\right)$ have to be also taken into account. By defining the operators

$$\mathcal{D}_+ = a^\dagger_{s'} v_{s'} \mathcal{G}_0 a^\dagger_s v_s, \quad \mathcal{D}_- = v^\dagger_{s'} a_{s'} \mathcal{G}_0 v^\dagger_s a_s$$

bearing in mind the rotating wave approximation, and resuming the series (17) to incorporate the diagonal terms and again making use of RWA, in the realm of $N_q = 3$ waveguide QED, we obtain

$$\begin{aligned}
&\left\langle N'_p, g \left| \mathcal{T}^{(3)} \right| N_p, g \right\rangle = \left\langle N'_p, g \left| a^\dagger_{s'_1} v_{s'_1} \frac{1}{\left(\mathcal{G}^{(1)}\right)^{-1} - \mathcal{R}^{(3)}} v^\dagger_{s_1} a_{s_1} \right| N_p, g \right\rangle \\
&\mathcal{R}^{(3)} = \mathcal{R}^{(2)} + \mathcal{D} \\
&\mathcal{D} = \mathcal{D}_+ \frac{1}{\left(\mathcal{G}^{(1)}\right)^{-1} - \mathcal{R}^{(2)}} \mathcal{D}_- = \mathcal{R}^{(2)} + \mathcal{D}_+ \mathcal{G}^{(1)} \mathcal{D}_- + \mathcal{D}_+ \mathcal{G}^{(1)} \mathcal{W}^{(2)} \mathcal{G}^{(1)} \mathcal{D}_-
\end{aligned}$$

As usual, we define the $\mathcal{W}^{(3)}$ operator according to

$$\mathcal{W}^{(3)} := \mathcal{D} + \mathcal{D}\left(\mathcal{G}^{(1)} + \mathcal{G}^{(1)} \mathcal{W}^{(2)} \mathcal{G}^{(1)}\right) \mathcal{W}^{(3)}$$

which brings the transition operator to the following form:

$$\left\langle N'_p, g \left| \mathcal{T}^{(3)} \right| N_p, g \right\rangle = \left\langle N'_p, g \left| \mathcal{T}^{(2)} + a^\dagger_{s'_1} v_{s'_1} \mathcal{G}^{(1)} \left(1 + \mathcal{W}^{(2)} \mathcal{G}^{(1)}\right) \mathcal{W}^{(3)} \left(\mathcal{G}^{(1)} \mathcal{W}^{(2)} + 1\right) \mathcal{G}^{(1)} v^\dagger_{s_1} a_{s_1} \right| N_p, g \right\rangle$$

Upon the projection, onto the three-photon subspace, we obtain the following set of equations governing the generic (see Sec. II B) three-particle T matrix (see Appendix C for the detailed derivation):

$$\begin{aligned}
T^{(3,3)}_{s'_1 s'_2 s'_3, s_1 s_2 s_3}(\epsilon) &= \langle g | v_{s'_1} G^{(1)}(\epsilon - \omega_{s'_2} - \omega_{s'_3}) \left[W^{(2,2)}_{s'_2 s_3, s_2 s_3}(\epsilon) + V^{(3,2)}_{s'_2 s'_3}(\epsilon) G^{(3,0)}(\epsilon) \bar{V}^{(3,2)}_{s_2 s_3}(\epsilon) \right] G^{(1)}(\epsilon - \omega_{s_2} - \omega_{s_3}) v^\dagger_{s_1} | g \rangle \\
&=: \langle g | v_{s'_1} G^{(1)}(\epsilon - \omega_{s'_2} - \omega_{s'_3}) \left[W^{(2,2)}_{s'_2 s'_3, s_2 s_3}(\epsilon) + W^{(3,2)}_{s'_2 s_3, s_2 s_3}(\epsilon) \right] G^{(1)}(\epsilon - \omega_{s_2} - \omega_{s_3}) v^\dagger_{s_1} | g \rangle
\end{aligned}$$

$$G^{(3,0)}(\epsilon) = G^{(1)}(\epsilon) + G^{(1)}(\epsilon) \Sigma^{(3,0)}(\epsilon) G^{(3,0)}(\epsilon)$$

$$\begin{aligned}
\Sigma^{(3,0)}(\epsilon) &= \left[v^\dagger_s G_0(\epsilon - \omega_s) v^\dagger_{s'} + v^\dagger_{s'} G_0(\epsilon - \omega_{s'}) v^\dagger_s \right] G^{(1)}(\epsilon - \omega_s - \omega_{s'}) V^{(3,2)}_{ss'}(\epsilon) \equiv \\
&\equiv \bar{V}^{(3,2)}_{ss'}(\epsilon) G^{(1)}(\epsilon - \omega_s - \omega_{s'}) \left[v_{s'} G_0(\epsilon - \omega_s) v_s + v_s G_0(\epsilon - \omega_{s'}) v_{s'} \right]
\end{aligned}$$

$$\bar{V}^{(3,2)}_{s_1 s_2}(\epsilon) = v^\dagger_{s_1} G^{(2,0)}(\epsilon) \bar{V}^{(2,1)}_{s_2}(\epsilon) + \bar{V}^{(3,2)}_{s s_1}(\epsilon) G^{(1)}(\epsilon - \omega_s) W^{(2,1)}_{s, s_2}(\epsilon)$$

$$V^{(3,2)}_{s'_1 s'_2}(\epsilon) = V^{(2,1)}_{s'_1}(\epsilon) G^{(2,0)}(\epsilon) v^\dagger_{s'_2} + W^{(2,1)}_{s'_1, s}(\epsilon) G^{(1)}(\epsilon - \omega_s) V^{(3,2)}_{s'_2 s}(\epsilon)$$

Here $G^{(2,0)}(\epsilon)$ is the projection of (56) onto the photon vacuum state. As usual, the above equation may be compactly represented diagrammatically as shown in Fig. 6.

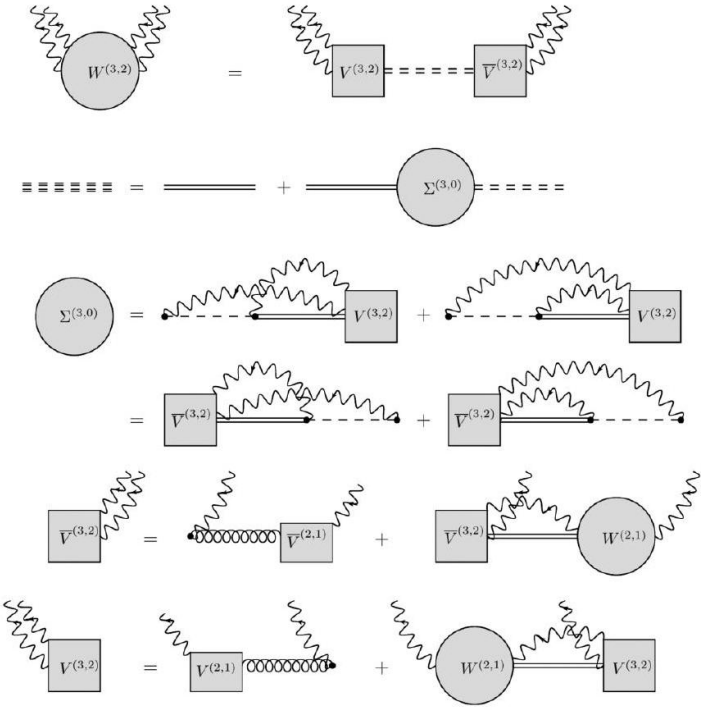

FIG. 6.
Equations corresponding to the general three-photon scattering problem. Here the first line defines the effective two-body vertex function $W^{(3,2)}$ in terms of the dressed Green's function in three-excitation subspace shown as a double dashed line as well as effective two-photon absorption and emission vertices depicted by square boxes with a pair of incoming and outgoing amputated photon legs (note that these vertices correspond to the absorption and emission of photon pairs by a system as a whole). As it is shown in the last five lines the effective two-photon emission and absorption vertices as well as the self-energy bubble defining the Green's function in the three-excitation subspace satisfy a closed hierarchy of self-consistent equations, the validity of which is directly proven in Appendix C. Curly lines as well as the rectangular boxes with single amputated photon lines are precisely defined in Fig. 5.

7.7.3 Derivation of the Diagrammatic Technique on a Simple Example (!?!?!?)

Вывод

(а то так в общем формализме и утонуть просто запросто можно. нет, пока не усвоил это.)

7.7.4 Diagrammatic representation of the generic 3-body transition operator (?????)

In this Appendix we start our analysis with Eq. (64). Taking matrix elements of (64) in the three-particle subspace we arrive at the following integral equation:

$$
\begin{aligned}
&W^{(3,2)}_{s_1 s_2', s_1 s_2}(\epsilon) = D^{(2)}_{s_1' s_2', s_1 s_2}(\epsilon) + \left[D^{(2)}_{s_1' s_2', \bar{s}_2' \bar{s}_1'}(\epsilon) + D^{(2)}_{s_1' s_2', \bar{s}_1' \bar{s}_2'}(\epsilon)\right] G^{(1)}\left(\epsilon - \omega_{\bar{s}_1'} - \omega_{\bar{s}_2'}\right) W^{(3,2)}_{\bar{s}_1' \bar{s}_2, s_1 s_2}(\epsilon) \\
&+ D^{(2)}_{s_1' s_2', \bar{s}_1' \bar{s}_2}(\epsilon) G^{(1)}\left(\epsilon - \omega_{\bar{s}_1'} - \omega_{\bar{s}_2}\right) W^{(2,1)}_{\bar{s}_2, \bar{s}_2'}(\epsilon) G^{(1)}\left(\epsilon - \omega_{\bar{s}_1'} - \omega_{\bar{s}_2'}\right) W^{(3,2)}_{\bar{s}_1' \bar{s}_2', s_1 s_2}(\epsilon) \\
&+ D^{(2)}_{s_1' s_2', \bar{s}_1 \bar{s}_1'}(\epsilon) G^{(1)}\left(\epsilon - \omega_{\bar{s}_1} - \omega_{\bar{s}_1'}\right) W^{(2,1)}_{\bar{s}_1, \bar{s}_2'}(\epsilon) G^{(1)}\left(\epsilon - \omega_{\bar{s}_1'} - \omega_{\bar{s}_2'}\right) W^{(3,2)}_{\bar{s}_1' s_2', s_1 s_2}(\epsilon) \\
&+ D^{(2)}_{s_1' s_2', \bar{s}_1 \bar{s}_2'}(\epsilon) G^{(1)}\left(\epsilon - \omega_{\bar{s}_1} - \omega_{\bar{s}_2'}\right) W^{(2,1)}_{\bar{s}_1, \bar{s}_1'}(\epsilon) G^{(1)}\left(\epsilon - \omega_{\bar{s}_1'} - \omega_{\bar{s}_2'}\right) W^{(3,2)}_{\bar{s}_1' \bar{s}_2', s_1 s_2}(\epsilon) \\
&+ D^{(2)}_{s_1' s_2', \bar{s}_2' \bar{s}_2}(\epsilon) G^{(1)}\left(\epsilon - \omega_{\bar{s}_2'} - \omega_{\bar{s}_2}\right) W^{(2,1)}_{\bar{s}_2, \bar{s}_1'}(\epsilon) G^{(1)}\left(\epsilon - \omega_{\bar{s}_1'} - \omega_{\bar{s}_2'}\right) W^{(3,2)}_{\bar{s}_1' \bar{s}_2', \mathcal{S}_1 s_2}(\epsilon) \\
&+ D^{(2)}_{s_1' s_2', \bar{s}_1 \bar{s}_2}(\epsilon) G^{(1)}(\epsilon - \omega_{\bar{s}_1} - \omega_{\bar{s}_2}) W^{(2,2)}_{\bar{s}_2 \bar{s}_1, \bar{s}_2' \bar{s}_1'}(\epsilon) G^{(1)}\left(\epsilon - \omega_{\bar{s}_1'} - \omega_{\bar{s}_2'}\right) W^{(3,2)}_{\bar{s}_1' \bar{s}_2', , 1 s_2}(\epsilon) \\
&+ D^{(2)}_{s_1' s_2', \bar{s}_1 \bar{s}_2}(\epsilon) G^{(1)}(\epsilon - \omega_{\bar{s}_1} - \omega_{\bar{s}_2}) W^{(2,2)}_{\bar{s}_1 \bar{s}_2, \bar{s}_2' \bar{s}_1'}(\epsilon) G^{(1)}\left(\epsilon - \omega_{\bar{s}_1'} - \omega_{\bar{s}_2'}\right) W^{(3,2)}_{\bar{s}_1' \bar{s}_2', s_1 s_2}(\epsilon) \\
&+ D^{(2)}_{s_1' s_2', \bar{s}_1 \bar{s}_2}(\epsilon) G^{(1)}(\epsilon - \omega_{\bar{s}_1} - \omega_{\bar{s}_2}) W^{(2,2)}_{\bar{s}_1 \bar{s}_2, \bar{s}_1' \bar{s}_2'}(\epsilon) G^{(1)}\left(\epsilon - \omega_{\bar{s}_1'} - \omega_{\bar{s}_2'}\right) W^{(3,2)}_{\bar{s}_1' \bar{s}_2', , 1 s_2}(\epsilon) \\
&+ D^{(2)}_{s_1' s_2', \bar{s}_1 \bar{s}_2}(\epsilon) G^{(1)}(\epsilon - \omega_{\bar{s}_1} - \omega_{\bar{s}_2}) W^{(2,2)}_{\bar{s}_2' \bar{s}_1, \bar{s}_1' \bar{s}_2'}(\epsilon) G^{(1)}\left(\epsilon - \omega_{\bar{s}_1'} - \omega_{\bar{s}_2'}\right) W^{(3,2)}_{\bar{s}_1' \bar{s}_2', s_1 s_2}(\epsilon),
\end{aligned}
$$

where the projection of $\mathcal{D}$ onto the two-particle subspace is given by

$$D^{(2)}_{s_1's_2',s_1s_2}(\epsilon) = v_{s_1'}G_0\left(\epsilon-\omega_{s_2'}\right)v_{s_2'}G^{(1)}(\epsilon)v^\dagger_{s_2}G_0\left(\epsilon-\omega_{s_2}\right)v^\dagger_{s_1}$$

Keeping this in mind we make the following ansatz:

$$W^{(3,2)}_{s_1's_2',s_1s_2}(\epsilon) = v_{s_1'}G_0\left(\epsilon-\omega_{s_2'}\right)v_{s_2'}G^{(3,0)}(\epsilon)v^\dagger_{s_2}G_0\left(\epsilon-\omega_{s_2}\right)v^\dagger_{s_1}$$

This, in turn, leads to the following Dyson equation:

$$G^{(3,0)}(\epsilon) = G^{(1)}(\epsilon) + G^{(1)}(\epsilon)\Sigma^{(3,0)}(\epsilon)G^{(3,0)}(\epsilon)$$

where the self-energy in the three-excitation subspace is given by

$$\begin{aligned}
\Sigma^{(3,0)}(\epsilon) &= \left[v^\dagger_{s_1'}G_0\left(\epsilon-\omega_{s_1'}\right)v^\dagger_{s_2'} + v^\dagger_{s_2'}G_0\left(\epsilon-\omega_{s_2'}\right)v^\dagger_{s_1'}\right]G^{(1)}\left(\epsilon-\omega_{s_1'}-\omega_{s_2'}\right)v_{s_1'}G_0\left(\epsilon-\omega_{s_2'}\right)v_{s_2'}\\
&+ v^\dagger_{s_2}G_0\left(\epsilon-\omega_{s_2}\right)v^\dagger_{s_1'}G^{(1)}\left(\epsilon-\omega_{s_1'}-\omega_{s_2}\right)W^{(2,1)}_{s_2,s_2'}(\epsilon)G^{(1)}\left(\epsilon-\omega_{s_1'}-\omega_{s_2'}\right)v_{s_1'}G_0\left(\epsilon-\omega_{s_2'}\right)v_{s_2'}\\
&+ v^\dagger_{s_1'}G_0\left(\epsilon-\omega_{s_1'}\right)v^\dagger_{s_1}G^{(1)}\left(\epsilon-\omega_{s_1}-\omega_{s_1'}\right)W^{(2,1)}_{s_1,s_2'}(\epsilon)G^{(1)}\left(\epsilon-\omega_{s_1'}-\omega_{s_2'}\right)v_{s_1'}G_0\left(\epsilon-\omega_{s_2'}\right)v_{s_2'}\\
&+ v^\dagger_{s_2'}G_0\left(\epsilon-\omega_{s_2'}\right)v^\dagger_{s_1}G^{(1)}\left(\epsilon-\omega_{s_1}-\omega_{s_2'}\right)W^{(2,1)}_{s_1,s_1'}(\epsilon)G^{(1)}\left(\epsilon-\omega_{s_1'}-\omega_{s_2'}\right)v_{s_1'}G_0\left(\epsilon-\omega_{s_2'}\right)v_{s_2'}\\
&+ v^\dagger_{s_2}G_0\left(\epsilon-\omega_{s_2}\right)v^\dagger_{s_2'}G^{(1)}\left(\epsilon-\omega_{s_2'}-\omega_{s_2}\right)W^{(2,1)}_{s_2,s_1'}(\epsilon)G^{(1)}\left(\epsilon-\omega_{s_1'}-\omega_{s_2'}\right)v_{s_1'}G_0\left(\epsilon-\omega_{s_2'}\right)v_{s_2'}\\
&+ v^\dagger_{s_2}G_0\left(\epsilon-\omega_{s_2}\right)v^\dagger_{s_1}G^{(1)}(\epsilon-\omega_{s_1}-\omega_{s_2})W^{(2,2)}_{s_2s_1,s_2's_1'}(\epsilon)G^{(1)}\left(\epsilon-\omega_{s_1'}-\omega_{s_2'}\right)v_{s_1'}G_0\left(\epsilon-\omega_{s_2'}\right)v_{s_2'}\\
&+ v^\dagger_{s_2}G_0\left(\epsilon-\omega_{s_2}\right)v^\dagger_{s_1}G^{(1)}(\epsilon-\omega_{s_1}-\omega_{s_2})W^{(2,2)}_{s_1s_2,s_2's_1'}(\epsilon)G^{(1)}\left(\epsilon-\omega_{s_1'}-\omega_{s_2'}\right)v_{s_1'}G_0\left(\epsilon-\omega_{s_2'}\right)v_{s_2'}\\
&+ v^\dagger_{s_2}G_0\left(\epsilon-\omega_{s_2}\right)v^\dagger_{s_1}G^{(1)}(\epsilon-\omega_{s_1}-\omega_{s_2})W^{(2,2)}_{s_1s_2,s_1's_2'}(\epsilon)G^{(1)}\left(\epsilon-\omega_{s_1'}-\omega_{s_2'}\right)v_{s_1'}G_0\left(\epsilon-\omega_{s_2'}\right)v_{s_2'}\\
&+ v^\dagger_{s_2}G_0\left(\epsilon-\omega_{s_2}\right)v^\dagger_{s_1}G^{(1)}(\epsilon-\omega_{s_1}-\omega_{s_2})W^{(2,2)}_{s_2s_1,s_1's_2'}(\epsilon)G^{(1)}\left(\epsilon-\omega_{s_1'}-\omega_{s_2'}\right)v_{s_1'}G_0\left(\epsilon-\omega_{s_2'}\right)v_{s_2'}.
\end{aligned}$$

Let us now consider the expression (65) for the transition operator. Concentrating on the three-photon subspace we obtain

$$\begin{aligned}
T^{(3)}_{s_1's_2's_3',s_1s_2s_3}(\epsilon) &= \left\langle g\left|v_{s_1'}G^{(1)}\left(\epsilon-\omega_{s_2'}-\omega_{s_3'}\right)\left[W^{(2,2)}_{s_2's_3',s_2s_3}(\epsilon) + V^{(3,2)}_{s_2's_3'}(\epsilon)G^{(3,0)}(\epsilon)\bar{V}^{(3,2)}_{s_2s_3}(\epsilon)\right]G^{(1)}(\epsilon-\omega_{s_2}-\omega_{s_3})\,v^\dagger_{s_1}\right|g\right\rangle,\\
V^{(3,2)}_{s_1's_2'} &= v_{s_1'}G_0(\epsilon)v_{s_2'} + W^{(2,1)}_{s_1',s}(\epsilon)G^{(1)}(\epsilon-\omega_s)v_sG_0(\epsilon)v_{s_2'} + W^{(2,1)}_{s_1',s}(\epsilon)G^{(1)}(\epsilon-\omega_s)v_{s_2'}G_0(\epsilon-\omega_s)v_s\\
&+ W^{(2,2)}_{s_1's_2',\bar{s}_1's_2'}(\epsilon)G^{(1)}\left(\epsilon-\omega_{\bar{s}_1'}-\omega_{\bar{s}_2'}\right)v_{\bar{s}_1'}G_0\left(\epsilon-\omega_{\bar{s}_2'}\right)v_{\bar{s}_2'}\\
&+ W^{(2)}_{s_1's_2,\bar{s}_2'\bar{s}_1'}(\epsilon)G^{(1)}\left(\epsilon-\omega_{\bar{s}_1'}-\omega_{\bar{s}_2'}\right)v_{\bar{s}_1'}G_0\left(\epsilon-\omega_{\bar{s}_2'}\right)v_{\bar{s}_2'}\\
\bar{V}^{(3,2)}_{s_1s_2} &= v_{s_1}G_0(\epsilon)v_{s_2} + v^\dagger_{s_1}G_0(\epsilon)v^\dagger_{s'}G^{(1)}(\epsilon-\omega_{s'})\,W^{(2,1)}_{s',s_2}(\epsilon) + v^\dagger_{s'}G_0\left(\epsilon-\omega_{s'}\right)v^\dagger_{s_1}G^{(1)}(\epsilon-\omega_{s'})\,W^{(2,1)}_{s',s_2}(\epsilon)\\
&+ v^\dagger_{\bar{s}_2}G_0\left(\epsilon-\omega_{\bar{s}_2}\right)v^\dagger_{\bar{s}_1}G^{(1)}(\epsilon-\omega_{\bar{s}_1}-\omega_{\bar{s}_2})\,W^{(2,2)}_{\bar{s}_1\bar{s}_2,s_1s_2}(\epsilon)\\
&+ v^\dagger_{\bar{s}_2}G_0\left(\epsilon-\omega_{\bar{s}_2}\right)v^\dagger_{\bar{s}_1}G^{(1)}(\epsilon-\omega_{\bar{s}_1}-\omega_{\bar{s}_2})\,W^{(2,2)}_{\bar{s}_2\bar{s}_1,s_1s_2}(\epsilon).
\end{aligned}$$

Now, our goal is to rewrite the renormalized two-particle emission $V_{s_1's_2'}$ and absorption $\bar{V}_{s_1s_2}$ vertices, as well as the self-energy in three-excitation subspace $\Sigma^{(3,3)}$ in terms of full Green's and vertex functions, as it is presented in the main text.

First, we note the following identity:

$$\begin{aligned}
&v_{s_1'}G_0(\epsilon)v_{s_2'} + W^{(2,1)}_{s_1',s}(\epsilon)G^{(1)}(\epsilon-\omega_s)v_sG_0(\epsilon)v_{s_2'} = v_{s_1'}G_0(\epsilon)v_{s_2'} + W^{(2,1,i)}_{s_1',s}(\epsilon)G^{(1)}(\epsilon-\omega_s)v_sG_0(\epsilon)v_{s_2'}\\
&\quad + V^{(2,1)}_{s_1'}(\epsilon)G^{(2,0)}(\epsilon)\bar{V}^{(2,1)}_s(\epsilon)G^{(1)}(\epsilon-\omega_s)v_sG_0(\epsilon)v_{s_2'} = v_{s_1'}G_0(\epsilon)v_{s_2'} + W^{(2,1,i)}_{s_1',s}G^{(1)}(\epsilon-\omega_s)v_sG_0(\epsilon)v_{s_2'}\\
&\quad + V^{(2,1)}_{s_1'}(\epsilon)G^{(2,0)}(\epsilon)\Sigma^{(2,0)}G_0(\epsilon)v_{s_2'} = v_{s_1'}G_0(\epsilon)v_{s_2'} + W^{(2,1,i)}_{s_1',s}(\epsilon)G^{(1)}(\epsilon-\omega_s)v_sG_0(\epsilon)v_{s_2'}\\
&\quad + V^{(2,1)}_{s_1'}(\epsilon)\left[G^{(2,0)}(\epsilon) - G_0(\epsilon)\right]v_{s_2'} = V^{(2,1)}_{s_1'}(\epsilon)G^{(2,0)}(\epsilon)v_{s_2'}.
\end{aligned}$$

Analogously

$$v^\dagger_{s_1}G_0(\epsilon)v^\dagger_{s_2} + v^\dagger_{s_1}G_0(\epsilon)v^\dagger_{s'}G^{(1)}(\epsilon-\omega_{s'})\,W^{(2,1)}_{s',s_2}(\epsilon) = v^\dagger_{s_1}G^{(2,0)}(\epsilon)\bar{V}^{(2,1)}_{s_2}(\epsilon)$$

Analyzing the structure of equations satisfied by $W^{(2,1)}$ and $W^{(2,2)}$ one easily concludes that

$$W^{(2,2)}_{s_1s_2',s_1s_2}(\epsilon) = W^{(2,1)}_{s_1',s_1}(\epsilon)G^{(1)}(\epsilon)W^{(2,1)}_{s_2',s_2}(\epsilon) + W^{(2,1)}_{s_1',s}(\epsilon)G^{(1)}(\epsilon-\omega_s)W^{(2,2)}_{s_2's,s_1s_2}(\epsilon)$$

$$W^{(2,2)}_{s_1's_2',s_1s_2}(\epsilon) = W^{(2,1)}_{s_1',s_1}(\epsilon)G^{(1)}(\epsilon)W^{(2,1)}_{s_2',s_2}(\epsilon) + W^{(2,2)}_{s_1's_2',ss_1}(\epsilon)G^{(1)}(\epsilon-\omega_s)W^{(2,1)}_{s,s_2}(\epsilon)$$

Multiplying (C11) and (C12) by $G^{(1)}(\epsilon)v_{s_2}G_0(\epsilon)v_{s_1}$ from the right and by $v^\dagger_{s_2'}G_0(\epsilon)v^\dagger_{s_1'}G^{(1)}(\epsilon)$ from the left, respectively, and contracting the relevant indices, we obtain

$$W^{(2,2)}_{s_1's_2',s_1s_2}(\epsilon)G^{(1)}(\epsilon-\omega_{s_1}-\omega_{s_2})\,v_{s_2}G_0\,(\epsilon-\omega_{s_2})\,v_{s_1}=W^{(2,1)}_{s_1',s_1}(\epsilon)G^{(1)}(\epsilon-\omega_{s_1})\left[V^{(2,1)}_{s_2'}(\epsilon)G^{(2,0)}(\epsilon-\omega_{s_1})\,v_{s_1}\right.$$
$$\left.-\,v_{s_2'}G_0\,(\epsilon-\omega_{s_1}\right]+W^{(2,1)}_{s_1',s}(\epsilon)G^{(1)}(\epsilon-\omega_s)W^{(2,2)}_{s_2's,s_1s_2}(\epsilon)G^{(1)}(\epsilon-\omega_{s_1}-\omega_{s_2})\,v_{s_2}G_0\,(\epsilon-\omega_{s_1})\,v_{s_1},$$
$$v^\dagger_{s_2'}G_0\left(\epsilon-\omega_{s_2'}\right)v^\dagger_{s_1'}G^{(1)}\left(\epsilon-\omega_{s_1'}-\omega_{s_2'}\right)W^{(2,2)}_{s_1's_2',s_1s_2}(\epsilon)=\left[v^\dagger_{s_2'}G^{(2,0)}\left(\epsilon-\omega_{s_2'}\right)\bar V^{(2,1)}_{s_1}(\epsilon)-v^\dagger_{s_2'}G_0\left(\epsilon-\omega_{s_2'}\right)v^\dagger_{s_1}\right]$$
$$\cdot\,G^{(1)}\left(\epsilon-\omega_{s_2'}\right)W^{(2,1)}_{s_2',s_2}+v^\dagger_{s_2'}G_0\left(\epsilon-\omega_{s_1'}\right)v^\dagger_{s_1'}G^{(1)}\left(\epsilon-\omega_{s_1'}-\omega_{s_2'}\right)W^{(2,2)}_{s_1's_2',ss_1}G^{(1)}(\epsilon-\omega_s)W^{(2,1)}_{s,s_2}(\epsilon).$$

Now, defining the objects

$$K^{(d)}_{s_1's_2'}(\epsilon)=W^{(\epsilon,2)}_{s_1's_2',s_1s_2}(\epsilon)G^{(1)}(\epsilon-\omega_{s_2}-\omega_{s_1})\,v_{s_2}G_0\,(\epsilon-\omega_{s_1})\,v_{s_1}+W^{(2,1)}_{s_1',s_1}(\epsilon)G^{(1)}(\epsilon-\omega_{s_1})\,v_{s_2'}G_0\,(\epsilon-\omega_{s_1})\,v_{s_1},$$
$$\bar K^{(d)}_{s_1s_2}(\epsilon)=v^\dagger_{s_2'}G_0\left(\epsilon-\omega_{s_2'}\right)v^\dagger_{s_1'}G^{(1)}\left(\epsilon-\omega_{s_1'}-\omega_{s_2'}\right)W^{(2,2)}_{s_1's_2',s_1s_2}(\epsilon)+v^\dagger_{s_2'}G_0\left(\epsilon-\omega_{s_2'}\right)v^\dagger_{s_1}G^{(1)}\left(\epsilon-\omega_{s_2'}\right)W^{(2,1)}_{s_2',s_2}(\epsilon),$$

we establish the following equations:

$$\begin{aligned}K^{(d)}_{s_1's_2'}(\epsilon)=&W^{(2,1)}_{s_1',s_1}(\epsilon)G^{(1)}(\epsilon-\omega_{s_1})\,V^{(2,1)}_{s_2'}(\epsilon-\omega_{s_1})\,G^{(2,0)}(\epsilon-\omega_{s_1})\,v_{s_1}\\&+W^{(2,1)}_{s_1',s}(\epsilon)G^{(1)}(\epsilon-\omega_s)\left[K^{(d)}_{s_2's}(\epsilon)-W^{(2,1)}_{s_2',s_1}(\epsilon-\omega_s)G^{(1)}(\epsilon-\omega_{s_1}-\omega_s)\,v_sG_0\,(\epsilon-\omega_{s_1})\,v_{s_1}\right],\\\bar K^{(d)}_{s_1s_2}(\epsilon)=&v^\dagger_{s_2'}G^{(2,0)}\left(\epsilon-\omega_{s_2'}\right)\bar V^{(2,1)}_{s_1}\left(\epsilon-\omega_{s_2'}\right)G^{(1)}\left(\epsilon-\omega_{s_2'}\right)W^{(1,0)}_{s_2',s_2}(\epsilon)\\&+\left[\bar K^{(d)}_{ss_1}(\epsilon)-v^\dagger_{s_2'}G_0\left(\epsilon-\omega_{s_2'}\right)v^\dagger_sG^{(1)}\left(\epsilon-\omega_{s_2'}-\omega_s\right)W^{(2,1)}_{s_2',s_1}(\epsilon-\omega_s)\right]G^{(1)}(\epsilon-\omega_s)W^{(2,1)}_{s,s_2}(\epsilon).\end{aligned}$$

Analogously, multiplying (C11) and (C12) by $G^{(1)}(\epsilon)v_{s_1}G_0(\epsilon)v_{s_2}$ from the right and by $v^\dagger_{s_1'}G_0(\epsilon)v^\dagger_{s_2'}G^{(1)}(\epsilon)$ from the left, respectively, contracting the $s_{1,2}$ indices, and defining

$$K^{(e)}_{s_1's_2'}(\epsilon)=W^{(2,2)}_{s_1's_2',s_1s_2}(\epsilon)G^{(1)}(\epsilon-\omega_{s_1}-\omega_{s_2})\,v_{s_1}G_0\,(\epsilon-\omega_{s_2})\,v_{s_2},$$
$$\bar K^{(e)}_{s_1s_2}(\epsilon)=v^\dagger_{s_1'}G_0\left(\epsilon-\omega_{s_1'}\right)v^\dagger_{s_2'}G^{(1)}\left(\epsilon-\omega_{s_1'}-\omega_{s_2'}\right)W^{(2,2)}_{s_1's_2',s_1s_2}(\epsilon),$$

we deduce

$$K^{(e)}_{s_1's_2'}(\epsilon)=W^{(2,1)}_{s_1',s_1}(\epsilon)G^{(1)}(\epsilon-\omega_{s_1})\,W^{(2,1)}_{s_2',s_2}(\epsilon-\omega_{s_1})\,G^{(1)}(\epsilon-\omega_{s_1}-\omega_{s_2})\,v_{s_1}G_0\,(\epsilon-\omega_{s_2})\,v_{s_2}+W^{(2,1)}_{s_1',s}(\epsilon)G^{(1)}(\epsilon-\omega_s)K^{(e)}_{s_2's}(\epsilon),$$
$$\bar K^{(e)}_{s_1s_2}(\epsilon)=v^\dagger_{s_1'}G_0\left(\epsilon-\omega_{s_1'}\right)v^\dagger_{s_2'}G^{(1)}\left(\epsilon-\omega_{s_1'}-\omega_{s_2'}\right)W^{(2,1)}_{s_1',s_1}\left(\epsilon-\omega_{s_2'}\right)G^{(1)}\left(\epsilon-\omega_{s_2'}\right)W^{(2,1)}_{s_2',s_2}(\epsilon)+\bar K^{(e)}_{ss_1}(\epsilon)G^{(1)}(\epsilon-\omega_s)W^{(2,1)}_{s,s_2}(\epsilon)$$

Further, we define

$$K_{s_1's_2'}(\epsilon)=K^{(d)}_{s_1's_2'}(\epsilon)+K^{(e)}_{s_1's_2'}(\epsilon),$$
$$\bar K_{s_1s_2}(\epsilon)=\bar K^{(d)}_{s_1s_2}(\epsilon)+\bar K^{(e)}_{s_1s_2}(\epsilon).$$

With these definitions it is easy to show that the two-particle emission and absorption vertices are given by

$$V^{(3,2)}_{s_1's_2'}(\epsilon)=V^{(2,1)}_{s_1'}(\epsilon)G^{(2,0)}(\epsilon)V^{(2,1)}_{s_2'}(\epsilon)+\tilde K_{s_1's_2'}(\epsilon),$$
$$\bar V^{(3,2)}_{s_1s_2}(\epsilon)=\bar V^{(2,1)}_{s_1}(\epsilon)G^{(2,0)}(\epsilon)\bar V^{(2,1)}_{s_2}(\epsilon)+\tilde{\bar K}_{s_1s_2}(\epsilon),$$

Where

$$\tilde K_{s_1's_2'}(\epsilon)=K_{s_1's_2'}(\epsilon)-V^{(2,1)}_{s_1'}(\epsilon)G^{(2,0)}(\epsilon)W^{(2,1,i)}_{s_2',s_1}(\epsilon)G^{(1)}(\epsilon-\omega_{s_1})\,v_{s_1},$$
$$\tilde{\bar K}_{s_1s_2}(\epsilon)=\bar K_{s_1s_2}(\epsilon)$$
$$-\,v^\dagger_{s_2'}G^{(1)}\left(\epsilon-\omega_{s_2'}\right)W^{(2,1,i)}_{s_2',s_1}(\epsilon)G^{(2,0)}(\epsilon)\bar V^{(2,1)}_{s_2}(\epsilon)$$

obey the following integral equations:

$$\begin{aligned}\tilde K_{s_1s_2'}(\epsilon)=&W^{(2,1)}_{s_1',s}(\epsilon)G^{(1)}(\epsilon-\omega_s)V^{(2,1)}_{s_2'}(\epsilon-\omega_s)G^{(2,0)}(\epsilon-\omega_s)V^{(2,1)}_s(\epsilon)-V^{(2,1)}_{s_1'}(\epsilon)G^{(2,0)}(\epsilon)W^{(2,1,i)}_{s_2',s}(\epsilon)G^{(1)}(\epsilon-\omega_s)v_s\\&+W^{(2,1)}_{s_1,s}(\epsilon)G^{(1)}(\epsilon-\omega_s)\tilde K_{s_2's}(\epsilon),\\\tilde{\bar K}_{s_1s_2}(\epsilon)=&\bar V^{(2,1)}_s(\epsilon)G^{(2,0)}(\epsilon-\omega_s)V^{(2,1)}_{s_1}(\epsilon-\omega_s)G^{(1)}(\epsilon-\omega_s)W^{(2,1)}_{s,s_2}(\epsilon)-v^\dagger_sG^{(1)}(\epsilon-\omega_s)W^{(2,1,i)}_{s,s_1}(\epsilon)G^{(2,0)}(\epsilon)\bar V^{(2,1)}_{s_2}(\epsilon)\\&+\tilde{\bar K}_{ss_1}(\epsilon)G^{(1)}(\epsilon-\omega_s)W^{(2,1)}_{s,s_2}(\epsilon).\end{aligned}$$

Using Eqs. (C25) and (C26) together with (C29) and (C30), we finally arrive at the following equations:

$$V^{(3,2)}_{s_1s_2'}(\epsilon)=V^{(2,1)}_{s_1'}(\epsilon)G^{(2,0)}(\epsilon)v_{s_2'}+W^{(2,1)}_{s_1,s}(\epsilon)G^{(1)}(\epsilon-\omega_s)V^{(3,2)}_{s_2'}(\epsilon),$$
$$\bar V^{(3,2)}_{s_1s_2}(\epsilon)=v_{s_1}G^{(2,1)}(\epsilon)\bar V_{s_2}(\epsilon)+\bar V^{(3,2)}_{ss_1}(\epsilon)G^{(1)}(\epsilon-\omega_s)W^{(2,1)}_{s,s_2}(\epsilon),$$

which are precisely Eqs. (70) and (71) stated in the main text.

Now, we turn our attention to the self-energy bubble. Let us show that Eqs. (68) and (69) hold via direct substitution. One has

$$
\begin{aligned}
\Sigma^{(3,0)}(\epsilon) &= \left[v^\dagger_{s'_1} G_0\left(\epsilon-\omega_{s'_1}\right) v^\dagger_{s'_2} + v^\dagger_{s'_2} G_0\left(\epsilon-\omega_{s'_2}\right) v^\dagger_{s'_1}\right] G^{(1)}\left(\epsilon-\omega_{s'_1}-\omega_{s'_2}\right) V^{(3,2)}_{s_1 s'_2}(\epsilon) \\
&= v^\dagger_{s'_2}\left[G^{(2,0)}\left(\epsilon-\omega_{s'_2}\right) - G_0\left(\epsilon-\omega_{s_2}\right)\right] v_{s'_2} - v^\dagger_{s'_1} G_0\left(\epsilon-\omega_{s'_1}\right) v^\dagger_s G^{(1)}\left(\epsilon-\omega_{s'_1}-\omega_s\right) v_{s'_1} G_0(\epsilon-\omega_s) v_s \\
&+ v^\dagger_{s'_1} G_0\left(\epsilon-\omega_{s_1}\right) v^\dagger_{s'_2} G^{(1)}\left(\epsilon-\omega_{s'_1}-\omega_{s_2}\right) V^{(2,1)}_{s'_1}\left(\epsilon-\omega'_{s_2}\right) G^{(2,0)}\left(\epsilon-\omega'_{s_2}\right) v_{s'_2} \\
&+ v^\dagger_{s'_1} G^{(2,0)}\left(\epsilon-\omega_{s'_1}\right) \bar{V}^{(2,1)}_s\left(\epsilon-\omega_{s'_1}\right) G^{(1)}\left(\epsilon-\omega_s-\omega_{s'_1}\right) v_{s'_1} G_0(\epsilon-\omega_s) v_s \\
&+ v^\dagger_{s'_2} G_0\left(\epsilon-\omega_{s'_2}\right) v^\dagger_{s'_1} G^{(1)}\left(\epsilon-\omega_{s'_1}-\omega_{s'_2}\right) W^{(2,1)}_{s'_2,s}\left(\epsilon-\omega_{s'_1}\right) G^{(1)}\left(\epsilon-\omega_{s'_1}-\omega_s\right) v_{s'_1} G_0(\epsilon-\omega_s) v_s \\
&+ v^\dagger_{s'_1} G_0\left(\epsilon-\omega_{s'_1}\right) v^\dagger_{s'_2} G^{(1)}\left(\epsilon-\omega_{s'_1}-\omega_{s'_2}\right) W^{(2,2)}_{s'_1 s_2, s' s}(\epsilon) G^{(1)}(\epsilon-\omega_{s'}-\omega_s) v_{s'} G_0(\epsilon-\omega_s) v_s \\
&+ v^\dagger_{s'_1} G_0\left(\epsilon-\omega_{s'_1}\right) v^\dagger_{s'_2} G^{(1)}\left(\epsilon-\omega_{s'_1}-\omega_{s'_2}\right) W^{(2,2)}_{s'_1 s'^2_2, s'}(\epsilon) G^{(1)}(\epsilon-\omega_{s'}-\omega_s) v_{s'} G_0(\epsilon-\omega_s) v_s \\
&+ v^\dagger_{s'_2} G_0\left(\epsilon-\omega_{s'_2}\right) v^\dagger_{s'_1} G^{(1)}\left(\epsilon-\omega_{s'_1}-\omega_{s'_2}\right) W^{(2,2)}_{s'_1 s_2, s'_s s}(\epsilon) G^{(1)}(\epsilon-\omega_{s'}-\omega_s) v_{s'} G_0(\epsilon-\omega_s) v_s \\
&+ v^\dagger_{s'_2} G_0\left(\epsilon-\omega_{s'_2}\right) v^\dagger_{s'_1} G^{(1)}\left(\epsilon-\omega_{s'_1}-\omega_{s'_2}\right) W^{(2,2)}_{s'_1 s_2, , s'}(\epsilon) G^{(1)}(\epsilon-\omega_{s'}-\omega_s) v_{s'} G_0(\epsilon-\omega_s) v_s, \\
\Sigma^{(3,0)}(\epsilon) &= \bar{V}^{(3,2)}_{s_1 s_2} G^{(1)}(\epsilon-\omega_{s_1}-\omega_{s_2})\left(v_{s_1} G_0\left(\epsilon-\omega_{s_2}\right) v_{s_2} + v_{s_2} G_0\left(\epsilon-\omega_{s_1}\right) v_{s_1}\right) \\
&= v^\dagger_{s_2}\left[G^{(2,0)}(\epsilon-\omega_{s_2}) - G_0\left(\epsilon-\omega_{s_2}\right)\right] v_{s_2} - v^\dagger_{s'} G_0\left(\epsilon-\omega_{s'}\right) v^\dagger_{s_1} G^{(1)}(\epsilon-\omega_{s_1}-\omega_{s'})\, v_{s'} G_0\left(\epsilon-\omega_{s_1}\right) v_{s_1} \\
&+ v^\dagger_{s'} G_0\left(\epsilon-\omega_{s'}\right) v^\dagger_{s_1} G^{(1)}(\epsilon-\omega_{s_1}-\omega_{s'})\, V^{(2,1)}_{s'}(\epsilon-\omega_{s_1})\, G^{(2,0)}(\epsilon-\omega_{s_1})\, v_{s_1} \\
&+ v^\dagger_{s_2} G^{(2,0)}(\epsilon-\omega_{s_2})\, \bar{V}^{(2,1)}_{s_1}(\epsilon-\omega_{s_2})\, G^{(1)}(\epsilon-\omega_{s_1}-\omega_{s_2})\, v_{s_2} G_0\left(\epsilon-\omega_{s_1}\right) v_{s_1} \\
&+ v^\dagger_{s'} G_0\left(\epsilon-\omega_{s'}\right) v^\dagger_{s_1} G^{(1)}(\epsilon-\omega_{s'}-\omega_{s_1})\, W^{(2,1)}_{s',s_2}(\epsilon-\omega_{s_1})\, G^{(1)}(\epsilon-\omega_{s_1}-\omega_{s_2})\, v_{s_1} G_0\left(\epsilon-\omega_{s_2}\right) v_{s_2} \\
&+ v^\dagger_{s'} G_0\left(\epsilon-\omega_{s'}\right) v^\dagger_s G^{(1)}(\epsilon-\omega_s-\omega_{s'})\, W^{(2,2)}_{ss',s_1 s_2}(\epsilon) G^{(1)}(\epsilon-\omega_{s_1}-\omega_{s_2})\, v_{s_1} G_0\left(\epsilon-\omega_{s_2}\right) v_{s_2} \\
&+ v^\dagger_{s'} G_0\left(\epsilon-\omega_{s'}\right) v^\dagger_s G^{(1)}(\epsilon-\omega_s-\omega_{s'})\, W^{(2,2)}_{s's,s_1 s_2}(\epsilon) G^{(1)}(\epsilon-\omega_{s_1}-\omega_{s_2})\, v_{s_1} G_0\left(\epsilon-\omega_{s_2}\right) v_{s_2} \\
&+ v^\dagger_{s'} G_0\left(\epsilon-\omega_{s'}\right) v^\dagger_s G^{(1)}(\epsilon-\omega_s-\omega_{s'})\, W^{(2,2)}_{ss',s_1 s_2}(\epsilon) G^{(1)}(\epsilon-\omega_{s_1}-\omega_{s_2})\, v_{s_2} G_0\left(\epsilon-\omega_{s_1}\right) v_{s_1} \\
&+ v^\dagger_{s'} G_0\left(\epsilon-\omega_{s'}\right) v^\dagger_s G^{(1)}(\epsilon-\omega_s-\omega_{s'})\, W^{(2)}_{s',s_1 s_2}(\epsilon) G^{(1)}(\epsilon-\omega_{s_1}-\omega_{s_2})\, v_{s_2} G_0\left(\epsilon-\omega_{s_1}\right) v_{s_1}.
\end{aligned}
$$

This, together with identities (C9) and (C10), justifies the proposed representation of the self-energy.

7.8 Coherence functions

Let's consider the non-Markovian scattering setup: A giant acoustic atom, extensively studied theoretically and experimentally in [19, 59, 60, 78 – 81] (see also [82] for a detailed review). (???? добавлю из этих статей теорию про это! мб там многое полезного!)

7.8.1 Model and conventions (!?!!??!)

(по идее это один из самых важных разделов!)

Theory

A giant acoustic atom may be defined as a two-level system coupled to an acoustical waveguide, in which the radiation is carried by the surface acoustic waves (SAW), at two distant points $x = \pm R/2$. The Hamiltonian of such a system may be written as $\mathcal{H} = \mathcal{H}_1 + \mathcal{V}$:

$$
\begin{aligned}
\mathcal{H}_0 &= \Omega\sigma_+\sigma_- - iv\sum_{\mu=1,2}\int dx c_\mu b^\dagger_\mu(x)\partial_x b_\mu(x), \\
\mathcal{V} &= \sum_{\mu=1,2}\left[\sqrt{\Gamma_1} b^\dagger_\mu(-R/2) + \sqrt{\Gamma_2} b^\dagger_\mu(R/2)\right]\sigma_- + \text{H.c.}
\end{aligned}
$$

Here $b_\mu(x), b^\dagger_\mu(x)$ are the position space field operators of phonons, the index μ distinguishes beetween the right $\mu = 1$ and left $\mu = 2$ moving fields, and $c_\mu = (-1)^{\mu-1}$. Note that we have made use of the common assumption of the mode dispersion being linear in the vicinity of the relevant energy scale $\sim \Omega$ and the bandwidth being infinite. Defining the Fourier transformation as

$$b_\mu(x) = \frac{1}{\sqrt{2\pi}} \int dk e^{ic_\mu kx} a_\mu(k),$$

we bring the Hamiltonian in to the forms (1) and (2):

$$\mathcal{H}_0 = \Omega\sigma_+\sigma_- + v \sum_{\mu=1,2} \int dk k a_\mu^\dagger(k) a_\mu(k),$$

$$\mathcal{V} = \sum_{\mu=1,2} \int dk g_\mu(k) a_\mu(k) \sigma_- + \text{H.c.} \ ,$$

$$g_\mu(k) = \sqrt{\frac{\Gamma_1}{2\pi}} e^{-ic_\mu kR/2} + \sqrt{\frac{\Gamma_1}{2\pi}} e^{ic_\mu kR/2}.$$

In the following subsections we are going to study the scattering of a coherent pulse in the form of a wave packet centered around the frequency vk_0 (see Sec. III B), for that sake it is convenient to perform the following time-dependent gauge transformation:

$$\mathcal{U}(t) = \exp\left(-ivk_0 \left[\int dk a_\mu^\dagger(k) a_\mu(k) + \sigma_+\sigma_-\right] t\right)$$

The Hamiltonian transforms as $\mathcal{H} \to \tilde{\mathcal{H}} = \mathcal{U}^\dagger(t)\mathcal{H}\mathcal{U}(t) - i\mathcal{U}^\dagger(t)\frac{d\mathcal{U}(t)}{dt} =: \tilde{\mathcal{H}}_0 + \tilde{\mathcal{V}}$, resulting in final form of the Hamiltonian we are going to work with:

$$\tilde{\mathcal{H}}_0 = -\Delta\sigma_+\sigma_- + v \sum_{\mu=1,2} \int dk k \tilde{a}_\mu^\dagger(k) \tilde{a}_\mu(k),$$

$$\tilde{\mathcal{V}} = \sum_{\mu=1,2} \int dk \tilde{g}_\mu(k) \tilde{a}_\mu(k) \sigma_- + \text{H.c.} \ ,$$

$$\tilde{g}_\mu(k) = \sqrt{\frac{\Gamma_1}{2\pi}} e^{-ic_\mu(k+k_0)R/2} + \sqrt{\frac{\Gamma_1}{2\pi}} e^{ic_\mu(k+k_0)R/2},$$
$$\tilde{a}_\mu(k) = a_\mu\left(k + k_0\right), \quad \Delta = \omega_0 - \omega, \quad \omega_0 = vk_0.$$

In the following we adopt the system of units such that $v = 1$, for simplicity we will also assume $\Gamma_1 = \Gamma_2 = \gamma/2$. Furthermore, we shall also drop the tilde symbols out of operators for notational convenience.

7.8.2 Problem formulation

Theory

In order to formulate the scattering problem, we define the following wave-packet operators:

$$A_\mu^\dagger = \int dk \varphi_L(k) a_\mu^\dagger(k)$$

where

$$\varphi_L(k) = \sqrt{\frac{2}{\pi L}} \frac{\sin(kL/2)}{k}$$

is the Fourier transform of the rectangular pulse of length L, with the property $\varphi_L(k) \sim \sqrt{\frac{2\pi}{L}}\delta(k), L \to \infty$ [obviously, it is possible to choose any other nascent δ function for $\varphi_L(k)$].

(!!! тут важные комментарии про то, что вообще происходит!)

Note that since we are working in the frame of reference rotating with frequency k_0, peaking of $\varphi_L(k)$ at $k = 0$ corresponds to a pulse centered at $k = k_0$ in the original one. Note that throughout this section we focus on the zero detuning setup $\Delta = 0$, i.e., the initial k_0 is chosen to be equal to Ω. The effect of nonzero detuning of atom from radiation is studied in Appendix D.

Definition of these wave-packet operators is crucial since the eigenstates of the bare Hamiltonian $\mathcal{H}_0$ are not normalizable. Hence, in order to avoid the ascent of the undefinable quantities such as $\delta(0), (\delta(0))^2, \ldots$ coming from the elastic clusters of the S matrix in the calculation of the observables, one has to work with the normalizable states and take the plane-wave limit $L \to \infty$ at the very end. Having defined the Fock creation operators $A_\mu^\dagger$, we can define the coherent state as a displaced vacuum

$$|\alpha\rangle_\mu = e^{-|\alpha|^2/2} e^{\alpha A_\mu^\dagger} |\Omega\rangle = e^{-|\alpha|^2/2} \sum_{n=0}^{\infty} \frac{\alpha^n}{\sqrt{n!}} \left|\Phi_\mu^{(n)}\right\rangle$$

where $\alpha \in \mathbb{C}$ is the so-called coherence parameter, defined such that $|\alpha|^2$ is the average photon number (power), and the normalized n-particle Fock states $\left|\Phi_\mu^{(n)}\right\rangle$ were defined according to

$$\left|\Phi_\mu^{(n)}\right\rangle = \frac{1}{\sqrt{n!}} \left(A_\mu^\dagger\right)^n |\Omega\rangle$$

In what follows, we assume that $|\alpha| \ll 1$ in such a way that the terms of order $|\alpha|^4$ are negligible:

$$|\alpha\rangle_\mu \approx e^{-|\alpha|^2/2} \left(|\Omega\rangle + \frac{\alpha}{\sqrt{1!}} \left|\Phi_\mu^{(1)}\right\rangle + \frac{\alpha^2}{\sqrt{2!}} \left|\Phi_\mu^{(2)}\right\rangle + \frac{\alpha^3}{\sqrt{3!}} \left|\Phi_\mu^{(3)}\right\rangle + O\left(|\alpha|^4\right) \right) \equiv |\alpha\rangle_\mu^{(3)}.$$

The factor $e^{-|\alpha|^2/2}$ has to be retained until various overlaps of states are calculated to ensure the normalization of both the initial and final states as well as the power conservation [here the normalization is again assumed in the power perturbative regime, that is up to order $O\left(|\alpha|^8\right)$]. With this in hand, we formulate the scattering problem as follows. We assume that the initial state of the system is given by $|\psi_i\rangle = |\alpha\rangle_1^{(3)} \otimes |0\rangle$, that is, a leftwards-propagating weakly coherent pulse $|\alpha\rangle_1^{(3)}$ is incident on a two-level system which is initially in its ground state $|0\rangle$. According to the theory developed above, the final state of the systems has the following form:

$$|\psi_f\rangle = e^{-|\alpha|^2/2} \left(|\Omega\rangle + \frac{\alpha}{\sqrt{1!}} \mathcal{S}_1 \left|\Phi_1^{(1)}\right\rangle + \frac{\alpha^2}{\sqrt{2!}} \mathcal{S}_2 \left|\Phi_1^{(2)}\right\rangle + \frac{\alpha^3}{\sqrt{3!}} \mathcal{S}_3 \left|\Phi_1^{(3)}\right\rangle \right) \otimes |0\rangle$$

Inelastic contributions to the n-phonon S matrices (discussed in Sec. IID) introduce a nontrivial momentum redistribution of the incident phonons (note that owing to the linear dispersion relation and our choice of units energy and momentum may be used interchangeably), leading to the nontrivial phonon correlations in the final state. As it is well known, the phononic correlations may be conveniently examined with the help of the so-called coherence functions introduced by Glauber [83] in 1963. Defining the Fourier transform of the field operators according to

$$a_\mu(\tau) = \int dk \frac{e^{ik\tau}}{\sqrt{2\pi}} a(k)$$

one constructs the first-order coherence function as

$$\begin{aligned} C_\mu^{(1)}(\tau) &= \left\langle \psi_f \left| a_\mu^\dagger(\tau) a_\mu(0) \right| \psi_f \right\rangle \\ &= \left(1 - |\alpha|^2 + \frac{|\alpha|^4}{2}\right) |\alpha|^2 C_\mu^{(1,1)}(\tau) + \left(1 - |\alpha|^2\right) \frac{|\alpha|^4}{2} C_\mu^{(1,2)}(\tau) + \frac{|\alpha|^6}{6} C_\mu^{(1,3)}(\tau) + O\left(|\alpha|^8\right), \end{aligned}$$

where we have introduced the n-particle Fock state first-order correlation functions as

$$C_\mu^{(1,n)}(\tau) = \left\langle \Phi_1^{(n)} \left| (\mathcal{S}_n)^\dagger a_\mu^\dagger(\tau) a_\mu(0) \mathcal{S}_n \right| \Phi_1^{(n)} \right\rangle.$$

With the help of the first-order coherence function, one may define the spectral power density as the Fourier transform of (89):

$$S_\mu(k) = \int d\tau \frac{e^{-ik\tau}}{2\pi} C_\mu^{(1)}(\tau)$$

$S_\mu(k)$ is understood as a momentum-space distribution of power in the scattered state of radiation, that is to a given mode k (supported by the μ th channel) it associates a certain power $S_\mu(k)$. The power conservation condition

$$\sum_{\mu=1,2} \int dk S_\mu(k) \to \Phi, \quad \Phi = \frac{|\alpha|^2}{L}$$

is automatically satisfied due to the unitarity of the S matrix. In a linear system, where the n-body S matrix factorizes into the product of single-particle S matrices, the first-order coherence function is a constant, thus leading to the purely elastic power density $S_\mu(k) \propto \delta(k)$. Since a qubit is an intrinsically nonlinear system, we are going to see that the spectral power density admits for the following decomposition $S(k) = S^{\text{el}}(k) + S^{\text{inel}}(k)$, where $S^{\text{el}}(k) \propto \delta(k)$ is the elastic contribution to the spectral density, and $S^{\text{inel}}(k)$, in turn, is the inelastic part of spectral power density with a nontrivial momentum dependence.

Further, we define the normalized second- and third-order coherence functions:

$$\begin{aligned}
C^{(2)}_{\mu,\mu'}(\tau) &= \frac{\left\langle \psi_f \left| a^\dagger_\mu(0) a^\dagger_{\mu'}(\tau) a_{\mu'}(\tau) a_\mu(0) \right| \psi_f \right\rangle}{C^{(1)}_\mu(0) C^{(1)}_{\mu'}(0)} = \\
&= \left(1 - \frac{|\alpha|^2}{2}\right) \frac{1}{2} C^{(2,2)}_{\mu,\mu'}(\tau) + \frac{|\alpha|^2}{6} C^{(2,3)}_{\mu,\mu'}(\tau) + O\left(|\alpha|^4\right), \\
C^{(3)}_{\mu,\mu',\mu''}(\tau,\tau') &= \frac{\left\langle \psi_f \left| a^\dagger_\mu(0) a^\dagger_{\mu'}(\tau) a^\dagger_{\mu''}(\tau') a_{\mu''}(\tau') a_{\mu'}(\tau) a_\mu(0) \right| \psi_f \right\rangle}{C^{(1)}_\mu(0) C^{(1)}_{\mu'}(0) C^{(1)}_{\mu''}(0)} = \\
&= \frac{1}{6} C^{(3,3)}_{\mu,\mu',\mu''}(\tau,\tau') + O\left(|\alpha|^2\right), \\
C^{(m,n)}_{\mu_1,\ldots,\mu_m}(\tau_1,\ldots,\tau_{m-1}) &= \frac{\left\langle \Phi_1^{(n)} \left| \mathcal{S}_n^\dagger a^\dagger_{\mu_1}(0) \ldots a^\dagger_{\mu_m}(\tau_{m-1}) a_{\mu_m}(\tau_{m-1}) \ldots a_{\mu_1}(0) \mathcal{S}_n \right| \Phi_1^{(n)} \right\rangle}{\prod_{l=1}^m C^{(1)}_{\mu_l}(0)}.
\end{aligned}$$

For pairs of phonons, the normalized second-order coherence function is defined as the arrival probability of the second particle as a function of the delay τ following the detection of the first one, normalized by the individual photon probabilities. Likewise, for particle triples, the normalized third-order coherence function is defined as the arrival probability of the third and second particle as a function of delays τ', τ following the detection of the first one, normalized by the individual phonon probabilities. A perfectly coherent source is characterized by a uniform arrival probability, yielding the correlation functions of all orders equal to unity. Whenever correlation functions exceed unity, particle statistics is said to be superPoissonian and the particles are said to be bunched together, whereas in the case of correlation functions falling below unity, the statistics of particles is said to be sub-Poissonian and particles are correspondingly said to be antibunched.

In the following subsections, we are going to use the ideas developed in Sec. II C in order to compute the abovediscussed observables to the lowest order in $|\alpha|$ exactly.

7.8.3 Spectral power density (???)

(???? я хз, что тут вообще происходит, это отдельно много учить еще нужно.)

Theory

Let us begin with the analysis of the power spectrum of the SAW scattered by the giant atom. We start by considering the Fock state first-order coherence functions defined via (90).

In order to establish $C_\mu^{(1,1)}(\tau)$ one first has to find the matrix elements of the single-particle S matrix, which, in turn, demands the knowledge of the dressed propagator in the single-excitation subspace $G^{(1)}(\epsilon)$. The self-energy diagram may be evaluated straightforwardly to yield

$$\Sigma^{(1)}(\epsilon) = -i\gamma\left(1 + e^{i(\epsilon+k_0)R}\right)\sigma_+\sigma_-,$$

in accordance with Ref. [59]. With this in hand, the singlephonon scattering operator may be easily established with the help of Eqs. (33), (37), and (38):

$$\begin{aligned}
\mathcal{S}_1 &= \sum_{\mu',\mu}\int dkdk' S^{(1)}_{\mu'k',\mu k} a^\dagger_{\mu'}(k')\, a_\mu(k),\\
S^{(1)}_{\mu'k',\mu k} &= \delta(k-k')\, S^{(1)}_{\mu',\mu}(k)\sigma_-\sigma_+\\
S^{(1)}_{\mu',\mu}(k) &= \left(\delta_{\mu,\mu'} - 2\pi i g^*_\mu(k) g_{\mu'}(k)\tilde{G}^{(1)}(k)\right)
\end{aligned}$$

Here the tilde symbol denotes the projection onto the excited state in the qubit space, and $G^{(1)}(\epsilon) = G_0^{-1}(\epsilon) - \Sigma^{(1)}(\epsilon)$ in accordance with the definition in Sec. IIC. Performing a straightforward calculation, we obtain

$$\begin{aligned}
C_\mu^{(1)}(\tau) &= |\alpha|^2 C_\mu^{(1,1)}(\tau) + O\left(|\alpha|^4\right)\\
&= \Phi\left|S^{(1)}_{\mu 0,10}\right|^2 + O\left(\Phi^2\right)\\
\to S_\mu(k) &= \Phi\left|S^{(1)}_{\mu 0,10}\right|^2 \delta(k) + O\left(\Phi^2\right).
\end{aligned}$$

As we can see there exists no inelastic contribution to the spectral density in single-photon sector. In general the phenomenon of resonance fluorescence [84], leading to the inelastic power spectrum, is underpinned by the possibility of the two-level system to emit into the modes other than the incident one. This naturally allows the photons incident on the atom to exchange their energy between one another (while conserving the total energy) due to the higher-order emission and absorption processes, leading to the inelastic power spectrum. In the case of the single-photon, however, the particle ought to conserve its energy individually [as mathematically prescribed by the δ function in Eq. (98)] leading to the purely elastic spectrum.

In order to obtain the leading-order inelastic contribution to the spectral power density, we thus have to consider the contribution of the multiparticle states in the expansion (87), so that to allow for the interparticle interaction. In this case, the information about the inelastic scattering is entirely contained in the connected component of the two-phonon T matrix (see Sec. IID), which captures the nonlinear acoustic effects via the effective single-particle vertex function. Contracting the cluster decomposed S matrix (45) with the two-particle Fock state we arrive at the following result:

$$\sum_{\mu,\mu'}\left(\frac{1}{\sqrt{2}}\int dkdk'\varphi(k)\varphi(k')\, S^{(1)}_{\mu,1}(k)S^{(1)}_{\mu',1}(k')\, a^\dagger_\mu(k)a^\dagger_{\mu'}(k') - \frac{8\pi^2 i}{L\sqrt{2}}\int dk T^{(2,C)}_{\mu k,\mu' -k,10,10}(0)a^\dagger_\mu(k)a^\dagger_{\mu'}(-k)\right)|\Omega\rangle\otimes|0\rangle$$

Again we would like to emphasize that at this point the planewave limit ($L\to\infty$) may only be taken in the term containing the connected component of the S matrix since in this limit the first part of the state (102) is clearly non-normalizable. With the help of the final two-particle state derived above one may easily establish

$$\begin{aligned}
C_\mu^{(1,2)}(\tau) =& 16\pi^2\sum_{\mu'}\mathrm{Im}\left\{M_{\mu',\mu}(0)\left(S^{(1)}_{\mu';1}(0)S^{(1)}_{\mu;1}(0)\right)^*\right\}\\
&+ 32\pi^3\sum_{\mu'}\int dk e^{ik\tau}\left|M_{\mu',\mu}(k)\right|^2,
\end{aligned}$$

where $M_{\mu',\mu}(k)$ is the symmetric part of $T^{(2,C)}_{\mu k,\mu' -k,10,10}(0)$, i.e., $M_{\mu',\mu}(k) = M_{\mu,\mu'}(-k) = \left[T^{(2,C)}_{\mu' k,\mu -k,10,10}(0) + T^{(2,C)}_{\mu -k,\mu' k,10,10}(0)\right]/2$. Performing the Fourier transform of (103) we arrive at

the following expressions for the elastic $S^{\mathrm{el}}(k)$ and inelastic $S^{\mathrm{inel}}(k)$ spectral power densities valid to order Φ^3:

$$S_{\mu}^{\mathrm{el}}(k) = \delta(k)\left(\Phi\left|S_{\mu;1}^{(1)}(0)\right|^2 + 16\pi^2\Phi^2 \cdot \sum_{\mu'} \mathrm{Im}\left\{M_{\mu',\mu}(0)\left(S_{\mu';1}^{(1)}(0)S_{\mu;1}^{(1)}(0)\right)^*\right\}\right),$$

$$S_{\mu}^{\mathrm{inel}}(k) = 32\pi^3\Phi^2\sum_{\mu'}\left|M_{\mu',\mu}(k)\right|^2.$$

The inelastic spectral densities are shown in Fig. 7 for different interleg separations ($R = 1, 3, 5$). As one can see, the inelastic power spectrum develops a couple of sharp peaks near the origin of momentum space followed by infinitely many smaller side peaks. In order to interpret the nature of these peaks, we adopt the physical picture discussed in [21, 85, 86] for an "atom in front of a mirror" system. One can interpret this system as a leaky cavity formed by the two connection points of a giant atom. In this picture these peaks may be thought of as being located at the renormalized excitation frequencies of the effective cavity broadened by the renormalized decay rates. The resulting effect is the formation of sharp, bound-state-like peaks in the intensity of the scattered phonons, corresponding to cavity resonances. As the delay γR increases, the peaks get closer to $\omega = 0$, and get sharper, corresponding to a decrease of the effective cavity linewidth $\simeq 1/(\gamma R)$, that is effective cavity resonances approach the resonance of the two-level system, thus making atomic connection points better and better mirrors and hence increasing the quality factor of the effective cavity (quality factor is a common physical measure of both the rate of Inelastic spectral power density (scaled by Φ^2) of SAW scattered by a giant acoustic atom as a function of frequency $\omega = k$ for a variety of interleg separations $\gamma R = 1, 3, 5$.

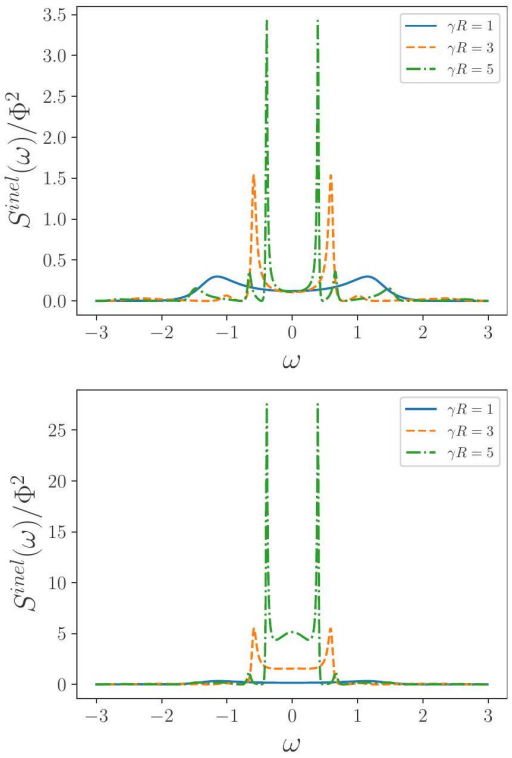

FIG. 7.
Top panel: Exact solution; bottom panel: Quasi-Markovian approximation. Other model parameters: $k_0 R = \pi/4 \bmod 2\pi$, and $\Delta = 0$. Here, the limit $L \to \infty$ was taken.

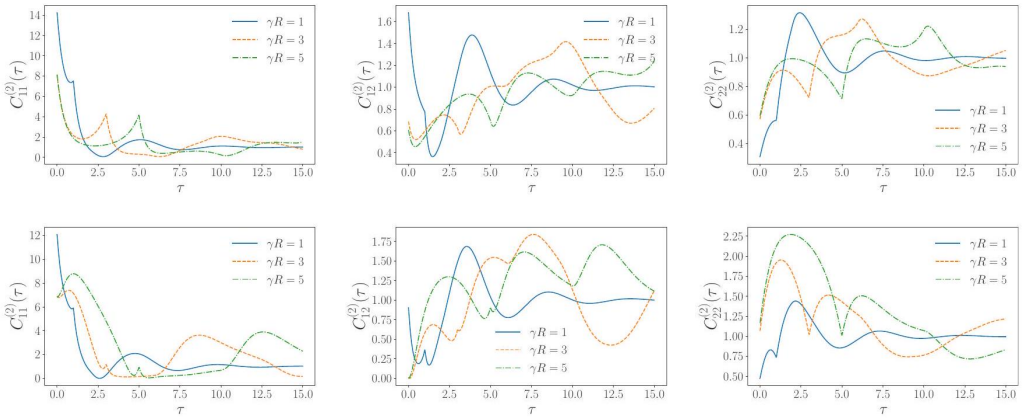

FIG. 8.

The figure demonstrates the independent components of the normalized second-order coherence function $C_{11}^{(2)}$, $C_{12}^{(2)}$, $C_{22}^{(2)}$ for various interleg separations $\gamma R = 1, 3, 5$. As before the top panel corresponds to an exact solution, the bottom one to its quasi-Markovian approximation, and $k_0 R = \pi/4 \bmod 2\pi, \Delta = 0$. Here the limit $L \to \infty$ was taken and by definition $C^{(2)}$ is dimensionless.

excitation damping and the rate of energy loss of an oscillator or a cavity)

Additionally, spectral densities based on the approximate solution of the scattering problem in the quasi-Markovian approximation are shown in Fig. 7. As it was mentioned in Sec. IIF, quasi-Markovian results show a good agreement with an exact solution in $\gamma R \ll 1$ parameter regime. As the delay time increases $\gamma R \geqslant 1$, the discrepancy between the approximate and complete solutions becomes dramatic. One can clearly see the tendency of the quasi-Markovian theory to enhance the scattering into the incoming frequency states $\omega = 0$. Indeed, in contrast to the exact solution, taking into account infinitely many excursions of phonons to the qubit, the quasi-Markovian approximation is based on the assumption of a single scattering event after which each phonon immediately leaves the system, thus leading to a more elastic result.

7.8.4 Second-order coherence

Theory

Let us now consider the second-order coherence function to the lowest order in $\Phi : O(\Phi^0)$. Performing the relevant Wick contractions we arrive at the following simple expression for the normalized second-order coherence:

$$C^{(2)}_{\mu',\mu}(\tau) = \left| 1 - \frac{4\pi i}{S^{(1)}_{\mu',1}(0) S^{(1)}_{\mu,1}(0)} \int dk e^{ik\tau} M_{\mu',\mu}(k) \right|^2 .$$

The independent components of second-order coherence function's components are presented in Fig. 8.

As it was mentioned above, the higher-order coherence functions provide the information about the information about the statistics of radiation scattered by a giant acoustic atom. Since $C^{(2)}_{1,1}(0) > 1$, one can clearly see that the statistics of back-scattered phonons is super-Poissonian, i.e., the particles tend to bunch together. Indeed, this result agrees with the physical expectation that at zero detuning $\Delta = 0$ the power extinction $1 - |S_{11}(0)|^2$ is enhanced even in the presence of pure dephasing [13, 87]. This assertion also explains the antibunching of forwardly scattered photons $C^{(2)}_{2,2}(0)$. Another clear feature of the second-order coherence function shown in Fig. 8 is presence of long-range quantum correlations of phonons, i.e., the components of $C^{(2)}$ do not decay to unity even for delays significantly exceeding the interleg separation $\tau \gg 1$. Note that this correlation effect becomes more and more pronounced with the increase in R, where correlation functions exhibit slightly damped oscillations around unity.

Another interesting feature of the second-order coherence is the presence of the nondifferentiable peaks at natural multiples of the interleg separation $\tau_n = nR, n \in \mathbb{N}$. Physically, this property may again be understood with the help of the simple picture of a leaky cavity formed

by the scatterer. Indeed, once a phonon is trapped between the legs of the atom, it may bounce off the cavity's walls back and forth multiple times, leading to the formation of the nonanalytical structures present in the second-order coherence. The fact that the nondifferentiable peaks are more pronounced at smaller values of n is a direct manifestation of the fact that the quality factor of the effective cavity is not infinite. This property is indeed of interest since the second-order coherence function is an experimentally measurable quantity which makes these sharp peaks a potentially observable effect.

Alongside the exact solution, the results based on the quasi-Markovian approximation are presented in Fig. 8 (lower panel). The discrepancy between the two is apparent. Another feature typical of this approximation is the tendency to overestimate the amplitudes of oscillation as was first pointed out in the Supplemental Material of Ref. [71].

7.8.5 Third-order coherence

Theory

Let us finally consider the third-order coherence function. The full expression for the third-order coherence function $C^{(3)}_{\mu,\mu',\mu''}(\tau,\tau')$ in terms of the symmetrized components of two- and three-particle transition matrices may be found in Appendix B. Although in general, $C^{(3)}_{\mu,\mu',\mu''}$ has eight

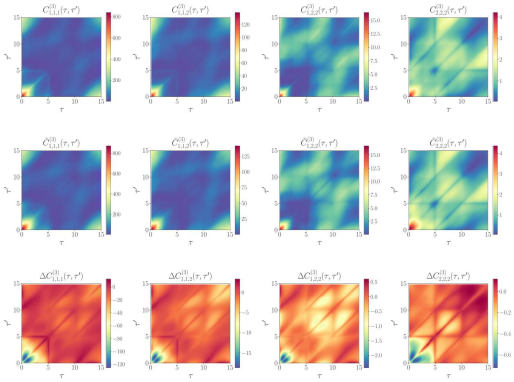

FIG. 9. Independent components $(\mu,\mu',\mu'') = (1,1,1), (1,1,2), (1,2,2), (2,2,2)$ of the third-order coherence function of phonons scattered by a giant acoustic atom. Top, central, and bottom panels correspond to the exact solution $C^{(3)}_{\mu,\mu',\mu''}(\tau,\tau')$, weak correlation approximation $\tilde{C}^{(3)}_{\mu,\mu',\mu''}(\tau,\tau')$, and their difference $\Delta C^{(3)}_{\mu,\mu',\mu''}(\tau,\tau') = C^{(3)}_{\mu,\mu',\mu''}(\tau,\tau') - \tilde{C}^{(3)}_{\mu,\mu',\mu''}(\tau,\tau')$, respectively. Here $\gamma R = 5, k_0 R = \pi/4 \bmod 2\pi$, and $\Delta = 0$. Here the limit $L \to \infty$ was taken and by definition $C^{(2)}$ is dimensionless.

independent components in the case of two radiation channels, due to our particular choice of the coupling $\Gamma_1 = \Gamma_2 = \gamma/2$, only four independent components remain:

$$C^{(3)}_{1,1,1}(\tau,\tau')\,, \quad C^{(3)}_{2,2,2}(\tau,\tau')\,,$$
$$C^{(3)}_{1,1,2}(\tau,\tau') = C^{(3)}_{1,2,1}(\tau,\tau') = C^{(3)}_{2,1,1}(\tau,\tau')\,,$$
$$C^{(3)}_{1,2,2}(\tau,\tau') = C^{(3)}_{2,2,1}(\tau,\tau') = C^{(3)}_{2,1,2}(\tau,\tau')\,.$$

Independent components of $C^{(3)}$ for a system with $R = 5$, $k_0 R = \pi/4 \bmod 2\pi$, and $\Delta = 0$ are shown in the top panel of Fig. 9. First, we note that the individual components of third-order coherence at $\tau,\tau' = 0$ significantly exceed unity, signifying the bunching of phonons. This effect can be attributed to the fact that a single two-level system can only emit and absorb a single quantum of radiation at a time, which, in turn, significantly increases the probability of simultaneous detection of a pair of phonons in the waveguide. Moreover, this effect is more pronounced in those components of the correlation function, describing correlations with phonons in the channel of incident radiation $\mu = 1$. This artifact again has to do with the fact of the enhancement of power extinction by an atom at zero detuning.

Another interesting feature of $C^{(3)}$ to be noticed is the presence of clear peak and downfall structures located on the lines $\tau' - \tau = nR, n \in \mathbb{Z}$. Physically, $\delta\tau = \tau' - \tau$ corresponds to the

average delay time between the second and third phonon detection events upon detection of the first one at zero time. The quantization of $\delta\tau$ in the units of deterministic time delay is the characteristic feature of the system under consideration and may be potentially observed in future experiments via the observation of enhancement or diminution of the conditional probability of arrival of the third particle. In fact, the peak and downfall structures discussed above are nondifferentiable, as it was the case with the second-order coherence function, and again this phenomenon may be understood with the help of a simple picture of an effective cavity discussed in Secs. IIIC1 and III C.

Aside from the exact solution $C^{(3)}_{\mu,\mu',\mu''}(\tau,\tau')$, the solution based on the weak-correlation (WC) approximation $\tilde{C}^{(3)}_{\mu,\mu',\mu''}(\tau,\tau')$ as well as the difference between the exact solution and the WC one

$$\Delta C^{(3)}_{\mu,\mu',\mu''} = C^{(3)}_{\mu,\mu',\mu''} - \tilde{C}^{(3)}_{\mu,\mu',\mu''}$$

are shown in Fig. 9 in central and bottom panels, respectively. As one can anticipate, the WC approximation tends to notably overestimate the amplitude of the third-order coherence function. This effect is especially apparent in the vicinity of $\tau,\tau' = 0$, where the WC approximation significantly overestimates the phononic bunching. Away from the temporal origin, though, the approximation becomes adequate and only slightly deviates from the exact result, as one may infer from the plots in the bottom panel of Fig. 9. The discrepancy between the exact solution and its WC approximation is not hard to understand. Weak-correlation approximation ignores an infinite diagrammatic channel, consisting of exchange interaction diagrams between the phonons, which are, of course, of importance when one studies the statistical properties of particles.

7.8.6 Effect of the non-zero detuning

In this Appendix we analyze the effect on nonzero detuning of the atom from radiation on the observable quantities. In particular, we focus on the spectral power density and the second-order coherence function. As it was discussed in Sec. III C, the sharp bound-state-like peaks in the line shape of spectral density may be understood with a simple physical picture of an effective cavity. When one increases (or de- creases) the detuning from zero value, one effectively changes the modes supported by the cavity and thus one expects the position of the peaks to be shifted. The precise location of the resonances in the spectral density as function of Δ and k for various values of k_0R is shown in Fig. 10. As we can see, for nonzero dephasing $k_0R \neq 0$, the spectrum is not a symmetric function of Δ. For negative dephasing we find that emission into the zero modes is enhanced for a negatively detuned atom $\Delta < 0$, whereas the picture is opposite for pos-

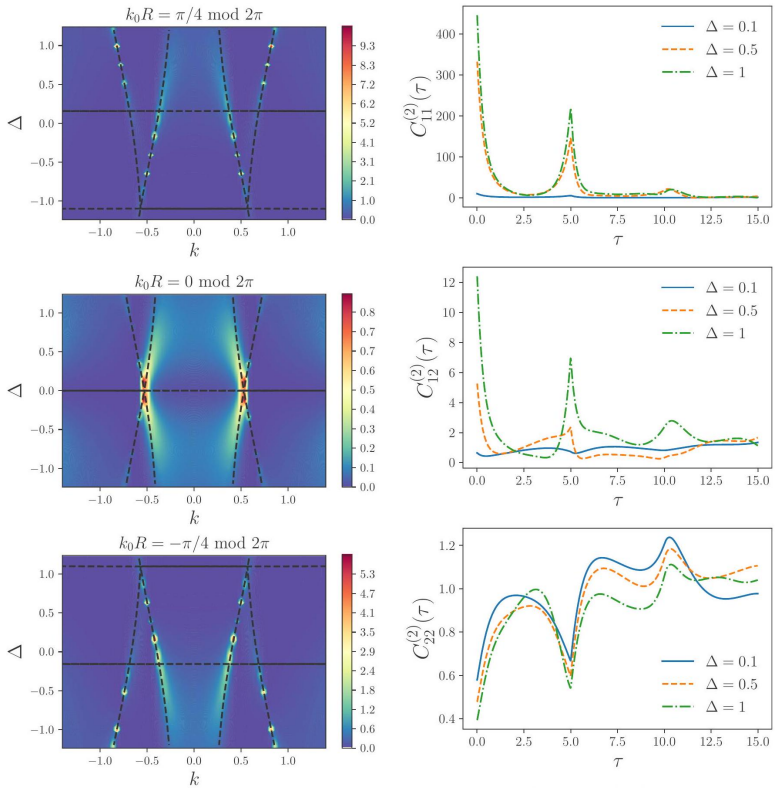

FIG. 10. Spectral power density (scaled by $1/\Phi^2$) for the giant atom model as a function of Δ, k for various values of k_0R and $\gamma R = 5$. Here the dashed black lines indicate the pole position of the dressed Green's function in the single-excitation subspace.

itive k_0R. In general, we can clearly resolve a pair of sharp peaks which eventually merge together at certain values of parameters (e.g., $k_0R = \Delta = 0$). It is interesting to note that the location of these peaks is almost entirely determined by the poles of the dressed propagator in the single-excitation subspace $\left(G^{(1)}(k)\right)^{-1} = k + \Delta + i\gamma\left(1 + e^{i(k+k_0)R}\right) = 0$. This

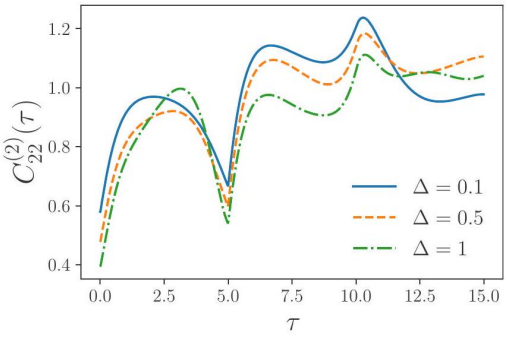

FIG. 11. Second-order coherence function for the system with $k_0R = 3\pi/11, \quad \gamma R = 5, \Delta = 0.1, 0.5, 1.0$ (as before, the the second-order coherence function is dimensionless).

equation is solved by

$$k = \pm i\frac{R\gamma - iR\Delta - W_n\left(-\gamma R e^{i(k_0 - \Delta - i\gamma)R}\right)}{R}$$

where $W_n(z)$ is the nth branch of the Lambert W function, also known as the product logarithm. The real part of (D1) with $n = 0, \pm 1$ is plotted as black dashed lines in Fig. 10. The vertical lines in Fig. 10 represent the discontinuous jumps of the Lambert function across the branch cut. As one may

7.8.7 Appendix on 3-order coherence function

The formula for the third-order coherence function of phonons in the giant atom model is obtained as follows. Using the formula (A28) with $\omega(k) = k$ along with the notations introduced in Sec. III, we obtain the following result upon contraction with

the three-phonon Fock state:

$$\mathcal{S}_3\left|\Phi_1^{(3)}\right\rangle = \frac{1}{\sqrt{6}}\sum_{\{\mu_i'\}}\left(A_{\Phi_1^{(3)}} - B_{\Phi_1^{(3)}} - C_{\Phi_1^{(3)}}\right),$$

where only here:

$$A_{\Phi_1^{(3)}} := \int\limits_{k_1k_2k_3} \varphi(k_1)\varphi(k_2)\varphi(k_3)\, S^{(1)}_{\mu_1',1}(k_1)\, S^{(1)}_{\mu_2',1}(k_2)\, S^{(1)}_{\mu_3',1}(k_3)\, a^\dagger_{\mu_1'}(k_1)\, a^\dagger_{\mu_2'}(k_2)\, a^\dagger_{\mu_3'}(k_3)\,|\Omega\rangle,$$

$$B_{\Phi_1^{(3)}} := -12\pi i \int\limits_{k_1'k_2'k_1k_2k_3} \varphi(k_1)\varphi(k_2)\varphi(k_3)\, T^{(2,C)}_{\mu_1'k_1',\mu_2'k_2',\mu_1k_1,\mu_2k_2}(k_1+k_2)\,\delta\left(k_1'+k_2'-k_1-k_2\right)\cdot S^{(1)}_{\mu_3';1}(k_3)\, a^\dagger_{\mu_1'}(k_1')\, a^\dagger_{\mu_2'}(k_2')\, a^\dagger_{\mu_3'}(k_3)\,|\Omega\rangle;$$

$$C_{\Phi_1^{(3)}} := -12\pi i\left(\frac{2\pi}{L}\right)^{3/2} \int\limits_{k_1'k_2'k_3'} Q\left(k_1',k_2',k_3'\right)\,\delta\left(k_1'+k_2'+k_3'\right) a^\dagger_{\mu_1'}(k_1')\, a^\dagger_{\mu_2'}(k_2')\, a^\dagger_{\mu_3'}(k_3')\,|\Omega\rangle.$$

and here we have introduced the following symmetrized version of the connected three-phonon transition operator:

$$\begin{aligned} Q\left(k_1',k_2',k_3'\right) :=& \frac{1}{6}\left[T^{)3,C)}_{\mu_1'k_1',\mu_2'k_2',\mu_3'k_3',10,10,10}(0) T^{(3)}_{\mu_1'k_1',\mu_3'k_3',\mu_2'k_2',10,10,10}(0) + T^{(3,C)}_{\mu_3'k_3',\mu_2'k_2',\mu_1'k_1',10,10,10}(0)\right. \\ &\left. + T^{(3,C)}_{\mu_3'k_3',\mu_1'k_1',\mu_2'k_2',10,10,10}(0) T^{(3,C)}_{\mu_2'k_2',\mu_1'k_1',\mu_3'k_3',10,10,10}(0) + T^{(3,C)}_{\mu_2'k_2',\mu_3'k_3',\mu_1'k_1',10,10,10}(0)\right]. \end{aligned}$$

Here we have suppressed the dependence of $Q\left(k_1',k_2',k_3'\right)$ on $\{\mu'\}$ since in the giant atom model the coupling constants are independent of the channel index.

Now we consider

$$a_{\mu''}(\tau_3)\, a_{\mu'}(\tau_2)\, a_{\mu}(\tau_1)\,\mathcal{S}_3\left|\Phi_1^{(3)}\right\rangle = \frac{\sqrt{6}}{L^{3/2}} S^{(1)}_{\mu'',1}(0) S^{(1)}_{\mu',1}(0) S^{(1)}_{\mu,1}(0)\,(1-A-B)$$

$$A := 4\pi i\left[\frac{I^{(1)}_{\mu'',\mu'}(\tau_3-\tau_2)}{S^{(1)}_{\mu'',1}(0)S^{(1)}_{\mu',1}(0)} + \frac{I^{(1)}_{\mu,\mu'}(\tau_2-\tau_1)}{S^{(1)}_{\mu,1}(0)S^{(1)}_{\mu',1}(0)} + \frac{I^{(1)}_{\mu'',\mu}(\tau_3-\tau_1)}{S^{(1)}_{\mu'',1}(0)S^{(1)}_{\mu,1}(0)}\right]; \qquad B := 12\pi i\frac{I^{(2)}(\tau_3-\tau_1,\tau_2-\tau_1)}{S^{(1)}_{\mu'',1}(0)S^{(1)}_{\mu',1}(0)S^{(1)}_{\mu,1}(0)}.$$

where the following functions were defined:

$$I^{(1)}_{\mu',\mu}(t_1) = \int\limits_k e^{ikt_1} M_{\mu',\mu}(k),$$

$$I^{(2)}(t_2,t_1) = \int\limits_{k,q} e^{iqt_2} e^{ikt_1} Q(-k-q,k,q),$$

where $M_{\mu,\mu'}(k) = \left[T^{(2,C)}_{\mu'k,\mu-k,10,10}(0) + T^{(2,C)}_{\mu-k,\mu'k,10,10}(0)\right]/2$, as before. By introducing the following variables $\tau' = \tau_3-\tau_1, \tau = \tau_2-\tau_1$, we can immediately write the normalized third-order coherence function to the lowest order in φ as

$$C^{(3)}_{\mu'',\mu',\mu}(t',t) = |1-A-B|^2,$$

where only here

$$A := 4\pi i\left[\frac{I^{(1)}_{\mu'',\mu'}(t'-t)}{S^{(1)}_{\mu'',1}(0)S^{(1)}_{\mu',1}(0)} + \frac{I^{(1)}_{\mu,\mu'}(t)}{S^{(1)}_{\mu,1}(0)S^{(1)}_{\mu',1}(0)} + \frac{I^{(1)}_{\mu'',\mu}(t')}{S^{(1)}_{\mu'',1}(0)S^{(1)}_{\mu;1}(0)}\right]; \qquad B := 12\pi i\frac{I^{(2)}(t',t)}{S^{(1)}_{\mu'',1}(0)S^{(1)}_{\mu',1}(0)S^{(1)}_{\mu,1}(0)}.$$

7.9 Scattering Theory in Waveguide QED

The outline of this Chapter is as follows. First of all, the general definition of the scattering operator, the most desired object in scattering theory, is introduced. Further, a short discussion of the properties of the scattering matrix specific to waveguide QED is presented. Next, these properties are used to exactly resum the perturbation theory for the transition operator in $Q = 1$ waveguide QED. Further, the generalized cluster decomposition principle is illustrated and a couple of approximate resummation routines are suggested. The formalism is then extended to higher Q systems by specific examples of $Q = 2$ and $Q = 3$ waveguide QED setups.

7.9.1 3.1 General Definition of the S-Matrix

The central problem of the scattering theory may be formulated as follows. Consider a quantum system described by the following Hamiltonian $\mathcal{H} = \mathcal{H}_0 + \mathcal{V}$, where $\mathcal{H}_0$ describes the free kinematics of the problem and $\mathcal{V}$ is the interaction potential. Furthermore, let us assume that the unperturbed Hamiltonian possesses a complete orthonormal set of eigenstates $\{|m\rangle\}_m$ with the corresponding eigenvalues given by $\{\epsilon_m\}_m$

$$\mathcal{H}_0|m\rangle = \epsilon_m|m\rangle, \quad \sum_m |m\rangle\langle m| = 1, \quad \langle m|n\rangle = \delta(m,n) \tag{3.1}$$

The basic assumption of the scattering theory is that one can canonically associate to each of the free states $|m\rangle$ the so-called incoming $\left|\psi_+^m\right\rangle$ and outgoing $\left|\psi_-^m\right\rangle$ states which possess the following two properties. Their dynamics is generated by the full Hamiltonian of the theory

$$\left|\psi_\pm^m\right\rangle(t) = \exp(-i\mathcal{H}t)\left|\psi_\pm^m\right\rangle \tag{3.2}$$

where $\left|\psi_\pm^m\right\rangle = \left|\psi_\pm^m\right\rangle(0^\mp)$. Additionally, in the far past and far future, $\left|\psi_+^m\right\rangle$ and $\left|\psi_-^m\right\rangle$ are respectively assumed to evolve under the free kinematics [11]:

$$\lim_{t\to\mp\infty} \| \left|\psi_\pm^m\right\rangle(t) - \exp\left(-i\mathcal{H}_0 t\right)|m\rangle \Big\| = \lim_{t\to\mp\infty} \Big\| \left|\psi_\pm^m\right\rangle - \exp(i\mathcal{H}t)\exp\left(-i\mathcal{H}_0 t\right)|m\rangle \| = 0 \tag{3.3}$$

The asymptotic freedom constraint (3.3) may be solved by the introduction of the Møller [38] operators

$$\left|\psi_\pm^m\right\rangle = \mathcal{M}_\pm|m\rangle, \quad \mathcal{M}_\pm = \lim_{t\to\mp\infty} \exp(i\mathcal{H}t)\exp\left(-i\mathcal{H}_0 t\right) \tag{3.4}$$

The limits in (3.4) are understood in the strong operator topology and the proof of their existence for the theory of our interest is far beyond the scope of this thesis. Now consider the following

$$\begin{aligned} e^{-i\mathcal{H}\tau}\mathcal{M}_\pm &= \lim_{t\to\mp\infty} e^{i\mathcal{H}(t-\tau)}e^{-i\mathcal{H}_0 t} = \lim_{t\to\mp\infty} e^{i\mathcal{H}(t-\tau)}e^{-i\mathcal{H}_0(t-\tau)}e^{-i\mathcal{H}_0\tau} = \mathcal{M}_\pm e^{-i\mathcal{H}_0\tau} \\ &\iff e^{-i\mathcal{H}\tau}\mathcal{M}_\pm = \mathcal{M}_\pm e^{-i\mathcal{H}_0\tau} \implies \mathcal{H}\mathcal{M}_\pm = \mathcal{M}_\pm\mathcal{H}_0 \implies \mathcal{H}\left|\psi_\pm^m\right\rangle = \epsilon_m\left|\psi_\pm^m\right\rangle. \end{aligned} \tag{3.5}$$

So we see that the incoming and outgoing states $\left|\psi_\pm^m\right\rangle$ are the eigenstates of the full Hamiltonian with the corresponding eigenvalues ϵ_m. Hermiticity of $\mathcal{H}$ (unitarity of $\mathcal{M}_\pm$) implies $\left\langle\psi_\pm^n|\psi_\pm^m\right\rangle = \delta(n,m)$. Using the above definitions we now can define the scattering operator's matrix elements $\mathcal{S}_{n,m}$ as the following transition probability amplidue $\left|\psi_+^m\right\rangle \to \left|\psi_-^n\right\rangle$

$$\mathcal{S}_{n,m} = \left\langle\psi_-^n|\psi_+^m\right\rangle = \left\langle n\left|\mathcal{M}_-^\dagger\mathcal{M}_+\right|m\right\rangle, \tag{3.6}$$

which helps us to identify

$$\mathcal{S} = \mathcal{M}_-^\dagger\mathcal{M}_+. \tag{3.7}$$

Let us now have a closer look at the Møller isometries (3.4). We note that

$$\begin{aligned} \mathcal{M}_- &= \lim_{t\to\infty}\exp(i\mathcal{H}t)\exp\left(-i\mathcal{H}_0 t\right) = 1 + \int_0^\infty d\tau \frac{\partial}{\partial\tau}\exp(i\mathcal{H}\tau)\exp\left(-i\mathcal{H}_0\tau\right) \\ &= 1 + i\int_0^\infty d\tau \exp(i\mathcal{H}\tau)\mathcal{V}\exp\left(-i\mathcal{H}_0\tau\right) = 1 + i\int_0^\infty d\tau\sum_m \exp\left(i\left(\mathcal{H}-\epsilon_m\right)\tau\right)\mathcal{V}|m\rangle\langle m| \\ &= 1 + i\lim_{\eta\searrow 0}\int_0^\infty d\tau\sum_m \exp\left(-i\left(\epsilon_m - \mathcal{H} - i\eta\right)\tau\right)\mathcal{V}|m\rangle\left\langle m\right| = 1 + \sum_m \mathcal{G}_A\left(\epsilon_m\right)\mathcal{V}\left|m\right\rangle\langle m|, \end{aligned}$$

where we have defined the advanced Green's operator as

$$\mathcal{G}_A(\epsilon) = \lim_{\eta \searrow 0} \frac{1}{\epsilon - \mathcal{H} - i\eta}. \tag{3.8}$$

Analogously we obtain

$$\mathcal{M}_+ = 1 + \sum_m \mathcal{G}_R(\epsilon_m)\, \mathcal{V}|m\rangle\langle m| \tag{3.9}$$

where the retarded Green's operator is defined according to $\mathcal{G}_R(\epsilon) = \mathcal{G}_A^\dagger(\epsilon)$. Using the above representation of $\mathcal{M}_\pm$we arrive at the well-known Lippmann-Schwinger equations

$$\left|\psi_\pm^m\right\rangle = |m\rangle + \mathcal{G}_{R/A}(\epsilon_m)\, \mathcal{V}|m\rangle \tag{3.10}$$

By subtracting these equations from one another and taking the adjoint of the result we obtain

$$\left\langle\psi_-^n\right| = \left\langle\psi_+^n\right| + \langle n|\mathcal{V}\left[\mathcal{G}_R(\epsilon_n) - \mathcal{G}_A(\epsilon_n)\right]. \tag{3.11}$$

Projecting this equation on $\left|\psi_+^n\right\rangle$ we deduce

$$S_{n,m} = \left\langle\psi_+^n|\psi_+^m\right\rangle + \left\langle n\left|\mathcal{V}\left[\mathcal{G}_R(\epsilon_n) - \mathcal{G}_A(\epsilon_n)\right]\right|\psi_+^m\right\rangle. \tag{3.12}$$

Using the fact that $\left|\psi_+^m\right\rangle$ is an eigenstate of $\mathcal{H}$ we see that

$$\begin{aligned}\langle n|\mathcal{V}\left[\mathcal{G}_R(\epsilon_n) - \mathcal{G}_A(\epsilon_n)\right]\left|\psi_+^m\right\rangle &= \left\langle n|\mathcal{V}|\psi_+^m\right\rangle \lim_{\eta\searrow 0}\left(\frac{1}{(\epsilon_n-\epsilon_m)+i\eta} - \frac{1}{(\epsilon_n-\epsilon_m)-i\eta}\right)\\ &= -2\pi i\delta(\epsilon_n-\epsilon_m)\left\langle n|\mathcal{V}|\psi_+^m\right\rangle = -2\pi i\delta(\epsilon_n-\epsilon_m)\left\langle n\left|\left(\mathcal{V}+\mathcal{V}\mathcal{G}_R(\epsilon_m)\,\mathcal{V}\right)\right|m\right\rangle\end{aligned} \tag{3.13}$$

By defining the retarded transition operator $\mathcal{T}^R(\epsilon)$ (a.k.a. T-matrix) as

$$\mathcal{T}^R(\epsilon) = \mathcal{V} + \mathcal{V}\mathcal{G}_R(\epsilon)\mathcal{V} \tag{3.14}$$

and exploiting the orthonormality of the outgoing states $\left\{\left|\psi_+^n\right\rangle\right\}_n$ we finally represent the S-matrix as

$$S_{n,m} = \delta(n,m) - 2\pi i\delta(\epsilon_n-\epsilon_m)\,\mathcal{T}^R_{n,m}(\epsilon_n) \tag{3.15}$$

Thus we see that all of the non-trivial information about the scattering process is contained in the retarded T-matrix.

7.9.2 3.2 General Properties of the Scattering Matrix in Waveguide QED

As we have seen above (3.15), the non-trivial information about the scattering process, is entirely contained in the matrix elements of the retarded on-shell T-matrix $\left\langle n\left|\mathcal{T}^R(\epsilon_n)\right|m\right\rangle$, where $\{|m\rangle\}_m$ are the eigenstates of the unperturbed Hamiltonian $\mathcal{H}_0$. Let us consider the scattering problem for the following initial state $|P\rangle\otimes|g\rangle$, where $|P\rangle$ is a P-photon state, and $|g\rangle = |0\rangle^{\otimes Q}$ is the ground state of the scatterer. Due to the conservation of excitation-number operator, all of the possible $D(P,Q)$ scattering outcomes must contain P excitations. Due to the fact that for any system of qubits the ground state $|g\rangle$ is the only non-decaying (subradiant) subspace, in the longtime limit (a priory assumed in scattering theory) all of the emitters will definitely decay into the continuum, leaving us with the only possibility for the system to end up in the state $|P'\rangle\otimes|g\rangle$ (here $|P'\rangle$ is again a P-photon state, with potentially redistributed momenta). Readers finding this assertion not convincing are referred to Chapter 5, where the statement is directly proven by showing that all of the on-shell matrix elements apart from $|g\rangle\to|g\rangle$ are zero. If one wishes to extend the scattering theory to the systems with metastable

ground states, such as e.g. a Λ three-level system, one then has to consider calculating more matrix elements of the transition operator [53].

Since the only matrix elements, we are interested in are diagonal in both the photon and qubit space, due to the RWA, the only terms contributing to the perturbation expansion of the T-matrix are those containing an even number of interactions $\mathcal{V}$, thus reducing the number of diagrams by half. Another important feature to be mentioned is the nilpotency of the photon-qubit interaction vertex operator $v_{s_1}^\dagger \dots v_{s_{Q+1}}^\dagger = v_{s_1} \dots v_{s_{Q+1}} = 0$, which along with the property $v_s|g\rangle = \langle g|v_s^\dagger = 0$ and the fact that the number of v 's and $v^\dagger$'s has to be equal in each graph contributing to the expansion, significantly reduces the number of non-zero diagrams at each order in perturbation theory. In fact, as we are going to see in this chapter, all of the diagrams contributing to the series for any fixed Q may be constructed out of a finite number of "clusters", in turn allowing, in principle for the exact resummation of the perturbation series. One can also organize the calculation differently, namely by fixing P and allowing Q to vary instead. Calculation within this approach is facilitated in its turn by the fact that $a_{s_1 \dots} \dots a_{s_{P+1}}|P\rangle = \langle P|a_{s_1}^\dagger \dots a_{s_{P+1}}^\dagger = 0$ and the fact that the number of a' 's and $a^\dagger$'s in each term of the perturbation series have to be equal. However, these two approaches turn out to be dual. This duality has to do with a couple of facts. First of all, $v_s\left(v_s^\dagger\right)$ by itself contains the sum of all of the single-qubit lowering (raising) operators, that means that the real dimension of the $E \in \{0, \dots, Q\}$-qubit excitation subspace $d(E,Q) = \frac{Q!}{E!(Q-E)!}$, is replaced in diagrammatic calculations by an effective dimension, which is equal to $d_{\text{eff}}(E,Q) = 1, \forall Q, E \in \{0, \dots, Q\}$. To see what do we mean by that, let us look at the particular case of $Q = 3$, in this case, $d(0,3) = 1, d(1,3) = 3, d(2,3) = 3$ and $d(3,3) = 1$, corresponding to the four sets of qubit states $\{|000\rangle\}, \{|100\rangle, |010\rangle, |001\rangle\}, \{|110\rangle, |101\rangle, |011\rangle\}$ and $\{|111\rangle\}$, but since only v s and $v^\dagger$s appear in the perturbation series all members of each one of the sets are indistinguishable: $|000\rangle \cong |0\rangle, |100\rangle \cong |010\rangle \cong |001\rangle \cong |1\rangle, |110\rangle \cong |101\rangle \cong |011\rangle \cong |2\rangle$ and $|111\rangle \cong |3\rangle$. Thus the real dimension of the space with N-excitations in the system (including both qubit and waveguide excitations) $D(N,Q) = \sum_{E=0}^{\min(N,Q)} d(E,Q)$ is replaced in practical calculations by an effective one $D_{\text{eff}}(N,Q) = \sum_{E=0}^{\min(N,Q)} d_{\text{eff}}(E,Q) = 1 + \min(N,Q)$ which is growing linearly not exponentially. Secondly, each time one encounters $v_s\left(v_s^\dagger\right)$ in the perturbation series, it is always multiplied by $a_s^\dagger(a_s)$. Combining these two facts, we see that once we calculate the $P = Q$-photon S-matrix for Q-qubits, this solution applies to any $Q' \geq Q$, i.e by solving say, a two-photon scattering problem on two qubits the solution to the two-photon scattering problem on 55 qubits follows the same lines, etc. Physically, this result is not of any surprise, of course, since the maximum state of a system of Q-qubits that could be excited by P-photons is the P-qubit excited state.

7.9.3 3.3 $Q = 1$ Waveguide QED

3.3.1 Transition Operator

Let us first consider the simplest imaginable scenario of a single qubit coupled to a waveguide. As it was anticipated above, to solve the P-photon scattering problem, we shall be hunting out $|P,g\rangle \to |P',g\rangle$ matrix elements of the retarded transition operator (note that in what follows we are going to omit the R superscripts, explicitly understanding that T-matrix and Green's operators are retarded)

$$\left\langle P',g\left|\mathcal{T}^{(1)}(\epsilon)\right|P,g\right\rangle = \langle P',g|\mathcal{V}|P,g\rangle + \langle P',g|\mathcal{V}\mathcal{G}(\epsilon)\mathcal{V}|P,g\rangle = \left\langle P',g\left|a_{s_1'}^\dagger v_{s_1'}\mathcal{G}(\epsilon)v_{s_1}^\dagger a_{s_1}\right|P,g\right\rangle$$
$$= \left\langle P',g\left|a_{s_1'}^\dagger v_{s_1'}\frac{1}{\epsilon - \mathcal{H}_0 - \mathcal{V} + i\eta}v_{s_1}^\dagger a_{s_1}\right|P,g\right\rangle = \sum_{n=0}^{\infty}\left\langle P',g\left|a_{s_1'}^\dagger v_{s_1'}\left(\mathcal{G}_0(\epsilon)\mathcal{V}\right)^n\mathcal{G}_0(\epsilon)v_{s_1}^\dagger a_{s_1}\right|P,g\right\rangle,$$

where we have used the fact that $\langle P',g|\mathcal{V}|P,g\rangle = 0$ and introduced the bare retarded Green's operator $\mathcal{G}_0^{-1}(\epsilon) = \epsilon - \mathcal{H}_0 + i\eta \quad (\eta \searrow 0)$, the superscript (1) refers to the $Q = 1$ waveguide QED.

As it was mentioned above, due to RWA, only even terms contribute to the above geometric series, so that

$$\left\langle P', g \left| \mathcal{T}^{(1)}(\epsilon) \right| P, g \right\rangle = \sum_{n=0}^{\infty} \left\langle P', g \left| a^{\dagger}_{s'_1} v_{s'_1} \left(\mathcal{G}_0(\epsilon) \mathcal{V} \mathcal{G}_0(\epsilon) \mathcal{V} \right)^n \mathcal{G}_0(\epsilon) v^{\dagger}_{s_1} a_{s_1} \right| P, g \right\rangle .$$

Now, let us consider the $\mathcal{V}\mathcal{G}_0\mathcal{V}$ term in the brackets above

$$\mathcal{V}\mathcal{G}_0(\epsilon)\mathcal{V} = a^{\dagger}_{s'} v_{s'} \mathcal{G}_0(\epsilon) a^{\dagger}_s v_s + a^{\dagger}_{s'} v_{s'} \mathcal{G}_0(\epsilon) v^{\dagger}_s a_s + v^{\dagger}_{s'} a_{s'} \mathcal{G}_0(\epsilon) v^{\dagger}_s a_s + v^{\dagger}_{s'} a_{s'} \mathcal{G}_0(\epsilon) a^{\dagger}_s v_s.$$

Clearly, the terms with two v s and two $v^{\dagger}$s do not contribute (they are in fact zero) by the single-qubit nilpotency condition $v^2 = \left(v^{\dagger}\right)^2 = 0$. Among the "diagonal" terms, the only non-zero contribution comes from the $v^{\dagger}v$ term since the term $vv^{\dagger}$ annihilates the state $v^{\dagger}|g\rangle$ and gives zero whenever it is multiplied with $v^{\dagger}v$ term. Hence, we arrive at

$$\left\langle P', g \left| \mathcal{T}^{(1)}(\epsilon) \right| P, g \right\rangle = \sum_{n=0}^{\infty} \left\langle P', g \left| a^{\dagger}_{s'_1} v_{s'_1} \left(\mathcal{G}_0(\epsilon) v^{\dagger}_{s'} a_{s'} \mathcal{G}_0(\epsilon) a^{\dagger}_s v_s \right)^n \mathcal{G}_0(\epsilon) v^{\dagger}_{s_1} a_{s_1} \right| P, g \right\rangle .$$

Now, by using the commutation relations (2.4), one may easily establish the following intertwining property of bosonic operators

$$a_s f\left(\mathcal{H}_0\right) = f\left(\mathcal{H}_0 - \omega_s\right) a_s, \quad f\left(\mathcal{H}_0\right) a^{\dagger}_s = a^{\dagger}_s f\left(\mathcal{H}_0 - \omega_s\right), \tag{3.16}$$

where f is some function addmitting for the Maclaurin expansion $f(z) = \sum\limits_{n=0}^{\infty} f_n z^n$. So, we see that

$$v^{\dagger}_{s'} a_{s'} \mathcal{G}_0(\epsilon) a^{\dagger}_s v_s = v^{\dagger}_{s'} \mathcal{G}_0\left(\epsilon - \omega'_s\right) v_s a_{s'} a^{\dagger}_s = v^{\dagger}_s \mathcal{G}_0\left(\epsilon - \omega_s\right) v_s + a^{\dagger}_{s'} v^{\dagger}_s \mathcal{G}_0\left(\epsilon - \omega_{s'} - \omega_s\right) v_{s'} a_s$$

By defining the self-energy operator $\Sigma^{(1)}$ and the effective potential energy operator $\mathcal{R}^{(1)}$ as

$$\Sigma^{(1)}(\epsilon) = v^{\dagger}_s \mathcal{G}_0\left(\epsilon - \omega_s\right) v_s, \quad \mathcal{R}^{(1)}(\epsilon) = a^{\dagger}_{s'} \mathcal{R}^{(1)}_{s',s}(\epsilon) a_s, \quad \mathcal{R}^{(1)}_{s',s}(\epsilon) = v^{\dagger}_s \mathcal{G}_0\left(\epsilon - \omega_{s'} - \omega_s\right) v_{s'} \tag{3.17}$$

we rewrite the matrix elements of the retarded T-matrix as

$$\begin{aligned}
&\left\langle P', g \left| \mathcal{T}^{(1)}(\epsilon) \right| P, g \right\rangle = \sum_{n=0}^{\infty} \left\langle P', g \left| a^{\dagger}_{s'_1} v_{s'_1} \left(\mathcal{G}_0(\epsilon) \left[\Sigma^{(1)}(\epsilon) + \mathcal{R}^{(1)}(\epsilon) \right] \right)^n \mathcal{G}_0(\epsilon) v^{\dagger}_{s_1} a_{s_1} \right| P, g \right\rangle \\
&= \left\langle P', g \left| a^{\dagger}_{s'_1} v_{s'_1} \frac{1}{\mathcal{G}_0^{-1}(\epsilon) - \Sigma^{(1)}(\epsilon) - \mathcal{R}^{(1)}(\epsilon)} v^{\dagger}_{s_1} a_{s_1} \right| P, g \right\rangle \\
&= \left\langle P', g \left| a^{\dagger}_{s'_1} v_{s'_1} \frac{1}{1 - \mathcal{G}^{(1)}(\epsilon) \mathcal{R}^{(1)}(\epsilon)} \mathcal{G}^{(1)}(\epsilon) v^{\dagger}_{s_1} a_{s_1} \right| P, g \right\rangle ,
\end{aligned}$$

where we have introduced the following Green's operator $\left(\mathcal{G}^{(1)}\right)^{-1}(\epsilon) = \mathcal{G}_0^{-1}(\epsilon) - \Sigma^{(1)}(\epsilon)$. Now, let us introduce the "vertex generating functional" $\mathcal{W}^{(1)}(\epsilon)$ as (we put this in quotes since $\mathcal{W}^{(1)}(\epsilon)$ is really an operator, but indeed has a similarity with vertex generating functional as we are going to see further)

$$\mathcal{W}^{(1)}(\epsilon) = \mathcal{R}^{(1)}(\epsilon) + \mathcal{R}^{(1)}(\epsilon) \mathcal{G}^{(1)}(\epsilon) \mathcal{W}^{(1)}(\epsilon) \tag{3.18}$$

By making use of the identity $(1 - AB)^{-1} A = A(1 - BA)^{-1}$, from equation (3.18) it follows

$$\frac{1}{1-\mathcal{G}^{(1)}(\epsilon)\mathcal{R}^{(1)}(\epsilon)} = \left(\mathcal{R}^{(1)}\right)^{-1}(\epsilon)\frac{1}{1-\mathcal{R}^{(1)}(\epsilon)\mathcal{G}^{(1)}(\epsilon)}\mathcal{R}^{(1)}(\epsilon) = \left(\mathcal{R}^{(1)}\right)^{-1}(\epsilon)\mathcal{W}^{(1)}(\epsilon)$$
$$= 1 + \mathcal{G}^{(1)}(\epsilon)\mathcal{W}^{(1)}(\epsilon).$$

So, finally, we arrive at the following result

$$\left\langle P', g \left| \mathcal{T}^{(1)}(\epsilon) \right| P, g \right\rangle = \left\langle P', g \left| a^\dagger_{s'_1} v_{s'_1} \mathcal{G}^{(1)}(\epsilon) v^\dagger_{s_1} a_{s_1} \right| P, g \right\rangle$$
$$+ \left\langle P', g \left| a^\dagger_{s'_1} v_{s'_1} \mathcal{G}^{(1)}(\epsilon) \mathcal{W}^{(1)}(\epsilon) \mathcal{G}^{(1)}(\epsilon) v^\dagger_{s_1} a_{s_1} \right| P, g \right\rangle . \tag{3.19}$$

Let us now have a closer look at the equation defining $\mathcal{W}^{(1)}(\epsilon)$. By iterating this equation and normal ordering it (here, by normal order, we understand the representation in which all the creation operators are on the left, whereas the annihilation operators are on the right) we obtain the subsequent expansion

$$\mathcal{W}^{(1)}(\epsilon) = a^\dagger_{s'_1}\mathcal{R}^{(1)}_{s'_1,s_1}(\epsilon)a_{s_1} + a^\dagger_{s'_1}\mathcal{R}^{(1)}_{s'_1,s}(\epsilon)\mathcal{G}^{(1)}\left(\epsilon-\omega_s\right)\mathcal{R}^{(1)}_{s,s_2}(\epsilon)a_{s_2}$$
$$+a^\dagger_{s'_1}a^\dagger_{s'_2}\mathcal{R}^{(1)}_{s'_1,s_1}\left(\epsilon-\omega_{s'_2}\right)\mathcal{G}^{(1)}\left(\epsilon-\omega_{s_1}-\omega_{s'_2}\right)\mathcal{R}^{(1)}_{s'_2,s_2}\left(\epsilon-\omega_{s_1}\right)a_{s_2}a_{s_1} + \dots$$

Hence, we deduce that $\mathcal{W}^{(1)}(\epsilon)$ can be represented in the form

$$\mathcal{W}^{(1)}(\epsilon) = \sum_{n=1}^{\infty} a^\dagger_{s'_1}\dots a^\dagger_{s'_n}\mathcal{W}^{(1,n)}_{s'_1\dots s'_n,s_1\dots s_n}(\epsilon)a_{s_n}\dots a_{s_1} \tag{3.20}$$

where $\mathcal{W}^{(1,n)}$ s are the operator-valued functions, which depend only on $\epsilon-\mathcal{H}_0$ and $2n$ multi-indicies $\{s'_1,\dots,s'_n,s_1,\dots,s_n\}$. By plugging this ansatz into the equation (3.18), we obtain

$$\sum_{n=1}^{\infty} a^\dagger_{s'_1}\dots a^\dagger_{s'_n}\mathcal{W}^{(1,n)}_{s'_1\dots s'_n,s_1\dots s_n}(\epsilon)a_{s_n\dots}\dots a_{s_1} = a^\dagger_{s'}\mathcal{R}^{(1)}_{s',s}(\epsilon)a_s$$
$$+a^\dagger_{s'}\mathcal{R}^{(1)}_{s',s}(\epsilon)a_s\mathcal{G}^{(1)}(\epsilon)\sum_{n=1}^{\infty} a^\dagger_{s'_1}\dots a^\dagger_{s'_n}\mathcal{W}^{(1,n)}_{s'_1\dots s'_n,s_1\dots s_n}(\epsilon)a_{s_n}\dots a_{s_1}$$
$$= a^\dagger_{s'}\mathcal{R}^{(1)}_{s',s}(\epsilon)a_s + a^\dagger_{s'}\mathcal{R}^{(1)}_{s',s}(\epsilon)\mathcal{G}^{(1)}\left(\epsilon-\omega_s\right)\sum_{n=1}^{\infty} a_s a^\dagger_{s'_1}\dots a^\dagger_{s'_n}\mathcal{W}^{(1,n)}_{s'_1\dots s'_n,s_1\dots s_n}(\epsilon)a_{s_n\dots}\dots a_{s_1}$$

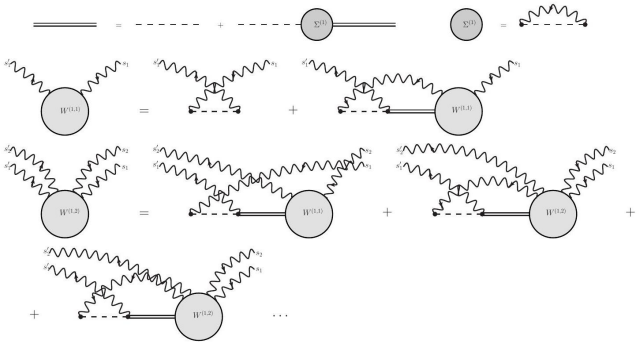

Figure 3.1: Graphical representation of integral equations for the effective multi-photon vertex functions in $Q = 1$ waveguide QED. Double line defines the dressed Green's function in the single excitation subspace. Photon emission and absorption vertices are denoted by wavy lines with outgoing and incoming arrows respectively. Effective n-particle vertices are represented by bubbles with n absorption and n emission photonic lines.

$$= a^\dagger_{s'}\mathcal{R}^{(1)}_{s',s}(\epsilon)a_s + a^\dagger_{s'}\mathcal{R}^{(1)}_{s',s}(\epsilon)\mathcal{G}\left(\epsilon-\omega_s\right)\sum_{n=1}^{\infty} a^\dagger_{s'_1\ldots}a^\dagger_{s'_n}\mathcal{W}^{(1,n)}_{s'_1\ldots s'_n,s_1\ldots s_n}\left(\epsilon-\omega_s\right)a_{s_n}\ldots a_{s_1}a_s$$

$$+a^\dagger_{s'}\mathcal{R}^{(1)}_{s',s}(\epsilon)\mathcal{G}^{(1)}(\epsilon-\omega_s)\sum_{n=1}^{\infty}\sum_{l=1}^{n} a^\dagger_{s'_1}\ldots a^\dagger_{s'_{l-1}}a^\dagger_{s'_{l+1}}\ldots a^\dagger_{s'_n}\mathcal{W}^{(1,n)}_{s'_1\ldots s'_{l-1}ss_{l+1}\ldots s'_n,s_1\ldots s_n}(\epsilon)a_{s_n}\ldots a_{s_1}$$

$$\begin{aligned}
&= a^\dagger_{s'}\mathcal{R}^{(1)}_{s',s}(\epsilon)a_s + \sum_{n=1}^{\infty} a^\dagger_{s'}a^\dagger_{s'_1}\ldots a^\dagger_{s'_n}\mathcal{R}^{(1)}_{s',s}\left(\epsilon-\sum_{r=1}^{n}\omega_{s'_r}\right)\mathcal{G}^{(1)}\left(\epsilon-\omega_s-\sum_{r=1}^{n}\omega_{s'_r}\right)\\
&\times\mathcal{W}^{(1,n)}_{s'_1\ldots s'_n,s_1\ldots s_n}\left(\epsilon-\omega_s\right)a_{s_n\ldots}a_{s_1}a_s\\
&+\sum_{n=1}^{\infty}\sum_{l=1}^{n} a^\dagger_{s'}a^\dagger_{s'_1}\ldots a^\dagger_{s'_{l-1}}a^\dagger_{s'_{l+1}}\ldots a^\dagger_{s'_n}\mathcal{R}^{(1)}_{s',s}\left(\epsilon-\sum_{r=1:r\neq l}^{n}\omega_{s'_r}\right)\mathcal{G}^{(1)}\left(\epsilon-\omega_s-\sum_{r=1:\neq l}^{n}\omega_{s'_n}\right)\\
&\times\mathcal{W}^{(1,n)}_{s'_1\ldots s'_{l-1}ss_{l-1}\ldots s'_n,s_1\ldots s_n}(\epsilon)a_{s_n}\ldots a_{s_1}.
\end{aligned}$$

Now, by taking the matrix elements in various n-particle subspaces, we arrive at the following set of integral equations

$$W^{(1,1)}_{s'_1,s_1}(\epsilon) = R^{(1)}_{s'_1,s_1}(\epsilon) + R^{(1)}_{s'_1,s}(\epsilon)G^{(1)}\left(\epsilon-\omega_s\right)W^{(1,1)}_{s,s_1}(\epsilon) \tag{3.21}$$

$$\begin{aligned}
W^{(1,2)}_{s'_1s'_2,s_1s_2}(\epsilon) &= R^{(1)}_{s'_1,s_1}\left(\epsilon-\omega_{s'_2}\right)G^{(1)}\left(\epsilon-\omega_{s_1}-\omega_{s'_2}\right)W^{(1,1)}_{s'_2,s_2}\left(\epsilon-\omega_{s_1}\right)\\
&+R^{(1)}_{s'_1,s}\left(\epsilon-\omega_{s'_2}\right)G^{(1)}\left(\epsilon-\omega_s-\omega_{s'_2}\right)\left[W^{(1,2)}_{ss'_2,s_1s_2}(\epsilon)+W^{(1,2)}_{s'_2s,s_1s_2}(\epsilon)\right]
\end{aligned} \tag{3.22}$$

$$\begin{aligned}
W^{(1,n)}_{s'_1\ldots s'_n,s_1\ldots s_n}(\epsilon) &= R^{(1)}_{s'_1,s_1}\left(\epsilon-\sum_{l=2}^{n}\omega_{s'_n}\right)G^{(1)}\left(\epsilon-\omega_{s_1}-\sum_{l=2}^{n}\omega_{s'_l}\right)W^{(1,n-1)}_{s'_2\ldots s'_n,s_2\ldots s_n}\left(\epsilon-\omega_{s_1}\right)\\
&+R^{(1)}_{s'_1,s}\left(\epsilon-\sum_{l=2}^{n}\omega_{s'_n}\right)G^{(1)}\left(\epsilon-\omega_s-\sum_{l=2}^{n}\omega_{s'_l}\right)\left[W^{(1,n)}_{ss'_2\ldots s'_n,s_1\ldots s_n}(\epsilon)+\ldots+W^{(1,n)}_{s'_2\ldots s'_ns,s_1\ldots s_n}(\epsilon)\right]
\end{aligned} \tag{3.23}$$

Here, we have used regular letters W, G, R instead of calligraphic ones to indicate that these objects are not operators but are rather their projections on the photonic vacuum (note that $W^{(1,n)}$s are still acting as operators on the qubit space). The collection of the integral equations above may be conveniently represented diagrammatically, see Figure 3.1. Diagrammatic rules may be formulated as follows. To each dotted line associate the bare propagator G_0. To each wavy line with incoming (outgoing) arrow associate the bare absorption $v^\dagger$ (emission v) vertex. Whenever two wavy lines are contracted together, one has to integrate over all momentum and sum over all channels. When a given wavy line passes over the propagator, its argument has to be shifted by the frequency carried by this line (which is a direct consequence of the intertwining property (3.16)).

Now having identified the equations defining the components of $\mathcal{W}^{(1)}$, we may express the transition operator as follows

$$\mathcal{T}^{(1)}(\epsilon) = \sum_{n=1}^{\infty} T^{(1,n)}_{s'_1\ldots s'_n,s_1\ldots s_n}(\epsilon)a^\dagger_{s'_1}\ldots a^\dagger_{s'_n}a_{s_n}\ldots a_{s_1} \tag{3.24}$$

where we have defined the following functions

$$T^{(1,1)}_{s'_1,s_1}(\epsilon) = \left\langle g \left| v_{s'_1} G^{(1)}(\epsilon) v^\dagger_{s_1} \right| g \right\rangle \tag{3.25}$$

$$T^{(1,n>1)}_{s'_1\ldots s'_n,s_1\ldots s_n}(\epsilon) = \left\langle g \left| v_{s'_1} G^{(1)}\left(\epsilon - \sum_{l=2}^{n}\omega_{s'_l}\right) W^{(1,n-1)}_{s'_2\ldots s'_n,s_2\ldots s_n}(\epsilon) G^{(1)}\left(\epsilon - \sum_{l=2}^{n}\omega_{s_l}\right) v^\dagger_{s_1} \right| g \right\rangle. \tag{3.26}$$

Diagrammatic representation of the components of T-matrix is presented in Figure (3.2). Note that throughout this thesis we work with the non-symmetrized forms of operators and perform the symmetrization only when doing actual calculations. Also note that the dependence of $\mathcal{T}^{(1,n)}_{s'_1\ldots s'_n,s_1\ldots s_n}$ on $\omega_s a^\dagger_s a_s$ may be omitted taking into account normal ordering, when S-matrix is going to be finally contracted with the initial state, all of the T-matrix components are going to be eventually projected onto the photonic vacuum and energies are going to be put on-shell. Using the above representation of the transition operator we immediately deduce that the scattering operator takes the following form

$$\mathcal{S} = 1 - 2\pi i \sum_{n=1}^{\infty} T^{(n)}_{s'_1\ldots s'_n,s_1\ldots s_n}\left(\sum_{l=1}^{n}\omega_{s_l}\right)\delta\left(\sum_{l=1}^{n}\omega_{s'_l} - \sum_{l=1}^{n}\omega_{s_l}\right) a^\dagger_{s'_1}\ldots a^\dagger_{s'_n} a_{s_n}\ldots a_{s_1} \tag{3.27}$$

Practically, when one contracts the S-matrix with the initial P-photon state, only first P terms in the above series contribute. It is, however, beneficial to represent the S-matrix in terms of the direct sum of N-body operators which act solely in the N-particle subspaces

$$\mathcal{S} = \bigoplus_{n=1}^{\infty} \mathcal{S}_n \tag{3.28}$$

where $\mathcal{S}_n$ may be written as

$$\mathcal{S}_n = S^{(n)}_{s'_1\ldots s'_n,s_1\ldots s_n} a^\dagger_{s'_1}\ldots a^\dagger_{s'_n} a_{s_n}\ldots a_{s_1} \tag{3.29}$$

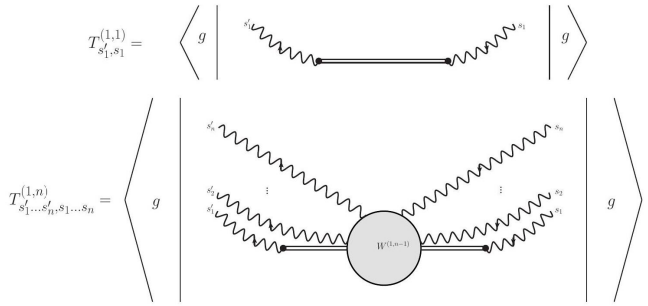

Figure 3.2: Diagrammatic representation of multi-photon T-matrix components. As one can see, n-particle T-matrix is completely determined by the $n-1$-particle vertex function, whereas the single-photon scattering matrix is completely determined by the dressed Green's function in the single excitation subspace. Such a representation is advantageous since it helps us to avoid formulating equations for $2n$-rank tensors, numerical integration of which would require greater computational efforts.

$$S^{(n)}_{s'_1\ldots s'_n,s_1\ldots s_n} = \left(\frac{1}{n!}\prod_{l=1}^{n}\delta_{s'_l,s_l} - 2\pi i \sum_{m=1}^{n}\frac{1}{(n-m)!} T^{(n)}_{s'_1\ldots s'_m,s_1\ldots s_m}\left(\sum_{l=1}^{m}\omega_{s_l}\right)\delta\left(\sum_{l=1}^{n}\omega_{s'_l} - \sum_{l=1}^{n}\omega_{s_l}\right)\prod_{r=m+1}^{n}\delta_{s'_r,s_r}\right). \tag{3.30}$$

Note that the combinatorial prefactors $\frac{1}{(n-m)!}$, $m \in \{0,\dots,n\}$ and additional δ functions $\delta_{s'_r,s_r}$ are chosen to take into account the excess number of $(n-m)$! Wick contractions. Let us now prove this statement for the states of our interest. Let us consider the action of an m-body operator $\mathcal{O} = O_{s'_1\dots s'_m,s_1\dots s_m} a^\dagger_{s'_1}\dots a^\dagger_{s'_m} a_{s_m}\dots a_{s_1}$ on an n-body ($n \geq m$) Fock state $\frac{1}{\sqrt{n!}}\left(\varphi_s a^\dagger_s\right)^n |\Omega\rangle$ (here and in what follows $|\Omega\rangle$ denotes the photonic vaccum state and φ_s stands for a normalized single-paricle wavefunction $\varphi^\dagger_s\varphi_s = 1$)

$$\begin{aligned}
&\frac{1}{\sqrt{n!}} O_{s'_1\dots s'_m,s_1\dots s_m} a^\dagger_{s'_1}\dots a^\dagger_{s'_m} a_{s_m}\dots a_{s_1}\left(\varphi_s a^\dagger_s\right)^n |\Omega\rangle \\
=&\frac{\prod_{l=0}^{m-1}(n-l)}{\sqrt{n!}} O_{s'_1\dots s'_m,s_1\dots s_m}\varphi_{s_1\dots}\dots\varphi_{s_m} a^\dagger_{s'_1}\dots a^\dagger_{s'_m}\left(\varphi_s a^\dagger_s\right)^{n-m}|\Omega\rangle \\
=&\frac{n!}{(n-m)!\sqrt{n!}} O_{s'_1\dots s'_m,s_1\dots s_m}\varphi_{s_1\dots\varphi_{s_m}} a^\dagger_{s'_1}\dots a^\dagger_{s'_m}\left(\varphi_s a^\dagger_s\right)^{n-m}|\Omega\rangle.
\end{aligned}$$

Now let us consider the contraction of the "promotion" of $\mathcal{O}$ to the n-particle subspace with the same state

$$\begin{aligned}
&\frac{1}{\sqrt{n!}}\frac{1}{(n-m)!} O_{s'_1\dots s'_m,s_1\dots s_m}\delta_{s'_{m+1},s_{m+1}}\dots\delta_{s'_n,s_n} a^\dagger_{s'_1}\dots a^\dagger_{s'_n} a_{s_n}\dots a_{s_1}\left(\varphi_s a^\dagger_s\right)^n|\Omega\rangle \\
&\quad= \frac{n!}{(n-m)!\sqrt{n!}} O_{s'_1\dots s'_m,s_1\dots s_m}\varphi_{s_1\dots}\dots\varphi_{s_m} a^\dagger_{s'_1}\dots a^\dagger_{s'_m}\left(\varphi_s a^\dagger_s\right)^{n-m}|\Omega\rangle \\
&\quad= \frac{1}{\sqrt{n!}} O_{s'_1\dots s'_m,s_1\dots s_m} a^\dagger_{s'_1\dots} a^\dagger_{s'_m} a_{s_m\dots}\dots a_{s_1}\left(\varphi_s a^\dagger_s\right)^n|\Omega\rangle
\end{aligned}$$

which, in turn, justifies the validity of our direct sum representation. In fact, by a tedious, but straightforward calculation, one can show that this representation holds for more general states, however, we shall not dwell on this point in the present thesis.

As it was mentioned above, the solution to the $P = Q'$-photon scattering problem on Q' qubits, provides the exact solution to the P-photon scattering problem on any number $Q \geq Q'$ of qubits, thus the expression for a single photon T-matrix for the case of a single emitter allows one to determine the exact single-photon T-matrix for any number of qubits. According to the above analysis $T^{(1)}_{s'_1,s_1}(\epsilon) = \left\langle g\left|v_{s'_1}G^{(1)}(\epsilon)v^\dagger_{s_1}\right|g\right\rangle$, with $G^{(1)}(\epsilon) = G_0(\epsilon)+G_0(\epsilon)\Sigma^{(1)}(\epsilon)G^{(1)}(\epsilon)$, where $G_0^{-1}(\epsilon) = \epsilon - \frac{1}{2}\sum\limits_{n=1}^{Q}\Delta_n\sigma_3^{(n)} + i\eta$ and

$$\Sigma^{(1)}(\epsilon) = v_s^\dagger G_0\left(\epsilon-\omega_s\right)v_s = \sum_{\alpha=1}^{C}\sum_{n=1}^{Q}\sum_{n'=1}^{Q}\int\limits_{B_\alpha} dk\sigma_+^{(n')}\frac{g^*_{\alpha,n'}(k)g_{\alpha,n}(k)}{\epsilon-\frac{1}{2}\sum\limits_{l=1}^{Q}\Delta_l\sigma_3^{(l)}-\omega_\alpha(k)+i\eta}\sigma_-^{(n)}. \tag{3.31}$$

3.3.2 Separation of Elastic Contributions, Parametrization of Effective Vertex Functions and Generalized Cluster Decomposition

It is worth noting that effective vertex functions $W^{(1,n)}$ are not entirely connected due to the presence of delta functions in the inhomogeneous terms of integral equations coming from $R_{s',s}(\epsilon)$. These delta function contributions, not only prohibit one to solve the resulting equations numerically, but also do not allow for the clear separation between the elastic and inelastic contributions to the respective S-matrices, since such a separation is crucial in the calculation of observables, it is the purpose of this subsection to address this problem. With the help of this separation, we are also going to illustrate the so-called generalized cluster decomposition principle in waveguide QED. Ordinary principle of cluster decomposition has its roots in relativistic quantum field theory and has a deep relation to the fundamental physical property of all field theories of particle physics - locality. In relativistic quantum field theories, locality implies that the scattering amplitude factorizes as a product of single-particle amplitudes for causally

disconnected input states [34]. Non-locality of waveguide quantum electrodynamics, in its turn, implies that the standard cluster decomposition principle has to be significantly modified as it was first shown in [57]. In [52], authors were able to demonstrate, that within the framework of waveguide QED, an N-particle S-matrix in no way can be written as a product of N single-particle S-matrices, instead, the absence of the exact causality in the theory, unavoidably leads to the presence of connected multiparticle components in the S-matrix. Another important issue discussed in this paragraph is the parametrization of effective vertex functions, which in turn allows reducing the solution of integral equations for 2×2 matrix-valued functions to the solution of scalar equations.

Let us for simplicity assume throughout this subsection that the dispersion relation and bandwidth are the same in all of the radiation channels $B_\alpha = B$, $\omega_\alpha(k) = \omega(k), \forall \alpha \in \{1, \ldots, C\}$ (although this assumption looks restrictive, in practice it is always satisfied). First, let us consider the lowest order equation

$$W^{(1,1)}_{s_1',s_1}(\epsilon) = R^{(1)}_{s_1',s_1}(\epsilon) + R^{(1)}_{s_1',s}(\epsilon) G^{(1)}(\epsilon - \omega_s) W^{(1,1)}_{s,s_1}(\epsilon) \tag{3.32}$$

With the following ansatz

$$\begin{aligned} W_{\mu_1' k_1', \mu_1 k_1}(\epsilon)^{(1,1)} &= |1\rangle\langle 1| g^*_{\mu_1}(k_1) g_{\mu_1'}(k_1') F^{(1,1)}(k_1', k_1, \epsilon) \\ &:= |1\rangle\langle 1| g^*_{\mu_1}(k_1) g_{\mu_1'}(k_1') \left(\hat{G}_0(\epsilon - \omega(k_1') - \omega(k_1)) + \bar{F}^{(1,1)}(k_1', k_1, \epsilon) \right) \end{aligned}$$

we obtain the following non-singular equation for a scalar function $\bar{F}^{(1,1)}$

$$\begin{aligned} \bar{F}^{(1,1)}(k_1', k_1, \epsilon) = &\sum_{\mu=1}^{C} \int_B dk \, |g_\mu(k)|^2 \hat{G}_0(\epsilon - \omega(k_1') - \omega(k)) \tilde{G}^{(1)}(\epsilon - \omega(k)) \hat{G}_0(\epsilon - \omega(k) - \omega(k_1)) \\ &+ \sum_{\mu=1}^{C} \int_B dk \, |g_\mu(k)|^2 \hat{G}_0(\epsilon - \omega(k_1') - \omega(k)) \tilde{G}^{(1)}(\epsilon - \omega(k)) \bar{F}^{(1,1)}(k_1', k_1, \epsilon) \,. \end{aligned} \tag{3.33}$$

Here, and in what follows, hat and tilde symbols over the objects denote respectively the ground and excited state (in the qubit space) diagonal matrix elements of the corresponding objects. Let us now consider the next equation in the ladder

$$\begin{aligned} W^{(1,2)}_{s_1' s_2', s_1 s_2}(\epsilon) = &R^{(1)}_{s_1', s_1}(\epsilon - \omega_{s_2'}) G^{(1)}(\epsilon - \omega_{s_1'} - \omega_{s_2'}) W^{(1,1)}_{s_2', s_2}(\epsilon - \omega_{s_1}) \\ &+ R^{(1)}_{s_1', s}(\epsilon - \omega_{s_2'}) G^{(1)}(\epsilon - \omega_s - \omega_{s_2'}) \left[W^{(1,2)}_{s s_2', s_1 s_2}(\epsilon) + W^{(1,2)}_{s_2' s, s_1 s_2}(\epsilon) \right] \end{aligned} \tag{3.34}$$

Baring in mind the parametrization of $W^{(1,1)}_{s_1',s_1}(\epsilon)$ and the equation which it satisfies, we make the following educated ansatz

$$\begin{aligned} W^{(1,2)}_{\mu_1' k_1' \mu_2' k_2', \mu_1 k_1 \mu_2 k_2} &= |1\rangle\langle 1| g^*_{\mu_1}(k_1) g_{\mu_1'}(k_1') g^*_{\mu_2}(k_2) g_{\mu_2'}(k_2') F^{(2,2)}(k_1', k_2', k_1, k_2, \epsilon) \\ := |1\rangle\langle 1| g^*_{\mu_1}(k_1) g_{\mu_1'}(k_1') g^*_{\mu_2}(k_2) g_{\mu_2'}(k_2') &\Big(F^{(1,1)}(k_1', k_1, \epsilon - \omega(k_2')) \tilde{G}^{(1)}(\epsilon - \omega(k_1) - \omega(k_2')) \\ &\times F^{(1,1)}(k_2', k_2, \epsilon - \omega(k_1)) + \bar{F}^{(2,2)}(k_1', k_2', k_1, k_2, \epsilon) \Big) \end{aligned}$$

again leading to the regular scalar equation for $\bar{F}^{(2,2)}$

$$\bar{F}^{(2,2)}\left(k_1',k_2',k_1,k_2,\epsilon\right)$$
$$=\sum_{\mu=1}^{C}\int_B dk\left|g_\mu(k)\right|^2\hat{G}_0\left(\epsilon-\omega\left(k_1'\right)-\omega\left(k_2'\right)-\omega(k)\right)\tilde{G}^{(1)}\left(\epsilon-\omega\left(k_2'\right)-\omega(k)\right)F^{(1,1)}\left(k_2',k_2,\epsilon-\omega(k)\right)$$
$$\times\tilde{G}^{(1)}\left(\epsilon-\omega\left(k_1\right)-\omega(k)\right)F^{(1,1)}\left(k,k_2,\epsilon-\omega\left(k_2\right)\right)$$
$$+\sum_{\mu=1}^{C}\int_B dk\left|g_\mu(k)\right|^2\hat{G}_0\left(\epsilon-\omega\left(k_1'\right)-\omega\left(k_2'\right)-\omega(k)\right)\tilde{G}^{(1)}\left(\epsilon-\omega\left(k_2'\right)-\omega(k)\right)$$
$$\times\left[\bar{F}^{(2,2)}\left(k,k_2',k_1,k_2,\epsilon\right)+\bar{F}^{(2,2)}\left(k_2',k,k_1,k_2,\epsilon\right)\right]. \tag{3.35}$$

Continuing this process, we see that to efficiently parametrize a general n-body vertex and remove the singular contributions from the inhomogeneous term, one has to make the following ansatz

$$W^{(1,n)}_{\mu_1'k_1'\ldots\mu_n'k_n',\mu_1k_1\ldots\mu_nk_n}(\epsilon)|1\rangle\langle 1|\prod_{l=1}^{n}g^*_{\mu_l}\left(k_l\right)g_{\mu_l'}\left(k_l'\right)\left(F^{(1,1)}\left(k_1',k_1,\epsilon-\sum_{s=2}^{n}\omega\left(k_s'\right)\right)\right.$$
$$\left.\times\tilde{G}\left(\epsilon-\omega_1-\sum_{m=2}^{n}\omega\left(k_m'\right)\right)F^{(1,n-1)}\left(k_2',\ldots,k_n',k_2,\ldots,k_n,\epsilon-\omega\left(k_1\right)\right)+\bar{F}^{(1,n)}\left(k_1',\ldots,k_n',k_1,\ldots,k_n,\epsilon\right)\right). \tag{3.36}$$

Let us now consider the effect of the separation of the singular contributions on the shape of the S-matrix. We again start by considering the lowest order case of two-photon scattering, the
scattering matrix in the two-excitation subspace has the following form

$$\mathcal{S}_2=(\frac{1}{2!}\delta_{s_1',s_1}\delta_{s_2',s_2}-2\pi iT^{(1,2)}_{s_1',s_1}\left(\omega\left(k_1\right)\right)\delta\left(\omega\left(k_1'\right)-\omega\left(k_1\right)\right)\frac{1}{1!}\delta_{s_2',s_2}$$
$$\left.-2\pi iT^{(1,2)}_{s_1's_2',s_1s_2}\left(\omega\left(k_1\right)+\omega\left(k_2\right)\right)\delta\left(\omega\left(k_1'\right)+\omega\left(k_2'\right)-\omega\left(k_1\right)-\omega\left(k_2\right)\right)\right)a^\dagger_{s_1'}a^\dagger_{s_2'}a_{s_2}a_{s_1} \tag{3.37}$$

where

$$T^{(1,1)}_{s_1',s_1}\left(\omega\left(k_1\right)\right)=\left\langle g\left|v_{s_1'}G^{(1)}\left(\omega\left(k_1\right)\right)v^\dagger_{s_1}\right|g\right\rangle,$$
$$T^{(1,2)}_{s_1's_2',s_1s_2}\left(\omega\left(k_1\right)+\omega\left(k_2\right)\right)=\left\langle g\left|v_{s_1'}G^{(1)}\left(\omega\left(k_1'\right)\right)W^{(1,1)}_{s_2',s_2}\left(\omega\left(k_1\right)+\omega\left(k_2\right)\right)G^{(1)}\left(\omega\left(k_1\right)\right)v^\dagger_{s_1}\right|g\right\rangle,$$

and all of the energies in above are implicitly shifted by $-\frac{\Delta}{2}$. Now we consider the above-defined decomposition of $W^{(1,1)}$

$$W^{(1,1)}_{s_2',s_2}\left(\omega\left(k_1\right)+\omega\left(k_2\right)\right)=v^\dagger_{s_2}v_{s_2'}\left(\hat{G}_0\left(\omega\left(k_1\right)-\omega\left(k_2'\right)\right)+\bar{F}^{(1,1)}\left(k_2',k_2,\omega\left(k_1\right)+\omega\left(k_2\right)\right)\right)$$
$$=-\pi iv^\dagger_{s_2}v_{s_2'}\delta\left(\omega\left(k_1\right)-\omega\left(k_2'\right)\right)+W^{(1,1,C)}_{s_2',s_2}\left(\omega\left(k_1\right)+\omega\left(k_2\right)\right),$$

where we have defined the connected part of the single-photon effective vertex as

$$W^{(1,1,C)}_{s_2',s_2}\left(\omega\left(k_1\right)+\omega\left(k_2\right)\right)=v^\dagger_{s_2}v_{s_2'}\left(P\left(\frac{1}{\omega\left(k_1\right)-\omega\left(k_2'\right)}\right)+\bar{F}^{(1,1)}\left(k_2',k_2,\omega\left(k_1\right)+\omega\left(k_2\right)\right)\right).$$

Here $P(\cdot)$ stands for the principal value in the distribution sense (principal value symbol can actually be removed when dealing with two-photon S-matrix since after symmetrization one can show that the singularity is gone). Two-body transition operator now takes the form

$$\begin{aligned} T^{(1,2}_{s_1's_2',s_1s_2}\left(\omega\left(k_1\right)+\omega\left(k_2\right)\right) &= -\pi i\delta\left(\omega\left(k_1\right)-\omega\left(k_2'\right)\right)\left\langle g\left|v_{s_1'}G^{(1)}\left(\omega\left(k_1'\right)\right)v^{\dagger}_{s_2}\right|g\right\rangle \\ &\times\left\langle g\left|v_{s_2'}G^{(1)}\left(\omega\left(k_1\right)\right)v^{\dagger}_{s_1}\right|g\right\rangle \\ &+\left\langle g\left|v_{s_1'}G^{(1)}\left(\omega\left(k_1'\right)\right)W^{(1,1,C)}_{s_2',s_2}\left(\omega\left(k_1\right)+\omega\left(k_2\right)\right)G^{(1)}\left(\omega\left(k_1\right)\right)v^{\dagger}_{s_1}\right|g\right\rangle \\ &= -\pi i\delta\left(\omega\left(k_1\right)-\omega\left(k_2'\right)\right)T^{(1,1)}_{s_1',s_1}\left(\omega\left(k_1\right)\right)T^{(1,1)}_{s_2',s_2}\left(\omega\left(k_2'\right)\right)+T^{(1,2,C)}_{s_1's_2',s_1s_2}\left(\omega\left(k_1\right)+\omega\left(k_2\right)\right). \end{aligned}$$

The equality sign in above is understood in the sense of permutation equivalence and on-shell condition. The connected part of the two-photon T-matrix $T^{(1,2,C)}$ is defined in the same manner as $T^{(1,2)}$, with $W^{(1,1,C)}$ replacing $W^{(1,1)}$. By plugging the above representation into the definition of $\mathcal{S}_2$ one obtains

$$\begin{aligned} &\mathcal{S}_2 \\ &=\left(\tfrac{1}{2}S^{(1)}_{s_1',s_1}S^{(1)}_{s_2',s_2}-2\pi iT^{(1,2)}_{s_1's_2',s_1s_2}\left(\omega\left(k_1\right)+\omega\left(k_2\right)\right)\delta\left(\omega\left(k_1'\right)+\omega\left(k_2'\right)-\omega\left(k_1\right)-\omega\left(k_2\right)\right)\right)a^{\dagger}_{s_1'}a^{\dagger}_{s_2'}a_{s_2}a_{s_1}, \end{aligned}$$

where the single-photon scattering operaotor's matrix elements are defined as $S^{(1)}_{s_1',s_1}=\frac{1}{1!}\delta_{s_1',s_1}$ - $2\pi i\delta\left(\omega\left(k_1'\right)-\omega\left(k_1\right)\right)T^{(1,1)}_{s_1',s_1}\left(\omega\left(k_1\right)\right)$. Such a representation of the scattering matrix is known as the generalized cluster decomposition.

Although the cluster decomposition principle is easily illustrated in the two-excitation subspace, it becomes completely non-apparent in higher-order sectors within the present approach. Namely, it seems like there is a lack of elastic contributions required to obtain appropriate combinatorial coefficients. The problem is though resolved by careful analysis of terms containing products of

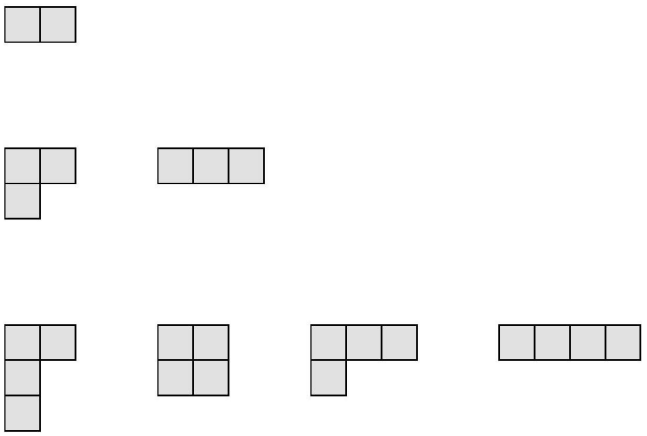

Figure 3.3: Young diagrams corresponding to partitions of 2, 3 and 4. In each of Young diagrams, n boxes are combined into $p(n)$ clusters, each corresponding to a separate partition (with $p(n)$ being the number of partitions of number n). Within each cluster, each row corresponds to an independent member of the given partition, whereas rows are understood to be added together, for example, $4=1+1+1+1, 4=2+1+1, 4=2+2, 4=3+1$ and $4=4$. Filling the boxes of Young diagrams with numbers (or sometimes more complicated objects, such as S-matrices, for example) obeying various rules, leads to a family of objects called Young tableaux, depending on the nature of such a filler, these tableaux may carry various meaning. We would also like to note, that depending on the context, Young diagrams may have a topology different from the one used in this thesis, for example, in molecular physics applications, individual clusters are usually organized vertically, instead of horizontally.

principal values of functions sharing their arguments. For example, in the view of the following distributional identity (Poincaré-Bertrand formula)

$$P\left(\frac{1}{x}\right)P\left(\frac{1}{y}\right)=P\left(\frac{1}{y-x}\right)\left[P\left(\frac{1}{x}\right)-P\left(\frac{1}{y}\right)\right]+\pi^2\delta(x)\delta(y) \tag{3.39}$$

one can establish the following relation in the three-photon sector (see Appendix B)

$$P\left(\frac{1}{\omega\left(k_3'\right)-\omega\left(k_3\right)}\right)P\left(\frac{1}{\omega\left(k_1\right)-\omega\left(k_1'\right)}\right)+P\left(\frac{1}{\omega\left(k_2'\right)-\omega\left(k_2\right)}\right)P\left(\frac{1}{\omega\left(k_3\right)-\omega\left(k_3'\right)}\right)$$
$$+P\left(\frac{1}{\omega\left(k_1'\right)-\omega\left(k_1\right)}\right)P\left(\frac{1}{\omega\left(k_2\right)-\omega\left(k_2'\right)}\right)=\pi^2\delta\left(\omega\left(k_3'\right)-\omega\left(k_3\right)\right)\delta\left(\omega\left(k_1'\right)-\omega\left(k_1\right)\right) \tag{3.40}$$

where equality sign in (3.40) is again understood in the sense of permutation equivalence and on-shell condition. With the help of this formula, one eventually arrives at the following cluster decomposition of the three-photon S-matrix

$$\begin{aligned}\mathcal{S}_3=&\left(\frac{1}{6}S^{(1)}_{s_1',s_1}S^{(1)}_{s_2',s_2}S^{(1)}_{s_3',s_3}\right.\\&-2\pi iT^{(1,2,C)}_{s_1's_2',s_1s_2}\left(\omega\left(k_1\right)+\omega\left(k_2\right)\right)\delta\left(\omega\left(k_1'\right)+\omega\left(k_2'\right)-\omega\left(k_1\right)-\omega\left(k_2\right)\right)S^{(1)}_{s_3',s_3}\\&\left.-2\pi iT^{(1,3,C)}_{s_1's_2's_3',s_1s_2s_3}\left(\omega\left(k_1\right)+\omega\left(k_2\right)+\omega\left(k_3\right)\right)\delta\left(\omega\left(k_1'\right)+\omega\left(k_2'\right)+\omega\left(k_3'\right)-\omega\left(k_1\right)-\omega\left(k_2\right)-\omega\left(k_3\right)\right)\right)\\&\times a^\dagger_{s_1'}a^\dagger_{s_2'}a^\dagger_{s_3'}a_{s_3}a_{s_2}a_{s_1},\end{aligned} \tag{3.41}$$

where the connected part of the three-photon T-matrix is given by the following nasty expression

$$\begin{aligned}&T^{(1,3,C}_{s_1's_2's_3',s_1s_2s_3}\left(\omega\left(k_1\right)+\omega\left(k_2\right)+\omega\left(k_3\right)\right)=g^*_{\mu_1}\left(k_1\right)g^*_{\mu_2}\left(k_2\right)g^*_{\mu_3}\left(k_3\right)g_{\mu_1'}\left(k_1'\right)g_{\mu_2'}\left(k_2'\right)g_{\mu_3'}\left(k_3'\right)\\&\left(\frac{1}{\omega)k_3')-\omega)k_3)}\frac{1}{\omega)k_1)-\omega)k_1')}\left[\tilde G\left(\omega\left(k_3'\right)\right)\tilde G\left(\omega\left(k_1\right)\right)\left(\tilde G\left(\omega\left(k_2\right)+\omega\left(k_1\right)-\omega\left(k_1'\right)\right)-\tilde G\left(\omega\left(k_2\right)\right)\right)\right.\\&\left.+\tilde G\left(\omega\left(k_2\right)\right)\tilde G\left(\omega\left(k_1\right)\right)\left(\tilde G\left(\omega\left(k_3'\right)\right)-\tilde G\left(\omega\left(k_3\right)\right)\right)\right]\\&+\frac{1}{\omega\left(k_1'\right)-\omega\left(k_1\right)}\left[\tilde G\left(\omega\left(k_1'\right)\right)\tilde G\left(\omega\left(k_3\right)\right)\tilde G\left(\omega\left(k_3'\right)+\omega\left(k_1'\right)-\omega\left(k_1\right)\right)\bar F^{(1,1)}\left(k_2',k_2,\omega\left(k_2\right)+\omega\left(k_3\right)\right)\right.\\&\left.-\tilde G\left(\omega\left(k_3'\right)\right)\tilde G\left(\omega\left(k_1\right)\right)\tilde G\left(\omega\left(k_1\right)+\omega\left(k_3\right)-\omega\left(k_1'\right)\right)\bar F^{(1,1)}\left(k_2',k_2,\omega\left(k_3'\right)+\omega\left(k_2'\right)\right)\right]\\&+\tilde G\left(\omega\left(k_1'\right)\right)\tilde G\left(\omega\left(k_1\right)+\omega\left(k_3\right)-\omega\left(k_3'\right)\right)\tilde G\left(\omega\left(k_1\right)\right)\bar F^{(1,1)}\left(k_2',k_2,\omega\left(k_1'\right)+\omega\left(k_2'\right)\right)\bar F^{(1,1)}\left(k_3',k_3,\omega\left(k_1\right)+\omega\left(k_3\right)\right.\\&\left.+\tilde G\left(\omega\left(k_1'\right)\right)\tilde G\left(\omega\left(k_1\right)\right)\bar F^{(2,2)}\left(k_2',k_3',k_2,k_3,\omega\left(k_1\right)+\omega\left(k_2\right)+\omega\left(k_3\right)\right)\right)\end{aligned}$$

All of the terms in this expression are non-singular as it may be shown by exploiting permutation equivalence and on-shell condition (see Appendix B).

Cluster decomposition is extremely beneficial in the calculation of observable quantities, not only because it allows for a clear separation between the elastic and inelastic contributions, but also because it significantly simplifies the calculation of the scattered state. The physical meaning of the cluster decomposition is rather apparent. In the two-photon sector, two particles may both scatter coherently (without interaction) which is represented by the product of two singleparticle S-matrices, or they can scatter incoherently by interacting and thus redistributing their initial momenta between one another. Analogously, in three-photon scattering there are three possibilities: all three particles scatter coherently, a single particle scatters coherently and the other two interact, or finally, all three particles may inseparably be involved in the scattering process. Interestingly enough, the problem of generalized cluster decomposition has a deep relationship with the famous problem of partitions of natural numbers in number theory. Namely, the number of clusters in the n-particle S-matrix is exactly equal to the number of partitions of a natural number $n-p(n)$. In number theory partitions are usually represented by Young diagrams which are shown in Figure 3.3.

3.3.3 Closed Form Solution in the Markovian Limit

Let us now consider the single-qubit scattering problem in the Markovian limit. Validity of Markovian approximation demands a number of assumptions: linear dispersion relation in all of the channels $\omega_\mu(k) = \omega_{0\mu} + v_\mu k$, broadband limit $B_\mu = \mathbb{R}, \forall \mu \in \{1, \ldots, C\}$ and local couplings (i.e. independent of frequency) $g_\mu(k) = \sqrt{\gamma_\mu/\pi}$. Within the above assumptions, the self-energy diagram reads as $\Sigma^{(1)}(\epsilon) = -i \sum_{\mu=1}^{C} \gamma_\mu |1\rangle\langle 1|$, which is independent of ϵ (here we have introduced the projector on the qubit's excited state $|1\rangle\langle 1| = \frac{1+\sigma_3}{2}$). By causality, all of the W functions are analytic in momentum (energy) variables in the lower (upper) half of the complex plane (a picky reader may verify this statement by evaluating any diagram contributing to the Neumann expansion of any of the above integral equations to see that it indeed possesses the above mentioned

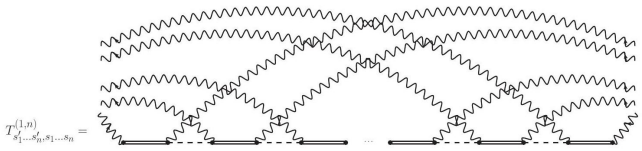

Figure 3.4: n-photon T-matrix in the non-crossing approximation.

analytical properties). By exploiting this analyticity along with the momentum independence of both coupling constants and self-energy, we can close all of the integration contours in the lower half of the complex momentum plane to render all of the integrals zero, thus promoting the integral equations into algebraic ones

$$W^{(1,1)}_{s'_1,s_1}(\epsilon) = R^{(1)}_{s'_1,s_1}(\epsilon), \quad W^{(1,2)}_{s'_1 s'_2,s_1 s_2}(\epsilon) = R^{(1)}_{s'_1,s_1}\left(\epsilon - \omega_{s'_2}\right) G^{(1)}\left(\epsilon - \omega_{s'_2} - \omega_{s_1}\right) R^{(1)}_{s'_2,s_2}\left(\epsilon - \omega_{s_1}\right),$$

$$W^{(1,n)}_{s'_1 \ldots s'_n,s_1 \ldots s_n}(\epsilon) = R^{(1)}_{s'_1,s_1}\left(\epsilon - \sum_{l=2}^{n} \omega_{s'_l}\right) G^{(1)}\left(\epsilon - \omega_{s_1} - \sum_{l=2}^{n} \omega_{s'_l}\right) R^{(1)}_{s'_2,s_2}\left(\epsilon - \omega_{s_1} - \sum_{l=3}^{n} \omega_{s'_l}\right)$$
$$\times G^{(1)}\left(\epsilon - \omega_{s_1} - \omega_{s_2} - \sum_{l=3}^{n} \omega_{s'_l}\right) \times \ldots \times G^{(1)}\left(\epsilon - \sum_{l=1}^{n-1} \omega_{s_l} - \omega_{s'_n}\right) R^{(1)}_{s'_n,s_n}\left(\epsilon - \sum_{l=1}^{n-1} \omega_{s_l}\right).$$

Plugging the above expressions into the definition of the components of the T-matrix we recover the solution obtained in [42] for a two-level system locally coupled to a one-dimensional transmission line. In their later work [43], the same authors used this solution for their tour-de-force calculation of the full-counting statistics, the evolution of the spectral density and entanglement entropy, thus demonstrating the power of the scattering approach. Diagrammatically the above solution is equivalent to the so-called non-crossing approximation (which becomes exact in the Markovian limit) and it is represented in Figure 3.4.

3.3.4 Approximation Strategies

Although it is possible to write an entire hierarchy of exact equations for the multi-photon vertex functions, which in turn parametrize the exact S-matrix, their analytical solution is in general only possible in the Markovian limit. As it is usually done in theoretical physics, to make some progress in solving a given physical problem, one has to resort to some kind of approximation routine. By taking inspiration from the theory of condensed matter, we propose a couple of physically motivated resummations, allowing one to avoid (or partially avoid) the solution of the above integral equations.

The first approximation which we suggest is the quasi-Markovian one, which is exactly based on the non-crossed diagrams shown in Figure 3.4. We call this approximation quasi-Markovian since it becomes exact in the Markov limit. Baring this in mind, we physically expect this approximation to be valid in the cases when the characteristic time delays in the system τ are such that $\gamma\tau \leq 1$, where γ is the characteristic decay rate of the system into the continuum. In this approximation, all of the non-trivial momentum dependence of the S-matrix, comes entirely from the frequency dependence of the self-energy diagram which may be easily computed in a

bunch of cases. We would also like to note that quasi-Markovian approximation becomes exact in a single-photon sector.

The second approximation routine we are proposing is based on the resummation of the full single-photon vertex functions $W^{(1,1)}_{s',s}(\epsilon)$. Diagrammatically, this approximation amounts to the replacement of the dotted lines in Figure 3.4 by the full single-particle bubbles, the resulting n photon T-matrix is shown in Figure 3.5. To understand the physics behind this approximation

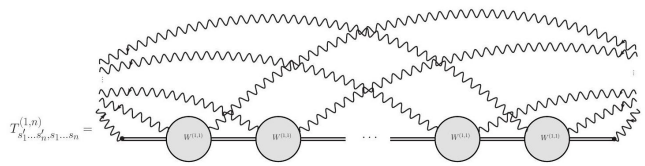

Figure 3.5: n-photon T-matrix in the weak correlation approximation. As one can see, this approximation effectively amounts to the replacement of bare single-particle vertices in the noncrossed diagrams by exact single-particle bubbles, which have to be determined by solving equation (3.21).

as well as the bounds for its validity, it is instructive to have a look at the exact equations of the theory. Consider the second equation for instance

$$W^{(1,2)}_{s'_1 s'_2, s_1 s_2}(\epsilon) = R^{(1)}_{s'_1, s_1}\left(\epsilon - \omega_{s'_2}\right) G^{(1)}\left(\epsilon - \omega_{s_1} - \omega_{s'_2}\right) W^{(1,1)}_{s'_2, s_2}\left(\epsilon - \omega_{s_1}\right)$$
$$+ R^{(1)}_{s'_1, s}\left(\epsilon - \omega_{s'_2}\right) G^{(1)}\left(\epsilon - \omega_{s} - \omega_{s'_2}\right) \left[W^{(1,2)}_{s s'_2, s_1 s_2}(\epsilon) + W^{(1,2)}_{s'_2 s, s_1 s_2}(\epsilon)\right]$$

We note that if we ignore the exchange symmetry (in the spirit of the Hartree approximation), we are led to the following equation

$$W^{(1,2)}_{s'_1 s'_2, s_1 s_2}(\epsilon) \approx R^{(1)}_{s'_1, s_1}\left(\epsilon - \omega_{s'_2}\right) G^{(1)}\left(\epsilon - \omega_{s_1} - \omega_{s'_2}\right) W^{(1,1)}_{s'_2, s_2}\left(\epsilon - \omega_{s_1}\right)$$
$$+ R^{(1)}_{s'_1, s}\left(\epsilon - \omega_{s'_2}\right) G^{(1)}\left(\epsilon - \omega_{s} - \omega_{s'_2}\right) W^{(1,2)}_{s s'_2, s_1 s_2}(\epsilon).$$

It is easy to see that its exact solution is given by

$$W^{(1,2)}_{s'_1 s'_2, s_1 s_2}(\epsilon) = W^{(1,1)}_{s'_1, s_1}\left(\epsilon - \omega_{s'_2}\right) G^{(1)}\left(\epsilon - \omega_{s_1} - \omega_{s'_2}\right) W^{(1,1)}_{s'_2, s_2}\left(\epsilon - \omega_{s_1}\right).$$

In exactly the same spirit we can consider the third equation

$$W^{(1,3)}_{s'_1 s'_2 s'_3, s_1 s_2 s_3}(\epsilon) = R^{(1)}_{s'_1, s_1}\left(\epsilon - \omega_{s'_2} - \omega_{s'_3}\right) G^{(1)}\left(\epsilon - \omega_{s_1} - \omega_{s'_2} - \omega_{s'_3}\right) W^{(1,2)}_{s'_2 s'_3, s_2 s_3}\left(\epsilon - \omega_{s_1}\right)$$
$$+ R^{(1)}_{s'_1, s}\left(\epsilon - \omega_{s'_2} - \omega_{s'_3}\right) \bar{G}\left(\epsilon - \omega_{s} - \omega_{s'_2} - \omega_{s'_3}\right) \left[W^{(1,3)}_{s s'_2 s'_3, s_1 s_2 s_3}(\epsilon) + W^{(1,3)}_{s'_2 s'_3, s_1 s_2 s_3}(\epsilon)\right.$$
$$\left. + W^{(1,3)}_{s'_2 s'_3 s, s_1 s_2 s_3}(\epsilon)\right]$$
$$\approx R^{(1)}_{s'_1, s_1}\left(\epsilon - \omega_{s'_2} - \omega_{s'_3}\right) G^{(1)}\left(\epsilon - \omega_{s_1} - \omega_{s'_2} - \omega_{s'_3}\right) W^{(1,2)}_{s'_2 s'_3, s_2 s_3}\left(\epsilon - \omega_{s_1}\right)$$
$$+ R^{(1)}_{s'_1, s}\left(\epsilon - \omega_{s'_2} - \omega_{s'_3}\right) \bar{G}\left(\epsilon - \omega_{s} - \omega_{s'_2} - \omega_{s'_3}\right) W^{(1,3)}_{s s'_2 s'_3, s_1 s_2 s_3}(\epsilon).$$

Again, it is easy to check that

$$W^{(1,3)}_{s'_1 s'_2 s'_3, s_1 s_2 s_3}(\epsilon) W^{(1,1)}_{s'_1, s_1}\left(\epsilon - \omega_{s'_2} - \omega_{s'_3}\right) G\left(\epsilon - \omega_{s_1} - \omega_{s'_2} - \omega_{s'_3}\right) W^{(1,2)}_{s'_2 s'_3, s_2 s_3}\left(\epsilon - \omega_{s_1}\right)$$
$$\approx W^{(1,1)}_{s'_1, s_1}\left(\epsilon - \omega_{s'_2} - \omega_{s'_3}\right) G\left(\epsilon - \omega_{s_1} - \omega_{s'_2} - \omega_{s'_3}\right) W^{(1,1)}_{s'_2, s_2}\left(\epsilon - \omega_{s_1} - \omega_{s'_3}\right)$$
$$\times G^{(1)}\left(\epsilon - \omega_{s_1} - \omega_{s_2} - \omega_{s'_3}\right) W^{(1,1)}_{s'_3, s_3}\left(\epsilon - \omega_{s_1} - \omega_{s_2}\right).$$

By continuing this process, we arrive at the following approximate result

$$W^{(1,n)}_{s'_1\ldots s'_n,s_1\ldots s_n}(\epsilon) \approx W^{(1,1)}_{s'_1,s_1}\left(\epsilon-\sum_{l=2}^{n}\omega_{s'_l}\right)G^{(1)}\left(\epsilon-\omega_{s_1}-\sum_{l=2}^{n}\omega_{s'_l}\right)W^{(1,1)}_{s'_2,s_2}\left(\epsilon-\omega_{s_1}-\sum_{l=3}^{n}\omega_{s'_l}\right)$$
$$\times G^{(1)}\left(\epsilon-\omega_{s_1}-\omega_{s_2}-\sum_{l=3}^{n}\omega_{s'_l}\right)\times\ldots\times G^{(1)}\left(\epsilon-\sum_{l=1}^{n-1}\omega_{s_l}-\omega_{s'_n}\right)W^{(1,1)}_{s'_n,s_n}\left(\epsilon-\sum_{l=1}^{n-1}\omega_{s_l}\right).$$

So we see that the above approximation corresponds to resummation of all of the direct interaction diagrams, completely ignoring the exchange processes. We expect this approximation to get worse as one increases the number of photons in the system since this approximation ignores larger and larger fraction of diagrams with the increase in the number of particles involved in a scattering process. This approximation is beneficial since an integral equation for $W^{(1,1)}$ may be frequently solved analytically by means of the method developed in the supplementary material of [29] (see Appendix A). Due to the non-trivial momentum dependence of $W^{(1,1)}$, we expect this approximation to be better than a quasi-Markovian one. In what follows we refer to this approximation as to the weak correlation one. Note that as the quasi-Markovian approximation is exact in the single-particle sector, the weak correlation approximation is exact in the two-particle sector, thus in order to test its validity, one has to consider at least a three-photon scattering problem.

7.9.4 Two Waveguide QED

General Two-Photon Scattering Theory for $Q = 2$

In the two-qubit case, our starting point remains the same

$$\left\langle P',g\left|\mathcal{T}^{(2)}(\epsilon)\right|P,g\right\rangle=\sum_{n=0}^{\infty}\left\langle P',g\left|a^{\dagger}_{s'_1}v_{s'_1}\left(\mathcal{G}_0(\epsilon)\mathcal{V}\mathcal{G}_0(\epsilon)\mathcal{V}\right)^n\mathcal{G}_0(\epsilon)v^{\dagger}_{s_1}a_{s_1}\right|P,g\right\rangle$$

Again, let us consider the $\mathcal{V}\mathcal{G}_0\mathcal{V}$ term in the brackets

$$\mathcal{V}\mathcal{G}_0(\epsilon)\mathcal{V}=a^{\dagger}_{s'}v_{s'}\mathcal{G}_0(\epsilon)a^{\dagger}_{s}v_{s}+a^{\dagger}_{s'}v_{s'}\mathcal{G}_0(\epsilon)v^{\dagger}_{s}a_{s}+v^{\dagger}_{s'}a_{s'}\mathcal{G}_0(\epsilon)v^{\dagger}_{s}a_{s}+v^{\dagger}_{s'}a_{s'}\mathcal{G}_0(\epsilon)a^{\dagger}_{s}v_{s}$$

Now, clearly, both diagonal terms $v^{\dagger}_{s'}a_{s'}\mathcal{G}_0(\epsilon)a^{\dagger}_{s}v_{s}$ and $a^{\dagger}_{s'}v_{s'}\mathcal{G}_0(\epsilon)v^{\dagger}_{s}a_{s}$ contribute to the above geometric series. Non-diagonal ones still give zero, since they both annihilate the state $v^{\dagger}|g\rangle$. By introducing

$$\mathcal{R}^{(2)}(\epsilon)=a^{\dagger}_{s'_1}\mathcal{R}^{(2)}_{s'_1,s_1}(\epsilon)a_{s_1},\quad \mathcal{R}^{(2)}_{s'_1,s_1}(\epsilon)=\mathcal{R}^{(1)}_{s'_1,s_1}(\epsilon)+v_{s'_1}\mathcal{G}_0(\epsilon)v^{\dagger}_{s_1} \tag{3.43}$$

we rewrite the series as

$$\left\langle P',g\left|\mathcal{T}^{(2)}(\epsilon)\right|P,g\right\rangle=\sum_{n=0}^{\infty}\left\langle P',g\left|a^{\dagger}_{s'_1}v_{s'_1}\left(\mathcal{G}_0(\epsilon)\left[\Sigma^{(1)}(\epsilon)+\mathcal{R}^{(2)}(\epsilon)\right]\right)^n\mathcal{G}_0(\epsilon)v^{\dagger}_{s_1}a_{s_1}\right|P,g\right\rangle$$
$$=\left\langle P',g\left|a^{\dagger}_{s'_1}v_{s'_1}\frac{1}{\left(\mathcal{G}^{(1)}(\epsilon)\right)^{-1}-\mathcal{R}^{(2)}(\epsilon)}v^{\dagger}_{s_1}a_{s_1}\right|P,g\right\rangle$$
$$=\left\langle P',g\left|a^{\dagger}_{s'_1}v_{s'_1}\frac{1}{1-\mathcal{G}^{(1)}(\epsilon)\mathcal{R}^{(2)}(\epsilon)}\mathcal{G}^{(1)}(\epsilon)v^{\dagger}_{s_1}a_{s_1}\right|P,g\right\rangle.$$

Similarly, by introducing the following "vertex generating functional"

$$\mathcal{W}^{(2)}(\epsilon)=\mathcal{R}^{(2)}(\epsilon)+\mathcal{R}^{(2)}(\epsilon)\mathcal{G}^{(1)}(\epsilon)\mathcal{W}^{(2)}(\epsilon) \tag{3.44}$$

we render the transition operator's matrix elements in the following form

$$\left\langle P', g \left| \mathcal{T}^{(2)}(\epsilon) \right| P, g \right\rangle = \left\langle P', g \left| a^\dagger_{s'_1} v_{s'_1} \mathcal{G}^{(1)}(\epsilon) v^\dagger_{s_1} a_{s_1} \right| P, g \right\rangle + \left\langle P', g \left| a^\dagger_{s'_1} v_{s'_1} \mathcal{G}^{(1)}(\epsilon) \mathcal{W}^{(2)}(\epsilon) \mathcal{G}^{(1)}(\epsilon) v^\dagger_{s_1} a_{s_1} \right| P, g \right\rangle .$$

This, in turn, leads us to

$$\mathcal{T}^{(2)}(\epsilon) = \sum_{n=1}^{\infty} T^{(2,n)}_{s'_1 \ldots s'_n, s_1 \ldots s_n}(\epsilon) a^\dagger_{s'_1} \ldots a^\dagger_{s'_n} a_{s_n} \ldots a_{s_1} \tag{3.45}$$

where

$$T^{(2,1)}_{s'_1, s_1}(\epsilon) = \left\langle g \left| v_{s'_1} G^{(1)}(\epsilon) v^\dagger_{s_1} \right| g \right\rangle \tag{3.46}$$

$$T^{(2,n)}_{s'_1 \ldots s'_n, s_1 \ldots s_n}(\epsilon) = \left\langle g \left| v_{s'_1} G^{(1)} \left(\epsilon - \sum_{l=2}^{n} \omega_{s'_l} \right) W^{(2,n-1)}_{s'_2 \ldots s'_n, s_2 \ldots s_n}(\epsilon) G^{(1)} \left(\epsilon - \sum_{l=2}^{n} \omega_{s_l} \right) v^\dagger_{s_1} \right| g \right\rangle . \tag{3.47}$$

Here, the effective n-particle vertex functions $W^{(2,n)}_{s'_1 \ldots s'_n, s_1 \ldots s_n}(\epsilon)$ are defined in the similar manner as before

$$\mathcal{W}^{(2)}(\epsilon) = \sum_{n=1}^{\infty} a^\dagger_{s'_1} \ldots a^\dagger_{s'_n} \mathcal{W}^{(2,n)}_{s'_1 \ldots s'_n, s_1 \ldots s_n}(\epsilon) a_{s_n} \ldots a_{s_1}$$

Due to the algebraic equivalence in the definitions of $\mathcal{W}^{(2)}(\epsilon)$ and $\mathcal{W}^{(1)}(\epsilon)$, the components of $\mathcal{W}^{(2)}(\epsilon)$ satisfy the same hierarchy of equations as those of $\mathcal{W}^{(1)}(\epsilon)$ with $\mathcal{R}^{(2)}_{s'_1, s_1}(\epsilon)$ replacing $\mathcal{R}^{(1)}_{s'_1, s_1}(\epsilon)$. In order to understand the difference between the single qubit and the two-qubit theories, let us have a closer look at the equation defining $\mathcal{W}^{(2)}(\epsilon)$

$$\begin{aligned} \mathcal{W}^{(2)}(\epsilon) &= \mathcal{R}^{(2)}(\epsilon) + \mathcal{R}^{(2)}(\epsilon) \mathcal{G}^{(1)}(\epsilon) \mathcal{W}^{(2)}(\epsilon) \\ &= \mathcal{R}^{(1)}(\epsilon) + a^\dagger_{s'_1} v_{s'_1} \mathcal{G}_0(\epsilon) v^\dagger_{s_1} a_{s_1} + \mathcal{R}^{(1)}(\epsilon) \mathcal{G}^{(1)}(\epsilon) \mathcal{W}^{(2)}(\epsilon) + a^\dagger_{s'_1} v_{s'_1} \mathcal{G}_0(\epsilon) v^\dagger_{s_1} a_{s_1} \mathcal{G}^{(1)}(\epsilon) \mathcal{W}^{(2)}(\epsilon) \end{aligned} \tag{3.48}$$

Now let us perform the following separation

$$\mathcal{W}^{(2)}(\epsilon) = \mathcal{W}^{(2,i)}(\epsilon) + \mathcal{W}^{(2,r)}(\epsilon) \tag{3.49}$$

where the superscripts i and r stand for the irreducible and reducible contributions respectively, and $\mathcal{W}^{(2,i)}(\epsilon)$ is chosen to satisfy the following equation

$$\mathcal{W}^{(2,i)}(\epsilon) = \mathcal{R}^{(1)}(\epsilon) + \mathcal{R}^{(1)}(\epsilon) \mathcal{G}^{(1)}(\epsilon) \mathcal{W}^{(2,i)}(\epsilon) \tag{3.50}$$

leading us to the following equation satisfied by the reducible part

$$\begin{aligned} \mathcal{W}^{(2,r)}(\epsilon) = a^\dagger_{s'_1} v_{s'_1} \mathcal{G}_0(\epsilon) v^\dagger_{s_1} a_{s_1} + \mathcal{R}^{(1)}(\epsilon) \mathcal{G}^{(1)}(\epsilon) \mathcal{W}^{(2,r)}(\epsilon) \\ + a^\dagger_{s'_1} v_{s'_1} \mathcal{G}_0(\epsilon) v^\dagger_{s_1} a_{s_1} \mathcal{G}^{(1)}(\epsilon) \mathcal{W}^{(2,i)}(\epsilon) + a^\dagger_{s'_1} v_{s'_1} \mathcal{G}_0(\epsilon) v^\dagger_{s_1} a_{s_1} \mathcal{G}^{(1)}(\epsilon) \mathcal{W}^{(2,r)}(\epsilon) \end{aligned} \tag{3.51}$$

The solution of equation (3.51) may then conveniently parameterized as

$$W^{(2,r)}(\epsilon) = \overline{\mathcal{V}}(\epsilon) \mathcal{G}^{(2)}(\epsilon) \mathcal{V}(\epsilon) \tag{3.52}$$

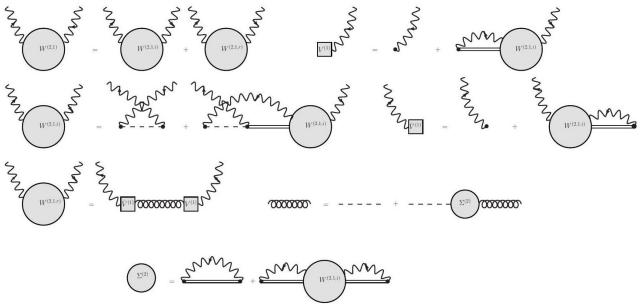

Figure 3.6: Equations corresponding to the general two-photon scattering problem.
where

$$\mathcal{G}^{(2)}(\epsilon) = \mathcal{G}_0(\epsilon) + \mathcal{G}_0(\epsilon)\Sigma^{(2)}(\epsilon)\mathcal{G}^{(2)}(\epsilon)$$

$$\Sigma^{(2)}(\epsilon) = a_s v_s^\dagger \mathcal{G}^{(1)}(\epsilon) v_{s'} a_{s'}^\dagger + a_s v_s^\dagger \mathcal{G}^{(1)}(\epsilon)\mathcal{W}^{(2,i)}\mathcal{G}^{(1)}(\epsilon) v_{s'} a_{s'}^\dagger \tag{3.53}$$

$$\mathcal{V}(\epsilon) = v_s^\dagger a_s + v_s^\dagger a_s \mathcal{G}(\epsilon)\mathcal{W}^{(2,i)}(\epsilon), \quad \overline{\mathcal{V}}(\epsilon) = a_s^\dagger v_s + \mathcal{W}^{(2,i)}(\epsilon)\mathcal{G}(\epsilon) v_s a_s^\dagger \tag{3.54}$$

The meaning of the above-defined objects is as follows. $\mathcal{G}^{(2)}(\epsilon)$ may be thought of as a Green's operator in the two-qubit excitation subspace since in practice, it is always projected there. $\Sigma^{(2)}(\epsilon)$ in its turn may be thought of as a self-energy operator in the two-qubit excitation subspace. $\mathcal{V}(\epsilon)$ and $\overline{\mathcal{V}}(\epsilon)$ may be understood as the renormalized absorption and emission vertex operators.

As in was anticipated above, the equations governing a two-photon scattering on a pair of qubits hold in the case of a two-photon scattering for a general Q system. Bearing this in mind, in Figure 3.6 we present the system of exact integral equations governing the general two-photon scattering problem in waveguide QED (i.e. equations defining $W^{(2,1)}$). These equations were first obtained in [29] in relation with the two-photon scattering problem on two distant qubits.

7.9.5 Three Waveguide QED

General Three-Photon Scattering Problem for $Q = 3$

Let us finally consider the problem of scattering on three qubits. Due to the high complexity of calculations, we restrict our attention to the lowest non-trivial result - a problem of three-photon scattering. As before, our starting point is

$$\left\langle P', g \left| \mathcal{T}^{(3)}(\epsilon) \right| P, g \right\rangle = \sum_{n=0}^{\infty} \left\langle P', g \left| a_{s_1'}^\dagger v_{s_1'} \left(\mathcal{G}_0(\epsilon)\mathcal{V}\mathcal{G}_0(\epsilon)\mathcal{V}\right)^n \mathcal{G}_0(\epsilon) v_{s_1}^\dagger a_{s_1} \right| P, g \right\rangle$$

Again the $\mathcal{V}\mathcal{G}_0\mathcal{V}$ term in the brackets is

$$\mathcal{V}\mathcal{G}_0(\epsilon)\mathcal{V} = \mathcal{R}^{(2)}(\epsilon) + \mathcal{O}_+(\epsilon) + \mathcal{O}_-(\epsilon) + \Sigma^{(1)}(\epsilon)$$

where the following notation was adopted

$$\mathcal{O}_+(\epsilon) = a_{s'}^\dagger v_{s'} \mathcal{G}_0(\epsilon) a_s^\dagger v_s, \quad \mathcal{O}_-(\epsilon) = v_{s'}^\dagger a_{s'} \mathcal{G}_0(\epsilon) v_s^\dagger a_s \tag{3.55}$$

By resumming the series to first incorporate the diagonal contribution we obtain

$$\left\langle P', g \left| \mathcal{T}^{(3)}(\epsilon) \right| P, g \right\rangle$$
$$= \sum_{n=0}^{\infty} \left\langle P', g \left| a_{s_1'}^\dagger v_{s_1'} \left(\frac{1}{\left(\mathcal{G}^{(1)}(\epsilon)\right)^{-1} - \mathcal{R}^{(2)}(\epsilon)} \left[\mathcal{O}_+(\epsilon) + \mathcal{O}_-(\epsilon)\right] \right)^n \frac{1}{\left(\mathcal{G}^{(1)}(\epsilon)\right)^{-1} - \mathcal{R}^{(2)}(\epsilon)} v_{s_1}^\dagger a_{s_1} \right| P, g \right\rangle.$$

Again, due to RWA, only even terms contribute to the above geometric series, so that

$$\left\langle P', g \left| \mathcal{T}^{(3)}(\epsilon) \right| P, g \right\rangle$$
$$= \sum_{n=0}^{\infty} \langle P', g| \, a^\dagger_{s'_1} v_{s'_1} \left(\frac{1}{\left(\mathcal{G}^{(1)}(\epsilon)\right)^{-1} - \mathcal{R}^{(2)}(\epsilon)} \left[\mathcal{O}_+(\epsilon) + \mathcal{O}_-(\epsilon)\right] \frac{1}{\left(\mathcal{G}^{(1)}(\epsilon)\right)^{-1} - \mathcal{R}^{(2)}(\epsilon)} \left[\mathcal{O}_+(\epsilon) + \mathcal{O}_-(\epsilon)\right] \right)^n$$
$$\times \frac{1}{\left(\mathcal{G}^{(1)}(\epsilon)\right)^{-1} - \mathcal{R}^{(2)}(\epsilon)} v^\dagger_{s_1} a_{s_1} |P, g\rangle.$$

Since $\frac{1}{\left(\mathcal{G}^{(1)}(\epsilon)\right)^{-1} - \mathcal{R}^{(2)}(\epsilon)}$ contains a projector onto the single-qubit excitation subspace $\sim v^\dagger v$, the only terms to retain in the brackets are

$$\frac{1}{\left(\mathcal{G}^{(1)}(\epsilon)\right)^{-1} - \mathcal{R}^{(2)}(\epsilon)} \mathcal{O}_+(\epsilon) \frac{1}{\left(\mathcal{G}^{(1)}(\epsilon)\right)^{-1} - \mathcal{R}^{(2)}(\epsilon)} \mathcal{O}_-(\epsilon)$$

The terms with two $\mathcal{O}_-(\epsilon)$ or two $\mathcal{O}_+(\epsilon)$ yield zero by three-qubit nilpotency condition and the terms with $\mathcal{O}_+(\epsilon)$ standing on the right annihilate the state $v^\dagger|g\rangle$ and give zero whenever multiplied by the "diagonal" term with $\mathcal{O}_+$standing on the left. So, we finally obtain

$$\left\langle P', g \left| \mathcal{T}^{(3)}(\epsilon) \right| P, g \right\rangle = \left\langle P', g \left| a^\dagger_{s'_1} v_{s'_1} \frac{1}{\left(\mathcal{G}^{(1)}(\epsilon)\right)^{-1} - \mathcal{R}^{(3)}(\epsilon)} v^\dagger_{s_1} a_{s_1} \right| P, g \right\rangle,$$

where we have defined

$$\mathcal{R}^{(3)}(\epsilon) = \mathcal{R}^{(2)}(\epsilon) + \mathcal{A}(\epsilon), \quad \mathcal{A}(\epsilon) = \mathcal{O}_+(\epsilon) \frac{1}{\left(\mathcal{G}^{(1)}(\epsilon)\right)^{-1} - \mathcal{R}^{(2)}(\epsilon)} \mathcal{O}_-(\epsilon)$$

Now we define the following operators

$$\mathcal{W}^{(2)}(\epsilon) = \mathcal{R}^{(2)}(\epsilon) + \mathcal{R}^{(2)}(\epsilon) \mathcal{G}^{(1)}(\epsilon) \mathcal{W}^{(2)}(\epsilon) \tag{3.56}$$
$$\mathcal{W}^{(3)}(\epsilon) = \mathcal{A}(\epsilon) + \mathcal{A}(\epsilon) \left(\mathcal{G}^{(1)}(\epsilon) + \mathcal{G}^{(1)}(\epsilon) \mathcal{W}^{(2)}(\epsilon) \mathcal{G}^{(1)}(\epsilon) \right) \mathcal{W}^{(3)}(\epsilon) \tag{3.57}$$

By successively applying the identity $(1-AB)^{-1}A = A(1-BA)^{-1}$, we arrive at the following results

$$\begin{aligned}
&\left\langle P', g \left| \mathcal{T}^{(3)}(\epsilon) \right| P, g \right\rangle = \left\langle P', g \left| a^\dagger_{s'_1} v_{s'_1} \mathcal{G}^{(1)}(\epsilon) v^\dagger_{s_1} a_{s_1} \right| P, g \right\rangle \\
&+ \left\langle P', g \left| a^\dagger_{s'_1} v_{s'_1} \mathcal{G}^{(1)}(\epsilon) \mathcal{W}^{(2)}(\epsilon) \mathcal{G}^{(1)}(\epsilon) v^\dagger_{s_1} a_{s_1} \right| P, g \right\rangle \\
&+ \left\langle P', g \left| a^\dagger_{s'_1} v_{s'_1} \mathcal{G}^{(1)}(\epsilon) \left(1 + \mathcal{W}^{(2)}(\epsilon) \mathcal{G}^{(1)}(\epsilon)\right) \mathcal{W}^{(3)}(\epsilon) \left(\mathcal{G}^{(1)}(\epsilon) \mathcal{W}^{(2)}(\epsilon) + 1\right) \mathcal{G}^{(1)}(\epsilon) v^\dagger_{s_1} a_{s_1} \right| P, g \right\rangle
\end{aligned} \tag{3.58}$$

$$\mathcal{A}(\epsilon) = \mathcal{O}_+(\epsilon) \mathcal{G}^{(1)}(\epsilon) \mathcal{O}_-(\epsilon) + \mathcal{O}_+(\epsilon) \mathcal{G}^{(1)}(\epsilon) \mathcal{W}^{(2)}(\epsilon) \mathcal{G}^{(1)}(\epsilon) \mathcal{O}_-(\epsilon) \tag{3.59}$$

As before we write

$$\mathcal{W}^{(2)}(\epsilon) = a^\dagger_{s'_1} \mathcal{W}^{(2,1)}_{s'_1, s_1}(\epsilon) a_{s_1} + a^\dagger_{s'_1} a^\dagger_{s'_2} \mathcal{W}^{(2,2)}_{s'_1 s'_2, s_1 s_2}(\epsilon) a_{s_2} a_{s_1} + \ldots$$

and

$$\mathcal{W}^{(3)}(\epsilon) = a^\dagger_{s'_1} a^\dagger_{s'_2} \mathcal{W}^{(3,2)}_{s'_1 s'_2, s_1 s_2}(\epsilon) a_{s_2} a_{s_1} + \ldots$$

Substituting these expansions into the equation defining $\mathcal{W}^{(3)}(\epsilon)$, we obtain the following integral equation

$$
\begin{aligned}
&W^{(3,2)}_{s_1's_2',s_1s_2}(\epsilon) = A^{(2)}_{s_1's_2',s_1s_2}(\epsilon) \\
&+ \left[A^{(2)}_{s_1's_2',w_2'w_1'}(\epsilon) + A^{(2)}_{s_1's_2',w_1'w_2'}(\epsilon)\right] G^{(1)}\left(\epsilon - \omega_{w_1'} - \omega_{w_2'}\right) W^{(3,2)}_{w_1'w_2',s_1s_2}(\epsilon) \\
&+ A^{(2)}_{s_1's_2',w_1'w_2}(\epsilon) G^{(1)}\left(\epsilon - \omega_{w_1'} - \omega_{w_2}\right) W^{(2,1)}_{w_2,w_2'}(\epsilon) G^{(1)}\left(\epsilon - \omega_{w_1'} - \omega_{w_2'}\right) W^{(3,2)}_{w_1'w_2',s_1s_2}(\epsilon) \\
&+ A^{(\epsilon)}_{s_1's_2',w_1w_1'}(\epsilon) G^{(1)}\left(\epsilon - \omega_{w_1} - \omega_{w_1'}\right) W^{(2,1)}_{w_1,w_2'}(\epsilon) G^{(1)}\left(\epsilon - \omega_{w_1'} - \omega_{w_2'}\right) W^{(3,2)}_{w_1'w_2',s_1s_2}(\epsilon) \\
&+ A^{(\epsilon)}_{s_1's_2',w_1w_2'}(\epsilon) G^{(1)}\left(\epsilon - \omega_{w_1} - \omega_{w_2'}\right) W^{(2,1)}_{w_1,w_1'}(\epsilon) G^{(1)}\left(\epsilon - \omega_{w_1'} - \omega_{w_2'}\right) W^{(3,2)}_{w_1'w_2',s_1s_2}(\epsilon) \\
&+ A^{(2)}_{s_1's_2',w_2'w_2}(\epsilon) G^{(1)}\left(\epsilon - \omega_{w_2'} - \omega_{w_2}\right) W^{(2,1)}_{w_2,w_1'}(\epsilon) G^{(1)}\left(\epsilon - \omega_{w_1'} - \omega_{w_2'}\right) W^{(3,2)}_{w_1'w_2',s_1s_2}(\epsilon) \\
&+ A^{(2)}_{s_1's_2',w_1w_2}(\epsilon) G^{(1)}\left(\epsilon - \omega_{w_1} - \omega_{w_2}\right) W^{(2,2)}_{w_2w_1,w_2'w_1'}(\epsilon) G^{(1)}\left(\epsilon - \omega_{w_1'} - \omega_{w_2'}\right) W^{(3,2)}_{w_1'w_2',s_1s_2}(\epsilon) \\
&+ A^{(2)}_{s_1's_2',w_1w_2}(\epsilon) G^{(1)}\left(\epsilon - \omega_{w_1} - \omega_{w_2}\right) W^{(2,2)}_{w_1w_2,w_2'w_1'}(\epsilon) G^{(1)}\left(\epsilon - \omega_{w_1'} - \omega_{w_2'}\right) W^{(3,2)}_{w_1'w_2',s_1s_2}(\epsilon) \\
&+ A^{(2)}_{s_1's_2',w_1w_2}(\epsilon) G^{(1)}\left(\epsilon - \omega_{w_1} - \omega_{w_2}\right) W^{(2,2)}_{w_1w_2,w_1'w_2'}(\epsilon) G^{(1)}\left(\epsilon - \omega_{w_1'} - \omega_{w_2'}\right) W^{(3,2)}_{w_1'w_2',s_1s_2}(\epsilon) \\
&+ A^{(2)}_{s_1's_2',w_1w_2}(\epsilon) G^{(1)}\left(\epsilon - \omega_{w_1} - \omega_{w_2}\right) W^{(2,2)}_{w_2'w_1,w_1'w_2'}(\epsilon) G^{(1)}\left(\epsilon - \omega_{w_1'} - \omega_{w_2'}\right) W^{(3,2)}_{w_1'w_2',s_1s_2}(\epsilon)
\end{aligned}
$$

where the projection of $\mathcal{A}$ on the two-photon subspace is defined as

$$
A^{(2)}_{s_1's_2',s_1s_2}(\epsilon) = v_{s_1'} G_0\left(\epsilon - \omega_{s_2'}\right) v_{s_2'} G^{(1)}(\epsilon) v^\dagger_{s_2} G_0\left(\epsilon - \omega_{s_2}\right) v^\dagger_{s_1} \tag{3.60}
$$

Bearing this in mind, we represent

$$
W^{(3,2)}_{s_1's_2',s_1s_2}(\epsilon) = v_{s_1'} G_0\left(\epsilon - \omega_{s_2'}\right) v_{s_2'} G^{(3)}(\epsilon) v^\dagger_{s_2} G_0\left(\epsilon - \omega_{s_2}\right) v^\dagger_{s_1} \tag{3.61}
$$

which, in turn, yields

$$
G^{(3)}(\epsilon) = G^{(1)}(\epsilon) + G^{(1)}(\epsilon)\Sigma^{(3)}(\epsilon)G^{(3)}(\epsilon), \tag{3.62}
$$

where the self-energy in the three-excitation subspace is given by

$$
\begin{aligned}
\Sigma^{(3)}(\epsilon) = &\left[v^\dagger_{w_1'} G_0\left(\epsilon - \omega_{w_1'}\right) v^\dagger_{w_2'} + v^\dagger_{w_2'} G_0\left(\epsilon - \omega_{w_2'}\right) v^\dagger_{w_1'}\right] G^{(1)}\left(\epsilon - \omega_{w_1'} - \omega_{w_2'}\right) v_{w_1'} G_0\left(\epsilon - \omega_{w_2'}\right) v_{w_2'} \\
&+ v^\dagger_{w_2} G_0\left(\epsilon - \omega_{w_2}\right) v^\dagger_{w_1'} G^{(1)}\left(\epsilon - \omega_{w_1'} - \omega_{w_2}\right) W^{(2,1)}_{w_2,w_2'}(\epsilon) G^{(1)}\left(\epsilon - \omega_{w_1'} - \omega_{w_2'}\right) v_{w_1'} G_0\left(\epsilon - \omega_{w_2'}\right) v_{w_2'} \\
&+ v^\dagger_{w_1'} G_0\left(\epsilon - \omega_{w_1'}\right) v^\dagger_{w_1} G^{(1)}\left(\epsilon - \omega_{w_1} - \omega_{w_1'}\right) W^{(2,1)}_{w_1,w_2'}(\epsilon) G^{(1)}\left(\epsilon - \omega_{w_1'} - \omega_{w_2'}\right) v_{w_1'} G_0\left(\epsilon - \omega_{w_2'}\right) v_{w_2'} \\
&+ v^\dagger_{w_2'} G_0\left(\epsilon - \omega_{w_2'}\right) v^\dagger_{w_1} G^{(1)}\left(\epsilon - \omega_{w_1} - \omega_{w_2'}\right) W^{(2,1)}_{w_1,w_1'}(\epsilon) G^{(1)}\left(\epsilon - \omega_{w_1'} - \omega_{w_2'}\right) v_{w_1'} G_0\left(\epsilon - \omega_{w_2'}\right) v_{w_2'} \\
&+ v^\dagger_{w_2} G_0\left(\epsilon - \omega_{w_2}\right) v^\dagger_{w_2'} G^{(1)}\left(\epsilon - \omega_{w_2'} - \omega_{w_2}\right) W^{(2,1)}_{w_2,w_1'}(\epsilon) G^{(1)}\left(\epsilon - \omega_{w_1'} - \omega_{w_2'}\right) v_{w_1'} G_0\left(\epsilon - \omega_{w_2'}\right) v_{w_2'} \\
&+ v^\dagger_{w_2} G_0\left(\epsilon - \omega_{w_2}\right) v^\dagger_{w_1} G^{(1)}\left(\epsilon - \omega_{w_1} - \omega_{w_2}\right) W^{(2,2)}_{w_2w_1,w_2'w_1'}(\epsilon) G^{(1)}\left(\epsilon - \omega_{w_1'} - \omega_{w_2'}\right) v_{w_1'} G_0\left(\epsilon - \omega_{w_2'}\right) v_{w_2'} \\
&+ v^\dagger_{w_2} G_0\left(\epsilon - \omega_{w_2}\right) v^\dagger_{w_1} G^{(1)}\left(\epsilon - \omega_{w_1} - \omega_{w_2}\right) W^{(2,2)}_{w_1w_2,w_2'w_1'}(\epsilon) G^{(1)}\left(\epsilon - \omega_{w_1'} - \omega_{w_2'}\right) v_{w_1'} G_0\left(\epsilon - \omega_{w_2'}\right) v_{w_2'} \\
&+ v^\dagger_{w_2} G_0\left(\epsilon - \omega_{w_2}\right) v^\dagger_{w_1} G^{(1)}\left(\epsilon - \omega_{w_1} - \omega_{w_2}\right) W^{(2,2)}_{w_1w_2,w_1'w_2'}(\epsilon)\left(\epsilon - \omega_{w_1'} - \omega_{w_2'}\right) v_{w_1'} G_0\left(\epsilon - \omega_{w_2'}\right) v_{w_2'} \\
&+ v^\dagger_{w_2} G_0\left(\epsilon - \omega_{w_2}\right) v^\dagger_{w_1} G^{(1)}\left(\epsilon - \omega_{w_1} - \omega_{w_2}\right) W^{(2,2)}_{w_2w_1'} G^{(1)}\left(\epsilon - \omega_{w_1'} - \omega_{w_2'}\right)
\end{aligned} \tag{3.63}
$$

Equations (3.61), (3.62) and (3.63) may be elegantly represented diagrammmatically as shown in Figure 3.7. Now, succeeding to identify the expressions defining $W^{(3,2)}$, the remaining bit is

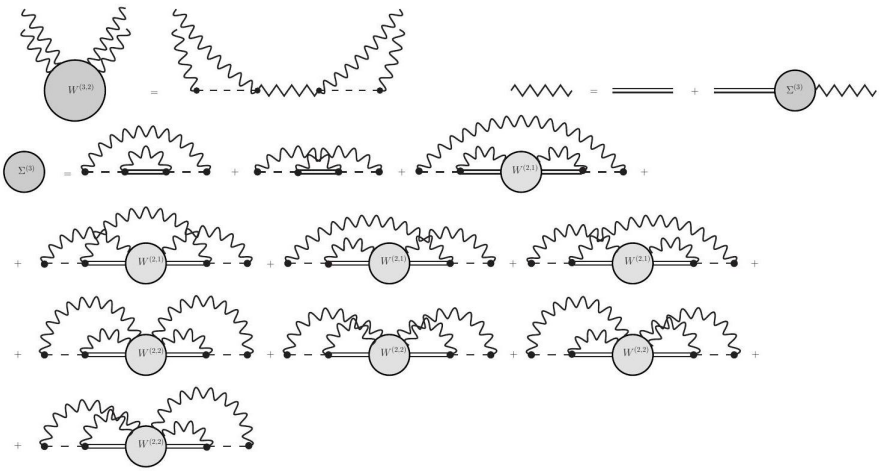

Figure 3.7: Diagrammatic representation of $W^{(3,2)}$.

to establish the expression for the generic three-particle transition operator. After a tedious but rather straightforward calculation, one obtains the following result

$$T^{(3)}_{s_1's_2's_3',s_1s_2s_3}(\epsilon) = \\ = \left\langle g \left| a^\dagger_{s_1'} v_{s_1'} G^{(1)}\left(\epsilon - \omega_{s_1'} - \omega_{s_2'}\right) \widehat{W}^{(2)}_{s_2's_3',s_2s_3}(\epsilon) G^{(1)}\left(\epsilon - \omega_{s_1} - \omega_{s_2}\right) v^\dagger_{s_1} a_{s_1} \right| g \right\rangle \tag{3.64}$$

where $\widehat{W}^{(2)}$ is defined as

$$\begin{aligned}
\widehat{W}^{(2)}_{s_1's_2',s_1s_2}(\epsilon) &= W^{(2,2)}_{s_1's_2',s_1s_2}(\epsilon) + W^{(3,2)}_{s_1's_2',s_1s_2}(\epsilon) + W^{(2,1)}_{s_1',s}(\epsilon) G^{(1)}\left(\epsilon - \omega_s\right) W^{(3,2)}_{ss_2',s_1s_2}(\epsilon) \\
&+ W^{(2,1)}_{s_2',s}(\epsilon) G^{(1)}\left(\epsilon - \omega_s\right) W^{(3,2)}_{s_1's,s_1s_2}(\epsilon) + W^{(3,2)}_{s_1's_2',ss_2}(\epsilon) G^{(1)}\left(\epsilon - \omega_s\right) W^{(2,1)}_{s,s_1}(\epsilon) \\
&+ W^{(2,1)}_{s_1',s}(\epsilon) G^{(1)}\left(\epsilon - \omega_s\right) W^{(3,2)}_{ss_2',s's_2}(\epsilon) G^{(1)}\left(\epsilon - \omega_{s'}\right) W^{(2,1)}_{s',s_1}(\epsilon) \\
&+ W^{(2,1)}_{s_2',s}(\epsilon) G^{(1)}\left(\epsilon - \omega_s\right) W^{(3,2)}_{s_1's,s's_2}(\epsilon) G^{(1)}\left(\epsilon - \omega_{s'}\right) W^{(2,1)}_{s',s_1}(\epsilon) \\
&+ W^{(3,2)}_{s_1's_2',s_1s}(\epsilon) G^{(1)}\left(\epsilon - \omega_s\right) W^{(2,1)}_{s,s_2}(\epsilon) + W^{(2,1)}_{s_1',s} G^{(1)} W^{(3,2)}_{ss_2',s_1s'} G^{(1)}\left(\epsilon - \omega_{s'}\right) W^{(2,1)}_{s',s_2}(\epsilon) \\
&+ W^{(2,1)}_{s_2',s}(\epsilon) G^{(1)}\left(\epsilon - \omega_s\right) W^{(3,2)}_{s_1's,s_1s'}(\epsilon) G^{(1)}\left(\epsilon - \omega_{s'}\right) W^{(2,1)}_{s',s_2}(\epsilon) \\
&+ W^{(2,2)}_{s_1's_2',ss'}(\epsilon) G^{(1)}\left(\epsilon - \omega_s - \omega_{s'}\right) W^{(3,2)}_{ss',s_1s_2}(\epsilon) + W^{(2,2)}_{s_1's_2',s's}(\epsilon) G^{(1)}\left(\epsilon - \omega_s - \omega_{s'}\right) W^{(3,2)}_{ss',s_1s_2}(\epsilon) \\
&+ W^{(3,2)}_{s_1's_2',ss'}(\epsilon) G^{(1)}\left(\epsilon - \omega_s - \omega_{s'}\right) W^{(2,2)}_{ss',s_1s_2}(\epsilon) + W^{(3,2)}_{s_1's_2',ss'}(\epsilon) G^{(1)}\left(\epsilon - \omega_s - \omega_{s'}\right) W^{(2,2)}_{s's,s_1s_2}(\epsilon) \\
&+ W^{(2,2)}_{s_1's_2',ss'}(\epsilon) G^{(1)}\left(\epsilon - \omega_s - \omega_{s'}\right) W^{(3,2)}_{ss',ww'}(\epsilon) G^{(1)}\left(\epsilon - \omega_w - \omega_{w'}\right) W^{(2,2)}_{ww',s_1s_2}(\epsilon) \\
&+ W^{(2,2)}_{s_1's_2',s's}(\epsilon) G^{(1)}\left(\epsilon - \omega_s - \omega_{s'}\right) W^{(3,2)}_{ss',ww'}(\epsilon) G^{(1)}\left(\epsilon - \omega_w - \omega_{w'}\right) W^{(2,2)}_{ww',s_1s_2}(\epsilon) \\
&+ W^{(2,2)}_{s_1's_2',ss'}(\epsilon) G^{(1)}\left(\epsilon - \omega_s - \omega_{s'}\right) W^{(3,2)}_{ss',ww'}(\epsilon) G^{(1)}\left(\epsilon - \omega_w - \omega_{w'}\right) W^{(2,2)}_{w'w,s_1s_2}(\epsilon) \\
&+ W^{(2,2)}_{s_1's_2',s's}(\epsilon) G^{(1)}\left(\epsilon - \omega_s - \omega_{s'}\right) W^{(3,2)}_{ss',ww'}(\epsilon) G^{(1)}\left(\epsilon - \omega_w - \omega_{w'}\right) W^{(2,2)}_{w'w,s_1s_2}(\epsilon).
\end{aligned}$$

This completes the specification of the general three-photon scattering matrix.

7.10 Giant Acustic Atom Model

Let's consider the non-Markovian scattering setup: A giant acoustic atom, extensively studied theoretically and experimentally in [19, 59, 60, 78 – 81] (see also [82] for a detailed review).

7.10.1 4.1 Study of Delayed Coherent Quantum Feedback in the Framework of Quantum Acoustics

The rapidity of the technological advancement in the area of superconducting quantum circuitry makes the development of large-scale quantum networks merely a question of time. As one may easily suspect, in a distributed quantum network significant distances between the nodes, and hence the propagation time delays are unavoidable [17,29]. This very feature had motivated a tremendous interest in the study of the systems with deterministic time delays, both on the theoretical and experimental sides [18]. Despite the fast pace of technological development in quantum electronics, practical study of the on-chip delayed coherent quantum feedback in superconducting quantum circuits is a rather challenging task. Such a complication has to do with purely dimensional reasons. The characteristic frequency ν of the excitations in the superconducting transmission line is of the order of couple GHz (as well as a typical transition rate of a transmon charge qubit), owing to the fact that those excitations propagate with nearly the speed of light c, the resulting wavelength $\lambda = \frac{c}{\nu}$ is commensurate with a centimeter, which is precisely a typical chip size.

Fortunately, there exists another possibility to investigate the on-chip propagation time delays, namely by transforming the quantum information into the surface acoustic waves (SAW) through the piezo-electric effect. The fact that the phase velocity of SAW is five orders of magnitude less than that of light, allows one to achieve the on-chip propagation time delays of couples of microseconds [20]. Another non-Markovian feature of the quantum acoustic systems arises from the qubit-SAW coupling mechanism utilized in modern experiments. Typically, the transfer of quantum information into the phonons is achieved by means of the interdigital transducer (IDT), which, in its turn, possesses a non-trivial periodic internal structure, thus rendering the coupling non-local and frequency-dependent [9,36]. Recently, an even more extreme system was proposed in [19, 27, 28] - a giant acoustic atom. In such a system, an IDT is split into two halves which are then used to connect the qubit to the piezoelectric substrate at two distant points. Such a non-local coupling allows one to extend the linear dimension of the emitter up to hundreds, and even thousands of SAW wavelengths [19]. Such a system is a prominent example of an open quantum system with closed time loops - a system where the radiation propagation time through the system exceeds its relaxation time. This proposition had eventually led to an experimental realization of a giant acoustic atom in 2018 at the Chalmers University of Technology [2]. Since the quantum acoustic systems intrinsically do not allow for a Markovian description (thus allowing us to showcase the theory developed in Chapter 3 in the full glory), we choose them to be the main focus of our considerations in this section.

The outline of this section is as follows. First of all, we are going to set up simple theoretical models of both ordinary and giant acoustic atoms. Next, a coherent state scattering problem is formulated in the power-perturbative regime. Further, an exact scattered state is going to be determined using the theory developed in Chapter 3. Knowledge of the scattered state then

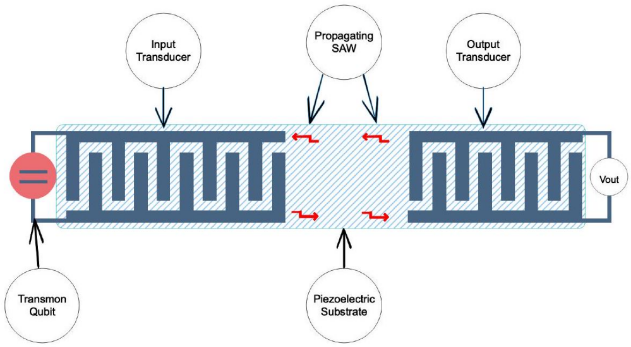

Figure 4.1: A schematic sketch of the typical quantum acoustics setup: a single qubit coupled to the piezoelectric substrate by means of an IDT.

allows us to compute the coherence functions of the output field, which, in turn, contain all of the information about the phonon statistics and, at the same time, reveal the non-Markovian behavior of the system under consideration. Exact results are then compared to the approximation routines developed above.

7.10.2 4.2 Model of a Non-locally Coupled Acoustic Atom

The system described above, consisting of a superconducting charge qubit coupled to the phononic waveguide by an IDT may be described as follows. An IDT may be practically thought of as a couple of forks each having n fork tines (see Figure 4.1), in the experimentalist's jargon tines are usually referred to as the fingers. In practice, an IDT is thus characterized by a pair of numbers $N = 2n$ and l where n is the number of fingers in each fork and l is half the distance between the neighboring fingers, $2l$ is dubbed as the periodicity of an IDT.

As it was mentioned above, in the giant atom problem, an IDT is split into two parts which are then put onto a piezoelectric substrate at two distant points (see Figure 4.2), separated by some distance R. Assuming that $R \gg l$, one can ignore the internal substructure of the IDT parts and model a giant atom as a system connected to a waveguide at two distant points. Moreover, the delay coming from the information transfer between the atom and these two connection points may be ignored since this information is transferred via superconducting leads and the velocity of its propagation is much larger than that of SAW.

Both of these situations may be viewed as limiting cases of the following model. Consider a two-level system coupled to an infinite one-dimensional bi-directional transmission line at a discrete set of points $\{x_n\}_{n\in\{1,\dots,N\}}$. Without loss of generality we assume that $x_n > x_m, \forall n > m$. Additionally, let us also denote the decay rate of the qubit into the transmission line at point x_n by Γ_n. The Hamiltonian in the rotating wave approximation is thus given by $\mathcal{H} = \mathcal{H}_0 + \mathcal{V}$, where

$$\mathcal{H}_0 = -\Delta\frac{1+\sigma_3}{2} + \sum_{\mu=1,2}\int_{\mathbb{R}} dk\omega_\mu(k)a^\dagger_\mu(k)a_\mu(k) \tag{4.1}$$

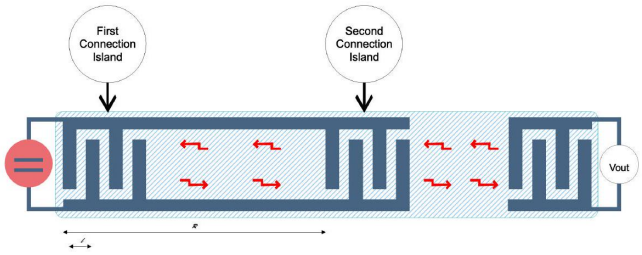

Figure 4.2: A schematic sketch of the giant atom experiment. Here an IDT used to couple an atom to SAW is split into two halves which are put onto a piezoelectric substrate at two distant points separated by a distance R assumed to significantly exceed the periodicity of an original IDT ($2l \ll R$), allowing to approximate the couplings to be point-like.

$$\mathcal{V} = \sum_{\mu=1,2}\int_{\mathbb{R}} dk\left[g_\mu(k)a^\dagger_\mu(k)\sigma_- + g^*_\mu(k)\sigma_+a_\mu(k)\right] \tag{4.2}$$

Here, μ labels the left ($\mu = 1$) and right ($\mu = 2$) propagation channels, $\omega_1(k) = \omega_2(k) = k$, $\Delta = k_0 - \Omega$ with k_0 being the linearization point of the SAW spectrum and Ω being the transition frequency between the ground and the first excited states of the qubit. As one may also note we have also taken the broad-band limit $B_1 = B_2 = \mathbb{R}$. It should be additionally emphasized that the ground state of the two-level system was chosen to be the reference energy $\epsilon_{gs} = 0$ in our problem. The aforementioned coupling mechanism may be encoded in the following form of the coupling constants

$$g_\mu(k) = \sum_{n=1}^{N}\sqrt{\frac{\Gamma_n}{2\pi}}e^{-ic_\mu(k+k_0)x_n} \tag{4.3}$$

where $c_\mu = (-1)^{\mu-1}$ distinguishes the coupling to the left and right movers. In the special case $\Gamma_n = \frac{\gamma}{N}, \forall n, x_n = \ln$ considered in [27], to which we refer to as maximally symmetric, one has

$$g_\mu^{ms}(k) = \sqrt{\frac{\gamma}{2\pi N}} \sum_{n=1}^{N} e^{-ic_\mu(k+k_0)ln} = \sqrt{\frac{\gamma}{2\pi N}} \frac{e^{-ic_\mu(k+k_0)lN} - 1}{1 - e^{ic_\mu(k+k_0)l}}. \tag{4.4}$$

In the case of the gigantic atom, on the other hand, one effectively has $N = 2$ with $x_1 = -x_2 = -R/2$, leading us to

$$g_\mu^{ga}(k) = \sqrt{\frac{\Gamma_1}{2\pi}} e^{-ic_\mu(k+k_0)R/2} + \sqrt{\frac{\Gamma_2}{2\pi}} e^{ic_\mu(k+k_0)R/2}. \tag{4.5}$$

In the symmetric situation $\Gamma_1 = \Gamma_2 = \frac{\gamma}{2}$, one simply has $g_\mu^{\text{gas}}(k) = \sqrt{\frac{\gamma}{\pi}} \cos\left((k + k_0) R/2\right)$.

7.10.3 4.3 Formulation of the Scattering Problem

4.3.1 Initializing the State

To formulate the scattering problem, let us first define the following wavepacket operators

$$A_\mu^\dagger = \int\limits_{\mathbb{R}} dk \varphi_L(k) a_\mu^\dagger(k) \tag{4.6}$$

Here $\varphi_L(k)$ may be chosen to be any normalized function with a nascent delta function quality to it $\varphi_L(k) \sim \delta(k), \quad L \to \infty$, one usually says a delta function broadened by $1/L$. Examples of such functions include Lorentzian (a.k.a Cauchy, a.k.a Breit-Wigner distributions), Gaussian, bump function, etc. Here, however, for no other reasons than personal preference we choose $\varphi_L(k)$ to be the Fourier image of a rectangular pulse of length L

$$\varphi_L(k) = \sqrt{\frac{2}{\pi L}} \frac{\sin(kL/2)}{k}, \quad \varphi_L(k) \sim \sqrt{\frac{2\pi}{L}} \delta(k), L \to \infty. \tag{4.7}$$

To condense the notation a little bit, we further denote $\varphi_L(k) = \varphi(k)$ omitting the L subscript and implicitly understanding the dependence of φ on L. Definition of these wave-packet operators is crucial since the eigenstates of the bare Hamiltonian $\mathcal{H}_0$ are non-normalizable. Hence, in order to avoid the ascent of the undefinable quantities such as $\delta(0), (\delta(0))^2, \ldots$ coming from the elastic clusters of the S-matrix in the calculation of the observables, one has to work with the normalizable states and take the plane-wave limit $L \to \infty$ at the very end. These complications lie in the very roots of the scattering theory and have to do with the non-commutativity of the long-time $\eta \searrow 0$ and plane wave $L \to \infty$ limits in multiparticle scattering problems.

Having defined the Fock creation operators $A_\mu^\dagger$, we can define the coherent state as a displaced vacuum

$$|\alpha\rangle_\mu = e^{-|\alpha|^2/2} e^{\alpha A_\mu^\dagger} |\Omega\rangle = e^{-|\alpha|^2/2} \sum_{n=0}^{\infty} \frac{\alpha^n}{\sqrt{n!}} \left|\Phi_\mu^{(n)}\right\rangle \tag{4.8}$$

where $\alpha \in \mathbb{C}$ is the so-called coherence parameter, defined such that $|\alpha|^2$ is the average photon number (power), and the normalized n-particle Fock states $\left|\Phi_\mu^{(n)}\right\rangle$ were defined according to

$$\left|\Phi_\mu^{(n)}\right\rangle = \frac{1}{\sqrt{n!}} \left(A_\mu^\dagger\right)^n |\Omega\rangle, \quad \left\langle \Phi_{\mu'}^{(n')} | \Phi_\mu^{(n)} \right\rangle = \delta_{\mu,\mu'} \delta_{n,n'} \tag{4.9}$$

In what follows, we assume that $|\alpha| \ll 1$ so that the terms of order $|\alpha|^4$ are negligible

$$|\alpha\rangle_\mu \approx |\alpha\rangle_\mu^{(3)} \equiv e^{-|\alpha|^2/2} \left(|\Omega\rangle + \frac{\alpha}{\sqrt{1!}} \left|\Phi_\mu^{(1)}\right\rangle + \frac{\alpha^2}{\sqrt{2!}} \left|\Phi_\mu^{(2)}\right\rangle + \frac{\alpha^3}{\sqrt{3!}} \left|\Phi_\mu^{(3)}\right\rangle + \mathcal{O}\left(|\alpha|^4\right) \right) \tag{4.10}$$

Note that the factor $e^{-|\alpha|^2/2}$ has to be retained until various overlaps of states are calculated, this is going to ensure the normalization of both the initial and final states as well as the power conservation (here the normalization is again assumed in the power perturbative regime, that is up to order $\mathcal{O}(|\alpha|^8)$). With this in hands, we formulate the scattering problem as follows. Let us assume that the initial state of the system is given by $|\psi_i\rangle = |\alpha\rangle_1^{(3)} \otimes |0\rangle$, that is a leftwardspropagating weakly coherent pulse $|\alpha\rangle_1^{(3)}$ is incident on a two-level system which is initially in its ground state $|0\rangle$. According to the scattering theory, the final state of the systems is thus

$$|\psi_f\rangle = e^{-|\alpha|^2/2}\left(|\Omega\rangle + \frac{\alpha}{\sqrt{1!}}\mathcal{S}_1\left|\Phi_1^{(1)}\right\rangle + \frac{\alpha^2}{\sqrt{2!}}\mathcal{S}_2\left|\Phi_1^{(2)}\right\rangle + \frac{\alpha^3}{\sqrt{3!}}\mathcal{S}_3\left|\Phi_1^{(3)}\right\rangle\right)\otimes|0\rangle \tag{4.11}$$

4.3.2 Identifying the Observables

Inelastic contributions to the n-phonon S-matrices introduce a non-trivial momentum redistribution of the incident phonons, which, in turn, results in the non-trivial phonon statistics and correlations in the final state. A way of probing the properties of these correlations was introduced by Roy Glauber in his groundbreaking work [13]. In this paper, Glauber introduced an infinite hierarchy of the so-called coherence functions. Adopting the definition of Glauber to our problem, we define the first-order coherence correlation function as

$$C_\mu^{(1)}(\tau_2,\tau_1) = \left\langle \psi_f \left| a_\mu^\dagger(\tau_2)\, a_\mu(\tau_1)\right| \psi_f\right\rangle, \tag{4.12}$$

where we have defined the following position space field operators

$$a_\mu(x) = \int\limits_{\mathbb{R}} dk \frac{e^{ikx}}{\sqrt{2\pi}} a_\mu(k), \quad a_\mu^\dagger(x) = \int\limits_{\mathbb{R}} dk \frac{e^{-ikx}}{\sqrt{2\pi}} a_\mu^\dagger(k), \quad \left[a_\mu(x), a_{\mu'}^\dagger(x')\right] = \delta_{\mu,\mu'}\delta(x-x'). \tag{4.13}$$

In the case of the linear dispersion relation, the first-order correlation function $C_\mu^{(1)}(\tau_2,\tau_1) = C_\mu^{(1)}(\tau_2-\tau_1)$ depends only on the difference of its arguments. In such a case one can define the so-called spectral power density as a Fourier transform of the first-order coherence function

$$S_\mu(k) = \int\limits_{\mathbb{R}} \frac{d\tau}{2\pi} C_\mu^{(1)}(\tau) e^{-ik\tau} \tag{4.14}$$

$S_\mu(k)$ should be understood as a momentum space distribution of power in the scattered state of radiation, that is to a given mode k (supported by the μ^{th} channel) it associates a certain power $S_\mu(k)$. Presence of the effective phonon-phonon interactions in our theory, in principle, allows for the scattering into the modes other than the initial momentum. Study of this phenomenon is usually facilitated by the decomposition of the power density into the elastic (coherent) and inelastic (incoherent) power densities $S_\mu(k) = S_\mu^{el}(k) + S_\mu^{\text{inel}}(k)$. As one may infer from its name, the elastic power density corresponds to the elastic part of the scattering spectra and is thus proportional to the delta function centered at the momentum of incident particles (in our case $S_\mu^{el}(k) \propto \delta(k)$). The inelastic contribution, however, in principle, contains some non-trivial momentum dependence and the complexity of its line-shape is a typical feature of the non-Markovian models. Using the form of the final state (4.11), we write the first-order correlation function as

$$C_\mu^{(1)}(\tau) = \left(1-|\alpha|^2+\frac{|\alpha|^4}{2}\right)|\alpha|^2 C_\mu^{(1,1)}(\tau) + \left(1-|\alpha|^2\right)\frac{|\alpha|^4}{2}C_\mu^{(1,2)}(\tau) + \frac{|\alpha|^6}{6}C_\mu^{(1,3)}(\tau) + \mathcal{O}\left(|\alpha|^8\right), \tag{4.15}$$

where we have introduced the n-particle Fock state first-order correlation functions as

$$C_\mu^{(1,n)}(\tau_2-\tau_1) = \left\langle \Phi_1^{(n)} \left| (\mathcal{S}_n)^\dagger\, a_\mu^\dagger(\tau_2)\, a_\mu(\tau_1)\, \mathcal{S}_n\right| \Phi_1^{(n)}\right\rangle. \tag{4.16}$$

An important validity test of our theory is the power conservation, which has to be fulfilled by the unitarity of the S-matrix. Power conservation demands that the total power is equal to the initial one, that is

$$\sum_{\mu=1,2}\int_{\mathbb{R}} dk S_\mu(k) = \sum_{\mu=1,2} C_\mu^{(1)}(0) \equiv \left\langle \psi_i \left| a_\mu^\dagger(0) a_\mu(0) \right| \psi_i \right\rangle \to \frac{|\alpha|^2}{L} \tag{4.17}$$

which may be easily verified numerically. Nonetheless we are here interested in computing all observables to the lowest order in $|\alpha|$ (for example, the lowest inelastic contribution to the spectral density comes to form the two-phonon sector), in what follows we are going to establish the formulas for the spectral densities in all particle sectors, since they are needed for the power conservation control.

Again, following Glauber [13] we can define higher-order coherence functions as ($n \geq 2$)

$$C^{(n)}_{\mu_1,\ldots,\mu_n}(\tau_n,\ldots,\tau_1) = \left\langle \psi_f \left| a^\dagger_{\mu_1}(\tau_1)\ldots a^\dagger_{\mu_n}(\tau_n)\, a_{\mu_n}(\tau_n)\ldots a_{\mu_1}(\tau_1) \right| \psi_f \right\rangle \tag{4.18}$$

These functions represent normally ordered correlations between intensities $\mathcal{I}_\mu(\tau) = a_\mu^\dagger(\tau)a_\mu(\tau)$ at n different points $\{\tau_1,\ldots,\tau_n\}$ in n different radiation channels $\{\mu_1,\ldots,\mu_n\}$. For practical purposes, it is also valuable to define the so-called normalized higher-order coherence functions as

$$c^{(n)}_{\mu_1,\ldots,\mu_n}(\tau_1,\ldots,\tau_n) = \frac{C^{(n)}_{\mu_1,\ldots,\mu_n}(\tau_n,\ldots,\tau_1)}{\prod_{s=1}^n C^{(1)}_{\mu_s}(\tau_s,\tau_s)} \tag{4.19}$$

Again, in systems with linear dispersion relation, these functions depend only on $n-1$ variables $\{\tau_n-\tau_{n-1},\tau_n-\tau_{n-2},\ldots,\tau_n-\tau_1\}$. As one may note, in our particular problem $c^{(n)}_{\mu_1,\ldots,\mu_n}(\tau_n,\ldots,\tau_1) =$

0, $\forall n > 3$, so in what follows we are going to focus our attention on $c^{(2)}_{\mu_1,\mu_2}(\tau_2-\tau_1)$ and $c^{(3)}_{\mu_1,\mu_2,\mu_3}(\tau_3-\tau_2,\tau_3-\tau_1)$.

For pairs of phonons, the normalized second-order coherence function is defined as the arrival probability of the second particle as a function of the delay $(\tau_2-\tau_1)$ following the detection of the first one, normalized by the individual photon probabilities. Likewise, for particle triples, the normalized third-order coherence function is defined as the arrival probability of the third and second particle as a function of delays $\tau_3-\tau_1, \tau_2-\tau_1$ following the detection of the first one, normalized by the individual phonon probabilities. A perfectly coherent source is characterized by a uniform arrival probability, yielding the correlation functions of all orders equal to unity. Whenever correlation functions exceed unity, particle statistics is said to be super-Poissonian and the particles are said to be bunched together, whereas in the case of correlation functions falling below unity, the statistics of particles is said to be sub-Poissonian and particles are correspondingly said to be anti-bunched.

Historically, the development of the quantum theory of optical coherence was motivated by the well known Hanbury Brown and Twiss experiment. In their experiment [7], Hanbury Brown and Twiss used an interferometer consisting of two photomultiplier tubes to which light originating from a distant galaxy was redirected from a searchlight. The experiment revealed intensity correlations of photocurrents from two spatially separated detectors and enhancement was observed when the difference of the optical wavelengths of the two signals disappeared (what is now known as photonic bunching phenomenon). This result was considered controversial by a number of physicists of the time, it was speculated that atoms excited at random, independently of one another, would subsequently emit light incoherently, additively contributing to the intensity observed at any given point in space, in this connection it was believed that no interference pattern could be formed by such a thermal light source. This apparent controversy was then resolved by Ugo Fano. In his gedankenexperiment [10], Fano considered a process of photoionization of a pair of distant atoms by a pair of photons emitted by the second pair of distant independently excited emitters. As Fano pointed out, the photoionization probability amplitude of both atoms cannot be expressed as a product of individual photoionization probability amplitudes, neither it is expressible as a function of individual probability amplitudes of any kind, instead, such a probability amplitude turns out to be a complicated oscillatory function of the distance between the receiving atoms. These ideas served as a key to the enigma of optical coherence on the quantum mechanical level, subsequently leading to

the ideas of Glauber and Mandel [12,13,35,39]. Indeed, based on the Glauber's theory, one can easily deduce that thermal light tends to arrive in clumps and is therefore bunched, the probability to detect a photon immediately after another one is higher than at a later moment in time $c^{(2)}(0) > c^{(2)}(t > 0)$. As we are going to see in the present Chapter, coherence functions of radiation in non-Markovian quantum systems exhibit very complicated behavior, which is not to be found in systems with local emitters, in turn, explaining our interest in these observables.

Finally, using the definition of the final state (4.11), we express the second and third-order coherence functions to the lowest order in $|\alpha|$ as

$$c^{(2)}_{\mu_1,\mu_2}(\tau) = \frac{1}{2} c^{(2,2)}_{\mu_1,\mu_2}(\tau) + \mathcal{O}\left(|\alpha|^2\right), \tag{4.20}$$

$$c^{(3)}_{\mu_1,\mu_2,\mu_3}(\tau',\tau) = \frac{1}{6} c^{(3,3)}_{\mu_1,\mu_2,\mu_3}(\tau',\tau) + \mathcal{O}\left(|\alpha|^2\right) \tag{4.21}$$

where the corresponding Fock state coherence functions were defined as

$$c^{(m,n)}_{\mu_1,\ldots,\mu_m}(\tau_1,..,\tau_m) = \\ = \frac{L^m}{\prod_{l=1}^m C^{(1)}_{\mu_l}(0)} \left\langle \Phi^{(n)}_1 \left| (\mathcal{S}_n)^\dagger a^\dagger_{\mu_1}(\tau_1) \ldots a^\dagger_{\mu_m}(\tau_m)\, a_{\mu_m}(\tau_m) \ldots a_{\mu_1}(\tau_1)\, \mathcal{S}_n \right| \Phi^{(n)}_1 \right\rangle. \tag{4.22}$$

7.10.4 4.4 Single-Phonon Processes: Reflectance and Transmittance

According to equation (3.30) (throughout this chapter we relax our summation convention), the single-phonon scattering matrix is given by

$$\mathcal{S}_1 = \sum_{\mu'=1,2} \sum_{\mu=1,2} \int_{\mathbb{R}} dk' \int_{\mathbb{R}} dk \delta(k-k')\, S^{(1)}_{\mu';\mu}(k) a^\dagger_{\mu'}(k')\, a_\mu(k) \otimes |0\rangle\langle 0| \tag{4.23}$$

where we have defined

$$S^{(1)}_{\mu';\mu}(k) = \delta_{\mu',\mu} - 2\pi i T^{(1)}_{\mu' k;\mu k}(k), \quad T^{(1)}_{\mu' k;\mu k}(k) = g^*_\mu(k) g_{\mu'}(k) \tilde{G}^{(1)}(k), \tag{4.24}$$

with the projection of the Green's function on the excited state of the qubit $\tilde{G}^{(1)}(k)$ is completely determined by the self-energy diagram (see equation (3.31))

$$\Sigma^{(1)}(E) = \lim_{\eta \searrow 0} \sum_{\mu=1,2} \int_{\mathbb{R}} dk \frac{|g_\mu(k)|^2}{E - k + i\eta} |1\rangle\langle 1| \tag{4.25}$$

Using the definition of the bare phonon-qubit vertex function (equation (4.3)) and performing the straight-forward integration, we obtain

$$\Sigma^{(1)}(E) = -i \left[\sum_{n=1}^N \Gamma_n + 2 \sum_{1 \le n < n' \le N} \sqrt{\Gamma_{n'} \Gamma_n} e^{i(E+k_0)(x_{n'} - x_n)} \right] |1\rangle\langle 1|. \tag{4.26}$$

Note that the real and imaginary parts of the self-energy determine the frequency dependent Lamb shift $\tilde{\Delta}(k) = \mathrm{Re}\{\Sigma(k)\}$ and renormalized decay rate $\tilde{\Gamma}(k) = \mathrm{Im}\{\Sigma(k)\}$ of the system. The non-trivial dependence of the self-energy on the frequency is a typical feature of non-Markovian systems and this frequency dependence is responsible for the non-trivial single-photon scattering properties. In the maximally symmetric case $x_n = \ln$ and $\Gamma_n = \gamma/N, \quad \forall n \in \{1, \ldots, N\}$ formula (4.26) simplifies to

$$\Sigma^{ms}(E) = -i\gamma \left(1 + \frac{2\left[\left(e^{i(E+k_0)Nl} - 1 \right) - N \left(e^{i(E+k_0)l} - 1 \right) \right] e^{i(E+k_0)l}}{N \left(e^{i(E+k_0)l} - 1 \right)^2} \right) \tag{4.27}$$

In the special case $N = 1$ this boils down to $\Sigma^{ms}_{N=1}(E) = -i\gamma$ which is the correct result for a local, i.e. Markovian scattering setup. In the case $N = 2$ we recover the result of [19] for a symmetric giant atom, namely $\Sigma^{gas}_{N=2}(E) = -i\gamma\left(1 + e^{i(E+k_0)R}\right)$.

In order to compute $C^{(1,1)}_{\mu}(\tau_2 - \tau_1)$, let us contract the single-phonon scattering operator with the single-phonon Fock state to yield

$$\mathcal{S}_1 \left|\Phi^{(1)}_1\right\rangle = \sum_{\mu'=1,2} \int_{\mathbb{R}} dk S^{(1)}_{\mu';1}(k)\varphi(k)a^{\dagger}_{\mu'}(k)|\Omega\rangle \otimes |0\rangle \tag{4.28}$$

Expansion of the sum in (4.28) leads us to

$$\mathcal{S}_1 \left|\Phi^{(1)}_1\right\rangle = \int_{\mathbb{R}} dk S^{(1)}_{1;1}(k)\varphi(k)a^{\dagger}_{1}(k)|\Omega\rangle \otimes |0\rangle + \int_{\mathbb{R}} dk S^{(1)}_{2;1}(k)\varphi(k)a^{\dagger}_{2}(k)|\Omega\rangle \otimes |0\rangle, \tag{4.29}$$

which, in turn, helps us to identify reflection $r(k)$ and transmission $t(k)$ amplitudes as follows

$$t(k) = S^{(1)}_{1;1}(k), \quad r(k) = S^{(1)}_{2;1}(k) \tag{4.30}$$

Note that the sum rule for reflectance and transmitance $|t(k)|^2 + |r(k)|^2 = 1$ is satisfied by the unitarity of the single-phonon S-matrix

$$\mathcal{S}^{\dagger}_1 \mathcal{S}_1 = 1 \tag{4.31}$$

$R = 0.5$

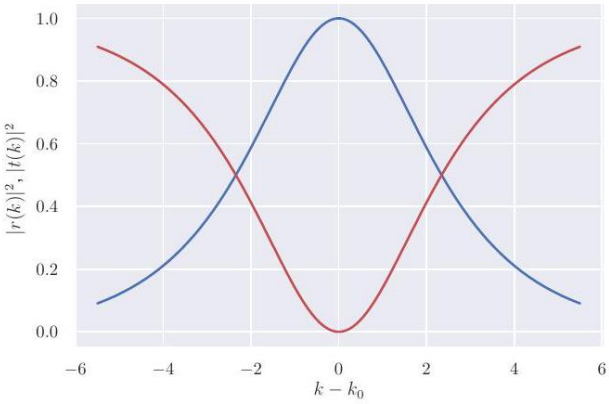

$R = 4$

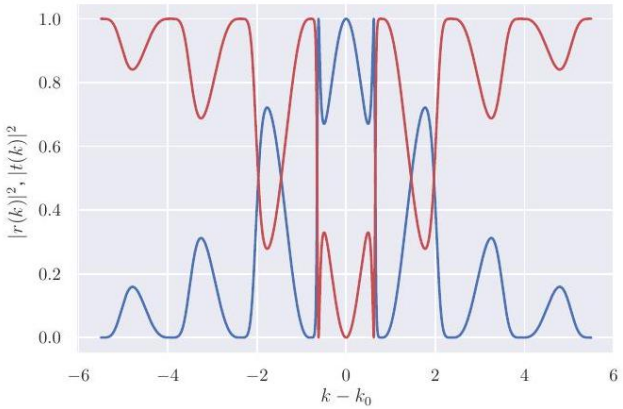

Figure 4.3: Transmittance (red) and reflectance (blue) of a giant atom for $R = 0.5$ and $R = 4$. Other parameters: $\Delta = 0, k_0 = 0$, and $\gamma = 1$.

Using equation (4.28) we can compute the first-order correlation function to the lowest order in $|\alpha|$, first we consider

$$a_\mu(\tau_1)\,\widehat{\mathcal{S}}^{(1)}\left|\Phi_1^{(1)}\right\rangle = \frac{1}{\sqrt{2\pi}}\int\limits_{\mathbb{R}} dk e^{ik\tau_1} S_{\mu;1}^{(1)}(k)\varphi(k)|\Omega\rangle\otimes|0\rangle \to \frac{1}{\sqrt{L}} S_{\mu;1}^{(1)}(0)|\Omega\rangle\otimes|0\rangle \tag{4.32}$$

leading us to the following result

$$C_\mu^{(1)}(\tau) = |\alpha|^2 C_\mu^{(1,1)}(\tau) + \mathcal{O}\left(|\alpha|^4\right) = \frac{|\alpha|^2}{L}\left|S_{\mu;1}^{(1)}(0)\right|^2 + \mathcal{O}\left(|\alpha|^4\right) \equiv f\left|S_{\mu;1}^{(1)}(0)\right|^2 + \mathcal{O}\left(f^2\right) \tag{4.33}$$

Here, we have defined the average phonon power density as the total incident power per unit pulse width $f = |\alpha|^2/L$, one may also write it in terms of the generalized Rabi-frequency Ω_R as follows $f = 4\pi\Omega_R^2/\Gamma_\sigma$, where $\Gamma_\sigma = \sum_{n=1}^{N}\Gamma_n$ is the total decay rate of the qubit into the continuum. One may also easily note that the power conservation sum condition (4.17) is automatically fulfilled (to the lowest order in $|\alpha|$) by the unitarity property (4.31). With this in hands, we may immediately compute the spectral power density to the lowest order in f

$$S_\mu(k) = f\left|S_{\mu;1}^{(1)}(0)\right|^2\delta(k) + \mathcal{O}\left(f^2\right) \tag{4.34}$$

We note that there exists no inelastic contribution to power density in the single-phonon sector. This result is a direct consequence of the energy-conserving delta function in the single-phonon S-matrix, which naturally prohibits any non-trivial momentum redistribution in the scattering process. In later sections of this chapter, we are going to see that this is not the case for the higher-order scattering processes, moreover, the presence of the multi-photon interactions in the higher-order S-matrices may, in general, render the resulting spectrum extremely non-trivial.

Let us now consider the following system - a qubit coupled to a piezoelectric substrate by an ideal interdigital transducer. By an ideal IDT, we here understand an equally spaced (with separation l) array of N fingers with decay rates being all equal, i.e. the maximally symmetric case. Using the self-energy given by the formula (4.27) the reflectance can be written as

$$|r(k)|^2 = \frac{4\gamma^2\left(1-\cos\left(\left(k+k_0\right)Nl\right)\right)^2}{\left|N\left(e^{i(k+k_0)l}-1\right)^2(k+\Delta) + i\gamma\left(N\left(1-e^{2i(k+k_0)l}\right)+2\left(e^{i(k+k_0)Nl}-1\right)e^{i(k+k_0)l}\right)\right|^2}. \tag{4.35}$$

The corresponding transmittance is simply $|t(k)|^2 = 1 - |r(k)|^2$. Note that this formula also covers the case of a symmetric giant atom with $N = 2$ and $l = R$ being the inter-leg separation.

Let us now find the condition for perfect transmittance $|t(k)|^2 = 1$, or equivalently, zero reflectance $|r(k)|^2 = 0$. It is easy to see that the numerator of expression (4.35) vanishes at $l = 0.2$

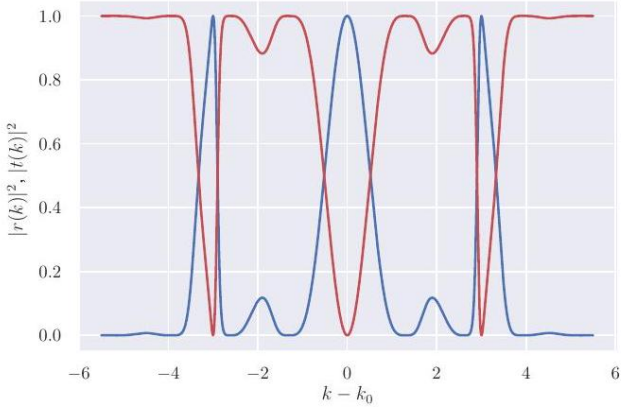

$l = 2$

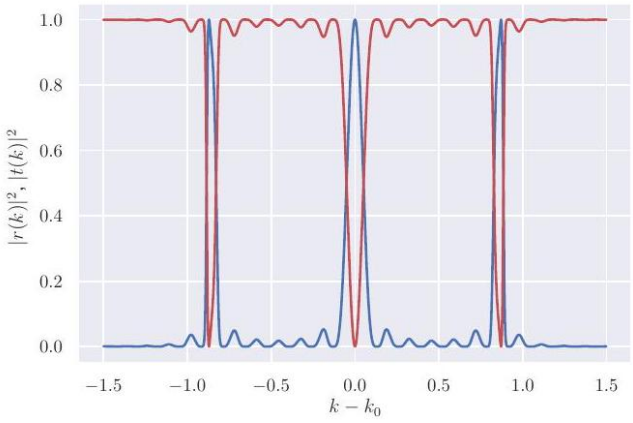

Figure 4.4: Transmittance (red) and reflectance (blue) of a qubit coupled to a piezoelectric substrate by an ideal IDT with $N = 24$ fingers. Other parameters: $\Delta = 0, k_0 = 0$, and $\gamma = 1$.

$(k + k_0) Nl = 2\pi n$ for $n \in \mathbb{Z}$, the denomenator, in its turn, at these points is equal to $N^2 \mid \left(e^{2\pi i n/N} - 1\right)^2 (k + \Delta) + i\gamma \left(1 - e^{4\pi i n/N}\right)\Big|^2$, so we see that if $\frac{n}{N} \in \mathbb{Z}$ the numerator also vanishes rendering the finite reflectance, hence the perfect transmittance condition may be stated as $k = \frac{2\pi m}{Nl} - k_0, \quad m \in \left\{n \in \mathbb{Z} \,\middle|\, \frac{n}{N} \notin \mathbb{Z}\right\}$, for practical purposes one can generate this set by introducing a generating function $f_N(n), \quad n \in \mathbb{N}$, such that $\left\{n \in \mathbb{Z} \,\middle|\, \frac{n}{N} \notin \mathbb{Z}\right\} = \{f_N(n) | n \in \mathbb{N}\} \cup \{-f_N(n) | n \in \mathbb{N}\}$. Clearly, this generating function is a solution to the following reccurence relation $f_N(n + N - 1) - f_N(n) = N$ (with appropriate boundary conditions), e.g. $f_2(n) = 2n - 1, f_3(n) = \frac{1}{4}\left(6n - 3 + (-1)^{n+1}\right)$, etc. The condition for perfect reflection may be found by setting the numerator being equal to the denomenator, which, in turn, leads to a complicated transendental equation. For the case of a symmetric giant atom, the condition of maximum reflection may be written as $k + \Delta = \gamma \sin\left((k + k_0) R\right)$, which always has a finite number of solutions. It is important to note that for $k_0 R = 2\pi n, n \in \mathbb{Z}, \Delta = 0$ we have $r(0) = 1$ for all N, which agrees with the physical expectation that in the absence of pure dephasing the power extinction $1 - |t(0)|^2$ reaches a maximum at zero detuning $\Delta = 0$[4].

Transmittance and reflectance for a symmetric giant atom are plotted in Figure 4.3 for the cases of small $\gamma R = 0.5$ and large $\gamma R = 4$ inter-leg separations. In the case of a small inter-leg separation, the system shows a typical Markovian transmittance/reflectance characteristic with reflectance following a simple Lorentzian curve $r \sim \frac{\gamma^2}{(k+\Delta)^2 + \gamma^2}$. In the case of a larger inter-leg separation, one sees that transmittance and reflectance show a rather non-trivial behavior typical to the non-Markovian systems, as one may additionally note, the transmittance maxima exactly lie at the points predicted in the above analysis $k_{tr-\max} = \pm\frac{\pi}{4}, \pm\frac{3\pi}{4}, \pm\frac{5\pi}{4}, \ldots$, whereas the reflectance maxima exactly correspond to the three solutions of $\frac{\sin(4k)}{k} = 1 : k_{re-\max} = 0, \pm 0.618644\ldots$

Figure 4.4, in its turn, shows the transmittance/reflectance characteristics for a single qubit coupled to a piezoelectric substrate by an ideal IDT with $N = 24$ fingers. In this case, one can clearly see that even in the case of comparatively small delay the response is still non-Markovian, thus showing that quantum acoustical systems do not intrinsically allow for a Markovian description. One can additionally see that transmission maxima and thus reflection minima exactly follow the above-prescribed formula $k_{tr-\max} = \pm\frac{\pi}{12l}, \pm\frac{\pi}{6l}, \pm\frac{\pi}{4l}, \ldots$.

7.10.5 4.5 Two-Phonon Processes: Inelastic Spectral Power Density and Second-Order Coherence Function

According to (3.37), the two-phonon S-matrix may be written as

$$\mathcal{S}_2 = \sum_{\mu_1',\mu_2',\mu_1,\mu_2} \int_{\mathbb{R}} dk_1' \int_{\mathbb{R}} dk_2' \int_{\mathbb{R}} dk_1 \int_{\mathbb{R}} dk_2 S^{2)}_{\mu_1' k_1', \mu_2' k_2'; \mu_1 k_1, \mu_2 k_2} \times a^\dagger_{\mu_1'}(k_1') a^\dagger_{\mu_2'}(k_2') a_{\mu_2}(k_2) a_{\mu_1}(k_1) \otimes |0\rangle\langle 0| \tag{4.36}$$

where

$$S^{(2)}_{\mu_1' k_1', \mu_2' k_2'; \mu_1 k_1, \mu_2 k_2} = \frac{1}{2!} S^{(1)}_{\mu_1';\mu_1}(k_1) S^{(1)}_{\mu_2';\mu_2}(k_2) \delta(k_1' - k_1) \delta(k_2' - k_2) - 2\pi i T^{(2,C)}_{\mu_1' k_1', \mu_2' k_2'; \mu_1 k_1, \mu_2 k_2}(k_1 + k_2) \delta(k_1' + k_2' - k_1 - k_2) \tag{4.37}$$

Contracting the S-matrix with the two-phonon Fock state we arrive at

$$\mathcal{S}_2 \left|\Phi_1^{(2)}\right\rangle \to \left(\frac{1}{\sqrt{2}} \sum_{\mu_1',\mu_2'} \int_{\mathbb{R}} dk_1 \int_{\mathbb{R}} dk_2 \varphi(k_1) \varphi(k_2) S^{(1)}_{\mu_1';1}(k_1) S^{(1)}_{\mu_2';1}(k_2) a^\dagger_{\mu_1'}(k_1) a^\dagger_{\mu_2'}(k_2) |\Omega\rangle - \frac{8\pi^2 i}{L\sqrt{2}} \sum_{\mu_1',\mu_2'} \int_{\mathbb{R}} dk T^{(2,C)}_{\mu_1' k, \mu_2' - k; 10, 10}(0) a^\dagger_{\mu_1'}(k) a^\dagger_{\mu_2'}(-k) |\Omega\rangle \right) \otimes |0\rangle. \tag{4.38}$$

To compute the first non-trivial correction to the power-density, we consider

$$a_\mu(\tau_1) \mathcal{S}_2 \left|\Phi_1^{(2)}\right\rangle \to \left(\sqrt{\frac{2}{L}} S^{(1)}_{\mu;1}(0) \sum_{\mu_1'} \int_{\mathbb{R}} dk_1 \varphi(k_1) S^{(1)}_{\mu_1';1}(k_1) a^\dagger_{\mu_1'}(k_1) |\Omega\rangle - \frac{8\pi^2 i}{L\sqrt{\pi}} \sum_{\mu_1'} \int_{\mathbb{R}} dk e^{-ik\tau_1} M_{\mu_1',\mu}(k) a^\dagger_{\mu_2'}(k) |\Omega\rangle \right) \otimes |0\rangle, \tag{4.39}$$

where we have introduced the following function

$$M_{\mu',\mu}(k) = M_{\mu,\mu'}(-k) = \frac{\left(T^{(2,C)}_{\mu - k, \mu' k; 10, 10}(0) + T^{(2,C)}_{\mu' k, \mu - k; 10, 10}(0) \right)}{2}. \tag{4.40}$$

Thus, the first-order coherence function up to order f^3 is given by

$$C^{(1)}_\mu(\tau) = f \left| S^{(1)}_{\mu;1}(0) \right|^2 + 16\pi^2 f^2 \sum_{\mu'} \mathrm{Im} \left\{ M_{\mu',\mu}(0) \left(S^{(1)}_{\mu';1}(0) S^{(1)}_{\mu;1}(0) \right)^* \right\} + 32\pi^3 f^2 \sum_{\mu'} \int_{\mathbb{R}} dk e^{ik\tau} |M_{\mu',\mu}(k)|^2 + \mathcal{O}\left(f^3\right) \tag{4.41}$$

By performing the Fourier transform of (4.41), we arrive at the following expressions for the elastic and inelastic power densities

$$S^{el}_\mu(k) = \delta(k) \left(f \left| S^{(1)}_{\mu;1}(0) \right|^2 + 16\pi^2 f^2 \sum_{\mu'} \mathrm{Im} \left\{ M_{\mu',\mu}(0) \left(S^{(1)}_{\mu';1}(0) S^{(1)}_{\mu;1}(0) \right)^* \right\} \right) + \mathcal{O}\left(f^3\right), \tag{4.42}$$

$$S^{\mathrm{inel}}_\mu(k) = 32\pi^3 f^2 \sum_{\mu'} |M_{\mu',\mu}(k)|^2 + \mathcal{O}\left(f^3\right). \tag{4.43}$$

The power conservation condition up to order f^3 leads to the following requirement in the twophonon sector

$$\sum_{\mu',\mu} \mathrm{Im}\left\{ M_{\mu',\mu}(0)\left(S^{(1)}_{\mu';1}(0)S^{(1)}_{\mu;1}(0)\right)^*\right\} = -2\pi \sum_{\mu',\mu}\int_{\mathbb{R}} dk\,|M_{\mu',\mu}(k)|^2 \tag{4.44}$$

Let us now compute the normalized second-order coherence to the lowest order in f, for that purpose we consider

$$a_{\mu'}(\tau_2)\,a_{\mu}(\tau_1)\,\widehat{\mathcal{S}}^{(2)}\left|\Phi^{(2)}_1\right\rangle \to \frac{\sqrt{2}}{L}\left(S^{(1)}_{\mu';1}(0)S^{(1)}_{\mu;1}(0)|\Omega\rangle - 4\pi i\int_{\mathbb{R}} dk e^{ik(\tau_2-\tau_1)}M_{\mu',\mu}(k)\right)|\Omega\rangle\otimes|0\rangle \tag{4.45}$$

Hence, the normalized second-order coherence function is given by

$$c^{(2)}_{\mu',\mu}(\tau) = \left|1 - \frac{4\pi i}{S^{(1)}_{\mu';1}(0)S^{(1)}_{\mu;1}(0)}\int_{\mathbb{R}} dk e^{ik\tau}M_{\mu',\mu}(k)\right|^2 + \mathcal{O}(f) \tag{4.46}$$

Let us first focus our attention on the giant atom model. Surprisingly enough, in this rather simple model, an analytical solution to the integral equation (3.21) may be obtained using the method developed in [19,29], see Appendix A. The above-defined M-function takes the following form

$$\begin{aligned} M_{\mu',\mu}(k) = g^*_1(0)g^*_1(0)\left\langle 1\left|G^{(1)}(0)\right|1\right\rangle g_\mu(k)g_{\mu'}(-k)[P(k) \\ +\frac{\left\langle 1\left|G^{(1)}(k)\right|1\right\rangle \bar{F}^{(1,1)}(k,0,0) + \left\langle 1\left|G^{(1)}(-k)\right|1\right\rangle \bar{F}^{(1,1)}(k,0,0)}{2}\Bigg] \end{aligned} \tag{4.47}$$

where $P(k)$ is the term purely associated with the quasi-Markovian contribution (non-crossed diagrams only, see Figure 3.4)

$$P(k) = \left\langle 1\left|G^{(1)}(k)\right|1\right\rangle\left\langle 1\left|G^{(1)}(-k)\right|1\right\rangle\left(\gamma R e^{ik_0R}\,\mathrm{sinc}(kR) - 1\right) \tag{4.48}$$

$\bar{F}^{(1,1)}(k,0,0)$, in its turn, is the solution of the integral equation (3.33), containing some non-trivial frequency dependence

$$\bar{F}^{(1,1)}(k,0,0) = -\frac{i\gamma e^{ik_0R}}{\lambda + i\gamma e^{ik_0R}}\sum_{\kappa\in\{-1,0,1\}} C_\kappa \frac{e^{-ikR} - e^{-i\kappa pR}}{\kappa p - k} \tag{4.49}$$

where

$$p^2 = \lambda^2 + \gamma^2 e^{2ik_0R},\quad C_\pm = \pm\frac{(\pm p - \lambda)e^{\pm ipR} - i\gamma e^{ik_0R}}{2(p\cos pR - i\lambda\sin pR)},\quad C_0 = -1,\quad \lambda = \Delta + i\gamma \tag{4.50}$$

As one can see, compared to the quasi-Markovian approximation, an exact solution contains a new parameter p providing us with new oscillation frequencies $\mathrm{Re}\{p\}$ and new decay rates $\mathrm{Im}\{p\}$ in the system.

To make a distinction between the responses of Markovian and non-Markovian systems more apparent, let us first consider a simple limiting case of a locally coupled (Markovian) system $R = 0$. In this case, we see that the purely non-Markovian contribution $\bar{F}^{(1,1)}(k,0,0)$ vanishes and quasiMarkovian approximation becomes exact enabling us to deduce the following simple formula for the inelastic spectral power density

$$S^{inel}_\mu(k) = \frac{\gamma^4}{\pi}\frac{64f^2}{\Delta^2 + 4\gamma^2}\frac{1}{\left|k^2 - (\Delta - 2i\gamma)^2\right|^2}, \tag{4.51}$$

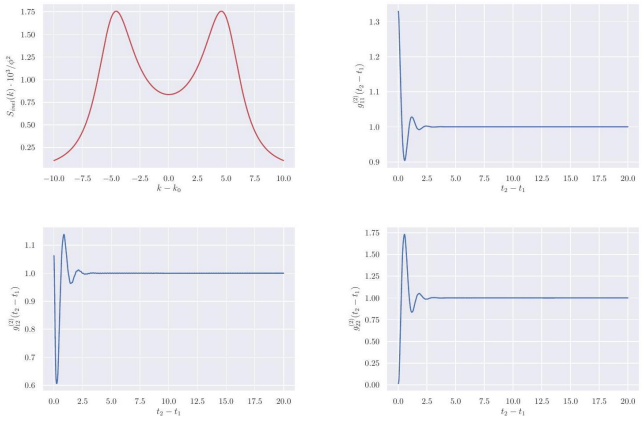

Figure 4.5: Two-photon observables in the Markovian limit. $\Delta = 5, \gamma = 1$.

which shows a pair of smooth peaks which merge together when the detuning of the qubit reaches zero. The second-order coherence function may be shown to be

$$c^{(2)}_{2,2}(\tau) = \left|1 - \mathrm{sign}(\tau) e^{i\Delta|\tau|} e^{-2\gamma|\tau|}\right|^2, \quad c^{(2)}_{1,1}(\tau) = \left|1 + \frac{4\gamma^2}{\Delta^2}\,\mathrm{sign}(\tau) e^{i\Delta|\tau|} e^{-2\gamma|\tau|}\right|^2$$
$$c^{(2)}_{2,1}(\tau) = \left|1 + \frac{2i\gamma}{\Delta}\,\mathrm{sign}(\tau) e^{i\Delta|\tau|} e^{-2\gamma|\tau|}\right|^2 \tag{4.52}$$

where $\mathrm{sign}(0) = 1$. We see that as $t \to \infty$ all of the components of the second-order correlation function tend to 1, leading to the Poissonian statistics for large values of the delay between phonon counting events. We also see that $c^{(2)}_{11}(0) > c^{(2)}_{21}(0) > 1$ leading to the tendency of the phonon bunching which is then followed by an ani-bunching dip at some intermediate delay $\tau > 0$. Since a local system can emit or absorb a single quantum of radiation at a time we essentially have $c^{(2)}_{22}(0) = 0$, leading to the anti-bunching of phonons. Components of the second-order coherence function, as well as the inelastic power spectrum in the Markovian limit, are displayed in Figure 4.5.

In the non-Markovian regime, the full solution of the integral equation (3.21) is required and the resulting spectrum, as well as the behavior of the second-order coherence correlation function, becomes much richer. To understand the inelastic power spectrum beyond the Markovian limit, for the sake of simplicity, let us focus on the case of a bright atom $\Delta = 0$ and $k_0 R \in 2\pi\mathbb{Z}$. In this case $p \to 0$, and after careful evaluation of this limit we find out the following formula for the inelastic power spectrum

$$S^{\mathrm{inel}}_{\mu}(k) = \frac{4(\gamma f)^2}{\pi(1+\gamma R)^2} \frac{(1+\cos kR)^2}{\left((k - \gamma \sin kR)^2 + \gamma^2(1+\cos kR)^2\right)^2} \tag{4.53}$$

In this limit, the inelastic power spectrum develops two sharp peaks near the origin followed by infinitely many smaller side peaks (see Figure 4.6). To understand the basic physics of these peaks, we can interpret this system as a leaky cavity formed by the two connection points of a giant atom. Let us first note that $S^{\mathrm{inel}}_{\mu}(k) = 0$ whenever $k = \frac{\pi n}{R}, \quad n \in \left\{m \in \mathbb{Z} \,\middle|\, \frac{m}{2} \notin \mathbb{Z}\right\}$. These frequencies also coincide with the modes supported by the effective cavity. The resulting effect is the formation of sharp, bound-state like peaks in the intensity of the scattered phonons very close to these zeros, corresponding to cavity resonances. As the delay increases, the peaks thus get closer to $k = 0$, and get sharper, corresponding to a decrease of the effective cavity linewidth $\simeq 1/R$, that is effective cavity resonances approach the resonance of the two-level system, thus making atomic connection points better and better mirrors and hence increasing the quality factor of the effective cavity (quality factor is a common physical measure of both the rate of excitation damping and the rate of energy loss of an oscillator or a cavity). If one goes away form $k_0 R \in 2\pi\mathbb{Z}, \quad \Delta = 0$ point in parameter space, one can find an even more sophisticated response of the system, since now the new renormalized decay poles $p = \sqrt{\lambda^2 + \gamma^2 e^{2ik_0 R}}$ appear in the power spectrum. A few examples are shown in Figure 4.7.

Additionally, spectral densities based on the approximate solution of the scattering problem in the quasi-Markovian approximation are shown in Figures 4.6 and 4.7. As it was mentioned

in the Chapter 3, quasi-Markovian results show a rather good agreement with an exact solution in $\gamma R \ll 1$ parameter regime. As the delay time increases $\gamma R \geq 1$, the discrepancy between the approximate and complete solutions becomes dramatic. One can clearly see the tendency of the quasi-Markovian theory to enhance the scattering into the incoming frequency states $k = 0$. Indeed, in contrast to the exact solution, taking into account infinitely many excursions of phonons to the qubit, the quasi-Markovian approximation is based on the assumption of a single scattering event after which each phonon immediately leaves the system, thus leading to a more elastic result.

Let us now consider the second-order coherence function in the non-Markovian setup. Secondorder coherence function's components are presented in Figure 4.8. As one can see, as compared to the Markovian system, components of the second-order coherence are not rapidly tending to unity, but instead, exhibit complicated oscillation patterns. As one may notice though some of the Markovian features are still present. Namely, $c_{11}^{(2)}(0)$ and $c_{12}^{(2)}(0)$ both exceed unity thus showing phononic bunching behaviour. Moreover, the property of $c_{11}^{(2)}(0)$ being greater than $c_{12}^{(2)}(0)$ is also retained, as well as the anti-bunching behavior of SAW in the second channel $c_{22}^{(2)}(0) < 1$, note that, now, however $c_{22}^{(2)}(0) \neq 0$. One may also apparently see the presence of non-differentiable peaks in the line-shapes of various coherence function's components. No surprise, the location of these $\mathbf{C}^0$ structures coincides with the integer multiples of the delay time in the system $\tau \in R \cdot \mathbb{Z}$. This phenomenon becomes apparent when one reminds himself about the presence of the single-particle preparators $\tilde{G}^{(1)}(\pm k)$ in the definition of $M_{\mu',\mu}(k)$, Fourier transform of which completely specifies $c_{\mu',\mu}^{(2)}(\tau)$. Indeed, the following mathematical argument shall sound like a reasonable justification. For instance, the following identity

$$\tilde{G}^{(1)}(\pm k) = \frac{1}{\pm k + \Delta + i\gamma\left[1 + e^{i(\pm k + k_0)R}\right]} = \sum_{n=0}^{\infty} \frac{\left(-i\gamma e^{ik_0 R}\right)^n e^{\pm iknR}}{(\pm k + \Delta + i\gamma)^{n+1}} \tag{4.54}$$

implies analyticity of $\tilde{G}^{(1)}(k)$ and $\tilde{G}^{(1)}(-k)$ in the upper and in the lower halves of the complex plane respectively. When calculating the residues coming from the essential singularities of $\tilde{G}^{(1)}(k)$ and $\tilde{G}^{(1)}(-k)$ one has first and foremost to close the integration contours in the lower and in the upper halves of the complex k plane correspondingly, the convergence of the integrand, in its turn, would respectively demand $\pm\tau > nR$ leading to the emergence of the discontinuous Heaviside functions $\Theta(\tau \pm nR)$ in the outcome of integration. The ascent of these non-differentiable structures is a characteristic feature of the quantum systems with delayed coherent quantum feedback. Baring in mind that coherence functions are experimentally measurable quantities, such peculiar features in their line-shape may manifest themselves in future experiments, making the theoretical understanding of their nature rather valuable.

Alongside the exact solution, the results based on the quasi-Markovian approximation are

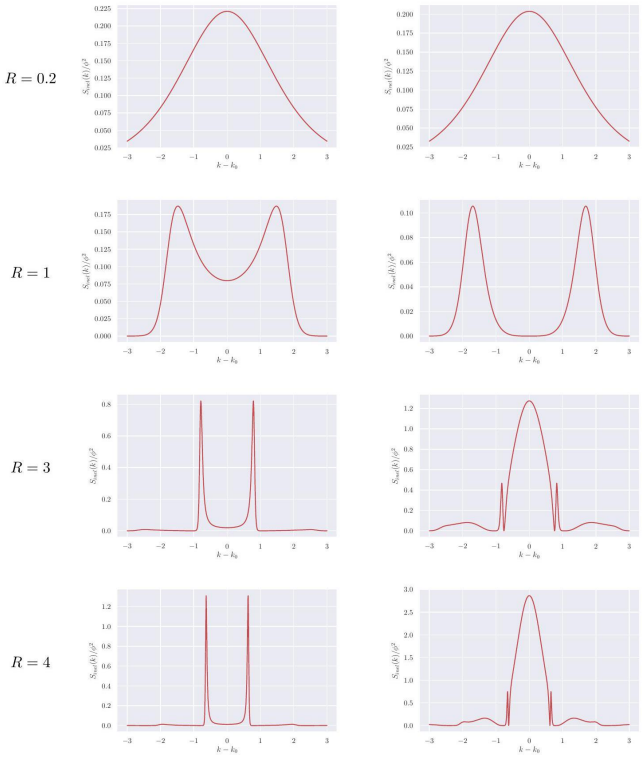

Figure 4.6: Inelastic spectral density of a bright giant atom wiht $\Delta = 0, k_0 R = 2\pi$, and $\gamma = 1$. Left: exact solution. Right: quasi-Markovian approximation.
$R = 4, k_0 = 3\pi/7, \Delta = 3$

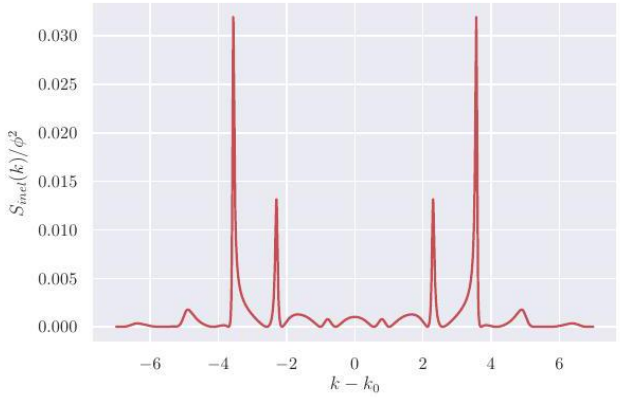

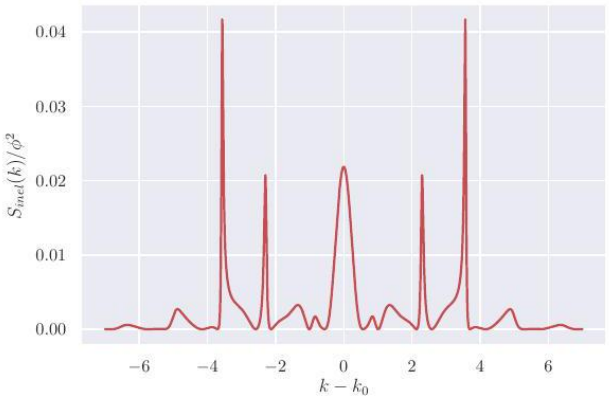

$R = 10, k_0 = 0, \Delta = 3$

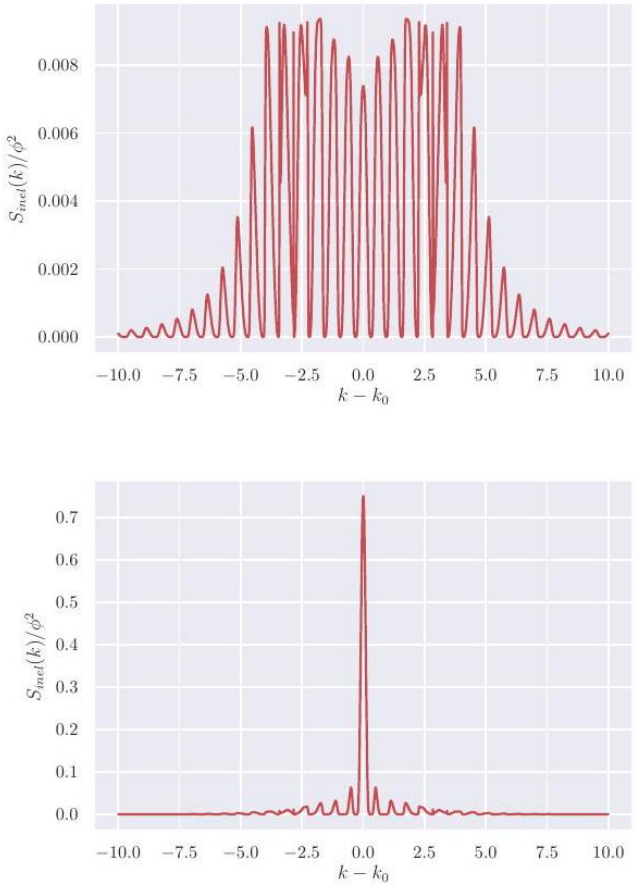

Figure 4.7: Inelastic spectral density away from the $\Delta = 0, k_0 R \in 2\pi\mathbb{Z}$ point in parameter space. Top: exact solution. Bottom: quasi-Markovian approximation. In all plots $\gamma = 1$.

presented. The discrepancy between the two is apparent. Despite the fact of the agreement in the node/antinode structure of both results, quasi-Markovian solution clearly shows incorrect trends in the long run. Another feature typical of this approximation is the tendency to overestimate the amplitudes of oscillation [29].

Now let us consider the observables in the IDT model. In this case, it is impossible to solve the resulting integral equation analytically, so one has to solve it by numerical means. In Figure 4.9, the resultant inelastic spectral densities, as well as the second-order coherence functions, are shown for two sets of parameters.

As one can see, as in the giant atom model, in the case of multiple coupling points ($N > 2$), spectral density also shows an infinite number of sharp peaks around the origin. Now, however, the number of visible peaks is greater. Using our picture of an effective cavity created by imperfect mirrors, we may attribute the emergence of additional resonances to the uprise in the number of resonant frequencies, corresponding to all of $(N-1)l$ inter-finger separations in the system. Namely one can see a variety of smaller peaks nesting near the origin of momentum space coming from the resonance frequencies associated with larger wavelengths supported by the cavity $k_{\min} \simeq 1/Nl$ followed by the sharper ones, corresponding to the smallest wavelength supported by the system $k_{\max} \simeq 1/l$. As one can see, the peaks which are closer to the origin are smaller and appear more broadened, this fact may be attributed to the significant attenuation of the field amplitude due to the presence of additional "leaky mirrors" in between the outermost fingers. Indeed, the typical characteristic of one-dimensional quantum electronic systems, high-quality mode matching, effectively suppresses processes where a particle emitted in the middle of the "finger forest" transverses a significant distance without being reabsorbed by a neighboring finger.

Now let us be concerned with a second-order coherence function. As one may notice, some of the features exhibited by the second-order coherence correlation function of a gigantic atom are retained, whereas the others are not. First of all, non-differentiability of $c^{(2)}_{\mu',\mu}(\tau)$ at $\tau \in l \cdot \mathbb{Z}$ is preserved, and in fact becomes more apparent. It is also interesting to observe that $c^{(2)}_{12}(\tau)$ component of both the coherence function of a giant atom and an IDT system at $\tau = 0$ start to

Exact

$c_{11}^{(2)}(t)$

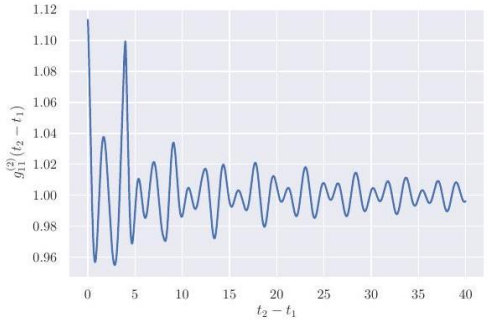

$c_{12}^{(2)}(t)$

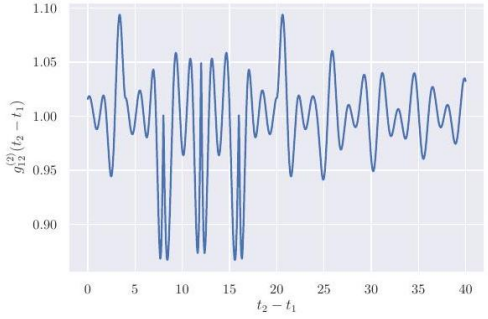

$c_{22}^{(2)}(t)$

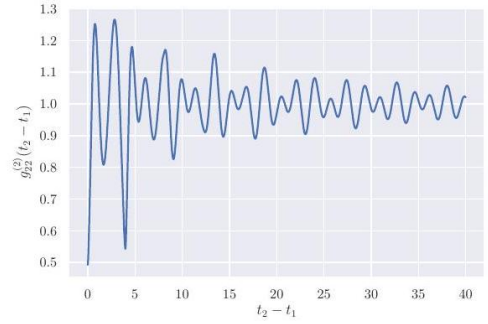

Approximate

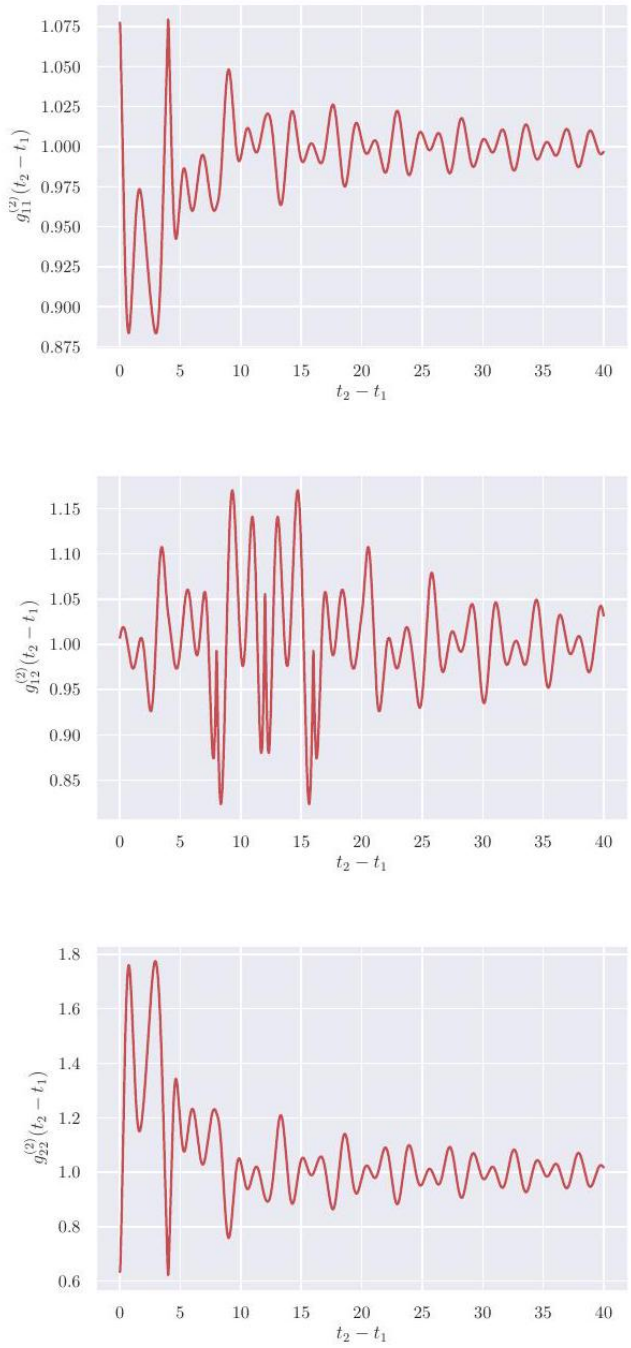

Figure 4.8: Independant components of a second-order coherence function for a giant acoustic atom with $R = 4, \Delta = 3, k_0 = 3\pi/7$, and $\gamma = 1$.

exhibit a complicated symmetric oscillation pattern, whereas $c_{22}^{(2)}(\tau)$ component of the coherence function of both systems drops down whenever the $c_{11}^{(2)}(\tau)$ component is increasing, which one would naturally expect for few phonon systems. The difference, however, emerges in the values of the second-order coherence correlation at $\tau = 0$. Indeed, as we have observed above, $c_{11}^{(2)}(0)$ and $c_{12}^{(2)}(0)$ used to show the bosonic bunching behavior, whereas in the IDT model one observes clear phononic ani-bunching behavior $c_{12}^{(2)}(0) < 1$ in the cross channel correlation function. Moreover, the $c_{22}^{(2)}(0)$ coherence function demonstrated anti-bunching of bosons $c_{22}^{(2)}(0) < 1$, however, in the multi-finger model one can observe $c_{22}^{(2)}(0)$ significantly exceeding 1 for the second set of parameters $(l = 2, k_0 = 3\pi/7, N = 6, \Delta = 2)$.

7.10.6 4.6 Three-Phonon Processes: Third-Order Coherence Function

Finally, let us consider the contribution from the three-body sector to the scattering process. Due to the high computational complexity, in this section, we are going to focus solely on the symmetric giant atom model. The observable we are going to concentrate on is the third-order coherence function, which is the observable only accessible in three and higher phonon sectors. According to formula (3.41) the cluster-decomposed three-phonon S-matrix is given by the following expression

$$\begin{aligned}\mathcal{S}_3 = \sum_{\{\mu_i'\},\{\mu_i\}} \int\limits_{\mathbb{R}} D_{k_1'k_2'k_3'k_1k_2k_3} \Big(& \frac{1}{6} S^{(1)}_{\mu_1';\mu_1}(k_1)\, S^{(1)}_{\mu_2';\mu_2}(k_2)\, S^{(1)}_{\mu_3';\mu_3}(k_3)\, \delta(k_1-k_1')\, \delta(k_2-k_2')\, \delta(k_3-k_3') \\ & -2\pi i T^{(2,C)}_{\mu_1'k_1',\mu_2'k_2';\mu_1k_1,\mu_2k_2}(k_1+k_2)\, \delta(k_1'+k_2'-k_1-k_2)\, S^{(1)}_{\mu_3';\mu_3}(k_3)\, \delta(k_3-k_3') \\ & -2\pi i T^{(3,C)}_{\mu_1'k_1',\mu_2'k_2',\mu_3'k_3';\mu_1k_1,\mu_2k_2,\mu_3k_3}(k_1+k_2+k_3)\, \delta(k_1'+k_2'+k_3'-k_1-k_2-k_3)\Big) \\ & \times a^\dagger_{\mu_1'}(k_1')\, a^\dagger_{\mu_2'}(k_2')\, a^\dagger_{\mu_3'}(k_3')\, a_{\mu_3}(k_3)\, a_{\mu_2}(k_2)\, a_{\mu_1}(k_1), \qquad (4.55)\end{aligned} \tag{4.55}$$

where we have introduced the following compact notations

$$\int\limits_{\mathbb{R}} D_{p_1\ldots p_n} \equiv \int\limits_{\mathbb{R}} dp_1 \ldots \int\limits_{\mathbb{R}} dp_n, \qquad \sum_{\{\mu_i'\},\{\mu_i\}} = \sum_{\mu_1',\mu_2',\mu_3',\mu_1,\mu_2,\mu_3}. \tag{4.56}$$

Upon contraction with the three-phonon Fock state one obtains

$$\begin{aligned}&\mathcal{S}_3 \left|\Phi_1^{(3)}\right\rangle = \\ &= \frac{1}{\sqrt{6}} \sum_{\{\mu_i'\}} \Bigg(\int\limits_{\mathbb{R}} D_{k_1k_2k_3} \varphi(k_1)\, \varphi(k_2)\, \varphi(k_3)\, S^{(1)}_{\mu_1';1}(k_1)\, S^{(1)}_{\mu_2';1}(k_2)\, S^{(1)}_{\mu_3',1}(k_3)\, a^\dagger_{\mu_1'}(k_1)\, a^\dagger_{\mu_2'}(k_2)\, a^\dagger_{\mu_3'}(k_3)\, |\Omega\rangle - \\ &- 12\pi i \int\limits_{\mathbb{R}} D_{k_1'k_2'k_1k_2k_3} \varphi(k_1)\, \varphi(k_2)\, \varphi(k_3)\, T^{(2,C}_{\mu_1'k_1',\mu_2'k_2';\mu_1k_1,\mu_2k_2}(k_1+k_2)\, \delta(k_1'+k_2'-k_1-k_2)\, S^{(1)}_{\mu_3';1}(k_3)\, a^\dagger_{\mu_1'}(k_1')\, a^\dagger_{\mu_2'}(k_2')\, a^\dagger_{\mu_3'}(k_3)\, |\Omega\rangle - \\ &- 12\pi i \left(\frac{2\pi}{L}\right)^{3/2} \int\limits_{\mathbb{R}} D_{k_1'k_2'k_3'} Q(k_1',k_2',k_3')\, \delta(k_1'+k_2'+k_3')\, a^\dagger_{\mu_1'}(k_1')\, a^\dagger_{\mu_2'}(k_2')\, a^\dagger_{\mu_3'}(k_3')\, |\Omega\rangle \Bigg),\end{aligned}$$

where we have introduced the following symmetrized version of the three-phonon transition operator

$$\begin{aligned}Q(k_1',k_2',k_3') = \frac{1}{6} \Big[& T^{(3,C)}_{\mu_1'k_1',\mu_2'k_2',\mu_3'k_3';10,10,10}(0) + T^{(3,C)}_{\mu_1'k_1',\mu_3'k_3',\mu_2'k_2';10,10,10}(0) + T^{(3,C)}_{\mu_3'k_3',\mu_2'k_2',\mu_1'k_1';10,10,10}(0) \\ & + T^{(3,C)}_{\mu_3'k_3',\mu_1'k_1',\mu_2'k_2';10,10,10}(0) + T^{(3,C)}_{\mu_2'k_2',\mu_1'k_1',\mu_3'k_3';10,10,10}(0) + T^{(3,C)}_{\mu_2'k_2',\mu_3'k_3',\mu_1'k_1';10,10,10}(0)\Big]\end{aligned}$$

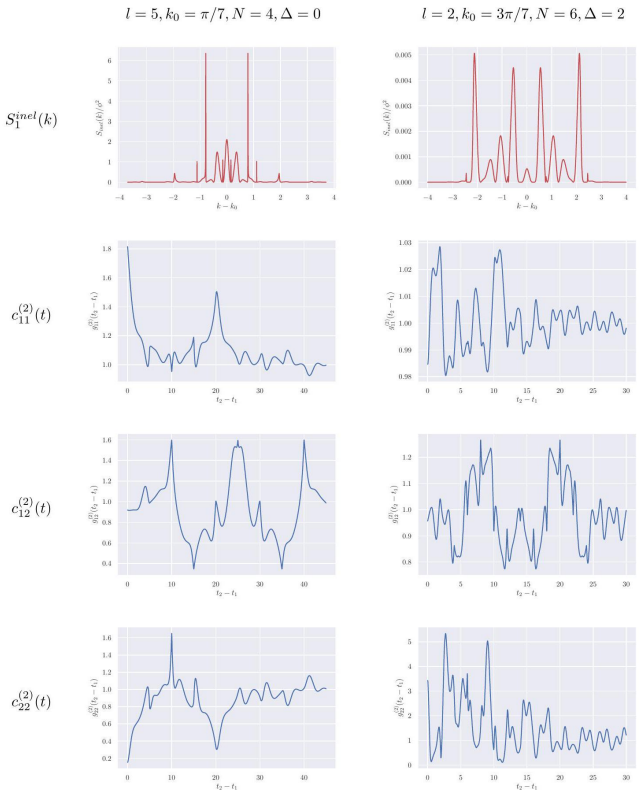

Figure 4.9: Observables for a system consisting of a qubit coupled to SAW by an ideal IDT. In all plots $\gamma = 1$.

Here we have suppressed the dependence of $Q\left(k_1', k_2', k_3'\right)$ on $\{\mu'\}$ since in the giant atom model the coupling constants are independent of the channel index. As before, in order to compute $C_\mu^{(1,3)}(\tau)$ we consider the action of the position space annihilation operator on (4.57)

$$
\begin{aligned}
a_\mu\left(\tau_1\right) \mathcal{S}_3 \left|\Phi_1^{(3)}\right\rangle &= \sqrt{\frac{3}{L}} S_{\mu,1}^{(1)}(0) \mathcal{S}_2 \left|\Phi_1^{(2)}\right\rangle \\
&- \frac{24\pi i}{\sqrt{6}} \frac{2\pi}{L} \frac{1}{\sqrt{2\pi}} \sum_{\mu_1', \mu_2'} \int_{\mathbb{R}} dk \int_{\mathbb{R}} dq e^{-k\tau_1} M(k) S_{\mu_2';1}^{(1)}(q) \varphi(q) a_{\mu_1'}^\dagger(k) a_{\mu_2'}^\dagger(k) |\Omega\rangle \\
&- \frac{72\pi^2 i}{\sqrt{6}} \frac{1}{L^{3/2}} \sum_{\mu_1', \mu_2'} \int_{\mathbb{R}} dk \int_{\mathbb{R}} dq e^{-i(k+q)\tau_1} Q(-k-q, k, q) a_{\mu_1'}^\dagger(k) a_{\mu_2'}^\dagger(q) |\Omega\rangle
\end{aligned} \tag{4.59}
$$

Here, $M(k)$ is defined in exactly the same manner as $M_{\mu',\mu}(k)$ (see equation (4.40)) with the dependence on the channel index being suppressed. With this in hands, we write the first-order coherence function up to the fourth-order in f as

$$C_{\mu}^{(1)}\left(\tau_1'-\tau_1\right)=f\left|S_{\mu;1}^{(1)}(0)\right|^2+16\pi^2f^2\sum_{\mu_1'}\mathrm{Im}\left\{M(0)\left(S_{\mu_1';1}^{(1)}(0)S_{\mu;1}^{(1)}(0)\right)^*\right\}$$
$$+256\pi^4f^3|M(0)|^2\sum_{\mu_1'}\mathrm{Re}\left\{S_{\mu;1}^{(1)}(0)\left(S_{\mu_1';1}^{(1)}(0)\right)^*\right\}+768\pi^4f^3\int\limits_{\mathbb{R}}dk\,\mathrm{Re}\left\{S_{\mu;1}^{(1)}(0)Q^*(0,k,-k)M(k)\right\}$$
$$48\pi^3f^3\sum_{\mu_1',\mu_2'}\mathrm{Im}\left\{Q(0,0,0)\left(S_{\mu_1';1}^{(1)}(0)S_{\mu_2';1}^{(1)}(0)S_{\mu;1}^{(1)}(0)\right)^*\right\}+64\pi^4f^3\sum_{\mu_1',\mu_2'}\left(S_{\mu_1';1}^{(1)}(0)\right)^*S_{\mu_2';1}^{(1)}(0)|M(0)|^2$$
$$+64\pi^3f^2\sum_{\mu'}\int\limits_{\mathbb{R}}dke^{ik\tau}|M(k)|^2+1152\pi^4f^3\int\limits_{\mathbb{R}}dk\int\limits_{\mathbb{R}}dqe^{i(k+q)\left(\tau_1'-\tau_1\right)}|Q(-k-q,k,q)|^2$$
$$+768\pi^4f^3\sum_{\mu_1'}\int\limits_{\mathbb{R}}dke^{ik\left(\tau_1'-\tau_1\right)}\mathrm{Re}\left\{Q(-k,k,0)\left(M(k)S_{\mu_1';1}^{(1)}(0)\right)^*\right\}. \tag{4.60}$$

Power conservation condition, in its turn, demands the following

$$0=16\pi|M(0)|^2\sum_{\mu_1',\mu_2'}\left[\mathrm{Re}\left\{S_{\mu_1';1}^{(1)}(0)\left(S_{\mu_2';1}^{(1)}(0)\right)^*\right\}+4\left(S_{\mu_1';1}^{(1)}(0)\right)^*S_{\mu_2';1}^{(1)}(0)\right]$$
$$+3\sum_{\mu_1',\mu_2',\mu_3'}\mathrm{Im}\left\{Q(0,0,0)\left(S_{\mu_1';1}^{(1)}(0)S_{\mu_2';1}^{(1)}(0)S_{\mu_3';1}^{(1)}(0)\right)^*\right\}$$
$$+144\pi\int\limits_{\mathbb{R}}dk\int\limits_{\mathbb{R}}dq|Q(-k-q,k,q)|^2+192\sum_{\mu_1'}\int\limits_{\mathbb{R}}dk\,\mathrm{Re}\left\{Q(-k,k,0)\left(M(k)S_{\mu_1';1}^{(1)}(0)\right)^*\right\} \tag{4.61}$$

For the two sets of parameters considered, the right-hand side of the above expression evaluated to zero within the numerical error, thus justifying the validity of our theory.

Now, let us focus on the third-order coherence function. One has

$$a_{\mu''}\left(\tau_3\right)a_{\mu'}\left(\tau_2\right)a_{\mu}\left(\tau_1\right)\mathcal{S}_3\left|\Phi_1^{(3)}\right\rangle=\frac{\sqrt{6}}{L^{3/2}}S_{\mu'',1}^{(1)}(0)S_{\mu',1}^{(1)}(0)S_{\mu,1}^{(1)}(0)\left(1-4\pi i\left[\frac{I_1\left(\tau_3-\tau_2\right)}{S_{\mu'';1}^{(1)}(0)S_{\mu';1}^{(1)}(0)}\right.\right.$$
$$\left.\left.+\frac{I_1\left(\tau_2-\tau_1\right)}{S_{\mu;1}^{(1)}(0)S_{\mu';1}^{(1)}(0)}+\frac{I_1\left(\tau_3-\tau_1\right)}{S_{\mu'';1}^{(1)}(0)S_{\mu;1}^{(1)}(0)}\right]-12\pi i\frac{I_2\left(\tau_3-\tau_1,\tau_2-\tau_1\right)}{S_{\mu'';1}^{(1)}(0)S_{\mu';1}^{(1)}(0)S_{\mu;1}^{(1)}(0)}\right)$$

where the following functions were defined

$$I_1(t)=\int\limits_{\mathbb{R}}dke^{ikt}M(k),\qquad I_2\left(t_2,t_1\right)=\int\limits_{\mathbb{R}}dk\int\limits_{\mathbb{R}}dqe^{iqt_2}e^{ikt_1}Q(-k-q,k,q). \tag{4.63}$$

By introducing the following variables $t'=\tau_3-\tau_1, t=\tau_2-\tau_1$, we can immediately write down the normalized third order coherence function as

$$c_{\mu'',\mu',\mu}^{(3)}\left(t',t\right)=\left|1-4\pi i\left[\frac{I_1\left(t'-t\right)}{S_{\mu'';1}^{(1)}(0)S_{\mu';1}^{(1)}(0)}+\frac{I_1(t)}{S_{\mu;1}^{(1)}(0)S_{\mu';1}^{(1)}(0)}+\frac{I_1\left(t'\right)}{S_{\mu'';1}^{(1)}(0)S_{\mu;1}^{(1)}(0)}\right]\right.$$
$$\left.-\,12\pi i\frac{I_2\left(t',t\right)}{S_{\mu'';1}^{(1)}(0)S_{\mu';1}^{(1)}(0)S_{\mu;1}^{(1)}(0)}\right|^2+\mathcal{O}(f). \tag{4.64}$$

As before, let us begin by considering the third-order coherence correlation in the small system $1 > \gamma R = 0.1$, the results for the four different components of $c^{(3)}$ are plotted for both $t = 0$ and $t' = t$ in Figure 4.10. As one can observe, one should expect significantly more simultaneous three-phonon counting events $c^{(3)}_{1,1,1}(0)$ than simultaneous two-particle counting ones $c^{(2)}_{1,1}(0)$ in the left channel, whereas the number of rightwards propagating three-photon detections is significantly less than the number of simultaneous two-phonon countings $c^{(3)}_{2,2,2}(0) < c^{(2)}_{2,2}(0)$. Although the delay in the system is comparatively small, one can still see that the components of $c^{(3)}$ exhibit some oscillations. As one may additionally notice, as it is expected, $c^{(3)}$ saturates at a constant value at large values of its arguments, however, as opposed to the second-order coherence function, this value is different from unity. Indeed, due to the poles of the integrands of both $I_1(t)$ and $I_2(t', t)$ one effectively has

$$\lim_{t\to\infty} I_1(t) = \lim_{t\to\infty} I_2(t', t) = \lim_{t'\to\infty} I_2(t', t) = 0, \tag{4.65}$$

leading to the following limiting values of $c^{(3)}$

$$\lim_{t\to\infty} c^{(3)}_{\mu'',\mu',\mu}(t, 0) = \left| 1 - 4\pi i \frac{I_1(0)}{S^{(1)}_{\mu;1}(0) S^{(1)}_{\mu';1}(0)} \right|^2 = c^{(2)}_{\mu',\mu}(0), \tag{4.66}$$

$$\lim_{t\to\infty} c^{(3)}_{\mu'',\mu',\mu}(t, t) = \left| 1 - 4\pi i \frac{I_1(0)}{S^{(1)}_{\mu'';1}(0) S^{(1)}_{\mu';1}(0)} \right|^2 = c^{(2)}_{\mu'',\mu'}(0). \tag{4.67}$$

Note that unless $\alpha'' = \alpha$ these two limits are different, however $\lim_{t\to\infty} c^{(3)}_{\mu'',\mu',\mu}(t, 0) = \lim_{t\to\infty} c^{(3)}_{\mu'',\mu',\mu}(0, t)$ due to the symmetrization. Interestingly enough, in a local (Markovian) system it is well known that the third-order coherence function factorizes into the product of two second-order coherence functions for all times (see e.g. [43])

$$c^{(3)}_{\mu'',\mu',\mu}(t', t) \propto c^{(2)}_{\mu'',\mu'}(t')\, c^{(2)}_{\mu',\mu}(t). \tag{4.68}$$

Baring this in mind, we may introduce the following measure of non-Markovianity in three-body sector

$$N_{\mu'',\mu',\mu}(t', t) = \frac{c^{(3)}_{\mu'',\mu',\mu}(t', t)}{c^{(2)}_{\mu'',\mu'}(t')\, c^{(2)}_{\mu',\mu}(t)} \tag{4.69}$$

For a perfectly Markovian emitter, this function has to remain constant for all values of its arguments, whereas one expects this function to possess non-zero gradients in a system with delayed coherent quantum feedback. For example, $N_{1,1,1}(t, 0)$ is shown in Figure 4.11. As one may notice, despite the fact of a comparatively small delay in the system, $c^{(3)}$ does not factorize into two $c^{(2)}$s, instead, for $t \leq 2$ we see significant deviations of $c^{(3)}_{1,1,1}(t, 0)$ from $c^{(2)}_{1,1}(t)c^{(2)}_{1,1}(0)$. However, owing to the fact that $c^{(3)}_{1,1,1}(t, 0) \to c^{(2)}_{1,1}(0)$ and $c^{(2)}_{1,1}(t) \to 1$ for $t \to \infty$, the N-fucntion effectively saturates at unit value.

Let us now consider the third-order coherence function in a non-Markovian system $\gamma R = 4$. The corresponding components of the third-order coherence are shown in Figure 4.12. In analogy with the second-order coherence function, in the non-Markovian regime, the components of the
$c^{(3)}_{\mu'',\mu',\mu}(t, 0)$

$c^{(3)}_{1,1,1}$

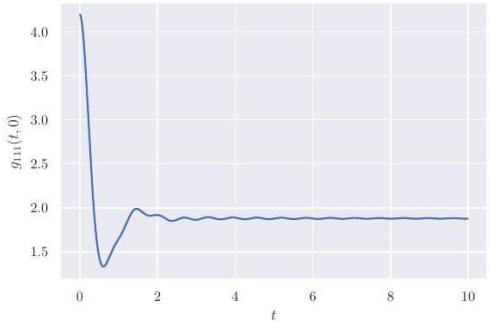

$c^{(3)}_{2,1,1}$

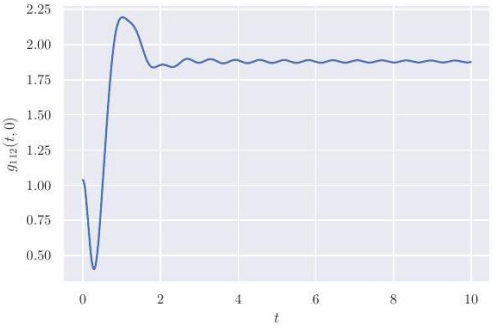

$c^{(3)}_{2,2,1}$

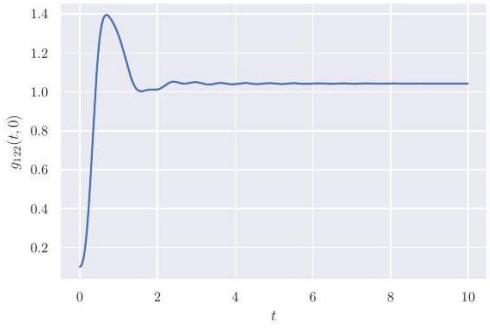

$c^{(3)}_{2,2,2}$

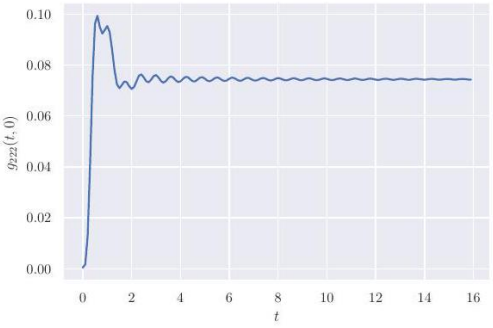

$c^{(3)}_{\mu'',\mu',\mu}(t,t)$

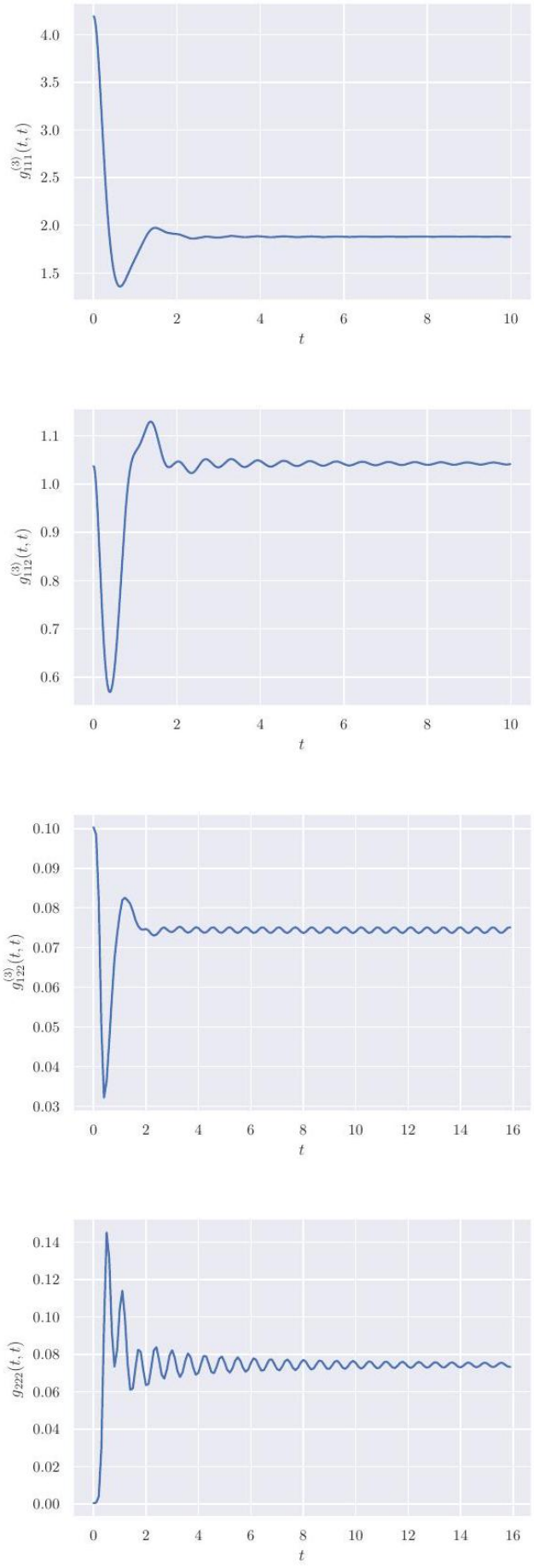

Figure 4.10: Third-order coherence function for a small atom: $R = 0.1, k_0 = 0, \Delta = 3$, and $\gamma = 1$.
$R = 0.1, k_0 = 0$

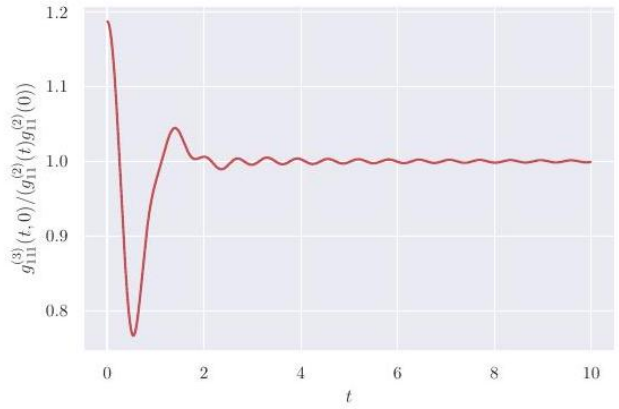

$R = 4, k_0 = 3\pi/7$

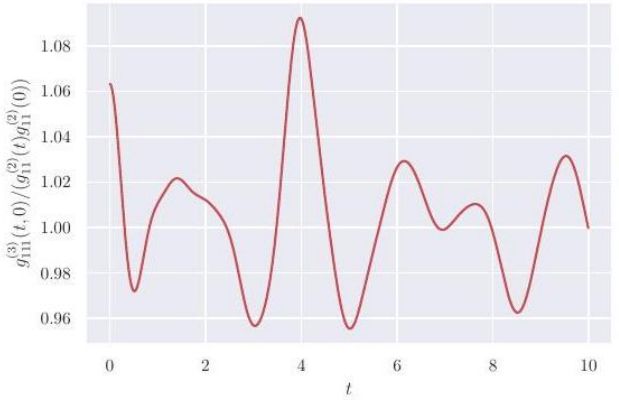

Figure 4.11: Plot of $N_{1,1,1}(t, 0)$ for both small (left) and large (right) systems. Other parameters: $\Delta = 3, \gamma = 1$.

third-order coherence correlation are not rapidly saturating at a constant value, but instead, demonstrate complicated oscillation patterns. Another apparent similarity is the presence of nondifferentiable structures at integer multiples of the delay time R. The nature of these features may again be attributed to the poles in the single-particle propagators, which naturally appear in the defenition of the three-phonon scattering matrix. However, some of the features of the more Markovian model discussed above are still retained. Namely, by reading off the values of $c^{(2)}$ at $\tau = 0$ from Figure 4.8, we see that one shall expect significantly more simultaneous three-phonon counting events in the first channel $c^{(3)}_{1,1,1}(0) > c^{(2)}_{1,1}(0)$. Analogously, in the second radiation channel triplets of phonons are clearly more antibunched than phonon doublets. The $N_{1,1,1}(t, 0)$-function corresponding to the non-Markovian parameter set is also presented in Figure 4.11. Now, we see that $c^{(3)}_{1,1,1}(t, 0)$ significantly deviates from the factorization into a pair of $c^{(2)}$s. This result is, of course, a reminiscence of the completely connected part of the two-body effective vertex function which shows itself non-zero, only in the non-Markovian systems.

In addition to the exact solution (red), an approximate solution based on the weak correlation approximation (magenta) is also shown in Figure 4.12. Although the agreement between the two may be said acceptable on average, certain discrepancies are still present. First of all, in most cases, we see that weak correlation approximation tends to show incorrect oscillation amplitudes by either over or underestimating them. Secondly, many features of the full exact solution, such as inflection and saddle points are either not present or appear to be suppressed in the approximate solution. Despite these apparent, but rather small disharmonies, one can say that weak correlation approximation shows itself rather successful, in turn proving the assertion about the domain of its validity made in Chapter 3.

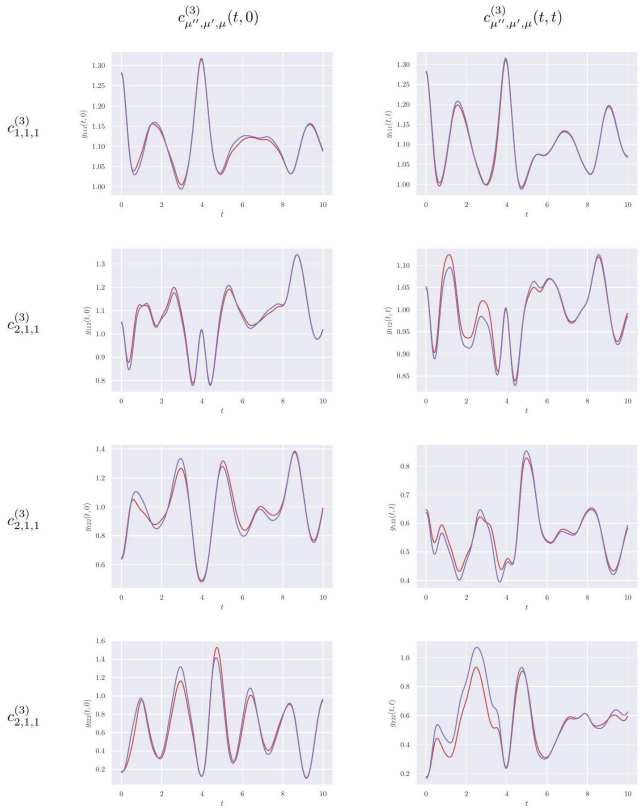

Figure 4.12: Third-order coherence function for a giant atom $R = 4, k_0 = 3\pi/7, \Delta = 3$, and $\gamma = 1$. Red: exact solution. Magneta: weak correlation approximation.

7.11 Real-Time Dynamics in Waveguide QED

7.11.1 Introduction and Generalities

In Schrödinger picture, these are states which evolve in time, as opposed to the operator evolution picture of Heisenberg. Whenever the dynamics of a quantum system is generated by an autonomous Hamiltonian $\partial_t \mathcal{H} = 0$, the following prescription holds true. Given a state of a system $|\psi\rangle(0)$ at time $t = 0$ (for an autonomous system initial time may always be set to 0 by time-translational invariance), state of the system at a later time $t, |\psi\rangle(t)$ is given by the action of a one-parameter family of unitary transformations $\mathcal{U}(t)$ on the initial state

$$|\psi\rangle(t) = \mathcal{U}(t)|\psi\rangle(0) \tag{5.1}$$

By unitarity the state of a system at a given preceding time is thus obtained by the action of the adjoint of $\mathcal{U}(t)$ on $|\psi\rangle(0)$, i.e. $\mathcal{U}(-t) = \mathcal{U}^\dagger(t)$. As an element of any unitary group admitting for projective representations, $\mathcal{U}(t)$ may be written as an exponential map of a certain anti-hermitian generator $\mathcal{U}(t) = \exp(-i\mathcal{H}t)$, it turns out the generator of the group of time translations is precisely ($-i$ times) the Hamiltonian operator of a quantum system, as it is the case in the classical description.

Here, we would like to develop a particularly convenient representation of the unitary evolution operator, which is going to allow us to extend the formalism of the scattering theory to include studies of real-time dynamics. Such a representation relies on the fact that one can relate any one-parameter family of unitary transformations to the resolvent of its generator. Namely, given a one-parameter family of unitary transformations $\mathcal{U}(t) = \exp(-i\mathcal{H}t)$, it may be written as an inverse Laplace transform of the resolvent of $\mathcal{H}$

$$\mathcal{U}(t) = \exp(-i\mathcal{H}t) = \int\limits_{C_+} \frac{dz}{2\pi i} \frac{e^{-izt}}{z - \mathcal{H}} := \lim_{\eta \searrow 0} \int\limits_{+\infty}^{-\infty} \frac{d\epsilon}{2\pi i} \frac{e^{-i\epsilon t}}{\epsilon - \mathcal{H} + i\eta} \equiv \int\limits_{+\infty}^{-\infty} \frac{d\epsilon}{2\pi i} e^{-i\epsilon t} \mathcal{G}_R(\epsilon) \tag{5.2}$$

It then follows that the backward evolution operator admits for the following representation

$$\mathcal{U}(-t)=\mathcal{U}^{\dagger}(t)=\int\limits_{C_-}\frac{dz}{2\pi i}\frac{e^{izt}}{z-\mathcal{H}}:=\lim_{\eta\searrow 0}\int\limits_{-\infty}^{+\infty}\frac{d\epsilon}{2\pi i}\frac{e^{i\epsilon t}}{\epsilon-\mathcal{H}-i\eta}\equiv\int\limits_{-\infty}^{+\infty}\frac{d\epsilon}{2\pi i}e^{i\epsilon t}\mathcal{G}_A(\epsilon) \tag{5.3}$$

Now, succeeding to represent the unitary evolution operator in terms of the retarded (advanced) Green's operator we reduce the problem of finding the former object to the determination of the
latter one. Not to restrict ourselves to consideration of retarded or advanced operators of Green, in what follows we are going to consider a generic resolvent $\mathcal{G}^{-1}(z)=z-\mathcal{H}$, for $z\in\mathbb{C}$.

Let us now consider the following Neumann series of the resolvent of $\mathcal{H}$, baring the perturbed/unperturbed decomposition $\mathcal{H}=\mathcal{H}_0+\mathcal{V}$ in mind

$$\mathcal{G}(z)=\frac{1}{z-\mathcal{H}}=\frac{1}{z-\mathcal{H}_0-\mathcal{V}}=\sum_{n=0}^{\infty}\left(\mathcal{G}_0(z)\mathcal{V}\right)^n\mathcal{G}_0(z)=\mathcal{G}_0(z)+\sum_{n=1}^{\infty}\left(\mathcal{G}_0(z)\mathcal{V}\right)^n\mathcal{G}_0(z)$$
$$=\mathcal{G}_0(z)+\begin{cases}\mathcal{G}_0(z)\mathcal{V}\sum\limits_{n=0}^{\infty}\left(\mathcal{G}_0(z)\mathcal{V}\right)^n\mathcal{G}_0(z)\\ \sum\limits_{n=0}^{\infty}\left(\mathcal{G}_0(z)\mathcal{V}\right)^n\mathcal{G}_0(z)\mathcal{V}\mathcal{G}_0(z)\end{cases}=\mathcal{G}_0(z)+\begin{cases}\mathcal{G}_0(z)\mathcal{V}\mathcal{G}(z)\\ \mathcal{G}(z)\mathcal{V}\mathcal{G}_0(z)\end{cases} \tag{5.4}$$

Here, the bare propagator $\mathcal{G}_0(z)$ was associated with the unperturbed Hamiltonian $\mathcal{H}_0$ in the usual manner $\mathcal{G}_0^{-1}(z)=z-\mathcal{H}_0$. Now by inserting the resulting left Dyson equation $\mathcal{G}(z)=\mathcal{G}_0(z)+\mathcal{G}(z)\mathcal{V}\mathcal{G}_0(z)$ into the right one $\mathcal{G}(z)=\mathcal{G}_0(z)+\mathcal{G}_0(z)\mathcal{V}\mathcal{G}(z)$, we arrive at the following result

$$\mathcal{G}(z)=\mathcal{G}_0(z)+\mathcal{G}_0(z)\mathcal{T}(z)\mathcal{G}_0(z),\quad \mathcal{T}(z)=\mathcal{V}+\mathcal{V}\mathcal{G}(z)\mathcal{V} \tag{5.5}$$

Thus, one sees that the search for $\mathcal{G}(z)$ is reducible to the problem of determination of the transition operator $\mathcal{T}(z)$, just as it is the case in the theory of scattering. However, there exists a major difference: in principle, much more matrix elements of $\mathcal{T}$ have to be computed. Namely, in order to study transient effects within a Q-qubit waveguide QED, given an initial state possessing N excitations, all of the $(D(N,Q))^2$ matrix elements between all of the $D(N,Q)$ basis elements spanning the N-excitation subspace have now to be computed.

7.11.2 Resummation of the Perturbation Series for the Propagator in $Q=1$ Waveguide QED

As in the case with the scattering theory, let us start with the simplest problem in waveguide QED - a single qubit setup. To completely determine $\mathcal{G}(z)$ in the P-excitation subspace of the system, one seeks the following four matrix elements of the transition operator

$$\begin{array}{ll}\langle P',0|\mathcal{T}(z)|P,0\rangle, & \langle (P-1)',1|\mathcal{T}(z)|(P-1),1\rangle\\ \langle (P-1)',1|\mathcal{T}(z)|P,0\rangle, & \langle P',0|\mathcal{T}(z)|(P-1),1\rangle.\end{array} \tag{5.6}$$

Our formalism tells us that

$$\left\langle P',0\left|\mathcal{T}^{(1)}(z)\right|P,0\right\rangle=\langle P',0|\,a^{\dagger}_{s_1'}v_{s_1'}\mathcal{G}^{(1)}(z)v^{\dagger}_{s_1}a_{s_1}|P,0\rangle$$
$$+\left\langle P',0\left|a^{\dagger}_{s_1'}v_{s_1'}\mathcal{G}^{(1)}(z)\mathcal{W}^{(1)}(z)\mathcal{G}^{(1)}(z)v^{\dagger}_{s_1}a_{s_1}\right|P,0\right\rangle, \tag{5.7}$$

where

$$\mathcal{G}^{(1)}(z)=\left(\mathcal{G}_0^{-1}(z)-\Sigma^{(1)}(z)\right)^{-1},$$
$$\Sigma^{(1)}(z)=v_s^{\dagger}\mathcal{G}_0\left(z-\omega_s\right)v_s$$
$$\mathcal{W}^{(1)}(z)=\mathcal{R}^{(1)}(z)+\mathcal{R}^{(1)}(z)\mathcal{G}^{(1)}(z)\mathcal{W}^{(1)}(z),$$

$$\mathcal{R}^{(1)}(z) = a^\dagger_{s'_1} v^\dagger_{s_1} \mathcal{G}_0 \left(z - \omega_{s_1} - \omega_{s'_1}\right) v_{s'_1} a_{s_1}$$

Another diagonal element is:

$$\begin{aligned}
\langle (P-1)', 1|\mathcal{T}(z)|(P-1), 1\rangle &= \left\langle (P-1)', 1 \left| a_{s'} v^\dagger_{s'} \mathcal{G}(z) v_s a^\dagger_s \right| (P-1), 1 \right\rangle \\
&= \sum_{n=0}^{\infty} \left\langle (P-1)', 1 \left| a_{s'} v^\dagger_{s'} \left(\mathcal{G}_0(z)\mathcal{V}\right)^n \mathcal{G}_0(z) v_s a^\dagger_s \right| (P-1), 1 \right\rangle \\
&= \sum_{n=0}^{\infty} \left\langle (P-1)', 1 \left| a_{s'} v^\dagger_{s'} \left(\mathcal{G}_0(z)\mathcal{V}\mathcal{G}_0(z)\mathcal{V}\right)^n \mathcal{G}_0(z) v_s a^\dagger_s \right| (P-1), 1 \right\rangle = \\
&= \sum_{n=0}^{\infty} \left\langle (P-1)', 1 \left| a_{s'} v^\dagger_{s'} \left(\mathcal{G}_0(z) v_{s'_1} a^\dagger_{s'_1} \mathcal{G}_0(z) a_{s_1} v^\dagger_{s_1}\right)^n \mathcal{G}_0(z) v_s a^\dagger_s \right| (P-1), 1 \right\rangle
\end{aligned}$$

where we have utilized our standard arguments of nilpotency and subtraction of odd terms from the above geometric series. Now, we rewrite the above as

$$\begin{aligned}
&\langle (P-1)', 1|\mathcal{T}(z)|(P-1), 1\rangle = \\
&= \sum_{n=0}^{\infty} \left\langle (P-1)', 1 \left| \mathcal{G}_0^{-1}(z)\mathcal{G}_0(z) a_{s'} v^\dagger_{s'} \left(\mathcal{G}_0(z) v_{s'_1} a^\dagger_{s'_1} \mathcal{G}_0(z) a_{s_1} v^\dagger_{s_1}\right)^n \mathcal{G}_0(z) v_s a^\dagger_s \mathcal{G}_0(z)\mathcal{G}_0^{-1}(z) \right| (P-1), 1 \right\rangle \\
&= \sum_{n=1}^{\infty} \left\langle (P-1)', 1 \left| \mathcal{G}_0^{-1}(z) \left(\mathcal{G}_0(z) a_{s_1} v^\dagger_{s_1} \mathcal{G}_0(z) v_{s'_1} a^\dagger_{s'_1}\right)^n \mathcal{G}_0(z)\mathcal{G}_0^{-1}(z) \right| (P-1), 1 \right\rangle \\
&= \sum_{n=0}^{\infty} \left\langle (P-1)', 1 \left| \mathcal{G}_0^{-1}(z) \left(\mathcal{G}_0(z) \left[\Sigma^{(1)}(z) + \mathcal{R}^{(1)}(z)\right]\right)^n \mathcal{G}_0(z)\mathcal{G}_0^{-1}(z) \right| (P-1), 1 \right\rangle \\
&\quad - \left\langle (P-1)', 1 \left| \mathcal{G}_0^{-1}(z) \right| (P-1), 1 \right\rangle = \\
&= \left\langle (P-1)', 1 \left| \mathcal{G}_0^{-1}(z)\mathcal{G}^{(1)}(z)\mathcal{G}_0^{-1}(z) \right| (P-1), 1 \right\rangle \\
&\quad + \left\langle (P-1)', 1 \left| \mathcal{G}_0^{-1}(z)\mathcal{G}^{(1)}(z)\mathcal{W}^{(1)}(z)\mathcal{G}^{(1)}(z)\mathcal{G}_0^{-1}(z) \right| (P-1), 1 \right\rangle - \\
&\quad - \left\langle (P-1)', 1 \left| \mathcal{G}_0^{-1}(z) \right| (P-1), 1 \right\rangle .
\end{aligned}$$

Note that this calculation proves our assertation, made in Chapter 3 about the vanishment of the $|1\rangle \to |1\rangle$ scattering processes, since $\mathcal{G}_0^{-1}(z)$ is annulled when being put on-shell.

Now, let us consider the off-diagonal matrix elements. As opposed to the diagonal case, the only terms in the Neumann series allowed by RWA are the odd ones

$$\begin{aligned}
&\langle (P-1)', 1|\mathcal{T}(z)|P, 0\rangle = \\
&= \langle (P-1)', 1|\mathcal{V}|P, 0\rangle + \langle (P-1)', 1|\mathcal{V}\mathcal{G}(z)\mathcal{V}|P, 0\rangle \\
&= \left\langle (P-1)', 1 \left| a_s v^\dagger_s \right| P, 0 \right\rangle + \sum_{n=0}^{\infty} \left\langle (P-1)', 1 \left| a_{s'} v^\dagger_{s'} \left(\mathcal{G}_0(z)\mathcal{V}\mathcal{G}_0(z)\mathcal{V}\right)^n \mathcal{G}_0(z)\mathcal{V}\mathcal{G}_0(z) a_s v^\dagger_s \right| P, 0 \right\rangle \\
&= \left\langle (P-1)', 1 \left| a_s v^\dagger_s \right| P, 0 \right\rangle + \\
&\quad + \sum_{n=0}^{\infty} \left\langle (P-1)', 1 \left| a_{s'} v^\dagger_{s'} \left(\mathcal{G}_0(z) v_{s_1} a^\dagger_{s_1} \mathcal{G}_0(z) v^\dagger_{s'_1} a_{s'_1}\right)^n \mathcal{G}_0(z) v_{s''} a^\dagger_{s''} \mathcal{G}_0(z) a_s v^\dagger_s \right| P, 0 \right\rangle \\
&= \sum_{n=0}^{\infty} \langle (P-1)', 1| \mathcal{G}_0^{-1}(z) \left(\mathcal{G}_0(z) a_{s_1} v^\dagger_{s_1} \mathcal{G}_0(z) v_{s'_1} a^\dagger_{s'_1}\right)^n \mathcal{G}_0(z) a_s v^\dagger_s |P, 0\rangle \\
&= \left\langle (P-1)', 1 \left| \mathcal{G}_0^{-1}(z)\mathcal{G}^{(1)}(z) a_s v^\dagger_s \right| P, 0 \right\rangle + \left\langle (P-1)', 1 \left| \mathcal{G}_0^{-1}(z)\mathcal{G}^{(1)}(z)\mathcal{W}^{(1)}(z)\mathcal{G}^{(1)}(z) a_s v^\dagger_s \right| P, 0 \right\rangle .
\end{aligned}$$

The last off-diagonal element is

$$
\begin{aligned}
&\langle P',0|\mathcal{T}(z)|(P-1),1\rangle = \\
&= \left\langle P',0\left|a_s^\dagger v_s\right|(P-1),1\right\rangle + \left\langle P',0\left|a_s^\dagger v_s \mathcal{G}(z) a_{s'}^\dagger v_{s'}\right|(P-1),1\right\rangle = \\
&= \left\langle P',0\left|a_s^\dagger v_s\right|(P-1),1\right\rangle + \sum_{n=0}^{\infty}\left\langle P',0\left|a_s^\dagger v_s \left(\mathcal{G}_0(z)\mathcal{V}\mathcal{G}_0(z)\mathcal{V}\right)^n \mathcal{G}_0(z)\mathcal{V}\mathcal{G}_0(z) a_{s'}^\dagger v_{s'}\right|(P-1),1\right\rangle = \\
&= \left\langle P',0\left|a_s^\dagger v_s\right|(P-1),1\right\rangle + \sum_{n=0}^{\infty}\left\langle P',0\left|a_s^\dagger v_s \left(\mathcal{G}_0(z) v_{s_2}^\dagger a_{s_2} \mathcal{G}_0(z) v_{s_1'} a_{s_1'}^\dagger\right)^n \mathcal{G}_0(z) v_{s_1}^\dagger a_{s_1} \mathcal{G}_0(z) a_{s'}^\dagger v_{s'}\right|(P-1),1\right\rangle = \\
&= \sum_{n=0}^{\infty}\left\langle P',0\left|a_s^\dagger v_s \left(\mathcal{G}_0(z) v_{s_1}^\dagger a_{s_1} \mathcal{G}_0(z) a_{s_1'}^\dagger v_{s_1'}\right)^n \mathcal{G}_0(z)\mathcal{G}_0^{-1}(z)\right|(P-1),1\right\rangle \\
&= \left\langle P',0\left|a_s^\dagger v_s \mathcal{G}^{(1)}(z)\mathcal{G}_0^{-1}(z)\right|(P-1),1\right\rangle + \left\langle P',0\left|a_s^\dagger v_s \mathcal{G}^{(1)}(z)\mathcal{W}^{(1)}(z)\mathcal{G}^{(1)}(z)\mathcal{G}_0^{-1}(z)\right|(P-1),1\right\rangle .
\end{aligned}
$$

So all of the non-trivial information about the dynamics may be drawn from the knowledge of $\mathcal{G}^{(1)}(z)$ and $\mathcal{W}^{(1)}(z)$ as it is the case in the theory of scattering!

Now, by making use of the relation between the Green's function and the transition operator, we are ready to write the former as

$$
\mathcal{G}(z) = \begin{pmatrix} \mathcal{G}_{11}(z) & \mathcal{G}_{10}(z) \\ \mathcal{G}_{01}(z) & \mathcal{G}_{00}(z) \end{pmatrix}
$$

where

$$
\begin{aligned}
\mathcal{G}_{11}(z) &= \left\langle 1\left|\mathcal{G}^{(1)}(z)\left[1+\mathcal{W}^{(1)}(z)\mathcal{G}^{(1)}(z)\right]\right|1\right\rangle, \\
\mathcal{G}_{00}(z) &= \left\langle 0\left|\mathcal{G}_0(z)\left(1+a_{s_1'}^\dagger v_{s_1'}\mathcal{G}^{(1)}(z)\left[1+\mathcal{W}^{(1)}(z)\mathcal{G}^{(1)}(z)\right]v_{s_1}^\dagger a_{s_1}\mathcal{G}_0(z)\right)\right|0\right\rangle, \\
\mathcal{G}_{10}(z) &= \left\langle 1\left|\left[1+\mathcal{W}^{(1)}(z)\mathcal{G}^{(1)}(z)\right]\mathcal{G}^{(1)}(z) a_s v_s^\dagger \mathcal{G}_0(z)\right|0\right\rangle, \\
\mathcal{G}_{01}(z) &= \left\langle 0\left|\mathcal{G}_0(z) a_s^\dagger v_s \mathcal{G}^{(1)}(z)\left[1+\mathcal{W}^{(1)}(z)\mathcal{G}^{(1)}(z)\right]\right|1\right\rangle .
\end{aligned}
$$

$$
\begin{aligned}
\mathcal{G}^{(1)}(z) &= \left(\mathcal{G}_0^{-1}(z) - \Sigma^{(1)}(z)\right)^{-1}, \\
\Sigma^{(1)}(z) &= v_s^\dagger \mathcal{G}_0\left(z-\omega_s\right) v_s \\
\mathcal{W}^{(1)}(z) &= \mathcal{R}^{(1)}(z) + \mathcal{R}^{(1)}(z)\mathcal{G}^{(1)}(z)\mathcal{W}^{(1)}(z), \\
\mathcal{R}^{(1)}(z) &= a_{s_1'}^\dagger v_{s_1}^\dagger \mathcal{G}_0\left(z-\omega_{s_1}-\omega_{s_1'}\right) v_{s_1'} a_{s_1}
\end{aligned}
$$

7.11.3 General Dynamics in Single Excitation Subspace

In this section, we would like to stress that once one established the general relations for the dynamics in the single excitation subspace of a single qubit, these relations hold in the case of a single excitation dynamics in multiple qubit systems, precisely as it was the case in the scattering theory. Namely, given a generic single excitation subspace sate at initial time $t = 0$

$$
|\psi\rangle(0) = \sum_{\mu=1}^{C}\int_{B_\mu} dk \psi_\mu(k) a_\mu^\dagger(k)|\Omega\rangle\otimes|g\rangle + \sum_{n=1}^{Q}\eta_n|\Omega\rangle\otimes\sigma_+^{(n)}|g\rangle. \tag{5.14}
$$

The state at any later time t is given by

$$
|\psi\rangle(t) = \sum_{\mu=1}^{C}\int_{B_\mu} dk \psi_\mu(t,k) a_\mu^\dagger(k)|\Omega\rangle\otimes|g\rangle + \sum_{n=1}^{Q}\eta_n(t)|\Omega\rangle\otimes\sigma_+^{(n)}|g\rangle, \tag{5.15}
$$

where

$$\eta_n(t) = \sum_{m=1}^{Q} \eta_m \int\limits_{C_+} \frac{dz}{2\pi i} \left\langle \Omega \right| \otimes \left\langle g \left| \sigma_-^{(n)} \mathcal{G}^{(1)}(z) \right| \Omega \right\rangle \otimes \sigma_+^{(m)} \left| g \right\rangle e^{-izt}$$
$$+ \sum_{\mu=1}^{C} \sum_{m=1}^{Q} \int\limits_{B_\mu} dk \int\limits_{C_+} \frac{dz}{2\pi i} g^*_{\mu,m}(k) \left\langle \Omega \right| \otimes \left\langle g \left| \sigma_-^{(n)} \mathcal{G}^{(1)}(z) \sigma_+^{(m)} \mathcal{G}_0\left(z - \omega_\mu(k)\right) \right| \Omega \right\rangle \otimes \left| g \right\rangle \psi_\mu(k) e^{-izt} \tag{5.16}$$

$$\psi_\mu(t,k) = \int\limits_{C_+} \frac{dz}{2\pi i} \left\langle \Omega \right| \otimes \left\langle g \left| \mathcal{G}_0\left(z - \omega_\mu(k)\right) \right| \Omega \right\rangle \otimes \left| g \right\rangle \psi_\mu(k) e^{-izt}$$
$$+ \int\limits_{C_+} \frac{dz}{2\pi i} \sum_{\nu=1}^{C} \sum_{n'=1}^{Q} \sum_{n=1}^{Q} \int\limits_{\mathbb{R}} dp g_{\mu,n'}(k) g^*_{\nu,n}(p) \langle \Omega | \otimes \langle g | \mathcal{G}_0\left(z - \omega_\mu(k)\right) \sigma_-^{(n')} \mathcal{G}^{(1)}(z) \sigma_+^{(n)} \mathcal{G}_0\left(z - \omega_\nu(p)\right)$$
$$\times |\Omega\rangle \otimes |g\rangle \psi_\nu(p) e^{-izt}$$
$$+ \int\limits_{C_+} \frac{dz}{2\pi i} \sum_{m=1}^{Q} \sum_{n=1}^{Q} \eta_n \left\langle \Omega \right| \otimes \left\langle g \left| \mathcal{G}_0\left(z - \omega_\mu(k)\right) g_{\mu,m}(k) \sigma_-^{(m)} \mathcal{G}^{(1)}(z) \sigma_+^{(n)} \right| \Omega \right\rangle \otimes \left| g \right\rangle e^{-izt}, \tag{5.17}$$

and

$$\mathcal{G}^{(1)}(z) = z - \mathcal{H}_0 - \Sigma^{(1)}(z) \tag{5.18}$$

Here, $\Sigma(z)$ is given by (3.31). So, we see that the only bit required to study dynamics in single excitation subspace is the dressed Green's function $\mathcal{G}^{(1)}$.

Of particular interest are the so-called spontaneous emission problems, whereby the initial conditions are chosen such that $\psi_\mu(k) = 0, \forall \mu$, whereas $\eta_n \neq 0$. In this class of problems, one can identify two types of observables, the single-qubit occupation probabilities

$$|\eta_n(t)|^2 = \left| \sum_{m=1}^{Q} \eta_m \int\limits_{C_+} \frac{dz}{2\pi i} \left\langle \Omega \right| \otimes \left\langle g \left| \sigma_-^{(n)} \mathcal{G}^{(1)}(z) \right| \Omega \right\rangle \otimes \sigma_+^{(m)} \left| g \right\rangle e^{-izt} \right|^2 \tag{5.19}$$

As well as the so-called emission spectral densities defined by the following limit

$$S_\mu^{\text{emission}}(k) = \left| \lim_{t\to\infty} \psi_\mu(t,k) \right|^2 =$$
$$= \left| \lim_{t\to\infty} \int\limits_{C_+} \frac{dz}{2\pi i} \sum_{m=1}^{Q} \sum_{n=1}^{Q} \eta_n \left\langle \Omega \right| \otimes \left\langle g \left| \mathcal{G}_0\left(z - \omega_\mu(k)\right) g_{\mu,m}(k) \sigma_-^{(m)} \mathcal{G}^{(1)}(z) \sigma_+^{(n)} \right| \Omega \right\rangle \otimes \left| g \right\rangle e^{-izt} \right|^2. \tag{5.20}$$

However, we would like to emphasize that emission spectral density is not always a well-defined quantity. In particular, it could not be made any sense of in the system with bound states, i.e. systems were the pole equation $\left(\tilde{G}^{(1)}(z_p)\right)^{-1} = 0$ admits for the zero imaginary part solutions $\text{Im}\{z_p\} = 0$. Indeed, in such a case neither $\lim_{t\to\infty} \eta_n(t) = 0$, nor the above limit (5.20) is well defined. Instead, such a system ends up in a superposition of bound states of a photon and emitters. For example, such a situation (where one encounters poles of the propagator on the real axis) frequently happens in the systems with nonlinear dispersion relation. In this class of systems, as one may easily anticipate, the scattering problem is not well defined either. In the long time run, the system is going to evolve into the bound state, thus not enabling

any meaningful definition of spectral densities or coherence functions. Mathematically, these complications are related to the fact that the limits (3.4) used to define the Møller operators are not well-posed, in a rather mathematically unrefined manner one can say that the domain of $\mathcal{H}$ is larger than that of $\mathcal{H}_0$. In the systems where the poles of $\tilde{G}^{(1)}(z)$ lie entirely in the lower half of the complex z plane, on the other hand, the excitation never remains localized in the emitter and decays into the continuum, in such a case, the emission spectral density is given by the sole contribution of the poles of $\hat{G}_0\left(z-\omega_\mu(k)\right)$ at $z=\omega_\mu(k)+\frac{1}{2}\sum_{n=1}^{Q}\Delta_n$ to the integral in (5.20).

7.11.4 Spontaneous Emission of a Giant Acoustic Atom

Let us now consider the problem of quantum decay of a symmetric giant acoustic atom into the surface acoustic waves, for that we assume the initial state of the following form

$$|\psi\rangle(0)=|1\rangle\otimes|\Omega\rangle. \tag{5.21}$$

The state of the system at a later time t is given by

$$|\psi\rangle(t)=\mathcal{U}(t)|\psi(0)\rangle=a(t)|1\rangle\otimes|\Omega\rangle+|0\rangle\otimes\sum_{\mu=1,2}\int_{\mathbb{R}}dk b_\mu(k,t)a_\mu^\dagger(k)|\Omega\rangle \tag{5.22}$$

Using the relations (5.10) and (5.13), we obtain

$$a(t)=\int_{C_+}\frac{dz}{2\pi i}\frac{e^{-izt}}{z+\Delta+i\gamma\left[1+\exp\left(i\left(z+k_0\right)R\right)\right]} \tag{5.23}$$

$$b_\mu(k,t)=g_\mu(k)\int_{C_+}\frac{dz}{2\pi i}\frac{1}{z-k}\frac{e^{-izt}}{z+\Delta+i\gamma\left[1+\exp\left(i\left(z+k_0\right)R\right)\right]} \tag{5.24}$$

Let us start by calculating the survival probability $P_s(t)=|a(t)|^2$, for that we consider the first of the above integrals

$$\begin{aligned}
a(t)&=e^{ik_0t}\int_{C_+}\frac{dz}{2\pi i}\frac{e^{-izt}}{z-\Omega+i\gamma\left[1+e^{izR}\right]}\\
&=e^{ik_0t}\sum_{n=0}^{\infty}(-i\gamma)^n\int_{C_+}\frac{dz}{2\pi i}\frac{e^{-iz(t-nR)}}{(z-\Omega+i\gamma)^{n+1}}\\
&=e^{ik_0t}\sum_{n=0}^{\infty}\frac{(-1)^n(\gamma(t-nR))^n}{n!}\Theta(t-nR)e^{-i(\Omega-i\gamma)(t-nR)}.
\end{aligned} \tag{5.25}$$

Non-Markovian nature of this expression is extremely apparent. Namely, one can see that this expression possesses an infinite number of non-differentiable revival peaks at all natural multiples of the delay time $t=nR,\quad n\in\mathbb{N}_0$. Let us now compute the momentum-space wavefunction of an emitted phonon given by integral

$$\begin{aligned}
b_\mu(k,t)&=g_\mu(k)\int_{C_+}\frac{dz}{2\pi i}\frac{1}{z-k}\frac{e^{-izt}}{z+\Delta+i\gamma\left[1+\exp\left(i\left(z+k_0\right)R\right)\right]}\\
&=g_\mu(k)\sum_{n=0}^{\infty}(-i\gamma)^ne^{ink_0R}\int_{C_+}\frac{dz}{2\pi i}\frac{1}{z-k}\frac{e^{-iz(t-nR)}}{(z+\Delta+i\gamma)^{n+1}}\\
&=g_\mu(k)\sum_{n=0}^{\infty}(-i\gamma)^ne^{ink_0R}\Theta(t-nR)\left(\frac{e^{-ik(t-nR)}}{(k+\Delta+i\gamma)^{n+1}}+\varphi_n(k,t)\right)
\end{aligned} \tag{5.26}$$

where we have defined

$$\varphi_n(k,t) = \frac{1}{n!}\frac{d^n}{dz^n}\frac{e^{-iz(t-nR)}}{z-k}\bigg|_{z=-\Delta-i\gamma} = -\sum_{m=0}^{n}\frac{(-i(t-nR))^m e^{i(\Delta+i\gamma)(t-nR)}}{m!(k+\Delta+i\gamma)^{n-m+1}}. \tag{5.27}$$

In the limit of large times one has $a(t) \to 0$ and $\varphi_n(k,t) \to 0$, so the phononic wavefunctions approach

$$b_\mu(k, t\to\infty) \to \frac{g_\mu(k)e^{-ikt}}{k+\Delta+i\gamma}\sum_{n=0}^{\infty}\frac{\left(-i\gamma e^{i(k+k_0)R}\right)^n}{(k+\Delta+i\gamma)^n} = \frac{g_\mu(k)e^{-ikt}}{k+\Delta+i\gamma\left[1+e^{i(k+k_0)R}\right]} \tag{5.28}$$

Thus the emission spectral density can be written as

$$S_\mu^{\text{emission}}(k) = |b_\mu(k,t\to\infty)|^2 = \frac{\gamma}{2\pi}\frac{1+\cos\left((k+k_0)R\right)}{\left|k+\Delta+i\gamma\left[1+e^{i(k+k_0)R}\right]\right|^2} \equiv -\frac{1}{2\pi}\operatorname{Im}\left\{\tilde{G}^{(1)}(k)\right\} \tag{5.29}$$

Both survival probabilities and the corresponding emission spectral densities are shown in Figure 5.1. As it is the case in the theory of scattering, spectral densities of emission show an infinite number of sharp, bound-state-like peaks residing near the origin of momentum space. Again, one can see that those peaks correspond to the resonances $k \sim \frac{\pi n}{R}$, $n \in \left\{m \in \mathbb{Z} \,\middle|\, \frac{m}{2} \notin \mathbb{Z}\right\}$ of the effective cavity formed by the two connection points of a giant atom. Survival probability, in its turn, demonstrates an infinite series of revival peaks at all natural multiples of R, as was anticipated above. For significant delay times, contributions to the survival probability coming from each interval $mT < t < (m+1)T$ are peaked near $t = mT$ and may be approximately thought of as not overlapping. Baring this in mind, for $\gamma R \gg 1$, to a good approximation we can write

$$|a(t)|^2 \approx \sum_{n=0}^{\infty}\Theta(t-nR)a_n(t), \quad a_n(t) = \frac{(\gamma(t-nR))^{2n}}{(n!)^2}e^{-2\gamma(t-nR)} \tag{5.30}$$

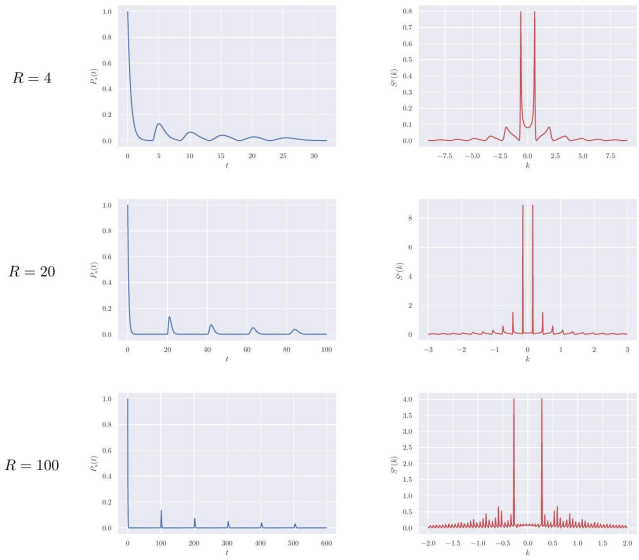

Figure 5.1: Left: survival probability of a giant atom. Right: emission power spectrum. Other parameters: $k_0 = 2\pi, \Delta = 0$, and $\gamma = 1$.

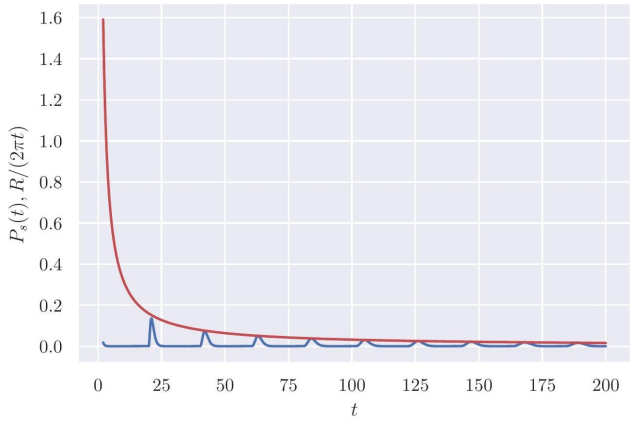

Figure 5.2: Blue: Survival probability of a giant atom for $\gamma = 1, k_0 = 2\pi, \Delta$, and $R = 20$. Red: Asymptotic formula (5.33).

This approximate result may be used to estimate the height and the position of the n^{th} peak. The position of the n^{th} peak is determined from the extremum condition $\frac{da_n(t)}{dt} = 0$ to be

$$t_n \approx n\left(R + \frac{1}{\gamma}\right) \tag{5.31}$$

which, in turn, leads to the following approximate expression for the height of the n^{th} peak

$$h_n \approx a_n\left(t_n\right) \approx \frac{n^{2n}}{(n!)^2} e^{-2n} \tag{5.32}$$

Using the Stirling's formula $n! \sim \sqrt{2\pi n} n^n e^{-n}$, we deduce the following asymptotic expression for the hight of the n^{th} peak

$$h_n \sim \frac{1}{2\pi n} \tag{5.33}$$

which shows a universal subexponential decay of a giant atom system $|\alpha(t)|^2 \sim \frac{R}{2\pi t}$. Comparison between the exact integration of dynamics and the asymptotic formula (5.33) is shown in Figure 5.2.

7.11.5 Dynamics of Single Excitation States in the System of Two Distant Qubits

Let's consider two distant qubits coupled to a one-dimensional bi-directional transmission line. Assuming broadband limit, linear dispersion of waveguide excitations and letting the distance between the emitters to be R we may write the corresponding Hamiltonian as $\mathcal{H} = \mathcal{H}_0 + \mathcal{V}$, where

$$\mathcal{H}_0 = \frac{1}{2}\sum_{n=1,2} \Delta_n \sigma_3^{(n)} + \sum_{\mu=1,2} \int_{\mathbb{R}} dk \omega_\mu(k) a_\mu^\dagger(k) a_\mu(k), \tag{5.34}$$

$$\mathcal{V} = \sum_{\mu=1,2}\sum_{n=1,2} \int_{\mathbb{R}} dk \left[g_{\mu,n}(k) a_\mu^\dagger(k) \sigma_-^{(n)} + g_{\mu,n}^*(k) \sigma_+^{(n)} a_\mu(k) \right], \tag{5.35}$$

where $\omega_\mu(k) = k$ and the detuning of the n^{th} qubit is defined as $\Delta_n = \Omega_n - k_0$. The radiation qubit couplings are assumed to have the following form

$$g_{\mu,n}(k) = \sqrt{\frac{\Gamma_n}{2\pi}} e^{-ic_\mu c_n (k+k_0)R/2} \tag{5.36}$$

Here, $c_\mu = (-1)^{\mu-1}$ and $c_n = (-1)^{n-1}$. In what follows, we find benificial the definition of the following quantities

$$\Delta_+ = \frac{1}{2}\left(\Delta_1 + \Delta_2\right), \quad \Delta_- = \frac{1}{2}\left(\Delta_1 - \Delta_2\right). \tag{5.37}$$

Suppose, that initially, the system is prepared in the following state

$$|\psi\rangle(0) = |\Omega\rangle \otimes \left(\cos\varphi|10\rangle + e^{i\vartheta/2}\sin\varphi|01\rangle\right). \tag{5.38}$$

The state at later times $t > 0$ is given by

$$|\psi\rangle(t) = \psi_{10}(t)|10\rangle + \psi_{01}(t)|01\rangle + \sum_\mu \int\limits_{\mathbb{R}} dk \psi^\mu_{00}(t,k) a^\dagger_\mu(k)|\Omega\rangle \otimes |00\rangle \tag{5.39}$$

where the corresponding wavefunctions are determined by expressions (5.16) and (5.17)

$$\begin{aligned}
\psi_{10}(t) &= \int\limits_{C_+} \frac{dz}{2\pi i} e^{-izt} \left\langle 10 \left| G^{(1)}(z) \right| \psi, 0 \right\rangle, \\
\psi_{01}(t) &= \int\limits_{C_+} \frac{dz}{2\pi i} e^{-izt} \left\langle 01 \left| G^{(1)}(z) \right| \psi, 0 \right\rangle,
\end{aligned} \tag{5.40}$$

$$\psi^\mu_{00}(t,k) = \sum_{n=1,2} \int\limits_{C_+} \frac{dz}{2\pi i} e^{-izt} \left\langle 00 \left| G_0(z-k) g_{\mu,n}(k) \sigma^{(n)}_- G^{(1)}(z) \right| \psi, 0 \right\rangle. \tag{5.41}$$

Here, the Green's function in the single excitation subspace is defined as $G^{(1)}(z) = G_0(z) + G_0(z)\Sigma^{(1)}(z)G^{(1)}(z)$, with the self-energy $\Sigma^{(1)}(z)$ given by the usual expression

$$\begin{aligned}
&\Sigma^{(1)}(z) = v_s^\dagger G_0\left(z - \omega_s\right) v_s = \sum_\mu \sum_{n',n} \int\limits_{\mathbb{R}} dk g^*_{\mu,n'}(k) g_{\mu,n}(k) \sigma^{(n')}_+ G_0(z-k) \sigma^{(n)}_- \\
&= -i\left(\left[\Gamma_1 + \Gamma_2\right]|11\rangle\langle 11| + \Gamma_1|10\rangle\langle 10| + \Gamma_2|01\rangle\langle 01| + \sqrt{\Gamma_1\Gamma_2} e^{i(z+\Delta_+ + k_0)R}\left[\sigma^{(1)}_+\sigma^{(2)}_- + \sigma^{(2)}_+\sigma^{(1)}_-\right]\right)
\end{aligned} \tag{5.42}$$

Here there are two different contributions to the self-energy. The first one $\propto -i\left(\left[\Gamma_1 + \Gamma_2\right]|11\rangle\langle 11| + \Gamma_1|10\rangle\langle 10| + \Gamma_2|01\rangle\langle 01|\right)$ is diagonal in qubit space and is independent of momentum, the second one, however, $\propto -i\sqrt{\Gamma_1\Gamma_2} e^{i(z+\Delta_+ + k_0)R}\left[\sigma^{(1)}_+\sigma^{(2)}_- + \sigma^{(2)}_+\sigma^{(1)}_-\right]$ describes the frequency dependent interatomic exchange interaction.

The dressed Green's function is thus

$$\begin{aligned}
&G^{(1)}(z) = \frac{1}{z - \Delta_+ + i\left(\Gamma_1 + \Gamma_2\right)}|11\rangle\left\langle 11\right| + \frac{1}{z + \Delta_+ + i\eta}\left|00\right\rangle\langle 00| + \\
&+ \frac{\left[z + \Delta_- + i\Gamma_2\right]|10\rangle\langle 10| + \left[z - \Delta_- + i\Gamma_1\right]|01\rangle\langle 01| - i\sqrt{\Gamma_1\Gamma_2} e^{i(z+\Delta_+ + k_0)R}\left[\sigma^{(1)}_+\sigma^{(2)}_- + \sigma^{(2)}_+\sigma^{(1)}_-\right]}{\left(z - \Delta_- + i\Gamma_1\right)\left(z + \Delta_- + i\Gamma_2\right) + \Gamma_1\Gamma_2 e^{2i(z+\Delta_+ + k_0)R}}
\end{aligned} \tag{5.43}$$

Using the fact that

$$G^{(1)}(z)|\psi, 0\rangle = \left\{\cos\varphi G_{e1}(z) + e^{i\vartheta/2}\sin\varphi G_o(z)\right\}|10\rangle + \left\{\cos\varphi G_o(z) + e^{i\vartheta/2}\sin\varphi G_{e2}(z)\right\}|01\rangle \tag{5.44}$$

with even "$G_{em}(m=1,2)$" and odd "G_o" Green's functions are defined as follows

$$G_{em}(z) := \frac{g_m(z)}{1+g_1(z)g_2(z)\Gamma_1\Gamma_2 e^{2i(z+\Delta_++k_0)R}}, \qquad g_m(z) := \frac{1}{(z+(-1)^m\Delta_- + i\Gamma_m)} \qquad (m=1,2)$$
$$G_o(z) := \frac{-ig_1(z)g_2(z)\sqrt{\Gamma_1\Gamma_2}e^{i(z+\Delta_++k_0)R}}{1+g_1(z)g_2(z)\Gamma_1\Gamma_2 e^{2i(z+\Delta_++k_0)R}},$$

we deduce that

$$\begin{aligned}
\psi_{10}(t) &= \cos\varphi G_{e1}(t) + e^{i\vartheta/2}\sin\varphi G_o(t), \\
\psi_{01}(t) &= \cos\varphi G_o(t) + e^{i\vartheta/2}\sin\varphi G_{e2}(t) \qquad (5.47)\\
\psi^{\mu}_{00}(t,k) &= \int\limits_{C_+}\frac{dz}{2\pi i}e^{-izt}\frac{g_{\mu,1}(k)}{z-k+\nabla}\left\{\cos\varphi G_{e1}(z) + e^{i\vartheta/2}\sin\varphi G_o(z)\right\} + \\
&\qquad + \int\limits_{C_+}\frac{dz}{2\pi i}e^{-izt}\frac{g_{\mu,2}(k)}{z-k+\nabla}\left\{\cos\varphi G_o(z) + e^{i\vartheta/2}\sin\varphi G_{e2}(z)\right\} \qquad (5.48)
\end{aligned}$$

where we have defined

$$G_l(t) = \int\limits_{C_+}\frac{dz}{2\pi i}G_l(z)e^{-izt}, \quad l=\{e1,e2,o\} \qquad (5.49)$$

In particular, one has

$$G_o(t) = -ie^{i(\Delta_++k_0)R}\sqrt{\Gamma_1\Gamma_2}\sum_{n=0}^{\infty}\left(-\Gamma_1\Gamma_2 e^{2i(\Delta_++k_0)R}\right)^n I(2n+1,n+1,n+1,t), \qquad (5.50)$$

$$G_{e1}(t) = e^{-i\Delta_+t}e^{-\Gamma_1 t} + \sum_{n=1}^{\infty}\left(-\Gamma_1\Gamma_2 e^{2i(\Delta_++k_0)R}\right)^n I(2n,n+1,n,t), \qquad (5.51)$$

$$G_{e2}(t) = e^{i\Delta_+t}e^{-\Gamma_2 t} + \sum_{n=1}^{\infty}\left(-\Gamma_1\Gamma_2 e^{2i(\Delta_++k_0)R}\right)^n I(2n,n,n+1,t), \qquad (5.52)$$

where

$$\begin{aligned}
I(L,M,N,t) &= \int\limits_{C_+}\frac{dz}{2\pi i}\frac{e^{-iz(t-LR)}}{(z-\Delta_-+i\Gamma_1)^M(z+\Delta_-+i\Gamma_2)^N} = \\
&= \Theta(t-LR)\left(\sum_{k=0}^{M-1}\frac{(-1)^k(N+k-1)!(-i(t-LR))^{M-k-1}}{k!(M-k-1)!(N-1)!}\frac{e^{-i\Delta_-(t-LR)}e^{-\Gamma_1(t-LR)}}{(2\Delta_- + i(\Gamma_2-\Gamma_1))^{N+k}}\right. \\
&\qquad \left. + \sum_{k=0}^{N-1}\frac{(-1)^k(M+k-1)!(-i(t-LR))^{N-k-1}}{k!(N-k-1)!(M-1)!}\frac{e^{i\Delta_-(t-LR)}e^{-\Gamma_2(t-LR)}}{(-2\Delta_- + i(\Gamma_1-\Gamma_2))^{M+k}}\right). \qquad (5.53)
\end{aligned}$$

Note that in the special case $\Gamma_1=\Gamma_2=\Gamma, \Delta_1=\Delta_2=\Delta$ this boils down to

$$I(L,M,N,t) = \Theta(t-LR)\frac{(-i(t-LR))^{M+N-1}}{(M+N-1)!}e^{-\Gamma(t-LR)} \qquad (5.54)$$

The emission spectral density may be written as follows

$$S_{\mu}^{\text{emission}}(k) = |g_{\mu,1}(k)\left\{\cos\varphi G_{e1}(k-\Delta_+) + e^{i\vartheta/2}\sin\varphi G_o(k-\Delta_+)\right\} + g_{\mu,2}(k)\left\{\cos\varphi G_o(k-\Delta_+) + e^{i\vartheta/2}\sin\varphi G_{e2}(k-\Delta_+)\right\}\Big|^2 \tag{5.55}$$

To understand the physics behind the quantum system described above, let us first consider a limiting case of equivalent qubits. As it is well known, in the case of two equivalent $\Gamma_1 = \Gamma_2 = \Gamma$ bright qubits $\Delta_1 = \Delta_2 = 0$ separated by an even number of wavelength $k_0 R \in 2\pi\mathbb{Z}$, Lindblad master equation approaches predict the states $|B\rangle = \frac{1}{\sqrt{2}}(|10\rangle + |01\rangle)$ and $|D\rangle = \frac{1}{\sqrt{2}}(|10\rangle - |01\rangle)$ to be super and subradiant states respectively, see e.g [30]. So let us see whether such a result is reproduced within the exact theory of dynamics developed above. For an initial state of the form

$$|\psi, 0\rangle = |B/D\rangle \equiv \frac{1}{\sqrt{2}}(|10\rangle \pm |01\rangle) \tag{5.56}$$

Occupation probability amplitudes of single-qubit excited states read as follows

$$\psi_{10}(t) = \frac{1}{\sqrt{2}}\left(G_e(t) \pm G_o(t)\right), \quad \psi_{01}(t) = \frac{1}{\sqrt{2}}\left(G_o(t) \pm G_e(t)\right) \tag{5.57}$$

where we have made use of the fact that for a system of equivalent qubits $G_{e1} = G_{e2} = G_e$. This, in turn, leads to the following expressions for the survival probabilities of bright $|B\rangle$ and dark $|D\rangle$ states respectively

$$p_B(t) = |G_e(t) + G_o(t)|^2 = \left|\sum_{n=0}^{\infty}\Theta(t-nR)\frac{(-\Gamma(t-nR))^n}{n!}e^{-\Gamma(t-nR)}\right|^2 \tag{5.58}$$

$$p_D(t) = |G_e(t) - G_o(t)|^2 = \left|\sum_{n=0}^{\infty}\Theta(t-nR)\frac{(\Gamma(t-nR))^n}{n!}e^{-\Gamma(t-nR)}\right|^2 \tag{5.59}$$

As one may notice, the survival probability of the superradiant (a.k.a. bright) state resembles one of the giant atom, which tends to zero as $t \to \infty$ in all parameter space.

Survival probability of the dark state, in its turn, requires some careful analysis. First, let us consider the Markovian case $\Gamma R \ll 1$. In this limit we obtain

$$\sum_{n=0}^{\infty}\Theta(t-nR)\frac{(\Gamma(t-nR))^n}{n!}e^{-\Gamma(t-nR)}\Big|_{R=0} = \sum_{n=0}^{\infty}\frac{(\Gamma t)^n}{n!}e^{-\Gamma t} = 1 \tag{5.60}$$

indeed showing the that in the Markovian limit $|D\rangle$ is a true subradiant state. When one goes to another extreme $\Gamma R \gg 1$, one effectively expects the individual contributions to the survival probability amplitude coming from each $mR < t < (m+1)R$ interval to overlap weakly and be peaked near $t \approx mR$. In this case, we thus expect a dark state to decay almost completely, in the same spirit as a giant atom, showing universal $R/(2\pi t)$ subexponential decay. In the intermediate regime $\Gamma R \leq 1, \quad R \neq 0$ one can expect a non-vanishing overlap between the contributions coming from each interval $mR < t < (m+1)R$, which for times chosen such that $\Gamma t \gg 1$, allows us to make the following approximation

$$\sum_{n=0}^{\infty}\Theta(t-nR)\frac{(\Gamma(t-nR))^n}{n!}e^{-\Gamma(t-nR)} \approx e^{-\Gamma t}\sum_{n=0}^{\infty}\frac{\left(\Gamma(t-nR)e^{\Gamma R}\right)^n}{n!} \tag{5.61}$$

$R = 0.0001$

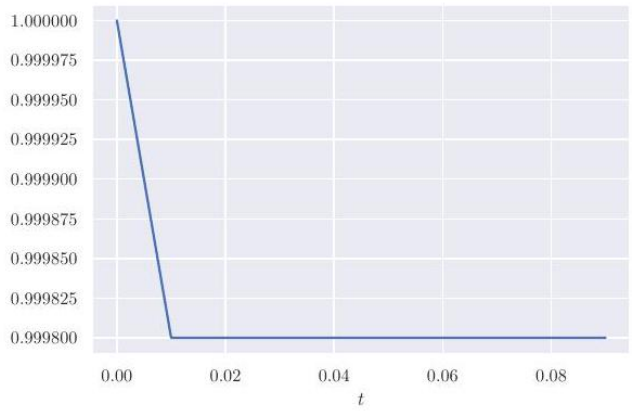
1.000000
0.999975
0.999950
0.999925
0.999900
0.999875
0.999850
0.999825
0.999800
0.00
0.02
0.04
0.06
0.08
t

$R = 2$

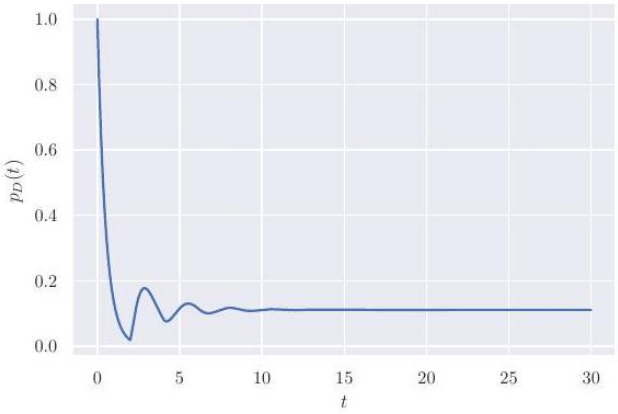
1.0
0.8
0.6
0.4
0.2
0.0
$p_D(t)$
0
5
10
15
20
25
30
t

$R = 0.5$

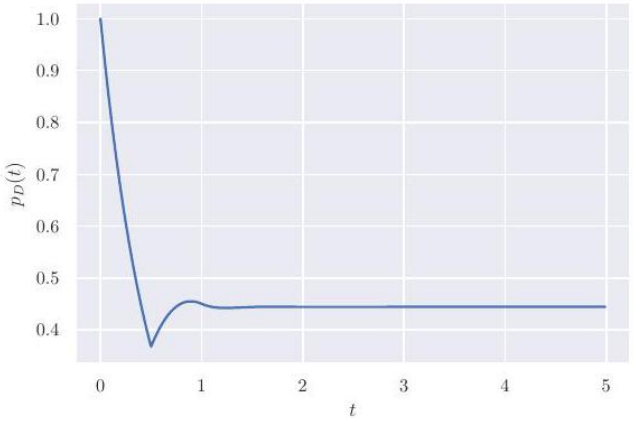
1.0
0.9
0.8
0.7
0.6
0.5
0.4
$p_D(t)$
0
1
2
3
4
5
t

$R = 20$

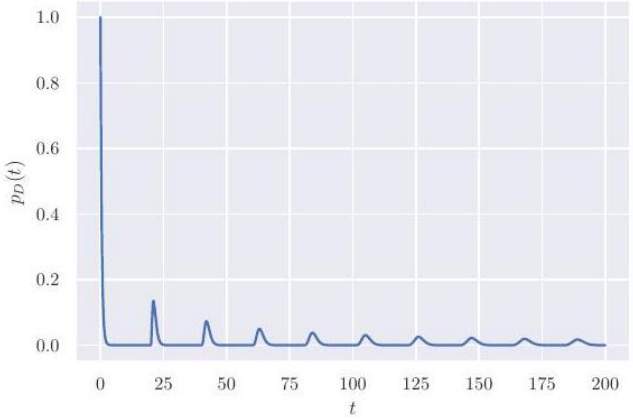
1.0
0.8
0.6
0.4
0.2
0.0
$p_D(t)$
0
25
50
75
100
125
150
175
200
t

Figure 5.3: Survival probability of a dark state for a range of delay times R. Other parameters: $\Gamma = 1, k_0 = 1$.

Now, further expanding the above expression in a Taylor series about $R = 0$ we obtain

$$\sum_{n=0}^{\infty} \Theta(t-nR)\, \frac{(\Gamma(t-nR))^n}{n!} e^{-\Gamma(t-nR)} \approx e^{-\Gamma t} \sum_{m=0}^{\infty}\sum_{n=0}^{\infty} \frac{d^m\left((t-nR)e^{\Gamma R}\right)^n}{dR^m}\bigg|_{R=0} \frac{\Gamma^n R^m}{n!m!}$$
$$= \sum_{m=0}^{\infty}(-\Gamma R)^m = \frac{1}{1+\Gamma R} \Longrightarrow p_D(t) \sim \frac{1}{(1+\Gamma R)^2}, \quad t\to\infty, \quad R\Gamma \leq 1 \quad (5.62)$$

where equality between the first and the second line may be easily sought by induction. So, finally, we arrive at the following conclusion. In the Markovian system, $|D\rangle$ is indeed a completely non-decaying state, following the Master equation-based predictions. In the intermediate regime, where the propagation time delays are chosen such that $\Gamma R \leq 1$ this state decays partially, thus already showing the inconsistency of the Lindblad equation-based approaches. In heavily nonMarkovian parameter regime, $\Gamma R \gg 1$, one shall expect the Dark state to become superradiant, completely invalidating expectations based on Master equations. Exact integration of dynamics in all three parameter regimes is shown in Figure 5.3. As one can see, the formula (5.62) provides an excellent estimate of the limiting value of survival probability at $t \to \infty$.

Now, let us turn our attention to the system of inequivalent qubits. Unfortunately, the complexity of general expressions for both survival probabilities and emission spectral densities (5.50)(5.55) naturally prohibit us to get an analytical insight into the dynamics of the system. So let us try to draw some conclusions from the plots of the respective formulas. First, let us consider a problem of emission of individual single-qubit excited states $\vartheta = 0, \varphi = 0, \frac{\pi}{2}$. The corresponding observables are presented in Figure 5.4 for $R = 4, k_0 = 2\pi/R, \Delta_1 = -\Delta_2 = 0.3$ and $\Gamma_1 = 2\Gamma_2 = 1$. The first thing one can notice is that the states $\varphi = 0$ and $\varphi = \frac{\pi}{2}$ indeed decay differently as one shall physically expect for an asymmetric system. Namely, since the decay rate of the second qubit into the continuum is two times less than that of the first one, the revival peaks of the $\frac{\pi}{2}$ state are significantly higher than that of $\varphi = 0$ state. On the other hand, the excitation

$\varphi = 0$

$|\psi_{10}(t)|^2$

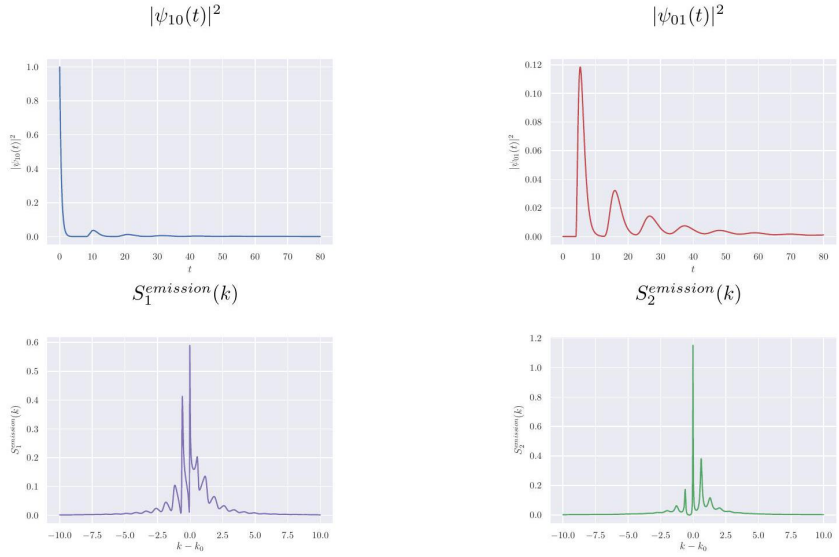

$$\varphi = \frac{\pi}{2}$$

$|\psi_{10}(t)|^2$

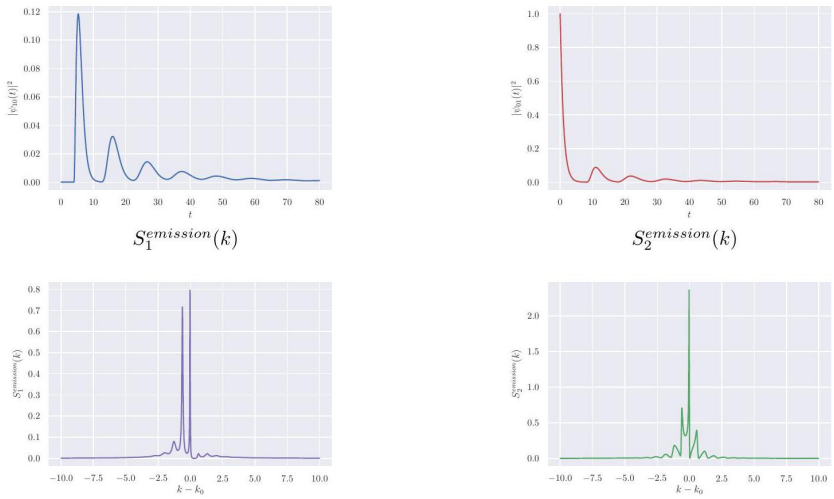

Figure 5.4: Observables corresponding to the decay of single-qubit excited states. In all plots: $R = 4, k_0 = 2\pi/R, \Delta_1 = -\Delta_2 = 0.3$, and $\Gamma_1 = 2\Gamma_2 = 1$.

probabilities of initially unexcited states ($|01\rangle$ for $\varphi = 0$ and $|10\rangle$ for $\varphi = \frac{\pi}{2}$) appear the same. This result is also not surprising since the mechanism of excitation of these states, an exchange interaction, is nonsensitive to the qubit asymmetry $\propto \sqrt{\Gamma_1\Gamma_2}e^{i\Delta_+ R}$. What concerns the emission spectral densities, we note that not only these are asymmetric around the linearization point of the spectrum, but also do they differ in both radiation channels. Asymmetry of the spectra can be easily attributed to the non-zero detuning of both qubits. Indeed, the first qubit being positively detuned from radiation has a tendency to emit more into the right moving modes, whereas the situation is opposite for the second one. The reason for the difference between the emission spectra in both channels is, of course, related to the difference in coupling constants of both qubits to left and right movers.

Let us now turn our attention to the problem of quantum decay of the second pair of the Bell states $\varphi = \frac{\pi}{4}, \frac{3\pi}{4}$ and $\vartheta = 0$. The corresponding observables are shown in Figure 5.5. The first thing we note is that opposed to the symmetric situation, $|B\rangle$ and $|D\rangle$ states are both decaying completely. Although qubits are still separated by a single wavelength, due to the asymmetry, the states $|10\rangle$ and $|01\rangle$ become distinguishable, thus not allowing for any cancelation of field amplitudes at $\pm R/2$ in the $\frac{3\pi}{4}$ case. Again, as in the previous example, one can observe clear differences in decay patterns of both qubits. Similarly, both the asymmetry of emission spectral density and dissimilarity of its line shape in different radiation channels is retained.

7.11.6 Spontaneous Emission of a Qubit Into an Array of Coupled Resonators

In this section, our goal is to show how our theory of dynamics can cope with photonic systems possessing nonlinear dispersion relation. Such systems are proposed to be realizable in both optical and microwave domains. The basic idea is to couple optical resonators or superconducting linear circuits to engineer artificial crystals with desired band structure [5,14-16,51]. Here, for the sake of simplicity, we are going to focus on the simplest photonic crystal, a single band system.

Infinite Single Band System

Let us consider the following problem. Suppose that we couple a single qubit to a single resonator, which itself is a unit cell of an infinite array of nearest-neighbour coupled resonators. The Hamiltonian modeling such a system may be written as $\mathcal{H} = \mathcal{H}_0 + \mathcal{V}$, whereby we have defined

$$\mathcal{H}_0 = \Omega|1\rangle\langle 1| + \omega_0 \sum_{n\in\mathbb{Z}} a_n^\dagger a_n - J\sum_{n\in\mathbb{Z}} \left[a_n^\dagger a_{n+1} + a_{n+1}^\dagger a_n\right] \tag{5.63}$$

$$\mathcal{V} = \sqrt{\gamma}\sum_{n\in\mathbb{Z}} \left[a_0^\dagger \sigma_- + \sigma_+ a_0\right] \tag{5.64}$$

Here, ω_0 is the resonant frequency of each cavity, $-J$ is the coupling strength, Ω is a transition frequency of the qubit and without any loss of generality, it is assumed that a qubit is coupled to the 0^{th} site. Now, by defining the momentum space field operators as follows

$$a(k) = \frac{1}{\sqrt{2\pi}}\sum_{n\in\mathbb{Z}} a_n e^{-ikn}, \quad a_n = \frac{1}{\sqrt{2\pi}}\int_{-\pi}^{\pi} dk e^{ikn} a(k), \quad \left[a(k), a^\dagger(k')\right] = \delta(k-k'),$$

and performing the time-dependent gauge transformation (2.7), we arrive at

$$\mathcal{H}_0 = -\Delta|1\rangle\langle 1| + \int_{-\pi}^{\pi} dk\omega(k)a^\dagger(k)a(k), \quad \mathcal{V} = \sqrt{\frac{\gamma}{2\pi}}\int_{-\pi}^{\pi} dk\left[a^\dagger(k)\sigma_- + \sigma_+ a(k)\right] \tag{5.65}$$

where we defined $\omega(k) = -2J\cos k$ and $\Delta = \omega_0 - \Omega$. Let us again consider the following scenario, suppose a qubit was initially prepared in an excited state $|1\rangle$ with a waveguide occupying its vacuum state, i.e.

$$|\psi\rangle(0) = |1\rangle \otimes |\Omega\rangle. \tag{5.66}$$

$$\varphi = \frac{\pi}{4}$$

$|\psi_{10}(t)|^2$

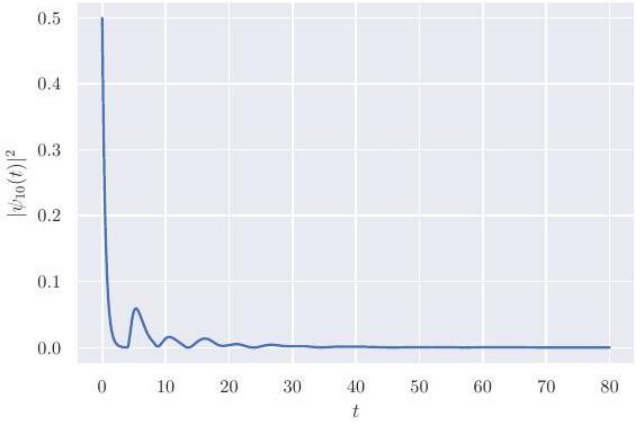

$|\psi_{10}(t)|^2$

$S_1^{emission}(k)$

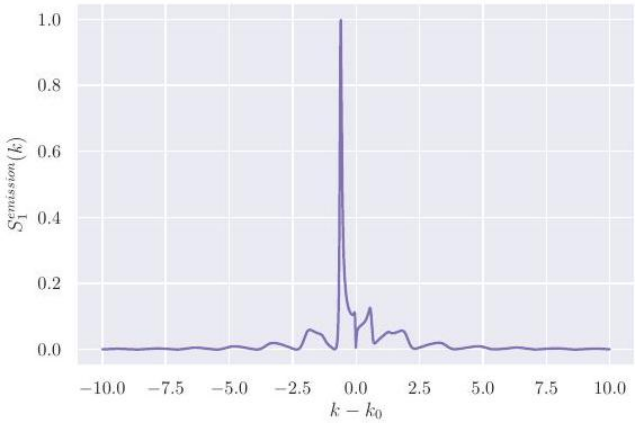

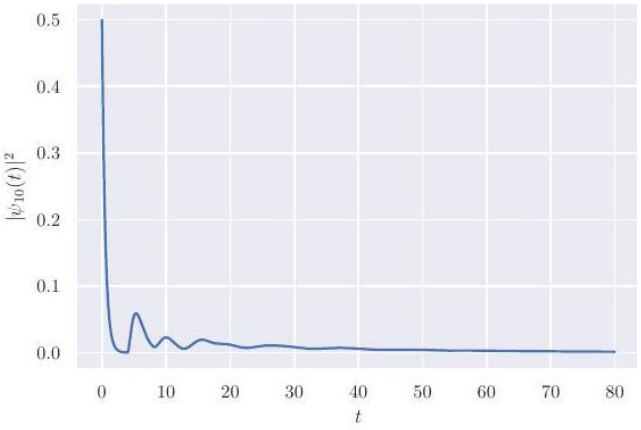

$|\psi_{01}(t)|^2$

$S_1^{emission}(k)$

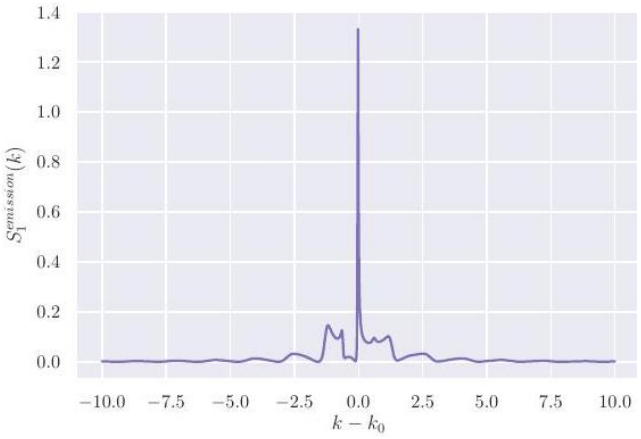

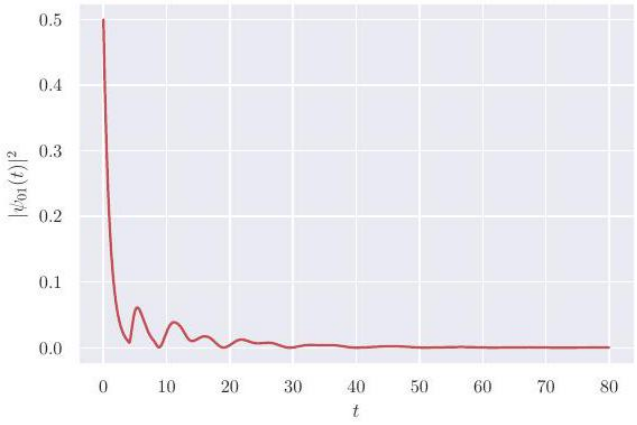

$$S_2^{emission}(k)$$

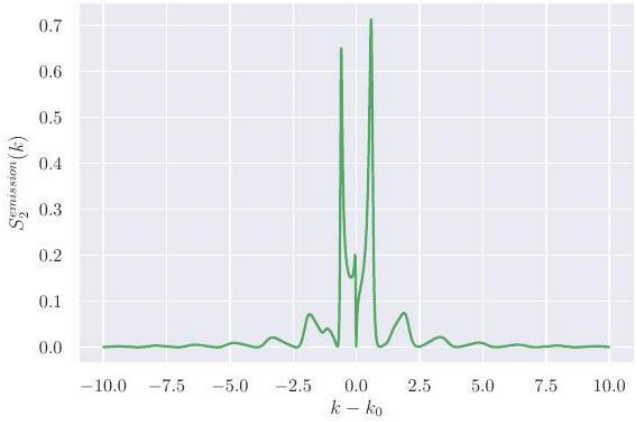

$$\varphi = \frac{3\pi}{4}$$

$|\psi_{01}(t)|^2$

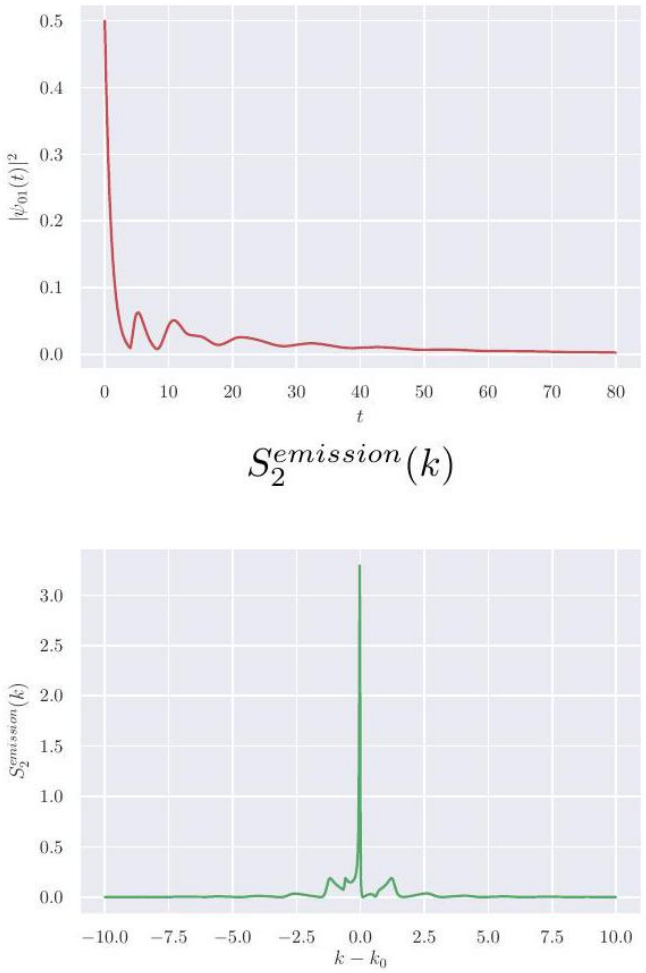

Figure 5.5: Observables corresponding to the decay of second pair of the Bell states. In all plots: $R = 4, k_0 = 2\pi/R, \Delta_1 = -\Delta_2 = 0.3$, and $\Gamma_1 = 2\Gamma_2 = 1$.

As before, the state of the system at any later time $t > 0$ can be written as

$$|\psi\rangle(t) = \alpha(t)|1\rangle \otimes |\Omega\rangle + \int_{-\pi}^{\pi} dk \beta(k,t) a^\dagger(k)|0\rangle \otimes |\Omega\rangle \tag{5.67}$$

where

$$\alpha(t) = \int_{C_+} \frac{dz}{2\pi i} \left\langle 1 \left| \frac{e^{-izt}}{z + \frac{\Delta}{2}(1+\sigma_3) - \Sigma^{(1)}(z)} \right| 1 \right\rangle \tag{5.68}$$

$$\beta(k,t) = \sqrt{\frac{\gamma}{2\pi}} \int_{C_+} \frac{dz}{2\pi i} \frac{1}{z - \omega(k)} \left\langle 1 \left| \frac{e^{-izt}}{z + \frac{\Delta}{2}(1+\sigma_3) - \Sigma^{(1)}(z)} \right| 1 \right\rangle. \tag{5.69}$$

The self-energy is given by the usual expression

$$\Sigma^{(1)}(z) = \gamma|1\rangle \left\langle 1 \left| \int_{-\pi}^{\pi} \frac{dk}{2\pi} \frac{1}{z - \omega(k)} = \frac{\gamma}{z\sqrt{1 - \frac{4J^2}{z^2}}} \right| 1 \right\rangle \langle 1| := \sigma(z)|1\rangle\langle 1| \tag{5.70}$$

Let us first focus on the calculation of the survival probability $P_s(t) = |\alpha(t)|^2$. We see that we need to evaluate the following integral

$$\alpha(t) = \int_{C_+} \frac{dz}{2\pi i} \frac{e^{-izt}}{z + \Delta - \sigma(z)}$$

We have a difficulty with evaluation of this integral due to the branch cut of $\sigma(z)$ on a real axis along $[-2J, 2J]$, to overcome such a complication one performs an analytic continuation of the self-energy to the lower half-plane $\sigma(z) \to \tilde{\sigma}(z)$, where

$$\tilde{\sigma}(z) = \frac{-i\gamma}{\sqrt{-i(z-2J)}\sqrt{-i(z+2J)}} \tag{5.71}$$

Such a replacement is possible since $\sigma(z) = \tilde{\sigma}(z), \quad \forall z = E + i\eta, \eta \in \mathbb{R}^+$. Now, with such a choice of $\tilde{\sigma}(z)$, the branch cuts are along $z = \pm 2J - iy$ where $y \in [0, \infty)$. So, we have three contributions to the survival probability amplitude $\alpha(t) = \alpha_{bs}(t) + \alpha_{dp}(t) + \alpha_{bc}(t), \alpha_{bs}$ coming from the poles of the integrand on the real axis - bound-state poles, α_{dp} arising from the existance of poles of the integrand in the region of the complex plane to which the self-energy was analytically continued, so-called decay poles, and fianlly, α_{bc} arising from the integration along the branch cuts. The resulting contour of integration is shown in Figure 5.6.

Poles of the integrand are the solutions of the following equation

$$z + \Delta = \tilde{\sigma}(z) \tag{5.72}$$

Analyzing (5.72), we find that there are always two solutions $z = \omega_{\pm}$on the real axis, one is larger than $2J$ (above the band), the other is smaller than $-2J$ (below the band). They correspond to the bound states. Besides, we can have a decay pole in the lower half-plane at $z = -i\Gamma/2$. In particular, let us focus on the special case of resonance $\Delta = 0$, in this situation all of the poles can be found explicitly

$$\omega_{\pm} = \pm\omega, \quad \omega = \sqrt{2J^2 + \sqrt{4J^4 + \gamma^2}}, \quad \Gamma = 2\sqrt{\sqrt{4J^4 + \gamma^2} - 2J^2} \tag{5.73}$$

Pole contribution to the dynamics is thus

$$\alpha_{bs}(t) = \frac{e^{-i\omega t}}{1 - \tilde{\sigma}'(\omega)} + \frac{e^{i\omega t}}{1 - \tilde{\sigma}'(-\omega)} = \frac{\sqrt{4J^4 + \gamma^2} - 2J^2}{\sqrt{4J^4 + \gamma^2}} \cos \omega t \tag{5.74}$$

$$\alpha_{dp}(t) = \frac{e^{-\Gamma t/2}}{1 - \tilde{\sigma}'(-i\Gamma/2)} = \frac{\sqrt{4J^4 + \gamma^2} + 2J^2}{2\sqrt{4J^4 + \gamma^2}} e^{-i\Gamma t/2} \tag{5.75}$$

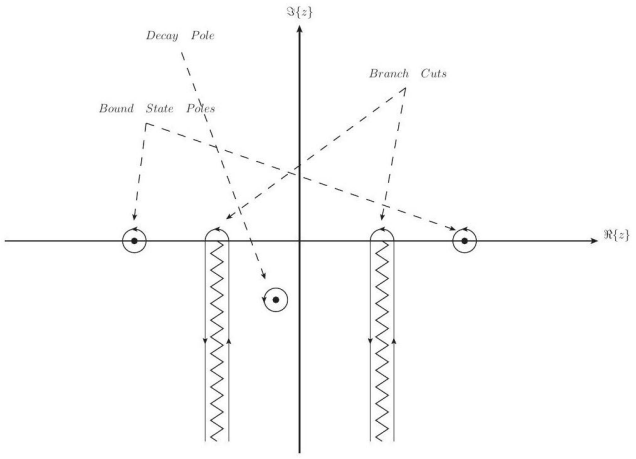

Figure 5.6: Integration contour for the survival probability of a qubit coupled to an array of coupled resonators.

Let us now focus on the branch cut contribution to the dynamics, we write

$$\alpha_{bc}(t) = \alpha_{bc}^{(1)}(t) + \alpha_{bc}^{(2)}(t) \tag{5.76}$$

where

$$\alpha_{bc}^{(n)}(t) = -e^{(-1)^n 2iJt} \lim_{\eta \searrow 0} \int_{\mathbb{R}^+} \frac{dy}{2\pi} e^{-ty} \{ \frac{1}{(-1)^{n+1}2J - iy - \tilde{\sigma}\left((-1)^{n+1}2J - iy - \eta\right)} - \frac{1}{(-1)^{n+1}2J - iy - \tilde{\sigma}\left((-1)^{n+1}2J - iy + \eta\right)} \Big\}. \quad (5.77)$$

Integration over branch cuts is a rather challenging problem and thus has to be accomplished numerically, though, one may still get an insight into the contribution arising from the existence of the branching points in the self-energy, by considering the asymptotic expansion of the integrals for times t chosen such that $\gamma t \gg 1$. In this limit one effectively has $\tilde{\sigma}(z) \sim \gamma \ll J$, yielding $y < \frac{1}{t} \ll \gamma$, so that the rightmost branch cut contribution is asymptotic to

$$\alpha_{bc}^{(1)}(t) \sim \frac{e^{-i2Jt}}{8\pi J^2} \lim_{\eta \searrow 0} \int_{\mathbb{R}^+} dy e^{-yt} [\tilde{\sigma}(2J - iy + \eta) - \tilde{\sigma}(2J - iy - \eta)] \quad (5.78)$$

Now, we consider the following

$$\lim_{\eta \searrow 0} \tilde{\sigma}(2J - iy \pm \eta) = \lim_{\eta \searrow 0} \frac{\gamma}{\sqrt{-y \mp \eta}\sqrt{-4iJ - y}} \sim \lim_{\eta \searrow 0} \frac{\gamma}{2i\sqrt{-y + i\eta}\sqrt{iJ}}$$
$$= \lim_{\eta \searrow 0} \frac{\gamma e^{-i\pi/4}}{2i\sqrt{J}} \exp\left(-\frac{\ln\{-y \mp i\eta\}}{2}\right) = \frac{\gamma e^{-i\pi/4}}{2i\sqrt{J}} \exp\left(-\frac{\ln y \mp i\pi}{2}\right) = \pm \frac{\gamma e^{-i\pi/4}}{2\sqrt{yJ}}.$$

This, in turn, has to be integrated, resulting in

$$\alpha_{bc}(t) \sim e^{-2iJt} \frac{\gamma e^{-i\pi/4} \Gamma\left(\frac{1}{2}\right)}{8\pi J^{5/2} t^{1/2}} \quad (5.79)$$

The analogous procedure has to be done with an integral over a leftmost branch cut, those two when combined produce the following result

$$\alpha_{bc}(t) \sim \frac{\Gamma\left(\frac{1}{2}\right)}{4\pi J^{5/2} t^{1/2}} \cos\left(2Jt + \frac{\pi}{4}\right) \quad (5.80)$$

which shows a universal sub-exponential decay. Exact integration of the dynamics is shown in Figure 5.7. Analyzing the analytical formulas we see that for $\gamma \ll J$ we expect the survival probability to be dominated by an exponential decay and the amplitude of bound state oscillations

to be strongly suppressed $\sim \mathcal{O}\left(\frac{\gamma^2}{J^4}\right)$. In the case of $\gamma \geq J$, we expect the system to decay algebraically and end up oscillating in the bound state. As one can see, numerical integration results exactly fulfill our expectations.

Let us now deduce the asymptotic state of the field emitted by the qubit. Analyzing 5.69 we see that there are three contributions to $\beta(t, k)$. First, arising from the bound-sate poles of the bare and dressed propagators, another one coming from the decay pole of the dressed propagator in the lower half of the complex z plane and finally, the third contribution coming from the branch cut integration. In the long-time limit, we expect the decay pole and branch cut contributions to be exponentially and subexponentially suppressed which allows us to deduce

$$\beta(k, t) \to \sqrt{\frac{\gamma}{2\pi}} \frac{2J|\sin k| e^{2Ji\cos kt}}{i\gamma - 4J^2|\sin k|\cos k} + \sqrt{\frac{\gamma}{2\pi}} \frac{\sqrt{4J^4 + \gamma^2} - 2J^2}{\sqrt{4J^4 + \gamma^2}} \frac{2i\omega \sin \omega t + 2J \cos k \cos \omega t}{4J^2 \cos^2 k - \omega^2} \quad (5.81)$$

This result shows that it is not meaningful to define the emission spectral density in this model.

Semi-Infinite Single Band System

Let us now consider a slightly more sophisticated problem - a single emitter coupled to a semiinfinite resonator array. The Hamiltonian $\mathcal{H} = \mathcal{H}_0 + \mathcal{V}$ now takes the following form

$$\mathcal{H}_0 = \Omega|1\rangle\langle 1| + \omega_0 \sum_{n=1}^{\infty} a_n^\dagger a_n - J \sum_{n\in\mathbb{N}} \left[a_n^\dagger a_{n+1} + a_{n+1}^\dagger a_n\right] \tag{5.82}$$

$$\mathcal{V} = \sqrt{\gamma} \sum_{n=1}^{\infty} \left[a_N^\dagger \sigma_- + \sigma_+ a_N\right] \tag{5.83}$$

Here, all of the parameters are defined as before, and N is the site to which an atom is coupled. Now, defining the Fourier transform for a semi-infinite lattice

$$a(k) = \sqrt{\frac{2}{\pi}} \sum_{n=1}^{\infty} \sin(kn) a_n, \quad a_n = \sqrt{\frac{2}{\pi}} \int_0^\pi dk \sin(kn) a(k), \quad \left[a(k), a^\dagger(k')\right] = \delta(k-k'), \tag{5.84}$$

and again performing our usual gauge transformation, we arrive at the following expression for the Hamiltonian

$$\mathcal{H}_0 = -\Delta|1\rangle\langle 1| + \int_0^\pi dk \omega(k) a^\dagger(k) a(k), \quad \mathcal{V} = \sqrt{\frac{2\gamma}{\pi}} \int_0^\pi dk \sin(kN) \left[a^\dagger(k)\sigma_- + \sigma_+ a(k)\right] \tag{5.85}$$

where $\omega(k) = -2J\cos k, \quad k \in [0, \pi)$. The self-energy is given by the usual expression

$$\begin{aligned}\Sigma_N^{(1)}(z) = 2\gamma|1\rangle \left\langle 1 \left| \int_0^\pi \frac{dk}{\pi} \frac{\sin^2(kN)}{z + 2J\cos k} = \gamma \right| 1 \right\rangle \langle 1| \int_0^\pi \frac{dk}{\pi} \frac{1}{z + 2J\cos k} \\ - \gamma|1\rangle \left\langle 1 \left| \int_0^\pi \frac{dk}{\pi} \frac{\cos(2kN)}{z + 2J\cos k} = \frac{\gamma}{z\sqrt{1 - \frac{4J^2}{z^2}}} \right| 1 \right\rangle \langle 1| \left(1 - \left(\frac{\sqrt{1 - \frac{4J^2}{z^2}} - 1}{\frac{2J}{z}}\right)^{2N}\right).\end{aligned} \tag{5.86}$$

$\gamma = 0, 1$

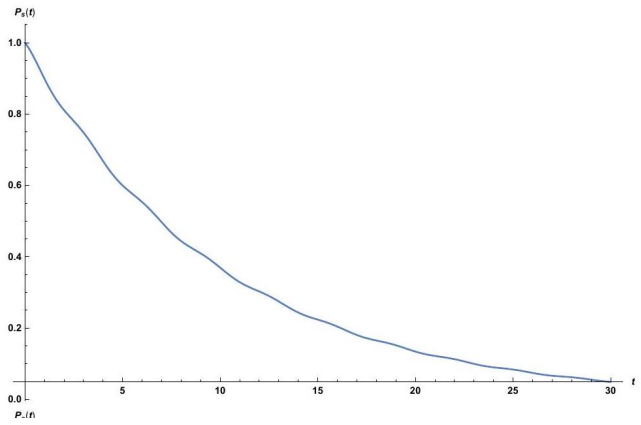

$\gamma = 0, 8$

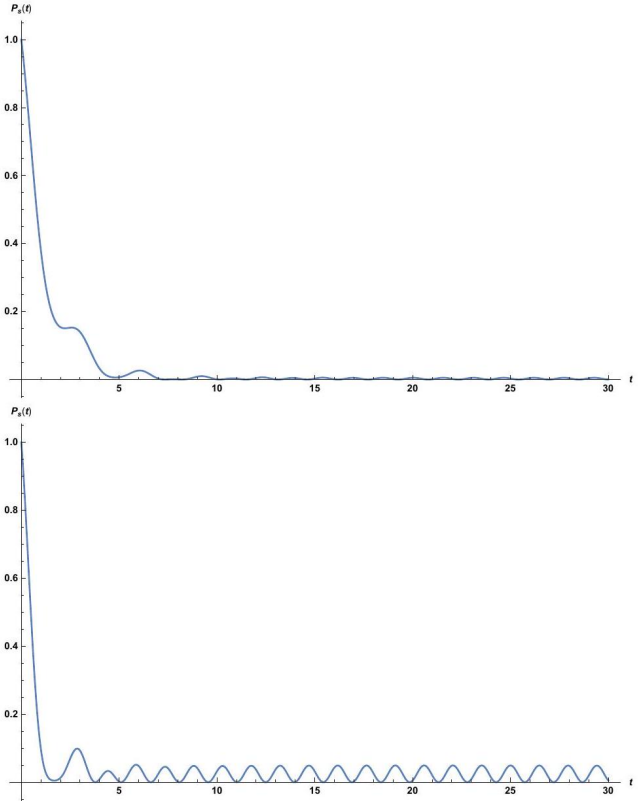

Figure 5.7: Survival probabilities of a qubit coupled to a resonator array for a range of bare decay rates. In all plots: $J = 1$ and $\Delta = 0$.

Let us now, for simplicity, specify to the case $N = 1$. In this case, the above formula simplifies to

$$\Sigma_1^{(1)}(z) = |1\rangle \left\langle 1 \left| \frac{\gamma z}{2J^2} \left(1 - \sqrt{1 - \frac{4J^2}{z^2}} \right) := \right| 1 \right\rangle \langle 1|\sigma_1(z) \tag{5.87}$$

Again, we have to analytically continue the self-energy $\sigma_1(z) \to \tilde{\sigma}_1(z)$ to the lower half-plane, such that the branch cuts again point along the negative imaginary axis. Now, we consider the following analytic continuation of the self-energy to the lower half-plane

$$\tilde{\sigma}_1(z) = \frac{\gamma}{2J^2}(z - \sqrt{z - 2J}\sqrt{z + 2J}) \tag{5.88}$$

Let us consider the process of spontaneous emission of an excited qubit. Survival probability $P_s(t) = |\alpha(t)|^2$ is determined by the evaluation of the following integral

$$\alpha(t) = \int\limits_{C_+} \frac{dz}{2\pi i} \frac{e^{-izt}}{z + \Delta - \tilde{\sigma}_1(z)} \tag{5.89}$$

As before, we have three contributions to the dynamics coming from bound-state and decay poles, as well as the contribution from the branch cuts of $\tilde{\sigma}_1(z)$. Poles of the integrand are determined from

$$z + \Delta = \tilde{\sigma}_1(z) \Longleftrightarrow z^2 + \tfrac{2J^2-\gamma}{J^2-\gamma}\Delta z + \tfrac{\Delta^2 J^2+\gamma^2}{J^2-\gamma} = 0 \Longrightarrow \begin{cases} z_\pm = \omega \pm i\Gamma/2, & \Delta^2 < 4\left(J^2-\gamma\right) \\ z_\pm = \omega \pm \Gamma/2, & \Delta^2 > 4\left(J^2-\gamma\right), \end{cases}$$
$$\omega = \Delta \tfrac{2J^2-\gamma}{2(J^2-\gamma)}, \quad \Gamma = \tfrac{\gamma}{J^2-\gamma}\sqrt{|\Delta^2 - 4\left(J^2-\gamma\right)|}.$$

Let us now specify to the case $\Delta = 0$. In this case, the pole contribution to the dynamics is given by

$$\begin{cases} \alpha_p(t) = \frac{2J^2-\gamma}{2J^2-2\gamma} e^{-\Gamma t/2}, & J^2-\gamma > 0, \\ \frac{\gamma}{2J^2-\gamma} e^{-i\Gamma t/2}, & J^2-\gamma < 0, \end{cases} \qquad \Gamma = \frac{2\gamma}{\sqrt{|J^2-\gamma|}}.$$

Further, let us consider the contribution of the branch cuts to the evolution of the state. As before, let us first have a look at the asymptotic long-time behavior. The rightmost branch cut contributes

$$\alpha_{bc}^{(1)}(t) \sim e^{-2iJt} \frac{1}{\left(2J+\frac{\gamma}{J}\right)^2} \int\limits_{\mathbb{R}^+} \frac{dx}{2\pi} e^{-xt} \left\{ \tilde{\sigma}_1(2J - ix - \eta) - \tilde{\sigma}_1(2J - ix + \eta) \right\}. \tag{5.92}$$

One has

$$\tilde{\sigma}_1(2J - ix \pm \eta) = \frac{\gamma}{2J^2}(2J - ix - \sqrt{-ix \pm \eta}\sqrt{4J - ix}) \sim \frac{\gamma}{J^2}\left(J \mp \sqrt{Jx} e^{-i\pi/4}\right)$$

resulting in

$$\alpha_{bc}^{(1)}(t) \sim \frac{\Gamma\left(\frac{3}{2}\right) e^{-i\pi/4} \gamma\sqrt{J}}{2\pi\left(2J^2+\gamma\right)^2} \frac{e^{-2iJt}}{t^{3/2}}. \tag{5.93}$$

Performing the analogous procedure with the integral over the left branch cut we find

$$\alpha_{bc}^{(2)}(t) \sim \frac{\Gamma\left(\frac{3}{2}\right) e^{i\pi/4} \gamma\sqrt{J}}{2\pi\left(-2J^2+\gamma\right)^2} \frac{e^{2iJt}}{t^{3/2}} \tag{5.94}$$

So we see that the long-time behavior in the semi-infinite model differs form the one found in the infinite one. Exact integration of the dynamics is shown in Figure 5.8.

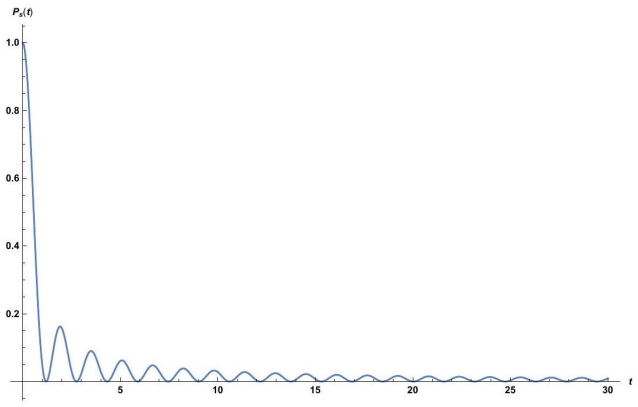

Figure 5.8: Survival probability of a qubit coupled to a semi-infinite resonator array with $J = 1$, $\gamma = 2$, and $\Delta = 0$.

7.12 Conclusions and Outlook

(выпишу это в начало скорее всего!!)

In this thesis, the theory of scattering of few-photon states in waveguide QED was developed. As opposed to many other studies, this theory is based on exact equations, which in turn allows one to investigate waveguide QED systems beyond the Born-Markov approximation. The theory was then successfully applied to a weakly coherent pulse scattering problem in non-Markovian quantum acoustic setup. The inelastic spectral density, as well as coherence functions of radiation of second and third-order in the exact scattered state, were then calculated. The non-Markovian nature of the system under consideration was shown to have a

drastic effect on the statistical properties of the scattered field. Exact results were also compared with approximate calculations where appropriate. Further, the resummation technique used in scattering theory was extrapolated to capture the study of real-time dynamics. The resulting dynamical theory was then showcased on some spontaneous emission problems in non-Markovian waveguide QED systems. Again the nonMarkovianity of the considered systems was shown to have a significant impact on the transient characteristics.

One of the many interesting non-Markovian waveguide QED problems to be solved in the future is the scattering of a coherent state in power non-perturbative regime. This problem is extremely non-trivial since its exact resolution demands the solution of an infinite hierarchy of integral equations. Baring this in mind, we propose that one solves this problem in the weak correlation approximation developed in the present thesis. Within this approximation, n-body vertex functions, parametrizing the $n+1$-particle transition operators, factorize into the product of n single-particle effective vertices and $n-1$ dressed Green's functions. Being cognizant of that the effective single-particle vertex may be often found analytically, the remaining challenge in coherent state scattering problem would be the evaluation of an infinite number of integrals in order to compute the full counting statistics. Although such a method of solution is of an approximate nature, the complicated energy-momentum dependence of the exact single-particle vertex function shall in principle capture the leading non-Markovian effects.

Amongst the dynamical problems, we may identify the following two. First, one can use the exact unitary evolution operator in single-qubit waveguide QED to study the real-time dynamics of a coherent pulse in a Markovian single qubit system. Since in Markovian systems the non-crossing approximation becomes exact, the remaining task would be the evaluation of an infinite number of rather simple integrals. Another long-standing dynamical problem in waveguide QED systems is the general dynamics of two-excitation states. As we know from our general considerations, this problem is equivalent to the solution of the two-excitation subspace dynamics in a two-qubit system. In principle, using the resummation theory, it should be possible to compute all of the 16 matrix elements of the unitary evolution operator in two-qubit waveguide QED.

7.13 Numerical And Analytical Solutions of Integral Equations

7.13.1 A. 1 Single-Photon Effective Vertex

7.13.2 A.1.1 Multi-Finger Coupled Qubit

According to our general theory, all of the non-trivial information about the two-photon scattering is contained in the single-photon effective vertex, which upon parametrization and separation of the singular contribution reads as follows

$$\bar{F}^{(1,1)}(k',k,E) = \sum_{\alpha\in\{1,2\}} \int_{\mathbb{R}} dp \frac{|g_\alpha(p)|^2}{E-k'-p+i\eta} \frac{1}{E-p+\Delta-\sigma(E-p)} \frac{1}{E-p-k+i\eta} + \sum_{\alpha\in\{1,2\}} \int_{\mathbb{R}} dp \frac{|g_\alpha(p)|^2}{E-k'-p+i\eta} \frac{1}{E-p+\Delta-\sigma(E-p)} \bar{F}^{(1,1)}(p,k,E), \quad \text{(A.1)}$$

where

$$\sigma(E) = -i\sum_{n=1}^{N}\Gamma_n - i\sum_{1<n<n'<N}\sqrt{\Gamma_n\Gamma_{n'}}e^{i(E+k_0)(x_{n'}-x_n)} \quad \text{(A.2)}$$

Now, let us consider the following

$$\sum_{\alpha\in\{1,2\}}|g_\alpha(p)|^2 = \frac{1}{2\pi}\sum_{\alpha\in\{1,2\}}\sum_{n'=1}^{N}\sum_{n=1}^{N}\sqrt{\Gamma_{n'}\Gamma_n}e^{ic_\alpha(p+k_0)(x_{n'}-x_n)}$$

$$= \frac{1}{2\pi}\sum_{n'=1}^{N}\sum_{n=1}^{N}\sqrt{\Gamma_{n'}\Gamma_n}e^{i(p+k_0)(x_{n'}-x_n)} + \frac{1}{2\pi}\sum_{n'=1}^{N}\sum_{n=1}^{N}\sqrt{\Gamma_{n'}\Gamma_n}e^{-i(p+k_0)(x_{n'}-x_n)}.$$

Since, by causality, $\bar{F}^{(1,1)}(k',k,E)$ is analytic in the lower half-plane in both k' and k, the only terms contributing to the first sum are those where $n'>n$ whereas the terms contributing to the second one are those where $n>n'$, hence

$$\sum_{\alpha\in\{1,2\}}|g_\alpha(p)|^2\to\tfrac{1}{2\pi}\sum_{1\le n<n'\le N}\sqrt{\Gamma_{n'}\Gamma_n}e^{i(p+k_0)(x_{n'}-x_n)}+\tfrac{1}{2\pi}\sum_{1\le n<n'\le N}\sqrt{\Gamma_n\Gamma_{n'}}e^{i(p+k_0)(x_{n'}-x_n)}$$
$$=\tfrac{1}{\pi}\sum_{1\le n<n'\le N}\sqrt{\Gamma_{n'}\Gamma_n}e^{i(p+k_0)(x_{n'}-x_n)}.$$

By putting the equation on shell $E=k=0$ (bearing in mind the particular form of the initial state it suffices to solve the equation for $E=k=0$) we thus obtain

$$\bar{F}^{(1,1)}(k',0,0)=-\frac{1}{\pi}\sum_{1\le n<n'\le N}\sqrt{\Gamma_{n'}\Gamma_n}\int\limits_{\mathbb{R}}dp\frac{e^{i(p+k_0)(x_{n'}-x_n)}}{k'+p-i\eta}\frac{1}{p-\Delta+\sigma(-p)}\frac{1}{p-i\eta}$$
$$+\frac{1}{\pi}\sum_{1\le n<n'\le N}\sqrt{\Gamma_{n'}\Gamma_n}\int\limits_{\mathbb{R}}dp\frac{e^{i(p+k_0)(x_{n'}-x_n)}}{k'+p-i\eta}\frac{1}{p-\Delta+\sigma(-p)}\bar{F}^{(1,1)}(p,0,0).\quad(A.4)$$

Let us now define the Fourier transform according to the following convention

$$f(x)=\frac{1}{2\pi}\int\limits_{\mathbb{R}}dk\bar{F}^{(1,1)}(k',0,0)\,e^{ikx},\quad\bar{F}^{(1,1)}(k',0,0)=\int\limits_{\mathbb{R}}dxf(x)e^{-ikx}\quad(A.5)$$

With these definitions, the position-space equation finally takes the following form

$$f(x)=I(x)+\int\limits_0^R dx'K(x,x')\,f(x')\quad(A.6)$$

where $R=\max\{|x_{n'}-x_n|\}=x_N-x_1$, and

$$K(x,x')=i\Theta(x)\frac{1}{\pi}\sum_{1\le n<n'\le N}\sqrt{\Gamma_{n'}\Gamma_n}e^{ik_0(x_{n'}-x_n)}\int\limits_{\mathbb{R}}dp\frac{e^{ip(x_{n'}-x_n-x-x')}}{p-\Delta+\sigma(-p)},\quad(A.7)$$

$$I(x,x')=\int\limits_0^R dx'K(x,x').\quad(A.8)$$

Here, we have made use of the fact that for $x>0$ one has

$$\int\limits_{\mathbb{R}}dp\frac{e^{ip(x_{n'}-x_n-x-x')}}{p-\Delta+\sigma(-p)}\propto\Theta(x_{n'}-x_n-x-x')\quad(A.9)$$

So, we see that the passage to the position space leads to the equation for the function with finite support, which, in turn, can be efficiently solved numerically, by e.g employing standard matrix inversion.

7.13.3 A.1.2 Giant Atom. Analytical Solution

In the case of the giant atom, we rewrite (A.4) for $E\neq0$ (this case is interesting since it is needed in three-photon calculations) as follows

$$\bar{F}^{(1,1)}(k',0,E) = -\frac{\gamma e^{ik_0 l}}{2\pi}\int\limits_{\mathbb{R}} dp \frac{e^{ipl}}{k'+p-E-i\eta}\frac{1}{p-\Delta-E-i\gamma\left[1+e^{ik_0 l}e^{-ipl}\right]}\frac{1}{p-E-i\eta}$$
$$+\frac{\gamma e^{ik_0 l}}{2\pi}\int\limits_{\mathbb{R}} dp \frac{e^{ipl}}{k'+p-E-i\eta}\frac{1}{p-E-\Delta-i\gamma\left[1+e^{ik_0 l}e^{-ipl}\right]}\bar{F}^{(1,1)}(p,0,E). \tag{A.10}$$

Now, given an analytic function $f(z)$ in the lower half of the complex z plane, it is easy to verify that for any $\xi \in (-\infty, l]$

$$\int\limits_{\mathbb{R}} dz e^{i\xi z} f(z)\left\{\frac{1}{z-E-\Delta-i\gamma\left[1+e^{ik_0 l}e^{-izl}\right]} - \frac{1}{z-E-\Delta-i\gamma}\right\} = 0 \tag{A.11}$$

which, in turn, leads us to the following simplification of (A.10)

$$\bar{F}^{(1,1)}(k',0,E) = -\frac{\gamma e^{ik_0 l}}{2\pi}\int\limits_{\mathbb{R}} dp \frac{e^{ipl}}{k'+p-E-i\eta}\frac{1}{p-\Delta-E-i\gamma}\frac{1}{p-E-i\eta}$$
$$+\frac{\gamma e^{ik_0 l}}{2\pi}\int\limits_{\mathbb{R}} dp \frac{e^{ipl}}{k'+p-E-i\eta}\frac{1}{p-\Delta-E-i\gamma}\bar{F}^{(1,1)}(p,0,E). \tag{A.12}$$

By defining the Fourier transform according to (A.5), we arrive at the following equation

$$f_E(x) = \Theta(x)\Theta(l-x)\frac{\gamma e^{iEl}e^{ik_0 l}}{\lambda}\left(e^{i\lambda(l-x)}-1\right)$$
$$-\Theta(x)\gamma e^{ik_0 l}\int\limits_0^l dx' e^{iE(l-x')}\Theta\left(l-x-x'\right)e^{i\lambda(l-x-x')}f_E\left(x'\right), \tag{A.13}$$

where we have introduced $\lambda = \Delta + i\gamma$. Now, we consider the following

$$\left(\frac{\partial}{\partial x}+i\lambda\right)f_E(x) = \delta(x)f_E\left(0^+\right) - i\Theta(x)\Theta(l-x)\gamma e^{iEl}e^{ik_0 l} + \Theta(x)\gamma e^{ik_0 l}e^{iEx}f_E(l-x). \tag{A.14}$$

On the other hand,

$$\left(\frac{\partial}{\partial x}-i\lambda\right)f_E(l-x) = -\delta(l-x)f_E\left(0^+\right) + i\Theta(x)\Theta(l-x)\gamma e^{iEl}e^{ik_0 l}$$
$$-\Theta(l-x)\gamma e^{ik_0 l}e^{iE(l-x)}f_E(x) \tag{A.15}$$

hence

$$\left(\frac{\partial^2}{\partial x^2} - iE\frac{\partial}{\partial x} + \lambda E + \lambda^2 + \Theta(x)\Theta(l-x)\gamma^2 e^{iEl}e^{2ik_0 l}\right)f_E(x) = \delta'(z)f_E(0)$$
$$+\delta(x)\left[\gamma e^{ik_0 l}f_E(l) - i\gamma e^{ik_0 l}e^{iEl} - i\lambda f_E\left(0^+\right) - iEf_E\left(0^+\right)\right] + \delta(l-x)\gamma e^{ik_0 l}e^{iEl}\left[i - f_E\left(0^+\right)\right]$$
$$+\Theta(x)\Theta(l-x)\gamma e^{iEl}e^{ik_0 l}\left[i-\lambda+\gamma e^{ik_0 l}e^{iEx}\right] \tag{A.16}$$

Solving this distributional differential equation, we finally obtain

$$f_E(x) = \Theta(x)\Theta(l-x)e^{iEx/2}\left[C_{1+}(E)e^{iEx/2} + C_{1-}(E)e^{-iEx/2} + \left(C_{2+}(E)e^{ip(E)x} + C_{2-}(E)e^{-ip(E)x}\right)\right] \tag{A.17}$$

where we have defined

$$C_{1+}(E) = \frac{i\gamma^2 e^{2ik_0 l}e^{iEl}}{(E+\lambda)\lambda + \gamma^2 e^{2ik_0 l}e^{iEl}}, \quad C_{1-}(E) = -\frac{(E+\lambda)\gamma e^{ik_0 l}e^{iEl}}{(E+\lambda)\lambda + \gamma^2 e^{2ik_0 l}e^{iEl}}, \tag{A.18}$$

$$p(E) = \sqrt{(E/2+\lambda)^2 + \gamma^2 e^{2ik_0 l}e^{iEl}}, \tag{A.19}$$

$$C_{2-}(E) = -i\gamma e^{ik_0 l}e^{iEl/2}\frac{i(E+\lambda)+\gamma e^{ik_0 l}e^{iEl}}{(E+\lambda)\lambda + \gamma^2 e^{2ik_0 l}e^{iEl}} \times \frac{[p(E)+(E/2+\lambda)] + i\gamma e^{ik_0 l}e^{iEl/2}e^{ip(E)l}}{2(p(E)\cos p(E)l - i(E/2+\lambda)\sin p(E)l)}, \tag{A.20}$$

$$C_{2+}(E) = -i\gamma e^{ik_0 l}e^{iEl/2}\frac{i(E+\lambda)+\gamma e^{ik_0 l}e^{iEl}}{(E+\lambda)\lambda + \gamma^2 e^{2ik_0 l}e^{iEl}} \times \frac{[p(E)-(E/2+\lambda)] - i\gamma e^{ik_0 l}e^{iEl/2}e^{-ip(E)l}}{2(p(E)\cos p(E)l - i(E/2+\lambda)\sin p(E)l)}. \tag{A.21}$$

Note, although there is a square root in the definition of $p(E)$, $f_E(x)$ function does not possess any branching points in E-plane since it is an even function of $p(E)$. With this in hands, we can
finally write down the solution in momentum space as

$$\bar{F}^{(1,1)}(k',0,E) = \int_{\mathbb{R}} dx f_E(x)e^{-ikx} = C_{1+}(E)\frac{e^{i(E-k)l}-1}{i(E-k)} + C_{1-}(E)\frac{e^{-ikl}-1}{-ik} + C_{2+}(E)\frac{e^{i(E/2+p(E)-k)l}-1}{i(E/2+p(E)-k)} + C_{2-}(E)\frac{e^{i(E/2-p(E)-k)l}-1}{i(E/2-p(E)-k)} \tag{A.22}$$

As one may additionally note, $\bar{F}^{(1,1)}(k',0,E)$ is an analytic function of k.

7.13.4 A. 2 Optimization Scheme for the Numerical Treatment of the Two-Body Effective Vertex Function Integral Equation

In this part of the Appendix, we would like to present a numerical, or rather semi-analytical, scheme applicable to the solution of the integral equation defining an effective two-body vertex function. As it was anticipated in the main body, in the three-photon sector, due to the high computational complexity, we are going to focus on the giant atom model exclusively. After separation of the singular contribution and parametrization introduced in the main body, we are left with the following integral equation for the on-shell vertex function ($k_1 = k_2 = \epsilon = 0$)

$$\bar{F}^{(2,2)}(k_1',k_2',0,0,0) = -\frac{\gamma e^{ik_0 l}}{2\pi}\int_{\mathbb{R}} dk \frac{e^{ikl}}{k_1'+k_2'+k-i\eta}\frac{1}{k_2'+k-\lambda}F^{(1,1)}(k_2',0,-k)\frac{1}{k-\lambda}F^{(1,1)}(k,0,0) + \frac{\gamma e^{ik_0 l}}{2\pi}\int_{\mathbb{R}} dk \frac{e^{ikl}}{k_1'+k_2'+k-i\eta}\frac{1}{k_2'+k-\lambda}\left[\bar{F}^{(2,2)}(k,k_2',0,0,0) + \bar{F}^{(2,2)}(k_2',k,0,0,0)\right], \tag{A.23}$$

where we have utilized the properties (A.3) and (A.11) discussed above, as before, we define the Fourier transform according to the following convention

$$h(x,y) = \frac{1}{(2\pi)^2}\int\limits_{\mathbb{R}} dk_1' \int\limits_{\mathbb{R}} dk_2' e^{ik_1'x} e^{ik_2'y} \bar{F}^{(2,2)}\left(k_1', k_2', 0, 0, 0\right),$$

$$\bar{F}^{(2,2)}\left(k_1', k_2', 0, 0, 0\right) = \int\limits_{\mathbb{R}} dk_1' \int\limits_{\mathbb{R}} dk_2' e^{-ik_1'x} e^{-ik_2'y} h(x,y). \tag{A.24}$$

Upon the Fourier transformation, the integral equation takes the following form

$$h(x,y) = -\int\limits_0^l dz K(x,z)[h(z, y+z-l) + h(y+z-l, z)] + P(x,y) \tag{A.25}$$

where we have defined the following two functions

$$K(x,z) = \gamma e^{ik_0 l}\Theta(x)\Theta(l-x-z)e^{i\lambda(l-x-z)} \tag{A.26}$$

$$P(x,y) = -\frac{\gamma e^{ik_0 l}}{2\pi}\frac{1}{(2\pi)^2}\int\limits_{\mathbb{R}} dk_1' \int\limits_{\mathbb{R}} dk_2' e^{ik_1'x} e^{ik_2'y} \int\limits_{\mathbb{R}} dk \frac{e^{ikl}}{k_1' + k_2' + k - i\eta}\frac{1}{k_2' + k - \lambda}$$

$$\times F^{(1,1)}\left(k_2', 0, -k\right)\frac{1}{k-\lambda}F^{(1,1)}(k,0,0). \tag{A.27}$$

Let us now compute $P(x,y)$, such a computation is facilitated through the following observation. First of all, we remind ourselves of the following decomposition

$$F^{(1,1)}\left(k_2', 0, -k\right) = -\frac{1}{k + k_2' - i\eta} + \bar{F}^{(1,1)}\left(k_2', 0, -k\right) \tag{A.28}$$

Secondly, from the equation (A.12), by iteration, we can deduce the following representation of $\bar{F}^{(1,1)}\left(k_2', 0, -k\right)$

$$\bar{F}^{(1,1)}\left(k_2', 0, -k\right) = \sum_{n=1}^{\infty} Q_n\left(k_2', k\right) e^{-ikln} \tag{A.29}$$

where $Q_n\left(k_2', k\right)$ are analytic functions of both arguments in their respective lower half-planes. Indeed, this assertion is in line with both an exact solution (A.22) and causality structure a priori built into the theory. By causality, we know that $\bar{F}^{(1,1)}\left(k_1', k_1, \epsilon\right)$ is an analytic function of momenta in the lower half of the complex plane and is an analytic function of ϵ in the upper-half, hence $\bar{F}^{(1,1)}\left(k_1', k_1, -\epsilon\right)$ is analytic in ϵ in the lower half. It hence follows

$$\int\limits_{\mathbb{R}} dk e^{ikl} L(k) \bar{F}^{(1,1)}\left(k_2', 0, -k\right) = 0 \tag{A.30}$$

where $L(k)$ is an analytic function of k in the lower half-plane. Now, using this result we rewrite (A.27) as follows

$$P(x,y) = \frac{\gamma e^{ik_0 l}}{2\pi}\frac{1}{(2\pi)^2}\int\limits_{\mathbb{R}} dk_1' \int\limits_{\mathbb{R}} dk_2' e^{ik_1'x} e^{ik_2'y} \int\limits_{\mathbb{R}} dk \frac{e^{ikl}}{k_1' + k_2' + k - i\eta}\frac{1}{k_2' + k - \lambda}$$

$$\times \frac{1}{k + k_2' - i\eta}\frac{1}{k-\lambda}F^{(1,1)}(k,0,0). \tag{A.31}$$

Now, performing the Fourier integrals, we arrive at the following rather simple result

$$P(x,y) = i\Theta(x)\Theta(y-x)\frac{1}{\lambda}\left(e^{i\lambda(y-x)}-1\right)f_0(y) \tag{A.32}$$

where $f_E(x)$ is defined as above.

By carefully analyzing the above equation, we deduce that the domain of $h(x,y)$ is the following semi-infinite wedge on the (x,y) plane $x \in [0,l], \quad y \in [x,\infty)$. Now, we make the following ansatz

$$h(x,y) = \sum_{n=1}^{\infty} \Theta(nl-y)\Theta(y-(n-1)l)h^{(n)}(x,y) \tag{A.33}$$

where $h^{(n)}(x,y)$ for $n>1$ are further decomposed according to

$$h^{(n)}(x,y) = \Theta((n-1)l-y+x)h^{(n,-)}(x,y) + \Theta(y-x-(n-1)l)h^{(n,+)}(x,y), \quad n>1 \tag{A.34}$$

leading us to the following hierarchy of integral equations

$$\begin{aligned}
h^{(1)}(x,y) \equiv h^{(1,+)}(x,y) &= -\int_0^l dz K(x,z)h^{(1,+)}(y+z-l,z) + P(x,y),\\
h^{(n,-)}(x,y) &= -\int_0^l K(x,z)h^{(n-1,+)}(z,y+x-l),\\
h^{(n,+)}(x,y) &= -\gamma e^{ik_0 l}\int_0^{nl-y} dz e^{i\lambda(l-x-z)}h^{(n-1,+)}(z,y+z-l) -\\
&-\gamma e^{ik_0 l}\int_{nl-y}^{l-x} dz e^{i\lambda(l-x-z)}h^{(n,-)}(z,y+z-l).
\end{aligned} \tag{A.35}$$

Thus, we see that we have to solve only the first equation in the hierarchy and the rest of the functions are given by appropriate convolutions. Such a representation of the solution is numerically beneficial since one can efficiently solve the equation for $h^{(1,+)}$ on a finite domain, and construct all the rest of the functions by simple tensor multiplication. The above functions are defined on their respective simplices, as shown in Figure A.1.

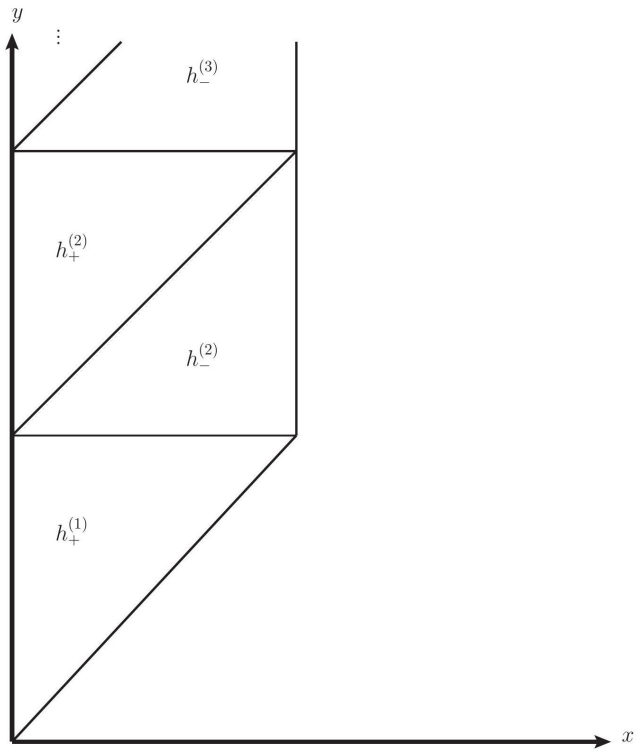

Figure A.1: Domains of the $h_\pm^{(n)}$ functions.

7.14 Other Features and Questions about PP21 Method

7.14.1 Connection of PP21 Method with known QFT and Quantum Optics Theory (????)

(потом пропишу, вопросы про это есть многие. мб уменьшу раздел, посмотрим.)

Вывод данного гамильтониана ил Лагранжиана КЭД (?????)

(пока это вообще не понимаю)

7.14.2 How Exactly the Experiment "Nonexponential decay of a giant artificial atom" by Andersson et. al. Is Explained by PP21 Method?

(???? answer it here????)

7.14.3 General properties of the scattering matrix in waveguide QED

(???? ничего пока не понял, супер сложно считается этот абзац)

Theory

Let us consider the scattering problem for the following initial state $|N_p\rangle \otimes |g\rangle$, where $|N_p\rangle$ is a N_p-photon state, and $|g\rangle = |0\rangle^{\otimes N_q}$ is the ground state of the scatterer. Due to the conservation of excitation-number operator, all of the possible $D\left(N_p, N_q\right)$ scattering outcomes must contain

N_p excitations. (???? это не совсем понимаю, у нас один фотон большой энергии разве не может создать два фотона???)

Due to the fact that for any system of qubits the ground state $|g\rangle$ is the only nondecaying (subradiant) subspace, in the long-time limit (a priori assumed in scattering theory) all of the emitters will definitely decay into the continuum, leaving us with the only possibility for the system to end up in the state $\left|N_p'\right\rangle \otimes |g\rangle$ (here $\left|N_p'\right\rangle$ is again a N_p-photon state, with potentially redistributed momenta) [74].

If one wishes to extend the scattering theory to the systems with metastable ground states, such as, e.g., a Λ three-level system, one then has to consider calculating more matrix elements of the transition operator [75, 76]. (?? потом еще раз прочитаю, не понял)

Since the only matrix elements we are interested in are diagonal in both the photon and qubit spaces, due to the RWA, the only terms contributing to the perturbation expansion of the T matrix are those containing an even number of interactions $\mathcal{V}$, thus reducing the number of diagrams by half.

Another important feature to be mentioned is the nilpotency of the photon-qubit interaction vertex operator $v_{s_1}^\dagger \dots v_{s_{N_q+1}}^\dagger = v_{s_1} \dots v_{s_{N_q+1}} = 0$, which along with the property $v_s|g\rangle = \langle g|v_s^\dagger = 0$ and the fact that the number of v's and $v^\dagger$'s have to be equal in each graph contributing to the expansion, significantly reduces the number of nonzero diagrams at each order in perturbation theory. In fact, as we are going to see in this section, all of the diagrams contributing to the series for any fixed N_q may be constructed out of a finite number of "clusters," in turn allowing, in principle, for the exact resummation of the perturbation series. One can also organize the calculation differently, namely, by fixing N_p and allowing N_q to vary instead. Calculation within this approach is facilitated in its turn by the fact that $a_{s_1} \dots a_{s_{N_p+1}} |N_p\rangle = \langle N_p| a_{s_1}^\dagger \dots a_{s_{N_p+1}}^\dagger = 0$ and the fact that the number of a's and $a^\dagger$'s in each term of the perturbation series have to be equal.

Although, these two approaches are clearly dual due to the structure of interaction potential in RWA. This approach is beneficial when studying few-photon scattering on a large number of qubits. This assertion has to do with the fact that once the solution of N_p photon scattering problem on $N_q = N_p$ the scattering of N_p particles on $N_q > N_p$ follows the same lines. Indeed, since v_s $\left(v_s^\dagger\right)$ by itself contains the sum of all of the single-qubit lowering (raising) operators and the highest number of qubits that the N_p-photon pulse can excite equals to N_p, the normal ordered N_p-photon S matrix cannot contain projectors on subspaces with higher-excitation number than N_p.

Using this fact in the following we are going to derive the generic two- and three-photon scattering matrices by considering two- and three-particle scattering on two and three atoms, respectively.

(крч, надеюсь, что выше - просто слова, ничего супер важного.)

8 Reliable multiphoton generation in waveguide QED by González-Tudela et al.

Abstract

In spite of decades of effort, it has not yet been possible to create single-mode multiphoton states of light with high success probability and near unity fidelity. Complex quantum states of propagating optical photons would be an enabling resource for diverse protocols in quantum information science, including for interconnecting quantum nodes in quantum networks. Here, we propose several methods to generate heralded mutipartite entangled atomic and photonic states by using the strong and long-range dissipative couplings between atoms emerging in waveguide QED setups. Our theoretical analysis demonstrates high success probabilities and fidelities are possible exploiting waveguide QED properties.

8.1 Main Theory

On-demand generation of optical propagating photons is at the basis of many applications in quantum information science, including multipartite teleportation [1], quantum repeaters [2], quantum cryptography

[3, 4], and quantum metrology [5]. While single photons are routinely produced in different experimental setups [6], *single–mode multiphoton states* are much harder to generate [7]. Current methods are limited by either an exponentially small success probabilities or by low fidelities. Here we show that reliable single-mode multiphoton sources can be constructed with emitters close to nano-photonic waveguides by combining both the strong coupling present in those systems and collective phenomena. In particular, we show how collective excitations can be efficiently loaded in a collection of atoms, which can then be released with a fast laser pulse to produce the desired multi-photon state [8, 9]. In order to boost the success probability and fidelity of each excitation process, our method utilizes atoms to both generate the excitations in the rest, as well as to herald the successful generation. Furthermore, to overcome the exponential scaling of the probability of success with the number of excitations, we design a protocol to merge excitations that are present in different internal atomic levels with a polynomial scaling.

The enhancement of light-matter interactions provided by quantum nanophotonics opens up new avenues to create high-fidelity multiphoton states. For example, m quantum emitters can be strongly coupled to structured waveguides, which show large Purcell factors, $P_{1\mathrm{d}}$, so that m atomic excitations can be mapped to a waveguide mode with an error (or infidelity, I_m) scaling as $m/P_{1\mathrm{d}}$. However, the resulting state is not a single mode, but a complex entangled state of several modes [9], so that it cannot be directly used for quantum information purposes. Single-mode multiphoton states can be created by storing m collective excitations in $N \gg m$ atoms, which are then mapped to a photonic state of the waveguide. While the latter process can be achieved with very low infidelity, scaling as $m^2/(NP_{1\mathrm{d}})$ [8, 9], present schemes for the first part scale like $I_m \propto m/\sqrt{P_{1\mathrm{d}}}$ [9], as they still do not fully exploit the strong coupling to the waveguide nor collective effects. This ultimately limits the fidelity of the whole procedure.

In this work we show how this limitation can be overcome with new schemes for the heralded generation of m collective excitations in $N \gg m$ atoms coupled to a waveguide. The basic idea is to use the atoms themselves to both create the excitations one-by-one, and to herald the success of the process. In this way, arbitrarily small infidelities, I_m, can be obtained at the expense of making the process non-deterministic. Depending on the scheme, we find that the global probability of success (or, inversely, the average number of operations, R_m) decreases (increases) exponentially with m, and thus it cannot be scaled to arbitrarily large photon production. Finally, we also show how to overcome this exponential law by using additional atomic states, atom number resolved detection, and a specific protocol to merge excitations, while keeping a very low global infidelity, $I_m \sim \mathrm{poly}(m)/(NP_{1\mathrm{d}})$.

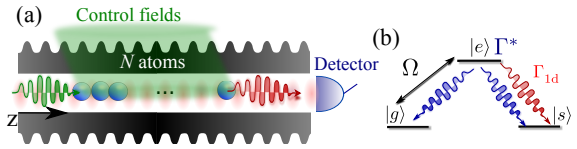

Figure 8.1: (a) Setup for the first protocol: N *target* atoms are collectively coupled to the waveguide. A photon detection heralds the addition of a collective excitation. (b) Atomic level structure: waveguide modes are coupled to the $e \leftrightarrow s$ transition with a spontaneous emission rate $\Gamma_{1\mathrm{d}}$. The transition $g \leftrightarrow e$ is driven by a Raman laser Ω and the spontaneous emission rate to other modes is denoted by Γ^*.

Structured waveguide setups with trapped atoms offer several interesting characteristics that we exploit to design our protocols, namely, i) regions of large Purcell Factor $P_{1\mathrm{d}} \gg 1$, e.g., due to slow light in engineered dielectrics [10, 11, 12, 13], while keeping at the same time ii) long-propagation lengths of the guided modes compared to the characteristic wavelength (λ_{a}) that give rise to long-range dissipative couplings [14]. Moreover, as shown in, e.g. Ref. [14], in order to avoid dipole-dipole interactions and fully exploit superradiance effects we assume iii) the atoms to be placed at distances $z_n = n\lambda_{\mathrm{a}}$, with $n \in \mathbb{N}$. [1]. Finally, iv) it is possible to read the collective atomic state very efficiently through the waveguide due to the naturally short timescales and large collection efficiencies. We use atomic detection for heralding, which has already reached accuracies of 10^{-4} [16] in trapped ion setups, where the collection efficiency is not enhanced by the presence of a waveguide, as in our scheme. Thus, here we assume the atomic detection to be perfect, and consider $P_{1\mathrm{d}}$ and N as the main resources to analyze the figures of merit of the protocols. For the analysis of three different schemes, we adopt the following strategy for each one: we analyze the process of generating a single collective excitation, assuming the atoms already store m excitations. We denote by p the probability of success, and $I_{m\to m+1}$ the corresponding infidelity. We finally analyze the average number of operations R_m and final infidelities I_m for accumulating all m excitations. To simplify the expressions along the main text, we assume to work in a regime with $N \gg m$ and $P_{1\mathrm{d}} \gg 1$, though complete expressions can be found in Supplementary Material [17].

Let us first analyze a protocol inspired in a method originally devised to create long-distant entangled states in atomic ensembles [18], that requires N atoms placed close to a 1d waveguide as depicted in Fig. 16.1(a). The atoms must have a level structure as depicted in Fig. 16.1(b), where the atomic transition $e \leftrightarrow s$ is coupled to the guided modes at a rate $\Gamma_{1\mathrm{d}}$ and the transition $g \leftrightarrow e$ is driven equally by a laser with Rabi frequency Ω. The excited states e also radiate into leaky modes (of the waveguide or outside) other than the relevant one, that give rise to a decay rate Γ^*, leading to the Purcell factor $P_{1\mathrm{d}} = \Gamma_{1\mathrm{d}}/\Gamma^*$. The excitations are stored in the states g and s, which are assumed to be decoherence-free like any other hyperfine ground state. The procedure assumes that we start with m collective excitations in level s, and the goal is to add another one. Thus, the

[1] In fact all results can be extended to separations of $\lambda_{\mathrm{a}}/2$

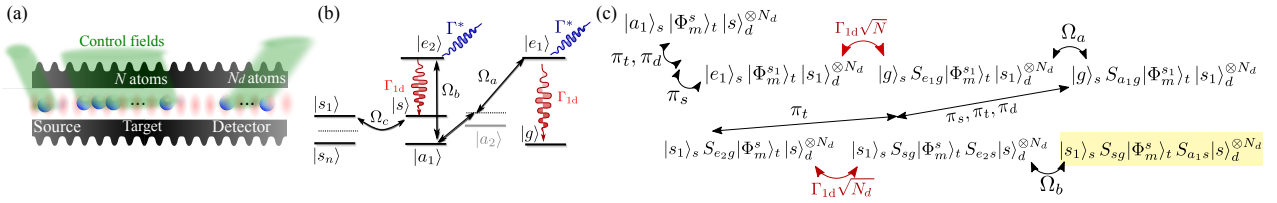

Figure 8.2: (a) Setup for the second and third protocol: N *target*, one *source* and N_d *detector* atoms are collectively coupled to the waveguide. The source atom creates a single excitation, and the detector atoms herald the success of the process. (b) Atomic level structure: waveguide modes are coupled to the $e_1 \leftrightarrow g$ and $e_2 \leftrightarrow s$ transition with a spontaneous emission rate Γ_{1d}. A two-photon transition $a_1 \leftrightarrow e_1$ is driven by laser light via level a_2 with effective Rabi frequency Ω_a. Transition $a_1 \leftrightarrow e_2$ is driven by a different laser with Rabi frequency Ω_b. Coupling between levels s, s_1 is characterized by a Rabi frequency Ω_c. Other levels $\{s_n\}$ can be manipulated using lasers/microwave fields. (c) Scheme for the second protocol, with $\pi_{c,t,d}$ denoting the π-pulses for the population transfers within the source/target/detector atoms. The driven transitions to the excited states are indicated by the Rabi frequencies $\Omega_{a,b}$. In shaded yellow the final state where we want to arrive is indicated.

initial state is $|\Phi^s_m\rangle \propto \mathrm{sym}\{|s\rangle^{\otimes m} \otimes |g\rangle^{N-m}\}$, where 'sym' denotes the symmetrizing operator. The idea is to weakly excite the atoms in g to level e with a short laser pulse of duration $T \ll 1/(N\Gamma_{1d})$ and if a photon in the waveguide is detected, it heralds the addition of an excitation in state s. As all the atoms are equally coupled to the waveguide, the excitation will be collective.

Let us denote by $x = \Omega\sqrt{N}T/2 \ll 1$, so that right after the pulse we have the state (up to a normalization constant), $\left[\mathbf{1} + x\, S_{eg} + x^2\, S^2_{eg} + O(x^3)\right] |\Phi^s_m\rangle$, where we used the notation $S_{\alpha\beta} = (N)^{-1/2} \sum_{n=1}^{N} \sigma^n_{\alpha\beta}$ for the collective spin operators and $\sigma^n_{\alpha\beta} = |\alpha\rangle_n \langle\beta|$ with atom number $n = 1, \ldots, N$. After the pulse, we leave the system free to evolve under the interaction with the waveguide for a time $t \gg 1/\Gamma^*$), in which case the wavefunction terms with excitations in e decay either to waveguide/leaky photons. If a waveguide photon is detected, either it comes from the lowest order term, $O(x)$, in which case the atomic state will be the desired one, i.e., $S_{sg}\,|\Phi^s_m\rangle$, or from the double excited state, in which case we will prepare the wrong state introducing an error. Emission of leaky photons also produces errors, but of smaller order [17]. Denoting by η the detection efficiency, the success probability in generating the desired state is $p \approx \eta x^2$ and the infidelity is $I_{m\to m+1} \propto (1-\eta)x^2$ [to lowest order in x]. To create m excitations, one has to detect m consecutive photons, leading to $R_m = p^{-m}$ and $I_m \propto m(1-\eta)x^2$. As in Ref. [18], the error can be made arbitrarily small at the expense of decreasing the success probability. If a high fidelity is required (e.g., 0.999) the method is practicable only for few excitations. One way of reducing R_m is by using an additional metastable state s_1 in which the heralded excitation is stored after each successful addition. This can be done by combining, e.g., a two-photon Raman transition, to make a beam splitter transformation between levels s and s_1, and post-selection conditioned on no atomic detection in s. Then, assuming that we have m excitations already stored in s_1, this procedure generates $m+1$ within the same level. It can be shown [17, 19] that this strategy leads to an average number of operations $R_m \propto e^m/p$.

To overcome the trade-off between probabilities and fidelities coming from zero and double excitations, we propose a protocol relying on a configuration as depicted in Fig. 16.2(a): we replace the write field of the previous scheme by a single *source* atom that guarantees the transfer of at most a single excitation to the *target* ensemble. Furthermore, in a second step, N_d *detector* atoms act as a detector to herald the transfer of excitations, replacing the photon detector. Both the source and detector atoms should be separated from the target ensemble by a multiple of $\lambda_a/2$ and sufficiently separated for independent addressing with external control fields. The protocol requires a level structure as shown in Fig. 16.2(b) where two dipolar transitions $e_1 \leftrightarrow g$ and $e_2 \leftrightarrow s$ are coupled to the same waveguide mode with rates that we set to be equal for simplicity and with a corresponding Purcell Factor P_{1d}. We require the use of other hyperfine, auxiliary levels, a_1, a_2, s_1. The transition $a_1 \leftrightarrow e_2$ is connected by a laser, whereas the $a_1 \leftrightarrow e_1$ is a two-photon transition mediated by a_2, with effective Rabi frequency Ω_a, so that direct spontaneous emission from $e_1 \to a_1$ is forbidden [20, 8, 21, 17]. The level s_1 is used to store excitations and decouple them from the dynamics induced by the waveguide. We require that s_1 is not connected to neither e_1 nor e_2 by a dipole transition, so that it will only be connected to s coherently through microwave fields.

As before, this protocol starts with a superposition in the target ensemble $|\Phi^s_m\rangle_t$, and with the source/detector atoms in a_1/s respectively. The heralded transfer of a single collective excitation consists of several steps [Fig. 16.2(c)]. The first one, coherently transfers the excitations from $s \to s_1$ in the target and detector ensemble to protect them from the waveguide dynamics. The second step uses a short laser pulse in the source atom to excite it to state e_1, and then switches on the lasers driving $e_1 \leftrightarrow a_1$ via a two-photon transition in the target ensemble with (effective) Rabi frequency Ω_a for a time T_a. Ideally, the source atom exchanges the excitation with the target ensemble by a virtual photon in the waveguide, thus generating a collective excitation in a_1-state of the target ensemble. After that, the laser Ω_a is turned off and one waits for a time $t \gg (\Gamma^*)^{-1}$ such that any (non-ideal) remaining population in the excited state decays. Thirdly, we apply π-pulses to decouple the

source atom and couple the target and detector ensemble. Another short pulse is applied to move the collective excitation in the target ensemble from a_1 to e_2 and we switch on the laser Ω_b driving the $e_2 \leftrightarrow a_1$ transition in the detector ensemble for a time T_b with Rabi frequency Ω_b. This transfers the collective excitation in the target ensemble to s and creates a collective excitation in a_1 in the detector ensemble. At the end, a measurement of that internal state, a_1, of the detector atoms (through fluorescence in the waveguide) heralds the successful preparation of a collective excitation in the target ensemble, i.e., $\left|\Phi^s_{m+1}\right\rangle_t$.

Let us now analyze the protocol in detail. In the second step, the evolution of the source/target atoms is described by a master equation [17], which can be analytically solved in the limit $NP_{1\mathrm{d}} \gg 1$. By choosing the Rabi frequency $\Omega_a \approx \sqrt{N\Gamma_{1\mathrm{d}}\Gamma^*}$, and $T_a = \pi/\sqrt{\Gamma_{1\mathrm{d}}\Gamma^*}$, the probability for the ensemble to end up in the desired state after the second step, $|g\rangle_s \otimes S_{a_1 g} \left|\Phi^{s_1}_m\right\rangle_t$, is maximized $p_\mathrm{a} \approx e^{-\pi/\sqrt{P_{1\mathrm{d}}}}$, which can be improved by appropriate pulse shaping [17]. Similarly, in the third step, the evolution of the source/detector atoms can be analytically solved in the limit $N_d P_{1\mathrm{d}} \gg 1$, obtaining a probability to end up in the desired state $S_{sg} \left|\Phi^s_m\right\rangle_t \otimes S_{a_1 s} |s\rangle_d^{\otimes N_d}$ given also by $p_\mathrm{b} \geq p_\mathrm{a}$. Thus, the total probability of success of the protocol is lower bounded by $p \gtrsim p_\mathrm{a}^2$, with a heralding infidelity $I_{m\to m+1} = 0$, as we rule out all the possible errors through post-selection. Indeed, the only way to have the detector atom in a_1 is that the steps two and three have occurred as desired. Any spontaneous emission in any of the atoms or photon absorption is incompatible with that event. Thus, to accumulate m excitations we need to repeat an average number of times $R_m \propto p^{-m}$, but with $I_m = 0$. As p can be very close to 1 for systems with $N, N_d, P_{1\mathrm{d}} \gg 1$, we can still expect to achieve big number of excitations $m \gg 1$ in spite of the exponential scaling of R_m as shown in Fig. 16.3 for systems with $N, N_d \gg m$. In case of unsuccessful detection, then, we pump all the target atoms back to $|g\rangle$ and re-initialize the process.

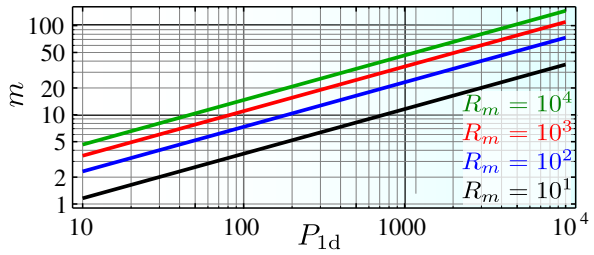

Figure 8.3: Approximate number m of collective excitations with $I_m = 0$ for a fixed number of repetitions R_m (see legend) for the method where we directly accumulate excitations such that $R_m = p^{-m}$ and $p \approx p_a^2$, with p_a as defined in the text and assuming $N, N_d \gg m$.

After this analysis one natural question arises, that is, whether the exponential number of operations is a fundamental problem of probabilistic protocols [19]. This leads to our third and final scheme in which we design a specific protocol which circumvents this exponential scaling with a judicious modification of the previous protocol using several additional atomic states s_n [see Fig. 16.2(b)] and atomic number resolved detection. The idea is that with each successful detection, we transfer the heralded collective excitation in s not to the same level s_1, but to one of several states $\{s_n\}$ to then *merge* them a posteriori with an adequate protocol that we explain below. For that note that, in contrast to our previous schemes, in case of unsuccessful detection, i.e., the detector atoms were not found in a_1, the m excitations stored in $\{s_n\}_n$ are not destroyed, but only the one we wanted to add. We can pump back the target atoms in s, a_1 to g and try again. The price one has to pay is that errors appear since one may not recover the original collective state in the ensemble, i.e., because a spontaneous emission event occurred within the target ensemble [17]. One can show that the main source of errors occurs when a collective excitation was indeed produced in the ensemble, but it was not detected (because, e.g., of spontaneous emission in the detector ensemble). In order to reduce this error, we have to ensure that undetected collective states return back to g coherently. For that, we apply the following repumping procedure: first, we pump all levels but $s, \{s_n\}_n$ back to g. Then we coherently transfer the potential excitations from $s \to a_1$, and then apply a pumping through the waveguide, $a_1 \to e_1 \to g$. In order to further minimize the errors introduced by repumping and obtain the desired scaling of infidelity $(1/(NP_{1\mathrm{d}}))$, we also need to modify the third step of the protocol for which then, interestingly, only a single detector atom is needed, $N_d = 1$. It can be shown that once we are in $S_{a_1 g} \left|\Phi^{\{s_n\}_n}_m\right\rangle |s\rangle_d$, the optimal strategy is to apply a fast π-pulse in the target atoms such $S_{e_2 g} \left|\Phi^{\{s_n\}_n}_m\right\rangle_t$ is prepared. Then, the system is left free to interact for a time $T_\mathrm{b} = 1/\Gamma_{1\mathrm{d}}$ without any external fields, and the dynamics are terminated by applying another π-pulse on the target and detector atoms. We find that the optimal probability for the system to be in $S_{sg} \left|\Phi^{\{s_n\}_n}_m\right\rangle_t \otimes |a_1\rangle_d$ is $p_\mathrm{b} \approx 0.1\,(1 - 1/P_{1\mathrm{d}})$, which can be improved up to $p_\mathrm{b} \sim 0.33$ by repeating the fast π-pulses several times [17]. Finally, if we fail, we apply the repumping and repeat the process until success, of the order of $1/p$ times with $p = p_\mathrm{a} p_\mathrm{b}$. In Ref. [17], we analyze the process in detail, identifying all errors and how they accumulate in the repetitions, leading to an (averaged) infidelity $I_{m\to m+1} \lesssim m/(pNP_{1\mathrm{d}})$ [17]. We confirm numerically (Fig. 16.4) the scaling of p and $I_{m\to m+1}$ integrating the corresponding master equation, showing that our analytical estimations capture the right scalings.

Thus, the problem is reduced to *merging* the atomic excitations distributed in the levels $\{s_n\}_n$. For example, if instead of adding excitations one by one, as we did for the first scheme, we use $\log_2 m$ metastable states s_n, and adopt a tree-like structure, we obtain a superpolynomial scaling [22, 17] in $R_m \propto m^{\log_2 m}/p$ to merge m collective

excitations in a single atomic level. The key step is to double the number of excitations in each step using beam splitter transformations and post-selection conditioned no atomic detection in one of the levels. Moreover, combining the beam splitters with displacement transformations, arbitrary superpositions of collective atomic excitations can be obtained [19, 22, 17].

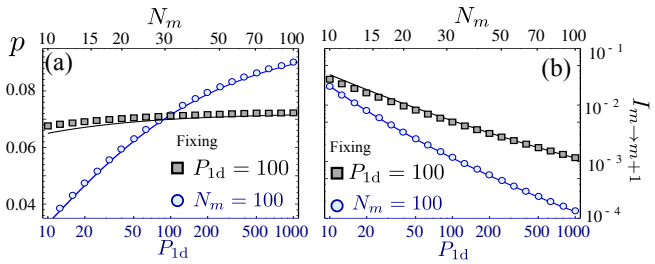

Figure 8.4: Numerical calculation (markers) and analytical approximation (solid lines) of total probability p and $I_{m\to m+1}$ for the third protocol discussed in the text in panel (a) and (b) respectively. We plot the variation with P_{1d} for fixed $N_m = 100$ (in blue) and with N_m for fixed $P_{1d} = 100$. The analytical approximations for p_a, p_b are given in the text and the analysis is made in Ref. [17]. The curves are obtained from full numerical integration of the master equation.

Finally, we go one step further by using number-resolved atomic detection to obtain a polynomial scaling. The key point is to realize that if we have n excitations stored in two atomic levels, after applying a beam splitter transformation, the probability to obtain exactly $2n$ excitations in one of them (by detecting no excitation in the other) decays with n; however, the probability of obtaining more than $3n/2$ in one level (by detecting $p < n/2$ in the other) is actually bounded below by $1/3$, independent of n [17]. Assuming the worst case scenario in which after detecting $q < m/2$ excitations in one of the two levels, we assume that the other state only goes up to $3n/2$ excitations, that gives us an upper bound for the number of operations [17] $R_m \lesssim m^{4.41}\log_{3/2}(m)/p$, that is already polynomial, and which in practical situations is better as the number of excitations in the other mode is always larger than $3n/2$. The number of atomic levels, $|s_i\rangle$, required to reach m excitations scales logarithmically $\log_{3/2} m$, and the final infidelity scales as $I_m \propto \text{poly}(m)/(NP_{1d})$. We note that atomic detection may itself introduce errors, however, the aim of this scheme is just to show that polynomial scaling can be achieved, despite not being currently the most efficient method. However, we expect that by suitable modification and adaptation to specific setups, polynomial and efficient scaling can be constructed.

State-of-the art technologies already provide systems with $N \sim 1-2$ emitters coupled to engineered dielectrics [23, 24, 12, 13, 10, 11] with $P_{1d} \sim 1-100$. Advances in both fabrication and trapping techniques foresee implementations with $N \sim 100$ atoms and $P_{1d} \gtrsim 100$ in the near future. The use of atomic internal levels may be replaced by motional levels of each of the atoms, if they are trapped in pseudo-harmonic potentials [25], since there can be many of them at our disposal. There are several sources of errors that have not been considered here and that will give limitations to our proposal, such as decoherence of hyperfine levels, laser fluctuations, non perfect atom-resolving detection, although we expect that they can be controlled to a large extent. Other effects such as retardation, imperfect atomic cooling, or fluctuations in atomic positions may have to be considered in the analysis to achieve large fidelities (see, however [9] where part of these errors were already considered).

In conclusion, we have presented several probabilistic protocols to generate heralded highly entangled atomic states that afterwards can be mapped to photonic states at will with very high fidelities. In particular, we show how to accumulate m collective atomic excitations with infidelity $I_m = 0$ and an exponential number of operations $R_m = p^{-m}$, being p the heralding probability for adding a single excitation. We design a protocol where p can be close to unity for systems with large N, P_{1d}, which would allow to accumulate $m \sim 20-50$ excitations with systems $P_{1d} \sim 10^2 - 10^3$ using $R_m \sim 10^4$ operations with unit fidelity [see Fig. 16.3]. Moreover, we also present a protocol with polynomial scaling in the number of operations R_m by using atomic excitation number resolved and overall low infidelity $I_m \propto \text{poly}(m)/(NP_{1d})$. Though, we discus our protocols in the context of waveguide QED, the ideas can also be exported to other systems such as low mode cavities [26, 23, 24, 27], superconducting circuits [28] or optical fibers [29, 30, 31, 32] with suitable modification of the protocols.

Acknowledgements. The work of AGT, VP and JIC was funded by the European Union integrated project *Simulators and Interfaces with Quantum Systems* (SIQS). AGT also acknowledges support from Intra-European Marie-Curie Fellowship NanoQuIS (625955). VP acknowledges the Cluster of Excellence NIM. HJK acknowledges funding by the Air Force Office of Scientific Research, Quantum Memories in Photon-Atomic-Solid State Systems (QuMPASS) Multidisciplinary University Research Initiative (MURI), by the Institute of Quantum Information and Matter, a National Science Foundation (NSF) Physics Frontier Center with support of the Moore Foundation by the Department of Defense National Security Science and Engineering Faculty Fellows (DoD NSSEFF) program, by NSF PHY1205729 and support as a Max Planck Institute for Quantum Optics Distinguished Scholar.

8.2 Supplemental Material: Reliable multiphoton generation in waveguide QED

In this Supplementary Material, we provide the full details on how to characterize the different protocols described within the main manuscript. For the sake of understanding, we devote different Sections to the each protocol including in all of them the atom-waveguide tools required and the calculation of probabilities and fidelities such that each Section is self-contained. The summary of the Supplementary Material reads as follows:

- In Section 8.3, we discuss the first protocol of the main manuscript which adapts a protocol envisioned for entangling atomic ensembles [18] to herald the generation of m collective excitations using single photon detections within the waveguide. We discuss both the situation where we accumulate directly the excitations into the same atomic level and where we store it in another hyperfine level and combine them a posteriori.

- In Section 8.4, we discuss the second protocol of the main manuscript which accumulate excitations directly within the same level using a two-step protocol. The protocol overcomes the trade-off between probability of success and fidelities of the first one but still requires an exponential number of operations.

- In Section 8.5, we discuss the third protocol which show to overcome the exponential scaling of the number of operations of the second protocol by using extra auxiliary levels to store the excitations after each heralded transfer while keeping the overall infidelity still low

- For completeness, in Section 8.6 we discuss a variation of the previous two protocol that relaxes part of the requirements of the protocols two and three, e.g., closed transition, at expense of slightly worse scaling of probabilities and infidelities.

- Finally, in Section 8.7 we discuss on how to use beam splitters transformations and atomic detection to merge atomic excitations and reach high photon numbers.

8.3 Heralding multiple collective atomic excitations in waveguide QED setups using single photon detectors.

In this Section is show how to adapt a protocol originally envisioned to generate entanglement between distant ensembles [18], to create multiphoton states in waveguide QED setups. The idea is to accumulate several collective atomic excitations, that can afterwards be mapped to m-photon states with very high fidelities [8, 9].

The protocol consists in heralding the transfer a single collective atomic excitations m times through m photon detection events within the waveguide. We discuss two different approaches: i) one where we store the heralded single excitation in a different level s_1 with methods that we revise in Section 8.7; ii) or where we store the excitation directly into the same level.

The key step in both cases is to study how an additional single collective excitation can be added to an atomic ensemble which already contains m excitations in another level, s_1, i.e.

$$|\Phi_m^{s_1}\rangle = \frac{1}{\sqrt{\binom{N}{m}}}\mathrm{sym}\{|s_1\rangle^{\otimes m}|g\rangle^{\otimes(N-m)}\}\,. \tag{8.1}$$

Notice, that due to low heralding efficiencies p of these kind of protocols [18], it is not clear whether the decoherence introduced when repeating the protocol $1/p$ times will spoil the coherence of the already stored excitations in $|\Phi_m^{s_1}\rangle$. In the following Sections, we analyze what are the atom-waveguide resources that we use to extend the protocol for multiple excitations. Then, we analyze the probabilities of the different processes that may occur in each attempt of generating an extra collective excitation, and finally, we take everything into account to estimate the fidelity of adding an extra excitation when the system is already in $|\Phi_m^{s_1}\rangle$. In a separate Section, we will consider the modifications of probabilities when we directly accumulate in s, such that the initial state is $|\Phi_m^{s}\rangle$.

8.3.1 Atom-waveguide resources

The tools/resources that we use are:

- We assume that we have N *target* atoms, in which we prepare the superposition, trapped close to a one-dimensional waveguide as depicted in Fig. 8.5 (a). Moreover, we assume that the atoms have an internal level structure, as shown in Fig. 8.5(b), where one optical transition $|e\rangle \leftrightarrow |s\rangle$ is coupled to a waveguide mode with a rate $\Gamma_{1\mathrm{d}}$, and the other leg $|e\rangle \rightarrow |g\rangle$ is controlled by a classical field Ω^n, with $n = 1, \ldots, N$. In one of the schemes that we explore, we also assume that we have an extra mode s_1, where the excitations can be stored and which can be combined through microwave or two-photon Raman transitions with Rabi frequency G.

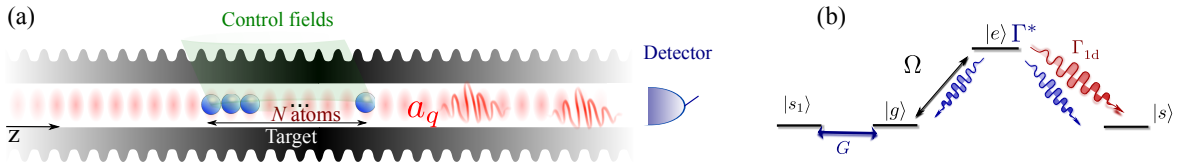

Figure 8.5: (a) General setup for first protocol discussed in the main manuscript which consists of a collective ensemble where we prepare superpositions and a single photon detector that we use to herald the excitations. (b) Internal level structure of emitters in which the transition $|e\rangle \leftrightarrow |s\rangle$ is coupled to a waveguide mode with rate Γ_{1d}. The transition $|g\rangle \leftrightarrow |e\rangle$ is controlled through the Raman laser Ω. We also include the possibility of having an extra auxiliary level $|s_1\rangle$ where excitations can be stored using microwave [or two-photon Raman] fields G.

- The atoms are placed at distances commensurate with the characteristic wavelength of the guided mode, λ_a, at the frequency of the transition $|e\rangle \to |g\rangle$, i.e. $z_n = n\lambda_a$. With that assumption, it is easy to show that effective atom dynamics induced by the interaction with the waveguide is solely driven by long-range dissipative couplings:

$$\mathcal{L}_{\text{coll}}[\rho] = \frac{\Gamma_{1d}}{2} D_{S_{ge}}[\rho], \tag{8.2}$$

  where ρ is the reduced density matrix of the atomic system, $D_O[\rho] = (2O\rho O^\dagger - O^\dagger O\rho - \rho O^\dagger O)$ is the dissipator associated to a given jump operator O, and where we defined the collective spin operator of the target ensemble as $S_{\alpha\beta} = \sum_{n=1}^{N} \sigma^n_{\alpha\beta}$, with $\sigma^n_{\alpha\beta} = |\alpha\rangle_n \langle\beta|$. Obviously, the excited state can also decay to other modes other than into the waveguide, which leads to extra Lindblad terms which read:

$$\mathcal{L}_*(\rho) = \sum_{n=1,\dots,N} \left(\frac{\Gamma^*}{4} D_{\sigma^n_{se}}[\rho] + \frac{\Gamma^*}{4} D_{\sigma^n_{ge}}[\rho] \right), \tag{8.3}$$

  which lead to finite Purcell factor $P_{1d} = \frac{\Gamma_{1d}}{\Gamma^*}$.

- A single photon detector with overall efficiency η at the end of the waveguide to detect the emission of waveguide photons.

8.3.2 Protocol and calculation of probabilities.

The protocol works as follows: we apply a short laser pulse $\Omega^n = \Omega$ such that we drive the collective dipole excitation coupled to the waveguide S_{ge}, during a short time T such that $\sqrt{N}\Omega T/2 = x \ll 1$. Then, the stored superposition $|\Phi^{s_1}_m\rangle$ evolves into:

$$|\Psi_0\rangle \propto |\Phi^{s_1}_m\rangle + x\frac{1}{\sqrt{N_m}} S_{eg} |\Phi^{s_1}_m\rangle + \frac{x^2}{2}\sqrt{\frac{2}{N_m(N_m-1)}} S^2_{eg} |\Phi^{s_1}_m\rangle + O(x^3). \tag{8.4}$$

If we leave the system free to decay for a time $t \gg (\Gamma^*)^{-1}$, the system evolves to (dropping normalization and coefficients):

$$\begin{aligned}
|\Psi_0\rangle \to\ & |\Phi^{s_1}_m\rangle + xS_{sg} |\Phi^{s_1}_m\rangle \otimes |1_k\rangle + x\sum_n \sigma^n_{gg} |\Phi^{s_1}_m\rangle \otimes |1^*_{k,n}\rangle + \sum_n \sigma^n_{sg} |\Phi^{s_1}_m\rangle \otimes |1^*_{k,n}\rangle + , \\
& + x^2 S^2_{sg} |\Phi^{s_1}_m\rangle \otimes |2_k\rangle + x^2 \sum_n \sigma^n_{gg} S_{sg} |\Phi^{s_1}_m\rangle \otimes |1_k\rangle \otimes |1^*_{k,n}\rangle + x^2 \sum_n \sigma^n_{sg} S_{sg} |\Phi^{s_1}_m\rangle \otimes |1_k\rangle \otimes |1^*_{k,n}\rangle + \\
& + x^2 \sum_{n,m} \sigma^n_{sg}\sigma^m_{gg} |\Phi^{s_1}_m\rangle \otimes |1^*_{k,m}\rangle \otimes |1^*_{k,n}\rangle + x^2 \sum_{n,m} \sigma^n_{gg}\sigma^m_{gg} |\Phi^{s_1}_m\rangle \otimes |1^*_{k,m}\rangle \otimes |1^*_{k,n}\rangle + x^2 \sum_{n,m} \sigma^n_{sg}\sigma^m_{sg} |\Phi^{s_1}_m\rangle \otimes |1^*_{k,m}\rangle \otimes |1^*_{k,n}\rangle
\end{aligned} \tag{8.5}$$

where the $|M_k\rangle$ [$|M^*_k\rangle$] denotes waveguide (leaky) photon states. The first line of the equation contains the processes where no photon ($|\Phi^{s_1}_m\rangle$) or only one photon is emitted either through the waveguide or through spontaneous emission. In the second and third lines we write the different processes associated with the existence of double quantum jumps. In order to obtain the different probabilities associated to each process, we use the

expansion of the master equation [33] distinguishing the evolution of the effective non-hermitian Hamiltonian, i.e., $S(t,t_0)\rho = e^{-iH_{\rm eff}t}\rho e^{iH_{\rm eff}^\dagger t}$, and the one resulting from quantum jumps evolution, i.e., $J\rho$, that is given in general by:

$$\rho(t) = S(t,t_0)\rho(t_0) + \sum_{n=1}^{\infty}\int_{t_0}^{t} dt_n S(t,t_n)J(t_n)\cdots\int_{t_0}^{t_2} dt_1 S(t_1,t_0)\rho(t_0)\,. \tag{8.6}$$

The non-hermitian evolution leads to:

$$|\Psi(t)\rangle \propto e^{-iH_{\rm eff}t}|\Psi_0\rangle \propto |\Phi_m^{s_1}\rangle + x\frac{e^{-(\Gamma_{1\rm d}+\Gamma^*)t}}{\sqrt{N_m}}S_{eg}\ |\Phi_m^{s_1}\rangle + \frac{x^2}{2}e^{-2(\Gamma_{1\rm d}+\Gamma^*)t}\sqrt{\frac{2}{N_m(N_m-1)}}S_{eg}^2|\Phi_m^{s_1}\rangle + O(x^3)\,, \tag{8.7}$$

where we see that if we wait a time long enough, i.e., $t \gg (\Gamma^*)^{-1}$ the only population remaining in $|\Psi(T)\rangle \to |\Phi_m^{s_1}\rangle$. The probability emitting a collective photon from $S_{eg}|\Phi_m^{s_1}\rangle$ is given by:

$$p_{\rm coll} = \frac{x^2}{1+\frac{1}{P_{1\rm d}}} \approx x^2\left(1-\frac{1}{P_{1\rm d}}\right)\,, \tag{8.8}$$

where in the last approximation we assumed to be in a regime with $P_{1\rm d} \gg 1$, whereas the one of emitting an spontaneous emission photon from the same state:

$$p_* = \frac{x^2}{P_{1\rm d}+1} \approx \frac{x^2}{P_{1\rm d}}\,. \tag{8.9}$$

We herald with the detection of a waveguide photon with efficiency η, such that the final success probability of heralding is:

$$p = p_{\rm coll}\times\eta \approx \eta x^2\left(1-\frac{1}{P_{1\rm d}}\right)\,, \tag{8.10}$$

In case of no detection it may have happened that our waveguide photon was emitted but not detected, that is, the atoms will indeed be in a superposition $S_{sg}\ |\Phi_m^{s_1}\rangle$. So, before making a new attempt, we need to ensure that we pump back any possible excitation in $|g\rangle$ to $|s\rangle$. However, to minimize the probability of emitting an leaky photon, which spoils the coherence of our stored superpositions, one needs to apply a repumping procedure in three steps:

- First, apply a π pulse with a microwave field that flips all the excitations $|g\rangle \to |s\rangle$. This switches $S_{sg}|\Phi_m^{s_1}\rangle$ into $S_{gs}|\Psi_m^{s_1}\rangle$, where $|\Psi_m^{s_1}\rangle$ is the same as $|\Phi_m^{s_1}\rangle$ but with levels $|s\rangle$ and $|g\rangle$ interchanged.

- Then, we apply a fast Raman π-pulse with $\Omega \gg N\Gamma_{1\rm d}$ such that $S_{gs}|\Psi_m^{s_1}\rangle \to S_{es}|\Psi_m^{s_1}\rangle \to |\Psi_m^{s_1}\rangle$. This incoherent transfer is done through a collective photon, such that the probability of emitting a leaky photon is:
$$p_{{\rm pump},*} \approx (1-\eta)\times p_{\rm coll}\times\frac{1}{N_m P_{1\rm d}} \approx (1-\eta)\frac{x^2}{N_m P_{1\rm d}}\,. \tag{8.11}$$

- Finally, we reverse the microwave π-pulse such that $|g\rangle \leftrightarrow |s\rangle$ and therefore $|\Psi_m^{s_1}\rangle \to |\Phi_m^{s_1}\rangle$.

8.3.3 Fidelities of the protocol.

In order to calculate the errors (and fidelities) of the protocol we have to distinguish between the errors introduced after successfully heralding the excitations, and the error per trial that we introduce when we repeat the protocol after failure.

- *Successful heralding:* From Eq. 8.5, it can be seen that if we detect a single photon in the waveguide, this means that the initial density matrix $\rho_m = |\Psi_m\rangle\langle\Psi_m|$ transforms into:
$$\rho_m \to \frac{1}{N_m}S_{gs}\rho_m S_{sg} + \frac{2x^2(1-\eta_{\rm d})}{N_m(N_m-1)}S_{gs}^2\rho_m S_{sg}^2\,, \tag{8.12}$$
where the first term is the desired process, whereas the second corresponds to the probability of detecting only one of the two photons emitted from the doubly excited terms $S_{es}^2\ |\Phi_m^{s_1}\rangle$. This introduces a large error as the state $S_{gs}\ |\Phi_m^{s_1}\rangle$ is orthogonal to the state that we want to create, such that the error when heralding is:
$$\varepsilon_{\rm double} = x^2(1-\eta)\,. \tag{8.13}$$

- *Failed heralding:* If we detect no photon, then, our state is projected to:

$$\rho_m \to (1-x^2)\rho_m + p_{\rm coll}(1-\eta)\frac{1}{N_m}S_{gs}\rho_m S_{sg} + p_*\mathbb{J}_*\rho_m + O(x^4)\,, \tag{8.14}$$

which corresponds to processes in which: i) we have not created any excitation in the system, with probability $(1-x^2)$, ii) we have created a single collective excitation emitting a collective photon but we have not detected it; iii) we have created a single excitation, but it has emitted a free space photon, represented through $\mathbb{J}_*\rho_m$. As we explained before, after appropriate repumping, the errors from undetected collective quantum jumps can be corrected introducing some extra spontaneous emission probability, such the final density matrix after repumping is given by:

$$\rho_m \to (1-x^2)\rho_m + (p_{\rm pump,*}+p_*)\,\mathbb{J}_*\rho_m + O(x^4)\,, \tag{8.15}$$

Fortunately, the errors from spontaneous emission are not so severe as the resulting state still have a big overlap with the original state:

$$\langle\Phi_m|\,\mathbb{J}_*[\rho_m]\,|\Phi_m\rangle = \frac{\binom{N-1}{m}}{\binom{N}{m}} \approx 1-\frac{2m}{N}\,. \tag{8.16}$$

Therefore, the error introduced per failed attempt is given by:

$$\varepsilon_{\rm fail,*} = (p_{\rm pump,*}+p)\,\frac{m}{N} \tag{8.17}$$

- *Complete process:* The complete process consists (in average) of a successful heralding event and $1/p$ repetitions such that the average final (in)fidelity to generate $S_{sg}\,|\Phi_m^{s_1}\rangle$ is given by:

$$I_{m\to m+1} \approx \frac{\varepsilon_{\rm fail,*}}{p} + \varepsilon_{\rm double} \approx \frac{m}{\eta N P_{\rm 1d}} + (1-\eta)x^2\,, \tag{8.18}$$

Therefore, the best fidelity that can be obtained is done by imposing: $x^2 = \frac{m}{\eta(1-\eta)NP_{\rm 1d}}$, however, at the price of bad scaling of probability: $p = \frac{m}{NP_{\rm 1d}(1-\eta)}$ [2]. This trade off between probabilities and fidelities comes from the well known problem of double excitations in these type of probabilistic protocols for atomic ensembles. The total error to accumulate m excitations depends on how to combine excitations from s_1 and s and will be discussed in Section 8.7.

Accumulating excitations in the same level.

If we accumulate excitations directly in s, the initial state in each step will be $|\Phi_m^s\rangle$ instead of $|\Phi_m^{s_1}\rangle$. The protocol works in the very same way, but the heralding probability has in this case a small correction in m which reads:

$$p_m = p_{{\rm coll},m}\times\eta \approx \eta x^2\left(1-\frac{1}{(m+1)P_{\rm 1d}}\right)\,. \tag{8.19}$$

Moreover, in case of failure we reinitialize the process from the beginning, pumping back all the atoms to g, which avoids the need of applying the repumping protocol discussed below. The infidelity at each step in this case only come from double excitations contributions scale as:

$$I_{m\to m+1} = \varepsilon_{\rm double} \approx (1-\eta)x^2\,. \tag{8.20}$$

The total error to accumulate m collective excitations will be directly $I_m = m(1-\eta)x^2$.

8.4 Heralding single collective excitations using atom-waveguide QED: two-step protocol with exponential scaling.

In this Section we discuss the second protocol of the main manuscript which overcomes the trade-off between heralding probabilities and fidelities. The starting point is that our target ensemble already contains m collective excitation in a given level s, i.e., our initial state is $|\Phi_m^s\rangle$. Then, the protocol is divided in two-steps: i) we use a single atom to provide single excitations to the target ensemble; ii) then, we use an independent ensemble to herald the successful transfer of the excitations to the target ensemble.

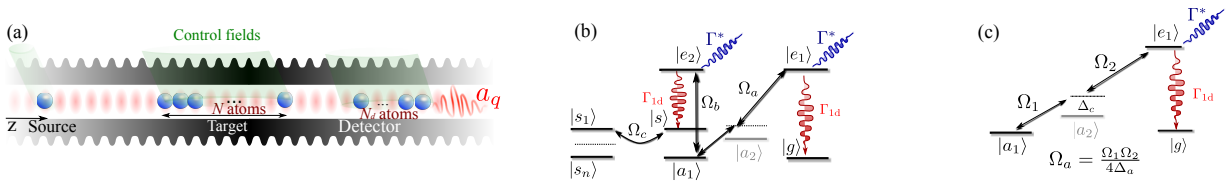

Figure 8.6: (a) General setup consisting in three individually ensembles: a single *source* atom and a *target*/*detector* ensembles and N/N_d atoms respectively. (b) Internal level structure of emitters in which the transition $e_1(, e_2) \leftrightarrow g(, s)$ is coupled to a waveguide mode with rate Γ_{1d}. The transition $e_1 \leftrightarrow a_1$ is driven by a two-photon off resonant process such that there is no spontaneous emission associated to it. The transition $e_2 \to s$ is controlled through a laser with Rabi frequency Ω_b, and the transition $s \leftrightarrow s_n$ is controlled through microwave/Raman laser Ω_c. In the case of the target atoms, we require extra hyperfine levels $\{|s_m\rangle\}_n$, to store atomic excitations. (c) Detail of closed transition implementation using a two photon Raman transition using $|a_2\rangle$ as the auxiliary intermediate state.

8.4.1 Atom-waveguide resources.

The requirements that we need for this protocol are:

- The general setup is depicted in Fig. 8.6(a): we have one individually addressable *source* atom, and two independently addressable ensembles with N, N_d atoms respectively, one where we store the collective excitations, namely, the *target* ensemble and another one that we use to herald the excitations, namely, the *detector* ensemble. We assume that the atoms have a general level structure as depicted in Fig. 8.6(b), with two dipolar transitions $e_1(, e_2) \leftrightarrow g(, s)$ coupled to a waveguide modes with an effective rate Γ_{1d}.

- The atoms must be placed at distances $z_n = n\lambda_a$, with $n \in \mathbb{N}$ and being λ_a the characteristic wavelength of the guided mode at the atomic frequency. With that choice, the dynamics induced by the waveguide is given only by long-range dissipative couplings, described by the following Lindblad terms:

$$\mathcal{L}_{\text{coll}}[\rho] = \frac{\Gamma_{1d}}{2} D_{\sigma^s_{ge_1} + S_{ge_1} + S^d_{ge_1}}[\rho] + \frac{\Gamma_{1d}}{2} D_{\sigma^s_{se_2} + S_{se_2} + S^d_{se_2}}[\rho]\,. \tag{8.21}$$

  where $S_{\alpha\beta}, S^d_{\alpha\beta}$ denote the collective spin operators $(\sum_n \sigma^n_{\alpha\beta})$ in the target/detector atoms. Note that in principle they will be expressed all in a collective jump operator as they are all coupled to the same guided mode. However, we separate them for convenience as in our protocol each term will act in the two different steps of the protocol.

- The excited states may also decay to other channels than the one inducing the long-range couplings, which we embedded in a single decay rate Γ^*. However, to obtain the desired scaling we use a closed transition [20, 8, 21], that we study more in detail in a separate section. Thus, the final spontaneous emitted photons are described by:

$$\mathcal{L}_*(\rho) = \sum_n \left(\frac{\Gamma^*}{4} D_{\sigma^n_{se_2}}[\rho] + \frac{\Gamma^*}{4} D_{\sigma^n_{a_1e_2}}[\rho] + \frac{\Gamma^*}{2} D_{\sigma^n_{ge_1}}[\rho] \right), \tag{8.22}$$

  where we define the coefficients accompanying the jump operators, such that both transitions have the same P_{1d}.

- Finally, we also require the existence of Raman/microwave fields, $\Omega_{a,b,c}$ as depicted in Fig. 8.6(a) that classically control the transition between different levels.

Example of closed transition

There have already been several proposals in the literature of closed transitions [20, 8, 21] but for completeness, we discuss here in detail one of particular realization sketched in Fig. 8.6(c). The state a_1 is connected to the excited state e_1 with a two-photon transition through the intermediate state a_2. The level a_1 is chosen, e.g., such that the direct transition $a_1 \leftrightarrow e_1$ is dipole forbidden. Then, denoting as $\Omega_1(\Omega_2)$ the Rabi frequency connecting $a_1 \leftrightarrow a_2(, a_2 \leftrightarrow e_1)$, and choosing a detuning $\Delta_a \gg \Omega_1, \Omega_2$, the microwave and Raman laser induce a two photon transition from $a_1 \leftrightarrow e_1$ with effective driving $\Omega_a = \frac{\Omega_1\Omega_2}{4\Delta_a}$.

[2] All the expressions are valid obviously for detectors with $0 < \eta < 1$

8.4.2 Protocol and calculation of probabilities

The protocol for heralding single collective excitation starts with the source/target/detector atoms in $|a_1\rangle_s \otimes |\Phi_m^s\rangle_t \otimes |s\rangle_d^N$ and it consists of several steps (as depicted in Fig. 2b of the main manuscript):

1. In the first step, we move the target/detector atoms in s to an auxiliary level s_1, such that we have $|a_1\rangle_s \otimes |\Phi_m^{s_1}\rangle_t \otimes |s_1\rangle^{N_d}$, avoiding that the excitations from the waveguide can be absorbed the detector level s.

2. In the second step, we excite the source atom to e_1, then, we switch on Ω_a^t under the Quantum Zeno dynamics conditions ($\Omega_b^d \ll N_d P_{1\mathrm{d}}$), such that the excitation is coherently transferred to the ensemble to a_1, i.e., $S_{a_1 g}|\Phi_m^{s_1}\rangle$.

3. Now, we move back the states in the target/detector ensemble from s_1 to s, such that, we prepare $S_{a_1 g}|\Phi_m^s\rangle_t \otimes |s\rangle_d^{\otimes N_d}$. Moreover, we move the source atom to, e.g., s_1, such that it plays no role in subsequent steps.

4. Then, we do a fast π-pulse in the ensemble with Ω_b, such that, $S_{a_1 g}|\Phi_m^s\rangle \to S_{e_2 g}|\Phi_m^s\rangle$. Afterwards, we apply Ω_b^d within the Zeno dynamics conditions ($\Omega_b^d \ll N_d P_{1\mathrm{d}}$), such that we arrive to a state in the target/detector atoms $\left|\Phi_{m+1}^s\right\rangle \otimes S_{a_1 s}|s\rangle^{\otimes N_d}$.

5. Thus, if we measure the detector atoms in a_1, we herald the transfer of a single collective excitation to s.

Assuming that π-pulses are perfect, the relevant steps of the protocols for the analysis of probabilities and fidelities are the second and the fourth. Interestingly, they can be analyzed in a common way as in each of them what happens is that a single excitation is transferred through the waveguide via Zeno dynamics to an ensemble with N/N_d atoms respectively. Therefore, in the following Section we analyze the general problem and then we will particularize for steps 2 and 4.

General Zeno step

The general problem consists of two ensembles (a and b) with three-level atoms (with metastable states $|0\rangle$, $|1\rangle$ and excited state $|2\rangle$) that contain N_a and N_b atoms each. The dynamics are governed by the collective decay on the $|2\rangle - |1\rangle$ transition, i.e., $\mathcal{L}[\rho] = \frac{1}{2}\Gamma_{1\mathrm{d}} D_{S_{12}^{(\mathrm{a})}+S_{12}^{(\mathrm{b})}}[\rho]$ and an external field on the second ensemble, i.e., $H_\mathrm{b} = \frac{1}{2}\Omega S_{21}^{(\mathrm{b})} + \mathrm{h.c.}$. Therefore the effective non-hermitian hamiltonian that drives the no-jump evolution is given by:

$$H_{\mathrm{eff}} = \frac{1}{2}\left(\Omega S_{21}^{(\mathrm{b})} + \mathrm{h.c.}\right) - \mathrm{i}\frac{\Gamma_{1\mathrm{d}}}{2}\left(S_{21}^{(\mathrm{a})} + S_{21}^{(\mathrm{b})}\right)\left(S_{12}^{(\mathrm{a})} + S_{12}^{(\mathrm{b})}\right) - \mathrm{i}\frac{\Gamma^*}{2}\sum_n \sigma_{ee}^n. \tag{8.23}$$

Denoting the collective symmetric excitations as $|\#_0, \#_1, \#_2\rangle_{\mathrm{a/b}}$, the initial state of the problem we want to analyze can be written $|0,0,1\rangle_\mathrm{a} \otimes |0, N-m, 0\rangle_\mathrm{b}$ and the goal state is $|0,1,0\rangle_\mathrm{a} \otimes |1, N-m-1, 0\rangle_\mathrm{b}$.

The decay operators couple an initial state $|\psi_1\rangle = |N_\mathrm{a}-k-1, k, 1\rangle_\mathrm{a} \otimes |0, N_b, 0\rangle$ to $|\psi_2\rangle = |N_\mathrm{a}-k-1, k+1, 0\rangle_\mathrm{a} \otimes |0, N_b, 1\rangle$ and the coherent terms couple the latter to $|\psi_3\rangle = |N_\mathrm{a}-k-1, k+1, 0\rangle_\mathrm{a} \otimes |1, N_b, 0\rangle$. In this basis, one can write the Hamiltonian as

$$H_{\mathrm{eff}} = \frac{1}{2}\begin{pmatrix} -i\left((k+1)\Gamma_{1\mathrm{d}} + \Gamma^*\right) & -i\sqrt{(k+1)N_\mathrm{b}}\Gamma_{1\mathrm{d}} & 0 \\ -i\sqrt{(k+1)N_\mathrm{b}}\Gamma_{1\mathrm{d}} & -i(N_\mathrm{b}\Gamma_{1\mathrm{d}} + \Gamma^*) & \Omega \\ 0 & \Omega & 0 \end{pmatrix}. \tag{8.24}$$

or equivalently in the basis of superradiant and dark states, that is $\{|\psi_s\rangle, |\psi_d\rangle, |\psi_3\rangle\}$ with $|\psi_s\rangle = \sqrt{\frac{k+1}{N_\mathrm{b}+k+1}}|\psi_1\rangle + \sqrt{\frac{N_\mathrm{b}}{N_\mathrm{b}+k+1}}|\psi_2\rangle$ and $|\psi_d\rangle = \sqrt{\frac{N_b}{N_\mathrm{b}+k+1}}|\psi_1\rangle - \sqrt{\frac{m+1}{N_\mathrm{b}+k+1}}|\psi_2\rangle$, as

$$\widetilde{H}_{\mathrm{eff}} = \frac{1}{2}\begin{pmatrix} -i\left((N_\mathrm{b}+k+1)\Gamma_{1\mathrm{d}} + \Gamma^*\right) & 0 & -\sqrt{\frac{N_\mathrm{b}}{N_\mathrm{b}+k+1}}\Omega \\ 0 & -i\Gamma^* & -\sqrt{\frac{k+1}{N_\mathrm{b}+k+1}}\Omega \\ -\sqrt{\frac{N_\mathrm{b}}{N_\mathrm{b}+k+1}}\Omega & -\sqrt{\frac{k+1}{N_\mathrm{b}+k+1}}\Omega & 0 \end{pmatrix}. \tag{8.25}$$

When the coherent driving is weak compared to the collective dissipation $\Omega \ll N_\mathrm{b}\Gamma_{1\mathrm{d}}$, the superradiant state can be adiabatically eliminated and an effective Zeno Dynamics between the dark states is obtained, which is governed by the Hamiltonian

$$H_{\mathrm{AE}} \approx \frac{1}{2}\begin{pmatrix} -i\left((N_\mathrm{b}+k+1)\Gamma_{1\mathrm{d}} + \Gamma^*\right) & 0 & 0 \\ 0 & -i\Gamma^* & -i\sqrt{\frac{k+1}{N_\mathrm{b}+k+1}}\Omega \\ 0 & -i\sqrt{\frac{m+1}{N_\mathrm{b}+k+1}}\Omega & -i\frac{N_\mathrm{b}|\Omega|^2}{(N_\mathrm{b}+k+1)^2\Gamma_{1\mathrm{d}}} \end{pmatrix}. \tag{8.26}$$

To minimize the errors, one chooses $\Omega = \sqrt{(N_\mathrm{b}+k+1)\Gamma_{1\mathrm{d}}\Gamma^*}$ such that $\frac{N_\mathrm{b}|\Omega|^2}{(N_\mathrm{b}+k+1)^2\Gamma_{1\mathrm{d}}} = \Gamma^*$. The dynamics for each state is then approximately given by

$$|\psi_d(t)|^2 \approx \frac{N_\mathrm{b}}{N_\mathrm{b}+k+1} e^{-\Gamma^* t}\cos^2\left(t\frac{\Gamma^*\sqrt{(k+1)P_{1\mathrm{d}}}}{2}\right), \tag{8.27}$$

$$|\psi_3(t)|^2 \approx \frac{N_\mathrm{b}}{N_\mathrm{b}+k+1} e^{-\Gamma^* t}\sin^2\left(t\frac{\Gamma^*\sqrt{(k+1)P_{1\mathrm{d}}}}{2}\right) \equiv p, \tag{8.28}$$

$$|\psi_s(t)|^2 \approx \frac{k+1}{N_\mathrm{b}+k+1} e^{-(\Gamma^*+(N_\mathrm{b}+k+1)\Gamma_{1\mathrm{d}})t}. \tag{8.29}$$

The success probability $p = |\psi_3(T)|^2$ is the maximized for $T = \pi\left(\sqrt{\frac{k+1}{N_\mathrm{b}+k+1}}\Omega\right)^{-1}$ and $\Omega = \sqrt{(N_\mathrm{b}+k+1)\Gamma_{1\mathrm{d}}\Gamma^*}$ for $k \ll N_\mathrm{b}$. In this case, one obtains

$$p = \frac{N_\mathrm{b}}{N_\mathrm{b}+k+1}\mathrm{e}^{-\pi/\sqrt{(k+1)P_{1\mathrm{d}}}}, \tag{8.30}$$

where the prefactor originates in the non-unit overlap of the initial state with the dark state, i.e., $|\langle\psi_d|\psi_1\rangle|^2 = \frac{N_\mathrm{b}}{N_\mathrm{b}+k+1}$.

For the repumping protocols that we will study in Section 8.5 it is important to know the probability of spontaneous jumps in both ensembles during the evolution. As we already saw in the first protocol, the problematic processes are the one associated to leaky photons. The quantum jump analysis shows that the probability for a spontaneous jump in the ensemble a or b is given by

$$p_{\mathrm{a},*} = p_{\mathrm{a}_1,*} + p_{\mathrm{a}_2,*} = \Gamma^*\int_0^T \mathrm{d}t_1|\psi_1(t_1)|^2 + \Gamma^*\int_0^\infty \mathrm{d}t_1|\psi_1(T)|^2 e^{-\Gamma^* t_1}, \tag{8.31}$$

$$p_{\mathrm{b},*} = p_{\mathrm{b}_1,*} + p_{\mathrm{b}_2,*} = \Gamma^*\int_0^T \mathrm{d}t_1|\psi_2(t_1)|^2 + \Gamma^*\int_0^\infty \mathrm{d}t_1|\psi_2(T)|^2 e^{-\Gamma^* t_1}, \tag{8.32}$$

where the first parts, $p_{\mathrm{a},\mathrm{b}_1,*}$, corresponds to the interval of time $(0,T)$ where Ω is switched on, and the second part, $p_{\mathrm{a}_2,*}$, the time $t \gg 1/\Gamma^*$ that we wait, with $\Omega = 0$, such that all the population in the excited state, if any, disappears. By using the approximations for H_eff, we can calculate the different contributions and upper bound the probabilities from these processes

$$p_{\mathrm{a}_1,*} \lesssim \frac{1}{2}(1-e^{-\pi/\sqrt{(k+1)P_{1\mathrm{d}}}}) \lesssim \frac{\pi}{2\sqrt{P_{1\mathrm{d}}}} \tag{8.33}$$

$$p_{\mathrm{b}_1,*} \lesssim \frac{k+1}{2N_\mathrm{b}}(1-e^{-\pi/\sqrt{(k+1)P_{1\mathrm{d}}}}) \lesssim \frac{\pi\sqrt{k+1}}{2N_\mathrm{b}\sqrt{P_{1\mathrm{d}}}}, \tag{8.34}$$

which mainly comes from the contribution of the dark state and where the last approximation is valid for $P_{1\mathrm{d}} \gg 1$.

Finally, we need to consider what happens with the contribution $p_{\mathrm{a}_2,*}$ when $P_{1\mathrm{d}} \gg 1$, and when we assume a perfect timing, $T = \pi/\sqrt{(k+1)\Gamma_{1\mathrm{d}}\Gamma^*}$ such that then $|\psi_d(T)|^2 = 0$. The only contribution remaining is the one of the superradiant $|\psi_s(T)\rangle = \sqrt{\frac{k+1}{N_\mathrm{b}+k+1}}e^{-(\Gamma^*+(N_\mathrm{b}+k+1)\Gamma_{1\mathrm{d}})T/2}$, which leads to

$$p_{\mathrm{a}_2,*} \lesssim \frac{(k+1)^2}{(N_\mathrm{b}+k+1)^2} e^{-\pi(N_\mathrm{b}+k+1)/\sqrt{(k+1)P_{1\mathrm{d}}}}, \tag{8.35}$$

$$p_{\mathrm{b}_2,*} \lesssim \frac{N_\mathrm{b}(k+1)}{(N_\mathrm{b}+k+1)^2} e^{-\pi(N_\mathrm{b}+k+1)/\sqrt{(k+1)P_{1\mathrm{d}}}}, \tag{8.36}$$

which are negligible compared to $p_{\mathrm{a},\mathrm{b}_1,*}$ for sufficiently large N_b.

Particularizing for the two step protocol: success probability and infidelity.

The second step of the protocol that we want to analyze corresponds to identifying in the general problem $|0\rangle = |a_1\rangle$, $|1\rangle = |g\rangle$, $|2\rangle = |e_1\rangle$, $\Omega = \Omega_\mathrm{a}$, where the ensembles have a size of $N_\mathrm{a} = 1$ and an effective size $N_\mathrm{b} = N - m$ because the m excitations in all other states are decoupled and effectively reduce the atom number. This results in a heralding probability:

$$p_\mathrm{a} = \frac{N-m}{N-m+1}\mathrm{e}^{-\pi/\sqrt{P_{1\mathrm{d}}}}. \tag{8.37}$$

In the fourth step, the equivalence reads $|0\rangle = |a_1\rangle$, $|1\rangle = |s\rangle$, $|2\rangle = |e_2\rangle$, $\Omega = \Omega_{\rm b}$ and the ensembles have a size of $N_{\rm a} = N$ and $N_{\rm b} = N_{\rm d}$. The initial state is $|N-m-1, m, 1\rangle_{\rm a} \otimes |0, N_{\rm d}, 0\rangle_{\rm b}$ and the goal state is $|N-m-1, m+1, 0\rangle_{\rm a} \otimes |1, N_{\rm d}-1, 0\rangle_{\rm b}$. Thus, the success probability reads:

$$p_{\rm b} = \frac{N_{\rm d}}{N_{\rm d}+m+1} {\rm e}^{-\pi/\sqrt{(m+1)P_{1\rm d}}}, \tag{8.38}$$

where it can be shown that in the limit of $N, N_d \gg m$, the total probability of success is lower bounded by: $p \gtrsim p_{\rm a}^2 \approx e^{-2\pi/\sqrt{P_{1\rm d}}}$.

Improving probability through pulse-shaping.

So far, we have restricted our attention to the case of constant pulse driving Ω. However, it is in principle possible to shape $\Omega(t)$ such that the excitation transfer from $|\psi_1\rangle$ to $|\psi_3\rangle$ is improved. The problem of optimizing $\Omega(t)$ can not be tackled analytically, however, we can choose a discretization of time $[t_1, t_2, \dots t_n]$, and try to find the optimal choice of Ω_i's such that it maximizes $|\langle\psi_1|\psi_3\rangle|^2$. In Fig. 8.7, we show an example that such optimization is possible by discretizing the optimal time found in the previous Section T in 10 steps. In Fig. 8.7(a), we show the ratio between the probability of success with/without pulse shaping $p_{\rm pulse}/p$ as a function of $P_{1\rm d}$ for a situation with $N = 100$ atoms in the ensemble receiving the excitations, where we show how probability can be increased, specially for moderate $P_{1\rm d}$. In panel (b), we show an example of such optimization for the case of $P_{1\rm d} = 50$, showing how the optimal shape found is bigger that the optimal $\Omega_{\rm opt}$ (in red) for a constant pulse at initial times and then smaller. The intuition for this shape can be understood by looking the effective Hamiltonian that drives the evolution. Within the Zeno dynamics, only the dark states $|\psi_d\rangle$ and $|\psi_3\rangle$ are relevant. If we project the dynamics within this subspace, we obtain a 2×2 hamiltonian:

$$\widetilde{H}_{\rm eff} \approx \frac{1}{2}\begin{pmatrix} -i\Gamma^* & \frac{\Omega}{\sqrt{N}} \\ \frac{\Omega}{\sqrt{N}} & -i\frac{|\Omega|^2}{N\Gamma_{1\rm d}} \end{pmatrix}. \tag{8.39}$$

From this effective Hamiltonian, we realize that while the initial state (mostly $|\psi_d\rangle$), which only decays with Γ^*, independent of Ω the final state where we want to arrive decays with an effective decay rate which increases with Ω, i.e., $\frac{|\Omega|^2}{N\Gamma_{1\rm d}}$. Therefore, it is more optimal to ramp up first Ω while the population in $|\psi_3\rangle$ is still small. By using more elaborate pulse shaping, even better improvements might be found.

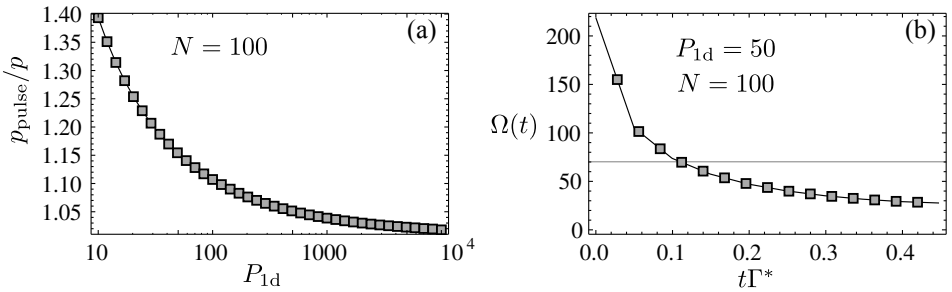

Figure 8.7: (a) Ratio between the probability of success with/without pulse shaping $p_{\rm pulse}/p$ as a function of $P_{1\rm d}$ for a situation with $N = 100$ atoms in the ensemble receiving the excitations. (b) Optimal $\Omega(t)$ for a situation with $N = 100$,$P_{1\rm d} = 50$ using 10 discretization steps. In red we plot the optimal Ω for the situation of constant pulses.

8.5 Heralding single collective excitations using atom-waveguide QED: two-step protocol for polynomial scaling.

In this Section we analyze the third protocol discussed in the manuscript. This protocol is a variation of the second protocol in which after each successful heralding we store the excitations in different levels $\{|s_n\rangle\}_n$ to combine them a posteriori. This however implies the modification of the previous protocol to obtain the desired $1/(NP_{1\rm d})$ scaling for the infidelity $I_{m\to m+1}$. In particular, the second step can not be done through Quantum Zeno dynamics, because the probability of emitting an spontaneous photon within the target ensemble is large, i.e., $p_{b,*} \propto 1/\sqrt{P_{1\rm d}}$, that would yield an infidelity $I_{m\to m+1} \propto 1/(N\sqrt{P_{1\rm d}})$. Therefore, in order to achieve subexponential scaling in the number of operations *and* infidelities still scaling with $I_m \propto 1/(NP_{1\rm d})$ one needs to make judicious modification of the setup as we will explain now.

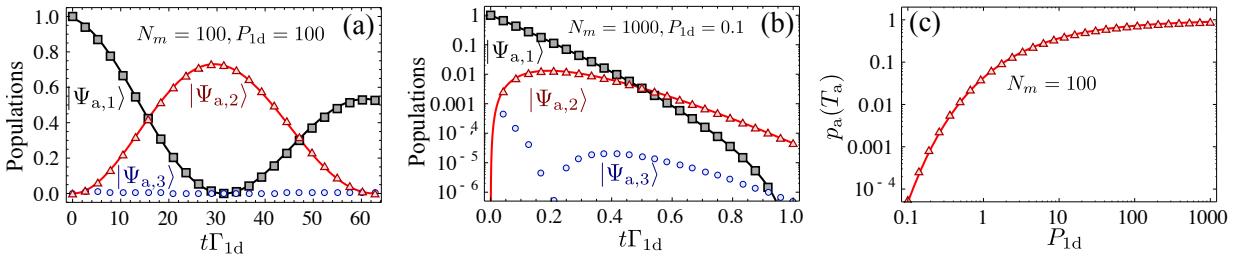

Figure 8.8: (a-b): Evolution of populations calculated with exact numerical integration (markers), together with the analytical approximations (solid lines, see text) by choosing the optimal $\Omega_a = \sqrt{N_m \Gamma_{1d} \Gamma^*}$. The two panels correspond to a situation with $N_m = 100 = P_{1d}$ (a) and $N_m = 1000$, $P_{1d} = 0.1$ (b). (c) Exact (solid lines) and analytical optimal probability using $T_a \approx \pi/\sqrt{\Gamma^* \Gamma_{1d}}$.

8.5.1 Atom-waveguide resources for two-step protocol.

The requirements of this protocol are exactly analogue to the ones of Section 8.4 with two modifications: i) we only require a single detector atom, i.e., $N_d = 1$[3]; ii) we require the existence of several hyperfine states $\{s_n\}$ to store the superpositions.

8.5.2 Protocol and calculation of probabilities

In this Section, we analyze the main protocol described for heralding the transfer of a single collective excitation to the target ensemble, assuming that is already in an entangled state $\left|\Phi_m^{\{s_n\}}\right\rangle$, with m excitations, which can be written as follows:

$$\left|\Phi_m^{\{s_n\}}\right\rangle = \frac{1}{\sqrt{\binom{N}{m_1, m_2, \ldots, m_n}}} \mathrm{sym}\{|s_1\rangle^{\otimes m_1} \ldots |s_n\rangle^{\otimes m_n} |g\rangle^{\otimes N_m}\} \tag{8.40}$$

where $\binom{N}{m_1, m_2, \ldots, m_n} = \frac{N!}{m_1! \ldots m_N N_m)!}$ is the number of states within the superposition, denoting $N_m = N - m$. The final goal state we want to create is:

$$|\Phi_{\mathrm{goal}}\rangle = \frac{1}{\sqrt{N_m}} S_{sg} \left|\Phi_m^{\{s_n\}}\right\rangle . \tag{8.41}$$

As we discussed in the main text, there are two steps that we also consider separately: (a) to move an excitation from the source to the target using Quantum Zeno Dynamics (which is analogue to the one discussed in Section 8.4); (b) herald the transfer by inducing a change in the detector atom state. The second step has to be done fast in order to get the desired scaling of infidelity. We will consider these processes separately. We assume the initial state of the detector is $|s\rangle_d$ such that it only participates in step (b).

Step (a): From source to target using Zeno dynamics (no-jump evolution).

This first step is exactly analogue to the first step of the second protocol discussed in Section 8.4. We start in an initial state $|\Psi_{0,a}\rangle = |e\rangle \otimes \left|\Phi_m^{\{s_n\}}\right\rangle = |\Psi_{a,1}\rangle$, which couples to other states, namely, $|\Psi_{a,2}\rangle = |g\rangle \otimes \frac{S_{e_1 g}}{\sqrt{N_m}} \left|\Phi_m^{\{s_n\}}\right\rangle$ and $|\Psi_{a,3}\rangle = |g\rangle \otimes \frac{S_{a_1 g}}{\sqrt{N_m}} \left|\Phi_m^{\{s_n\}}\right\rangle$. For completeness, we compare the analytical expression of the dynamics obtained in Section 8.4 with the full integration of master equation in Figs. 8.8(a-b), where we observe that they are a good approximation even for systems with $P_{1d} < 1$, as long as $N_m P_{1d}$. The optimal heralding probability

$$p_a \approx \frac{N_m}{N_m + 1} e^{-\pi/\sqrt{P_{1d}}}, \tag{8.42}$$

that we compare to the exact result in Fig. 8.8(c), being a good approximation even when $P_{1d} < 1$.

[3] Actually the source atom can also play the role of the detector atom with appropriate modification of the protocol.

Step (b): heralding the transfer using fast π-pulses (no-jump evolution).

This second step of the protocol do not rely on quantum Zeno dynamics, and it will take place between the target and detector atoms. As we explained in the main text the idea is to: i) first do a fast π pulse with $\Omega_b^{\rm t} \gg \Gamma_{1\rm d}$ such that the possible excitation in $S_{a_1 g}\left|\Phi_m^{\{s_n\}}\right\rangle \to S_{e_2 g}\left|\Phi_m^{\{s_n\}}\right\rangle$; ii) let the system evolve only through the couplings induced by the waveguide; iii) do a π pulse in both the target and detector ensemble, i.e., $\Omega_b^{\rm t}, \Omega_b^{\rm d} \gg \Gamma_{1\rm d}$, such that any remaining excitation in the excited states $|e_2\rangle$ go back to $|a_1\rangle$. It is important to notice that if no excitation has been transferred to $|a_1\rangle$ in step (a), nothing will happen in this step. Therefore, we consider our initial state to be: $|\Psi_{0,\rm b}\rangle = |\Psi_{b,1}\rangle = \frac{1}{\sqrt{N_m}} S_{e_2 g}\left|\Phi_m^{\{s_n\}}\right\rangle \otimes |s\rangle$. The effective Hamiltonian in this case is then given by:

$$H_{\rm b,eff} = -i\frac{\Gamma^*}{2}\sum_n \sigma^n_{e_2 e_2} - i\frac{\Gamma_{1\rm d}}{2}\left(S_{e_2 s} + \sigma^{\rm d}_{e_2 s}\right)\left(S_{s e_2} + \sigma^{\rm d}_{s e_2}\right), \tag{8.43}$$

which connects $|\Psi_{b,1}\rangle$ only to $|\Psi_{b,2}\rangle = \frac{1}{\sqrt{N_m}} S_{sg}\left|\Phi_m^{\{s_n\}}\right\rangle \otimes |e_2\rangle$. In this basis the effective Hamiltonian reads:

$$H_{\rm b,eff} = \frac{1}{2}\begin{pmatrix} -i(\Gamma^* + \Gamma_{1\rm d}) & -i\Gamma_{1\rm d} \\ -i\Gamma_{1\rm d} & -i(\Gamma^* + \Gamma_{1\rm d}) \end{pmatrix}. \tag{8.44}$$

It is again instructive to rewrite it in the basis of sub/superradiant state: $\{|\Psi_{{\rm b},D}\rangle = \frac{1}{\sqrt{2}}\left(|\Psi_{\rm b,1}\rangle - |\Psi_{\rm b,2}\rangle\right), |\Psi_{{\rm b},S}\rangle = \frac{1}{\sqrt{2}}\left(|\Psi_{\rm b,1}\rangle + |\Psi_{\rm b,2}\rangle\right)\}$, arriving to:

$$H_{\rm b,eff} = \frac{1}{2}\begin{pmatrix} -i\Gamma^* & 0 \\ 0 & -i(\Gamma^* + 2\Gamma_{1\rm d}) \end{pmatrix}. \tag{8.45}$$

where the Hamiltonian is diagonal. From here, it is simple to arrive to the solution of the dynamics: $|\Psi_{\rm b}(t)\rangle = e^{-iH_{\rm b,eff}t}|\Psi_{0,\rm b}\rangle = \sum_j \beta_j(t)|\Psi_{{\rm b},j}\rangle$, which read:

$$|\beta_1(t)|^2 = \frac{1}{4}e^{-\Gamma^* t}\left[1 + e^{-\Gamma_{1\rm d}t}\right]^2 \tag{8.46}$$

$$|\beta_2(t)|^2 = \frac{1}{4}e^{-\Gamma^* t}\left[1 - e^{-\Gamma_{1\rm d}t}\right]^2 \equiv p_{\rm b}, \tag{8.47}$$

in the original basis. Notice that $p_{\rm b}$ will be the probability of having transferred the collective excitation to the target while changing the detector atom state to a_1, if we assume that the second π pulse is perfect. If we choose a time $T_{\rm b} = 1/\Gamma_{1\rm d}$, then

$$|\beta_1(T_{\rm b})|^2 \approx \frac{(e+1)^2}{4e^2}\left(1 - \frac{1}{P_{1\rm d}}\right) = 0.46\left(1 - \frac{1}{P_{1\rm d}}\right), \tag{8.48}$$

$$p_{\rm b} \approx \frac{(e-1)^2}{4e^2}\left(1 - \frac{1}{P_{1\rm d}}\right) \approx 0.1\left(1 - \frac{1}{P_{1\rm d}}\right), \tag{8.49}$$

Interestingly, there is a sizeable probability of remaining in the initial state of this step. So instead of start from the beginning every time that we fail, it is possible to repeat this step several times, which increases probability to $p_b \approx 1/3$.

Step a: Using Zeno dynamics (quantum jump analysis).

As we already calculated in Section 8.4, the probability of having an individual quantum jump in the target ensemble is given by:

$$p_{{\rm a},*} \lesssim \frac{\pi}{(N_m+1)\sqrt{P_{1\rm d}}}, \text{ if } \quad P_{1\rm d} \gg 1 \tag{8.50}$$

$$p_{{\rm a},*} \lesssim \frac{3}{(N_m+1)}, \text{ if } \quad P_{1\rm d} \ll 1\ . \tag{8.51}$$

In Fig. 8.9 we compare the exact results (markers) with the upper bound (solid lines) for ε_a, showing that actually we get the right scalings both with $P_{1\rm d}$ and N_m.

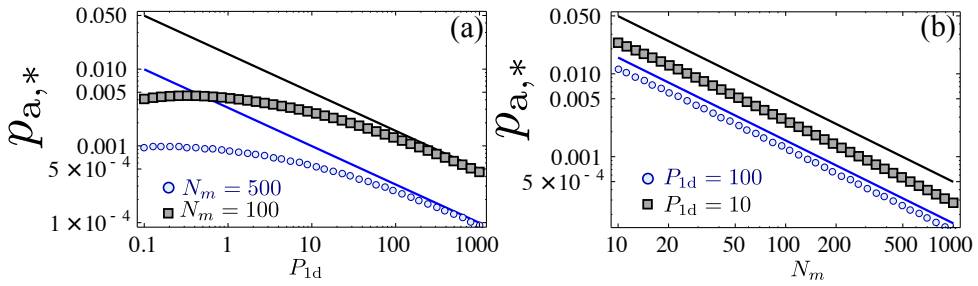

Figure 8.9: (a-b): Exact (markers) vs estimated upper bound (solid lines) $p_{a,*}$ as a function of P_{1d} (a) and N_m (b). The exact calculation is obtained from integrating populations in Eq. 8.48, whereas for the analytical upper bound we use the leading order contribution: $\frac{\pi}{2(N_m+1)\sqrt{P_{1d}}}$. The T_a is chosen to be the optimal one as in Fig. 8.8.

Step b: heralding the transfer using fast π-pulses (quantum jump analysis).

The relevant quantum jumps in this step are $J_b\rho = J_{b,*}\rho + J_{b,coll}\rho$, with

$$J_{b,*}\rho = \frac{\Gamma^*}{2}\sum_n \sigma^n_{se_2}\rho\sigma^n_{e_2s} + \frac{\Gamma^*}{2}\sum_n \sigma^n_{a_1e_2}\rho\sigma^n_{e_2a_1}\,,$$
$$J_{b,coll}\rho = \Gamma_{1d}\big(S_{se_2} + \sigma^d_{se_2}\big)\rho\big(S_{e_2s} + \sigma^d_{e_2s}\big)\,. \tag{8.52}$$

In this second step, we make a π-pulse with Ω^t_b, such that the initial state $|\Psi_{b,0}\rangle = |\Psi_{b,1}\rangle = \frac{1}{\sqrt{N_m}} S_{e_2g}\left|\Phi^{\{s_n\}_n}_m\right\rangle$. Then the system is left free to evolve for a time $T_b = \frac{1}{\Gamma_{1d}}$, and switching the Ω^t_b, Ω^d_b such that no population remains in the excited state e_2. Therefore, the quantum jumps could only occur within a small time interval giving rise to

$$p_{b,*} = \Gamma^* \int_0^{T_b} dt_1 |\beta_1|^2 \approx \frac{0.67}{P_{1d}}\,. \tag{8.53}$$

In this regime, with $P_{1d} \gg 1$ and $T_b = \frac{1}{\Gamma_{1d}}$, it is also instructive to consider the probability of other quantum jumps. For example, to calculate the probability that the excitation is transferred to $S_{sg}\left|\Phi^{\{s_n\}}_m\right\rangle$ but the state of the detector is unchanged, i.e., remains in s, one needs to sum up the probability of making a collective quantum jump in the target together with the probability of making any jump in the $f \to s$ transition:

$$p_{b,coll} = \Gamma_{1d}\int_0^{T_b} dt_1|\beta_1|^2 + (\Gamma_{1d} + \frac{\Gamma^*}{2})\int_0^{T_b} dt_1|\beta_2|^2 \approx 0.71\,, \tag{8.54}$$

which biggest contribution comes from the emission in the target ensemble. These states have not destroyed the coherence of $\left|\Phi^{\{s_n\}}_m\right\rangle$ but they need to be properly taken care of with the repumping process. In order to avoid that these states also lead to error, we have to make a repumping process back to $|g\rangle$ in the way depicted in Fig. 8.10:

1. First we pump incoherently back any possible excitation in $|c\rangle$ through the waveguide, namely, $S_{a_1g}\left|\Phi^{\{s_n\}}_m\right\rangle \to S_{e_1g}\left|\Phi^{\{s_n\}}_m\right\rangle \to \left|\Phi^{\{s_n\}}_m\right\rangle$. Because this process is done through a collective photon the error introduced in this step $p_{pump,*} \propto \frac{1}{NP_{1d}}$.

2. Once, we have make sure that there are no excitation in $|a_1\rangle$ we can move the excitations from $S_{sg}\left|\Phi^{\{s_n\}}_m\right\rangle \to S_{a_1g}\left|\Phi^{\{s_n\}}_m\right\rangle$ with π pulse using a microwave or two-photon Raman transition.

3. Now, after having transferred the excitation to $|a_1\rangle$, we repeat the incoherent transfer through the waveguide that will only introduce errors of the order $p_{pump,*}$.

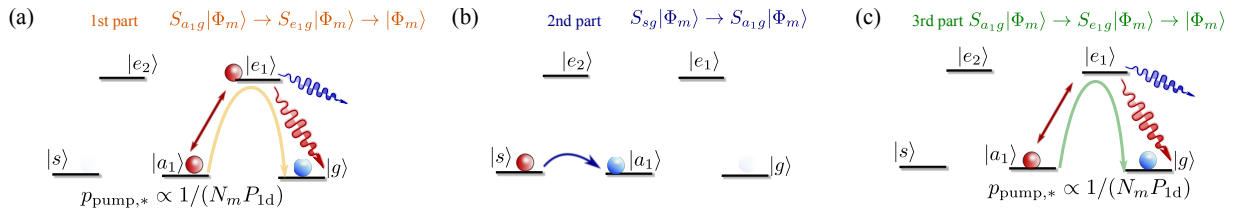

Figure 8.10: General scheme of repumping process to correct collective quantum jump errors (see details in the text).

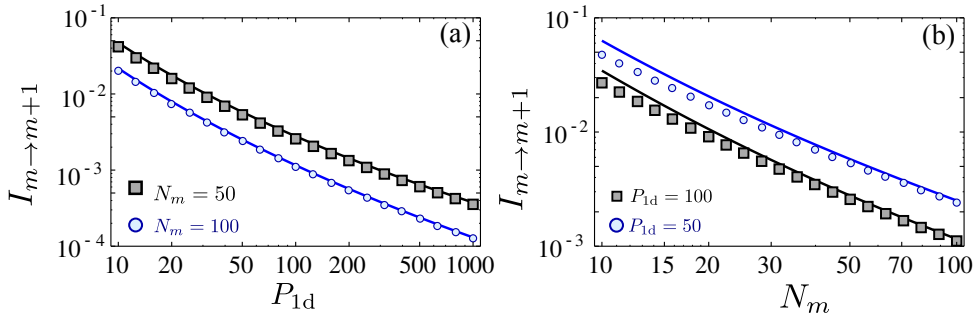

Figure 8.11: Scaling of the exact (solid lines) and approximated (markers) infidelities with $P_{1\mathrm{d}}$ (Panel a) and N_m (Panel (b)) for different N_m and $P_{1\mathrm{d}}$ respectively as depicted in the legends.

8.5.3 Fidelities of the protocol.

From the calculation of probabilities of the previous Section, we are prepared to estimate the average fidelity when detecting an atomic excitation in the detector atom in a_1. The errors appear:

- *Successful heralding:* As shown in the main manuscript, in the case where the transition $e_1 \to |a_1\rangle$ is closed the only way of measuring detector atom in $|a_1\rangle$ is by successfully generating $|\Phi_{\mathrm{goal}}\rangle$. If we have a spurious spontaneous emission $\sim \alpha\Gamma^*$, then, it is possible that we herald the transfer of an incoherent excitation of s, i.e., σ^n_{sg}, which have an overlap $\propto 1/N$ with the state we want to create. Thus, the possible error after heralding is given by:

$$\varepsilon_{\mathrm{closed}} = \frac{\alpha}{N\sqrt{P_{1\mathrm{d}}}}\,. \tag{8.55}$$

- *Failed heralding:* As it occurred in the first protocol, in each failed attempt we introduce an error in our initial state $\left|\Phi_m^{\{s_n\}}\right\rangle$ due to the probability of emitting free space, which in this protocol may occur in step (a), (b) and the repumping. The error per attempt can be estimated to be:

$$\varepsilon_* \approx (p_{\mathrm{a},*} + p_{\mathrm{b},*} + p_{\mathrm{pump},*})\frac{m}{N} \approx \frac{0.67m}{NP_{1\mathrm{d}}}\,. \tag{8.56}$$

  where in the last approximation we assumed to be in a regime where $p_{\mathrm{b},*} \gg p_{\mathrm{a},*}, p_{\mathrm{pump},*}$.

- *Complete process:* As in the first protocol, the average complete process consist of a successful heralding and $1/p$ failed attempts, such that the average fidelities of the process:

$$I_{m\to m+1} = \varepsilon_{\mathrm{closed}} + \frac{\varepsilon_*}{p} = \frac{\alpha}{N\sqrt{P_{1\mathrm{d}}}} + \frac{m}{pNP_{1\mathrm{d}}}\,, \tag{8.57}$$

  where one sees that to reach the $I_{m->m+1} \propto 1/(NP_{1\mathrm{d}})$ scaling, we do not need a perfectly closed transition, but it is enough to demand a cancellation of spontaneous emission (α) of at least $\alpha = 1/\sqrt{P_{1\mathrm{d}}}$ which can be achieved as well, e.g., by using a quadrupole transition.

In Fig. 8.11, we compare the analytical approximation of infidelities of Eq. 8.57 (markers) together with exact results (solid lines) as a function of $P_{1\mathrm{d}}$ and N_m.

8.6 Heralding single photon excitations using atom-waveguide QED: single-step protocol for polynomial scaling.

In this Section, we study a modification of the previous protocol such that we can do the heralded transfer in a single step and without the need of the closed transition at expense of showing a worse scaling of the success probabilities and infidelities and with the requirement of two different guided modes. These protocol is not discussed in the main manuscript, though we include here for completeness.

8.6.1 Atom waveguide resources.

The requirements for this protocol are:

- We need to have an atomic configuration of source/target/detector atom as in the previous protocol. However, the internal level structure must be modified, as shown in Fig. 8.12 to have an excited state $|e\rangle$ coupled directly to two waveguide modes through the transitions $|e\rangle \leftrightarrow |g[,s]\rangle$ with rates $\Gamma_{1\mathrm{d}}^{g[,s]}$. As we will see afterwards in this case it is important that $\Gamma_{1\mathrm{d}}^{g} \neq \Gamma_{1\mathrm{d}}^{s}$. The modes can differ either in polarization or frequency, but they must satisfy that their characteristic wavelength λ_{a} is approximately the same.

- To guarantee the heralding, it will be important that the transition $|e\rangle \rightarrow |s\rangle$ $[|e\rangle \rightarrow |g\rangle]$ of the source [detector] atom to be largely off-resonant. This must be satisfied to avoid a direct transfer of the excitation from the source to the detector atom that would spoil the heralding.

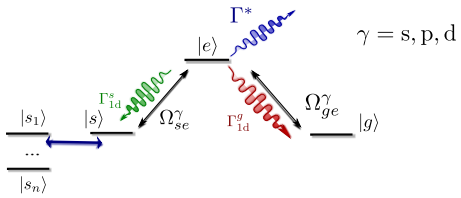

Figure 8.12: Variation of the internal level structure of emitters of the different ensembles in which the transition $|e\rangle \leftrightarrow |g\rangle$ $[|e\rangle \leftrightarrow |g\rangle$ is coupled to a single waveguide mode with $\Gamma_{1\mathrm{d}}$. We also require an extra intermediate level $|c\rangle$, which forms a closed transition with $|e\rangle$. We also assume that we can control the $|e\rangle \leftrightarrow |g\rangle$ $[|s\rangle]$ transition with a classical laser Ω_{ge}^{α} $[\Omega_{se}^{\alpha}]$.

8.6.2 Protocol and calculation of probabilities.

The main difference with the previous protocol is that is done in a single step. We start with $|\Psi_{0,\mathrm{a}}\rangle = |\Psi_{\mathrm{a},1}\rangle = |e\rangle \otimes \left|\Phi_m^{\{s_n\}}\right\rangle \otimes |s\rangle$ and consider that only the classical field $\Omega_{ge}^{\mathrm{d}} \equiv \Omega^{\mathrm{d}} \neq 0$, such that the dynamics governed by the effective Hamiltonian:

$$H_{\mathrm{a,eff}} = \frac{\Omega^{\mathrm{d}}}{2}\left(\sigma_{ge}^{\mathrm{d}} + \sigma_{eg}^{\mathrm{d}}\right) - i\frac{\Gamma^*}{2}\sum_n \sigma_{ee}^n - i\frac{\Gamma_{1\mathrm{d}}^{\mathrm{g}}}{2}\left(\sigma_{eg}^{\mathrm{s}} + S_{eg}\right)\left(\sigma_{ge}^{\mathrm{s}} + S_{ge}\right) - i\frac{\Gamma_{1\mathrm{d}}^{\mathrm{s}}}{2}\left(\sigma_{es}^{\mathrm{d}} + S_{es}\right)\left(\sigma_{se}^{\mathrm{d}} + S_{se}\right), \quad (8.58)$$

that couples our initial state to $|\Psi_{\mathrm{a},2}\rangle = |g\rangle \otimes \frac{1}{\sqrt{N_m}} S_{eg} \left|\Phi_m^{\{s_n\}}\right\rangle \otimes |s\rangle$, $|\Psi_{\mathrm{a},3}\rangle = |g\rangle \otimes \frac{1}{\sqrt{N_m}} S_{sg} \left|\Phi_m^{\{s_n\}}\right\rangle \otimes |e\rangle$ and $|\Psi_{\mathrm{a},4}\rangle = |g\rangle \otimes \frac{1}{\sqrt{N_m}} S_{sg} \left|\Phi_m^{\{s_n\}}\right\rangle \otimes |g\rangle$. In this basis the Hamiltonian can be written as:

$$H_{\mathrm{eff}} = \frac{1}{2}\begin{pmatrix} -i(\Gamma_{1\mathrm{d}}^{\mathrm{g}} + \Gamma^*) & -i\sqrt{N_m}\Gamma_{1\mathrm{d}}^{\mathrm{g}} & 0 & 0 \\ -i\sqrt{N_m}\Gamma_{1\mathrm{d}}^{\mathrm{g}} & -i(N_m\Gamma_{1\mathrm{d}}^{\mathrm{g}} + \Gamma_{1\mathrm{d}}^{\mathrm{s}} + \Gamma^*) & -i\Gamma_{1\mathrm{d}}^{\mathrm{s}} & 0 \\ 0 & -i\Gamma_{1\mathrm{d}}^{\mathrm{s}} & -i(\Gamma_{1\mathrm{d}}^{\mathrm{s}} + \Gamma^*) & \Omega^{\mathrm{d}} \\ 0 & 0 & \Omega^{\mathrm{d}} & 0 \end{pmatrix}, \quad (8.59)$$

The goal is to find $|\Psi(t)\rangle = e^{-iH_{\mathrm{a,eff}}t}|\Psi_0\rangle = \sum_j \alpha_j(t)|\Psi_j\rangle$, which can always be done numerically as it is only a 4x4 matrix. However, in order to gain more insight it is useful to write it in a basis with sub and superradiant states. Interestingly, the system always contains a dark state $|\Psi_{\mathrm{a},D}\rangle = \frac{1}{\sqrt{N_m+2}}\left(\sqrt{N_m}|\Psi_{\mathrm{a},1}\rangle - |\Psi_{\mathrm{a},2}\rangle + |\Psi_{\mathrm{a},3}\rangle\right)$, which is dark for all values of $\Gamma_{1\mathrm{d}}^{\mathrm{g}}, \Gamma_{1\mathrm{d}}^{\mathrm{s}} \neq 0$. However, the two orthogonal excited states depend on the ratio $\Gamma_{1\mathrm{d}}^{\mathrm{s}}/\Gamma_{1\mathrm{d}}^{\mathrm{g}}$. After a careful study, we found the optimal choice for the maximum transfer to $|\Psi_{\mathrm{a},4}\rangle$ was to choose $\Gamma_{1\mathrm{d}}^{\mathrm{s}}/\Gamma_{1\mathrm{d}}^{\mathrm{g}} = \frac{N_m+1}{2}$, and the reason is that in that case the two decay channels to $|g\rangle$ and $|s\rangle$ show the same

"superradiant" decay $(N_m+1)\Gamma^{\rm g}_{\rm 1d}$. From now one, we use that ratio and $\Gamma^{g}_{\rm 1d}=\Gamma_{\rm 1d}$. For this ratio, the adiabatic elimination of the superradiant states give rise to an effective 2×2 between the dark state and the goal state

$$H_{\rm eff}\approx\begin{pmatrix} -\frac{i\Gamma^*}{2} & \frac{\Omega^{\rm d}}{2\sqrt{N_m}} \\ \frac{\Omega^{\rm d}}{2\sqrt{N_m}} & -i\frac{3(\Omega^{\rm d})^2}{2N_m\Gamma_{\rm 1d}}\end{pmatrix}. \tag{8.60}$$

where we have used $N_m\gg 1$ to simplify the expressions. As we know from the previous Sections, the more convenient is to choose an $\Omega^{\rm d}$ such that the contribution of Γ^* and the effective losses induced by superradiant states, i.e., $\frac{3(\Omega^{\rm d})^2}{2N_m\Gamma_{\rm 1d}}$, is the same. Thus, by choosing $\Omega^{\rm d}=\sqrt{N_m\Gamma_{\rm 1d}\Gamma^*/3}$, it is easy to find that:

$$\begin{aligned}|\alpha_D(t)|^2&\approx\frac{N_m}{N_m+2}e^{-\Gamma^* t}\cos^2(\frac{\sqrt{\Gamma_{\rm 1d}\Gamma^*}t}{2\sqrt{3}}),\\ |\alpha_4(t)|^2&\approx\frac{N_m}{N_m+2}e^{-\Gamma^* t}\sin^2(\frac{\sqrt{\Gamma_{\rm 1d}\Gamma^*}t}{2\sqrt{3}})=p(t).\end{aligned} \tag{8.61}$$

Therefore, if $P_{\rm 1d}\gg 1$ and $T_{\rm a}=\frac{\pi\sqrt{3}}{\sqrt{\Gamma_{\rm 1d}\Gamma^*}}$ then the probability of heralding reads:

$$p\approx\frac{N_m}{N_m+2}e^{-\sqrt{3}\pi/\sqrt{P_{\rm 1d}}}, \tag{8.62}$$

In Fig. 8.13 we compare the results from the exact integration of the complete non-hermitian hamiltonian together with the analytical approximation (markers) obtained from the Quantum Zeno dynamics (solid lines).

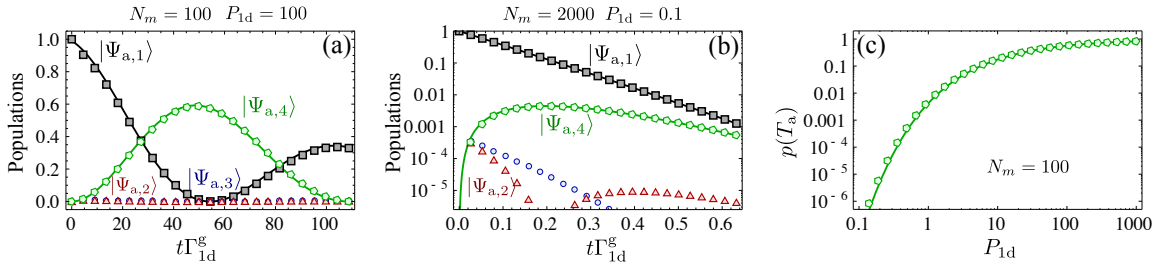

Figure 8.13: (a-b): Evolution of populations calculated with exact non-hermitian hamiltonian (markers) of Eq. 8.59, together with the analytical approximations (solid lines) by using the superradiant/subradiant decoupling of Eq. 8.60 by choosing the optimal $\Omega_{\rm a}=\sqrt{N_m\Gamma_{\rm 1d}\Gamma^*/3}$. The two panels correspond to a situation with $N_m=100=P_{\rm 1d}$ (a) and $N_m=2000$, $P_{\rm 1d}=0.1$ (b). (c) Exact (solid lines) and analytical optimal probability using $T_{\rm a}\approx\pi\sqrt{3}/\sqrt{\Gamma^*\Gamma_{\rm 1d}}$.

The problematic quantum jump in this case is related to the probability of having an excitation $|e\rangle$ in the *target* ensemble, i.e., coming from the population of state $|\Psi_{\rm a,2}\rangle$ that reads

$$p_*=\Gamma^*\int_0^{T_{\rm a}}dt_1|\alpha_2(t_1)|^2+\Gamma^*\int_0^{\infty}dt_1|\alpha_2(T_{\rm a})|^2e^{-\Gamma^*t_1}, \tag{8.63}$$

where the first part corresponds to the interval of time $(0,T_{\rm a})$ where $\Omega^{\rm d}$ is switched on, and the second part, the time $t\gg 1/\Gamma^*$ that we wait, with $\Omega^{\rm d}=0$, such that all the population in the dark state vanishes. The contributions of the superradiant/subradiant states to $|\Psi_{\rm a,2}\rangle$ can be obtained in the asymptotic limit $N_m\gg 1$, where:

$$\begin{aligned}|\langle\Psi_{{\rm a},D}|\Psi_{\rm a,2}\rangle|&\sim\frac{1}{\sqrt{N_m}}\\ |\langle\Psi_{{\rm a},S_+}|\Psi_{\rm a,2}\rangle|&\sim\frac{\sqrt{2+\sqrt{2}}}{2}\sim O(1)\\ |\langle\Psi_{{\rm a},S_-}|\Psi_{\rm a,2}\rangle|&\sim\frac{\sqrt{2-\sqrt{2}}}{2}\sim O(1)\end{aligned} \tag{8.64}$$

Using that information we can estimate the contribution of the dark state within the time interval: $(0,T_{\rm a})$.

$$p_{*,D}\lesssim\frac{\Gamma^*}{N_m}\int_0^{T_{\rm a}}dt_1e^{-\Gamma^*t_1}\lesssim\frac{1-e^{-\Gamma^*T_{\rm a}}}{N_m}, \tag{8.65}$$

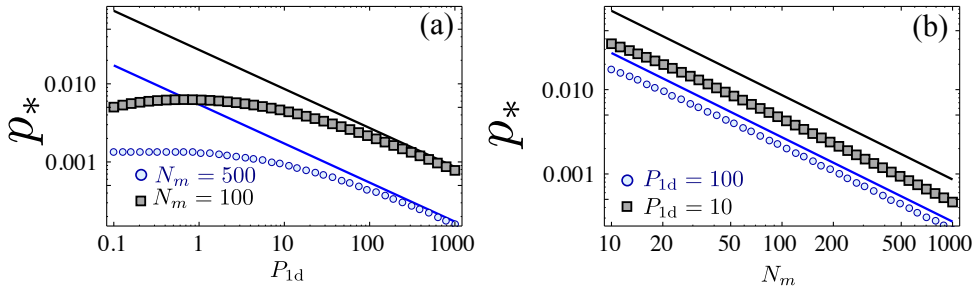

Figure 8.14: (a-b): Exact (markers) vs estimated upper bound (solid lines) p_* as a function of P_{1d} (a) and N_m (b). The exact calculation is obtained from integrating populations in Eq. 8.63, whereas for the analytical upper bound we use the leading order contribution of Eq. 8.67. The T_a is chosen to be the optimal one as in Fig. 8.13.

that is:

$$p_{*,D} \approx \frac{\pi\sqrt{3}}{2N_m\sqrt{P_{1d}}}\,, \text{ if } \ , P_{1d} \gg 1\,, \tag{8.66}$$

whereas the contribution of (T_a, ∞) can always be shown to be smaller order: when $P_{1d} \gg 1$. Therefore, we the overall probability of emitting a quantum jump in the target ensemble for this protocol

$$p_* \propto \frac{\pi\sqrt{3}}{2N_m\sqrt{P_{1d}}}\,, \text{ if } \ , P_{1d} \gg 1\,, \tag{8.67}$$

which are confirmed numerically in Fig. 8.14. The repumping process to correct the collective quantum jump errors can be done as well in a single step by pumping collectively the atoms from $|s\rangle \to |g\rangle$, which moves $S_{sg}\,|\Phi_m\rangle \to S_{eg}\,|\Phi_m\rangle \to |\Phi_m\rangle$. Because this process is done through a collective photon the probability of emitting a free space photon is given by $p_{\text{pump},*} \propto \frac{1}{NP_{1d}}$.

8.6.3 Fidelity of the protocol.

The analysis of the fidelity will be very similar to the one performed for the previous protocol. In this case, if we detect an excitation in g in the detector atom, no error may appear. Therefore, the only contribution to the infidelity is the error coming from free space photons in each attempt after $1/p$ repetitions, which finally scale:

$$I_{m\to m+1} \approx \frac{1}{p} \times (p_* + p_{\text{pump},*}) \times \frac{m}{N} \propto \frac{m}{N^2\sqrt{P_{1d}}}\,, \tag{8.68}$$

for systems with $P_{1d}, N_m \gg 1$. In Fig. 8.15 we confirm numerically that the analytical approximations capture the right scaling. If we consider as a reference the largest Purcell factor (the one associated to Γ^s_{1d}), then, the scaling of probabilities and fidelities should read equivalently:

$$\begin{aligned} p &\approx \frac{N_m}{N_m+2} e^{-\sqrt{3}\pi\sqrt{N_m}/\sqrt{P_{1d}}} \\ I_{m\to m+1} &\propto \frac{m}{N^{3/2}\sqrt{P_{1d}}}\,, \end{aligned} \tag{8.69}$$

8.7 Merging protocols for combining collective atomic excitations.

In this Section we show how to combine the excitations stored in the target atoms after the first part of the process, that is, when our atomic state has the form $\left|\Phi_m^{\{s_n\}}\right\rangle \propto \text{sym}\{|s_1\rangle^{m_1} \otimes \cdots \otimes |s_n\rangle^{m_n} \otimes |g\rangle^{N_m}\}$, with $N_m = N - m = N - \sum_i m_i$ such that we can build up higher excitation numbers into a single level. For that purposes we use several tools and assumptions:

- We are interested in the so called Holstein-Primakoff limit where $m \ll N$, such that the collective atomic dipoles $S_{\alpha g}\sqrt{N_m} \approx a_\alpha^\dagger$ can be approximated by bosonic operators.
- Using the microwave/Raman lasers connecting an atomic level α with g, we can do displacement transformations $D(\alpha)$ on the α level. Moreover, using microwave/Raman transition between α and β levels, we can also engineer beam splitter transformations between these modes.

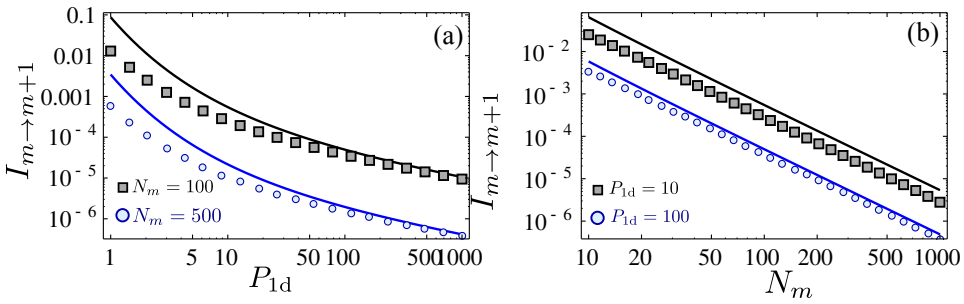

Figure 8.15: Scaling of the exact (solid lines) and approximated (markers) infidelities with P_{1d} (Panel a) and N_m (Panel (b)) for different N_m and P_{1d} respectively as depicted in the legends.

- Moreover, we can read the atomic state very efficiently by pumping to an excited state that emits a collective photon through the waveguide in a cyclic transition. This will allow do to very efficient detection and potentially number resolved as we explain in the last Section. Together with the beam splitter and displacement transformations, they provide a similar set of tools as the ones used in linear optics protocol with the advantage of having the excitations stored.

Using all those assumptions, our goal is to build a given arbitrary atomic state of m excitations, that we know it can be afterwards be mapped to a photonic state with very high efficiency [9]. The general form of this state typically reads:

$$|\Psi_m\rangle = \sum_n \frac{f_n}{\sqrt{n!}}(a^\dagger)^n |\text{vac}\rangle \propto \prod_{i=1}^{n}(a^\dagger - \alpha_i^*)|\text{vac}\rangle \ , \tag{8.70}$$

and we will put particular emphasis in the simple Dicke states with m excitations, as this will be mapped to photonic Fock states. We discuss two different types of merging protocols separately.

1. If the number of metastable states $|s_i\rangle$ is limited, we only use two levels and add excitations one by one. This is the kind of protocols typically used in linear optics protocols where it is not possible to store several atomic excitations [19].

2. Using several hyperfine levels and adopting a tree-like structure that will allow us to avoid the exponential scaling of the number of operations.

8.7.1 Adding excitations one by one.

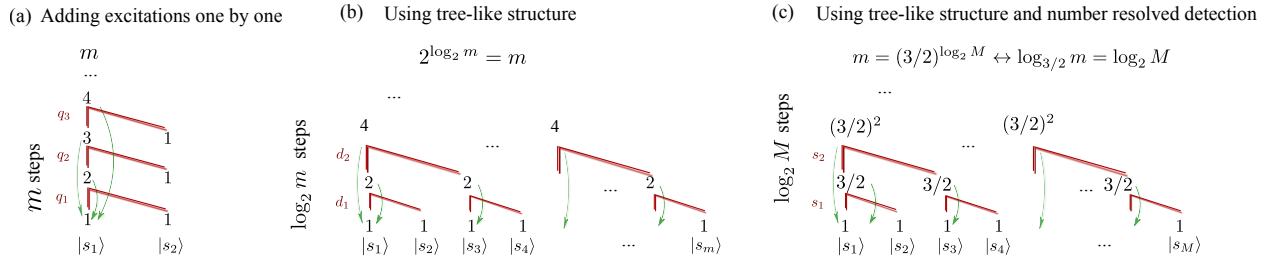

Figure 8.16: Scheme to build up m collective atomic states combining heralded single collective excitations plus beam splitters and postselection. The red arrows indicates the path adding excitations, whereas the green ones how one needs to reinitialize the process if we fail in given step. (a) Scheme using two atomic levels to add excitations one by one with probability q_n in each step. (b) [(c)] Scheme using $\log_2 m$ [$\log_{3/2} m$] with probability q_n [s_n] in each step using a tree-like structure that avoids starting the whole process from the beginning in case of failure.

Here we show how to create a photonic state of m excitations by combining beam splitters (B), displacements transformations ($D(\alpha)$) and post-selection condition on no detection in a particular level $\mathbb{P}_{0_i}$ by using only two atomic levels. For the sake of discussion, we analyze first in detail the case of single Dicke states and leave the analysis of the superpositions afterwards.

The general scheme to build a given atomic state with m collective excitations is depicted in Fig. 8.16(a). The main step consists of going from an state with m excitations in one level and a single one in the other,

$|\phi_n\rangle = |n\rangle \otimes |1\rangle$, to an state $n+1$ excitation in one of them conditioned on detecting no excitation in the other one, i.e., $|n+1\rangle \otimes |0\rangle_1$. The idea is to apply a beam splitter transformation of $|\phi_n\rangle$, followed by a projection of the state conditioned on detecting no excitations in the a_2 level:

$$\left|\tilde{\phi}_n\right\rangle = \mathbb{P}_{0_2} B\,|\phi_n\rangle = \frac{1}{\sqrt{n!}} T^n R (a_1^\dagger)^{n+1}\,|\text{vac}\rangle \tag{8.71}$$

(not normalized) and the probability of finding it is given by

$$\left\langle \tilde{\phi}_n \middle| \tilde{\phi}_n \right\rangle = (n+1)|T|^{2n}|R|^2 \leq \left(\frac{n}{n+1}\right)^m = q_n, \tag{8.72}$$

which is maximized for a transmitivity $|T|^2 = n/(n+1)$. Interestingly, $\lim_{n\to\infty} q_n = e^{-1}$ such that it does not decay with n. However, if we fail, we have to repeat the process from the beginning, such that the mean number of operations to create a state with m excitations can be obtained:

$$R_m = \frac{1+R_{m-1}}{q_{m-1}} = \frac{1}{q_{m-1}} + \frac{1}{q_{m-1}q_{m-2}} + \cdots + \frac{1}{\prod_n^{m-1} q_n}\,. \tag{8.73}$$

Taking into account that $2 = q_1 > q_2 > \cdots > q_n > e^{-1}$ and $q_0 = p$ the probability to generate a single heralded excitation, the mean number of states can be lower and upper bounded by:

$$\begin{aligned} R_m &< \frac{m}{\prod_n^{m-1} q_n} < \frac{m}{\prod_n^{m-1} q_n} < \frac{m e^m}{p}\,, \\ R_m &> \frac{1}{\prod_n^{m-1} q_n} > \frac{1}{p\prod_{n=1}^{m-1} q_1} > \frac{2^{m-1}}{p}\,. \end{aligned} \tag{8.74}$$

which increase exponentially to increase the number of excitations m. Moreover, it was shown in Ref. [19] that by combining single photon addition with displacement transformation before and after the addition, lead to a conditional outcome after starting with a state $|\phi\rangle$, that is, $D(\alpha)a^\dagger D(\alpha)^\dagger\,|\phi\rangle$. Combining m of these operations and using the fact that $D(\alpha)a^\dagger D(\alpha)^\dagger = a^\dagger - \alpha$ it can be shown that one arrives to $|\Psi_{\text{ph},m}\rangle$ as in Eq. 8.70, but also with an exponential number of operations.

8.7.2 Doubling the number of excitations post-selecting on no detection.

The key difference with respect to the previous protocol is that we are going to adopt a tree-like structures as depicted in Fig. 8.16(b), where we can reach the m excitations in $\log_2 m$ steps and we do not have to repeat all of them if we fail. The first building block is to study the process that add up two states with $|n\rangle$ excitations to go to $|n\rangle \otimes |n\rangle \to |2n, 0\rangle$. It can be shown that the conditional outcome after a beam splitter and detecting no excitations in the second atomic level is given by:

$$\left|\tilde{\phi}_{2n}\right\rangle = \frac{1}{n!} T^n R^n (a_1^\dagger)^{2n}\,|\text{vac}\rangle\,, \tag{8.75}$$

which yields an (approximated) optimal probability for a $50-50$ beam splitter transformation:

$$d_n = \left\langle \tilde{\phi}_{2n} \middle| \tilde{\phi}_{2n} \right\rangle = \frac{(2n)!}{2^{2n}(n!)^2} \approx 1/\sqrt{\pi n}\,, \tag{8.76}$$

where we used Stirling's approximation $n! \approx \sqrt{2\pi n}\, n^n \mathrm{e}^{-n}$ in the last step. Therefore, in this case the optimal d_n does decay with $1/\sqrt{n}$ but only polynomially. However, in spite of this decay, the use of of a tree-like structure is enough to circumvent the exponential scaling of adding excitations one by one. The average number of operations to arrive to an state of m excitations can be calculated iteratively, i.e.,

$$R_m = d_{m/2}^{-1}\left(1 + 2R_{m/2}\right) = d_{m/2}^{-1} + 2d_{m/2}^{-1}d_{m/4}^{-1} + 2^2 d_{m/2}^{-1}d_{m/4}^{-1}d_{m/8}^{-1} + \ldots\,, \tag{8.77}$$

where the $d_{m/2}^{-1}$ terms represents the number of times we need to try in the step $m/2$ to succeed and the one with $2R_{m/2}$ is the number of steps we need to repeat at the m-th step to get the the two branches of the tree. We lower and upper bound this number of operations to get m excitations by:

$$\begin{aligned} R_m &< \frac{\log_2 m}{p} \frac{2^{\log_2 m - 1}}{\prod_{n=1}^{\log_2 m - 1} d_{m/2^n}} < \frac{\log_2 m}{p} \frac{2^{\log_2 m - 1}}{d_{m/2}^{\log_2 m}} \approx \frac{m^{(\log_2 m)/2+1}\log_2 m}{2p}\,, \\ R_m &> \frac{2^{\log_2 m - 1}}{p\prod_{n=1}^{\log_2 m - 1} d_{m/2^n}} > \frac{m^2}{4p}\,, \end{aligned} \tag{8.78}$$

where we use that $d_m < d_{m/2}$ and $d_1 = 1/2$ and that we require $\log_2 m$ steps to arrive to m excitations. Thus, R_m is superpolynomial in m because the probability in each step, d_m, decays with m. If we had a way of making d_m independent of m as it occurs for the single excitation case q_m, then we would have a polynomial scaling.

For completeness it will be interesting to prove that one can also get arbitrary superpositions [22] using the tree-like structure of Fig. 8.16(b). As a resource we assume we can build any superposition of 0 and 1 photon, i.e., which we know is possible from the previous section. Then, we prove first that using $50-50$ beam splitter and detecting no excitations in the a_2-mode we can arrive to any arbitrary state as follows:

$$P_{0_2} B\,|\Psi_{a_1,m}\rangle \otimes |\Psi_{a_2,m}\rangle = P_{0_2} B \prod_{i=1}^{m}\left(a_1^\dagger - \frac{\alpha_i^*}{\sqrt{2}}\right)\prod_{i=1}^{m}\left(a_2^\dagger - \frac{\alpha_{i+m}^*}{\sqrt{2}}\right)|\text{vac}\rangle =$$
$$= \frac{1}{2^m}\prod_{i=1}^{m}\left((a_1^\dagger)^2 - (\alpha_i^* + \alpha_{i+m}^*)a_1^\dagger + \alpha_i^*\alpha_{i+m}^*\right)|\text{vac}\rangle \propto \prod_{i=1}^{2m}(a_1^\dagger - \alpha_i^*)\,|\text{vac}\rangle \propto |\Psi_{2m,\text{goal}}\rangle\,. \tag{8.79}$$

Now, it is important to check the conditions under which the probability of doubling the excitations is not exponentially small. It is easy to show from the previous equations that he probability of success in each step of the doubling is lower bounded by

$$d_m \gtrsim \frac{1}{\sqrt{2\pi m}}|\,\langle m|\Psi_{a_1,m}\rangle\,|^2 |\,\langle m|\Psi_{a_2,m}\rangle\,|^2\,, \tag{8.80}$$

such that it does not decay exponentially if the contribution $|\,\langle m|\Psi_{a_{1,2},m}\rangle\,|^2$ do not decay exponentially either. This is a reasonable assumption as if $|\,\langle m|\Psi_{a_{1,2},m}\rangle\,|$ would be exponentially small we could approximate the photonic state without doubling with an exponentially small error. Both Eqs. 8.79 and 8.80 show that we can create any arbitrary state with a non-exponentially small probability. Using that $|\,\langle m|\Psi_{a_{1,2},m}\rangle\,|^2 \propto 1/m^\alpha$, it is then easy to show the superpolynomial scaling of probability:

$$R_m \lesssim \frac{m^{\alpha(\log_2 m)+1}\log_2 m}{2p}\,. \tag{8.81}$$

8.7.3 Increasing the number of excitations with number resolved detection.

In this last Section, we show how by using atomic number resolved detection, we can overcome the superpolynomial scaling of the previous section. Instead of starting the process again when we detect some excitation in the a_2, we can think of using some of these states that still have a non-negligible number of excitations in the a_1 mode that we can use a posteriori. To further explore this possibility, we generalize the operation of Eq. 8.75 to see what is the resulting state after 50/50 beam splitter transformation when we want to sum up m and n excitations in the $a_{1,2}$ modes when we detect the p excitations in the a_2 mode:

$$f_p(m,n) =_1 \langle m+n-p\left|\tilde{\phi}_{m+n-p}\right\rangle =_1 \langle m+n-p|\,\mathbb{P}_{p_2} B\frac{(a_1^\dagger)^m(a_2^\dagger)^n}{\sqrt{m!}\sqrt{n!}}\,|\text{vac}\rangle$$
$$= \sum_{k=0}^{m}\frac{(-1)^{m-k}}{2^{(m+n)/2}\sqrt{m!}\sqrt{n!}}\binom{m}{k}\binom{n}{m+n-k-p}\sqrt{p!}\sqrt{(m+n-p)!}\,. \tag{8.82}$$

In Fig. 8.17(a) we plot the distribution of probabilities $|f_p(m,n)|^2$ as a function of p for different m and n. In solid black, we depict the the case with $m=n$ which is the symmetric situation that we consider before. For this symmetric situation the expression of Eq. 8.82 can be simplified as follows:

$$|f_{2n}(m,m)|^2 = \frac{(2m-2n)!(2n)!}{2^{2m}(m!)^2}\binom{m}{n}^2 \approx \frac{1}{\pi}\frac{1}{\sqrt{n(m-n)}}\,. \tag{8.83}$$

and $f_{2n-1}(m,m) \equiv 0$ for $n \in \mathbb{N}$, and where in the last approximation we assumed $m,n \gg 1$ to use Stirling approximation. By integrating this expression it can be obtained that the probability of detecting an state $p < m/2$ lead to:

$$s_{p<m/2} = \sum_{p=0}^{m/2}|f_p(m,m)|^2 \approx \int_0^{m/4} dn|f_{2n}(m,m)|^2 = \int_0^{m/4} dn\frac{1}{\pi}\frac{1}{\sqrt{n(m-n)}} = 1/3 \equiv s\,, \tag{8.84}$$

which means that there is a probability s independent of m of going from $|m\rangle_1 \otimes |m\rangle_2 \to |2m-p > 3m/2\rangle_1 \otimes |p\rangle_2$. In order to make a worst case estimation, we assume that in each step we go only to $|m\rangle_1 \otimes |m\rangle_2 \to |3m/2\rangle_1$.

This in principle can be done because if one obtains a higher excitation number it can be decreased by applying infinitesimal beam splitter transformations with an empty mode as:

$$\begin{aligned}\mathbb{P}_{0_2} B(\theta \ll 1)\,|n\rangle_1 \otimes |0\rangle_2 &\approx \left(1-\frac{\theta^2 n}{2}\right)|n\rangle\ ,\\ \mathbb{P}_{0_2} B(\theta \ll 1)\,|n\rangle_1 \otimes |0\rangle_2 &\approx i\theta\sqrt{n}\,|n-1\rangle_1\ ,\end{aligned} \tag{8.85}$$

which show that by switching $\theta^2 n \ll 1$, we do not alter $|n\rangle_1$, until we decrease one excitation. This can be applied several times until we arrive to $|3m/2\rangle$. In this worst case scenario, starting again with M single excitations [see Fig. 8.16(c)] we will arrive at least to $m \geq \left(\frac{3}{2}\right)^{\log_2(M)}$ [which lead $\log_{3/2} m = \log_2 M$] in $\log_2(M)$ steps, which means that with this protocol

$$R_m \lesssim \frac{\log_2(M) 2^{\log_2 M - 1}}{p s^{\log_2 M}} \approx \frac{m^{4.41}\log_{3/2} m}{2p}\ , \tag{8.86}$$

where we used $\log_b x = \frac{\log_a x}{\log_a b}$. Thus, by using number resolved detection we turn the superpolynomial scaling into polynomial which is big improvement if we want to scale our protocol for larger excitation numbers. In practical situations, the scaling will be better as one will never decrease the excitations to arrive to $3n/2$, but will use the larger excitation numbers. The consequence of that is that within the tree we will need to add up excitation in an asymmetric way, i.e., (m, n) as we showed in Fig. 8.17(b). However, even in this case it can also be shown that

$$\sum_{p=1}^{m/2} |f_p(m+\alpha, m-\alpha)|^2 \approx 1/3 \equiv s\,, \tag{8.87}$$

for approximately all α as shown numerically in Fig. 8.17(b). This proves that the number resolved excitation also helps even in the asymmetric configuration as it also may give rise to a probability in each step independent of the number of excitations we add up.

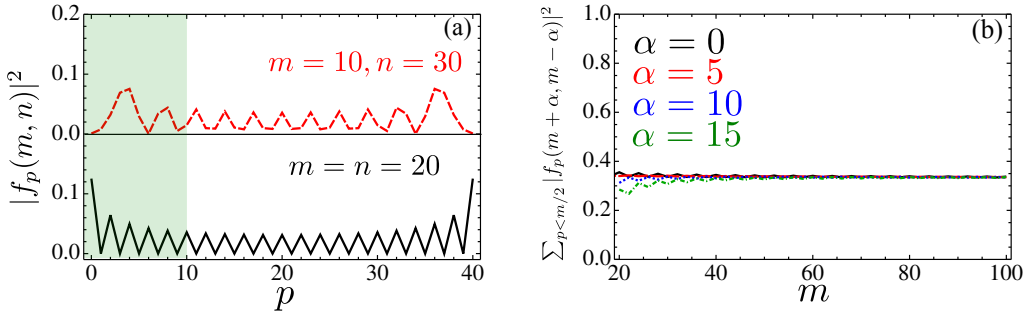

Figure 8.17: (a) Distribution of probabilities $|f_p(m,n)|^2$ as a function of p for $m = n = 20$ (lower panel) and $m = 10, n = 30$. (b) $\sum_{p<m/2} |f_p(m+\alpha, m-\alpha)|^2$ as a function of m for different degrees of asymmetry given by α as shown in the legend. It can be easily checked that all the cases converges to a constant $s \approx 1/3$.

8.7.4 Atomic number resolved detection using waveguide QED.

Though standard linear optics setups can already distinguish between photon numbers using superconducting detectors, current technologies are far from obtaining the desired detection efficiencies for optical photons. In our case, we can benefit directly from our atomic detection which naturally give rise to ways of having number resolved detection. In this Section, we make a short discussion of how one can do it.

The goal is to be able to distinguish in one atomic level between having m or $m+1$ excitations. In order to do it, we can drive a closed atomic transition to an excited state such that we emit photons through the waveguide. Using the fact that $P_{1\mathrm{d}} \gg 1$, we will be able to obtain the photon counting distribution $P[n,T]$ of having detected n photons after a time interval T. Interestingly, this photon counting distribution is given by a Poisson process with different parameter $\lambda_m = m\Gamma_{1\mathrm{d}}T$, being m the number of excitations, i.e., $P[n,T] = \frac{\lambda_m^n}{n!}e^{-\lambda_m}$. In Fig. 8.18, we see this distribution quickly converges to a Gaussian with mean value λ_m and width $\sqrt{\lambda_m}$, such that for large T (or equivalently large λ_m), the overlap between the two distribution, ε vanishes approximately with T approximately $\varepsilon \propto e^{-(\Gamma_{1\mathrm{d}}T)^2}$, which give as some bounds of the T required to minimize the error introduced in the number resolved detection.

Depending on the particular implementation, a more thorough analysis of the errors has to be performed, to estimate the final fidelities of the protocol, though our paper serves as an optimistic basis for future research.

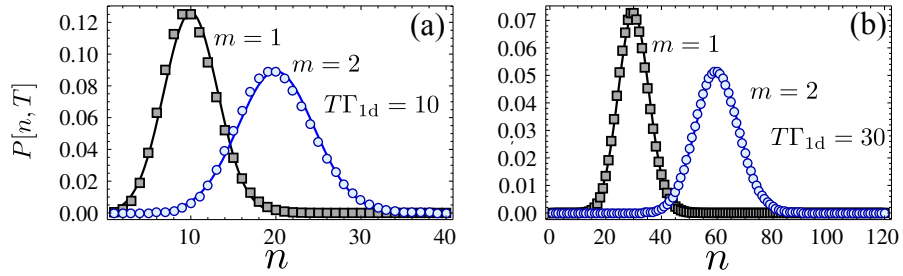

Figure 8.18: (a-b) Photon counting probabilities $P[n, T]$ for $T\Gamma_{1d} = 10 - 30$ for two different atomic levels with $m = 1$ [black] and $m = 2$ excitations.

9 The giant acoustic atom – a single quantum system with a deterministic time delay by Guo et. al.

Abstract

We investigate the quantum dynamics of a single transmon qubit coupled to surface acoustic waves (SAWs) via two distant connection points. Since the acoustic speed is five orders of magnitude slower than the speed of light, the travelling time between the two connection points needs to be taken into account. Therefore, we treat the transmon qubit as a giant atom with a deterministic time delay. We find that the spontaneous emission of the system, formed by the giant atom and the SAWs between its connection points, initially decays polynomially in the form of pulses instead of a continuous exponential decay behaviour, as would be the case for a small atom. We obtain exact analytical results for the scattering properties of the giant atom up to two-phonon processes by using a diagrammatic approach. We find that two peaks appear in the inelastic (incoherent) power spectrum of the giant atom, a phenomenon which does not exist for a small atom. The time delay also gives rise to novel features in the reflectance, transmittance, and second-order correlation functions of the system. Furthermore, we find the short-time dynamics of the giant atom for arbitrary drive strength by a numerically exact method for open quantum systems with a finite-time-delay feedback loop.

9.1 Introduction

Superconducting circuits [1, 2] form a promising technology for realising the computational nodes of a large-scale quantum network [3, 4].

In a large network, time delays are unavoidable and have to be understood and handled with care. The on-chip delays of standard superconducting microwave circuits, however, are negligible due to the cm chip size and the speed of light.

A key element to realize a quantum network is a coherent transducer capable of converting quantum information from the microwave regime to the optical regime, where it could be transmitted over large distances. While many different designs for such a transducer are very actively investigated [5, 6, 7, 7, 9, 10], no high-efficiency solution has been experimentally realized so far.

However, there is another possibility to investigate time delays due to propagation on-chip. By transforming the quantum information into surface acoustic waves (SAWs) [16, 12, 13, 14, 17], *i.e.*, sound waves travelling with a velocity five orders of magnitude lower than the speed of light, microsecond propagation-time delays can easily be achieved. Delay lines is indeed also one of the main applications of SAWs in microwave technology [14].

The theoretical description of open quantum systems including propagation time delays has until recently focussed on so-called cascaded quantum systems [16, 17, 18, 19, 20], where no closed loops for quantum information are created.

There are also tools to describe systems with closed loops, but where the dynamics of quantum systems is approximatively coherent during the short time-delay, which can then be included in terms of signal phase shifts [19, 20, 21, 24]. Recently, there has been an increased interest in longer time delays and closed loops,

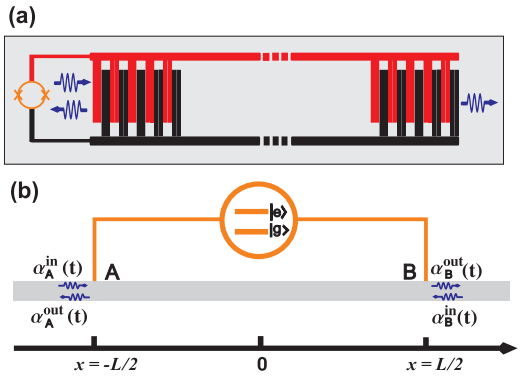

Figure 9.1: **Giant atom coupled to SAWs.** (a) The giant atom is a transmon (orange SQUID circle) with large interdigitated capacitance (red and black structures) from its two islands. The giant atom couples to SAWs propagating on the piezoelectric substrate (grey color) through the piezoelectric effect. (b) The transmon qubit is modelled by a two-level atom with two legs (labelled by A and B, respectively) coupled to a one-dimensional (1D) transmission line. The distance between the two legs is L. In- and out-going phonons, including external drive fields, near the two connection points are shown as blue arrows.

where the quantum systems have time to evolve dissipatively and really emit energy into the transmission line before that energy returns [23, 24, 27, 26, 27, 26, 29].

In this paper, we analyze one of the simplest examples of an open quantum system with a deterministic propagation-time delay. It consists of a single two-level atom, connected at two points to a single open transmission line. This is not only conceptually one of the simplest examples but also straightforward to implement experimentally [16, 12, 17]. The single two-level quantum system is realized by a transmon qubit [15] with strong nonlinearity, which serves as an artificial atom. Compared to the SAW wavelength ($\lesssim$1 m), the transmon can be designed to extend over distances at least several hundred, or even a thousand, times greater($>$100 m). Since the speed of SAWs is five orders of magnitude slower than the speed of light, we need to consider the time delay between the two connection points. However, we neglect the time delay in the connections themselves and the transmon, since they are metallic and signals travel through them at the speed of light. Therefore, we refer to our single two-level quantum system as a *giant atom*. Other examples of simple systems that can exhibit time delay are a two-level atom in front of a mirror [23, 24, 26, 31] and two two-level atoms at a long distance from each other in an open transmission line [32, 33, 8, 27, 19, 27, 26].

The two connection points of the giant atom introduce boundary conditions for the SAWs propagating in the open transmission line, making the area between the connection points reminiscent of a cavity. However, it is different from both the cavities used for optical photons in cavity quantum electrodynamics (QED) and the transmission line resonators used for microwave photons in circuit QED, as well as from the effective cavities for single photons that can be formed by several small atoms in an open transmission line [33, 36, 37]. For example, we find that the total energy stored in atom and the SAWs between the connection points exhibits an intially polynomial decay process before reverting to exponential decay in the long-time limit.

9.2 The Model

In Fig. 9.1(a), we show the setup investigated in this work. A transmon is coupled to a piezoelectric substrate (grey color). The interdigitated capacitance forming the two islands of the transmon also forms a transducer which couples to the SAWs propagating on the substrate. In our case, the whole interdigital transducer (IDT) consists of two local IDTs at its two ends, far away from each other. Each IDT has N pairs of fingers ($N = 5$ pairs are shown in Fig. 9.1(a)). The fork configuration of each finger is designed to minimize internal mechanical reflections [16, 12, 13, 14].

In this paper, we will explore the transmon dynamics in the qubit regime, *i.e.*, where only the lowest two transmon levels with energy splitting $\hbar\omega_0$ are involved. Considering just one of the two local IDTs, we assume the relaxation rate corresponding to a single IDT finger pair is γ_0. Due to the interference of all the finger pairs, the total effective relaxation rate of each local IDT is given by [24]

$$\gamma = \gamma_0 \frac{1 - \cos(N\omega_0\tau)}{1 - \cos(\omega_0\tau)}, \tag{9.1}$$

where τ is the travelling time (negligible in this case) between neighbouring finger pairs (of the same colour shown in Fig. 9.1(a)). We now consider the distance between neighbouring finger pairs to match the wavelength of the corresponding phonons, so that the transmon-phonon coupling is maximized, *i.e.*, $\omega_0\tau = 2n\pi$, $n \in \mathbb{Z}^+$, leading to $\gamma = N^2\gamma_0$. The bandwidth of phonons involved in the qubit dynamics will be determined by the coupling γ. In the following, we will consider the regime $\gamma \ll \omega_0/N$, so that we can neglect the weak frequency dependence of the coupling around the maximum in Eq. (9.1).

The distance L between the centers of the two local IDTs can be made long, straightforwardly up to a few thousands of SAW wavelengths [12], which is the regime of interest in this paper. We characterize this distance by the corresponding time delay $T = L/v_g$ for the SAWs travelling with the velocity v_g on the piezoelectric substrate.We thus arrive at the model of a two-legged giant atom, as sketched in Fig. 9.1(b), with two legs labelled by A and B, respectively. The model Hamiltonian is

$$\begin{aligned}\mathscr{H} &= \hbar\omega_0 \left|e\right\rangle\!\left\langle e\right| + \sum_{\alpha=1,2}\int \hbar\omega_p a^\dagger_{\alpha\omega_p} a_{\alpha\omega_p} d\omega_p \\ &+ \sum_{\alpha=1,2}\int \hbar\sqrt{\frac{\gamma}{4\pi}}\left[\sigma_- a^\dagger_{\alpha\omega_p}\left(e^{-ic_\alpha k_p \frac{L}{2}} + e^{ic_\alpha k_p \frac{L}{2}}\right) + \text{h.c.}\right] d\omega_p, \end{aligned} \tag{9.2}$$

where $a_{\alpha\omega_p}$ are phonon field operators for the right- ($\alpha = 1$) and left-propagating ($\alpha = 2$) phonons satisfying $\left[a_{\alpha\omega_p}, a^\dagger_{\alpha'\omega'_p}\right] = \delta_{\alpha\alpha'}\delta(\omega_p - \omega'_p)$, and ω_p represents the frequency of phonon modes. We have defined atomic operators $\sigma_- \equiv \left|g\right\rangle\!\left\langle e\right|$ and $\sigma_+ \equiv (\sigma_-)^\dagger$ where $\left|g\right\rangle$ and $\left|e\right\rangle$ are the atomic ground and excited states. The coupling term in the second line of Eq. (9.2) has included the phase difference between two legs of giant atom at positions $x = -L/2$ and $x = L/2$. The parameter k_p is the wave vector of the SAWs, *i.e.*, $k_p = \omega_p/v_g$ or $k_p = 2\pi/\lambda_{SAW}$ with λ_{SAW} being the wavelength of the SAWs. Since the typical value of γ is tens of MHz, which is small compared to ω_0 (several GHz), it is reasonable to assume that the SAW dispersion is flat over the atom's bandwidth. The notation $c_{\alpha=1} = +1$, $c_{\alpha=2} = -1$ is used to distinguish the interaction of the giant atom with the right- and left-propagating phonon fields, respectively.

In Section 9.3, we will explore the spontaneous-emission dynamics of the giant atom when it is excited directly by an electrical gate [16], and also the single-phonon scattering properties of the giant atom when it is driven by SAWs emanating from external IDTs. We then extend the scattering calculations to two-phonon processes in Section 9.4, allowing us to study second-order correlation functions for the scattered phonons. Finally, in Section 9.5, we investigate the short-time dynamics of the giant atom when it is subjected to coherent driving of arbitrary strength.

9.3 Single-phonon processes

We will first consider the single-excitation subspace of the giant atom's dynamics, since this is amenable to analytic solutions. In this subspace, the total state of the two-level giant atom and SAW field in the transmission line can be described by [38]

$$\left|\Psi(t)\right\rangle = \int d\omega \left[\alpha_{1\omega}(t) a^\dagger_{1\omega} + \alpha_{2\omega}(t) a^\dagger_{2\omega}\right] \left|g, vac\right\rangle + e(t)\left|e, vac\right\rangle, \tag{9.3}$$

where $\left|vac\right\rangle$ represents the ground state of SAW field in the transmission line. The integral part describes the state of a single phonon propagating in the transmission line towards the right, $\alpha_{1\omega}$, or the left, $\alpha_{2\omega}$, with the giant atom in the ground state $\left|g\right\rangle$. When the phonon is absorbed, the giant atom is in the excited state $\left|e\right\rangle$ with the probability amplitude $e(t)$. From the Schrödinger equation $i\hbar\partial/\partial t\left|\Psi(t)\right\rangle = \mathscr{H}\left|\Psi(t)\right\rangle$, we obtain the evolution of $e(t)$ (see Appendix 9.7.1 for details)

$$\begin{aligned}\frac{\partial e(t)}{\partial t} &= -i\omega_0 e(t) - \gamma\left[e(t) + e(t-T)\right] \\ &\quad -iV\left[\alpha^{in}_A(t) + \alpha^{in}_A(t-T) + \alpha^{in}_B(t) + \alpha^{in}_B(t-T)\right]. \end{aligned} \tag{9.4}$$

The first term in the right-hand side (RHS) of Eq. (9.4) describes the unitary evolution of the giant atom without dissipation and driving. The second term in the RHS of Eq. (9.4) describes the relaxation process via the two legs of the giant atom, which includes the time delay between the two legs. The last term in the RHS of Eq. (9.4) describes the dynamics due to external driving sources exciting the atom through both leg A and leg B. If a plane-wave driving field only comes from the leg A, as shown in Fig. 9.1(a), the driving terms in Eq. (9.4) is $\alpha^{in}_A(t) = Ae^{-i\omega_d t}$ and $\alpha^{in}_B(t) = 0$ with A the amplitude of the drive. The coherent coupling amplitude V is determined by the relaxation rate γ through $V = \sqrt{\gamma v_g/2}$ (details are given in Appendix 9.7.1). Previous work on the giant atom only considered the Markov limit, where the time delay T is negligible [24]. In this article, on the other hand, we are mainly interested in understanding the effect of a nonnegligible T. Below, we specify the parameter regimes that will be considered.

9.3.1 Spontaneous Emission

Overview of parameter regimes

Equation (9.4) is a time-delay differential equation. Without the external driving, *i.e.*, setting $\alpha^{in}_A(t) = 0$ and $\alpha^{in}_B(t) = 0$, we straightforwardly find the analytical solution describing the spontaneous relaxation of the

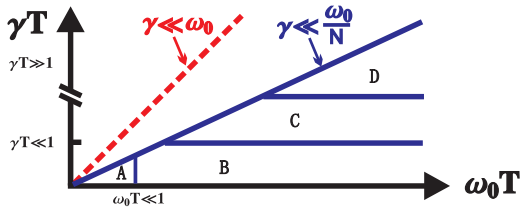

Figure 9.2: **Parameter space**. The parameter region under the line $\gamma \ll \omega_0/N$, where the RWA holds, is divided into several different subregions. Region A: The limit of both long wavelength, $\omega_0 T = kL \ll 1$, and Markovian dynamics, $\gamma T \ll 1$. Region B: Still Markovian dynamics, but arbitrary phase difference $\omega_0 T$. Region C: The moderately non-Markovian regime $\gamma T \sim 1$. Region D: The deep non-Markovian regime, $\gamma T \gg 1$.

giant atom's excitation amplitude (see Appendix 9.7.2, and also Ref. [23], for details)

$$e(t) = e(0)e^{-i(\omega_0 T - i\gamma T)\frac{t}{T}} \sum_{n=0}^{[t/T]} \frac{(\gamma T)^n}{n!} \left(n - \frac{t}{T}\right)^n e^{in(\omega_0 T - i\gamma T)}, \tag{9.5}$$

where $e(0)$ is the initial probability amplitude of giant atom and $[t/T]$ is the integer part of t/T. From Eq. (9.5), we see that $e(t)$ is a function of the dimensionless time t/T, depending on the two dimensionless parameters γT and $\omega_0 T$. Therefore, the relaxation properties of the giant atom is determined by the parameter plane spanned by γT and $\omega_0 T$, which can be divided into several regions as shown in Fig. 9.2. Since we work in the rotating wave approximation (RWA), we only consider the region under the line $\gamma \ll \omega_0$. Furthermore, we neglect the frequency dependence of the local IDTs (see Eq. (9.1)), implying that $\gamma \ll \omega_0/N$. We divide the remaining region into several different subregions marked by A, B, C and D, respectively.

The corner region A is defined by the condition $\omega_0 T \ll 1$. Since $\omega_0 T = k_p L = 2\pi L/\lambda_{SAW}$, the condition $\omega_0 T \ll 1$ corresponds to the long wavelength limit $\lambda_{SAW} \gg 2\pi L$, which means we can neglect the phase acquired by SAWs travelling between the connection points. Due to the RWA condition $\gamma \ll \omega_0$, this region is also in the Markov limit, *i.e.*, $\gamma T \ll \omega_0 T \ll 1$. Thus, we can neglect high orders of γT ($n \geq 1$) in Eq. (9.5) and obtain an approximate result, $e(t) \approx e(0)\exp(-i\omega_0 t - 2\gamma t)$. This is indeed the result for a small atom with total relaxation rate 2γ, since the inter-leg distance is much smaller than the phonon wavelength. Here, we also note that this regime cannot be accessed experimentally in the SAW-transmon system, since each individual local IDT already consists of N legs separated by the phonon wavelength. However, since the wavelength of microwave photons is usually much longer than the dimensions of a superconducting qubit, most circuit-QED setups work inside this regime.

Parameter region B is also in the Markov limit $\gamma T \ll 1$, but with an arbitrary $\omega_0 T$, which means the phase acquired by SAWs travelling in the transmission line between the two legs needs to be considered [24]. In this case, the main contribution comes from the low orders in the series of Eq. (9.5). Therefore, by taking $n - t/T \approx -t/T$ in the limit $t \gg T$, we have the asymptotic behaviour $e(t) \approx e(0)\exp(-i\bar{\omega}_0 t - \bar{\gamma} t)$, where the effective frequency is $\bar{\omega}_0 = \omega_0 + \gamma e^{\gamma T}\sin(\omega_0 T)$ and the effective decay rate is given by $\bar{\gamma} = \gamma[1 + e^{\gamma T}\cos(\omega_0 T)]$. Considering the Markov limit $\gamma T \ll 1$, we can further take $e^{\gamma T} \approx 1$ in $\bar{\omega}_0$ and $\bar{\gamma}$. We see that $\bar{\omega}_0$ and $\bar{\gamma}$ are both modified by the phase factor $\omega_0 T$ and the results coincide with those given in Ref. [24], where the distances between the legs were represented by frequency-dependent phase shifts.

The parameter regions C and D are both beyond the Markov approximation. Region C corresponds to a moderate non-Markovian regime $\gamma T \sim 1$ while region D is the deep non-Markovian regime $\gamma T \gg 1$. In region D, the dominant term is the highest order in the series of Eq. (9.5). Thus we have the approximate solution in the time interval $mT \leq t < (m+1)T$, with $m \in \mathbb{Z}^+$,

$$e_m(t) \approx e(0)e^{-i(\omega_0 T - i\gamma T)\frac{t}{T}} \frac{(\gamma T)^m}{m!} \left(m - \frac{t}{T}\right)^m e^{im(\omega_0 T - i\gamma T)}. \tag{9.6}$$

In region C, no such simplifications are possible and the complete time evolution, given by Eq.(9.5), must be used. Examples of relaxation dynamics in the experimentally accessible parameter regions B, C and D are given in Figs. 9.3(a1), (b1) and (c1), respectively, which we will discuss in detail below. However, to understand the dynamics better, it is useful to first also study the power spectrum of the giant atom.

Power spectra

We now study the solution of Eq. (9.4) from another point of view by decomposing $e(t)$ into a superposition of many independent modes, *i.e.*, $e(t) = \sum_k c_k e^{-i\omega_{(k)}t}$. In general, the mode frequencies $\omega_{(k)}$ can be complex numbers where the imaginary part gives the relaxation rate of each mode. Plugging this form into Eq. (9.4) without driving terms, we obtain the analytical solution

$$\omega_{(k)} = \omega_0 - i\gamma + i\frac{1}{T}W_k\left(-\gamma T e^{\gamma T + i\omega_0 T}\right), \tag{9.7}$$

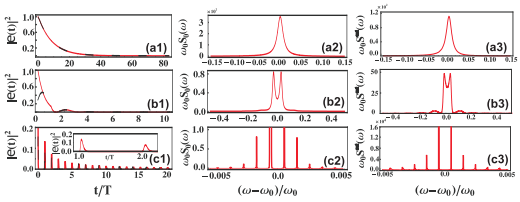

Figure 9.3: **Time evolutions and power spectra of giant atom**. (a1) Time evolution of $|e(t)|^2$ in parameter region B with $\gamma T = 0.045, \omega_0 T = 2.4\pi$. The red line is a numerical simulation and the black dashed line is the analytical result from Eq. (9.8) with a single mode $\omega_{(0)}$. (a2), (a3) The corresponding power spectra of the giant atom and the outgoing phonons, respectively. (b1) Time evolution of $|e(t)|^2$ in parameter region C with $\gamma T = 1.0, \omega_0 T = 20\pi$. The black dashed line is the analytical result from Eq. (9.8) including the two modes $\omega_{(0)}$ and $\omega_{(-1)}$. (b2), (b3) The corresponding power spectra of the giant atom and the outgoing phonons, respectively. (c1) Time evolution of $|e(t)|^2$ in parameter region D with $\gamma T = 37.5, \omega_0 T = 2000\pi$. The black dashed line is the analytical result from Eq. (9.8) including eleven modes, *i.e.*, from $\omega_{(-10)}$ to $\omega_{(10)}$. The evolution exhibits revival peaks, the first two of which are shown in more detail in the inset. (c2), (c3) The corresponding power spectra of the giant atom and the outgoing phonons, respectively.

with $k \in \mathbb{Z}$. Here, $W(z)$ is the Lambert W-function [39] defined by the equation $z = W(z)e^{W(z)}$, which in general is a multivalued function with branches $W_k(z)$, $k \in \mathbb{Z}$. By Fourier transforming Eq. (9.4), we obtain the solution of $e(t)$ for $t > 0$ (details are given in Appendix 9.7.2)

$$e(t) = e(0) \sum_k \frac{e^{-i\omega_{(k)} t}}{1 - \gamma T e^{i\omega_{(k)} T}}. \tag{9.8}$$

We assume the giant atom is initially in the excited state and set $e(0) = 1$ in the following. We now define the power spectrum of the giant atom by

$$S_0(\omega) \equiv \omega_0 \left| \int_{-\infty}^{+\infty} e(t) e^{i\omega t} dt \right|^2. \tag{9.9}$$

According to the Wiener-Khinchin theorem [40, 41, 42], the power spectrum can be obtained by Fourier transform of the autocorrelation function $C_{ee^*}(\tau) \equiv \int e^*(t) e(t+\tau) dt$, i.e., $S_0(\omega) = \omega_0 \int C_{ee^*}(\tau) e^{i\omega\tau} d\tau$ [43]. From Parseval's theorem, we have the identity $(2\pi)^{-1} \int S_0(\omega) d\omega = \omega_0 \int |e(t)|^2 dt$, which is a reflection of energy conservation, i.e., the energy in the time domain is equal to the energy in the frequency domain. Therefore, the power spectrum $S_0(\omega)$ (normalized by a factor) is the density of the atom's energy distribution over the frequency domain.

From Eq. (9.8), we can calculate the atomic power spectrum as following

$$\begin{aligned} S_0(\omega) &= \omega_0 \left| \sum_k \frac{i}{1 - \gamma T e^{i\omega_{(k)} T}} \frac{1}{\omega - \omega_{(k)}} \right|^2 \\ &= \omega_0 \frac{1}{\left| \omega - \omega_0 + i\gamma (1 + e^{i\omega T}) \right|^2}. \end{aligned} \tag{9.10}$$

Here, we have used Eq. (9.107) in Appendix 9.7.2 to arrive at the second expression. In Fig. 9.3, we show the time evolution of $|e(t)|^2$ in different parameter regions and the corresponding power spectra. The red curve in Fig. 9.3(a1) shows the time evolution of $|e(t)|^2$ from a numerical simulation with parameters in region B. The time evolution can be well fit by an exponential decay (black dashed curve) obtained from Eq. (9.8) including only one frequency mode $\omega_{(0)}$. The corresponding atomic power spectrum in Fig. 9.3(a2) shows a single peak. The red curve in Fig. 9.3(b1) shows the time evolution of $|e(t)|^2$ with parameters in region C. In the atomic power spectrum shown in Fig. 9.3(b2), we see that there are two dominant modes, corresponding to $\omega_{(-1)}$ and $\omega_{(0)}$. The long-time behaviour of $|e(t)|^2$ can be fit well by Eq. (9.8) including the two modes $\omega_{(-1)}$ and $\omega_{(0)}$ (black dashed curve in Fig. 9.3(b1)). To fit the short-time dynamics, we need to include more modes.

In Fig. 9.3(c1), the red curves show the time evolution of $|e(t)|^2$ with parameters in region D. We see that the giant atom exhibits revivals during the evolution in intervals spaced by T. Here, the distance between the

two IDTs is one thousand SAW wavelengths, *i.e.*, $L = 1000\lambda_{SAW}$. The giant atom decays to the ground state between revivals since the travelling time between the IDTs is much larger than the decay time of the giant atom ($T \gg 1/\gamma$). The corresponding atomic power spectrum, shown in Fig. 9.3(c2), has a more complicated structure of multiple peaks with narrow widths. The higher-frequency modes correspond to shorter wavelengths. In Appendix 9.7.2, we derive the approximate solution for complex mode $\omega_{(k)} = \mathrm{Re}[\omega_{(k)}]+i\mathrm{Im}[\omega_{(k)}]$ in parameter region D:

$$\begin{aligned} \mathrm{Re}[\omega_{(k)}] &\approx \omega_0 - \frac{1}{T}\left[\pi(2k+1+\Delta) - \arctan\frac{\pi(2k+1+\Delta)}{\gamma T}\right] \\ \mathrm{Im}[\omega_{(k)}] &\approx -\frac{1}{2T}\ln\left(1+\left[\frac{(2k+1+\Delta)\pi}{\gamma T}\right]^2\right). \end{aligned} \tag{9.11}$$

Here, the residual phase is defined by $\Delta = \omega_0 T/\pi - 2n \in [0,2)$ with $n \in \mathbb{Z}$. The real part of kth mode $\mathrm{Re}[\omega_{(k)}]$ gives the position of the center of the corresponding peak in the power spectrum. The positions of the peaks are roughly equally spaced; the frequency spacing is given by $\Delta\omega \approx 2\pi/T$ when $\gamma T \gg (2k+1+\Delta)\pi$. The imaginary part of kth mode $\mathrm{Im}[\omega_{(k)}]$ gives the width of each peak in the power spectrum. In the limit $\gamma T \gg (2k+1+\Delta)\pi$, the width of each peak is approximately given by $\pi^2(2k+1+\Delta)^2/\gamma^2 T^3$.

In an experiment, it is more convenient to measure the power spectrum of the outgoing phonons $\alpha^{out}(t) \equiv \alpha_A^{out}(t) = \alpha_B^{out}(t)$, which is given by the interference of the phonons emitted from the two legs

$$\alpha^{out}(t) = -i\frac{V}{v_g}\left[e(t) + e(t-T)\right]. \tag{9.12}$$

Similar to the definition of the atomic power spectrum in Eq. (9.9), we define the power spectrum of $\alpha^{out}(t)$ (fluorescence spectrum) and calculate it as (see Appendix 9.7.2 and Ref. [38] for details)

$$\begin{aligned} S^{out}(\omega) &\equiv v_g\left|\int_{-\infty}^{+\infty}\alpha^{out}(t)e^{i\omega t}dt\right|^2 \\ &= v_g\left|\frac{\gamma}{2V}\sum_k \frac{1}{1-\gamma T e^{i\omega_{(k)}T}}\frac{1+e^{i\omega T}}{\omega-\omega_{(k)}}\right|^2 \\ &= \gamma\frac{1+\cos\omega T}{\left|\omega-\omega_0+i\gamma(1+e^{i\omega T})\right|^2}. \end{aligned} \tag{9.13}$$

Compared to Eq. (9.10), there is an additional factor $(1+\cos\omega T)$, which comes from the interference of outgoing photons from the two legs of the giant atom. In Figs. 9.3(a3), (b3), and (c3), we calculate the power spectra of the outgoing phonons in the three parameter regimes B, C, and D, respectively. The fluorescence spectrum $S^{out}(\omega)$ can be directly obtained by measuring the autocorrelation function of outgoing phonon fields $C_{\alpha\alpha^*}(\tau) \equiv \int \alpha^{out*}(t)\alpha^{out}(t+\tau)dt$. According to the Wiener-Khinchin theorem, the quantity $S^{out}(\omega)$ is given by the Fourier transform of the above autocorrelation function, i.e., $S^{out}(\omega) = v_g\int C_{\alpha\alpha^*}(\tau)e^{i\omega\tau}d\tau$ [43]. The fluorescence spectrum $S^{out}(\omega)$ is the energy distribution of outgoing phonons over the frequency domain.

In the above discussion, we assumed a general case where the parameters were chosen to satisfy $\omega_0 T \neq (2n+1)\pi$, such that all the modes die out in the end and the giant atom decays to the ground state. In the case of $\omega_0 T = (2n+1)\pi$, from the definition of the Lambert W-function and Eq. (9.7), we have a real frequency mode $\omega_{(0)} = \omega_0$ with zero imaginary part. In the long-time limit, this mode survives while all the other modes die out. Therefore, we have the stationary solution $e(t\to+\infty) = \frac{1}{1+\gamma T}e^{-i\omega_0 t}$. This corresponds to a *dark state* which does not decay to the ground state in spite of the coupling to the open transmission line. The reason is that the emissions from the two legs cancel each other due to the phase difference $\omega_0 T = (2n+1)\pi$, reminiscent of how two or more atoms in waveguides can form dark states [44, 45, 46, 47]. Therefore, the stationary values of $|e(+\infty)|^2$ will be finite and the corresponding spectra $|S_0(\omega)|^2$ will show a singularity at $\omega = \omega_0$ due to the zero imaginary part of the dark mode.

Polynomial decay

As discussed in the introduction, the whole structure shown in Fig. 9.1(a) is reminiscent of a cavity for SAW phonons, since the two connection points of the giant atom introduce boundary conditions that can act as semitransparent mirrors. The energy stored in the atom and in the SAWs between the connection points is gradually lost to SAWs propagating out from the two connection points. In the case of an ordinary cavity with a small atom inside, and in the case of a small atom coupled to an open transmission line, the damping follows an exponential decay law. In our setup, however, we here show that the decay process in parameter region D exhibits a different behaviour.

In Fig. 9.4, we plot the numerical results for the time evolution of the energy stored in the form of phonons between the connection points, $E_P(t)$, and the total energy of the giant atom, $E_T(t) \equiv E_P(t) + \hbar\omega_0|e(t)|^2$, for parameters $\omega_0 T = 2001\pi$ (dark state) and $\omega_0 T = 2000\pi$ (bright state). In the long-time limit, the decaying

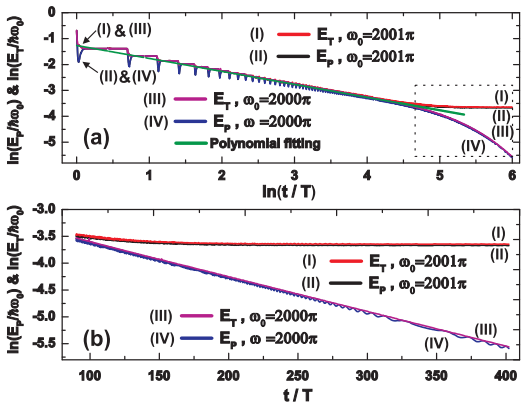

Figure 9.4: **Spontaneous decay of giant atom.** (a) The initial decay of the phonon energy stored between the connection points of the giant atom $E_P(t)$ [curves (II) and (IV)] and the total energy of giant atom $E_T(t)$ [curves (I) and (III)] exhibit universal polynomial behaviours on the time scale of T. However, the long-time behaviour (the part indicated by the dashed box) deviates from this polynomial behaviour. (b) The long-time decay follows exponential decay laws. The slope (decay exponent) for $\omega_0 T = 2000\pi$ (bright state) is given by $\pi^2/(\gamma^2 T^2)$. The slope for $\omega_0 T = 2001\pi$ (dark state) is zero.

behaviour depends on the parameter $\omega_0 T$ [see the part in the dashed box in Fig. 9.4(a)]. However, before this stage, there is a universal energy damping following a polynomial law. From Fig. 9.4(a), we see that the total energy $E_T(t)$ [curves (I) and (III)] decays monotonically in a staircase-like function. The decay of the phonon energy $E_P(t)$ [curves (II) and (IV)] overlaps with $E_T(t)$ most of the time except around integer multiples of T, where a dip of $E_P(t)$ appears on the time scale of $\gamma^{-1} \ll T$. On the large time scale T, we find that the energy decay of the stairs shown in $E_P(t)$ and $E_T(t)$ obeys (see Appendix 9.7.4 for details)

$$E_{P/T} \approx \frac{\hbar\omega_0}{2\sqrt{\pi}} \left(\frac{t}{T}\right)^{-1/2}. \tag{9.14}$$

It is interesting to note that the timescale for the polynomial decay, which here follows an inverse square-root law, is not set by the coupling strength γ but is instead determined solely by the propagation time T. In contrast, the timescale of the exponential decay of a small atom in an open transmission line would be completely fixed by γ.

The spontaneous emission of a small atom is a continuous process. However, the staircase behavior of the total energy $E_T(t)$ indicates that the giant atom emits energy in the form of phonon pulses with time period T. In an experiment, it should be straightforward to measure the outgoing phonons from the two legs of the giant atom, $\alpha^{out}(t)$. One can measure the total energy of each outgoing phonon pulse, i.e., $E^{out}(m) \equiv v_g \int_{mT}^{(m+1)T} |\alpha^{out}(t)|^2 dt$ for $m \leq t/T < m+1$. We find that the total pulse energy $E^{out}(m)$ as a function of the pulse number m also decays polynomially, i.e., $E^{out}(m)/\hbar\omega_0 \approx \frac{1}{8\sqrt{\pi}} m^{-3/2}$ [see Eq. (9.125) in Appendix 9.7.4]. Beside the polynomial behaviours of $E_P(t)$, $E_T(t)$ and $E^{out}(m)$, we find that the revival peaks shown in Fig. 9.3(c1) also exhibit polynomial decay. In Appendix 9.7.4, we calculate the time position of the revival peaks' maxima $t_m = mT + m/\gamma$ for $t \in [mT, (m+1)T)$ and the values of the revival peaks $P_e^{max}(t_m)$. As given by Eq. (9.122) in Appendix 9.7.4, the decay of revival peaks follows a polynomial law $P_e^{max}(t_m) \propto t_m^{-1}$. From Fig. 9.3(c1), we also see that the width of the revival peak becomes broader and broader. In fact, from the revival peaks' maxima $t_m = mT + m/\gamma$, we see that the peak will spread over the whole time interval $[mT, (m+1)T]$ when $m > \gamma T$, which implies that the polynomial decay is valid only for $t < \gamma T^2$.

For sufficiently long time $t > \gamma T^2$, the decaying behaviour deviates from the polynomial law. In parameter region D, the total system energy is mainly stored in the form of propagating phonon wave packets excited at both legs of the giant atom as shown in Fig. 9.3(c1). A wave packet contains many frequency modes, given by Eq. (9.11). Each mode k decays at a different rate as described by its imaginary part $\mathrm{Im}[\omega_{(k)}]$. The initial polynomial decaying behaviour is the collective effect of multiple modes decaying. In the long-time limit, however, only the mode with the slowest (exponential) decay rate survives. In Fig. 9.4(b), we show the long-time decaying behaviour in two cases, both following an exponential decay law. From the analytical expression of $\omega_{(k)}$ given by Eq. (9.11), we see the slope for $\omega_0 T = 2000\pi$ is $\pi^2/(\gamma^2 T^2)$. For the dark state case $\omega_0 T = 2001\pi$, the smallest imaginary part is zero, explaining the finite remaining energy and zero decay rate.

9.3.2 Single-phonon scattering

Above, we studied the spontaneous emission of the undriven giant atom. Now, we investigate the scattering process in the weak-driving limit, *i.e.*, single-phonon driving. In experiments, it is convenient to measure

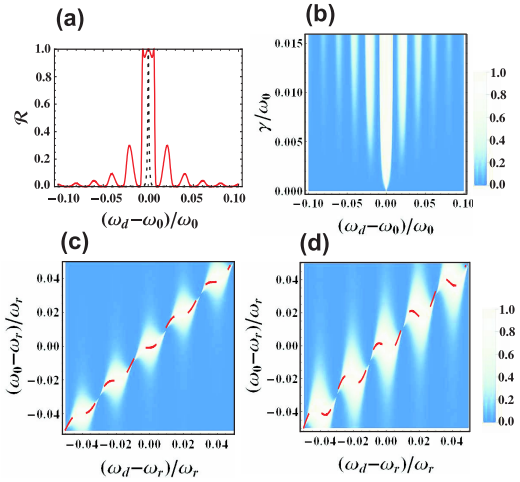

Figure 9.5: **Reflectances**. (a) Reflectance $\mathcal{R}$ as a function of the scaled driving detuning $(\omega_d-\omega_0)/\omega_0$ for $\gamma T=0.1$ (dashed black line) and $\gamma T=2$ (red line). (b) Reflectance $\mathcal{R}$ as a function of the scaled detuning $(\omega_d-\omega_0)/\omega_0$ and the scaled decay rate γ/ω_0. (c) Reflectance $\mathcal{R}$ as a function of the scaled driving frequency detuning $(\omega_d-\omega_r)/\omega_r$ and the scaled transition frequency detuning $(\omega_0-\omega_r)/\omega_r$ for $\gamma T=1$, where ω_r is the reference frequency. (d) The same as (c), but with $\gamma T=2$. Other parameters: $\omega_0 T=100\pi$ for (a) and (b), $\omega_r T=100\pi$ for (c) and (d).

transmittance and reflectance of such a weak drive. We consider SAWs incoming towards leg A and transmitted to leg B, *i.e.*, the driving terms in Eq. (9.4) are set to be $\alpha_A^{in}(t)=Ae^{-i\omega_d t}$ and $\alpha_B^{in}(t)=0$ (see also Fig. 9.1(a)). Using the method of Laplace transformation, the reflectance in the long-time limit, defined as $\mathcal{R}=|\alpha_A^{out}(\infty)|^2/|\alpha_A^{in}(t)|^2$, is calculated to be (see Appendix 9.7.5 for details)

$$\mathcal{R}=\frac{\gamma^2\left(1+\cos\omega_d T\right)^2}{\left[(\omega_d-\omega_0)-\gamma\sin\omega_d T\right]^2+\gamma^2(1+\cos\omega_d T)^2}. \tag{9.15}$$

The transmittance in the long-time limit is given by $\mathcal{T}=|\alpha_B^{out}(\infty)|^2/|\alpha_A^{in}(t)|^2=1-\mathcal{R}$. From Eq. (9.1), we see that the effective relaxation rate γ also depends on the driving frequency ω_d (In the driven case, ω_0 appearing in Eq. (9.1) needs to be replaced by ω_d.). However, as long as the change of ω_d is small enough, *i.e.*, $\Delta\omega_d\ll 2\pi/(N\tau)\sim\omega_0/N$, we can view γ as approximately constant in the full range of driving frequencies. From Eq. (9.15), we see that the condition for total reflection, $\mathcal{R}=1$, is given by

$$\omega_d=\omega_0+\gamma\sin(\omega_d T), \tag{9.16}$$

and the condition for total transmission, $\mathcal{R}=0$, is given by $\omega_d T=(2n+1)\pi$, $n\in\mathbb{Z}$. In case the phase difference between the two legs is a multiple of 2π, *i.e.*, $\omega_0 T=2n\pi$, Eq. (9.16) has only one solution ($\omega_d=\omega_0$) for $\gamma T<1$, but two additional solutions exist for $\gamma T>1$.

In Fig. 9.5(a), we plot the reflectance $\mathcal{R}$ as a function of the scaled detuning $(\omega_d-\omega_0)/\omega_0$ for $\omega_0 T=100\pi$. The black curve corresponds to $\gamma T=0.1$ and exhibits the typical features of a small atom: a single peak with perfect reflection at $\omega_d=\omega_0$. The red curve corresponds to $\gamma T=2$ and shows some new features characteristic of the giant atom: (1) $\mathcal{R}$ exhibits a multi-peak structure as a function of detuning; (2) there are two additional driving frequencies resulting in $\mathcal{R}=1$ beside the central peak at $\omega_d=\omega_0$. In fact, the multiple peaks correspond to the frequency peaks shown in Fig. 9.3(c2). When the driving frequency ω_d resonates with one of the modes $\omega_{(k)}$, the reflectance shows a local maximum in Fig. 9.5(a). However, the central peak at $\omega_d=\omega_0$ does not correspond to any mode $\omega_{(k)}$. This peak is instead the result of a new pole in the complex plane due to the driving. The side peaks of $\mathcal{R}=1$ can also be understood using Eq. (9.16). The transition frequency of the giant atom is shifted by $\gamma\sin(\omega_d T)$. Therefore, the driving frequency can be resonant with the shifted transition frequency of the giant atom again (if $\gamma T>1$) when it deviates from $\omega_d=\omega_0$. In Fig. 9.5(b), we plot the reflectance $\mathcal{R}$ as functions of the scaled detuning $(\omega_d-\omega_0)/\omega_0$ and the scaled decay rate γ/ω_0 for $\omega_0 T=100\pi$.

In experiments, the transition frequency ω_0 of the transmon qubit can be easily tuned *in situ*; tuning the decay rate γ is considerably more difficult. (As discussed below Eq.(9.1), we have neglected the frequency dependence of the effective decay rate γ. Thus, the only way to tune the effective decay rate γ is to change the single-finger decay rate γ_0 which is, however, fixed by the design of the device.) Thus, we plot the reflectance $\mathcal{R}$ as a function of both drive detuning $(\omega_d-\omega_r)/\omega_r$ and transmon detuning $(\omega_0-\omega_r)/\omega_r$ in Figs. 9.5(c) and (d) for $\gamma T=1$ and $\gamma T=2$, respectively. Here, the reference frequency ω_r is given by $\omega_r=100\pi/T$. The dashed red curves correspond to the condition of total reflection given by Eq. (9.16).

9.4 Two-phonon processes

In this section, we study the scattering of a weakly coherent pulse from the giant atom, focusing on two-phonon processes. We construct the exact two-phonon scattering matrix following the diagrammatic approach of Ref. [27] and use it to compute the leading-order contribution (in the phononic flux) to the second-order coherence functions and to the inelastic power spectrum of the scattered phonons. In addition, we find the first-order correction to the transmittance, extending the result of Section 9.3.2 beyond the single-phonon approximation.

9.4.1 Two-phonon scattering matrix

We assume that the phonon field is initially prepared in a coherent state in the form of a wavepacket centered around the driving frequency ω_d. By defining a unitary operator

$$U \equiv \exp\left[-i\omega_d t\left(\sigma_+\sigma_- + \sum_{\alpha=1,2}\int a^\dagger_{\alpha\omega_p}a_{\alpha\omega_p}d\omega_p\right)\right], \tag{9.17}$$

the Hamiltonian in Eq. (9.2) is transformed into $H_{RF} \equiv U^\dagger \mathscr{H} U + i\hbar\frac{dU^\dagger}{dt}U$ in the frame rotating with frequency ω_d. Dropping the fast oscillating terms in H_{RF} and setting $\hbar = 1$, we arrive at the Hamiltonian under the RWA,

$$\begin{aligned} H &= -\frac{1+\sigma_z}{2}\delta + \sum_{\alpha=1,2}\int d\omega\omega a^\dagger_{\alpha\omega}a_{\alpha\omega} \\ &+ \sum_{\alpha=1,2}\int d\omega\left(\nu_{\alpha\omega}a^\dagger_{\alpha\omega} + \text{H.c.}\right). \end{aligned} \tag{9.18}$$

Here, we have defined the atomic detuning $\delta \equiv \omega_d - \omega_0$ and $\sigma_z \equiv |e\rangle\langle e| - |g\rangle\langle g|$. The phonon frequency is also shifted by the driving frequency, *i.e.*, $\omega \equiv \omega_p - \omega_d$. We have introduced the interacting operator $\nu_{\alpha\omega}$, which we call bare vertex operator,

$$\nu_{\alpha\omega} \equiv \sqrt{\frac{\gamma}{4\pi}}\sum_{\beta=1,2}\sigma_- e^{-ic_\alpha c_\beta(\omega T+\varphi)/2}. \tag{9.19}$$

The parameter $\varphi = \omega_d T = \omega_d L/v_g$ is the phase accumulated by the phonons during propagation from one leg to the other (we have used the relationship $kL = \omega_p T$ for SAWs).

We consider a rectangular pulse of spatial length d, initially created at a large distance ($\gg d$) to the left of the giant atom, propagating rightwards with a constant group velocity v_g. Keeping contributions from up to two phonons, we can write the initial phonon state

$$\begin{aligned} |\Psi_i\rangle &= e^{-\bar{n}/2}e^{\sqrt{\bar{n}}b_1^\dagger}|0\rangle \\ &\approx e^{-\bar{n}/2}\left[|0\rangle + \sqrt{\bar{n}}b_1^\dagger|0\rangle + \frac{\bar{n}}{2}b_1^{\dagger\,2}|0\rangle + O\left(\bar{n}^{3/2}\right)\right], \end{aligned} \tag{9.20}$$

where $\bar{n} \ll 1$ is the mean number of phonons in the coherent state, and $b_1^\dagger$ is a normalized wavepacket operator

$$b_1^\dagger = \int d\omega\phi(\omega)a^\dagger_{1\omega}, \quad \phi(\omega) = \sqrt{\frac{2v_g}{\pi d}}\frac{\sin(\omega d/2v_g)}{\omega}, \tag{9.21}$$

defined in terms of the plane-wave operator $a^\dagger_{1\omega}$ which creates a right-propagating phonon of frequency $\omega + \omega_d$ (the frequency ω in $a^\dagger_{1\omega}$ is measured from the driving frequency ω_d). We also assume that the wavepacket $\phi(\omega)$ has a narrow bandwidth $\frac{2\pi v_g}{d} \ll \gamma$, which implies that we can make the replacement $\phi(\omega) \to \sqrt{\frac{2\pi v_g}{d}}\delta(\omega)$ whenever $\phi(\omega)$ is convolved with a function varying slowly on the bandwidth scale.

After scattering from the giant atom, the initial phonon state in Eq. (9.20) becomes the final one

$$|\Psi_f\rangle = e^{-\bar{n}/2}\left[|0\rangle + \sqrt{\bar{n}}S^{(1)}b_1^\dagger|0\rangle + \frac{\bar{n}}{2}S^{(2)}b_1^{\dagger\,2}|0\rangle + O\left(\bar{n}^{3/2}\right)\right], \tag{9.22}$$

where $S^{(1)}$ and $S^{(2)}$ are the one- and two-phonon scattering operators. They can be expressed as [27]

$$S^{(1)} = \left\{\delta_{s's} - 2\pi i P_- v_{s'}M(\omega)v_s^\dagger P_-\delta_{\omega'\omega}\right\}a^\dagger_{s'}a_s, \tag{9.23}$$

$$\begin{aligned} S^{(2)} = \Bigg\{&\frac{1}{2}\delta_{s_1's_1}\delta_{s_2's_2} - 2\pi i P_- v_{s_1'}M(\omega_1')\left[\delta_{\omega_1'\omega_1}\delta_{s_2's_2} + \right. \\ &\left. + W_{s_2's_2}(E)M(\omega_1)\delta_{\omega_1'+\omega_2',\omega_1+\omega_2}\right]v_{s_1}^\dagger P_-\Bigg\}a^\dagger_{s_1'}a^\dagger_{s_2'}a_{s_2}a_{s_1}, \end{aligned} \tag{9.24}$$

where $s=(\alpha,\omega)$ is a multi-index, and we implicitly assume summation/integration over it, when it is repeated. The parameter E must eventually be set to the value of an incoming-state energy $\omega_1+\omega_2$; for the initial state (Eq. (9.20)) in our convention about the energy reference point it equals $E=0$. The Green's functions of the qubit in the ground $G(E)=\frac{P_-}{E+i\eta}$ and excited $M(E)=\frac{P_+}{E+\delta+\Sigma(E)}$ states are spanned by the corresponding projectors $P_\pm=\sigma_\pm\sigma_\mp=\frac{1\pm\sigma_z}{2}$. The self-energy of the ground state is infinitesimally small ($\eta\to 0^+$), while the self-energy of the excited state $\Sigma(E)$ has to be established. The effective two-phonon vertex $W_{s_2's_2}(E)$ also requires specification.

We note that the Hilbert space of the qubit is two-dimensional, and, in addition, the Hamiltonian in Eq. (9.18) is written in the RWA. This means that in a diagrammatic representation of $\Sigma(E)$ and $W_{s's}(E)$, the bare vertices v and $v^\dagger$ must alternate each other. Along with an application of Wick's theorem, this leads to the following exact equations:

$$\Sigma(E) = v_s^\dagger G(E-\omega)v_s, \tag{9.25}$$
$$W_{s's}(E) = w_{s's}(E)+w_{s's_1}(E)M(E-\omega_1)W_{s_1s}(E), \tag{9.26}$$

where $w_{s's}(E)=v_s^\dagger G(E-\omega-\omega')v_{s'}$, and Eq. (9.26) is obtained from the iteration $w+wMw+\ldots$.

A simple calculation shows that Eq. (9.25) yields $\Sigma(E)=-iP_+\gamma\left[1+e^{i(ET+\varphi)}\right]$, and this is sufficient to recover the single-phonon scattering matrix. Thus, we obtain

$$S^{(1)}b_1^\dagger|0\rangle = s_{\alpha_1',1}\phi(\omega_1')a^\dagger_{\alpha_1',\omega_1'}|0\rangle, \tag{9.27}$$

where the matrix elements

$$s_{1,1} = \frac{\delta-\gamma\sin\varphi}{\delta+i\gamma(1+e^{i\varphi})}, \tag{9.28}$$
$$s_{2,1} = -i\gamma\frac{1+\cos\varphi}{\delta+i\gamma(1+e^{i\varphi})}. \tag{9.29}$$

Note that the scattering matrix elements $s_{1,1}$ and $s_{2,1}$ connect the incident right-propagating phonons to the scattered right-propagating and left-propagating phonons, respectively. Therefore, the reflectance and transmittance are given by $\mathcal{T}=|s_{1,1}|^2$ and $\mathcal{R}=|s_{2,1}|^2$, which coincides with the definitions found in the previous section and in Appendix 9.7.5.

The effective two-phonon vertex $W_{s's}(E)$ obeying Eq. (9.26) accounts for multiple excursions of two correlated phonons between the two legs. Parameterizing

$$W_{s's}(E)=\sum_{\beta',\beta}\frac{\gamma P_+}{4\pi}e^{-ic_{\alpha'}c_{\beta'}(\omega'T+\varphi)/2}e^{ic_\alpha c_\beta(\omega T+\varphi)/2}\overline{W}(\omega',\omega), \tag{9.30}$$

we simplify Eq. (9.26) down to

$$\overline{W}(\omega',\omega) = \frac{1}{E-\omega'-\omega+i\eta} + \frac{\gamma}{2\pi}\int d\omega_1\frac{1}{E-\omega'-\omega_1+i\eta}\times\frac{e^{i\omega_1T+i\varphi}}{E-\omega_1+\delta+i\gamma}\overline{W}(\omega_1,\omega). \tag{9.31}$$

The first term on the RHS of Eq. (9.31) does not depend on the travel time $T=L/v_g$ between the legs. The function $\overline{W}(\omega',\omega)$ is analytic in the lower half-plane in both its arguments. In the regime $\gamma T\ll 1$, we can neglect the term $e^{i\omega_1T}$ under the integral and close the integration contour in the lower half-plane, which leads to the second term vanishing. Therefore, at short inter-leg distances we can approximate $\overline{W}(\omega',\omega)\approx\frac{1}{E-\omega'-\omega+i\eta}$, identifying this term with the Markovian contribution.

For larger separations $\gamma T\gtrsim 1$, we need the full solution of Eq. (9.31). Taking into account the particular form of the initial state in Eq. (9.20), it suffices to solve Eq. (9.31) for $E=\omega=0$. This can be done analytically, and we find

$$\overline{W}(-q,0)|_{E=0} = \frac{1}{q+i\eta}+F(q), \tag{9.32}$$
$$F(q) = -\frac{i\gamma e^{i\varphi}}{\lambda+i\gamma e^{i\varphi}}\sum_{\sigma=\pm,0}C_\sigma\frac{e^{iqT}-e^{-i\sigma pT}}{q+\sigma p}, \tag{9.33}$$

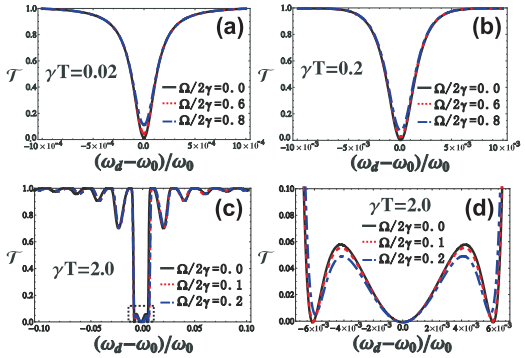

Figure 9.6: **Transmittance including two-phonon processes.** The plots show $\mathcal{T} = |s_{1,1} + \delta s_{1,1}|^2$ as a function of normalized driving detuning $(\omega_d - \omega_0)/\omega_0$. In all figures, $\omega_0 T = 100\pi$. (a) $\mathcal{T}$ for $\gamma T = 0.02$ and various scaled driving parameters $\Omega/(2\gamma)$. (b) Same as (a), but with $\gamma T = 0.2$. (c) $\mathcal{T}$ for $\gamma T = 2.0$ and various scaled driving parameters $\Omega/(2\gamma)$. (d) Zoom-in of the dashed box in (c).

where

$$p = \sqrt{\lambda^2 + \gamma^2 e^{2i\varphi}}, \quad \lambda = \delta + i\gamma, \tag{9.34}$$

$$C_\pm = \pm \frac{(\pm p - \lambda)e^{\pm ipT} - i\gamma e^{i\varphi}}{2(p\cos pT - i\lambda \sin pT)}, \quad C_0 = -1. \tag{9.35}$$

The parameter p appears only in the non-Markovian part $F(q)$ of the term (32). Its real and imaginary parts contain a new oscillation frequency $\mathrm{Re}(p)$ and a new relaxation rate $\mathrm{Im}(p)$, which can only manifest themselves in the two-photon inelastic scattering processes in the non-Markovian regime $|p| \cdot T \gg 1$.

Finally, we derive

$$\begin{aligned} \frac{1}{2} S^{(2)} b_1^{\dagger 2} |0\rangle &= \sum_{\alpha_1', \alpha_2'} \frac{1}{2} s_{\alpha_1',1} s_{\alpha_2',1} \phi(\omega_1')\phi(\omega_2') a^\dagger_{\alpha_1',\omega_1'} a^\dagger_{\alpha_2',\omega_2'} |0\rangle \\ &+ \sum_{\alpha_1', \alpha_2'} \frac{2v_g\gamma}{d} s_{2,1} \int dq \cos\frac{qT+\varphi}{2} \cos\frac{-qT+\varphi}{2} \\ &\times M(q) \left[\frac{1}{q} + F(q)\right] a^\dagger_{\alpha_1',q} a^\dagger_{\alpha_2',-q} |0\rangle , \end{aligned} \tag{9.36}$$

thus completing the determination of the scattering state in Eq. (9.22). In this expression (and in the following), we use the notation $M(q)$ for $\frac{1}{q+\lambda+i\gamma e^{iqT+i\varphi}}$, omitting the associated matrix structure.

In the Markovian regime $|p| \cdot T \ll 1$, the second – inelastic – contribution to Eq. (9.36) is approximated by

$$\sum_{\alpha_1', \alpha_2'} \frac{2v_g\gamma}{d} s_{2,1} \cos^2\frac{\varphi}{2} \int dq \frac{a^\dagger_{\alpha_1',q} a^\dagger_{\alpha_2',-q}}{(q+\lambda+i\gamma e^{i\varphi})q} |0\rangle,$$

where the q-dependence of the integrand features only simple poles. We also note the absence of the parameter p in this expression.

9.4.2 Correction to the transmittance

Knowing the exact two-photon S-matrix (Eq. (16.20)), we can find the first nonlinear correction to the transmittance. We calculate $\langle \Psi_f | a_1(x) | \Psi_f \rangle = e^{i\omega_0 x/v_g}\sqrt{f}[s_{1,1} + \delta s_{1,1} + O(f^2)]$, where $f = \bar{n} v_g/d$ is a phonon flux. To compare our results for a giant atom to known results for a small atom, we introduce the driving amplitude $\Omega \equiv \sqrt{8\gamma f}$ (Rabi frequency in the small-atom limit $\gamma T \to 0$), which is widely used in the study of quantum optics. Then, we write the correction $\delta s_{1,1}$ to the single-phonon transmittance

$$\delta s_{1,1} = \frac{1}{2}\left(\frac{\Omega}{2\gamma}\right)^2 \frac{8ip\gamma^3 \cos^4\frac{\varphi}{2}(\lambda\cos pT - ip\sin pT + i\gamma e^{i\varphi})}{|\lambda + i\gamma e^{i\varphi}|^2 (\lambda + i\gamma e^{i\varphi})^2 (p\cos pT - i\lambda\sin pT)}. \tag{9.37}$$

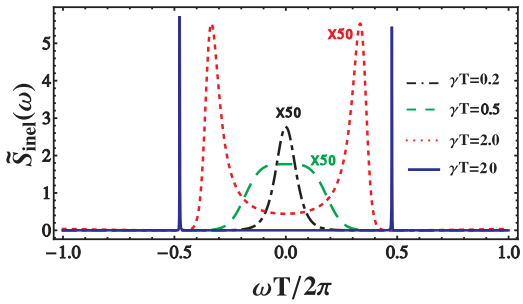

Figure 9.7: **Inelastic power spectra.** The black dotted dashed, green long dashed, red short dashed, and blue solid curves are the scaled inelastic power spectra $\tilde{S}_{\rm inel}(\omega) \equiv (2\gamma/\Omega)^4 S_{\rm inel}(\omega)$ for $\gamma T = 0.2$ (enlarged 50 times), $\gamma T = 0.5$ (enlarged 50 times), $\gamma T = 2.0$ (enlarged 50 times) and $\gamma T = 20$, respectively. Other parameters: $\delta/\omega_0 = 0.0$, $\varphi = 2k\pi, k \in Z^+$.

While the linear transmittance $s_{1,1}$ corresponds to the transition $|1\rangle \to |0\rangle$ (elimination of a single phonon), the correction $\delta s_{1,1}$ corresponds to a measurement of a phonon in a two-phonon state, $|2\rangle \to |1\rangle$. Let us analyze $\delta s_{1,1}$ in different limiting cases.

For $\gamma T \ll 1$, we obtain

$$\delta s_{1,1} \approx \frac{1}{2}\left(\frac{\Omega}{2\gamma}\right)^2 \frac{8i\gamma^3 \cos^4\frac{\varphi}{2}}{|\lambda + i\gamma e^{i\varphi}|^2 (\lambda + i\gamma e^{i\varphi})}. \tag{9.38}$$

In the small-atom limit $\varphi \to 0$, we can furthermore simplify the above correction

$$\delta s_{1,1} \approx \frac{1}{2}\left(\frac{\Omega}{2\gamma}\right)^2 \frac{1 + i\frac{\delta}{2\gamma}}{\left[1 + \left(\frac{\delta}{2\gamma}\right)^2\right]^2}, \tag{9.39}$$

which is consistent with the result in Ref. [43] for the study of a small artificial atom (recall that the total relaxation rate of our atom in this limit is 2γ).

For $\gamma T \gg 1$ and $p \neq 0$ ($\mathrm{Im}\, p > 0$), we find that

$$\delta s_{1,1} \approx \frac{1}{2}\left(\frac{\Omega}{2\gamma}\right)^2 \frac{8i\gamma^3 \cos^4\frac{\varphi}{2}}{|\lambda + i\gamma e^{i\varphi}|^2 (\lambda + i\gamma e^{i\varphi})} \frac{p}{\lambda + i\gamma e^{i\varphi}}, \tag{9.40}$$

which differs from its short-distance counterpart in Eq. (9.38) by the additional factor at the end.

For $p = 0$ (resonance $\delta = 0$ and bright state $\varphi = 2k\pi, k \in \mathbb{N}$), we derive the expression directly from Eq. (9.37)

$$\delta s_{1,1} = \frac{1}{2}\left(\frac{\Omega}{2\gamma}\right)^2 \frac{1}{1 + \gamma T}, \tag{9.41}$$

valid for arbitrary T. Since in this case $s_{1,1} = 0$, Eq. (9.41) represents the leading contribution to the transmittance. Unlike Eq. (9.40), it vanishes at large T.

We plot the corrected transmittance $\mathcal{T} = |s_{1,1} + \delta s_{1,1}|^2$ in Fig. 9.6 for different parameter regimes. Fig. 9.6(a) and (b) show the transmittance for $\gamma T = 0.02$ and $\gamma T = 0.2$, respectively. We see that the two-phonon process basically enhances the transmittance. The reason is that the atom can only interact with a single phonon at any given time. When γT is small, corresponding to the limit of a small atom with Markovian dynamics, a second incoming phonon will thus not interact with the atom and simply be transmitted forward [16, 6, 51]. However, for larger $\gamma T = 2.0$, when the Markov approximation breaks down, the transmittance through the giant atom shows a more complicated structure as can be seen in Figs. 9.6(c) and (d). In particular, we observe that the two-phonon process does not always enhance the transmttance, but instead sometimes suppresses it. This is due to the fact that the giant atom can interact with one phonon while the other phonon travels between the two connection points. These two phonons can then interfere constructively or destructively in a way that is not possible with a small atom.

9.4.3 Inelastic power spectrum

At weak coherence $\bar{n} \ll 1$, the elastic scattering dominates over the inelastic scattering: the former receives the leading $O(\Omega^2)$ contribution from a single-phonon process, while the latter starts to happen when at least two phonons are involved. This gives the $O(\Omega^4)$ contribution.

Let us compute these leading terms in the power spectrum of the giant atom in the state from Eq. (9.22). We consider $g_\alpha^{(1)}(\tau) = \langle \Psi_f \left| a_\alpha^\dagger(x - v_g\tau) a_\alpha(x) \right| \Psi_f \rangle$, where $a_\alpha(x) = \sqrt{\frac{v_g}{2\pi}} \int d\omega a_{\alpha\omega} e^{i(\omega+\omega_0)x/v_g}$, and establish

$$\begin{aligned} g_\alpha^{(1)}(\tau) &= e^{i\omega_0\tau} \left\{ (8\gamma)^{-1} \Omega^2 \left| s_{\alpha,1} \right|^2 - (4\gamma)^{-2} \Omega^4 \mathcal{R} \mathrm{Im} \left[s_{\alpha,1}^* \Lambda M(0) \right] \right\} \\ &+ \int d\omega e^{i(\omega_0+\omega)\tau} S_{\mathrm{inel}}(\omega) + O\left(\Omega^6\right), \end{aligned} \tag{9.42}$$

where $\mathcal{R} = \left| s_{2,1} \right|^2$ and

$$\Lambda = 1 + \frac{i\gamma e^{i\varphi}}{p} \left[C_+ \left(1 - e^{-ipT} \right) - C_- \left(1 - e^{ipT} \right) \right]. \tag{9.43}$$

The leading inelastic contribution is given in terms of the corresponding power spectrum

$$\begin{aligned} S_{\mathrm{inel}}(\omega) &= \frac{\Omega^4}{4\pi} \mathcal{R} \cos^2 \frac{\omega T + \varphi}{2} \cos^2 \frac{-\omega T + \varphi}{2} \\ &\times \left| \frac{M(\omega) - M(-\omega)}{2\omega} + \frac{M(\omega)F(\omega) + M(-\omega)F(-\omega)}{2} \right|^2. \end{aligned} \tag{9.44}$$

We see that the inelastic power is on the order of $O(\Omega^4)$.

It is important to check the power conservation. Summing $g_\alpha^{(1)}(0)$ over the channels α and using the unitarity of the single-phonon matrix from Eq. (9.23), we obtain the incoming power up to leading order $O(\Omega^2)$. Therefore, the elastic and inelastic contributions to the power in $O(\Omega^4)$ must cancel each other, *i.e.*,

$$-(4\gamma)^{-2} \Omega^4 \mathcal{R} \sum_\alpha \mathrm{Im} \left[s_{\alpha,1}^* \Lambda M(0) \right] + 2 \int d\omega S_{\mathrm{inel}}(\omega) = 0. \tag{9.45}$$

This relationship indeed holds due to the unitarity of the two-phonon scattering matrix in Eq. (16.20). In the resonant case $\delta/\omega_0 = 0.0$ and for the bright state $\varphi = 2k\pi, k \in Z^+$, we have $M(0) = -i(2\gamma)^{-1}$ and $\Lambda = 1/(1+\gamma T)$ from Eqs. (9.35) and (9.43). From Eqs. (9.28) and (9.29), we have the scattering matrix elements $s_{2,1} = -1$ and $s_{1,1} = 0$. The total power of the inelastic spectrum can be calculated from Eq. (9.45):

$$\int d\omega S_{\mathrm{inel}}(\omega) = \left(\frac{\Omega}{2\gamma} \right)^4 \frac{\gamma}{4(1+\gamma T)}. \tag{9.46}$$

In the small-atom limit $\gamma T \to 0$, the total power of the inelastic spectrum is $\frac{\gamma}{4} \left(\frac{\Omega}{2\gamma} \right)^4$. However, in the giant-atom limit $\gamma T \gg 1$, the total inelastic power is $\frac{1}{4T} \left(\frac{\Omega}{2\gamma} \right)^4$. In Fig. 9.7, we plot the scaled inelastic power spectrum $\tilde{S}_{\mathrm{inel}}(\omega) \equiv (2\gamma/\Omega)^4 S_{\mathrm{inel}}(\omega)$ as a function of the dimensionless frequency $\omega T/2\pi$. Due to the narrow bandwidths and the high peaks in the large-atom limit $\gamma T = 20$, we enlarge the plots for $\gamma T = 0.2$, $\gamma T = 0.5$ and $\gamma T = 2.0$ by fifty times.

For point-like atoms ($T = 0$), we can simplify the inelastic power spectrum Eq. (9.44) on resonance $\delta/\omega_0 = 0$ and bright state $\varphi = 2k\pi, k \in Z^+$

$$S_{\mathrm{inel}}(\omega) = \frac{1}{4\pi} \left(\frac{\Omega}{2\gamma} \right)^4 \left(\frac{4\gamma^2}{\omega^2 + 4\gamma^2} \right)^2. \tag{9.47}$$

This gives a single peak around the central resonant frequency in the elastic spectrum as shown by the black dot-dashed line in Fig. 9.7. However, if we increase the size of the atom, the central peak will split into two peaks. In the general case $\gamma T > 0$, we have the inelastic power spectrum

$$\begin{aligned} &S_{\mathrm{inel}}(\omega) = \\ &\frac{\Omega^4}{16\pi(1+\gamma T)^2} \left[\frac{1 + \cos\omega T}{(\omega - \gamma \sin\omega T)^2 + \gamma^2 (1 + \cos\omega T)^2} \right]^2. \end{aligned} \tag{9.48}$$

The critical point where the central peak splits into two peaks can be determined by the second derivative of the inelastic power spectrum, i.e., $\frac{d^2}{d\omega^2} S_{\mathrm{inel}}(\omega)|_{\omega=0} = 0$, which gives the critical value $(\gamma T)_c = 1/2$. The mechanism of two peaks appearing here is different from that of two side peaks in the famous Mollow triplet [52], which comes from relatively large driving $\Omega/(2\gamma) > 1$ [52, 53]. In fact, our two-phonon expansion is only valid for $\Omega/(2\gamma) < 1$. The two peaks found here come from the time delay of the giant atom, not from strong driving.

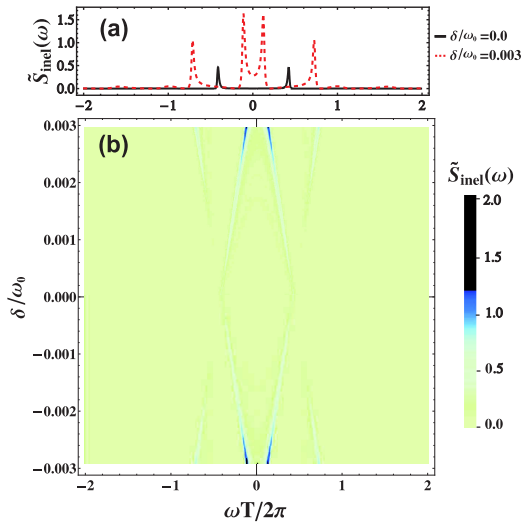

Figure 9.8: **Inelastic power spectra vs detunings.** (a) The black solid and red dashed curves are the scaled inelastic power spectra $\tilde{S}_{inel}(\omega)$ for $\delta/\omega_0 = 0$ and $\delta/\omega_0 = 0.003$, respectively. (b) Density plot of $\tilde{S}_{inel}(\omega)$ with the detuning $\delta/\omega_0 \in [-0.003, 0.003]$. Other parameters: $\gamma T = 5.0$, $\varphi = 200\pi$ for both figures.

9.4.4 Production of phonon pairs

To further understand the meaning of the inelastic power spectrum $S_{inel}(\omega)$, we rewrite the scattered two-phonon state from Eq. (9.36) as

$$\begin{aligned} S^{(2)} b_1^{\dagger 2} |0\rangle &= \frac{2\pi v_g}{d} \sum_{\alpha_1,\alpha_2} s_{\alpha_1,1} s_{\alpha_2,1} a^\dagger_{\alpha_1,0} a^\dagger_{\alpha_2,0} |0\rangle \\ &+ \int d\omega \psi(\omega) \left(a^\dagger_{1,\omega} a^\dagger_{1,-\omega} + a^\dagger_{2,\omega} a^\dagger_{2,-\omega} \right) |0\rangle \\ &+ \int d\omega \psi(\omega) \left(a^\dagger_{1,\omega} a^\dagger_{2,-\omega} + a^\dagger_{2,\omega} a^\dagger_{1,-\omega} \right) |0\rangle . \end{aligned} \tag{9.49}$$

Here we have used the narrow bandwidth assumption, *i.e.*, $\phi(\omega) = \sqrt{\frac{2\pi v_g}{d}}\delta(\omega)$. The first line on the RHS of Eq. (9.49) means that the two phonons travel through the transmission line independently. The second and third lines on the RHS of Eq. (9.49) represent the final states of two phonons after inelastic scattering (exchanging energy). Due to energy conservation, the two scattered phonons are always generated in pairs with frequencies of opposite signs (with reference to the driving frequency ω_d). The second line on the RHS of Eq. (9.49) represents the superposition state of a right-propagating phonon pair and a left-propagating phonon pair. The third line on the RHS of Eq. (9.49) represents the phonon pair of a right-propagating phonon and a left-propagating phonon. The coefficient of these photon-pair states at frequency ω is given by

$$\begin{aligned} \psi(\omega) \equiv s_{2,1} \frac{2 v_g \gamma}{d} \cos\frac{\omega T + \varphi}{2} \cos\frac{-\omega T + \varphi}{2} \\ \times \left[\frac{M(\omega) - M(-\omega)}{2\omega} + \frac{M(\omega)F(\omega) + M(-\omega)F(-\omega)}{2} \right]. \end{aligned} \tag{9.50}$$

Compared to Eq. (9.44), we see that the inelastic power spectrum $S_{inel} \propto |\psi(\omega)|^2$ is a direct measure of the production of phonon pairs with frequency ω.

In Fig. 9.7, we plot the scaled inelastic power spectrum $\tilde{S}_{inel}(\omega)$ with the parameters $\delta/\omega_0 = 0$ and $\varphi = 2k\pi$, $k \in Z^+$, which corresponds to perfect reflection $\mathcal{R} = |s_{2,1}|^2 = 1$ and zero transmission $\mathcal{T} = |s_{1,1}|^2 = 0$ in the single-phonon approximation. In this case, no phonons are transmitted by elastic scattering, *i.e.*, the first line on the RHS of Eq. (9.49) gives no contribution to the transmission channel. However, phonons are still allowed to transmit through inelastic scattering as described by the second line on the RHS of Eq. (9.49) (two phonons are transmitted) and the third line on the RHS of Eq. (9.49) (one phonon is transmitted and the other is reflected). From Fig. 9.7, we see that, in the small-atom limit $\gamma T = 0.2$, the production of phonon pairs centres at $\omega = 0$ decreasing with frequency on both sides. However, when the atom becomes larger, *e.g.*, $\gamma T = 2$, the phonon pair production centres around two well-separated frequency regions. For the giant atom with $\gamma T = 20$, we generate phonon pairs of frequencies $\omega \approx \pm\pi/T$ with a narrow bandwidth.

We further plot the scaled inelastic power spectrum as a function of the dimensionless driving detuning δ/ω_0 in Fig. 9.8. We set the parameters as $\gamma T = 5.0$ and $\varphi = 200\pi$ and change the detuning value continuously

from $\delta/\omega_0 = -0.003$ to $\delta/\omega_0 = 0.003$ in Fig. 9.8(b). It is shown that the inelastic power spectrum is symmetric with respect to the detuning. At zero detuning, $\delta/\omega_0 = 0$, we see two peaks in the inelastic power spectrum as shown by the black curve in Fig. 9.8(a). For a small detuning $\delta/\omega_0 = 0.003$, however, we see four peaks as shown by the red curve in Fig. 9.8(a). This means we can generate phonon pairs at two different frequencies. From the third line on the RHS of Eq. (9.49) and Eq. (9.50), we see that the production of phonon pairs is proportional to the reflectance $\mathcal{R} = |s_{2,1}|^2$. Note that at $\varphi = \pi + 2\pi k$, $k \in \mathbb{Z}^+$, the backward scattering is absent ($\mathcal{R} = 0$), and the inelastic scattering vanishes – all phonons propagate forward without any obstruction due to the formation of a dark state in the giant atom. In this case, as a result, no phonon pairs are generated.

9.4.5 Second-order coherence correlation functions

A further important quantity is the second-order coherence correlation function defined by

$$G^{(2)}_{\alpha'\alpha}(\tau) \equiv \left\langle \Psi_f \left| a^\dagger_\alpha(x) a^\dagger_{\alpha'}(x - v_g\tau) a_{\alpha'}(x - v_g\tau) a_\alpha(x) \right| \Psi_f \right\rangle . \tag{9.51}$$

This correlation function corresponds to the probability of detecting a phonon in channel α at time τ after detecting a first one in channel α' for the final state $|\Psi_f\rangle$ (see, *e.g.*, [53, 23]). It is also useful to introduce the normalized second-order coherence correlation function

$$g^{(2)}_{\alpha'\alpha}(\tau) = \frac{\left\langle \Psi_f \left| a^\dagger_\alpha(x) a^\dagger_{\alpha'}(x - v_g\tau) a_{\alpha'}(x - v_g\tau) a_\alpha(x) \right| \Psi_f \right\rangle}{g^{(1)}_{\alpha'}(0) g^{(1)}_{\alpha}(0)}. \tag{9.52}$$

In the two-phonon approximation, it becomes

$$g^{(2)}_{\alpha'\alpha}(\tau) = \left| 1 + \kappa_{\alpha'\alpha}(\varphi) \left[\cos\varphi I_0(\tau) + I_1(\tau) \right] \right|^2 , \tag{9.53}$$

where the coefficients

$$\kappa_{11}(\varphi) = \frac{\gamma^2(1+\cos\varphi)}{(\delta - \gamma\sin\varphi)^2}, \tag{9.54}$$

$$\kappa_{22}(\varphi) = -\frac{1}{1+\cos\varphi}, \tag{9.55}$$

$$\kappa_{12}(\varphi) = \kappa_{21}(\varphi) = \frac{i\gamma}{\delta - \gamma\sin\varphi} \tag{9.56}$$

specify the coherence correlations in the transmitted ($g^{(2)}_{11}$) and reflected ($g^{(2)}_{22}$) channels, as well as the cross-correlations ($g^{(2)}_{12} = g^{(2)}_{21}$).

The delay-time dependence enters in Eq. (16.58) via the functions

$$I_0(\tau) = \frac{M^{-1}(0)}{\pi i} \int dq M(q) \left(\frac{1}{q} + F(q) \right) \cos q\tau, \tag{9.57}$$

$$I_1(\tau) = \frac{I_0(\tau - T) + I_0(\tau + T)}{2}. \tag{9.58}$$

Performing the integral, we obtain them in the explicit form

$$\begin{aligned} I_0(\tau) &= \frac{1}{2(p\cos pT - i\lambda\sin pT)} \\ &\times \{ e^{-ip(|\tau|+T)} M^{-1}(p) - e^{ip(|\tau|+T)} M^{-1}(-p) \\ &+ \sum_{n=0}^{\infty} \Theta(|\tau| - nT)[g^{(-)}_n(\tau) - g^{(+)}_n(\tau)] \}, \end{aligned} \tag{9.59}$$

where

$$\begin{aligned} g^{(\pm)}_n(\tau) &= (-i\gamma e^{i\varphi})^n e^{\mp ipT} \frac{(\pm p + \lambda + i\gamma e^{i\varphi} e^{\pm ipT})^2}{(\pm p + \lambda)^{n+1}} \\ &\times \left[e^{\mp ip(|\tau| - nT)} - e^{i\lambda(|\tau| - nT)} f^{(\pm)}_n(\tau) \right], \end{aligned} \tag{9.60}$$

$$f^{(\pm)}_n(\tau) = \sum_{m=0}^{n} \frac{[-i(|\tau| - nT)(\pm p + \lambda)]^m}{m!}. \tag{9.61}$$

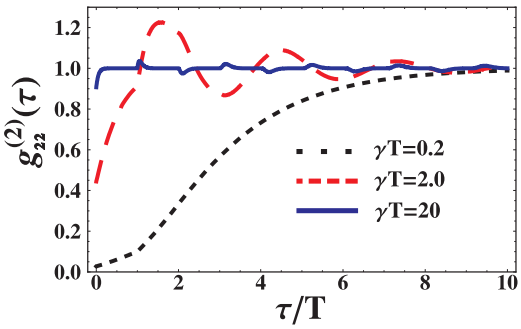

Figure 9.9: **Second-order correlation function for phonons reflected from a giant atom.** The plot shows the correlation function $g_{22}^{(2)}(\tau)$ for three choices of γT, taken from regions B, C, and D of the parameter space shown in Fig. 9.2. For the other parameters, we have chosen the resonance condition $\delta/\omega_0 = 0$ and the constructive-interference condition $\omega_0 T = 2k\pi$, $k \in \mathbb{Z}$.

For small T, *i.e.*, $\gamma T \ll 1$, we can neglect the explicit T dependence, keeping only φ finite. Thus, we obtain

$$I_0(\tau) \approx I_1(\tau) \approx e^{i(\lambda + i\gamma e^{i\varphi})\tau}, \tag{9.62}$$

which leads to

$$g_{22}^{(2)}(\tau) = \left|1 - e^{i(\delta - \gamma \sin\varphi)\tau} e^{-\gamma(1+\cos\varphi)\tau}\right|^2. \tag{9.63}$$

The small atom can only absorb and emit one phonon at a time, which results in $g_{22}^{(2)}(0) = 0$, exhibiting the typical antibunching behaviour of a single-phonon state.

For large T, *i.e.*, $\gamma T \gg 1$, we neglect the terms containing $\left|e^{ipT}\right| \ll 1$ (without loss of generality we assume $\operatorname{Im} p > 0$, since Eq. (16.59) is invariant under $p \to -p$). For $\tau > 0$, this yields

$$\begin{aligned} I_0(\tau) \;\approx\; & \sum_{n=0}^{\infty} \Theta(nT < \tau < (n+1)T)(-i\gamma e^{i\varphi})^n \\ \times\; & \left[\frac{e^{ip(\tau - nT)}}{(-p+\lambda)^n} - i\gamma e^{i\varphi} \frac{e^{-ip(\tau-(n+1)T)}}{(p+\lambda)^{n+1}}\right. \\ & \left. - e^{i\lambda(\tau - nT)} \left(\frac{f_n^{(-)}(\tau)}{(-p+\lambda)^n} - \frac{f_n^{(+)}(\tau)}{(p+\lambda)^n}\right)\right], \end{aligned} \tag{9.64}$$

i.e., in a given interval $[nT, (n+1)T]$ there are terms which exponentially decay inward the interval at rate $\operatorname{Im} p$ from both ends, and in addition there is a term exponentially decaying at rate γ from the left end and multiplied by a polynomial of a degree $n-1$.

There is, however, a special case $p \to 0$, in which the approximation of Eq. (9.64) is not applicable. It is realized when $\delta = 0$ and $\varphi = 2\pi k, k \in \mathbb{Z}$. For these parameters a single phonon is fully reflected, so we focus on the correlation function for two phonons in the reflected channel as well. Its exact expression reads

$$g_{22}^{(2)}(\tau) = \left(1 + \frac{1}{1+\gamma T} \sum_{n=0}^{\infty} \Theta(\tau - nT) K_n(\tau - nT)\right)^2, \tag{9.65}$$

$$K_n(z) = (-1)^{n+1} e^{-\gamma z} \frac{(\gamma z)^n}{n!}. \tag{9.66}$$

In Fig. 9.9, we plot the this correlation function for different choices of γT. For $\gamma T \ll 1$ (short dashed black line), we see that the behaviour is close to that of a small atom, which displays perfect antibunching ($g_{22}^{(2)}(0) = 0$) on resonance [6, 51]. For larger values of γT (long dashed red and solid blue lines), there is a possibility that a photon was emitted from the right leg of the giant atom at an earlier time, which results in $g_{22}^{(2)}(0) \neq 0$.

For $\gamma T \gg 1$, each contribution $K_n(\tau - nT)$ is localized in the beginning of the corresponding interval, being exponentially small at its end. Therefore, the contributions from different intervals do not overlap, and $g_{22}^{(2)}$ is represented by a sequence of kinks attached to the line of unity height. The shape of the nth kink ($n \geq 1$) is given by

$$g_{22}^{(2)}(nT + z) - 1 \approx \frac{2}{\gamma T} K_n(z). \tag{9.67}$$

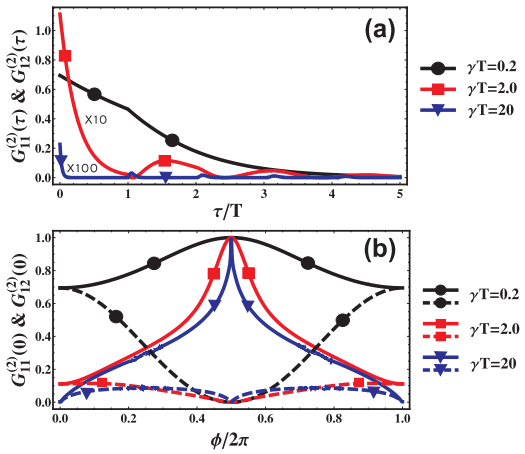

Figure 9.10: **Transmitted and cross second-order correlation functions.** (a) Correlation functions $G_{11}^{(2)}(\tau) = G_{12}^{(2)}(\tau)$. To be visible, we enlarge the correlation functions by 10 and 100 times for $\gamma T = 2.0$ and $\gamma T = 20$, respectively. (b) Correlation functions at $\tau = 0$, $G_{11}^{(2)}(0)$ (solid lines) and $G_{12}^{(2)}(0)$ (dashed lines), as functions of the reduced phase $\phi = \varphi - 2k\pi \in [0, 2\pi]$. Parameters: $\delta/\omega_0 = 0$ and $\omega_0 T = 2k\pi$, $k \in \mathbb{Z}$ for both figures.

Because of the sign factor in Eq. (9.66), every odd kink rises upwards, while every even kink dips downwards, and we observe an alternation of bunching and antibunching properties of the reflected phonons.

In Fig. 9.10, we plot the unrenormalized transmitted correlation function $G_{11}^{(2)}(\tau) \approx \mathcal{T}^2 g_{11}^{(2)}(\tau)$ and the unrenormalized cross correlation function $G_{12}^{(2)}(\tau) \approx \mathcal{R}\mathcal{T} g_{12}^{(2)}(\tau)$, where we only keep the leading order in Eq. (9.42). In the special case $\delta = 0$ and $\omega_0 T = 2k\pi$, $k \in \mathbb{Z}$, we have $G_{11}^{(2)}(\tau) = G_{12}^{(2)}(\tau) = \frac{1}{4}\left|I_0(\tau) + I_1(\tau)\right|^2$ as plotted in Fig. 9.10(a). The equality of $G_{11}^{(2)}(\tau)$ and $G_{12}^{(2)}(\tau)$ can be understood from Eq. (9.49), which indicates that there is no contribution to the transmitted channel from the first line on the RHS of Eq. (9.49). Therefore, the second and third lines on the RHS of Eq. (9.49) give equal contribution to the correlation functions $G_{11}^{(2)}(\tau)$ and $G_{12}^{(2)}(\tau)$, respectively. Another feature revealed by Fig. 9.10(a) is that $G_{11}^{(2)}(\tau)$ and $G_{12}^{(2)}(\tau)$ always show bunching behaviours initially, irrespective of the size of the atom, which comes from the fact that phonons are always created in pairs and there is no contribution to the transmitted channel from singe phonon scattering. If we change the phase $\varphi = 2k\pi + \phi$, $\phi \in [0, 2\pi]$ and $k \in \mathbb{Z}$, however, the contributions to the correlation functions $G_{11}^{(2)}(\tau)$ and $G_{12}^{(2)}(\tau)$, from the first line on the RHS of Eq. (9.49), are no longer equal to each other. In Fig. 9.10(b), we plot the initial value of the correlation functions, *i.e.*, $G_{11}^{(2)}(0)$ (solid lines) and $G_{12}^{(2)}(0)$ (dashed lines) as functions of phase ϕ for $\gamma T = 0.2$ (black, labelled by solid circle), $\gamma T = 2.0$ (red, labelled by solid square) and $\gamma T = 20$ (blue, labelled by solid triangle). We see that the transmitted correlation function $G_{11}^{(2)}(0)$ is always larger than the cross-correlation function $G_{12}^{(2)}(0)$. In particular, for $\phi = \pi$ we have we have $G_{11}^{(2)}(0) = 1$ and $G_{12}^{(2)}(0) = 0$, which means that all the phonons are perfectly transmitted and no phonon is reflected back.

9.5 Transient dynamics with arbitrary drive strength

The finite time delay makes the dynamics of the giant atom highly non-Markovian and with more than a few phonons present in the delay-loop the dynamics is correspondingly complex. Recently, a numerically exact method for integrating the dynamics of open quantum systems with deterministic time-delays was introduced in Ref. [26]. The method is based on mapping the problem onto a Markovian problem in an extended system space: It was shown that the problem can be solved by integrating the dynamics of a fictitious quantum cascade [16, 17] of system copies, where each copy represents a past version of the atom. This is analogous to how classical stochastic dynamical systems with finite delays can be solved by recasting them in terms of multivariate Markov processes [54, 55]. In the following, we use this method to study the atom's dynamics, including properties of the scattered output field, for arbitrary drive strengths.

As discussed in Section 9.2, the giant atom couples to two fields—a left-propagating and a right-propagating—each of which couples to the atom's legs at two different locations, $x = -L/2$ and $x = L/2$. The fields can be treated as independent (correlations between the left- and right-propagating phonons only arise through scattering via the atom), and the atom can thus be seen as being subject to two independent coherent feedback loops [26], each with the same time-delay $T = L/v_g$.

We note that only a single feedback field was considered in Ref. [26], but the extension to multiple fields with commensurate delays is straightforward [55]. The case we consider here, with two feedback fields with identical delays and a decay rate of $\gamma/2$ into each feedback loop, is particularly straightforward, as from the atom's point of view this is no different than a single feedback loop with a decay rate of γ. Experimentally,

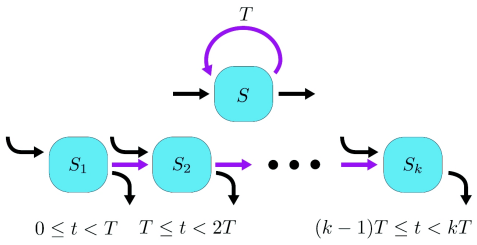

Figure 9.11: Mapping from a quantum system with deterministic time-delay (top) to the fictitious quantum cascade of k identical system copies, described by Eq. (9.69) (bottom). The lth copy represents the interval $(l-1)T \leq t < lT$.

there is of course a difference since the atom has two distinct input-output ports through which a scattered signal can be measured.

In this section, we will explore the giant-atom dynamics beyond the few-phonon limit by considering a monochromatic coherent drive of arbitrary strength applied to the atom. Experimentally this can be achieved by driving the atom through the phonon waveguide, as has been explored for one and two phonons in the previous sections, but one can also consider a drive applied directly on the atom through a voltage side gate. The latter option is more flexible in the sense that a drive with arbitrary frequency can be applied, while a drive with a π phase shift between the two legs would cancel if applied through the phonon waveguide.

In either case, the drive can be accounted for by including a drive term in the atom's Hamiltonian (see Appendix 9.8 for more details)

$$H_S = \hbar\delta \left|e\right\rangle \left\langle e\right| + \frac{1}{2}\hbar\left(\Omega\sigma_- + \text{H.c.}\right), \tag{9.68}$$

where we have moved to a rotating frame at the drive frequency, $\delta = \omega_d - \omega_0$ is the detuning and Ω is the drive strength (Rabi frequency). To connect with the treatment in the previous sections, if a drive is applied through the phonon waveguide we have that $\Omega = 2VA^*\left(1 + e^{-i\varphi}\right)$ where $\varphi = \omega_d T$ is the phase shift of the drive, and the coherent input drive is $\alpha_A^{\text{in}}(t) = Ae^{-i\omega_d t}$ as before. Below we however take Ω to be independent of φ since the drive can be applied through a voltage side gate as already mentioned.

Following Ref. [26], to find the atomic state at a time $(k-1)T \leq t < kT$ with $k \in \mathbb{Z}^+$, we numerically solve the cascaded master equation

$$\frac{d}{ds}\mathcal{E}_s(t) = \sum_{l=0}^{k}\left\{-\frac{i}{2\hbar}\mathcal{H}\left[H_{l,l+1}(s)\right] + \mathcal{D}\left[L_{l,l+1}(s)\right]\right\}\mathcal{E}_s(t), \tag{9.69}$$

for the atomic time-propagator $\mathcal{E}_s(t)$. This time-propagator is a superoperator on a k-fold system space $S_1 \otimes \cdots \otimes S_k$, as are the superoperators

$$\mathcal{H}[A]\bullet = [A, \bullet], \tag{9.70}$$

$$\mathcal{D}[A]\bullet = A\bullet A^\dagger - \frac{1}{2}A^\dagger A\bullet - \frac{1}{2}\bullet A^\dagger A. \tag{9.71}$$

The system operators $H_{l,l+1}$ and $L_{l,l+1}$ are given by

$$H_{l,l+1} = H_S^{(l)} + H_S^{(l+1)} + i\gamma(e^{-i\varphi}\sigma_-^{(l)\dagger}\sigma_-^{(l+1)} - \text{H.c.}), \tag{9.72}$$

$$L_{l,l+1} = \sqrt{\gamma}\sigma_-^{(l)} + \sqrt{\gamma}e^{-i\varphi}\sigma_-^{(l+1)}, \tag{9.73}$$

except for $H_{0,1} = H_S^{(1)}$, $H_{k,k+1} = H_S^{(k)}$, $L_{0,1} = \sqrt{\gamma}e^{-i\varphi}\sigma_-^{(1)}$ and $L_{k,k+1} = \sqrt{\gamma}\sigma_-^{(k)}$, where we use a superscript to denote the system on which an operator acts. Finally, we have defined $A^{(l)}(s) = A^{(l)}$ for all $l < k$, and $A^{(k)}(s) = \Theta\left[t - (k-1)T - s\right]A^{(k)}$, where $\Theta(s)$ is the Heaviside step function, for any system operator A.

The cascaded chain given by Eq. (9.69) is illustrated in Fig. 9.11. The mapping from a single system with feedback to a cascaded chain is analogous to the "method of steps" used to solve classical delay-differential equations [54]: the lth system copy in the cascade can be interpreted as representing the time-interval $(l-1)T \leq t < lT$. A system with feedback is, however, not equivalent to a conventional quantum cascade, since the identical copies do not represent physically distinct systems. This has to be taken into account when the *true* reduced density matrix for the system, $\rho_S(t)$, is found by tracing out the auxiliary degrees of freedom. As explained in more detail in Ref. [26], the reduced density matrix is found by first integrating Eq. (9.69) up to $s = T$, where s is an auxiliary time variable, to find $\mathcal{E}_T(t)$ and then acting on the given initial state $\rho_{S_1}(0)$ for system S_1 and taking a generalized partial trace:

$$\rho_S(t) = \text{Tr}_{(S_k,S_{k-1})}\ldots\text{Tr}_{(S_2,S_1)}\,\mathcal{E}_T(t)\rho_{S_1}(0), \tag{9.74}$$

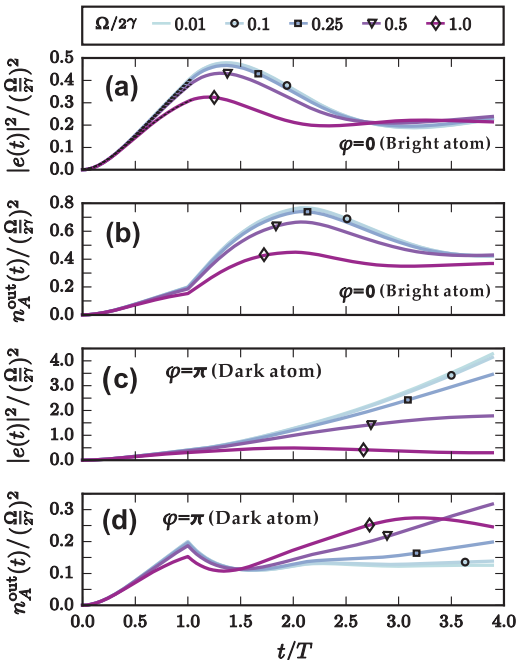

Figure 9.12: **Transient dynamics for a giant atom starting in the ground state with $\gamma T = 1.0$ (region C).** Solid lines show numerically exact results for various drive strengths $\Omega/(2\gamma)$ in the range 0.01 to 1.0. The plotted quantities $|e(t)|^2$ and $n_A^{out}(t)$ (normalized by $(\Omega/2\gamma)^2$) are the atomic excited-state probability and outgoing phonon number at leg A, respectively. Black dashed lines shown in (a) are the analytical results from Eq. (9.76) for $0 < t < T$. Parameters: $\varphi = 0$ (bright atom) for (a) and (b), $\varphi = \pi$ (dark atom) for (c) and (d).

where the generalized trace $\mathrm{Tr}_{(S_{l'},S_l)}$ acts on a superoperator in the following way

$$\mathrm{Tr}_{(S_{l'},S_l)}\,\mathcal{A}\bullet = \sum_{ij} \langle i_l|\mathcal{A}\left(\bullet \otimes |i_{l'}\rangle\langle j_{l'}|\right)|j_l\rangle\,, \tag{9.75}$$

where $|i_l\rangle$ and $|i_{l'}\rangle$ are orthonormal bases for the two respective systems, S_l and $S_{l'}$. This operation can be understood as mapping the output of system S_l to the input of system $S_{l'}$ [26].

This method is a powerful tool for exploring the transition from essentially linear dynamics in the single-phonon regime to strongly nonlinear dynamics with multiple phonons. We focus in the following on the giant atom's transient dynamics and the field it emits into the phonon waveguide when the atom is starting in the ground state and driven on resonance with varying drive strengths. The emitted radiation is a phononic analog to resonance fluorescence. To explore the consequences of non-Markovian effects due to the propagation delay between the two legs we consider two values of the time-delay, $\gamma T = 1.0$ and $\gamma T = 10$, corresponding to regions C and D in Fig. 9.2, respectively.

In Figs. 9.12 ($\gamma T = 1.0$) and 9.13 ($\gamma T = 10$), we display the transient atomic dynamics, starting from the ground state for various drive strengths and an on-resonant drive, $\omega_d = \omega_0$. We plot the short-time evolutions of the atomic excited-state probability $|e(t)|^2$ and the output phonon number at leg A, $n_A^{\mathrm{out}}(t) \equiv \left\langle a_A^{\mathrm{out}\,\dagger}(t) a_A^{\mathrm{out}}(t)\right\rangle$ where the output field $a_A^{\mathrm{out}}(t)$ is defined in Appendix 9.8. We normalize our data by $(\Omega/2\gamma)^2$. We consider two distinct cases with phase shifts of $\varphi = 0$ (bright atom) and $\varphi = \pi$ (dark atom), respectively.

The figures show a clear transition from a linear regime to a nonlinear regime. For low drive strengths, the atomic population as well as the output-field phonon number is proportional to the drive power: the lines with $\Omega/(2\gamma) = 0.01$ and 0.1 coincide. As the drive power is increased we enter the nonlinear regime where the two-level nature of the atom starts to be important. The transient dynamics is initially essentially Markovian for $t < T$, as the atom does not feel any feedback effects. Therefore, the atom can be viewed as an ordinary atom with two connections to the waveguide. The probability of excited state has an analytical result [53]

$$|e(t)|^2 = \frac{\Omega^2}{(2\gamma)^2 + 2\Omega^2}\left[1 - e^{-\frac{3\gamma t}{2}}\left(\cosh\zeta t + \frac{3\gamma}{2\kappa}\sinh\zeta t\right)\right], \tag{9.76}$$

where $\zeta = \sqrt{(\gamma/2) - \Omega^2}$. In Figs. 9.12(a) and 9.13(a), we plot the curve (9.76) and compare it with numerical simulation for $0 < t < T$. Actually, the time evolutions of $|e(t)|^2$ and $n_A^{out}(t)$ of the bright and dark atoms

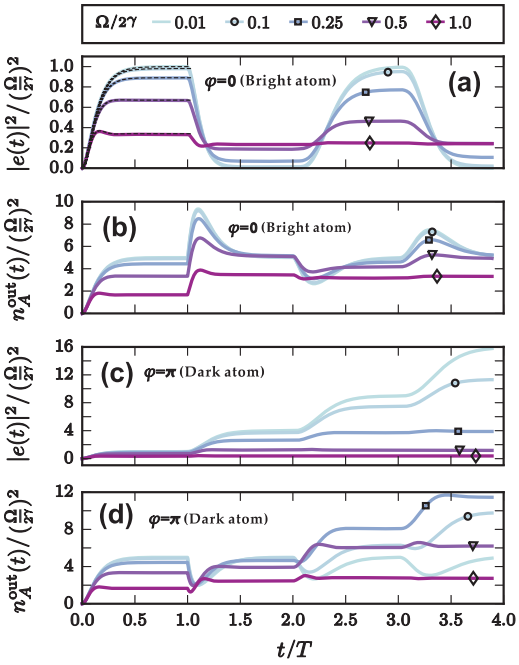

Figure 9.13: **Transient dynamics for a giant atom starting in the ground state with $\gamma T = 10$ (region D).** Solid lines show numerically exact results for various drive strengths $\Omega/(2\gamma)$ in the range 0.01 to 1.0. The plotted quantities $|e(t)|^2$ and $n_A^{out}(t)$ (normalized by $(\Omega/2\gamma)^2$) are the atomic excited-state probability and outgoing phonon number at leg A, respectively. Black dashed lines shown in (a) are the analytical results from Eq. (9.76) for $0 < t < T$. Parameters: $\varphi = 0$ (bright atom) for (a) and (b), $\varphi = \pi$ (dark atom) for (c) and (d). Note that the outgoing phonon numbers are larger than that in Fig. 9.12 due to the drive being an order of magnitude larger.

for $0 < t < T$ are the same regardless of the phase φ across the two legs. At $t = T$, the atom enters the non-Markovian regime, marked by a sharp kink in the observables, best visible in the output-field phonon number.

In the moderately non-Markovian regime (Fig. 9.12), we see that the feedback interferes constructively with the outfield for the bright atom (Fig. 9.12(b)). For the dark atom (Fig. 9.12(d)), the destructive interferences instead leads to a reduction of the output field. The bright atom approaches a steady-state within the simulation time, due to the comparatively strong dissipation. The dark atom has an effectively weaker coupling to the outgoing phonons, leading to an increase of the atom population during the whole simulation for all but the strongest drive. For the strongest drive, the atom population changes noticeably during the propagation time T, which makes the destructive interference of the feedback less efficient.

In the deep non-Markovian regime (Fig. 9.13), we find transient dynamics with plateaus of constant population and output field amplitude, interrupted approximately at integer values of t/T with steps on the timescale of $1/\gamma$. This pattern can be understood starting from the initial Markovian regime $t < T$, where the steady state of the driven, damped atom is established on the timescale of the local coupling strength $1/\gamma$. At $t = T$ the feedback changes the effective drive and damping, which gives a transient period until a new steady state is established. The length of the transient periods increase with each period, probably allowing the system to approach a global steady state at very long times. For the bright atom (Fig. 9.13(a)), we note a pattern of alternating high and low population where the relative amplitude of the steps decrease with increasing drive strength and increasing time. For the dark atom (Fig. 9.13(c)), we instead see a population increasing with time, again due to destructive interference in the output fields.

It is also interesting to look at higher-order correlation functions for the atom's output field. In Fig. 9.14 we show the second-order correlation function

$$G_{22}^{(2)}(t_0, \tau) \equiv \left\langle {a_A^{\text{out}}}^{\dagger}(t_0) {a_A^{\text{out}}}^{\dagger}(t_0+\tau) a_A^{\text{out}}(t_0+\tau) a_A^{\text{out}}(t_0) \right\rangle . \tag{9.77}$$

In our previous definition of second-order correlation function in Eq. (9.51), we have implicitly chosen the average over the stationary state after scattering $|\Psi_f\rangle$, *i.e.*, we calculated the correlation function in Eq. (9.77) at $t_0 = +\infty$. Since $G_{22}^{(2)}(t_0, \tau) = 0$ for an atom starting in the ground state, we show in Fig. 9.14 the behaviour when starting from the excited state instead. We again show results for two values of the time-delay, $\gamma T = 1.0$ and $\gamma T = 10.0$, as well as two values of the phase shift $\varphi = 0$ (bright atom) and $\varphi = \pi$ (dark atom). From the definition of the second-order correlation function, $G_{22}^{(2)}(0, \tau)$ is proportional to the joint probability density of observing one phonon at $t = 0$ and another at $t = \tau$ [41]. We have assumed that the atom is in the excited state and the entire waveguide (including the part between the atom's legs) is in the vacuum state at initial time $t = 0$. Thus the atom is in the ground state when the first phonon is observed at $t = 0$. Then the probability to observe another phonon at $t = \tau$ is proportional to the phonon field emitted by the atom at leg A. Therefore, the second-order correlation functions $G_{22}^{(2)}(0, \tau)$ scaled by $(\Omega/2\gamma)^2$ in Fig. 9.14 exhibit exactly the same behaviors of $n_A^{out}(t)$, up to a normalization factor, as shown in Figs. 9.12 and 9.13. The second-order correlation function shows particularly strong signatures of the feedback force at times $\tau = nT$ for integer n.

Output field properties are calculated using a generalization of the well-known quantum regression formula for systems with time-delays, given in Appendix 9.9. The numerical simulations were performed using an open source implementation of the method from Ref. [26] in QuTiP [56, 57].

9.6 Summary and outlook

We have investigated the quantum dynamics of a single two-level quantum system (a transmon qubit) coupled to a SAW transmission line via two connection points separated by a large distance L, which introduces a deterministic time delay T. We explored how the non-Markovian dynamics that arises due to a long time delay affects the spontaneous emission and scattering properties of this system, which we call a giant atom. We found several notable differences to the more common case of a small atom coupled to a transmission line at a single point. Both the large time delay and the phase acquired by phonons travelling between the connection points, resulting in interference effects, are important to explain these differences.

For single-phonon processes, we obtained analytical solutions by solving a differential time-delay equation. Using these solutions, we first studied the power spectrum of the spontaneous emission from the giant atom. This revealed the presence of several frequency modes, something not seen for a small atom. Furthermore, interference between these modes was shown to make the energy decay from the system polynomial at first; only after a long time, when all modes but one has decayed, does the giant atom follow an exponential decay law. During this process, the atom experiences revivals as it emits energy from one connection point and later reabsorbs some of it at the other one. The presence of multiple modes at large T was also shown to cause multiple peaks in the single-phonon reflection of the giant atom, another feature distinguishing it from a small atom, which only has a single reflection peak at its resonance frequency.

For two-phonon processes, we obtained an exact analytical solution of the scattering matrix by using the diagrammatic Lippmann-Schwinger-equation approach given in Ref. [27]. Using the two-phonon scattering matrix, we calculated the lowest-order correction to the transmittance of the system. For a small atom, increasing the driving always increases the transmittance, but for the case of a giant atom, we show that the transmittance sometimes decreases instead. This is due to interference effects between phonons emitted at the two different connection points. We also calculated the inelastic (incoherent) power spectrum. For a small atom ($\gamma T < 1$), the inelastic power spectrum showed a central peak around the driving frequency. For $\gamma T > 1$, the central peak splits into two peaks due to the time delay of the giant atom. This is different from the Mollow triplet, which is due to strong driving.

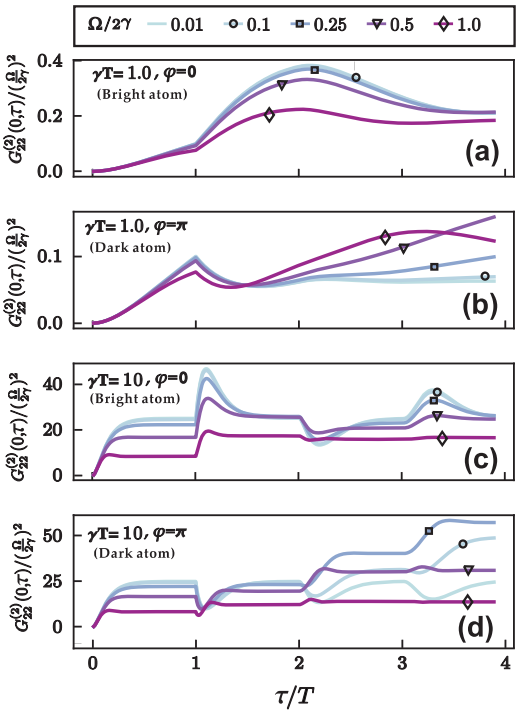

Figure 9.14: **Phonon correlation function $G_{22}^{(2)}(0,\tau)$ scaled by $(\Omega/2\gamma)^2$ for a giant atom starting in the excited state.** (a) $\gamma T = 1.0$, $\varphi = 0$ (bright atom), (b) $\gamma T = 1.0$, $\varphi = \pi$ (dark atom), (c) $\gamma T = 10.0$, $\varphi = 0$ (bright atom), (d) $\gamma T = 10.0$, $\varphi = \pi$ (dark atom).

We discussed the second-order correlation functions for phonons scattered by the giant atom. While phonons (or photons) reflected from a small atom will display perfect antibunching, this effect is diminished for a giant atom since a second phonon can be emitted from the second connection point at an earlier time. However, the second-order correlation function for the reflected phonons from a giant atom has a richer structure than for the case of a small atom; both bunching and antibunching occur, and the function has kinks at integer multiples of T.

Finally, we also considered coherent driving of arbitrary strength being applied to the giant atom. In this case, an analytical solution is beyond the reach of the diagrammatic approach. Therefore, we instead used the exact numerical method for integrating the dynamics of open quantum systems with deterministic time delays introduced in Ref. [26]. This allowed us to numerically simulate the short-time dynamics of the giant atom and calculate second-order correlation functions.

There are several possible directions of research beyond our present work. When it comes to an experimental implementation, we believe that the parameter regimes we have considered here are rather straightforward to reach with a transmon coupled to SAWs by modifying the experimental setup of Ref. [16]. A pure circuit-QED setup might also be able to reach a regime with long enough time delays to demonstrate differences from the small-atom case, but to achieve truly long time delays SAWs seem more promising. One potential obstacle for measurements in such experiments is the low conversion efficiency of SAWs to electric microwave signals in conventional symmetric IDTs. However, the recent work in Ref. [58] demonstrated unidirectional transducers (UDTs), which can increase the conversion efficiency up to 99.4% at GHz frequencies and millikelvin temperatures. From a technical perspective, it is of interest whether the diagrammatic Lippmann-Schwinger approach can be extended to scattering with more than two phonons. In a similar vein, it would be desirable to extend the numerical technique used to simulate the short-time dynamics to work for longer times. Finally, the system under investigation could also be extended, *e.g.*, to include more than two connection points of the atom or to include several giant atoms coupled to the SAW transmission line.

9.7 Single-phonon processes

9.7.1 Equations of motion

We start from the RWA Hamiltonian based on Eq. (9.18)

$$\begin{aligned}H=&-\frac{1+\sigma_z}{2}\delta+\sum_{\alpha=1,2}\int d\omega\omega a_{\alpha\omega}^{\dagger}a_{\alpha\omega}\\&+\sqrt{\frac{\gamma}{4\pi}}\int d\omega\left\{\sigma_-\left[a_{1\omega}^{\dagger}e^{-i(\omega T+\varphi)/2}+a_{2\omega}^{\dagger}e^{i(\omega T+\varphi)/2}\right]+\text{H.c.}\right\}\\&+\sqrt{\frac{\gamma}{4\pi}}\int d\omega\left\{\sigma_-\left[a_{1\omega}^{\dagger}e^{i(\omega T+\varphi)/2}+a_{2\omega}^{\dagger}e^{-i(\omega T+\varphi)/2}\right]+\text{H.c.}\right\},\end{aligned}\tag{9.78}$$

where $\delta\equiv\omega_d-\omega_0$ is the atomic detuning and $\sigma_z\equiv|e\rangle\langle e|-|g\rangle\langle g|$. The phonon frequency $\omega\equiv\omega_p-\omega_d$ is also shifted by the rotating frequency. The phase difference between two legs is given by $\varphi=\omega_d T=\omega_d L/v_g$.

As discussed in Section 9.2, we make the following ansatz for the single-phonon process

$$|\Psi(t)\rangle=\int d\omega\left[\alpha_{1\omega}(t)a_{1\omega}^{\dagger}+\alpha_{2\omega}(t)a_{2\omega}^{\dagger}\right]|g,vac\rangle+e(t)\,|e,vac\rangle\,.\tag{9.79}$$

Then, the Schrödinger equation gives

$$\begin{aligned}&H\,|\Psi(t)\rangle=-\delta e(t)\,|e,vac\rangle\\&+\int d\omega\left[\omega\alpha_{1\omega}(t)a_{1\omega}^{\dagger}+\omega\alpha_{2\omega}(t)a_{2\omega}^{\dagger}\right]|g,vac\rangle\\&+e(t)\sqrt{\frac{\gamma}{4\pi}}\int d\omega\left[a_{1\omega}^{\dagger}e^{-i(\omega T+\varphi)/2}+a_{2\omega}^{\dagger}e^{i(\omega T+\varphi)/2}\right]|g,vac\rangle\\&+e(t)\sqrt{\frac{\gamma}{4\pi}}\int d\omega\left[a_{1\omega}^{\dagger}e^{i(\omega T+\varphi)/2}+a_{2\omega}^{\dagger}e^{-i(\omega T+\varphi)/2}\right]|g,vac\rangle\\&+\sqrt{\frac{\gamma}{4\pi}}\int d\omega\left[\alpha_{1\omega}e^{i(\omega T+\varphi)/2}+\alpha_{2\omega}e^{-i(\omega T+\varphi)/2}\right]|e,vac\rangle\\&+\sqrt{\frac{\gamma}{4\pi}}\int d\omega\left[\alpha_{1\omega}e^{-i(\omega T+\varphi)/2}+\alpha_{2\omega}e^{i(\omega T+\varphi)/2}\right]|e,vac\rangle\\&=i\int d\omega\left[\dot{\alpha}_{1\omega}(t)a_{1\omega}^{\dagger}+\dot{\alpha}_{2\omega}(t)a_{2\omega}^{\dagger}\right]|g,vac\rangle+i\dot{e}(t)\,|e,vac\rangle\,.\end{aligned}\tag{9.80}$$

Therefore, we have the dynamical equations for the giant atom

$$\begin{aligned}&\frac{d}{dt}e(t)=i\delta e(t)\\&-i\sqrt{\frac{\gamma}{4\pi}}\int d\omega\left[e^{i(\omega T+\varphi)/2}+e^{-i(\omega T+\varphi)/2}\right]\alpha_{1\omega}(t)\\&-i\sqrt{\frac{\gamma}{4\pi}}\int d\omega\left[e^{-i(\omega T+\varphi)/2}+e^{i(\omega T+\varphi)/2}\right]\alpha_{2\omega}(t),\end{aligned}\tag{9.81}$$

right-propagating phonon fields in the transmission line

$$\frac{d}{dt}\alpha_{1\omega}(t)=-i\omega\alpha_{1\omega}(t)-ie(t)\sqrt{\frac{\gamma}{4\pi}}\left[e^{-i(\omega T+\varphi)/2}+e^{i(\omega T+\varphi)/2}\right],\tag{9.82}$$

and left-propagating phonon fields in the transmission line

$$\frac{d}{dt}\alpha_{2\omega}(t)=-i\omega\alpha_{2\omega}(t)-ie(t)\sqrt{\frac{\gamma}{4\pi}}\left[e^{i(\omega T+\varphi)/2}+e^{-i(\omega T+\varphi)/2}\right].\tag{9.83}$$

Integrating Eqs. (9.82) and (9.83), we have

$$\begin{aligned}\alpha_{1\omega}(t)=&\,e^{-i\omega t}\Big\{\alpha_{1\omega}(0)\\&-i\sqrt{\frac{\gamma}{4\pi}}\left[e^{-i(\omega T+\varphi)/2}+e^{i(\omega T+\varphi)/2}\right]\int_0^t dt'e(t')e^{i\omega t'}\Big\}\end{aligned}\tag{9.84}$$

and

$$\alpha_{2\omega}(t) = e^{-i\omega t}\Big\{\alpha_{2\omega}(0) \\ -i\sqrt{\frac{\gamma}{4\pi}}\left[e^{i(\omega T+\varphi)/2} + e^{-i(\omega T+\varphi)/2}\right]\int_0^t dt' e(t')e^{i\omega t'}\Big\}. \tag{9.85}$$

Inserting the two equations above into Eq. (9.81), we have

$$\begin{aligned}
&\frac{d}{dt}e(t) = i\delta e(t) \\
&-i\sqrt{\frac{\gamma}{4\pi}}\int d\omega\left[e^{i(\omega T+\varphi)/2} + e^{-i(\omega T+\varphi)/2}\right]e^{-i\omega t}\alpha_{1\omega}(0) \\
&-i\sqrt{\frac{\gamma}{4\pi}}\int d\omega\left[e^{-i(\omega T+\varphi)/2} + e^{i(\omega T+\varphi)/2}\right]e^{-i\omega t}\alpha_{2\omega}(0) \\
&-\frac{\gamma}{2\pi}\int d\omega\left|e^{i(\omega T+\varphi)/2} + e^{-i(\omega T+\varphi)/2}\right|^2\int_0^t dt' e(t')e^{-i\omega(t-t')}.
\end{aligned} \tag{9.86}$$

If the amplitude of one plane wave at time t is $\alpha_{1(2)\omega}(t)$, then the total SAW field in the transmission line at position x is

$$\alpha_{1(2)}(x,t) \equiv \frac{1}{\sqrt{2\pi v_g}}\int d\omega e^{\pm i\omega x/v_g}\alpha_{1(2)\omega}(t). \tag{9.87}$$

For right- (left-) propagating fields we take positive (negative) sign in the phase. Using this notation, we can continue massaging Eq. (9.86):

$$\begin{aligned}
&\frac{d}{dt}e(t) = i\delta e(t) \\
&-i\sqrt{\frac{\gamma v_g}{2}}\left[e^{i\varphi/2}\alpha_1(L/2-v_gt,0) + e^{-i\varphi/2}\alpha_1(-L/2-v_gt,0)\right] \\
&-i\sqrt{\frac{\gamma v_g}{2}}\left[e^{-i\varphi/2}\alpha_2(L/2-v_gt,0) + e^{i\varphi/2}\alpha_2(-L/2-v_gt,0)\right] \\
&-\gamma\int_0^t dt' e(t')\left[2\delta(t-t') + e^{i\varphi}\delta(T-t+t')\right. \\
&\left.+e^{-i\varphi}\delta(-T-t+t')\right] \\
&= i\delta e(t) - \gamma\left[e(t) - \Theta(t-T)e^{i\varphi}e(t-T)\right] \\
&-i\sqrt{\frac{\gamma v_g}{2}}\left[e^{i\varphi/2}\alpha_1(L/2-v_gt,0) + e^{-i\varphi/2}\alpha_1(-L/2-v_gt,0)\right] \\
&-i\sqrt{\frac{\gamma v_g}{2}}\left[e^{-i\varphi/2}\alpha_2(L/2-v_gt,0) + e^{i\varphi/2}\alpha_2(-L/2-v_gt,0)\right],
\end{aligned} \tag{9.88}$$

where $\Theta(x)$ is the Heaviside step function ($\Theta(x) = 0$ for $x < 0$ and $\Theta(x) = 1$ for $x > 0$). We can transform Eq. (9.88) into the original frame by making the replacement $\tilde{e}(t) \to e^{-i\omega_d t}e(t)$. We then get

$$\begin{aligned}
\frac{d}{dt}\tilde{e}(t) \;=\; & -i\omega_0\tilde{e}(t) - \gamma\left[\tilde{e}(t) - \Theta(t-T)\tilde{e}(t-T)\right] \\
& -iV\left[\tilde{\alpha}_1(L/2-v_gt,0) + \tilde{\alpha}_1(-L/2-v_gt,0)\right. \\
& \left.+\tilde{\alpha}_2(L/2-v_gt,0) + \tilde{\alpha}_2(-L/2-v_gt,0)\right],
\end{aligned} \tag{9.89}$$

where $V = \sqrt{\frac{\gamma v_g}{2}}$ is the coupling strength and

$$\tilde{\alpha}_{1(2)}(x,0) \equiv e^{\pm i\omega_d x/v_g}\alpha_{1(2)}(x,0) \tag{9.90}$$

are the SAW fields in the rest frame. For simplicity in the following, we further omit the tildes. Then, we have

$$\begin{aligned}
\frac{\partial e(t)}{\partial t} \;=\; & -i\omega_0 e(t) - \gamma\left[e(t) + e(t-T)\right] \\
& -iV\left[\alpha_1(L/2-v_gt,0) + \alpha_1(-L/2-v_gt,0)\right. \\
& \left.+\alpha_2(L/2-v_gt,0) + \alpha_2(-L/2-v_gt,0)\right].
\end{aligned} \tag{9.91}$$

Here, we have assumed $e(t) = 0$ for $t < 0$ and thus neglected the Heaviside step function $\Theta(t - T)$. By Fourier transforming Eq. (9.91), *i.e.*,

$$e(\omega) = \int_{-\infty}^{+\infty} dt e(t) e^{i\omega t}, \quad e(t < 0) = 0 \tag{9.92}$$

$$e(t) = \frac{1}{2\pi} \int d\omega e(\omega) e^{-i\omega t}, \quad t > 0 \tag{9.93}$$

and using Eq. (9.87), we have

$$\begin{aligned} &-e(0) - i\omega e(\omega) = -i\omega_0 e(\omega) - \gamma e(\omega) - \gamma e^{i\omega T} e(\omega) \\ &-iV\sqrt{\frac{2\pi}{v_g}} \left[\alpha_{1\omega}(0) + \alpha_{2\omega}(0)\right] \left(e^{i\omega T/2} + e^{-i\omega T/2}\right). \end{aligned} \tag{9.94}$$

Therefore, we have the solutions

$$e(\omega) = \frac{ie(0) + V\sqrt{2\pi/v_g} \left[\alpha_{1\omega}(0) + \alpha_{2\omega}(0)\right] \left(e^{i\omega T/2} + e^{-i\omega T/2}\right)}{\omega - \omega_0 + i\gamma + i\gamma e^{i\omega T}} \tag{9.95}$$

and

$$\begin{aligned} e(t) = &\frac{ie(0)}{2\pi} \int d\omega \frac{e^{-i\omega t}}{\omega - \omega_0 + i\gamma + i\gamma e^{i\omega T}} \\ + &\frac{V}{\sqrt{2\pi v_g}} \int d\omega \frac{\left[\alpha_{1\omega}(0) + \alpha_{2\omega}(0)\right] \left(e^{i\omega T/2} + e^{-i\omega T/2}\right)}{\omega - \omega_0 + i\gamma + i\gamma e^{i\omega T}} e^{-i\omega t}. \end{aligned} \tag{9.96}$$

9.7.2 Spontaneous emission

Assuming the initial condition $e(0) = 1$ for the giant atom and no driving, *i.e.*, $\alpha_{1\omega}(0) = \alpha_{2\omega}(0) = 0$, we have from Eq. (9.96)

$$\begin{aligned} e(t) &= \frac{i}{2\pi} \int d\omega \frac{e^{-i\omega t}}{\omega - \omega_0 + i\gamma + i\gamma e^{i\omega T}} \\ &= \frac{i}{2\pi} \int d\omega \frac{e^{-i\omega t}}{\omega - \omega_0 + i\gamma} \left(1 + \frac{i\gamma e^{i\omega T}}{\omega - \omega_0 + i\gamma}\right)^{-1} \\ &= \frac{i}{2\pi} \int d\omega \frac{e^{-i\omega t}}{\omega - \omega_0 + i\gamma} \sum_{n=0}^{+\infty} \left(-\frac{i\gamma e^{i\omega T}}{\omega - \omega_0 + i\gamma}\right)^n \\ &= \sum_{n=0}^{+\infty} \frac{i}{2\pi} \int d\omega \frac{(-i\gamma)^n e^{-i\omega(t-nT)}}{(\omega - \omega_0 + i\gamma)^{n+1}} \\ &= \sum_{n=0}^{+\infty} \Theta(t - nT) \frac{[-\gamma(t - nT)]^n}{n!} e^{-i(\omega_0 - i\gamma)(t-nT)}. \end{aligned} \tag{9.97}$$

This is in fact equivalent to the solution given as Eq. (9.5) in the main text. The solution can also be put into the alternative form

$$\begin{aligned} e(t) &= \frac{i}{2\pi} \int d\omega \frac{e^{-i\omega t}}{\omega - \omega_0 + i\gamma + i\gamma e^{i\omega T}} \\ &= \sum_k \frac{e^{-i\omega_{(k)} t}}{1 - \gamma T e^{i\omega_{(k)} T}}. \end{aligned} \tag{9.98}$$

Here, we have used the residue theorem and the poles $\omega_{(k)}$ are given by equation

$$\omega_{(k)} - \omega_0 + i\gamma + i\gamma e^{i\omega_{(k)} T} = 0, \tag{9.99}$$

or the following equivalent form:

$$\left[-i(\omega_{(k)} - \omega_0 + i\gamma)T\right] e^{-i(\omega_{(k)} - \omega_0 + i\gamma)T} = -\gamma T e^{\gamma T + i\omega_0 T}. \tag{9.100}$$

The solutions are given by Eq. (9.7) in the main text, *i.e.*,

$$\omega_{(k)} = \omega_0 - i\gamma + i\frac{1}{T}W_k\left(-\gamma T e^{\gamma T + i\omega_0 T}\right), \tag{9.101}$$

with $k \in \mathbb{Z}$. Here, $W(z)$ is the Lambert W-function [39] defined by $z = W(z)e^{W(z)}$, which in general is a multivalued function with branches $W_k(z)$, $\in \mathbb{Z}$. The asymptotic behaviour of $W(-re^{i\theta})$ in the limit $r \gg 1$ can be obtained in the following way. Starting from the definition $-re^{i\theta} = W(-re^{i\theta})e^{W(-re^{i\theta})}$ and $-re^{i\theta} = re^{i(2k+1)\pi+i\theta}$ with $\theta \in [0, 2\pi)$, we have

$$W_k = \ln r + i[(2k+1)\pi + \theta] - \ln W_k. \tag{9.102}$$

As the lowest-order approximation we can neglect $\ln W_k$ and have $W_k \approx \ln r + i[(2k+1)\pi + \theta]$. Plugging this solution back into Eq. (9.102), we get the higher-order solution

$$\begin{aligned} W(-r) &\approx \ln \frac{r}{\sqrt{(\ln r)^2 + [(2k+1)\pi+\theta]^2}} \\ &\quad + i\left[\pi(2k+1) + \theta - \arctan\frac{\pi(2k+1)+\theta}{\ln r}\right]. \end{aligned} \tag{9.103}$$

This approximate solution is valid for $r \gg 1$. It can be obtained from Eq. (4.20) in Ref. [39]. We now apply this approximate solution to Eq. (9.7). By replacing $r = \gamma T e^{\gamma T}$ and assuming $\omega_0 T = 2n\pi + \Delta\pi$ with $n \in \mathbb{Z}$ and $\Delta \in [0, 2)$, we have the frequency modes for $\gamma T e^{\gamma T} \gg 1$

$$\begin{aligned} \omega_{(k)} &\approx \omega_0 - \frac{1}{T}\left[\pi(2k+1+\Delta) - \arctan\frac{\pi(2k+1+\Delta)}{\gamma T}\right] \\ &\quad - i\frac{1}{2T}\ln\left(1 + \left[\frac{(2k+1+\Delta)\pi}{\gamma T}\right]^2\right). \end{aligned} \tag{9.104}$$

For $\gamma T \gg 1$, the frequency interval is $\Delta\omega \approx 2\pi/T$.

We now study the emission spectrum of outgoing phonons. By defining the variables in the original frame, *i.e.*, $\tilde{\alpha}_{1(2)\omega} \equiv e^{-i\omega_d t}\alpha_{1(2)\omega}(t)$, $\tilde{e}(t') = e^{-i\omega_d t'}e(t')$ and $\tilde{\omega} \equiv \omega + \omega_d$, Eqs. (9.84) and (9.85) can be written as

$$\begin{aligned} &\alpha_{1(2)\omega}(t) = e^{-i\omega t}\alpha_{1(2)\omega}(0) \\ &-i\sqrt{\frac{\gamma}{4\pi}}\left(e^{-i\omega T/2} + e^{i\omega T/2}\right)\int_0^t dt' e(t') e^{i\omega(t'-t)}. \end{aligned} \tag{9.105}$$

As done in Eq. (9.91), we have omitted the tildes for simplicity. Without driving (*i.e.*, $\alpha_{1\omega}(0) = 0$ and $\alpha_{2\omega}(0) = 0$), we have $\alpha^{out}_{\omega}(t) = \alpha_{1\omega}(t) = \alpha_{2\omega}(t)$ from symmetry and

$$\begin{aligned} \alpha^{out}_{\omega}(t) &= -i\sqrt{\frac{\gamma}{4\pi}}\left(e^{-i\omega T/2} + e^{i\omega T/2}\right)\int_0^t dt' e(t') e^{i\omega(t'-t)} \\ &= \frac{1}{2\pi}\sqrt{\frac{\gamma}{4\pi}}\left(e^{-i\omega T/2} + e^{i\omega T/2}\right) \\ &\times \int d\omega' \frac{e^{-i\omega' t}}{\omega' - \omega_0 + i\gamma + i\gamma e^{i\omega' T}}\int_0^t dt' e^{i(\omega-\omega')(t'-t)} \\ &= \frac{1}{2\pi}\sqrt{\frac{\gamma}{4\pi}}\left(e^{-i\omega T/2} + e^{i\omega T/2}\right) \\ &\times \int d\omega' \frac{1}{\omega' - \omega_0 + i\gamma + i\gamma e^{i\omega' T}}\frac{e^{-i\omega' t} - e^{-i\omega t}}{i(\omega - \omega')} \\ &= -\sqrt{\frac{\gamma}{4\pi}}\left(e^{-i\omega T/2} + e^{i\omega T/2}\right) \\ &\times \sum_k \frac{1}{1 - \gamma T e^{i\omega_{(k)} T}}\frac{e^{-i\omega_{(k)} t} - e^{-i\omega t}}{\omega - \omega_{(k)}}. \end{aligned} \tag{9.106}$$

Here, we have assumed $e^{i\omega_0 T} \neq -1$. Then all the poles given by Eq. (9.101) are in the lower half-plane, and we can write

$$\frac{1}{\omega' - \omega_0 + i\gamma + i\gamma e^{i\omega' T}} = \sum_k \frac{1}{1 - \gamma T e^{i\omega_{(k)} T}}\frac{1}{\omega - \omega_{(k)}}. \tag{9.107}$$

In the long-time limit, $e^{-i\omega_{(k)}t} \to 0$ due to the negative imaginary part of $\omega_{(k)}$, and therefore

$$\begin{aligned}\alpha_\omega^{out}(+\infty) &= e^{-i\omega t}\sqrt{\frac{\gamma}{\pi}}\cos(\omega T/2)\sum_k \frac{1}{1-\gamma T e^{i\omega_{(k)}T}}\frac{1}{\omega-\omega_{(k)}} \\ &= e^{-i\omega t}\sqrt{\frac{\gamma}{\pi}}\frac{\cos(\omega T/2)}{\omega-\omega_0+i\gamma+i\gamma e^{i\omega T}}. \end{aligned} \tag{9.108}$$

We define the emission spectrum of outgoing phonons

$$S^{out}(\omega) \equiv 2\pi\left|\alpha_\omega^{out}(+\infty)\right|^2 = \frac{\gamma(1+\cos\omega T)}{\left|\omega-\omega_0+i\gamma+i\gamma e^{i\omega T}\right|^2}, \tag{9.109}$$

which can be proven to be equivalent to Eq. (9.13) in the main text using the identity in Eq. (9.107).

9.7.3 Boundary conditions

Using Eqs. (9.87) and (9.105), we compute the SAW fields in the transmission line

$$\begin{aligned}\alpha_1(x,t) &= \alpha_1(x-v_g t,0) \\ &\quad -i\sqrt{\frac{\gamma}{2v_g}}\left[\Theta(x-L/2)e(t+T/2-x/v_g)\right. \\ &\quad \left.+\Theta(x+L/2)e(t-T/2-x/v_g)\right], \end{aligned} \tag{9.110}$$

$$\begin{aligned}\alpha_2(x,t) &= \alpha_2(x-v_g t,0) \\ &\quad -i\sqrt{\frac{\gamma}{2v_g}}\left[\Theta(-x-L/2)e(t+T/2+x/v_g)\right. \\ &\quad \left.+\Theta(-x+L/2)e(t-T/2+x/v_g)\right]. \end{aligned} \tag{9.111}$$

In particular, we have the boundary conditions at the two legs for the right-propagating SAW field

$$\begin{aligned}\alpha_1(+L/2+0^+,t) &= \alpha_1(+L/2-v_g t,0) \\ &\quad -i\sqrt{\frac{\gamma}{2v_g}}\left[e(t)+e(t-T)\right], \\ \alpha_1(-L/2-0^-,t) &= \alpha_1(-L/2-v_g t,0), \end{aligned} \tag{9.112}$$

and for the left-propagating SAW field

$$\begin{aligned}\alpha_2(-L/2-0^-,t) &= \alpha_2(-L/2-v_g t,0) \\ &\quad -i\sqrt{\frac{\gamma}{2v_g}}\left[e(t)+e(t-T)\right], \\ \alpha_2(+L/2+0^+,t) &= \alpha_2(+L/2-v_g t,0). \end{aligned} \tag{9.113}$$

Introducing the following notation

$$\begin{aligned}\alpha_A^{in}(t) &\equiv \alpha_1(-L/2-0^-,t) = \alpha_1(-L/2-v_g t,0), \\ \alpha_B^{in}(t) &\equiv \alpha_2(+L/2-0^+,t) = \alpha_2(+L/2-v_g t,0), \\ \alpha_A^{out} &\equiv \alpha_2(-L/2-0^+,t), \\ \alpha_B^{out} &\equiv \alpha_1(+L/2+0^+,t), \end{aligned}$$

we can rewrite the boundary conditions as

$$\alpha_B^{out}(t) \equiv \alpha_A^{in}(t-T) - i\sqrt{\frac{\gamma}{2v_g}}\left[e(t)+e(t-T)\right], \tag{9.114}$$

$$\alpha_A^{out}(t) \equiv \alpha_B^{in}(t-T) - i\sqrt{\frac{\gamma}{2v_g}}\left[e(t)+e(t-T)\right]. \tag{9.115}$$

With this notation, Eq. (9.91) recovers Eq. (9.4) in the main text.

9.7.4 Polynomial decay

Without driving, the spontaneous emission of the giant atom excites SAW wave-packets in both directions at the two legs. We are interested in the phonon field excited between the two legs, *i.e.*, $-L/2 < x < L/2$. The total field is the superposition of the two fields which can be obtained from Eqs. (9.110) and (9.111),

$$\begin{aligned}\alpha(x,t) = \alpha_1\left(-\frac{L}{2} < x < \frac{L}{2}, t\right) + \alpha_2\left(-\frac{L}{2} < x < \frac{L}{2}, t\right)\\ -i\sqrt{\frac{\gamma}{2v_g}}\left[e\left(t - \left[x+\frac{L}{2}\right]/v_g\right) + e\left(t - \left|x-\frac{L}{2}\right|/v_g\right)\right].\end{aligned} \tag{9.116}$$

The total energy stored as SAW phonons between the two legs is

$$\begin{aligned}E_P &= \hbar\omega_0\int_{-L/2}^{L/2}|\alpha(x,t)|^2\,dx\\ &= \hbar\omega_0\int_0^L|\alpha(x-L/2,t)|^2\,dx\\ &= \frac{\gamma\hbar\omega_0}{2v_g}\int_0^L|e\left(t-x/v_g\right)+e\left(t-|x-L|/v_g\right)|^2\,dx\\ &= \frac{\gamma\hbar\omega_0}{2v_g}\left[\int_0^L|e(t-x/v_g)|^2\,dx+\int_0^L|e\left(t-|x-L|/v_g\right)|^2\,dx\right]\\ &\quad+\frac{\gamma\hbar\omega_0}{v_g}\mathrm{Re}\left[\int_0^L e(t-x/v_g)e^*(t-|x-L|/v_g)dx\right].\end{aligned} \tag{9.117}$$

In parameter region D, two SAW wave-packets are generated from the two legs of giant atom. When the two wave packets are well separated, we can neglect the overlap integral and have

$$\begin{aligned}E_P(t) &\approx \frac{\gamma\hbar\omega_0}{2v_g}\left[\int_0^L|e(t-x/v_g)|^2\,dx\right.\\ &\quad\left.+\int_0^L|e(t-|x-L|/v_g)|^2\,dx\right]\\ &\approx \gamma\hbar\omega_0\int_0^T|e(t-\tau)|^2\,d\tau.\end{aligned} \tag{9.118}$$

For $m \le t/T < m+1$, the time evolution of giant atom is $e(t) = \sum_{m=0} e_m(t)$ with $e_m(t)$ given by Eq. (9.6). We neglect the overlap between different $e_m(t)$. The stored SAW energy at time $t = (m+1)T$ can then be calculated as

$$\begin{aligned}E_P &\approx \gamma\hbar\omega_0\int_0^T|e(t-\tau)|^2\,d\tau\\ &\approx \gamma\hbar\omega_0|e(0)|^2\int_{mT}^{(m+1)T}|e_m(t)|^2\,dt\\ &\approx \gamma\hbar\omega_0|e(0)|^2\frac{\left(\gamma Te^{\gamma T}\right)^{2m}}{(m!)^2}\int_{mT}^{(m+1)T}e^{-2\gamma T\frac{t}{T}}\left(m-\frac{t}{T}\right)^{2m}dt\\ &\approx \gamma\hbar\omega_0|e(0)|^2T\frac{\left(\gamma Te^{\gamma T}\right)^{2m}}{(m!)^2}\frac{(2m)!}{(-2\gamma T)^{2m}}\int_m^{m+1}e^{-2\gamma Tx}dx\\ &\approx \gamma\hbar\omega_0|e(0)|^2T\frac{\left(\gamma Te^{\gamma T}\right)^{2m}}{(m!)^2}\frac{(2m)!}{(-2\gamma T)^{2m}}\frac{1}{2\gamma T}e^{-2m\gamma T}\\ &\approx \frac{\gamma\hbar\omega_0|e(0)|^2}{2\gamma}\frac{\left(\gamma Te^{\gamma T}\right)^{2m}}{2\pi m(m/e)^{2m}}\frac{\sqrt{4\pi m}(2m/e)^{2m}}{(-2\gamma T)^{2m}}e^{-2m\gamma T}\\ &\approx \frac{\hbar\omega_0|e(0)|^2}{2\sqrt{\pi}}\frac{1}{\sqrt{m}} \approx \frac{\hbar\omega_0|e(0)|^2}{2\sqrt{\pi}}\left(\frac{t}{T}-1\right)^{-1/2}\\ &\approx \frac{\hbar\omega_0|e(0)|^2}{2\sqrt{\pi}}\left(\frac{t}{T}\right)^{-1/2}.\end{aligned} \tag{9.119}$$

Here, we have used Stirling's formula $m! = \sqrt{2\pi m}(m/e)^m$ and the fact that $\gamma T \gg 1$ in parameter region D. Therefore, the stored energy follows a universal polynomial decay law $\propto t^{-1/2}$.

In parameter region D, as shown in Fig. 9.3(c1), the giant atom exhibits revival behaviour. We find that the revival peaks also decay polynomially. From Eq. (9.6), the probability of the giant atom to be in the excited state in the time interval $mT \leq t < (m+1)T$, with $m \in \mathbb{Z}^+$, is

$$P_e(t) \equiv |e_m(t)|^2 \approx e^{-2(\gamma T)\frac{t}{T}} \frac{(\gamma T e^{\gamma T})^{2m}}{(m!)^2} \left(m - \frac{t}{T}\right)^{2m}. \tag{9.120}$$

Here, we have assumed the giant atom is in the excited state initially, i.e., $e(0) = 1$. From Eq. (A43), we see that the atom follows the following general behaviour in each time interval: it starts in the ground state $[P_e(mT) = 0]$, revives to a peak value P_e^{max}, and then decays exponentially at a rate 2γ. The peak's position in the time interval $mT \leq t < (m+1)T$ is readily found to be

$$\frac{t_m}{T} = m + \frac{m}{\gamma T}. \tag{9.121}$$

The peak value $P_e^{max}(t_m)$ is given by

$$P_e^{max}(t_m) \approx \left(\frac{m^m}{e^m m!}\right)^2 \approx \frac{1}{2\pi m} = (1 + \frac{1}{\gamma T})\frac{T}{2\pi t_m}. \tag{9.122}$$

Here, we have used $m! \approx \sqrt{2\pi m}(m/e)^m$ for $m \gg 1$. We see that $P_e^{max}(t_m)$ follows a polynomial decay law $\propto t_m^{-1}$. We also see from Eq.(9.121) that the time of the peak shifts with m. When $m \approx \gamma T$, the peak is at $(m+1)T$, the boundary of the interval, which indicates that the decay behaviour changes around this value of m.

In the experiment, one can measure the outgoing phonons from the two legs of the giant atom. The outgoing phonon field for $m \leq t/T < m+1$ $(m \geq 1)$ is given by

$$\alpha^{out}(t) = -i\sqrt{\frac{\gamma}{2v_g}}\Big[e_m(t) + e_{m-1}(t-T)\Big]. \tag{9.123}$$

Using Eq. (9.6), we have

$$\alpha^{out}(t) \approx -i\sqrt{\frac{\gamma}{2v_g}} e_m(t)\Big[1 + \frac{m}{\gamma T(m - t/T)}\Big]. \tag{9.124}$$

We calculate energy accumulation of outgoing phonons during the time $m \leq t/T < m+1$:

$$\begin{aligned}
\frac{E^{out}(m)}{\hbar\omega_0} &\equiv v_g \int_{mT}^{(m+1)T} |\alpha^{out}(t)|^2 dt \\
&= \frac{\gamma}{2}\Big[\int_{mT}^{(m+1)T} |e_m(t)|^2 dt + \int_{(m-1)T}^{mT} |e_{m-1}(t)|^2 dt \\
&\quad + \int_{mT}^{(m+1)T} \Big(e_m(t)e_{m-1}^*(t) + e_m^*(t)e_{m-1}(t)\Big)dt\Big] \\
&= \frac{\gamma}{2}\Big[\frac{1}{2\gamma\sqrt{\pi}}\frac{1}{\sqrt{m}} + \frac{1}{2\gamma\sqrt{\pi}}\frac{1}{\sqrt{m-1}} \\
&\quad + \int_{mT}^{(m+1)T} |e_m(t)|^2 \frac{2m}{\gamma T(m - t/T)} dt\Big] \\
&= \frac{\gamma}{2}\Big[\frac{1}{2\gamma\sqrt{\pi}}\frac{1}{\sqrt{m}} + \frac{1}{2\gamma\sqrt{\pi}}\frac{1}{\sqrt{m-1}} \\
&\quad + \frac{2m(\gamma T e^{\gamma T})^{2m}}{\gamma T(m!)^2} \int_{mT}^{(m+1)T} e^{-2(\gamma T)\frac{t}{T}}(m - \frac{t}{T})^{2m-1} dt\Big] \\
&\approx \frac{\gamma}{2}\Big[\frac{1}{2\gamma\sqrt{\pi}}\frac{1}{\sqrt{m}} + \frac{1}{2\gamma\sqrt{\pi}}\frac{1}{\sqrt{m-1}} \\
&\quad + \frac{2m(\gamma T e^{\gamma T})^{2m}}{\gamma T(m!)^2} T \frac{(2m-1)!}{(-2\gamma T)^{2m-1}} \frac{e^{-2m\gamma T}}{2\gamma T}\Big] \\
&= \frac{\gamma}{2}\Big[\frac{1}{2\gamma\sqrt{\pi}}\frac{1}{\sqrt{m-1}} - \frac{1}{2\gamma\sqrt{\pi}}\frac{1}{\sqrt{m}}\Big] \\
&\approx \frac{1}{8\sqrt{\pi}} m^{-\frac{3}{2}}.
\end{aligned} \tag{9.125}$$

The above result shows that the energy of the outgoing phonons also follows a polynomial decay law $\propto m^{-\frac{3}{2}}$.

9.7.5 Reflectance and transmittance

To study the scattering properties of the giant atom, we send a right-propagating SAW towards the left leg, *i.e.*, $\alpha_{1\omega}(0) \neq 0$ and $\alpha_{2\omega}(0) = 0$. Assuming the giant atom to be in the ground state initially, we have from Eq. (9.96) that its dynamics are given by

$$e(t) = 2\sqrt{\frac{\gamma}{4\pi}} \int d\omega \frac{\alpha_{1\omega}(0)\cos(\omega T/2)}{\omega - \omega_0 + i\gamma + i\gamma e^{i\omega T}} e^{-i\omega t}. \tag{9.126}$$

From Eq. (9.105) we obtain the dynamics of forward-scattered SAWs

$$\begin{aligned} \alpha_{1\omega}(t) = e^{-i\omega t}\alpha_{1\omega}(0) - i\frac{\gamma}{\pi}\cos\left(\frac{\omega T}{2}\right) \times \\ \int d\omega' \frac{\alpha_{1\omega'}(0)\cos\left(\frac{\omega' T}{2}\right)}{\omega' - \omega_0 + i\gamma + i\gamma e^{i\omega' T}} e^{-i\omega t} \int_0^t dt' e^{i(\omega-\omega')t'}, \end{aligned} \tag{9.127}$$

and the backward-scattered SAWs

$$\begin{aligned} \alpha_{2\omega}(t) = -i\frac{\gamma}{\pi}\cos\left(\frac{\omega T}{2}\right) \times \\ \int d\omega' \frac{\alpha_{1\omega'}(0)\cos\left(\frac{\omega' T}{2}\right)}{\omega' - \omega_0 + i\gamma + i\gamma e^{i\omega' T}} e^{-i\omega t} \int_0^t dt' e^{i(\omega-\omega')t'}. \end{aligned} \tag{9.128}$$

In the long-time limit, we have

$$\alpha_{1\omega}(\infty) = e^{-i\omega t}\alpha_{1\omega}(0)\left(1 - i\gamma\frac{1+\cos\omega T}{\omega - \omega_0 + i\gamma + i\gamma e^{i\omega T}}\right), \tag{9.129}$$

$$\alpha_{2\omega}(\infty) = e^{-i\omega t}\alpha_{1\omega}(0)\left(-i\gamma\frac{1+\cos\omega T}{\omega - \omega_0 + i\gamma + i\gamma e^{i\omega T}}\right). \tag{9.130}$$

We define the transmittance and reflectance as $\mathcal{T} \equiv \frac{|\alpha_{1\omega}(+\infty)|^2}{|\alpha_{1\omega}(0)|^2}$ and $\mathcal{R} \equiv \frac{|\alpha_{2\omega}(+\infty)|^2}{|\alpha_{1\omega}(0)|^2}$, respectively. They can be calculated from Eqs. (9.129) and (9.130), giving

$$\mathcal{T} = \frac{(\omega_d - \omega_0 - \gamma\sin\omega_d T)^2}{(\omega_d - \omega_0 - \gamma\sin\omega_d T)^2 + \gamma^2(1+\cos\omega_d T)^2}, \tag{9.131}$$

$$\mathcal{R} = \frac{\gamma^2(1+\cos\omega_d T)^2}{(\omega_d - \omega_0 - \gamma\sin\omega_d T)^2 + \gamma^2(1+\cos\omega_d T)^2}. \tag{9.132}$$

It is easily seen that $\mathcal{T} + \mathcal{R} = 1$.

9.8 Input-output theory for a giant atom

In this appendix we give some further details on the input-output theory for the giant atom with arbitrary driving strength. We write the model atom-phonon Hamiltonian from Eq. (9.2) in the main text as

$$\begin{aligned} \mathscr{H} = H_S + \sum_{\alpha=1,2}\int_0^\infty d\omega \hbar\omega a_{\alpha\omega}^\dagger a_{\alpha\omega} \\ + \hbar\sum_{\alpha=1,2}\int_{-\infty}^\infty d\omega\sqrt{\frac{\gamma}{4\pi}}\left[\sigma_- a_{\alpha\omega}^\dagger\left(e^{-i\omega T/2} + e^{i\omega T/2}\right) + \text{H.c.}\right], \end{aligned} \tag{9.133}$$

where $H_S = \hbar\omega_0 |e\rangle\langle e|$ is the bare atom Hamiltonian. In Eq. (9.133), we have made the standard Markov approximations of taking the atom's decay rate to be frequency independent and extended the lower integration limit to minus infinity for the interaction term [59].

How the phonon transmission line serves as a feedback loop for the atom is apparent when the equations of motion are formulated using the usual quantum optics input-output formalism. Following the standard approach

[59], we find from the Hamiltonian in Eq. (9.133) that the quantum Langevin equation for an aribtrary atomic operator x is

$$\begin{aligned}\dot{x}(t) = \frac{i}{\hbar}[H_S, x] \\ + \sum_{i=A,B} \Bigg\{ [\sigma_+, x] \Bigg[\frac{\gamma}{2} \left(\sigma_-(t) + \sigma_-(t-T)\right) \\ + i\sqrt{\frac{\gamma}{2}} \left(a_i^{\text{in}}(t) + a_i^{\text{in}}(t-T)\right) \Bigg] \\ - \Bigg[\frac{\gamma}{2} \left(\sigma_+(t) + \sigma_+(t-T)\right) \\ - i\sqrt{\frac{\gamma}{2}} \left(a_i^{\text{in}\dagger}(t) + a_i^{\text{in}\dagger}(t-T)\right) \Bigg] [\sigma_-, x] \Bigg\},\end{aligned} \tag{9.134}$$

where we have defined input free phonon fields incident on the atom at leg A and leg B

$$a_A^{\text{in}}(t) \equiv \quad \tfrac{1}{\sqrt{2\pi}} \textstyle\int_{-\infty}^{\infty} d\omega e^{-i\omega(t-t_0)} a_{1\omega}(t_0), \tag{9.135}$$

$$a_B^{\text{in}}(t) \equiv \quad \tfrac{1}{\sqrt{2\pi}} \textstyle\int_{-\infty}^{\infty} d\omega e^{-i\omega(t+T-t_0)} a_{2\omega}(t_0), \tag{9.136}$$

where t_0 is some early time where the Heisenberg picture and Schrödinger picture operators coincide (we assume $t_0 < t - T$ for all t). We can similarly define output fields at leg A and leg B of the giant atom

$$a_A^{\text{out}}(t) \equiv \quad \tfrac{1}{\sqrt{2\pi}} \textstyle\int_{-\infty}^{\infty} d\omega e^{-i\omega(t-t_1)} a_{2\omega}(t_1), \tag{9.137}$$

$$a_B^{\text{out}}(t) \equiv \quad \tfrac{1}{\sqrt{2\pi}} \textstyle\int_{-\infty}^{\infty} d\omega e^{-i\omega(t-T-t_1)} a_{1\omega}(t_1), \tag{9.138}$$

where $t_1 > t + T$ is some late time. The output fields are given by the inputs and the atomic dynamics through input-output equations

$$a_A^{\text{out}}(t) = \quad a_B^{\text{in}}(t-T) - i\sqrt{\tfrac{\gamma}{2}} \left[\sigma_-(t) + \sigma_-(t-\tau)\right], \tag{9.139}$$

$$a_B^{\text{out}}(t) = \quad a_A^{\text{in}}(t-T) - i\sqrt{\tfrac{\gamma}{2}} \left[\sigma_-(t) + \sigma_-(t-\tau)\right]. \tag{9.140}$$

These boundary conditions are similar to the boundary conditions (9.114) and (9.115) but replacing the single phonon excitation amplitude $e(t)$ by the lowering operator $\sigma_-(t)$.

Equation (9.134) is a non-linear quantum Langevin delay differential equation, making the feedback mechanism of the transmission line quite clear. It is, however, not easily solved in general. Note that in the presence of coherent input drives, these can conveniently be moved into the system Hamiltonian

$$\begin{aligned}H_S = \hbar\omega_0 |e\rangle\langle e| \\ + \hbar V \sum_\alpha \left[\left(\alpha_\alpha^{\text{in}}(t)^* + e^{-i\varphi} \alpha_\alpha^{\text{in}}(t-T)^*\right) \sigma_- + \text{H.c.} \right],\end{aligned} \tag{9.141}$$

by displacing the phonon fields $a_{\alpha\omega} \to a_{\alpha\omega} + \sqrt{4\pi/\gamma} V \alpha_\alpha^{\text{in}}(t) \delta(\omega - \omega_{d_\alpha})$ with $\alpha_1^{\text{in}}(t) = A_1 e^{-i\omega_{d_1} t}$ and $\alpha_2^{\text{in}}(t) = A_2 e^{-i\omega_{d_2}(t+T)}$.

In Section 9.5 we also used the fact that the problem can be mapped onto a setup with only a single feedback loop. This is easily seen from Eq. (9.133) by defining a new phonon operator $b_\omega \equiv \left(a_{1\omega} + a_{2\omega} e^{-i\omega T}\right)/\sqrt{2}$. In terms of this new field, the quantum Langevin equation can be written

$$\begin{aligned}\dot{x}(t) = \frac{i}{\hbar}[H_S, x] \\ + \Bigg\{ [\sigma_+, x] \Bigg[\gamma \left(\sigma_-(t) + \sigma_-(t-T)\right) \\ + i\sqrt{\gamma} \left(b^{\text{in}}(t) + b^{\text{in}}(t-T)\right) \Bigg] \\ - \Bigg[\gamma \left(\sigma_+(t) + \sigma_+(t-T)\right) \\ - i\sqrt{\gamma} \left(b^{\text{in}\dagger}(t) + b^{\text{in}\dagger}(t-T)\right) \Bigg] [\sigma_-, x] \Bigg\},\end{aligned} \tag{9.142}$$

where

$$b^{\text{in}}(t) \equiv \frac{1}{\sqrt{2\pi}} \int_{-\infty}^{\infty} d\omega e^{-i\omega(t-t_0)} b_\omega(t_0) = \frac{1}{\sqrt{2}} \left[a_A^{\text{in}}(t) + a_B^{\text{in}}(t) \right]. \tag{9.143}$$

We can also define an output field given by the usual input-output equation

$$\begin{aligned} b^{\text{out}}(t) &= b^{\text{in}}(t-T) - i\sqrt{\gamma} \left[\sigma_-(t) + \sigma_-(t-\tau) \right] \\ &= \frac{1}{\sqrt{2}} \left[a_A^{\text{out}}(t) + a_B^{\text{out}}(t) \right]. \end{aligned} \tag{9.144}$$

Note that in a situation where the left and right input fields are identical, we have, based on symmetry, that $a_A^{\text{out}}(t) = a_B^{\text{out}}(t) = b^{\text{out}}(t)/\sqrt{2}$.

9.9 Computing output-field correlation functions from the cascaded master equation

In this appendix, we outline how output field correlation functions can be computed from Eq. (9.69) building on the method presented in Ref. [26]. We want to calculate an output field correlation function of the type

$$\langle c_1(t_1) c_2(t_2) \dots c_n(t_n) \rangle, \tag{9.145}$$

where $c_i(t_i)$ is one of $b^{\text{out}}(t_i)$ or $b^{\text{out}}(t_i)^\dagger$ (see Appendix 9.8) and we assume that all the times are different, $t_i \neq t_j$, such that the time-ordering is arbitrary (equal times can be taken as a limit). First, it is illustrative to recall how this can be done for a conventional Markovian open quantum system where the evolution is given by a Lindblad master equation

$$\frac{d}{dt}\mathcal{E}(t) = \left\{ -\frac{i}{\hbar}\mathcal{H}[H_s(t)] + \mathcal{D}[L] \right\} \mathcal{E}(t), \tag{9.146}$$

for the time-propagator $\mathcal{E}(t)$ [*i.e.*, the state at time t is given by $\rho(t) = \mathcal{E}(t)\rho(0)$] and where the output field is given by the input field and the system dynamics through an input-output equation

$$b^{\text{out}}(t) = b^{\text{in}}(t) + L(t). \tag{9.147}$$

As is well known, Eq. (9.145) can be computed through the so-called quantum regression formula [59, 18]

$$\begin{aligned} &\langle c_1(t_1) c_2(t_2) \dots c_n(t_n) \rangle \\ &= \langle \mathcal{F}_n \mathcal{E}(s_n - s_{n-1}) \dots \mathcal{F}_2 \mathcal{E}(s_2 - s_1) \mathcal{F}_1 \mathcal{E}(s_1) \rho(0) \rangle, \end{aligned} \tag{9.148}$$

where we have time-ordered the times and relabelled them by $s_1 < s_2 < \dots < s_n$, and defined

$$\mathcal{F}_j \rho = L\rho \qquad \text{for } c_j(s_j) = b^{\text{out}}(s_j), \tag{9.149}$$

$$\mathcal{F}_j \rho = \rho L^\dagger \qquad \text{for } c_i(s_j) = b^{\text{out}}(s_j)^\dagger. \tag{9.150}$$

The computation for a system with time-delay, with the time-propagator master equation Eq. (9.69), is entirely analogous. First, we define new time-variables t_i^* through

$$t_i^* = t - l_i T, \tag{9.151}$$

where $l_i = \left[\frac{t}{T} \right]$ is the largest integer less than or equal to $\frac{t}{T}$, and time-order these auxiliary time-variables from earliest to latest and call them $s_1^* < s_2^* < \dots < s_n^*$. The correlation function in Eq. (9.145) is then given by

$$\begin{aligned} &\langle c_1(t_1) c_2(t_2) \dots c_n(t_n) \rangle \\ &= \left\langle \mathcal{F}_n \mathcal{E}_T(s_n^* - s_{n-1}^*) \dots \mathcal{F}_2 \mathcal{E}_T(s_2^* - s_1^*) \mathcal{F}_1 \mathcal{E}_T(s_1^*) \rho(0) \right\rangle, \end{aligned} \tag{9.152}$$

where now

$$\mathcal{F}_j \rho = L_{l_{j-1}, l_j} \rho \qquad \text{for } c_j(t_j) = b^{\text{out}}(t_j), \tag{9.153}$$

$$\mathcal{F}_j \rho = \rho L_{l_{j-1}, l_j}^\dagger \qquad \text{for } c_j(t_j) = b^{\text{out}}(t_j)^\dagger, \tag{9.154}$$

and the index j refers to the time-ordering of s_j^*. A formal proof of Eq. (9.152) can be given using the tensor-network representation of the time-propagator used in Ref. [26] and will be presented in a future work [55].

Part VI
Old, Fundamental Theories

Part VII
Multiphoton Processes: Main Articles

10 Few photon scattering on Bose-Hubbard lattices by Pedersen, Pletyukhov

Abstract

We theoretically investigate the scattering of few photon light on Bose-Hubbard lattices using diagrammatic scattering theory. We explicitly derive general analytical expressions for the lowest order photonic correlation functions, which we apply numerically to several different lattices. We focus specifically on non-linear effects visible in the intensity-intensity correlation function and explain bunching and anti-bunching effects in dimers, chains, rings and planes.

The numerical implementation can be applied to arbitrary Bose-Hubbard graphs, and we provide it as an attachment to this publication.

10.0.1 Introduction

Experimentalists have in the last decade realized ever more complex quantum many-body photonic systems. This progress depends on several innovations, like the controlled guiding of photons in one-dimensional channels, their subsequent coupling to cavities, the coupling of multiple such cavities [1, 2, 3, 4, 5], and the creation of an effective interaction between photons through their mutual coupling to discrete quantum systems [6, 7, 8] or other non-linear media [9].

These experiments have attracted a lot of attention because of the possibility of realizing complex many-body quantum states [10, 11, 12, 13, 14]; but this goal also has a backside, since the (exponentially) complex quantum many-body problem makes it increasingly difficult to perform meaningful theoretical calculations or exact numerical simulations. Theory and experiment can, however, be brought on equal grounds by reducing the complexity of the involved quantum many-body states, as realized in the limit of weak input power, where only a few photons inhabit the scatterer at a time.

We consider complex photonic systems composed of a distributed scatterer coupled to one or more one-dimensional chiral channels and operated in the few photon limit. Figure 10.1 shows a general example of such a system, where the distributed scatterer is represented by connected dots, the chiral channels are symbolized by directed lines, while dashed lines indicate the couplings between the scatterer and channels.

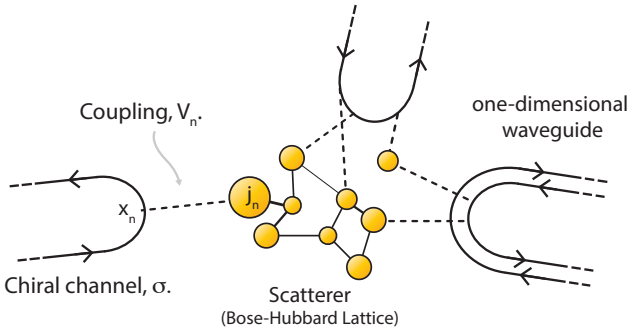

Figure 10.1: Example of a scattering setup: Four chiral channels (two of them forming a one-dimensional waveguide) couple at multiple points to an extended scatterer consisting of multiple sites.

The theory developed to describe such systems in the few photon limit exists in various incarnations as e.g. scattering theory [15, 16, 17, 18, 19], Lehmann-Symanzik-Zimmermann formalism [20], generalized master equations [21, 22], SLH formalism [23, 24], and input-output theory [19, 25]. We here provide a generalization of the scattering theory methods to more complex local and quasi-local scatterers. While we here stop short of explicitly going beyond the Markov approximation [26, 27, 28], our results can be used to numerically solve a large class of photonic scattering problems, and used to understand and interpret many different photonic experiments operated in the weak power limit.

We here perform explicit numerical calculations for several different setups modeled as Bose-Hubbard graphs. While some of the distributed scatterer geometries have received some attention [19, 18, 29, 30, 31], we also show how our method can be applied to larger systems such as chains, rings and square lattices. The paper is structured as follows:

Section 11.2 describes the relevant theoretical models and discuss some of their possible experimental realizations.

Section 10.0.3 reviews diagrammatic scattering theory within the Markov approximation. The diagrammatics are applied directly to the scattering of few photons states on distributed quantum systems coupled locally and quasi-locally to the chiral channels. We explicitly derive the one-photon and two-photon scattering matrices, and finally find expressions for the first and second order correlation functions for coherent photonic input states.

Section 10.0.4 investigates few photon scattering in several different Bose-Hubbard graphs using a numerical implementation of the results of the previous sections called `babusca` [4] and available in the supplementary information. For some simple systems we show that we easily reproduce the well-known results, and we then turn to more complicated geometries including dimers, chains and rings. We analyze the results and explain the main effects visible in the first and second order coherence functions, such as photon blockade, photon bunching and anti-bunching, and discuss their relationship to the geometry of the scatterer. We end the paper by demonstrating the capability of the `babusca` approach by considering scattering an 8 by 8 square lattice scatterer.

10.0.2 Model

We describe the relevant photonic systems by the general Hamiltonian,

$$H = H_0 + V = H_{\rm sc} + H_{\rm chs} + V. \tag{10.1}$$

Here $H_{\rm sc}$ describes the scatterer, which in our discussion is explicitly represented by a Bose-Hubbard lattice graph. $H_{\rm chs}$ is a free Hamiltonian describing all the chiral one-dimensional channels, and V describes the coupling between the channels and the scatterer.

Such photonic systems can be built in various experimental platforms, but one of the most direct implementations uses coupled cavity arrays based on either optical [3] or superconducting microwave resonators [1, 2], which in the presence of local non-linearities directly realize a Bose-Hubbard lattice model, as is also the case for multiple coupled qubits or emitters [33]. Other emitters - like atoms with intricate level structures - can also be modeled as effective Bose-Hubbard graphs, provided they support only a single ground state.

The Bose-Hubbard lattice Hamiltonian can be written as the sum of three terms,

$$\begin{aligned} H_{\rm sc} &= H_\varepsilon + H_t + H_U \\ &= \sum_i \varepsilon_i b_i^\dagger b_i + \sum_{i>j} (t_{ij} b_i^\dagger b_j + h.c.) \\ &\quad + \sum_i \tfrac{1}{2} U_i b_i^\dagger b_i (b_i^\dagger b_i - 1). \end{aligned} \tag{10.2}$$

Here the second quantization operators $b_i^\dagger$ (b_i) create (annihilate) an excitation on the lattice site i. Each lattice site has a local excitation energy, ε_i, an onsite photon-photon interaction, U_i, also referred to as a nonlinearity; while the hopping between two neighbor lattices sites is captured by the amplitudes, t_{ij}.

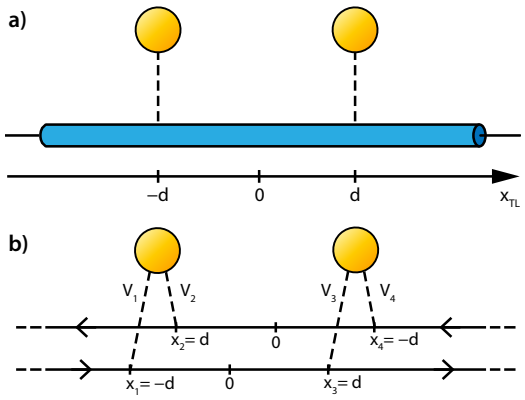

Figure 10.2: Representation of left- and right-propagating modes of the bi-directional waveguide as a pair of two chiral channels. Each channel requires its own coordinate axis co-directed with the propagation of the photons.

[4] `babusca` is also available at .

Existing photonic experiments often rely on one-dimensional waveguides which naturally accommodate two counter-propagating (left- and right-moving) one-dimensional channels. They can be modeled as a pair of chiral channels, as shown in Fig. 10.2. This modeling requires the introduction of a separate coordinate axis for each channel, which is co-directed with the propagation direction of the photons. However, this does not reduce the complexity of the problem, since the representation in Fig. 10.2(b) explicitly shows that the ordering of the coupling points along one channel is opposite to their ordering along the other channel.

Single chiral channels can also be realized as e.g. edge states in topological photonic lattice systems exhibiting the photonic spin-Hall effect [4], and in systems of linear optical resonator arrays with an induced artificial magnetic field [3]. Additionally, chiral propagation may emerge in cascaded systems like tapered fibers coupled asymmetrically to the two directions of propagation due the "spin orbit effect for light" [34], or in photonic crystal lattices using similar effects [35]. Several theoretical proposals now rely explicitly on chiral quantum optics models [36, 37, 38]. Thus, by modeling the guiding of photons using chiral channels, we may describe both traditional waveguides as well as more exotic chiral propagation modes.

We model a general chiral channel, σ, in the wide band limit where its dispersion $\omega_{\sigma k}$ has been linearized around the working frequency, ω_0, such that $\omega_{\sigma k} = v_\sigma(k - k_0) + \omega_0$, v_σ being the group velocity in the channel σ. Introducing the bosonic creation operator, $a^\dagger_{\sigma\omega} = (2\pi v_\sigma)^{-1/2} \int_{-\infty}^{\infty} \mathrm{d}x\, e^{i(\omega_0+\omega)x/v_\sigma} a^\dagger_\sigma(x)$, which creates a single photonic excitation with a frequency $\omega_0 + \omega$ in channel σ, we end up with the single channel Hamiltonian,

$$H_\sigma = \int \mathrm{d}\omega\, (\omega_0 + \omega) a^\dagger_{\sigma\omega} a_{\sigma\omega}. \tag{10.3}$$

In the following we assume for simplicity that all v_σ are the same in all channels, and use convenient units where $\hbar = v_\sigma = 1$. In this way, $H_{\mathrm{chs}} = \sum_\sigma H_\sigma$.

The dynamics of the chiral channels, H_{chs}, or the scatterer, H_{sc}, are solvable in themselves, and all of our difficulty arises from their mutual coupling, V. A single coupling term, V_n, connects a point, x_n, along a chiral channel, σ_n to the j_n'th site on the scatterer with the overall coupling strength, g_n. We define it through the dipole coupling operator in the rotating wave approximation (RWA),

$$\begin{aligned} V_n &= g_n b^\dagger_{j_n} a_{\sigma_n}(x_n) + h.c. \\ &= \int \mathrm{d}\omega\, (g_n e^{i(\omega_0+\omega)x_n} b^\dagger_{j_n} a_{\sigma_n,\omega} + h.c.). \end{aligned} \tag{10.4}$$

For the sake of brevity we also define the total effective coupling between one channel, σ, and the scatterer,

$$V_\sigma = \sum_n \delta_{\sigma,\sigma_n} V_n = \int \mathrm{d}\omega\, (\tilde{b}^\dagger_\sigma a_{\sigma,\omega} + h.c.). \tag{10.5}$$

In the last line we introduced the shorthand $\tilde{b}^\dagger_\sigma = \sum_n \delta_{\sigma,\sigma_n} g_n e^{i(\omega_0+\omega)x_n} b^\dagger_{j_n}$ that describe the collective excitation originating from channel σ.

10.0.3 Diagrammatic scattering theory

In this section we briefly remind the reader of diagrammatic Lippmann-Schwinger scattering theory and its application to photonic systems as derived in Refs. [15, 39]. We then apply diagrammatic scattering theory to our general photonic system; a Bose-Hubbard graph coupled to multiple chiral channels.

Photons begin their journey in the channels far away from the scatterer. They propagate freely along their original channel, then encounter the scatterer and interact with it until finally leaving the scatterer through the (same or possibly other) channels.

This time-evolution from the initial photonic state at time t_i, to the final scattered state at time t_f is defined by the time-evolution operator in the interaction picture, $U(t_f, t_i) = \mathcal{T} \exp\left(-i \int_{t_i}^{t_f} \mathrm{d}\tau\, V(\tau)\right)$. Scattering theory considers the full time evolution from the distant past, $t_i \to -\infty$ where the incoming state is far away from the scatterer, and to the far future, $t_f \to +\infty$ where the outgoing state has not only left the scatterer but is also far away from it.

In this limit, the time-evolution operator is simply known as the S-matrix. When working explicitly in the interaction picture, it expresses scattering transitions between eigenstates of the uncoupled system, $H_0 = H_{\mathrm{chs}} + H_{\mathrm{sc}}$, under the physical constraint that the energy of the scattered state is conserved, $E_i = E_f$.

The trivial part of the S-matrix can be separated out through the introduction of the T-matrix [40],

$$S = I - 2\pi i T(E_i)\delta(E_f - E_i). \tag{10.6}$$

The T-matrix can be perturbatively expanded in the interaction V,

$$\begin{aligned} T(E) &= V + V\frac{1}{E - H_0 - V + i0^+}V \\ &= \sum_{j=0}^{\infty} V\left(\frac{1}{E - H_0 + i0^+}V\right)^j \\ &= \sum_{j=0}^{\infty} V\left(G_0(E)V\right)^j, \end{aligned} \tag{10.7}$$

and this expression forms the basis for the diagrammatic approach. In the last line we introduced the bare Green's function $G_0(E) = (E - H_0 + i0^+)^{-1}$ that propagate the system in between consecutive scattering events.

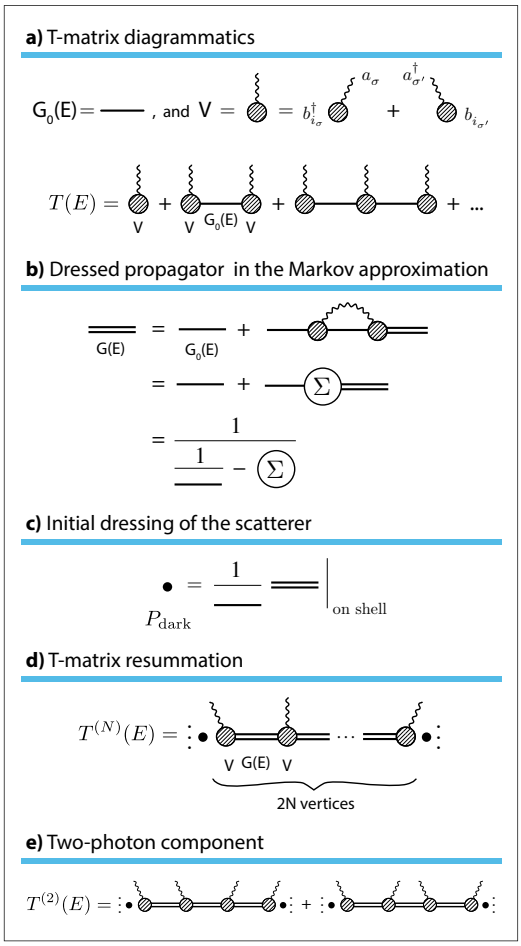

Figure 10.3: Diagrammatic form of the scattering theory developed in Ref. [15]. **(a)** The expression for T-matrix as derived in Eq. (10.7). **(b)** Diagrammatic expression of the dressing of the bare Greens function by the emission and immediate re-absorption of virtual photons. **(c)** The dressing of the initial state of the scatterer, which effectively projects onto the dark state subspace. **(d)** The N-photon operator contribution to the T-operator. Notice the modified normal ordering, ⋮ ⋮, which signifies an additional shift to the Green's function arguments as described in the main text. **(e)** Diagrams for the two-photon T-operator.

We draw a scattering event, V, as a filled circle with an additional wiggly lines pointing to the right (left) and symbolizing the absorption (emission) of a photon by the scatterer. The bare propagation, $G_0(E)$, is drawn as a solid line. The T-matrix in Eq. (10.7) can then be drawn as shown in Fig. 11.3(a).

A photon that is emitted during a scattering event, V, can either belong directly to the outcoming state; or it can be a virtual photon which is later re-arbsorbed by the scatterer. Diagrammatic scattering theory deals with the problem of how to correctly describe these virtual photon processes.

Pletyukhov and Gritsev [15] showed that under the assumption of two Markovianity conditions only a single type of virtual processes become important to scattering. The Markovianity conditions demand that

1. all channels have linear dispersions, and

2. dipole couplings are independent of the photonic mode, ω;

and they ensure that the whole scattering problem can be captured exactly within the Markov approximation.

The only virtual processes that contribute to the scattering amplitudes under these conditions involve virtual photons which are re-absorbed immediately after their emission [15]. These virtual processes are then be reincorporated as a dressing of the bare propagator, giving rise to a Dyson equation for the dressed Green's function as shown in Fig. 11.3(b).

Direct inversion of the the Dyson equation gives access to the dressed Green's function, $G(E)^{-1} = G_0(E)^{-1} - \Sigma(E)$, where $\Sigma(E)$ is the scatterer's self-energy which captures all possible consecutive processes involving the emission of a virtual photon and its immediate absorption. It equals

$$\Sigma(E) = \tilde{\Sigma}(E - H_{\text{chs}}), \tag{10.8}$$

where

$$\tilde{\Sigma}(E) = \langle V G_0(E) V \rangle_{\text{chs}}\,, \tag{10.9}$$

with the average performed in the vacuum state of the channels.

Additionally, these virtual processes also lead to a projection of the initial and final state of the scatterer onto its dark state subspace, when the expression for the S-matrix is put on-shell (i.e. it respects energy conservation). Formally, this projection is given by the operator $P_{\text{dark}} = G_0^{-1} G|_{\text{on shell}} = G G_0^{-1}|_{\text{on shell}}$, which is depicted in Fig. 11.3(c). Assuming that the empty scatterer is the *only* state in the dark-state subspace, this projection – along with the RWA – ensures the conservation of the number of photons in the incoming and outgoing states. The T-matrix can then be split up into the sum $T = \sum_{N=1}^{\infty} T^{(N)}$, where the contribution

$$T^{(N)}(E) = P_{\text{dark}} \left\{ \vdots \left(\prod_{i=1}^{2N-1} V G(E) \right) V \vdots \right\} P_{\text{dark}} \tag{10.10}$$

represents the N-photon operator multiplied by the dark-state projector. Here, we introduced a modified normal ordering of the chiral channel field operators, $\vdots(\cdots)\vdots$, which differs from the conventional normal ordering by the implementation of additional shifts in the Green's functions energy argument, as dictated by $G(E + \omega_0 + \omega) a^\dagger_{\sigma\omega} = a^\dagger_{\sigma\omega} G(E)$ and $a_{\sigma\omega} G(E) = G(E - \omega_0 - \omega) a_{\sigma\omega}$. While obscure, this modified normal ordering presents a simplified way to deal with all the possible diagrams. A graphical representation of Eq. (10.10) is shown in Fig. 11.3(d).

Note that this formulation of few photon scattering is almost equivalent the cluster form in input-output theory [25].

Local scatterers

The main obstacle in directly applying diagrammatic scattering theory to the relevant models, is that the coupling in Eq. (10.4), depends explicitly on the mode, ω, and hence does not fulfill the second Markovianity condition. One way around this, is to limit ourselves to *local* scatterers, where any given chiral channel, σ, only couples to the scatterer at a single point x_σ along the channel. The coordinate of the coupling point can then be *gauged* away, i.e. by setting $x_\sigma = 0$ in the expression for the coupling elements in Eq. (10.4). This allows us to write the couplings as

$$V_n = \int \mathrm{d}\omega \, (g_n b^\dagger_{j_n} a_{\sigma_n,\omega} + h.c.). \tag{10.11}$$

Both Markovianity conditions can then be satisfied, and the diagrammatic approach of Pletyukhov and Gritsev [15] allows us to solve the scattering problem exactly for an arbitrary number of incoming of photons. This subsection shows the derivation of the single photon and two-photon S-matrices for locally coupled scatterers.

The first step in this derivation concerns the scatterer self-energy as defined by Eq. (10.8). The self-energy is naturally split up in its contributions from any two coupling terms, $\Sigma = \sum_{n,m} \Sigma_{nm}$, where

$$\begin{aligned}
\Sigma_{nm} = \tilde{\Sigma}_{nm} &= \left\langle V_n \frac{1}{E - H_0 + i0^+} V_m \right\rangle_{\text{chs}} \\
&= g_n g_m^* b^\dagger_{j_n} \int_{-\infty}^{\infty} \mathrm{d}\omega \, \frac{1}{E - \omega_0 - \omega - H_{\text{sc}} + i0^+} b_{j_m} \\
&= -i\pi g_n g_m^* \delta_{\sigma_n,\sigma_m} b^\dagger_{j_n} b_{j_m}.
\end{aligned} \tag{10.12}$$

The total effective scatterer Hamiltonian is the concatenation of the bare scatterer Hamiltonian and the self-energy, $H_{\text{eff}} = H_{\text{sc}} + \Sigma$. Both the scatterer Hamiltonian and the self-energy conserve the number of photons in the scatterer, $M = \sum_j b_j^\dagger b_j$, i.e. $[H_{\text{sc}}, M] = [\Sigma, M] = 0$. Hence we can perform a spectral decomposition of the effective scatterer Hamiltonian for every photon number m, which is the eigenvalue of M. Since the self-energy is non-Hermitian, this decomposition,

$$\begin{aligned} H_{\text{eff}}^{(M)} &= \sum_{l_M=1}^{d_M} \lambda_{l_M}^{(M)} |M, l_M\rangle\langle\overline{m, l_M}| \\ &= \sum_{l_M=1}^{d_M} \lambda_{l_M}^{(M)} P_{l_M}^{(M)}, \end{aligned} \tag{10.13}$$

contains both right $|m, l_m\rangle$ and left $\langle\overline{m, l_m}|$ eigenvectors of $H_{\text{eff}}^{(M)}$, corresponding to the (possibly complex) eigenvalue $\lambda_{l_M}^{(M)}$ and obeying the bi-orthogonality relations $\langle\overline{M, l_M}|M, l'_M\rangle = \delta_{l_M, l'_M}$. Here, d_m denotes the dimension of the M-photon scatterer subspace, and $P_{l_M}^{(M)}$ is a projector onto the eigenspace of the eigenvalue $\lambda_{l_M}^{(M)}$.

The corresponding dressed Green's function has the form

$$\begin{aligned} G^{(M)}(E) &= \frac{1}{E - H_{\text{chs}} - H_{\text{eff}}^{(M)}} \\ &= \sum_{l_M=1}^{d_M} \frac{P_{l_M}^{(M)}}{E - H_{\text{chs}} - \lambda_{l_M}^{(M)}}. \end{aligned} \tag{10.14}$$

Note that it is important to keep H_{chs} in this definition in order to maintain the diagrammatic rules discussed in the paragraph following Eq. (10.10).

The single photon S-matrix describes how an incoming single photon state, $|\nu_1\rangle = a_{\nu_1}^\dagger |0\rangle_{\text{chs}}$, scatters into multiple outgoing single photon states, $|\nu'_1\rangle$. Note that we refer to photonic states in the channels using a multi-index, $\nu = (\sigma, \omega)$, labelling both the channel, σ and the mode, ω. We may write $S^{(1)} = \sum_{\nu'_1, \nu_1} S^{(1)}_{\nu'_1, \nu_1} a_{\nu'_1}^\dagger a_{\nu_1}$, where

$$\begin{aligned} S^{(1)}_{\nu'_1, \nu_1} &= S^{(1)}_{\sigma'_1\omega'_1, \sigma_1\omega_1} \\ &= \delta_{\omega'_1\omega_1} \left(\delta_{\sigma'_1\sigma_1} - 2\pi i T^{(1)}_{\sigma'_1\omega'_1, \sigma_1\omega_1} \right). \end{aligned} \tag{10.15}$$

Applying Eq. (10.10), we find

$$\begin{aligned} T^{(1)} &= P^{(0)} \vdots VGV \vdots P^{(0)} \\ &= \sum_{\sigma'_1\omega'_1, \sigma_1\omega_1} P^{(0)} \tilde{b}_{\sigma'_1} G^{(1)}(E + \omega_0 + \omega'_1) \tilde{b}_{\sigma_1}^\dagger P^{(0)} \\ &\qquad \times a_{\sigma'_1\omega'_1}^\dagger a_{\sigma_1\omega_1}. \end{aligned}$$

Enforcing the on-shell condition, $\omega'_1 = \omega_1$, and applying the spectral decomposition to the single-photon dressed Green's function, we obtain an expression for the matrix elements appearing in Eq. (10.15),

$$T^{(1)}_{\sigma'_1\omega'_1, \sigma_1\omega_1} = P^{(0)} \sum_{l_1=1}^{d_1} \frac{\langle 0|\tilde{b}_{\sigma'_1}|1, l_1\rangle\langle\overline{1, l_1}|\tilde{b}_{\sigma_1}^\dagger|0\rangle}{\omega_1 + \omega_0 - \lambda_{l_1}^{(1)}}. \tag{10.16}$$

The effects of photonic correlations first show up in the scattering of two-photon states $|\nu_1, \nu_2\rangle = a_{\nu_1}^\dagger a_{\nu_2}^\dagger |0\rangle_{\text{chs}}$ into other two photon states, $|\nu'_1, \nu'_2\rangle$. One can generally show [15, 27] that the two-photon scattering matrix

$$\begin{aligned} S^{(2)} = &\sum_{\nu'_1, \nu'_2} \sum_{\nu_1, \nu_2} a_{\nu'_1}^\dagger a_{\nu'_2}^\dagger a_{\nu_2} a_{\nu_1} \\ &\times \left(\frac{1}{2} S^{(1)}_{\nu'_1, \nu_1} S^{(1)}_{\nu'_2, \nu_2} - 2\pi i T^{(2)\mathcal{P}}_{\nu'_1, \nu'_2; \nu_1, \nu_2} \delta_{\omega'_1 + \omega'_2, \omega_1 + \omega_2} \right) \end{aligned} \tag{10.17}$$

can be expressed in terms of the single-photon matrices from Eq. (10.15) and the principal value part ($\mathcal{P}$) of the two-photon T-matrix calculated on the basis of Eq. (10.10). The first contribution describes elastic scattering of two photons (i.e. without energy exchange between them), while the second contribution captures inelastic effects arising due to the effective interaction between the two photons.

A direct calculation of the two-photon inelastic matrix components, which is based on the diagrams in Fig. 11.3(e) and presented in Appendix 10.0.7, yields the following result

$$T^{(2)\mathcal{P}}_{\nu_1',\nu_2';\nu_1,\nu_2} = P^{(0)} \sum_{l_1,l_1'} \frac{\langle 0|\tilde{b}_{\sigma_1'}|1,l_1'\rangle}{\omega_1' + \omega_0 - \lambda^{(1)}_{l_1'}} \Bigg\{ \sum_{l_2} \frac{\langle \overline{1,l_1'}|\tilde{b}_{\sigma_2'}|2,l_2\rangle\langle \overline{2,l_2}|\tilde{b}^\dagger_{\sigma_2}|1,l_1\rangle}{\omega_1+\omega_2+2\omega_0-\lambda^{(2)}_{l_2}} - \frac{1}{2}\frac{\omega_1+\omega_2+2\omega_0-\lambda^{(1)}_{l_1'}-\lambda^{(1)}_{l_1}}{(\omega_2'+\omega_0-\lambda^{(1)}_{l_1})(\omega_2+\omega_0-\lambda^{(1)}_{l_1'})}\langle \overline{1,l_1'}|\tilde{b}^\dagger_{\sigma_2}|0\rangle\langle 0|\tilde{b}_{\sigma_2'}|1,l_1\rangle \Bigg\} \frac{\langle \overline{1,l_1}|\tilde{b}^\dagger_{\sigma_1}|0\rangle}{\omega_1+\omega_0-\lambda^{(1)}_{l_1}}. \tag{10.18}$$

This expression provides an exact description of two-photon scattering, and while it is unwieldy for all but the simplest scatterers, it does allow for an efficient numerical calculation of photonic correlation effects showing up in two photon scattering.

Quasi-local scatterers

In the previous section we ensured the fulfillment of the Markovianity conditions by restricting ourselves to local scatterers, and this approach provided us with both a simple and exact solution of the scattering problem.

We now turn to systems where the channels couple non-locally to the scatterer, such that coupling points on some channel are separated by distances greater than the relevant wave-length, $\omega_0|x_n - x_m| \gtrsim 1$. The dynamics of such systems is in general non-Markovian.

However, there exists a quasi-local regime, where we can still obtain trustworthy results by applying Markov-type simplifications to the dynamics. In this regime, the non-Markovian effects originating from higher order scattering diagrams, which renormalize bare vertices and therefore lie beyond the set of diagrams shown in Fig. 11.3, are perturbatively small, as long as the condition

$$D_{nm} = \pi|g_n g_m||x_n - x_m| \ll 1 \tag{10.19}$$

is fulfilled. This condition means that the scatterer's state is unlikely to decay on time scales of a field propagation between two coupling points. In addition to Eq. (10.19) we also assume that

$$||M\omega_0 - H^{(M)}_{\rm sc}|| \cdot |x_n - x_m| \ll 1, \text{ for all } m \tag{10.20}$$

This condition implies that the scatterer's internal energy scales – as characterized by its detunings and nonlinearities – do not substantially contribute to the propagation phase on a typical distance between two coupling points. In other words, the scatterer dynamics in the co-rotating frame is frozen during the field propagation from one coupling point to the next one.

The insignificance of non-Markovian effects in the regime of parameters restricted by the conditions in Eq. (10.19) and Eq. (10.20) has been explicitly checked in Ref. [27] for a model of two two-level systems coupled to a bi-directional waveguide at different points by considering the quasi-local limit of the exact analytic non-Markovian solution derived for this model.

The Markovian approximation in the quasi-local case – relying on the conditions Eq. (10.19) and Eq. (10.20) – is achieved on the basis of the same diagrams, shown in Fig. 11.3, as in the local case. However, it is necessary to additionally specify the values of their constituent dressed Green's functions and bare vertices.

At the outset, a model with a quasi-local coupling–in contrast to its local counterpart–allows for the coupling to have mode-dependent phase factors, as appearing in Eq. (10.4). This dependence is essential in calculating the self-energy from Eq. (10.9). It leads to the dependence of $\tilde{\Sigma}_{nm}$ on the ordering of the coupling points along the coordinate axis of the relevant channel. In particular,

$$\begin{aligned}
\tilde{\Sigma}_{nm}(E) &= \left\langle V_n \frac{1}{E - H_0 + i0^+} V_m \right\rangle_{\rm chs} \\
&= \delta_{\sigma_n,\sigma_m} g_n g_m^* \\
&\times b^\dagger_{j_n} \left(\int_{-\infty}^{\infty} {\rm d}\omega \, \frac{e^{i(\omega_0+\omega)(x_n-x_m)}}{E - \omega - \omega_0 - H_{\rm sc} + i0^+} \right) b_{j_m} \\
&= -2i\pi g_n g_m^* \delta_{\sigma_n,\sigma_m} \Theta(x_n - x_m) \\
&\quad \times b^\dagger_{j_n} e^{i)E - H_{\rm sc})(x_n - x_m)} b_{j_m}.
\end{aligned} \tag{10.21}$$

Here the Heaviside step function is conveniently defined such that $\Theta(0) = \frac{1}{2}$. In the derivation of Eq. (10.21) we made use of a linear channel dispersion. Mathematically the difference between the two possible orderings of

the coupling points stems from the condition whether the phase factor allows us to close the integration contour in either the upper or lower complex half-plane.

According to Eq. (10.8) we find the dressed Green's function of the scatterer

$$G(E) = \frac{1}{E - H_{\rm chs} - H_{\rm sc} - \tilde{\Sigma}(E - H_{\rm chs})}, \tag{10.22}$$

where $\tilde{\Sigma} = \sum_{n,m} \tilde{\Sigma}_{nm}$. It can be also decomposed into a sum of contributions with different photon numbers M,

$$G^{(M)}(E) = \frac{1}{E - H_{\rm chs} - H_{\rm sc}^{(M)} - \tilde{\Sigma}^{(M)}(E - H_{\rm chs})}. \tag{10.23}$$

We see that Eq. (10.23), however, does not have the Markovian form inherent to its local counterpart Eq. (10.14): because of the functional dependence of $\tilde{\Sigma}^{(M)}$ on $E - H_{\rm chs}$ the Green's function in Eq. (10.23) might have more than d_M poles.

We can enforce the Markov approximation for quasi-local scatterers, assuming that the initial state consists of N photons, all having the same frequency ω_0. Then, the approximation

$$G^{(M)}(N\omega_0) \approx \frac{1}{N\omega_0 - H_{\rm chs} - H_{\rm sc}^{(M)} - \tilde{\Sigma}^{(M)}(M\omega_0)} \tag{10.24}$$

allows us to introduce the effective scatterer Hamiltonian $H_{\rm eff}^{(M)} = H_{\rm sc}^{(M)} + \tilde{\Sigma}^{(M)}(M\omega_0)$ and to finally bring Eq. (10.23) to the form of Eq. (10.14).

We note that the approximation in Eq. (10.24) is consistent with the quasi-local condition of Eq. (10.19). Indeed, expanding $\tilde{\Sigma}^{(M)}(E - H_{\rm chs})$ around $M\omega_0$ up to a linear term, we obtain a correction to $E - H_{\rm chs} - H_{\rm sc}^{(M)}$ in Eq. (10.14), which is smaller by a factor of the order of D_{nm} than the leading term.

Using the condition in Eq. (10.20), we can additionally simplify $\tilde{\Sigma}^{(M)}(M\omega_0)$. From Eq. (10.21) it follows

$$\begin{aligned}\tilde{\Sigma}_{nm}^{(M)}(M\omega_0) &= -2i\pi g_n g_m^* \delta_{\sigma_n,\sigma_m} \Theta(x_n - x_m) \\ &\quad \times b_{j_n}^\dagger e^{i)M\omega_0 - H_{\rm sc}^{(M-1)})(x_n - x_m)} b_{j_m} \\ &\approx -2i\pi g_n g_m^* \delta_{\sigma_n,\sigma_m} \Theta(x_n - x_m) \\ &\quad \times b_{j_n}^\dagger b_{j_m} e^{i\omega_0(x_n - x_m)}.\end{aligned} \tag{10.25}$$

Thus, computing a scattering matrix for a quasi-local scatterer is possible on the basis of the diagrams in Fig. 11.3 and the associated diagrammatic rules described in the previous subsection. Additionally, the dressed Green's functions must be approximated by Eq. (10.24), where the self-energies are given by Eq. (10.25) instead of Eq. (10.12). Finally, bare vertices in the diagrams of Fig. 11.3(d,e) must be replaced by

$$V_n \to \tilde{V}_n = \int \mathrm{d}\omega \, (g_n e^{i\omega_0 x_n} b_{j_n}^\dagger a_{\sigma_n,\omega} + h.c.). \tag{10.26}$$

The reason for neglecting the phase factor $e^{i\omega x_n}$ in the above expression is based on the observation that the diagrams in Fig. 11.3 produce poles in the functional dependence of T matrix on frequencies $\omega_1', \omega_2', \ldots$, which are located at points $\lambda_{l_M}^{(M)} - M\omega_0$ in the lower half of the frequency complex plane (see e.g. Eq. (10.18)). Therefore, the contribution of the aforementioned phase factors can be estimated by $\exp\left(-i(\lambda_{l_M}^{(M)} - M\omega_0)|\Delta x|\right) \approx 1$, in accordance with Eq. (10.19) and Eq. (10.20). Note that these two quasi-locality conditions can be combined into a single one

$$|\lambda_{l_M}^{(M)} - M\omega_0||\Delta x| \ll 1. \tag{10.27}$$

Observables

Since scattering matrices are naturally expressed in terms of the non-normalizable eigenbases of the channels, special care must be taken in applying scattering theory to real, physical states. We construct such physical incoming states as rectangular wave packets quantified by their width L, central coordinate x_c, channel σ_0, and working frequency ω_0

$$\begin{aligned}\mathcal{A}_{\sigma_0,\omega_0;x_c}^\dagger &= \frac{1}{\sqrt{L}} \int_{x_c - L/2}^{x_c + L/2} \mathrm{d}x \, a_{\sigma_0}^\dagger(x) e^{i\omega_0 x} \\ &= \int_{-\infty}^{\infty} \mathrm{d}\omega \, e^{-i\omega x_c} \phi(\omega) a_{\sigma_0\omega}^\dagger.\end{aligned} \tag{10.28}$$

In the interaction picture, in which the scattering formalism is formulated, we have

$$e^{iH_0t}\mathcal{A}^\dagger_{\sigma_0,\omega_0;x_c}e^{-iH_0t} = e^{i\omega_0 t}\mathcal{A}^\dagger_{\sigma_0,\omega_0;x_c-t}. \tag{10.29}$$

The convolution function, $\phi(\omega) = \sqrt{L/(2\pi)}\,\mathrm{sinc}(\omega L/2)$, approaches $\sqrt{2\pi/L}\delta(\omega)$ in the wide packet limit, $L \to \infty$. Therefore Eq. (10.29) can be approximated by $e^{i\omega_0 t}\mathcal{A}^\dagger_{\nu_0} = \mathcal{A}^\dagger_{\nu_0}(t)$, where $\mathcal{A}^\dagger_{\nu_0}$ is the normalized wavepacket operator,

$$\mathcal{A}^\dagger_{\nu_0} = \int_{-\infty}^{\infty} \mathrm{d}\omega\, \phi(\omega) a^\dagger_{\sigma_0\omega}, \quad \int_{-\infty}^{\infty} \mathrm{d}\omega\, |\phi(\omega)|^2 = 1. \tag{10.30}$$

We focus in the following exclusively on the scattering of weakly coherent states. Creating an incoming coherent state, which is written in the interaction picture as

$$|\phi_{\nu_0}\rangle = e^{-\bar{n}/2}e^{-\sqrt{\bar{n}}\mathcal{A}^\dagger_{\nu_0}(t)}|0,0\rangle, \quad |0,0\rangle = |0\rangle_{\mathrm{chs}}|0\rangle, \tag{10.31}$$

we assume that the mean number of photons $\bar{n}$ is small, and perform an expansion of $|\phi_{\nu_0}\rangle$ in this parameter. The resulting scattering state $|S\phi_{\nu_0}\rangle$ is given by the scattering matrix, and up to two-photon contribution we find

$$\begin{aligned}&|S\phi_{\nu_0}\rangle \\ &\approx e^{-\bar{n}/2}\left(1 + \sqrt{\bar{n}}S^{(1)}\mathcal{A}^\dagger_{\nu_0}(t) + \frac{\bar{n}}{2}S^{(2)}(\mathcal{A}^\dagger_{\nu_0}(t))^2\right)|0,0\rangle\,.\end{aligned} \tag{10.32}$$

The properties of this state can be characterized through the measurement of the first and second order correlation functions.

The first order correlation function is given by

$$g^{(1)}_{\sigma_0,\sigma}(\tau) = \langle S\phi_{\nu_0}|a^\dagger_\sigma(x-t-\tau)a_\sigma(x-t)|S\phi_{\nu_0}\rangle, \tag{10.33}$$

where the operators $a^\dagger_\sigma$, a_σ are also written in the interaction picture. To leading order in $\bar{n}$, it can be expressed

$$\begin{aligned}g^{(1)}_\sigma(\tau) &\approx \bar{n}\langle 0,0|\mathcal{A}_{\nu_0}(t)S^{(1)\,\dagger}a^\dagger_\sigma(x-t-\tau) \\ &\qquad \times a_\sigma(x-t)S^{(1)}\mathcal{A}^\dagger_{\nu_0}(t)|0,0\rangle \\ &\approx f e^{i\omega_0\tau}|s^{(1)}_{\sigma\sigma_0}|^2,\end{aligned} \tag{10.34}$$

where $f = \bar{n}/L$ is the photonic flux and

$$s^{(1)}_{\sigma_0,\sigma} = \delta_{\sigma\sigma_0} - 2\pi i\sum_{l_1=1}^{d_1}\frac{\langle 0|\tilde{b}_\sigma|1,l_1\rangle\langle\overline{1,l_1}|\tilde{b}^\dagger_{\sigma_0}|0\rangle}{\omega_0 - \lambda^{(1)}_{l_1}}, \tag{10.35}$$

originates in Eq. (10.15) and Eq. (10.16). The components of Eq. (10.35) contain the single-photon transmission ($\sigma \neq \sigma_0$) or reflection ($\sigma = \sigma_0$) amplitudes. This expression is general and well-known from any single particle transport theory, and due to the Fisher-Lee relation it is identical to the Landauer-Büttiker scattering matrix [41]. Unless stated otherwise we discuss $g^{(1)}_{\sigma\sigma_0}(0)$, i.e. does not include the phase factor.

Interaction effects within two-photon scattering are available to experiments through the second order intensity correlation function, measurable in a Hanbury Brown and Twiss setup [42], where the time offset, τ, is directly translatable into real-space detection points, Δx, due to our assumption of a linear channel dispersion. The correlation of the scattered state is directly given by,

$$\begin{aligned}g^{(2)}_{\sigma_0\sigma_0,\sigma\sigma'}(\tau) = \frac{1}{g^{(1)}_\sigma(0)g^{(1)}_{\sigma'}(0)}&\langle S\phi_{\nu_0}|a^\dagger_{\sigma'}(x-t)a^\dagger_\sigma(x-t-\tau) \\ &\cdot a_\sigma(x-t-\tau)a_{\sigma'}(x-t)|S\phi_{\nu_0}\rangle.\end{aligned} \tag{10.36}$$

Appendix 10.0.8 details the analytical calculation of the $g^{(2)}$ correlation function for complex scatterers. The intensity-intensity correlation function probes the effects of photon-photon interaction present within the scattering structure: Such correlations disappear in the absence of such photon-photon interactions ($g^{(2)} = 1$), while the presence of any photon-photon interactions may either lead to photon bunching ($g^{(2)} > 1$) or photon anti-bunching ($g^{(2)} < 1$).

When the $g^{(1)}$ or $g^{(2)}$correlation functions involves different incoming and outgoing channels, their analytical expressions can be written very compactly. Specifically the expressions in Eq. (10.33) and Eq. (10.75) simplify to,

$$g^{(1)}_{1,2}(\tau) = f e^{i\omega_0\tau}\left|A^{(1)}_{1,2}(0)\right|^2, \tag{10.37}$$

$$g^{(2)}_{11,22})\tau) = \left|1 - \frac{A^{(1)}_{1,2}(\tau)}{A^{(1)}_{1,2}(0)} + \frac{A^{(2)}_{11,22}(\tau)}{)A^{(1)}_{1,2}(0))^2}\right|^2, \tag{10.38}$$

Here the one- and two-photon amplitudes are given by,

$$A^{(1)}_{1,2}(\tau) = \langle 0|\tilde{b}_2 e^{i(\omega_0 - H_{\text{eff}})\tau} G^{(1)} \tilde{b}^\dagger_1|0\rangle, \tag{10.39}$$

$$A^{(2)}_{11,22}(\tau) = \langle 0|\tilde{b}_2 e^{i(\omega_0 - H_{\text{eff}})\tau} \tilde{b}_2 G^{(2)} \tilde{b}^\dagger_1 G^{(1)} \tilde{b}^\dagger_1|0\rangle. \tag{10.40}$$

Here, it is worth noting that $g^{(2)}$ is a relative measure of correlation, and strong correlation effects in $g^{(2)}$ are caused by dramatic changes happening in either the $A^{(1)}$ amplitude in the denominator of Eq. (10.38) or the two-photon amplitude $A^{(2)}$ in the numerator of Eq. (10.38). In the results section we find that dramatic two photon correlation effects are most often associated with destructive interference effects in the single photon amplitude, $A^{(1)}$ leading to (relatively speaking) strong bunching of photons. Strong anti-bunching ($g^{(2)} < 1$) is the less common (hence, also more interesting) effect to achieve since it is most often associated with destructive two-photon interference phenomena (as expressed by the $A^{(2)}$ numerator of Eq. (10.38)).

10.0.4 Results

While the above expression can be evaluated analytically for simple systems, our final goal is to study complex extended scattering structures. To this end we have implemented the single and two photon correlation functions numerically in the Python programming language using the numpy package. The babusca code – made available in the supplementary material – is modular and flexible and makes it possible to construct arbitrary scattering systems composed of multiple chiral channels coupled to a Bose-Hubbard scatterer. For weakly coherent incident photons the code computes the single and two-photon correlation functions in the Markov approximation for systems with up to approximately a hundred sites on current standard equipment.

As a pedagogical prelude, we consider transport through a single non-linear cavity; then turn to the dimer, which we discuss thoroughly, including an example of quasi-local coupling. We then investigate chain and ring geometries, and then finish by demonstrating how the scattering method also easily deals with larger scatterers by considering an 8 by 8 square lattice penetrated by an artificial magnetic field and supporting quantum Hall edge states.

We fix the channel couplings of the incoming and outgoing channels, $\sum_\sigma \frac{1}{2}\Gamma_\sigma = \sum_\sigma \frac{1}{2}\pi g^2_\sigma = 1$, effectively expressing the Bose-Hubbard parameters in units of this channel coupling. Because the Bose-Hubbard hopping amplitudes, t, determine the relevant bandwidth of the scatterer, we may in general associate strong channel coupling with weak hopping, $t \sim \Gamma$, and weak channel coupling with strong hopping, $t \sim 10\Gamma$.

For each lattice we compute both the single-photon and two-photon correlations for weakly coherent incident photonic states, and plot the results as a function of the two-photon detuning, $2\delta = 2(\omega_0 - \langle\varepsilon\rangle)$, where the averaged onsite energy $\langle\varepsilon\rangle = 1/N_s \sum_{i=1}^{N_s} \varepsilon_i$.

The Kerr non-linear element

We begin with a discussion of the simplest possible scattering setup: a single Bose-Hubbard site coupled symmetrically to two chiral channels. The scatterer Hamiltonian,

$$H_{\text{sc}} = \varepsilon b^\dagger_1 b_1 + \frac{U}{2} b^\dagger_1 b_1 (b^\dagger_1 b_1 - 1), \tag{10.41}$$

is characterized by a single resonance frequency, ε, and the photon-photon interaction, U.

Due to its simplicity, this scattering setup have been realized on several experimental platforms by e.g. coupling a non-linear cavity to a one-dimensional transmission line [43]. Consequently, the analytical form of the coherence functions are well-known when driving the setup at both high and low power [44, 16, 45, 15]. Thus, our goal in this section is pedagogical: to show how to derive the coherence functions in diagrammatic scattering theory, and to interpret the physics behind these results.

Our single site scatterer is locally coupled, and its effective Hamiltonian, $H_{\text{eff}} = H_{\text{sc}} + \Sigma$, trivially supports a single (right) eigenstate in each M-photon sector, $|\lambda^{(M)}\rangle$, with eigenvalue, $\lambda^{(M)}$, as given by

$$|\lambda^{(0)}\rangle = |0\rangle, \qquad \lambda^{(0)} = 0, \tag{10.42}$$

$$|\lambda^{(1)}\rangle = b^\dagger_1 |0\rangle, \qquad \lambda^{(1)} = \varepsilon - i\Gamma, \tag{10.43}$$

$$|\lambda^{(2)}\rangle = \tfrac{1}{\sqrt{2}}(b^\dagger_1)^2 |0\rangle, \qquad \lambda^{(2)} = 2\varepsilon + U - 2i\Gamma. \tag{10.44}$$

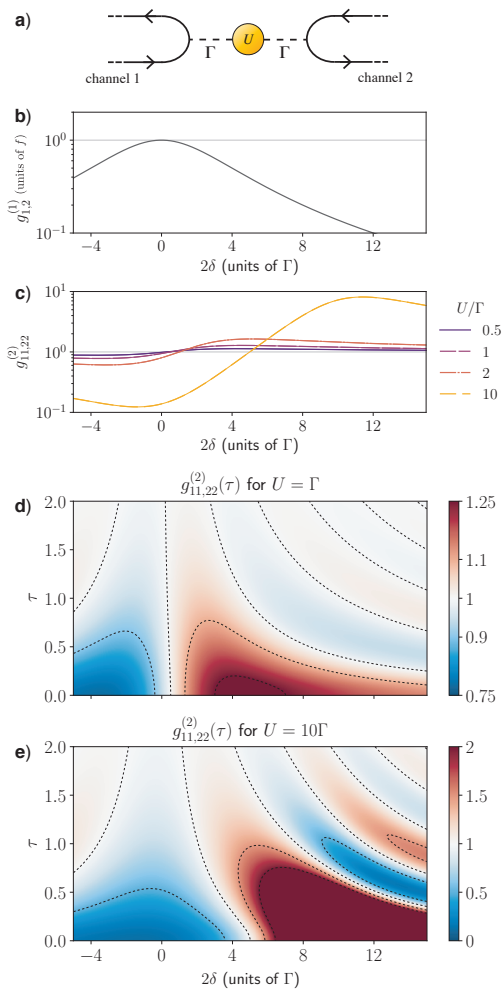

Figure 10.4: A single Bose-Hubbard site with an interaction, U, coupled to two chiral channels. (**a**) The Lorentz shaped $g^{(1)}_{12}$ correlation (or transmission) between channel 1 and 2, with a resonant peak around zero detuning, $\delta = 0$. (**b**) The second order correlation function $g^{(2)}_{11,22}$ showing an anti-bunching dip around the single photon resonance and a bunching top around the two-photon resonance at $2\delta \approx U$. A large interaction, U, effectively disadvantages the doubly-occupied state, producing an effective two-level system and giving rise to strong photon anti-bunching. (**c**) Delayed $g^{(2)}$ for intermediate $U = \Gamma$ exponential and oscillating falloff with increased delay, τ. (**d**) Delayed $g^{(2)}$ for strong $U = 10\Gamma$ showing the clear asymmetry but identical oscillating period in the decay of the correlations with respect to delay time, τ.

We imagine sending in photons in one channel and measuring the scattered photons in the second channel. The low order coherence functions are given by the scattering amplitudes of Eq. (10.39)-(10.40), which are calculated to be,

$$A^{(1)}_{1,2} = e^{i(\delta+2i\Gamma)}\frac{2i\Gamma}{\delta+2i\Gamma} \tag{10.45}$$

$$A^{(2)}_{11,22} = 4\Gamma^2 e^{i(\delta+2i\Gamma)\tau}\frac{1}{\delta+2i\Gamma-U/2}\frac{1}{\delta+2i\Gamma} \tag{10.46}$$

Allowing us to calculate the correlation functions,

$$g^{(1)}_{1,2} = f e^{i\omega_0\tau}\left|\frac{2\Gamma}{\delta+2i\Gamma}\right|^2 \tag{10.47}$$

$$g^{(2)}_{11,22} = \left|1 - e^{i(\delta+2i\Gamma)\tau}\left(1 - \frac{\delta+2i\Gamma}{\delta+2i\Gamma-U/2}\right)\right|^2 \tag{10.48}$$

The single photon correlation function, as given by Eq. (10.47), is a simple Lorentzian which allows for a single photon on resonance, $\delta = \omega_0 - \varepsilon = 0$, to perfectly transmit between the two attached channel. Figure 10.4(b) shows this first order correlation as a function of the detuning.

The $g^{(2)}$ correlation function, Eq. (10.48), has a more complicated shape, as shown in Fig. 10.4(c) for different interaction strengths, U/Γ. The dip-peak shape – which we later refer to as a Kerr signature – shows how the photon-photon interaction shifts the two-photon resonance at $2\delta = U$ away from the single photon resonance. At a large enough non-linear strength $U \gg \delta$ the system can effectively be modeled as a two-level emitter, showing up in the correlations through a strong anti-bunching, $g^{(2)} \ll 1$, of the transmitted photons as shown in Fig. 10.4(c) for $U = 10\Gamma$.

For finite delay times between the detected photons, the two-photon correlation, $g^{(2)}(\tau)$, is plotted in Fig. 10.4(d-e) as functions of both detuning and delay time. The correlations oscillate between bunching and anti-bunching with a frequency set by the detuning, δ, and a fall-off towards unity set by the total coupling strength, 2Γ.

This oscillation can be interpreted as arising from the extra phase picked up by the second photon during the delay after the first one left the scatterer. For detunings, $\delta \sim U/2$, the photons are bunched at zero delay $\tau = 0$ because the two photons scatter close to resonance, while the two photons anti-bunch at longer delay times. The multiple terms of Eq. (10.48) can be directly interpreted as either the elastic or the inelastic scattering amplitudes. The scattering phase shift between the inelastic an elastic contributions then readily creates the more complex oscillations patterns in the delayed correlations as shown for $U = 10\Gamma$ in Fig. 10.4(d-e).

The Dimer

Next, consider a Bose-Hubbard dimer consisting of two coupled Bose-Hubbard sites characterized by their resonance energies $\varepsilon_{1/2}$, nonlinear strengths, $U_{1/2}$, and mutual coupling strength, t.

The dimer parameters and the possible contacting combinations already presents an impossibly large parameter space to explore. So far, parts of this space have been investigated numerically for both weak input power [18, 31, 30], and for coherent input states of arbitrary power [46]. In the following we show how to obtain and interpret some of these results for three different contacting geometries: parallel, perpendicular and side-coupled quasi-local.

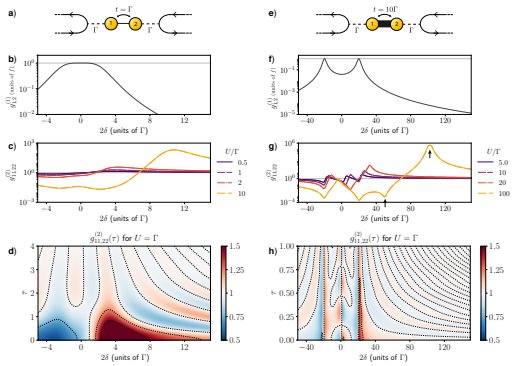

Figure 10.5: Single-particle transmission and intensity-intensity correlation $g^{(2)}$ as a function of detunings for various strength of the interaction, U, through **(a - d)** the dimer with intermediate hopping, $t = \Gamma$, which behaves like a single non-linear cavity with an effectively smaller coupling. **(e-h)** The dimer with strong hopping, $t = 10\Gamma$, where **(g)** shows interference features between the sharply resolved two-photon resonances, and **(h)** shows how the delayed correlation for $U = \Gamma$ distinguishes the three resonances, showing a clear difference to the single-cavity case in the oscillations around $2\delta = U = \Gamma$.

The isolated ($\Gamma = 0$) and isotropic ($\varepsilon_1 = \varepsilon_2 = \varepsilon$ and $U_1 = U_2 = U$) dimer supports two single-photon states,

$$|\psi^{(1)}_{l_1=\pm}\rangle = \frac{1}{\sqrt{2}}(|1,0\rangle \pm |0,1\rangle), \qquad E^{(1)}_{l_1=\pm} = \varepsilon \pm t. \tag{10.49}$$

and three (here unnormalized) two-photon states:

$$\begin{aligned} |\psi^{(2)}_{l_2=0}\rangle &\propto |2,0\rangle - |0,2\rangle, \\ |\psi^{(2)}_{l_2=\pm}\rangle &\propto \alpha_\pm)|2,0\rangle + |0,2\rangle) \pm |1,1\rangle, \end{aligned} \tag{10.50}$$

with eigenenergies

$$\begin{aligned} E^{(2)}_{l_2=0} &= 2\varepsilon + U, \\ E^{(2)}_{l_2=\pm} &= 2\varepsilon + 2\sqrt{2}t\alpha_\pm, \end{aligned} \tag{10.51}$$

given by the parameters,

$$\alpha_{\pm} = \frac{1}{\sqrt{2}}\left(U/(4t) \pm \sqrt{U^2/16t^2+1}\right). \tag{10.52}$$

First, we couple each of the two dimer sites uniformly to their own separate chiral channel as shown in Fig. 11.9(a). For this contacting geometry, the self-energy is proportional to the total photon number, $\Sigma^{(M)} = -iM\Gamma$, which shifts the effective Hamiltonian within each photon number block, $H^{(M)} = H_{\rm sc}^{(M)} + \Sigma^{(M)}$, the corresponding constant. The coupled and the isolated dimers then share eigenstates, $|M, l_M\rangle = |\psi_{l_M}^{(M)}\rangle$, with eigenvalues offset by the imaginary contribution from the self-energy, $\lambda_{l_M}^{(M)} = E_{l_M}^{(M)} - iM\Gamma$.

The uniformly coupled dimer allows for simple analytical expressions of the zero-delay amplitudes,

$$A_{1,2}^{(1)} = -2i\Gamma\frac{t}{(\delta+i\Gamma)^2 - t^2} \tag{10.53}$$

$$A_{11,22}^{(2)} = 4\Gamma^2\frac{1}{4(\delta+i\Gamma)^2 - (\delta+i\Gamma)U - 4t^2} \times \frac{2t^2}{(\delta+i\Gamma)^2 - t^2}\left(\frac{2(\delta+i\Gamma)}{2(\delta+i\Gamma)-U} + 1\right) \tag{10.54}$$

with corresponding zero-delay correlation functions,

$$g_{1,2}^{(1)} = f|A_{1,2}^{(1)}|^2, \tag{10.55}$$

$$g_{11,22}^{(2)} = \left|\frac{A_{11,22}^{(2)}}{(A_{1,2}^{(1)})^2}\right|^2. \tag{10.56}$$

Note that Eq. (10.54) now contain two terms. It turns out these terms originate in Eq. (10.40) from two pathways the two-photon system can follow. The two pathways split off after the first photon enters the site, and either propagate to its initial site or to the other site before the second photon enters. This interpretation is also depicted graphically in Fig. 10.6.

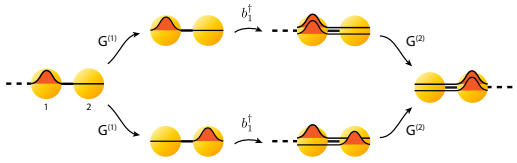

Figure 10.6: Dimer interference pathways interpretation of the numerator of the last term in Eq. (10.38) as given by Eq. (10.40). Starting from the left the first photon enters the dimer, and propagation of the single photon Green's function places the photon in a superposition between the two sites of the dimer. In the site basis the two dimer sites then represent the two paths which in this case gives rise to destructive interference.

We now distinguish between dimers with intermediate and strong hopping, t. For intermediate hopping $t \sim \Gamma$ we plot the first and second order correlation functions in Fig. 11.9(b-d). The qualitative similarity with the single non-linear cavity in Fig. 10.4 is obvious. It arises from the coupling induced level broadening for weak hopping, $t \leq \Gamma$, which does not allow the resolution of the individual dimer states. Instead the dimer behaves as a single collective level with an reduced effective coupling, $\tilde{\Gamma} = (\Gamma^2 + t^2)/(2\Gamma) < \Gamma$, due to the total coupling being distributed over two sites instead of one. This effectively reduced coupling increases the magnitude of the correlation effects compared to that of a single non-linear Kerr element, as shown in Fig. 11.9(b) for the uniformly coupled dimer with an intermediate hopping.

For strong hopping, $t = 10\Gamma$, the correlation functions easily resolve the individual levels as seen in Fig. 11.9(f-g). For weak interaction strengths, $U < \Gamma$, the two-photon correlation function maintains characteristic dip-peak Kerr signatures for each of the three two-photon states.

While each of the three Kerr signatures correspond to a two-photon state, the delayed two-photon correlations clearly distinguishes the three. For weak interactions, $U \sim \Gamma$, the two side signatures at $2\delta \approx \pm 2t$ both arise from coinciding one- and two-photon states. The signature around $2\delta \approx U$ arises from a single two-photon state which does not correspond to any single-photon state. In the delayed second order correlations this difference shows up in the oscillations, since only the middle signature oscillates rapidly between bunching and anti-bunching.

The physical explanation of this oscillation is straightforward. The relevant two-photon state is the doublonic, $|2,0\rangle$, which has no components with only one photon per site. After the first photon has left the dimer,

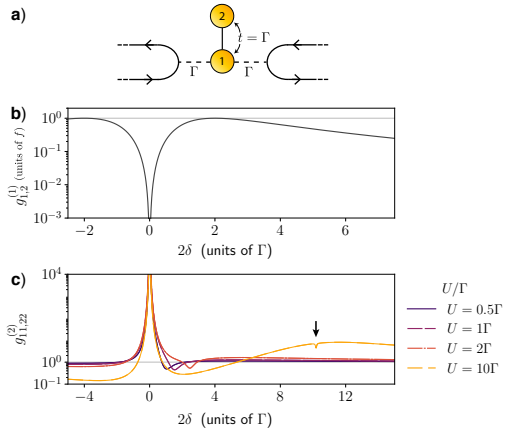

Figure 10.7: The strongly coupled dimer in the side-coupled configuration. A strong destructive interference node is induced in the single-photon transmission at zero detuning as predicted by the MST rules [48]. This induces a strong bunching effect in the $g^{(2)}$ correlations. Likewise, another interference node – of the same geometric origin – appears in the two-photon correlation function around $2\delta = U$ when adequately separated from the single photon resonances.

the remaining photon may perform Rabi-like oscillations between the two dimer states, thus changing the statistics at a rate proportional to the hopping between the dimer sites. For the strong hopping case ($t = 10\Gamma$) this induces oscillations of a period $T = 2\pi/10 \approx 1.59$ which fits the plot in Fig. 11.9(h).

At strong photon-photon interactions, $U \geq 4t$, however, the $g^{(2)}$ correlations undergoes a qualitative change due to quantum interference arising from the mixing of the two-photon states as described by Eq. (10.54); this is also briefly mentioned in Ref. [18]. The last parenthesis in Eq. (10.54) is the origin of the interference, which is destructive for small detunings $\delta < U$, and reaches a minimum value of $4i\Gamma/(-U/2 + 2i\Gamma)$ at $\delta = U/4$, thus confirming that the destructive interference becomes most pronounced in the limit of large interactions $U \gg \Gamma$, as already evident in Fig. 11.9(g). We shall see that this destructive interference in the two-photon sector is a common trait of all parallel coupled chains.

A Perpendicularly Coupled Dimer

Quantum interference effects within the scatterer may render it completely transparent to single photons. A uniform Bose-Hubbard dimer connected in a perpendicular configuration, Fig. 10.7(a), constitutes a simple example of interference induced transparency.

As shown in Fig. 10.7(b) this setup is transparent to single photons at zero detuning, meaning that the transmission between the two connected channels vanishes, and single photons are allowed to propagate in their initial channel as if uninterrupted by the scatterer.

Even slight non-linearities make the setup less transparent to two-photon states. This small discrepancy in the transparency of one- and two-photon states filters out the single-photon component of the incoming light, visible in Fig. 10.7)(c) as a strong bunching peak in $g^{(2)}$ for the "reflected" weakly coherent light around zero detuning. For coherent input this huge bunching peak is to be "cut off" at a scale set by the inverse photon flux $1/f = L/(v\bar{n})$ due to higher order contributions to the few-photon expansion of $g^{(2)}$ [28].

The transparency is perhaps unsurprising since our perpendicularly coupled dimer realizes a dressed state picture of the pumped three-level system (in a V or linear configuration). These three level systems serve as the prime example of electromagnetically induced transparency, as found experimentally by e.g. Abdumalikov *et al.* [47].

Transparency due to destructive single-photon interference also shows up in more elaborate lattice geometries, when the overall one-dimensionality of the scatterer and the coupling is broken, as for the perpendicularly coupled dimer. Such interference nodes can partly be predicted by the Markussen-Stadler-Thygesen (MST) rules [48], as we will discuss later for the ring geometry.

For strong enough non-linearities the transparency node in the single-photon transmission also shows up in the two-photon correlations. The transparency is visible in Fig. 10.7 as a dip in the $g^{(2)}$ correlation around detunings $2\delta \sim U$. We can explain this behavior by looking at the generalized two-photon eigenstates. At large non-linear strengths, $U \gg t$, the three two-photon states in Eq. (10.50) split into the doublonic states, $|0, 2\rangle$ and $|2, 0\rangle$, which energetically decouple from the hardcore photonic state, $|1, 1\rangle$. The doublonic subsystem is effectively similar to the single photon system, $|0, 1\rangle$ and $|1, 0\rangle$, with a mutual coupling $4t/U$. This similarity carries the single-photon transparency over to the two-photon sector, and similarly induces a two-photon transparency that is offset by the doublon energy, $2\delta \sim U$. This correspondence between single photon and doublonic two-photon states is a general feature of few-photon scattering, and we will address it explicitly when discussing chain scatterers.

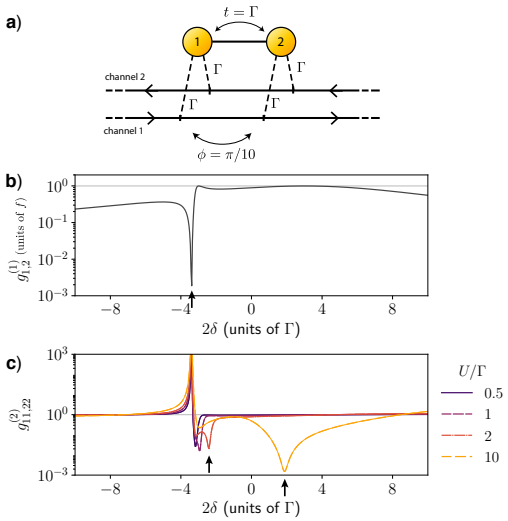

Figure 10.8: **(a)** Quasi-locally coupled dimer, where each channel couples at multiple points. Within the quasi-local regime the coupling points are fully characterized by the phase difference, ϕ. **(b)** The transmission between the two channels show a destructive interference induced transparency around $\delta = -t$

A Quasi-Locally Coupled Dimer

The dimer can also be coupled to the channels at multiple points, a setup which we can model in the quasi-local limit. We consider side-coupling the dimer symmetrically to both channels, where

$$V = \sum_{\sigma} \sum_{i \in \{1,2\}} (g e^{i\omega_0 x_i^\sigma} a_\sigma^\dagger b_i + h.c.), \tag{10.57}$$

The setup is shown schematically in Fig. 10.8(a) with the relevant phase-shift, $\phi = (x_2^1 - x_1^1)\omega_0 = (x_1^2 - x_2^2)\omega_0$, between the two coupling points.

The self-energy then becomes non-diagonal in the scatterer basis,

$$\Sigma^{(M)} = -2i\Gamma(M + b_2^\dagger b_1 e^{i\phi} + b_1^\dagger b_2 e^{-i\phi}). \tag{10.58}$$

This self-energy modifies the generalized eigenvalues of the dimer in a different way than for the linearly coupled dimer. For vanishing phase shifts, $\phi \approx 0$, the single-photons eigenfunctions are still given by the symmetric and anti-symmetric states of Eq. (10.50), while the generalized eigenvalues become,

$$\lambda_\pm^{(1)} = \varepsilon \pm t - 2i(1 \pm 1)\Gamma. \tag{10.59}$$

This means that the anti-symmetric $|\psi_-^{(1)}\rangle$ state has a vanishing imaginary part and hence decouples from the channels, making the symmetric state the only accessible single-photon state.

When the phase shift ϕ is non-zero the anti-symmetric state is no longer completely isolated. The single photon transmission between channels is shown in Fig. 10.8(b) for $\phi = \pi/10$. For small phase differences the re-coupling to the anti-symmetric state also gives rise to destructive quantum interference and an accompanying single photon transparency.

However, in contrast to the side-coupled dimer, the two-photon correlations also develop a strong and distinct anti-bunching feature around detunings $2\delta \approx U - 2(t + \Gamma)$ as shown in Fig. 10.8(c), and visible for even very small interaction strengths. While we do not go into details here, the results can be interpreted using a diagram similar to Fig. 10.6.

The Parallel Coupled Chain

Longer Bose-Hubbard chains support many more single and two-photon states.

Starting our analysis with an (isolated) uniform Bose-Hubbard chain of length, N_s, its single particle eigenstates are naturally indexed by their standing wave numbers $k = n\pi/(N_s + 1)$ also corresponding to the number of wave-function anti-nodes, $n = 1, \ldots, N_s$. The eigenenergies follow a cosine spectrum, $E_k^{(1)} = \varepsilon + 2t\cos(k)$, and by numbering the chain sites sequentially the corresponding single-photon eigenstates can be written as,

$$|\psi_k^{(1)}\rangle = \sum_{i=1}^{N_s} \sqrt{\frac{2}{N_s + 1}} \sin(ki)\, b_i^\dagger |0\rangle, \tag{10.60}$$

We seek to understand the few photon states of the generalized Hamiltonian for uniform Bose-Hubbard chains with their first and last sites coupled to chiral channels. The generalized single photon states can be found exactly [49], but such solutions allow for little concrete interpretation and we instead choose to analyze the one photon and two photon states perturbatively in the limits of either weak or strong coupling, Γ, combined with either a weak, $U/\Gamma \ll 1$, or a strong nonlinearity $U/\Gamma \gg 1$. We will focus on their similarity with the dimer eigenstates.

In the limit of both weak coupling and weak nonlinearity, our starting point is the eigenstates of the non-interacting chain. Here, the one-photon states are given by Eq. 10.60 and the two-photon eigenstates are the direct products of two one-photon eigenstates,

$$|\psi^{(2)}_{k,q}\rangle_0 = \frac{2}{N_s+1}\sum_{i,j=1}^{N_s}\sin(qi)\sin(kj)b_i^\dagger b_j^\dagger|0\rangle, (k<q)$$
$$|\psi^{(2)}_{k,k}\rangle_0 = \frac{1}{\sqrt{2}}\frac{2}{N_s+1}\sum_{i,j=1}^{N_s}\sin(ki)\sin(kj)b_i^\dagger b_j^\dagger|0\rangle. \tag{10.61}$$

At first, we focus on the zero energy subspace spanned by the $N_s/2$ two photon states (for even N_s) which combine two single photon states of opposite wave numbers, $|\psi^{(2)}_{k,\pi-k}\rangle_0$, $k<\frac{\pi}{2}$. The non-linearity partially lifts their zero energy degeneracy, which can be seen by writing the interaction Hamiltonian in the basis of the subspace states,

$$\langle\psi^{(2)}_{k,\pi-k}|H_U|\psi^{(2)}_{q,\pi-q}\rangle =)1+\tfrac{1}{2}\delta_{k,q})\frac{2U}{N_s+1}. \tag{10.62}$$

A single two-photon state splits off from the rest of this subspace. Like the dimer doublon state, $|2,0\rangle$, this splinter state is also exclusively doublonic, and given by

$$|\phi^{(2)}_0\rangle = \sqrt{\frac{2}{N_s}}\sum_{n=1}^{N_s/2}|\psi^{(2)}_{k_n,\pi-k_n}\rangle$$
$$= \frac{1}{\sqrt{2N_s}}\sum_{i=1}^{N_s}(-1)^{i+1})b_i^\dagger)^2\,|0\rangle\,. \tag{10.63}$$

This is actually an exact eigenstate on the isotropic Bose-Hubbard chain, with the photon-photon interaction contributing to its eigenenergy $E^{(2)}_0 = 2\varepsilon+U$. In the perturbative analysis the rest $N_s/2-1$ states are degenerate with an energy $2\varepsilon+U/(N_s+1)$ despite the finite nonlinearity.

In the regime of strong photon-photon interactions, we focus on the doublonic subspace consisting solely of states where the two photons always occupy the same site. The effective subspace Hamiltonian can be expressed through the projection, $\mathcal{P}$, onto this doublonic subspace, and the projection, $\mathcal{Q}=1-\mathcal{P}$, onto its complement: the subspace containing "hard core" photonic states.

$$H^d = \mathcal{P}H_U\mathcal{P} + \mathcal{P}H_t\mathcal{Q}\frac{1}{E-H_t-H_U}\mathcal{Q}H_t\mathcal{P} \tag{10.64}$$
$$\approx U + \mathcal{P}H_t\mathcal{Q}\frac{1}{E}\mathcal{Q}H_t\mathcal{P}, \tag{10.65}$$

where in the last line we ignored contributions from additional hops beyond the initial hop which "splits" a doublon and the final hop which recreates it. The effective Hamiltonian for doublons on the lattice, spanned by $|2_i\rangle = \frac{(b_i^\dagger)^2}{\sqrt{2}}|0\rangle$, becomes

$$H^d \approx U + \frac{2t^2}{E}\sum_{i=1}^{N_s-1}(|2_{i+1}\rangle\langle 2_i| + h.c.)$$
$$+\frac{2t^2}{E}\sum_{i=1}^{N_s})2-\delta_{i,1}-\delta_{i,N_s})|2_i\rangle\langle 2_i|. \tag{10.66}$$

For long chains, $N_s \gg 1$, and strong interaction, $U \gg t$, the energy difference between the two subspaces is $E\approx U$, except for a small non-uniform onsite energy at the chain ends. This roughly demonstrates that the effective doublon Hamiltonian is similar to that of a single photon on the same chain with a slight discrepancy in the on-site energies at the chain ends. The two-photon eigenenergies in this subspace then form a cosine spectrum $E^d_k = 2\varepsilon+U+4t^2/U(1+\cos(k))$, and the eigenstates are here standing waves of doublons, $|\psi^d_k\rangle = \sqrt{2/(N_s+1)}\sum_{i=1}^{N_s}\sin(ki)|2_i\rangle$.

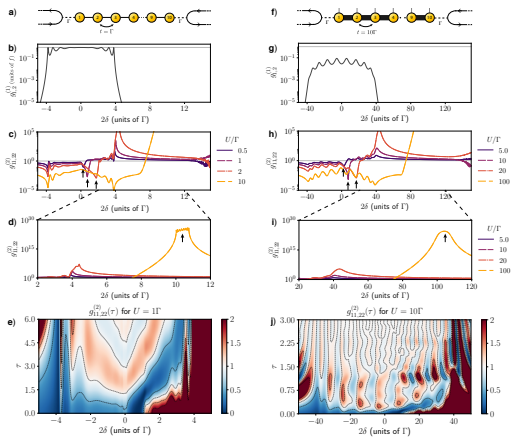

Figure 10.9: Transport through 10-site chains. **(a)** The weak hopping ($t = \Gamma$) chain and corresponding **(b)** single-photon transmission and **(c-e)** second order correlation for various values of the onsite interaction strength U. Note the strong anti-bunching effect just below $2\delta = U$ marked with arrows. **(d)** The shape of the $g^{(2)}$ correlations for large U resembles the single photon correlations as discussed in the text. Note, however, the discrepancy in the number of peaks. **(f)** The strongly coupled ($t = 10\Gamma$) chain with additional decay channels, each with a decay rate $\Gamma_d = \Gamma/4$. **(g)** The clearly separated single-photon transmission peaks. **(h-j)** The two-photon correlation function still exhibits anti-bunching around $2\delta = U$ marked with arrows. The delayed correlation in **(j)** shows oscillations and reappearance of correlations as a function the delay time, τ.

In the limit of an infinitely strong photon-photon repulsion, $U/t \to \infty$, the remaining $\frac{N_s(N_s-1)}{2}$ two-photon states describe hard core photons forming the lattice equivalent of a Tonks-Girardeaux gas [50]. Their eigenfunctions are analogous to those of non-interacting fermions, but with bosonic statistics,

$$|\psi^{TG}_{k,q}\rangle = \sum_{i,j} S(i,j)\langle i|\psi^{(1)}_k\rangle\langle j|\psi^{(1)}_q\rangle b_i^\dagger b_j^\dagger|0\rangle, \quad k < q. \tag{10.67}$$

The fermionized behavior is captured by the exchange sign $S(i,j) = 2\Theta(i-j) - 1$, with Θ being the Heaviside step function. Obviously, $S(i,i) = 0$. These states play the same role as the $|\psi^{(2)}_{l_2=\pm}\rangle$ dimer eigenstates from Eq. (10.50).

This picture becomes more complicated when we wish to include the self-energy arising from the coupling to the chiral channels as discussed in Eq. (10.12). Starting from the non-interacting limit, we may consider the case of a perturbatively small coupling Γ (compared to the relevant energy scales). To lowest order the eigenenergies are modified through the wavefunction density at the coupling sites (located at the chain ends),

$$E^{(1)}_k - \varepsilon \approx 2t\cos(k) - \frac{4}{N_s+1} i\Gamma \sin^2(k). \tag{10.68}$$

In the strong coupling (weak hopping) limit one may instead start from the subsystem that excludes the coupling sites. The subsystem quasi-momenta are then given by $k = \pi m/(N_s-1)$, with integer $m = 1, \ldots, N_s-2$ and eigen-energies $E^{(1)}_k - \varepsilon = 2t\cos(k)$. The system also supports two additional eigenstates localized around the coupling sites and with imaginary eigen-energies approximately given by $E^{(1)}_\sigma - \varepsilon = -i\Gamma_\sigma$.

Figure 10.9 shows the few-photon correlation function for 10-site chains with intermediate hopping $t = \Gamma$ and strong hopping $t = 10\Gamma$. In the case of strong hopping, we also attach additional decay channels to each of the chain sites with a decay strength, $\Gamma_d = \Gamma/4$, in order to both demonstrate the capability of the scattering method to deal with such systems, and to smooth out the otherwise sharp features of the correlation functions.

The two-photon correlations for both chains develops a strong anti-bunching feature around $2\delta = U$ present for even small values of the photon-photon interaction. We speculate that this feature has the same origin as the anti-bunching feature for the parallel coupled dimer, and is connected to the exclusively doublonic state $|\phi^{(2)}_0\rangle$ with the energy $E = U$. It shows up for chains of all lengths, but is most pronounced for longer chains. We also note the robustness of this feature, as it is present even for a chain with strong hopping and additional decays.

The similarity between the doublonic subspace at large values of the photon-photon interaction strengths and the single photon Hilbert space is visible in Fig. 10.9(d) and (i). The band-width of the doublonic spectrum in Fig. 10.9(d) is here roughly $8t^2/U = 0.8$ for the case of intermediate hopping, $t = \Gamma$. However, we already

discussed that the coupling at the ends, means that the end sites do not contribute in the same way to the Hilbert space, and we may partly exclude them when calculating the Green's function; and when counting, the two-photon correlation function only shows eight resonance peaks as opposed to the ten resonance peaks in the single-photon correlation function.

For large hopping the additional decays smears our the shape of the correlations as in Fig. 10.9(i).

The delayed two-photon correlation functions are shown in Fig. 10.9(e) and (j) for $U = \Gamma$ and $U = 10\Gamma$ respectively. Both show the decay of the anti-bunching feature around $2\delta = U$, and both show oscillations on a time-scale set by $U + |2\delta|$. For large hoppings the oscillations only lasts for one or two periods before decaying through the additional channels. However, the oscillations here are reminiscent of revivals with strong correlations suddenly emerging at finite delay times from previously weak values. While reminding us of previous results [27], we speculate that one may solve the full non-Markovian dynamics by simulating a one-dimensional waveguide using scattering theory on a discrete chain. A notion one may pursue in further work.

10.0.5 Rings

Next, we consider six sites arranged in a ring geometry with two chiral channels coupling to two different sites on the ring as shown in Fig. 10.10(a). By coupling channels at different sites, one may induce destructive quantum interference effects which block single-photon transport. This is clearly visible in Fig. 10.10(b) where the transmission through the six-sited ring shows three interference nodes. As already discussed in our analysis of the perpendicularly coupled dimer, this effect is geometrical and can be found in many other lattice geometries where the one-dimensionality of the combined channel-lattice system has been broken.

The blocking of single photon transport around the interference nodes again induces a large relative bunching effect as seen in the plot of the two-photon correlation in Figure 10.10(c), because the finite photon-photon interaction lifts the transport blockade and allows the two-photon states to transmit.

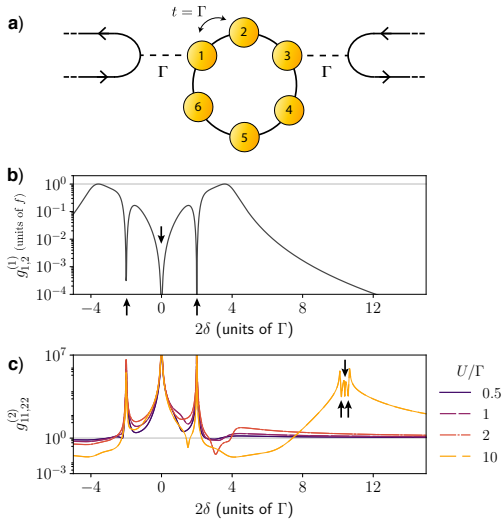

Figure 10.10: Transmission and second order intensity correlation for the six site ring lattice with weak hopping, $t = 1\Gamma$. **(a)** The single-photon transmission with the characteristic three dip structure arising as a consequence of quantum transport interference. **(b)** The intensity-intensity correlation function as a function of detuning for various values of the interaction, U. For strong repulsion, $U \geq 4\Gamma$, the three dip structure of the single-photon transmission is replicated in the intensity-intensity correlation due dominance of the (mostly) doublonic subspace at those detunings as annotated with arrows.

The perturbative analysis for weak non-linearity performed for the chain geometry easily carries over to the ring geometry: Again a single two-photon state consisting entirely of doublons, factors out, and creates a deficit of bunched states around zero detuning visible in the $g^{(2)}$ function as an anti-bunching dip.

In the regime of strong non-linearity, the states separate again into two subspaces describing doublons and hardcore photons. Figure. 10.10 shows that the characteristic three node pattern int the single photon transmission is now also visible in the doublonic part of the two-photon correlation at detunings $2\delta \approx U$.

Planes and Edge States

A Bose-Hubbard lattice plane penetrated by a magnetic field is known to support single-particle topological quantum Hall edge states [51] as has also been investigated experimentally [3].

We consider a uniform 8 by 8 square lattice of Bose-Hubbard sites shown schematically in Fig. 10.11, where the hopping Hamiltonian takes the form

$$H_t = \sum_{\langle i,j \rangle} \left(t_{i,j} b_i^\dagger b_j + h.c. \right), \tag{10.69}$$

with hopping amplitudes

$$t_{i,j} = \begin{cases} t & \text{if } i \text{ and } j \text{ in different rows.} \\ t_k = te^{ik\phi} & \text{if } i \text{ and } j \text{ oth in row } k. \end{cases} \tag{10.70}$$

Such a row-increasing phase has already been artificially induced in optical resonator circuits [3], and can be interpreted as an effective magnetic field. The system should then exhibit the quantum Hall effect, and its single particle states should separate into either edge or bulk states.

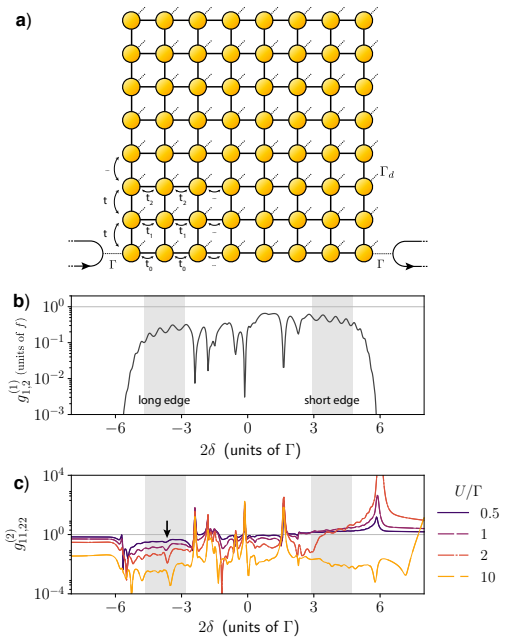

Figure 10.11: Transmission and $g^{(2)}$ function for a plane penetrated by a (artificial) magnetic field. **(b)** The single photon transmission amplitude between the attached channels. Such systems support single-photon edge states that in our case follow the lattice edge either the long or the short way around. The parts of the spectrum where edge states dominate have been shaded gray. **(c)** The $g^{(2)}$ correlation for transport along the long edge clearly resembles the correlations of a simple chain with the characteristic anti-bunching dip, thus making the one-dimensionality of the edge state clearly discernible (compare Fig. 10.9).

In order to make the setup more experimentally realistic we added an additional decay channel to each of the Bose-Hubbard sites–although with a rather small coupling rate, $\Gamma_d = \Gamma/100$.

We finally attach chiral channels to two lattice corners at the usual coupling strength, $\Gamma = t$. For an effective phase per plaquette of $\phi = 2\pi/5$, the resulting first and second order correlation function is shown in Fig. 10.11. We have explicitly marked the part of the spectrum containing edge states in the the single-photon transmission in Fig. 10.11(b). The absence of interference nodes in those parts of the spectrum makes the qualitative resemblance to the transmission through a linear chain in Fig. 10.9 obvious. The bulk spectrum on the other hand shows several transmission nodes at irregular values of the detuning.

The edge states at the two ends of the total spectrum propagate in opposite directions, with the edge states in the low end of the spectrum traveling the long way around the lattice, while the high end edge states travel the short way around.

The $g^{(2)}$ correlation for transport along the long edge clearly resembles the correlations of a simple chain with the distinct anti-bunching dip in the middle of the edge state spectrum clearly visible, thus further demonstrating the one-dimensionality of the chiral edge states.

10.0.6 Conclusion

In conclusion, we have investigated few photon scattering in systems with many internal degrees of freedom. Specifically we have focused on systems with multiple chiral channels coupling to extended Bose-Hubbard

lattices. In the case of local couplings – coupling to each channel at a single local point – we have derived exact analytical expressions for the single-photon and two-photon scattering matrices. In the case of multiple coupling points we have derived similar expressions for the single-photon and two-photon scattering matrices in the quasi-local regime, which we have argued is equivalent to invoking the Markov approximation.

We have implemented the analytical expression numerically and shown results for the scattering of weakly coherent light on several different Bose-Hubbard graphs.

Obviously, we have by no means exhausted the possibilities for analyzing photon scattering on Bose-Hubbard graphs. We therefore offer babusca – a Python implementation of the results obtained in this paper – for download online [5] and as an attachment to the supplementary material for this paper. Babusca makes it straightforward to analyze the low-order coherence functions for photon transport through chiral channels that couple locally or quasi-locally to an arbitrary Bose-Hubbard lattice.

During the finishing stages of this manuscript, we became aware of similar work carried out by See *et al.* [53], and we refer to their manuscript for a complementary but equivalent formulation of few photon scattering on Bose-Hubbard lattices.

10.0.7 Appendix: Two photon scattering

The two-photon T matrix is given by (10.10). In explicit form it reads

$$
\begin{aligned}
T^{(2)} &= P^{(0)} \vdots VGVGVGV \vdots P^{(0)} \\
&= P^{(0)} \vdots a^\dagger_{\nu_1'} \tilde{b}_{\sigma_1'} G(E) \left[a^\dagger_{\nu_2'} \tilde{b}_{\sigma_2'} + \tilde{b}^\dagger_{\sigma_2} a_{\nu_2} \right] G(E) \left[a^\dagger_{\nu_2'} \tilde{b}_{\sigma_2'} + \tilde{b}^\dagger_{\sigma_2} a_{\nu_2} \right] G(E) \tilde{b}^\dagger_{\sigma_1} a_{\nu_1} \vdots P^{(0)} \\
&\overset{\text{o.s.}}{=} P^{(0)} \tilde{b}_{\sigma_1'} G^{(1)}(E+\omega_1'+\omega_0) \tilde{b}_{\sigma_2'} G^{(2)}(E+\omega_1'+\omega_2'+2\omega_0) \tilde{b}^\dagger_{\sigma_2} G^{(1)}(E+\omega_1+\omega_0) \tilde{b}^\dagger_{\sigma_1} P^{(0)} a^\dagger_{\nu_1'} a^\dagger_{\nu_2'} a_{\nu_2} a_{\nu_1} \\
&\quad + P^{(0)} \tilde{b}_{\sigma_1'} G^{(1)}(E+\omega_1'+\omega_0) \tilde{b}^\dagger_{\sigma_2} G^{(0)}(E+\omega_1'-\omega_2) \tilde{b}_{\sigma_2'} G^{(1)}(E+\omega_1+\omega_0) \tilde{b}^\dagger_{\sigma_1} P^{(0)} a^\dagger_{\nu_1'} a^\dagger_{\nu_2'} a_{\nu_2} a_{\nu_1} \\
&= P^{(0)} \tilde{b}_{\sigma_1'} \sum_{l_1'} \frac{P^{(1)}_{l_1'}}{\omega_1'+\omega_0-\lambda^{(1)}_{l_1'}} \tilde{b}_{\sigma_2'} \sum_{l_2} \frac{P^{(2)}_{l_2}}{\omega_1'+\omega_2'+2\omega_0-\lambda^{(2)}_{l_2}} \tilde{b}^\dagger_{\sigma_2} \sum_{l_1} \frac{P^{(1)}_{l_1}}{\omega_1+\omega_0-\lambda^{(1)}_{l_1}} \tilde{b}^\dagger_{\sigma_1} P^{(0)} a^\dagger_{\nu_1'} a^\dagger_{\nu_2'} a_{\nu_2} a_{\nu_1} \\
&\quad + P^{(0)} \tilde{b}_{\sigma_1'} \sum_{l_1'} \frac{P^{(1)}_{l_1'}}{\omega_1'+\omega_0-\lambda^{(1)}_{l_1'}} \tilde{b}^\dagger_{\sigma_2} \frac{P^{(0)}}{\omega_1'-\omega_2+i0^+} \tilde{b}_{\sigma_2'} \sum_{l_1} \frac{P^{(1)}_{l_1}}{\omega_1+\omega_0-\lambda^{(1)}_{l_1}} \tilde{b}^\dagger_{\sigma_1} P^{(0)} a^\dagger_{\nu_1'} a^\dagger_{\nu_2'} a_{\nu_2} a_{\nu_1}. \qquad (10.71)
\end{aligned}
$$

Note the implicit summation over all four channel state indices, $\nu_1', \nu_2', \nu_1, \nu_2$. From the third line on we make use of the on-shell (o.s.) condition $E = \omega_1' + \omega_2' = \omega_1 + \omega_2$. In the last two lines we set $E - H_{\text{chs}} = E -)\omega_1' + \omega_2') = 0$, since the operator $E - H_{\text{chs}}$ after the (modified) normal ordering acts on the final state.

In the following we consider only the principal value part of $(\omega_1' - \omega_2 + i0^+)^{-1} = (\omega_1' - \omega_2)^{-1} - i\pi\delta(\omega_1' - \omega_2)$ in (10.71), because the delta function part contributes to the elastic two-photon scattering accounted by the term $\propto S^{(1)} S^{(1)}$ in (10.17). The spurious divergence $\omega_1' = \omega_2$ in $(\omega_1' - \omega_2)^{-1}$ is removed after symmetrization of the last line term in (10.71) under permutation of the field indices ν_1' and ν_2'. Thus we obtain

$$
\begin{aligned}
T^{(2)\mathcal{P}} = \frac{P^{(0)}}{2} a^\dagger_{\nu_1'} a^\dagger_{\nu_2'} a_{\nu_2} a_{\nu_1} \sum_{l_1', l_1} \Bigg\{ & 2 \sum_{l_2} \frac{\langle 0 | \tilde{b}_{\sigma_1'} P^{(1)}_{l_1'} \tilde{b}_{\sigma_2'} P^{(2)}_{l_2} \tilde{b}^\dagger_{\sigma_2} P^{(1)}_{l_1} \tilde{b}^\dagger_{\sigma_1} | 0 \rangle}{(\omega_1'+\omega_0-\lambda^{(1)}_{l_1'})(\omega_1+\omega_2+2\omega_0-\lambda^{(2)}_{l_2})(\omega_1+\omega_0-\lambda^{(1)}_{l_1})} \\
& + \frac{\langle 0 | \tilde{b}_{\sigma_1'} P^{(1)}_{l_1'} \tilde{b}^\dagger_{\sigma_2} | 0 \rangle \langle 0 | \tilde{b}_{\sigma_2'} P^{(1)}_{l_1} \tilde{b}^\dagger_{\sigma_1} | 0 \rangle}{(\omega_1'+\omega_0-\lambda^{(1)}_{l_1'})(\omega_1'-\omega_2)(\omega_1+\omega_0-\lambda^{(1)}_{l_1})} - \frac{\langle 0 | \tilde{b}_{\sigma_2'} P^{(1)}_{l_1} \tilde{b}^\dagger_{\sigma_1} | 0 \rangle \langle 0 | \tilde{b}_{\sigma_1'} P^{(1)}_{l_1'} \tilde{b}^\dagger_{\sigma_2} | 0 \rangle}{(\omega_2'+\omega_0-\lambda^{(1)}_{l_1})(\omega_1'-\omega_2)(\omega_2+\omega_0-\lambda^{(1)}_{l_1'})} \Bigg\}. \qquad (10.72)
\end{aligned}
$$

Combined with the identity

$$
\begin{aligned}
&\frac{1}{(\omega_1'+\omega_0-\lambda^{(1)}_{l_1'})(\omega_1+\omega_0-\lambda^{(1)}_{l_1})} - \frac{1}{(\omega_2'+\omega_0-\lambda^{(1)}_{l_1})(\omega_2+\omega_0-\lambda^{(1)}_{l_1'})} \\
&\overset{\text{o.s.}}{=} -\frac{(\omega_1'-\omega_2)(E-\lambda^{(1)}_{l_1'}-\lambda^{(1)}_{l_1})}{(\omega_1'+\omega_0-\lambda^{(1)}_{l_1'})(\omega_2'+\omega_0-\lambda^{(1)}_{l_1})(\omega_2+\omega_0-\lambda^{(1)}_{l_1'})(\omega_1+\omega_0-\lambda^{(1)}_{l_1})},
\end{aligned}
$$

this directly produces Eq. (10.18).

[5] The latest babusca library is available at .

10.0.8 Appendix: Second-order intensity correlation function

This sections details the derivation of the second order intensity correlation function, $g^{(2)}$, for weakly coherent light. The lowest order contribution to $g^{(2)}$ involves the two photon component of the coherent state, $|\phi^{(2)}_{\nu_0}\rangle = \frac{1}{2}\bar{n}(\mathcal{A}^\dagger_{\nu_0}(t))^2\,|0,0\rangle$, which scatters into the state $|S\phi^{(2)}_{\nu_0}\rangle = S^{(2)}|\phi^{(2)}_{\nu_0}\rangle$. The latter is constructed using Eqs. (10.17) and (10.18), resulting in

$$|S^{(2)}\phi^{(2)}_{\nu_0}\rangle = \bar{n}e^{2i\omega_0 t}\left(\frac{1}{2}s^{(1)}_{\sigma_2'\sigma_0}s^{(1)}_{\sigma_1'\sigma_0}\mathcal{A}^\dagger_{\sigma_2'\omega_0}\mathcal{A}^\dagger_{\sigma_1'\omega_0} - 2\pi i T^{(2)\mathcal{P}}_{\sigma_1'\sigma_2';\sigma_0\sigma_0}(\omega_1',\omega_2';0,0)\frac{2\pi}{L}a^\dagger_{\sigma_2'\omega_2'}a^\dagger_{\sigma_1'\omega_1'}\,\delta_{\omega_1'+\omega_2',0}\right)|0,0\rangle, \tag{10.73}$$

with implicit summations over repeated indices.

Next step involves the evaluation

$$\begin{aligned} &a_\sigma(x-t-\tau)a_{\sigma'}(x-t)|S^{(2)}\phi^{(2)}_{\nu_0}\rangle \\ &\quad= \frac{\bar{n}}{L}e^{i\omega_0(2x+\tau)}\left[s^{(1)}_{\sigma'\sigma_0}s^{(1)}_{\sigma\sigma_0} - 2\pi i\int_{-\infty}^{\infty}\mathrm{d}\omega\,(\delta_{\sigma,\sigma_1'}\delta_{\sigma',\sigma_2'}e^{-i\omega\tau}+\delta_{\sigma,\sigma_2'}\delta_{\sigma',\sigma_1'}e^{i\omega\tau})T^{(2)\mathcal{P}}_{\sigma_1'\sigma_2';\sigma_0\sigma_0}(\omega,-\omega;0,0)\right]|0,0\rangle\,. \end{aligned} \tag{10.74}$$

The ω integral can be performed by closing the contour of integration in either the upper or lower complex half-plane depending on the exponential prefactor (also recall that $\mathrm{Im}\lambda^{(M)}_{l_M} < 0$). After the proper normalization we obtain

$$\begin{aligned} g^{(2)}_{\sigma\sigma'}(\tau) &= \frac{\left|\left|a_\sigma(x-t-\tau)a_{\sigma'}(x-t)|S^{(2)}\phi^{(2)}_{\nu_0}\rangle\right|\right|^2}{\frac{\bar{n}^2}{L^2}\left|s^{(1)}_{\sigma'\sigma_0}s^{(1)}_{\sigma\sigma_0}\right|^2} \\ &= \Bigg|1 - \frac{4\pi^2}{s^{(1)}_{\sigma'\sigma_0}s^{(1)}_{\sigma\sigma_0}}\sum_{l_1',l_1}e^{-i(\lambda^{(1)}_{l_1'}-\omega_0)\tau} \\ &\qquad\times\langle 0|\tilde{b}_\sigma|1,l_1'\rangle\left\{\frac{\langle\overline{1,l_1'}|\tilde{b}_{\sigma'}|2,l_2\rangle\langle\overline{2,l_2}|\tilde{b}^\dagger_{\sigma_0}|1,l_1\rangle}{2\omega_0-\lambda^{(2)}_{l_2}} - \frac{\langle\overline{1,l_1'}|\tilde{b}^\dagger_{\sigma_0}|0\rangle\langle 0|\tilde{b}_{\sigma'}|1,l_1\rangle}{\omega_0-\lambda^{(1)}_{l_1'}}\right\}\frac{\langle\overline{1,l_1}|\tilde{b}^\dagger_{\sigma_0}|0\rangle}{\omega_0-\lambda^{(1)}_{l_1}}\Bigg|^2. \end{aligned} \tag{10.75}$$

Note that the correlations are exponentially suppressed at large delay times τ with the decay rates $-\mathrm{Im}\lambda^{(1)}_{l_1'}$.

11 Diagrammatic Approach to Multiphoton Scattering by See, et al.

Abstract

We present a method to systematically study multi-photon transmission in one dimensional systems comprised of correlated quantum emitters coupled to input and output waveguides. Within the Green's function approach of the scattering matrix (S-matrix), we develop a diagrammatic technique to analytically obtain the system's scattering amplitudes while at the same time visualise all the possible absorption and emission processes. Our method helps to reduce the significant effort in finding the general response of a many-body bosonic system, particularly the nonlinear response embedded in the Green's functions. We demonstrate our proposal through physically relevant examples involving scattering of multi-photon states from two-level emitters as well as from arrays of correlated Kerr nonlinear resonators in the Bose-Hubbard model.

11.1 Introduction

Engineering strong photon-photon interactions [1] is important in numerous areas such as quantum information processing and computing [2]. To achieve that, strong coupling between light and matter at the quantum level is often required. For this matter, different approaches have been explored using a variety of quantum technological platforms including atoms in optical and microwave cavities [3], semiconductor based devices [4], superconducting circuits [5], and Rydberg media [6].

Among other applications, strong photon-photon interactions allow generation and manipulation of non-classical states of light with applications in single photon transistors and quantum photonic switches [7, 8, 9, 10] . It can also be used to create strongly correlated states of light with applications in quantum simulations [11, 12].

To determine if an atomic or a general quantum optical system can be used to manipulate light as above, one usually analyses its transmission spectra and photon statistics. Different theoretical methods have been used to retrieve such information in various setups. Since we are dealing with photons, it is natural to use quantum optical methods like master equations and the input-output formalism [13, 14] to connect experimental observables such as the intensity and correlation functions of the transmitted or scatteredred light to the behaviour of the system probed. Tools that are not traditionally from quantum optics like Lippmann-Schwinger equation [15] or equivalently Bethe ansatz [16] and quantum field theory [17], have also been incorporated recently when one is seeking exact analytical descriptions [18, 19, 20**? ?** , 23, 24, 25, 26, 27, 28]. For the case of photonic Fock state inputs, while it is relatively easy to calculate the part of the S-matrix due to elastic scattering, where the momenta of the photons are simply rearranged at the output, it is usually tedious and complicated to calculate the part due to inelastic scattering, where the output momenta are a continuum. The latter is particularly true for cases where more than two photons and/or several emitters are involved.

One of the main focuses in this paper is to provide a systematic method to calculate these non-trivial terms. To do so, we use input-output operators to define the S-matrix and with inspiration from quantum field theory, we develop a diagrammatic method to evaluate the S-matrix in a setup where single-mode waveguides are coupled locally to an arbitrary system. Using this method, scattering elements are calculated more intuitively, especially their inelastic parts representing the nonlinear responses. We first present the model and the necessary background of S-matrix in section 11.2. Next, in section 11.3, we illustrate rules for drawing diagrams which allow their associated Green's functions to be written. We demonstrate our method with a few concrete examples in section 11.4 before concluding the paper. In particular, we will first discuss two non-interacting systems — a two-level emitter and two collocated two-level emitters, before moving on to a many emitters interacting system described by the Bose-Hubbard model. In the latter, we consider open and closed boundary conditions. Through these examples, we aim to illuminate how the diagrammatic approach can help one understand the physics of the systems both qualitatively and quantitatively.

11.2 Model and background of S-matrix

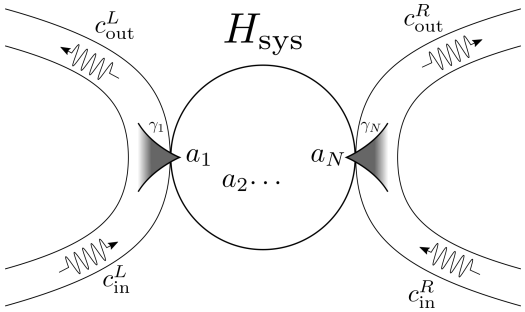

Figure 11.1: Two photonic waveguides coupled to a many-body system with Hamiltonian, H_{sys} that is described by the operators $a_1, \ldots, a_N$. The left and right waveguides are bilinearly coupled to a_1 and a_N respectively.

To study the transport and scattering properties of a system, we couple single-mode waveguides to the system (Fig. 11.1), insert photons through the waveguides, and observe the reflection and transmission spectra. Such a setup is described by a total Hamiltonian ($\hbar = 1$)

$$H_{\text{tot}} = H_{\text{w}} + H_{\text{ws}} + H_{\text{sys}}.$$

The free propagation of photons in the left and right waveguides is described by

$$H_{\text{w}} = \int \mathrm{d}k\, \omega(k) \left(c_k^{L\dagger} c_k^L + c_k^{R\dagger} c_k^R \right)$$

where $c_k^{L/R\dagger}$ and $c_k^{L/R}$ are the creation and annihilation operators of k-mode photons in the left/right waveguides respectively. We assume linear dispersion relation in the waveguides and take the group velocity to be one, i.e. $\omega(k) = k$. This allows us to use momentum and energy interchangeably throughout this paper.

Next, we model the coupling between the waveguides and local system operators a_1 and a_N as

$$H_{\rm ws} = \int \mathrm{d}k \left(\xi_1 a_1^\dagger c_k^L + \xi_N a_N^\dagger c_k^R + h.c. \right). \tag{11.1}$$

We have made the rotating wave approximation and assumed frequency-independent coupling constants ξ_1 and ξ_N, which is valid when the coupling constant is small compared to the typical frequency of the system and the bandwidths of the waveguides are large. This assumption, along with the linear dispersion relation of the waveguides, is equivalent to making the Markov approximation, yielding the input-output relation to be derived shortly.

Finally, $H_{\rm sys}$ is the Hamiltonian of the system of interest and has a form $H_{\rm sys} = H_0 + H_{\rm int}$, where $H_0 = \sum_{j=1}^N \omega_j a_j^\dagger a_j$ describes the free energy of all its constituents, a_j's and $H_{\rm int}$ describes interactions between them. We restrict our discussion to interactions where the system Hamiltonian is total-particle-number conserving, i.e. $[H_{\rm sys}, N_{\rm tot}] = 0$, where $N_{\rm tot}$ = total particle number $= \sum_{j=1}^N a_j^\dagger a_j$. Such feature is common in many physical models. Generalisation of the method to non-particle-number-conserving interactions is straightforward.

From the above model Hamiltonian, one can derive the following input-output relations for the waveguides [29],

$$\begin{aligned} c_{\rm out}^L(t) &= c_{\rm in}^L(t) - \mathrm{i}\sqrt{\gamma_1} a_1(t) \\ c_{\rm out}^R(t) &= c_{\rm in}^R(t) - \mathrm{i}\sqrt{\gamma_N} a_N(t) \end{aligned} \tag{11.2}$$

where $\gamma_i = 2\pi\xi_i^2$, for $i = 1, N$ and $c_{\rm in}^{L/R}$ and $c_{\rm out}^{L/R}$ are the input and output operators in the left/right waveguides. Using these operators, the S-matrix, which is a unitary matrix mapping the asymptotic free initial state $|\mathbf{k}\rangle = \prod_i c_{k_i}^\dagger |0\rangle$ to the asymptotic free final state $|\mathbf{p}\rangle = \prod_i c_{p_i}^\dagger |0\rangle$ with incoming and outgoing particle momenta of $\mathbf{k}$ and $\mathbf{p}$, is as follows,

$$\begin{aligned} S(\mathbf{p};\mathbf{k}) &= \langle \mathbf{p}|S|\mathbf{k}|\mathbf{p}|S|\mathbf{k}\rangle \\ &= \mathscr{F} \left\langle 0|c_{\rm out}(t_1')\dots c_{\rm out}(t_n') c_{\rm in}^\dagger(t_1)\dots c_{\rm in}^\dagger(t_n)|0 \middle| 0|c_{\rm out}(t_1')\dots c_{\rm out}(t_n') c_{\rm in}^\dagger(t_1)\dots c_{\rm in}^\dagger(t_n)|0 \right\rangle \end{aligned}$$

where $\mathscr{F} = \left(\prod_{i=1}^n \int \frac{\mathrm{d}t_i'}{\sqrt{2\pi}} \mathrm{e}^{\mathrm{i}p_i t_i'} \prod_{j=1}^n \int \frac{\mathrm{d}t_j}{\sqrt{2\pi}} \mathrm{e}^{-\mathrm{i}k_j t_j} \right)$ is the Fourier transform operation. We have omitted the labels for the incoming and outgoing photon paths, i.e. the L and R labels, on the input and output operators [6].

As noted in Ref. [27], the S-matrix can be cluster decomposed into a sum of the products of connected parts, i.e.

$$S_{\mathbf{p};\mathbf{k}} = \sum_{\mathcal{B}} \sum_{P} \prod_{i=1}^{M_{\mathcal{B}}} S^C_{p_{\mathcal{B}_i};k_{P\mathcal{B}_i}} \tag{11.3}$$

where the summation is taken over all partitions $\mathcal{B}$ of $\{1, 2, \dots, n\}$, with $M_{\mathcal{B}}$ number of subsets $\mathcal{B}_i$, and all permutations (denoted P) of the subset elements $P\mathcal{B}_i$. Note that the connected part of a function is defined as the part of the function that is proportional to only one delta function. Furthermore, a connected n-photon S-matrix, $S^C_{\mathbf{p};\mathbf{k}}$ is equal to a connected $2n$-point Green's function for $n > 1$. For $n = 1$, there is an extra delta function if there is an input from that channel (section 11.6). Omitting the incoming and outgoing photon paths, the $2n$-point Green's function is defined as

$$\begin{aligned} &G(p_1 \dots p_n; k_1 \dots k_n) \\ =&(-1)^n \mathscr{F} \langle 0| \mathcal{T} a(t_1') \dots a(t_n') a^\dagger(t_1) \dots a^\dagger(t_n) |0\rangle \end{aligned} \tag{11.4}$$

where $\mathcal{T}$ is the time ordering operator and all γ's in the definition have been set to one. The correct factor of γ's could be recovered easily as each a_j contributes a factor of $\sqrt{\gamma_j}$. The system operators evolve under the effective Hamiltonian,

$$H_{\rm eff} = H_{\rm sys} - \mathrm{i}\frac{\gamma_1}{2} a_1^\dagger a_1 - \mathrm{i}\frac{\gamma_N}{2} a_N^\dagger a_N$$

as

$$a(t) = \mathrm{e}^{iH_{\rm eff}t} a \mathrm{e}^{-iH_{\rm eff}t}, \qquad a^\dagger(t) = \mathrm{e}^{iH_{\rm eff}t} a^\dagger \mathrm{e}^{-iH_{\rm eff}t}.$$

For $n > 1$, the $2n$-point Green's function defined above is nonzero only when the system is nonlinear. It represents inelastic scattering processes when multiple photons are sent into the system. Elastic scattering processes, on the other hand, are fully described by products of single-photon S-matrix elements.

In summary, to compute the S-matrix, we need to consider only the effective Hamiltonian described solely by the system operators. Moreover, any additional waveguide couplings via say a_j is dealt with by adding a

[6] For example, for a one-photon process, there are four different S-matrix elements for incoming and outgoing photons from the left and right waveguides, i.e. ${}_L\langle p|S|k|p|S|k\rangle_L$, ${}_R\langle p|S|k|p|S|k\rangle_L$, ${}_L\langle p|S|k|p|S|k\rangle_R$ and ${}_R\langle p|S|k|p|S|k\rangle_R$.

term $-\mathrm{i}\frac{\gamma_j}{2}a_j^\dagger a_j$ to the effective Hamiltonian. Similarly, any loss to free space through the system operator, a_j is taken care of by adding a term $-\mathrm{i}\frac{\Gamma_j}{2}a_j^\dagger a_j$ to the effective Hamiltonian.

In this work, we stay in the weak waveguide-local system coupling limit by assuming that $\gamma \ll$ the smallest energy gap of the local system and ignoring the effects of extra decay into free space. All of our results in Section 11.4 have been worked out within this regime and remain valid as long as the effects of the bandwidth and dispersion of the waveguides can be ignored.

11.3 Diagrammatic approach

As we discussed, the problem of calculating the n-photon S-matrix has been reduced to calculating all $2m$-point Green's functions, for $m \leqslant n$. Here, we aim to provide a quick and straightforward recipe to compute them. As a gentle introduction, let us start by describing how a 2-point Green's function is calculated. The latter is defined as

$$\begin{aligned} G(p;k) &= -\mathscr{F}\,\langle 0|\,\mathcal{T}a(t')a^\dagger(t)\,|0\rangle \\ &= -\mathscr{F}\Big\{\,\langle 0|\,a(t')a^\dagger(t)\,|0\rangle\,\theta(t'-t)\Big\}. \end{aligned}$$

To proceed, the system operators need to be expressed in the Heisenberg form under the effective Hamiltonian. If the spectrum of the effective Hamiltonian is $H_{\text{eff}}\,|\epsilon\rangle = \epsilon\,|\epsilon\rangle$, $\langle\bar{\epsilon}|\,H_{\text{eff}} = \epsilon\,\langle\bar{\epsilon}|$, with normalisation conditions $\langle\epsilon|\bar{\epsilon'}\rangle\langle\epsilon|\bar{\epsilon'}\rangle = \delta_{\epsilon\epsilon'}$, where ϵ denote the eigenenergies and $|\epsilon\rangle$ and $\langle\bar{\epsilon}|$ denote the right and left eigenvectors respectively, the above step gives us

$$G(p;k) = -\mathscr{F}\Big\{\sum_{\epsilon}\langle 0|a|\epsilon\rangle\langle 0|a|\epsilon\rangle\,\langle\bar{\epsilon}|a^\dagger|0\rangle\langle\bar{\epsilon}|a^\dagger|0\rangle\,\mathrm{e}^{-\mathrm{i}\epsilon(t'-t)}\theta(t'-t)\Big\}.$$

The sum is taken over all eigenenergies of H_{eff}. The calculation is completed by performing the Fourier transformation.

Although it is seemingly straightforward to do, it gets cumbersome quickly as the number of photons increases. This motivates us to develop a diagrammatic technique to calculate the quantity which at the same time is able to provide us an intuitive picture of the processes that happen during an inelastic scattering. The diagrammatic method to compute the $2m$-point Green's function, $G(p_1 \ldots p_m; k_1 \ldots k_m)$ is as follows: (proof is given in section 11.7)

1. Draw all possible diagrams in the excitation space where each diagram corresponds to a particular time ordering of the Green's function. All diagrams start and end at the vacuum state (zero excitations) and consist of m input momenta (upwards arrows representing creation of excitation, $a^\dagger$) and m output momenta (downwards arrows representing annihilation of excitation, a). Input and output momenta are labeled with k's and p's respectively. Figure 11.2 shows the only possible diagram for the 2-point Green's function while Fig. 11.3 shows all the possible diagrams for 4- and 6-point Green's functions.

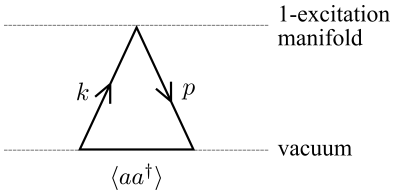

Figure 11.2: Diagram for 2-point Green's function.

2. For each diagram, assign a factor of

$$\frac{-\mathrm{i}}{(2\pi)^{m-1}}\,\delta\left(\sum_{i=1}^{m}k_i - \sum_{i=1}^{m}p_i\right)$$

for momentum conservation. As a consequence of this, at every node between two momenta, the sum of all upwards momenta to the left of the node is equal the sum of all downwards momenta to the right of the node. We label such sums by K_i for $i = 1, \ldots, (2m-1)$. For example, with the diagram $\langle aaa^\dagger a^\dagger aa^\dagger|aaa^\dagger a^\dagger aa^\dagger\rangle$ in Fig. 11.3(b), we have the sums, $K_1 = k_1 = p_1 + p_2 + p_3 - k_2 - k_3$, $K_2 = k_1 - p_1 = p_2 + p_3 - k_2 - k_3$, $K_3 = k_1 + k_2 - p_1 = p_2 + p_3 - k_3$, $K_4 = k_1 + k_2 + k_3 - p_1 = p_2 + p_3$ and $K_5 = k_1 + k_2 + k_3 - p_1 - p_2 = p_3$.

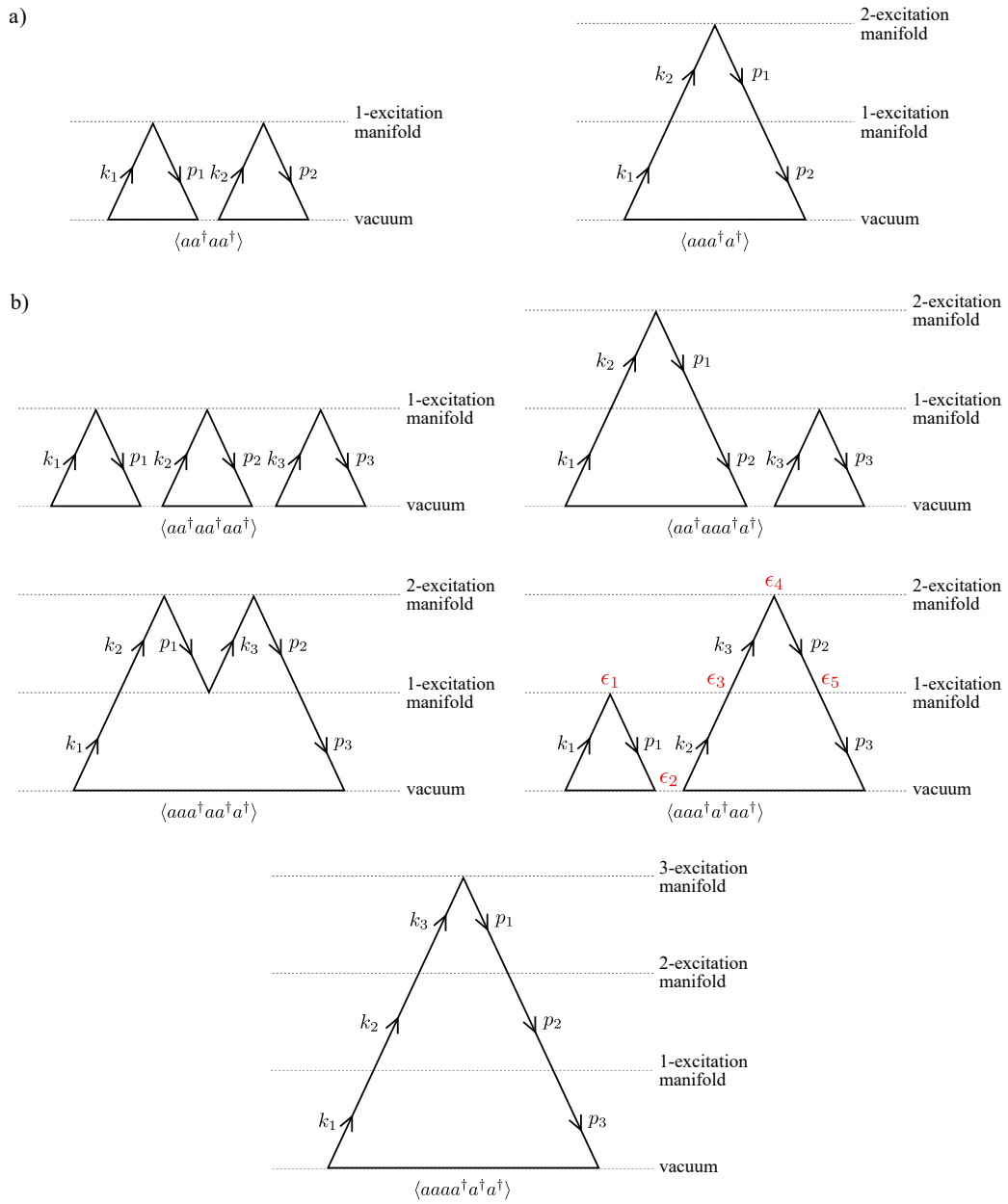

Figure 11.3: Examples of all possible diagrams for a) 4-point Green's funtion and b) 6-point Green's function. Note that some of the diagrams drawn here are simply the disconnected products of the lower order diagrams. Generally, one can construct all diagrams for higher order Green's functions by building upon the lower order diagrams and drawing purely connected ones.

3. Next, assign a 'propagator' for each arrow except the last one. It is written as

$$\prod_{j=1}^{2m-1} \frac{1}{K_j - \epsilon_j},$$

where ϵ_j's are dummy variables for the eigenenergies of H_{eff} that will be summed over in the next step.

4. Finally, sum over all the eigenenergies with the respective weights

$$\sum_{\epsilon_1,\ldots,\epsilon_{2m-1}} \langle 0| \cdot |\epsilon_{2m-1}|0| \cdot |\epsilon_{2m-1}\rangle \, \langle \bar{\epsilon}_{2m-1}| \ldots |\epsilon_1|\bar{\epsilon}_{2m-1}| \ldots |\epsilon_1\rangle \, \langle \bar{\epsilon}_1| \cdot |0|\bar{\epsilon}_1| \cdot |0\rangle$$

and over all permutations of input and output momenta which leave the diagram unchanged. For example,

in Fig. 11.3(b), the Green's function corresponding to the diagram $\langle aaa^\dagger a^\dagger aa^\dagger | aaa^\dagger a^\dagger aa^\dagger \rangle$ yields

$$
\begin{aligned}
&-\frac{\mathrm{i}}{4\pi^2}\delta(k_1+k_2+k_3-p_1-p_2-p_3)\cdot \\
&\sum_{\epsilon_1,\epsilon_3,\epsilon_4,\epsilon_5} \langle 0|a|\epsilon_5\rangle\langle 0|a|\epsilon_5\rangle \langle \bar{\epsilon}_5|a|\epsilon_4\rangle\langle \bar{\epsilon}_5|a|\epsilon_4\rangle \langle \bar{\epsilon}_4|a^\dagger|\epsilon_3\rangle\langle \bar{\epsilon}_4|a^\dagger|\epsilon_3\rangle \langle \bar{\epsilon}_3|a^\dagger|0\rangle\langle \bar{\epsilon}_3|a^\dagger|0\rangle \\
&\langle 0|a|\epsilon_1\rangle\langle 0|a|\epsilon_1\rangle \langle \bar{\epsilon}_1|a^\dagger|0\rangle\langle \bar{\epsilon}_1|a^\dagger|0\rangle \frac{1}{k_1-\epsilon_1}\frac{1}{k_1-p_1} \\
&\frac{1}{k_1+k_2-p_1-\epsilon_3}\frac{1}{p_2+p_3-\epsilon_4}\frac{1}{p3-\epsilon_5} \\
&+ \text{all permutations of } \{k_1,k_2,k_3\} \text{ and } \{p_1,p_2,p_3\}
\end{aligned}
$$

where the summation is over all eigenenergies for ϵ_1, ϵ_3, ϵ_4 and ϵ_5. Since the ground state is unique and is always set to have zero energy, ϵ_2 (which has been left out in the expression) is zero.

Following these four steps, one can write down the connected parts of the Green's function (which is also the connected parts of the S-matrix) in a systematic way. Once they are found, the cluster decomposition structure illustrated in Eq. (11.3) and section 11.6 is used to calculate the full S-matrix.

11.4 Paradigmatic examples

In this section, several examples are presented to demonstrate the diagrammatic approach detailed above. The examples consist of systems that are total-particle-number conserving, $[H_{\text{sys}}, N_{\text{tot}}] = 0$, starting from non-interacting systems, $H_{\text{int}} = 0$ with a two-level emitter and two collocated two-level emitters and ending with a many-emitter interacting system described by the Bose-Hubbard model. Implementations of such systems have been explored in areas such as superconducting circuits [5], cold atoms [31], and cavity systems [3].

11.4.1 Two-level system

First, we consider a simple example — a two-level system described by $H_{\text{sys}} = H_{\text{2-lvl}} = \omega\sigma_{ee}$ where $\sigma_{ee} = |e\rangle\langle e|$, embedded between two waveguides (Fig. 11.4). The effective Hamiltonian is simply given by

$$H_{\text{eff}} = (\omega - \mathrm{i}\gamma)\sigma_{ee}.$$

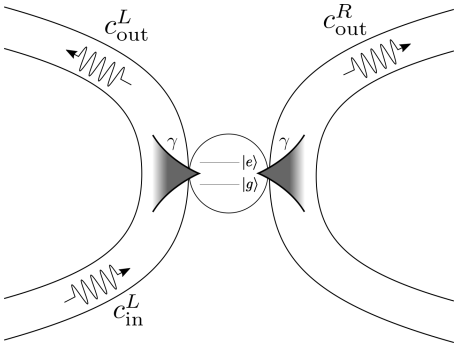

Figure 11.4: Scattering photons from a two-level system.

Following the first step in section 11.3, we start by drawing all possible diagrams for Green's functions. Since the effective Hamiltonian is diagonal, comprised of only the ground state $|g\rangle$ and a single excitation state $|e\rangle$, only possible diagrams are the ones that are products of the triangular loop diagram of the 2-point Green's function (Fig. 11.5). The corresponding $2m$-point Green's function is

$$
\begin{aligned}
G_{\mathbf{i};\mathbf{j}}(\mathbf{p};\mathbf{k}) = &-\frac{\mathrm{i}\gamma^m}{(2\pi)^{m-1}}\delta(\mathbf{p}-\mathbf{k})\Bigg(\frac{1}{k_1-\omega+\mathrm{i}\gamma}\frac{1}{k_1-p_1}\cdot \\
&\frac{1}{k_1+k_2-p_1-\omega+\mathrm{i}\gamma}\cdots\frac{1}{p_m-\omega+\mathrm{i}\gamma} \\
&+ \text{permutations of } \{\mathbf{p}\} \text{ and } \{\mathbf{k}\}\Bigg).
\end{aligned} \tag{11.5}
$$

i and **j** are the labels L/R, for the outgoing and incoming photon channels with corresponding outgoing momenta **p** and incoming momenta **k**, respectively. Note that the expressions of the Green's functions for different sets of outgoing and incoming photon channels are identical and are distinguished by the corresponding **i** and **j** labels associated to the momenta. Furthermore, inserting photons only from the left channel gives no extra delta function in the one-photon S-matrix of the right channel output, because there is no event where a photon would pass by the right channel without going through the two-level atom.

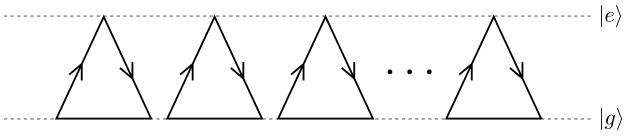

Figure 11.5: The only possible scattering diagram of the $2m$-point Green's functions for a two level quantum emitter being probed by m photons.

Following the rest of the steps in section 11.3, we obtain the one-photon S-matrices

$$\begin{array}{rcccl} S_{L;L}(p;k) & = & \delta(p-k)+G_{L;L}(p;k) & = & r_k\delta(p-k), \\ S_{R;L}(p;k) & = & G_{R;L}(p;k) & = & t_k\delta(p-k), \end{array} \tag{11.6}$$

where

$$r_k = 1-\mathrm{i}\gamma\frac{1}{k-\omega+\mathrm{i}\gamma}, \qquad t_k = -\mathrm{i}\gamma\frac{1}{k-\omega+\mathrm{i}\gamma},$$

are the reflection and transmission coefficients. Using the cluster decomposition relation, one can derive the two-photon S-matrices

$$\begin{aligned} S_{ij;LL}(p_1,p_2;k_1,k_2) &= G_{ij;LL}(p_1,p_2;k_1,k_2)+ \\ &\quad (S_{i;L}(p_1;k_1)S_{j;L}(p_2;k_2)+(k_1\leftrightarrow k_2)) \end{aligned} \tag{11.7}$$

with the 4-point Green's functions defined in Eq. (11.5) and have expressions

$$\begin{aligned} &G_{ij;LL}(p_1,p_2;k_1,k_2) \\ =&\frac{\mathrm{i}\gamma^2(k_1+k_2-2\omega+2\mathrm{i}\gamma)}{\pi(k_1-\omega+\mathrm{i}\gamma)(k_2-\omega+\mathrm{i}\gamma)(p_1-\omega+\mathrm{i}\gamma)(p_2-\omega+\mathrm{i}\gamma)}\cdot \\ &\delta(p_1+p_2-k_1-k_2) \end{aligned} \tag{11.8}$$

where i and j are the labels L/R for outgoing photon channels with output momenta p_1 and p_2 respectively. Within our diagrammatic approach, the aforementioned 4-point Green's function is visualised in Fig. 11.5 but with two loops only. Higher-order S-matrices can be written down similarly using the cluster decomposition relation with the Green's functions in Eq. (11.5).

To see the significance of this result, consider first a linear system (for example, a simple harmonic oscillator). Such systems have all the connected $2m$-point Green's functions being identically zero for $m \geq 2$ and hence the n-photon S-matrices are just products of the one-photon S-matrix for $n \geq 2$. For the case where n photons come in from the left and exits to the right, the n-photon S-matrix is $S_{\mathbf{p};\mathbf{k}} \propto t_{k_1}t_{k_2}\ldots t_{k_n}$. In particular, if the input field is coherent, $S_{\mathbf{p};\mathbf{k}} \propto (t_k)^n$, yielding a coherent output field. Therefore, in order to obtain a non-classical output, some kind of nonlinearity in the system is a must. In this example, the two-level atom is strongly nonlinear. Hence, the output is modified from being classical-like by the presence of nonzero Green's functions. Moreover, the diagrams of the Green's functions (Fig. 11.5) match the description of the photon blockade effect where photons are being absorbed and emitted one at a time [32, 33]. Of course one could then proceed with the calculation of the transmitted light correlation functions using the S-matrix derived above to reproduce the anti-bunching correlation/photon blockade effect well known to this system. We would like to point out here that such an effect is intuitive and obvious from the diagrams of the Green's functions (see Fig. 11.5). Calculation of the S-matrix using other methods without these diagrams would not give us such an insight.

11.4.2 Two collocated atoms

Before moving into a many-correlated-emitter example, we step up the complexity of the previous example by looking at two collocated non-interacting two-level atoms [34], with $H_{\text{sys}} = H_{2\text{-coll}} = \omega_1\sigma_{ee}^{(1)} + \omega_2\sigma_{ee}^{(2)}$. This example, in the limiting case of two identical atoms and coupling strengths, describes the two-atom Dicke model [35]. Working with only one channel that both atoms are coupled to (Fig. 11.6), we have the total Hamiltonian

$$\begin{aligned} H_{\text{tot}} = H_{2\text{-coll}} &+ \int \mathrm{d}k\; kc_k^\dagger c_k \\ &+ \int \mathrm{d}k\; \left(c_k^\dagger(\xi_1\sigma_{ge}^{(1)}+\xi_2\sigma_{ge}^{(2)})+h.c.\right), \end{aligned}$$

where ξ_i is the coupling strength between the the ith atom and the waveguide modes, for $i = 1, 2$. This gives rise to an input-output relation

$$c_{\text{out}}(t) = c_{\text{in}}(t) - \mathrm{i}\sqrt{\gamma_1}\sigma_{ge}^{(1)}(t) - \mathrm{i}\sqrt{\gamma_2}\sigma_{ge}^{(2)}(t). \tag{11.9}$$

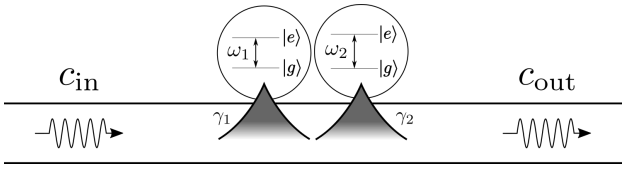

Figure 11.6: Schematic diagram of two collocated (ignore the distance in the sketch) two-level atoms coupled to a waveguide.

Comparing the forms of Eqs. (11.9) and (18.8), we see that the $\sqrt{\gamma}a$ in Eq. (18.8) is replaced by $\sqrt{\gamma_1}\sigma_{ge}^{(1)} + \sqrt{\gamma_2}\sigma_{ge}^{(2)}$. Therefore, the effective Hamiltonian can be deduced and takes the form:

$$\begin{aligned} H_{\text{eff}} &= \omega_1\sigma_{ee}^{(1)} + \omega_2\sigma_{ee}^{(2)} \\ &\quad - \frac{\mathrm{i}}{2}(\sqrt{\gamma_1}\sigma_{ge}^{(1)} + \sqrt{\gamma_2}\sigma_{ge}^{(2)})^\dagger(\sqrt{\gamma_1}\sigma_{ge}^{(1)} + \sqrt{\gamma_2}\sigma_{ge}^{(2)}) \\ &= (\omega_1 - \mathrm{i}\frac{\gamma_1}{2})\sigma_{ee}^{(1)} + (\omega_2 - \mathrm{i}\frac{\gamma_2}{2})\sigma_{ee}^{(2)} \\ &\quad - \mathrm{i}\frac{\sqrt{\gamma_1\gamma_2}}{2}(\sigma_{eg}^{(1)}\sigma_{ge}^{(2)} + \sigma_{ge}^{(1)}\sigma_{eg}^{(2)}) \end{aligned}$$

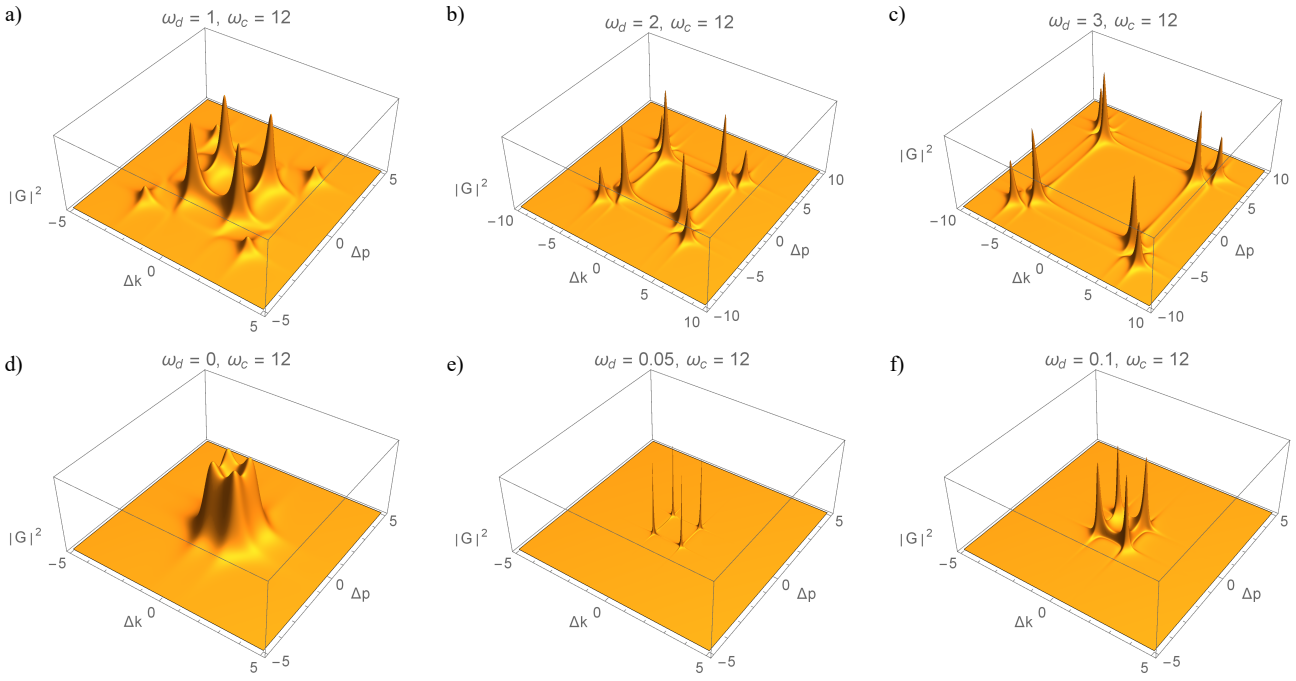

Figure 11.7: **Two collocated atoms:** Plots of $|G(p_1, p_2; k_1, k_2)|^2$ where i) $\omega_d^2 > \gamma_c^2/4$ with $\omega_d = 1, 2$ and 3 (figures (a–c)); and ii) $\omega_d^2 < \gamma_c^2/4$ with $\omega_d = 0, 0.05$ and 0.1 (figures (d–f)). For all the plots, $\omega_c = 12$, $\gamma_c = 0.25$ and the total incoming momentum, $E_i = 2\omega_c + 3\gamma_c$. We define $\Delta k \equiv k_1 - k_2$ and $\Delta p \equiv p_1 - p_2$. In figures (a–c), under i), the spectra exhibit eight peaks with the same width while in figures (d–f), under ii), the spectra exhibit only four peaks with the width becoming smaller as the detuning, ω_d decreases except at zero detuning where the width is much wider.

The effective Hamiltonian shows that even though the two collocated atoms do not interact directly, coupling to the same waveguide induces an effective dissipative interaction between them. Moreover, it has a spectrum:

$\epsilon^{(0)}=0, \epsilon^{(1)}_{\pm}=\omega_c-\mathrm{i}\gamma_c/2\pm\sqrt{\omega_d^2-\mathrm{i}\omega_d\gamma_d-\gamma_c^2/4}, \epsilon^{(2)}=2\omega_c-\mathrm{i}\gamma_c$, where $\omega_c=\frac{\omega_1+\omega_2}{2}$, $\omega_d=\frac{\omega_1-\omega_2}{2}$, $\gamma_c=\frac{\gamma_1+\gamma_2}{2}$, and $\gamma_d=\frac{\gamma_1-\gamma_2}{2}$. The corresponding right eigenvectors are $\left|\epsilon^{(0)}\right\rangle=|gg\rangle$, $\left|\epsilon^{(1)}_{\pm}\right\rangle\propto \mathrm{i}\sqrt{\gamma_c^2-\gamma_d^2}/4\,|eg\rangle+(\omega_d-\mathrm{i}\gamma_d/2\mp\sqrt{\omega_d^2-\mathrm{i}\omega_d\gamma_d-\gamma_c^2/4})\,|ge\rangle$ and $\left|\epsilon^{(2)}\right\rangle=|ee\rangle$. The left eigenvectors have the same coefficients but with the corresponding $\langle\cdot|$. The single excitation manifold, $\epsilon^{(1)}_{\pm}$ becomes degenerate when

$$\gamma_d=0,\ \omega_d^2=\gamma_c^2/4 \tag{11.10}$$

and the effective Hamiltonian becomes undiagonalisable. Hence, the theory cannot be applied under this condition. However, we can still study how the system behaves when $\gamma_d=0$ (i.e. $\gamma_1=\gamma_2=\gamma_c$), but $\omega_d^2\neq\gamma_c^2/4$. We noticed that when, i) $\omega_d^2>\gamma_c^2/4$, $\epsilon^{(1)}_{\pm}=\omega_{1,2}-\mathrm{i}\gamma_c/2+\mathcal{O}(\frac{\gamma_c^2}{\omega_d^2})$; and when ii) $\omega_d^2<\gamma_c^2/4$,

$$\epsilon^{(1)}_{\pm}=\begin{cases}\omega_c-\mathrm{i}\omega_d^2/\gamma_c+\mathcal{O}(\frac{\omega_d^4}{\gamma_c^4})\\ \omega_c-\mathrm{i}\gamma_c+\mathcal{O}(\frac{\omega_d^2}{\gamma_c^2})\end{cases}.$$

Since the peaks we observe in the S-matrix are closely related to the spectrum of the effective Hamiltonian, the condition in Eq. (11.10) defines some sort of critical point separating the region where i) the atoms decay as independent atoms and ii) the atoms decay collectively either with a subradiant (radiation reduction) or superradiant (radiation enhancement) profile. Moreover, in ii) when detuning is zero, $\omega_d=0$, the superradiant state, $\left|\epsilon^{(1)}_{-}\right\rangle=(|eg\rangle+|ge\rangle)/\sqrt{2}$, that decays as γ_c is the only state that is coupled to the input field. To visualise the two different situations, we first write the 2-point Green's function and one-photon S-matrix,

$$\begin{aligned}G(p;k)&=\sum_{\epsilon^{(1)}}\left\langle 0|a|\epsilon^{(1)}\right|0|a|\epsilon^{(1)}\right\rangle\left\langle\bar{\epsilon}^{(1)}|a^\dagger|0\right|\bar{\epsilon}^{(1)}|a^\dagger|0\right\rangle\frac{-\mathrm{i}}{k-\epsilon^{(1)}}\delta(k-p)\\&=\frac{-2\mathrm{i}\gamma_c(k-\omega_c)}{(k-\omega_1+\frac{\mathrm{i}\gamma_c}{2})(k-\omega_2+\frac{\mathrm{i}\gamma_c}{2})+\frac{\gamma_c^2}{4}}\delta(k-p)\\&\equiv g_k\delta(k-p)\end{aligned}$$

and

$$\begin{aligned}S(p;k)&=\delta(k-p)+G(p;k)\\&=\frac{(k-\omega_1-\frac{\mathrm{i}\gamma_c}{2})(k-\omega_2-\frac{\mathrm{i}\gamma_c}{2})+\frac{\gamma_c^2}{4}}{(k-\omega_1+\frac{\mathrm{i}\gamma_c}{2})(k-\omega_2+\frac{\mathrm{i}\gamma_c}{2})+\frac{\gamma_c^2}{4}}\delta(k-p).\end{aligned}$$

Next, the 4-point Green's function can be computed following the steps in section 11.3 with the aid of the diagrams in Fig. 11.3.

$$\begin{aligned}&G(p_1,p_2;k_1,k_2)\\&=\sum_{l=1}^{2}G^{(l)}(p_1,p_2;k_1,k_2)\delta(E_o-E_i)\end{aligned}\tag{11.11}$$

where $E_i=k_1+k_2$, $E_o=p_1+p_2$, and $G^{(1)}$, $G^{(2)}$ represent the diagrams $\left\langle aa^\dagger aa^\dagger\right|aa^\dagger aa^\dagger\rangle$, $\left\langle aaa^\dagger a^\dagger\right|aaa^\dagger a^\dagger\rangle$ respectively, with expressions

$$\begin{aligned}&G^{(1)}(p_1,p_2;k_1,k_2)\\&=-\frac{\mathrm{i}}{2\pi}\sum_{\epsilon_1^{(1)},\epsilon_2^{(1)}}\left(\frac{\left\langle 0|a|\epsilon_2^{(1)}\right|0|a|\epsilon_2^{(1)}\right\rangle\left\langle\bar{\epsilon}_2^{(1)}|a^\dagger|0\right|\bar{\epsilon}_2^{(1)}|a^\dagger|0\right\rangle}{p_2-\epsilon_2^{(1)}}\frac{1}{k_1-p_1}\cdot\right.\\&\qquad\left.\frac{\left\langle 0|a|\epsilon_1^{(1)}\right|0|a|\epsilon_1^{(1)}\right\rangle\left\langle\bar{\epsilon}_1^{(1)}|a^\dagger|0\right|\bar{\epsilon}_1^{(1)}|a^\dagger|0\right\rangle}{k_1-\epsilon_1^{(1)}}\right)\\&\quad+\text{ all permutations of }\{k_1,k_2\}\text{ and }\{p_1,p_2\}\end{aligned}\tag{11.12}$$

and

$$\begin{aligned}&G^{(2)}(p_1,p_2;k_1,k_2)\\&=-\frac{\mathrm{i}}{2\pi}\sum_{\epsilon_1^{(1)},\epsilon_2^{(2)},\epsilon_3^{(1)}}\left(\left\langle 0|a|\epsilon_3^{(1)}\right|0|a|\epsilon_3^{(1)}\right\rangle\left\langle\bar{\epsilon}_3^{(1)}|a|\epsilon_2^{(2)}\right|\bar{\epsilon}_3^{(1)}|a|\epsilon_2^{(2)}\right\rangle\left\langle\bar{\epsilon}_2^{(2)}|a^\dagger|\epsilon_1^{(1)}\right|\bar{\epsilon}_2^{(2)}|a^\dagger|\epsilon_1^{(1)}\right\rangle\cdot\\&\qquad\left\langle\bar{\epsilon}_1^{(1)}|a^\dagger|0\right|\bar{\epsilon}_1^{(1)}|a^\dagger|0\right\rangle\frac{1}{k_1-\epsilon_1^{(1)}}\frac{1}{k_1+k_2-\epsilon_2^{(2)}}\frac{1}{p_2-\epsilon_3^{(1)}}\Bigg)\\&\quad+\text{ all permutations of }\{k_1,k_2\}\text{ and }\{p_1,p_2\}.\end{aligned}\tag{11.13}$$

The exact expression for the 4-point Green's function is listed in section 11.8. Finally, the two-photon S-matrix is given by

$$S(p_1,p_2;k_1,k_2) = G(p_1,p_2;k_1,k_2)+ \\ (S(p_1;k_1)S(p_2;k_2) + (k_1 \leftrightarrow k_2))\,. \tag{11.14}$$

Graphs of $|G(p_1,p_2;k_1,k_2)|^2$ are plotted in Fig. 11.7 under two different conditions i) $\omega_d^2 > \gamma_c^2/4$ and ii) $\omega_d^2 < \gamma_c^2/4$. The plots are generated with the total incoming momentum going slightly off the two-photon resonance ($E_i = 2\omega_c$) because the 4-point Green's function is identically zero at resonance (section 11.8). This means that two photons inserted into the system at the two-photon resonance will scatter off as independent photons. In Fig. 11.7(a–c), under i), the spectra exhibit eight peaks with the same width while in Fig. 11.7(d–f), under ii), the spectra exhibit only four peaks and the width of the peaks becomes smaller as the detuning ω_d decreases except at zero detuning where the peaks are wider. This observation is consistent with the above arguments that under i) the atoms decay like independent particles, hence the spectra exhibit eight peaks and with the same decay rate which is represented by the width of the peaks while under ii) the atoms decay collectively hence the spectra exhibit only half the number of peaks as compared to i) and with a dominant subradiant profile (narrow peaks) except at $\omega_d = 0$ where only the superradiant state is coupled, and the superradiant effect can be observed (wide peaks).

11.4.3 Bose-Hubbard model

Finally, we consider a fully interacting, many-body scenario — the Bose-Hubbard model,

$$H_{\rm sys} = H_{\rm bh} = \sum_{j=1}^{N}\left(\omega_j a_j^\dagger a_j + \frac{U_j}{2}a_j^\dagger a_j^\dagger a_j a_j\right) \\ + J\sum_{j=1}^{N-1}\left(a_j^\dagger a_{j+1} + a_{j+1}^\dagger a_j\right)$$

The Bose-Hubbard model has been realised in experiments with ultracold atoms [36] and there are many proposals to realise it in different platforms, notably the one using coupled cavity arrays [37, 38, 39]. This model is interesting as it exhibits rich quantum phases. We study the model assuming two input photons and a mesoscopic number of sites as studied in Refs. [11, 40].

Figure 11.8 illustrates a realisation of the Bose-Hubbard model with the open boundary condition, $H_{\rm bh}$ coupled to two waveguides via operators a_1 and a_N. The effective Hamiltonian can be written as

$$H_{\rm eff} = H_{\rm bh} - {\rm i}\frac{\gamma_1}{2}a_1^\dagger a_1 - {\rm i}\frac{\gamma_N}{2}a_N^\dagger a_N.$$

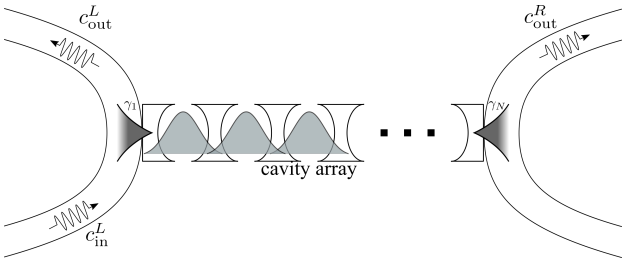

Figure 11.8: Sketch of a one-dimensional nonlinear cavity array coupled to input and output waveguides.

As before we consider only inputs from the left waveguide. To calculate the one- and two-photon S-matrix, we first compute the 2- and 4-point Green's functions. Following the steps in section 11.3 with Fig. 11.2, the 2-point Green's functions are

$$G_{L;L}(p;k) = \sum_{\epsilon^{(1)}}\left\langle 0|a_1|\epsilon^{(1)}\right|0|a_1|\epsilon^{(1)}\Big\rangle\left\langle\bar\epsilon^{(1)}|a_1^\dagger|0\right|\bar\epsilon^{(1)}|a_1^\dagger|0\Big\rangle\frac{-{\rm i}\gamma_1}{k-\epsilon^{(1)}}\delta(p-k)$$

$$G_{R;L}(p;k) = \sum_{\epsilon^{(1)}}\left\langle 0|a_N|\epsilon^{(1)}\right|0|a_N|\epsilon^{(1)}\Big\rangle\left\langle\bar\epsilon^{(1)}|a_1^\dagger|0\right|\bar\epsilon^{(1)}|a_1^\dagger|0\Big\rangle\frac{-{\rm i}\sqrt{\gamma_1\gamma_N}}{k-\epsilon^{(1)}}\delta(p-k) \tag{11.15}$$

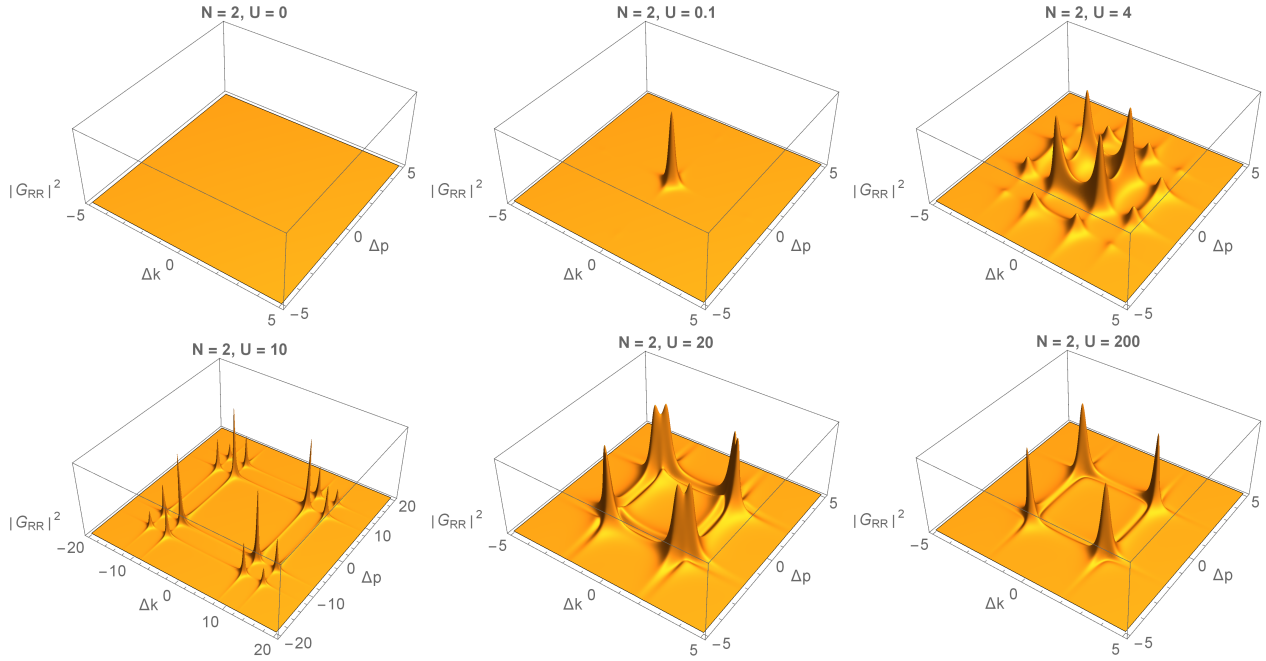

Figure 11.9: **Bose-Hubbard model with $N = 2$:** Plots of $|G_{RR;LL}|^2$ (incoming photon channel labels, LL are dropped) of Bose-Hubbard model with $N = 2$. $U = 0, 0.1, 4, 10, 20$ and 200 respectively above. $\Delta k \equiv k_1 - k_2$ and $\Delta p \equiv p_1 - p_2$. $\omega_0 = 100$, $\gamma = 0.25$ and the total incoming momentum, $k_1 + k_2 = 2\omega_0 + \frac{U}{2} - \sqrt{4J^2 + \frac{U^2}{4}}$, all in units of J.

where the superscript on ϵ denotes the particle-number manifold we are summing over. The one-photon S-matrix elements are as shown in Eq. (11.6) with the 2-point Green's functions in Eq. (11.15). Next, from Fig. 11.3(a), we have

$$\begin{aligned} &G_{i_1 i_2;LL}(p_1, p_2; k_1, k_2) \\ =&\sum_{l=1}^{2} G^{(l)}_{i_1 i_2;LL}(p_1, p_2; k_1, k_2)\delta(p_1 + p_2 - k_1 - k_2) \end{aligned} \tag{11.16}$$

where $G^{(1)}$ and $G^{(2)}$ represent the diagrams $\langle aa^\dagger aa^\dagger | aa^\dagger aa^\dagger \rangle$ and $\langle aaa^\dagger a^\dagger | aaa^\dagger a^\dagger \rangle$ respectively and have expressions

$$\begin{aligned} &G^{(1)}_{i_1 i_2;LL}(p_1, p_2; k_1, k_2) \\ =&\frac{-\mathrm{i}\gamma_1\sqrt{\gamma_{i_1}\gamma_{i_2}}}{2\pi} \sum_{\epsilon_1^{(1)}, \epsilon_2^{(1)}} \left(\frac{\left\langle 0|a_{i_2}|\epsilon_2^{(1)}\right\rangle \left|0|a_{i_2}|\epsilon_2^{(1)}\right\rangle \left\langle \bar{\epsilon}_2^{(1)}|a_1^\dagger|0\right\rangle \left|\bar{\epsilon}_2^{(1)}|a_1^\dagger|0\right\rangle}{p_2 - \epsilon_2^{(1)}} \frac{1}{k_1 - p_1} \cdot \right. \\ &\left. \frac{\left\langle 0|a_{i_1}|\epsilon_1^{(1)}\right\rangle \left|0|a_{i_1}|\epsilon_1^{(1)}\right\rangle \left\langle \bar{\epsilon}_1^{(1)}|a_1^\dagger|0\right\rangle \left|\bar{\epsilon}_1^{(1)}|a_1^\dagger|0\right\rangle}{k_1 - \epsilon_1^{(1)}} \right) \\ &+ \text{ all permutations of } \{k_1, k_2\} \text{ and } \{p_1, p_2\} \end{aligned}$$

and

$$\begin{aligned} &G^{(2)}_{i_1 i_2;LL}(p_1, p_2; k_1, k_2) \\ =&\frac{-\mathrm{i}\gamma_1\sqrt{\gamma_{i_1}\gamma_{i_2}}}{2\pi} \sum_{\epsilon_1^{(1)}, \epsilon_2^{(2)}, \epsilon_3^{(1)}} \left(\left\langle 0|a_{i_2}|\epsilon_3^{(1)}\right\rangle \left|0|a_{i_2}|\epsilon_3^{(1)}\right\rangle \left\langle \bar{\epsilon}_3^{(1)}|a_{i_1}|\epsilon_2^{(2)}\right\rangle \left|\bar{\epsilon}_3^{(1)}|a_{i_1}|\epsilon_2^{(2)}\right\rangle \cdot \right. \\ &\left. \left\langle \bar{\epsilon}_2^{(2)}|a_1^\dagger|\epsilon_1^{(1)}\right\rangle \left|\bar{\epsilon}_2^{(2)}|a_1^\dagger|\epsilon_1^{(1)}\right\rangle \left\langle \bar{\epsilon}_1^{(1)}|a_1^\dagger|0\right\rangle \left|\bar{\epsilon}_1^{(1)}|a_1^\dagger|0\right\rangle \frac{1}{k_1 - \epsilon_1^{(1)}} \frac{1}{k_1 + k_2 - \epsilon_2^{(2)}} \frac{1}{p_2 - \epsilon_3^{(1)}} \right) \\ &+ \text{ all permutations of } \{k_1, k_2\} \text{ and } \{p_1, p_2\}, \end{aligned} \tag{11.17}$$

where it is understood that the channel L (R) corresponds to the operator a_1 (a_N). The two-photon S-matrix elements are then written down as Eq. (11.7) with the 4-point Green's functions in Eq. (11.17). In the following discussion, we will consider the case where all the cavities are identical, i.e. $\omega_i = \omega_0$, $U_i = U\ \forall i$, with identical coupling to both waveguides, i.e. $\gamma_1 = \gamma_N = \gamma$.

Probing the dimer ($N = 2$) with two photons. Using the calculation above, the Bose-Hubbard model with unit filling can be studied in a dimer ($N = 2$) with two photons. We study the behaviour of the resonant peaks of the S-matrix in Fig. 11.9 as we vary U/J from the superfluid regime, $U/J \ll 1$, to the Mott insulator regime, $U/J \gg 1$, with total incoming momentum, $k_1 + k_2 = 2\omega_0 + \frac{U}{2} - \sqrt{4J^2 + \frac{U^2}{4}}$. The total incoming momentum corresponds to the state $\left|\epsilon_-^{(2)}\right\rangle \propto |20\rangle + |02\rangle - \frac{U+\sqrt{16J^2+U^2}}{2\sqrt{2}J}|11\rangle$, which becomes the 'Mott state' $|11\rangle$ as $U/J \to \infty$. As expected, when $U = 0$, the system is linear and hence the nonlinear part described by the Green's function is identically zero. When $U/J \ll 1$, the function exhibits only a single peak. As U/J increases, more peaks are visible, i.e. four peaks in each quadrant, with the two off-diagonal peaks in each quadrant becoming more prominent and finally merging into one at $U/J \gg 1$.

Several points are noteworthy. First, notice that in order for the 4-point Green's function to be identically zero at $U = 0$, either both contributions from $G^{(1)}$ ($\langle aa^\dagger aa^\dagger | aa^\dagger aa^\dagger \rangle$) and $G^{(2)}$ ($\langle aaa^\dagger a^\dagger | aaa^\dagger a^\dagger \rangle$) are identically zero or the contributions from $G^{(1)}$ and $G^{(2)}$ are equal and opposite. However, $G^{(1)}$ is independent of U and is in general nonzero. This can be seen from Fig. 11.3 where its diagram involves only the first excitation manifold that is independent of U. Hence, contributions from $G^{(1)}$ and $G^{(2)}$ must be equal and opposite at $U = 0$, so as to interfere destructively to give a zero 4-point Green's function.

Second, the positions of the peaks are determined by the following equation:

$$|\Delta k(\Delta p)| = \pm 2J - \frac{U}{2} + \sqrt{4J^2 + \frac{U^2}{4}}. \tag{11.18}$$

Figure 11.10 shows a visualisation of Eq. (11.18) together with the corresponding paths represented by different colours.

Third, when $U/J \ll 1$, Eq. (11.18) becomes $|\Delta k(\Delta p)| \approx 0, 4J$. However, in Fig. 11.9, only one peak ($|\Delta k(\Delta p)| \approx 0$) corresponding to paths that go through $\left|\epsilon_-^{(1)}\right\rangle$ twice (red dots in Fig. 11.10) is visible in the transmission spectra. One can understand this by first defining symmetric and anti-symmetric operators, $a_\pm = \frac{1}{\sqrt{2}}(a_1 \pm a_2)$. Then, note that when $U/J \ll 1$ but $U \neq 0$, the contribution from $G^{(1)}$ only cancels part of the contribution from $G^{(2)}$. Hence, we can focus on the diagram represented by $G^{(2)}$, $\langle aaa^\dagger a^\dagger | aaa^\dagger a^\dagger \rangle$, which is the only term that depends on U. The state that we are probing can be very closely approximated by the state that is created by two anti-symmetric operators:

$$\left|\epsilon_-^{(2)}\right\rangle \approx \frac{1}{\sqrt{2}} a_-^{\dagger 2} |0\rangle = \frac{1}{\sqrt{2}} a_-^\dagger \left|\epsilon_-^{(1)}\right\rangle.$$

Because of this symmetry of the system, the paths through $\left|\epsilon_-^{(1)}\right\rangle$ twice are favoured, even though the system is not pumped using the anti-symmetric operator. By choosing to pump the state, $\left|\epsilon_-^{(2)}\right\rangle$, this particular path is automatically preferred as dictated by the symmetry of the system.

Fourth, when $U/J \gg 1$, Eq. (11.18) becomes $|\Delta k(\Delta p)| \approx \pm 2J$, making all four peak positions in each quadrant to become one, as seen in Fig. 11.9. Moreover, before the four peaks in each quadrant become indistinguishable, peaks corresponding to paths that go through both $\left|\epsilon_\pm^{(1)}\right\rangle$ (blue dots in Fig. 11.10) are more dominant. This is because when U/J is large, the symmetry described above is no longer present and different paths have similar contributions in $G^{(2)}$, however, different paths contribute differently in $G^{(1)}$ with diagram $\langle aa^\dagger aa^\dagger | aa^\dagger aa^\dagger \rangle$. In $\langle aa^\dagger aa^\dagger | aa^\dagger aa^\dagger \rangle$, the first excitation manifold is excited twice and hence the paths that go through both $\left|\epsilon_\pm^{(1)}\right\rangle$ are favoured since the other paths go through the same state twice which require the state to decay before it is able to be excited again.

Last, in the intermediate regime where $U/J \sim 1$, the behaviour in Fig. 11.9 can be understood as an interplay and continuation between the two extreme regimes. Further note that the height of the peaks representing the strength of the nonlinearity increases with U as expected.

Many sites regime. Finally, $|G_{RR;LL}|^2$ is plotted in Figs. 11.11 and 11.12 with different numbers of cavities, N and different nonlinearities, U at a total energy of two incoming photons, $k_1 + k_2$ equal to the highest doubly excited state. In Fig. 11.11, off-diagonal peaks ($|\Delta k| \neq |\Delta p|$) that can only result from nonlinear scattering processes are clearly visible. Also, the positions of peaks in Fig. 11.11 correspond to the eigenenergies in the single excitation manifold. Hence, as N increases, the number of peaks increases. Figure 11.12 focuses on the positive quadrant with $N = 5$ and varying U, going from the weakly interacting to strongly interacting regimes. We note three features: with increasing nonlinearity, i) the peaks are located at progressively larger values (refer to Fig. 11.11 in which the clusters of peaks move further apart as U increases); ii) the heights of the peaks become more and more uniform; iii) the relative spacings between the peaks are maintained and when $U/J \ll 1$ only one peak is visible. These features reflect the following facts: i) the highest doubly excited state has a larger energy as the nonlinearity increases; ii) the overlaps between the highest doubly excited state with $a_1 \left|\epsilon^{(1)}\right\rangle$ and $a_N \left|\epsilon^{(1)}\right\rangle$ become more uniform as the nonlinearity increases; iii) the spacings between the peaks

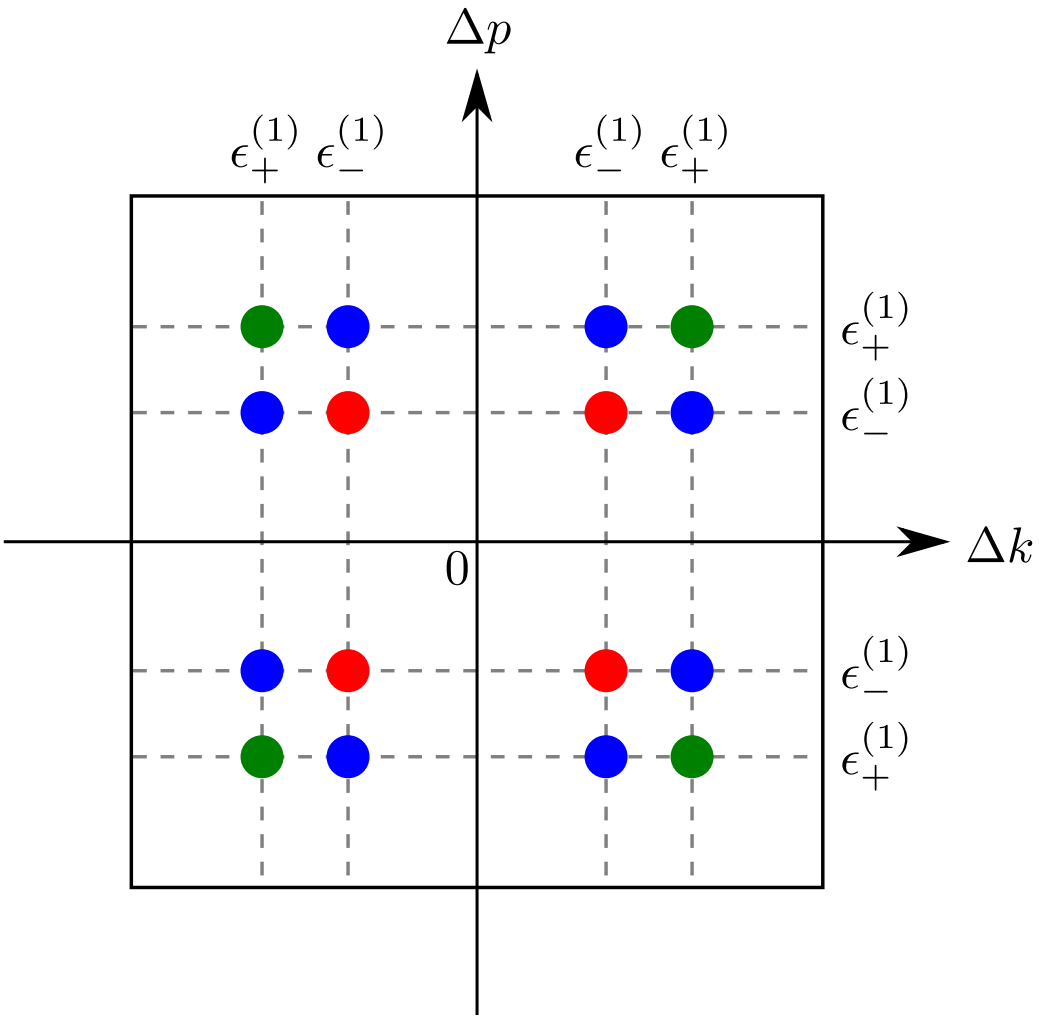

Figure 11.10: Positions of the peaks on the Δk-Δp plane as determined by Eq. (11.18). The different colours denote different paths: red represents paths that go through $\left|\epsilon_-^{(1)}\right\rangle$ twice, blue represents paths that go through both $\left|\epsilon_\pm^{(1)}\right\rangle$ and green represents paths that go through $\left|\epsilon_+^{(1)}\right\rangle$ twice.

reflect the relative gaps between the singly excited states which are independent of U and the single peak at $U/J \ll 1$ can be explained by the same symmetry argument as in the case of two cavities.

11.5 Conclusion

In summary, we have presented a diagrammatic approach to construct the Green's functions (and in turn the S-matrix) required to study multi-photon transmission in one dimensional systems comprised of correlated quantum emitters. Our method can be used for any bosonic many-body systems probed by corresponding leads. The method is especially useful in working out inelastic parts of the scattering matrix. We have demonstrated the usefulness of our technique by going through the calculations of the S-matrix for a few paradigmatic examples including cases of single and many correlated emitters. Through them, we showed that the method simplifies calculations considerably, especially when we are dealing with interacting many-body problems, even at the two-photon level. We also discussed the applicability of our method when one deals with multi-photons scattering from non-interacting emitters, by providing an intuitive way to visualise the scattering processes that map one-to-one to Green's functions. Having the ability to write down expressions of the Green's functions directly and to visualise them will be useful in guessing a system's response qualitatively without computing the exact form.

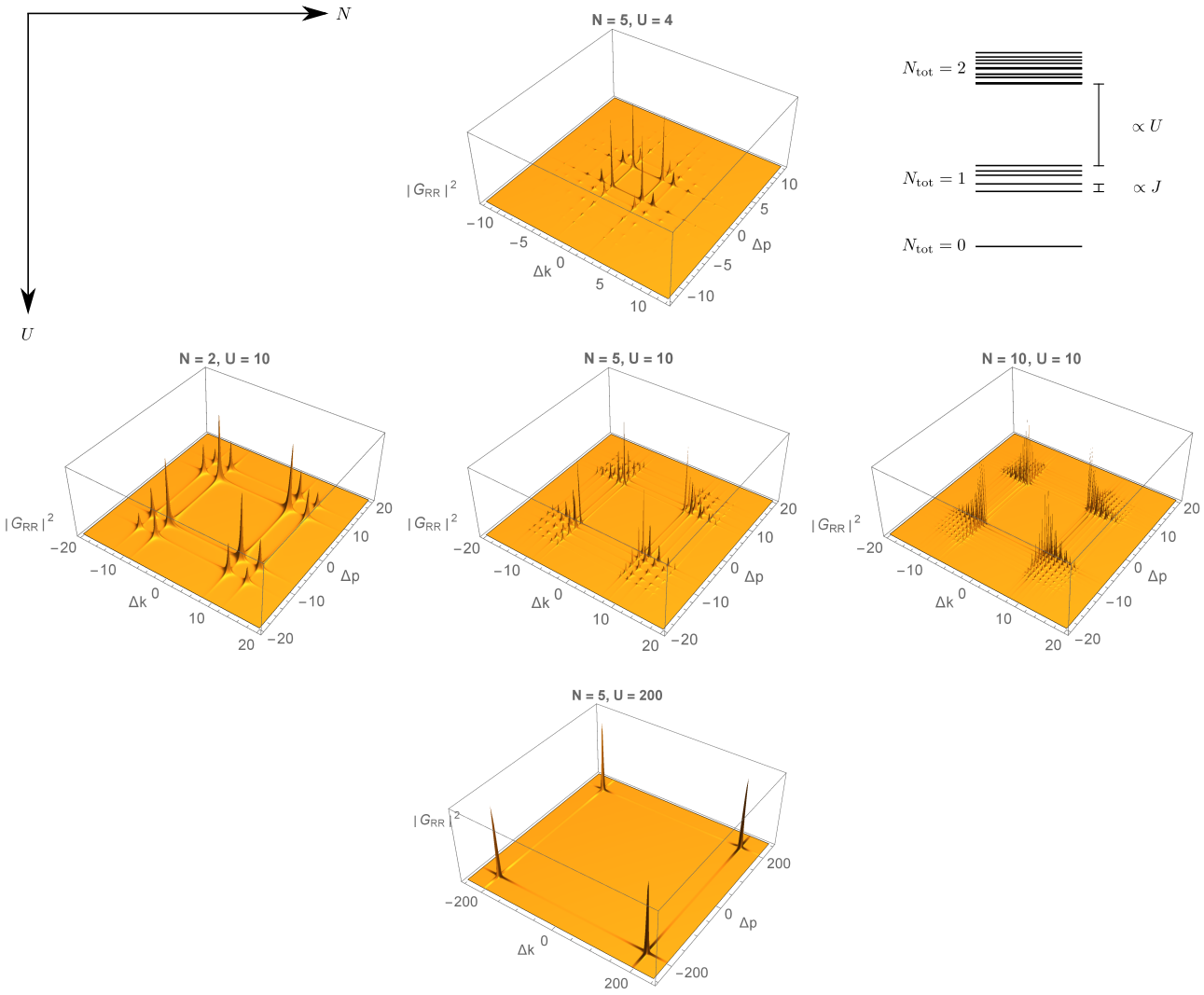

Figure 11.11: **Bose-Hubbard model:** Plots of $|G_{RR;LL}|^2$ (incoming photon channel labels LL are dropped) of the Bose-Hubbard model with the open boundary condition. $N = 2, 5, 10$ and $U = 4, 10, 200$ are shown. $\Delta k \equiv k_1 - k_2$ and $\Delta p \equiv p_1 - p_2$. $\omega_0 = 100$, $\gamma = 0.25$ and the total incoming momentum, $k_1 + k_2 =$ highest doubly excited eigenvalue, all in units of J. The schematic diagram at the top right corner depicts the scaling of the level spacings.

11.6 Cluster decomposition of the S-matrix

Figure 11.13 illustrates the cluster decomposition structure of the S-matrix for up to three photons. We can see that an elastic scattering, in which the photon momenta are simply rearranged at the output, is fully described by the single-photon S-matrix and a larger-photon-number elastic scattering amplitude is just the product of it. This, however, only describes the linear part of the system's response. If the system is nonlinear, there will be inelastic scatterings as well, which gives the S-matrix a richer structure. This is encoded in the Green's functions. Therefore, in order to see the effects of nonlinearity, we need to calculate the Green's functions which form the important part of the S-matrix.

11.7 Proof

Here, we will prove the steps outlined in section 11.3. The time ordering in Eq. (11.4) gives rise to different diagrams. To see this, consider a particular time ordering, $\langle a \dots a a^\dagger \dots a^\dagger | a \dots a a^\dagger \dots a^\dagger \rangle$, up to interchanges of the a's or $a^\dagger$'s at different times that do not change the form. Then, we insert identities, $\mathbb{1} = \sum_\epsilon |\epsilon\rangle \langle\bar{\epsilon}|$ in

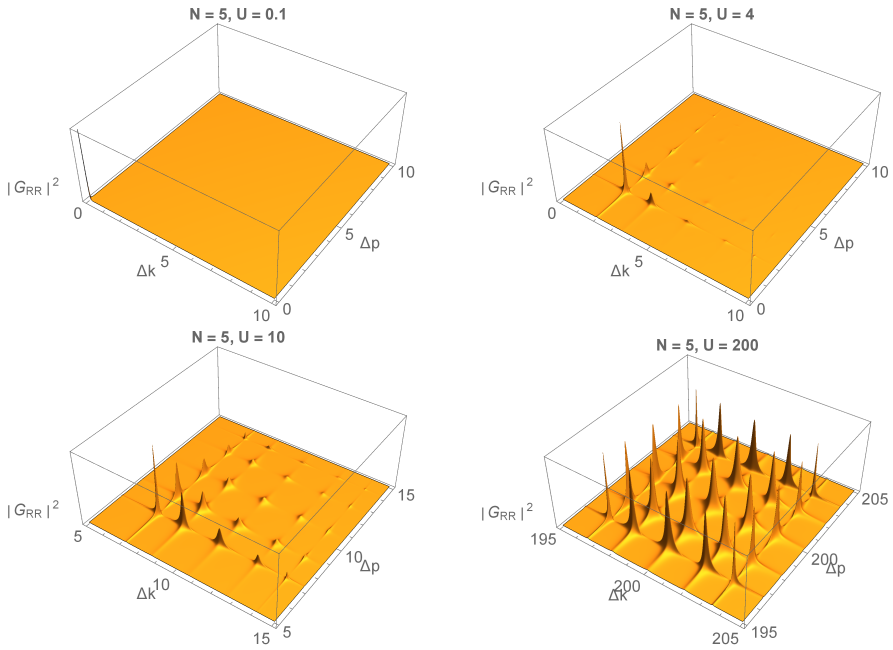

Figure 11.12: **Bose-Hubbard model with $N = 5$:** Plots of $|G_{RR;LL}|^2$ (incoming photon channel labels LL are dropped) of the Bose-Hubbard model with the open boundary condition. $N = 5$ and $U = 0.1, 4, 10$ and 200 respectively. $\Delta k \equiv k_1 - k_2$ and $\Delta p \equiv p_1 - p_2$. $\omega_0 = 100$, $\gamma = 0.25$ and the total incoming momentum, $k_1 + k_2 =$ highest doubly excited eigenvalue, all in units of J.

between two operators to evaluate the expression.

$$
\begin{aligned}
&\langle 0|a(t_1')\dots a(t_m')a^\dagger(t_1)\dots a^\dagger(t_m)|0\big|0|a(t_1')\dots a(t_m')a^\dagger(t_1)\dots a^\dagger(t_m)|0\rangle \\
&\cdot\theta(t_1'-t_2')\dots\theta(t_{m-1}-t_m)(-1)^m \\
=&\sum_{\epsilon_1\dots\epsilon_{2m-1}} \langle 0|a(t_1')|\epsilon_{2m-1}|0|a(t_1')|\epsilon_{2m-1}\rangle\,\langle\bar\epsilon_{2m-1}|\dots|\epsilon_1|\bar\epsilon_{2m-1}|\dots|\epsilon_1\rangle\,\langle\bar\epsilon_1|a^\dagger(t_m)|0\big|\bar\epsilon_1|a^\dagger(t_m)|0\rangle \\
&\qquad\cdot\theta(t_1'-t_2')\dots\theta(t_{m-1}-t_m)(-1)^m \\
=&\sum_{\epsilon_1\dots\epsilon_{2m-1}} \langle 0|a|\epsilon_{2m-1}|0|a|\epsilon_{2m-1}\rangle\,\langle\bar\epsilon_{2m-1}|\dots|\epsilon_1|\bar\epsilon_{2m-1}|\dots|\epsilon_1\rangle\,\langle\bar\epsilon_1|a^\dagger|0\big|\bar\epsilon_1|a^\dagger|0\rangle \\
&\qquad\cdot \mathrm{e}^{-\mathrm{i}\epsilon_{2m-1}(t_1'-t_2')}\dots\mathrm{e}^{-\mathrm{i}\epsilon_1(t_{m-1}-t_m)} \\
&\qquad\cdot\theta(t_1'-t_2')\dots\theta(t_{m-1}-t_m)(-1)^m
\end{aligned}
\tag{11.19}
$$

where we have taken just one particular variant of the form $\langle a\dots aa^\dagger\dots a^\dagger\big|a\dots aa^\dagger\dots a^\dagger\rangle$. To find the Green's function in the momentum space, we perform a Fourier transformation of Eq. (11.19). Since only the exponential and Heaviside step functions are time-dependent, all we need to do is

$$
\mathscr{F}\Big(\mathrm{e}^{-\mathrm{i}\epsilon_{2m-1}(t_1'-t_2')}\dots\mathrm{e}^{-\mathrm{i}\epsilon_1(t_{m-1}-t_m)}\,\theta(t_1'-t_2')\dots\theta(t_{m-1}-t_m)(-1)^m\Big). \tag{11.20}
$$

To calculate this, we perform a change of variables,

$$
\begin{aligned}
\tau_i &= t_{m-i} - t_{m-i+1} && \text{for } i = 1,\dots,m-1 \\
\tau_m &= t_m' - t_1 \\
\tau_{m+i} &= t_{m-i}' - t_{m-i+1}' && \text{for } i = 1,\dots,m-1 \\
\tau_{2m} &= t_m
\end{aligned}
$$

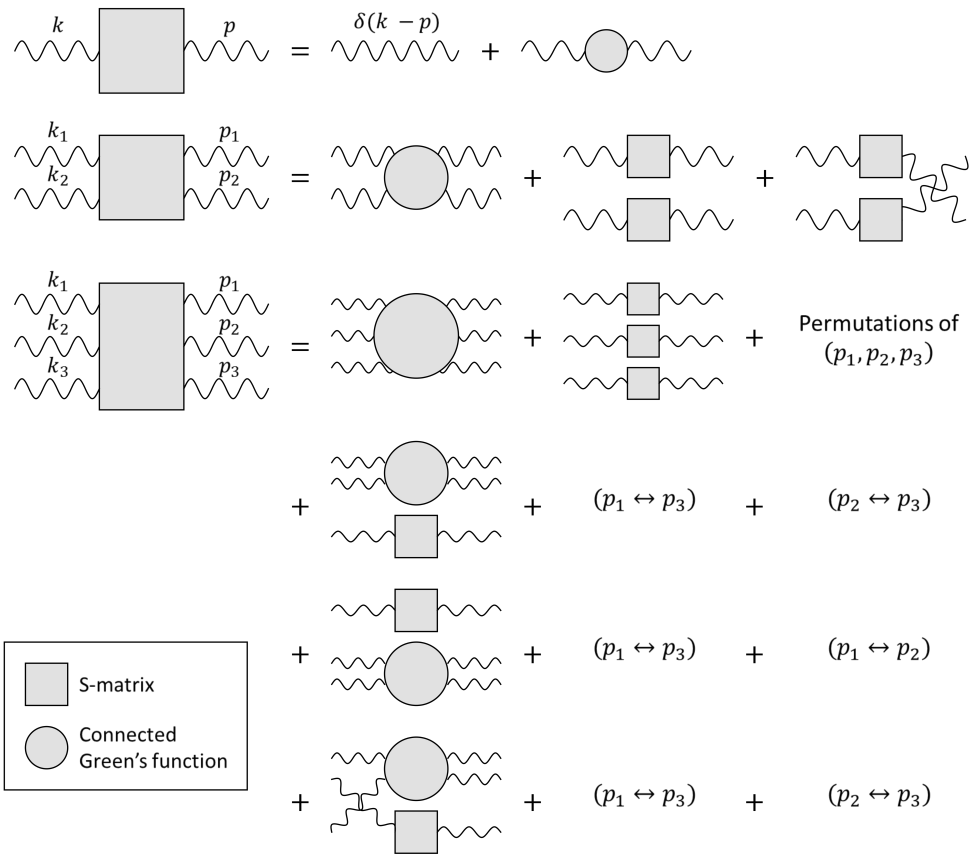

Figure 11.13: Cluster decomposition structure of the one-, two-, and three-photon S-matrix. The n-photon S-matrix is made up of $2m$-point connected Green's functions, for $m \leqslant n$. The delta function in the one-photon S-matrix is present only if the input from the corresponding waveguide is nonzero.

and define

$$\mathbf{t} = \begin{pmatrix} t_m \\ \vdots \\ t_1 \\ t'_m \\ \vdots \\ t'_1 \end{pmatrix}, \qquad \boldsymbol{\alpha} = \begin{pmatrix} k_m \\ \vdots \\ k_1 \\ -p_m \\ \vdots \\ -p_1 \end{pmatrix},$$

$$\boldsymbol{\tau} = \begin{pmatrix} \tau_1 \\ \vdots \\ \tau_{2m} \end{pmatrix}, \qquad M = \begin{pmatrix} 0 & 0 & 0 & \dots & 0 & 1 \\ 1 & 0 & 0 & \dots & 0 & 1 \\ 1 & 1 & 0 & \dots & 0 & 1 \\ \vdots & \vdots & \vdots & \ddots & \vdots & \vdots \\ 1 & 1 & 1 & \dots & 1 & 1 \end{pmatrix}$$

where $\mathbf{t} = M\boldsymbol{\tau}$ and $\mathscr{F} = \int \frac{\mathrm{d}^{2m}\mathbf{t}}{(2\pi)^m}\, \mathrm{e}^{-\mathrm{i}\boldsymbol{\alpha}.\mathbf{t}}$. Eq. (11.20) now becomes

$$\begin{aligned}
&\left(\frac{-1}{2\pi}\right)^m \left(\prod_{i=1}^{2m-1} \int_0^\infty \mathrm{d}\tau_i \int_{-\infty}^\infty \mathrm{d}\tau_{2m}\right) \mathrm{e}^{-\mathrm{i}\boldsymbol{\alpha}.\mathbf{t}} \prod_{j=1}^{2m-1} \mathrm{e}^{-\mathrm{i}\epsilon_j\tau_j} \\
=&\left(\frac{-1}{2\pi}\right)^m \left(\prod_{i=1}^{2m-1} \int_0^\infty \mathrm{d}\tau_i \mathrm{e}^{-\mathrm{i}(\sum_{j=i+1}^{2m}\alpha_j+\epsilon_i)\tau_i}\right) \cdot \\
&\qquad \left(\int_{-\infty}^\infty \mathrm{d}\tau_{2m} \mathrm{e}^{-\mathrm{i}\sum_{j=1}^{2m}\alpha_j\tau_{2m}}\right) \\
=&\frac{(-1)^m}{(2\pi)^{m-1}}\, \delta\left(\sum_{j=1}^{2m}\alpha_j\right) \left(\prod_{i=1}^{2m-1} \frac{-\mathrm{i}}{\sum_{j=i+1}^{2m}\alpha_j + \epsilon_i}\right) \\
=&\frac{-\mathrm{i}}{(2\pi)^{m-1}}\, \delta\left(\sum_{i=1}^{m} k_i - \sum_{i=1}^{m} p_i\right) \left(\prod_{i=1}^{2m-1} \frac{1}{\sum_{j=1}^{i}\alpha_j - \epsilon_i}\right)
\end{aligned}$$

The other variants in $\langle a \dots aa^\dagger \dots a^\dagger | a \dots aa^\dagger \dots a^\dagger \rangle$ are accounted for by permutations of the k's and p's of the previous line. This together with the sum over weights in Eq. (11.19) gives us all the factors detailed in section 11.3. If instead we have a different time ordering, the weights that we sum over in Eq. (11.19) will be different but will take a straight forward form. Moreover, the Heaviside step functions in Eq. (11.20) will be such that they show the time ordering together with the exponential functions. For example, if we consider an ordering like $\langle aa^\dagger aa^\dagger \dots aa^\dagger | aa^\dagger aa^\dagger \dots aa^\dagger \rangle$, the weights to sum over will look like

$$\sum_{\epsilon_1 \dots \epsilon_{2m-1}} \langle 0|a|\epsilon_{2m-1}|0|a|\epsilon_{2m-1}\rangle \left\langle \bar{\epsilon}_{2m-1}|a^\dagger \dots a|\epsilon_1 \middle| \bar{\epsilon}_{2m-1}|a^\dagger \dots a|\epsilon_1 \right\rangle \left\langle \bar{\epsilon}_1|a^\dagger|0 \middle| \bar{\epsilon}_1|a^\dagger|0\right\rangle$$

and Eq. (11.20) will look like

$$\mathscr{F}\Big(\mathrm{e}^{-\mathrm{i}\epsilon_{2m-1}(t'_1-t_1)}\mathrm{e}^{-\mathrm{i}\epsilon_{2m-2}(t'_2-t_2)} \dots \mathrm{e}^{-\mathrm{i}\epsilon_1(t'_m-t_m)} \theta(t'_1-t_1)\theta(t'_2-t_2)\dots\theta(t'_m-t_m)(-1)^m\Big) \tag{11.21}$$

up to permutations of a's and $a^\dagger$'s at different times. The proof can then be proceeded as before by defining $\boldsymbol{\tau}$ in a similar fashion, and $\mathbf{t}$ as a list from earliest time to latest time and $\boldsymbol{\alpha}$ accordingly. It is now obvious to see that different time orderings give the same general expression but can be represented with different diagrams. For non-particle number conserving Hamiltonians, the same expression holds but the sum will now have to be taken over all eigenenergies instead of a particular manifold and the interpretation of the diagrams will be different.

11.8 4-point Green's function for two collocated atoms

The exact expression of the 4-point Green's function for two collocated atoms coupled to a waveguide (section 11.4.2) is as below:

$$\begin{aligned} &G(p_1, p_2; k_1, k_2) \\ =&\frac{\mathrm{i}}{32\pi\gamma_c^2}\frac{E_i - 2\omega_c}{E_i - 2\omega_c + \mathrm{i}\gamma_c} g_{k_1} g_{k_2} g_{p_1} g_{p_2} \Big(4(E_i - 2\omega_c + 2\mathrm{i}\gamma_c) \\ &+ \omega_d^2 f^{(2)}(\mathbf{p};\mathbf{k}) + \omega_d^4 f^{(4)}(\mathbf{p};\mathbf{k}) \Big) \delta(E_i - E_o) \end{aligned}$$

where

$$\begin{aligned} f^{(2)}(\mathbf{p};\mathbf{k}) &= \frac{(E_i - 2\omega_c)\Big((k_1 - k_2)^2 + (p_1 - p_2)^2 \\ &\qquad + 4\gamma_c^2 + 2(E_i - 2\omega_c + 2\mathrm{i}\gamma_c)^2 \Big)}{(k_1 - \omega_c)(k_2 - \omega_c)(p_1 - \omega_c)(p_2 - \omega_c)} \\ f^{(4)}(\mathbf{p};\mathbf{k}) &= -\frac{4(3(E_i - 2\omega_c) + 2\mathrm{i}\gamma_c)}{(k_1 - \omega_c)(k_2 - \omega_c)(p_1 - \omega_c)(p_2 - \omega_c)}. \end{aligned}$$

Part VIII
Experiments: Main Articles

12 Nonexponential decay of a giant artificial atom by Andersson et. al.

In quantum optics, light-matter interaction has conventionally been studied using small atoms interacting with electromagnetic fields with wavelength several orders of magnitude larger than the atomic dimensions [1, 2].
(why?)
In contrast, here we experimentally demonstrate the vastly different *giant atom* regime, where an artificial atom interacts with acoustic fields with wavelength several orders of magnitude *smaller* than the atomic dimensions.
This is achieved by coupling a superconducting qubit [3] to surface acoustic waves at two points with separation on the order of 100 wavelengths.
(read the Schoelkopf2008 article!)
This approach is comparable to controlling the radiation of an atom by attaching it to an antenna.
(antenna?)
The slow velocity of sound leads to a significant internal time-delay for the field to propagate across the giant atom, giving rise to non-Markovian dynamics [4].
(why non-Markovian dynamics??? they cite Pletyukhov, so it is explained in this note somwehere)
We demonstrate the non-Markovian character of the giant atom in the frequency spectrum as well as nonexponential relaxation in the time domain.

Cavity Quantum Electrodynamics (cavity QED) studies the interaction between atoms and photons in configurations where the atom is placed inside a cavity to enhance the interaction strength with the radiation field[5, 6].
In parallel, artificial atoms based on superconducting circuits have emerged in the last 20 years and over the past 15 years, superconducting circuit quantum electrodynamics has developed as an analogue to the cavity QED experiments[7].
This has enabled probing the strong and ultrastrong coupling regimes of atom - light interaction to study exotic phenomena including vacuum Rabi splitting [8] and the controlled generation of non-classical photon states [9, 10].
(never heard about it, I'll read later)
A later development was waveguide QED where superconducting circuits were coupled to open transmission lines [11, 47, 13].
These experiments replace natural atoms and optical cavities with Josephson junction-based superconducting circuits behaving as artificial atoms strongly coupled to the field in open transmission lines or planar or 3D microwave resonators [14, 13].
(I'll create a section about how exactly superconducting circuits simulators work? very not obvious that these systems behave same way (SC circuits, atoms))

For atoms coupled to laser light in optical cavity QED and the interaction of microwaves with either Rydberg atoms in cavities or artificial atoms in circuit QED, treating the atom as a pointlike dipole is a valid approximation.
(maybe it is not answer anywhere, why it is so, but still it is a good question, why (about dipole)?)
In fact, in all the experiments mentioned above (SC circuits) the size of the atom L is at least an order of magnitude smaller than the wavelength λ of the interacting radiation.

More recently, a superconducting transmon qubit [15] was coupled to propagating surface acoustic waves (SAW) on a piezoelectric substrate [16], demonstrating qubit decay by SAW emission and nonlinear reflection of SAW beams.
(I'll read later)
Analogues of resonator QED architectures were realized in later experiments [17, 18, 19, 20, 21] where an artificial atom was coupled to the phonons inside an acoustic cavity [22].
(I'll read later)
Further work exploited superconducting qubits to generate and characterize phononic Fock states in SAW cavities as well as in bulk acoustic cavities [18, 23].
(I'll read later)
Owing to the slow propagation speed of sound in solids (3000 m/s), for a given frequency the wavelength of sound is five orders of magnitude smaller than that of light in vacuum.
This property allow artificial atoms to interact with propagating acoustic fields beyond the small-atom approximation such that $L > \lambda$ [24].
(what is in Kockum2014?)
Crucially to the experimental results presented here, the slow velocity of SAW further enables the engineering of time delays that are significant compared to the relaxation time as laid out in ref. [4] proposing the giant atom configuration we have implemented here. In this case the emitted excitation can be reabsorbed by the atom leading to non-Markovian effects.

Growing interest in quantum information science has spurred substantial theoretical investigations of non-Markovian open quantum systems, characterized by information back-flow from the environment [25]. In this context, the physical origin of the non-Markovianity is typically the coupling to a structured or finite reservoir. In contrast, we have realized a non-Markovian system by introducing deterministic time-delayed feedback through coupling a single quantum emitter at two distant points to a radiation field in one dimension. This feedback is intrinsic to the giant atom itself and can be engineered. In addition to enabling new parameter regimes in atom-field interactions, time-delayed feedback has potential applications in quantum information processing [26, 27]. It has been suggested that this form of non-Markovianity could be exploited to generate cluster states for universal measurement-based quantum computation requiring considerably less hardware resources than gate-based approaches [27]. Recent work [28] has also demonstrated that architectures involving multiple giant atoms can be designed to realize inter-atomic interactions while protecting the atoms from decohering into the waveguide, provided their coupling points overlap in a braided configuration. This makes giant atoms a relevant candidate for applications in quantum simulation.

The giant atom

The artificial atom in this experiment is a transmon qubit, consisting of a superconducting quantum interference device (SQUID) loop connected in parallel with an interdigital transducer (IDT) [16, 29].

(interdigital transducer ???)

This interdigitated finger structure provides a shunt capacitance for the transmon as well as coupling to SAW at wavelengths matching the periodicity of the IDT, 1.25 µm.

(shunt capacitance???)

Due to the fixed periodicity of the finger structure, the coupling is frequency dependent and given by [supplementary]

$$\gamma(\omega) = \frac{N_p K^2 \omega_{01}}{4} \left(\frac{\sin X}{X} \right)^2 , \tag{12.1}$$

where $\omega_{01}/2\pi$ is the qubit resonance frequency and $X = N_p \pi(\omega_{\mathrm{IDT}} - \omega)/\omega_{\mathrm{IDT}}$.

(in which formula there is this coupling ?)

This gives rise to a coupling strength that is proportional to the number of finger pairs N_p, with a coupling bandwidth that scales inversely with N_p. Our devices are fabricated using aluminium on GaAs which has a SAW velocity of $v_{\mathrm{SAW}} = 2900\,\mathrm{m/s}$.

The piezo-electric coupling coefficient ($K^2 = 0.07\,\%$) of GaAs, while relatively low compared to materials such as lithium niobate and quartz [29], is still strong enough to ensure that the qubit lifetime τ is dominated by the acoustic coupling.

(why piezo-electric is here?)

The giant atom is realized by splitting the IDT into two electrically connected coupling points separated a by a distance L.

Relevant sample parameters are listed in table 1.

Due to the strong electromechanical coupling and slow propagation velocity of SAW, the propagation time $T = L/v_{\mathrm{SAW}}$ can be orders of magnitude larger than the excited state lifetime.

(why?)

In such a case, a phonon emitted into the transmission line at one coupling point of the qubit due to the spontaneous decay may later be reabsorbed by the qubit at the second point.

Considering the local IDT as a pointlike coupling center with coupling strength γ, the time-delay dynamics of the excited state amplitude a_e in the absence of external driving is given by [4]

$$\frac{\partial a_e(t)}{\partial t} = -i\omega_{01} a_e(t) - \gamma \left(a_e(t) + a_e(t-T) \right). \tag{12.2}$$

(check that work, how this formula is deriven?)

(what is the plot of this function???)

In the giant atom regime, characterised by $\gamma T \gtrsim 1$, the time delayed coupling term in eq. (12.2) introduces markedly non-Markovian effects, which is the subject of this paper.

The SAW-giant atom interaction is characterized using two different device designs. In design A, shown in Fig. 12.1a, the transmon is embedded in a SAW transmission line with IDTs to generate and pick up acoustic signals. In addition to IDTs on either side, a capacitively coupled gate provides electrical control. Using this design we first measure the SAW scattering properties to verify acoustic coupling. The steady-state emission properties are then characterized for a range of giant atom parameters by measurements via the electrical gate. For a chosen set of giant atom parameters, we implement a second device, design B, where the transmon is capacitively coupled to a coplanar waveguide $\lambda/4$ resonator. This enables us to read-out the state of the transmon by probing the resonator, which we exploit to perform spectroscopy on the giant atom as well as time domain relaxation measurements. All the measured results are obtained at the 10 mK base temperature of a dilution refrigerator. The qubit resonance frequency is tuned into the SAW coupling band ($\omega_{01}/2\pi \approx 2.3\,\mathrm{GHz}$) using an applied external magnetic flux.

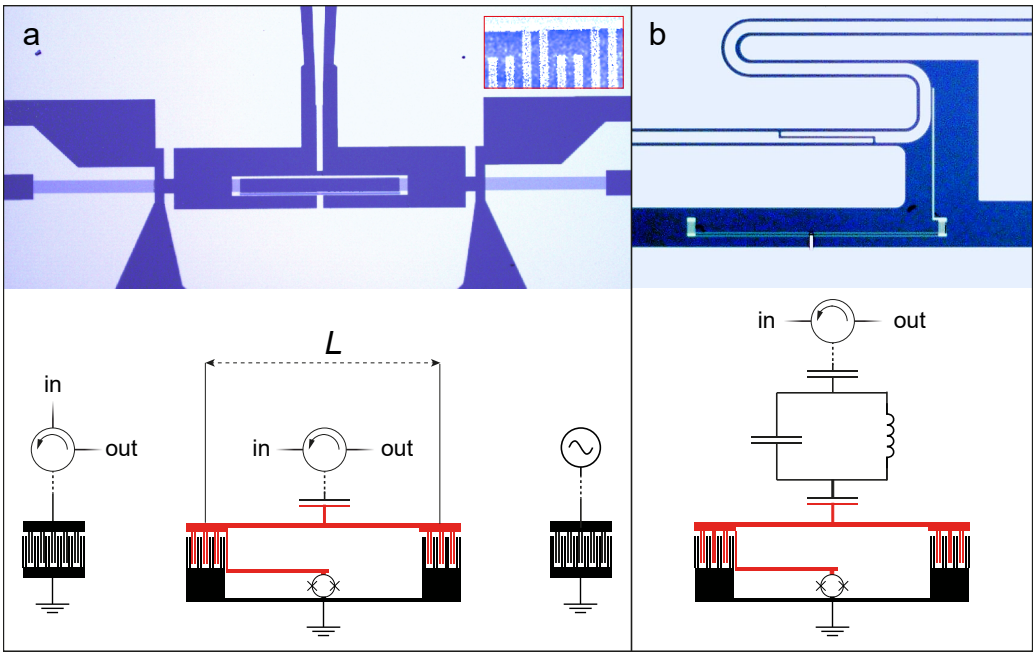

Figure 12.1: **Device layouts.** **a**, false-color optical micrograph and circuit schematic of a giant atom capacitively coupled to an electrical gate. The GaAs substrate is shown in blue and the aluminum circuit and ground planes are white. The transmon circuit that makes up the giant atom is grounded and has two Josephson junctions forming a SQUID loop to enable frequency tuning via an external coil. The acoustic reflection and transmission properties are probed via IDTs on either side of the giant atom. A circulator routes the reflected gate signal to a cryogenic amplifier. Inset shows a false-color scanning electron micrograph of the finger structure of the giant atom IDTs. **b**, false-color optical micrograph and circuit schematic of giant atom coupled to a coplanar waveguide resonator. Excitation and readout tones are sent via a circulator to the resonator input. The reflected readout signal is amplified and measured similarly to the gate reflecion in **a**.

Scattering Measurements

The steady state acoustic transmission amplitude is measured at the pick-up IDT while a continous weak SAW drive is applied to the giant atom using the launcher IDT. In Fig. 12.2a we map the acoustic transmission amplitude for sample A4 as a function of drive frequency $\omega_d/2\pi$ while tuning the qubit resonance frequency $\omega_{01}/2\pi$. At weak driving powers, we expect to approach the limit of near-perfect extinction of transmitted SAWs when ω_d matches ω_{01} [43, 11]. However, for our giant atom, we observe that interference between the scattering of each point causes the the condition for total reflection of a coherent beam to be modified from $\omega_d = \omega_{01}$. A right-propagating SAW beam of frequency $\omega/2\pi$ transmitted at $x = 0$ (left coupling point) will pick up a phase factor $e^{i\omega T}$ before interacting with the giant atom again at $x = L$. The phase factors add up to yield a maximum reflection condition of [4]

$$\omega_{01} = \omega_d - \gamma \sin \omega_d T. \tag{12.3}$$

The coupling point separation of sample A4 ($L = 550\,\mu\text{m}$) is sufficiently large that interference fringes are visible within the bandwidth constrained by the launcher and pickup IDTs.

Next, we study the the SAW emission from the giant atom. A continuous drive of frequency $\omega_d/2\pi$ is applied to the capacitively coupled electrical gate while measuring the reflected amplitude of the drive tone. Efficient conversion of the input signal to SAW will result in a dip in the gate reflection, allowing for the characterization of the steady state emission of the giant atom (Fig. 12.2b). Similarly to the acoustic reflection off a giant atom, this does not generally occur for $\omega_{01} = \omega_d$ [supplementary].

The condition for maximal transduction of the electrical signal to outgoing SAW coincides with maximal acoustic reflection and is given by eq. (12.3). In addition, the giant atom coupling to SAW depends on the drive frequency as

$$\gamma_{\text{eff}} = \gamma \left(1 + \cos \omega_d T\right). \tag{12.4}$$

As this measurement is not limited by the bandwidth of the launcher IDTs, the giant atom properties may be probed across a wider frequency range than in the purely acoustic case. We exploit this to measure gate reflection for three samples with intrinsic time delays of $T \approx \{19\,\text{ns}, 45\,\text{ns}, 190\,\text{ns}\}$. Going deeper into the giant

sample	N_p	$\gamma/2\pi$	T	γT	L	$\gamma_{\text{gate}}/2\pi$	$2\gamma/\gamma_{\text{ext}}$
A1	14	6.1 MHz	19 ns	0.8	55 µm	1.25 MHz	4.4
A2	14	4.4 MHz	46 ns	1.4	125 µm	1.5 MHz	1.8
A3	18	5.8 MHz	190 ns	7.0	550 µm	2.2 MHz	1.9
A4	18	5.3 MHz	190 ns	6.3	550 µm	-	-
B1	14	4.8 MHz	160 ns	4.8	450 µm	-	1.4

Table 1: **Giant atom sample parameters**. IDT finger pairs per coupling point N_p, Acoustic coupling strength per coupling point γ, time delay T and coupling point separation L for the giant atom samples. All samples have an IDT center frequency of 2.3 GHz. The resonator in sample B1 has a resonance frequency of 2.77 GHz. The coupling strength to the electrical gate γ_{gate} is shown for samples A1, A2, A3 in the second column from the right. The rightmost column shows the ratio of the total SAW coupling 2γ to the sum of non-acoustic decay rates $\gamma_{\text{ext}} = \gamma_{\text{res}} + \gamma_{\text{gate}}$. The parameters for samples A1, A2, A3 are extracted from fits to the gate reflection measurements shown in Fig. 12.2b, where γ is estimated by a fit of the resonance frequency to eq. (12.3). The gate coupling γ_{gate} is estimated from the linewidth. The parameters for sample B1, which is coupled to a microwave resonator (with coupling strength $g = 18$ MHz) rather than an electrical gate, are determined by two-tone spectroscopy of the absorption (Fig. 12.3a).

atom regime, i.e. increasing T, leads to a finer interference structure in the gate reflection, which is shown in Fig. 12.2b. Fitting the resonance frequency modulation to data from the largest atom, the designed separation distance (550 µm) yields a SAW velocity of 2906 m/s on GaAs, consistent with literature values at millikelvin temperatures [29].

Qubit readout measurements

Coupling the giant atom to an electromagnetic resonator in addition to the SAW field enables spectroscopy in the dispersive regime of circuit QED. This allows us to measure the excited state population. In sample B1, a $\lambda/4$ resonator with resonance frequency $f_r = 2.77$ GHz is capacitively coupled to the giant atom with coupling strength $g/2\pi = 15$ MHz. Operating the giant atom at IDT resonance (2.29 GHz) gives an atom-cavity detuning of 480 MHz, resulting in a dispersive shift $\chi/2\pi = 0.47$ MHz. This is small compared to the SAW-atom interaction strength but sufficiently large to read out the qubit state via the resonator phase response. The spectrum of sample B1 is probed in two-tone spectroscopy with a weak, fixed-frequency readout tone applied at f_r while a drive tone is swept across the resonance of the giant atom. The interaction with phonons already emitted into the SAW channel gives rise to a multi-peak structure in the absorption very different from the Lorentzian lineshape of ordinary (small) atoms. In Fig. 12.3a the phase of the readout tone is shown along with a fit to the expression

$$S_0(\omega) = \frac{\omega_{01}}{\left|\omega - \omega_{01} + i\gamma\left(1 + e^{i\omega T}\right) + i\gamma_{\text{res}}\right|^2} \tag{12.5}$$

where $\gamma_{\text{res}} \approx 2\pi \cdot 6.85$ MHz represents residual broadening of the spectral lineshape induced by non-acoustic decay as well as the finite spectroscopic drive power.

The spectrum of the giant atom excitation is related to its time evolution via the Fourier transform, such that $S_0 = \left|\int_{-\infty}^{\infty} a_e(t) e^{i\omega t} dt\right|^2$. The excitation amplitude of an initially excited giant atom evolves according to

$$a_e(t) = \sum_{n=0}^{\infty} \Theta(t - nT) \frac{(-\gamma(t - nT))^n}{n!} e^{-i(\omega_{01} - i\gamma - i\gamma_{\text{res}})(t - nT)} \tag{12.6}$$

where $\Theta(t)$ is the Heaviside function. For times $t > T$, interference between the instantaneous relaxation and the amplitude already emitted into the acoustic field gives rise to subexponential decay. While the inital decay is exponential with a rate fixed by γ, each revival peak decays slower than exponentially and, on sufficiently short timescales, the peak amplitude is only polynomially damped. The time evolution of $|a_e(t)|$ that corresponds to the power spectrum of Fig. 12.3a is shown as the red line in Fig. 12.3b. It captures well the features of the Inverse Fourier Transform (IFT) of the measured giant atom power spectrum (black dotted line, Fig. 12.3b). In the supplementary materials we show that the trace distance between the initially excited state and the ground state evolves non-monotonically in time, providing a quantitative measure of the non-Markovianity of the giant atom [31].

To directly probe the non-exponential decay in the time domain, we monitor continuously the phase response of the readout resonator while applying an approximate π-pulse to the giant atom. The data is averaged

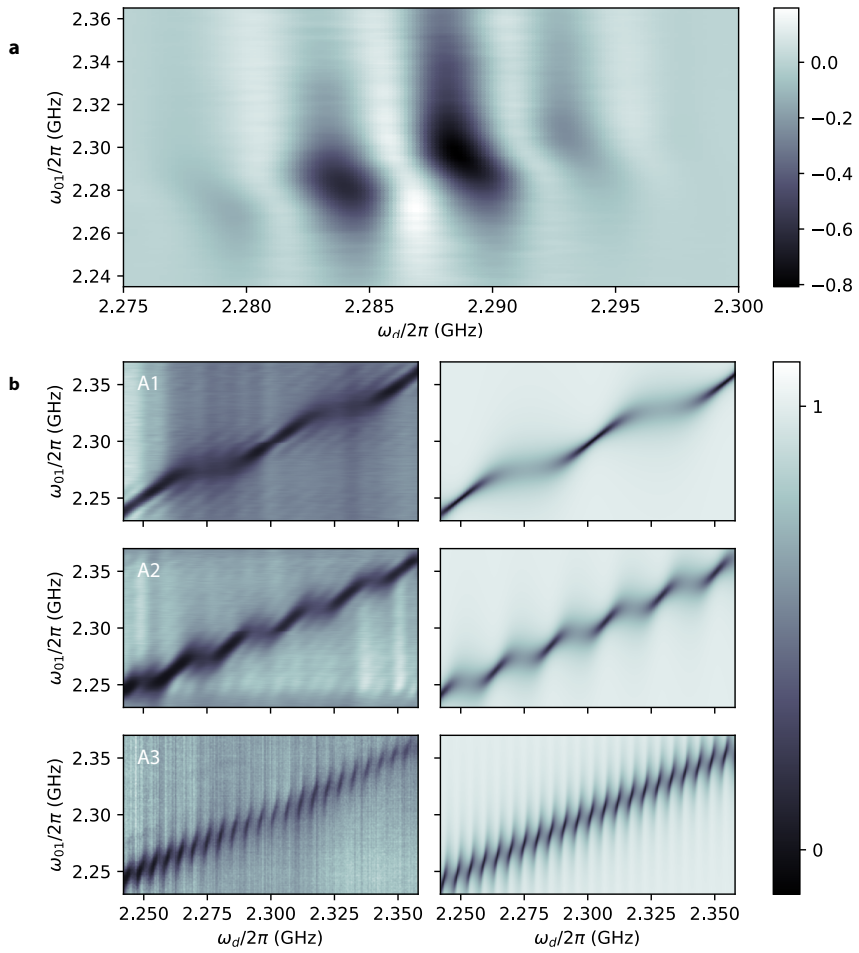

Figure 12.2: **Scattering properties of the giant atom**. **a**, Acoustic power transmission (normalized) of a SAW signal from launcher IDT to pickup IDT measured as function of SAW frequency $\omega_d/2\pi$ and giant atom frequency $\omega_{01}/2\pi$ for sample A4. The background transmission when the giant atom is far detuned from the SAW frequency range has been subtracted. The small positive values for certain frequencies is an artefact of this subtraction [supplementary]. The magnitude is normalized to the maximal SAW transmission of the subtracted, far-detuned trace. The two visible dips in transmission are separated by $1/T \approx 5\,\mathrm{MHz}$. The limited bandwidth of the launcher and pickup IDTs allows the acoustic scattering to be mapped across a frequency span of approximately 14 MHz. **b**, Reflected electromagnetic power (normalized) off the capacitively coupled electrical gate for three different giant atoms. (A1-A3) The reflectance is measured while sweeping the drive frequency ω_d and giant atom frequency ω_{01} (left panel). Theoretical reflectance given by eq. (8) of [supplementary] (right panel). Sample parameters are listed in table 1. The residual dissipation included to generate the theory plots are $\gamma_q/2\pi = \{1.5\,\mathrm{MHz}, 3.5\,\mathrm{MHz}, 4.0\,\mathrm{MHz}\}$ for A1, A2, A3. Increasing the coupling point separation, and thereby the time delay T, gives rise to finer structure in the interference pattern. The background reflection when the giant atom is far detuned from the SAW frequency range has been subtracted.

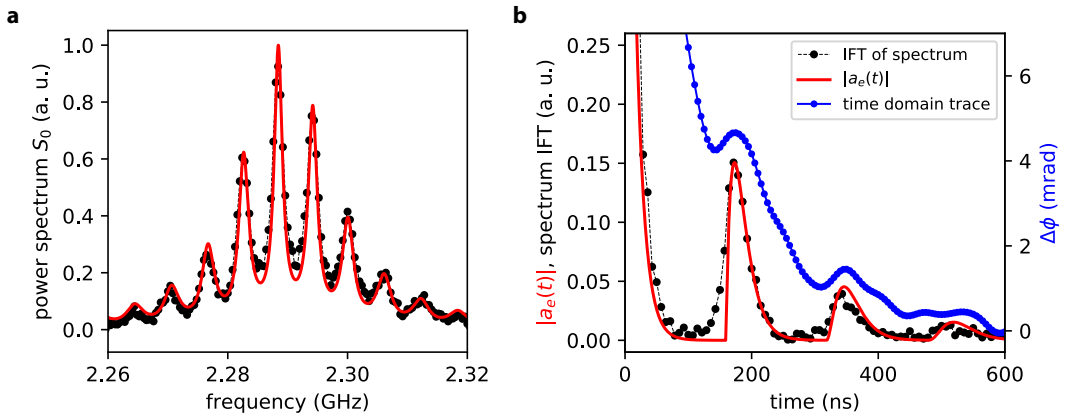

Figure 12.3: **Frequency response and dynamics of the giant atom.** **a**, Two-tone spectroscopy of the giant atom measured through the electromagnetic resonator. A fixed-frequency readout is applied on resonance with the resonator, while a probe tone is swept across the giant atom resonance $\omega_{01}/2\pi = 2.29\,\mathrm{GHz}$. The dotted black line shows the spectrum (normalized) of a giant atom with $L = 450\,\mu\mathrm{m}$ (sample B1) obtained from the readout phase response. A fit to eq. (12.5) is shown as a red line. The multi-peak structure arises due to the interference of SAW emission from the giant atom coupling points. **b**, Time evolution of the giant atom excited state population. The dotted black line shows the magnitude of the inverse Fourier transform of the (complex-valued) spectrum plotted in **a**. The red line shows the time evolution of $|a_e(t)|$ corresponding to the spectrum S_0 in **a**. This implies the (magnitude square) Fourier transform of a_e gives the fit to S_0. The relaxation obtained in the time domain via a readout tone to the resonator is shown in blue. The elevated power in the readout tone causes slowdown in the qubit-resonator interaction, leading to the slowly decaying envelope in the response.

approximately 10^7 times and shown as the blue line in Fig. 12.3a. The readout tone is applied with high power [32] such that the qubit-cavity system enters the nonlinear regime where switching between meta-stable states occur. In this regime the resonator acquires a memory of the qubit state longer than the qubit relaxation time, giving rise to a slowly decaying exponential envelope. This appears as a smearing effect in the time trace. Two revivals of the giant atom are clearly visible in this measurement, occurring at times consistent with the spectroscopic data.

Summary and outlook

Our results show that the acousto-electric interaction can be exploited to investigate previously unexplored parameter regimes of light-matter interaction. We have demonstrated that superconducting qubits can be strongly coupled to SAW such that the giant atom regime can be reached with significant internal time delays giving rise to non-Markovian dynamics. In the present experiment we have studied spontaneous emission from a single giant atom. Further new physics can be expected in circuit- and waveguide-QED settings for systems that break the Markov approximation. For example, it would be interesting to study waveguide-mediated interactions between quantum emitters in the non-Markovian regime, or the quantum properties of sound reflected from a giant atom.

Part IX
Bound States with Photons: Main Articles

13 Waveguide QED: Many-Body Bound State Effects in Coherent and Fock State Scattering from a Two-Level System by Zheng, Gauthier, Baranger

Abstract

Strong coupling between a two-level system (TLS) and bosonic modes produces dramatic quantum optics effects. We consider a one-dimensional continuum of bosons coupled to a single localized TLS, a system which may be realized in a variety of plasmonic, photonic, or electronic contexts. We present the exact many-body scattering eigenstate obtained by imposing open boundary conditions. *Multi-photon bound states* appear in the scattering of two or more photons due to the coupling between the photons and the TLS. Such bound states are shown to have a large effect on scattering of both Fock and coherent state wavepackets, especially in the intermediate coupling strength regime. We compare the statistics of the transmitted light with a coherent state having the same mean photon number: as the interaction strength increases, the one-photon probability is suppressed rapidly, and the two- and three-photon probabilities are greatly enhanced due to the many-body bound states. This results in non-Poissonian light.

13.1 Introduction

Recently, there has been increasing interest in designing quantum optical elements based on the strong coupling between light and matter [1, 2, 3, 4, 5, 6, 7, 8, 9]. The strong coupling regime has been realized in the classic cavity quantum electrodynamics (QED) systems [10, 11, 12], as well as in circuit-QED experiments [13, 14, 15, 16]. Several experimental systems have been proposed for realizing devices such as a single-photon transistor [4, 8] or a quantum switch [6, 7, 17], including surface plasmons coupled to a single two-level emitter [4], a superconducting transmission line resonator coupled to a local superconducting charge qubit [6, 7], and propagating photons in a 1D waveguide coupled to a two-level system [18, 19]. Most of the theoretical work focuses on a single-photon coupled to a local quantum system modeled as a two-level system (TLS). The key property used in the device proposals is that, if the energy of the incident photon is tuned to be on resonance with the TLS, the system will block the transmission of photons due to destructive interference between the directly transmitted photon and the photon reemitted by the impurity [4, 6].

A more challenging task is to study the two or more photon scattering problem in such systems. The two-photon problem has been addressed by Shen and Fan using a generalized Bethe-ansatz [18, 19]. They showed that two-photon bound states emerge as the photons interact with the two-level system. Effective attractive and repulsive interactions can be induced depending on the energy of the photons [18]. Such effective interactions between photons may provide new avenues for controlling photon entanglement [20]. However, the scattering eigenstates were not constructed explicitly in Ref. [19]: the bound states were found by first constructing Bethe-type scattering eigenstates and then deducing the bound states via the completeness of the basis. It is difficult to generalize the method in Ref. [19] to solve the three-photon (or more) scattering problem in which we expect more complicated and interesting photon correlations.

Here, we present a method to explicitly construct exact n-photon scattering eigenstates and then use the eigenstates to analyze the scattering of Fock- and coherent-state wavepackets. The system consists of a 1D bosonic continuum coupled to a local two-level-system as shown in Figure 13.1. First, we explicitly construct the n-photon ($n = 1$ to 4) scattering eigenstates by imposing open boundary conditions while requiring that the incoming wavefunctions consist entirely of plane waves [21, 22]. In addition to two-photon bound states, three-photon bound states appear in the three-photon scattering eigenstates, and likewise n-photon bound states appear in the n-photon scattering eigenstates. Second, to show the significance of these bound states in the scattering of practical light sources, we study the scattering of one-, two-, and three-photon Fock state wavepackets. It is shown that the two- and three-photon bound states dramatically enhance the transmission of two- and three-photon wavepackets, respectively. Third, we study the scattering of coherent states to determine the impact of the bound states on both the photon correlation and the statistics of the transmitted and reflected photons. Strong bunching and antibunching effects appear, and the statistics are non-Poissonian.

The paper is organized as follows. In Sec. II, we introduce the model, solve for the n-photon scattering eigenstates in the $n = 1$ to 4 cases, and construct the corresponding S-matrix based on the Lippmann-Schwinger

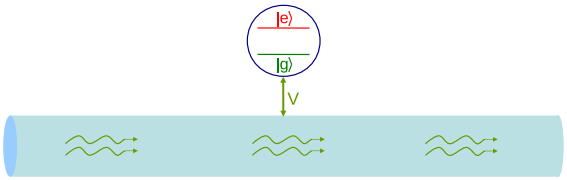

Figure 13.1: (color online) Sketch of the structure considered: a 1D continuum of bosons coupled to a two-level-system.

formalism [23]. In Sec. III, the impact of bound states on the photon transmission is studied for initial Fock-state wavepackets with photon number of one, two, and three. In Sec. IV, we present the analysis of photon correlation and statistics for coherent state scattering. Finally, we conclude in Sec. V.

13.2 Scattering Eigenstates

The system we study consists of a two-level system coupled to photons propagating in both directions in a one-dimensional waveguide [18, 19, 9]. The system is modeled by the Hamiltonian [18]

$$H = \int dx \frac{1}{i}\Big[a_R^\dagger(x)\frac{d}{dx}a_R(x) - a_L^\dagger(x)\frac{d}{dx}a_L(x)\Big] + \Big(\epsilon - \frac{i\Gamma'}{2}\Big)|e\rangle\langle e| + \int dx V\delta(x)\Big\{\big[a_R^\dagger(x) + a_L^\dagger(x)\big]S^- + h.c.\Big\}, \tag{13.1}$$

where $a_R^\dagger(x)/a_L^\dagger(x)$ is the creation operator for a right-going/left-going photon at position x, ϵ is the level splitting between the ground state $|g\rangle$ and the excited state $|e\rangle$ of the two level system, Γ' is the decay rate into channels other than the 1D continuum, V is the frequncy-independent coupling strength, and $S^- = |g\rangle\langle e|$ is the atomic lowering operator. Throughout the paper, we set the group velocity c and Plank's constant $\hbar$ to 1 for simplicity.

It is natural to transform to modes which are either even or odd about the origin, $a_{e/o}^\dagger(x) \equiv \big[a_R^\dagger(x) \pm a_L^\dagger(-x)\big]/\sqrt{2}$. The Hamiltonian (13.1) is then decomposed into two decoupled modes: $H = H_e + H_o$ with

$$H_e = \int dx \frac{1}{i}a_e^\dagger(x)\frac{d}{dx}a_e(x) + (\epsilon - i\Gamma'/2)\,|e\rangle\langle e| + \int dx\,\bar{V}\,\delta(x)\big[a_e^\dagger(x)S^- + h.c.\big], \tag{13.2a}$$

$$H_o = \int dx \frac{1}{i}a_o^\dagger(x)\frac{d}{dx}a_o(x), \tag{13.2b}$$

where the effective coupling strength becomes $\bar{V} = \sqrt{2}V$. Note that the odd mode is free. The number operator for even bosons is $n_e = \int dx\, a_e^\dagger(x)a_e(x)$, that for the odd bosons is $n_o = \int dx\, a_o^\dagger(x)a_o(x)$, and the occupation number of the two-level system is $n_{tls} = |e\rangle\langle e|$. Because H commutes with certain number operators, $[H,\, n_e + n_{tls}] = [H,\, n_o] = 0$, the total number of excitations in both the even and odd spaces are separately conserved. We will now focus on finding the non-trivial even-mode solution and then transform back to the left/right representation.

A n-excitation state ($n = n_e + n_{tls}$) is given by

$$|\psi_n\rangle = \int dx_1\cdots dx_n\, g_n(x_1,\cdots,x_n)\, a_e^\dagger(x_1)\cdots a_e^\dagger(x_n)|0,g\rangle + \int dx_1\cdots dx_{n-1}\, e_n(x_1,\cdots,x_{n-1})\, a_e^\dagger(x_1)\cdots a_e^\dagger(x_{n-1})|0,e\rangle, \tag{13.3}$$

where $|0,g\rangle$ is the zero photon state with the atom in the ground state. From $H_e|\psi_n\rangle = E_n|\psi_n\rangle$, we obtain

the Schrödinger equations

$$\begin{aligned}&\Big[\frac{1}{i}(\partial_1+\cdots+\partial_n)-E_n\Big]g_n(x_1,\cdots,x_n)\\&+\frac{\bar{V}}{n}\Big[\delta(x_1)e_n(x_2,\cdots,x_n)+\cdots+\delta(x_n)e_n(x_1,\cdots,x_{n-1})\Big]=0,\\&\Big[\frac{1}{i}(\partial_1+\cdots+\partial_{n-1})-E_n+\epsilon-i\Gamma'/2\Big]e_n(x_1,\cdots,x_{n-1})\\&\qquad+n\bar{V}g_n(0,x_1,\cdots,x_{n-1})=0,\end{aligned}\tag{13.4}$$

where the eigenvalue $E_n=k_1+k_2+\cdots k_n$, and $g_n(x_1,\cdots,x_n)$ is discontinuous at $x_i=0$, $i=1,\cdots n$. In all the following calculations, we set $g_n(0,x_1,\cdots,x_{n-1})=[g_n(0^+,x_1,\cdots,x_{n-1})+g_n(0^-,x_1,\cdots,x_{n-1})]/2$ [21, 22]. The scattering eigenstates $g_n(x_1,\cdots,x_n)$ and $e_n(x_1,\cdots,x_{n-1})$ are constructed by imposing the boundary condition that, in the incident region, $g_n(x_1,\cdots,x_n)$ is free-bosonic plane wave. That is to say, for $x_1,\cdots,x_n<0$,

$$g_n(x_1,\cdots,x_n) = \frac{1}{n!}\sum_Q h_{k_1}(x_{Q_1})\cdots h_{k_n}(x_{Q_n}),\tag{13.5a}$$

$$h_k(x) = \frac{1}{\sqrt{2\pi}}e^{ikx}\,.\tag{13.5b}$$

For $n=1$, plane-wave solutions are sufficient to satisfy Eq. (13.4) with eigenenergy $E=k$:

$$g_1(x) = g_k(x)=h_k(x)[\theta(-x)+\bar{t}_k\theta(x)],\tag{13.6a}$$

$$e_1 = \frac{i}{2\sqrt{\pi}V}(\bar{t}_k-1),\tag{13.6b}$$

$$\bar{t}_k = \frac{k-\epsilon+i\Gamma'/2-i\Gamma_c/2}{k-\epsilon+i\Gamma'/2+i\Gamma_c/2},\tag{13.6c}$$

where $\theta(x)$ is the step function and $\Gamma_c=\bar{V}^2=2V^2$ is the spontaneous emission rate from the two-level-system to the 1D continuum. Note that $\bar{t}_k$ is the transmission coefficient for the even problem; because the even mode is chiral, $|\bar{t}_k|=1$ when $\Gamma'=0$.

For $n=2$, plane-wave solutions are not sufficient to satisfy Eq. (13.4). As discussed by Shen and Fan [18, 19], a two-photon bound state must be included to guarantee the completeness of the basis. Here, instead of extracting the bound state through a completeness check [18, 19], we construct the scattering eigenstate explicitly and find a two-photon bound state contribution to the solution, as has been done in the open interacting resonant-level model [21]. We require the two-photon solution to satisfy Eq. (13.5a) in the region $x_1,x_2<0$ and solve for the solution in other regions using Eq. (13.4). This method of constructing scattering eigenstates can be generalized to three-, four-, and even more photon cases. In the Appendix, it is shown that the two-photon eigenstate with eigenenergy $E=k_1+k_2$ is

$$\begin{aligned}g_2(x_1,x_2) &= g_{k_1,k_2}(x_1,x_2)=\frac{1}{2!}\Big[\sum_Q g_{k_1}(x_{Q_1})g_{k_2}(x_{Q_2})\\&\quad+\sum_{PQ}B^{(2)}_{k_{P_1},k_{P_2}}(x_{Q_1},x_{Q_2})\theta(x_{Q_1})\Big],\end{aligned}\tag{13.7a}$$

$$e_2(x) = \frac{\sqrt{2}i}{V}[g_2(0^+,x)-g_2(0^-,x)],\tag{13.7b}$$

$$\begin{aligned}B^{(2)}_{k_{P_1},k_{P_2}}(x_{Q_1},x_{Q_2}) &\equiv -(\bar{t}_{k_{P_1}}-1)(\bar{t}_{k_{P_2}}-1)h_{k_{P_1}}(x_{Q_2})h_{k_{P_2}}(x_{Q_2})\\&\quad\times e^{(-\Gamma/2-i\epsilon)|x_{Q2}-x_{Q1}|}\theta(x_{Q_2}-x_{Q_1}).\end{aligned}\tag{13.7c}$$

Here, $P=(P_1,P_2)$ and $Q=(Q_1,Q_2)$ are permutations of $(1,2)$ needed to account for the bosonic symmetry of the wavefuntion, and $\Gamma=\Gamma_c+\Gamma'$ is the total spontaneous emission rate. The two-body bound-state term $B^{(2)}_{k_{P_1},k_{P_2}}(x_{Q1},x_{Q_2})\theta(x_{Q_1})$ is generated when there are two photons interacting with the same two-level-system (TLS), while the TLS can only absorb one photon at one time. The binding strength of the two photons depends on the total spontaneous emission rate Γ. Conceptually, two photons have two ways of going through the TLS. One way is to pass by the TLS independently as plane waves and gain a phase factor, which is described by the first term of $g_2(x_1,x_2)$. The other way is to bind together and form a bound state, which is described by the second term. The formation of the bound state can be viewed as a result of stimulated emission: the first photon excites the TLS and the passing of the second photon stimulates emission of the first photon into the same right-going state, hence producing the bound state.

For $n = 3$, a procedure similar to that used to solve the $n = 2$ case yields

$$g_3(x_1, x_2, x_3) = g_{k_1,k_2,k_3}(x_1, x_2, x_3)$$
$$= \frac{1}{3!}\Big[\sum_Q g_{k_1}(x_{Q_1})g_{k_2}(x_{Q_2})g_{k_3}(x_{Q_3}) + \sum_{PQ} g_{k_{P_1}}(x_{Q_1})B^{(2)}_{k_{P_2},k_{P_3}}(x_{Q_2}, x_{Q_3})\theta(x_{Q_2}) + \sum_{PQ} B^{(3)}_{k_{P_1},k_{P_2},k_{P_3}}(x_{Q_1}, x_{Q_2}, x_{Q_3})\theta(x_Q$$

$$e_3(x_1, x_2) = \frac{3i}{\sqrt{2}V}[g_3(0^+, x_1, x_2) - g_3(0^-, x_1, x_2)],$$

$$B^{(3)}_{k_{P_1},k_{P_2},k_{P_3}}(x_{Q_1}, x_{Q_2}, x_{Q_3}) \equiv 2(\bar{t}_{k_{P_1}} - 1)(\bar{t}_{k_{P_2}} - 1)(\bar{t}_{k_{P_3}} - 1)h_{k_{P_1}}(x_{Q_2})h_{k_{P_2}}(x_{Q_3})h_{k_{P_3}}(x_{Q_3})e^{(-\Gamma/2-i\epsilon)|x_{Q_3}-x_{Q_1}|}\theta(x_{Q_{32}})\theta(x$$

where $P = (P_1, P_2, P_3)$ and $Q = (Q_1, Q_2, Q_3)$ are permutations of $(1, 2, 3)$ and $\theta(x_{Q_{ij}}) = \theta(x_{Q_i}) - \theta(x_{Q_j})$ for short. In addition to the two-photon bound state, there emerges a three-body bound state $B^{(3)}_{k_{P_1},k_{P_2},k_{P_3}}(x_{Q_1}, x_{Q_2}, x_{Q_3})\theta(x_{Q_1})$ in the region $x_1, x_2, x_3 > 0$. Conceptually, there are three ways for the three photons to pass by the atom: (i) all three photons propagate as independent plane waves; (ii) two photons form a two-body bound state, while the other one propagates independently as a plane wave; and (iii) all three photons bind together and form a three-body bound state. These three processes are described by the first, second, and third terms of $g_3(x_1, x_2, x_3)$, respectively.

This simple picture can be applied to a general n-photon scattering process. For example, in the case of four-photon scattering, there are five ways for the four photons to pass by the atom as illustrated in Figure 13.2: (i) all four propagate as independent plane waves; (ii) two photons form a two-body bound state, while the other two propagate independently as plane waves; (iii) three photons form a three-body bound state, while the other one propagate independently as a plane wave; (iv) four photons form two independent two-body bound states; and (v) four photons form a four-body bound state. These five processes can be identified as the five terms of $g_4(x_1, x_2, x_3, x_4)$ in the four-photon solution, which is given by

$$g_4(x_1, x_2, x_3, x_4) = \frac{1}{4!}\Big[\sum_Q g_{k_1}(x_{Q_1})g_{k_2}(x_{Q_2})g_{k_3}(x_{Q_3})g_{k_4}(x_{Q_4}) + \sum_{PQ} g_{k_{P_1}}(x_{Q_1})g_{k_{P_2}}(x_{Q_2})B^{(2)}_{k_{P_3},k_{P_4}}(x_{Q_3}, x_{Q_4})\theta(x_{Q_3})$$
$$+ \sum_{PQ} g_{k_{P_1}}(x_{Q_1})B^{(3)}_{k_{P_2},k_{P_3},k_{P_4}}(x_{Q_2}, x_{Q_3}, x_{Q_4})\theta(x_{Q_2}) + \sum_{PQ} B^{(2)}_{k_{P_1},k_{P_2}}(x_{Q1}, x_{Q_2})B^{(2)}_{k_{P_3},k_{P_4}}(x_{Q_3}, x_{Q_4})\theta(x_{Q_1})\theta$$
$$+ \sum_{PQ} B^{(4)}_{k_{P_1},k_{P_2},k_{P_3},k_{P_4}}(x_{Q_1}, x_{Q_2}, x_{Q_3}, x_{Q_4})\theta(x_{Q_1})\Big],$$

$$e_4(x_1, x_2, x_3) = \frac{4i}{\sqrt{2}V}[g_4(0^+, x_1, x_2, x_3) - g_4(0^-, x_1, x_2, x_3)],$$

$$B^{(4)}_{k_{P_1},k_{P_2},k_{P_3},k_{P_4}}(x_{Q_1}, x_{Q_2}, x_{Q_3}, x_{Q_4}) \equiv -2^2(\bar{t}_{k_{P_1}} - 1)(\bar{t}_{k_{P_2}} - 1)(\bar{t}_{k_{P_3}} - 1)(\bar{t}_{k_{P_4}} - 1)h_{k_{P_1}}(x_{Q_2})h_{k_{P_2}}(x_{Q_3})h_{k_{P_3}}(x_{Q_4})h_{k_{P_4}}(x_{Q_4}$$
$$\times e^{(-\Gamma/2-i\epsilon)|x_{Q_4}-x_{Q_1}|}\theta(x_{Q_4} - x_{Q_3})\theta(x_{Q_3} - x_{Q_2})\theta(x_{Q_2} - x_{Q_1}).$$

The scattering eigenstates of a general n-photon problem can be constructed recursively in a similar way: the only unknown term in $g_n(x_1, \cdots, x_n)$ is the $n-$photon bound state as all the other terms can be constructed from the solutions of the $1, 2, \cdots, (n-1)$-photon problems. We extrapolate from the results of $n =$ 2-4 that,

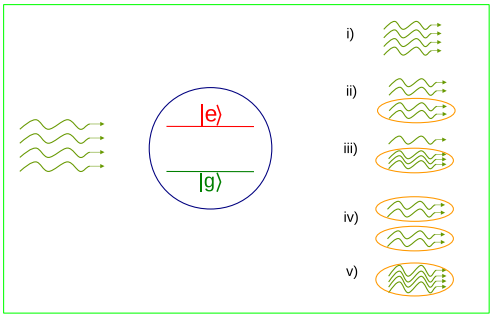

Figure 13.2: (color online) Schematic of different processes in four-photon scattering by a two-level system. The plane waves are represented by wiggly lines, while the many-body bound states are represented by the ovals.

for general n (≥ 2), the n-body bound state assumes the form

$$B_{k_1,\ldots,k_n}(x_1,\ldots,x_n) = -(-2)^{n-2}\prod_{i=1}^{n}(\bar{t}_{k_i}-1)\prod_{i=1}^{n-1}\theta(x_{i+1}-x_i)$$
$$\times h_{k_1}(x_n)h_{k_2}(x_2)\cdots h_{k_{n-1}}(x_{n-1})h_{k_n}(x_n)e^{(-\Gamma/2-i\epsilon)|x_n-x_1|}. \tag{13.10}$$

We have verified this expression for $n = 5$. Thus we have given explicit formulas for constructing the exact n-photon scattering eigenstates.

The exact scattering eigenstates can be used to construct the scattering matrix. According to the Lippmann-Schwinger formalism [23], one can read off the "in" state (before scattering) and the "out" state (after scattering) of a general n-photon S-matrix from $g_n(x_1,\cdots,x_n)$ in the input region $(x_1<0,\cdots,x_n<0)$ and in the output region $(x_1>0,\cdots,x_n>0)$, respectively. The "in" and "out" states of one and two photon scattering matrices are given by

$$|\phi_{in}^{(1)}\rangle_e = \int dx\, h_k(x)a_e^\dagger(x)|0\rangle \tag{13.11a}$$
$$|\phi_{out}^{(1)}\rangle_e = \int dx\, \bar{t}_k h_k(x)a_e^\dagger(x)|0\rangle, \tag{13.11b}$$

and

$$|\phi_{in}^{(2)}\rangle_e = \int dx_1dx_2\frac{1}{2!}\Big[\sum_Q h_{k_1}(x_{Q_1})h_{k_2}(x_{Q_2})\Big]a_e^\dagger(x_1)a_e^\dagger(x_2)|0\rangle$$
$$|\phi_{out}^{(2)}\rangle_e = \int dx_1dx_2\frac{1}{2!}\Big[\sum_Q \bar{t}_{k_1}\bar{t}_{k_2}h_{k_1}(x_{Q_1})h_{k_2}(x_{Q_2})$$
$$+\sum_{PQ}B_{k_{P_1},k_{P_2}}(x_{Q_1},x_{Q_2})\Big]a_e^\dagger(x_1)a_e^\dagger(x_2)|0\rangle, \tag{13.12}$$

and similarly for three and four photons. The corresponding S-matrices are

$$S_e^{(n)} = \int dk_1\cdots dk_n\frac{1}{n!}|\phi_{out}^{(n)}\rangle_{ee}\langle\phi_{in}^{(n)}|. \tag{13.13}$$

Notice that the unitarity of the S-matrix is automatically satisfied since the incoming state $|\phi_{in}^{(n)}\rangle_e$ is a complete basis set in the even space [19, 23].

The S-matrix in the odd space is just the identity operator because the odd mode is free and decoupled from the impurity and the even mode,

$$S_o^{(n)} = \int dk_1\cdots dk_n\frac{1}{n!}|\phi_{in}^{(n)}\rangle_{oo}\langle\phi_{in}^{(n)}|, \tag{13.14a}$$
$$|\phi_{in}^{(n)}\rangle_o = \int dx_1\cdots dx_n\frac{1}{n!}\sum_Q\prod_{i=1}^{n}h_{k_i}(x_{Q_i})a_e^\dagger(x_i)|0\rangle\ . \tag{13.14b}$$

Finally, we wish to construct the scattering matrix in the right/left representation based on the S-matrices in the even/odd representation. For a general n-photon scattering problem, the possible scattering channels are that i photons undergo scattering in the even space and $n-i$ photons undergo scattering in the odd space, with i running from 0 to n. In addition, the even and odd spaces are decoupled from each other. Therefore, the n-photon S-matrix is

$$S^{(n)} = \sum_{i=0}^{n}S_e^{(i)}\otimes S_o^{(n-i)}\ . \tag{13.15}$$

We will use this S-matrix to study the scattering of Fock states and coherent state wave packets in the right/left space in the subsequent sections.

13.3 Scattering of Fock States

In order to show the significance of the many-body bound states, we study the scattering of a Fock state off of a two-level system. We assume that the incident mode propagates to the right and the two level system is initially in the ground state. We use the S-matrices defined in Eq. (13.15) to evaluate the transmission and reflection coefficients. In practice, any state that contains a finite number of photons must have the form of a

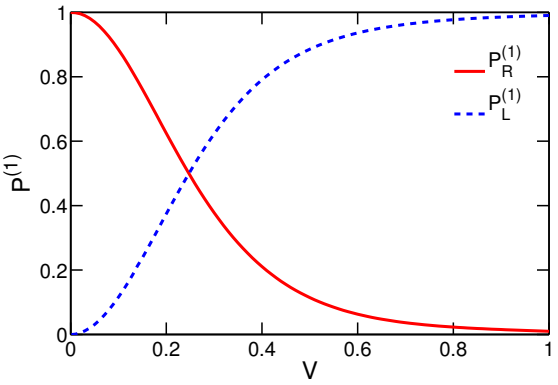

Figure 13.3: (color online) Single-photon transmission ($P_R^{(1)}$) and reflection ($P_L^{(1)}$) probabilities as a function of coupling strength V. The incident photon is on resonance with the two level system ($k_0 = \epsilon$) and we have considered the lossless case $\Gamma' = 0$. ($\Delta = 0.1$.)

wave-packet. Thus, we start with the definition of the continuous-mode photon wave-packet creation operator in momentum space [24]

$$a_\alpha^\dagger = \int dk\, \alpha(k) a^\dagger(k)|0\rangle, \tag{13.16}$$

with the normalization condition $\int dk\, |\alpha(k)|^2 = 1$. The corresponding continuous-mode n-photon Fock state is

$$|n_\alpha\rangle = \frac{(a_\alpha^\dagger)^n}{\sqrt{n!}}|0\rangle\ , \tag{13.17}$$

and the output state after it scatters off the TLS is

$$|\text{out}_\alpha^{(n)}\rangle = S^{(n)}|n_\alpha\rangle. \tag{13.18}$$

To obtain the scattering probabilities of a Fock state from the S-matrix found in Section II, we follow the following general procedure. (i) First, we write an n-photon input Fock state traveling to the right in momentum space: $|n_\alpha\rangle = (1/\sqrt{n!}) \int dk_1 \cdots dk_n\ \alpha(k_1)\cdots\alpha(k_n)|k_1,\cdots,k_n\rangle$; (ii) Next, we apply the S-matrix on the input state and find the output state $|\text{out}_\alpha^{(n)}\rangle = S^{(n)}|n_\alpha\rangle = (1/\sqrt{n!}) \int dk_1 \cdots dk_n\, \alpha(k_1)\cdots\alpha(k_n) S^{(n)}|k_1,\cdots,k_n\rangle$ in the even/odd basis; (iii) We transform back to the right/left basis. Then we project the output state onto the n-photon (right/left-going) momentum basis $|k_1,\cdots,k_n\rangle_R,\cdots,|k_1,\cdots,k_i\rangle_R \otimes |k_{i+1},\cdots,k_n\rangle_L,\cdots,|k_1,\cdots,k_n\rangle_L$ and take the absolute value square to obtain the probabilities $P(k_1,\cdots,k_n)$ of finding the output state in $|k_1,\cdots,k_n\rangle$; (iv) Finally, we integrate $P(k_1,\cdots,k_n)$ over $k_1,\cdots,k_n$ to obtain the total transmission and reflection probabilities. Here, a right/left-going state is defined by a positive/negative momentum, i.e., $k_1 > 0,\cdots,k_n > 0$ for $|k_1,\cdots,k_n\rangle_R$ and $k_1 < 0,\cdots,k_n < 0$ for $|k_1,\cdots,k_n\rangle_L$.

For convenience, we choose Gaussian type wavepackets with the spectral amplitude

$$\alpha(k) = (2\pi\Delta^2)^{-1/4} \exp\left\{\left(-\frac{(k-k_0)^2}{4\Delta^2}\right)\right\}. \tag{13.19}$$

For all of the numerical examples in this paper, we choose $k_0 = \epsilon$: the central frequency of the wavepacket is on resonance with the TLS, a condition which makes the interaction between the photons and the TLS strongest. We take the central momentum $k_0 \gg \Delta$ so that the narrow-band condition is satisfied. In particular, we choose $\Delta = 0.1$. However, we emphasize that all the conclusions we draw are independent of the choice of Δ. That is because all the transmission and reflection probabilities are functions of Γ/Δ, where $\Gamma = 2V^2$. A different choice of Δ does not change any of the qualitative results, but merely rescales the spontaneous emission rate Γ.

13.3.1 Single-Photon Fock State Scattering

The probabilities of transmission ($P_R^{(1)}$) and reflection ($P_L^{(1)}$) for a single-photon Fock state are found as

$$P_R^{(1)} = \int_{k>0} dk\, |\langle k|\text{out}_\alpha^{(1)}\rangle|^2 = \int_{k>0} dk\, \alpha(k)^2 |t_k|^2, \tag{13.20a}$$

$$P_L^{(1)} = \int_{k<0} dk\, |\langle k|\text{out}_\alpha^{(1)}\rangle|^2 = \int_{k>0} dk\, \alpha(k)^2 |r_k|^2, \tag{13.20b}$$

where $t_k = (\bar{t}_k + 1)/2$ and $r_k = (\bar{t}_k - 1)/2$ and $\bar{t}_k$ is the transmission coefficient defined above for the even mode [Eq. (13.6c)].

Note that the propagation of a single-photon is strongly modulated by the TLS as we turn on the coupling. In the strong-coupling limit, a single-photon is perfectly reflected and the two-level atom acts as a mirror. This perfect reflection is due to destructive interference between the directly transmitted state and the state re-emitted from the TLS. A single-photon transistor [4] and a quantum switch [6] have been proposed based on this perfect reflection.

13.3.2 Two-Photon Fock State Scattering

For two incident photons, following the general procedure above, we find that the transmission and reflection probabilities are

$$P_{RR}^{(2)} = \int_{k_1>0,k_2>0} dk_1 dk_2 \ \frac{1}{2!} |\langle k_1, k_2 | \mathrm{out}_\alpha^{(2)} \rangle|^2, \tag{13.21a}$$

$$P_{RL}^{(2)} = \int_{k_1>0,k_2<0} dk_1 dk_2 \ |\langle k_1, k_2 | \mathrm{out}_\alpha^{(2)} \rangle|^2, \tag{13.21b}$$

$$P_{LL}^{(2)} = \int_{k_1<0,k_2<0} dk_1 dk_2 \ \frac{1}{2!} |\langle k_1, k_2 | \mathrm{out}_\alpha^{(2)} \rangle|^2, \tag{13.21c}$$

where $P_{RR}^{(2)}$, $P_{RL}^{(2)}$ and $P_{LL}^{(2)}$ are, respectively, the probability for two photons to be transmitted (right-going), one transmitted and one reflected, and two photons reflected (left-going).

To show the significance of the bound state in the propagation of multi-photon Fock states, we separate each of the probabilities $P_{RR}^{(2)}$, $P_{RL}^{(2)}$ and $P_{LL}^{(2)}$ into two parts. One part is the contribution from only the plane wave term (labeled PW), which is the direct transmission or reflection. The other is the contribution from all the other terms (labeled BS), including the bound state term as well as the interference term between the plane wave and bound state. Notice that the BS part vanishes in the absence of bound state, as in the case of single-photon scattering. Therefore, it is a manifestation of the nonlinear effect caused by the interaction between the TLS and two or more photons. As an example, $P_{RR}^{(2)}$ split into PW and BS parts is

$$P_{RR}^{(2)} = \int_{k_1>0,k_2>0} dk_1 dk_2 |t(k_1,k_2) + B(k_1,k_2)|^2 \tag{13.22a}$$

$$= (P_{RR}^{(2)})_{\mathrm{PW}} + (P_{RR}^{(2)})_{\mathrm{BS}}, \tag{13.22b}$$

$$(P_{RR}^{(2)})_{\mathrm{PW}} = \int_{k_1>0,k_2>0} dk_1 dk_2 |t(k_1,k_2)|^2, \tag{13.22c}$$

$$(P_{RR}^{(2)})_{\mathrm{BS}} = \int_{k_1>0,k_2>0} dk_1 dk_2 \big[t^*(k_1,k_2) B(k_1,k_2) + t(k_1,k_2) B^*(k_1,k_2) + |B(k_1,k_2)|^2 \big] \tag{13.22d}$$

$$t(k_1,k_2) = \alpha(k_1)\alpha(k_2) t_{k_1} t_{k_2}, \tag{13.22e}$$

$$B(k_1,k_2) = \Big[\frac{-i/2\pi}{k_1 - \epsilon + \frac{i\Gamma}{2}} + \frac{-i/2\pi}{k_2 - \epsilon + \frac{i\Gamma}{2}} \Big] \times \int_{k'>0} dk' \, \alpha(k') \alpha(k_1 + k_2 - k') r_{k'} r_{k_1+k_2-k'} \ . \tag{13.22f}$$

Figure 13.4 shows the three transmission probabilities $P_{RR}^{(2)}$, $P_{RL}^{(2)}$, and $P_{LL}^{(2)}$ for our standard parameters, with the contributions from the plane wave and bound state plotted separately in panels (a)-(c). *Note that the presence of the bound state has a very substantial effect on these transmission probabilities.* As shown in panels (a) and (b), $P_{RR}^{(2)}$ and $P_{RL}^{(2)}$ are enhanced by the formation of the bound state. This is mainly due to constructive interference between the plane wave and bound state. In contrast, panel (c) shows that $P_{LL}^{(2)}$ is strongly reduced in the presence of the bound state because of destructive interference between the plane wave and bound state (change from ~ 0.8 to ~ 0.4 at $V = 0.5$). Therefore, the presence of the bound state tends to *increase* the one-photon and two-photon transmission, while *suppressing* the two-photon reflection.

A particularly interesting aspect of the results in Fig 13.4 is that the effect of the bound state is most prominent in the *intermediate* coupling regime, not at the strongest coupling. This is because, first, in the weak coupling limit, the interaction is too weak to produce a pronounced bound state for two-photon scattering, while, second, in the strong coupling limit, the TLS responds to the first photon too quickly (in a duration of order $1/\Gamma$ with $\Gamma = 2V^2$) for the second photon to produce a significant nonlinear effect. (The formation of the bound state requires the presence of both photons at the two-level system.) The optimal coupling strength V_m for producing nonlinear (bound state) effects lies at intermediate coupling, when the spontaneous emission rate Γ is on the order of the wavepacket width Δ ($V_m \sim 0.4$ when $\Delta = 0.1$).

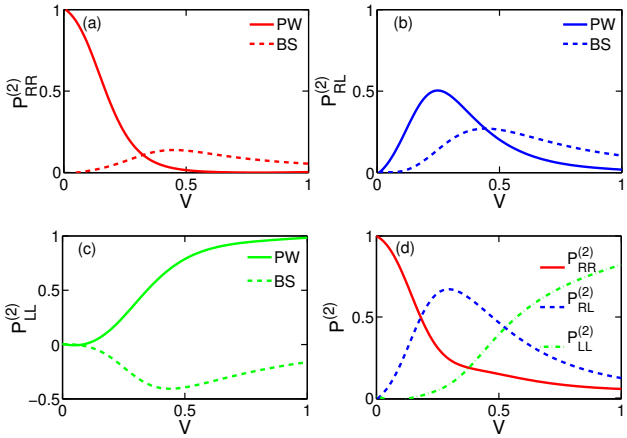

Figure 13.4: (color online) Two-photon transmission and reflection probabilities as a function of coupling strength V. (a) Probability that both photons are transmitted (and hence are right-going, $P^{(2)}_{RR}$). (b) Probability that one photon is transmitted and one reflected (right-left, $P^{(2)}_{RL}$). (c) Probability that both photons are reflected (both left-going, $P^{(2)}_{LL}$). (d) The three processes on a single plot. The label PW refers to the contribution from the plane-wave term only, while BS refers to all the other contributions involving bound-state terms. The incident photons are on resonance with the two-level system ($k_0 = \epsilon$), we consider the lossless case $\Gamma' = 0$, and $\Delta = 0.1$. Notice the large effect of the bound state on these quantities.

13.3.3 Three-Photon Fock State Scattering

Following the general procedure for obtaining scattering probabilities, the transmission and reflection probabilities for three-photon Fock state scattering are defined as

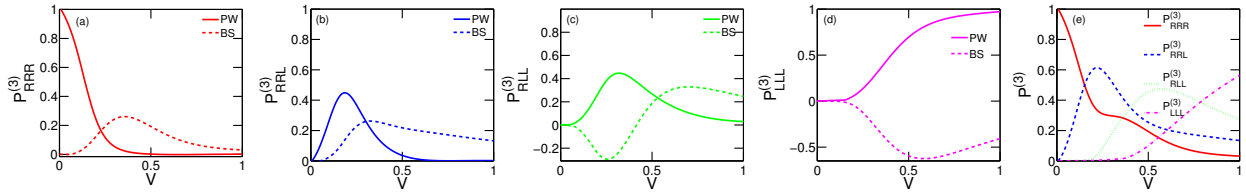

Figure 13.5: (color online) Three-photon transmission and reflection probabilities as a function of coupling strength V. (a) Probability of all three photons transmitted ($P^{(3)}_{RRR}$). (b) Probability of two photons transmitted and one reflected ($P^{(3)}_{RRL}$). (c) Probability of one photon transmitted and two photons reflected ($P^{(3)}_{RLL}$). (d) Probability of all three photons reflected ($P^{(3)}_{LLL}$). (e) P^3 all together. The label PW refers to the contribution from only the plane wave term, while BS refers to all the other contributions, involving bound state terms. The incident photons are on resonance with the two level system ($k_0 = \epsilon$), we consider the lossless case $\Gamma' = 0$, and $\Delta = 0.1$. Note the large bound state effects.

$$
\begin{aligned}
P^{(3)}_{RRR} &= \int_{k_1>0,k_2>0,k_3>0} dk_1 dk_2 dk_3 \; \frac{1}{3!} |\langle k_1, k_2, k_3 | \mathrm{out}^{(3)}_\alpha \rangle|^2, \\
P^{(3)}_{RRL} &= \int_{k_1>0,k_2>0,k_3<0} dk_1 dk_2 dk_3 \; \frac{1}{2!} |\langle k_1, k_2, k_3 | \mathrm{out}^{(3)}_\alpha \rangle|^2, \\
P^{(3)}_{RLL} &= \int_{k_1>0,k_2<0,k_3<0} dk_1 dk_2 dk_3 \; \frac{1}{2!} |\langle k_1, k_2, k_3 | \mathrm{out}^{(3)}_\alpha \rangle|^2, \\
P^{(3)}_{LLL} &= \int_{k_1<0,k_2<0,k_3<0} dk_1 dk_2 dk_3 \; \frac{1}{3!} |\langle k_1, k_2, k_3 | \mathrm{out}^{(3)}_\alpha \rangle|^2,
\end{aligned}
\tag{13.23}
$$

where $P^{(3)}_{RRR}$, $P^{(3)}_{RRL}$, $P^{(3)}_{RLL}$, and $P^{(3)}_{LLL}$ are the probabilities for three photons being transmitted (all right-going), two transmitted and one reflected, one transmitted and two reflected, and all three reflected (left-going), respectively. As in the two-photon scattering case, we separate each probability into two parts: the contribution of only the plane wave term (labeled PW) and the contribution from all the other terms (labeled BS), including the bound states as well as the interference between the plane wave and bound states. The probabilities and the decomposition into PW and BS parts are plotted in Figure 13.5 for our usual parameters.

Figure 13.5 shows that the bound state contribution to the transmission probabilities is, as for two photons, very substantial. In panels (a) and (b), the BS parts of $P^{(3)}_{RRR}$ and $P^{(3)}_{RRL}$ are positive; thus, these probabilities are enhanced by the bound states. Panel (d) shows that $P^{(3)}_{LLL}$ is suppressed by the bound state contribution for arbitrary coupling strength. In contrast, as we increase the coupling strength, $P^{(3)}_{RLL}$ is first suppressed and then enhanced by the BS part as shown in Figure 13.5(c). Tuning the coupling strength changes the relative phase between the plane wave and bound state parts; for $P^{(3)}_{RLL}$, the interference between them happens to change from destructive to constructive as the coupling strength increases. Finally, as in the two-photon case, the most pronounced bound state effects occur in the intermediate coupling regime instead of the strong coupling limit.

To sum up this section, we point out that all the curves plotted in Figs. 13.3-13.5 are universal in terms of the choice of Δ. Because Δ appears in the scattering probabilities [$P^{(1)}_R$, etc.] only in the ratio Γ/Δ, a different choice of Δ (i.e., other than 0.1 used in the figures) is equivalent to rescaling V and does not change the shape of the curves. Therefore, the substantial bound state effects observed here are intrinsic for multi-photon scattering processes in this system, independent of the details of the wavepackets.

13.4 Scattering of coherent-states

We now turn to studying the scattering of coherent states in order to show, first, the strong photon-photon correlation induced by the the two-level system and, second, the change in photon number statistics. The incident coherent state wavepacket is defined by [24]

$$
|\alpha\rangle = e^{a^\dagger_\alpha - \bar{n}/2} |0\rangle, \tag{13.24}
$$

with $a^\dagger_\alpha = \int dk\, \alpha(k) a^\dagger(k)|0\rangle$, and mean photon number $\bar{n} = \int dk |\alpha(k)|^2$. A Gaussian type wavepacket is chosen

$$
\alpha(k) = \frac{\sqrt{\bar{n}}}{(2\pi\Delta^2)^{1/4}} \exp\left\{ \left(- \frac{(k-k_0)^2}{4\Delta^2} \right) \right\}; \tag{13.25}
$$

for numerical evaluations, we use, as before, $\Delta = 0.1$ and $k_0 = \epsilon \gg \Delta$. The output state $|\mathrm{out}_\alpha\rangle$ is then

$$
|\mathrm{out}_\alpha\rangle = \sum_n S^{(n)} |\alpha\rangle \tag{13.26}
$$

We assume the incident coherent state is right-going and the two-level system is in the ground state initially. We present the analysis of second-order correlation and photon number statistics in the transmitted field.

13.4.1 Correlation

The second-order correlation function of the transmitted field is defined as [24]

$$
g^{(2)}_R(x_2 - x_1) = \frac{\langle \mathrm{out}_\alpha | a^\dagger_R(x_1) a^\dagger_R(x_2) a_R(x_2) a_R(x_1) | \mathrm{out}_\alpha \rangle}{\langle \mathrm{out}_\alpha | a^\dagger_R(x_1) a_R(x_1) | \mathrm{out}_\alpha \rangle^2}. \tag{13.27}
$$

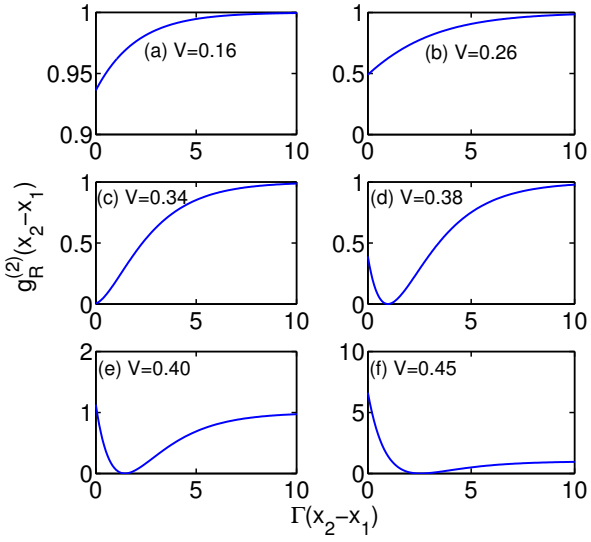

Figure 13.6: (color online) Second-order correlation of the transmitted field given an incident coherent state with $\bar{n} \leq 1$ at various coupling strengths V to the 1D continuum. (a) $V = 0.16$, (b) $V = 0.26$, (c) $V = 0.34$, (d) $V = 0.38$, (e) $V = 0.40$, (f) $V = 0.45$. The spontaneous emission rate to channels other than the 1D continuum is set to $\Gamma' = 0.10$. Notice that the correlation behavior is very sensitive to the coupling strength to 1D continuum, showing both bunching and antibunching.

We consider the mean photon number $\bar{n} \leq 1.0$. In this case, the probability to find $n \geq 3$ number states is much smaller than that of $n = 2$ number states. Moreover, the contributions from $n \geq 3$ states to $g^{(2)}$ are at least one order of Δ $(= 0.1)$ smaller than that from the $n = 2$ state. Therefore, we neglect the contributions from $n \geq 3$ number states. The second-order correlation function simplifies to

$$g_R^{(2)}(x_2 - x_1) = \frac{\left| \int dk_1 dk_2 \, \alpha(k_1)\alpha(k_2)(t_{k_1}t_{k_2} - r_{k_1}r_{k_2}e^{-\frac{\Gamma(x_2-x_1)}{2}}) \right|^2}{\left| \int dk_1 dk_2 \, \alpha(k_1)\alpha(k_2)t_{k_1}t_{k_2} \right|^2}. \tag{13.28}$$

The contributions from the directly transmitted state and the bound state can be identified as the first term and second term in the numerator of $g_R^{(2)}(x_2 - x_1)$ in Eq. (13.28). In the absence of the bound state, $g_R^{(2)}(x_2 - x_1)$ is always equal to unity. As we turn on the interaction, the interference between the directly transmitted state and the bound state will give rise to interesting correlation behavior. Figure 13.6 shows the second-order correlation as a function of $\Gamma(x_2 - x_1)$ at various coupling strengths, V, to the 1D mode with $\Gamma' = 0.1$. In the weak coupling limit $(V = 0.16)$ as shown in Figure 13.6(a), the directly transmitted state dominates and $g_R^{(2)}(0)$ is slightly smaller than 1. We observe a slight initial antibunching. As V increases [Figure 13.6(b)-(c)], $g_R^{(2)}(0)$ further decreases and the initial antibunching gets stronger and becomes strongest at $V = 0.34$ when $g_R^{(2)}(0) = 0$. Notice that the antibunching is getting weaker as one moves away from the origin for $V \leq 0.34$. Further increase of V starts to change the initial antibunching [$V = 0.38$, $g_R^{(2)}(0) < 1$] to bunching [$V = 0.45$, $g_R^{(2)}(0) > 1$] as shown in Figure 13.6(d)-(f). In this case, the bound state starts to dominate the correlation behavior. It is remarkable that, for $V > 0.34$, the initial antibunching ($V < 0.40$) or bunching ($V > 0.40$) is followed by a later antibunching $g_R^{(2)}(0) = 0$, which is caused by the cancellation of the directly transmitted state and the bound state. The formation of the bound state gives rise to a rich phenomenon of photon-photon correlation, which is very sensitive to the coupling strength V to the 1D mode. *Effective attractive or repulsive interaction between photons is induced by the presence of a single two-level system* [18].

Our findings agree with the results obtained by Chang *et al.* [4] using a very different approach. In the lossless $\Gamma' = 0$ case, as we increase the coupling strength, the transmission for individual photons is reduced rapidly [see, for example, Figure 13.3 and Figure 13.4(a)]. But the two-photon bound state can strongly enhance the transmission. Therefore, we will observe a strong initial bunching followed by a later antibunching, similar to Figure 13.6(f).

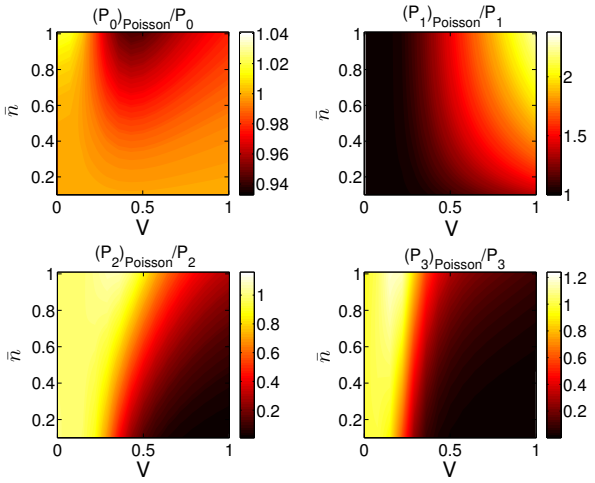

Figure 13.7: (color online) Photon number distribution of the transmitted field compared with a coherent state. We considered the lossless case $\Gamma' = 0$. The statistics is non-Possonian with the 2 and 3 photon content enhanced.

13.4.2 Photon Number Distribution

Given the output state $|\text{out}_\alpha\rangle$, we measure the photon number distribution in the transmitted field following the general procedure described in Sec. III.

$$\begin{aligned} P_0 &= |\langle \text{out}_\alpha|(|0\rangle_R \otimes |I\rangle_L)|^2, \\ P_1 &= \int_{k>0} dk |\langle \text{out}_\alpha|(|k\rangle_R \otimes |I\rangle_L)|^2, \\ P_2 &= \int_{k_1,k_2>0} dk_1 dk_2 \frac{1}{2!} |\langle \text{out}_\alpha|(|k_1,k_2\rangle_R \otimes |I\rangle_L)|^2, \\ P_3 &= \int_{k_1,k_2,k_3>0} dk_1 dk_2 dk_3 \frac{1}{3!} |\langle \text{out}_\alpha|(|k_1,k_2,k_3\rangle_R \otimes |I\rangle_L)|^2, \end{aligned} \tag{13.29}$$

where $|I\rangle_L$ is the complete basis set in the left-going photon space. We consider a mean photon number $\bar{n} \leq 1.0$ in the incident coherent state. In this case, the probability to find the four photon state is negligible ($\leq 1.6\%$). We compare the photon number distribution P_n of the output state with $(P_n)_{\text{Poisson}}$ of a coherent state having the same mean photon number.

Figure 13.7 shows the ratio between $(P_n)_{\text{Poisson}}$ and P_n as a function of the coupling strength V and the mean photon number $\bar{n}$ of the incident coherent state. The zero-photon probability does not deviate from that of a coherent state much in the whole parameter region we considered. The one-photon probability is smaller than the corresponding probability in a coherent state. In contrast, the two- and three-photon probabilities are much larger than the ones in a coherent state, especially in the strong coupling regime. This is to say, the interaction between photons and the two-level system redistributes the probabilities among different photon numbers. *The one-photon probability is reduced and is redistributed to the two- and three-photon probabilities.* This is mainly because the bound states enhance the transmission of multi-photon states as we have shown in Sec. III B and C. In conclusion, we obtain a non-Poissonian light source after the scattering. It is perhaps possible to use this strongly-correlated light source to perform passive decoy-state quantum key distribution in order to raise the key generation rate [25, 26, 27, 28].

13.5 Conclusion

In this paper, we present a general method to construct the exact scattering eigenstates for the problem of n-photons interacting with a two-level system. Many-body bound states appear in the presence of the coupling between photons and the two-level system. Furthermore, the scattering matrices are extracted using the Lippmann-Schwinger formalism. We emphasize that the completeness of the S-matrices is guaranteed by imposing open boundary conditions and requiring the incident field to be free plane waves. Based on the S-matrices, we study the scattering of the Fock states and coherent states. The bound states are shown to enhance the transmission of multi-photon states and suppress the transmission of single-photon states. In the transmitted field of coherent state scattering, the photons exhibit strong bunching or antibunching effects depending on the coupling strength. This is a manifestation of the many-body bound states. Finally, we determine the photon number distribution and find that the one-photon state is transferred to two- and three-photon states. This results in a non-Poissonian light source which might have applications in quantum information.

13.6 Appendix: Two-photon Scattering Eigenstate

In this appendix, we show in detail how we obtain the two-photon scattering eigenstate [Eq. (13.7)] by imposing the open boundary condition Eq. (13.5). The equations of motion for the two-photon case read

$$\Big[\frac{1}{i}(\partial_1+\partial_2)-E_2\Big]g_2(x_1,x_2)+ \frac{\bar{V}}{2}\Big[\delta(x_1)e_2(x_2)+\delta(x_2)e_2(x_1)\Big]=0, \tag{13.30a}$$

$$\Big[\frac{1}{i}\frac{d}{dx}-E_2+\epsilon-i\Gamma'/2\Big]e_2(x)+2\bar{V}g_2(0,x)=0, \tag{13.30b}$$

which can be cast into the following set of equations

$$\Big[\frac{1}{i}(\partial_1+\partial_2)-E_2\Big]g_2(x_1,x_2)=0, \tag{13.31a}$$

$$e_2(x)=\frac{2i}{\bar{V}}[g_2(0^+,x)-g_2(0^-,x)], \tag{13.31b}$$

$$\Big[\frac{1}{i}\frac{d}{dx}-E_2+\epsilon-i\Gamma'/2\Big]e_2(x) +\bar{V}[g_2(0^+,x)+g_2(0^-,x)]=0, \tag{13.31c}$$

$$e_2(0^+)=e_2(0^-). \tag{13.31d}$$

Here, $g_2(x_1,x_2)$ is discontinuous at $x_1=0, x_2=0$ and we set $g_2(x,0)=[g_2(x,0^+)+g_2(x,0^-)]/2$. We eliminate $e_2(x)$ from the above equations and obtain

$$\Big[\frac{1}{i}(\partial_1+\partial_2)-E_2\Big]g_2(x_1,x_2)=0, \tag{13.32a}$$

$$\Big[\frac{1}{i}\frac{d}{dx}-E_2+\epsilon-i\Gamma'/2-i\Gamma_c/2\Big]g_2(0^+,x) =\Big[\frac{1}{i}\frac{d}{dx}-E_2+\epsilon-i\Gamma'/2+i\Gamma_c/2\Big]g_2(0^-,x), \tag{13.32b}$$

$$g_2(0^+,0^+)-g_2(0^-,0^+)=g_2(0^-,0^+)-g_2(0^-,0^-). \tag{13.32c}$$

Because of the bosonic symmetry, we can solve for $g_2(x_1,x_2)$ by first considering the half space $x_1\le x_2$ and then extending the result to the full sapce. In this case, there are three quadrants in real space: ① $x_1\le x_2<0$; ② $x_1<0<x_2$; ③ $0<x_1\le x_2$. Eq. (13.32b) can be rewritten as two separate equations

$$\Big[\frac{1}{i}\frac{d}{dx}-E_2+\epsilon-i\Gamma'/2-i\Gamma_c/2\Big]g_2^{②}(x,0^+) = \Big[\frac{1}{i}\frac{d}{dx}-E_2+\epsilon-i\Gamma'/2+i\Gamma_c/2\Big]g_2^{①}(x,0^-),\ \text{for } x<0, \tag{13.33a}$$

$$\Big[\frac{1}{i}\frac{d}{dx}-E_2+\epsilon-i\Gamma'/2-i\Gamma_c/2\Big]g_2^{③}(0^+,x) = \Big[\frac{1}{i}\frac{d}{dx}-E_2+\epsilon-i\Gamma'/2+i\Gamma_c/2\Big]g_2^{②}(0^-,x),\ \text{for } x>0. \tag{13.33b}$$

Substituting $g_2^{①}(x_1,0^-)$ [Eq. (13.5)] into Eq. (13.33a), we solve to find

$$g_2^{②}(x,0^+)=\frac{1}{2!}\Big[\bar{t}_{k_2}\frac{e^{ik_1x}}{2\pi}+\bar{t}_{k_1}\frac{e^{ik_2x}}{2\pi}\Big]+Ae^{[-\Gamma/2+i(k_1+k_2-\epsilon)]x}, \tag{13.34}$$

where A is a constant to be determined. Applying the constraint Eq. (13.32a) to $g_2^{②}(x,0^+)$, we obtain

$$g_2^{②}(x_1,x_2)=\frac{1}{2!}\Big[\bar{t}_{k_2}\frac{e^{i(k_1x_1+k_2x_2)}}{2\pi}+\bar{t}_{k_1}\frac{e^{i(k_2x_1+k_1x_2)}}{2\pi}\Big] +Ae^{(\Gamma/2+i\epsilon)(x_2-x_1)}e^{i(k_1+k_2)x_1}. \tag{13.35}$$

From Eq. (13.35), we can identify A to be zero: otherwise, the solution is not normalizable [$e^{\Gamma(x_2-x_1)/2}$ is divergent when $x_2 - x_1 \to \infty$]. Hence, $g_2(x_1, x_2)$ in region ② is given by

$$g_2^{②}(x_1, x_2) = \frac{1}{2!}\Big[\bar{t}_{k_2}\frac{e^{i(k_1x_1+k_2x_2)}}{2\pi} + \bar{t}_{k_1}\frac{e^{i(k_2x_1+k_1x_2)}}{2\pi}\Big]. \tag{13.36}$$

Substituting Eq. (13.36) into Eq. (13.33b) yields

$$g_2^{③}(0^+, x) = \frac{1}{2!}\bar{t}_{k_1}\bar{t}_{k_2}\Big[\frac{e^{ik_2x}}{2\pi} + \frac{e^{ik_1x}}{2\pi}\Big] + Be^{[-\Gamma/2+i(k_1+k_2-\epsilon)]x}, \tag{13.37}$$

where B is a constant to be determined. Again, applying the constraint Eq. (13.32a) to $g_2^{③}(0^+, x)$, we obtain

$$g_2^{③}(x_1, x_2) = \frac{1}{2!}\bar{t}_{k_1}\bar{t}_{k_2}\Big[\frac{e^{i(k_1x_1+k_2x_2)}}{2\pi} + \frac{e^{i(k_1x_2+k_2x_1)}}{2\pi}\Big] + Be^{(-\Gamma/2-i\epsilon)(x_2-x_1)}e^{i(k_1+k_2)x_2}. \tag{13.38}$$

Finally, B is found by substituting Eq. (13.5), Eq. (13.36), and Eq. (13.38) into the continuity condition Eq. (13.32c), yielding

$$B = -\frac{(\bar{t}_{k_1} - 1)(\bar{t}_{k_2} - 1)}{2\pi}. \tag{13.39}$$

Extending these solutions from the half space to the full space using the bosonic symmetry gives rise to the two-photon scattering eigenstate given in Eq. (13.7) of the main text.

14 Bound states and entanglement generation in waveguide quantum electrodynamics by Facchi, Kim, et al.

Abstract

We investigate the behavior of two quantum emitters (two-level atoms) embedded in a linear waveguide, in a quasi-one-dimensional configuration. Since the atoms can emit, absorb and reflect radiation, the pair can spontaneously relax towards an entangled bound state, under conditions in which a single atom would instead decay. Exploting the resolvent formalism, we analyze the properties of these bound states, which occur for resonant values of the interatomic distance, and discuss their relevance with respect to entanglement generation. The stability of such states close to the resonance is studied, as well as the properties of non-resonant bound states, whose energy is below the threshold for photon propagation.

14.1 Introduction

An excited atom in free space unavoidably decays towards its ground state through spontaneous emission. Boundary conditions and artificial dimensional reduction can drastically modify the picture, providing situations in which the decay is enhanced, inhibited or even completely hindered [1, 2, 3, 4, 5, 6, 7, 8, 9]. While confinement in optical cavities has long been a common way to study the effects of geometry [10, 11, 12], one-dimensional systems have recently emerged as another promising stage for the observation of interesting quantum electrodynamics (QED) phenomena. Nowadays a variety of quantum emitters (atoms for brevity) can be coupled to quasi one-dimensional fields such as waveguides, optical fibers and microwave transmission lines [13, 14, 15, 16, 17, 18, 19]. Alternatively, the effective reduction to one dimension can be obtained by tightly focusing photons [20, 21, 22]. These impressive experimental advances have opened the way to unexplored non-perturbative regimes of QED, and have motivated work on the interaction between atoms and waveguides in different geometries [23, 24, 25, 26, 27, 28, 29, 30].

In this context, an interesting problem is the study of atoms in semi-infinite linear waveguides, where one end of the guide behaves as a perfect mirror [31, 32, 33]. For selected values of the atom-mirror distance a nontrivial bound state exists, in which the probability of atomic excitation is finite, even when photons emitted through spontaneous decay can propagate in the guide [34, 35]. The optical path between the atom and the mirror is crucial for the existence of this kind of resonance. It is worth noting that even a single atom exhibits a mirror-like behavior in one dimension [21, 22, 36, 37, 38, 39]. One may thus consider the interaction of

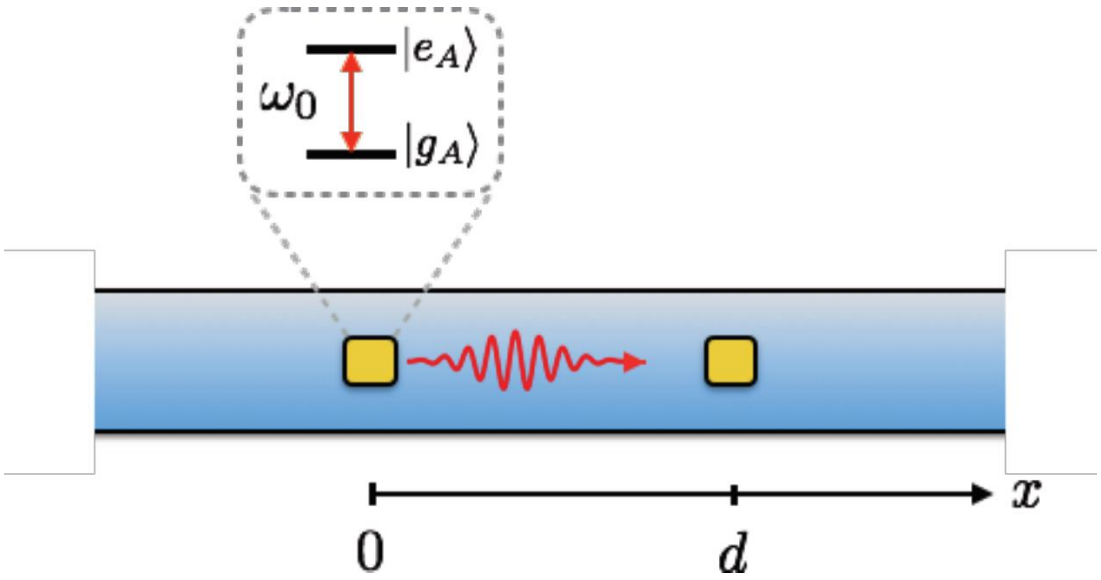

Figure 14.1: Two two-level atoms are placed at relative distance d in a one-dimensional waveguide, with propagation direction along the x axis. Both atoms possess the same internal structure (for brevity we only sketch the levels of emitter A) and interact through the mediation of waveguide photons. The waveguide is characterized by its one-dimensional photon dispersion relation $\omega(k)$, with k being the photon momentum. We first focus on the $\mathrm{TE}_{1,0}$ mode of an infinite waveguide of rectangular cross section, and then generalize to a wide class of one-dimensional dispersion relations in Sec. 14.5.

two atoms, mediated by the exchange of photons propagating in one dimension, and exploit the dual behavior of each atom as both an emitter and a mirror. Such interaction can give rise to stable configurations in which the atoms display significant entanglement, while the field is confined between the atoms and does not propagate [39, 40, 41]. Besides the fundamental interest of few-body QED in quasi 1D geometries, where non-Markovian effects easily come into play [42], such a system is thus interesting from the point of view of generating entanglement, an important resource in Quantum Information, by *relaxation*. Indeed, if a bound state exists in which the two atoms are entangled, an initially factorized atomic state can spontaneously relax towards a state with finite entanglement. Relaxation occurs after an initial transient in which photon exchange builds up quantum correlations. Differently from other methods of entanglement generation in waveguide-QED [43], this process would not require a continuous pumping of energy into the system, and would ideally provide a constant entanglement in time after the initial transient.

In this paper we show how the properties of bound and quasi-bound entangled states in waveguide-QED can be studied in great depth and generality by exploiting the resolvent formalism [44, 46]. Studying the resolvent, one notices the presence of a number of poles in the so-called *complex-energy plane*. Each pole can be associated with a (generally unstable) state, and the imaginary part of a pole is proportional to the inverse lifetime of the state. This allows us to immediately identify a favorable situation for entanglement generation by relaxation: we need one of these poles to be a long-lived entangled state (i.e., the pole must have a negligible imaginary part), while the remaining poles must be fast-decaying states. Under such conditions, a separable atomic state would quickly relax onto an entangled metastable state. While the metastable state will eventually decay due to losses and imperfections, our analysis allows to clearly identify the relevant timescales of the problem. Thus, we can give a clear indication of what degree of losses and imperfections a given system is able to tolerate while still allowing the generation of long-lived entanglement. Importantly, our formalism automatically takes into account a number of physical effect that are often neglected: these include non-markovian effects, time-delay (due to the finite propagation speed of photons), threshold effects (due to the presence of either high- or low-frequency cutoffs in the dispersion relation). Even though, for definiteness, we focus for the most part on the dispersion relation typical of rectangular waveguides, we will also outline how a wide class of physically relevant dispersion relations can be tackled within the same framework.

Our paper is organized as follows. In section 14.2 we introduce the Hamiltonian of our model, and illustrate how a suitable choice of the inter-atomic distance gives rise to entangled bound states above the frequency threshold for photon propagation. Section 14.3 is devoted to the study of poles in the complex-energy plane, which allows us to extract crucial information relevant to the entanglement-by-relaxation protocol. In section 14.4 we extend our analysis to off-resonant bound states, whose energy is below the low-frequency cutoff of the waveguide. We outline in section 14.5 how our study can be generalized in a straightforward manner to any dispersion relation that satisfies appropriate conditions. Finally, we draw our conclusions in section 14.6.

14.2 The model

We describe the dynamics of two two-level atoms A and B, situated in an infinite waveguide of rectangular cross section, with sides $L_y < L_z$, see Fig. 14.1. When longitudinal propagation occurs with long wavelength compared to the transverse size, interaction between atoms and field can be reduced to a coupling with the lowest-cutoff-energy $\mathrm{TE}_{1,0}$ mode, in which the electric field vibrates along the z direction and has a sine modulation in the y direction [48]. In this situation, the electromagnetic field is effectively scalar and massive. The interacting atoms and photons are described, in dipolar and rotating wave approximations, by the Hamiltonian

$$\begin{aligned} H &= H_0 + \lambda V \\ &= \omega_0(|e_A\rangle\langle e_A| + |e_B\rangle\langle e_B|) + \int dk\, \omega(k) b^\dagger(k) b(k) \\ &\quad + \lambda \int \frac{dk}{\omega(k)^{1/2}} \Big[|e_A\rangle\langle g_A|\, b(k) + |g_A\rangle\langle e_A|\, b^\dagger(k) \\ &\quad + |e_B\rangle\langle g_B|\, b(k) \mathrm{e}^{\mathrm{i}kd} + |g_B\rangle\langle e_B|\, b^\dagger(k) \mathrm{e}^{-\mathrm{i}kd} \Big], \end{aligned} \tag{14.1}$$

where ω_0 is the bare energy separation between the atomic ground $|g\rangle$ and first-excited states $|e\rangle$, λ is the coupling constant (see Appendix B), d is the A-B distance, $\omega(k)$ is the photon dispersion relation, and $b(k)$ ($b^\dagger(k)$) is the annihilation (creation) field operator, satisfying the canonical commutation relation $[b(k), b^\dagger(k')] = \delta(k-k')$. Henceforth, we will focus on the dispersion $\omega(k) = \sqrt{k^2 + M^2}$ of the $\mathrm{TE}_{1,0}$ mode in the waveguide, characterized by a mass $M \propto L_y^{-1}$. However, as discussed in section 14.5, our approach is applicable to a wide class of one-dimensional dispersion relations. The effective mass M provides a natural cutoff to the coupling. The Hamiltonian (14.1) commutes with the excitation number

$$\mathcal{N} = \mathcal{N}_{\mathrm{at}} + \int dk\, b^\dagger(k) b(k), \tag{14.2}$$

where $\mathcal{N}_{\mathrm{at}} = |e_A\rangle\langle e_A| + |e_B\rangle\langle e_B|$ is the atomic excitation number. The $\mathcal{N} = 0$ sector is 1-dimensional and is spanned by the bare ground state $|g_A, g_B; \mathrm{vac}\rangle$. We shall focus instead on the dynamics in the $\mathcal{N} = 1$ sector, where the states read

$$|\psi\rangle = \big(c_A\, |e_A, g_B\rangle + c_B\, |g_A, e_B\rangle\big) \otimes |\mathrm{vac}\rangle + |g_A, g_B\rangle \otimes |\varphi\rangle \tag{14.3}$$

where $|\varphi\rangle := \int dk\, \varphi(k) b^\dagger(k) |\mathrm{vac}\rangle$ is a one-photon state, and $|c_A|^2 + |c_B|^2 + \int dk |\varphi(k)|^2 = 1$.

In the small-coupling regime, an isolated excited atom with $\omega_0 \gtrsim M$ would decay to the ground state. We shall demonstrate that, when two atoms are considered, a resonance effect emerges, yielding a bound state. Using the expansion (14.3) the eigenvalue equation, $H|\psi\rangle = E|\psi\rangle$, reads

$$E c_A = \omega_0 c_A + \lambda \int dk \frac{\varphi(k)}{\omega(k)^{1/2}}, \tag{14.4}$$

$$E c_B = \omega_0 c_B + \lambda \int dk \frac{\varphi(k) \mathrm{e}^{\mathrm{i}kd}}{\omega(k)^{1/2}}, \tag{14.5}$$

$$\varphi(k) = \frac{\lambda}{\omega(k)^{1/2}} \frac{c_A + c_B \mathrm{e}^{-\mathrm{i}kd}}{E - \omega(k)}. \tag{14.6}$$

The field amplitude $\varphi(k)$ has two simple poles at $k = \pm\bar{k} = \pm\sqrt{E^2 - M^2}$. Thus, when $E > M$, the integrals in (14.4)-(14.5) are finite only if $c_A + c_B \mathrm{e}^{\pm \mathrm{i}\bar{k}d} = 0$, yielding $\bar{k}d = n\pi$ for positive integers n. This implies that a bound state can exist only for discrete values of the interatomic distance d. Moreover, in the first component of such an eigenstate (14.3), the atoms are in a maximally entangled (singlet or triplet) state, namely $c_A = (-1)^{n+1} c_B$. To determine the distances at which the bound state exists, let us first compute the energy eigenvalue, which after the resonance condition is the solution of

$$\begin{aligned} E &= \omega_0 + \lambda^2 \int dk \frac{1 - (-1)^n \mathrm{e}^{-\mathrm{i}kd}}{\omega(k)(E - \omega(k))} \\ &= \omega_0 + \frac{2\lambda^2}{M} \left[1 + O\left(\frac{E-M}{M}\right) + O\left(\frac{\mathrm{e}^{-Md}}{\sqrt{Md}}\right) \right]. \end{aligned} \tag{14.7}$$

Corrections in the second line are negligible if $|\omega_0 - M| \ll M$. This will result as a special case of the ensuing analysis of the complex poles of the resolvent. [See Eq. (14.28) and following ones.] Thus for large M, a bound state with $E > M$ is present only if the distance d takes one of the discrete and equally spaced values

$$d_n = \frac{n\pi}{\bar{k}}, \quad \text{with} \quad \bar{k} := \sqrt{\left(\omega_0 + \frac{2\lambda^2}{M}\right)^2 - M^2}, \tag{14.8}$$

and if the wavenumber $\bar{k}$ is real ($\omega_0 > M - 2\lambda^2/M$). The properties of states with $E < M$, to which an imaginary wavenumber can be associated, will be discussed in Section 14.4.

To complete the characterization of the bound state, we shall analyze the atomic populations and the field energy density. The former can be immediately obtained using the normalization condition on the states (14.3) as

$$1 = 2|c_A^{(n)}|^2 \left(1 + \lambda^2 \int dk \frac{1-(-1)^n \cos(kd_n)}{\omega(k)(E-\omega(k))^2}\right), \tag{14.9}$$

Where we use the shorthands $c_A^{(n)}, c_B^{(n)}$ to indicate the coefficients of the bound state with $d = d_n$. Retaining only the highest order in M and defining $p_n := |c_A^{(n)}|^2 + |c_B^{(n)}|^2$ as the probability associated to the $\mathcal{N}_{\rm at} = 1$ sector, one gets

$$p_n \simeq \left(1 + n\pi \frac{2\pi\lambda^2 M}{\bar{k}^3}\right)^{-1}. \tag{14.10}$$

Notice that, despite being apparently of order λ^2, the correction to unity is given by the ratio between powers of two small quantities, namely the effective coupling constant λ/M, and the wavenumbers ratio $\bar{k}/M$. The resulting number can be of order one, even at small coupling constants. Observe that the probability vanishes like $\bar{k}^3/n$ at very small $\bar{k}$: this behavior is physically motivated by the fact that, as the energy approaches the cutoff, the distance between the atoms must increase to infinity in all bound states. Let us finally analyze the energy density of the electromagnetic fields. Neglecting the exponentially suppressed contribution of the square-root cuts, the energy density turns out to be related to the Fourier transform of the photon amplitude,

$$\begin{aligned} \widetilde{\varphi}_n(x) &= \int \frac{dk}{2\pi} \varphi_n(k) \mathrm{e}^{\mathrm{i}kx} \\ &\simeq \frac{\lambda c_A^{(n)} 2M}{\sqrt{2\pi E}} \int dk \frac{1-(-1)^n \mathrm{e}^{-\mathrm{i}kd_n}}{\bar{k}^2 - k^2} \mathrm{e}^{\mathrm{i}kx}, \end{aligned} \tag{14.11}$$

as

$$\mathcal{E}_n(x) \simeq E|\widetilde{\varphi}_n(x)|^2 \simeq \left(\frac{2\sqrt{\pi}\lambda M}{\bar{k}}\right)^2 p_n \sin\left(\bar{k}x\right)^2, \tag{14.12}$$

for $x \in [0, d_n]$, and $\mathcal{E}_n(x) \simeq 0$ outside. Thus, the field is confined between the two atoms, and modulated with periodicity $\pi/\bar{k}$, with nodes at the positions of the atoms which act as mirrors. This explains the occurrence of such bound states for discrete values (14.8) of the interatomic distance.

Moreover, the structure of the bound state is

$$|\psi_n\rangle = \sqrt{p_n}\, |\Psi^s\rangle \otimes |\mathrm{vac}\rangle + |g_A, g_B\rangle \otimes |\varphi_n\rangle\,, \tag{14.13}$$

where $s = (-1)^{n+1}$ and $|\Psi^\pm\rangle = (|e_A, g_B\rangle \pm |g_A, e_B\rangle)/\sqrt{2}$ are (maximally entangled) Bell states. This is a key feature which enables entanglement generation by atom-photon interaction. Indeed, suppose that $d = d_n$: a factorized initial state, say $|\psi(0)\rangle = |e_A, g_B\rangle \otimes |\mathrm{vac}\rangle$, can be expanded into a "stable" and a "decaying" part as

$$|e_A, g_B; \mathrm{vac}\rangle = \sqrt{\frac{p_n}{2}}\, |\psi_n\rangle + \sqrt{1 - \frac{p_n}{2}}\, |\psi_n^\perp\rangle\,, \tag{14.14}$$

with $\langle \psi_n^\perp | \psi_n \rangle = 0$. After a transient of the order of $|\psi_n^\perp\rangle$'s lifetime (see discussion in the following), the atomic density matrix $\rho_{\rm at}(t) := \mathrm{Tr}_{\rm field}\, |\psi(t)\rangle \langle\psi(t)|$ approaches

$$\rho_{\rm at}(\infty) = \frac{p_n^2}{2} |\Psi^s\rangle \langle\Psi^s| + \left(1 - \frac{p_n^2}{2}\right) |g_A, g_B\rangle \langle g_A, g_B|\,, \tag{14.15}$$

in which the atoms have a finite probability, determined by (14.10), to be maximally entangled. In Figure 14.2 we display the atomic entanglement in the asymptotic state, as measured by the concurrence [45]. However, one could also measure the photon state and obtain, with a finite probability, a maximally entangled atomic state. The strategy is therefore the following: one prepares a factorized state, and measures whether a photon is emitted. If (after a few lifetimes) no photon has been observed, the atomic state is projected over the maximally entangled Bell state $|\Psi^s\rangle$. This can be achieved with higher probabilities for larger values of ω_0. In realistic scenarios this simplified picture is challenged by the presence of losses, such that it is no longer possible to prepare an exact Bell state. Nevertheless, if losses occur on sufficiently long timescales (as compared to the decay rate of the fast pole — see section 14.3 below), and provided the detector efficiency is high enough, it remains possible to achieve high fidelity with a Bell state.

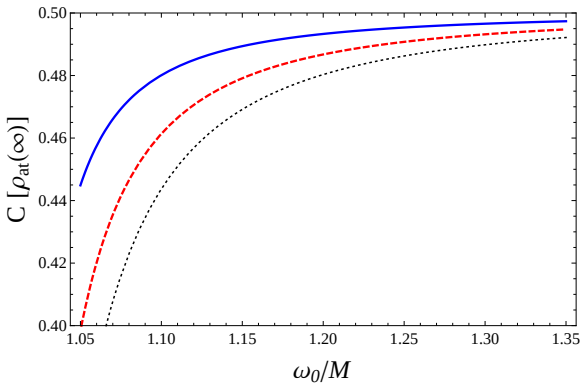

Figure 14.2: Behavior of the concurrence $C = p_n^2/2$ of the asymptotic states $\rho_{\rm at}(\infty)$ as a function of the atomic excitation energy, for $\lambda = 10^{-2}M$ and a factorized initial state. The solid (blue) line, dashed (red) line and dotted (black) line are referred to the resonant states with $n = 1, 2, 3$, respectively.

14.3 Time evolution and bound state stability

Let us now study the general evolution of an initial state in the atomic sector $\mathcal{N}_{\rm at} = 1$. We will use the resolvent formalism [44, 46] to illustrate that the system relaxes towards the bound state, and to quantify the robustness of the bound state against small variations in the model parameters (such as the A-B distance). We remark that the usefulness of the resolvent formalism goes beyond the analysis of stable states, in that it provides crucial information on the relevant timescales of the problem. Indeed, the entanglement-by-relaxation protocol described in the previous section relies on the fast decay of the unstable Bell state. The analysis of the resolvent enables to determine the lifetime of this unstable state, which must be much shorter than the typical timescales of waveguide or atomic losses, as well as the inevitably finite lifetime of the bound state (due for example to imperfect control of the A-B distance). Whenever these conditions are met, the effectiveness of the protocol is guaranteed and a long-lived entangled state may be prepared by relaxation.

The resolvent $\mathcal{G}(z) = (z - H)^{-1}$, with z the complex energy variable, has singularities only on the real axis (on the first Riemann sheet) and the study of additional singularities (on the other Riemann sheets) yields crucial information about the dynamical stability of the system: in particular, a pole with a non-vanishing imaginary component signals a decay process. The resolvent approach yields results that are consistent with those obtained from the analysis of the Laplace transform of the time evolution [41].

For $\lambda = 0$, the free resolvent $\mathcal{G}_0(z) = (z - H_0)^{-1}$ has a pole on the real axis, at $z = \omega_0$, corresponding to the excited states of atoms A or B. When interaction is turned on, this singularity splits into two simple poles, which generally migrate into the second Riemann sheet. We shall see from a non-perturbative analysis that, under resonance conditions, one of the poles falls on the real axis (and is therefore very long-lived), while the other one has a very short lifetime. Let $G(z)$ and $G_0(z)$ be the restrictions to the $\mathcal{N}_{\rm at} = 1$ sector of the interacting and free resolvent, respectively. In the basis $\{|e_A, g_B\rangle, |g_A, e_B\rangle\}$ one gets

$$G_0(z) = \frac{1}{z - \omega_0} \begin{pmatrix} 1 & 0 \\ 0 & 1 \end{pmatrix} \tag{14.16}$$

and

$$G(z) = [G_0(z)^{-1} - \lambda^2 \Sigma(z)]^{-1} = [z - \omega_0 - \lambda^2 \Sigma(z)]^{-1}, \tag{14.17}$$

where

$$\Sigma(z) = \begin{pmatrix} \Sigma_{AA}(z) & \Sigma_{AB}(z) \\ \Sigma_{BA}(z) & \Sigma_{BB}(z) \end{pmatrix} \tag{14.18}$$

is called self energy.

The resolvent $G(z)$ is analytic in the whole complex energy plane, except at points on the real axis that belong to the spectrum of the Hamiltonian H. In particular it exhibits simple poles at the eigenvalues of H and cuts along its continuous spectrum [44, 46]. However, it can happen that some complex poles show up on the second Riemann sheet, through the analytic continuation of the resolvent $G_{\rm II}(z)$ from the upper half-plane to the lower half-plane under the cut [46, 47]. These poles physically correspond to unstable states with energy and decay rates given by their real and imaginary part, respectively.

The particular form of the interaction Hamiltonian V in (14.1) enables one to exactly evaluate the self energy:

$$\Sigma_{AA}(z) = \Sigma_{BB}(z) = \int dk \frac{1}{\omega(k)(z - \omega(k))}, \tag{14.19}$$

$$\Sigma_{AB}(z) = \Sigma_{BA}(z) = \int dk \frac{\cos(kd)}{\omega(k)(z - \omega(k))}. \tag{14.20}$$

Due to the bare energy degeneracy and the symmetric structure of the self energy, the propagator can be diagonalized as

$$G(z) = \frac{|\Psi^+\rangle\langle\Psi^+|}{z-\omega_0-\lambda^2\Sigma_+(z)} + \frac{|\Psi^-\rangle\langle\Psi^-|}{z-\omega_0-\lambda^2\Sigma_-(z)}, \tag{14.21}$$

where

$$\Sigma_s(z) = 2\int_M^\infty d\omega \frac{\kappa_s(\omega)}{z-\omega}, \qquad s=\pm 1, \tag{14.22}$$

with spectral densities

$$\kappa_\pm(E) = \frac{1\pm\cos\left(\sqrt{E^2-M^2}d\right)}{\sqrt{E^2-M^2}}\chi_{[M,\infty)(E)}. \tag{14.23}$$

The self-energy functions $\Sigma_\pm(z)$ are analytic in the cut complex energy plane $\mathbb{C}\setminus[M,+\infty)$ and have a purely imaginary discontinuity across the cut proportional to the spectral density:

$$\Sigma_s(E-\mathrm{i}0^+) - \Sigma_s(E+\mathrm{i}0^+) = 2\pi\mathrm{i}\kappa_s(E). \tag{14.24}$$

During the continuation process into the second Riemann sheet through the cut, the self energy (14.22) will thus get an additional term

$$\Sigma_s(z) \longrightarrow \Sigma_s^{\mathrm{II}}(z) = \Sigma_s(z) - 2\pi i\kappa_s(z), \qquad z\in\mathbb{C}. \tag{14.25}$$

Note that the new term has in general a nonvanishing imaginary part and is the analytical continuation of the discontinuity of the self-energy function across the cut. Now, a pole

$$z_\mathrm{p} = E_\mathrm{p} - \mathrm{i}\gamma_\mathrm{p}/2 \tag{14.26}$$

of $G(z)$ on the second sheet must satisfy the equation

$$z_\mathrm{p} = \omega_0 + \lambda^2\Sigma_s^{\mathrm{II}}(z_\mathrm{p}), \tag{14.27}$$

for $s=+1$ or $s=-1$, where $\Sigma_s^{\mathrm{II}}(z)$ is the branch (14.25) of the self energy in the second sheet. By plugging (14.25) and (14.23) into (14.27) we get

$$z_\mathrm{p} = \omega_0 + \lambda^2\left(\Sigma_\pm(z_\mathrm{p}) - 4\pi\mathrm{i}\frac{1\pm\cos\left(\sqrt{z_\mathrm{p}^2-M^2}d\right)}{\sqrt{z_\mathrm{p}^2-M^2}}\right). \tag{14.28}$$

It is evident from (14.28) how the energetic degeneracy at $\lambda=0$ is lifted by interactions. Notice the presence of an imaginary component, detecting decay.

The last ingredient we need in order to get a closed expression for the complex energy poles is the evaluation of $\Sigma_s(z)$ in (14.28). Thus, let us rewrite (14.22) as an integral over k:

$$\Sigma_\pm(z) = \int_{-\infty}^{+\infty}\frac{dk}{\sqrt{k^2+M^2}}\frac{1\pm e^{ikd}}{z-\sqrt{k^2+M^2}}. \tag{14.29}$$

The integrand function can be analytically continued to the complex k plane using the principal determination of the square root, which has nonnegative real part for all values of its argument, and is characterized by a branch cut for $k^2+M^2<0$, that is

$$k = \pm\mathrm{i}\chi, \quad \text{with } \chi\in(M,\infty). \tag{14.30}$$

Two first-order poles, symmetric with respect to the origin of the k plane, are also present whenever $\mathrm{Re}(z)>0$:

$$k = \pm k_0(z) = \pm\sqrt{z^2-M^2}. \tag{14.31}$$

By deforming the integration contours as in Figure 14.3 and applying Jordan's theorem, Σ_s is split in two terms

$$\Sigma_s(z) = \Sigma_s^{\mathrm{cut}}(z) + \Sigma_s^{\mathrm{pole}}(z). \tag{14.32}$$

coming from the upper branch cut and from one of the two poles (see Figure 14.3). Specifically, when $\mathrm{Im}(z)>0$, the pole $k_0(z)$ lies in the upper half plane, and the integral involves the residue

$$\begin{aligned}\Sigma_\pm^{\mathrm{pole}}(z) &= 2\pi\mathrm{i}\lim_{k\to k_0(z)}\frac{(k-k_0(z))(1\pm e^{ikd})}{\sqrt{k^2+M^2}(z-\sqrt{k^2+M^2})}\\ &= -2\pi\mathrm{i}\frac{1\pm e^{\mathrm{i}\sqrt{z^2-M^2}d}}{\sqrt{z^2-M^2}}.\end{aligned} \tag{14.33}$$

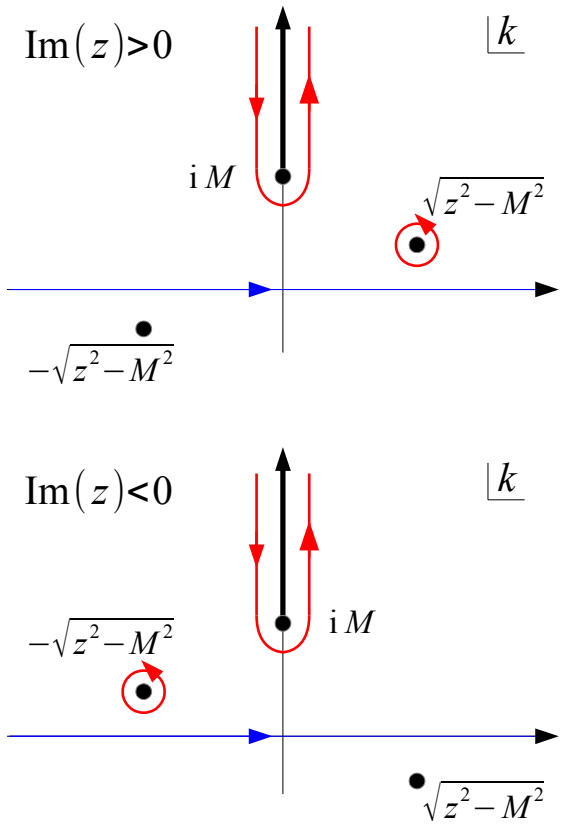

Figure 14.3: Integration contours (red) in the complex k plane for the computation of the integral in Eq. (14.22) with $\mathrm{Im}(z) > 0$ (upper panel) and $\mathrm{Im}(z) < 0$ (lower panel).

Instead, when $\mathrm{Im}(z) < 0$, the deformed contour in the upper plane encircles $-k_0(z)$, where the residue yields

$$\begin{aligned}\Sigma_{\pm}^{\mathrm{pole}}(z) &= 2\pi\mathrm{i}\lim_{k\to -k_0(z)}\frac{(k+k_0(z))(1\pm e^{\mathrm{i}kd})}{\sqrt{k^2+M^2}(z-\sqrt{k^2+M^2})}\\ &= 2\pi\mathrm{i}\frac{1\pm e^{-\mathrm{i}\sqrt{z^2-M^2}d}}{\sqrt{z^2-M^2}}.\end{aligned} \tag{14.34}$$

Finally, the integrals along the cut read

$$\begin{aligned}\Sigma_{\pm}^{\mathrm{cut}}(z) &= 2z\int_M^\infty d\chi\frac{1\pm e^{-\chi d}}{\sqrt{\chi^2-M^2}(z^2+\chi^2-M^2)}\\ &= \frac{2}{\sqrt{z^2-M^2}}\mathrm{Log}\left(\frac{z+\sqrt{z^2-M^2}}{M}\right)\pm O(e^{-Md}),\end{aligned} \tag{14.35}$$

where the contribution from $e^{-\chi d}$, that is not amenable to an explicit closed form in terms of simple functions, is nevertheless suppressed like e^{-Md} and can be neglected for large values of Md.

We are now able to recognize the real resonant poles discussed in the first part of the paper as special solutions of Eq. (14.28). Indeed, assuming that the complex energy pole (14.26) is far from the branching point $z = M$ and that its imaginary part is almost vanishing, one can decouple the real and imaginary parts of (14.28) and obtain from Eqs. (14.32)-(14.35)

$$E_{\mathrm{p}} \simeq \omega_0 + \frac{2\lambda^2}{k_{\mathrm{p}}}\mathrm{Log}\left(\frac{E_{\mathrm{p}}+k_{\mathrm{p}}}{M}\right)\pm 2\pi\lambda^2\frac{\sin(k_{\mathrm{p}}d)}{k_{\mathrm{p}}}, \tag{14.36}$$

$$\gamma_{\mathrm{p}} \simeq 4\pi\lambda^2\frac{1\pm\cos(k_{\mathrm{p}}d)}{k_{\mathrm{p}}}, \tag{14.37}$$

where $k_{\mathrm{p}} = \sqrt{E_{\mathrm{p}}^2 - M^2}$. Hence, we find that the poles in the second Riemann sheet have a cyclic behavior with respect to d. This result is in agreement with the one obtained in Ref. [40] in the Markovian approximation. In

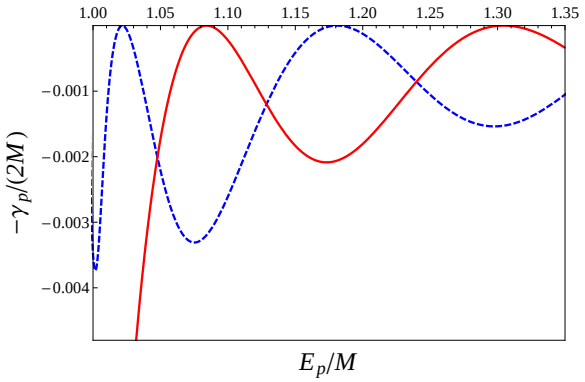

Figure 14.4: Trajectories of the poles $E_{\rm p}^{(+)} - {\rm i}\gamma_{\rm p}^{(+)}/2$ (dashed blue line) and $E_{\rm p}^{(-)} - {\rm i}\gamma_{\rm p}^{(-)}/2$ (solid red line) on the second Riemann sheet of the complex energy plane, for $Md = 15$ and $\lambda = 10^{-2}M$, with varying $.95 \leq \omega_0/M \leq 1.35$. The trajectories are tangent to the real axis (they touch it whenever condition (14.8) is satisfied), showing that the approximate bound states are robust against variation of ω_0. Notice that the behaviour of both poles becomes non perturbative in λ as $\omega_0 \sim M$.

particular, when $d = d_n$, as defined in Eq. (14.8), the real part of the pole equations is solved by $E_{\rm p} = \sqrt{\bar{k}^2 + M^2}$. In this case, one of the poles corresponds to the entangled bound state, and has vanishing imaginary part, while the other signals an unstable state with associated decay rate

$$\gamma_{\rm p}^{(u)} = 8\pi\lambda^2/\bar{k} \tag{14.38}$$

Even if, strictly speaking, bound states only occur for discrete values of d, it can be readily checked that while the energy shift is linear, the decay rate of the stable pole is quadratic for $d \to d_n$

$$\gamma_{\rm p}^{(s)} \simeq 2\pi\lambda^2\bar{k}(d - d_n)^2, \tag{14.39}$$

implying that the state $|\psi_n\rangle$ remains very long-lived close to resonance. Eq. (14.39) quantifies the robustness of the bound states against variations of the parameter d. Note how Eqs. (14.38) and (14.39) provide essential information on the feasibility and effectiveness of the entanglement generation protocol: firstly, it is necessary that the condition $\gamma_{\rm p}^{(s)} \ll \gamma_{\rm p}^{(u)}$ is satisfied, which is equivalent to the condition $\bar{k}^2(d - d_n)^2 \ll 1$. Secondly, $\gamma_{\rm p}^{(u)}$ must be much larger than any decay rate associated with loss processes (e.g. waveguide losses). Even though approximate analytical expressions such as Eqs. (14.38) and (14.39) are extremely valuable, we emphasize that our methodology is capable of capturing the *exact* behaviour of the poles against variations in the model parameters. To illustrate this, in Fig. 14.4 we show the trajectories of the poles (14.26) in the complex energy plane, obtained by fixing M and d and varying the bare excitation energy ω_0. On the one hand, we are thus able to assess quantitatively the robustness of bound states against variations in ω_0. On the other hand, Fig. 14.4 demonstrates how our methodology allows one to interpolate seamlessly between perturbative and non-perturbative regimes.

14.4 Off-resonant bound states

Let us briefly discuss the behavior of bound states with $E < M$. In this case, the atoms are not expected to decay. Nonetheless, they interact by coupling to the evanescent modes of the waveguide. Scrutiny of Eqs. (14.4)-(14.5) shows that there are bound states for all d, whose energy satisfies

$$\begin{pmatrix} E - \omega_0 - \alpha(E) & -\beta(E) \\ -\beta(E) & E - \omega_0 - \alpha(E) \end{pmatrix} \begin{pmatrix} c_A \\ c_B \end{pmatrix} = 0, \tag{14.40}$$

with

$$\alpha(E) = -\frac{\lambda^2}{\sqrt{M^2 - E^2}} \left(\pi + 2\arctan\frac{E}{\sqrt{M^2 - E^2}} \right), \tag{14.41}$$

$$\beta(E) = -\frac{\lambda^2}{\sqrt{M^2 - E^2}}\, 2\pi e^{-\sqrt{M^2 - E^2}\, d}. \tag{14.42}$$

where we have again neglected the $O(e^{-Md})$ contributions from branch-cut integration in the complex k plane. If the coupling is small and the excitation energy ω_0 is far from the threshold M for photon emission, the above equations reduce to an effective Hamiltonian eigenvalue equation in the $\mathcal{N}_{\rm at} = 1$ sector. The eigenvalues read

$$E^{(\pm)} = \omega_0 + \alpha(\omega_0) \pm \beta(\omega_0), \tag{14.43}$$

with $c_A = c_B$ for the plus sign (ground state) and $c_A = -c_B$ for the minus sign. These bound states are not associated to any resonance. It is also possible to check that the electromagnetic energy density falls like $\exp\left(-\sqrt{M^2 - E^2}|x|\right)$ away from the atoms.

Since the eigenstates of the effective Hamiltonian are Bell states, the evolution of an initially factorized state is characterized by oscillations between two orthogonal maximally entangled states with period $2\pi/\beta(\omega)$. Compared to entanglement by relaxation, this mechanism yields unit concurrence [41]. On the other hand, the process can be very slow, since the energy splitting is exponentially suppressed with the interatomic distance, and requires the fine tuning of an optimal time to stop the interactions, which is not required in the spontaneous entanglement process described in Section 14.2.

The case $E \to M$ is more interesting, since the physics becomes nonperturbative. Equations (14.4)-(14.5) admit a singlet and a triplet solution. For the singlet case, the bound state with $E = M$ is obtained at a finite excitation energy:

$$\omega_0 = M - \frac{2\lambda^2}{M} + 2\pi\lambda^2 d, \tag{14.44}$$

in which, due to a cancellation of divergences, the correction to the bare energy is still perturbative in λ^2. This singlet solution approximates the dark eigenstate $|\Psi^-\rangle \otimes |\text{vac}\rangle$ occurring at $d = 0$. The triplet, instead, survives as a real eigenstate even for $\omega_0 \geq M$. However, since $c_A = c_B$ implies that the integrals over the field become divergent in this limit, the population in the $\mathcal{N}_{\rm at} = 1$ sector is suppressed to fulfill normalization, and the contribution of this pole to the expansion (14.14) can be safely neglected.

14.5 Extension to generic dispersion relations

While we have worked out in detail the case of a rectangular waveguide, we emphasize that our methods can be applied to a generic dispersion relation $\omega(k)$. We start by noticing that Eqs. (14.4)-(14.6) lead in full generality to the implicit condition

$$E = \omega_0 + \lambda^2 \int dk \frac{1 - (-1)^n \mathrm{e}^{-\mathrm{i}kd}}{\omega(k)(E - \omega(k))}, \tag{14.45}$$

which must be satisfied by the bound state energy E. For the existence of a resonant (i.e. above threshold) bound state, it is evident that also the condition $\bar{k}d = n\pi$, $n \in \mathbb{N}$ must hold, where $\bar{k} > 0$ satisfies $E = \omega(\pm\bar{k})$. If this were not the case, the right hand side of Eq. (14.45) would diverge. We assume that such $\bar{k}$ exists and is unique. This is the case, for example, when $\omega(k)$ is an increasing lower-bounded function of $|k|$. Moreover, the possibility of non-resonant eigenstates below threshold follows as in the case of a rectangular waveguide.

Moving on to the complex energy plane, the analysis of poles proceeds along the same lines as in section 14.3, albeit the existence of compact analytical expressions will rely on the specific functional form of $\omega(k)$. The pole contribution to the self energies can be generalized by replacing the denominators in Eqs. (14.33)-(14.34) with $\omega(k_0)\omega'(k_0)$, and the square root in the exponentials with k_0. In the perturbative regime, this change does not affect formally the ratio of the decay rates of stable and unstable poles close to a resonance, namely [see Eqs. (14.38)-(14.39)]

$$\frac{\gamma_{\rm p}^{(s)}}{\gamma_{\rm p}^{(u)}} = \frac{1}{4}\bar{k}^2(d - d_n)^2, \tag{14.46}$$

where $d_n = n\pi/\bar{k}$. We can see that quantitative differences between models arise in the inversion of the dispersion relation as a function of the energy. The quantity in Eq. (14.46) gives a clear indication of the potential of a given model to generate entanglement by relaxation. While losses would inevitably degrade the quality of the achievable entangled state, Eq. (14.46) may be seen as posing a fundamental limit to the entangling capabilities of a given system, a limit which would persist even in an idealized lossless scenario.

14.6 Conclusions and outlook

We analyzed stable and unstable states of a pair of atoms in a waveguide, finding that an entangled bound state exists for discrete values of the interatomic distance. This implies that an initially factorized atomic state can spontaneously relax towards a long-lived entangled state. By analyzing the poles of the resolvent operator, we have shown how to quantify the robustness of the entangled bound state to small variations in the model parameters, and how to identify the timescales that are crucial for the preparation of an entangled state by relaxation.

While it has been pointed out that quantum computation may be achievable in waveguide-QED trough effective photon-photon interactions [49], focusing on the atomic degrees of freedom may also hold significant potential for applications in Quantum Information [50]. Further investigation will thus be devoted to the analysis of many-atom systems [51, 52, 53, 54], in which photon-mediated interactions could possibly produce stable configurations such as W states or cluster states.

14.7 Derivation of the quasi-1D free field Hamiltonian

We derive here the Hamiltonian in Eq. (1) of the main text from first principles. Let us consider a waveguide of infinite length, parallel to the x axis, characterized by a rectangular cross section with $y \in [0, L_y]$ and $z \in [0, L_z]$. We conventionally assume that $L_y > L_z$. A common choice is $L_y/L_z = 2$. In a generic guide made of a linear dielectric with uniform density and coated by a conducting material, the boundary conditions for the electric and magnetic fields on the surface S read

$$E_x|_S = 0 \qquad \text{and} \qquad \left.\frac{\partial B_x}{\partial n}\right|_S = 0, \tag{14.47}$$

with $\partial/\partial n$ denoting the normal derivative with respect to the surface. Transverse electric (TE) modes are characterized by $E_x = 0$ everywhere in the guide and obtained by imposing $\partial B_x/\partial n = 0$ on the surface. On the other hand, transverse magnetic (TM) modes have $B_x = 0$ identically. If the waveguide is rectangular, the boundary conditions for TE modes reduce to

$$\left.\frac{\partial B_x}{\partial y}\right|_{y=0} = \left.\frac{\partial B_x}{\partial y}\right|_{y=L_y} = \left.\frac{\partial B_x}{\partial z}\right|_{z=0} = \left.\frac{\partial B_x}{\partial z}\right|_{z=L_z} = 0, \tag{14.48}$$

which limits the form of the longitudinal magnetic field to the real part of

$$B_x = B_0 \cos\left(\frac{m\pi y}{L_y}\right) \cos\left(\frac{n\pi z}{L_z}\right) e^{i(kx - \omega_{m,n}(k)t)}, \tag{14.49}$$

with $m, n \in \mathbb{N}^2 \backslash \{(0,0)\}$ and B_0 a constant.
The integers m and n label the mode $\mathrm{TE}_{m,n}$. The dispersion relation with respect to the longitudinal momentum has the same form as a massive relativistic particle,

$$\omega_{m,n}(k) = \sqrt{(vk)^2 + \omega_{m,n}(0)^2}, \tag{14.50}$$

with $\omega_{m,n}(0) = v\left[\left(\frac{m\pi y}{L_y}\right)^2 + \left(\frac{n\pi z}{L_z}\right)^2\right]^{\frac{1}{2}}$, where the mass term is called the *cutoff frequency* of the mode, and $v = (\mu\epsilon)^{-1/2}$ is the phase velocity in the waveguide, assumed isotropic and nondispersive with magnetic permeability μ and dielectric constant ϵ. Since $L_y < L_z$, the $\mathrm{TE}_{1,0}$ mode has the lowest cutoff frequency. It can be proved [48] that $\omega_{1,0}(0)$ is also lower than the cutoffs of all TM modes. Thus, at sufficiently low energy the contribution of the higher energy modes can be neglected, and propagation occurs effectively in one dimension.

The $\mathrm{TE}_{1,0}$ mode is characterized by the following behavior of the fields

$$B_x = B_0 \cos\left(\frac{\pi y}{L_y}\right) e^{i(kx - \omega_{1,0}(k)t)}, \tag{14.51}$$

$$B_y = -i\frac{kL_yB_0}{\pi} \sin\left(\frac{\pi y}{L_y}\right) e^{i(kx - \omega_{1,0}(k)t)}, \tag{14.52}$$

$$E_z = i\frac{\omega_{1,0}(k)L_yB_0}{\pi} \sin\left(\frac{\pi y}{L_y}\right) e^{i(kx - \omega_{1,0}(k)t)}, \tag{14.53}$$

with the other three components vanishing. These fields can be derived from the (transverse) vector potential

$$A_z = \frac{L_yB_0}{\pi} \sin\left(\frac{\pi y}{L_y}\right) e^{i(kx - \omega_{1,0}(k)t)}. \tag{14.54}$$

The mode can be quantized by introducing the time-0 field operators

$$\boldsymbol{A}^{(1,0)}(\boldsymbol{r}) = \int dk \left(\frac{\hbar}{2\pi\epsilon\omega_{1,0}(k)L_yL_z}\right)^{\frac{1}{2}} \sin\left(\frac{\pi y}{L_y}\right) \times \left[a(k)e^{ikx} + a^\dagger(k)e^{-ikx}\right] \hat{u}_z, \tag{14.55}$$

$$\boldsymbol{E}^{(1,0)}(\boldsymbol{r}) = i\int dk \left(\frac{\hbar\omega_{1,0}(k)}{2\pi\epsilon L_yL_z}\right)^{\frac{1}{2}} \sin\left(\frac{\pi y}{L_y}\right) \times \left[a(k)e^{ikx} - a^\dagger(k)e^{-ikx}\right] \hat{u}_z, \tag{14.56}$$

with $[a(k), a^\dagger(k')] = \delta(k-k')$ and $\hat{u}_z = (0,0,1)$. The electric field energy operator associated to the mode thus reads

$$\begin{aligned}\mathcal{E}_{el}^{(1,0)} &= \frac{\epsilon}{2}\int d\boldsymbol{r} : \left(E_z^{(1,0)}(\boldsymbol{r})\right)^2 : \\ &= \frac{1}{2}\int dk\, \hbar\omega_{1,0}(k)\Big[a^\dagger(k)a(k) \\ &\qquad -\frac{a(k)a(-k)+a^\dagger(k)a^\dagger(-k)}{2}\Big]\end{aligned} \tag{14.57}$$

with : (...) : denoting normal ordering, while the magnetic field energy can be evaluated using the relation $\boldsymbol{B}^{(1,0)} = \boldsymbol{\nabla}\times\boldsymbol{A}^{(1,0)}$:

$$\begin{aligned}\mathcal{E}_{mag}^{(1,0)} &= \frac{\epsilon}{2}\int d\boldsymbol{r} : \left(\partial_y A_z^{(1,0)}(\boldsymbol{r})\right)^2 + \left(-\partial_x A_z^{(1,0)}(\boldsymbol{r})\right)^2 : \\ &= \frac{1}{2}\int dk\, \hbar\omega_{1,0}(k)\Big[a^\dagger(k)a(k) \\ &\qquad +\frac{a(k)a(-k)+a^\dagger(k)a^\dagger(-k)}{2}\Big].\end{aligned} \tag{14.58}$$

Thus, the free Hamiltonian for the electromagnetic field takes the diagonal form

$$\begin{aligned}H^{(1,0)} &= \mathcal{E}_{el}^{(1,0)} + \mathcal{E}_{mag}^{(1,0)} \\ &= \int dk\, \hbar\omega_{1,0}(k)a^\dagger(k)a(k) \\ &= \hbar v\int dk\, \sqrt{k^2+\left(\frac{\pi}{L_y}\right)^2}\, a^\dagger(k)a(k).\end{aligned} \tag{14.59}$$

It is worth noticing that the analogy with a massive boson is not limited to the dispersion relation. Indeed, the quantum theory of the mode can be mapped onto a real scalar theory in one dimension, by introducing the operators

$$\begin{aligned}\alpha(x) &= \int dx \sqrt{\frac{\hbar}{2(2\pi)\omega_{1,0}(k)}}\left[a(k)e^{ikx}+a^\dagger(k)e^{-ikx}\right], \\ \Pi(x) &= -i\int dx \sqrt{\frac{\hbar\omega_{1,0}(k)}{2(2\pi)}}\left[a(k)e^{ikx}-a^\dagger(k)e^{-ikx}\right],\end{aligned} \tag{14.60}$$

satisfying

$$[\alpha(x), \Pi(x')] = i\hbar\delta(x-x') \tag{14.61}$$

and related to the vector potential and the electric field by multiplication. The Hamiltonian can be expressed in terms of the field operator $\alpha(x)$ and its canonically conjugated momentum $\Pi(x')$ as

$$\begin{aligned}H^{(1,0)} &= \frac{1}{2}\int dx : \Big[(\Pi(x))^2 + v^2\left(\partial_x\alpha(x)\right)^2 \\ &\qquad +v^4\left(\frac{M}{\hbar}\right)^2\left(\partial_x\alpha(x)\right)^2\Big] :\end{aligned} \tag{14.62}$$

with $M := \frac{\pi\hbar}{vL_y}$, which also allows to identify a linear Hamiltonian density $\mathcal{H}(x)$ such that $H^{(1,0)} = \int dx\mathcal{H}$.

14.8 Interaction Hamiltonian

The interaction between the field and an artificial atom, made up of a particle trapped in a potential $V(\boldsymbol{r})$, can be obtained by the minimal coupling prescription:

$$\begin{aligned}H_{\text{at}} &= \frac{1}{2m_e}\left(\boldsymbol{p}-e\boldsymbol{A}^{(1,0)}(\boldsymbol{r})\right)^2 + V(\boldsymbol{r}) \\ &= H_{\text{at}}^0 - \frac{e}{m_e}\boldsymbol{p}\cdot\boldsymbol{A}^{(1,0)}(\boldsymbol{r}) + \frac{e^2}{2m_e}\left(\boldsymbol{A}^{(1,0)}(\boldsymbol{r})\right)^2,\end{aligned} \tag{14.63}$$

with $\boldsymbol{r}$ and $\boldsymbol{p}$ the canonically conjugated position and momentum of the artificial "electron". The transverse choice $\boldsymbol{\nabla}\cdot\boldsymbol{A}=0$ for the vector potential makes the ordering with respect to $\boldsymbol{p}$ immaterial. We adopt a two-level approximation for the atom, retaining only the ground state $|g\rangle$ and the first excited state $|e\rangle$, satisfying

$$H^0_{\rm at}\,|g\rangle = 0, \qquad H^0_{\rm at}\,|e\rangle = \hbar\omega_0\,|e\rangle\,. \tag{14.64}$$

Furthermore, we apply long-wavelength approximations to the interaction terms, which enable one to neglect the $O(e^2)$ contribution, whose relevance is suppressed like the ratio of the photon momentum to the particle momentum [44], and to apply a dipolar approximation to the $O(e)$ term. The position operator $\boldsymbol{r}$ is replaced by a non dynamical center-of-mass position $\boldsymbol{r}_0$. The interaction Hamiltonian thus reads

$$\begin{aligned} H^{(dip)}_{\rm int} &= -\frac{e}{m_e}A^{(1,0)}_z(\boldsymbol{r}_0)\Big[\langle g|\,p_z\,|g\rangle\,|g\rangle\,\langle g| + \langle e|\,p_z\,|e\rangle\,|e\rangle\,\langle e| \\ &\quad + \langle g|\,p_z\,|e\rangle\,|g\rangle\,\langle e| + \langle e|\,p_z\,|g\rangle\,|e\rangle\,\langle g|\Big]. \end{aligned} \tag{14.65}$$

The assumption that the expectation value of momentum vanishes in the eigenstates of the free Hamiltonian simplifies the interaction. Moreover, the canonical commutation relation can be used to obtain

$$\begin{aligned} \langle e|\,p_z\,|g\rangle &= \frac{im}{\hbar}\,\langle e|\,[H^0_{\rm at}, z]\,|g\rangle = im\omega_0\,\langle e|\,z\,|g\rangle =: im\omega z_{eg} \\ &= im\omega_0|z_{eg}|e^{i\theta_{eg}}, \end{aligned} \tag{14.66}$$

by which the mass m_e disappears from the theory, and the Hamiltonian takes the form of a coupling between the dipole moment $D_{eg}=e|z_{eg}|$ and the electric field. Finally, we can define new canonically conjugated field operators $b(k) := e^{-i(\theta_{eg}+\pi/2)}a(k)$ and retain only the rotating-wave terms $b(k)\,|e\rangle\,\langle g|$ and $b^\dagger(k)\,|g\rangle\,\langle e|$, to obtain the interaction operator

$$\begin{aligned} H^{(dip,RW)}_{\rm int} &= \omega_0 D_{eg}\left(\frac{\hbar}{2\pi\epsilon v L_y L_z}\right)^{\frac{1}{2}}\int\frac{dk}{(k^2+(vM/\hbar)^2)^{1/4}} \\ &\quad\times\left[b(k)\,|e\rangle\,\langle g|\,e^{ikx_0} + b^\dagger(k)\,|g\rangle\,\langle e|\,e^{-ikx_0}\right]. \end{aligned} \tag{14.67}$$

Notice that $y_0 = L_y/2$ has been used. The dynamics for the atom pair is thus determined by

$$H = H^0_{{\rm at},A} + H^0_{{\rm at},B} + H^{(1,0)} + H^{(dip,RW)}_{{\rm int},A} + H^{(dip,RW)}_{{\rm int},B} \tag{14.68}$$

with atom A in $x_0=0$ and atom B in $x_0=d$.

14.9 Energy density

The study in the main text has been focused on the $\mathcal{N}=1$ sector, spanned by the wavefunctions

$$\begin{aligned} |\psi_1\rangle &= c_A\,|e_A, g_B; vac\rangle + c_B\,|g_A, e_B; vac\rangle \\ &\quad + \int dk F(k)\,|g_A, g_B; k\rangle\,. \end{aligned} \tag{14.69}$$

Using the scalar Hamiltonian density defined in Section 14.7, one can compute the energy density

$$\begin{aligned} \langle\psi_1|\,\mathcal{H}(x)\,|\psi_1\rangle &= \frac{1}{2}\Big[\langle\psi_1| : (\Pi(x))^2 : |\psi_1\rangle \\ &\qquad + v^2\,\langle\psi_1| : (\partial_x\alpha(x))^2 : |\psi_1\rangle \\ &\qquad + v^4\left(\frac{M}{\hbar}\right)^2\langle\psi_1| : (\partial_x\alpha(x))^2 : |\psi_1\rangle\Big] \\ &= \left|\int dk\sqrt{\frac{\hbar\omega_{1,0}(k)}{2(2\pi)}}F(k)e^{ikx}\right|^2 \\ &\quad + \left|\int dk\frac{\hbar v k}{\sqrt{2(2\pi)\hbar\omega_{1,0}(k)}}F(k)e^{ikx}\right|^2 \\ &\quad + \left|\int dk\frac{v^2 M}{\sqrt{2(2\pi)\hbar\omega_{1,0}(k)}}F(k)e^{ikx}\right|^2. \end{aligned} \tag{14.70}$$

This stucture can be simplified if one assumes that the dominant contribution to the integrals comes from the poles of $F(k) \sim A_+(k-k_0)^{-1} + A_-(k+k_0)^{-1}$. Neglecting the corrections yielded by square-root branch-cut integration, one obtains

$$\begin{aligned} \langle\psi_1|\,\mathcal{H}(x)\,|\psi_1\rangle &\simeq \hbar\omega_{1,0}(k_0)\left|\int \frac{dk}{2\pi}F(k)e^{ikx}\right|^2 \\ &=: \hbar\omega_{1,0}(k_0)\left|\tilde{F}(x)\right|^2, \end{aligned} \tag{14.71}$$

which is used to compute the energy density for the resonant states.

Part X
Exact Solutions in wQED: Main Articles

(???? they were not in archive and I am not into this topic yet, so I'll add them later)

Part XI
Other, Non-Typical Theory

15 Scattering of massless particles in one-dimensional chiral channel by Pletyukhov, Gritsev

Abstract

We present a general formalism describing a propagation of an arbitrary multiparticle wave packet in a one-dimensional multimode chiral channel coupled to an ensemble of emitters which are distributed at arbitrary positions. The formalism is based on a direct and exact resummation of diagrammatic series for the multiparticle scattering matrix. It is complimentary to the Bethe Ansatz and to approaches based on equations of motion, and it reveals a simple and transparent structure of scattering states. In particular, we demonstrate how this formalism works on various examples, including scattering of one- and two-photon states off two- and three-level emitters, off an array of emitters as well as scattering of coherent light. We argue that this formalism can be constructively used for study of scattering of an arbitrary initial photonic state off emitters with arbitrary degree of complexity.

15.1 Introduction

Recent advance in fabricating quasi one-dimensional (1D) nanostructures has stimulated and motivated extensive theoretical works on propagating photons in reduced dimensions. One of the goals of this research is to achieve considerable photonic nonlinearities for a single photon pass through the structure which would become a fertile platform for variety of applications in future technology and quantum information [1]. The only way nonlinear effects may show up in the photonic component of scattering is through interaction with ensemble of emitters. This can be achieved by inserting emitters into the 1D channel or by side coupling to evanescent modes of the channel. The scattering probability of an individual quantum particle of wavelength λ in the 1D channel is controlled by the ratio λ^2/A where A is the effective scattering area of the channel. Therefore reducing the effective scattering area makes nonlinear effects feasible in the range of wavelengths close to λ. Several physical realizations of such kind of scattering have been recently suggested: tapered optical fibers with atomic ensemble coupled to the evanescent field (currently tapered region can have optical sub wavelength diameters down to 50 nm) [2]; hollow optical fibers, "stuffed" with cold atoms [3], photonic crystals [4]. Besides conventional atomic ensembles, various artificial emitters and channels can be used as well. Thus, superconducting q-bits coupled to transmission lines have been engineered to demonstrate two- and three-level emitters (see [5] for extensive recent review). Moreover, photons can be replaced by surface plasmons coupled to quantum dots [6].

Having in mind these and other physical realizations we consider the model Hamiltonian which describes interaction of a massless multimode quantized bosonic field propagating unidirectionally in 1D geometry with an array of emitters. The coupling between bosons and emitters has the standard dipole-like form. The emitters are assumed to have a multilevel structure (in particular, in this paper we focus on two- and three-level structures, although our formalism allows for a straightforward generalization to more complicated cases as well). We do not impose any specific details on the spatial distribution of emitters in the 1D channel. However, we distinguish between the case of Dicke arrangement (when all emitters are placed in a space region of the size smaller than a typical wavelength) and the case of remotely distributed emitters. The problem we focus on is of the scattering type: an initial state consists of a direct product of the photonic state and the ground state of an atomic ensemble. Typically, this state is an eigenstate of the free (noninteracting) Hamiltonian. An interaction between light and matter is assumed to be switched on adiabatically in the infinite past and switched off adiabatically in the infinite future. The adiabaticity parameter controls the so-called on-shell condition which plays an important role in the scattering matrix approach (more precisely, the adiabaticity parameter defines an uncertainty in the energy conservation condition). The outgoing state is obtained from the incoming state by an application of a multiparticle scattering matrix. The main goal is to evaluate the scattering matrix, and this is the primary goal of our paper.

We provide a generic solution of the problem (see Eq. (15.3) below) under the assumptions specified above. It can be further extended to the case of multiple emitters. The coupling constant, detuning, and the level structure may vary from emitter to emitter. Arbitrary initial condition can also be studied, however we specifically focus here on the Fock and coherent states. We found that the multiparticle scattering matrix generically contains many-body bound states in the photonic sector, while in the atomic sector it has a projector-like structure. The result of the scattering consists in preparing the ensemble of scatterers in a specific linear combination of levels, which is nothing else but the dark state, i.e. the state which does not emit.

Previous studies in eighties [7],[8],[9], nineties [10], and 00's [11],[12],[13],[14],[15],[16] have already clarified a number of theoretical questions related to propagating of photons in 1D geometry. Many of these studies have been based on the property of integrability. Our analysis here extends these studies in various directions: we consider arrays of emitters with multilevel structures and arbitrary coupling constants, and treat the problem in full generality using the methodology of the scattering formalism. Our approach does not require any apriori knowledge about system's integrability. Nevertheless, our results agree with those obtained by integrability methods, whenever the latter are available.

In the next section we first present our general result with outline of its derivation. In the following sections we demonstrate its application on specific examples of light scattering off two- and three- level systems. We consider separately the scattering of Fock states with a well-defined number of photons N and the scattering of coherent light. The latter study serves the two purposes: first, the scattering matrix in the coherent state basis describes a scattering problem of coherent light itself, and, second, it can be considered as a generating functional for scattering problems in sectors with a well-defined number of photons.

15.2 General solution

15.2.1 Main result

We consider the following Hamiltonian

$$H = \int d\nu\, \nu\, a^\dagger(\nu)a(\nu) + \sum_i \epsilon_i P_i + \sum_{j=1}^{M} \int d\nu g_j \{a^\dagger(\nu) S_j^- + a(\nu) S_j^+\} \equiv H_0 + a_{\alpha\nu} S_{\bar\alpha}, \tag{15.1}$$

where the spectrum of photons is chiral, that is it contains a single branch $\omega = +\nu$ corresponding to a unidirectional propagation of right-moving photons created by $a^\dagger(\nu)$. Diagonal P_i and off-diagonal $S_j^+ = (S_j^-)^\dagger$ operators act in the Hilbert space of the atomic system, and we use the notations $a^\dagger = a_+$, $a = a_-$, $\alpha = \pm$, $\bar\alpha = -\alpha$. Here M is the number of atoms (emitters) which are localized in a small spatial region close to $x = 0$. The precise form of operators S^a is determined by the level structure of an emitter. Thus, for the two-level system in the rotating wave approximation (RWA) they read $S_j^a = \frac{\sigma_j^a}{2}$, where σ^a are the Pauli matrices. In case of three-level emitters the form of operators S^a depends on a specific type of levels' structure, being either of Λ, V, or Σ-type, which will be introduced below. Moreover, eventual counterrotating terms may be also included in these generic notations (in particular, for the two-level system beyond the RWA we would then have $S^+ = S^- = \sigma^x/2$).

The main assumptions we make by writing up the Hamiltonian (15.1) are the following: 1) a linear, unidirectional nature of the photon's spectrum and an absence of its lower and upper bounds; 2) the interaction is linear in a_α; 3) a coupling constant (absorbed in $S_{\bar\alpha}$) is independent of momentum (energy) ν.

Generically, the scattering matrix is defined as a limit $t \to -\infty$, $t' \to +\infty$ of the unitary evolution exponent $U(t,t') = \mathcal{T}\exp\left(-i\int_t^{t'} H(\tau)d\tau\right)$ and contains different scattering channels. The nontrivial part of scattering is contained in the so-called T-matrix, which is related to the scattering matrix S via the expression

$$S = \hat 1 - 2\pi i \delta(E_{in} - E_{out}) T(E_{in}), \tag{15.2}$$

E_{in} and E_{out} being the energies of incoming and outgoing states.

Under the assumptions we stated above we show that the T-matrix in the N-particle sector equals

$$T^{(N)}(\omega) = G_0^{-1} G(\hat a_{\alpha_1\nu_1} S_{\bar\alpha_1}) G \dots G(\hat a_{\alpha_{2N}\nu_{2N}} S_{\bar\alpha_{2N}}) G G_0^{-1}, \tag{15.3}$$

where the summation over the set of $\alpha_i = \pm$ and integration over the set of ν_i is implicitly assumed. The hats over the operators a mean that they can only be contracted with *external* operators (that is, operators creating incoming and outgoing states). The operators $\hat a$ are effectively normal-ordered in (15.3), but it is still necessary to account for their commutation relations with $a^\dagger a$ appearing in the bare $G_0^{-1} = \omega - H_0$ and dressed G^{-1} Green's functions. In turn, the latter amounts to

$$G^{-1}(\omega) = G_0^{-1}(\omega) - \Sigma = \omega - H_0 + i\pi S_+ S_-. \tag{15.4}$$

We state that if the *self-energy* $\Sigma = -i\pi S_+ S_-$ does not have a zero eigenvalue, then $T(\omega)$ identically vanishes when being put on shell ($\omega = E_{in} = E_{out}$): since both E_{in} and E_{out} are the eigenstates of H_0, then $G_0^{-1}|_{\rm os} = 0$, while $G|_{\rm os}$ has finite eigenvalues in all atomic states. To better clarify this important statement we note that the combination $G_0^{-1}G$ is nothing else, but the projector onto the atomic states with zero broadening (dark states). Therefore the first task is to evaluate this building block of (15.3).

We also note that from the diagrammatic point of view, the class of models we study here does not allow for diagrams with intersection and overlapping of photonic lines, what follows from the spectrum linearity and the causality imposed by the absence of backscattering for propagating chiral modes. It is naturally possible to extend a diagrammatic approach beyond this class, but then the non-crossing approximation no longer provides an exact solution, and one should expect effects associated with vertex corrections to the vertices V.

15.2.2 Derivation of the main result

Below we derive our main expression (15.3). First we remind several basic facts about the scattering matrix approach illustrating them on a simple example of scattering off the two-level system. After that, we outline the main steps of our derivation.

Scattering problem

The main goal of the scattering theory is to calculate the scattering matrix

$$S = \mathcal{T} \exp\left[-i \int_{-\infty}^{+\infty} V(t) dt\right], \tag{15.5}$$

where the interaction term $V(t)$ is evaluated in the interaction picture. The matrix elements of the scattering matrix $S_{n'n} = \langle n'|S|n\rangle$ are defined in the states of the non-interacting Hamiltonian, which in our case have the following form

$$|n\rangle = a^\dagger_{k_1} \dots a^\dagger_{k_n} |0\rangle_b |\sigma\rangle, \quad \varepsilon_n = \sum_{i=1}^{n} k_i + \sigma \frac{\Omega}{2}, \tag{15.6}$$

$$|n'\rangle = a^\dagger_{p_1} \dots a^\dagger_{p_{n'}} |0\rangle_b |\sigma'\rangle, \quad \varepsilon_{n'} = \sum_{i=1}^{n'} p_i + \sigma' \frac{\Omega}{2}, \tag{15.7}$$

where $|0\rangle_b$ is the photon vacuum state, and $\sigma = \pm$ labels the states of the two-level system, and Ω is the level splitting.

By definition the T-matrix is

$$T(\omega) = V + V\hat{G}(\omega)V, \tag{15.8}$$

where the full Green's function is defined as $\hat{G}(\omega) = (\omega - H + i\eta)^{-1}$. The parameter η controls the adiabaticity of switching the interaction on and off in the far past and far future, respectively. The matrix elements of the S-matrix (15.5) and the T-matrix (15.8) are related to each other by the the following equation, $\langle n'|S|n\rangle = \langle n'|n\rangle - 2\pi i \delta(\varepsilon_n - \varepsilon_{n'}) \langle n'|T(\varepsilon_n)|n\rangle$. Therefore, it is sufficient to calculate the matrix elements of the on-shell T-matrix (that is, at $\omega = \varepsilon_n$).

Calculation of the T-matrix

We expand $\hat{G}$ in (15.8) in a series of the interaction V

$$\hat{G}(\omega) = G_0(\omega) + G_0(\omega) V G_0(\omega) + G_0(\omega) V G_0(\omega) V G_0(\omega) + \dots, \tag{15.9}$$

where

$$G_0(\omega) = \frac{1}{\omega - H_0 + i\eta} = \frac{P_+}{\omega - \frac{\Omega}{2} - H_b + i\eta} + \frac{P_-}{\omega + \frac{\Omega}{2} - H_b + i\eta}. \tag{15.10}$$

is the bare Green's function. The projectors $P_\pm = \sigma_\pm \sigma_\mp = \frac{1}{2}(1 \pm \sigma_z)$ map onto the spin states $|\pm\rangle$, respectively. We note that $P_\pm \sigma_\mp = \sigma_\pm P_\pm = 0$, and $P_\pm \sigma_\pm = \sigma_\pm P_\mp$, and therefore $T = V + VG_0V + VG_0VG_0V + \dots$. As V is linear in bosonic operators, we can omit odd powers of V in this expansion: they do not conserve the number of photons and will vanish in the calculation of matrix elements. Then $T = W + WG_0W + \dots$, where $W = VG_0V$.

Using the properties of $P_\pm$, one can show that only diagonal elements $T_{\pm\pm} = \langle \pm|T|\pm\rangle$ in spin space are nonzero

$$T_{++}(\omega) = g^2 a_{\nu_1'} \frac{1}{\omega + \frac{\Omega}{2} - H_b + i\eta} a^\dagger_{\nu_1} \tag{15.11}$$
$$+ g^4 \left(a_{\nu_1'} \frac{1}{\omega + \frac{\Omega}{2} - H_b + i\eta} a^\dagger_{\nu_1} \right) \frac{1}{\omega - \frac{\Omega}{2} - H_b + i\eta} \left(a_{\nu_2'} \frac{1}{\omega + \frac{\Omega}{2} - H_b + i\eta} a^\dagger_{\nu_2} \right) + \dots,$$

$$T_{--}(\omega) = g^2 a^\dagger_{\nu_1} \frac{1}{\omega - \frac{\Omega}{2} - H_b + i\eta} a_{\nu_1'} \tag{15.12}$$
$$+ g^4 \left(a^\dagger_{\nu_1} \frac{1}{\omega - \frac{\Omega}{2} - H_b + i\eta} a_{\nu_1'} \right) \frac{1}{\omega + \frac{\Omega}{2} - H_b + i\eta} \left(a^\dagger_{\nu_2} \frac{1}{\omega - \frac{\Omega}{2} - H_b + i\eta} a_{\nu_2'} \right) + \dots.$$

Here the integration over the frequencies $\{\nu_i, \nu_i'\}$ is implicitly assumed.

Let us put T_{++} and T_{--} partially on-shell introducing $\omega = \omega_b + \frac{\Omega}{2}$ in (15.11), and $\omega = \omega_b - \frac{\Omega}{2}$ in (15.12), where ω_b is the energy of photons, $\omega_b = \sum_i k_i = \sum_i p_i$. Then, we can rewrite

$$\begin{aligned} T_{++}(\omega_b) &= g^2 a_{\nu_1'} \frac{1}{\omega_b + \Omega - H_b + i\eta} a^\dagger_{\nu_1} \qquad (15.13)\\ &+ g^4 \left(a_{\nu_1'} \frac{1}{\omega_b + \Omega - H_b + i\eta} a^\dagger_{\nu_1} \right) \frac{1}{\omega_b - H_b + i\eta} \left(a_{\nu_2'} \frac{1}{\omega_b + \Omega - H_b + i\eta} a^\dagger_{\nu_2} \right) + \dots, \\ T_{--}(\omega_b) &= g^2 a^\dagger_{\nu_1} \frac{1}{\omega_b - \Omega - H_b + i\eta} a_{\nu_1'} \qquad (15.14)\\ &+ g^4 \left(a^\dagger_{\nu_1} \frac{1}{\omega_b - \Omega - H_b + i\eta} a_{\nu_1'} \right) \frac{1}{\omega_b - H_b + i\eta} \left(a^\dagger_{\nu_2} \frac{1}{\omega_b - \Omega - H_b + i\eta} a_{\nu_2'} \right) + \dots . \end{aligned}$$

As we are interested in evaluation of average values in the bosonic eigenstates $\langle a_{p_n} \dots a_{p_1} T_{\pm\pm} a^\dagger_{k_1} \dots a^\dagger_{k_n} \rangle$, it is natural to exploit the Wick's theorem, implying $\langle a_{\nu'} a^\dagger_\nu \rangle = \delta(\nu - \nu')$ and $\langle a^\dagger_\nu a_{\nu'} \rangle = 0$. We also note the following intertwining properties of bosonic operators

$$a^\dagger_\nu \frac{1}{\omega - H_b - \nu} = \frac{1}{\omega - H_b} a^\dagger_\nu, \quad a_{\nu'} \frac{1}{\omega - H_b + \nu'} = \frac{1}{\omega - H_b} a_{\nu'}. \qquad (15.15)$$

An application of the Wick's theorem implies that we have to contract pairwise the operators $a_{\nu'}$ and $a^\dagger_\nu$. In order to do that, it necessary to move $a_{\nu'}$ to the right, commuting it by means of (15.15) with all propagators appearing in between its initial position and the position of $a^\dagger_\nu$. There are only the two possibilities for such a contraction: 1) a_ν is contracted with an *adjacent* operator $a^\dagger_{\nu'}$ standing to the right from it; 2) a_ν is contracted with some *external* operator $a^\dagger_{k_i}$. In the diagrammatic representation this means that only diagrams with non-crossing lines of contraction are allowed.

The reason for this restriction is the following. If $a_{\nu'}$ is reshuffled with more than one propagator, and after that it is contracted to some *internal* operator, we obtain an integral over ν' with more than one pole lying in the same half-plane. Such an integral identically vanishes. The operator $a_{\nu'}$ can then be loosely reshuffled to the right end, which provides the second possibility. A contraction of the two adjacent operators yields

$$\langle a_{\nu'} \frac{1}{\omega - H_b + i\eta} a^\dagger_\nu \rangle = \langle \int d\nu d\nu' \frac{\delta(\nu - \nu')}{\omega - H_b - \nu' + i\eta} \rangle = -i\pi. \qquad (15.16)$$

This generates the self-energy insertion Σ.

Let us denote by $a_{\mu'}$ and $a^\dagger_\mu$ the operators which are contracted to the *external* operators. In the N-photon sector we have the number N of both species, moreover for the two-level system they alternate (due to $\sigma_+^2 = \sigma_-^2 = 0$), that is after $a_{\mu'}$ we must have $a^\dagger_\mu$, not $a_{\mu''}$. All self-energy insertions between such pairs can be resummed, and we obtain for T_{++} and T_{--} the following result in the N-particle sector

$$\begin{aligned} T^{(N)}_{++}(\omega_b) &= g^{2N} (\omega_b - H_b + i\eta) \frac{1}{\omega_b - H_b + i\pi g^2} \left(a_{\mu_1'} \frac{1}{\omega_b + \Omega - H_b + i\eta} a^\dagger_{\mu_1} \right) \\ &\times \frac{1}{\omega_b - H_b + i\pi g^2} \cdots \frac{1}{\omega_b - H_b + i\pi g^2} \\ &\times \left(a_{\mu_N'} \frac{1}{\omega_b + \Omega - H_b + i\eta} a^\dagger_{\mu_N} \right) \frac{1}{\omega_b - H_b + i\pi g^2} (\omega_b - H_b + i\eta), \qquad (15.17) \end{aligned}$$

$$\begin{aligned} T^{(N)}_{--}(\omega_b) &= g^{2N} a^\dagger_{\mu_1} \frac{1}{\omega_b - \Omega - H_b + i\pi g^2} \left(a_{\mu_1'} \frac{1}{\omega_b - H_b + i\eta} a^\dagger_{\mu_2} \right) \\ &\times \frac{1}{\omega_b - \Omega - H_b + i\pi g^2} \cdots \frac{1}{\omega_b - \Omega - H_b + i\pi g^2} \\ &\times \left(a_{\mu_{N-1}'} \frac{1}{\omega_b - H_b + i\eta} a^\dagger_{\mu_N} \right) \frac{1}{\omega_b - \Omega - H_b + i\pi g^2} a_{\mu_N'}. \qquad (15.18) \end{aligned}$$

In these relations operators a and $a^\dagger$ effectively commute with each other, and one has only to take carefully into account permutations of $a(a^\dagger)$ with the propagators using (15.15). Note that $T_{++}(\omega_b)$ vanishes, when it is put on-shell, because of the factors $(\omega_b - H_b + i\eta)$ in the beginning and in the end of the corresponding expression.

Let us now consider $T^{(N)}_{--}(\omega_b)$. Moving all propagators to the left and putting them on-shell, we obtain

$$\begin{aligned} T^{(N)}_{--} &= g^{2N} \frac{1}{\mu_1 - \alpha} \frac{1}{\Delta_{11'} + i\eta} \frac{1}{\Delta_{11'} + \mu_2 - \alpha} \cdots \frac{1}{\sum_{i=1}^{N-2} \Delta_{ii'} + \mu_{N-1} - \alpha} \\ &\times \frac{1}{\sum_{i=1}^{N-1} \Delta_{ii'} + i\eta} \frac{1}{\sum_{i=1}^{N-1} \Delta_{ii'} + \mu_N - \alpha} a^\dagger_{\mu_1} \dots a^\dagger_{\mu_N} a_{\mu_N'} \dots a_{\mu_1'}, \qquad (15.19) \end{aligned}$$

where $\Delta_{ii'} = \mu_i - \mu_{i'}$ and $\alpha = \Omega - i\pi g^2$.

A direct generalization of this derivation to cases with a more complicated level structure leads to our main equation (15.3).

15.3 Examples

Here we consider several important examples and compute the scattering matrix for the cases of a single emitter coupled to a 1D waveguide within and beyond the RWA. We focus on the two-level and three-level cases.

15.3.1 One emitter in the RWA

For pedagogical reasons, we repeat here the derivation of (15.19) from the general expression (15.3).

In the case of a single atom interacting with a 1D field in the RWA we define $\epsilon_\pm = \pm\frac{\Omega}{2}$, $P_\pm = \sigma_\pm\sigma_\mp$, and $S_\pm = g\sigma_\pm = g\frac{\sigma_x \pm i\sigma_y}{2}$. We find then $\Sigma = -i\pi S_+S_- = -i\pi g^2 P_+$ and $G(\omega) = P_+(\omega - \frac{\Omega}{2} - H_b + i\pi g^2)^{-1} + P_-(\omega + \frac{\Omega}{2} - H_b + i\eta)^{-1} = P_+G_+ + P_-G_-$. Therefore, the main building blocks of the equation for the T-matrix are given by

$$G_0^{-1}G = (\omega - \frac{\Omega}{2} - H_b + i\eta)\frac{P_+}{\omega - \frac{\Omega}{2} - H_b + i\pi g^2} + P_-, \tag{15.20}$$

$$GG_0^{-1} = \frac{P_+}{\omega - \frac{\Omega}{2} - H_b + i\pi g^2}(\omega - \frac{\Omega}{2} - H_b + i\eta) + P_-. \tag{15.21}$$

Putting them on-shell we find

$$G_0^{-1}G|_{\rm os} = GG_0^{-1}|_{\rm os} = P_-, \tag{15.22}$$

and therefore

$$\begin{aligned} T(\omega) &= g^{2N}P_-(\hat{a}_{+,\nu_1}\sigma_-)P_+G_+(\hat{a}_{-,\nu_2}\sigma_+)P_-G_-\ldots P_-G_-(\hat{a}_{+,\nu_{2N-1}}\sigma_-)P_+G_+(\hat{a}_{-,\nu_{2N}}\sigma_+)P_- \\ &= P_-g^{2N}\hat{a}^\dagger_{\nu_1}G_+\hat{a}_{\nu_2}G_-\ldots G_-\hat{a}^\dagger_{\nu_{2N-1}}G_+\hat{a}_{\nu_{2N}}. \end{aligned} \tag{15.23}$$

Introducing $\omega = \omega_b - \frac{\Omega}{2}$, we can rewrite $G_\pm$ as $G_+ = (\omega_b - H_b - \Omega + i\pi g^2)^{-1}$ and $G_- = (\omega - H_b + i\eta)^{-1}$.

15.3.2 M emitters in the RWA (Dicke case)

In the case of many emitters confined in a small (compared to the typical wavelength) region of space we have $\epsilon_m = m\Omega$, $P_m = |m\rangle\langle m|$, while $S_\pm \to gS_\pm$. The total effective spin is conserved, $S_aS_a = l(l+1)$. If the system is initially in the ground state, that is $S_z = -M/2$, then it is sufficient to consider the representation with the largest weight $l = M/2$, to which the ground state belongs. In this case we find

$$\Sigma = -i\pi g^2 S_+S_- = -i\pi g^2(S_a^2 - S_z^2 + S_z) = -i\pi g^2\sum_{m=-l}^{l} P_m[l(l+1) - m(m-1)], \tag{15.24}$$

and therefore for the dressed Green's function we find

$$G(\omega) = \sum_{m=-l}^{l}\frac{P_m}{\omega - H_b - m\Omega + i\pi g^2(l+m)(l-m+1)}. \tag{15.25}$$

The main building block is therefore equal to

$$G_0^{-1}G|_{\rm os} = GG_0^{-1}|_{\rm os} = P_{-l} = |-l\rangle\langle -l|. \tag{15.26}$$

In the one-photon sector we immediately get

$$\begin{aligned} T^{(1)}(\omega) &= g^2P_{-l}(a^\dagger_{\nu_1}S_-)P_{-l+1}G_{-l+1}(a_{\nu_2}S_+)P_{-l} \\ &= g^2P_{-l}|\langle -l|S_-|-l+1\rangle|^2a^\dagger_{\nu_1}\frac{1}{\omega - H_b + (l-1)\Omega + i2\pi g^2 l}a_{\nu_2}. \end{aligned} \tag{15.27}$$

Using the action of the collective spin operators on the states of emitters

$$S_\pm|m\rangle = \sqrt{(l\mp m)(l\pm m+1)}|m\pm 1\rangle, \tag{15.28}$$

we obtain that $|\langle -l|S_-|-l+1\rangle|^2 = 2l$. Introducing $\omega = \omega_b - \Omega l = \omega_b - \Omega M/2$ as well as $\alpha_M = \Omega - i\pi g^2 M$, and omitting P_{-l}, we obtain $T^{(1)}(\omega_b) = g^2 M a^\dagger_{\nu_1}(\omega_b - H_b - \alpha_M)^{-1} a_{\nu_2}$. Putting this expression on-shell results in

$$T^{(1)} = g^2 M \frac{1}{\nu_1 - \alpha_M} a^\dagger_{\nu_1} a_{\nu_2}. \tag{15.29}$$

In the two-photon sector

$$\begin{aligned} T^{(2)}(\omega) &= g^4 P_{-l}(a^\dagger_{\nu_1} S_-) P_{-l+1} G_{-l+1}(a_{\alpha_2\nu_2} S_{\bar\alpha_2}) P_{m_2} G_{m_2}(a_{\alpha_3\nu_3} S_{\bar\alpha_3}) P_{-l+1} G_{-l+1}(a_{\nu_4} S_+) P_{-l} \\ &= g^4 P_{-l} |\langle -l|S_-|-l+1\rangle|^2 \langle -l+1|S_{\bar\alpha_2}|m_2\rangle\langle m_2|S_{\bar\alpha_3}|-l+1\rangle \\ &\times a^\dagger_{\nu_1} \frac{1}{\omega - H_b + (l-1)\Omega + i2\pi g^2 l} a_{\alpha_2\nu_2} \frac{1}{\omega - H_b - m_2\Omega + i\pi g^2 (l+m_2)(l-m_2+1)} \\ &\times a_{\alpha_3\nu_3} \frac{1}{\omega - H_b + (l-1)\Omega + i2\pi g^2 l} a_{\nu_4}. \end{aligned} \tag{15.30}$$

Using (15.28) we obtain

$$\begin{aligned} & |\langle -l|S_-|-l+1\rangle|^2 \langle -l+1|S_{\bar\alpha_2}|m_2\rangle\langle m_2|S_{\bar\alpha_3}|-l+1\rangle \\ = \; & (2l)(\delta_{\alpha_2-}\delta_{m_2,-l}\sqrt{2l} + \delta_{\alpha_2+}\delta_{m_2,-l+2}\sqrt{2(2l-1)})(\delta_{\alpha_3+}\delta_{m_2,-l}\sqrt{2l} + \delta_{\alpha_3-}\delta_{m_2,-l+2}\sqrt{2(2l-1)}) \\ = \; & 2l[2l\delta_{\alpha_2-}\delta_{\alpha_3+}\delta_{m_2,-l} + 2(2l-1)\delta_{\alpha_2+}\delta_{\alpha_3-}\delta_{m_2,-l+2}] \end{aligned} \tag{15.31}$$

and

$$\begin{aligned} T^{(2)}(\omega) &= P_{-l} g^4 4l^2 a^\dagger_{\nu_1} \frac{1}{\omega - H_b + (l-1)\Omega + i2\pi g^2 l} a_{\nu_2} \frac{1}{\omega - H_b + l\Omega + i\eta} \\ &\times a^\dagger_{\nu_3} \frac{1}{\omega - H_b + (l-1)\Omega + i2\pi g^2 l} a_{\nu_4} \\ &+ P_{-l} g^4 4l(2l-1) a^\dagger_{\nu_1} \frac{1}{\omega - H_b + (l-1)\Omega + i2\pi g^2 l} a^\dagger_{\nu_2} \frac{1}{\omega - H_b + (l-2)\Omega + i\pi g^2 2(2l-1)} \\ &\times a_{\nu_3} \frac{1}{\omega - H_b + (l-1)\Omega + i2\pi g^2 l} a_{\nu_4}. \end{aligned} \tag{15.32}$$

Introducing $\alpha_{M-1} = \Omega - i\pi g^2 (M-1)$ and omitting P_{-l}, we arrive at

$$\begin{aligned} T^{(2)}(\omega_b) &= g^4 M^2 a^\dagger_{\nu_1} \frac{1}{\omega_b - H_b - \alpha_M} a_{\nu_2} \frac{1}{\omega_b - H_b + i\eta} a^\dagger_{\nu_3} \frac{1}{\omega_b - H_b - \alpha_M} a_{\nu_4} \\ &+ g^4 M(M-1) a^\dagger_{\nu_1} \frac{1}{\omega_b - H_b - \alpha_M} a^\dagger_{\nu_2} \frac{1}{\frac{1}{2}(\omega_b - H_b) - \alpha_{M-1}} a_{\nu_3} \frac{1}{\omega_b - H_b - \alpha_M} a_{\nu_4}. \end{aligned} \tag{15.33}$$

Putting $T^{(2)}$ on-shell, we obtain (note relabeling $\nu_2 \leftrightarrow \nu_3$ in the first term which is allowed because of the symmetric nature of the photonic wavefunction)

$$T^{(2)} = g^4 M \frac{1}{\nu_1 - \alpha_M} \frac{1}{\nu_1 + \nu_2 - \nu_3 - \alpha_M} \left[\frac{M}{\nu_1 - \nu_3 + i\eta} + \frac{M-1}{\frac{1}{2}(\nu_1+\nu_2) - \alpha_{M-1}} \right] a^\dagger_{\nu_1} a^\dagger_{\nu_2} a_{\nu_3} a_{\nu_4}. \tag{15.34}$$

In the one-photon sector we have

$$t_{p_1 k_1} = \delta_{p_1 k_1} \langle a_{p_1} T^{(1)} a^\dagger_{k_1}\rangle = \delta_{p_1 k_1} \frac{Mg^2}{\nu_1 - \alpha_M} \langle a_{p_1} a^\dagger_{\nu_1} a_{\nu_2} a^\dagger_{k_1}\rangle = \delta_{p_1 k_1} \frac{Mg^2}{p_1 - \alpha_M}, \tag{15.35}$$

and therefore the scattering matrix is

$$S_{p_1 k_1} = \delta_{p_1 k_1} - 2\pi i t_{p_1 k_1} = \delta_{p_1 k_1} \left(1 - 2\frac{i\pi M g^2}{p_1 - \alpha_M}\right). \tag{15.36}$$

Let us consider the scattering matrix in the two-photon sector. First, we consider

$$\delta_{p_1+p_2,k_1+k_2} \langle a_{p_2} a_{p_1} T^{(1)} a^\dagger_{k_1} a^\dagger_{k_2}\rangle = \delta_{p_2 k_2} t_{p_1 k_1} + \delta_{p_1 k_1} t_{p_2 k_2} + \delta_{p_2 k_1} t_{p_1 k_2} + \delta_{p_1 k_2} t_{p_2 k_1}. \tag{15.37}$$

Second,

$$\delta_{p_1+p_2,k_1+k_2}\langle a_{p_2}a_{p_1}T^{(2)}a^\dagger_{k_1}a^\dagger_{k_2}\rangle = \delta_{p_1+p_2,k_1+k_2}g^4M\frac{1}{\nu_1-\alpha_M}\frac{1}{\nu_4-\alpha_M}$$
$$\times\left[\frac{M}{\nu_1-\nu_3}-iM\pi\delta_{\nu_1\nu_3}+\frac{M-1}{\frac{1}{2}(\nu_1+\nu_2)-\alpha_{M-1}}\right]$$
$$\times(\delta_{p_1\nu_1}\delta_{p_2\nu_2}+\delta_{p_1\nu_2}\delta_{p_2\nu_1})(\delta_{k_1\nu_4}\delta_{k_2\nu_3}+\delta_{k_1\nu_3}\delta_{k_2\nu_4}), \tag{15.38}$$

and therefore

$$S_{p_1p_2,k_1k_2} = S_{p_1k_1}S_{p_2k_2}+S_{p_2k_1}S_{p_1k_2}+i\mathcal{T}^{(2)}_{p_1p_2,k_1k_2}, \tag{15.39}$$

where

$$\begin{aligned}\mathcal{T}^{(2)}_{p_1p_2,k_1k_2} &= -2\pi\delta_{p_1+p_2,k_1+k_2}g^4M\\ &\times\frac{1}{\nu_1-\alpha_M}\frac{1}{\nu_4-\alpha_M}\left[\frac{M}{\nu_1-\nu_3}+\frac{M-1}{\frac{1}{2}(\nu_1+\nu_2)-\alpha_{M-1}}\right]\\ &\times(\delta_{p_1\nu_1}\delta_{p_2\nu_2}+\delta_{p_1\nu_2}\delta_{p_2\nu_1})(\delta_{k_1\nu_4}\delta_{k_2\nu_3}+\delta_{k_1\nu_3}\delta_{k_2\nu_4}).\end{aligned} \tag{15.40}$$

Defining $E=p_1+p_2=k_1+k_2$, $\Delta=\frac{1}{2}(k_1-k_2)$, and $\Delta'=\frac{1}{2}(p_1-p_2)$ we find that $k_{1,2}=\frac{E}{2}\pm\Delta$, $p_{1,2}=\frac{E}{2}\pm\Delta'$. Therefore the T-matrix is

$$\begin{aligned}\mathcal{T}^{(2)}_{p_1p_2,k_1k_2} &= \frac{8\pi\delta_{p_1+p_2,k_1+k_2}g^4M(\frac{E}{2}-\alpha_M)}{[(\frac{E}{2}-\alpha_M)^2-\Delta^2][(\frac{E}{2}-\alpha_M)^2-\Delta'^2]}\left\{M-(M-1)\frac{\frac{E}{2}-\alpha_M}{\frac{E}{2}-\alpha_{M-1}}\right\}\\ &= \frac{8\pi\delta_{p_1+p_2,k_1+k_2}g^4M(\frac{E}{2}-\alpha_M)}{[(\frac{E}{2}-\alpha_M)^2-\Delta^2][(\frac{E}{2}-\alpha_M)^2-\Delta'^2]}\frac{\frac{E}{2}}{\frac{E}{2}-\alpha_{M-1}},\end{aligned} \tag{15.41}$$

which is in agreement with the result of Ref. [16]. The emergence of the poles in (15.41) involving more than one individual photon's energy reflects a formation of the photonic bound state.

15.3.3 One emitter beyond the RWA

For the case of an emitter interacting with the field beyond the RWA we have $S_+=g\sigma_++g'\sigma_-$ and $S_-=g\sigma_-+g'\sigma_+$. Calculating the self-energy we find $\Sigma=-i\pi S_+S_-=-i\pi g^2P_+-i\pi(g')^2P_-$, and therefore $G_0^{-1}G|_{\rm os}=GG_0^{-1}|_{\rm os}=0$. This implies that the T-matrix identically vanishes.

Thus, we observe that the non-RWA model is not analytically connected to the RWA one. The nonanalyticity is hidden in the noncommutativity of the limits $\eta\to0$ (which should be taken first for the non-RWA model) and $g'\to0$: the corresponding eigenvalue $\eta/(\pi(g')^2+\eta)$ of the projector onto the emitter's groundstate is sensitive to the order of these limits, and a smooth crossover between the non-RWA and the RWA models would be only possible for the finite value of η.

15.3.4 Three-level system, Λ-scheme

For the three-level scheme of Λ-type (see Fig. 15.1) we have $S_+=g_{31}|3\rangle\langle1|+g_{32}|3\rangle\langle2|$, and $S_-=g_{31}|1\rangle\langle3|+g_{32}|2\rangle\langle3|$. The self-energy is $\Sigma=-i\pi(g_{31}^2+g_{32}^2)P_3\equiv-i\pi g^2P_3$, hence the dressed Green's function acquires the following form

$$G=\frac{P_1}{\omega-\epsilon_1-H_b+i\eta}+\frac{P_2}{\omega-\epsilon_2-H_b+i\eta}+\frac{P_3}{\omega-\epsilon_3-H_b+i\pi g^2}=P_iG_i. \tag{15.42}$$

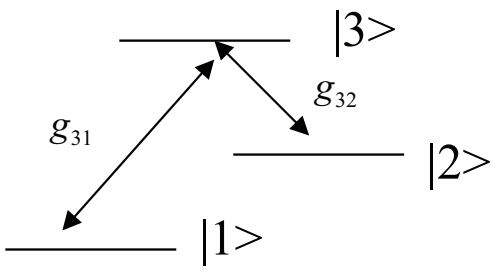

Figure 15.1: Three-level Λ-scheme

Therefore the building block is

$$G_0^{-1}G|_{\rm os} = GG_0^{-1}|_{\rm os} = P_1 + P_2. \tag{15.43}$$

The T-matrix in the single-photon sector is

$$\begin{aligned} T^{(1)}(\omega) &= (P_1+P_2)(\hat{a}^\dagger_{\nu_1}S_-)P_3G_3(\hat{a}_{\nu_2}S_+)(P_1+P_2) \\ &= \left\{g_{31}^2P_1 + g_{32}^2P_2 + g_{31}g_{32}(|2\rangle\langle 1| + |1\rangle\langle 2|)\right\}\hat{a}^\dagger_{\nu_1}\frac{1}{\omega-\epsilon_3-H_b+i\pi g^2}\hat{a}_{\nu_2}, \end{aligned} \tag{15.44}$$

and therefore

$$\begin{aligned} S_{pk} &= \delta_{pk} - 2\pi i g_{31}^2\delta_{pk}\frac{P_1}{p+\epsilon_1-\epsilon_3+i\pi g^2} - 2\pi i g_{32}^2\delta_{pk}\frac{P_2}{p+\epsilon_2-\epsilon_3+i\pi g^2} \\ &\quad -2\pi i g_{31}g_{32}\left[\delta_{k+\epsilon_1,p+\epsilon_2}\frac{|2\rangle\langle 1|}{p+\epsilon_2-\epsilon_3+i\pi g^2} + \delta_{p+\epsilon_1,k+\epsilon_2}\frac{|1\rangle\langle 2|}{p+\epsilon_1-\epsilon_3+i\pi g^2}\right]. \end{aligned} \tag{15.45}$$

In the two-photon sector of scattering we obtain (cf. Ref. [13])

$$\begin{aligned} T^{(2)}(\omega) &= (P_1+P_2)(\hat{a}^\dagger_{\nu_1}S_-)P_3G_3(\hat{a}_{\nu_2}S_+)(P_1G_1+P_2G_2)(\hat{a}^\dagger_{\nu_3}S_-)P_3G_3(\hat{a}_{\nu_4}S_+)(P_1+P_2) \\ &= \left\{g_{31}^2P_1 + g_{32}^2P_2 + g_{31}g_{32}(|2\rangle\langle 1| + |1\rangle\langle 2|)\right\}\hat{a}^\dagger_{\nu_1}G_3\hat{a}_{\nu_2}(g_{31}^2G_1+g_{32}^2G_2)\hat{a}^\dagger_{\nu_3}G_3\hat{a}_{\nu_4}. \end{aligned} \tag{15.46}$$

15.3.5 Three-level system, V-scheme

In the case of three-level V-scheme (see Fig. 15.2) the $S_\pm$ operators are $S_+ = g_{31}|3\rangle\langle 1| + g_{21}|2\rangle\langle 1|$, and $S_- = g_{31}|1\rangle\langle 3| + g_{21}|1\rangle\langle 2|$. The corresponding self-energy is therefore $\Sigma = -i\pi g_{31}^2P_3 - i\pi g_{21}^2P_2 - i\pi g_{21}g_{31}(|2\rangle\langle 3| + |3\rangle\langle 2|)$, while the dressed Green's function is $G = P_1(\omega-\epsilon_1-H_b+i\eta)^{-1} + \sum_{a=2,3}\tilde{P}_a(\omega-H_b-\lambda_a)^{-1}$, where

$$\begin{aligned} \tilde{P}_2 &= \xi_{22}^2P_2 + \xi_{23}^2P_3 + \xi_{22}\xi_{23}|2\rangle\langle 3| + \xi_{23}\xi_{22}|3\rangle\langle 2|, \\ \tilde{P}_3 &= \xi_{33}^2P_3 + \xi_{32}^2P_2 + \xi_{32}\xi_{33}|2\rangle\langle 3| + \xi_{33}\xi_{32}|3\rangle\langle 2|, \\ \xi_{22} &= \xi_{33} = \cos\frac{\phi}{2}, \quad \xi_{23} = -\xi_{32} = \sin\frac{\phi}{2}, \\ \frac{\lambda_2-\lambda_3}{2}\cos\phi &= \frac{\epsilon_2-\epsilon_3}{2} - i\pi\frac{g_{21}^2-g_{31}^2}{2}, \quad \frac{\lambda_2-\lambda_3}{2}\sin\phi = -i\pi g_{21}g_{31}, \\ \frac{\lambda_2+\lambda_3}{2} &= \frac{\epsilon_2+\epsilon_3}{2} - i\pi\frac{g_{21}^2+g_{31}^2}{2}, \quad \lambda_2\lambda_3 = (\epsilon_2-i\pi g_{21}^2)(\epsilon_3-i\pi g_{31}^2) + \pi^2g_{21}^2g_{31}^2, \\ (\lambda-\lambda_2)(\lambda-\lambda_3) &= (\lambda-\epsilon_2+i\pi g_{21}^2)(\lambda-\epsilon_3+i\pi g_{31}^2) + \pi^2g_{21}^2g_{31}^2. \end{aligned} \tag{15.47}$$

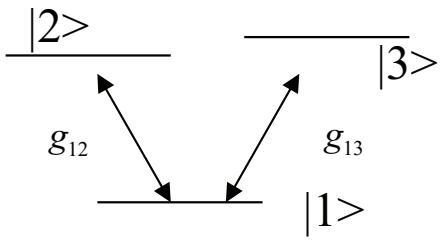

Figure 15.2: Three-level V-scheme

Using these relations we observe that our basic building block $G_0^{-1}G|_{\rm os} = GG_0^{-1}|_{\rm os} = P_1$, and therefore

$$\begin{aligned} T^{(1)}(\omega) &= P_1(\hat{a}^\dagger_{\nu_1}S_-)\tilde{P}_aG_a(\hat{a}_{\nu_2}S_+)P_1 \\ &= P_1\hat{a}^\dagger_{\nu_1}\left[\frac{\frac{1+\cos\phi}{2}g_{21}^2 + \frac{1-\cos\phi}{2}g_{31}^2 + g_{21}g_{31}\sin\phi}{\omega-H_b-\lambda_2}\right. \\ &\quad \left. + \frac{\frac{1-\cos\phi}{2}g_{21}^2 + \frac{1+\cos\phi}{2}g_{31}^2 - g_{21}g_{31}\sin\phi}{\omega-H_b-\lambda_3}\right]\hat{a}_{\nu_2}. \end{aligned} \tag{15.48}$$

Combining the terms in square brackets, we obtain for the single-particle scattering matrix

$$\begin{aligned} S_{pk} &= \delta_{pk}\left[1-2\frac{i\pi g_{21}^2(p+\epsilon_1-\epsilon_3)+i\pi g_{31}^2(p+\epsilon_1-\epsilon_2)}{(p+\epsilon_1-\epsilon_2+i\pi g_{21}^2)(p+\epsilon_1-\epsilon_3+i\pi g_{31}^2)+\pi^2 g_{21}^2 g_{31}^2}\right] \\ &= \delta_{pk}\frac{(p+\epsilon_1-\epsilon_2-i\pi g_{21}^2)(p+\epsilon_1-\epsilon_3-i\pi g_{31}^2)+\pi^2 g_{21}^2 g_{31}^2}{(p+\epsilon_1-\epsilon_2+i\pi g_{21}^2)(p+\epsilon_1-\epsilon_3+i\pi g_{31}^2)+\pi^2 g_{21}^2 g_{31}^2}. \end{aligned} \tag{15.49}$$

15.3.6 Three-level system, Σ-scheme

In the case of Σ-scheme (see Fig. 15.3) the role of $S_\pm$ operators is played by $S_+ = g_{32}|3\rangle\langle 2| + g_{21}|2\rangle\langle 1|$, and $S_- = g_{32}|2\rangle\langle 3| + g_{21}|1\rangle\langle 2|$. The corresponding self-energy is $\Sigma = -i\pi g_{32}^2 P_3 - i\pi g_{21}^2 P_2$ and therefore $G = P_1(\omega-\epsilon_1-H_b+i\eta)^{-1} + P_2(\omega-\epsilon_2-H_b+i\pi g_{21}^2)^{-1} + P_3(\omega-\epsilon_3-H_b+i\pi g_{32}^2)^{-1} = P_i G_i$.

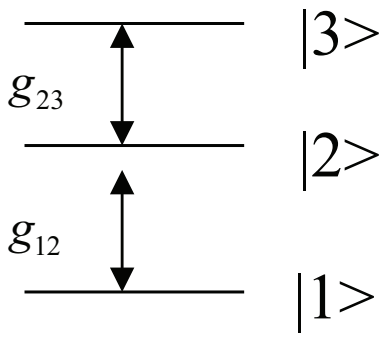

Figure 15.3: Three-level Σ-scheme

The building block is $G_0^{-1}G|_{\rm os} = GG_0^{-1}|_{\rm os} = P_1$, and therefore

$$T^{(1)}(\omega) = P_1(\hat{a}^\dagger_{\nu_1}S_-)P_2G_2(\hat{a}_{\nu_2}S_+)P_1 = P_1 g_{21}^2\hat{a}^\dagger_{\nu_1}\frac{1}{\omega-\epsilon_2+i\pi g_{21}^2}\hat{a}_{\nu_2}, \tag{15.50}$$

while

$$S_{pk} = \delta_{pk}\left[1-2\pi i\frac{g_{21}^2}{p+\epsilon_1-\epsilon_2+i\pi g_{21}^2}\right] = \delta_{pk}\frac{p+\epsilon_1-\epsilon_2-i\pi g_{21}^2}{p+\epsilon_1-\epsilon_2+i\pi g_{21}^2}. \tag{15.51}$$

We note that for Σ-scheme the one-photon scattering is the same as in the case of the two-level model, the third level being inefficient.

The results for the one-photon scattering of subsections D, E, and F agree with the ones derived in Ref. [12].

15.4 A model with several emitters

Here we apply the same formalism to the case of several emitters. We will distinguish the case of distributed emitters from the case of concentrated system (located at the same point). Moreover we will mostly focus on the case of two-level systems and discuss the cases of single- and two-photon scattering separately. We show that our main result works even when different emitters have different coupling constants. These calculations explicitly prove one of our main statements about an independent character of scattering of unidirectional photons in distributed systems.

15.4.1 The case of two atoms

To be specific we will focus on the following model Hamiltonian with two emitters

$$\begin{aligned} H &= \int d\nu\,\nu\,a^\dagger(\nu)a(\nu) + \frac{\Omega_1}{2}\sigma_z^{(1)} + \frac{\Omega_2}{2}\sigma_z^{(2)} + \int d\nu\{a^\dagger(\nu)S_-(\nu) + a(\nu)S_+(\nu)\} \\ &\equiv H_0 + a_{\alpha\nu}S_{\bar{\alpha}\nu}, \end{aligned} \tag{15.52}$$

where the following combinations play now the role of spin operators

$$S_+(\nu) = g_1\sigma_+^{(1)}e^{i\nu r_1} + g_2\sigma_+^{(2)}e^{i\nu r_2}, \tag{15.53}$$
$$S_-(\nu) = g_1\sigma_-^{(1)}e^{-i\nu r_1} + g_2\sigma_-^{(2)}e^{-i\nu r_2}. \tag{15.54}$$

It is important to remark that this form of coupling is effectively energy (momentum) dependent, and for $r_1 \neq r_2$ it does not fulfill one of the assumptions we used to derive (15.3). Therefore, an extension of (15.3) is required, which will be done below.

It is convenient to introduce the following projection operators $P_{ab} = P_a^{(1)}P_b^{(2)}$, $a, b = \pm$, such that $\sum_{a,b} P_{ab} = 1$. We find then

$$\begin{aligned}\frac{\Omega_1}{2}\sigma_z^{(1)} + \frac{\Omega_2}{2}\sigma_z^{(2)} &= \frac{\Omega_1}{2}(P_+^{(1)} - P_-^{(1)})(P_+^{(2)} + P_-^{(2)}) + \frac{\Omega_2}{2}(P_+^{(1)} + P_-^{(1)})(P_+^{(2)} - P_-^{(2)}) \\ &= \frac{\Omega_1+\Omega_2}{2}P_{++} + \frac{\Omega_1-\Omega_2}{2}(P_{+-} - P_{-+}) - \frac{\Omega_1+\Omega_2}{2}P_{--}.\end{aligned} \tag{15.55}$$

It follows that the bare Green's function is

$$\begin{aligned}G_0(\omega) &= \frac{P_{++}}{\omega - H_b - \frac{\Omega_1+\Omega_2}{2} + i\eta} + \frac{P_{+-}}{\omega - H_b - \frac{\Omega_1-\Omega_2}{2} + i\eta} \\ &+ \frac{P_{-+}}{\omega - H_b + \frac{\Omega_1-\Omega_2}{2} + i\eta} + \frac{P_{--}}{\omega - H_b + \frac{\Omega_1+\Omega_2}{2} + i\eta} = P_{ab}G_{ab}.\end{aligned} \tag{15.56}$$

15.4.2 Calculation of the self-energy and scattering matrices

There is the only allowed diagram for the self-energy

$$\begin{aligned}&\Sigma^{(2)}(\omega) = \overbrace{a_\nu S_{+\nu}P_{ab}G_{ab}(\omega)a_\nu^\dagger}S_{-\nu} = S_{+\nu}P_{ab}G_{ab}(\omega-\nu)S_{-\nu} \\ =\ &\left[g_1\sigma_+^{(1)}e^{i\nu r_1} + g_2\sigma_+^{(2)}e^{i\nu r_2}\right]P_{ab}G_{ab}\left[g_1\sigma_-^{(1)}e^{-i\nu r_1} + g_2\sigma_-^{(2)}e^{-i\nu r_2}\right] \\ =\ &\left[g_1e^{i\nu r_1}\sigma_+^{(1)}P_b^{(2)}G_{-,b} + g_2e^{i\nu r_2}P_a^{(1)}\sigma_+^{(2)}G_{a,-}\right]\left[g_1\sigma_-^{(1)}e^{-i\nu r_1} + g_2\sigma_-^{(2)}e^{-i\nu r_2}\right] \\ =\ &\int d\nu[g_1^2P_{+b}G_{-b} + g_1g_2e^{i\nu(r_2-r_1)}\sigma_-^{(1)}\sigma_+^{(2)}G_{--} + g_1g_2e^{i\nu(r_1-r_2)}\sigma_+^{(1)}\sigma_-^{(2)}G_{--} + g_2^2P_{a,+}G_{a,-}] \\ =\ &-i\pi\left[(g_1^2+g_2^2)P_{++} + g_1^2P_{+-} + g_2^2P_{-+} + g_1g_2f(r_2,r_1)\sigma_-^{(1)}\sigma_+^{(2)} + g_1g_2f(r_1,r_2)\sigma_+^{(1)}\sigma_-^{(2)}\right],\end{aligned} \tag{15.57}$$

where $f(r_1, r_2; \omega_b - H_b) = f(r_1, r_2) = 2\exp[i(\omega_b - H_b)(r_1 - r_2)]\Theta(r_1 - r_2)$, and $\omega = \omega_b - \Omega$, ω_b being the energy of incoming (outgoing) photons. The standard symbol for the Wick contraction is also used. The dressed Green's function is therefore

$$G(\omega) = G(\omega_b - H_b) = \frac{P_{++}}{\omega_b - H_b - \Omega_1 - \Omega_2 + i\pi(g_1^2+g_2^2)} + \frac{P_{--}}{\omega_b - H_b + i\eta} + \mathcal{M}, \tag{15.58}$$

where $\mathcal{M}$ is the matrix to be specified below.

Now we consider the two cases separately: the case of concentrated system (when positions of two emitters r_1 and r_2 coincide) and the case of distributed system when the coordinates of emitters are different. In the former case the analysis based on Eq. (15.3) is sufficient, while the latter case requires its extension.

Concentrated case

For coinciding positions of emitters $r_1 = r_2$ and we have $f_{12} = f_{21} = 1$ and

$$\begin{aligned}\mathcal{M} &= \left\{\left[(G_{+-}^0)^{-1} + i\pi g_1^2\right]P_{+-} + \left[(G_{-+}^0)^{-1} + i\pi g_2^2\right]P_{-+} + i\pi g_1g_2\frac{\sigma_-^{(1)}\sigma_+^{(2)} + \sigma_+^{(1)}\sigma_-^{(2)}}{2}\right\}^{-1} \\ &= \frac{1}{\det\mathcal{M}}\left\{\left[(G_{-+}^0)^{-1} + i\pi g_2^2\right]P_{+-} + \left[(G_{+-}^0)^{-1} + i\pi g_1^2\right]P_{-+} - i\pi g_1g_2\frac{\sigma_-^{(1)}\sigma_+^{(2)} + \sigma_+^{(1)}\sigma_-^{(2)}}{2}\right\},\end{aligned} \tag{15.59}$$

where

$$\begin{aligned}\det\mathcal{M} &= (G_{+-}^0)^{-1}(G_{-+}^0)^{-1} + i\pi\left[g_2^2(G_{+-}^0)^{-1} + g_1^2(G_{-+}^0)^{-1}\right] \\ &= \left(\omega_b - H_b - \frac{\Omega_1+\Omega_2}{2} - \Lambda_+\right)\left(\omega_b - H_b - \frac{\Omega_1+\Omega_2}{2} - \Lambda_-\right),\end{aligned} \tag{15.60}$$

$$\Lambda_\pm = -\frac{i\pi(g_1^2+g_2^2)}{2} \pm \frac{1}{2}\sqrt{-\pi^2(g_1^2+g_2^2)^2 + (\Omega_1-\Omega_2)^2 - 2i\pi(\Omega_1-\Omega_2)(g_1^2-g_2^2)}. \tag{15.61}$$

In the limiting case $\Omega_1 = \Omega_2 = \Omega$

$$\begin{aligned}\mathcal{M} &= \frac{P_{+-}+P_{-+}}{2}\left[\frac{1}{\omega_b - H_b - \Omega + i\pi(g_1^2+g_2^2)} + \frac{1}{\omega_b - H_b - \Omega + i\eta}\right] \\ &+ \frac{P_{+-}-P_{-+}}{2}\cos\theta\left[\frac{1}{\omega_b - H_b - \Omega + i\pi(g_1^2+g_2^2)} - \frac{1}{\omega_b - H_b - \Omega + i\eta}\right] \\ &+ \frac{\sigma_-^{(1)}\sigma_+^{(2)}+\sigma_+^{(1)}\sigma_-^{(2)}}{2}\sin\theta\left[\frac{1}{\omega_b - H_b - \Omega + i\pi(g_1^2+g_2^2)} - \frac{1}{\omega_b - H_b - \Omega + i\eta}\right], \end{aligned} \tag{15.62}$$

where $\tan\frac{\theta}{2} = \frac{g_2}{g_1}$. Then

$$T^{(1)} = \left[g_1\sigma_-^{(1)}P_-^{(2)} + g_2P_-^{(1)}\sigma_-^{(2)}\right]G(\nu_1)\left[g_1\sigma_+^{(1)}P_-^{(2)} + g_2P_-^{(1)}\sigma_+^{(2)}\right]a_{\nu_1}^\dagger a_{\nu_2} = a_{\nu_1}^\dagger a_{\nu_2}P_{--}\frac{g_1^2+g_2^2}{\nu_1 - \Omega + i\pi(g_1^2+g_2^2)} \tag{15.63}$$

and the corresponding scattering matrix is

$$S_{pk} = \delta_{pk}\left(1 - 2\frac{i\pi(g_1^2+g_2^2)}{p - \Omega + i\pi(g_1^2+g_2^2)}\right) = \delta_{pk}\frac{p - \Omega - i\pi(g_1^2+g_2^2)}{p - \Omega + i\pi(g_1^2+g_2^2)}. \tag{15.64}$$

Distributed system

For distributed system $r_1 \neq r_2$ we obtain

$$\begin{aligned}\mathcal{M} &= \frac{P_{+-}}{\omega_b - H_b - \Omega_1 + i\pi g_1^2} + \frac{P_{-+}}{\omega_b - H_b - \Omega_2 + i\pi g_2^2} \\ &- i\pi g_1 g_2\frac{f(r_2,r_1)\sigma_-^{(1)}\sigma_+^{(2)} + f(r_1,r_2)\sigma_+^{(1)}\sigma_-^{(2)}}{(\omega_b - H_b - \Omega_1 + i\pi g_1^2)(\omega_b - H_b - \Omega_2 + i\pi g_2^2)} \\ &= M_1P_{+-} + M_2P_{-+} + M_{12}\sigma_+^{(1)}\sigma_-^{(2)} + M_{21}\sigma_-^{(1)}\sigma_+^{(2)}. \end{aligned} \tag{15.65}$$

The one-photon T-matrix amounts to

$$\begin{aligned}T^{(1)} &= P_{--}a_{\nu_1}^\dagger S_{-,\nu_1}Ga_{\nu_2}S_{+,\nu_2}P_{--} \\ &= \left[g_1\sigma_-^{(1)}P_-^{(2)}e^{-i\nu_1 r_1} + g_2P_-^{(1)}\sigma_-^{(2)}e^{-i\nu_1 r_2}\right]G(\nu_1)\left[g_1\sigma_+^{(1)}P_-^{(2)}e^{i\nu_2 r_1} + g_2P_-^{(1)}\sigma_+^{(2)}e^{i\nu_2 r_2}\right]a_{\nu_1}^\dagger a_{\nu_2} \\ &= a_{\nu_1}^\dagger a_{\nu_2}P_{--}\frac{g_1^2(\nu_1 - \Omega_2) + g_2^2(\nu_1 - \Omega_1)}{(\nu_1 - \Omega_1 + i\pi g_1^2)(\nu_1 - \Omega_2 + i\pi g_2^2)}, \end{aligned} \tag{15.66}$$

and the corresponding scattering matrix reads

$$S_{pk} = \delta_{pk}\left(1 - 2\frac{i\pi g_1^2(p - \Omega_2) + i\pi g_2^2(p - \Omega_1)}{(p - \Omega_1 + i\pi g_1^2)(p - \Omega_2 + i\pi g_2^2)}\right) = \delta_{pk}\prod_{i=1}^{2}\frac{(p - \Omega_i - i\pi g_i^2)}{(p - \Omega_i + i\pi g_i^2)}. \tag{15.67}$$

We note that (15.67) can be represented as a convolution

$$S_{pk} = \int dk' S_{2;pk'}S_{1;k'k} \tag{15.68}$$

of the scattering matrices S_1 and S_2 on the first and the second emitters, respectively. This property is a consequence of the absent backscattering for chiral photons, and it will be later on generalized to the arbitrary N-photon sector.

We also make the two following observations: 1) In the absence of backscattering there is no interference between counter-propagating waves, and therefore the outgoing state contains no information about positions of emitters, that is there is no dependence on $r_1 - r_2$ in (15.67). 2) The result (15.67) would smoothly cross over to (15.64) on a scale of the phononic wavelength. The latter quantity is of the order of an inverse bandwidth, which is effectively set to zero in our theory. Therefore, (15.64) and (15.67) are not analytically connected with each other in the limit of the vanishing distance $r_1 - r_2$ between the emitters.

15.4.3 General approach: One-photon scattering

Here we present a general approach aimed at calculation of the scattering matrices for the distributed system. Therefore in the following we consider only the model with two emitters located in different positions and having different Ω_i and g_i,

$$H = \int d\nu\, \nu\, a^\dagger(\nu)a(\nu) + \frac{\Omega_1}{2}\sigma_z^{(1)} + \frac{\Omega_2}{2}\sigma_z^{(2)} + V_1 + V_2, \tag{15.69}$$

where $V_i = v_i + v_i^\dagger$, where $i = 1, 2$. Here $v_i = g_i\sigma_+^{(i)} \int d\nu e^{i\nu r_i} a(\nu) \equiv g_i\sigma_+^{(i)} A_i$. Let us label the atoms in such a way that $r_1 > r_2$. Our aim is to calculate the T-matrix

$$T(\omega) = V + V\frac{1}{\omega - H + i\eta}V, \tag{15.70}$$

where $V = V_1 + V_2$, in the ground state of the atomic system $|\downarrow\downarrow\rangle$. In the following we omit $i\eta$ assuming $\omega \to \omega + i\eta$.

The first term in (15.70) can be neglected as it is off-diagonal in spin states. In calculation of the second term $(V_1 + V_2)\frac{1}{\omega - H_0 - V_1 + V_2}(V_1 + V_2)$ we can retain only $(v_1^\dagger + v_2^\dagger)$ in the left factor and $(v_1 + v_2)$ in the right factor, respectively, since $\sigma_-^i|\downarrow\downarrow\rangle = 0$ and $\langle\downarrow\downarrow|\sigma_+^{(i)} = 0$. Thus we have a sum of four terms

$$T = v_1^\dagger \frac{1}{\omega - H_0 - V_1 - V_2} v_1 \tag{15.71}$$

$$+ v_2^\dagger \frac{1}{\omega - H_0 - V_1 - V_2} v_2 \tag{15.72}$$

$$+ v_1^\dagger \frac{1}{\omega - H_0 - V_1 - V_2} v_2 \tag{15.73}$$

$$+ v_2^\dagger \frac{1}{\omega - H_0 - V_1 - V_2} v_1. \tag{15.74}$$

As a consequence of the RWA we obtain the operators $A_i^\dagger \sim v_i^\dagger$ to the left from the resolvent, and the operators $A_i \sim v_i$ to the right from the resolvent in each term of this sum.

Let us now consider term by term expanding them first in V_1, and then in V_2. In the following we will use an important observation that v_1 can be only paired with the adjacent $v_1^\dagger$, while any contraction of v_2 and $v_1^\dagger$ always yields zero. More generally, the contraction

$$\overbrace{v_i v_j^\dagger} = 0, \quad i > j. \tag{15.75}$$

vanishes as it typically implies an integral of the kind

$$\int d\nu \frac{e^{i\nu(r_i - r_j)}}{(\ldots - \nu + i\eta)\ldots(\ldots - \nu + i\eta)} = 0. \tag{15.76}$$

This integral is zero as it has all poles in the upper half-plane, and the exponential function $e^{i\nu(r_i - r_j)}$ decays sufficiently fast in the lower half-plane for $r_i < r_j$. Therefore we can close the integration contour in the lower half-plane and get zero.

Let us consider different components (15.71)-(15.74) of the T-matrix in more detail. In the contribution T_{11} given by (15.71)

$$T_{11} = v_1^\dagger \left(\frac{1}{\omega - H_0 - V_2} + \frac{1}{\omega - H_0 - V_2} v_1 \frac{1}{\omega - H_0 - V_2} v_1^\dagger \frac{1}{\omega - H_0 - V_2} + \ldots \right) v_1 \tag{15.77}$$

we can omit the terms in parentheses which are odd in V_1, as they are off-diagonal in the spin states of the $i = 1$ atom. Moreover, the operators v_1 and $v_1^\dagger$ must alternate.

If we are exclusively interested in the single-photon scattering, then we should only consider terms with the single creation (annihilation) operator in the left (right) side. For this reason we can neglect V_2 everywhere in (15.77): an expansion in V_2 cannot contain v_2 in the leftmost position because of the spin state of the second atom, and it cannot contain $v_2^\dagger$ because of the photon state. Note that this argument is implicitly based on the RWA.

Resumming the remaining series we obtain in the one-photon sector

$$T_{11}^{(1)} = v_1^\dagger \frac{1}{\omega - H_0 - \Sigma_1} v_1 = g_1^2 A_1^\dagger \frac{1}{\omega - H_0 - \Omega_1 - \Sigma_1} A_1, \tag{15.78}$$

where $\Sigma_1 = -i\pi g_1^2 \equiv -i\Gamma_1$.

Applying similar arguments to T_{22} (15.72), we find

$$T_{22}^{(1)} = v_2^\dagger \frac{1}{\omega - H_0 - \Sigma_2} v_2 = g_2^2 A_2^\dagger \frac{1}{\omega - H_0 - \Omega_2 - \Sigma_2} A_2, \tag{15.79}$$

where $\Sigma_2 = -i\pi g_2^2 \equiv -i\Gamma_2$.

Analogously we find for T_{12} (15.73) that

$$T_{12} = v_1^\dagger \left(\frac{1}{\omega - H_0 - V_2} v_1 \frac{1}{\omega - H_0 - V_2} + \dots \right) v_2. \tag{15.80}$$

The terms in parentheses which are even in V_1 are omitted; an expansion starts from v_1. Once a term containing $v_1^\dagger$ occurs (e.g. $\sim v_1 v_1^\dagger v_1$), a pairing of adjacent v_1 and $v_1^\dagger$ should be performed, as there is no any other possibility for $v_1^\dagger$ to be paired in the one-photon sector (the latter implies that $v_1^\dagger$ can not be either paired to an external vertex). This leads to an expression

$$T_{12}^{(1)} = v_1^\dagger \frac{1}{\omega - H_0 - V_2 - \Sigma_1} v_1 \frac{1}{\omega - H_0 - V_2} v_2. \tag{15.81}$$

In the first propagator one can neglect V_2 as the corresponding expansion can start neither form v_2 nor from $v_2^\dagger$. After expanding the second propagator in V_2 one keeps only the terms odd in V_2, the expansion starting from $v_2^\dagger$. Resumming the series containing the power of contraction between v_2 and $v_2^\dagger$, one transforms (15.81) into

$$T_{12}^{(1)} = v_1^\dagger \frac{1}{\omega - H_0 - \Sigma_1} v_1 \frac{1}{\omega - H_0} v_2^\dagger \frac{1}{\omega - H_0 - \Sigma_2} v_2. \tag{15.82}$$

It now only remains to pair v_1 and $v_2^\dagger$ which results in

$$T_{12}^{(1)} = -2\pi i g_1^2 g_2^2 A_1^\dagger \frac{1}{\omega - H_0 - \Omega_1 - \Sigma_1} e^{i(\omega - H_0)(r_1 - r_2)} \frac{1}{\omega - H_0 - \Omega_2 - \Sigma_2} A_2, \tag{15.83}$$

where we have also used that

$$\sigma_- \frac{1}{\omega - \frac{\Omega}{2}\sigma_z} = \frac{1}{\omega - \frac{\Omega}{2}\sigma_z - \Omega} \sigma_-. \tag{15.84}$$

Finally, we consider T_{21} (15.74)

$$T_{21} = v_2^\dagger \left(\frac{1}{\omega - H_0 - V_2} v_1^\dagger \frac{1}{\omega - H_0 - V_2} + \dots \right) v_1. \tag{15.85}$$

The terms in parentheses which are even in V_1 are omitted; an expansion starts from $v_1^\dagger$. However, this operator cannot be paired to any operator standing to the left from it as follows from (15.75). Therefore, T_{21} identically vanishes in the one-photon sector, $T_{21}^{(1)} = 0$.

Let us now collect all the terms and calculate the scattering matrix in the one-photon sector

$$\begin{aligned} S_{pk} &= \delta_{pk} - 2i\delta_{pk} \left[\frac{\Gamma_1}{p - \Omega_1 + i\Gamma_1} + \frac{\Gamma_2}{p - \Omega_2 + i\Gamma_2} - 2i\Gamma_1\Gamma_2 e^{-ipr_1} \frac{1}{p - \Omega_1 + i\Gamma_1} e^{ip(r_1 - r_2)} \frac{1}{p - \Omega_2 + i\Gamma_2} e^{ipr_2} \right] \\ &= \delta_{pk} \left[1 - 2\frac{i\Gamma_1(p - \Omega_2) + i\Gamma_2(p - \Omega_1)}{(p - \Omega_1 + i\Gamma_1)(p - \Omega_2 + i\Gamma_2)} \right] = \delta_{pk} \frac{(p - \Omega_1 - i\Gamma_1)(p - \Omega_2 - i\Gamma_2)}{(p - \Omega_1 + i\Gamma_1)(p - \Omega_2 + i\Gamma_2)}. \end{aligned} \tag{15.86}$$

which coincides with the result (15.67) from the previous subsection.

15.4.4 Two-photon sector

In order to find an exact expression for a scattering matrix in the two-photon sector it is necessary to classify all possible arrangements of external vertices with their eventual renormalization which are allowed by the algebra of spin operators. In between vertices one can insert the dressed Green's functions given by Eqs. (15.58) and (15.65).

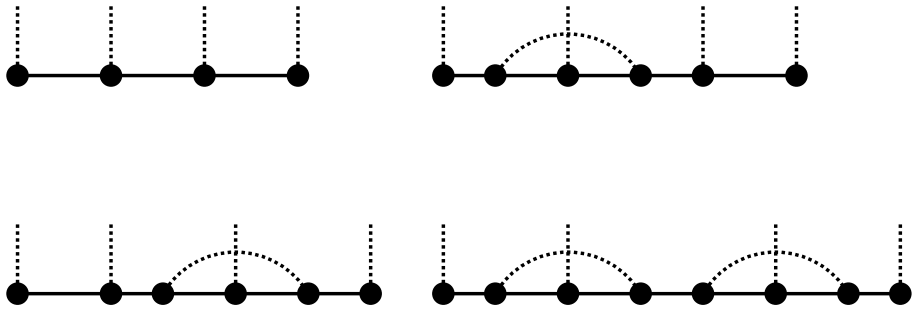

Figure 15.4: Diagrams without renormalization of vertices and with renormalization of a single vertex. Solid lines correspond to the dressed Green's functions, circles denote spin operators, dotted lines are (paired and unpaired) photonic lines.

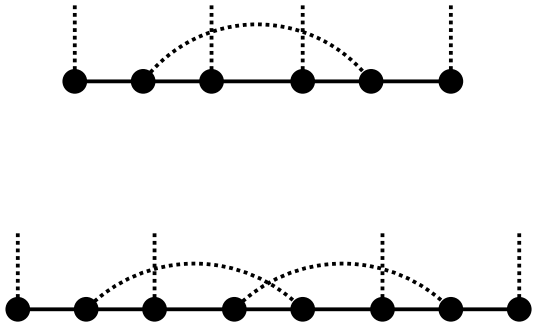

Figure 15.5: Diagrams with renormalization of double vertices. Notations are the same as before.

The diagrams which do not vanish in the two-photon sector are shown in Figs. 15.4 and 15.5. The first and the forth vertices in these diagrams are not renormalized, which is a consequence of the RWA. This allows us to evaluate the part which is the same for all diagrams

$$\begin{aligned} & a^\dagger_{\nu_1}(g_1\sigma^{(1)}_- P^{(2)}_- e^{-i\nu_1 r_1} + g_2 P^{(1)}_- \sigma^{(2)}_- e^{-i\nu_1 r_2}) G \dots G a_{\nu_4}(g_1\sigma^{(1)}_+ P^{(2)}_- e^{i\nu_4 r_1} + g_2 P^{(1)}_- \sigma^{(2)}_+ e^{i\nu_4 r_2}) \\ = \;& a^\dagger_{\nu_1}(g_1 M_1 \sigma^{(1)}_- P^{(2)}_- e^{-i\nu_1 r_1} + g_2 M_2 P^{(1)}_- \sigma^{(2)}_- e^{-i\nu_1 r_2} + g_1 M_{12} P^{(1)}_- \sigma^{(2)}_- e^{-i\nu_1 r_1}) \times \\ & \times \dots \times a_{\nu_4}(M_1 g_1 \sigma^{(1)}_+ P^{(2)}_- e^{i\nu_4 r_1} + M_2 g_2 P^{(1)}_- \sigma^{(2)}_+ e^{i\nu_4 r_2} + M_{12} g_2 \sigma^{(1)}_+ P^{(2)}_- e^{i\nu_4 r_2}) \\ = \;& a^\dagger_{\nu_1}(g_1 M_1 \sigma^{(1)}_- P^{(2)}_- e^{-i\nu_1 r_1} + g_2 M_2 S_1 P^{(1)}_- \sigma^{(2)}_- e^{-i\nu_1 r_2}) \\ & \times \dots \times a_{\nu_4}(M_1 g_1 S_2 \sigma^{(1)}_+ P^{(2)}_- e^{i\nu_4 r_1} + M_2 g_2 P^{(1)}_- \sigma^{(2)}_+ e^{i\nu_4 r_2}), \end{aligned} \tag{15.87}$$

where $S_{1,2} = 1 - 2\pi i g^2_{1,2} M_{1,2}$, and $M_{1,2}$ are defined in (15.65).

Let us first evaluate the diagrams shown in Fig. 15.4. The diagram without vertex renormalization is given by the expression

$$\begin{aligned} & P_{--} a^\dagger_{\nu_1} S_{-,\nu_1} G a_{\nu_2} S_{+,\nu_2} G a^\dagger_{\nu_3} S_{-,\nu_3} G a_{\nu_4} S_{+,\nu_4} P_{--} \\ + \;& P_{--} a^\dagger_{\nu_1} S_{-,\nu_1} G a^\dagger_{\nu_2} S_{-,\nu_2} G a_{\nu_3} S_{+,\nu_3} G a_{\nu_4} S_{+,\nu_4} P_{--}. \end{aligned} \tag{15.88}$$

The first term in (15.88) reads

$$\begin{aligned}
& P_{--}a^\dagger_{\nu_1}\left(g_1^2M_1e^{-i(\nu_1-\nu_2)r_1}+g_2^2M_2S_1e^{-i(\nu_1-\nu_2)r_2}\right)a_{\nu_2}\\
\times\ & \frac{1}{\omega_b-H_b+i\eta}a^\dagger_{\nu_3}\left(g_1^2M_1S_2e^{-i(\nu_3-\nu_4)r_1}+g_2^2M_2e^{-i(\nu_3-\nu_4)r_2}\right)a_{\nu_4}\\
=\ & P_{--}\left(g_1^2M_1(\nu_1)e^{-i(\nu_1-\nu_3)r_1}+g_2^2M_2(\nu_1)S_1(\nu_1)e^{-i(\nu_1-\nu_3)r_2}\right)\frac{1}{\nu_1-\nu_3+i\eta}\\
\times\ & \left(g_1^2M_1(\nu_4)S_2(\nu_4)e^{i(\nu_1-\nu_3)r_1}+g_2^2M_2(\nu_4)e^{i(\nu_1-\nu_3)r_2}\right)a^\dagger_{\nu_1}a^\dagger_{\nu_2}a_{\nu_3}a_{\nu_4}\\
=\ & \big(g_1^4M_1(\nu_1)M_1(\nu_4)S_2(\nu_4)+g_2^4S_1(\nu_1)M_2(\nu_1)M_2(\nu_4)\\
& +g_1^2g_2^2M_1(\nu_1)M_2(\nu_4)e^{-i(\nu_1-\nu_3)(r_1-r_2)}+g_1^2g_2^2M_1(\nu_4)S_2(\nu_4)M_2(\nu_1)S_1(\nu_1)e^{i(\nu_1-\nu_3)(r_1-r_2)}\big)\\
\times\ & \frac{P_{--}}{\nu_1-\nu_3+i\eta}a^\dagger_{\nu_1}a^\dagger_{\nu_2}a_{\nu_3}a_{\nu_4}.
\end{aligned}\tag{15.89}$$

The second term in (15.88) reads

$$\begin{aligned}
& P_{--}a^\dagger_{\nu_1}g_1g_2(M_1e^{-i\nu_1r_1-i\nu_2r_2}+M_2S_1e^{-i\nu_1r_2-i\nu_2r_1})a^\dagger_{\nu_2}\\
\times\ & \frac{1}{\omega_b-H_b-\alpha_1-\alpha_2}a_{\nu_3}g_1g_2(M_1S_2e^{i\nu_3r_2+i\nu_4r_1}+M_2e^{i\nu_3r_1+i\nu_4r_2})a_{\nu_4}\qquad(15.90)\\
=\ & P_{--}g_1^2g_2^2\left(M_1(\nu_1)e^{-i\nu_1r_1-i\nu_2r_2}+M_2(\nu_1)S_1(\nu_1)e^{-i\nu_1r_2-i\nu_2r_1}\right)\\
\times\ & \frac{1}{E-\alpha_1-\alpha_2}(M_1(\nu_4)S_2(\nu_4)e^{i\nu_3r_2+i\nu_4r_1}+M_2(\nu_4)e^{i\nu_3r_1+i\nu_4r_2})a^\dagger_{\nu_1}a^\dagger_{\nu_2}a_{\nu_3}a_{\nu_4}\\
=\ & \Big(M_1(\nu_1)M_1(\nu_4)S_2(\nu_4)e^{-i(\nu_1-\nu_4)(r_1-r_2)}+M_2(\nu_1)S_1(\nu_1)M_2(\nu_4)e^{i(\nu_1-\nu_4)(r_1-r_2)}\\
& +M_2(\nu_1)S_1(\nu_1)M_1(\nu_4)S_2(\nu_4)e^{i(\nu_1-\nu_3)(r_1-r_2)}+M_1(\nu_1)M_2(\nu_4)e^{-i(\nu_1-\nu_3)(r_1-r_2)}\Big)\\
\times\ & \frac{P_{--}g_1^2g_2^2}{E-\alpha_1-\alpha_2}a^\dagger_{\nu_1}a^\dagger_{\nu_2}a_{\nu_3}a_{\nu_4},\qquad(15.91)
\end{aligned}$$

where $\alpha_{1,2}=\Omega_{1,2}-i\pi g_{1,2}^2$ and $E=\nu_1+\nu_2=\nu_3+\nu_4$.

In order to evaluate the diagram with renormalization of the second vertex we find the following vertex correction to the second vertex

$$\begin{aligned}
& \left(g_1\sigma^{(1)}_+a_\nu e^{i\nu r_1}\right)G\left(g_1\sigma^{(1)}_-a^\dagger_{\nu_2}e^{-i\nu_2r_1}\right)G\left(g_2\sigma^{(2)}_-a^\dagger_\nu e^{-i\nu r_2}\right)\\
=\ & g_1^2g_2\overbrace{a_\nu G_{--}a^\dagger_{\nu_2}G_{+-}}a^\dagger_\nu P^{(1)}_+\sigma^{(2)}_-e^{i\nu(r_1-r_2)}e^{-i\nu_2r_1}\\
=\ & P^{(1)}_+\sigma^{(2)}_-e^{-i\nu_2r_1}g_1^2g_2\int d\nu\frac{e^{i\nu(r_1-r_2)}}{(\omega_b-H_b-\nu+i\eta)(\omega_b-H_b-\nu+\nu_2-\alpha_1)}a^\dagger_{\nu_2}.
\end{aligned}\tag{15.92}$$

Such vertex correction can only occur in the diagram which has $v_1^\dagger$ in the first position (from the left). Therefore we can effectively replace $\omega_b-H_b\to\nu_1$. Evaluating the integral we obtain

$$\begin{aligned}
& P^{(1)}_+\sigma^{(2)}_-e^{-i\nu_2r_1}g_1^2g_2(-2\pi i)e^{i\nu_1(r_1-r_2)}M_1(\nu_2)\left[1-e^{i(\nu_2-\alpha_1)(r_1-r_2)}\right]a^\dagger_{\nu_2}\\
=\ & P^{(1)}_+\sigma^{(2)}_-e^{-i\nu_2r_1}g_2e^{i\nu_1(r_1-r_2)}[S_1(\nu_2)-1]\left[1-e^{i(\nu_2-\alpha_1)(r_1-r_2)}\right]a^\dagger_{\nu_2}.
\end{aligned}\tag{15.93}$$

Now we can evaluate the whole diagram with this vertex correction

$$\begin{aligned}
& M_1(\nu_1)\left[S_1(\nu_2)-1\right]\left[1-e^{i(\nu_2-\alpha_1)(r_1-r_2)}\right]\\
\times\ & (M_1(\nu_4)S_2(\nu_4)e^{i(\nu_1-\nu_3)(r_1-r_2)}+M_2(\nu_4)e^{i(\nu_1-\nu_4)(r_1-r_2)})\\
\times\ & \frac{P_{--}g_1^2g_2^2}{E-\alpha_1-\alpha_2}a^\dagger_{\nu_1}a^\dagger_{\nu_2}a_{\nu_3}a_{\nu_4}.
\end{aligned}\tag{15.94}$$

In order to evaluate the diagram with renormalization of the third vertex we find the following vertex correction to the third vertex

$$\begin{aligned}
& \left(g_1\sigma^{(1)}_+a_\nu e^{i\nu r_1}\right)G\left(g_2\sigma^{(2)}_+a_{\nu_3}e^{i\nu_3r_2}\right)G\left(g_2\sigma^{(2)}_-a^\dagger_\nu e^{-i\nu r_2}\right)\\
=\ & g_1g_2^2\overbrace{a_\nu G_{-+}a_{\nu_3}G_{--}}a^\dagger_\nu\sigma^{(1)}_+P^{(2)}_+e^{i\nu(r_1-r_2)}e^{i\nu_3r_2}\\
=\ & \sigma^{(1)}_+P^{(2)}_+e^{i\nu_3r_2}g_1g_2^2a_{\nu_3}\int d\nu\frac{e^{i\nu(r_1-r_2)}}{(\omega_b-H_b-\nu+\nu_3-\alpha_2)(\omega_b-H_b-\nu+i\eta)}.
\end{aligned}\tag{15.95}$$

Such vertex correction can only occur in the diagram which has v_2 in the forth position (from the left). Therefore we can effectively replace $\omega_b - H_b \to \nu_4$. Evaluating the integral we obtain

$$\begin{aligned} & \sigma_+^{(1)} P_+^{(2)} e^{i\nu_3 r_2} g_1 g_2^2 a_{\nu_3} (-2\pi i) e^{i\nu_4 (r_1 - r_2)} M_2(\nu_3) \left[1 - e^{i(\nu_3 - \alpha_2)(r_1 - r_2)}\right] \\ = \; & \sigma_+^{(1)} P_+^{(2)} e^{i\nu_3 r_2} g_1 e^{i\nu_4 (r_1 - r_2)} \left[S_2(\nu_3) - 1\right] \left[1 - e^{i(\nu_3 - \alpha_2)(r_1 - r_2)}\right] a_{\nu_3}. \end{aligned} \tag{15.96}$$

Now we can evaluate the whole diagram with this vertex correction

$$\begin{aligned} & \left(M_1(\nu_1) e^{-i(\nu_1 - \nu_4)(r_1 - r_2)} + M_2(\nu_1) S_1(\nu_1) e^{i(\nu_1 - \nu_3)(r_1 - r_2)}\right) \\ \times \; & \left[S_2(\nu_3) - 1\right] \left[1 - e^{i(\nu_3 - \alpha_2)(r_1 - r_2)}\right] M_2(\nu_4) \frac{P_{--} g_1^2 g_2^2}{E - \alpha_1 - \alpha_2} a_{\nu_1}^\dagger a_{\nu_2}^\dagger a_{\nu_3} a_{\nu_4}. \end{aligned} \tag{15.97}$$

The diagram with renormalization of both the second and the third vertices is given by

$$\begin{aligned} & e^{i(\nu_1 - \nu_3)(r_1 - r_2)} \left[1 - e^{i(\nu_2 - \alpha_1)(r_1 - r_2)}\right] \left[1 - e^{i(\nu_3 - \alpha_2)(r_1 - r_2)}\right] \\ \times \; & M_1(\nu_1) \left[S_1(\nu_2) - 1\right] \left[S_2(\nu_3) - 1\right] M_2(\nu_4) \frac{P_{--} g_1^2 g_2^2}{E - \alpha_1 - \alpha_2} a_{\nu_1}^\dagger a_{\nu_2}^\dagger a_{\nu_3} a_{\nu_4}. \end{aligned} \tag{15.98}$$

Summarizing the results of Eqs. (15.91), (15.94), (15.97), and (15.98) we obtain the following intermediate expression for $T^{(2)}$

$$\begin{aligned} & - \; i\pi \delta_{\nu_1 \nu_3} \left[g_1^4 M_1(\nu_1) M_1(\nu_4) S_2(\nu_4) + g_2^4 S_1(\nu_1) M_2(\nu_1) M_2(\nu_4)\right] \\ & - \; i\pi \delta_{\nu_1 \nu_3} g_1^2 g_2^2 \left[M_1(\nu_1) M_2(\nu_4) + M_1(\nu_4) S_2(\nu_4) M_2(\nu_1) S_1(\nu_1)\right] \\ & + \; \frac{1}{\nu_1 - \nu_3} \left[g_1^4 M_1(\nu_1) M_1(\nu_4) S_2(\nu_4) + g_2^4 S_1(\nu_1) M_2(\nu_1) M_2(\nu_4)\right] \\ & + \; \frac{g_1^2 g_2^2}{\nu_1 - \nu_3} \left[M_1(\nu_1) M_2(\nu_4) - M_1(\nu_3) S_2(\nu_3) M_2(\nu_2) S_1(\nu_2)\right] e^{-i(\nu_1 - \nu_3)(r_1 - r_2)} \\ & + \; \frac{g_1^2 g_2^2}{E - \alpha_1 - \alpha_2} e^{-i(\nu_1 - \nu_3)(r_1 - r_2)} \\ & \times \; \left\{M_1(\nu_1) + M_2(\nu_2) S_1(\nu_2) + M_1(\nu_2) [S_1(\nu_1) - 1][1 - e^{i(\nu_1 - \alpha_1)(r_1 - r_2)}]\right\} \\ & \times \; \left\{M_2(\nu_4) + M_1(\nu_3) S_2(\nu_3) + M_2(\nu_3) [S_2(\nu_4) - 1][1 - e^{i(\nu_4 - \alpha_2)(r_1 - r_2)}]\right\}, \end{aligned} \tag{15.99}$$

which has to be convoluted with $a_{\nu_1}^\dagger a_{\nu_2}^\dagger a_{\nu_3} a_{\nu_4}$. The projector P_{--} onto the ground state of the atomic system is also omitted.

We see that the dependence on atomic positions is still present in (15.99). Exchanging the dummy frequencies $\nu_1 \leftrightarrow \nu_2$ and $\nu_3 \leftrightarrow \nu_4$, when necessary, and exploiting obvious identities

$$M_1(\nu_2)[S_1(\nu_1) - 1] = M_1(\nu_1)[S_1(\nu_2) - 1], \tag{15.100}$$

$$M_2(\nu_3)[S_2(\nu_4) - 1] = M_2(\nu_4)[S_2(\nu_3) - 1], \tag{15.101}$$

we can cast the position-dependent part of (15.99) to

$$\begin{aligned} & \frac{g_1^2 g_2^2}{\nu_1 - \nu_3} M_1(\nu_1) M_2(\nu_4) \left[1 - S_1(\nu_2) S_2(\nu_3)\right] e^{-i(\nu_1 - \nu_3)(r_1 - r_2)} \\ & - \; g_1^2 g_2^2 M_1(\nu_1) [S_1(\nu_2) - 1] M_1(\nu_3) M_2(\nu_4) S_2(\nu_3) e^{i(\nu_3 - \alpha_1)(r_1 - r_2)} \\ & - \; g_1^2 g_2^2 M_2(\nu_4) [S_2(\nu_3) - 1] M_1(\nu_1) M_2(\nu_2) S_1(\nu_2) e^{i(\nu_2 - \alpha_2)(r_1 - r_2)} \\ & + \; \frac{g_1^2 g_2^2}{E - \alpha_1 - \alpha_2} M_1(\nu_1) M_2(\nu_4) [S_1(\nu_2) - 1][S_2(\nu_3) - 1] e^{i(E - \alpha_1 - \alpha_2)(r_1 - r_2)}. \end{aligned} \tag{15.102}$$

A cancellation of (15.102) is achieved by an account of diagrams containing double vertices shown in Fig. 15.5. The first possibility to generate a double vertex is provided by one photon line covering the second

and third vertices (upper panel of Fig. 15.5). The corresponding double vertex reads

$$
\begin{aligned}
&\left(g_1\sigma_+^{(1)}a_\nu e^{i\nu r_1}\right)G\left(g_i\sigma_-^{(i)}a_{\nu_2}^\dagger e^{-i\nu_2 r_i}\right)G\left(g_i\sigma_+^{(i)}a_{\nu_3}e^{i\nu_3 r_i}\right)G\left(g_2\sigma_-^{(2)}a_\nu^\dagger e^{-i\nu r_2}\right)\\
=\;& g_1^3 g_2 \sigma_+^{(1)}\sigma_-^{(2)}\overbrace{a_\nu G_{--}a_{\nu_2}^\dagger G_{+-}a_{\nu_3}G_{--}a_\nu^\dagger} e^{i\nu(r_1-r_2)}e^{-i(\nu_2-\nu_3)r_1}\\
+\;& g_1 g_2^3 \sigma_+^{(1)}\sigma_-^{(2)}\overbrace{a_\nu G_{--}a_{\nu_2}^\dagger G_{-+}a_{\nu_3}G_{--}a_\nu^\dagger} e^{i\nu(r_1-r_2)}e^{-i(\nu_2-\nu_3)r_2}\\
=\;& -g_1 g_2 \sigma_+^{(1)}\sigma_-^{(2)}a_{\nu_2}^\dagger a_{\nu_3}\left\{g_1^2 e^{-i(\nu_2-\nu_3)r_1}\int d\nu \frac{e^{i\nu(r_1-r_2)}}{(\nu-\nu_1-i\eta)(\nu-E+\alpha_1)(\nu-\nu_4-i\eta)}\right.\\
&\left.+g_2^2 e^{-i(\nu_2-\nu_3)r_2}\int d\nu\frac{e^{i\nu(r_1-r_2)}}{(\nu-\nu_1-i\eta)(\nu-E+\alpha_2)(\nu-\nu_4-i\eta)}\right\}\\
=\;& 2\pi i g_1 g_2 \sigma_+^{(1)}\sigma_-^{(2)}a_{\nu_2}^\dagger a_{\nu_3} \qquad (15.103)\\
\times\;&\left\{g_1^2 e^{-i(\nu_2-\nu_3)r_1}\left[\frac{M_1(\nu_2)e^{i\nu_1(r_1-r_2)}-M_1(\nu_3)e^{i\nu_4(r_1-r_2)}}{\nu_1-\nu_4}-M_1(\nu_2)M_1(\nu_3)e^{i(E-\alpha_1)(r_1-r_2)}\right]\right.\\
&\left.+g_2^2 e^{-i(\nu_2-\nu_3)r_2}\left[\frac{M_2(\nu_2)e^{i\nu_1(r_1-r_2)}-M_2(\nu_3)e^{i\nu_4(r_1-r_2)}}{\nu_1-\nu_4}-M_2(\nu_2)M_2(\nu_3)e^{i(E-\alpha_2)(r_1-r_2)}\right]\right\}.
\end{aligned}
$$

The whole diagram amounts to

$$
\begin{aligned}
&g_1^2 g_2^2 a_{\nu_1}^\dagger a_{\nu_2}^\dagger a_{\nu_3}a_{\nu_4}\\
\times\;&\left\{[S_1(\nu_2)-1]M_2(\nu_4)\frac{M_1(\nu_1)e^{-i(\nu_1-\nu_3)(r_1-r_2)}}{\nu_1-\nu_3}+[S_1(\nu_1)-1]M_2(\nu_3)\frac{M_1(\nu_4)}{\nu_1-\nu_3}\right.\\
&+M_1(\nu_1)M_2(\nu_4)[S_1(\nu_2)-1]M_1(\nu_3)e^{i(\nu_3-\alpha_1)(r_1-r_2)}\\
&+M_1(\nu_2)[S_2(\nu_4)-1]\frac{M_2(\nu_1)}{\nu_1-\nu_3}+M_1(\nu_1)[S_2(\nu_3)-1]\frac{M_2(\nu_4)e^{-i(\nu_1-\nu_3)(r_1-r_2)}}{\nu_1-\nu_3}\\
&\left.+M_1(\nu_1)M_2(\nu_4)M_2(\nu_2)[S_2(\nu_3)-1]e^{i(\nu_2-\alpha_2)(r_1-r_2)}\right\}. \qquad (15.104)
\end{aligned}
$$

The second possibility to generate a double vertex is provided by two photon lines covering the second and the third vertices, respectively, and at the same time intersecting each other (lower panel of of Fig. 15.5). The corresponding expression reads

$$
\begin{aligned}
&\left(g_1\sigma_+^{(1)}a_\nu e^{i\nu r_1}\right)G\left(g_1\sigma_-^{(1)}a_{\nu_2}^\dagger e^{-i\nu_2 r_1}\right)G\left(g_1\sigma_+^{(1)}a_\mu e^{i\mu r_1}\right)\\
\times\;& G\left(g_2\sigma_-^{(2)}a_\nu^\dagger e^{-i\nu r_2}\right)G\left(g_2\sigma_+^{(2)}a_{\nu_3}e^{i\nu_3 r_2}\right)G\left(g_2\sigma_-^{(2)}a_\mu^\dagger e^{-i\mu r_2}\right)\\
=\;& g_1^3 g_2^3 \sigma_+^{(1)}\sigma_-^{(2)}\overbrace{a_\nu G_{--}a_{\nu_2}^\dagger G_{+-}\overbrace{a_\mu G_{--}a_\nu^\dagger} G_{-+}a_{\nu_3}G_{--}a_\mu^\dagger} e^{i\nu(r_1-r_2)}e^{i\mu(r_1-r_2)}e^{-i\nu_2 r_1+i\nu_3 r_2}\\
=\;& -g_1^3 g_2^3 e^{-i\nu_2 r_1+i\nu_3 r_2}\sigma_+^{(1)}\sigma_-^{(2)}a_{\nu_2}^\dagger a_{\nu_3}\\
\times\;&\int d\nu\int d\mu\frac{e^{i\nu(r_1-r_2)}e^{i\mu(r_1-r_2)}}{(\nu-\nu_1-i\eta)(\nu-E+\alpha_1)(\nu+\mu-E-i\eta)(\mu-E+\alpha_2)(\mu-\nu_4-i\eta)}. \qquad (15.105)
\end{aligned}
$$

Let us first evaluate the integral over μ

$$
\begin{aligned}
&\int d\mu\frac{e^{i\mu(r_1-r_2)}}{(\nu+\mu-E-i\eta)(\mu-E+\alpha_2)(\mu-\nu_4-i\eta)}\\
=\;& 2\pi i\left[\frac{e^{i(E-\nu)(r_1-r_2)}}{(-\nu+\nu_2)(\nu_3-\nu)}+\frac{e^{i(E-\alpha_2)(r_1-r_2)}}{(\nu-\alpha_2)(\nu_3-\alpha_2)}+\frac{e^{i\nu_4(r_1-r_2)}}{(\nu-\nu_3)(-\nu_3+\alpha_2)}\right]\\
=\;& 2\pi i e^{i(E-\nu)(r_1-r_2)}M_2(\nu_3)\left[\frac{1-e^{i(\nu-\nu_3)(r_1-r_2)}}{\nu-\nu_3}-\frac{1-e^{i(\nu-\alpha_2)(r_1-r_2)}}{\nu-\alpha_2}\right]. \qquad (15.106)
\end{aligned}
$$

Now we have to perform integration over ν. Note that there is no pole at $\nu=\nu_3$ and $\nu=\alpha_2$. Collecting the contributions from the poles at $\nu=\nu_1+i\eta$ and $\nu=E-\alpha_1$, we cast (15.105) to

$$
\begin{aligned}
&(2\pi i)^2 g_1^3 g_2^3 e^{i\nu_1 r_1-i\nu_4 r_2}\sigma_+^{(1)}\sigma_-^{(2)}a_{\nu_2}^\dagger a_{\nu_3}M_2(\nu_3)M_1(\nu_2)\\
\times\;&\left\{\frac{1-e^{i(\nu_1-\nu_3)(r_1-r_2)}}{\nu_1-\nu_3}+\frac{1-e^{i(E-\alpha_1-\alpha_2)(r_1-r_2)}}{E-\alpha_1-\alpha_2}\right.\\
&\left.-M_2(\nu_1)[1-e^{i(\nu_1-\alpha_2)(r_1-r_2)}]-M_1(\nu_4)[1-e^{i(\nu_4-\alpha_1)(r_1-r_2)}]\right\}. \qquad (15.107)
\end{aligned}
$$

The whole diagram with this vertex amounts to

$$\begin{aligned}
& (2\pi i)^2 g_1^4 g_2^4 P_{--} a^\dagger_{\nu_1} a^\dagger_{\nu_2} a_{\nu_3} a_{\nu_4} M_1(\nu_1) M_2(\nu_3) M_1(\nu_2) M_2(\nu_4) \\
\times \quad & \left\{ \frac{1 - e^{i(\nu_1-\nu_3)(r_1-r_2)}}{\nu_1 - \nu_3} + \frac{1 - e^{i(E-\alpha_1-\alpha_2)(r_1-r_2)}}{E - \alpha_1 - \alpha_2} \right. \\
& \left. - M_2(\nu_1)[1 - e^{i(\nu_1-\alpha_2)(r_1-r_2)}] - M_1(\nu_4)[1 - e^{i(\nu_4-\alpha_1)(r_1-r_2)}] \right\} \\
= \quad & g_1^2 g_2^2 P_{--} a^\dagger_{\nu_1} a^\dagger_{\nu_2} a_{\nu_3} a_{\nu_4} \left\{ -M_1(\nu_2) M_2(\nu_4) [S_1(\nu_1) - 1][S_2(\nu_3) - 1] \frac{1 - e^{-i(\nu_1-\nu_3)(r_1-r_2)}}{\nu_1 - \nu_3} \right. \\
& + M_1(\nu_1)[S_2(\nu_3) - 1][S_1(\nu_2) - 1] M_2(\nu_4) \frac{1 - e^{i(E-\alpha_1-\alpha_2)(r_1-r_2)}}{E - \alpha_1 - \alpha_2} \\
& - [S_1(\nu_2) - 1][S_2(\nu_3) - 1] M_1(\nu_1) M_2(\nu_4) M_2(\nu_2)[1 - e^{i(\nu_2-\alpha_2)(r_1-r_2)}] \\
& \left. - M_1(\nu_1) M_2(\nu_4)[S_1(\nu_2) - 1][S_2(\nu_3) - 1] M_1(\nu_3)[1 - e^{i(\nu_3-\alpha_1)(r_1-r_2)}] \right\}. \qquad (15.108)
\end{aligned}$$

Collecting all contributions to $T^{(2)}$, namely (15.102), (15.104), (15.108), and the terms $\sim g_1^4, g_2^4$ from (15.99), we obtain

$$\begin{aligned}
-2\pi i T^{(2)} \quad = \quad & -\frac{2\pi i}{\nu_1 - \nu_3} \left[g_1^4 M_1(\nu_1) M_1(\nu_4) S_2(\nu_4) + g_2^4 S_1(\nu_1) M_2(\nu_1) M_2(\nu_4) \right] \\
- \quad & 2\pi i g_1^2 g_2^2 \left\{ [S_1(\nu_1) - 1] M_2(\nu_3) \frac{M_1(\nu_4)}{\nu_1 - \nu_3} + M_1(\nu_2)[S_2(\nu_4) - 1] \frac{M_2(\nu_1)}{\nu_1 - \nu_3} \right. \\
& - M_1(\nu_2) M_2(\nu_4)[S_1(\nu_1) - 1][S_2(\nu_3) - 1] \frac{1}{\nu_1 - \nu_3} \\
& + M_1(\nu_1)[S_2(\nu_3) - 1][S_1(\nu_2) - 1] M_2(\nu_4) \frac{1}{E - \alpha_1 - \alpha_2} \\
& - [S_1(\nu_2) - 1][S_2(\nu_3) - 1] M_1(\nu_1) M_2(\nu_4) M_2(\nu_2) \\
& \left. - M_1(\nu_1) M_2(\nu_4)[S_1(\nu_2) - 1][S_2(\nu_3) - 1] M_1(\nu_3) \right\}. \qquad (15.109)
\end{aligned}$$

One can observe the dependence on atomic coordinates has disappeared. Transforming $T^{(2)}$ further, we find

$$\begin{aligned}
-2\pi i T^{(2)} \quad = \quad & \frac{E - 2\alpha_2}{4\pi i} S_1(\nu_1) S_1(\nu_2) M_2(\nu_1) M_2(\nu_2)[S_2(\nu_4) - 1][S_2(\nu_3) - 1] \\
+ \quad & \frac{E - 2\alpha_1}{4\pi i} M_1(\nu_4) M_1(\nu_3)[S_1(\nu_2) - 1] S_2(\nu_4)[S_1(\nu_1) - 1] S_2(\nu_3) \\
- \quad & \frac{1}{2\pi i} [S_1(\nu_1) - 1][S_2(\nu_3) - 1][S_1(\nu_2) - 1][S_2(\nu_4) - 1] \frac{1}{E - \alpha_1 - \alpha_2}. \qquad (15.110)
\end{aligned}$$

This expression should be multiplied by $a^\dagger_{\nu_1} a^\dagger_{\nu_2} a_{\nu_3} a_{\nu_4}$. Then the irreducible part of $S^{(2)}$ equals

$$S^{(2)irred}_{p_1 p_2, k_1 k_2} = -2\pi i \delta_{p_1+p_2, k_1+k_2} \langle a_{p_2} a_{p_1} T^{(2)} a^\dagger_{k_1} a^\dagger_{k_2} \rangle. \qquad (15.111)$$

Note that if one of the atoms is decoupled (say, $g_2 = 0$), then $S_2 \equiv 1$, and one recovers from (15.110) the already known result for the two-photon scattering matrix on a single atom.

It now remains to evaluate a reducible contribution to the two-photon scattering. To this end we use an expression for $T^{(1)}$ and the δ-part of (15.102) and find that the corresponding expression factorizes into products

of the one-photon scattering matrices

$$\begin{aligned}
S^{(2)red}_{p_1p_2,k_1k_2} &= (\delta_{p_1k_1}\delta_{p_2k_2}+\delta_{p_1k_2}\delta_{p_2k_1})\left\{1-2\pi i\left[g_1^2M_1(p_2)+g_2^2M_2(p_2)-2\pi i g_1^2g_2^2M_1(p_2)M_2(p_2)\right]\right.\\
&\quad -2\pi i\left[g_1^2M_1(p_1)+g_2^2M_2(p_1)-2\pi i g_1^2g_2^2M_1(p_1)M_2(p_1)\right]\\
&\quad +\frac{1}{2}(2\pi i)^2\left[g_1^4M_1(p_1)M_1(p_2)S_2(p_2)+g_2^4S_1(p_1)M_2(p_1)M_2(p_2)\right]\\
&\quad +\frac{1}{2}(2\pi i)^2g_1^2g_2^2\left[M_1(p_1)M_2(p_2)+M_1(p_2)S_2(p_2)M_2(p_1)S_1(p_1)\right]\\
&\quad +\frac{1}{2}(2\pi i)^2\left[g_1^4M_1(p_2)M_1(p_1)S_2(p_1)+g_2^4S_1(p_2)M_2(p_2)M_2(p_1)\right]\\
&\quad \left.+\frac{1}{2}(2\pi i)^2g_1^2g_2^2\left[M_1(p_2)M_2(p_1)+M_1(p_1)S_2(p_1)M_2(p_2)S_1(p_2)\right]\right\}\\
&= \frac{1}{2}(\delta_{p_1k_1}\delta_{p_2k_2}+\delta_{p_1k_2}\delta_{p_2k_1})\left\{2+\right.\\
&\quad +2(S_1(p_2)-1)+2(S_2(p_2)-1)+2[S_1(p_2)-1][S_2(p_2)-1]\\
&\quad +2(S_1(p_1)-1)+2(S_2(p_1)-1)+2[S_1(p_1)-1][S_2(p_1)-1]\\
&\quad +[S_1(p_1)-1][S_1(p_2)-1]S_2(p_2)+S_1(p_1)[S_2(p_1)-1][S_2(p_2)-1]\\
&\quad +[S_1(p_1)-1][S_2(p_2)-1]+[S_1(p_2)-1]S_2(p_2)[S_2(p_1)-1]S_1(p_1)\\
&\quad +[S_1(p_2)-1][S_1(p_1)-1]S_2(p_1)+S_1(p_2)[S_2(p_2)-1][S_2(p_1)-1]\\
&\quad \left.+[S_1(p_2)-1][S_2(p_1)-1]+[S_1(p_1)-1]S_2(p_1)[S_2(p_2)-1]S_1(p_2)\right\}\\
&= (\delta_{p_1k_1}\delta_{p_2k_2}+\delta_{p_1k_2}\delta_{p_2k_1})S_1(p_1)S_2(p_1)S_2(p_2)S_1(p_2)=S^{(1)}_{p_1k_1}S^{(1)}_{p_2k_2}+S^{(1)}_{p_1k_2}S^{(1)}_{p_2k_1}. \qquad (15.112)
\end{aligned}$$

Let us now prove that the two-photon scattering matrix on two atoms can be represented as a convolution of the two-photon scattering matrices on individual atoms, that is

$$\begin{aligned}
S^{(2)}_{p_1p_2,k_1k_2} &\stackrel{!}{=} \frac{1}{2!}\int dk_1'dk_2'S^{(2)}_{2;p_1p_2,k_1'k_2'}S^{(2)}_{1;k_1'k_2',k_1k_2}\\
&= \frac{1}{2!}\int dk_1'dk_2'\left(S^{(1)}_{2;p_1k_1'}S^{(1)}_{2;p_2k_2'}+S^{(1)}_{2;p_2k_1'}S^{(1)}_{2;p_1k_2'}+i\mathcal{T}^{(2)}_{2;p_1p_2,k_1'k_2'}\right)\\
&\quad \times\left(S^{(1)}_{1;k_1'k_1}S^{(1)}_{1;k_2'k_2}+S^{(1)}_{1;k_1'k_2}S^{(1)}_{1;k_2'k_1}+i\mathcal{T}^{(2)}_{1;k_1'k_2',k_1k_2}\right)\\
&= (\delta_{p_1k_1}\delta_{p_2k_2}+\delta_{p_1k_2}\delta_{p_2k_1})S_2(p_1)S_2(p_2)S_1(p_1)S_1(p_2)\\
&+ S_2(p_1)S_2(p_2)i\mathcal{T}_{1;p_1p_2,k_1k_2}+S_1(k_1)S_1(k_2)i\mathcal{T}_{2;p_1p_2,k_1k_2}\\
&- \frac{1}{2}\int dk_1'dk_2'\mathcal{T}^{(2)}_{2;p_1p_2,k_1'k_2'}\mathcal{T}^{(2)}_{1;k_1'k_2',k_1k_2}. \qquad (15.113)
\end{aligned}$$

The first term is obviously equal to the reducible contribution (15.112). Let us now show that the second and the third terms together yield $S^{(2)irred}_{p_1p_2,k_1k_2}$. We get

$$\begin{aligned}
&4\delta_{p_1+p_2,k_1+k_2}\left[\frac{(2\pi ig_1^2)^2}{4\pi i}(E-2\alpha_1)M_1(p_1)M_1(p_2)M_1(k_1)M_1(k_2)S_2(p_1)S_2(p_2)\right.\\
&\left.+\frac{(2\pi ig_2^2)^2}{4\pi i}(E-2\alpha_2)M_2(p_1)M_2(p_2)M_2(k_1)M_2(k_2)S_1(k_1)S_1(k_2)\right]\\
&-\frac{1}{2}(4\pi)^2g_1^4g_2^4\delta_{p_1+p_2,k_1+k_2}(E-2\alpha_1)(E-2\alpha_2)M_2(p_1)M_2(p_2)M_1(k_1)M_1(k_2)\\
&\times\int dk_1'M_2(k_1')M_2(E-k_1')M_1(k_1')M_1(E-k_1'). \qquad (15.114)
\end{aligned}$$

Evaluating the last integral we find

$$\int dk_1'M_2(k_1')M_2(E-k_1')M_1(k_1')M_1(E-k_1')=-\frac{4\pi i}{(E-\alpha_1-\alpha_2)(E-2\alpha_1)(E-2\alpha_2)}, \qquad (15.115)$$

and therefore

$$\begin{aligned}
&4\delta_{p_1+p_2,k_1+k_2}\left[\frac{(2\pi ig_1^2)^2}{4\pi i}(E-2\alpha_1)M_1(p_1)M_1(p_2)M_1(k_1)M_1(k_2)S_2(p_1)S_2(p_2)\right.\\
&+\frac{(2\pi ig_2^2)^2}{4\pi i}(E-2\alpha_2)M_2(p_1)M_2(p_2)M_2(k_1)M_2(k_2)S_1(k_1)S_1(k_2)\\
&\left.-\frac{(2\pi ig_1^2)^2(2\pi ig_2^2)^2}{2\pi i}\delta_{p_1+p_2,k_1+k_2}\frac{M_2(p_1)M_2(p_2)M_1(k_1)M_1(k_2)}{E-\alpha_1-\alpha_2}\right]=S^{(2)irred}_{p_1p_2,k_1k_2}, \qquad (15.116)
\end{aligned}$$

which reproduces the result contained in Eqs. (15.110) and (15.111).

Note that the sequence of S_1 and S_2 in the convolution (15.113) corresponds to the order in which the right-moving photons encounter the atoms 1 and 2 along the line of propagation. The presence of the irreducible part $\mathcal{T}^{(2)}$ in the two-photon scattering makes the convolution (15.113) noncommutative $S_2^{(2)} * S_1^{(2)} \neq S_1^{(2)} * S_2^{(2)}$, in contrast to the case of single-photon scattering (15.68), where the scattering is commutative, $S_2^{(1)} * S_1^{(1)} = S_1^{(1)} * S_2^{(1)}$.

The result (15.110)-(15.112) generalizes the corresponding expressions of Ref. [9] to arbitrary coupling strengths $g_1 \neq g_2$. Being equipped with the convolution property, one can write down as well an expression for the two-photon scattering on M emitters with different g_i's.

The calculations outlined above allows us to make the following general statement: the two-particle scattering matrix on an array of distributed emitters is a momentum space convolution of scattering matrices on individual emitters. This property has a deep reason: the absence of backscattering for unidirectionally propagating photons. Therefore, it is expected to hold also in arbitrary N-photon sector of scattering.

15.5 Coherent light scattering

In this section we consider scattering of coherent light off a single two-level emitter. The aim of this calculation is twofold: at first, we describe the certain physical situation relevant for a discussion of the resonant fluorescence [17] in nanostructures, and, at second, we provide a generating functional for a N-particle scattering matrix.

We start from introducing operators of photons propagating inside a waveguide of a finite length L

$$c_k = \frac{1}{\sqrt{2\pi}} \int_{-L/2}^{L/2} dx a(x) e^{-ikx}, \quad c_k^\dagger = \frac{1}{\sqrt{2\pi}} \int_{-L/2}^{L/2} dx a^\dagger(x) e^{ikx}, \tag{15.117}$$

where $a(x)$ and $a^\dagger(x)$ are the Fourier transforms of the operators a_k and $a_k^\dagger$

$$a(x) = \frac{1}{\sqrt{2\pi}} \int dk a_k e^{ikx}, \quad a^\dagger(x) = \frac{1}{\sqrt{2\pi}} \int dk a_k^\dagger e^{-ikx}. \tag{15.118}$$

The construction (15.117) explicitly containing the finite length L is very useful as it allows for a treatment of different limits such as a finite photon number limit ($\bar{N} \equiv |\alpha_k|^2$=const, $L \to \infty$) and a finite photon density limit ($\bar{N}/L$=const at $\bar{N}, L \to \infty$).

The operators (15.117) obey the commutation relations

$$\left[c_k, c_p^\dagger\right] = \left[c_k, a_p^\dagger\right] = \left[a_p, c_k^\dagger\right] = \frac{1}{2\pi i} \frac{e^{i(k-p)L/2} - e^{-i(k-p)L/2}}{k-p} \equiv \delta_\Delta(k-p), \tag{15.119}$$

$$\left[a(x), c_k^\dagger\right] = \frac{e^{ikx}}{\sqrt{2\pi}} \Theta(-L/2 < x < L/2). \tag{15.120}$$

where $\delta_\Delta(k-p)$ is a delta function broadened by $\Delta \equiv 2\pi/L$ and reaching the peak value $1/\Delta$ at $k = p$. An expression of the operator c_k in terms of a_k is given by

$$c_k = \int dp a_p \delta_\Delta(p-k). \tag{15.121}$$

As an initial state we choose a coherent state in the mode k

$$|\alpha_k\rangle = e^{-|\alpha_k|^2/2} \sum_{n_k=0}^{\infty} \left(\frac{2\pi}{L}\right)^{n_k/2} \frac{\alpha_k^{n_k} (c_k^\dagger)^{n_k}}{n_k!} |0\rangle = e^{-|\alpha_k|^2/2} \sum_{n_k=0}^{\infty} \frac{\alpha_k^{n_k}}{\sqrt{n_k!}} |n_k\rangle. \tag{15.122}$$

This state is normalized to unity, which is ensured by the finite waveguide's length L. It is a superposition of Fock states with different numbers of photons n_k, and therefore we introduce an operator O which projects on-shell and accounts for the energy conservation in each photons' number sector. An outgoing state after the scattering off a two-level system is thus obtained by applying the operator O followed by an action of the T-matrix, as prescribed by (15.19),

$$\begin{aligned}
|\beta_k\rangle &= (1 - 2\pi i T O)|\alpha_k\rangle = |\alpha_k\rangle - 2\pi i e^{-|\alpha_k|^2/2} \sum_{n_k=1}^{\infty} \left(\frac{2\pi}{L}\right)^{n_k/2} \alpha_k^{n_k} \sum_{n=1}^{n_k} g^{2n} \int \left(\prod_{i=1}^{n} dq_i dp_i\right) \delta\left(\sum_{i=1}^{n} p_i - \sum_{i=1}^{n} q_i\right) \\
&\times a_{p_1}^\dagger \frac{1}{kn_k - H_b - \alpha} a_{q_1} \frac{1}{kn_k - H_b + i\eta} \dots a_{p_n}^\dagger \frac{1}{kn_k - H_b - \alpha} a_{q_n} \frac{(c_k^\dagger)^{n_k}}{n_k!} |0\rangle \qquad (15.123) \\
&= |\alpha_k\rangle - 2\pi i e^{-|\alpha_k|^2/2} \sum_{n_k=1}^{\infty} \left(\frac{2\pi}{L}\right)^{n_k/2} \alpha_k^{n_k} \sum_{n=1}^{n_k} \frac{(c_k^\dagger)^{n_k-n}}{(n_k-n)!} g^{2n} \int \left(\prod_{i=1}^{n} dq_i dp_i\right) \delta\left(\sum_{i=1}^{n} (p_i - q_i)\right) \left(\prod_{i=1}^{n} \delta_\Delta(q_i - k)\right) \\
&\times a_{p_1}^\dagger \frac{1}{[q_1 + \sum_{i=2}^{n}(q_i - p_i) - \alpha][\sum_{i=2}^{n}(q_i - p_i) + i\eta]} a_{p_2}^\dagger \dots a_{p_{n-1}}^\dagger \frac{1}{[q_{n-1} + q_n - p_n - \alpha][q_n - p_n + i\eta]} a_{p_n}^\dagger \frac{1}{q_n - \alpha} |0\rangle.
\end{aligned}$$

Exchanging the order of summations $\sum_{n_k=1}^{\infty}\sum_{n=1}^{n_k}=\sum_{n=1}^{\infty}\sum_{n_k=n}^{\infty}$ and shifting $n_k\to n_k+n$ we find

$$
\begin{aligned}
|\beta_k\rangle &= |\alpha_k\rangle - 2\pi i e^{-|\alpha_k|^2/2}\sum_{n=1}^{\infty}\sum_{n_k=0}^{\infty}\left(\frac{2\pi}{L}\right)^{(n_k+n)/2}\alpha_k^{n_k+n}\frac{(c_k^\dagger)^{n_k}}{n_k!}g^{2n}\int\left(\prod_{i=1}^{n}dq_i dp_i\right)\delta\left(\sum_{i=1}^{n}(p_i-q_i)\right)\left(\prod_{i=1}^{n}\delta_\Delta(q_i-k)\right)\\
&\times\ a_{p_1}^\dagger\frac{1}{[q_1+\sum_{i=2}^{n}(q_i-p_i)-\alpha][\sum_{i=2}^{n}(q_i-p_i)+i\eta]}a_{p_2}^\dagger\ldots a_{p_{n-1}}^\dagger\frac{1}{[q_{n-1}+q_n-p_n-\alpha][q_n-p_n+i\eta]}a_{p_n}^\dagger\frac{1}{q_n-\alpha}|0\rangle\\
&= |\alpha_k\rangle - 2\pi i\sum_{n=1}^{\infty}\left(\frac{2\pi}{L}\right)^{n/2}\alpha_k^n g^{2n}\int\left(\prod_{i=1}^{n}dq_i dp_i\right)\delta\left(\sum_{i=1}^{n}(p_i-q_i)\right)\left(\prod_{i=1}^{n}\delta_\Delta(q_i-k)\right) \qquad (15.124)\\
&\times\ a_{p_1}^\dagger\frac{1}{[q_1+\sum_{i=2}^{n}(q_i-p_i)-\alpha][\sum_{i=2}^{n}(q_i-p_i)+i\eta]}a_{p_2}^\dagger\ldots a_{p_{n-1}}^\dagger\frac{1}{[q_{n-1}+q_n-p_n-\alpha][q_n-p_n+i\eta]}a_{p_n}^\dagger\frac{1}{q_n-\alpha}|\alpha_k\rangle.
\end{aligned}
$$

Let us now consider the state

$$
\begin{aligned}
|\gamma_k^{(n)}\rangle &= \int dp_1\ldots dp_n\int dq_1\ldots dq_n\delta\left(\sum_{i=1}^{n}(p_i-q_i)\right)\left(\prod_{i=1}^{n}\delta_\Delta(q_i-k)\right) \qquad (15.125)\\
&\times\ \frac{1}{[q_1+\sum_{i=2}^{n}(q_i-p_i)-\alpha][\sum_{i=2}^{n}(q_i-p_i)+i\eta]}\cdots\frac{1}{[q_{n-1}+q_n-p_n-\alpha][q_n-p_n+i\eta]}\frac{1}{q_n-\alpha}a_{p_1}^\dagger\ldots a_{p_n}^\dagger|\alpha_k\rangle.
\end{aligned}
$$

Performing the inverse Fourier transformation [cf. (15.118)]

$$
a_{p_i}^\dagger=\frac{1}{\sqrt{2\pi}}\int dx_i a^\dagger(x_i)e^{ip_i x_i}, \qquad (15.126)
$$

and substituting it into (15.125), we obtain

$$
\begin{aligned}
|\gamma_k^{(n)}\rangle &= \frac{1}{(2\pi)^{n/2}}\int dx_1\ldots dx_n\int dp_1\ldots dp_n\int dq_1\ldots dq_n\delta\left(\sum_{i=1}^{n}(p_i-q_i)\right)\left(\prod_{i=1}^{n}\delta_\Delta(q_i-k)\right)\\
&\times\ \frac{1}{[q_1+\sum_{i=2}^{n}(q_i-p_i)-\alpha][\sum_{i=2}^{n}(q_i-p_i)+i\eta]}\cdots\frac{1}{[q_{n-1}+q_n-p_n-\alpha][q_n-p_n+i\eta]}\frac{1}{q_n-\alpha}\\
&\times\ e^{ip_1x_1+\ldots+ip_nx_n}a^\dagger(x_1)\ldots a^\dagger(x_n)|\alpha_k\rangle. \qquad (15.127)
\end{aligned}
$$

Introducing new variables $P_j=\sum_{i=j}^{n}p_i$ and $Q_j=\sum_{i=j}^{n}q_i$, such that $p_i=P_i-P_{i+1}$ and $q_i=Q_i-Q_{i+1}$, we cast (15.127) to

$$
\begin{aligned}
|\gamma_k^{(n)}\rangle &= \frac{1}{(2\pi)^{n/2}}\int dx_1\ldots dx_n\int dP_1\ldots dP_n\int dq_1\ldots dq_n\delta\left(P_1-Q_1\right)\left(\prod_{i=1}^{n}\delta_\Delta(q_i-k)\right)\\
&\times\ e^{i(P_1-P_2)x_1}\frac{1}{[Q_1-P_2-\alpha][Q_2-P_2+i\eta]}\cdots\frac{1}{[Q_{n-1}-P_n-\alpha][Q_n-P_n+i\eta]}e^{iP_nx_n}\frac{1}{Q_n-\alpha}\\
&\times\ a^\dagger(x_1)\ldots a^\dagger(x_n)|\alpha_k\rangle \qquad (15.128)\\
&= \frac{1}{(2\pi)^{n/2}}\int dx_1\ldots dx_n\int dq_1\ldots dq_n\left(\prod_{i=1}^{n}\delta_\Delta(q_i-k)\right)e^{iQ_1x_1}\frac{1}{Q_n-\alpha}\\
&\times\ \left(\int dP_2\frac{e^{-iP_2(x_1-x_2)}}{[Q_1-P_2-\alpha][Q_2-P_2+i\eta]}\right)\cdots\left(\int dP_n\frac{e^{-iP_n(x_{n-1}-x_n)}}{[Q_{n-1}-P_n-\alpha][Q_n-P_n+i\eta]}\right)a^\dagger(x_1)\ldots a^\dagger(x_n)|\alpha_k\rangle.
\end{aligned}
$$

Each integral over dP_j does not vanish, if one can close the contour of integration in the upper half plane. It is only possible for $\Delta x_j\equiv x_j-x_{j-1}>0$. Then we get

$$
\int dP_j\frac{e^{iP_j\Delta x_j}}{[Q_{j-1}-P_j-\alpha][Q_j-P_j+i\eta]}=\Theta(x_j-x_{j-1})2\pi i e^{iQ_j\Delta x_j}\frac{e^{i(q_{j-1}-\alpha)\Delta x_j}-1}{q_{j-1}-\alpha}, \qquad (15.129)
$$

and therefore

$$
\begin{aligned}
|\beta_k\rangle &= |\alpha_k\rangle + \sum_{n=1}^{\infty} \left(-2\pi i g^2 \bar{\alpha}_k\right)^n \int dx_1 \dots dx_n \int dq_1 \dots dq_n \left(\prod_{i=1}^{n} \delta_\Delta(q_i - k)\right) \Theta(x_n > \dots > x_1) \\
&\times e^{iq_1 x_1 + \dots + iq_n x_n} \frac{1}{q_n - \alpha} \prod_{j=2}^{n} \frac{1 - e^{i(q_{j-1} - \alpha)\Delta x_j}}{q_{j-1} - \alpha} a^\dagger(x_1) \dots a^\dagger(x_n) |\alpha_k\rangle \\
&= |\alpha_k\rangle + \sum_{n=1}^{\infty} \left(-2\pi i g^2 \bar{\alpha}_k\right)^n \int dx_1 \dots dx_n \Theta(x_n > \dots > x_1) \\
&\times \left(\int dq_n \frac{e^{iq_n x_n}}{q_n - \alpha} \delta_\Delta(q_n - k)\right) \left(\prod_{j=1}^{n-1} \int dq_j e^{iq_j x_j} \frac{1 - e^{i(q_j - \alpha)\Delta x_{j+1}}}{q_j - \alpha} \delta_\Delta(q_j - k)\right) a^\dagger(x_1) \dots a^\dagger(x_n) |\alpha_k\rangle
\end{aligned} \tag{15.130}
$$

where $\bar{\alpha}_k = \alpha_k / \sqrt{L}$.

It remains to evaluate integrals

$$
\begin{aligned}
&\int dq_j \frac{e^{iq_j x_j}}{q_j - \alpha} \delta_\Delta(q_j - k) = \frac{e^{ikx_j}}{4\pi i} \int dq_j \frac{e^{iq_j(x_j + L/2)} - e^{-iq_j(L/2 - x_j)}}{q_j + k - \alpha} \left[\frac{1}{q_j + i0^+} + \frac{1}{q_j - i0^+}\right] \\
&= \frac{1}{2} e^{ikx_j} \left[\frac{1}{k - \alpha} \Theta(x_j + L/2) + \left(\frac{2}{k - \alpha} e^{-i(k-\alpha)(x_j + L/2)} - \frac{1}{k - \alpha}\right) \Theta(-x_j - L/2)\right. \\
&\qquad \left. + \left(-\frac{2}{k - \alpha} e^{i(k-\alpha)(L/2 - x_j)} + \frac{1}{k - \alpha}\right) \Theta(L/2 - x_j) - \frac{1}{k - \alpha} \Theta(x_j - L/2)\right] \\
&= \frac{e^{ikx_j}}{k - \alpha} \left[1 - e^{i(k-\alpha)(L/2 - x_j)}\right] \Theta(-L/2 < x_j < L/2) \\
&+ \frac{e^{ikx_j}}{k - \alpha} \left[e^{-i(k-\alpha)(x_j + L/2)} - e^{i(k-\alpha)(L/2 - x_j)}\right] \Theta(x_j < -L/2)
\end{aligned} \tag{15.131}
$$

and

$$
\begin{aligned}
&-\int dq_j \frac{e^{iq_j x_j} e^{i(q_j - \alpha)\Delta x_{j+1}}}{q_j - \alpha} \delta_\Delta(q_j - k) = -e^{-i\alpha \Delta x_{j+1}} \int dq_j \frac{e^{iq_j x_{j+1}}}{q_j - \alpha} \delta_\Delta(q_j - k) \\
&= -e^{-i\alpha \Delta x_{j+1}} \frac{e^{ikx_{j+1}}}{k - \alpha} \left[1 - e^{i(k-\alpha)(L/2 - x_{j+1})}\right] \Theta(-L/2 < x_{j+1} < L/2) \\
&\quad -e^{-i\alpha \Delta x_{j+1}} \frac{e^{ikx_{j+1}}}{k - \alpha} \left[e^{-i(k-\alpha)(x_{j+1} + L/2)} - e^{i(k-\alpha)(L/2 - x_{j+1})}\right] \Theta(x_{j+1} < -L/2).
\end{aligned} \tag{15.132}
$$

Summing up the both terms (15.131) and (15.132) yields

$$
\begin{aligned}
&\Theta(x_{j+1} - x_j) \int dq_j \frac{e^{iq_j x_j} [1 - e^{i(q_j - \alpha)\Delta x_{j+1}}]}{q_j - \alpha} \delta_\Delta(q_j - k) \\
&= \Theta(-L/2 < x_j < x_{j+1} < L/2) \frac{e^{ikx_j}}{k - \alpha} \left[1 - e^{i(k-\alpha)\Delta x_{j+1}}\right] \\
&+ \Theta(x_j < -L/2 < x_{j+1} < L/2) \frac{e^{ikx_j}}{k - \alpha} \left[e^{-i(k-\alpha)(x_j + L/2)} - e^{i(k-\alpha)\Delta x_{j+1}}\right].
\end{aligned} \tag{15.133}
$$

Note that there is no contribution to (15.133) when both x_j and x_{j+1} are smaller than $-L/2$.

Thus, we finally obtain an expression for the state $|\beta_k\rangle$ which emerges after scattering of the initially prepared coherent state (15.122) off the two-level system

$$
\begin{aligned}
|\beta_k\rangle &= |\alpha_k\rangle + \sum_{n=1}^{\infty} \left(-\frac{2\pi i g^2 \bar{\alpha}_k}{k - \alpha}\right)^n \int dx_1 \dots dx_n e^{ik(x_1 + \dots + x_n)} \\
&\times \left[\Theta(L/2 > x_n > \dots > x_2 > x_1 > -L/2) \prod_{j=1}^{n} \left(1 - e^{i(k-\alpha)\Delta x_{j+1}}\right)\right. \\
&\quad \left. + \Theta(L/2 > x_n > \dots > x_2 > -L/2 > x_1) e^{-i(k-\alpha)(x_1 + L/2)} \left(1 - e^{i(k-\alpha)(x_2 + L/2)}\right) \prod_{j=2}^{n} \left(1 - e^{i(k-\alpha)\Delta x_{j+1}}\right)\right] \\
&\times a^\dagger(x_1) \dots a^\dagger(x_n) |\alpha_k\rangle,
\end{aligned} \tag{15.134}
$$

where $x_{n+1} \equiv L/2$.

The state (15.134) has a remarkable property: when two coordinates in the integrand approach each other, it vanishes. This property lies in the origin of antibunching of photons which is conventionally observed in the density-density correlation functions [17],[8]. An occurrence of the two contributions with $x_1 > -L/2$ and $x_1 < -L/2$ has been previously remarked in [8], both being important for a proper normalization of the state (15.134).

The explicit expression for the outgoing state (15.134) opens a possibility for a study of correlation functions as well as photons' statistics in all parametric regimes, which will be a subject of a subsequent publication [18].

15.6 Conclusions

We have developed the scattering approach to problems of propagating bosons in one dimensional geometry. We have derived the general form of the T-matrix (non-trivial part of the scattering matrix), Eq. (15.3), under the following assumptions about the spectrum of bosons: the spectrum is linear, chiral, and infinite. Our formalism is complimentary to the Bethe ansatz solutions [7] and to the traditional approaches based on the equations of motion.

We have applied the developed formalism to several specific examples including emitters with two- and three-level structures. The emitters can be either distributed across the 1D channel or concentrated in a tiny region of space. We have shown that the scattering results in projecting the state of the emitter onto the specific – dark – state which does not emit.

We have also shown that the one- and two-particle scattering matrices off two emitters can be represented as a convolution of scattering matrices corresponding to individual emitters. Hereby the microscopic properties of different emitters can vary (i.e. coupling constants to photons, detunings, level structure). We conjecture that this property generically holds for multi-emitter arrays as well as for the multiparticle scattering with $N > 2$ photons. We are going to elaborate more on these issues in future studies [18].

The developed approach can be applied to the arbitrary initial state, which can either conserve the particle number or not. In the case of number-conserving initial state, we observe the formation of photonic bound states, which is reflected in the emergence of a pole of the S-matrix involving in its argument an energy of more than one individual photon. In the case of the coherent light scattering, we clearly observe the fermionized behavior typical to the Tonks-Girardeau gas [19] discussed in the photonic context in [20].

16 Delayed Coherent Quantum Feedback

Delayed Coherent Quantum Feedback from a Scattering Theory and a Matrix Product State Perspective by Guimond, Pletyukhov et al.

Abstract

We study the scattering of photons propagating in a semi-infinite waveguide terminated by a mirror and interacting with a quantum emitter. This paradigm constitutes an example of coherent quantum feedback, where light emitted towards the mirror gets redirected back to the emitter. We derive an analytical solution for the scattering of two-photon states, which is based on an exact resummation of the perturbative expansion of the scattering matrix, in a regime where the time delay of the coherent feedback is comparable to the timescale of the quantum emitter's dynamics. We compare the results with numerical simulations based on matrix product state techniques simulating the full dynamics of the system, and extend the study to the scattering of coherent states beyond the low-power limit.

16.1 Introduction

One of the paradigmatic models in quantum optics consists of a quantum emitter coupled to a one-dimensional photonic waveguide. This forms the basic block for the description of more complex quantum optical systems such as quantum networks, where multiple emitters exchange quantum information via photons propagating in one-dimensional quantum channels. Recent experimental realizations in the optical domain include single atoms coupled to nanofibers [1] or nanostructured waveguides [2, 3], as well as artificial atoms such as quantum dots or color centers in diamond [4] embedded in photonic crystal waveguides [5, 6]. The same model also describes the physics of superconducting qubits coupled to microwave transmission lines [7, 8], and of systems where bosonic excitations other than photons are used, such as surface acoustic waves [9] or phonons in cold quantum gases [10].

From a theoretical point of view, the atom-photon interaction can often be treated in a Born-Markov approximation, and the description in terms of a master equation is excellent. However, many interesting problems require going beyond this Markovian paradigm [11, 12]. In particular, in the description of problems

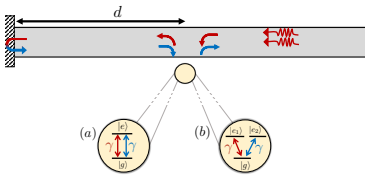

Figure 16.1: Schematic of the setup. Incoming photons scatter off of a quantum emitter coupled to a one-dimensional waveguide and located at a distance d from a mirror. We consider the following two examples. (a) The atom realizes a two-level system. (b) Chiral setup where the atom realizes a V-level system with one transition coupling to the waveguide modes propagating to the left and one transition coupling to the ones propagating to the right.

involving coherent quantum feedback the finite propagation speed of photons and the corresponding *time delays* invalidate one of the assumptions of a Markovian master equation treatment [13] by introducing an effective memory.

In recent years several theoretical methods have been developed to address different aspects of problems involving such time delays [14, 15, 16, 17, 18, 19, 20, 21, 22]. In particular, notable progress has been made in analyzing so-called *scattering problems*. There, one is interested in injecting (few) photons into a network of distributed passive emitters and characterizing the properties of transmitted and reflected photons. While this type of problems is well studied in the Markovian regime [23, 24, 25, 26], exact numerical and analytical solutions have been derived only recently for specific examples that include time delays [17, 18, 19]. These solutions are based on methods that are tailored to the scattering problem, such as a direct integration of the Lippmann-Schwinger equation or diagrammatic techniques. Due to the complexity increasing with the photon number, these approaches are however limited to incident states consisting of few-photon states.

In the present work we first apply these methods to study the two-photon scattering problem. The system we consider consists of a single quantum emitter coupled to a semi-infinite 1D waveguide terminated by a mirror, and constitutes a paradigmatic example of quantum feedback in a quantum optical system, where the photons emitted towards the mirror are redirected towards the emitter. The non-Markovian element is introduced here by the finite propagation time of the coherent feedback photons relative to the timescale of the emitter's dynamics. We present analytical and numerical solutions for different types of emitters. Explicitly we consider two types of emitters: a two-level system, and a V-level system where one transition couples only to the photons propagating towards the mirror while the other transition couples only to the ones propagating outwards. This assumes chiral (*i.e.* unidirectional) coupling between emitter and waveguide, as has been demonstrated in recent experiments with optical setups [1, 5]. Arguably, these two scenarios can be considered the most simple quantum optical examples exhibiting essential non-Markovian character due to time-delayed coherent feedback. The former because of the structure of the emitter, the latter because an incoming photon scattering on the emitter will necessarily undergo only a single roundtrip between the emitter and the mirror before leaving the system [27].

In a different approach, some of us have recently developed numerical techniques to describe the *full time-dependent dynamics* of photonic quantum networks with time delays [16]. This method makes use of matrix product state techniques [28, 29, 30, 31] to represent the entangled state of the propagating photons. Due to this efficient representation of the effective many-body Hilbert space these methods are not limited by the number of photons, and can be used to analyze systems where the photon number is not conserved. This includes the important case of coherent input fields, with a finite photon intensity. In this work we make use of these techniques to study the scattering of coherent states, beyond the low-power regime usually assumed when using analytical methods. Further we verify that simulations of two-photon state scattering yield results in agreement with the analytical predictions.

The paper is organized as follows. In section 16.2 we formally introduce our model and formulate the scattering problem. In section 16.3 we develop our analytical approach for the scattering of two-photon states, performing a resummation of the expansion of the scattering matrix. Section 16.4 provides details on the numerical approach. In section 16.5 we discuss the solutions obtained with both techniques. We present the solution of the two-photon scattering problem, and extend the study to coherent driving fields, discussing the limit in which an analytical approximation based on a truncation of the driving field to few-photon components captures the results.

16.2 Model

16.2.1 Hamiltonian

The system we consider is depicted in Fig. 16.1, where an atom as quantum emitter is coupled to a semi-infinite waveguide terminated by a mirror. The dynamics of the system of atom and waveguide is dictated by the Hamiltonian $H = H_a + H_B + V$ [14], where H_a is the free atomic Hamiltonian (discussed below),

$H_B = \int d\omega\, \omega\, b^\dagger(\omega) b(\omega)$ is the free waveguide Hamiltonian (in units with $\hbar = 1$), and

$$V = i\sqrt{\gamma/2\pi} \int d\omega \big(b^\dagger(\omega)(\sigma_1 e^{i\omega\tau/2} - \sigma_2 e^{-i\omega\tau/2}) - \text{H.C.} \big), \tag{16.1}$$

describes the coupling of the atom to the waveguide. Here the integrals run over a broad bandwidth around a characteristic optical frequency $\bar{\omega}$ close to the frequencies of the scattered photons and the atomic transitions. The operator $b^\dagger(\omega)$ is the creation operator for a photon with frequency ω in the waveguide, satisfying $[b(\omega), b^\dagger(\omega')] = \delta(\omega - \omega')$, and σ_1 and σ_2 are the atomic transition operators coupling to left and right moving photons respectively [16]. The finite time delay of the coherent feedback $\tau = 2d/c > 0$ introduces frequency-dependent phase factors in the coupling strength. The interaction Hamiltonian (16.1) assumes a linear dispersion relation $\omega(k) \approx c|k|$ over the relevant bandwidth, with the speed of light in the waveguide denoted by c and the distance of the atom to the mirror by d. The opposite sign in the coupling to left- and right-moving photons accounts for the π-shift in the phase of the photons reflected by the mirror. We also made use of the rotating wave approximation (RWA) and considered the absolute values of the coupling strengths, γ, to be independent of the frequency in the relevant bandwidth. Moreover, we neglect waveguide losses and couplings of the atom to modes outside of the waveguide.

We consider two examples for the atomic structure and its coupling to the waveguide. First, we consider an atom that is described by a two-level system (TLS) with ground state $|g\rangle$ and excited state $|e\rangle$ (see Fig. 16.1(a)). We naturally assume that this two-level system couples equally to both left and right moving photons. In this case, the atomic operators are given by $\sigma_1 = \sigma_2 = |g\rangle\langle e|$ and $H_a = \omega_a |e\rangle\langle e|$, where ω_a is the two-level transition frequency. Since the excited state $|e\rangle$ can decay by emission of photons into both directions, its total decay rate is 2γ (in the absence of the mirror). In the second example, the atomic level structure is represented by a V-level system with ground state $|g\rangle$ and excited states $|e_1\rangle$ and $|e_2\rangle$ (see Fig. 16.1(b)). In this case the atomic operators are defined as $\sigma_1 = |g\rangle\langle e_1|, \sigma_2 = |g\rangle\langle e_2|$ and $H_a = \omega_1 |e_1\rangle\langle e_1| + \omega_2 |e_2\rangle\langle e_2|$, where $\omega_{1,2}$ is the frequency of each atomic transition. Note that in this example photons emitted from the atom in state $|e\rangle_1$ propagate towards the mirror, while photons emitted from state $|e_2\rangle$ propagate away from the mirror, as realized by a chiral coupling [32]. Thus, in this case both excited states decay with a rate γ (in the absence of the mirror). In the following we will use a generic notation for these two examples, denoting the excited states as $|e_\chi\rangle$, with χ labelling the transitions, and writing the Hamiltonian as $H_a = \sum_\chi \omega_\chi |e_\chi\rangle\langle e_\chi|$.

For convenience we move to a frame rotating with the characteristic frequency $\bar{\omega}$. In addition we rescale the photon frequencies as $\omega - \bar{\omega} \to \nu$, and correspondingly redefine $b(\omega) \to b(\nu)$. In this frame the free Hamiltonians for the atom and the waveguide now read

$$H_a = -\sum_\chi \delta_\chi |e_\chi\rangle\langle e_\chi| \text{ and } H_B = \int d\nu\, \nu\, b^\dagger(\nu) b(\nu), \tag{16.2}$$

where the detuning is $\delta_\chi = \bar{\omega} - \omega_\chi$ and the interaction Hamiltonian reads

$$V = i\sqrt{\gamma/2\pi} \int d\nu \big(b^\dagger(\nu)(\sigma_1 e^{i(\bar{\omega}+\nu)\tau/2} - \sigma_2 e^{-i(\bar{\omega}+\nu)\tau/2}) - \text{H.C.} \big). \tag{16.3}$$

We can identify two physically relevant dimensionless quantities characterizing the delayed interactions in this system. These are the delay-bandwidth product $\gamma\tau$, quantifying the degree of non-Markovianity, and the roundtrip propagation phase that a photon acquires when traveling from the atom to the mirror and back, $\phi \equiv \bar{\omega}\tau + \pi$ (modulo 2π).

16.2.2 Scattering problem

In the scattering problem we consider a state $|\Psi_i\rangle$ of free incident photons propagating in the waveguide towards the quantum emitter that is initially in the ground state. After the interaction with the emitter, the photons are scattered back into the waveguide in a final state $|\Psi_f\rangle$ with the emitter returning to its initial state. The goal is then to calculate this output state, *i.e.* the *scattering operator* S, with $|\Psi_f\rangle = S|\Psi_i\rangle$. Its matrix elements are typically computed in the eigenbasis of H_B, which is the basis of states with definite photon numbers and frequencies and corresponding to infinitely extended wave packets. In practice we approximate an incident photon of a given frequency ν_1 by a wave packet with a finite length L, e.g. by the square pulse with spectrum

$$\phi_{\nu_1}(\nu) = \sqrt{\frac{2c}{\pi L}} \frac{\sin((\nu - \nu_1)L/2c)}{\nu - \nu_1}, \tag{16.4}$$

which approaches $\sqrt{\frac{2\pi c}{L}}\delta(\nu - \nu_1)$ for L large. For the scattering of incoming states consisting of two such photons with frequency ν_1, the initial state is of the form $|\Psi_i\rangle = \frac{1}{\sqrt{2}}\big(\int d\nu \phi_{\nu_1}(\nu) b^\dagger(\nu)\big)^2 |g, \text{vac}\rangle$, where $|g, \text{vac}\rangle$ corresponds to the ground state for the emitter and the vacuum state for the waveguide. Due to the fact that the number of excitations is conserved by the Hamiltonian in the RWA, the final state then also consists of two photons in the waveguide.

16.3 Scattering theory approach

16.3.1 Scattering matrix

In the interaction picture with $H_0 \equiv H_a + H_B$, the unitary evolution from time t' to t is given by the operator

$$U(t,t') = \mathcal{T}\exp\Big(-i\int_{t'}^{t} dt'' V(t'')\Big), \tag{16.5}$$

where $\mathcal{T}$ denotes the time-ordering superoperator, and $V(t) = e^{iH_0 t} V e^{-iH_0 t}$. The scattering operator is then defined as $S \equiv \lim_{t\to\infty} U(t,-t)$. This scattering operator is conveniently expressed as [33]

$$S = \mathbb{1} - 2\pi i\, \delta(E_f - E_i)\, T(E_i). \tag{16.6}$$

Here E_i and E_f are the energies of the initial and final state, *i.e.* $H_0 |\psi_i\rangle = E_i |\psi_i\rangle$ and $H_0 |\psi_f\rangle = E_f |\psi_f\rangle$. The $\delta-$function ensures energy conservation in the scattering process. The first term in (16.6) describes the free evolution, while the interacting part is contained in the *T-operator* $T(E)$, which is defined with the infinite perturbative series

$$T(E) = \sum_{n=0}^{\infty} V\left(\frac{1}{E - H_0 + i\eta} V\right)^n \tag{16.7}$$

with $\eta = 0^+$ and V given in (16.3). Since we consider problems with a conserved number of excitations, we can decompose the scattering operator into a direct sum $S = \bigoplus_{N=0}^{\infty} S^{(N)}$, where each term $S^{(N)}$ acts solely in the corresponding N-photon subspace. Analogously we can decompose $T(E) = \bigoplus_{N=0}^{\infty} T^{(N)}(E)$. Below we explicitly calculate analytical expressions for matrix elements of $T^{(1)}(E)$ and $T^{(2)}(E)$. To keep notation in the following derivation as compact as possible we abbreviate the interaction Hamiltonian by $V = b_\nu^\dagger v_\nu + v_\nu^\dagger b_\nu$, where $b_\nu \equiv b(\nu)$, and $v_\nu = i\sqrt{\gamma/2\pi}(\sigma_1 e^{i(\bar\omega+\nu)\tau/2} - \sigma_2 e^{-i(\bar\omega+\nu)\tau/2})$ is the bare interaction vertex. The integration over repeated ν is implicit.

Single-photon subspace.

We first start with the simpler case of a single-photon scattering ($N = 1$). Using the expansion (16.7), we can calculate all matrix elements in this sector as

$$\begin{aligned}
\langle g,\nu_1'|\, T^{(1)}(E)\, |g,\nu_1\rangle &= \langle g,\nu_1'| \sum_{n=0}^{\infty} V\left(\frac{1}{E-H_0+i\eta}V\right)^n |g,\nu_1\rangle \\
&= \langle g,\nu_1'|\, V \sum_{n=0}^{\infty}\left(\frac{1}{E-H_0+i\eta}V\right)^n \frac{1}{E-H_0+i\eta} V\, |g,\nu_1\rangle \\
&= \sum_{\chi',\chi} g^*_{\chi'}(\nu_1')\, \langle e_{\chi'}, \mathrm{vac}| \sum_{n=0}^{\infty}\left(\frac{1}{E-H_0+i\eta}V\right)^n |e_\chi, \mathrm{vac}\rangle\, \frac{g_\chi(\nu_1)}{E+\delta_\chi+i\eta} \\
&\equiv \sum_{\chi',\chi} g_\chi(\nu_1) g^*_{\chi'}(\nu_1')\, \langle e_{\chi'}|\, M(E)\, |e_\chi\rangle\,,
\end{aligned} \tag{16.8}$$

where $|g,\nu\rangle$ denotes the state with the atom in the ground state and a single photon with frequency ν in the waveguide. In the second line we used $\langle g,\nu'|\, V\, |g,\nu\rangle = 0$ and shifted the sum. In the third line we defined

$$g_\chi(\nu) \equiv \langle e_\chi|\, v_\nu^\dagger\, |g\rangle = -i\sqrt{\gamma/2\pi}\left(\langle e_\chi|\, \sigma_1^\dagger\, |g\rangle\, e^{-i(\bar\omega+\nu)\tau/2} - \langle e_\chi|\, \sigma_2^\dagger\, |g\rangle\, e^{i(\bar\omega+\nu)\tau/2}\right), \tag{16.9}$$

and in the fourth line we defined the dressed atomic Green's function projected on the excited subspace

$$M(E) = \sum_{n=0}^{\infty} \langle \mathrm{vac}|\left(\frac{1}{E-H_0+i\eta}V\right)^n |\mathrm{vac}\rangle\, M^0(E), \tag{16.10}$$

with $M^0(E) = \sum_\chi \frac{1}{E+\delta_\chi+i\eta} |e_\chi\rangle\langle e_\chi|$ the corresponding bare atomic Green's function. To obtain an explicit expression for $M(E)$, we note that only the even powers of n contribute to the sum, since $\langle \mathrm{vac}|\, V\, |\mathrm{vac}\rangle = 0$. We

then obtain the Dyson equation

$$M(E) = \sum_{n=0}^{\infty} \langle \mathrm{vac} | \left(\frac{1}{E - H_0 + i\eta} V \frac{1}{E - H_0 + i\eta} V \right)^n |\mathrm{vac}\rangle \, M^0(E) \tag{16.11}$$
$$= \sum_{n=0}^{\infty} \left(M^0(E) \langle \mathrm{vac} | V \frac{1}{E - H_0 + i\eta} V |\mathrm{vac}\rangle \right)^n M^0(E)$$
$$= \sum_{n=0}^{\infty} \left(M^0(E)\Sigma(E) \right)^n M^0(E) = \frac{1}{1 - M^0(E)\Sigma(E)} M^0(E).$$

In the last line we defined the *self-energy* of the atom

$$\Sigma(E) = \langle \mathrm{vac} | V \frac{1}{E - H_0 + i\eta} V |\mathrm{vac}\rangle = \sum_{\chi,\chi'} \int d\nu \frac{g_\chi(\nu) g^*_{\chi'}(\nu)}{E - \nu + i\eta} |e_\chi\rangle \langle e_{\chi'}| \tag{16.12}$$
$$= -i\gamma \sum_{\chi,\chi'} \left(\frac{1}{2} \langle e_\chi | \left(\sigma_1^\dagger \sigma_1 + \sigma_2^\dagger \sigma_2 \right) |e'_\chi\rangle - e^{i(\bar{\omega}+E)\tau} \langle e_\chi | \sigma_2^\dagger \sigma_1 |e_{\chi'}\rangle \right) |e_\chi\rangle \langle e_{\chi'}| \,,$$

where we used the explicit expression for $g_\chi(\nu)$ given in (16.9). The self-energy is interpreted as the energy of the atom arising from the interaction with the waveguide, restricted to the excited subspace. The first component is purely imaginary and corresponds here to the deterministic decay of an excitation via photon emission at the rate γ. The second component on the other hand is the dipole-dipole interaction between the two transitions, which depicts the driving of the second transition by the first one via the delayed exchange of photons with frequency $\bar{\omega} + E$. Note that in the Markovian limit, that is, for $\gamma \ll 1/\tau$, the phase factor $e^{i(\bar{\omega}+E)\tau}$ in (16.12) is approximately constant over the relevant bandwidth, and $\Sigma(E)$ becomes independent of the frequency E. Using (16.11) and (16.12) we finally obtain the single-photon scattering matrix from (16.6) via

$$\langle g | S^{(1)}_{\nu'_1,\nu_1} | g \rangle = \delta_{\nu'_1\nu_1} \left(1 - 2\pi i \langle g | v_{\nu_1} M(\nu_1) v^\dagger_{\nu_1} | g \rangle \right). \tag{16.13}$$

Two-photon subspace.

We now apply the same approach for two-photon scattered states ($N = 2$). Let us consider an input state $|\Psi_i\rangle$ and an output state $|\Psi_f\rangle$ with the atom in the ground state and two photons in the waveguide. The expansion (16.7) then reads

$$\langle \Psi_f | T^{(2)}(E) |\Psi_i\rangle = \langle \Psi_f | \sum_{n=0}^{\infty} V \left(\frac{1}{E - H_0 + i\eta} V \right)^n |\Psi_i\rangle \tag{16.14}$$
$$= \langle \Psi_f | V \sum_{n=0}^{\infty} \left(\frac{1}{E - H_0 + i\eta} V \right)^n \frac{1}{E - H_0 + i\eta} V |\Psi_i\rangle \,.$$

Using the fact that $V|\Psi_i\rangle$ has one photon and belongs to the atomic excited subspace, and noting that once again only even values of n contribute to the sum, this expression can be rewritten as

$$\langle \Psi_f | V \sum_{n=0}^{\infty} \left(M^0(E - H_B) V \frac{1}{E - H_0 + i\eta} V \right)^n M^0(E - H_B) V |\Psi_i\rangle \,, \tag{16.15}$$

where M^0 is now evaluated at $E - H_B$ due to the presence of an additional photon. Let us now consider the term $V \frac{1}{E - H_0 + i\eta} V$, which in (16.15) is also an operator acting on the subspace with one photon and the atom in an excited state. Its matrix elements are given by

$$\langle e_{\chi'}, \nu' | V \frac{1}{E - H_0 + i\eta} V |e_\chi, \nu\rangle = \langle e_{\chi'}, \mathrm{vac} | \, b_{\nu'} v^\dagger_{\nu_3} b_{\nu_3} \frac{1}{E - H_0 + i\eta} b^\dagger_{\nu_4} v_{\nu_4} b^\dagger_\nu |e_\chi, \mathrm{vac}\rangle \tag{16.16}$$
$$= \langle e_{\chi'} | \, v^\dagger_{\nu_3} v_{\nu_4} |e_\chi\rangle \frac{\delta_{\nu_3,\nu_4}\delta_{\nu,\nu'} + \delta_{\nu',\nu_4}\delta_{\nu,\nu_3}}{E - \nu_4 - \nu + i\eta} = \langle e_{\chi'}, \nu' | \, \Sigma(E - H_B) + \Omega(E) |e_\chi, \nu\rangle \,.$$

Here $\Sigma(E)$ corresponds to the path without interaction between the atom and the photon, where $\nu' = \nu$ and $\nu_3 = \nu_4$, and is defined in (16.12). On the other hand, $\Omega(E)$ corresponds to the path with interaction, with $\nu_4 = \nu'$ and $\nu_3 = \nu$, and is expressed as

$$\Omega(E) = b^\dagger_{\nu'} v^\dagger_\nu \frac{1}{E - \nu - \nu' + i\eta} v_{\nu'} b_\nu. \tag{16.17}$$

The T-operator in (16.15) can then be written as

$$\begin{aligned}\langle\Psi_f|\,T^{(2)}(E)\,|\Psi_i\rangle &= \langle\Psi_f|\,V\frac{1}{1-M^0(E-H_B)(\Sigma(E-H_B)+\Omega(E))}M^0(E-H_B)V\,|\Psi_i\rangle\\ &= \langle\Psi_f|\,V\frac{1}{1-M(E-H_B)\Omega(E)}M(E-H_B)V\,|\Psi_i\rangle\\ &= \langle\Psi_f|\,V\sum_{n=0}^{\infty}\Big(M(E-H_B)\Omega(E)\Big)^n M(E-H_B)V\,|\Psi_i\rangle\\ &= \langle\Psi_f|\,VM(E-H_B)V\,|\Psi_i\rangle\\ &\quad+\langle\Psi_f|\,VM(E-H_B)W(E)M(E-H_B)V\,|\Psi_i\rangle\,,\end{aligned}\tag{16.18}$$

where in the second line we made use of the Dyson equation (16.11), and $W(E)$ is defined implicitly via the recursive relation

$$W(E)=\Omega(E)+\Omega(E)M(E-H_B)W(E).\tag{16.19}$$

Finally, from (16.6) we obtain that the coefficients of the two-photon scattering matrix are given by

$$\begin{aligned}\langle g|S^{(2)}_{\nu_1'\nu_2',\nu_1\nu_2}|g\rangle =&\frac{1}{2}\delta_{\nu_1'\nu_1}\delta_{\nu_2'\nu_2}-2\pi i\,\langle g|\,v_{\nu_1'}M(\nu_1)v^\dagger_{\nu_1}\,|g\rangle\,\delta_{\nu_1'\nu_1}\delta_{\nu_2'\nu_2}\\ &-2\pi i\,\langle g|\,v_{\nu_1'}M(\nu_1')W_{\nu_2',\nu_2}(\nu_1+\nu_2)M(\nu_1)v^\dagger_{\nu_1}\,|g\rangle\,\delta_{\nu_1'+\nu_2',\nu_1+\nu_2}\,,\end{aligned}\tag{16.20}$$

where $W_{\nu',\nu}(E)\equiv\langle\nu'|\,W(E)\,|\nu\rangle$. From (16.17), the contribution $\langle\nu'|\,\Omega(E)\,|\nu\rangle$ to (16.19) can be decomposed into the elastic part $-i\pi v^\dagger_\nu v_{\nu'}\delta(E-\nu-\nu')$ and the inelastic part $\mathcal{P}v^\dagger_\nu\frac{1}{E-\nu-\nu'}v_{\nu'}$, with $\mathcal{P}$ the principal value. We can then alternatively represent (16.20) by

$$\begin{aligned}\langle g|S^{(2)}_{\nu_1'\nu_2',\nu_1\nu_2}|g\rangle =&\frac{1}{2}\langle g|S^{(1)}_{\nu_1',\nu_1}|g\rangle\langle g|S^{(1)}_{\nu_2',\nu_2}|g\rangle\\ &-2\pi i\,\langle g|\,v_{\nu_1'}M(\nu_1')W^{\mathcal{P}}_{\nu_2',\nu_2}(\nu_1+\nu_2)M(\nu_1)v^\dagger_{\nu_1}\,|g\rangle\,\delta_{\nu_1'+\nu_2',\nu_1+\nu_2}\,,\end{aligned}\tag{16.21}$$

where $W^{\mathcal{P}}_{\nu',\nu}(E)\equiv W_{\nu',\nu}(E)+i\pi v^\dagger_\nu v_{\nu'}\delta(E-\nu-\nu')$. This representation is convenient for the clear separation between elastic and inelastic scattering processes, respectively in the first and second term of (16.21).

16.3.2 Observables

In the following we will consider an initial state consisting of two photons with the same frequency, to which we will set the rotating frame frequency $\bar\omega$. The initial state is approximated by the wavepacket $|\Psi_i\rangle=\frac{1}{\sqrt{2}}\Big)\int d\nu\,\phi_0(\nu)b^\dagger(\nu)\Big)^2|g,\mathrm{vac}\rangle$, with $\phi_0(\nu)$ defined in (16.4). Using the relation given in eq. (16.21), the final state can be expressed as

$$|\Psi_f\rangle=S^{(2)}\,|\Psi_i\rangle=\frac{1}{\sqrt{2}}\Big(\int d\nu\,s\,\phi_0(\nu)b^\dagger(\nu)\Big)^2|g,\mathrm{vac}\rangle+\frac{c}{\sqrt{2}L}\int d\nu\,\hat t(\nu)b^\dagger(\nu)b^\dagger(-\nu)|g,\mathrm{vac}\rangle,\tag{16.22}$$

where we defined

$$s=1-2\pi i\langle g|v_0M(0)v_0^\dagger|g\rangle,\quad\text{and}\quad\hat t(\nu)=\frac{1}{2}\left[t(\nu)+t(-\nu)\right],\tag{16.23}$$

with $t(\nu)=-8i\pi^2\langle g|v_\nu M(\nu)W^{\mathcal{P}}_{-\nu,0}(0)M(0)v_0^\dagger|g\rangle$. Here s is a phase factor acquired by each photon during an elastic scattering, and the second term contains the inelastic part which generates entangled states of photons with opposite frequencies. In the derivation of the second term of (16.22) we have assumed the limit $L\to\infty$, hence replaced $\phi_0(\nu)\to\sqrt{\frac{2\pi c}{L}}\delta(\nu)$. However, we have retained the full form of ϕ in the first term, as it will be needed to regularize the expression of observables in which products of the form $\phi_0^*(\nu)\phi_0(\nu)$ appear. In this situation it is necessary to employ the normalization condition $\int d\nu|\phi_0(\nu)|^2=1$. Below we express observables as a function of s and $\hat t(\nu)$.

Power spectrum.

From (16.22), we find

$$b(x)|\Psi_f\rangle=\sqrt{\frac{2}{L}}s^2\int d\nu\,\phi_0(\nu)b^\dagger(\nu)|g,\mathrm{vac}\rangle+\frac{\sqrt{c}}{L\sqrt{\pi}}\int d\nu\,e^{i\nu x/c}\,\hat t(\nu)b^\dagger(-\nu)|g,\mathrm{vac}\rangle,\tag{16.24}$$

where $b(x) \equiv \frac{1}{\sqrt{2\pi c}} \int d\nu\, b_\nu e^{i\nu x/c}$ is the field operator in the position representation. We then obtain the first-order field correlation as

$$G^{(1)}(t) \equiv c\,\langle \Psi_f|\, b^\dagger(x-ct)b(x)\,|\Psi_f\rangle = \frac{2c}{L} + \frac{4c^2}{L^2}\mathrm{Re}[(s^*)^2\hat{t}(0)] + \frac{c^2}{L^2\pi}\int d\nu\, e^{i\nu t}|\hat{t}(\nu)|^2. \tag{16.25}$$

The Fourier transform of this expression yields the elastic and inelastic power spectra, which read

$$S_{\mathrm{el}}(\nu) = \left(\frac{2c}{L} + \frac{4c^2}{L^2}\mathrm{Re}[(s^*)^2\hat{t}(0)]\right)\delta(\nu),\ S_{\mathrm{inel}}(\nu) = \frac{c^2}{L^2\pi}|\hat{t}(\nu)|^2, \tag{16.26}$$

where the elastic part is obtained from the first two terms of (16.25), which are time-independent, and the inelastic part from the last term.

Second order field correlation.

Similarly, we establish

$$b(x-ct)b(x)\,|\Psi_f\rangle = \frac{\sqrt{2}}{L}\Big[s^2 + \frac{1}{2\pi}\int d\nu\, e^{i\nu t}\hat{t}(\nu)\Big]\,|\mathrm{vac}\rangle\,. \tag{16.27}$$

Combining this result with (16.24), we obtain the normalized second order auto-correlation function, which reads (in the limit $L \to \infty$)

$$g^{(2)}(t) = \frac{\langle\Psi_f|b^\dagger(x)b^\dagger(x-ct)b(x-ct)b(x)|\Psi_f\rangle}{\langle\Psi_f|b^\dagger(x)b(x)|\Psi_f\rangle^2} = \frac{1}{2}\left|1 + \frac{1}{2\pi s^2}\int d\nu\,\hat{t}(\nu)\cos(\nu t)\right|^2. \tag{16.28}$$

We have thus derived analytical expressions for the observables in our scattering problem in terms of the components of the scattering matrix. The explicit expressions for the cases where the quantum emitter is a two-level or a V-level system are given in 16.7.

16.3.3 Scattering of coherent states in the low-power limit

In quantum optical experiments one typically studies the scattering of coherent states. There the photon number is not conserved, and the input states contain a constant photon intensity rather than a fixed photon number. The previous results can be easily adapted to the scattering of coherent states with low amplitude, as only the few-photon components contribute to the dynamics in the limit of weak coherent driving fields. In this regime we can expand the weak coherent input state in different photon number sectors. Keeping only contributions up to two-photon states we can approximate a weak coherent field with amplitude α as

$$\begin{aligned}|\Psi_i\rangle &= e^{-|\alpha|^2/2}\sum_{n=0}^{\infty}\frac{\alpha^n}{n!}\Big(\int d\nu\,\phi_0(\nu)b^\dagger(\nu)\Big)^n\,|g,\mathrm{vac}\rangle \\ &\approx e^{-|\alpha|^2/2}\Big[1 + \alpha\int d\nu\,\phi_0(\nu)b^\dagger(\nu) + \frac{\alpha^2}{2}\Big(\int d\nu\,\phi_0(\nu)b^\dagger(\nu)\Big)^2\Big]\,|g,\mathrm{vac}\rangle\,.\end{aligned} \tag{16.29}$$

With the scattering theory approach we can calculate the corresponding output state in terms of the variables (16.23),

$$\begin{aligned}|\Psi_f\rangle \approx e^{-|\alpha|^2/2}\Big[1 &+ \alpha s\int d\nu\,\phi_0(\nu)b^\dagger(\nu) \\ &+ \frac{\alpha^2}{2}\Big(\int d\nu\, s\,\phi_0(\nu)b^\dagger(\nu)\Big)^2 + \frac{c}{2L}\int d\nu\,\hat{t}(\nu)b^\dagger(\nu)b^\dagger(-\nu)\Big]\,|g,\mathrm{vac}\rangle\,.\end{aligned} \tag{16.30}$$

The previous analytical derivations can then be readily reproduced using these states. In terms of (16.26), the inelastic part of the power spectrum then reads $S^{\mathrm{coh}}_{\mathrm{inel}}(\nu) = (|\alpha|^4/2)S_{\mathrm{inel}}$, to leading order in $|\alpha|$. Conversely, the second order field correlation from (16.28) now reads $g^{(2)}_{\mathrm{coh}}(t) = 2g^{(2)}(t)$.

16.4 Matrix product state approach

We now turn to our numerical approach, which employs matrix product state (MPS) techniques to simulate the evolution of the entangled state of photonic field and emitter, allowing to go beyond the two photon limit. It is based on the methods developed in [16] where the authors studied non-Markovian dynamics of quantum systems strongly driven by a continuous classical field. Here we adapt these methods in order to calculate also the scattering of states with fixed photon number.

16.4.1 Stroboscopic evolution

In order to apply our matrix product state approach we cast the Hamiltonian given in (16.2) and (16.3) in the interaction picture with respect to H_B. Moreover, we define quantum noise operators as $b(t) = \frac{1}{\sqrt{2\pi}} \int d\nu\, b(\nu) e^{-i\nu t}$ such that the Hamiltonian now depends explicitly on time and becomes

$$H(t) = H_a + i\sqrt{\gamma}\big(b^\dagger(t+\tau/2)\sigma_1 e^{i\bar{\omega}\tau/2} - b^\dagger(t-\tau/2)\sigma_2 e^{-i\bar{\omega}\tau/2} - \text{H.C.}\big), \tag{16.31}$$

or, under the transformation $b(t) \to b(t-\tau/2)e^{i\bar{\omega}\tau/2}$,

$$H(t) = H_a + i\sqrt{\gamma}\big(b^\dagger(t)\sigma_1 - b^\dagger(t-\tau)\sigma_2 e^{-i\bar{\omega}\tau} - \text{H.C.}\big). \tag{16.32}$$

The dynamics of the system is then given by the Quantum Stochastic Schrödinger Equation (QSSE) $i\frac{d}{dt}|\Psi(t)\rangle = H(t)|\Psi(t)\rangle$.

The MPS-algorithm approximates the dynamics as a stroboscopic evolution at discrete times $t_k = t_{k-1} + \Delta t$ for $k = 1, ..., N$ with t_0 the initial time, Δt the time step interval and N the total number of time steps during the evolution. In order to approximate the continuous evolution we choose a step size that is much smaller than the time scales on which the atom evolves, *i.e.* $\gamma\Delta t \ll 1$. In each time-step k we define operators $\Delta B_k = \int_{t_{k-1}}^{t_k} dt\, b(t)$, which are known as *noise increments* in the context of quantum stochastic calculus and satisfy bosonic commutation relations $[\Delta B_k, \Delta B_{k'}^\dagger] = \Delta t\, \delta_{k,k'}$. The operator $\Delta B_k^\dagger/\sqrt{\Delta t}$ is therefore interpreted as the creation operator for the photons in time-bin k, *i.e.* the photons associated to times included in the interval $[t_k, t_{k+1}[$. We thus define the corresponding Fock states $|n\rangle_k \equiv \frac{(\Delta B_k^\dagger)^n}{\sqrt{n!}\sqrt{\Delta t^n}}|\text{vac}\rangle_k$ and write the state of the system at each time-step k as

$$|\Psi(t_k)\rangle = \sum_{i_S, n_1, n_2, ..., n_N} \psi_{i_S, n_1, n_2, ..., n_N}(t_k)\, |i_S\rangle_S \otimes |n_1\rangle_1 \otimes |n_2\rangle_2 \otimes ... |n_N\rangle_N\,, \tag{16.33}$$

where i_S labels the state of the quantum emitter and n_j denotes the photon number in time-bin j. The evolution of the system is then obtained by integrating the QSSE to lowest order in Δt, which provides the stroboscopic map $|\Psi(t_k)\rangle = U_k|\Psi(t_{k-1})\rangle$ with

$$U_k = \exp\Big(-iH_a\,\Delta t + \sqrt{\gamma}\big(\Delta B_k^\dagger\sigma_1 - \Delta B_{k-m}^\dagger\sigma_2 e^{-i\bar{\omega}\tau} - \text{H.C.}\big)\Big), \tag{16.34}$$

where the time step interval was chosen such that $\tau = m\Delta t$ with m an integer.

16.4.2 Matrix product state ansatz

The MPS ansatz consists in writing the amplitudes defined in (16.33) as products of matrices. In particular, let us express the initial state as

$$\psi_{i_S, n_1, n_2, ..., n_N}(t_0) = A[S]^{i_S} \cdot A[1]^{n_1} \cdot A[2]^{n_2} \cdot ... \cdot A[N]^{n_N}. \tag{16.35}$$

Here $A[k]^{n_k}$ is a matrix of dimension $D_k \times D_{k+1}$. Note that $A[S]^{i_S}$ is a vector of dimension $1 \times D_1$, and similarly $A[N]^{n_N}$ is of dimension $D_N \times 1$. The maximum bond dimension $D \equiv \max_k(D_k)$ determines the maximal amount of entanglement that can be represented with this ansatz.

Two-photon initial state.

Our MPS approach is naturally formulated in the time domain. To address the two-photon scattering problem, which is formulated in frequency space, we approximate the initial state of two photons (with a given frequency $\bar{\omega}$) by an incident two-photon wave packet of duration $T = N\Delta t$. This approximation is valid if this duration T is much larger than $1/\gamma$ and τ, hence $N \gg \max(m, 1/(\gamma\Delta t))$. Denoting the vacuum state in all time-bins by $|\text{vac}\rangle$, we thus consider the two-photon initial state

$$\begin{aligned} |\Psi(t_0)\rangle &= \frac{1}{\sqrt{2}}\Big(\frac{1}{\sqrt{N\Delta t}}\sum_{k=1}^{N}\Delta B_k^\dagger\Big)^2 |g\rangle_S \otimes |\text{vac}\rangle \\ &= \frac{1}{\sqrt{2}N\Delta t}\Big(\sum_{k=1}^{N}(\Delta B_k^\dagger)^2 + 2\sum_{k=1}^{N}\sum_{l=k+1}^{N}\Delta B_k^\dagger \Delta B_l^\dagger\Big)|g\rangle_S \otimes |\text{vac}\rangle\,. \end{aligned} \tag{16.36}$$

In order to express this state in the form of (16.35) we note that it can be written as

$$|\Psi(t_0)\rangle = \frac{1}{\sqrt{2}N} \sum_{n_1,n_2,\ldots,n_N} \prod_{k=1}^{N} M[k]^{n_k} |g\rangle_S \otimes |n_1\rangle_1 \otimes |n_2\rangle_2 \otimes \cdots , \tag{16.37}$$

where the matrices $M[k]^{n_k}$ are matrices given by

$$M[1]^0 = (1 \quad 0 \quad 0)\,,\ M[1]^1 = \begin{pmatrix}0 & \sqrt{2} & 0\end{pmatrix},\ M[1]^2 = \begin{pmatrix}0 & 0 & \sqrt{2}\end{pmatrix} \tag{16.38}$$

for $k = 1$,

$$M[k]^0 = \begin{pmatrix}1 & 0 & 0\\ 0 & 1 & 0\\ 0 & 0 & 1\end{pmatrix},\ M[k]^1 = \begin{pmatrix}0 & \sqrt{2} & 0\\ 0 & 0 & \sqrt{2}\\ 0 & 0 & 0\end{pmatrix},\ M[k]^2 = \begin{pmatrix}0 & 0 & \sqrt{2}\\ 0 & 0 & 0\\ 0 & 0 & 0\end{pmatrix} \tag{16.39}$$

for $1 < k < N$, and

$$M[N]^0 = (0 \quad 0 \quad 1)^\top,\ M[N]^1 = \begin{pmatrix}0 & \sqrt{2} & 0\end{pmatrix}^\top,\ M[N]^2 = \begin{pmatrix}\sqrt{2} & 0 & 0\end{pmatrix}^\top \tag{16.40}$$

for $k = N$. The initial state can thus be represented as an MPS state of the form (16.35) with bond dimension $D = 3$, with the normalized matrices $A[S]^{i_S} = \delta_{i_S,g}$ and $A[k]^{n_k} = M[k]^{n_k}/(\sqrt{2}N)^{1/N}$ for $1 \le k \le N$. This expression can be brought to a canonical form in the standard way [31]. The time evolution is then performed by applying the unitary operator (16.34) at each time step, hence updating these matrices. For details regarding the implementation, and in particular the long-range interactions arising from the time delay, we refer the reader to [16]. We note that it is straightforward to generalize this to states with larger number of photons.

Observables.

At the end of the scattering, the MPS state can be analyzed to obtain the properties of the output field. The first order correlation function reads

$$G^{(1)}(t_{k+m}, t_k) = \langle b^\dagger(t_{k+l}) b(t_k)\rangle \approx \langle \Delta B_{k+l}^\dagger \Delta B_k\rangle/(\Delta t)^2, \tag{16.41}$$

and the inelastic output spectrum is given by

$$S_{\text{inel}}(\nu) = \frac{1}{\pi}\int_0^\infty dt' \mathrm{Re}\Big(\tilde{G}^{(1)}(t', t_k) e^{i\nu t'}\Big) \approx \frac{\Delta t}{\pi}\sum_{l=0}^{M} \mathrm{Re}\Big(\tilde{G}^{(1)}(t_{k+l}, t_k) e^{i\nu l \Delta t}\Big), \tag{16.42}$$

where k and M should be taken large enough so that the system is in the steady-state and $\tilde{G}^{(1)}$ is obtained from $G^{(1)}$ by subtracting the time-independent offset corresponding to the elastic part of the spectrum. The normalized second order auto-correlation function on the other hand reads

$$g^{(2)}(t_{k+l}, t_k) = \frac{\langle b^\dagger(t_k) b^\dagger(t_{k+l}) b(t_{k+l}) b(t_k)\rangle}{\langle b^\dagger(t_k) b(t_k)\rangle \langle b^\dagger(t_{k+l}) b(t_{k+l})\rangle} \approx \frac{\langle \Delta B_k^\dagger \Delta B_{k+l}^\dagger \Delta B_{k+l} \Delta B_k\rangle}{\langle \Delta B_k^\dagger \Delta B_k\rangle \langle \Delta B_{k+l}^\dagger \Delta B_{k+l}\rangle}. \tag{16.43}$$

These correlation functions of the output state can be calculated using standard MPS routines [31]. In our simulations presented below we calculate these observables using the MPS parameters $\gamma\Delta t = 0.1$, $D = 200$ and $\gamma T = 300$.

Coherent initial state.

Within the MPS formalism coherent input fields can be naturally included by a Mollow transformation [34] where the noise increments are redefined as $\Delta B_k = \int_{t_{k-1}}^{t_k} dt\, b(t) - \beta\,\Delta t$ for a finite photon intensity of $|\beta|^2$ (with $\beta \equiv \alpha/\sqrt{T}$). Correspondingly the unitary operator of (16.34) that induces the evolution now reads

$$\begin{aligned} U_k = \exp\Big(&- iH_a\,\Delta t + \big(\Omega_R(\sigma_1 - \sigma_2 e^{-i\bar{\omega}\tau}) - \text{H.C.}\big)\Delta t \\ &+ \sqrt{\gamma}\big(\Delta B_k^\dagger \sigma_1 - \Delta B_{k-m}^\dagger \sigma_2 e^{-i\bar{\omega}\tau} - \text{H.C.}\big)\Big). \end{aligned} \tag{16.44}$$

The additional terms that appear under this transformation act as a classical driving field with Rabi frequency $\Omega_R \equiv \beta^*\sqrt{\gamma}$ on the atomic degrees of freedom. Moreover the input state of the waveguide in this transformed picture is simply the vacuum state. In a MPS description it is trivially represented by $A[j]^{n_j} = \delta_{n_j,0}$. The observables (16.41) and (16.43) are then redefined with $\Delta B_k \to \Delta B_k + \beta\,\Delta t$. With this approach arbitrarily strong coherent driving fields can be handled numerically [16].

16.5 Results

In the previous sections we developed an analytical solution and a numerical method to tackle the scattering problem. In this section we display and discuss the results obtained using these two approaches. We start out with presenting the properties of the field scattered by a two-level emitter, and then discuss the similarities and differences to the case of a chiral V-level emitter. As expected, the numerical calculations and the analytical solutions show a perfect agreement in the 2-photon sector.

16.5.1 First order correlation function: inelastic spectrum

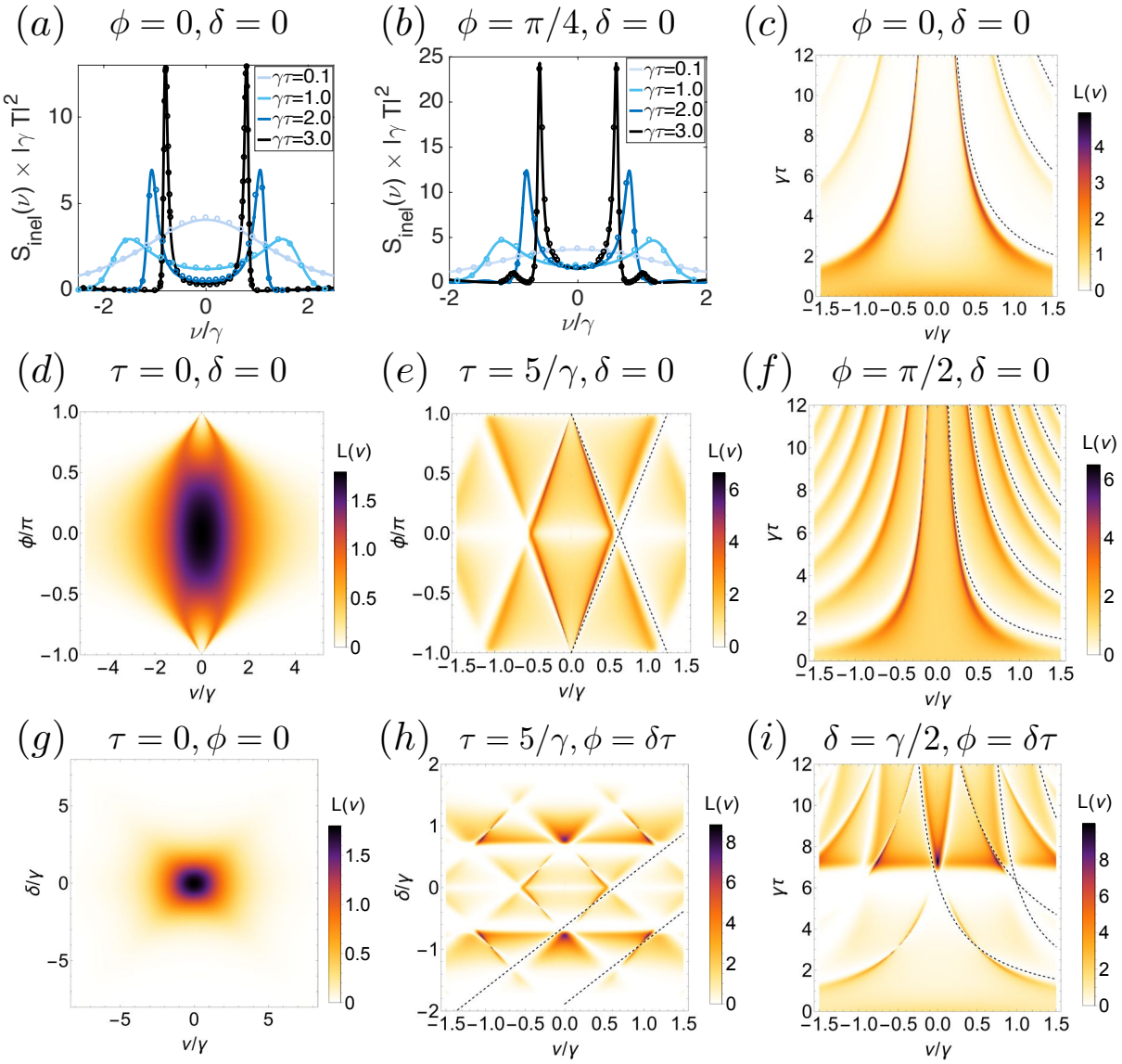

Figure 16.2: Inelastic spectrum of the 2-photon state scattered by a two-level quantum emitter. We consider various values of the coherent quantum feedback delay τ with $\delta = 0$, and $\phi \equiv \bar{\omega}\tau + \pi = 0$ in (a) and $\phi = \pi/4$ in (b). The solid lines are obtained using the MPS approach, and we compare the results with the scattering theory approach, in circles. In (c)-(i) we plot the logarithm of the spectrum $L(\nu) \equiv \log(1 + S_{\text{inel}}(\nu)|\gamma T|^2)$ calculated via the scattering theory approach. The various expressions for the dashed black lines are given in the text.

The inelastic spectrum of the output field is sensitive to processes in which the photons change frequency during the scattering. Due to energy conservation this can happen only if more than one photon is involved

in the scattering process. For the case of two incident photons of the same frequency considered here, this leads to a pair of photons with opposite frequencies in the scattered field. The inelastic spectrum is therefore necessarily symmetric around $\nu = 0$. In Figs. 16.2(a)-(b) we show examples of the inelastic spectra for different delay times. To understand the basic physics we discuss the two limiting cases of the Markovian regime and the non-Markovian regime separately.

Markovian regime

If the delay time is much smaller than the inverse bandwidth of the transition, *i.e.* $\gamma\tau \ll 1$, the system is effectively Markovian, as the delay line is too short to introduce significant memory. In this regime the system is effectively described by a master equation, where the mirror only renormalizes the transition frequency of the two-level system and its coupling to the field, as $\delta_{\text{eff}} = \delta - \gamma\sin(\phi)$ and $\gamma_{\text{eff}} = 4\gamma\cos^2(\phi/2)$ [14]. These effective parameters essentially depend on the distance of the atom from the mirror, via the propagation phase ϕ. For $\phi = \pi$ the incident field interferes destructively with the field reflected from the mirror and the atom decouples from the waveguide. On the other hand, for $\phi = 0$ the interference is constructive, leading to an enhanced emission of photons. The renormalization of the transition frequency can be interpreted as a dipole interaction of the atom with its mirror image.

The scattering problem of a Markovian two-level system is well understood, and can be calculated via the optical Bloch equations. From the general formula (16.26) we recover the expression for the inelastic spectrum in the Markovian limit:

$$S_{\text{inel}} \xrightarrow{\gamma\tau\to 0} \frac{64}{\pi(\gamma T)^2}\frac{\gamma_{\text{eff}}^2/4}{\delta_{\text{eff}}^2+\gamma_{\text{eff}}^2/4}\frac{\gamma_{\text{eff}}^2/4}{((\nu+\delta_{\text{eff}})^2+\gamma_{\text{eff}}^2/4)\,((\nu-\delta_{\text{eff}})^2+\gamma_{\text{eff}}^2/4)}. \tag{16.45}$$

If the incident photons are on resonance with the atom ($\delta = 0$) the spectrum can have one or two peaks, depending on ϕ, (see Fig. 16.2(d)). This depends on whether the effective level shift introduced by the mirror δ_{eff} is resolved on the scale of the effective decay rate γ_{eff}. For $\phi \approx 0$ the spectrum has a single maximum at $\nu = 0$ and is dominated by the broad effective decay rate γ_{eff}. Away from $\phi = 0$, the central peak becomes accordingly more narrow, until eventually one can resolve two peaks at $\nu = \pm\delta_{\text{eff}}$. These two peaks stem from the fact that the feedback shifts the atom out of resonance: incoherent scattering into photons resonant with the renormalized frequency is enhanced. That is, one of the two incoherently scattered photons is then resonant with the renormalized atomic transition frequency. If the atom is placed exactly at $\phi = \pi$ the coupling to the waveguide and correspondingly the inelastic spectrum vanishes. Finally, if the photons are off resonance with the atom, the results have a similar interpretation (see Fig. 16.2(g)): for a finite value of the detuning δ one resolves peaks at $\nu = \pm\delta$, albeit with lower amplitude than in the resonant case.

Non-Markovian regime

In the non-Markovian regime $\gamma\tau \gg 1$ the inelastic spectrum is much richer. In the simplest case of $\phi = 0$, $\delta = 0$ it can be expressed as

$$S_{\text{inel}}(\nu) = \Big(\frac{8}{\sqrt{\pi}\gamma T(1+\gamma\tau)}\frac{1+\cos(\nu\tau)}{(\nu/\gamma-\sin(\nu\tau))^2+(1+\cos(\nu\tau))^2}\Big)^2. \tag{16.46}$$

and displays a prominent pair of sharp peaks (see Fig. 16.2(a)) and an infinite number of smaller side peaks (see Fig. 16.2(c)). To understand the basic physics in this non-Markovian limit we can interpret this systems as a leaky cavity formed by the real perfect mirror on one side and the two-level atom playing the role of an imperfect mirror on the other side [35, 36]. The resonance frequencies and the effective linewidth of this cavity depend on the delay time and the propagation phase. For $\phi = 0$ and $\delta = 0$, the atom is completely decoupled from photons with frequencies ν given by an odd multiple of π/τ: indeed, all of these photons pick up a phase π when propagating to the mirror and back, such that their contribution to the electric field vanishes at the atomic position due to destructive interference. This is shown in Fig. 16.2(c), where the dashed lines display these frequencies as a function of $\gamma\tau$. Along these lines the inelastic spectrum vanishes, since the atom cannot scatter incoming photons into these modes. These frequencies however also coincide with the frequency of the modes supported by the effective cavity. The resulting effect is the formation of peaks in the intensity of the scattered photons very close to these zeros, corresponding to cavity resonances. As the delay increases, the peaks thus get closer to $\nu = 0$, and get sharper, corresponding to a decrease of the effective cavity linewidth. This is due to the fact that the effective cavity mode frequency approaches the two-level resonance, which improves the efficiency of the atom as a mirror, leading to an effective high finesse cavity.

Similarly, for a general ϕ the propagation phase acquired by a photon of frequency ν propagating from the atom to the mirror and back is given by $\phi+\nu\tau$. Thus, the atom decouples from photons with frequencies given by $((2l-1)\pi+\phi)/\tau$, with l an integer. In Figs. 16.2(e),(f) this is visible as the vanishing of S_{inel} along these curves, represented in dashed lines. Due to the symmetry of the spectrum, it must also vanish at $\nu = ((2l-1)\pi-\phi)/\tau$. This decoupling comes again hand in hand with resonances of the effective cavity close to these frequencies and we observe the corresponding sharp peaks of the inelastic spectrum.

Finally, for a finite value of the detuning δ between photons and atom we can apply a similar reasoning. In order for the modes supported by the effective cavity to be independent of the incoming photon detuning, in Figs. 16.2(h),(i) we choose to set the atomic phase $\omega_a\tau + \pi$ to 0 (modulo 2π), rather than ϕ, which then reads $\phi = \delta\tau$. The frequencies of the decoupled photons are now shifted by $\pm\delta$, as is shown in Figs. 16.2(h),(i) where the dashed lines corresponds to $\nu = (2l-1)\pi/\tau \pm \delta$ (with l an integer). Further we notice that the spectrum identically vanishes whenever $\phi = \delta\tau$ is an odd multiple of π (see Fig. 16.2(i)), as expected.

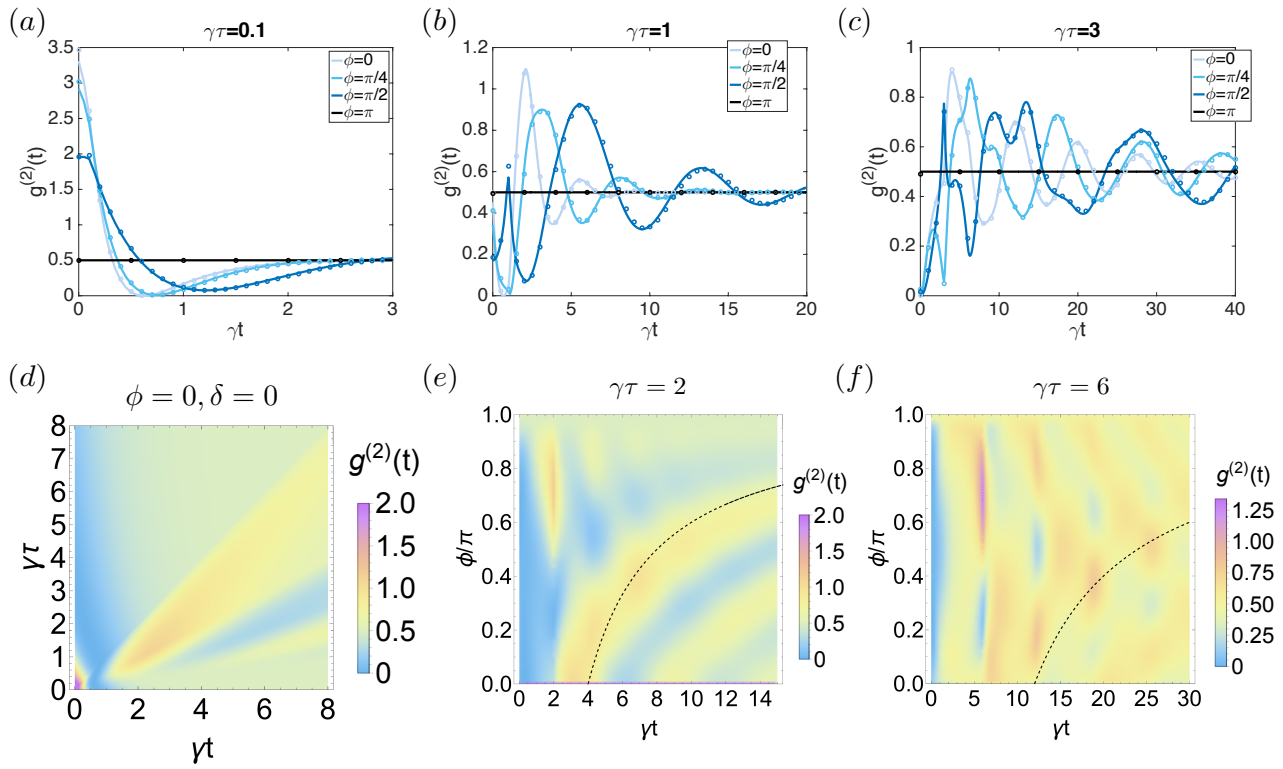

Figure 16.3: Second order correlation of the 2-photon state scattered by a two-level quantum emitter with $\delta = 0$. In (a)-(c) the solid lines are obtained using the MPS approach, and we compare the results with the scattering theory approach, in circles. In (d)-(f) we use the scattering theory approach. The dashed black lines in (e),(f) are given in the text.

16.5.2 Second order correlation function

To understand the temporal statistics of the two photons, we analyse the second order auto-correlation function $g^{(2)}(t)$. For the two-photon input state the correlation function is flat and evaluates to $g^{(2)} = 1/2$, *i.e.* there are no correlations (apart from those given by the fixed total photon number). The atom as a non-linear element can induce non-trivial correlations between photons as a result of the scattering process.

Again, we first discuss the results in the Markovian limit $\gamma\tau \ll 1$, shown in Fig. 16.3(a), where the entire setup can be understood as an effective two-level system as described above. In this limit the output field exhibits bunching of the photons at equal times, $g^{(2)}(t = 0) > 1/2$. This can be understood as follows: once the first photon is absorbed the second photon leads to an elastic stimulated emission. This increases the probability for observing the two photons at the same time at the output port of the waveguide, as signaled by $g^{(2)}(t = 0) > 1/2$. The same effect leads to a decrease of the probability to detect two photons separated by $t \sim 1/\gamma$, as visible in Fig. 16.3(a): the fast stimulated emission of the first absorbed photon by the second photon depletes the output field at later times (with respect to the uncorrelated state) leading to an almost perfect anti-bunching dip. Note that again the point $\phi = \pi$ is special: the atom decouples from the photons in this case and accordingly photons stay uncorrelated.

Remarkably, when one increases the time delay and leaves the Markovian limit, the auto-correlation function becomes non-analytic at each integer multiple of the delay time $t = n\tau$, $n = 1, 2, 3, \ldots$. This is most prominently visible at $t = \tau$, where the first derivative of $g^{(2)}(t)$ is dicontinuous (see Figs. 16.3(b)-(d)). These non-analyticities arise from the fact that a photon can "bounce" multiple times between the atom and the mirror. We note that these non-analyticities are always present for any nonzero τ, however they become less pronounced for short delay times $\tau \to 0$, such that $g^{(2)}$ eventually approaches a continuous function, as predicted in the Markovian approximation.

One of the most striking features of the auto-correlation function deep in the non-Markovian regime are "long-ranging" correlations between the photons as indicated by $g^{(2)}(t) \neq 1/2$ even for $t \gg 1/\gamma$. In particular, for $t \gg \tau$, $g^{(2)}(t)$ displays damped oscillations, where the oscillation frequency and their decay rate depend on ϕ (for simplicity we consider here only $\delta = 0$). To understand this behavior we recall that the output state for $\gamma\tau \gg 1$ is a superposition of the elastically scattered photons, and a state containing two photons at opposite frequency $\pm\nu$. From the discussion in the previous section we know that the distribution of the frequencies of these incoherently scattered photons, $\hat{t}(\nu)$, is strongly peaked around $\nu = \pm(\pi - |\phi|)/\tau$, corresponding to the supported frequency of the cavity formed by the atom and the distant mirror (see Fig. 16.2(e)). From

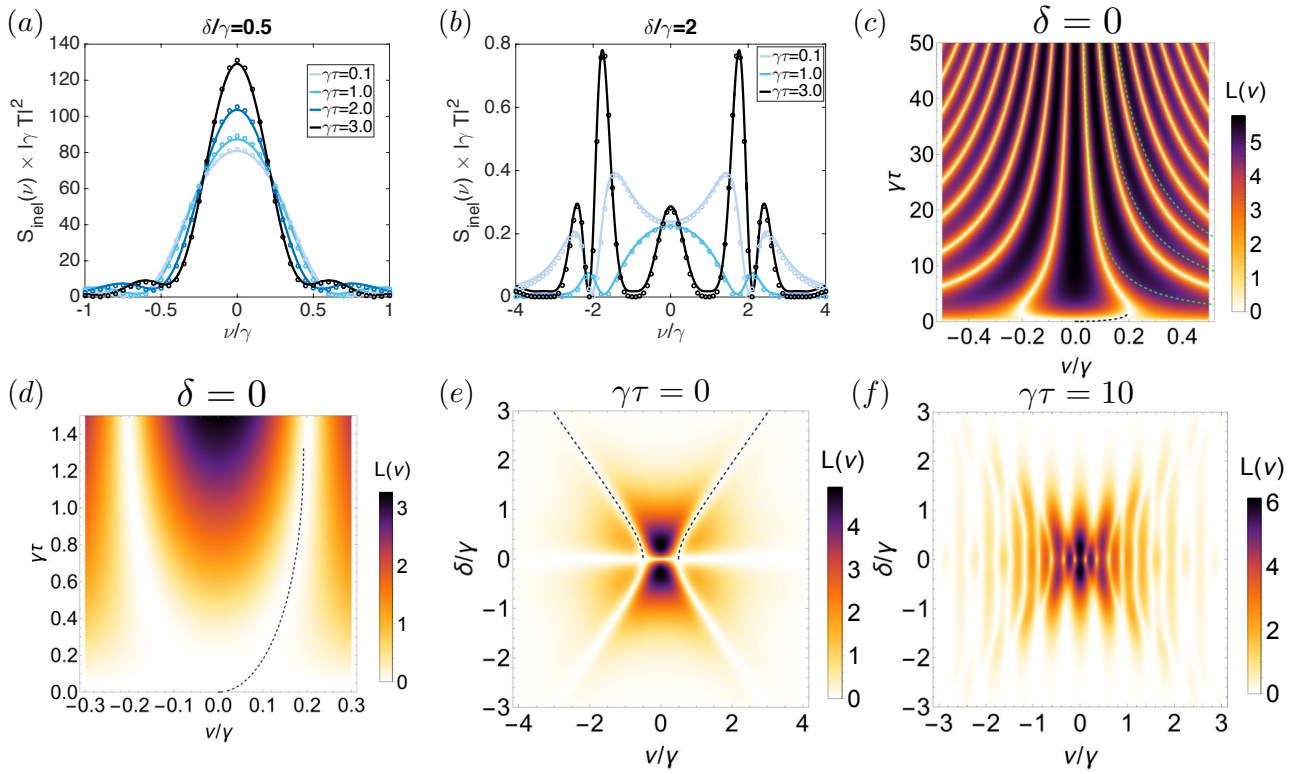

Figure 16.4: Inelastic spectrum of the 2-photon state scattered by a V-level quantum emitter. In (a) and (b), the solid lines are obtained using the MPS approach, and we compare the results with the scattering theory approach, in circles. In (c)-(f) we plot the logarithm of the spectrum $L(\nu) \equiv \log(1 + S_{\text{inel}}(\nu)|\gamma T|^2)$ using the scattering theory approach. The dashed lines are given in the text.

Eq. (16.28) it is clear that the auto-correlation function in such a state exhibits oscillations $\sim \cos(\nu t)$, *i.e.* $g^{(2)}$ is approximately periodic with period $\frac{2\pi\tau}{\pi-|\phi|}$. In Figs. 16.3(e),(f), we see that the oscillation period follows well this predicted curve as a function of ϕ, plotted in dashed lines. For $\phi \to \pi$ this period diverges, but at the same time the amplitude of the oscillations vanishes, such that $g^{(2)}(t) = 1/2$, *i.e.* the atom decouples from the waveguide as in the Markovian case.

The decay of the oscillations in the auto-correlation function is directly related to the finite linewidth of the effective cavity modes supported by the mirror and the atom. This is also consistent with the expectation that correlations between the two photons in the output field can not extend over longer times than the timescale over which the effective cavity can store a photon and in this way introduces a long memory time. Indeed the reflectivity of the atom as a mirror reads [35, 36] $R = 1/(1 + (\nu/\gamma)^2)$ for a frequency mismatch ν between the atomic transition and the photon. We can thus estimate the lifetime for a single photon inside the cavity in a mode with frequency ν as $t_{\text{eff}} \sim \tau(1-R)\sum_{n=0}^{\infty}(n+1)R^n = \frac{\tau}{1-R} = \tau(1+(\frac{\gamma}{\nu})^2)$. Here each term of the sum corresponds to the probability for a photon to be reflected n times (with probability R), before leaving the system (with probability $1-R$). The fact that the correlations extend over long times, is thus a direct consequence of the sharpness of the resonance peaks in the inelastic spectrum close to $\nu = 0$. As the mode frequency reads $\nu = \pm(\pi - |\phi|)/\tau$, we conclude that the oscillation decays slowly for large τ or for ϕ close to π, as can be observed in Fig. 16.3.

16.5.3 V-level system

If we replace the two-level scatterer by a chiral V-level system the situation changes both in the Markovian and in the non-Markovian regime (see Figs. 16.4 and 16.5). First we note that the propagation phase ϕ picked up by the incident photons when traveling from the atom to the mirror and back can be gauged away in this setting and thus has no measurable physical consequences. A second crucial difference to the previous case is that due to the chiral interactions, photons can only be scattered forward by the atom. Therefore each photon can only interact with the atom twice. As a consequence the atom can not form an effective cavity with the mirror, such that none of the above discussion can be transferred to the case of a chiral V-level scatterer. For simplicity we limit the discussion in what follows to the case of equal detunings for the two transitions $\delta_1 = \delta_2 \equiv \delta$.

Markovian regime

First, in the Markovian limit ($\gamma\tau \to 0^+$) the system can again be described by a master equation. In this case the mirror however does not only renormalize the coupling to the photon field and the transition frequencies, but it also induces an effective coherent coupling between the two excited states, as was shown in [27]. In particular for $\delta = 0$ there exists a dark state such that the atom completely decouples from the photon field, in which case the inelastic spectrum identically vanishes (see Figs. 16.4(d),(e)). Thus in the Markovian regime nontrivial features in the scattered field can only be obtained with a finite detuning δ. In Fig. 16.4(e), we show the inelastic spectrum in this case. One would expect an enhanced scattering into photons with resonant frequencies $\nu = \pm\delta$. However, most strikingly the atom here decouples from photons at frequencies satisfying $(\nu/\gamma)^2 + (\delta/\gamma)^2 = 1/4$ as plotted in dashed lines, which is due to a destructive interference effect. For $\delta \gtrsim \gamma/2$ this results into a splitting of the two resonant peaks $\nu = \pm\delta$ into four, as can be observed in the examples of Figs. 16.4(a),(b).

Non-Markovian regime

If one increases the delay τ, the scattered field is non-trivial even at $\delta = 0$. The expression of the inelastic spectrum for $\delta = 0$ now reads

$$S_{\text{inel}}(\nu) = \frac{4e^{-2\gamma\tau}(4\gamma)^4(e^{\gamma\tau/2}-1)^2}{\pi(\gamma T)^2\left(4\nu^2+\gamma^2\right)^4}\left[4\nu^2+\gamma^2+e^{\gamma\tau/2}\left((4\nu^2-\gamma^2)\cos(\nu\tau)+4\nu\gamma\sin(\nu\tau)\right)\right]^2. \tag{16.47}$$

For small values of the delay an expansion in $\gamma\tau$ provides an expression for the zeros of the spectrum at $\nu/\gamma = \frac{1}{4}\sqrt{\gamma\tau} - \frac{1}{16}(\gamma\tau)^{3/2} + \mathcal{O}(\gamma\tau)^{5/2}$, as pictured in black dashed lines in Figs. 16.4(c),(d). For larger delays the spectrum is dominated by the non-Markovian contributions. Similar to the case of the two-level system it displays a series of peaks separated by points where the spectrum vanishes, which display a $1/\tau$ dependency. This effect arises here because of interference between photons scattered by the different atomic transitions. More precisely, in an inelastic event pairs of photons with frequencies $\pm\nu$ can be produced. Let us consider an event where the photon with frequency ν is generated in a scattering event from transition 1 while the photon with frequency $-\nu$ is created by transition 2. The amplitude of this event acquires a phase $e^{i\nu\tau}$ due to the propagation of the first photon in the delay line. Conversely, the amplitude for the event with opposite frequencies acquires a phase $e^{-i\nu\tau}$, hence, for $\nu\tau = \pi/2$ (modulo π) these contributions cancel, and correspondingly no photons are created at these frequencies. The dashed green lines in Fig. 16.4(c) display these frequencies as a function of τ, which shows agreement in the limit of large delays.

Finally, for finite values of the detuning δ, we observe a rich variety of peaks in the inelastic spectrum (see Fig. 16.4(f)) which strongly depend on δ, similarly to the Markovian case (Fig. 16.4(e)). However the density of peaks is now much higher due to the behavior of their frequencies in $1/\tau$. Again, for small values of $\delta \lesssim \gamma/2$ the central peak at $\nu = 0$ is dominant (see also Fig. 16.4(a)), while for $\delta \gtrsim \gamma/2$ the stronger peaks are located close to $\nu = \pm\delta$ (see also Fig. 16.4(b)).

Second order correlation function

We now analyse the temporal statistics of the photons in the second order correlation function for the case of a V-level emitter. In the Markovian regime (see Fig. 16.5(a)), the situation is similar to the case of a two-level emitter, and the photons are bunched (*i.e.* $g^{(2)}(0) > 1/2$) as an effect of stimulated emission. Here we additionally show results for a finite detuning δ, which generates small decaying oscillations. Again, from Eq. (16.28) the oscillation frequencies are given by the positions of the most prominent peaks in the inelastic spectrum (Fig. 16.4(e)). The period of the oscillations is thus approximately given here by $2\pi/\delta$.

In the non-Markovian regime however, the system displays different results with respect to the response of a two-level emitter. Indeed, due to the chiral interactions the scattered photons cannot bounce back indefinitely between atom and mirror, but rather interact only once with each atomic transition. Here $g^{(2)}(t)$ is thus non-analytic only at $t = \tau$ (see Fig. 16.5(b)), as the absence of an effective cavity forbids the storage of a photon for long times and consequently prevents long lasting oscillations in $g^{(2)}$. In order to gain more insight in the shape of the correlation function, let us first assume $\delta = 0$ (see Fig. 16.5(c)). The non-analyticity here displays a strong contrast only along the line $t = \tau$. When the delay increases, the bunching vanishes as $g^{(2)}(0) \to 1/2$, indicating that photons are scattered mostly by different transitions. This can be further observed as there is a strong correlation in $g^{(2)}$ right after time $t = \tau$ for large values of the delay. Finally, for a finite detuning we observe, on top of these features, oscillations, once again with a period approximately given by $2\pi/\delta$. While with $\delta = 0$ the auto-correlation $g^{(2)}(t)$ converges towards $1/2$ for $t < \tau$ in Fig. 16.5(d), a value of $\delta \approx \gamma$ generates richer correlations as $g^{(2)}(t)$ undergoes oscillations with a large amplitude. The decrease of the oscillation period as $1/\delta$ is there clearly visible for $t > \tau$.

16.5.4 Finite coherent driving

Up to now we have analysed only the scattering of two-photon states, which in theory have an infinite spread and thus a vanishing intensity. In this final section we conclude our analysis by considering, on the other hand, the effect of a *finite* driving, that is, the scattering of coherent states with a nonzero photon intensity. In Fig. 16.6

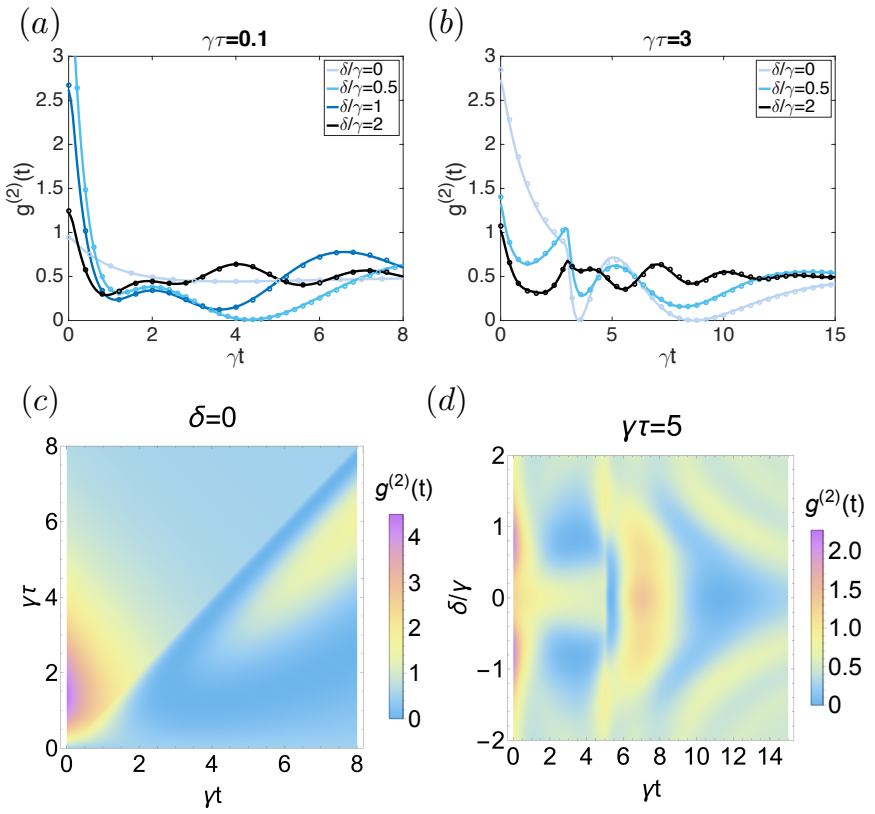

Figure 16.5: Second order correlation of the 2-photon state scattered by a V-level quantum emitter. In (a) and (b) the solid lines are obtained using the MPS approach, and we compare the results with the scattering theory approach, in circles. In (c) and (d) we use the scattering theory approach.

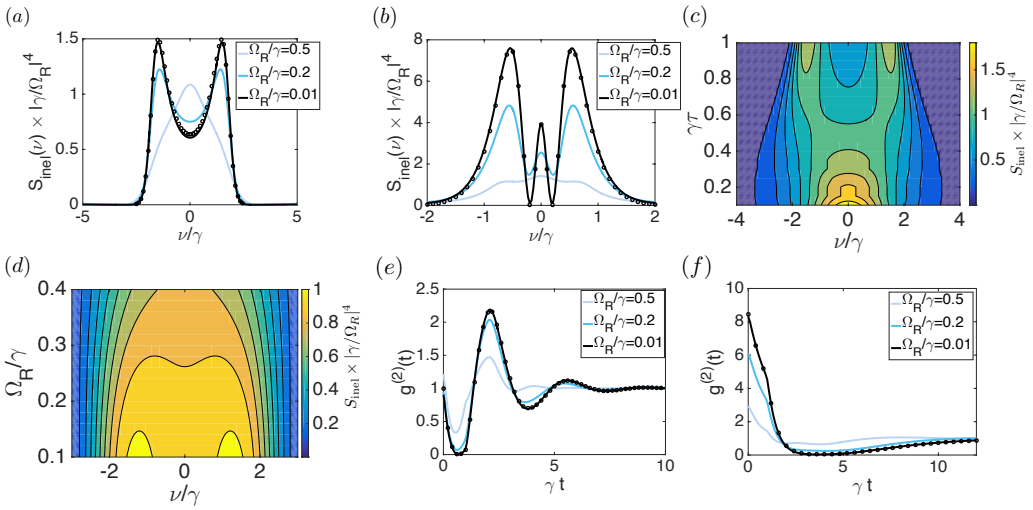

Figure 16.6: (a)-(d) Inelastic spectrum and (e),(f) second order correlation of the output field of a coherently driven quantum emitter, with $\phi = 0$ and $\delta = 0$. In (a),(c)-(e) we consider a two-level emitter, and in (b),(f) a V-level emitter. In (a),(b),(e),(f), the solid lines are obtained using the MPS approach with $\gamma\tau = 1$, and are compared with the predictions of the scattering theory approach in the weak field limit, in black circles. In (c),(d) we use the MPS approach with (c) $\Omega_R/\gamma = 0.1$ and (d) $\gamma\tau = 0.6$.

we calculate the spectrum and the second order correlation function for different values of the Rabi frequency Ω_R of the driven atom, in the non-Markovian regime. We see that the analytical formulas, based on a truncation of the state of the driving field to few-photon components, agree well with the quasi-exact numerical results in the limit $\Omega_R \to 0$. On the other hand, for finite coherent driving intensities, contributions from components with more than two photons become more and more significant. We observe in Figs. 16.6(a),(b) that the inelastic portion of the spectrum decreases for strong driving. This can be understood as the saturation of the atom, which prevents most of the driving field to be inelastically scattered. For the same reason, the second order auto-correlation function, shown here in Figs. 16.6(e),(f), identically convergences towards 1, corresponding to a perfectly coherent output.

As we showed in the previous sections, the physics underlying the results is vastly different between Markovian and non-Markovian regimes. Here the transition between these two regimes is displayed in Fig. 16.6(c) for a fixed driving intensity, showing at large delays the presence of the peaks characteristic of the first modes of the cavity formed by the mirror and the atom. However, in Figs. 16.6(a),(b) we also observe that by increasing the driving intensity, the shape of the spectrum converges towards the usual Lorentzian centred around $\nu = 0$, as in the Markovian regime. This can be understood as the saturation of the system preventing the existence of all interference effects discussed in the previous sections. This effect is further shown in Fig. 16.6(d) for a fixed value of the time delay. This shows that the threshold for the transition between Markovian and non-Markovian behavior depends on the competition between time delay and driving intensity.

16.6 Conclusion

In this work we have studied the scattering problem in a setup with delayed coherent quantum feedback, where light propagating in a semi-infinite waveguide scatters off of an atom located in front of a mirror. In particular we have analyzed the inelastic scattering of two photons and shown how the output spectrum strongly depends on the delay of the coherent feedback. We used a scattering theory approach, which provides analytical insight and is suitable for few-photon problems, and a numerical method based on matrix product states, which is designed to simulate complex problems involving larger numbers of photons. While these methods are tailored for different questions, their predictions can be compared and have shown strong agreement in the weak driving limit.

16.7 appendix: Explicit analytic expressions

Here we provide expressions for the variables defined in section 16.3 for the two types of quantum emitter we consider.

16.7.1 Two-level atom

Let us first consider the atom as a two-level system, as is represented in Fig. 16.1(a). If we define $\sigma \equiv |g\rangle\langle e| = \sigma_1 = \sigma_2$, the self-energy in (16.12) reads $\Sigma(E) = -i\gamma(1 - e^{i(\bar{\omega}+E)\tau})\,|e\rangle\langle e|$, and the atomic dressed Green's function in the excited state from (16.11) becomes $M(E) = |e\rangle\langle e|\,(E + \lambda - i\gamma e^{i(\bar{\omega}+E)\tau})^{-1}$, where $\lambda = \delta + i\gamma$, with δ the atomic detuning. The scattering phase in (16.23) then expresses as

$$s = (\lambda^* + i\gamma e^{-i\bar{\omega}\tau})/(\lambda - i\gamma e^{i\bar{\omega}\tau}). \tag{16.48}$$

From the definition in (16.17), we also obtain

$$\langle\nu'|\,\Omega(E)\,|\nu\rangle = |e\rangle\langle e|\,\frac{\gamma}{2\pi}\frac{(e^{i(\bar{\omega}+\nu)\tau/2} - e^{-i(\bar{\omega}+\nu)\tau/2})(e^{-i(\bar{\omega}+\nu')\tau/2} - e^{i(\bar{\omega}+\nu')\tau/2})}{E - \nu' - \nu + i\eta}. \tag{16.49}$$

In order to obtain an expression for $t(\nu)$ in (16.23), we first solve for $W(E)$ in the recursive equation (16.19). Details of the method can be found in the Suppl. Mat. of [18]. The solution can be expressed as

$$\langle\nu'|\,W(E)\,|\nu\rangle = |e\rangle\langle e|\,\frac{\gamma}{2\pi}(e^{i(\bar{\omega}+\nu)\tau/2} - e^{-i(\bar{\omega}+\nu)\tau/2})(e^{-i(\bar{\omega}+\nu')\tau/2} - e^{i(\bar{\omega}+\nu')\tau/2})\overline{W}_{\nu',\nu}(E), \tag{16.50}$$

where $\overline{W}_{\nu',\nu}(E)$ satisfies

$$\overline{W}_{\nu',\nu}(E) = \frac{1}{E - \nu' - \nu + i\eta} - \frac{\gamma}{2\pi}\int d\nu_1 \frac{1}{E - \nu' - \nu_1 + i\eta}\frac{e^{i(\bar{\omega}+\nu_1)\tau}}{E - \nu_1 + \lambda}\overline{W}_{\nu_1,\nu}(E). \tag{16.51}$$

Note that the first term corresponds to the Markovian contribution, whereas the second term is non-negligible only when $\gamma \gtrsim 1/\tau$. For an input state with $E = 0$, we then obtain (see also [9])

$$\overline{W}_{-\nu,0}(0) = \frac{1}{\nu + i\eta} + \frac{i\gamma e^{i\bar{\omega}\tau}}{\lambda - i\gamma e^{i\bar{\omega}\tau}}\sum_{\sigma=\pm,0} C_\sigma \frac{e^{i\nu\tau} - e^{-i\sigma p\tau}}{\nu + \sigma p}, \tag{16.52}$$

where $p \equiv \sqrt{\lambda^2+\gamma^2 e^{2i\bar{\omega}\tau}}$, and the coefficients are defined as $C_0=-1$ and $C_\pm = \pm([\pm p-\lambda]e^{\pm ip\tau}+i\gamma e^{i\bar{\omega}\tau})/(2p\cos p\tau - 2i\lambda\sin p\tau)$.

In terms of this solution we finally evaluate the output power spectra in (16.26) as

$$S_{\rm el}(\nu) = \left[\frac{2c}{L} - \frac{4c^2}{L^2}16\,\gamma^2\big(1-\cos\bar{\omega}\tau\big)^2{\rm Im}\big)[s^*]^2\Lambda\, m^3(0)\big)\right]\delta(\nu), \tag{16.53}$$

$$\begin{aligned} S_{\rm inel}(\nu) =& \frac{(4c)^2}{L^2\pi}\gamma^4(1-\cos\bar{\omega}\tau)^2|m(0)|^2(\cos\nu\tau-\cos\bar{\omega}\tau)^2 \\ &\times\left|\frac{m(\nu)-m(-\nu)}{\nu}+m(\nu)F(\nu)+m(-\nu)F(-\nu)\right|^2, \end{aligned} \tag{16.54}$$

where we defined the variables

$$F(\nu) \equiv -\,(ie^{-i\bar{\omega}\tau}\lambda/\gamma+1)^{-1}\sum_{\sigma=\pm,0}C_\sigma(e^{i\nu\tau}-e^{-i\sigma p\tau})/(\nu+\sigma p), \tag{16.55}$$

$$m(\nu) \equiv (\nu+\lambda-i\gamma e^{i(\bar{\omega}+\nu)\tau})^{-1}, \tag{16.56}$$

$$\Lambda \equiv 1-i\gamma e^{i\bar{\omega}\tau}\left[C_+(1-e^{-ip\tau})-C_-(1-e^{ip\tau})\right]/p. \tag{16.57}$$

From (16.28) we also find the expression for the second order field correlation function, which reads

$$g^{(2)}(t) = \frac{1}{2}\left|1+\frac{4\gamma^2\big(1-\cos(\bar{\omega}\tau)\big)}{(\lambda^*+i\gamma e^{-i\bar{\omega}\tau})^2}\left[I_1(t)-\cos(\bar{\omega}\tau)I_0(t)\right]\right|^2, \tag{16.58}$$

where we defined $I_1(t)=\big(I_0(t-\tau)+I_0(t+\tau)\big)/2$ and

$$\begin{aligned} I_0(t) =& \frac{1}{2(p\cos(p\tau)-i\lambda\sin(p\tau))}\Big)e^{-ip(|t|+\tau)}m^{-1}(p)-e^{ip(|t|+\tau)}m^{-1}(-p) \\ &+\sum_{n=0}^{\infty}\Theta(|t|-n\tau)[g_n^{(-)}(t)-g_n^{(+)}(t)]\Big), \end{aligned} \tag{16.59}$$

with

$$g_n^{(\pm)}(t) =)i\gamma e^{i\bar{\omega}\tau})^n e^{\mp ip\tau}\frac{(\pm p+\lambda-i\gamma e^{i\bar{\omega}\tau}e^{\pm ip\tau})^2}{(\pm p+\lambda)^{n+1}}\left[e^{\mp ip(|t|-n\tau)}-e^{i\lambda(|t|-n\tau)}f_n^{(\pm)}(t)\right], \tag{16.60}$$

$$f_n^{(\pm)}(t) = \sum_{l=0}^{n}\frac{1}{l!}[-i(|t|-n\tau)(\pm p+\lambda)]^l. \tag{16.61}$$

Here the non-Markovian behavior manifests itself in the occurrence of additional contributions to $g^{(2)}(t)$ at every multiple of the delay time τ, which create discontinuities in the derivative of $g^{(2)}(t)$.

16.7.2 V-level atom

We now consider the atom as a V-level system, as represented in figure 16.1(b). In the single excitation subspace, the self-energy expresses as

$$\Sigma(E) = -\frac{i}{2}\gamma(|e_1\rangle\langle e_1|+|e_2\rangle\langle e_2|)+i\gamma e^{i(\bar{\omega}+E)\tau}|e_2\rangle\langle e_1|. \tag{16.62}$$

From (16.11), it provides the dressed Green's function

$$M(E) = \frac{1}{E+\lambda_1}|e_1\rangle\langle e_1|+\frac{1}{E+\lambda_2}|e_2\rangle\langle e_2|+\frac{i\gamma e^{i(\bar{\omega}+E)\tau}}{(E+\lambda_1)(E+\lambda_2)}|e_2\rangle\langle e_1|, \tag{16.63}$$

where we defined $\lambda_{1,2}=\delta_{1,2}+i\gamma/2$. In this case we obtain from (16.23) the single-photon scattering phase $s=\lambda_1^*\lambda_2^*/(\lambda_1\lambda_2)$. From (16.17), we also get

$$\langle\nu'|\,\Omega(E)\,|\nu\rangle = \frac{\gamma}{2\pi}\frac{\left(e^{i(\bar{\omega}+\nu)\tau/2}\,|e_2\rangle-e^{-i(\bar{\omega}+\nu)\tau/2}\,|e_1\rangle\right)\left(e^{-i(\bar{\omega}+\nu')\tau/2}\,\langle e_2|-e^{i(\bar{\omega}+\nu')\tau/2}\,\langle e_1|\right)}{E-\nu'-\nu+i\eta}. \tag{16.64}$$

We recall that each photon interacts only once with each transition in the scattering event, in contrast to the case of the two-level system where it can be reemitted towards the mirror an arbitrary number of times. As a consequence, the iterative equation (16.19) identically terminates after the third iteration, providing the expression

$$\begin{aligned} W^{\mathcal{P}}_{-\nu,0}(0) = &\frac{\gamma}{2\pi}\frac{\left(e^{i\bar{\omega}\tau/2}\left|e_2\right\rangle - e^{-i\bar{\omega}\tau/2}\left|e_1\right\rangle\right)\left(e^{-i(\bar{\omega}-\nu)\tau/2}\left\langle e_2\right| - e^{i(\bar{\omega}-\nu)\tau/2}\left\langle e_1\right|\right)}{\nu} \\ &- \left(\frac{\gamma}{2\pi}\right)^2 e^{i\bar{\omega}\tau}|e_2\rangle\langle e_1|)e^{-i\nu\tau/2}F_1^{(1)}(\nu) + e^{i\nu\tau/2}F_1^{(2)}(\nu)) \\ &- \left(\frac{\gamma}{2\pi}\right)^3 e^{i\bar{\omega}\tau}|e_2\rangle\langle e_1|e^{i\nu\tau/2}F_2(\nu), \end{aligned} \tag{16.65}$$

where

$$F_1^{(\chi)}(\nu) = -\frac{2\pi i}{\lambda_\chi}\left[\frac{e^{i\nu\tau}-e^{i\lambda_\chi\tau}}{\nu-\lambda_\chi} - \frac{e^{i\omega\tau}-1}{\nu}\right], \quad (\chi=1,2) \tag{16.66}$$

$$F_2(\nu) = \frac{4\pi^2}{\lambda_1(\nu-\lambda_2)}\left[\frac{e^{i(\nu+\lambda_1)\tau}-1}{\nu+\lambda_1} - \frac{e^{i(\lambda_1+\lambda_2)\tau}-1}{\lambda_1+\lambda_2} - \frac{e^{i\nu\tau}-1}{\nu} + \frac{e^{i\lambda_2\tau}-1}{\lambda_2}\right]. \tag{16.67}$$

Combining (16.23) and (16.65) we deduce the inelastic part of the scattering as

$$\begin{aligned} \hat{t}(\nu) = &-\frac{2i\gamma^2}{\lambda_1}\frac{\lambda_2^{*2}-\lambda_1^2}{\lambda_2^2-\lambda_1^2}\frac{1}{\nu^2-\lambda_1^2} - \left[\frac{\lambda_1^{*2}}{\lambda_1^2}\frac{\gamma}{2\lambda_2} - \frac{i\gamma^2}{\lambda_1^2}\frac{\lambda_2}{\lambda_1+\lambda_2}\right. \\ &\left.+\frac{i\gamma^2}{\lambda_1^2}\frac{\delta_2\lambda_2}{\lambda_2^2-\lambda_1^2} + \frac{i\gamma^2}{2\lambda_1\lambda_2}e^{i\lambda_2\tau}\left(\frac{\lambda_1^*}{\lambda_1} + \frac{i\gamma\lambda_2 e^{i\lambda_1\tau}}{\lambda_1(\lambda_1+\lambda_2)}\right)\right]\frac{4i\gamma}{\nu^2-\lambda_2^2} \\ &-\frac{2i\gamma^2}{\lambda_1\lambda_2}\left(\frac{\lambda_1^*}{\lambda_1} + \frac{i\gamma\lambda_2 e^{i\lambda_1\tau}}{\lambda_1(\lambda_1+\lambda_2)}\right)\left[\frac{\lambda_2^*-\lambda_1}{\lambda_2-\lambda_1}\frac{\lambda_1\cos\nu\tau - i\nu\sin\nu\tau}{\nu^2-\lambda_1^2}\right. \\ &\left.+\frac{i\gamma}{2\lambda_2}\frac{\lambda_1+\lambda_2}{\lambda_2-\lambda_1}\frac{\lambda_2\cos\nu\tau - i\nu\sin\nu\tau}{\nu^2-\lambda_2^2} + \frac{\delta_2}{\lambda_2}\frac{\lambda_2\cos\nu\tau + i\nu\sin\nu\tau}{\nu^2-\lambda_2^2}\right]. \end{aligned} \tag{16.68}$$

Note that in this expression there is no dependence on the phase factor $e^{i\bar{\omega}\tau}$, since it can be absorbed in the redefinition of the atomic excited states, but there is a nontrivial dependence on τ. This means that the distance to the mirror becomes a relevant parameter only in the non-Markovian regime.

With the expression of $\hat{t}(\nu)$ we find readily the elastic and inelastic power spectra in (16.26). The second order field correlation is finally evaluated from (16.28) in terms of

$$\begin{aligned} \frac{1}{2\pi}\int d\nu\,\hat{t}(\nu)\cos(\nu t) = &\frac{\gamma^2}{\lambda_1^2}\frac{\lambda_2^{*2}-\lambda_1^2}{\lambda_2^2-\lambda_1^2}e^{i\lambda_1 t} \\ &+\frac{2\gamma}{\lambda_2}\left[\frac{\lambda_1^{*2}}{\lambda_1^2}\frac{\gamma}{2\lambda_2} - \frac{i\gamma^2}{\lambda_1^2}\frac{\lambda_2}{\lambda_1+\lambda_2} + \frac{i\gamma^2}{\lambda_1^2}\frac{\delta_2\lambda_2}{\lambda_2^2-\lambda_1^2} + \frac{i\gamma^2}{2\lambda_1\lambda_2}e^{i\lambda_2\tau}\left(\frac{\lambda_1^*}{\lambda_1} + \frac{i\gamma\lambda_2 e^{i\lambda_1\tau}}{\lambda_1(\lambda_1+\lambda_2)}\right)\right]e^{i\lambda_2 t} \\ &+\frac{\gamma^2}{\lambda_1\lambda_2}\left(\frac{\lambda_1^*}{\lambda_1} + \frac{i\gamma\lambda_2 e^{i\lambda_1\tau}}{\lambda_1(\lambda_1+\lambda_2)}\right)\left[\frac{\lambda_2^*-\lambda_1}{\lambda_2-\lambda_1}\Theta(t-\tau)e^{i\lambda_1(t-\tau)}\right. \\ &\left.+\frac{i\gamma}{2\lambda_2}\frac{\lambda_1+\lambda_2}{\lambda_2-\lambda_1}\Theta(t-\tau)e^{i\lambda_2(t-\tau)} + \frac{\delta_2}{\lambda_2}e^{i\lambda_2(\tau+t)} + \frac{\delta_2}{\lambda_2}\Theta(\tau-t)e^{i\lambda_2(\tau-t)}\right]. \end{aligned} \tag{16.69}$$

Once again, this function also features a discontinuity of the first derivative at $t=\tau$, which shows the effect of the delay. However, there is no discontinuity for $t>\tau$ as here the photon immediately leaves the feedback loop after this delay.

17 Input-output theory for waveguide QED with an ensemble of inhomogeneous atoms

by Kevin Lalumière, Barry C. Sanders, et al

Abstract

We study the collective effects that emerge in waveguide quantum electrodynamics where several (artificial) atoms are coupled to a one-dimensional superconducting transmission line. Since single microwave photons can travel without loss for a long distance along the line, real and virtual photons emitted by one atom can be reabsorbed or scattered by a second atom. Depending on the distance between the atoms, this collective effect can lead to super- and subradiance or to a coherent exchange-type interaction between the atoms. Changing the artificial atoms transition frequencies, something which can be easily done with superconducting qubits (two levels artificial atoms), is equivalent to changing the atom-atom separation and thereby opens the possibility to study the characteristics of these collective effects. To study this waveguide quantum electrodynamics system, we extend previous work and present an effective master equation valid for an ensemble of inhomogeneous atoms driven by a coherent state. Using input-output theory, we compute analytically and numerically the elastic and inelastic scattering and show how these quantities reveal information about collective effects. These theoretical results are compatible with recent experimental results using transmon qubits coupled to a superconducting one-dimensional transmission line [A. F. van Loo *et al.*].

17.1 Introduction

By confining the electromagnetic field in space, cavity quantum electrodynamics (QED), and more recently circuit QED, have opened the opportunity to study the interaction of light and matter in the strong-coupling regime where the light-matter interaction strength overwhelms decay rates [1, 2]. Strong interaction between matter and propagating photons is of interest for applications such as quantum networks [3, 4, 5] and single-photon transistors [6, 7]. Strong light-matter interaction in an open three-dimensional (3D) setting is made possible by tightly focusing the optical field [8]. An important signature of the interaction in this situation is the extinction of the transmitted light field by a single atom or molecule. Indeed, the light beam interferes destructively with the co-linearly emitted light from the atom or molecule, resulting ideally in 100% reflection. However, because of poor spatial mode-matching (i.e. the atom or molecule emits light in all directions while the incoming beam is tightly focused), only about 10% reflection is currently observed with single atoms [4].

The situation can be very different with artificial atoms in a circuit [9]. Indeed, as first shown experimentally by Astafiev *et al.* [10], almost ideal mode matching can be realized with a superconducting flux qubit coupled to a one-dimensional (1D) transmission line. In that experiment, 94% extinction of the transmitted signal was observed showing that a single qubit can act as a near ideal mirror for (low-intensity) microwave light. Deviation from the ideal result was caused by pure dephasing and qubit decay into nonradiative channels. Although this extra channel is present, the significant extinction of the transmitted signal implies that nonradiative decay is overwhelmed by radiative decay into the line. This is the signature of strong coupling for such a system. Experiments with transmon qubits [11] in the same regime have also been realized by the Chalmers group [12, 13, 14]. Interaction of a superconducting qubit with photons propagating in a 1D line has also been studied theoretically [9, 15, 16, 17, 18, 19].

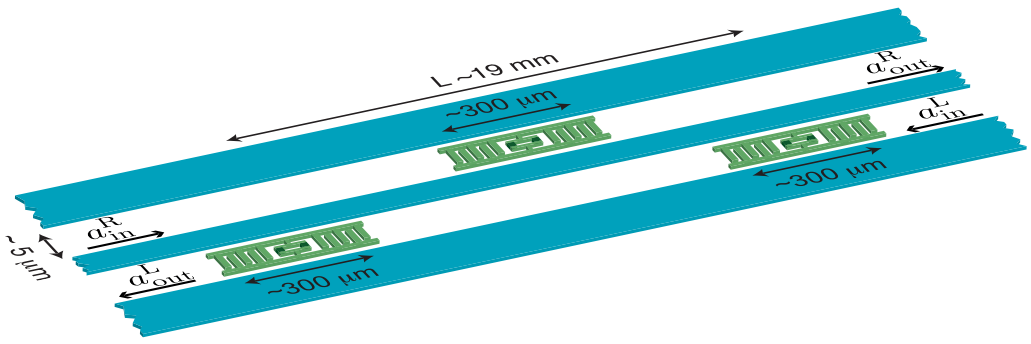

Figure 17.1: Waveguide QED realization with superconducting circuits: transmon qubits acting as artificial atoms (in green) are coupled to a 1D superconducting transmission line (in blue).

In this paper, we study theoretically the situation where several multi-level superconducting qubits (artificial atoms) interact with the same 1D transmission line. Experimental results on this waveguide QED system are presented in a companion paper [20]. To understand the main results, it is useful to first consider the well known and simpler case of a single free atom in 3D space. There, interaction of the atom with vacuum fluctuations leads to relaxation, due to emission by the atom of a photon at the atomic transition frequency, and to a Lamb shift of the atomic energy levels, due to emission of virtual photons. In the presence of a second atom, real and

virtual photons emitted by the first atom can be absorbed by the second, leading to a nontrivial interaction between the two. Therefore, while a single atom acts as a mirror reflecting incident light, two or more atoms will behave in a more complex way [21, 22]. However, because of poor mode-matching this interaction is rather weak in 3D.

With near-perfect mode matching, artificial atoms in a 1D transmission line provide an ideal system to study this interaction. Indeed, a single microwave photon could, in principle, travel for several kilometers along a superconducting transmission line before being lost. In this setting the above-mentioned qubit-qubit interaction is therefore long-range and emission of real photons modifies the single-qubit relaxation time [23]. As a result, collective decay or, in other words, super- and subradiance will be observed in the presence of several atoms. On the other hand, emission of virtual photons leads to exchange-type interactions between the qubits. Whereas these interactions can be long-range, their characteristics depend on the distance between the qubits. The character of the qubit-qubit interaction therefore changes with the distance between them. To change the distance between the qubits *in situ* is not feasible for a given sample, but changing the wavelength λ at which the qubits emit has an equivalent effect. Consequently, it is possible to study the distance dependence of the interaction simply by tuning the qubit transitions frequencies.

A system of two (artificial) atoms interacting via 3D [21, 24, 25, 26, 27, 28, 29, 30] and 1D [30, 31, 32, 33, 34] open space has been theoretically studied previously. In particular, non-Markovian effects (which are not relevant to the particular case of interest here) have been studied [35]. Here, we adapt Lehmberg's derivation for 3D space [21] to an ensemble of inhomogeneous (artificial) atoms coupled to a 1D transmission line. After eliminating the field degrees of freedom, an effective master equation for the atoms alone is obtained. Some approximations that were reasonable for atoms in 3D [21] must be revisited. In order to model reflection and transmission of an input beam by the system, we use input-output theory [36]. This allows us to calculate the elastic and inelastic scattering, which we show reveal the effects mentioned above.

The paper is organized as follows. In Sec. 17.2, we present a theory of waveguide QED. We first present a reduced master equation describing an arbitrary number of many-levels (artificial) atoms coupled to the 1D line and driven by a coherent state. We then apply input-output theory to this system, thereby allowing us to compute elastic and inelastic scattering. The dressed basis, which is useful for understanding collective effects, is discussed. Focusing on the situation where only two qubits are coupled to the line, we show how elastic and inelastic spectra reveal information about collective effects mediated by the open line. This is done in Sec. 17.3 considering a $\lambda/2$ separation between the qubits and in Sec. 17.5 a $\lambda/4$ separation. We summarize our work in Sec. 17.6.

In all cases, details of the calculations are relegated to the appendices. In Appendix 17.7.1, we present a derivation of the Hamiltonian for the cases of superconducting transmon qubits coupled to a 1D transmission line. The reduced master equation is derived in Appendix 17.7.2 and the input-output theory is discussed in Appendix 17.7.6. An in-depth discussion of the various approximations, and their validity in the context of waveguide QED with superconducting qubits, is presented in Appendix 17.7.3. Additional details on the derivation of the reduced master equation can be found in Appendices 17.7.4, 17.7.5, and 17.7.7.

17.2 Waveguide QED

17.2.1 General effective master equation for the inhomogeneous system

As illustrated in Fig. ?? with transmon qubits, we consider an ensemble of N inhomogeneous (artificial) atoms, each with M levels. They are dipole coupled to a 1D transmission line. The electromagnetic field in the transmission line can be described by the Hamiltonian [9]

$$H_{\mathrm{F}} = \int_0^\infty d\omega \hbar\omega \left[a_{\mathrm{R}}^\dagger(\omega) a_{\mathrm{R}}(\omega) + a_{\mathrm{L}}^\dagger(\omega) a_{\mathrm{L}}(\omega) \right], \tag{17.1}$$

where $a_{\mathrm{R(L)}}^\dagger(\omega)$ creates right- (left-) moving excitations at frequency ω in the line. The Hamiltonian of the artificial atoms is

$$H_{\mathrm{A}} = \sum_{j=0}^{N-1} \sum_{m=0}^{M-1} E_{mj} \left| m_j \right\rangle \left\langle m_j \right|, \tag{17.2}$$

where E_{mj} is the energy of the mth state of the jth atom. The interaction Hamiltonian between the line's electric field and the electric dipole for the free artificial atoms can be described as

$$H_{\mathrm{I}} = \sum_{j=0}^{N-1} \sum_{m=0}^{M-1} \hbar g_j \sqrt{m+1} \left(\Xi_j + \Xi_j^\dagger \right) \sigma_x^{mj}. \tag{17.3}$$

In this expression, Ξ_j is related to the electric field at the location x_j of the jth artificial atom,

$$\Xi_j = -i \int_0^\infty d\omega \sqrt{\omega} \left[a_{\mathrm{L}}(\omega) e^{-i\omega x_j/v} + a_{\mathrm{R}}(\omega) e^{i\omega x_j/v} \right], \tag{17.4}$$

with v the speed of light in the transmission line. We define

$$\sigma_x^{mj} = \sigma_-^{mj} + \sigma_+^{mj}, \tag{17.5}$$

with

$$\sigma_-^{mj} = |m_j\rangle \langle (m+1)_j| = \left(\sigma_+^{mj}\right)^\dagger, \tag{17.6}$$

the lowering operator for the $(m+1)$th state of the jth atom. The interaction only involves transitions between adjacent states of the atoms, which is a valid approximation for the transmon superconducting qubit behaving as a weakly nonlinear oscillator [11]. Finally, g_j is the (dimensionless) coupling strength between atom j and the field. The expression of g_j for transmon qubits is given in Appendix 17.7.3.

Following Lehmberg [21], and as shown in Appendix 17.7.2, the effective master equation for the artificial atoms after tracing out the field degrees of freedom can be expressed as [21, 24, 25, 27, 26, 28, 29, 30, 32, 33, 35]

$$\begin{aligned}\dot{\rho} = &-\frac{i}{\hbar}[H,\rho] \\ &+ \sum_{mj,nk} \gamma_{mj,nk}\left[\sigma_-^{mj}\rho\sigma_+^{nk} - \frac{1}{2}\left\{\sigma_+^{nk}\sigma_-^{mj},\rho\right\}\right],\end{aligned} \tag{17.7}$$

with the effective Hamiltonian

$$H = H_\mathrm{A} + \hbar\sum_{mj} d_{mj}(t)\sigma_x^{mj} + \hbar\sum_{mj,nk} J_{mj,nk}\sigma_-^{mj}\sigma_+^{nk}. \tag{17.8}$$

This effective Hamiltonian contains a drive on the atoms proportional to $d_{mj}(t)$. For input coherent states incoming from the left (right) and of frequency ω_d, phase $\theta_{\mathrm{L(R)}}$ and power $P_{\mathrm{L(R)}}$ we show in Appendix 17.7.4 that

$$\begin{aligned}d_{mj}(t) = &-2\sqrt{\frac{\gamma_{mj,mj}}{2}}\left(\sqrt{\frac{P_\mathrm{L}}{\hbar\omega_{mj}}}\sin\left[\omega_d(t+t_j+\theta_\mathrm{L})\right]\right. \\ &\left.+\sqrt{\frac{P_\mathrm{R}}{\hbar\omega_{mj}}}\sin\left[\omega_d(t-t_j+\theta_\mathrm{R})\right]\right)\end{aligned} \tag{17.9}$$

with $t_j = x_j/v$.

Hamiltonian of Eq. (17.8) is Hermitian since $J_{mj,nk} = J^*_{nk,mj}$. As discussed in Appendix 17.7.2, in obtaining this expression, we have used the rotating-wave approximation, dropped small non-positive terms in the dissipators and absorbed Lamb shifts in the definition of H_A (see Appendix 17.7.2 for the full expression). As seen from Eq. (17.7), the effect of the interaction with the transmission line is to damp atoms at the rate

$$\gamma_{mj,nk} = 2\pi g_k g_j\sqrt{(m+1)(n+1)}\left(\chi_{mjk} + \chi^*_{nkj}\right). \tag{17.10}$$

with

$$\chi_{mjk} = \omega_{mj}e^{i\omega_{mj}t_{kj}}, \tag{17.11}$$

$$\hbar\omega_{mj} = E_{m+1,j} - E_{mj} \tag{17.12}$$

and $t_{kj} = |x_k - x_j|/v$ the time it takes the signal to propagate from atom k to atom j. For $j = k$, Eq. (17.10) corresponds to standard relaxation rates of the atoms. As discussed below, for $j \neq k$ this however corresponds to correlated decay.

The last term of Eq. (17.8) is an exchange interaction between the atoms being mediated by virtual excitations in the line with amplitude

$$J_{mj,nk} = -i\pi g_k g_j\sqrt{(m+1)(n+1)}\left(\chi_{mjk} - \chi^*_{nkj}\right). \tag{17.13}$$

For the particular case of a pair of levels in two atoms that are tuned to resonance, $\omega_{mj} = \omega_{nk}$, the expressions for $\gamma_{mj,nk}$ and $J_{mj,nk}$ take a simpler form [28, 29, 30, 32, 33]:

$$\gamma_{mj,nk} = 4\pi g_k g_j\omega_{mj}\sqrt{(m+1)(n+1)}\cos\left(\omega_{mj}t_{kj}\right), \tag{17.14}$$

and

$$J_{mj,nk} = 2\pi g_k g_j\omega_{mj}\sqrt{(m+1)(n+1)}\sin\left(\omega_{mj}t_{kj}\right). \tag{17.15}$$

This form makes it clear that the magnitude of these two quantities has an oscillatory dependence on interatomic separation.

17.2.2 Input-output theory

To compare theoretical predictions to experiments measuring reflection and transmission of light by the system, we derive in Appendix 17.7.6 the input-output boundary condition in the presence of artificial atoms coupled to the line. Only the main results are presented in this section. Following the standard prescription [36], we find

$$a^{\mathrm{R}}_{\mathrm{out}}(t) = a^{\mathrm{R}}_{\mathrm{in}}(t) + \sum_{mj} e^{-i\omega_{mj}t_j}\sqrt{\frac{\gamma_{mj,mj}}{2}}\sigma^{mj}_{-} \tag{17.16}$$

and

$$a^{\mathrm{L}}_{\mathrm{out}}(t) = a^{\mathrm{L}}_{\mathrm{in}}(t) + \sum_{mj} e^{i\omega_{mj}t_j}\sqrt{\frac{\gamma_{mj,mj}}{2}}\sigma^{mj}_{-}, \tag{17.17}$$

where

$$a^{\mathrm{R}}_{\mathrm{in}}(t) = \int_0^\infty \frac{d\omega}{\sqrt{2\pi}} a_{\mathrm{R}}(\omega, t_0)e^{-i\omega t} \tag{17.18}$$

represents the input field arriving at the atoms from the left and

$$a^{\mathrm{R}}_{\mathrm{out}}(t) = \int_0^\infty \frac{d\omega}{\sqrt{2\pi}} a_{\mathrm{R}}(\omega, t_1)e^{-i\omega t} \tag{17.19}$$

the output field propagating to the right after interaction with the system. As is standard in input-output formalism, $t_0 < t$ and $t_1 > t$ refer to a time respectively before or after interaction with the system. Similar expressions can be found for the left-moving fields.

Assuming for example that the system is driven from the left, it is possible to compute using Eqs. (17.16) and (17.17) the transmission coefficient

$$|t|^2 = |\left\langle a^{\mathrm{L}}_{\mathrm{out}}\right\rangle / \left\langle a^{\mathrm{L}}_{\mathrm{in}}\right\rangle|^2 \tag{17.20}$$

and the reflection coefficient

$$|r|^2 = |\left\langle a^{\mathrm{R}}_{\mathrm{out}}\right\rangle / \left\langle a^{\mathrm{L}}_{\mathrm{in}}\right\rangle|^2 \tag{17.21}$$

corresponding to elastic scattering. Another useful quantity is the power spectrum of the output field

$$S^{\alpha}[\omega] = \int_{-\infty}^{\infty} dt e^{i\omega t}\langle a^{\alpha\dagger}_{\mathrm{out}}(t)a^{\alpha}_{\mathrm{out}}(0)\rangle \tag{17.22}$$

for $\alpha = \mathrm{R}, \mathrm{L}$ and which corresponds to inelastic scattering for $\omega \neq 0$. Analytical or numerical predictions for both the elastic and inelastic scattering will be presented below for two choices of interatomic separations.

17.2.3 Dressed basis

Elsewhere [20], we report measurements of $|t|^2$, $|r|^2$, and $S^{\alpha}[\omega]$ for $N = 2$ transmons coupled to the line. There, quantitative agreement with numerical calculations is presented. Here, we take $M = N = 2$ in the reduced master equation (17.7) and focus on the analytical results. Quantitative agreement between the theoretical description below and the experimental results of Ref. [20] can be obtained.

In a frame rotating at drive frequency ω_d, taking $N = M = 2$ leads to

$$\dot{\rho} = -\frac{i}{\hbar}[H, \rho] + \sum_{jk}\gamma_{jk}\left[\sigma^j_{-}\rho\sigma^k_{+} - \frac{1}{2}\left\{\sigma^k_{+}\sigma^j_{-}, \rho\right\}\right], \tag{17.23}$$

where

$$\begin{aligned} H/\hbar = &\sum_j \Delta_j |e_j\rangle\langle e_j| + \sum_j\left(\epsilon_j\sigma^j_{+} + \mathrm{H.c.}\right) \\ &+ J(\sigma^1_{-}\sigma^2_{+} + \sigma^1_{+}\sigma^2_{-}), \end{aligned} \tag{17.24}$$

with $|e_j\rangle$ the excited state of qubit j, $\Delta_j = \omega_{0j} - \omega_d$, $J = J_{0j,0k}$ and $\gamma_{jk} = \gamma_{0j,0k} + \gamma^j_{\mathrm{nr}}\delta_{jk}$. The rate γ^j_{nr} represents nonradiative decay of qubit j. In practice, it is easy to realize a situation where qubit decay will be dominated by emission into the line, that is $\gamma_{jj} \gg \gamma^j_{\mathrm{nr}}$. In this open-line setting, satisfying this inequality corresponds to

the strong-coupling regime [37]. Assuming that the qubits are driven from the left only, Eq. (17.9) for the drive amplitude now takes the simpler form

$$\epsilon_j = -i\sqrt{\frac{\gamma_{0j,0j}\omega_d}{2\omega_{0j}}}\left\langle a_{\rm in}^{\rm L}\right\rangle e^{-i\omega_d t_j}. \tag{17.25}$$

To deal with correlated decay described by the last term of Eq. (17.23), it is useful to move to a basis that diagonalizes the dissipation matrix with components $\gamma_{j,k}$. As shown in Appendix 17.7.7, this leads to the more standard form for the last term of Eq. (17.23), which now reads

$$\sum_{\mu=B,D}\Gamma_\mu\mathcal{D}\left[\sigma_-^\mu\right]\rho, \tag{17.26}$$

where $\mathcal{D}[x]\rho = x\rho x^\dagger - \left\{x^\dagger x,\rho\right\}/2$ is the standard dissipator that is now acting on the dressed lowering operators

$$\sigma_-^\mu = \frac{\left(\Gamma_\mu-\gamma_{11}\right)\sigma_-^0 + \gamma_{01}^*\sigma_-^1}{\sqrt{\left(\Gamma_\mu-\gamma_{11}\right)^2+|\gamma_{01}|^2}}, \tag{17.27}$$

with $\mu = B, D$ and with correlated decay rates

$$\Gamma_{B/D} = \frac{\gamma_{00}+\gamma_{11}}{2} \pm \sqrt{\left(\frac{\gamma_{00}-\gamma_{11}}{2}\right)^2+|\gamma_{01}|^2}. \tag{17.28}$$

The subscripts B and D refer to bright and dark respectively. Due to dependence on the qubit separation, both the correlated qubit decay Γ_μ and exchange interaction J can be tuned by a modification of the qubit's transition frequency.

Below we consider the case of two qubits tuned in resonance at a frequency ω_0 such that the distance d between them corresponds to λ_0 or $3\lambda_0/4$, with $\lambda_0 = 2\pi v/\omega_0$. In both cases, reflection and transmission coefficients are calculated as well as the corresponding power spectra.

17.3 $\lambda/2$ separation: Sub- and Superradiance

17.3.1 Discussion

We first consider a pair of qubits tuned in resonance at a frequency ω_0, whose associated wavelength λ_0 is equal to $d = \lambda_0/2$. To simplify the discussion, we let $\gamma_{\rm nr} \equiv \gamma_{\rm nr}^0 \sim \gamma_{\rm nr}^1$. In the strong-coupling regime, $\gamma_{\rm nr}^j \ll \gamma_{00},\gamma_{11}$, and the nonradiative relaxation rate is a small perturbation. The above assumption that the nonradiative rates are equivalent for both qubits will therefore not affect the results much.

With this simplification and the choice $d = \lambda_0/2$, the off-diagonal decay rate γ_{01} defined in Eq. (17.10) can be written as

$$\gamma_{01} = \pm\sqrt{(\gamma_{00}-\gamma_{\rm nr})(\gamma_{11}-\gamma_{\rm nr})}. \tag{17.29}$$

This leads to

$$\Gamma_D = \gamma_{\rm nr} \ll \Gamma_B = \gamma_{00}+\gamma_{11}-\gamma_{\rm nr}. \tag{17.30}$$

In other words, for $d = \lambda_0/2$ the state $|D\rangle$ defined by $\sigma_-^D|D\rangle = 0$ is dark as its decay rate is purely nonradiative. On the other hand, the state $|B\rangle$ defined by $\sigma_-^B|B\rangle = 0$ is bright. This corresponds, respectively, to sub- and superradiance [25, 28, 29, 38]. Moreover, for this half-wavelength setting, the exchange interaction is absent with $J = 0$.

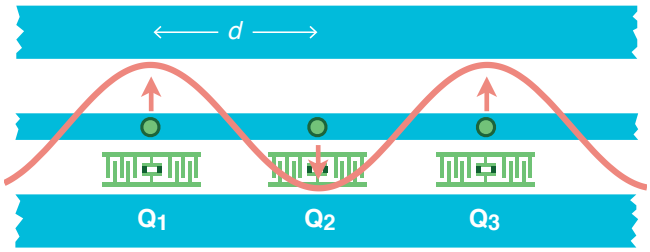

Figure 17.2: Schematic representation of three transmon qubits in a 1D transmission line. Qubits are considered as point-like objects and their locations x_j along the line are represented by circles. Q_1 and Q_2 are separated by $\lambda_0/2$ while Q_1 and Q_3 by λ_0. If Q_1 and Q_3 are identical, only symmetric superpositions of these two qubits can be excited by an external drive of wavelength λ_0. On the other hand, since they are separated by $\lambda_0/2$, only antisymmetric superpositions of Q_1 and Q_2 can be excited.

That $|B\rangle$ and $|D\rangle$ are bright and dark, respectively, can also be seen from the Hamiltonian. Indeed, by inverting Eq. (17.27), it is possible to rewrite the driving term in Eq. (17.24) as

$$\sum_{\mu=B,D} \hbar \left(\epsilon_\mu \sigma_+^\mu + \text{H.c.}\right). \tag{17.31}$$

For $|\Delta_j|/\omega_0 \ll 1$, which is easily satisfied, the drive amplitudes now take the forms

$$\begin{aligned} \epsilon_D &\approx 0, \\ \epsilon_B &\approx -i\langle a_{\text{in}}^{\text{L}}\rangle e^{-i\omega_d t_0}\sqrt{\frac{\gamma_{00}+\gamma_{11}}{2}-\gamma_{\text{nr}}}. \end{aligned} \tag{17.32}$$

Clearly, $|D\rangle$ cannot be driven from the ground state $|gg\rangle$. This can be understood intuitively from Fig. 17.2 in the case $\gamma_{00} = \gamma_{11}$. First, only consider the two leftmost qubits, Q_1 and Q_2. As illustrated in Fig. 17.2, when driven on resonance, Q_1 and Q_2 experience opposite phases of the driving field as they are separated by $d = \lambda_0/2$. In this case, transitions between $|gg\rangle$ and $|B\rangle = (|ge\rangle - |eg\rangle)/\sqrt{2}$ are allowed while transitions between $|gg\rangle$ and $|D\rangle = (|ge\rangle + |eg\rangle)/\sqrt{2}$ are forbidden. These selection rules are captured by Eq. (17.32) and are akin to what is observed in circuit QED in the presence of two qubits in the same resonator [39, 40]. As damping, just like driving, is an interaction of the qubits with the line, we also find in Eq. (17.30) that $\Gamma_D = \gamma_{\text{nr}}$ or, in other words, that $|D\rangle$ does not decay radiatively. As expected from these simple arguments, the situation is reversed for Q_1 and Q_3 in Fig. 17.2, which are separated by $d = \lambda_0$. In this case, $|B\rangle = (|ge\rangle + |eg\rangle)/\sqrt{2}$ and $|D\rangle = (|ge\rangle - |eg\rangle)/\sqrt{2}$.

It is important to point out that, since $\left[\sigma_\pm^{B/D}, \sigma_\mp^{B/D}\right] \neq 0$ and $\left[\sigma_\pm^{B/D}, \sigma_\mp^{D/B}\right] \neq 0$, $|D\rangle$ will not be completely dark in practice and especially not in the presence of finite nonradiative decay γ_{nr}. Indeed, as illustrated in Fig. 17.3(a), the joint excited state $|ee\rangle$ can be reached from $|B\rangle$ by driving with σ_+^B. From this state, $|D\rangle$ can be populated with the action of σ_-^B when $\gamma_{00} \neq \gamma_{11}$. This is because the matrix element of σ_-^B between $|ee\rangle$ and $|D\rangle$ is proportional to the asymmetry $(\gamma_{00}-\gamma_{11})/(\gamma_{00}+\gamma_{11})$, as shown in Fig. 17.3(b). The dark state can also be populated by nonradiative decay. It is interesting to point out that, while nonradiative relaxation cannot be controlled in this system, the indirect driving of $|D\rangle$ from $|ee\rangle$ can be tuned by controlling the asymmetry between γ_{00} and γ_{11}, something that can be done by tuning the qubit frequency.

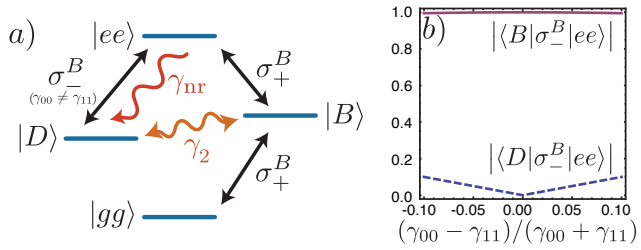

Figure 17.3: (a) Schematic energy level diagram for two qubits in a transmission line. The dark state $|D\rangle$ cannot be driven directly from the ground state $|gg\rangle$. If the qubits are identical, it can however be excited by nonradiative relaxation γ_{nr} from $|ee\rangle$. In the situation where the qubit relaxation rates are different ($\gamma_{00} \neq \gamma_{11}$), it can be excited indirectly from $|B\rangle$ via $|ee\rangle$. Dephasing (γ_2) can also cause transition between $|B\rangle$ and $|D\rangle$. (b) Matrix elements of σ_-^B as a function of the relaxation rate asymmetry $(\gamma_{00}-\gamma_{11})/(\gamma_{00}+\gamma_{11})$.

17.4 Elastic scattering

In this section, we compute the elastic scattering or, more precisely, the transmission, Eq. (17.20), and reflection coefficients, Eq. (17.21), assuming the two-qubit system to be driven from the left. To simplify the discussion, as before we take both qubits to have the same frequency, such that $\Delta = \Delta_j$, and have the same total decay rate $\gamma = \gamma_{jj}$. It is also useful to introduce $\gamma_{\text{r}} = |\gamma_{01}| = \gamma - \gamma_{\text{nr}}$, the radiative contribution to the decay rate. With these definitions and Eq. (17.16), we find for the outgoing field that

$$a_{\text{out}}^{\text{R/L}} = a_{\text{in}}^{\text{R/L}} \pm i\sqrt{\gamma_{\text{r}}}\sigma_-^B. \tag{17.33}$$

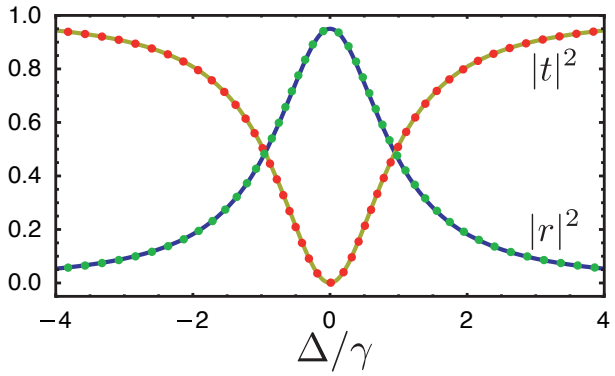

Figure 17.4: Transmission and reflection coefficients as a function of normalized detuning Δ/γ between the qubits equal transition frequencies and drive. The qubits are tuned such that they are separated by $d = \lambda_0$. There is full transmission extinction on resonance. The width of both $|t|^2$ and $|r|^2$ is given by the superradiant rate $\Gamma_B \sim 2\gamma$. Solid lines are obtained from analytical results whereas the dotted lines are obtained from numerical simulations of the reduced master equation. The selected parameters are $\gamma_r = 0.95\gamma$ and $\gamma/2\pi = 18.8$ MHz.

Solving for $\langle \sigma_-^B \rangle$ in steady state using the master equation (17.23), we have, to first order in the drive amplitude $\langle a_{\rm in}^{\rm L} \rangle$,

$$\langle a_{\rm out}^{\rm R} \rangle = \langle a_{\rm in}^{\rm L} \rangle \frac{-i(\Gamma_B - \gamma_{\rm nr})/2}{\Delta - i\Gamma_B/2}, \tag{17.34}$$

$$\langle a_{\rm out}^{\rm L} \rangle = \langle a_{\rm in}^{\rm L} \rangle \left(1 - \frac{-i(\Gamma_B - \gamma_{\rm nr})/2}{\Delta - i\Gamma_B/2} \right). \tag{17.35}$$

These equations are expected for a single qubit with relaxation rate Γ_B [10]. Indeed, in the absence of nonradiative decay, there is full extinction of the transmission and complete reflection when driving (with low power) on resonance $\Delta = 0$. While we are dealing here with a four-level system, this simple behavior is observed because, as illustrated in Fig. 17.3, at low irradiation power and in the absence of nonradiative decay or additional dephasing, only two levels are relevant, $\{|gg\rangle, |B\rangle\}$. The two qubits behave like a single two-level system coupled to the line and with decay rate Γ_B.

The output fields can also be obtained exactly analytically, but this leads to expressions that are too long to be worth reproducing here. The transmission $|t|^2$ and reflection coefficients $|r|^2$ obtained from these exact expressions are illustrated in Fig. 17.4. These are in excellent agreement with results obtained from numerical integration of the reduced master equation Eq. (17.7). As expected from the above discussion, the width of the transmission dip is given by the superradiant rate $\Gamma_B \sim 2\gamma$.

17.4.1 Inelastic scattering

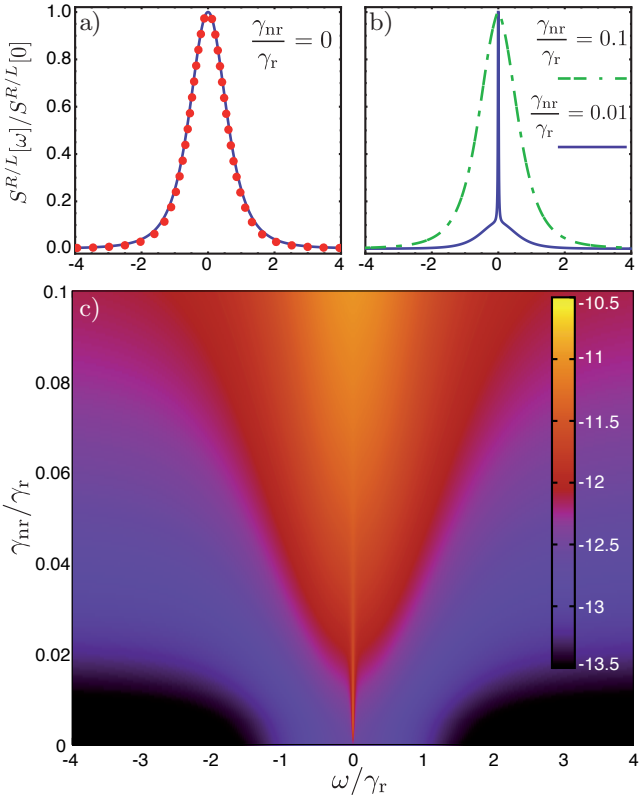

Figure 17.5: Power spectral density $S^{\alpha}[\omega]$ as a function of normalized frequency ω/γ_r and for a weak coherent tone corresponding to an amplitude $\epsilon_B/\gamma_r = 0.005$. The qubits are tuned such that they are separated by $d = \lambda_0$. In the absence of nonradiative relaxation or asymmetry in the qubit decay rates, a squared Lorentzian of width $\Gamma_B = 2\gamma_r$ is observed. In the presence of nonradiative relaxation the dark state can be populated and a narrow peak appears in the spectrum. (a) Analytical (solid blue line) and numerical (red dots) power spectral densities for $\gamma_{nr} = 0$. (b) Numerical power spectral density for $\gamma_{nr}/\gamma_r = 0.1$ (green dashed line) and $\gamma_{nr}/\gamma_r = 0.01$ (solid blue line). (c) Log_{10} of the numerical power spectral density vs frequency and as a function of nonradiative relaxation γ_{nr}/γ_r. $\gamma_r/2\pi = 17.9$ MHz.

As argued above, for $\gamma_{nr}/\gamma_r = 0$ and in the absence of pure dephasing, the state $|D\rangle$ is unpopulated and at low enough power, we are left with an effective two-level system $\{|gg\rangle, |B\rangle\}$. In this case, the normalized power spectral density takes the simple form [41]

$$S^{R/L}[\omega] = \frac{8\epsilon_B^{\text{eff}4}}{[(\Gamma_B/2)^2 + \omega^2]^2}, \tag{17.36}$$

with ϵ_B^{eff} the effective driving strength of the superradiant state. Figure 17.5(a) plots this expression with ϵ_B^{eff} evaluated as a fit parameter for results obtained from numerical integration of the master equation (17.7) and Eq. (17.22) in the limit $\gamma_{nr}/\gamma_r = 0$. As illustrated in Fig. 17.5(b), for γ_{nr}/γ_r finite but small, results obtained from numerical integration deviate from the above simple expression and show a sharp peak in the spectral density centered at zero (solid blue line). This is a signature of the subradiant state $|D\rangle$ that can become populated, as illustrated schematically in Fig. 17.3, via $|ee\rangle$ by nonradiative decay γ_{nr} and via $|B\rangle$ by dephasing $\gamma_2 = \gamma_{nr}/2 + \gamma_\varphi$. This peak should not be confused with the Rayleigh-scattered radiation which results in a δ peak at $\omega = 0$ and which we have removed here.

As illustrated in Fig. 17.5(b), the signature of the dark state disappears in the presence of large nonradiative decay. The evolution of this feature as a function of γ_{nr}/γ_r is presented in Fig. 17.5(c). Whereas a finite nonradiative decay rate is useful to observe both the signature of super- and subradiance, it is required for the system to be in the strong-coupling regime for both features to be observable. As shown in Ref. [20], this can be achieved with transmon qubits.

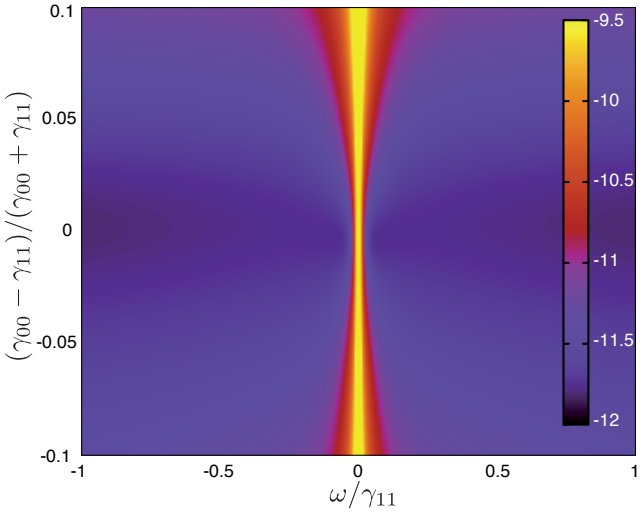

Figure 17.6: Log_{10} of the numerical power spectral density $S^{\alpha}[\omega]$ as a function of normalized frequency ω/γ_{11} and relaxation rate asymmetry $(\gamma_{00}-\gamma_{11})/(\gamma_{00}+\gamma_{11})$. The drive power and nonradiative decay are chosen such that $\epsilon_B/\gamma_{11}=0.005$ and $\gamma_{\text{nr}}/\gamma_{11}=0.01$, corresponding to a weak coherent drive tone in the strong-coupling limit. The qubits are tuned such that they are separated by $d=\lambda_0$. Asymmetry between the relaxation rates opens a new drive channel for the dark state $|D\rangle$, causing power broadening. $\gamma_{11}/2\pi=18.1$ MHz.

The above results have been obtained in the idealized case where $\gamma_{00}=\gamma_{11}$. These decay rates, defined below Eq. (17.24), contain both the radiative and the nonradiative contributions. Some asymmetry in the decay rates is to be expected in practice. As illustrated in Fig. 17.3, this leads to a finite transition matrix element between $|ee\rangle$ and the dark state $|D\rangle$. The effect of this asymmetry is illustrated in Fig. 17.6, which presents the numerically computed power spectral density as a function of both frequency and asymmetry $(\gamma_{00}-\gamma_{11})/(\gamma_{00}+\gamma_{11})$. These results are obtained for a constant $\gamma_{\text{nr}}/\gamma_{11}=0.01$ corresponding to the strong coupling limit. This additional population mechanism for the dark state leads to power broadening of the sharp feature centered around $\omega=0$. However, with up to 10% asymmetry, this signature of superradiance is expected to be clearly observable at low power. This is confirmed experimentally [20].

17.5 $\lambda/4$ separation: Exchange interaction

17.5.1 Discussion

We now consider the situation where the transition frequency of both qubits is chosen such that the qubit separation d is an odd multiple of $\lambda_0/4$. This is illustrated in Fig. 17.7 where Q_1 and Q_3 are separated by $3\lambda/4$. As can be seen from Eqs. (17.14) and (17.15), in this case the correlated decay rate $\gamma_{01}\propto\cos(2\pi d/\lambda_0)$ is zero and the exchange interaction $\propto\sin(2\pi d/\lambda_0)$ takes its maximal value $|J|=\gamma_{\text{r}}/2$.

That this interaction is at a maximum for this separation can be understood intuitively from Fig. 17.7 and by going back to the origin of the virtual interaction term in the derivation of the effective master equation. Indeed, as can be seen in detailed calculation presented in Appendix 17.7.2, the exchange interaction J is a modification of the Lamb shift in the presence of multiple qubits coupled to the line. Basically, virtual photons emitted and reabsorbed by a given qubit contribute to the qubit's Lamb shift. In the presence of two (or more) qubits, virtual photons can be emitted by one qubit and absorbed by the other, leading to an effective qubit-qubit interaction. This type of exchange interaction is well known in circuit QED where the qubits interact strongly with a single mode of a resonator leading to $J=g_1g_2/\delta$, with δ the detuning of both qubits to the resonator [39, 40]. In the present open-line context where the qubits interact with a continuum of modes, J is of the same form but is now an integral over all continuous modes *except* the continuous modes lying at qubit transition frequency [7].

As illustrated in Fig. 17.7 for Q_1 and Q_3, the continuous modes at longer wavelength than $3\lambda_0/4$ (dashed line) have a phase of opposite sign at the location of the second qubit with respect to continuous-modes of shorter wavelength than $3\lambda_0/4$ (dotted line). Moreover, since these continuous modes are, respectively, below and above the qubit frequency, their respective detuning δ is also of opposite sign. This double change of sign results in a finite exchange interaction because the contribution to J of the modes around $3\lambda_0/4$ all have the same overall (negative) sign. In contrast, for Q_1 and Q_2 which are separated by $\lambda_0/2$, the phases of all the

[7] The exclusion of the qubit transition frequency comes from the principal part in Eq. (17.65). Indeed, in this equation, the Dirac delta is responsible for relaxation (by emission of photons at the qubit transition frequency) while the principal part is responsible for the Lamb shift and the exchange interaction.

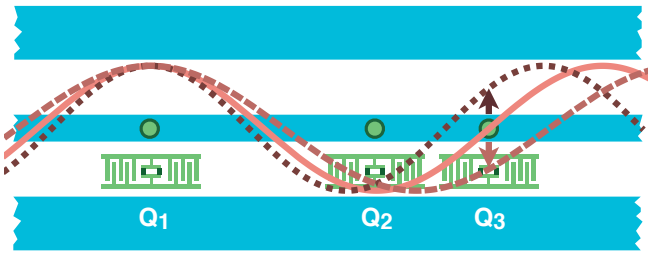

Figure 17.7: Schematic representation of three transmon qubits in a 1D transmission line. Qubits are considered as point-like objects and their location x_j along the line is represented by circles. As illustrated by the solid line, the distance between Q_1 and Q_3 corresponds to $3\lambda_0/4$. At the location of Q_3, modes of frequency around $3\lambda_0/4$ have opposite signs (see dashed and dotted line). On the other hand, for a separation corresponding to $\lambda_0/2$ just like Q_1 and Q_2, all modes have the same sign around Q_2.

continuous-modes at Q_2 have the same sign while the detuning δ changes sign. In this case, the exchange interaction vanishes when integrating over all continuous-modes above and below $\lambda_0/2$.

Assuming that the qubits are in resonance, and taking $\gamma = \gamma_{jj}$ for simplicity, this discussion can be made more formal by working in the dressed basis, which diagonalizes the effective Hamiltonian, Eq. (17.24). In this situation, the dressed lowering operators, Eq. (17.27), take the simple form

$$\sigma_-^{B/D} = \frac{\sigma_-^1 \pm \sigma_-^0}{\sqrt{2}}. \tag{17.37}$$

The master equation then reads

$$\dot{\rho} = -\frac{i}{\hbar}[H,\rho] + \gamma \sum_{i=B,D} \mathcal{D}\left[\sigma_-^i\right]\rho, \tag{17.38}$$

where

$$H = \sum_{i=B,D} \hbar\omega_i \sigma_+^i \sigma_-^i + \sum_{i=B,D} \hbar\left(\epsilon_i \sigma_+^i + \text{H.c.}\right), \tag{17.39}$$

and $\omega_{B/D} = \Delta \pm J$, $\epsilon_{B/D} = (\epsilon_1 \pm \epsilon_0)/\sqrt{2}$. As expected, in the dressed basis, the system is described by two driven eigenstates whose frequencies differ by $2J$.

17.5.2 Elastic scattering

We now turn to elastic scattering. Using Eqs. (17.17) and (17.16), the output fields can be expressed as

$$a_{\text{out}}^{\text{R}}(t) = \sqrt{\frac{\gamma_{\text{r}}}{2}} e^{-i\omega_0 t_0}\left[\sigma_-^0 - i\,\text{sgn}\,(J)\,\sigma_-^1\right], \tag{17.40}$$

$$a_{\text{out}}^{\text{L}}(t) = a_{\text{in}}^{\text{L}} + \sqrt{\frac{\gamma_{\text{r}}}{2}} e^{i\omega_0 t_0}\left[\sigma_-^0 + i\,\text{sgn}\,(J)\,\sigma_-^1\right]. \tag{17.41}$$

To first order in the drive amplitude $\langle a_{\text{in}}^{\text{L}}\rangle$, we then find the expectation values of these two quantities:

$$\langle a_{\text{out}}^{\text{L}}\rangle = \langle a_{\text{in}}^{\text{L}}\rangle \frac{J^2 - [\Delta - i\gamma/2][\Delta + i(\gamma_{\text{r}} - \gamma/2)]}{J^2 - (\Delta - i\gamma/2)^2}, \tag{17.42}$$

$$\langle a_{\text{out}}^{\text{R}}\rangle = \langle a_{\text{in}}^{\text{L}}\rangle \frac{-|J|\gamma_{\text{r}}}{J^2-)\Delta - i\gamma/2)^2}. \tag{17.43}$$

As $|J| = \gamma_{\text{r}}/2$, we expect transmission extinction if $\gamma_{\text{nr}}/\gamma \ll 1$ as in the $\lambda/2$ case. However, here the width of the extinction is given by γ, whereas this width was superradiant ($\Gamma_B = 2\gamma$) in the $\lambda/2$ case.

Using these expressions, we plot in Fig. 17.8(a) the reflection $|r|^2$ and transmission $|t|^2$ coefficients along with the corresponding results obtained from numerical simulations of the reduced master equation (17.7). The agreement is excellent, with transmission extinction at $\Delta = 0$. It is also interesting to observe that these coefficients do not have a Lorentzian profile when nonradiative decay is weak. Indeed, in this situation both $|r|^2$ and $|t|^2$ are rather flat around $\Delta = 0$. This is a consequence of the coupling J. Since the maximal magnitude of J is $\gamma_{\text{r}}/2$ and the width is $\gamma \geq \gamma_{\text{r}}$, a double peak structure is never resolved and instead leads to the non-Lorentzian profile seen in panel (a).

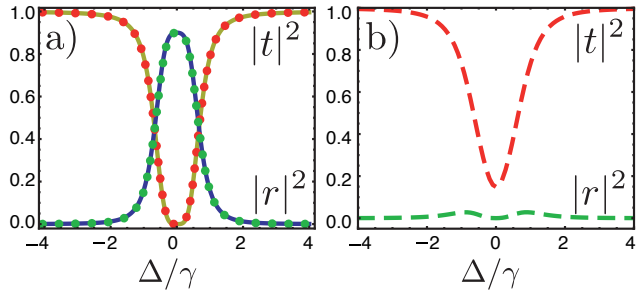

Figure 17.8: Transmission and reflection coefficients as a function of normalized detuning Δ/γ between the qubits transition frequencies and drive. The qubits are tuned such that $d = 3\lambda_0/4$. Full lines are analytical results while dotted lines are numerical results. (a) $|\epsilon_0|/\gamma = 0.005$. At low power, $|t|^2 + |r|^2 \sim 1$. (b) $|\epsilon_0|/\gamma = 0.35$. At high power, inelastic scattering is more important so that $|t|^2 + |r|^2 < 1$ around $\Delta = 0$. Radiative decay $\gamma_r = 0.95\gamma$ and $\gamma_r/2\pi = 10.3$ MHz in the numerical simulations.

In Fig. 17.8(b), we show results obtained from numerical simulations of the reduced master equation (17.7) at a larger power. Because of the increased power broadening, the transmission dip is more Lorentzian-like than in panel (a). Interestingly, at this higher power we find that $|t|^2 + |r|^2 < 1$ for $|\Delta| \lesssim \gamma$. This is because at these powers the effective two-level system becomes strongly dressed by the incoming light, leading to significant inelastic scattering. As expected, in this situation the power spectrum shows a Mollow triplet structure [20, 10, 14]. A signature of this dressing can be found in the reflection coefficient which shows two small peaks whose separation is tuned by the input power. For even larger power, the effective two-level system becomes saturated and $|t|^2 \to 1$ for all values of Δ (not shown). This is also observed experimentally [20].

17.5.3 Inelastic scattering

Taking $\gamma = \gamma_{jj}$ as in the previous section, the power spectrum, Eq. (17.22), vanishes to second order in ϵ_B/Γ_D, where ϵ_B is the drive amplitude. In this section, we therefore rely on numerical integration of the master equation (17.7). Figure 17.9(a) shows the simulated power spectrum in transmission $S^{\rm L}[\omega]$ (red dashed line) and in reflection $S^{\rm R}[\omega]$ (green dashed line) in the absence of nonradiative damping. The yellow dashed line corresponds to the power spectrum $S[\omega]$ obtained by combining the transmitted and reflected components of the output fields with a phase shift of $\pi/2$. In all cases, a clear signature of the exchange interaction J can be seen in the form of a doublet feature in the spectrum. The splitting of this doublet is exactly $2J$ for $S[\omega]$, while it is *larger* than $2J$ when measured only in transmission and *smaller* than $2J$ in reflection. In the presence of nonradiative damping, we thus expect the doublet structure to be easier to resolve in transmission.

To understand the differences between $S^{\rm R}[\omega]$, $S^{\rm L}[\omega]$, and $S[\omega]$, it is useful to consider the expected spectrum as a function of an additional phase shift. For this reason, we introduce

$$S[\omega,\phi] = \frac{\gamma_r}{2}\int_{-\infty}^{\infty} dt e^{i\omega t}\langle A^\dagger(t,\phi)A(0,\phi)\rangle, \tag{17.44}$$

where we have defined

$$A(t,\phi) = \sigma_-^B(t) + e^{i\phi}\sigma_-^D(t). \tag{17.45}$$

This spectrum is plotted as a function of frequency and phase in Fig. 17.9(c). As noted earlier, the transmitted signal $S^{\rm L}[\omega] = S[\omega,\pi/2]$ shows a splitting larger than $2J$, the reflected signal $S^{\rm R}[\omega] = S[\omega,3\pi/2]$ a splitting smaller than $2J$, while the splitting of $2J$ is recovered for $S[\omega] = S[\omega,\pi]$. We note that in the above expression for $S[\omega,\phi]$ we have removed the contribution of the in-field for clarity [see Eq. (17.22) for the full expression].

We explore in Fig. 17.9(b) the effect of asymmetry between relaxation rates and of nonradiative decay on $S[\omega]$. The only significant contribution is a rescaling of the power spectral density. In the case of asymmetry, this rescaling occurs because the coupling $\gamma_{r0} = \gamma_{00} - \gamma_{\rm nr}$ between the qubits and the line is changing, whereas in the case of nonradiative decay the rescaling is due to the increased losses.

17.6 Conclusion

Based on Lehmberg's work [21], we have obtained an effective master equation describing an arbitrary number of inhomogeneous many-level (artificial) atoms coupled to a 1D transmission line and driven by a coherent state. Elastic and inelastic scattering of an input beam are calculated for two qubits using input-output theory. While individual atoms act as simple mirrors at low power, reflecting incident light, collective

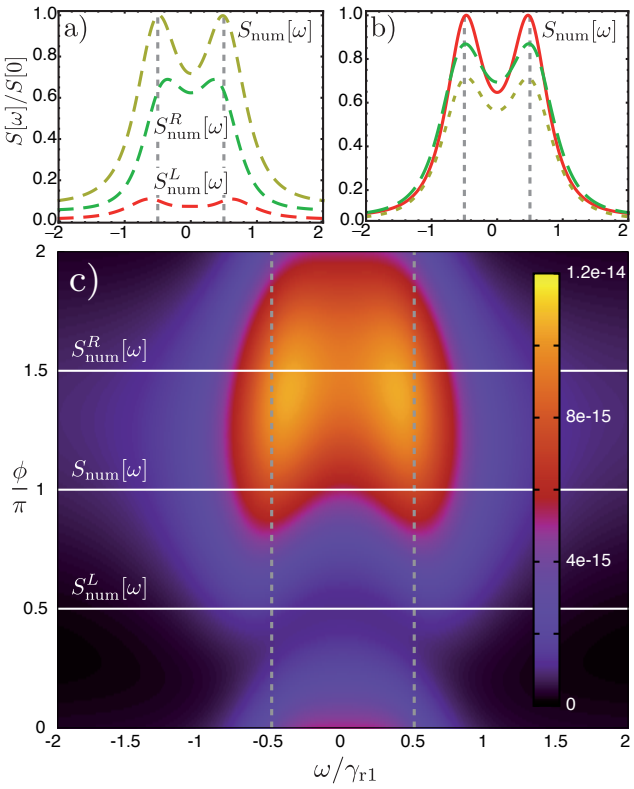

Figure 17.9: Spectral density as a function of normalized frequency $\omega/\gamma_{\rm r1}$ where $\gamma_{{\rm r}j} = \gamma_{jj} - \gamma_{\rm nr}$. The qubits are tuned such that $d = 3\lambda_0/4$. The spectral density of the transmitted power $S^{\rm L}(\omega)$ shows a signature of the exchange interaction J while it is less obvious in reflection $S^{\rm R}(\omega)$. The spectral density of the total signal $S[\omega]$ shows a splitting of $2J$ (indicated by the vertical dashed lines) (a) $\gamma_{\rm nr} = 0$. (b) $(\gamma_{00} - \gamma_{11})/(\gamma_{00} + \gamma_{11}) = (0.9, 1.1)$ for the solid red line and the long-dashed green line respectively. $\gamma_{\rm nr}/\gamma_{\rm r1} = 0.1$ for the dashed yellow line. (c) $S[\omega, \phi]$ as a function of ω and ϕ with $\gamma_{\rm nr} = 0$ and $\gamma_{\rm r0} = \gamma_{\rm r1}$. In all cases, $\gamma_{\rm r1}/2\pi = 10.3$ MHz.

effects emerge in the presence of several atoms coupled to the same line. The nature of these effects changes with qubit separation or equivalently with the qubit transition frequency. When the qubits are separated by λ_0, elastic and inelastic scattering show signatures of super- and subradiance. The dark state associated with subradiance can be made not completely dark by changing the asymmetry between the qubits' relaxation rates. This can be done by tuning the qubits' transition frequencies. On the other hand, for a separation corresponding to $3\lambda_0/4$, the inelastic scattering shows a doublet structure. This is a signature of the coherent exchange of virtual photons between the atoms. These results are in excellent agreement with experimental results [20].

Interesting directions for future work include exploring interaction of atoms with a squeezed electromagnetic field in a transmission line [43], studying correlation function measurements of the transmitted or reflected fields, and considering a network of atoms in a one-dimensional waveguide.

17.7 Appendix

17.7.1 Derivation of the waveguide QED Hamiltonian with superconducting qubits

In this appendix, we derive the Hamiltonian for an ensemble of N transmon qubits capacitively coupled to an open transmission line. A similar calculation for a single qubit can be found in Ref. [17]. As illustrated in Fig. 17.10, we use a lumped element description of the line, which is characterized by a capacitance per unit length c and inductance per unit length l, with x_0 the length of a single LC unit which will be taken to zero below. The jth qubit, of Josephson energy E_{Jj} and capacitance C_{Jj}, is coupled to the line at positions x_j

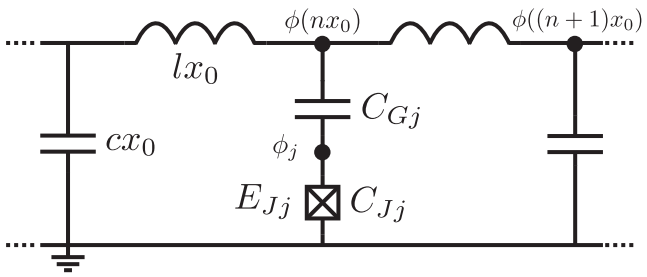

Figure 17.10: Lumped element representation of a transmission line, capacitively coupled to a transmon qubit.

through a gate capacitor C_{Gj}. The corresponding Lagrangian is

$$\begin{aligned} L =& \sum_n \left[\frac{cx_0}{2}\dot{\phi}(nx_0)^2 + \sum_j \frac{C_{Gj}\delta_{nx_0,x_j}}{2}[\dot{\phi}(nx_0) - \dot{\phi}_j]^2 \right. \\ & \left. - \frac{\{\phi[(n+1)x_0] - \phi(nx_0)\}^2}{2lx_0} \right] \\ & + \sum_{j=0}^{N-1} \left[\frac{C_{Jj}}{2}\dot{\phi}_j^2 + E_{Jj}\cos\left(\frac{2\pi}{\Phi_0}\phi_j\right) \right], \end{aligned} \tag{17.46}$$

where $\phi(x)$ and ϕ_j are the generalized fluxes, as defined in Ref. [44]. Φ_0 is the magnetic flux quantum. Introducing the charges $p(x_j)$ and p_j conjugate to the generalized fluxes, the Hamiltonian takes the form

$$H_{\mathrm{T}} = H_{\mathrm{A}} + H_{\mathrm{F}} + \sum_j \frac{p_j p(x_j) + \mathrm{H.c.}}{2c_{gj}}. \tag{17.47}$$

In this expression,

$$H_{\mathrm{A}} = \sum_j \left[\frac{p_j^2}{2C_j} - E_{Jj}\cos\left(\frac{2\pi}{\Phi_0}\phi_j\right) \right] \tag{17.48}$$

is the free-transmon Hamiltonian with

$$C_j = \frac{(C_{Gj} + C_{Jj})cx_0 + C_{Gj}C_{Jj}}{C_{Gj} + cx_0}. \tag{17.49}$$

The transmission line Hamiltonian reads

$$H_{\mathrm{F}} = \sum_n \left(\frac{x_0 p(nx_0)^2}{2c_L(nx_0)} + \frac{\{\phi[(n+1)x_0] - \phi(nx_0)\}^2}{2lx_0} \right), \tag{17.50}$$

where we have defined the effective transmission line capacitance per unit of length

$$c_L(nx_0) = c + \sum_j \frac{C_{Gj}C_{Jj}}{C_{Gj} + C_{Jj}} \frac{\delta_{nx_0,x_j}}{x_0}, \tag{17.51}$$

and the effective coupling capacitance per unit of length

$$c_{gj} = \frac{(C_{Gj} + C_{Jj})\, c + C_{Gj}C_{Jj}/x_0}{C_{Gj}}. \tag{17.52}$$

Letting $x_0 \to 0$, we obtain

$$H_{\mathrm{F}} = \int dx \left(\frac{p(x)^2}{2c_L(x)} + \frac{[\partial_x \phi(x)]^2}{2l} \right), \tag{17.53}$$

with

$$C_j = \frac{(C_{Gj}+C_{Jj})cL_A + C_{Gj}C_{Jj}}{C_{Gj}+cL_A}, \tag{17.54}$$

$$c_L(x) = c + \sum_j \frac{C_{Gj}C_{Jj}}{C_{Gj}+C_{Jj}}\delta(x-x_j), \tag{17.55}$$

$$c_{gj} = \frac{(C_{Gj}+C_{Jj})\,c + C_{Gj}C_{Jj}/L_{\rm A}}{C_{Gj}}, \tag{17.56}$$

with $L_{\rm A}$ the length of the Josephson junctions.

Using the expression for $c_L(x)$ above, the average capacitance of the transmission line over a length d extending over all of the qubits is

$$\begin{aligned}\bar{c}_L &= \frac{1}{d}\int_0^d dx\left(c + \sum_j \frac{C_{Gj}C_{Jj}}{C_{Gj}+C_{Jj}}\delta(x-x_j)\right)\\ &= c + \frac{1}{d}\sum_j \frac{C_{Gj}C_{Jj}}{C_{Gj}+C_{Jj}}.\end{aligned} \tag{17.57}$$

In practice, $cd \gg \sum_j C_{Gj}C_{Jj}/(C_{Gj}+C_{Jj})$ and the qubit's capacitances are small perturbations on the transmission line. In other words, $c_L(x) \sim c$ and the standard quantization procedure leads to the Hamiltonians of Eqs. (17.1) - (17.3) in the main text [45].

17.7.2 Master equation for ensemble of inhomogeneous atoms in open 1D space

For completeness, we derive in this appendix the master equation presented in Eq. (17.7) of the main text. The different approximations used in obtaining this result are mentioned here, but discussed in more detail in Appendix 17.7.3. As discussed in Sec. 17.2, we consider an ensemble of N multi-level (artificial) atoms dipole coupled to a 1D transmission line. The total Hamiltonian takes the form $H_{\rm T} = H_{\rm F} + H_{\rm A} + H_{\rm I}$, where the field Hamiltonian $H_{\rm F}$ is given in Eq. (17.1), the artificial atom Hamiltonian $H_{\rm A}$ in Eq. (17.2), and their interaction $H_{\rm I}$ in Eq. (17.3).

Following Lehmberg [21], to obtain an effective master equation for the artificial atoms we first move to the Heisenberg picture where the field operator $\dot{a}_{\rm R}(\omega)$ obeys the equation

$$\dot{a}_{\rm R}(\omega) = -i\omega a_{\rm R}(\omega) + \sum_{mj} g_j\sqrt{m+1}\sqrt{\omega}e^{-i\omega x_j/v}\sigma_x^{mj}. \tag{17.58}$$

Integrating from an initial time $t_0 = 0$ before the interaction, the above equation yields

$$\begin{aligned}a_{\rm R}(\omega,t) =& a_{\rm R}(\omega,0)e^{-i\omega t}\\ &+ \sum_{mj} g_j\sqrt{m+1}\sqrt{\omega}\int_0^t d\tau e^{-i\omega(t-\tau+t_j)}\sigma_x^{mj}(\tau),\end{aligned} \tag{17.59}$$

with $t_j = x_j/v$. The expression for $a_{\rm L}(\omega,t)$ is obtained with the replacement $t_j \to -t_j$. Using these results we can express $\Xi_j(t)$ defined in Eq. (17.4) as

$$\begin{aligned}\Xi_j(t) =& \Xi_j^{\rm in}(t)\\ &- i\sum_{nk}\sum_{\sigma=\pm1} g_k\sqrt{n+1}\int_0^t d\tau I_{nk}(t,\tau,\sigma t_{kj}),\end{aligned} \tag{17.60}$$

with $t_{kj} = |x_k - x_j|/v$ the time a signal takes to propagate from atom k to atom j and where we have defined

$$\begin{aligned}\Xi_j^{\rm in}(t) = -i\int_0^\infty d\omega\sqrt{\omega}\Big[&a_{\rm L}(\omega,0)e^{-i\omega(t+t_j)}\\ &+a_{\rm R}(\omega,0)e^{-i\omega(t-t_j)}\Big]\end{aligned} \tag{17.61}$$

and

$$I_{nk}(t,\tau,t_{kj}) = \int_0^\infty d\omega\omega e^{i\omega(\tau-t-t_{kj})}\sigma_x^{nk}(\tau). \tag{17.62}$$

Since the integrand of $I_{nk}(t,\tau,t_{kj})$ is proportional to ω, the integral is dominated by high frequencies where the exponential is, however, oscillating rapidly. As argued in Appendix 17.7.3, it is then reasonable to take

$$\sigma_-^{nk}(\tau) \approx \sigma_-^{nk}(t)e^{-i\omega_{nk}(\tau-t)}, \tag{17.63}$$

and $\omega_{nk}t \to \infty$, where

$$\omega_{nk} = \left(E_{(n+1)k} - E_{nk}\right)/\hbar \tag{17.64}$$

is the transition frequency between levels $n+1$ and n of atom k.

Using the standard identity

$$\int_0^\infty dx e^{-ikx} = \pi\delta(k) - i\mathrm{P}\left(\frac{1}{k}\right), \tag{17.65}$$

with P the Cauchy principal value, we obtain

$$\begin{aligned}\Xi_j(t) =& \Xi_j^{\mathrm{in}}(t) \\ &- \frac{1}{g_j}\sum_{nk}\left[\Omega_{kj}^{n+}\sigma_+^{nk} + \left(\Omega_{kj}^{n-} + i\gamma_{kj}^n/2\right)\sigma_-^{nk}\right].\end{aligned} \tag{17.66}$$

In this expression, we have defined

$$\Omega_{kj}^{n\pm} = 2g_kg_j\sqrt{n+1}\,\mathrm{P}\int_0^\infty \frac{\omega\cos\left[\omega t_{kj}\right]}{\omega \pm \omega_{nk}}d\omega \tag{17.67}$$

and

$$\gamma_{kj}^n = 4\pi g_k g_j \omega_{nk}\sqrt{n+1}\cos\left[\omega_{nk}t_{kj}\right]. \tag{17.68}$$

Again following Lehmberg [21], a reduced master equation for the atoms is obtained by first considering the Heisenberg equation of motion of an arbitrary operator Q acting on the atoms only. Given that $[Q(t),\Xi_j(t)] = 0$ at all times [this is more clearly seen from the form of Eq. (17.4) of $\Xi_j(t)$], we find

$$\begin{aligned}\dot{Q}(t) =& \frac{i}{\hbar}\left[H_A + \hbar\sum_{mj}\sqrt{m+1}g_j\left(\Xi_j^{\mathrm{in}} + \mathrm{H.c.}\right)\sigma_x^{mj}, Q\right] \\ &+ \sum_{mj}\sum_{nk}\sqrt{m+1} \\ &\times\Big[-i\Omega_{kj}^{n+}\left(\sigma_x^{mj}Q\sigma_+^{nk} - Q\sigma_x^{mj}\sigma_+^{nk} - \mathrm{H.c.}\right) \\ &- i\Omega_{kj}^{n-}\left(\sigma_x^{mj}Q\sigma_-^{nk} - Q\sigma_x^{mj}\sigma_-^{nk} - \mathrm{H.c.}\right) \\ &+ \frac{\gamma_{kj}^n}{2}\left(\sigma_x^{mj}Q\sigma_-^{nk} - Q\sigma_x^{mj}\sigma_-^{nk} + \mathrm{H.c.}\right)\Big].\end{aligned} \tag{17.69}$$

With $\mathrm{Tr}(\dot{Q}\rho_T) = \mathrm{Tr_A}(Q\dot{\rho})$, where $\rho = \mathrm{Tr_R}(\rho_T)$ is the reduced master equation of the atoms, we finally obtain after using the rotating-wave approximation

$$\begin{aligned}\dot{\rho} =& -i\left[\frac{H_\mathrm{A}}{\hbar} + \sum_{mj}L_{mj}\left|m_j\right\rangle\left\langle m_j\right|, \rho\right] \\ &- i\left[\sum_{mj}d_{mj}(t)\sigma_x^{mj} + \sum_{mj}\sum_{nk}J_{mj,nk}\sigma_+^{nk}\sigma_-^{mj}, \rho\right] \\ &+ \sum_{mj}\sum_{nk}\Big[\gamma_{mj,nk}\left(\sigma_-^{mj}\rho\sigma_+^{nk} - \frac{1}{2}\left\{\sigma_+^{nk}\sigma_-^{mj}, \rho\right\}\right) \\ &+ \Omega_{mj,nk}\left(\sigma_+^{mj}\rho\sigma_-^{nk} + \sigma_-^{nk}\rho\sigma_+^{mj} - \left\{\sigma_-^{nk}\sigma_+^{mj}, \rho\right\}\right)\Big].\end{aligned} \tag{17.70}$$

To obtain this expression, we have assumed that the system is driven from the left and the right by coherent fields of frequency ω_d, phase $\theta_{\mathrm{L(R)}}$ and power $P_{\mathrm{L(R)}}$. As shown in Appendix 17.7.4, the resulting amplitude of the qubit driving term in the above master equation takes the form

$$d_{mj}(t) = -2\sqrt{\frac{\gamma_{mj,mj}}{2}}\left(\sqrt{\frac{P_{\mathrm{L}}}{\hbar\omega_{mj}}}\sin\left[\omega_d(t+t_j+\theta_{\mathrm{L}})\right] + \sqrt{\frac{P_{\mathrm{R}}}{\hbar\omega_{mj}}}\sin\left[\omega_d(t-t_j+\theta_{\mathrm{R}})\right]\right). \tag{17.71}$$

We have also defined the Lamb shift

$$L_{mj} = -\left(\sqrt{m+1}\Omega_{jj}^{m+} - \sqrt{m}\Omega_{jj}^{(m-1)-}\right), \tag{17.72}$$

the (joint) decay rate

$$\frac{\gamma_{mj,nk}}{2\pi} = g_k g_j\sqrt{(m+1)(n+1)}\left(\chi_{mkj} + \chi_{nkj}^*\right), \tag{17.73}$$

with $\chi_{mjk} = \omega_{mj}e^{i\omega_{mj}t_{kj}}$, the atom-atom exchange interaction amplitude

$$\frac{J_{mj,nk}}{2\pi} = -i\frac{g_k g_j}{2}\sqrt{(m+1)(n+1)}\left(\chi_{njk} - \chi_{mkj}^*\right), \tag{17.74}$$

and

$$\Omega_{mj,nk} = -i\left(\sqrt{n+1}\Omega_{jk}^{m+} - \sqrt{m+1}\Omega_{kj}^{n+}\right). \tag{17.75}$$

The reader interested in (even) more details will find the evaluation of the integrals needed to find these coefficients in Appendix 17.7.5.

In the main text, we absorb the Lamb shift L_{mj} into the definition of the atomic transition frequency. As usual for point like atoms, this contribution is formally infinite. A nondiverging result can be obtained by taking into account the finite size of the atoms [46]. In any case, experimentally, the Lamb shift is always present in the evaluation of the various transition frequencies and absorbing it in the definition here does not cause any problems.

We also note that the matrix of components $\Omega_{mj,nk}$ is traceless, Hermitian, and nonzero. As a result, it is not semipositive as is required to express the master equation in Lindbladian form. Fortunately, and as discussed in Appendix 17.7.3, the various $\Omega_{mj,nk}$ are in practice small and can safely be neglected. Doing so, we finally arrive at the the master equation, Eq. (17.7), with an effective Hamiltonian given in Eq. (17.8).

17.7.3 Discussion of the approximations

In this appendix, we discuss in more detail the main approximations that have been used to obtain the reduced master equation. These approximations are certainly not original to this work and this discussion is added for completeness.

Markov approximation

We first start with $I_{nk}(t,\tau,t_{kj})$ defined in Eq. (17.62). The complexity in this expression is the dependence of the integrand σ_x^{nk} on the integration variable τ. This can be simplified by rewriting $I_{nk}(t,\tau,t_{kj})$ as

$$\begin{aligned} I_{nk}(t,\tau,t_{kj}) &= \int_0^\infty d\omega\omega e^{i\omega(\tau-t-t_{kj})}\sigma_x^{nk}(\tau) \\ &= \int_0^\infty d\omega\omega e^{-i\omega(\tau-t-t_{kj})} \\ &\times\left[e^{iH_{\mathrm{T}}(\tau-t)/\hbar}\sigma_-^{nk}(t)e^{-iH_{\mathrm{T}}(\tau-t)/\hbar} + \mathrm{H.c.}\right]. \end{aligned}$$

with $H_{\mathrm{T}} = H_{\mathrm{A}} + H_{\mathrm{I}} + H_{\mathrm{F}}$. Since the integrand is proportional to ω, high frequencies contribute most. However, at high frequency, the exponential is oscillating rapidly and the contribution averages out to zero. The only situation where the exponential does not oscillate is when $\tau = t + t_{kj}$ and this is the only value of τ that we retain.

To simplify this expression further, we neglect the interaction Hamiltonian $H_{\rm I}$ compared to the free Hamiltonian $H_{\rm A}$. More formally, the error $\mathcal{E}$ that is made in neglecting the interaction goes as [47]

$$\mathcal{E} \sim \left\langle \frac{H_{\rm I}^2}{H_{\rm A}} \right\rangle \frac{t_{kj}}{h}. \tag{17.76}$$

Evaluating the expectation value of the field operators appearing in $H_{\rm I}$ by assuming a coherent drive of power P, this error can be expressed as

$$\mathcal{E} \sim \frac{32\pi g_k^2 L}{v\omega_{nk}} \frac{P}{h}, \tag{17.77}$$

with L the maximum distance between two atoms.

For waveguide QED with transmon qubits, we find

$$g_k = \left(\sqrt{\frac{e^2 c}{2\hbar\pi v c_{gk}^2}} \right) \left(\frac{E_{Jk}}{8E_{Ck}} \right)^{(1/4)}, \tag{17.78}$$

with E_{Jk} and E_{Ck} the Josephson and charging energy of the kth transmon [11], c the capacitance per unit length of the transmission line, and where c_{gk} is defined in Eq. (17.56). Using typical experimental values for these parameters [48], we find that $g_k \sim 0.02$. The numerical value of g_k can also be estimated from the experimentally measured value of the relaxation rate $\gamma_{nk,nk}$. Doing so using recent experimental results [20, 13, 10] gives consistent results. Now, given that the speed of light in the transmission line is $v \sim 10^8$ m/s and assuming a separation $L \sim 1$ cm between two transmons of transition frequency $\omega_{nk} \sim 2\pi \times 6$ GHz, we find $\mathcal{E} \sim 0.02$ for $P \sim -100$ dBm. Since this power is large in practice [20], dropping the contribution of $H_{\rm I}$ from Eq. (17.76) is reasonable. Doing so we can rewrite $\sigma_-^{nk}(\tau)$ in $I_{nk}(t,\tau,t_{kj})$ as

$$\sigma_-^{nk}(\tau) \approx \sigma_-^{nk}(t) e^{-i\omega_{nk}(\tau - t)}. \tag{17.79}$$

This corresponds to a Markov approximation. It breaks down for larger separation, i.e., for $\omega_{nk} t_{kj}/(2\pi) \sim 10$, something that was studied in Ref. [35].

It is interesting to note that, even if we recover a result similar to Lehmberg's [21], here we used a different justification. Indeed, Lehmberg assumed that the atoms are close enough such that the time it takes for a signal to propagate from one atom to the other is small compared to the Larmor frequencies, $L \ll v/\omega_{nk}$. This is inapplicable in a waveguide QED setup with superconducting qubits.

Long-time approximation and causality

The identity (17.65) is essential in deriving the master equation (17.7). To use this identity, we need the upper bound of the time integral in Eq. (17.60) to go to infinity. Using approximation (17.63),

$$\begin{aligned} \int_0^t d\tau I_{nk}(t,\tau,t_{kj}) = \int_0^t d\tau \int_0^\infty d\omega \omega e^{-i\omega(\tau - t - t_{kj})} \\ \times \left(\sigma_-^{nk} e^{-i\omega_{nk}(\tau - t)} + \text{H.c.} \right), \end{aligned} \tag{17.80}$$

and with a change of variable $x = \omega_{nk}(t - \tau)$,

$$\begin{aligned} \int_0^t d\tau I_{nk}(t,\tau,t_{kj}) = \int_0^\infty d\omega \int_0^{\omega_{nk} t} dx \frac{\omega e^{-i\omega t_{kj}}}{\omega_{nk}} \\ \times \left[\sigma_-^{nk} e^{-i(\omega - \omega_{nk})x/\omega_{nk}} + \sigma_+^{nk} e^{-i(\omega_{nk} + \omega)x/\omega_{nk}} \right]. \end{aligned} \tag{17.81}$$

The integrand of x is an oscillating function. If $\omega_{nk} t \gg 1$, the integration is already over many periods of this function, so it is a good approximation to let $\omega_{nk} t \to \infty$. For waveguide QED with superconducting qubits, this condition requires that $t \gg 0.02$ ns. Since we are not interested in dynamics at this very fast time scale, this approximation holds here. In fact, the electronics in typical experiments have a bandwidth of less than ~ 1 GHz [48]. The same argument justifies taking $\omega_{mj}(t - t_f) \to -\infty$.

With this approximation, the atoms are treated as interacting instantaneously. This is not a major problem because the phase shift associated with the delays it takes for light to travel from one atom to another is taken into account by the factor $\exp(-i\omega t_{kj})$. Hence, interaction between two atoms at time t is mediated through light that has been emitted by the atoms at an earlier time $t - t_{kj} \sim t - L/v$. A more important problem arises during transients. For example, assume a drive is suddenly turned on such that it affects a first atom at time t. Our model causes the drive to affect the second atom at this very time t with a phase delay $\exp(-i\omega t_{kj})$ rather than at a time $t + t_{kj}$. As a result, we do not expect transient effects on a time scale smaller than L/v to be correctly captured. This is not an issue for the steady-state quantities that are computed here and measured in Ref. [20].

RWA, infinite terms, and Lindblad form

In this section, we justify the approximations that were made in going from the Heisenberg equation of motion (17.69) to the master equation (17.7). The error made by making the rotating-wave approximation can be expressed as [49]

$$\mathcal{E} \sim \frac{8M^2\left[\left(\gamma_{kj}^{n}\right)^2+\left(\Omega_{kj}^{n+}\right)^2+\left(\Omega_{kj}^{n-}\right)^2\right]}{3(\omega_{mj}+\omega_{nk})^2}. \tag{17.82}$$

This error is formally infinitely large simply because $\Omega_{jj}^{n\pm}\to\infty$ as shown in Appendix 17.7.5. This divergence is present because we did not take into account the physical dimensions of the artificial atoms (either explicitly or with a cut-off frequency). Ignoring this unphysical problem and using typical circuit QED parameters yields $\mathcal{E}\sim 0.001$. Considering this, we can safely make the rotating-wave approximation.

To go from Eq. (17.70) to its Lindblad form, Eq. (17.7), we also need to neglect terms proportional to $\Omega_{mj,nk}$ since this matrix is not semipositive. These terms are either small or quickly rotating. The error made by dropping them is, considering that the relevant time scale goes as $\gamma_{mj,mj}^{-1}$ [49],

$$\mathcal{E} \sim \frac{8M^2|\Omega_{mj,nk}|^2}{3(\gamma_{mj,mj})^2} \tag{17.83}$$

so that $\mathcal{E}\sim 0.002$. Hence, once more, it is a very good approximation to neglect these terms.

17.7.4 Driving term

To proceed from Eq. (17.69) to (17.70), we need to take care of the terms proportional to Ξ_j^{in} and $\Xi_j^{\text{in}\dagger}$ since these operators contain contributions from the field operator $a_{\text{in}}^{\text{R/L}}$. We regroup these terms under what we call the drive superoperator D acting on ρ in the master equation such that

$$\begin{aligned}\text{Tr}_{\text{A}}\left[QD\rho\right] =& i\sum_{mj} g_j\sqrt{m+1}\\ &\times \text{Tr}_{\text{A}}\left[\text{Tr}_{\text{R}}\left[\left(\left[\sigma_x^{mj},Q\right]\Xi_j^{\text{in}}-\text{H.c.}\right)\rho_{\text{T}}\right]\right]\\ =&\left\langle i\sum_{mj} g_j\sqrt{m+1}\left(\left[\sigma_x^{mj},Q\right]\Xi_j^{\text{in}}-\text{H.c.}\right)\right\rangle.\end{aligned} \tag{17.84}$$

Here, all operators are evaluated at time t. Because of causality, the input field operator Ξ_j^{in} cannot be correlated with any atomic operator when they are both evaluated at the same time. Therefore,

$$\begin{aligned}\text{Tr}_{\text{A}}\left[QD\rho\right] =& \sum_{mj}\left\langle ig_j\sqrt{m+1}\left(\left[\sigma_x^{mj},Q\right]\Xi_j^{\text{in}}-\text{H.c.}\right)\right\rangle\\ =& i\sum_{mj} g_j\sqrt{m+1}\left(\left\langle\left[\sigma_x^{mj},Q\right]\right\rangle\left\langle\Xi_j^{\text{in}}\right\rangle-\text{H.c.}\right)\\ =& i\sum_{mj} g_j\sqrt{m+1}\\ &\times \text{Tr}_{\text{A}}\left[\left[\left(\left\langle\Xi_j^{\text{in}}\right\rangle+\text{c.c.}\right)\sigma_x^{mj},Q\right]\rho\right],\end{aligned} \tag{17.85}$$

which leads to

$$\begin{aligned}\dot{\rho} =& -i\left[\frac{H_{\text{A}}}{\hbar}+\sum_{mj} d_{mj}(t)\sigma_x^{mj},\rho\right]+\sum_{mj}\sum_{nk}\sqrt{m+1}\\ &\times\Big[-i\Omega_{kj}^{n+}\left(\sigma_+^{nk}\rho\sigma_x^{mj}-\sigma_x^{mj}\sigma_+^{nk}\rho-\text{H.c.}\right)\\ &-i\Omega_{kj}^{n-}\left(\sigma_-^{nk}\rho\sigma_x^{mj}-\sigma_x^{mj}\sigma_-^{nk}\rho-\text{H.c.}\right)\\ &+\frac{\gamma_{kj}^{n}}{2}\left(\sigma_-^{nk}\rho\sigma_x^{mj}-\sigma_x^{mj}\sigma_-^{nk}\rho-\text{H.c.}\right)\Big],\end{aligned} \tag{17.86}$$

with

$$d_{mj}(t)=g_j\sqrt{m+1}\left(\left\langle\Xi_j^{\text{in}}(t)\right\rangle+\left\langle\Xi_j^{\text{in}}(t)\right\rangle^*\right). \tag{17.87}$$

We make the assumption that we are driving at frequency ω_d with a coherent state $|\{\alpha\}\rangle$ such that [50]

$$a_{\mathrm{L(R)}}(\omega,0)\,|\{\alpha\}\rangle = \sqrt{\frac{P_{\mathrm{L(R)}}}{\hbar\omega_d}}e^{-i\omega_d\theta_{\mathrm{L(R)}}}\delta(\omega-\omega_d)\,|\{\alpha\}\rangle\,, \tag{17.88}$$

with $P_{\mathrm{L(R)}}$ and $\theta_{\mathrm{L(R)}}$, respectively, the power and phase of left (right) movers. Using this, we have

$$\begin{aligned}\left\langle \Xi_j^{\mathrm{in}}(t)\right\rangle &= \langle\{\alpha\}|\,\Xi_j^{\mathrm{in}}\,|\{\alpha\}\rangle \\ &= -\,i\left[e^{-i\omega_d(t+t_j+\theta_{\mathrm{L}})}\sqrt{2\pi P_{\mathrm{L}}/\hbar}\right. \\ &\quad \left.+e^{-i\omega_d(t-t_j+\theta_{\mathrm{R}})}\sqrt{2\pi P_{\mathrm{R}}/\hbar}\right].\end{aligned} \tag{17.89}$$

Finally, the drive rate can be written as

$$\begin{aligned}d_{mj}(t) = -\,2\sqrt{\frac{\gamma_{mj,mj}}{2}}\left(\sqrt{\frac{P_{\mathrm{L}}}{\hbar\omega_{mj}}}\sin\left[\omega_d(t+t_j+\theta_{\mathrm{L}})\right]\right. \\ \left.+\sqrt{\frac{P_{\mathrm{R}}}{\hbar\omega_{mj}}}\sin\left[\omega_d(t-t_j+\theta_{\mathrm{R}})\right]\right).\end{aligned} \tag{17.90}$$

17.7.5 Evaluation of formula for Omega

this formula:

$$\boldsymbol{\Omega_{kj}^{n\pm}}$$

In this section, we present details of the integration of Eq. (17.67). With the change of variables $x = (\omega \pm \omega_{nk})/\omega_{nk}$ and $y = x \mp 1$, Eq. (17.67) can be expressed as

$$\begin{aligned}\Omega_{kj}^{n\pm} =& 2g_k g_j\omega_{nk}\sqrt{n+1}\left(\int_0^\infty dy\cos\left(\omega_{nk}t_{kj}y\right)\right. \\ &\left.\mp\mathrm{P}\int_{\pm1}^\infty dx\frac{\cos\left[\omega_{nk}t_{kj}(x\mp1)\right]}{x}\right).\end{aligned} \tag{17.91}$$

To deal with the first term of the right-hand-side, we add a converging factor. This reflects the fact that the system stops to respond at infinite frequencies. In this way, we find that this first term vanishes

$$\begin{aligned}&\lim_{\eta\to0^+}\int_0^\infty dy\cos\left(\omega_{nk}t_{kj}y\right)e^{-\eta y} \\ &\qquad = \lim_{\eta\to0^+}\frac{\eta}{(\omega_{nk}t_{kj})^2+\eta^2} = 0.\end{aligned} \tag{17.92}$$

On the other hand, for the second term, which we denote $I^{\pm}$, we find

$$\begin{aligned}I^{\pm} =& \mathrm{P}\int_{\pm1}^\infty dx\frac{\cos\left[\omega_{nk}t_{kj}(x\mp1)\right]}{x} \\ =& \cos\left(\omega_{nk}t_{kj}\right)\mathrm{P}\int_{\pm1}^\infty dx\frac{\cos\left(\omega_{nk}t_{kj}x\right)}{x} \\ &\pm\sin\left(\omega_{nk}t_{kj}\right)\mathrm{P}\int_{\pm1}^\infty dx\frac{\sin\left(\omega_{nk}t_{kj}x\right)}{x} \\ =& -\cos\left(\omega_{nk}t_{kj}\right)\mathrm{Ci}\left(|\omega_{nk}t_{kj}|\right) \\ &+\frac{\sin\left(\omega_{nk}t_{kj}\right)}{2}\left(\pm\pi\mathrm{sgn}\left(\omega_{nk}t_{kj}\right)-2\mathrm{Si}\left(\omega_{nk}t_{kj}\right)\right),\end{aligned} \tag{17.93}$$

where $\mathrm{Ci}\,(x)$ and $\mathrm{Si}\,(x)$ are the cosine and sine integral functions:

$$\mathrm{Ci}\,(x) = -\int_x^\infty dt \frac{\cos t}{t}, \quad \mathrm{Si}\,(x) = \int_0^x dt \frac{\sin t}{t}. \tag{17.94}$$

Using these results, we finally obtain

$$\begin{aligned}\Omega_{kj}^{n\pm} =& 2\pi g_k g_j \omega_{nk}\sqrt{n+1} \\ &\times \left[\mp p(\omega_{nk}t_{kj}) + \sin\left(\omega_{nk}t_{kj}\right)\left(\frac{\pm 1 - 1}{2}\right)\right],\end{aligned} \tag{17.95}$$

where we have defined a "proximity" function

$$p(x) \equiv \frac{\sin\left(|x|\right)\left[\pi - 2\mathrm{Si}\left(|x|\right)\right] - 2\cos\left(x\right)\mathrm{Ci}\left(|x|\right)}{2\pi}. \tag{17.96}$$

This choice of name reflects the fact $p(x)$ goes to ∞ as $x \to 0$, and rapidly approaches 0 as $x \to 1$.

17.7.6 Input-output theory

In this section, we derive the input-output boundary condition in the presence of the artificial atoms in the line. This will allow us to compare the theoretical predictions to experiments measuring reflection and transmission. To derive the reduced master equation, we used the formal solution to the Heisenberg equation of motion for $a_{\mathrm{R/L}}(\omega, t)$. In Eq. (17.59), this solution was given for the case where the equation of motion is integrated starting from a time $t_0 = 0 < t$ before the interaction. Following the standard input-output prescription [36], it is also useful to obtain this solution by integrating up to a time $t_f > t$ after the interaction:

$$\begin{aligned}a_{\mathrm{R}}(\omega, t) =& a_{\mathrm{R}}(\omega, t_f)e^{-i\omega t} \\ &- \sum_{mj} g_j\sqrt{m+1}\sqrt{\omega}\int_t^{t_f} d\tau e^{-i\omega(t-\tau+x_j/v)}\sigma_x^{mj}(\tau).\end{aligned} \tag{17.97}$$

Adding this expression to Eq. (17.59) and integrating over ω, we arrive at the input-output boundary condition

$$\begin{aligned}a_{\mathrm{out}}^{\mathrm{R}}(t) =& a_{\mathrm{in}}^{\mathrm{R}}(t) + \sum_{mj} g_j\sqrt{m+1} \\ &\times \int_0^\infty \frac{d\omega}{\sqrt{2\pi}}\sqrt{\omega}\int_0^{t_f} d\tau e^{-i\omega(t-\tau+x_j/v)}\sigma_x^{mj}(\tau),\end{aligned} \tag{17.98}$$

where, similarly to Eq. (17.61), we have defined the input field

$$a_{\mathrm{in}}^{\mathrm{R}}(t) = \int_0^\infty \frac{d\omega}{\sqrt{2\pi}} a_{\mathrm{R}}(\omega, 0)e^{-i\omega t}, \tag{17.99}$$

and the output field

$$a_{\mathrm{out}}^{\mathrm{R}}(t) = \int_0^\infty \frac{d\omega}{\sqrt{2\pi}} a_{\mathrm{R}}(\omega, t_f)e^{-i\omega t}. \tag{17.100}$$

While $a_{\mathrm{in}}^{\mathrm{R}}(t)$ can be interpreted as the field incident on the system from the left, $a_{\mathrm{out}}^{\mathrm{R}}(t)$ represents the field propagating to the right after interaction with the system.

It is possible to express the boundary condition in a more useful form by using the approximation of Eq. (17.63). Indeed, making the change of variable $y = \omega_{mj}(t-\tau)$ and taking $\omega_{mj}(t-t_f) \to -\infty$, we find the simpler form

$$a_{\mathrm{out}}^{\mathrm{R}}(t) = a_{\mathrm{in}}^{\mathrm{R}}(t) + \sum_{mj} e^{-i\omega_{mj}t_j}\sqrt{\frac{\gamma_{mj,mj}}{2}}\sigma_-^{mj}. \tag{17.101}$$

In the same way, we find

$$a_{\mathrm{out}}^{\mathrm{L}}(t) = a_{\mathrm{in}}^{\mathrm{L}}(t) + \sum_{mj} e^{+i\omega_{mj}t_j}\sqrt{\frac{\gamma_{mj,mj}}{2}}\sigma_-^{mj} \tag{17.102}$$

for the output field propagating to the left.

17.7.7 Relaxation diagonalization

In Sec. 17.2.3 of the main text we have shown that for a pair of qubits the master equation in its Lindblad form is

$$\begin{aligned}\dot{\rho} =& \frac{-i}{\hbar}\left[H,\rho\right] + \sum_{j,k=0,1}\gamma_{jk}\left[\sigma_-^j\rho\sigma_+^k - \frac{1}{2}\left\{\sigma_+^k\sigma_-^j,\rho\right\}\right] \\ \equiv& \frac{-i}{\hbar}\left[H,\rho\right] + \mathcal{L}_\gamma\rho,\end{aligned} \tag{17.103}$$

where H is given in Eq. (17.24). In this appendix, we diagonalize the dissipator $\mathcal{L}_\gamma$ in order to find the dressed basis.

Diagonalization is achieved by using the standard approach of expressing the density matrix ρ as a column vector in which case the dissipator takes the form

$$\mathcal{L}_\gamma\vec{\rho} = \sum_{kj}\gamma_{k,j}\left[\sigma_{b-}^k\sigma_{f+}^{Tj} - \frac{1}{2}\sigma_{b+}^j\sigma_{b-}^k - \frac{1}{2}\sigma_{f+}^{Tj}\sigma_{f-}^{Tk}\right]\vec{\rho}, \tag{17.104}$$

with

$$\begin{aligned}A\rho \to 1\otimes A\vec{\rho} = A_b\vec{\rho}, \\ \rho A \to A^T\otimes 1\vec{\rho} = A_f^T\vec{\rho},\end{aligned} \tag{17.105}$$

where T refers to matrix transposition. In this way, the dissipator can be expressed as

$$\mathcal{L}_\gamma\vec{\rho} = \left[\sigma_{b-}\Upsilon\sigma_{f+}^T - \frac{1}{2}\sigma_{b+}\Upsilon\sigma_{b-}^T - \frac{1}{2}\sigma_{f+}\Upsilon\sigma_{f-}^T\right]\vec{\rho}, \tag{17.106}$$

with the Hermitian relaxation rate matrix

$$\Upsilon = \begin{pmatrix}\gamma_{00} & \gamma_{01}\\ \gamma_{01}^* & \gamma_{11}\end{pmatrix}, \tag{17.107}$$

and where we have defined

$$\sigma_{b\pm} = \begin{pmatrix}\sigma_{b\pm}^0 & \sigma_{b\pm}^1\end{pmatrix}, \quad \sigma_{f\pm} = \begin{pmatrix}\sigma_{f\pm}^{T0} & \sigma_{f\pm}^{T1}\end{pmatrix}. \tag{17.108}$$

After diagonalizing Υ and going back to matrix form of the density matrix we find

$$\mathcal{L}_\gamma\rho = \sum_{i=B,D}\Gamma_i\mathcal{D}\left[\sigma_-^i\right]\rho, \tag{17.109}$$

with the rates

$$\Gamma_{B/D} = \frac{\gamma_{00}+\gamma_{11}}{2} \pm \sqrt{\left(\frac{\gamma_{00}-\gamma_{11}}{2}\right)^2 + |\gamma_{01}|^2}, \tag{17.110}$$

and dressed operators

$$\sigma_-^\mu = \frac{\left(\Gamma_\mu-\gamma_{11}\right)\sigma_-^0 + \gamma_{01}^*\sigma_-^1}{\sqrt{\left(\Gamma_\mu-\gamma_{11}\right)^2+|\gamma_{01}|^2}}, \tag{17.111}$$

for $\mu = B, D$.

4.5 Diagrammatic Approach to Multiphoton Scattering See, Noh, Angelakis

Part XII
Typical Theory: Another Explanations

18 Few-photon scattering and emission from open quantum systems by Trivedi et. al.

Abstract

We show how to use the input-output formalism compute the propagator for an open quantum system, i.e. quantum networks with a low dimensional quantum system coupled to one or more loss channels. The total propagator is expressed entirely in terms of the Green's functions of the low dimensional quantum system, and it is shown that these Green's functions can be computed entirely from the evolution of the low-dimensional system with an effective non-hermitian Hamiltonian. Our formalism generalizes the previous works that have focused on time independent Hamiltonians to systems with time dependent Hamiltonians, making it a suitable computational tool for the analysis of a number of experimentally interesting quantum systems. We illustrate our formalism by applying it to analyze photon emission and scattering from driven and undriven two-level system and three-level lambda system.

18.1 Introduction

Single photon sources [1, 2, 3, 4, 5] and single and two-photon optical gates [6, 7, 8, 9, 10, 11, 12] are the basic building blocks of optical quantum information processing and quantum communication systems. Implementing any of these building blocks involves interfacing a low-dimensional quantum system (e.g. a two level system such as quantum dots, color centers, superconducting qubits, atomic ensembles) with the high-dimensional optical field (which often propagates in optical structures such as waveguides) – the resulting system is called an open-quantum system [13, 14, 15] and such systems have been a topic of theoretical interest since the inception of quantum optics. Analyzing open-quantum systems has always been a challenging task due to the huge and continuous Hilbert Space of the optical fields, and the non-linearity induced by the low-dimensional quantum system.

Traditional computational methods for analyzing open quantum systems fall under two broad classes – master equation based methods and the scattering matrix based methods. The master-equation based methods [16, 17, 18] exactly compute the dynamics of the low-dimensional system while tracing out the Hilbert space of the optical fields. Within the master-equation framework, it is only possible to computationally extract the correlators in the optical fields. To extract the full state of the optical field, correlators of arbitrary orders are required and computing them becomes exponentially more complex with the order of the correlator. The scattering matrix based methods [19, 20, 21, 22, 23, 24, 25, 26, 27, 28, 29, 30, 31] attempt to resolve this problem by treating the low-dimensional system as a scatterer for the optical fields and attempting to relate the incoming and outgoing optical fields. However, most of the scattering matrix methods are restricted to time-independent Hamiltonians – in particular, they are unable to analyze coherently driven systems which are extremely important from an experimental standpoint. Moreover, the scattering matrix methods often only relate the input state at distant past to the output state at distant future, and don't have the capability to model the dynamics of the system during the interaction of the optical field with the low-dimensional system.

In this paper, we present a full calculation of the few-photon elements of the propagator for an arbitrary open quantum system coupled to a optical field. The central result of this paper is a relation between the propagator and time-ordered expectations of system operators over states where the bath is in the vacuum state (labeled as the 'Green's functions'). By resorting to a discrete approximation of the bath Hilbert space, we show that Green's functions can be evaluated by computing the dynamics of the low-dimensional system under an effective non-Hermitian Hamiltonian. It can be noted that our formalism is valid for both time-independent and time-dependent Hamiltonians, allowing it to efficiently model not only few-photon transport through the low-dimensional system, but also photon-emission and scattering from coherently driven systems. Our formalism provides a set of computational tools that are complementary to the master-equation framework, wherein the focus is on exactly computing the dynamics of the few-photon states emitted from the low-dimensional system, as opposed to capturing the exact dynamics of the low-dimensional system. Our formalism will thus be of relevance to design and analysis of quantum information processing systems in which the 'information' is encoded in the state of the bath, with the low-dimensional system implementing either a source for the bath state or a unitary operation on the bath state.

Finally, we show how to extract the scattering matrices of the low-dimensional system from the full propagator. In particular, we show that for the case of a time-independent low-dimensional system Hamiltonian, our method reduces to scattering matrices derived in past works [19, 20]. Our formalism also allows us to define a scattering matrix for systems with time-dependent Hamiltonians, as long as they are asymptotically time

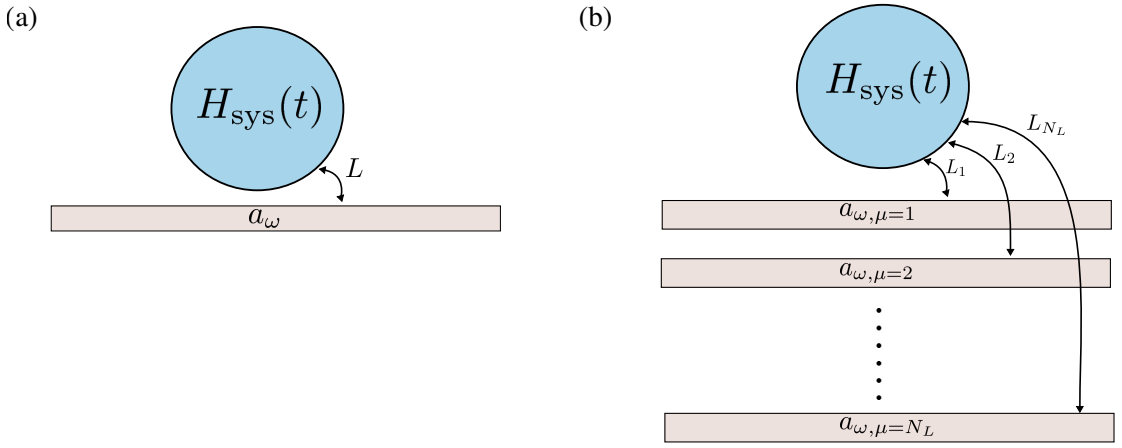

Figure 18.1: Schematic of the quantum systems being considered, with a low-dimensional system coupled to (a) a single waveguide (b) multiple waveguides.

independent. Such a quantity might be of interest while analyzing photon scattering from coherently driven low-dimensional systems.

This paper is organized as follows – Section 18.2 describes the propagator computation starting from the input-output equations, Section 18.3 shows how to extract the scattering matrix for the system from the propagator and Section 18.4 uses the formalism developed in sections II and III to analyze scattering and emission from a two-level system and a lambda system.

18.2 Quantum optical systems coupled to waveguides

The general quantum networks being considered in this paper include a low dimensional quantum-optical system coupled to one or more waveguides (Fig. 18.1). In our calculations, we will be concerned with not only the state of the quantum-optical system, but also with the state of the waveguides. Section 18.2.1 introduces the Hamiltonians studied in this paper and the associated input-output equations, section 18.2.2 shows how to use the input-output formalism to relate the propagator matrix elements to Green's functions of the low dimensional system, 18.2.3 extends the result to multiple input and output waveguides and 18.2.4 shows how to efficiently compute the Green's functions required for computing the propagator matrix elements.

18.2.1 Hamiltonian and input-output formalism

As a starting point, we consider only one waveguide [Fig. 18.1(a)] — the generalization to multiple waveguides is a straightforward extension. The total Hamiltonian we are interested in can be expressed as the local system Hamiltonian H_{sys}, the waveguide Hamiltonian H_{wg} and an interaction Hamiltonian between the local system and waveguide H_{int}:

$$H = H_{\text{sys}}(t) + H_{\text{wg}} + H_{\text{int}}. \tag{18.1}$$

The Hilbert space of the low dimensional system can often be captured by a finite or countably infinite basis, which we denote by $\{|\sigma_1\rangle, |\sigma_2\rangle \dots |\sigma_S\rangle\}$. It is typically straightforward and computationally tractable to analyze the dynamics of the low-dimensional system in isolation.

The dynamics of the waveguide can be modeled by the following Hamiltonian:

$$H_{\text{wg}} = \int \omega a_\omega^\dagger a_\omega \mathrm{d}\omega \tag{18.2}$$

where a_ω is the annihilation operator for an excitation of the waveguide mode at frequency ω. They satisfy the standard commutation relation $[a_\omega, a_{\omega'}] = 0$ and $[a_\omega, a_{\omega'}^\dagger] = \delta(\omega - \omega')$. A suitable basis for the waveguide's Hilbert space is the Fock state basis:

$$|\omega_1, \omega_2 \dots \omega_N\rangle = \prod_{n=1}^{N} a_{\omega_n}^\dagger |\text{vac}\rangle \quad \forall N \in \mathbb{N}. \tag{18.3}$$

It is also convenient to define a spatial annihilation operator for the waveguide mode:

$$a_x = \int a_\omega \exp\left(\mathrm{i}\frac{\omega x}{v_g}\right) \frac{\mathrm{d}\omega}{\sqrt{2\pi v_g}} \tag{18.4}$$

where v_g is the group velocity of the waveguide mode under consideration, which we will take as unity ($v_g = 1$) for the rest of this paper (note that this is equivalent to rescaling the position x to have units of time). It follows from the commutators for the operators a_ω that $[a_x, a_{x'}] = 0$ and $[a_x, a^\dagger_{x'}] = \delta(x - x')$. These operators can be used to construct another basis for the waveguide's Hilbert space, which we refer to as the spatial Fock states:

$$|x_1, x_2 \dots x_N\rangle = \prod_{n=1}^{N} a^\dagger_{x_n} |\text{vac}\rangle \,. \tag{18.5}$$

The system-waveguide interaction, in the rotating wave approximation, can be described by the following Hamiltonian:

$$H_{\text{int}} = \int \left(a_\omega L^\dagger + L a^\dagger_\omega\right) \frac{\mathrm{d}\omega}{\sqrt{2\pi}} \tag{18.6}$$

where L is the operator through which the low-dimensional system couples to the waveguide. In writing this Hamiltonian, we make the standard Markov approximation of assuming that the low-dimensional system couples equally to waveguide modes at all frequency — this is equivalent to assuming that the physical process inducing an interaction between the waveguide and the low-dimensional system has a bandwidth much larger than any excitation that will be used to probe the low-dimensional system.

In the Heisenberg picture, this system can be modeled via well known input-output equations [32]:

$$a_\omega(t) = a_\omega(\tau_-) \exp(-\mathrm{i}\omega(t - \tau_-)) - \mathrm{i} \int_{\tau_-}^{t} L(t') \exp(-\mathrm{i}\omega(t - t')) \frac{\mathrm{d}t'}{\sqrt{2\pi}} \tag{18.7a}$$

$$\dot{L}(t) = -\mathrm{i}[L(t), H_{\text{sys}}] - \mathrm{i}[L(t), L^\dagger(t)] \left(a_{\text{in}}(t) - \frac{\mathrm{i}}{2} L(t)\right) \tag{18.7b}$$

where $a_{\text{in}}(t) = \int a_\omega(\tau_-) \exp(-\mathrm{i}\omega(t - \tau_-))\, \mathrm{d}\omega/\sqrt{2\pi}$ is the input operator which, in the Heisenberg picture, captures the state of the system at time $t = \tau_-$. After the evolution of the system to a time instant $t = \tau_+ > \tau_-$ in the future, the state of the system is described by the output operator $a_{\text{out}}(t) = \int a_\omega(\tau_+) \exp(-\mathrm{i}\omega(t - \tau_+))\, \mathrm{d}\omega/\sqrt{2\pi}$. Using Eq. 18.7a, we can relate the input operator to the output operator via:

$$a_{\text{out}}(t) = a_{\text{in}}(t) - \mathrm{i} L(t) \mathcal{I}(\tau_- < t < \tau_+) \tag{18.8}$$

where $\mathcal{I}(\cdot)$ is the indicator function, which is 1 if its argument is true or else is 0. Intuitively, this expresses the field in the waveguide after the input has interacted with the system as a sum of the input field and field emitted by the low-dimensional system.

A useful set of commutators between the input operator, output operator and the low-dimensional system's Heisenberg operators can be derived using the quantum-causality conditions [32]:

$$[a_{\text{out}}(t), s(t')] = 0 \text{ if } t < t' \text{ and } [a_{\text{in}}(t), s(t')] = 0 \text{ if } t > t' \tag{18.9}$$

where s is an operator in the Hilbert space of the low-dimensional system. From these causality conditions, it immediately follows that [19]:

$$\mathcal{T}\left[\prod_{l=1}^{L} o(t_l) \prod_{m=1}^{M} s_m(t'_m)\right] = \mathcal{T}\left[\prod_{l=1}^{L} o(t_l)\right] \mathcal{T}\left[\prod_{m=1}^{M} s_m(t'_m)\right] \tag{18.10a}$$

$$\mathcal{T}\left[\prod_{l=1}^{L} i(t_l) \prod_{m=1}^{M} s_m(t'_m)\right] = \mathcal{T}\left[\prod_{m=1}^{M} s_m(t'_m)\right] \mathcal{T}\left[\prod_{l=1}^{L} i(t_l)\right] \tag{18.10b}$$

where $o(t)$ is an output operator evaluated at time t (i.e. $a_{\text{out}}(t)$, $a^\dagger_{\text{out}}(t)$ or their combination), $i(t)$ is an input operator evaluated at time t (i.e. $a_{\text{in}}(t)$, $a^\dagger_{\text{in}}(t)$ or their combination), $s_m(t)$ is a low-dimensional system operator evaluated at time t in the Heisenberg picture and $\mathcal{T}$ is the chronological time-ordering operator.

18.2.2 Calculating the propagator matrix elements

The dynamics of a quantum system with a Hamiltonian $H(t)$ is completely characterized by its propagator – in particular, if the propagator is known, then the time evolution of the quantum state of the system can be completely derived from the initial state of the system. In this section, we will focus on computing the interaction picture propagator $U_I(\tau_+, \tau_-)$ defined by:

$$U_{\text{I}}(\tau_+, \tau_-) = \exp(\mathrm{i} H_{\text{wg}} \tau_+) U(\tau_+, \tau_-) \exp(-\mathrm{i} H_{\text{wg}} \tau_-) \tag{18.11}$$

where $U(\tau_+, \tau_-)$ is the Schrödinger picture propagator for the system:

$$U(\tau_+, \tau_-) = \mathcal{T}\exp\left[-\mathrm{i}\int_{\tau_-}^{\tau_+} H(t)\mathrm{d}t\right] \tag{18.12}$$

and $\mathcal{T}$ is the chronological operator that time-orders the infinitesimal products of Eq. 18.12. In particular, we will compute the matrix elements of the interaction picture propagator in the form:

$$U^{\sigma',\sigma}_{\tau_+,\tau_-}(x'_1, x'_2 \dots x'_M; x_1, x_2 \dots x_N) \equiv \langle x'_1, x'_2 \dots x'_M; \sigma' | \, U_{\mathrm{I}}(\tau_+, \tau_-) \, | x_1, x_2 \dots x_N; \sigma\rangle \tag{18.13}$$

where $|x_1, x_2 \dots x_P; \sigma\rangle = |x_1, x_2 \dots x_P\rangle \otimes |\sigma\rangle$ with $x_i \in \mathbb{R}$ and $\sigma \in \{\sigma_1, \sigma_2 \dots\}$. Since the spatial Fock state basis for the waveguide is complete, and the basis $\{|\sigma_1\rangle, |\sigma_2\rangle \dots\}$ is a complete basis for the system state by construction, these matrix elements are sufficient to characterize the entire propagator.

Writing out $U^{\sigma',\sigma}_{\tau_+,\tau_-}(x'_1, x'_2 \dots x'_M; x_1, x_2 \dots x_N)$ in terms of the spatial annihilation operators:

$$\begin{aligned} U^{\sigma',\sigma}_{\tau_+,\tau_-}(x'_1 \dots x'_M; x_1 \dots x_N) &= \langle \mathrm{vac}; \sigma' | \left[\prod_{i=1}^{M} a_{x'_i}\right] U_{\mathrm{I}}(\tau_+, \tau_-) \left[\prod_{j=1}^{N} a^\dagger_{x_j}\right] | \mathrm{vac}; \sigma\rangle \\ &= \langle \mathrm{vac}; \sigma' | \left[\prod_{i=1}^{M} a_{x'_i}\right] U_{\mathrm{I}}(\tau_+, 0) U(0, \tau_-) \left[\prod_{j=1}^{N} a^\dagger_{x_j}\right] | \mathrm{vac}; \sigma\rangle \, . \end{aligned} \tag{18.14}$$

Noting that

$$\exp(-\mathrm{i}H_{\mathrm{wg}}\tau) a_x \exp(\mathrm{i}H_{\mathrm{wg}}\tau) = \int a_\omega \exp(\mathrm{i}\omega(x+\tau)) \frac{\mathrm{d}\omega}{\sqrt{2\pi}} \tag{18.15}$$

and since $U(0,\tau) a_\omega U(\tau, 0) = a_\omega(\tau)$,

$$U_{\mathrm{I}}(0, \tau_+) a_x U_{\mathrm{I}}(\tau_+, 0) = a_{\mathrm{out}}(-x) \quad \text{and} \quad U_{\mathrm{I}}(0, \tau_-) a_x U_{\mathrm{I}}(\tau_-, 0) = a_{\mathrm{in}}(-x). \tag{18.16}$$

Therefore

$$\left[\prod_{i=1}^{M} a_{x'_i}\right] U_{\mathrm{I}}(\tau_+, 0) = U_{\mathrm{I}}(\tau_+, 0) \left[\prod_{i=1}^{M} a_{\mathrm{out}}(-x'_i)\right] \tag{18.17a}$$

$$U_{\mathrm{I}}(0, \tau_-) \left[\prod_{j=1}^{M} a^\dagger_{x_j}\right] = \left[\prod_{j=1}^{M} a^\dagger_{\mathrm{in}}(-x_j)\right] U_{\mathrm{I}}(0, \tau_-). \tag{18.17b}$$

Eq. 18.14 can thus be expressed as

$$U^{\sigma',\sigma}_{\tau_+,\tau_-}(x'_1 \dots x'_M; x_1 \dots x_N) = \langle \mathrm{vac}; \sigma' | \, U_{\mathrm{I}}(\tau_+, 0) \prod_{i=1}^{M} a_{\mathrm{out}}(-x'_i) \prod_{j=1}^{N} a^\dagger_{\mathrm{in}}(-x_j) U_{\mathrm{I}}(0, \tau_-) \, | \mathrm{vac}; \sigma\rangle \, . \tag{18.18}$$

Since all the input or output operators commute with each other, we can introduce a time ordering operator as shown below:

$$\begin{aligned} &\prod_{j=1}^{N} a^\dagger_{\mathrm{in}}(-x_j) = \mathcal{T}\left[\prod_{j=1}^{N} a^\dagger_{\mathrm{in}}(-x_j)\right] \\ &= \mathcal{T}\left[\prod_{j=1}^{N} \left(a^\dagger_{\mathrm{out}}(-x_j) - \mathrm{i}L^\dagger(-x_j)\mathcal{I}(-\tau_+ < x_j < -\tau_-)\right)\right] \\ &= \sum_{k=0}^{N} (-\mathrm{i})^{N-k} \sum_{B_k^N} \mathcal{T}\left[\prod_{i=1}^{k} a^\dagger_{\mathrm{out}}(-x_{B_k^N(i)}) \prod_{j=1}^{N-k} L^\dagger(-x_{\bar{B}_k^N(j)})\right] \left[\prod_{j=1}^{N-k} \mathcal{I}(-\tau_+ < x_{\bar{B}_k^N(j)} < -\tau_-)\right] \\ &= \sum_{k=0}^{N} (-\mathrm{i})^{N-k} \sum_{B_k^N} \left[\prod_{i=1}^{k} a^\dagger_{\mathrm{out}}(-x_{B_k^N(i)})\right] \mathcal{T}\left[\prod_{j=1}^{N-k} L^\dagger(-x_{\bar{B}_k^N(j)})\right] \left[\prod_{j=1}^{N-k} \mathcal{I}(-\tau_+ < x_{\bar{B}_k^N(j)} < -\tau_-)\right] \end{aligned} \tag{18.19}$$

where B_k^N is a $k-$element unordered subset of $\{1, 2 \dots N\}$ and $\bar{B}_k^N$ is its complement. In the last step, we have used Eq. 18.10a and the fact that output operators evaluated at different time instances commute. From

Eq. 18.16, it follows that $a_{\rm out}(-x)U_{\rm I}(0,\tau_+)\,|{\rm vac};\sigma'\rangle = U_{\rm I}(0,\tau_+)a_x\,|{\rm vac};\sigma\rangle = 0$. Together with the commutator $[a_{\rm out}(t), a^\dagger_{\rm out}(t')] = \delta(t-t')$, this can be used to prove that:

$$\begin{aligned}
&\prod_{i=1}^{k} a_{\rm out}(-x_{B_k^N(i)}) \prod_{j=1}^{M} a^\dagger_{\rm out}(-x'_j) U_{\rm I}(0,\tau_+)|{\rm vac};\sigma'\rangle \\
&= \mathcal{I}(M\geq k)\sum_{B_k^M}\left[\sum_{P_k}\prod_{i=1}^{k}\delta(x'_{P_kB_k^M(i)} - x_{B_k^N(i)})\right]\prod_{j=1}^{M-k} a^\dagger_{\rm out}(-x'_{\bar{B}_k^M(j)})U_{\rm I}(0,\tau_+)\,|{\rm vac};\sigma'\rangle
\end{aligned} \tag{18.20}$$

where P_k denotes a permutation of a set of k elements, e.g. $P_kB_k^M$ is a permutation of B_k^M which itself is an unordered k-element subset of $\{1,2\ldots M\}$. Substituting Eqs. 18.19 and 18.20 into Eq. 18.18, we obtain:

$$\begin{aligned}
&U^{\sigma',\sigma}_{\tau_+,\tau_-}(x'_1\ldots x'_M; x_1\ldots x_N) \\
&= \sum_{k=0}^{N}(-{\rm i})^{N-k}\mathcal{I}(M\geq k)\sum_{B_k^N,B_k^M}\left[\sum_{P_k}\prod_{i=1}^{k}\delta(x'_{P_kB_k^M(i)} - x_{B_k^N(i)})\right]\times \\
&\quad \langle{\rm vac};\sigma'|\,U_{\rm I}(\tau_+,0)\left[\prod_{j=1}^{M-k} a_{\rm out}(-x'_{\bar{B}_k^M(j)})\right]\mathcal{T}\left[\prod_{s=1}^{N-k} L^\dagger(-x_{\bar{B}_k^N(s)})\right]U_{\rm I}(0,\tau_-)\,|{\rm vac};\sigma\rangle\times \\
&\quad \prod_{s=1}^{N-k}\mathcal{I}(-\tau_+ < x_{\bar{B}_k^N(s)} < -\tau_-) \\
&= \sum_{k=0}^{N}(-{\rm i})^{N-k}\mathcal{I}(M\geq k)\sum_{B_k^N,B_k^M}\left[\sum_{P_k}\prod_{i=1}^{k}\delta(x'_{P_kB_k^M(i)} - x_{B_k^N(i)})\right]\times \\
&\quad \langle{\rm vac};\sigma'|\,U_{\rm I}(\tau_+,0)\mathcal{T}\left[\prod_{j=1}^{M-k} a_{\rm out}(-x'_{\bar{B}_k^M(j)})\prod_{s=1}^{N-k} L^\dagger(-x_{\bar{B}_k^N(s)})\right]U_{\rm I}(0,\tau_-)\,|{\rm vac};\sigma\rangle\times \\
&\quad \prod_{s=1}^{N-k}\mathcal{I}(-\tau_+ < x_{\bar{B}_k^N(s)} < -\tau_-)
\end{aligned} \tag{18.21}$$

wherein we have used Eq. 18.10b in the last step to pull the output operators into the time-ordering operator. Using Eq. 18.8:

$$\begin{aligned}
&\mathcal{T}\left[\prod_{j=1}^{M-k} a_{\rm out}(-x'_{\bar{B}_k^M(j)})\prod_{s=1}^{N-k} L^\dagger(-x_{\bar{B}_k^N(s)})\right]U_{\rm I}(0,\tau_-)\,|{\rm vac};\sigma\rangle \\
&= \mathcal{T}\left[\prod_{j=1}^{M-k}(a_{\rm in}(-x'_{\bar{B}_k^M(j)}) - {\rm i}L(-x'_{\bar{B}_k^M(j)})\mathcal{I}(-\tau_+ < x'_{\bar{B}_k^M(k)} < \tau_-))\prod_{s=1}^{N-k} L^\dagger(-x_{\bar{B}_k^N(s)})\right]U_{\rm I}(0,\tau_-)\,|{\rm vac};\sigma\rangle \\
&= (-{\rm i})^{M-k}\mathcal{T}\left[\prod_{j=1}^{M-k} L(-x'_{\bar{B}_k^M(j)})\prod_{s=1}^{N-k} L^\dagger(-x_{\bar{B}_k^N(s)})\right]U_{\rm I}(0,\tau_-)\,|{\rm vac};\sigma\rangle\prod_{s=1}^{M-k}\mathcal{I}(-\tau_+ < x'_{\bar{B}_k^M(s)} < -\tau_-)
\end{aligned} \tag{18.22}$$

wherein we have used Eq. 18.10b and the fact that input operators at different time instances commute to move all the input operators in the time ordered product to the right and Eq. 18.16 to set $a_{\rm in}(-x)U_I(0,\tau_-)\,|{\rm vac};\sigma\rangle = U_I(0,\tau_-)a_x\,|{\rm vac};\sigma\rangle = 0$. Substituting Eq. 18.22 into Eq. 18.21

$$\begin{aligned}
&U^{\sigma',\sigma}_{\tau_+,\tau_-}(x'_1\ldots x'_M; x_1\ldots x_N) = \sum_{k=0}^{N}(-{\rm i})^{M+N-2k}\mathcal{I}(M\geq k)\times \\
&\quad \sum_{B_k^N,B_k^M}\left[\sum_{P_k}\prod_{i=1}^{k}\delta(x'_{P_kB_k^M(i)} - x_{B_k^N(i)})\right]\left[\prod_{i=1}^{M-k}\mathcal{I}(-\tau_+ < x'_{\bar{B}_k^M(i)} < -\tau_-)\right]\left[\prod_{j=1}^{N-k}\mathcal{I}(-\tau_+ < x_{\bar{B}_k^N(j)} < -\tau_-)\right]\times \\
&\quad \mathcal{G}^{\sigma',\sigma}_{\tau_+,\tau_-}(-x'_{\bar{B}_k^M(1)}, -x'_{\bar{B}_k^M(2)}\cdots - x'_{\bar{B}_k^M(M-k)}; -x_{\bar{B}_k^N(1)}, -x_{\bar{B}_k^N(2)}\cdots - x_{\bar{B}_k^N(N-k)})
\end{aligned} \tag{18.23}$$

where $\mathcal{G}^{\sigma',\sigma}_{\tau_+,\tau_-}(t'_1\ldots t'_M; t_1\ldots t_N)$ is the system Green's function defined by:

$$\mathcal{G}^{\sigma',\sigma}_{\tau_+,\tau_-}(t'_1\ldots t'_M; t_1\ldots t_N) = \langle{\rm vac};\sigma'|\,U_I(\tau_+,0)\mathcal{T}\left[\prod_{i=1}^{M} L(t'_i)\prod_{j=1}^{N} L^\dagger(t_j)\right]U_I(0,\tau_-)\,|{\rm vac};\sigma\rangle\,. \tag{18.24}$$

Note that the Green's function depends entirely on the dynamics of the low-dimensional system under consideration — we have thus reduced the problem of computing the propagator for the entire system to the problem of computing the dynamics of only the low-dimensional system.

Finally, after having computed the propagator in the interaction picture, $U_I(\tau_+, \tau_-)$, it is a simple matter to compute the propagator in the Schrödinger picture $U(\tau_+, \tau_-)$. To do so, we use the following property of the spatial Fock state:

$$\exp(-\mathrm{i}H_{\mathrm{wg}}\tau)\,|x_1, x_2 \ldots x_N\rangle = |x_1 + \tau, x_2 + \tau \ldots x_N + \tau\rangle \tag{18.25}$$

which intuitively states that an excitation created at a position x in the waveguide propagates along the positive x direction with velocity equal to the group velocity of the waveguide mode (which in this case is taken to be 1). Thus:

$$\langle x'_1 \ldots x'_M; \sigma'|\, U(\tau_+, \tau_-)\,|x_1 \ldots x_N; \sigma\rangle = U^{\sigma',\sigma}_{\tau_+,\tau_-}(x'_1 - \tau_+, x_2 - \tau_+ \ldots x'_M - \tau_+; x_1 - \tau_-, x_2 - \tau_- \ldots x_N - \tau_-). \tag{18.26}$$

18.2.3 Extension to multiple waveguides

Local systems coupled to multiple waveguide modes (which can either be physically separate waveguides or orthogonal modes of the same waveguide), diagrammatically shown in Fig. 18.1(b), can be described by Hamiltonians of the form:

$$H = H_{\mathrm{sys}}(t) + \sum_{\mu=1}^{N_L} \int \omega a^\dagger_{\omega,\mu} a_{\omega,\mu} \mathrm{d}\omega + \sum_{\mu=1}^{N_L} \int \left(a_{\omega,\mu} L^\dagger_\mu + L_\mu a^\dagger_{\omega,\mu}\right) \frac{\mathrm{d}\omega}{\sqrt{2\pi}} \tag{18.27}$$

where N_L is the total number of loss channels, $a_{\omega,\mu}$ is the plane wave annihilation operator for the μ^{th} waveguide which couples to the low dimensional system through the operator L_μ. A complete basis for the waveguide modes can now be constructed using the creation operators for the different waveguides:

$$|\{x_1, \mu_1\}, \{x_2, \mu_2\} \ldots \{x_N, \mu_N\}\rangle = \prod_{i=1}^{N} a^\dagger_{x_i,\mu_i} |\mathrm{vac}\rangle \tag{18.28}$$

where $a_{x,\mu} = \int a_{\omega,\mu} \exp(\mathrm{i}\omega x)\mathrm{d}\omega/\sqrt{2\pi}$ is the spatial annihilation operator for the μ^{th} waveguide mode. These annihilation operator have the commutators $[a_{x,\mu}, a_{x',\mu'}] = 0$ and $[a_{x,\mu}, a^\dagger_{x',\mu'}] = \delta(x - x')\delta_{\mu,\mu'}$. The propagator can thus be completely characterized by matrix elements of the form:

$$\begin{aligned} &U^{\sigma',\sigma}_{\tau_+,\tau_-}(\{x'_1, \mu'_1\}, \{x'_2, \mu'_2\} \ldots \{x'_M, \mu'_M\}; \{x_1, \mu_1\}, \{x_2, \mu_2\} \ldots \{x_N, \mu_N\}) \\ &= \langle \mathrm{vac}; \sigma'|\, a_{x'_1,\mu'_1} a_{x'_2,\mu'_2} \ldots a_{x'_M,\mu'_M} U_{\mathrm{I}}(\tau_+, \tau_-) a^\dagger_{x_1,\mu_1} a^\dagger_{x_2,\mu_2} \ldots a^\dagger_{x_M,\mu_M} |\mathrm{vac}; \sigma\rangle\,. \end{aligned} \tag{18.29}$$

Repeating the procedure described in Section 18.2.2, it can easily be shown that:

$$\begin{aligned} U^{\sigma',\sigma}_{\tau_+,\tau_-}(\{x'_1, \mu'_1\} \ldots \{x'_M, \mu'_M\}; \{x_1, \mu_1\} \ldots \{x_N, \mu_N\}) &= \sum_{k=0}^{N} (-\mathrm{i})^{M+N-2k} \mathcal{I}(M \geq k) \times \\ \sum_{B^N_k, B^M_k} \left[\sum_{P_k} \prod_{i=1}^{k} \delta(x'_{P_k B^M_k(i)} - x_{B^N_k(i)}) \delta_{\mu'_{P_k B^M_k(i)}, \mu_{B^N_k(i)}}\right] &\times \\ \left[\prod_{i=1}^{M-k} \mathcal{I}(-\tau_+ < x_{\bar{B}^M_k(i)} < -\tau_-)\right] \left[\prod_{j=1}^{N-k} \mathcal{I}(-\tau_+ < x_{\bar{B}^N_k(j)} < -\tau_-)\right] &\times \\ \mathcal{G}^{\sigma',\sigma}_{\tau_+,\tau_-}(\{-x'_{\bar{B}^M_k(1)}, \mu'_{\bar{B}^M_k(1)}\}, \ldots \{-x'_{\bar{B}^M_k(M-k)}, \mu'_{\bar{B}^M_k(M-k)}\}; \{-x_{\bar{B}^N_k(1)}, \mu_{\bar{B}^N_k(1)}\} \ldots \{-x_{\bar{B}^N_k(N-k)}, \mu_{\bar{B}^N_k(N-k)}\}) & \end{aligned} \tag{18.30}$$

where:

$$\mathcal{G}^{\sigma',\sigma}_{\tau_+,\tau_-}(\{t'_1, \mu'_1\} \ldots \{t'_M, \mu'_M\}; \{t_1, \mu_1\} \ldots \{t_N, \mu_N\}) = \langle \mathrm{vac}; \sigma'|\, U_{\mathrm{I}}(\tau_+, 0) \mathcal{T} \left[\prod_{i=1}^{M} L_{\mu'_i}(t'_i) \prod_{j=1}^{N} L^\dagger_{\mu_j}(t_j)\right] U_{\mathrm{I}}(0, \tau_-)\,|\mathrm{vac}; \sigma\rangle\,. \tag{18.31}$$

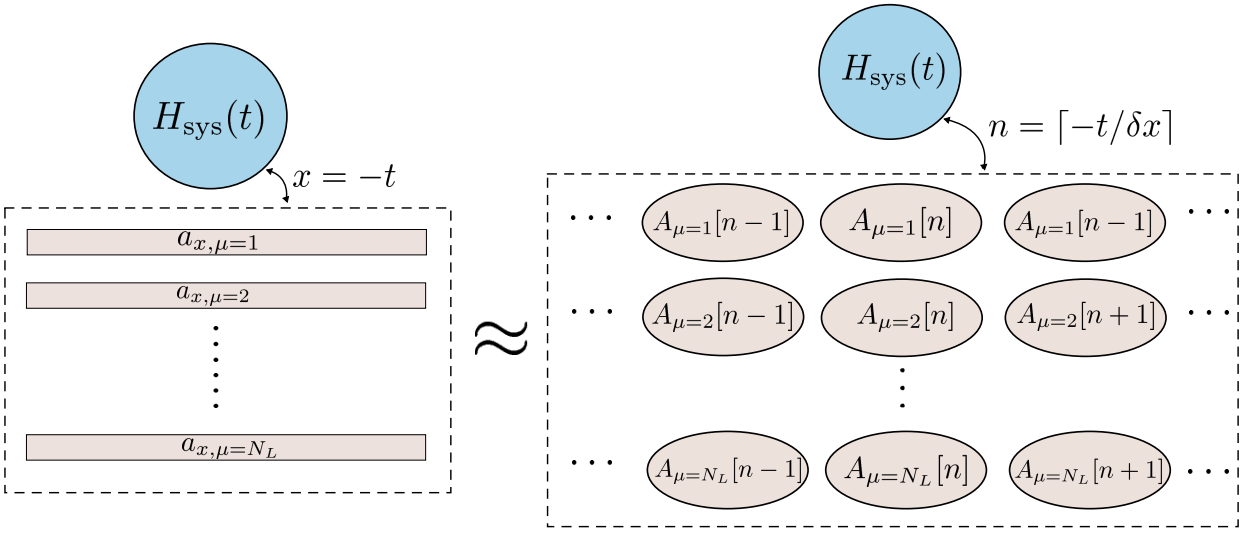

Figure 18.2: Diagrammatic representation of approximating the Hilbert space of the bath modes with a discrete Hilbert space.

18.2.4 Efficient computation of the Green's functions

While Eqs. 18.23 and 18.30 express the propagator entirely in terms of the low-dimensional system operators, the time evolution of these operators requires computing the time evolution of the entire system which remains computationally intractable due to the high dimensionality of the Hilbert space of the waveguide modes. In this section, we show that these Green's functions can equivalently be computed by evolving the low dimensional system under an effective non-hermitian Hamiltonian. We consider a general Green's function of the form:

$$\mathcal{G}^{\sigma',\sigma}_{\tau_+,\tau_-}(t_1,t_2\dots t_N) = \langle \text{vac};\sigma'|\, U_{\rm I}(\tau_+,0)\mathcal{T}\big[s_1(t_1)s_2(t_2)\dots s_N(t_N)\big]U_{\rm I}(0,\tau_-)\,|\text{vac};\sigma\rangle \tag{18.32}$$

where s_i are operators defined in the low-dimensional system's Hilbert space and $\tau_- < t_i < \tau_+ \;\forall\; i \in \{1,2\dots N\}$. Let P be a permutation of $\{1,2,3\dots N\}$ such that $t_{P(1)} \geq t_{P(2)} \cdots \geq t_{P(N)}$, then

$$\mathcal{G}^{\sigma',\sigma}_{\tau_+,\tau_-}(t_1,t_2\dots t_N) = \langle \text{vac};\sigma'|U_{\rm I}(\tau_+,0)\Big[\prod_{i=1}^{N} s_{P(i)}(t_{P(i)})\Big]U_{\rm I}(0,\tau_-)|\text{vac};\sigma\rangle. \tag{18.33}$$

We note that the system operators s_i commute with the waveguide Hamiltonian $H_{\rm wg}$ and thus $s_i(t) = U(0,t)s_iU(t,0) = U(0,t)\exp(-{\rm i}H_{\rm wg}t)s_i\exp({\rm i}H_{\rm wg}t)U(t,0) = U_{\rm I}(0,t)s_iU_{\rm I}(t,0)$. The Green's function can thus be expressed as:

$$\mathcal{G}^{\sigma',\sigma}_{\tau_-,\tau_+}(t_1,t_2\dots t_N) = \langle \text{vac};\sigma'|U_{\rm I}(\tau_+,t_{P(1)})\Big[\prod_{i=1}^{N-1} s_{P(i)}U_{\rm I}(t_{P(i)},t_{P(i+1)})\Big]s_{P(N)}U_{\rm I}(t_{P(N)},\tau_-)|\text{vac};\sigma\rangle. \tag{18.34}$$

We next show that the vacuum expectation in this equation can be explicitly evaluated — as a starting point, we express the interaction picture propagator in terms of the interaction picture Hamiltonian:

$$U_{\rm I}(t_1,t_2) = \mathcal{T}\exp\left[-{\rm i}\int_{t_2}^{t_1} H_{\rm I}(t'){\rm d}t'\right] \tag{18.35}$$

where

$$H_{\rm I}(t) = H_{\rm sys}(t) + \sum_{\mu=1}^{N_L}\int \big(a_{\omega,\mu}L^\dagger_\mu\exp(-{\rm i}\omega t) + L_\mu a^\dagger_{\omega,\mu}\exp({\rm i}\omega t)\big)\frac{{\rm d}\omega}{\sqrt{2\pi}}. \tag{18.36}$$

In terms of the spatial annihilation operator, $a_{x,\mu}$, the interaction picture Hamiltonian can be rewritten as:

$$H_{\rm I}(t) = H_{\rm sys}(t) + \sum_{\mu=1}^{N_L}\big(a_{x=-t,\mu}L^\dagger_\mu + L_\mu a^\dagger_{x=-t,\mu}\big). \tag{18.37}$$

To proceed, we approximate the high-dimensional continuum Hilbert space of the waveguides by a discrete Hilbert Space with a countably infinite basis (Fig. 18.2). This is achieved by introducing a coarse graining parameter δx, and defining the 'coarse grained operators' $A_{\mu,n}$ via:

$$A_\mu[n] = \int_{(n-1)\delta x}^{n\delta x} a_{x,\mu} \frac{\mathrm{d}x}{\sqrt{\delta x}}. \tag{18.38}$$

These operators satisfy the commutators $[A_\mu[n], A^\dagger_{\mu'}[n']] = \delta_{\mu,\mu'}\delta_{n,n'}$, $[A_\mu[n], A_{\mu'}[n']] = 0$ and in the limit of $\delta x \to 0$, $A_\mu[n]/\sqrt{\delta x}$ would approach the continuum operator $a_{x=n\delta x,\mu}$. The discrete Hilbert space approximating the waveguide's Hilbert space would then be the space spanned by the tensor product of the Fock states created by each of the operators $A^\dagger_\mu[n]$, $\forall \mu \in \{1, 2 \dots N_L\}$ and $n \in \mathbb{Z}$. In particular, the vacuum state $|\mathrm{vac}\rangle$ for the Hilbert space of the waveguide is approximated by

$$\bigotimes_{\mu=1}^{N_L} \bigotimes_{n=-\infty}^{\infty} |\mathrm{vac}_{n,\mu}\rangle \tag{18.39}$$

where $|\mathrm{vac}_{n,\mu}\rangle$ is the vacuum state corresponding to the operator $A_\mu[n]$. Moreover, this interaction Hamiltonian (Eq. 18.36) is then expressed as $H_\mathrm{I}(t;\delta x)$ in the limit of $\delta x \to 0$, where $H_\mathrm{I}(t;\delta x)$ is given by:

$$H_\mathrm{I}(t;\delta x) = H_\mathrm{sys}(t) + \frac{1}{\sqrt{\delta x}} \left\{ \sum_{\mu=1}^{N_L} \left(A_\mu\left[\lceil -t/\delta x \rceil\right] L^\dagger_\mu + L_\mu A^\dagger_\mu\left[\lceil -t/\delta x \rceil\right] \right) \right\}. \tag{18.40}$$

Using the notation $n_+ = \lceil \tau_+/\delta x \rceil$, $n_- = \lceil \tau_-/\delta x \rceil$, $n_i = \lceil t_i/\delta x \rceil$ and defining

$$U_\mathrm{I}[n_1, n_2] = \mathcal{T} \exp\left(-\mathrm{i} \int_{n_1\delta x}^{n_2\delta x} H_\mathrm{I}(t;\delta x)\mathrm{d}x \right) \tag{18.41}$$

the Green's function in Eq. 18.34 can be expressed as:

$$\begin{aligned}\mathcal{G}^{\sigma',\sigma}_{\tau_+,\tau_-}(t_1, t_2 \dots t_N) = \lim_{\delta x \to 0} \left[\left\{ \bigotimes_{\mu=1}^{N_L} \bigotimes_{n=-\infty}^{\infty} \langle \mathrm{vac}_{n,\mu}| \right\} \otimes \langle \sigma'| \right] U_\mathrm{I}[n_+, n_{P(1)}] \left[\prod_{i=1}^{N-1} s_{P(i)} U_\mathrm{I}[n_{P(i)}, n_{P(i+1)}] \right] \times \\ s_{P(N)} U_\mathrm{I}[n_{P(N)}, n_-] \left[\left\{ \bigotimes_{\mu=1}^{N_L} \bigotimes_{n=-\infty}^{\infty} |\mathrm{vac}_{n,\mu}\rangle \right\} \otimes |\sigma\rangle \right].\end{aligned} \tag{18.42}$$

Noting that since for $n\delta x < t < (n+1)\delta x$, $H_\mathrm{I}(t)$ depends only on $A_\mu[-n]$, $U_\mathrm{I}[n+1, n]$ would only act on $|\mathrm{vac}_{-n,\mu}\rangle$ $\forall \mu$. Using this together with the decomposition $U_\mathrm{I}[n_1, n_2] = U_\mathrm{I}[n_1, n_1 - 1]U_\mathrm{I}[n_1 - 1, n_1 - 2] \dots U_\mathrm{I}[n_2 - 1, n_2]$, we can rewrite Eq. 18.42 as:

$$\begin{aligned}\mathcal{G}^{\sigma',\sigma}_{\tau_+,\tau_-}(t_1, t_2 \dots t_N) = \lim_{\delta t \to 0} \langle \sigma'| \left[\prod_{j=-n_+-1}^{-n_{P(1)}} U_\mathrm{eff}[-j+1, -j] \right] \left[\prod_{i=1}^{N-1} \left\{ s_{P(i)} \prod_{j=-n_{P(i)}-1}^{-n_{P(i+1)}} U_\mathrm{eff}[-j+1, -j] \right\} \right] \times \\ s_{P(N)} \left[\prod_{j=-n_{P(N)}-1}^{-n_-} U_\mathrm{eff}[-j+1, -j] \right] |\sigma\rangle\end{aligned} \tag{18.43}$$

where

$$U_\mathrm{eff}[n+1, n] = \left[\bigotimes_{\mu=1}^{N_L} \langle \mathrm{vac}_{-n,\mu}| \right] U_\mathrm{I}[n+1, n] \left[\bigotimes_{\mu=1}^{N_L} |\mathrm{vac}_{-n,\mu}\rangle \right]. \tag{18.44}$$

This expression can be further simplified by expanding $U_\mathrm{I}[n+1, n]$ into a Dyson series in terms of the interaction Hamiltonian:

$$U_\mathrm{I}[n+1, n] = \mathrm{I} + \sum_{n=1}^{\infty} (-\mathrm{i})^n \int_{t_1=n\delta x}^{(n+1)\delta x} \int_{t_2=t_1}^{(n+1)\delta x} \cdots \int_{t_n=t_{n-1}}^{(n+1)\delta x} H_\mathrm{I}(t_n;\delta x) H_\mathrm{I}(t_{n-1};\delta x) \dots H_\mathrm{I}(t_1;\delta x) \mathrm{d}t_1 \dots \mathrm{d}t_n. \tag{18.45}$$

It follows from Eq. 18.40 that the vacuum expectations corresponding to the first two terms in the summation in the Dyson series evaluate to:

$$\left[\bigotimes_{\mu=1}^{N_L}\langle \mathrm{vac}_{-n,\mu}|\right]\int_{t=n\delta x}^{(n+1)\delta x} H_{\mathrm{I}}(t';\delta x)\mathrm{d}t'\left[\bigotimes_{\mu=1}^{N_L}|\mathrm{vac}_{-n,\mu}\rangle\right] = \int_{n\delta x}^{(n+1)\delta x} H_{\mathrm{sys}}(t)\mathrm{d}t \tag{18.46a}$$

$$\left[\bigotimes_{\mu=1}^{N_L}\langle \mathrm{vac}_{-n,\mu}|\right]\int_{t_1=n\delta x}^{(n+1)\delta x}\int_{t_2=t_1}^{(n+1)\delta x} H_{\mathrm{I}}(t_2;\delta x)H_{\mathrm{I}}(t_1;\delta x)\mathrm{d}t_1\mathrm{d}t_2\left[\bigotimes_{\mu=1}^{N_L}|\mathrm{vac}_{-n,\mu}\rangle\right] = \frac{1}{2}\sum_{\mu=1}^{N_L} L_\mu^\dagger L_\mu \delta x + \mathcal{O}(\delta x^2). \tag{18.46b}$$

Moreover, it can easily be seen from Eq. 18.36 that the vacuum expectations of higher order terms in the Dyson series do not have any contributions that are first order in δx. Therefore,

$$U_{\mathrm{eff}}[n+1,n] = \mathrm{I} - \mathrm{i}\int_{t=n\delta x}^{(n+1)\delta x} H_{\mathrm{eff}}(t')\mathrm{d}t' + \mathcal{O}(\delta x^2) = \mathcal{T}\exp\left[-\mathrm{i}\int_{n\delta x}^{(n+1)\delta x} H_{\mathrm{eff}}(t)\mathrm{d}t\right] + \mathcal{O}(\delta x^2) \tag{18.47}$$

where

$$H_{\mathrm{eff}}(t) = H_{\mathrm{sys}}(t) - \frac{\mathrm{i}}{2}\sum_{\mu} L_\mu^\dagger L_\mu. \tag{18.48}$$

Finally, substituting Eq. 18.47 into Eq. 18.43 and evaluating the limit, we obtain:

$$\mathcal{G}^{\sigma',\sigma}_{\tau_-,\tau_+}(t_1,t_2\ldots t_N) = \langle\sigma'|U_{\mathrm{eff}}(\tau_+,t_{P(1)})\left[\prod_{i=1}^{N-1} s_{P(i)}U_{\mathrm{eff}}(t_{P(i)},t_{P(i+1)})\right]s_{P(N)}U_{\mathrm{eff}}(t_{P(N)},\tau_-)|\sigma\rangle \tag{18.49}$$

where

$$U_{\mathrm{eff}}(t_1,t_2) = \mathcal{T}\exp\left[-\mathrm{i}\int_{t_2}^{t_1} H_{\mathrm{eff}}(t)\mathrm{d}t\right]. \tag{18.50}$$

Eq. 18.49 is an expectation evaluated entirely in the Hilbert space of the low-dimensional system, which makes it computationally tractable. For many systems of interest, it is often easier to work with a Heisenberg-like form of the Green's function, which can be obtained by defining $\tilde{s}_i(t) = U_{\mathrm{eff}}(0,t)s_iU_{\mathrm{eff}}(t,0)$, which satisfies the Heisenberg-like equations of motion:

$$\dot{\tilde{s}}_i(t) = -\mathrm{i}[\tilde{H}_{\mathrm{eff}}(t),\tilde{s}_i(t)] \tag{18.51}$$

where $\tilde{H}_{\mathrm{eff}}(t) = U_{\mathrm{eff}}(0,t)H_{\mathrm{eff}}(t)U_{\mathrm{eff}}(t,0)$. In terms of these operators, Eq. 18.49 can be reduced to

$$\begin{aligned}\mathcal{G}^{\sigma',\sigma}_{\tau_+,\tau_-}(t_1,t_2\ldots t_N) &= \langle\sigma'|U_{\mathrm{eff}}(\tau_+,0)\left[\prod_{i=1}^{N}\tilde{s}_{P}(i)(t_{P(i)})\right]U_{\mathrm{eff}}(0,\tau_-)\,|\sigma\rangle \\ &= \langle\sigma'|U_{\mathrm{eff}}(\tau_+,0)\mathcal{T}\left[\prod_{i=1}^{N}\tilde{s}_i(t_i)\right]U_{\mathrm{eff}}(0,\tau_-)\,|\sigma\rangle\,.\end{aligned} \tag{18.52}$$

18.3 Scattering matrices

The scattering matrix is a useful quantity to characterize the response of the low dimensional system to wave-packets incident from the waveguide modes coupling to it. The scattering matrix Σ can be computed from the interaction picture operator by taking the limits $\tau_- \to -\infty$ and $\tau_+ \to \infty$:

$$\Sigma = \lim_{\substack{\tau_+\to\infty \\ \tau_-\to-\infty}} U_I(\tau_+,\tau_-). \tag{18.53}$$

The scattering matrix can be completely characterized by matrix elements of the form:

$$\begin{aligned}&\Sigma^{\sigma',\sigma}(\{x_1',\mu_1'\}\ldots\{x_M',\mu_M'\};\{x_1,\mu_1\}\ldots\{x_N,\mu_N\}) \\ &= \langle\{x_1',\mu_1'\}\ldots\{x_M',\mu_M'\};\sigma'|\,\Sigma\,|\{x_1,\mu_1\}\ldots\{x_N,\mu_N\};\sigma\rangle\,.\end{aligned} \tag{18.54}$$

In order to compute the scattering matrix from the propagator analyzed in the previous section, we make the definition of the system Hamiltonian $H_{\text{sys}}(t)$ more explicit — in particular, we assume that it is 'time dependent' only if $t \in [0, T_P]$. Physically, this might correspond to a system like a two-level atom being driven by a coherent pulse which vanishes outside $[0, T_P]$. Mathematically, this is equivalent to writing $H_{\text{sys}}(t)$ as:

$$H_{\text{sys}}(t) = \begin{cases} H^0_{\text{sys}} + H^P_{\text{sys}}(t) & \text{for } 0 \leq t \leq T_P \\ H^0_{\text{sys}} & \text{otherwise} \end{cases}. \tag{18.55}$$

For a low-dimensional system Hamiltonian of this form and by using Eq. 18.23 the scattering matrix element can be expressed as:

$$\Sigma_{\sigma',\sigma}(\{x'_1,\mu'_1\}\dots\{x'_M,\mu'_M\};\{x_1,\mu_1\}\dots\{x_N,\mu_N\}) = \sum_{k=0}^{N}(-\mathrm{i})^{M+N-2k}\mathcal{I}(M\geq k)\times \tag{18.56}$$
$$\sum_{B_k^N,B_k^M}\left[\sum_{P_k}\prod_{i=1}^{k}\delta(x'_{P_kB_k^M(i)}-x_{B_k^N(i)})\delta_{\mu'_{P_kB_k^M(i)},\mu_{B_k^N(i)}}\right]\times$$
$$\mathcal{G}^{\sigma',\sigma}_{\infty,-\infty}(\{-x'_{\bar{B}_k^M(1)},\mu'_{\bar{B}_k^M(1)}\},\dots\{-x'_{\bar{B}_k^M(M-k)},\mu'_{\bar{B}_k^M(M-k)}\};\{-x_{\bar{B}_k^N(1)},\mu_{\bar{B}_k^N(1)}\}\dots\{-x_{\bar{B}_k^N(N-k)},\mu_{\bar{B}_k^N(N-k)}\})$$

where

$$\begin{aligned}&\mathcal{G}^{\sigma',\sigma}_{\infty,-\infty}(\{t'_1,\mu'_1\}\dots\{t'_M,\mu'_M\};\{t_1,\mu_1\}\dots\{t_N,\mu_N\})\\ &=\langle\sigma'|\,U^0_{\text{eff}}(\tau_+,T_P)U_{\text{eff}}(T_P,0)\mathcal{T}\left[\prod_{i=1}^{M}\tilde{L}_{\mu'_i}(t'_i)\prod_{j=1}^{N}\widetilde{L^\dagger}_{\mu_j}(t_j)\right]U^0_{\text{eff}}(0,\tau_-)\,|\sigma\rangle\end{aligned} \tag{18.57}$$

with

$$U^0_{\text{eff}}(t_1,t_2) = \exp\left[-\left(\mathrm{i}H^0_{\text{sys}}+\sum_\mu\frac{1}{2}L^\dagger_\mu L_\mu\right)(t_1-t_2)\right]. \tag{18.58}$$

While the orthonormal basis $\{|\sigma_1\rangle, |\sigma_2\rangle \dots |\sigma_S\rangle\}$ for the low-dimensional system's Hilbert space used for computing the propagator could be arbitrarily chosen as long as it is complete, for the purpose of computing the scattering matrix, we make this basis more explicit by expressing it as a union of a set of 'ground states' $\{|g_1\rangle, |g_2\rangle \dots |g_{S_g}\rangle\}$ and 'excited states' $\{|e_1\rangle, |e_2\rangle \dots |e_{S_e}\rangle\}$ which are all eigen-states of the Hamiltonian H^0_{sys}:

$$H^0_{\text{sys}}|g_n\rangle = \varepsilon_{g_n}|g_n\rangle \text{ and } H^0_{\text{sys}}|e_n\rangle = \varepsilon_{e_n}|e_n\rangle. \tag{18.59}$$

Moreover, the ground states and the excited states also satisfy:

$$L_\mu|g_n\rangle = 0\ \forall\ \mu\in\{1,2\dots N_L\}, n\in\{1,2\dots S_g\}, m\in\{1,2\dots S_e\} \tag{18.60a}$$
$$\exists\mu\in\{1,2\dots N_L\}\mid L_\mu|e_n\rangle\neq 0\ \forall\ n\in\{1,2\dots S_e\} \tag{18.60b}$$
$$\langle e_m|g_n|e_m|g_n\rangle = 0\ \forall\ m\in\{1,2\dots S_e\}, n\in\{1,2\dots S_g\} \tag{18.60c}$$

where L_μ are the operators through which the low dimensional system couples to the waveguide modes. An immediate consequence of the definition of ground and excited states (Eq. 18.60) and the positive-definiteness of the operator $\sum_\mu L^\dagger_\mu L_\mu$ (which is also the non-hermitian part of the effective Hamiltonian) within the subspace spanned by the excited states, is that if evolved with the propagator $U^0_{\text{eff}}(t_1,t_2)$ an excited state would decay to 0 and a ground state would remain unchanged except for accumulating a phase:

$$\lim_{\tau_-\to-\infty}U^0_{\text{eff}}(0,\tau_-)|e_n\rangle = 0 \text{ and } \lim_{\tau_-\to-\infty}U^0_{\text{eff}}(0,\tau_-)|g_n\rangle = \exp(\mathrm{i}\varepsilon_{g_n}\tau_-)|g_n\rangle \tag{18.61a}$$
$$\lim_{\tau_+\to\infty}\langle e_n|\,U^0_{\text{eff}}(\tau_+,T_P) = 0 \text{ and } \lim_{\tau_+\to-\infty}\langle g_n|\,U^0_{\text{eff}}(\tau_+,T_P) = \exp(-\mathrm{i}\varepsilon_{g_n}(\tau_+-T_P))\langle g_n|. \tag{18.61b}$$

Therefore, only the scattering matrix elements corresponding to the low-dimensional system going from one ground state to another ground state are non zero and are given by:

$$\Sigma_{g_m,g_n}(\{x'_1,\mu'_1\}\dots\{x'_M,\mu'_M\};\{x_1,\mu_1\}\dots\{x_N,\mu_N\}) = \sum_{k=0}^{N}(-\mathrm{i})^{M+N-2k}\mathcal{I}(M\geq k)\times \tag{18.62}$$
$$\sum_{B_k^N,B_k^M}\left[\sum_{P_k}\prod_{i=1}^{k}\delta(x'_{P_kB_k^M(i)}-x_{B_k^N(i)})\delta_{\mu'_{P_kB_k^M(i)},\mu_{B_k^N(i)}}\right]\times$$
$$\mathcal{G}^{\sigma',\sigma}_{\infty,-\infty}(\{-x'_{\bar{B}_k^M(1)},\mu'_{\bar{B}_k^M(1)}\},\dots\{-x'_{\bar{B}_k^M(M-k)},\mu'_{\bar{B}_k^M(M-k)}\};\{-x_{\bar{B}_k^N(1)},\mu_{\bar{B}_k^N(1)}\}\dots\{-x_{\bar{B}_k^N(N-k)},\mu_{\bar{B}_k^N(N-k)}\})$$

where

$$\mathcal{G}^{g_m,g_n}_{\infty,-\infty}(\{t'_1,\mu'_1\}\dots\{t'_M,\mu'_M\};\{t_1,\mu_1\}\dots\{t_N,\mu_N\}) = \langle g_m|\, U_{\text{eff}}(T_P,0)\mathcal{T}\left[\prod_{i=1}^{M}\tilde{L}_{\mu'_i}(t'_i)\prod_{j=1}^{N}\widetilde{L^\dagger}_{\mu_j}(t_j)\right]|g_n\rangle \quad (18.63)$$

wherein we have dropped the phase factors depending on τ_+ and τ_- corresponding to the phase accumulated by the ground states from the scattering matrix element. Previous calculation of the scattering matrix [19, 20] for systems with time-independent Hamiltonians arrived at exactly the same form as in Eqs. 18.62 and 18.63 with $T_P = 0$. However, as previously emphasized, the formalism introduced here allows us to model systems with time-dependent Hamiltonians, thereby increasing its applicability in modeling experimentally relevant systems.

18.4 Examples

In this section, we show how to use the formalism developed in the previous sections to analyze some open-quantum systems of interest. The examples we choose to analyze include a two-level system and a lambda three-level system. We calculate both emission from these systems when they are coherently driven, and scattering of single-photon pulses from these systems.

18.4.1 Two-level System

As our first example, we consider a coherently driven two-level system coupled to a single waveguide with coupling decay rate γ. Denoting the ground state of the two-level system with $|g\rangle$ and the excited state with $|e\rangle$, the two-level system can be modeled with the following Hamiltonian:

$$H_{\text{sys}} = \delta_a\sigma^\dagger\sigma + \Omega(t)(\sigma+\sigma^\dagger) \quad (18.64)$$

where $\sigma = |g\rangle\langle e|$ and $\sigma^\dagger = |e\rangle\langle g|$ are the annihilation and creation operators for the two-level system, δ_a is the detuning of the resonant frequency of the two level atom from the frequency of the coherent drive and $\Omega(t)$ is the amplitude of the coherent drive, which we assume to be of the form:

$$\Omega(t) = \begin{cases}\Omega_0 & 0\le t\le T_P\\ 0 & \text{otherwise}\end{cases}. \quad (18.65)$$

We first analyze emission from this driven two-level system — we consider the two-level system coupled to a single waveguide, with it being in the ground state and the waveguide to be in the vacuum state at $t = 0$ [Fig. 18.3(a)]. This amounts to computing the propagator $U_I(\tau,0)$, from which it is easy to extract the state of the waveguide and the two-level system as a function of τ. Of particular interest are the probabilities of finding 0 and 1 photon in the waveguide with the two-level system being in the excited or ground state as a function of τ:

$$P_{0,g}(\tau) = |\langle\text{vac};g|U(\tau,0)\,|\text{vac};g\rangle\,|^2, \quad P_{0,e}(\tau) = |\langle\text{vac};e|U(\tau,0)\,|\text{vac};g\rangle\,|^2 \quad (18.66a)$$

$$P_{1,g}(\tau) = \int|\langle x;g|U(\tau,0)\,|\text{vac};g\rangle\,|^2\mathrm{d}x; \quad P_{1,e}(\tau) = \int|\langle x;e|U(\tau,0)\,|\text{vac};g\rangle\,|^2\mathrm{d}x. \quad (18.66b)$$

Fig. 18.3(b) shows the steady state probabilities $P_{1,g}(\infty)$ and $P_{0,g}(\infty)$ of a two-level system emitting a single photon or not emitting any photons after being excited by a short pulse as a function of the pulse area. We observe the well understood rabi-oscillations in these probabilities with the pulse area. Fig. 18.3(c) shows the time-dependence of the probabilities defined in Eq. 18.66 for a long pulse — again, we observe oscillation in these probabilities while the two-level system is being driven, followed by a decay of the two-level system to its ground state and emission of photons into the waveguide. The full space-time dependence of the propagator matrix elements corresponding to a single photon in the waveguide is shown in Fig. 18.3(d) — we clearly see signatures of rabi-oscillation during the time interval in which the two-level system is being driven by the coherent pulse. During this time interval, the two-level system state and the waveguide state are entangled to each other, and after the coherent pulse goes to 0 the two-level system completely decays into the waveguide mode and the resulting excitation propagates along the waveguide. It can also be noted that the matrix elements are always zero outside the light-cone (i.e. for $x > t$), which is intuitively expected since the group velocity is an upper bound on the speed at which photons emitted by the two-level system can propagate in the waveguide.

Next, we analyze scattering of a single-photon pulse from a coherently driven two-level system (Fig. 18.4) — this amounts to computing the scattering matrix for the time dependent Hamiltonian in Eq. 18.64 using Eq. 18.62. We consider a two-level system coupled to two waveguides (Fig. 18.4), and excite it with an input pulse from the first waveguide (labeled as 1), and compute the single-photon component of the output state in the second waveguide (labeled as 2). Fig. 18.4(b) shows the single-photon scattering matrix for a two-level system, with and without the coherent drive. The two scattering matrices differ in the region $-T_P < x_1, x_2 < 0$, which corresponds to incident pulses that arrive at the two-level system while it is being driven. To analyze the

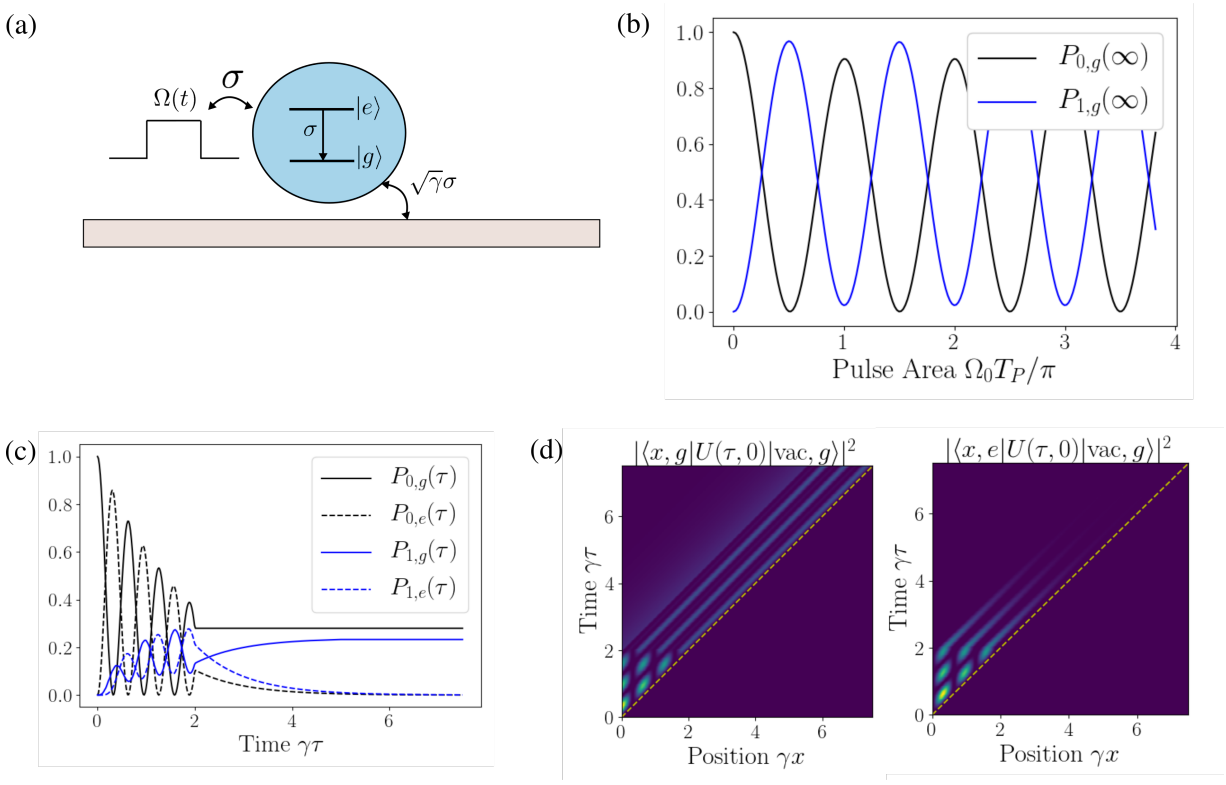

Figure 18.3: Emission from a coherently driven two-level system. (a) Schematic of a two-level system driven with a pulse $\Omega(t)$. (b) Probability of emission of a single photon $P_{0,g}(\infty)$ and of no emission $P_{1,g}(\infty)$ from a two-level system driven by a short pulse ($\gamma T_P = 0.2$) as a function of the pulse area. (c) Time dependence of the probabilities $P_{0,g}, P_{1,g}, P_{0,e}$ and $P_{1,e}$ for a two-level system driven by a long pulse ($\gamma T_P = 2$ and $\Omega_0 = 5\gamma$). (d) Space-time dependence of the propagator matrix elements corresponding to a single photon in the waveguide (dotted line is the light line $x = \tau$).

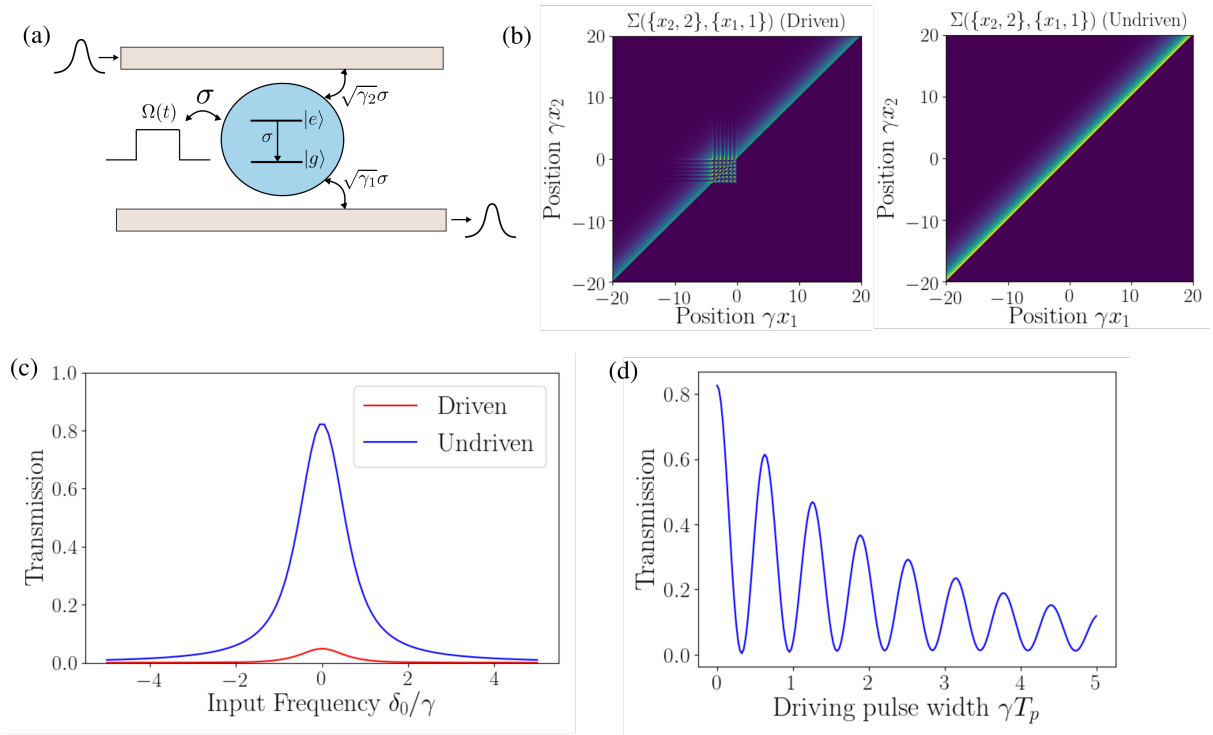

Figure 18.4: Scattering of a single-photon wave-packet from a coherently driven two-level system. (a) Schematic of a coherently driven two-level system coupled to an input and output waveguide. (b) Single-photon scattering matrix for the driven and undriven two-level system. (c) Variation of the transmission of the coherently driven two-level system with the central frequency δ_0 of the input single-photon state. (d) Variation of the transmission of a coherently driven two-level system with the length of the coherent drive for a resonant input single photon state ($\delta = 0$). For (b) and (c), it is assumed that $\gamma T_P = 4$ and $\Omega_0 = 5\gamma$. $\gamma_1 = \gamma_2 = \gamma/2$ and $\Delta x = 2.0/\gamma$ is assumed in all the calculations.

transmission spectra of the driven two-level system, we consider exciting the first waveguide with a single-photon state (in the interaction picture) at time $-\infty$ of the form:

$$|\psi(-\infty)\rangle = \int \psi_{\text{in}}(x_1) a^\dagger_{x_1,1} |\text{vac}\rangle \, \mathrm{d}x_1, \quad \psi_{\text{in}}(x_1) = \frac{1}{(\pi\Delta x^2)^{1/4}} \exp\left(-\frac{x_1^2}{2\Delta x^2} + \mathrm{i}\delta_0 x_1 \right) \tag{18.67}$$

where δ_0 is the central frequency of the incident wave-packet, and Δx is its spatial extent. We compute the single-photon component in the output waveguide by applying the scattering matrix to the input state:

$$\psi_{\text{out}}(x_2) = \int \Sigma(\{x_2, 2\}, \{x_1, 1\}) \psi_{\text{in}}(x_1) \mathrm{d}x_1 \tag{18.68}$$

and the transmission of the single-photon state via:

$$\text{Transmission} = \int |\psi_{\text{out}}(x_2)|^2 \mathrm{d}x_2. \tag{18.69}$$

Figure 18.4(c) shows the transmission spectrum of the two-level system with and without the coherent drive — the driven two-level system clearly shows a suppression in transmission. Intuitively, this is a consequence of the coherent pulse transferring the two-level system into its excited state when the single-photon pulse arrives at the two-level system, thereby resulting in low transmission into the output waveguide. Figure 18.4 shows the dependence of the transmission of the two-level system for a resonant input single-photon wave-packet ($\delta_0 = 0$) on the length of the coherent drive T_P. Again, we see a signature of the rabi-oscillation in the transmission — the probability of the two-level system being in the excited state oscillates with the input pulse, and this oscillation translates to the oscillation in the transmission of the driven two-level system.

18.4.2 Lambda system

As our next example, we consider a coherently driven three-level lambda-system. This system has two ground states, denoted by $|g_1\rangle$ and $|g_2\rangle$, and one excited state, denoted by $|e\rangle$. The Hamiltonian for this system is given by:

$$H_{\text{sys}} = \delta_e |e\rangle\langle e| + \delta_{12} |g_1\rangle\langle g_1| + \Omega(t)(\sigma_1 + \sigma_1^\dagger) \tag{18.70}$$

where $\sigma_i = |g_i\rangle\langle e|$ is the operator that annihilates the excited state $|e\rangle$ to the ground state $|g_i\rangle$, δ_e is the detuning of the frequency difference between $|e\rangle$ and $|g_2\rangle$ from the frequency of the coherent drive, δ_{12} is the frequency difference between the states $|g_2\rangle$ and $|g_1\rangle$, and $\Omega(t)$ is the amplitude of the coherent drive which we again assume to be a rectangular pulse as given by Eq. 18.65.

We first analyze photon emission from this driven lambda system — the lambda system is assumed to couple to a single waveguide through an operator $\sqrt{\gamma}\sigma_2$, with it being in the ground state $|g_1\rangle$ and the waveguide being in the vacuum state at time 0 [Fig. 18.5(a)]. The probabilities of interest that we compute include the following:

$$\begin{aligned} &P_{0,g1}(\tau) = |\langle \text{vac}; g_1| U_{\text{I}}(\tau, 0) |\text{vac}; g_1\rangle|^2, P_{0,e}(\tau) = |\langle \text{vac}; e| U_{\text{I}}(\tau, 0) |\text{vac}; g_1\rangle|^2 \\ &P_{1,g2} = \int |\langle x; g_2| U_{\text{I}}(\tau, 0) |\text{vac}; g_1\rangle|^2 \mathrm{d}x \end{aligned} \tag{18.71}$$

Figure 18.5(b) shows the dependence of the probabilities of single photon emission and no emission as a function of the pulse area for a short driving pulse – we again observe the expected rabi-oscillations in these probabilities. Fig. 18.5(c) shows the time evolution of the probabilities defined in Eq. 18.71 for a long driving pulse — we clearly observe an oscillation in these probabilities while the lambda system is being driven followed by emission of a single photon into the waveguide. We note that for a lambda system, once a photon emission into the waveguide occurs, the lambda system would necessarily transition to the state $|g_2\rangle$, and will no longer be driven by $\Omega(t)$. As a consequence of this structure of the lambda system, only a single photon can be emitted into the waveguide — this is numerically validated in Fig. 18.5(c) from which it can be seen that $P_{0,g1}(\infty) + P_{1,g2}(\infty) = 1$. Figure 18.5(d) shows the propagator matrix element $|\langle x; g_2| U(\tau, 0) |\text{vac}; g_1\rangle|^2$ — we clearly see a stark difference from the corresponding matrix element for a two-level system (Fig. 18.3) due to the system not interacting with the coherent pulse following the emission of a photon into the waveguide.

As our final example, we analyze photon subtraction using a lambda system — the system under consideration is shown in Fig. 18.6(a). A lambda system is coupled to an input waveguide through the operator σ_1 and to an output waveguide through σ_2 to an output waveguide, with lambda system initially being in the state $|g_1\rangle$. A single photon is incident from the input waveguide which drives the system from $|g_1\rangle$ to $|e\rangle$ to $|g_2\rangle$, with the photon finally being emitted into the output waveguide. For a lambda system with $\delta_{12} = 0$ and the incoming photon being resonant with the ground state to excited state transition, the incoming photon is completely transfered from the input waveguide to the output waveguide. Subsequently, a photon incident from the input waveguide does not interact with the lambda system, since the lambda system is now in the state $|g_2\rangle$ which cannot be driven with an excitation from the input waveguide. This allows the lambda system to be used as a photon subtracter [33] — for a stream of spatially separated single photons incident on the lambda system, the

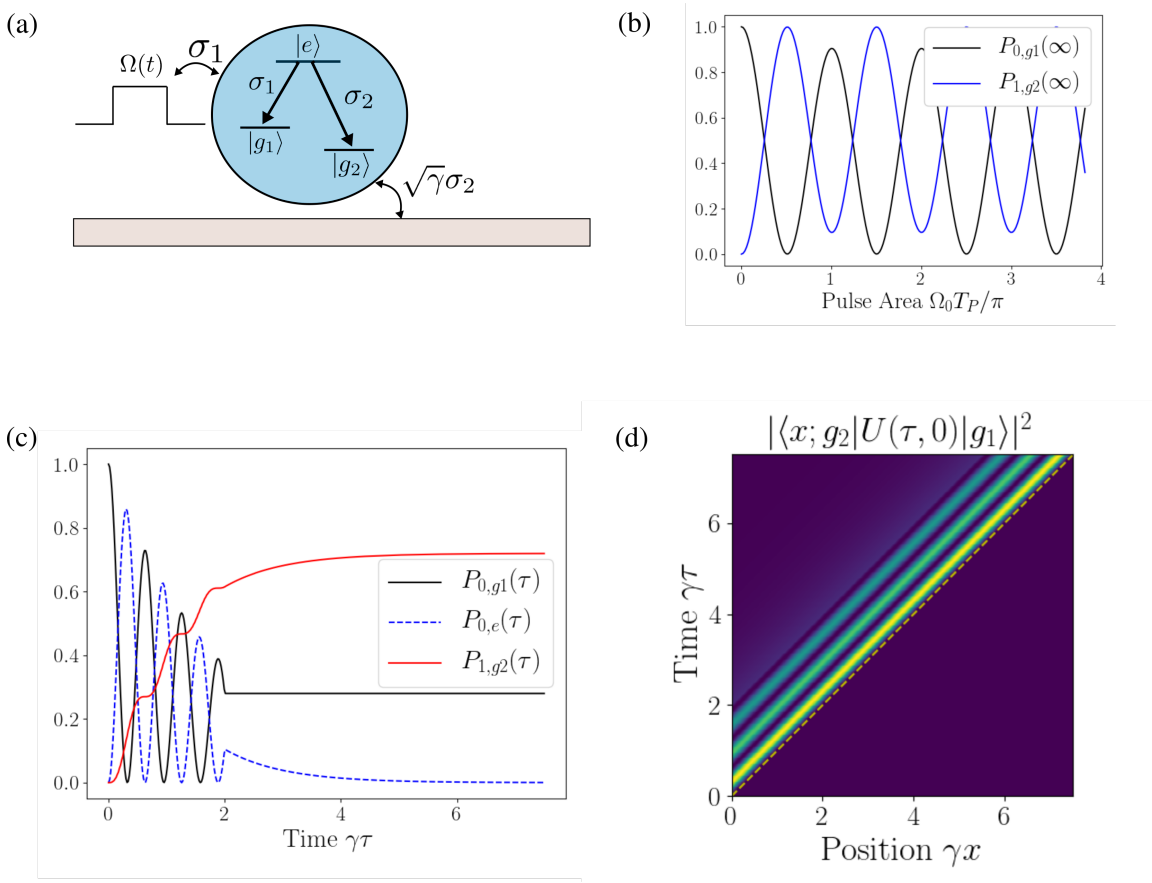

Figure 18.5: Emission from a coherently driven three-level lambda system. (a) Schematic of the system being analyzed. (b) Probability of emission of a single photon $P_{1,g_2}(\infty)$ and of no emission $P_{0,g_1}(\infty)$ from the lambda system driven by a short pulse ($\gamma T_P = 0.2$) as a function of the pulse area. (c) Time dependence of the probabilities P_{0,g_1}, P_{1,g_2} and $P_{0,e}$ for a three-level lambda system driven by a long pulse ($\gamma T_P = 2$ and $\Omega_0 = 5\gamma$). (d) Space-time dependence of the propagator matrix elements corresponding to a single photon in the waveguide (dotted line is the light line $x = \tau$). $\delta_{12} = 0$ and $\delta_e = 0$ are assumed in all the simulations.

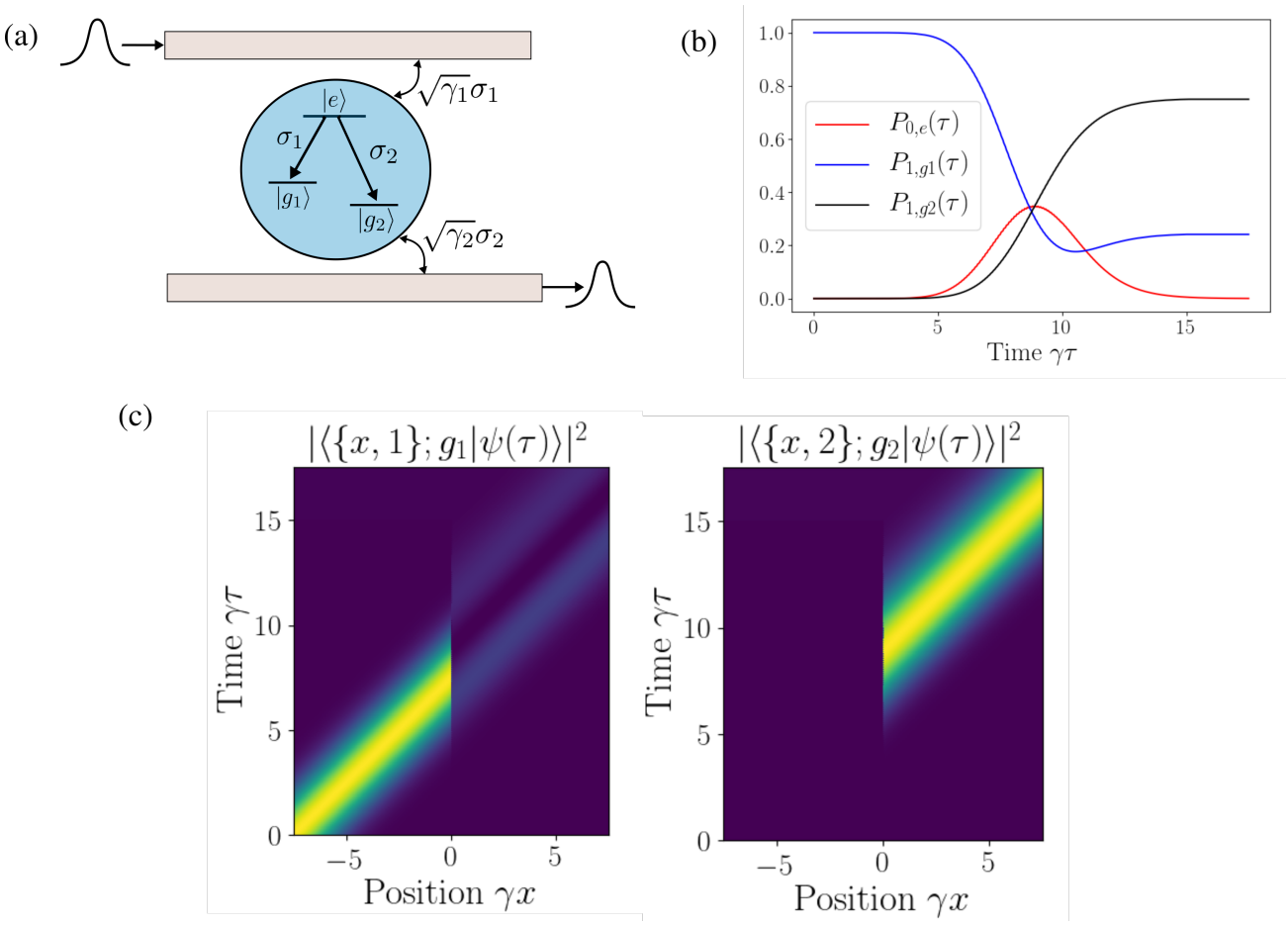

Figure 18.6: Scattering of a single-photon wave-packet from a three-level lambda system. (a) Schematic of the system being analyzed. (b) Time dependence of the probabilities P_e, P_{1,g_1} and P_{2,g_2} for a three-level lambda system excited by an incident single-photon state. (c) Space-time dependence of the single-photon component of the system state in both the input and output waveguides. $\gamma_1 = \gamma_2 = \gamma/2$, $\Delta x = 2/\gamma$ and $\delta_e = \delta_{12} = 0$ is assumed in all the simulations.

lambda system would remove the first photon from the stream, and transmit the rest. To numerically reproduce this effect, we consider the system to be in the following initial state:

$$|\psi(0)\rangle = \int \psi_{\text{in}}(x_1) a^\dagger_{x_1,1} |\text{vac}; g_1\rangle \, \mathrm{d}x_1, \quad \psi_{\text{in}}(x_1) = \frac{1}{(\pi\Delta x^2)^{1/4}} \exp\left(- \frac{(x_1 + L)^2}{2\Delta x^2} \right) \tag{18.72}$$

where Δx is its spatial extent of the incoming photon wave-packet and L is the distance of the center of the wave-packet from the lambda system at $t = 0$. The state of the system at $t = \tau$ can then be expressed in terms of the propagator matrix elements:

$$\begin{aligned} |\psi(\tau)\rangle = &\int \langle \text{vac}; e| \, U(\tau, 0) \, |\{x'_1, 1\}; g_1\rangle \, \psi_{\text{in}}(x'_1) \mathrm{d}x'_1 \\ &+ \int\int \langle \{x_1, 1\}; g_1| \, U(\tau, 0) \, |\{x'_1, 1\}; g_1\rangle \, \psi_{\text{in}}(x'_1) a^\dagger_{x,1} |\text{vac}; g_1\rangle \, \mathrm{d}x'_1 \mathrm{d}x_1 \\ &+ \int\int \langle \{x_2, 2\}; g_2| \, U(\tau, 0) \, |\{x'_1, 1\}; g_1\rangle \, \psi_{\text{in}}(x'_1) a^\dagger_{x,2} |\text{vac}; g_2\rangle \, \mathrm{d}x'_1 \mathrm{d}x_2. \end{aligned} \tag{18.73}$$

The probabilities of interest, denoted by P_e, P_{1,g_1} and P_{2,g_2}, that we simulate for this system are defined by:

$$P_e(\tau) = |\langle \text{vac}; e|\psi(\tau)|\text{vac}; e|\psi(\tau)\rangle|^2, \quad P_{1,g_1} = \int |\langle \{x_1, 1\}; g_1|\psi(\tau)|\{x_1, 1\}; g_1|\psi(\tau)\rangle|^2 \mathrm{d}x_1 \quad \text{and} \quad P_{2,g_2} = \int |\langle \{x_2, 1\}; g_2|\psi(\tau) \tag{18.74}$$

Figure 18.6(b) shows the time evolution of these probabilities — clearly, the lamba-system transitions from initially being in $|g_1\rangle$ to the excited state $|e\rangle$ and then to $|g_2\rangle$ with photon transfering from the input to the output waveguide. However, we note that the photon wave-packet is not completely transmitted into the second waveguide, which is a consequence of wave-packet having a finite spread in frequency, and therefore not being completely resonant with the lambda system. Figure 18.6(c) shows the space-time dependence of the single-photon wave packet in the input and output waveguides — clearly, the initial wave-packet propagates along the input waveguide till it reaches the lambda system at $x = 0$ and then transmits to the second waveguide.

18.5 Conclusion and outlook

We have completely described the unitary propagator for a composite quantum network comprising waveguides and a low-dimensional system. Our method is strongly connected to the linearity of the waveguide dispersions and the Markovian coupling approximation. This linearity allows us to always express the initial (time τ_-) and final (time τ_+) waveguide states in terms of Heisenberg field operators. As a result, we are able to use the input-output boundary conditions to arrive at an expression between the states in terms of system Heisenberg operators only. The culminating expectations are with respect to vacuum states, otherwise known as a Green's functions. These Green's functions can be expressed entirely in the Hilbert space of system operators, which we showed by coarse-graining the waveguides' spatial dimensions. Hence, our expression proves tractable for many systems of interest and provides insight into the connections between input-output theory, scattering matrices, and propagators for Markovian open-quantum systems.

Part XIII
Other Experiments

Part XIV
Adds

A Введение и обзор

A.0.1 Другая мотивация

Польза в плане развития как профессионала

(потом раскрою)

Польза в плане саморазвития

(потом раскрою)

A.0.2 Мышление профессионала в КЭД волноводах

(потом напишу, пока не до этого раздела)

Взгляд на КЭД волноводов

Для начала не так уж обязательно знать много другой физики и математики для КЭД волноводов, потому что в статьях очень схожий формализм и делают они почти одно и то же

Так что можно просто начать читать статьи и крутиться в этой теме. В 2023м году (да и скорее всего последние 10 лет тоже это так) очень много статей, так что можно читать их и понимать глубже и глубже этот предмет. Вообще не сложно.

И просто начинаешь про это думать, пару раз в неделю додумываешь детали - так за пару месяцев вообще без проблем и напрягов все понимается. Просто не нужно заниматься лишним и не нужно общие основы предметов собирать, можно спокойно исследовать многое, не так уж глубоко понимая основы, которые стоят за методами, которые тут используются.

А то можно и не дойти до этого предмета, если рыться в основах физики. По факту все тут нужное в статьях и написано.

(?? мб это общее соображение для всех предметов, тогда это в орг записи оставлю.)

Появление предмета в нашей картине мира

Использование предмета в обычной жизни (!)

Укажем, как предмет используется в обычной жизни.

Особенности работы с КЭД волноводов

Для первой записи формул пишем без индексов и упрощенно, потому что иначе индексы и детали займут очень много времени

(раскрою эту мысль, так и делаю. слишком уж тут много индексов. Окажется, что я неправ - изменю этот раздел.)

Все-таки, диаграммы для описания КЭД волноводов нужны и полезны или нет?

(по идее там будет раздел с приложениями вдали, тут обзорно, словами)

О применениях в квантовой когерентности, квантовых компьютерах (????)

(воспроизведу ответ Кирилла, я слишком мало про это думал, чтобы понять пока что.)

Актуальнейшие приложения

Построение КЭД волноводов с нуля или как догадаться об этих методах?

(потом раскрою, еще я не профессионал, а вопрос этот самый профессиональный)

Общие соображения, позволяющие догадаться

(тут абзац про то, что много индексов появляется, и казалось бы, тупик, но можно свернуть их в один мульти индекс.)
(и про другие общие организационные мелочи. без них тоже задачу не решить было бы)
(потом раскрою, еще я не профессионал, а вопрос этот самый профессиональный)

Способы догадаться до всех главных идей

незаменимая часть нормального понимания предмета.
(потом раскрою)

Мышление для эффективного изучения

Осудим, какое мышление наиболее эффективное для усвоение предмета.

Полезно начать смотреть на формулы, понять их, потом понять их смысл и описание задачи

То есть вообще смотреть только на формулы сперва, текст вообще почти не читать. Такой подход эффективнее, чем читать текст, потому что иначе завязнуть прямо очень легко.
(!! напишу лучше эту мысль, понятно, что не только это нужно делать вначале)
(убеждусь, действительно ли это полезно??? пока думаю, что скорее всего так и есть.)

Необходимые темы для

(потом раскрою)

Дополнительные темы для

(потом раскрою)

A.0.3 Literature

Основная

[**?**] K. Piasotski, M. Pletyukhov Diagrammatic approach to scattering of multiphoton states in waveguide QED
То, откуда я начинаю изучать формализм для этих задач
Piasotski, Kiryl Master's degree thesis
Много объяснений происходящего и много теории. В открытом доступе нет, нужно Кириллу писать для нее.
[**?**] Mikhail Pletyukhov, Vladimir Gritsev Scattering of massless particles in one-dimensional chiral channel 2012
Еще одна статья, которую смотрел, мб там тоже много очень хорошего сделано, просто пока не до нее, отдельную минимум неделю нужно на ней сидеть, чтобы понять.
K. Lalumiere, B. C. Sanders, A. F. van Loo, A. Fedorov, A. Wallraff, and A. Blais, Input-output theory for waveguide QED with an ensemble of inhomogeneous atoms, Phys. Rev. A 88, 043806 (2013)
Известная статья, первая, на которую Кирилл ссылается, почитаю тоже ее.

Другие тоже содержательные статьи

[?] P-O Guimond and M Pletyukhov and H Pichler and P Zoller Delayed coherent quantum feedback from a scattering theory and a matrix product state perspective

Очень полезная тоже статья, вроде о том же, что уже пройдено, но посидеть над ней тоже нужно.

R. H. Lehmberg, Radiation from an N-atom system. I. general formalism, Phys. Rev. A 2, 883 (1970)

Первая статья про формализм излучения (так говорил Кирилл), и в 3д пространстве аж! Потом почитаю, в открытом доступе нет, так что нужно просить кого-то скачать ее.

Books With Many Solved Problems

Статьи по схожим темам и методам

В помощь по физике и математике (!!!)

(тут скорее всего много всего будет)

О приложениях

A.0.4 Обзор

(потом раскрою)

Обзор применений и моделей описания

(тут то, что можно и потом прочитать супер внимательно, суть метода в частях ниже)

Waveguide quantum electrodynamics (QED) is a modern field of research focused on the study of light-matter interactions in one dimension. The confinement of electromagnetic radiation to a single spatial dimension allows one to achieve a significant enhancement of the coupling between atoms and fields, as well as to attain a better matching between the spatial modes of the emitting and absorbing atoms [1,2].

Apart from the purely academic interest in the study of strong light-matter coupling, a great deal of motivation in this field of research comes from the technological sector, namely, from the quantum computing [3-8]. One of the most prominent examples is the so-called quantum network: a system of quantum processors interconnected by quantum radiation channels propagating quantum information and entanglement between them [9].

Although photons are the excellent carriers of quantum information, capable of high-fidelity entanglement and information transfer [10-12], recent advancement in quantum electronics offers a large variety of alternatives. Most commonly, in 2020-s waveguide QED setups are realized in the experiments with superconducting quantum circuits, where superconducting transmission lines act as quantum radiation channels, whereas the Josephson-junction-based superconducting quantum bits play the role of quantum emitters [13-15]. Other examples include superconducting qubits coupled to propagating phonons (surface acoustic waves) employing the piezoelectric effect [16-19], and surface plasmons coupled to quantum dots [20].

Theoretically, the atom-field interactions in waveguide QED can often be accurately treated in the so-called Markovian limit $\gamma\tau \ll 1$, where γ and τ stand for the characteristic decay rate and time delay in the system [21] (??? разберусь, что они конкретно значат??). In the course of the last few decades, a significant number of theoretical approaches allowing one to tackle the waveguide QED problems within this limit was proposed. In particular, the Markovian waveguide QED systems are commonly examined theoretically with help of master-equation-based approaches [1,22-27]. Indeed, within the framework of the associated input-output formalism [1,28,29], Lindblad-type equation approaches allow one to study transmission and reflection characteristics, as well as the photonic correlations for arbitrary initial photon states, including coherent, thermal, and Fock ones. Moreover, at a rather modest expense, a substantial variety of theoretical tools are available for a derivation of master equations:

(??? окей, посмотрю их потом, мб сделаю разделы на эти методы. тут просто обзор, типа ну такое вот разное вообще есть. Интересно, конечно, но это можно вообще не знать и 1 метод додумать и все.)

Equation-of-motionbased methods [1,22,23], path-integral techniques [30], SLH formalism [31] (a popular formalism for the systematic construction of markovian master equations governing the evolution of cascaded quantum systems from S-matrix, coupling vector - L, and the Hamiltonian $-H$), to mention just a few. In 2020-s, master-equation-based approach was generalized to capture the effects of temporal modulation of the system parameters [32, 33], such as the light-matter coupling strength and the transition frequencies of quantum emitters.

Another frequenter method of studying waveguide QED systems within Markov approximation is the coordinate space Bethe ansatz [34-41]. Within this approach, one is able to determine the exact stationary eigenstates of the system's Hamiltonian in a subspace of a given excitation number, which, in turn, enables one to calculate stationary observables as well as photonic correlation functions exactly. Moreover, the Bethe ansatz technique was shown to be applicable to the studies of real-time dynamics of few-photon states [36, 42, 43], systems where the photon-photon bound states occur [41, 44], and systems with delayed coherent feedback [45]. Despite its scalability to the cases of multiple emitters and emitters with complicated level structures, this approach is known to be strongly limited by the number of excitations in the system due to the rapid increase of complexity of the resulting Bethe wave functions [34, 36, 46, 47].

Another group of systematic methods of studying the waveguide QED systems in the limit of the negligible delay times is comprised of the field-theory-based approaches. For example, in [48-50], by representing the atomic operators in terms of the slave fermions, the authors were able to employ the path-integral representation of the field correlation functions, from which the S matrix may be established by means of the celebrated Lehmann-Symanzik-Zimmermann reduction formula. Another field-theoretical method to be mentioned is the so-called diagrammatic resummation theory developed in [51-54]. Within the framework of resummation theory, one sums the perturbative series of Feynman diagrams for the matrix elements of the transition operator to infinite orders, which, in turn, allows one to determine the exact S matrix, with the help of which all of the stationary observables may be calculated [52].

(в абзаце ниже - хз, что, что-то не легко читается, оставил.)

Although the physics behind waveguide QED systems is easily accessible in the Markovian limit using a large variety of theoretical tools, there exist a number of problems forcing one to go beyond this approximation [21,55-58]. As it is well known, in the single-excitation subspace, all of the dynamical and stationary information about the system may be easily obtained (either analytically or numerically) by means of Bethe ansatz for a system of arbitrary complexity [59-62]. Primarily, this assertion has to do with the fact that it is relatively easy to conceive a closed system of (delay) differential equations governing the evolution of the system. Even though it is possible to proceed in the same manner in higher excitation subspaces [63], the calculations become much more cumbersome and lack systematicity. In the course of the last decade, a number of theoretical approaches allowing one to overcome these difficulties were put forward. On the numerical side, for example, significant progress in the dynamical simulation of the non-Markovian one-dimensional (1D) quantum systems was achieved within the framework of matrix product state ansatz [64-67]. Despite the complexity associated with the non-Markovian waveguide QED systems, a few analytical methods were also recently suggested. In particular, it is a common practice to generalize the Lindblad-type equation approaches to the non-Markovian realm [30,68-70]. Although generalized master equations can only provide exact results in the case of linear scatterers, they allow for systematic approximate treatment of systems with nonlinearities such as qubits.

Another common approach to waveguide QED problems with delayed coherent quantum feedback is based on the diagrammatic resummation theory. In recent years resummation ideas were successfully applied to solve the two-photon scat- tering and dynamics in the systems with two distant qubits [71], a single qubit in front of a mirror [21], a giant acoustic atom [59], and a qubit coupled to a resonator array [72].

Описние метода (!??!??!!)

(!??! тут нужно внимательно почитать!!)

In this paper, we present a systematic generalizattion of the diagrammatic approach to scattering of multi-photon states in waveguide QED. Our approach is based on the exact resummation of the perturbation theory for the transition operator which turns out to be possible due to the conservation of excitation number guaranteed by the rotating wave approximation.

The advantage of our approach is its insensitivity to the form of light-matter coupling constants, thus allowing one to potentially examine any kinds of waveguide QED systems, including the systems with delayed coherent quantum feedback. We start by making an exposure of the method by the direct example of one-qubit waveguide QED. This framework lays down a basis for further calculations, in particular general qubit number two and three-photon scattering theory. We then apply the developed theory to a weakly coherent pulse scattering on a giant acoustic atom, an intrinsically non-Markovian system.

In particular, we consider the scattering of a coherent state with small enough coherence parameter $|\alpha| \ll 1$ chosen such that the terms of order $|\alpha|^4$ can be ignored.

With the help of the general methods developed in Sec. II we compute an exact output state of radiation and study the particle correlations in it with the help of the theory of optical coherence. In particular, we compute the first-, second-, and third-order coherence functions to the lowest order in $|\alpha|$ and discuss the impact of the non-Markovianity of the scatterer on the observable quantities.

SCATTERING THEORY section description

In this section, we first set up the notations used throughout the paper. Next, we introduce the general formalism in the framework of the single-qubit waveguide QED. In particular, we extend the findings of the preceding papers [21, 51, 53, 59] to the realm of non-Markovian models by allowing for arbitrary momentum dependence of waveguide modes and radiation-qubit couplings. This development, in turn, allows one to study multiphoton scattering problems in systems with nonlinear dispersion of the modes supported by the radiation channels, as well as the systems with artificial feedback loops, such as a qubit placed in front of a mirror or a giant acoustic atom, for example.

Further on, we generalize the scattering formalism to the systems with a higher number of qubits, where the quantum feedback loops a naturally present due to the finiteness of time required for a photon to propagate between a given pair of distant emitters. Specifically, we discuss two- and three-photon scattering problems on an arbitrary number of emitters, extending the approach of [71].

Alongside this, we discuss several practical issues, such as the separation of elastic contributions to the scattering matrices and the generalized cluster decomposition.

Введение в двух словах (?????)

We give an exposure to diagrammatic techniques in waveguide quantum electrodynamics (QED) systems. A particular emphasis is placed on the systems with delayed coherent quantum feedback. Specifically, we

show that the N-photon scattering matrices in single-qubit waveguide QED systems, within the rotating wave approximation, admit for a parametrization in terms of $(N-1)$-photon effective vertex functions and provide a detailed derivation of a closed hierarchy of generalized Bethe-Salpeter equations satisfied by these vertex functions. (???? про Бете-Солпитера отдельный разговор, я в этом не разбираюсь, пока считаю, что нет, это ложь, тут нет этого уравнения, оно о чем-то другом.)

The advantage of this method is that the above-mentioned integral equations hold independently of the number of radiation channels, their bandwidth, the dispersion of the modes they are supporting, and the structure of the radiation-qubit coupling interaction, thus enabling one to study multiphoton scattering problems beyond the Born-Markov approximation. Further, we generalize the diagrammatic techniques to the systems containing more than a single emitter by presenting an exact set of equations governing the generic two- and three-photon scattering operators. The above-described theoretical machinery is then showcased on the example of a three-photon scattering on a giant acoustic atom, recently studied experimentally [G. Andersson et al., Nat.

Обзор диаграммных техник

один большой раздел

такой-то набор следствий

Связи с другими науками

Обсудим связи с разделами
(потом раскрою)

Обзор дальнейших развитий

Обзор теоретических подходов

такие-то есть, такие полезные, такие - нет.

Описание записи

Общее описание записи

Общие особенности записи

Особенности глав и разделов

Первая часть про предмет в двух словах

Вторая часть

Часть про приложения

какие вообще приложения я разбирал?

Обозначения и константы

A.0.5 Головоломки

Обсудим в порядке интересности задачки и вопросы

Бытовые головоломки

Принципиальные головоломки

Головоломки о деталях

A.0.6 Короткий исторический обзор

Обсудим вкратце историю развития электродинамики волноводов.

A.1 Mathematics for Waveguide QED

On Poincare-Bertrand identity

B Bibliography

References

B.1 From Main Most Useful Articles

From PP21

References

[1] K. Lalumiere, B. C. Sanders, A. F. V. Loo, A. Fedorov, A. Wallraff, and A. Blais, "Input-output theory for waveguide QED with an ensemble of inhomogeneous atoms", Phys. Rev. A **88**, 043806 (2013).

[2] M. Arcari, I. Söllner, A. Javadi, S. Lindskov Hansen, S. Mahmoodian, J. Liu, H. Thyrrestrup, E. H. Lee, J. D. Song, S. Stobbe, and P. Lodahl, "Near-Unity Coupling Efficiency of a Quantum Emitter to a Photonic Crystal Waveguide", Phys. Rev. Lett. **113**, 093603 (2014).

[3] D. G. Angelakis, M. F. Santos, V. Yannopapas, and A. Ekert, "A proposal for the implementation of quantum gates with photonic-crystal waveguides", Phys. Lett. A **362**, 377 (2007).

[4] V. Paulisch, H. J. Kimble, and A. Gonzalez-Tudela, "Universal quantum computation in waveguide QED using decoherence free subspaces", New J. Phys. **18**, 043041 (2016).

[5] B. Vermersch, P.-O. Guimond, H. Pichler, and P. Zoller, "Quantum State Transfer via Noisy Photonic and Phononic Waveguides", Phys. Rev. Lett. **118**, 133601 (2017).

[6] S. Xu and S. Fan, "Generate tensor network state by sequential single-photon scattering in waveguide QED systems", APL Photonics **3**, 116102 (2018).

[7] H. Zheng, D. J. Gauthier, and H. U. Baranger, "Waveguide-QED-Based Photonic Quantum Computation", Phys. Rev. Lett. **111**, 090502 (2013).

[8] A. F. Kockum, G. Johansson, and F. Nori, "Decoherence-Free Interaction between Giant Atoms in Waveguide Quantum Electrodynamics", Phys. Rev. Lett. **120**, 140404 (2018).

[9] H. J. Kimble, "The quantum internet", Nature **453**, 1023 (2008).

[10] J. Kimble, "Atom-Light Interactions in Photonic Crystals", Frontiers in Optics 2014 (OSA Publishing, Tucson, 2014).

[11] R. Mitsch, C. Sayrin, B. Albrecht, P. Schneeweiss, and A. Rauschenbeutel, "Quantum state-controlled directional spontaneous emission of photons into a nanophotonic waveguide", Nat. Commun. **5**, 5713 (2014).

[12] A. Sipahigil, "An Integrated Diamond Nanophotonics Platform for Quantum Optical Networks", Conference on Lasers and Electro-Optics (OSA Publishing, San Jose, 2017).

[13] O. Astafiev, A. M. Zagoskin, A. A. Abdumalikov, Y. A. Pashkin, T. Yamamoto, K. Inomata, Y. Nakamura, and J. S. Tsai, "Resonance Fluorescence of a Single Artificial Atom", Science **327**, 840 (2010).

[14] I. C. Hoi, A. F. Kockum, L. Tornberg, A. Pourkabirian, G. Johansson, P. Delsing, and C. M. Wilson, "Probing the quantum vacuum with an artificial atom in front of a mirror", Nat. Phys. **11**, 1045 (2015).

[15] A. F. V. Loo, A. Fedorov, K. Lalumiere, B. C. Sanders, A. Blais, and A. Wallraff, "Photon-Mediated Interactions Between Distant Artificial Atoms", Science **342**, 1494 (2013).

[16] Y. Chu, P. Kharel, W. H. Renninger, L. D. Burkhart, L. Frunzio, P. T. Rakich, and R. J. Schoelkopf, "Quantum acoustics with superconducting qubits", Science **358**, 199 (2017).

[17] M. V. Gustafsson, T. Aref, A. F. Kockum, M. K. Ekstrom, G. Johansson, and P. Delsing, "Propagating phonons coupled to an artificial atom ", Science **346**, 207 (2014).

[18] R. Manenti, A. F. Kockum, A. Patterson, T. Behrle, J. Rahamim, G. Tancredi, F. Nori, and P. J. Leek, "Circuit quantum acoustodynamics with surface acoustic waves", Nat. Commun. **8**, 975 (2017).

[19] G. Andersson, B. Suri, L. Guo, T. Aref, and P. Delsing, "Non-exponential decay of a giant artificial atom", Nat. Phys. **15**, 1123 (2019).

[20] A. V. Akimov, A. Mukherjee, C. L. Yu, D. E. Chang, A. S. Zibrov, P. R. Hemmer, H. Park, and M. D. Lukin, "Generation of single optical plasmons in metallic nanowires coupled to quantum dots", Nature **450**, 402 (2007).

[21] P.O. Guimond, M. Pletyukhov, H. Pichler, and P. Zoller, "Delayed coherent quantum feedback from a scattering theory and a matrix product state perspective", Quantum Sci. Technol. **2**, 044012 (2017).

[22] R. H. Lehmberg, "Radiation from an N-Atom System. I. General Formalism", Phys. Rev. A **2**, 883 (1970).

[23] R. H. Lehmberg, "Radiation from an N-Atom System. II. Spontaneous Emission from a Pair of Atoms", Phys. Rev. A **2**, 889 (1970).

[24] J. You, Z. Liao, S. -W. Li, and M. S. Zubairy, "Waveguide quantum electrodynamics in squeezed vacuum", Phys. Rev. A **97**, 023810 (2018).

[25] I. M. Mirza and J. C. Schotland "Multiqubit entanglement in bidirectional-chiral-waveguide QED", Phys. Rev. A **94**, 012302 (2016)

[26] P.-B. Li, Y. Gu, Q.-H. Gong, and G.-C. Guo, "Quantum-information transfer in a coupled resonator waveguide", Phys. Rev. A **79**, 042339 (2009).

[27] K.-T. Lin, T. Hsu, C.-Y. Lee, I.-C. Hoi, and G.-D. Lin, "Scalable collective Lamb shift of a 1D superconducting qubit array in front of a mirror", Sci. Rep. **9**, 19175 (2019).

[28] S. Fan, S. E. Kocabas, and J.-T. Shen, "Input-output formalism for few-photon transport in one-dimensional nanophotonic waveguides coupled to a qubit", Phys. Rev. A **82**, 063821 (2010).

[29] S. Xu and S. Fan, "Input-output formalism for few-photon transport: a systematic treatment beyond two photons", Phys. Rev. A **91**, 043845 (2015).

[30] T. Shi, D. E. Chang, and J. I. Cirac, "Multiphoton-scattering theory and generalized master equations", Phys. Rev. A **92**, 053834 (2015).

[31] J. Combes, J. Kerckhoff , and M. Sarovar, "The SLH framework for modeling quantum input-output networks", Advances in Physics X **2**, 784 (2017).

[32] M. Pletyukhov, K. G. L. Pedersen, and V. Gritsev, "Control over few-photon pulses by a time-periodic modulation of the photon emitter coupling", Phys. Rev. A **95**, 043814 (2017).

[33] Z. Liao, Y. Lu, and M. S. Zubairy, "Multiphoton pulses interacting with multiple emitters in a one-dimensional waveguide", Phys. Rev. A **102**, 053702 (2020).

[34] Y. Shen, and J.-T. Shen, "Photonic-Fock-state scattering in a waveguide-QED system and their correlation functions", Phys. Rev. A **92**, 033803 (2015).

[35] V. I. Yudson and P. Reineker, "Multiphoton scattering in a one-dimensional waveguide with resonant atoms", Phys. Rev. A **78**, 052713 (2008).

[36] V. Yudson, "Dynamics of the integrable one-dimensional system: photons + two-level atoms", Phys. Lett. A **129**, 17 (1988).

[37] J. T. Shen and S. Fan, "Coherent photon transport from spontaneous emission in one-dimensional waveguides", Opt. Lett. **30**, 2001 (2005).

[38] T. S. Tsoi and C. K. Law, "Quantum interference effects of a single photon interacting with an atomic chain inside a one-dimensional waveguide", Phys. Rev. A **78**, 063832 (2008).

[39] M. T. Cheng, J. Xu, and G. S. Agarwal, "Waveguide transport mediated by strong coupling with atoms", Phys. Rev. A **95**, 053807 (2017).

[40] Z. Liao, X. Zeng, H. Nha, and M. S. Zubairy, "Photon transport in a one-dimensional nanophotonic waveguide QED system", Phys. Scr. **91**, 063004 (2016).

[41] H. Zheng, D. J. Gauthier, and H. U. Baranger, "Waveguide QED: Many-body bound-state effects in coherent and Fock-state scattering from a two-level system", Phys. Rev. A **82**, 063816 (2010).

[42] Y. Chen, M. Wubs, J. Mørk, and A. F. Koenderink, "Coherent single-photon absorption by single emitters coupled to one-dimensional nanophotonic waveguides", New J. Phys. **13**, 103010 (2011).

[43] F. Dinc, I. Ercan, and A. M. Branczyk, "Exact Markovian and non-Markovian time dynamics in waveguide QED: collective interactions, bound states in continuum, superradiance and subradiance", Quantum **3**, 213 (2019).

[44] P. Facchi, M. S. Kim, S. Pascazio, F. V. Pepe, D. Pomarico, and T. Tufarelli, "Bound states and entanglement generation in waveguide quantum electrodynamics", Phys. Rev. A **94**, 043839 (2016).

[45] G. Calajo, Y.-L. L. Fang, H. U. Baranger, and F. Ciccarello, "Exciting a bound state in the continuum through multiphoton scattering plus delayed quantum feedback", Phys. Rev. Lett. **122**, 073601 (2019).

[46] Y.-L. L. Fang, H. Zheng, and H. U. Baranger, "One-dimensional waveguide coupled to multiple qubits: photon-photon correlations", EPJ Quantum Technol. **1**, 3 (2014).

[47] Y.-L. L. Fang and H. U. Baranger, "Multiple emitters in a waveguide: non-reciprocity and correlated photons at perfect elastic transmission", Phys. Rev. A **96**, 013842 (2017).

[48] T. Shi and C. P. Sun, "Lehmann-Symanzik-Zimmermann reduction approach to multiphoton scattering in coupled-resonator arrays", Phys. Rev. B **79**, 205111 (2009).

[49] T. Shi, S. Fan, and C. P. Sun, Two-photon transport in a waveguide coupled to a cavity in a two-level system, Phys. Rev. A **84**, 063803 (2011).

[50] T. Shi and S. Fan, "Two-photon transport through a waveguide coupling to a whispering-gallery resonator containing an atom and photon-blockade effect", Phys. Rev. A **87**, 063818 (2013).

[51] M. Pletyukhov and V. Gritsev, "Scattering of massless particles in one-dimensional chiral channel", New J. Phys. **14**, 095028 (2012).

[52] M. Pletyukhov and V. Gritsev, "Quantum theory of light scattering in a one-dimensional channel: Interaction effect on photon statistics and entanglement entropy", Phys. Rev. A **91**, 063841 (2015).

[53] K. G. L. Pedersen and M. Pletyukhov, "Few-photon scattering on Bose-Hubbard lattices", Phys. Rev. A **96**, 023815 (2017).

[54] T. F. See, C. Noh, and D. G. Angelakis, "Diagrammatic approach to multiphoton scattering", Phys. Rev. A **95**, 053845 (2017).

[55] A. Rivas, S. F. Huelga, and M. B. Plenio, "Quantum non-Markovianity: characterization, quantification and detection", Rep. Prog. Phys. **77**, 094001 (2014).

[56] H. P. Breuer, E. M. Laine, J. Piilo, and B. Vacchini, "Colloquium: Non-Markovian dynamics in open quantum systems", Rev. Mod.Phys. **88**, 021002 (2016).

[57] K. Sinha, P. Meystre, E. A. Goldschmidt, F. K. Fatemi, S. L. Rolston, and P. Solano, "Non-Markovian Collective Emission from Macroscopically Separated Emitters", Phys. Rev. Lett. **124**, 043603 (2020).

[58] K. Sinha, A. González-Tudela, Y. Lu, and P. Solano, "Collective radiation from distant emitters", Phys. Rev. A, **102**, 043718 (2020).

[59] L. Guo, A. Grimsmo, A. F. Kockum, M. Pletyukhov, and G. Johansson, "Giant acoustic atom: A single quantum system with a deterministic time delay", Phys. Rev. A **95**, 053821 (2017).

[60] L. Guo, A. F. Kockum, F. Marquardt, and G. Johansson, "Oscillating bound states for a giant atom", Phys. Rev. Research **2**, 043014 (2020).

[61] F. Dinc, "Diagrammatic approach for analytical non-Markovian time evolution: Fermi's two-atom problem and causality in waveguide quantum electrodynamics", Phys. Rev. A **102**, 013727 (2020).

[62] U. Dorner and P. Zoller, "Laser-driven atoms in half-cavities", Phys. Rev. A **66**, 023816 (2002).

[63] E. S. Redchenko and V. I. Yudson, "Decay of metastable excited states of two qubits in a waveguide", Phys. Rev. A **90**, 063829 (2014).

[64] A. L. Grimsmo, "Time-Delayed Quantum Feedback Control", Phys. Rev. Lett. 115, 060402 (2015).

[65] H. Pichler and P. Zoller, "Photonic Circuits with Time Delays and Quantum Feedback", Phys. Rev. Lett. **116**, 093601 (2016).

[66] R. Finsterhölzl, M. Katzer, A. Knorr, and A. Carmele, "Using Matrix-Product States for Open Quantum Many-Body Systems: Efficient Algorithms for Markovian and Non-Markovian Time-Evolution", Entropy 22, **9**, 984 (2020).

[67] Z. Wang and A. H. Safavi-Naeini, "Enhancing a slow and weak optomechanical nonlinearity with delayed quantum feedback", Nat. Commun. **8**, 15886 (2017).

[68] X.-Y. Chen, W.-Z. Zhang, and C. Li, "Non-Markovian Master Equation for Distant Resonators Embedded in a One-Dimensional Waveguide", Commun. Theor. Phys. **70** 273 (2018).

[69] M.-H. Wu, C. U. Lei, W.-M. Zhang, and H.-N. Xiong, "Non-Markovian dynamics of a microcavity coupled to a waveguide in photonic crystals", Optics Express **18**, 18407 (2010).

[70] H.-T. Tan and W.-M. Zhang, "Non-Markovian dynamics of an open quantum system with initial system-reservoir correlations: A nanocavity coupled to a coupled-resonator optical waveguide", Phys. Rev. A **83**, 032102 (2011).

[71] M. Laakso and M. Pletyukhov, "Scattering of Two Photons from Two Distant Qubits: Exact Solution", Phys. Rev. Lett. **113**, 183601 (2014).

[72] S. E. Kocabas, "Effects of modal dispersion on few-photon–qubit scattering in one-dimensional waveguides", Phys. Rev. A **93**, 033829 (2016).

[73] L. Mandel and E.Wolf, "Optical Coherence and Quantum Optics" (Cambridge University Press, Cambridge, 2013).

[74] K. Piasotski and M. Pletyukhov, unpublished.

[75] R. Trivedi, K. Fischer, S. Xu, S. Fan, and J. Vuckovic, "Few-photon scattering and emission from low-dimensional quantum systems", Phys. Rev. B **98**, 144112 (2018).

[76] S. Xu and S. Fan, "Generalized cluster decomposition principle illustrated in waveguide quantum electrodynamics", Phys. Rev. A **95**, 063809 (2017).

[77] E. Sanchez-Burillo, A. Cadarso, L. Martin-Moreno, J. J. Garcia-Ripoll, and D. Zueco, "Emergent causality and the N-photon scattering matrix in waveguide QED", New J. Phys. **20**, 013017 (2018).

[78] A. F. Kockum, P. Delsing, and G. Johansson, "Designing frequency-dependent relaxation rates and Lamb shifts for a giant artificial atom", Phys. Rev. A **90**, 013837 (2014).

[79] A. M. Vadiraj et al, "Engineering the Level Structure of a Giant Artificial Atom in Waveguide Quantum Electrodynamics", arXiv:2003.14167 (2020).

[80] B. Kannan et al, "Waveguide Quantum Electrodynamics with Giant Superconducting Artificial Atoms", Nature **583**, 775 (2020).

[81] D. Cilluffo, A. Carollo, S. Lorenzo, J. A. Gross, G. M. Palma, and F. Ciccarello, "Collisional picture of quantum optics with giant emitters", Phys. Rev. Research **2**, 043070 (2020).

[82] A. F. Kockum (2021) "Quantum Optics with Giant Atoms—the First Five Years." In: "International Symposium on Mathematics, Quantum Theory, and Cryptography. Mathematics for Industry, vol 33" (Springer, Singapore, 2020).

[83] R. J. Glauber, "The Quantum Theory of Optical Coherence", Phys. Rev. **130**, 2529 (1963).

[84] B. R. Mollow, "Power Spectrum of Light Scattered by Two-Level Systems", Phys. Rev. **188**, 1969 (1969).

[85] D. E. Chang, L. Jiang, A. V. Gorshkov, and H. J. Kimble, "Cavity QED with atomic mirrors", New J. Phys. **14**, 063003 (2012).

[86] P. O. Guimond, A. Roulet, H. N. Le, and V. Scarani, "Rabi oscillation in a quantum cavity: Markovian and non-Markovian dynamics", Phys. Rev. A **93**, 023808 (2016).

[87] H. J. Kimble and L. Mandel, "Theory of resonance fluorescence", Phys. Rev. A **13**, 2123 (1976).

From Scattering of massless particles in one-dimensional chiral channel

References

[1] I. Schuster et al, Nature Physics **4**, 382 (2008); B. Dayan et al, Science **319**, 1062 (2008); J. M. Fink et al, Nature **454**, 315 (2008); I.-C. Hoi et al, Phys. Rev. Lett. **107**, 073601 (2011); J. Hwang et al., Nature **460**, 76 (2009); A. Reinhard et al., arXiv 1108.3053v1 (2011); H. Tanji-Suzuki, W. Chen, R. Landig, J. Simon, and V. Vuletic, Science **333**, 1266-1269 (2011).

[2] K. P. Nayak, K. Hakuta, New J. Phys. **10**, 053003 (2008); K. P. Nayak, Fam Le Kien, M. Morinaga, and K. Hakuta, Phys. Rev. A **79**, 021801(R) (2009); G. Brambilla, J. Opt. **12** 043001 (2010); Fam Le Kien, S. Dutta Gupta, K. P. Nayak, and K. Hakuta, Phys. Rev. A **72**, 063815 (2005); G. Sague, E. Vetsch, W. Alt, D. Meschede, and A. Rauschenbeutel, Phys. Rev. Lett. **99**, 163602 (2007); Fam Le Kien, V. I. Balykin, and K. Hakuta, Phys. Rev. A **70**, 063403 (2004); V. I. Balykin, K. Hakuta, Fam Le Kien, J. Q. Liang, and M. Morinaga, Phys. Rev. A **70**, 011401(R) (2004). K. P. Nayak, P. N. Melentiev, M. Morinaga, Fam Le Kien, V. I. Balykin, and K. Hakuta, http://arxiv.org/abs/quant-ph/0610136v1.

[3] M. Bajcsy et al, Phys. Rev. Lett. 102, 203902 (2009).

[4] T. van der Sar et al, App. Phys. Lett. **98**, 193103 (2011).

[5] J. Q. You and F. Nori, Nature **474**, 589 (2011).

[6] A. Akimov et al, Nature **450**, 402 (1997).

[7] V. I. Rupasov, JETP Lett. **36**, 142 (1982); V. I Rupasov and V. I Yudson, Sov. Phys. JETP **59**, 478 (1984); V. I. Yudson, Sov. Phys. JETP **61**, 1043 (1985).

[8] V. I. Rupasov and V. I. Yudson, Preprint No. 26 of the Institute of Spectroscopy of the USSR, (1987).

[9] V. I. Yudson, Phys. Lett. A **129**, 17 (1988).

[10] A. LeClair, Phys.Rev. A **56**, 782 (1997); A. Leclair, F. Lesage, S. Lukyanov, and H. Saleur, Phys. Lett. A **235**, 203 (1997); R. Konik and A. LeClair, Phys. Rev. B **58** 1872 (1998); A. LeClair, Ann. Phys. **271**, 268 (1999); Z. S. Bassi and A. LeClair, J. Math. Phys. **40** 3723 (1999).

[11] H. F. Hofmann, K. Kojima, S. Takeuchi, and K. Sasaki, Phys. Rev. A **68**, 013803 (2003); quant-ph/0301146; J. T. Shen and S. Fan, Opt. Lett. **30**, 2001 (2005); J. T. Shen and S. Fan, Phys. Rev. Lett. 95, 213001 (2005); J. T. Shen and S. Fan, Phys. Rev. A **76**, 062709 (2007).

[12] T. S. Tsoi and C. K. Law, Phys. Rev. A **80**, 033823 (2009); D. Witthaut and A. S. Sorensen, New J. Phys. **12**, 043052 (2010).

[13] D. Roy, Phys. Rev. Lett. **106**, 053601 (2011).

[14] T. Shi and C. P. Sun, Phys. Rev. B **79**, 205111 (2009).

[15] P. Longo, P. Schmitteckert, and K. Busch, J. Opt. A: Pure Appl. Opt. **11**, 114009 (2009); Phys. Rev. Lett. **104**, 023602 (2010).

[16] V. I. Yudson and P. Reineker, Phys. Rev. A **78**, 052713 (2008); Optics and Spectroscopy, **108**, 362 (2010).

[17] B. R. Mollow, Phys. Rev. **188**, 1969 (1969).

[18] M. Pletyukhov, M. Ringel, V. Yudson, and V. Gritsev, to appear.

[19] M. Girardeau, J. Math. Phys. **1**, 516 (1960); L. Tonks, Phys. Rev. **50**, 955 (1936).

[20] D. E. Chang, V. Gritsev, G. Morigi, V. Vuletic, M.D. Lukin, and E.A. Demler, Nature Physics **4**, 884 (2008).

References from The gaint acoustic atom

References

[1] A. Blais, R.-S. Huang, A. Wallraff, S. M. Girvin, and R. J. Schoelkopf, "Cavity quantum electrodynamics for superconducting electrical circuits: An architecture for quantum computation," Physical Review A **69**, 062320 (2004), arXiv:0402216 [cond-mat] .

[2] M. H. Devoret and R. J. Schoelkopf, "Superconducting Circuits for Quantum Information: An Outlook," Science **339**, 1169 (2013).

[3] H. J. Kimble, "The quantum internet," Nature **453**, 1023 (2008), arXiv:0806.4195 .

[4] T. D. Ladd, F. Jelezko, R. Laflamme, Y. Nakamura, C. Monroe, and J. L. O'Brien, "Quantum computers," Nature **464**, 45 (2010), arXiv:1009.2267 .

[5] T. A. Palomaki, J. W. Harlow, J. D. Teufel, R. W. Simmonds, and K. W. Lehnert, "Coherent state transfer between itinerant microwave fields and a mechanical oscillator," Nature **495**, 210 (2013), arXiv:1206.5562 .

[6] R. W. Andrews, R. W. Peterson, T. P. Purdy, K. Cicak, R. W. Simmonds, C. A. Regal, and K. W. Lehnert, "Bidirectional and efficient conversion between microwave and optical light," Nature Physics **10**, 321 (2014), arXiv:1310.5276 .

[7] J. Bochmann, A. Vainsencher, D. D. Awschalom, and A. N. Cleland, "Nanomechanical coupling between microwave and optical photons," Nature Physics **9**, 712 (2013).

[7] M. Hafezi, Z. Kim, S. L. Rolston, L. A. Orozco, B. L. Lev, and J. M. Taylor, "Atomic interface between microwave and optical photons," Physical Review A **85**, 020302 (2012), arXiv:1110.3537 .

[9] R. Hisatomi, A. Osada, Y. Tabuchi, T. Ishikawa, A. Noguchi, R. Yamazaki, K. Usami, and Y. Nakamura, "Bidirectional conversion between microwave and light via ferromagnetic magnons," Physical Review B **93**, 174427 (2016), arXiv:1601.03908 .

[10] V. S. Shumeiko, "Quantum acousto-optic transducer for superconducting qubits," Physical Review A **93**, 023838 (2016), arXiv:1511.03819 .

[16] M. V. Gustafsson, T. Aref, A. F. Kockum, M. K. Ekström, G. Johansson, and P. Delsing, "Propagating phonons coupled to an artificial atom," Science **346**, 207 (2014), arXiv:1404.0401 .

[12] T. Aref, P. Delsing, M. K. Ekström, A. F. Kockum, M. V. Gustafsson, G. Johansson, P. J. Leek, E. Magnusson, and R. Manenti, "Quantum Acoustics with Surface Acoustic Waves," in *Superconducting Devices in Quantum Optics*, edited by R. H. Hadfield and G. Johansson (Springer, 2016) arXiv:1506.01631 .

[13] S. Datta, *Surface Acoustic Wave Devices* (Prentice Hall, 1986).

[14] D. Morgan, *Surface Acoustic Wave Filters*, 2nd ed. (Academic Press, 2007).

[17] R. Manenti, A. F. Kockum, A. Patterson, T. Behrle, J. Rahamim, G. Tancredi, F. Nori, and P. J. Leek, "Circuit quantum acoustodynamics with surface acoustic waves," arXiv:1703.04495 (2017).

[16] C. W. Gardiner, "Driving a quantum system with the output field from another driven quantum system," Physical Review Letters **70**, 2269 (1993).

[17] H. J. Carmichael, "Quantum trajectory theory for cascaded open systems," Physical Review Letters **70**, 2273 (1993).

[18] C. W. Gardiner and P. Zoller, *Quantum Noise*, 3rd ed. (Springer, 2004).

[19] J. Gough and M. R. James, "Quantum Feedback Networks: Hamiltonian Formulation," Communications in Mathematical Physics **287**, 1109 (2009), arXiv:0804.3442 .

[20] J. Gough and M. R. James, "The Series Product and Its Application to Quantum Feedforward and Feedback Networks," IEEE Transactions on Automatic Control **54**, 2530 (2009), arXiv:0707.0048 .

[21] J. Kerckhoff and K. W. Lehnert, "Superconducting Microwave Multivibrator Produced by Coherent Feedback," Physical Review Letters **109**, 153602 (2012), arXiv:1204.0024 .

[24] A. F. Kockum, P. Delsing, and G. Johansson, "Designing frequency-dependent relaxation rates and Lamb shifts for a giant artificial atom," Physical Review A **90**, 013837 (2014), arXiv:1406.0350 .

[23] U. Dorner and P. Zoller, "Laser-driven atoms in half-cavities," Physical Review A **66**, 023816 (2002).

[24] T. Tufarelli, F. Ciccarello, and M. S. Kim, "Dynamics of spontaneous emission in a single-end photonic waveguide," Physical Review A **87**, 013820 (2013), arXiv:1208.0969 .

[27] M. Laakso and M. Pletyukhov, "Scattering of Two Photons from Two Distant Qubits: Exact Solution," Physical Review Letters **113**, 183601 (2014), arXiv:1406.1664 .

[26] A. L. Grimsmo, "Time-Delayed Quantum Feedback Control," Physical Review Letters **115**, 060402 (2015), arXiv:1502.06959 .

[27] Y.-L. L. Fang and H. U. Baranger, "Waveguide QED: Power spectra and correlations of two photons scattered off multiple distant qubits and a mirror," Physical Review A **91**, 053845 (2015), arXiv:1502.03803 .

[26] H. Pichler and P. Zoller, "Photonic Circuits with Time Delays and Quantum Feedback," Physical Review Letters **116**, 093601 (2016), arXiv:1510.04646 .

[29] T. Ramos, B. Vermersch, P. Hauke, H. Pichler, and P. Zoller, "Non-Markovian dynamics in chiral quantum networks with spins and photons," Physical Review A **93**, 062104 (2016), arXiv:1602.00926 .

[15] J. Koch, T. M. Yu, J. Gambetta, A. A. Houck, D. I. Schuster, J. Majer, A. Blais, M. H. Devoret, S. M. Girvin, and R. J. Schoelkopf, "Charge-insensitive qubit design derived from the Cooper pair box," Physical Review A **76**, 042319 (2007), arXiv:0703002 [cond-mat] .

[31] Pierre-Olivier Guimond, Alexandre Roulet, Huy Nguyen Le, and Valerio Scarani, "Rabi oscillation in a quantum cavity: Markovian and non-Markovian dynamics," Physical Review A **93**, 023808 (2016).

[32] P. W. Milonni and P. L. Knight, "Retardation in the resonant interaction of two identical atoms," Physical Review A **10**, 1096 (1974).

[33] S. Rist, J. Eschner, M. Hennrich, and G. Morigi, "Photon-mediated interaction between two distant atoms," Physical Review A **78**, 013808 (2008), arXiv:0805.0655 .

[8] A. F. van Loo, A. Fedorov, K. Lalumiere, B. C. Sanders, A. Blais, and A. Wallraff, "Photon-Mediated Interactions Between Distant Artificial Atoms," Science **342**, 1494 (2013), arXiv:1407.6747 .

[19] Y.-L. L. Fang, H. Zheng, and H. U. Baranger, "One-dimensional waveguide coupled to multiple qubits: photon-photon correlations," EPJ Quantum Technology **1**, 3 (2014), arXiv:1308.6551 .

[36] D. E. Chang, L. Jiang, A. V. Gorshkov, and H. J. Kimble, "Cavity QED with atomic mirrors," New Journal of Physics **14**, 063003 (2012), arXiv:1201.0643 .

[37] F. Fratini, E. Mascarenhas, L. Safari, J.-P. Poizat, D. Valente, A. Auffèves, D. Gerace, and M. F. Santos, "Fabry-Perot Interferometer with Quantum Mirrors: Nonlinear Light Transport and Rectification," Physical Review Letters **113**, 243601 (2014), arXiv:1410.5972 .

[38] B. Peropadre, G. Romero, G. Johansson, C. M. Wilson, E. Solano, and J. J. García-Ripoll, "Approaching perfect microwave photodetection in circuit QED," Physical Review A **84**, 063834 (2011), arXiv:1101.0016 .

[39] R. M. Corless, G. H. Gonnet, D. E. G. Hare, D. J. Jeffrey, and D. E. Knuth, "On the Lambert W function," Advances in Computational Mathematics **5**, 329 (1996).

[40] H. J. Carmichael, *Statistical Methods in Quantum Optics 2* (Springer-Verlag Berlin Heidelberg, 2008).

[41] Marlan O. Scully and M. Suhail Zubairy, *Quantum Optics, p.321*, 1st ed. (Cambridge University Press, 1997).

[42] Scott Millers and Donald Childers, *Probability and Random Processes, p.373*, 2nd ed. (Academic Press, 2012).

[43] Jean-Michel Gèrard Alexia Aufféves, Benjamin Besga and Jean-Philippe Poizat, "Spontaneous emission spectrum of a two-level atom in a very-high-Q cavity," Physical Review A **77**, 063833 (2008).

[44] R. H. Lehmberg, "Radiation from an N-Atom System. II. Spontaneous Emission from a Pair of Atoms," Physical Review A **2**, 889 (1970).

[45] K. Stannigel, P. Rabl, and P. Zoller, "Driven-dissipative preparation of entangled states in cascaded quantum-optical networks," New Journal of Physics **14**, 063014 (2012), arXiv:1112.1690 .

[46] K. Lalumière, B. C. Sanders, A. F. van Loo, A. Fedorov, A. Wallraff, and A. Blais, "Input-output theory for waveguide QED with an ensemble of inhomogeneous atoms," Physical Review A **88**, 043806 (2013), arXiv:1305.7135 .

[47] H. Pichler, T. Ramos, A. J. Daley, and P. Zoller, "Quantum Optics of Chiral Spin Networks," Physical Review A **91**, 042116 (2015), arXiv:1411.2963 .

[43] O. Astafiev, A. M. Zagoskin, A. A. Abdumalikov Jr., Yu. A. Pashkin, T. Yamamoto, K. Inomata, Y. Nakamura, and J. S. Tsai, "Resonance Fluorescence of a Single Artificial Atom," Science **327**, 840–843 (2010).

[16] J.-T. Shen and S. Fan, "Strongly Correlated Two-Photon Transport in a One-Dimensional Waveguide Coupled to a Two-Level System," Physical Review Letters **98**, 153003 (2007), arXiv:0701170 [quant-ph] .

[6] D. E. Chang, A. S. Sørensen, E. A. Demler, and M. D. Lukin, "A single-photon transistor using nanoscale surface plasmons," Nature Physics **3**, 807 (2007), arXiv:0706.4335 .

[51] I.-C. Hoi, T. Palomaki, J. Lindkvist, G. Johansson, P. Delsing, and C. M. Wilson, "Generation of Nonclassical Microwave States Using an Artificial Atom in 1D Open Space," Physical Review Letters **108**, 263601 (2012), arXiv:1201.2269 .

[52] B. R. Mollow, "Power Spectrum of Light Scattered by Two-Level Systems," Physical Review **188** (1969), 10.1103/PhysRev.188.1969.

[53] D. F. Walls and G. J. Milburn, *Quantum Optics*, 2nd ed. (Springer-Verlag Berlin Heidelberg, 2008).

[54] T. D. Frank, "Multivariate Markov processes for stochastic systems with delays: Application to the stochastic Gompertz model with delay," Physical Review E **66**, 011914 (2002).

[55] S. Whalen, A. L. Grimsmo, and H. J. Carmichael, "in preparation," (2016).

[56] J. R. Johansson, P. D. Nation, and F. Nori, "QuTiP: An open-source Python framework for the dynamics of open quantum systems," Computer Physics Communications **183**, 1760 (2012), arXiv:1110.0573 .

[57] J. R. Johansson, P. D. Nation, and F. Nori, "QuTiP 2: A Python framework for the dynamics of open quantum systems," Computer Physics Communications **184**, 1234 (2013), arXiv:1211.6518 .

[58] Maria K. Ekström, Thomas Aref, Johan Runeson, Johan Björck, Isac Boström, and Per Delsing, "Surface acoustic wave unidirectional transducers for quantum applications," arXiv:1611.06018 (2016).

[59] M. J. Collett and C. W. Gardiner, "Squeezing of intracavity and traveling-wave light fields produced in parametric amplification," Physical Review A **30**, 1386 (1984).

References from delayed coherent feedback

References

[1] Mitsch R, Sayrin C, Albrecht B, Schneeweiss P and Rauschenbeutel A 2014 *Nature Communications* **5** 5713

[2] Tiecke T G, Thompson J D, de Leon N P, Liu L R, Vuletic V and Lukin M 2014 *Nature* **508** 241–244

[3] Goban A, Hung C L, Yu S P, Hood J D, Muniz J A, Lee J H, Martin M J, McClung A C, Choi K S, Chang D E, Painter O and Kimble H J 2014 *Nature Communications* **5** 3808

[4] Sipahigil A, Evans R E, Sukachev D D, Burek M J, Borregaard J, Bhaskar M K, Nguyen C T, Pacheco J L, Atikian H A, Meuwly C, Camacho R M, Jelezko F, Bielejec E, Park H, Loncar M and Lukin M 2016 *Science* **354** 847–850

[5] Söllner I, Mahmoodian S, Hansen S L, Midolo L, Javadi A, Kiršansk . e G, Pregnolato T, El-Ella H, Lee E H, Song J D, Stobbe S and Lodahl P 2015 *Nature Nanotechnology* **10** 775–778

[6] Lodahl P, Mahmoodian S and Stobbe S 2015 *Reviews of Modern Physics* **87** 347–400

[7] van Loo A F, Fedorov A, Lalumiere K, Sanders B C, Blais A and Wallraff A 2013 *Science* **342** 1494–1496

[8] Hoi I C, Kockum A F, Tornberg L, Pourkabirian A, Johansson G, Delsing P and Wilson C M 2015 *Nature Physics* **11** 1045–1049

[9] Guo L, Grimsmo A, Kockum A F, Pletyukhov M and Johansson G 2017 *Phys. Rev. A* **95**(5) 053821

[10] Ramos T, Pichler H, Daley A J and Zoller P 2014 *Physical Review Letters* **113** 237203

[11] Rivas Á, Huelga S F and Plenio M B 2014 *Reports on Progress in Physics* **77** 094001

[12] Breuer H P, Laine E M, Piilo J and Vacchini B 2016 *Reviews of Modern Physics* **88** 021002

[13] Gardiner C W and Zoller P *Quantum Noise* 3rd ed (Berlin Heidelberg (2004): Springer)

[14] Dorner U and Zoller P 2002 *Physical Review A* **66** 023816

[15] Grimsmo A L 2015 *Physical Review Letters* **115** 060402

[16] Pichler H and Zoller P 2016 *Physical Review Letters* **116** 093601

[17] Zheng H and Baranger H U 2013 *Physical Review Letters* **110** 113601

[18] Laakso M and Pletyukhov M 2014 *Physical Review Letters* **113** 183601

[19] Fang Y L L and Baranger H U 2015 *Physical Review A* **91** 053845

[20] Díaz-Camacho G, Porras D and García-Ripoll J J 2015 *Physical Review A*

[21] Ramos T, Vermersch B, Hauke P, Pichler H and Zoller P 2016 *Physical Review A* **93** 062104

[22] Pichler H, Choi S, Zoller P and Lukin M D 2017 *arXiv.org* (*Preprint* 1702.02119v1)

[23] Shen J T and Fan S 2007 *Physical Review Letters* **98** 153003

[24] Shi T and Sun C P 2009 *Physical Review B* **79** 205111

[25] Pletyukhov M and Gritsev V 2012 *New Journal of Physics* **14** 095028

[26] Shi T, Chang D E and Cirac J I 2015 *Physical Review A* **92** 053834

[27] Guimond P O, Pichler H, Rauschenbeutel A and Zoller P 2016 *Physical Review A* **94** 033829

[28] Vidal G 2003 *Physical Review Letters* **91** 147902

[29] Daley A J, Kollath C, Schollwock U and Vidal G 2004 *Journal of Statistical Mechanics: Theory and Experiment* **2004** P04005

[30] Verstraete F and Cirac J I 2010 *Physical Review Letters* **104** 190405

[31] Schollwöck U 2011 *Annals of Physics* **326** 96–192

[32] Lodahl P, Mahmoodian S, Stobbe S, Rauschenbeutel A, Schneeweiss P, Volz J, Pichler H and Zoller P 2017 *Nature* **541** 473–480

[33] Taylor J R 2006 *Scattering Theory: The Quantum Theory of Nonrelativistic Collisions* (New York: Dover)

[34] Gardiner C and Zoller P 2015 *The Quantum World of Ultra-Cold Atoms and Light Book II: The Physics of Quantum-Optical Devices* 1st ed (London: Imperial College Press)

[35] Chang D E, Jiang L, Gorshkov A V and Kimble H J 2012 *New Journal of Physics* **14** 063003

[36] Guimond P O, Roulet A, Le H N and Scarani V 2016 *Phys. Rev. A* **93**(2) 023808

References from "transmission line.."

References

[1] S. Haroche and J.-M. Raimond, *Exploring the Quantum: Atoms, Cavities, and Photons* (Oxford University Press, Oxford, 2006).

[2] A. Wallraff, D. I. Schuster, A. Blais, L. Frunzio, R.-S. Huang, J. Majer, S. Kumar, S. M. Girvin, and R. J. Schoelkopf, Nature **431**, 162 (2004).

[3] H. J. Kimble, Nature **453**, 1023 (2008).

[4] M. K. Tey, Z. Chen, S. A. Aljunid, B. Chng, F. Huber, G. Maslennikov, and C. Kurtsiefer, Nat. Phys. **4**, 924 (2008).

[5] J. L. O'Brien, A. Furusawa, and J. Vuckovic, Nat Photonics **3**, 687 (2009).

[6] D. E. Chang, A. S. Sorensen, E. A. Demler, and M. D. Lukin, Nat. Phys. **3**, 807 (2007).

[7] J. Hwang, M. Pototschnig, R. Lettow, G. Zumofen, A. Renn, S. Gotzinger, and V. Sandoghdar, Nature **460**, 76 (2009).

[8] J. A. Schuller, E. S. Barnard, W. Cai, Y. C. Jun, J. S. White, and M. L. Brongersma, Nat. Mater. **9**, 193 (2010).

[9] J.-T. Shen and S. Fan, Phys. Rev. Lett. **95**, 213001 (2005).

[10] O. Astafiev, A. M. Zagoskin, A. A. Abdumalikov Jr., Y. A. Pashkin, T. Yamamoto, K. Inomata, Y. Nakamura, and J. S. Tsai, Science **327**, 840 (2010).

[11] J. Koch, T. M. Yu, J. Gambetta, A. A. Houck, D. I. Schuster, J. Majer, A. Blais, M. H. Devoret, S. M. Girvin, and R. J. Schoelkopf, Phys. Rev. A **76**, 042319 (2007).

[12] I.-C. Hoi, C. M. Wilson, G. Johansson, T. Palomaki, B. Peropadre, and P. Delsing, Phys. Rev. Lett. **107**, 073601 (2011).

[13] I.-C. Hoi, T. Palomaki, J. Lindkvist, G. Johansson, P. Delsing, and C. M. Wilson, Phys. Rev. Lett. **108**, 263601 (2012).

[14] I.-C. Hoi, C. M. Wilson, G. Johansson, J. Lindkvist, B. Peropadre, T. Palomaki, and P. Delsing, New Journal of Physics **15**, 025011 (2013).

[15] J.-T. Shen, M. L. Povinelli, S. Sandhu, and S. Fan, Phys. Rev. B **75**, 035320 (2007).

[16] H. Zheng, D. J. Gauthier, and H. U. Baranger, Phys. Rev. A **82**, 063816 (2010).

[17] B. Peropadre, J. Lindkvist, I.-C. Hoi, C. M. Wilson, J. J. Garcia-Ripoll, P. Delsing, and G. Johansson, New Journal of Physics **15**, 035009 (2013).

[18] E. Rephaeli and S. Fan, Phys. Rev. Lett. **108**, 143602 (2012).

[19] K. Koshino and Y. Nakamura, New Journal of Physics **14**, 043005 (2012).

[20] A. F. van Loo, A. Fedorov, K. Lalumière, B. C. Sanders, A. Blais, and A. Wallraff, Science **342**, 1494 (2013).

[21] R. H. Lehmberg, Phys. Rev. A **2**, 883 (1970).

[22] Z. Ficek and B. C. Sanders, Phys. Rev. A **41**, 359 (1990).

[23] G. Ordonez and S. Kim, Phys. Rev. A **70**, 032702 (2004).

[24] G. Agarwal, *Quantum Statistical Theories of Spontaneous Emission and Their Relation to Other Approaches*, vol. 70 of *Springer Tracts in Modern Physics* (Springer, Berlin / Heidelberg, 1974).

[25] G. Lenz and P. Meystre, Phys. Rev. A **48**, 3365 (1993).

[26] T. G. Rudolph, Z. Ficek, and B. J. Dalton, Phys. Rev. A **52**, 636 (1995).

[27] Z. Ficek and R. Tanas, Phys. Rep. **372**, 369 (2002).

[28] F. Le Kien, S. Dutta Gupta, K. P. Nayak, and K. Hakuta, Phys. Rev. A **72**, 063815 (2005).

[29] D. Dzsotjan, A. S. Sørensen, and M. Fleischhauer, Phys. Rev. B **82**, 075427 (2010).

[30] A. Gonzalez-Tudela, D. Martin-Cano, E. Moreno, L. Martin-Moreno, C. Tejedor, and F. J. Garcia-Vidal, Phys. Rev. Lett. **106**, 020501 (2011).

[31] K. Xia, M. Macovei, and J. Evers, Phys. Rev. B **84**, 184510 (2011).

[32] D. Zueco, J. J. Mazo, E. Solano, and J. J. Garcia-Ripoll, Phys. Rev. B **86**, 024503 (2012).

[33] D. E. Chang, L. Jiang, A. V. Gorshkov, and H. J. Kimble, New Journal of Physics **14**, 063003 (2012).

[34] E. Shahmoon and G. Kurizki, Phys. Rev. A **87**, 033831 (2013).

[35] H. Zheng and H. U. Baranger, Phys. Rev. Lett. **110**, 113601 (2013).

[36] M. J. Collett and C. W. Gardiner, Phys. Rev. A **30**, 1386 (1984).

[37] A. A. Abdumalikov, O. V. Astafiev, Y. A. Pashkin, Y. Nakamura, and J. S. Tsai, Phys. Rev. Lett. **107**, 043604 (2011).

[38] A. Gonzalez-Tudela and D. Porras, Phys. Rev. Lett. **110**, 080502 (2013).

[39] J. Majer, J. M. Chow, J. M. Gambetta, J. Koch, B. R. Johnson, J. A. Schreier, L. Frunzio, D. I. Schuster, A. A. Houck, A. Wallraff, A. Blais, M. H. Devoret, S. M. Girvin, and R. J. Schoelkopf, Nature **449**, 443 (2007).

[40] S. Filipp, M. Göppl, J. M. Fink, M. Baur, R. Bianchetti, L. Steffen, and A. Wallraff, Phys. Rev. A **83**, 063827 (2011).

[41] D. Walls and G. J. Milburn, *Quantum Optics* (Springer, Berlin, 2008), 2nd ed.

[42] The exclusion of the qubit transition frequency comes from the principal part in Eq. (17.65). Indeed, in this equation, the Dirac delta is responsible for relaxation (by emission of photons at the qubit transition frequency) while the principal part is responsible for the Lamb shift and the exchange interaction.

[43] K. W. Murch, S. J. Weber, K. M. Beck, E. Ginossar, and I. Siddiqi, Nature **499**, 62 (2013).

[44] M. Devoret, in *Quantum Fluctuations*, edited by S. Reynaud, E. Giacobino, and J. Zinn-Justin (Elsevier, 1995), p. 351.

[45] G. Romero, J. J. Garcia-Ripoll, and E. Solano, Phys. Scr. **T137**, 014004 (2009).

[46] J. Bourassa, J. M. Gambetta, and A. Blais, (unpublished).

[47] D. Poulin, A. Qarry, R. Somma, and F. Verstraete, Phys. Rev. Lett. **106**, 170501 (2011).

[48] J. M. Fink, *Quantum Nonlinearities in Strong Coupling Circuit QED*, Ph.D. thesis, ETH Zurich (2010).

[49] M. Kliesch, T. Barthel, C. Gogolin, M. Kastoryano, and J. Eisert, Phys. Rev. Lett. **107**, 120501 (2011).

[50] R. Loudon, *The Quantum Theory of Light* (Oxford University Press, 2000), 3rd ed.

From Reliable multiphoton generation in waveguide QED by González-Tudela et al.

References

[1] Murao, M., Jonathan, D., Plenio, M. B. & Vedral, V. Quantum telecloning and multiparticle entanglement. *Phys. Rev. A* **59**, 156–161 (1999).

[2] Briegel, H.-J., Dür, W., Cirac, J. I. & Zoller, P. Quantum Repeaters: The Role of Imperfect Local Operations in Quantum Communication. *Phys. Rev. Lett.* **81**, 5932 (1998).

[3] Gisin, N., Ribordy, G., Tittel, W. & Zbinden, H. Quantum cryptography. *Rev. Mod. Phys.* **74**, 145 (2002).

[4] Durkin, G. A., Simon, C. & Bouwmeester, D. Multiphoton entanglement concentration and quantum cryptography. *Phys. Rev. Lett.* **88**, 187902 (2002).

[5] Giovannetti, V., Lloyd, S. & Maccone, L. Quantum metrology. *Phys. Rev. Lett.* **96**, 010401 (2006).

[6] Lounis, B. & Orrit, M. Single-photon sources. *Reports on Progress in Physics* **68**, 1129 (2005).

[7] Dell'Anno, F., De Siena, S. & Illuminati, F. Multiphoton quantum optics and quantum state engineering. *Physics reports* **428**, 53–168 (2006).

[8] Porras, D. & Cirac, J. Collective generation of quantum states of light by entangled atoms. *Physical Review A* **78**, 053816 (2008).

[9] González-Tudela, A., Paulisch, V., Chang, D. E., Kimble, H. J. & Cirac, J. I. Deterministic generation of arbitrary photonic states assisted by dissipation. *Phys. Rev. Lett.* **115**, 163603 (2015).

[10] Laucht, A. *et al.* A Waveguide-Coupled On-Chip Single-Photon Source. *Phys. Rev. X* **2**, 011014 (2012).

[11] Lodahl, P., Mahmoodian, S. & Stobbe, S. Interfacing single photons and single quantum dots with photonic nanostructures. *Rev. Mod. Phys.* **87**, 347–400 (2015).

[12] Yu, S.-P. *et al.* Nanowire photonic crystal waveguides for single-atom trapping and strong light-matter interactions. *Appl. Phys. Lett.* **104**, 111103 (2014).

[13] Goban, A. *et al.* Superradiance for atoms trapped along a photonic crystal waveguide. *Phys. Rev. Lett.* **115**, 063601 (2015).

[14] Chang, D., Jiang, L., Gorshkov, A. & Kimble, H. Cavity qed with atomic mirrors. *New Journal of Physics* **14**, 063003 (2012).

[15] In fact all results can be extended to separations of $\lambda_a/2$.

[16] Myerson, A. H. *et al.* High-fidelity readout of trapped-ion qubits. *Phys. Rev. Lett.* **100**, 200502 (2008).

[17] See Supplementary material for full details of the calculations of probabilities and fidelities of the protocols discussed in the main text.

[18] Duan, L.-M., Lukin, M. D., Cirac, J. I. & Zoller, P. Long-distance quantum communication with atomic ensembles and linear optics. *Nature* **414**, 413 (2001).

[19] Dakna, M., Clausen, J., Knöll, L. & Welsch, D.-G. Generation of arbitrary quantum states of traveling fields. *Phys. Rev. A* **59**, 1658–1661 (1999).

[20] van Enk, S. J., Cirac, J. I. & Zoller, P. Ideal quantum communication over noisy channels: A quantum optical implementation. *Phys. Rev. Lett.* **78**, 4293–4296 (1997).

[21] Borregaard, J., Kómár, P., Kessler, E. M., Sørensen, A. S. & Lukin, M. D. Heralded quantum gates with integrated error detection in optical cavities. *Phys. Rev. Lett.* **114**, 110502 (2015).

[22] Fiurášek, J., García-Patrón, R. & Cerf, N. J. Conditional generation of arbitrary single-mode quantum states of light by repeated photon subtractions. *Phys. Rev. A* **72**, 033822 (2005).

[23] Thompson, J. D. *et al.* Coupling a single trapped atom to a nanoscale optical cavity. *Science* **340**, 1202–1205 (2013).

[24] Tiecke, T. *et al.* Nanophotonic quantum phase switch with a single atom. *Nature* **508**, 241–244 (2014).

[25] Parkins, A. S., Marte, P., Zoller, P., Carnal, O. & Kimble, H. J. Quantum-state mapping between multilevel atoms and cavity light fields. *Phys. Rev. A* **51**, 1578–1596 (1995).

[26] Specht, H. P. *et al.* A single-atom quantum memory. *Nature* **473**, 190–193 (2011).

[27] Haas, F., Volz, J., Gehr, R., Reichel, J. & Estève, J. Entangled states of more than 40 atoms in an optical fiber cavity. *Science* **344**, 180–183 (2014).

[28] Mlynek, J., Abdumalikov, A., Eichler, C. & Wallraff, A. Observation of dicke superradiance for two artificial atoms in a cavity with high decay rate. *Nat. Communications* **5**, 5186 (2014).

[29] Vetsch, E. *et al.* Optical interface created by laser-cooled atoms trapped in the evanescent field surrounding an optical nanofiber. *Phys. Rev. Lett.* **104**, 203603 (2010).

[30] Goban, A. *et al.* Demonstration of a State-Insensitive, Compensated Nanofiber Trap. *Phys. Rev. Lett.* **109**, 033603 (2012).

[31] Petersen, J., Volz, J. & Rauschenbeutel, A. Chiral nanophotonic waveguide interface based on spin-orbit interaction of light. *Science* **346**, 67–71 (2014).

[32] Béguin, J.-B. *et al.* Generation and detection of a sub-poissonian atom number distribution in a one-dimensional optical lattice. *Phys. Rev. Lett.* **113**, 263603 (2014).

[33] Gardiner, G. W. & Zoller, P. *Quantum Noise* (Springer-Verlag, Berlin, 2000), 2nd edn.

[34] All the expressions are valid obviously for detectors with $0 < \eta < 1$.

[35] Actually the source atom can also play the role of the detector atom with appropriate modification of the protocol.

From Waveguide QED: Many-Body Bound State Effects on Coherent and Fock State Scattering from a Two-Level System

References

[1] A. Politi, M. J. Cryan, J. G. Rarity, S. Yu, and J. L. O'Brien, Science **320**, 646 (2008).

[2] M. Hofheinz, E. M. Weig, M. Ansmann, R. C. Bialczak, E. Lucero, M. Neeley, A. D. O'Connell, H. Wang, J. M. Martinis, and A. N. Cleland, Nature **454**, 310 (2008).

[3] D. E. Chang, A. S. Sørensen, P. R. Hemmer, and M. D. Lukin, Phys. Rev. Lett. **97**, 053002 (2006).

[4] D. E. Chang, A. S. Sørensen, E. A. Demler, and M. D. Lukin, Nature Phys. **3**, 807 (2007).

[5] J.-Q. Liao, J.-F. Huang, Y.-X. Liu, L.-M. Kuang, and C. P. Sun, Phys. Rev. A **80**, 014301 (2009).

[6] L. Zhou, Z. R. Gong, Y.-X. Liu, C. P. Sun, and F. Nori, Phys. Rev. Lett. **101**, 100501 (2008).

[7] L. Zhou, S. Yang, Y.-x. Liu, C. P. Sun, and F. Nori, Phys. Rev. A **80**, 062109 (2009).

[8] D. Witthaut and A. S. Sørensen, New J. Phys. **12**, 043052 (2010).

[9] P. Longo, P. Schmitteckert, and K. Busch, Phys. Rev. Lett. **104**, 023602 (2010).

[10] W. Vogel, D. G. Welsch, and S. Wallentowitz, *Quantum Optics-An Introduction* (WILEY-VCH, Berlin, 2001), 2nd ed.

[11] R. J. Thompson, G. Rempe, and H. J. Kimble, Phys. Rev. Lett. **68**, 1132 (1992).

[12] J. P. Reithmaier, G. Sek, A. Löffler, C. Hofmann, S. Kuhn, S. Reitzenstein, L. V. Keldysh, V. D. Kulakovskii, T. L. Reinecke, and A. Forchel, Nature **432**, 197 (2004).

[13] A. Wallraff, D. I. Schuster, A. Blais, L. Frunzio, R.-S. Huang, J. Majer, S. Kumar, S. M. Girvin, and R. J. Schoelkopf, Nature **431**, 162 (2004).

[14] I. Chiorescu, P. Bertet, K. Semba, Y. Nakamura, C. J. P. M. Harmans, and J. E. Mooij, Nature **431**, 159 (2004).

[15] O. Astafiev, A. M. Zagoskin, A. A. J. Abdumalikov, Y. A. Pashkin, T. Yamamoto, K. Inomata, Y. Nakamura, and J. S. Tsai, Science **327**, 840 (2010).

[16] R. J. Schoelkopf and S. M. Girvin, Nature **451**, 664 (2008).

[17] P. Longo, P. Schmittechert, and K. Busch, J. Opt. A **11**, 114009 (2009).

[18] J.-T. Shen and S. Fan, Phys. Rev. Lett. **98**, 153003 (2007).

[19] J.-T. Shen and S. Fan, Phys. Rev. A **76**, 062709 (2007).

[20] P. Maunz, D. L. Moehring, S. Olmschenk, K. C. Younge, D. N. Matsukevich, and C. Monroe, Nature Phys. **3**, 538 (2007).

[21] A. Nishino, T. Imamura, and N. Hatano, Phys. Rev. Lett. **102**, 146803 (2009).

[22] T. Imamura, A. Nishino, and N. Hatano, Phys. Rev. B **80**, 245323 (2009).

[23] J. J. Sakurai, *Modern Quantum Mechanics* (Addison-Wesley, Reading, MA, 1994).

[24] R. Loudon, *The Quantum Theory of Light* (Oxford University Press, New York, 2003), 3rd ed.

[25] W.-Y. Hwang, Phys. Rev. Lett. **91**, 057901 (2003).

[26] H.-K. Lo, X. Ma, and K. Chen, Phys. Rev. Lett. **94**, 230504 (2005).

[27] X.-B. Wang, Phys. Rev. Lett. **94**, 230503 (2005).

[28] M. Curty, T. Moroder, X. Ma, and N. Lütkenhaus, Opt. Lett. **34**, 3238 (2009).

B.2 From Articles about Main Experiments

From Non-exponential decay of a giant artificial atom

References

[1] Brune, M., Haroche, S., Lefevre, V., Raimond, J. M. & Zagury, N. Quantum nondemolition measurement of small photon numbers by Rydberg-atom phase-sensitive detection. *Physical Review Letters* **65**, 976–979 (1990).

[2] Raimond, J. M., Brune, M. & Haroche, S. Manipulating quantum entanglement with atoms and photons in a cavity. *Reviews of Modern Physics* **73**, 565–582 (2001).

[3] Schoelkopf, R. J. & Girvin, S. M. Wiring up quantum systems. *Nature* **451**, 664–669 (2008).

[4] Guo, L., Grimsmo, A. L., Kockum, A. F., Pletyukhov, M. & Johansson, G. Giant acoustic atom: A single quantum system with a deterministic time delay. *Physical Review A* **95**, 053821 (2017).

[5] Goy, P., Raimond, J. M., Gross, M. & Haroche, S. Observation of cavity-enhanced single-atom spontaneous emission. *Physical Review Letters* **50**, 1903–1906 (1983).

[6] Miller, R. *et al.* Trapped atoms in cavity QED: coupling quantized light and matter. *Journal of Physics B: Atomic, Molecular and Optical Physics* **38**, S551 (2005).

[7] Gu, X., Kockum, A., Miranowicz, A., Liu, Y. & Nori, F. Microwave photonics with superconducting quantum circuits. *Physics Reports* **718**, 1–102 (2017).

[8] Wallraff, A. *et al.* Strong coupling of a single photon to a superconducting qubit using circuit quantum electrodynamics. *Nature* **431**, 162–167 (2004).

[9] Hofheinz, M. *et al.* Synthesizing arbitrary quantum states in a superconducting resonator. *Nature* **459**, 546–549 (2009).

[10] Wang, C. *et al.* A Schrödinger cat living in two boxes. *Science* **352**, 1087–1091 (2016).

[11] Hoi, I. C. *et al.* Demonstration of a single-photon router in the microwave regime. *Physical Review Letters* **107**, 073601 (2011).

[12] Abdumalikov, A. A. *et al.* Electromagnetically induced transparency on a single artificial atom. *Physical Review Letters* **104**, 193601 (2010).

[13] Roy, D., Wilson, C. M. & Firstenberg, O. Colloquium: Strongly interacting photons in one-dimensional continuum. *Rev. Mod. Phys.* **89**, 021001 (2017).

[14] Paik, H. *et al.* Observation of high coherence in Josephson junction qubits measured in a three-dimensional circuit QED architecture. *Physical Review Letters* **107**, 240501 (2011).

[15] Koch, J. *et al.* Charge-insensitive qubit design derived from the Cooper pair box. *Physical Review A* **76**, 042319 (2007).

[16] Gustafsson, M. V. *et al.* Propagating phonons coupled to an artificial atom. *Science* **346**, 207–211 (2014).

[17] Manenti, R. *et al.* Circuit quantum acoustodynamics with surface acoustic waves. *Nature Communications* **8**, 975 (2017).

[18] Chu, Y. *et al.* Quantum acoustics with superconducting qubits. *Science* **358**, 199–202 (2017).

[19] Moores, B. A., Sletten, L. R., Viennot, J. J. & Lehnert, K. W. Cavity quantum acoustic device in the multimode strong coupling regime. *Physical Review Letters* **120**, 227701 (2018).

[20] Bolgar, A. N. *et al.* Quantum regime of a two-dimensional phonon cavity. *Physical Review Letters* **120**, 223603 (2018).

[21] Noguchi, A., Yamazaki, R., Tabuchi, Y. & Nakamura, Y. Qubit-assisted transduction for a detection of surface acoustic waves near the quantum limit. *Physical Review Letters* **119**, 180505 (2017).

[22] Manenti, R. *et al.* Surface acoustic wave resonators in the quantum regime. *Physical Review B* **93**, 041411 (2016).

[23] Satzinger, K. J. *et al.* Quantum control of surface acoustic wave phonons. *Nature* **563**, 661–665 (2018).

[24] Kockum, A. F., Delsing, P. & Johansson, G. Designing frequency-dependent relaxation rates and Lamb shifts for a giant artificial atom. *Physical Review A* **90**, 013837 (2014).

[25] Breuer, H.-P., Laine, E.-M., Piilo, J. & Vacchini, B. Colloquium: Non-markovian dynamics in open quantum systems. *Reviews of Modern Physics* **88**, 021002 (2016).

[26] Pichler, H. & Zoller, P. Photonic circuits with time delays and quantum feedback. *Physical Review Letters* **116**, 093601 (2016).

[27] Pichler, H., Choi, S., Zoller, P. & Lukin, M. D. Universal photonic quantum computation via time-delayed feedback. *Proceedings of the National Academy of Sciences* **114**, 11362–11367 (2017).

[28] Kockum, A. F., Johansson, G. & Nori, F. Decoherence-free interaction between giant atoms in waveguide quantum electrodynamics. *Physical Review Letters* **120**, 140404 (2018).

[29] Aref, T. *et al.* Quantum acoustics with surface acoustic waves. In Hadfield, R. H. & Johansson, G. (eds.) *Superconducting Devices in Quantum Optics*, 217–244 (Springer International Publishing, Cham, 2016).

[30] Astafiev, O. *et al.* Resonance fluorescence of a single artificial atom. *Science* **327**, 840–843 (2010).

[31] Breuer, H.-P., Laine, E.-M. & Piilo, J. Measure for the degree of non-Markovian behavior of quantum processes in open systems. *Physical Review Letters* **103**, 210401 (2009).

[32] Reed, M. D. *et al.* High-fidelity readout in circuit quantum electrodynamics using the Jaynes-Cummings nonlinearity. *Physical Review Letters* **105**, 173601 (2010).

B.3 From Main Articles about Multiphoton Scattering

From Few-photon scattering and emission fr open Q systems

References

[1] P. Lodahl, S. Mahmoodian, and S. Stobbe, Reviews of Modern Physics **87**, 347 (2015).

[2] X. Ding, Y. He, Z.-C. Duan, N. Gregersen, M.-C. Chen, S. Unsleber, S. Maier, C. Schneider, M. Kamp, S. Höfling, *et al.*, Physical Review Letters **116**, 020401 (2016).

[3] P. Michler, ed., *Quantum Dots for Quantum Information Technologies* (Springer, 2017).

[4] P. Senellart, G. Solomon, and A. White, Nature Nanotechnology **12**, nnano (2017).

[5] J. L. Zhang, S. Sun, M. J. Burek, C. Dory, Y.-K. Tzeng, K. A. Fischer, Y. Kelaita, K. G. Lagoudakis, M. Radulaski, Z.-X. Shen, *et al.*, Nano letters **18**, 1360 (2018).

[6] P. Kok, W. J. Munro, K. Nemoto, T. C. Ralph, J. P. Dowling, and G. J. Milburn, Reviews of Modern Physics **79**, 135 (2007).

[7] J. L. O'brien, A. Furusawa, and J. Vučković, Nature Photonics **3**, 687 (2009).

[8] D. Roy, C. M. Wilson, and O. Firstenberg, Reviews of Modern Physics **89**, 021001 (2017).

[9] A. Reiserer and G. Rempe, Reviews of Modern Physics **87**, 1379 (2015).

[10] L.-M. Duan and C. Monroe, Reviews of Modern Physics **82**, 1209 (2010).

[11] N. Sangouard, C. Simon, H. De Riedmatten, and N. Gisin, Reviews of Modern Physics **83**, 33 (2011).

[12] K. Nemoto, M. Trupke, S. J. Devitt, A. M. Stephens, B. Scharfenberger, K. Buczak, T. Nöbauer, M. S. Everitt, J. Schmiedmayer, and W. J. Munro, Physical Review X **4**, 031022 (2014).

[13] C. Gardiner and P. Zoller, *Quantum noise: a handbook of Markovian and non-Markovian quantum stochastic methods with applications to quantum optics*, Vol. 56 (Springer Science & Business Media, 2004).

[14] C. Gardiner and P. Zoller, in *The Quantum World of Ultra-Cold Atoms and Light Book II: The Physics of Quantum-Optical Devices* (World Scientific, 2015) pp. 1–524.

[15] H. M. Wiseman and G. J. Milburn, *Quantum measurement and control* (Cambridge university press, 2009).

[16] H.-P. Breuer and F. Petruccione, *The theory of open quantum systems* (Oxford University Press on Demand, 2002).

[17] H. Carmichael, *An open systems approach to quantum optics: lectures presented at the Université Libre de Bruxelles, October 28 to November 4, 1991*, Vol. 18 (Springer Science & Business Media, 2009).

[18] A. Isar, A. Sandulescu, H. Scutaru, E. Stefanescu, and W. Scheid, International Journal of Modern Physics E **3**, 635 (1994).

[19] S. Xu and S. Fan, Physical Review A **91**, 043845 (2015).

[20] S. Xu and S. Fan, in *Quantum Plasmonics* (Springer, 2017) pp. 1–23.

[21] K. A. Fischer, R. Trivedi, V. Ramasesh, I. Siddiqi, and J. Vučković, arXiv preprint arXiv:1710.02875 (2017).

[22] M. Pletyukhov and V. Gritsev, Physical Review A **91**, 063841 (2015).

[23] Y. Pan, D. Dong, and G. Zhang, New Journal of Physics **18**, 033004 (2016).

[24] T. Caneva, M. T. Manzoni, T. Shi, J. S. Douglas, J. I. Cirac, and D. E. Chang, New Journal of Physics **17**, 113001 (2015).

[25] T. Shi, D. E. Chang, and J. I. Cirac, Physical Review A **92**, 053834 (2015).

[26] J. Kiukas, M. Guţă, I. Lesanovsky, and J. P. Garrahan, Physical Review E **92**, 012132 (2015).

[27] S. Fan, Ş. E. Kocabaş, and J.-T. Shen, Physical Review A **82**, 063821 (2010).

[28] T. Shi, S. Fan, C. Sun, *et al.*, Physical Review A **84**, 063803 (2011).

[29] J.-T. Shen and S. Fan, Physical review letters **95**, 213001 (2005).

[30] S. Xu, E. Rephaeli, and S. Fan, Physical review letters **111**, 223602 (2013).

[31] J.-T. Shen and S. Fan, Physical review letters **98**, 153003 (2007).

[32] C. Gardiner and M. Collett, Physical Review A **31**, 3761 (1985).

[33] S. Rosenblum, O. Bechler, I. Shomroni, Y. Lovsky, G. Guendelman, and B. Dayan, Nature Photonics **10**, 19 (2016).

From Diagrammatic Approach to Multiphoton Scattering See, Noh, Angelakis

References

[1] D. E. Chang, V. Vuletic, and M. D. Lukin, Nat Photon **8**, 685 (2014).

[2] C. Gardiner and P. Zoller, *The Quantum World of Ultra-Cold Atoms and Light Book II: The Physics of Quantum-Optical Devices (Cold Atoms - Volume 4)* (Imperial College Press, 2015).

[3] S. Haroche and J.-M. Raimond, *Exploring the quantum : atoms, cavities and photons* (Oxford University Press, 2006).

[4] Y. Yamamoto, F. Tassone, and H. Cao, *Semiconductor cavity quantum electrodynamics* (Springer Berlin Heidelberg, 2000).

[5] A. Wallraff, D. I. Schuster, A. Blais, L. Frunzio, R.-S. Huang, J. Majer, S. Kumar, S. M. Girvin, and R. J. Schoelkopf, Nature **431**, 162 (2004).

[6] O. Firstenberg, C. S. Adams, and S. Hofferberth, Journal of Physics B: Atomic, Molecular and Optical Physics **49**, 152003 (2016).

[7] D. E. Chang, A. S. Sorensen, E. A. Demler, and M. D. Lukin, Nat Phys **3**, 807 (2007).

[8] P. Michler, A. Kiraz, C. Becher, W. V. Schoenfeld, P. M. Petroff, L. Zhang, E. Hu, and A. Imamoglu, Science **290**, 2282 (2000).

[9] T. Volz, A. Reinhard, M. Winger, A. Badolato, K. J. Hennessy, E. L. Hu, and A. Imamoglu, Nat Photon **6**, 605 (2012).

[10] T. G. Tiecke, J. D. Thompson, N. P. de Leon, L. R. Liu, V. Vuletic, and M. D. Lukin, Nature **508**, 241 (2014), letter.

[11] C. Noh and D. G. Angelakis, Reports on Progress in Physics **80**, 016401 (2017).

[12] M. J. Hartmann, Journal of Optics **18**, 104005 (2016).

[13] C. Gardiner and P. Zoller, *Quantum Noise*, 3rd ed. (Springer-Verlag Berlin Heidelberg, 2004).

[14] H. J. Carmichael, *Statistical Methods in Quantum Optics 1: Master Equations and Fokker-Planck Equations (Theoretical and Mathematical Physics) (v. 1)* (Springer, 2003).

[15] B. A. Lippmann and J. Schwinger, Phys. Rev. **79**, 469 (1950).

[16] H. Bethe, Zeitschrift für Physik **71**, 205 (1931).

[17] M. E. Peskin and D. V. Schroeder, *An Introduction To Quantum Field Theory (Frontiers in Physics)* (Westview Press, 1995).

[18] J.-T. Shen and S. Fan, Phys. Rev. Lett. **98**, 153003 (2007).

[19] T. Shi and C. P. Sun, Phys. Rev. B **79**, 205111 (2009).

[20] M. Pletyukhov and V. Gritsev, New Journal of Physics **14**, 095028 (2012).

[21] M. P. Schneider, T. Sproll, C. Stawiarski, P. Schmitteckert, and K. Busch, Phys. Rev. A **93**, 013828 (2016).

[22] Ş. E. Kocabaş, Phys. Rev. A **93**, 033829 (2016).

[23] H. Zheng, D. J. Gauthier, and H. U. Baranger, Phys. Rev. A **85**, 043832 (2012).

[24] C. Lee, C. Noh, N. Schetakis, and D. G. Angelakis, Phys. Rev. A **92**, 063817 (2015).

[25] T. Shi, D. E. Chang, and J. I. Cirac, Phys. Rev. A **92**, 053834 (2015).

[26] T. Caneva, M. T. Manzoni, T. Shi, J. S. Douglas, J. I. Cirac, and D. E. Chang, New Journal of Physics **17**, 113001 (2015).

[27] S. Xu and S. Fan, Phys. Rev. A **91**, 043845 (2015).

[28] A. Roulet and V. Scarani, New Journal of Physics **18**, 093035 (2016).

[29] C. W. Gardiner and M. J. Collett, Phys. Rev. A **31**, 3761 (1985).

[30] For example, for a one-photon process, there are four different S-matrix elements for incoming and outgoing photons from the left and right waveguides, i.e. ${}_L\langle p|S|k\rangle_L$, ${}_R\langle p|S|k\rangle_L$, ${}_L\langle p|S|k\rangle_R$ and ${}_R\langle p|S|k\rangle_R$.

[31] I. Bloch, J. Dalibard, and S. Nascimbene, Nat Phys **8**, 267 (2012).

[32] K. M. Birnbaum, A. Boca, R. Miller, A. D. Boozer, T. E. Northup, and H. J. Kimble, Nature **436**, 87 (2005).

[33] K. M. Birnbaum, A. Boca, R. Miller, A. D. Boozer, T. E. Northup, and H. J. Kimble, (2005), quant-ph/0507065 .

[34] E. Rephaeli, Ş. E. Kocabaş, and S. Fan, Phys. Rev. A **84**, 063832 (2011).

[35] B. M. Garraway, Philosophical Transactions of the Royal Society of London A: Mathematical, Physical and Engineering Sciences **369**, 1137 (2011).

[36] M. Greiner, O. Mandel, T. Esslinger, T. W. Hansch, and I. Bloch, Nature **415**, 39 (2002).

[37] D. G. Angelakis, M. F. Santos, and S. Bose, Phys. Rev. A **76**, 031805 (2007).

[38] M. J. Hartmann, F. G. S. L. Brandao, and M. B. Plenio, Nat Phys **2**, 849 (2006).

[39] A. D. Greentree, C. Tahan, J. H. Cole, and L. C. L. Hollenberg, Nat Phys **2**, 856 (2006).

[40] M. Fitzpatrick, N. M. Sundaresan, A. C. Y. Li, J. Koch, and A. A. Houck, Phys. Rev. X **7**, 011016 (2017).

References from "scattering on Bose-Hubbard lattices"

References

[1] A. A. Houck, H. E. Türeci, and J. Koch, Nature Physics **8**, 292 (2012) .

[2] I. C. Hoi, C. M. Wilson, G. Johansson, J. Lindkvist, B. Peropadre, T. Palomaki, and P. Delsing, New Journal of Physics **15**, 025011 (2013) .

[3] M. Hafezi, S. Mittal, J. Fan, a. Migdall, and J. M. Taylor, Nature Photonics **7**, 1001 (2013) .

[4] Y. Plotnik, M. C. Rechtsman, D. Song, M. Heinrich, J. M. Zeuner, S. Nolte, Y. Lumer, N. Malkova, J. Xu, A. Szameit, Z. Chen, and M. Segev, Nature Materials **13**, 57 (2014) .

[5] D. N. Christodoulides, F. Lederer, and Y. Silberberg, Nature **424**, 817 (2003) .

[6] D. E. Chang, A. S. Sorensen, E. A. Demler, and M. D. Lukin, Nature Physics **3**, 807 (2007) .

[7] M. Hafezi, D. E. Chang, V. Gritsev, E. Demler, and M. D. Lukin, Physical Review A **85**, 013822 (2012) .

[8] A. F. van Loo, A. Fedorov, K. Lalumiere, B. C. Sanders, A. Blais, and A. Wallraff, Science **342**, 1494 (2013) .

[9] S. Gupta, K. L. Moore, K. W. Murch, and D. M. Stamper-Kurn, Physical Review Letters **99**, 213601 (2007) .

[10] D. G. Angelakis, M. F. Santos, and S. Bose, Physical Review A **76**, 031805 (2007) .

[11] M. J. Hartmann, F. G. S. L. Brandão, and M. B. Plenio, Nature Physics **2**, 849 (2006) .

[12] A. D. Greentree, C. Tahan, J. H. Cole, and L. C. L. Hollenberg, Nature Physics **2**, 856 (2006) .

[13] A. Tomadin, V. Giovannetti, R. Fazio, D. Gerace, I. Carusotto, H. E. Türeci, and A. Imamoglu, Physical Review A **81**, 061801 (2010) .

[14] C. Noh and D. G. Angelakis, Rep. Prog. Phys. **80**, 016401 (2017) .

[15] M. Pletyukhov and V. Gritsev, New Journal of Physics **14**, 095028 (2012) .

[16] J. T. Shen and S. Fan, Physical Review Letters **98**, 153003 (2007) .

[17] J. T. Shen and S. Fan, Physical Review A **76**, 062709 (2007) .

[18] C. Lee, C. Noh, N. Schetakis, and D. G. Angelakis, Physical Review A **92**, 063817 (2015) .

[19] Y.-L. L. Fang, H. Zheng, and H. U. Baranger, EPJ Quantum Technology **1**, 3 (2014) .

[20] T. Shi and C. P. Sun, Physical Review B **79**, 205111 (2009) .

[21] T. Shi, D. E. Chang, and J. I. Cirac, Physical Review A **92**, 053834 (2015) .

[22] T. Caneva, M. T. Manzoni, T. Shi, J. S. Douglas, J. I. Cirac, and D. E. Chang, New Journal of Physics **17**, 113001 (2015) .

[23] D. J. Brod and J. Combes, Physical Review Letters **117**, 080502 (2016) .

[24] D. J. Brod, J. Combes, and J. Gea-Banacloche, Physical Review A **94**, 023833 (2016) .

[25] S. Xu and S. Fan, Physical Review A **91**, 043845 (2015) .

[26] H. Zheng and H. U. Baranger, Physical Review Letters **110**, 113601 (2013) .

[27] M. Laakso and M. Pletyukhov, Physical Review Letters **113**, 183601 (2014) .

[28] Y. L. L. Fang and H. U. Baranger, Physical Review A **91**, 053845 (2015) .

[29] Y.-L. L. Fang and H. U. Baranger, Phys. Rev. A **96**, 013842 (2017) .

[30] D. Roy, Scientific reports **3**, 2337 (2013) .

[31] T. C. H. Liew and V. Savona, Physical Review Letters **104**, 183601 (2010) .

[32] `babusca` is also available at .

[33] J. M. Fink, R. Bianchetti, M. Baur, M. Göppl, L. Steffen, S. Filipp, P. J. Leek, A. Blais, and A. Wallraff, Physical Review Letters **103**, 083601 (2009) .

[34] J. Petersen, J. Volz, and A. Rauschenbeutel, Science **346**, 67 (2014) .

[35] I. Söllner, S. Mahmoodian, S. L. Hansen, L. Midolo, A. Javadi, G. Kiršanske, T. Pregnolato, H. El-Ella, E. H. Lee, J. D. Song, S. Stobbe, and P. Lodahl, Nature Nanotechnology **10**, 775 (2015) .

[36] M. Hafezi, E. Demler, M. Lukin, and J. Taylor, Nature Physics **7**, 9 (2011) .

[37] P. Lodahl, S. Mahmoodian, S. Stobbe, A. Rauschenbeutel, P. Schneeweiss, J. Volz, H. Pichler, and P. Zoller, Nature Publishing Group **541**, 473 (2017) .

[38] H. Pichler, T. Ramos, A. J. Daley, and P. Zoller, Physical Review A **91**, 042116 (2015) .

[39] M. Pletyukhov and V. Gritsev, Physical Review A **91**, 063841 (2015) .

[40] J. R. Taylor, *Scattering Theory* (Dover Publications, 2006).

[41] R. Landauer, IBM Journal of Research and Development **1**, 223 (1957) .

[42] R. Hanbury Brown and R. Q. Twiss, Nature **178**, 1076 (1956) .

[43] O. Astafiev, A. M. Zagoskin, A. A. Abdumalikov, Y. A. Pashkin, T. Yamamoto, K. Inomata, Y. Nakamura, and J. S. Tsai, Science **327**, 840 (2010) .

[44] P. D. Drummond and D. F. Walls, Phys. Rev. A **23**, 2563 (1981) .

[45] J.-Q. Liao and C. K. Law, Physical Review A **82**, 053836 (2010) .

[46] F. Nissen, S. Schmidt, M. Biondi, G. Blatter, H. E. Türeci, and J. Keeling, Physical Review Letters **108**, 233603 (2012) .

[47] A. A. Abdumalikov, O. Astafiev, A. M. Zagoskin, Y. A. Pashkin, Y. Nakamura, and J. S. Tsai, Phys. Rev. Lett. **104**, 193601 (2010) .

[48] T. Markussen, R. Stadler, and K. S. Thygesen, Nano Lett. **10**, 4260 (2010) .

[49] L. Jin and Z. Song, Phys. Rev. A **80**, 052107 (2009) .

[50] M. A. Cazalilla, R. Citro, T. Giamarchi, E. Orignac, and M. Rigol, Rev. Mod. Phys. **83**, 1405 (2011) .

[51] D. R. Hofstadter, Physical Review B **14**, 2239 (1976) .

[52] The latest babusca library is available at .

[53] T. F. See, C. Noh, and D. G. Angelakis, Physical Review A **95**, 053845 (2017) .

B.4 From Articles about Other Special Models and Effects

From Bound states and entanglement generation in waveguide quantum electrodynamics by Facchi, Kim, et al.

References

[1] *Cavity Quantum Electrodynamics*, Adv. At. Mol. Opt. Phys., Suppl. 2, edited by P.R. Berman (Academic Press, Boston, 1994).

[2] E. A. Hinds, Adv. At., Mol., Opt. Phys. **28**, 237 (1991).

[3] S. Haroche, in *Fundamental Systems in Quantum Optics*, Proceedings of the Les Houches Summer School of Theoretical Physics, edited by J. Dalibard, J.-M. Raimond, and J. Zinn-Justin (North-Holland, Amsterdam, 1990), p. 767.

[4] D. J. Heinzen, J. J. Childs, J. E. Thomas, and M. S. Feld, Phys. Rev. Lett. **58**, 1320 (1987).

[5] D. J. Heinzen and M. S. Feld, Phys. Rev. Lett. **59**, 2623 (1987).

[6] W. Jhe, A. Anderson, E. A. Hinds, D. Meschede, L. Moi, and S. Haroche, Phys. Rev. Lett. **58**, 666 (1987).

[7] R. G. Hulet, E. S. Hilfer, and D. Kleppner, Phys. Rev. Lett. **55**, 2137 (1985).

[8] P. Goy, J. M. Raimond, M. Gross, and S. Haroche, Phys. Rev. Lett. **50**, 1903 (1983).

[9] F. DeMartini, G. Innocenti, G.R. Jacobovitz, and P. Mataloni, Phys. Rev. Lett. **59**, 2955 (1987).

[10] C. J. Hood, T. W. Lynn, A. C. Doherty, A. S. Parkins, and H. J. Kimble, Science **287**, 1447 (2000).

[11] P. W. H. Pinkse, T. Fischer, P. Maunz, and G. Rempe, Nature (London) **404**, 365 (2000).

[12] J. M. Raimond, M. Brune, and S. Haroche, Rev. Mod. Phys. **73**, 565 (2001).

[13] A. Faraon, E. Waks, D. Englund, I. Fushman, and J. Vučković, Appl. Phys. Lett. **90**, 073102 (2007).

[14] B. Dayan, A. S. Parkins, Takao Aoki, E. P. Ostby, K. J. Vahala, and H. J. Kimble, Science **319**, 1062 (2008).

[15] E. Vetsch, D. Reitz, G. Sague, R. Schmidt, S. T. Dawkins, and A. Rauschenbeutel, Phys. Rev. Lett. **104**, 203603 (2010).

[16] M. Bajcsy, S. Hofferberth, V. Balic, T. Peyronel, M. Hafezi, A. S. Zibrov, V. Vuletic, and M. D. Lukin, Phys. Rev. Lett. **102**, 203902 (2009).

[17] A. Wallraff, D. I. Schuster, A. Blais, L. Frunzio, R.-S. Huang, J. Majer, S. Kumar, S. M. Girvin, and R. J. Schoelkopf, Nature (London) **431**, 162 (2004).

[18] O. Astafiev, A. M. Zagoskin, A. A. Abdumalikov, Jr., Yu. A. Pashkin, T. Yamamoto, K. Inomata, Y. Nakamura, and J. S. Tsai, Science **327**, 840 (2010).

[19] D.Witthaut and A. S. Sørensen, New J. Phys. **12**, 043052 (2010).

[20] U. Dorner and P. Zoller, Phys. Rev. A **66**, 023816 (2002)

[21] G. Zumofen, N. M. Mojarad, V. Sandoghdar, and M. Agio, Phys. Rev. Lett. **101**, 180404 (2008).

[22] N. Lindlein, R. Maiwald, H. Konermann, M. Sondermann, U. Peschel, and G. Leuchs, Laser Phys. **17**, 927 (2007).

[23] T. Shi, D. E. Chang, and J. I. Cirac, Phys. Rev. A **92**, 053834 (2015).

[24] T. Shi, Y.-H. Wu, A. Gonzalez-Tudela, J. I. Cirac, *Bound states in boson impurity models*, arXiv:1512.07238 (2015).

[25] J. S. Douglas, H. Habibian, C.-L. Hung, A. V. Gorshkov, H. J. Kimble, D. E. Chang, Nature Photonics **9**, 326 (2015).

[26] A. Goban, C.-L. Hung, J. D. Hood, S.-P. Yu, J. A. Muniz, O. Painter, H. J. Kimble, Phys. Rev. Lett. **115**, 063601 (2015).

[27] A. González-Tudela, V. Paulisch, H. J. Kimble, and J. I. Cirac, *Reliable multiphoton generation in waveguide QED*, arXiv:1603.01243 (2016).

[28] F. Lombardo, F. Ciccarello, and G. M. Palma, Phys. Rev. A **89**, 053826 (2014).

[29] E. Sanchez-Burillo, D. Zueco, L. Martin-Moreno, J. J. Garcia-Ripoll, *Dynamical signatures of bound states in waveguide QED*, arXiv:1603.09408 (2016).

[30] J. T. Shen and S. Fan, Opt. Lett. **30**, 2001 (2005).

[31] J. Bleuse, J. Claudon, M. Creasey, N. S. Malik, J. M. Gerard, I. Maksymov, J. P. Hugonin, and P. Lalanne, Phys. Rev. Lett. **106**, 103601 (2011).

[32] M. E. Reimer, G. Bulgarini, N. Akopian, M. Hocevar, M. B. Bavinck, M. A. Verheijen, E. P. A. M. Bakkers, L. P. Kouwenhoven, and Val Zwiller, Nat. Commun. **3**, 737 (2012).

[33] I.-C. Hoi, A. F. Kockum, L. Tornberg, A. Pourkabirian, G. Johansson, P. Delsing, and C. M. Wilson, Nat. Phys. **11**, 1045 (2015).

[34] H. Dong, Z. R. Gong, H. Ian, L. Zhou, and C. P. Sun, Phys. Rev. A **79**, 063847 (2009).

[35] T. Tufarelli, F. Ciccarello, and M. S. Kim, Phys. Rev. A **87**, 013820 (2013).

[36] J.-T. Shen and S. Fan, Phys. Rev. Lett. **95**, 213001 (2005).

[37] L. Zhou, Z. R. Gong, Y. X. Liu, C. P. Sun, and F. Nori, Phys. Rev. Lett. **101**, 100501 (2008).

[38] L. Zhou, H. Dong, Y. X. Liu, C. P. Sun, and F. Nori, Phys. Rev. A **78**, 063827 (2008).

[39] C. Gonzalez-Ballestero, F. J. Garcia-Vidal, and E. Moreno, New J. Phys. **15**, 073015 (2013).

[40] A. Gonzalez-Tudela, D. Martin-Cano, E. Moreno, L. Martin-Moreno, C. Tejedor, and F. J. Garcia-Vidal, Phys. Rev. Lett. **106**, 020501 (2011).

[41] E. Shahmoon and G. Kurizki, Phys. Rev. A **87**, 033831 (2013).

[42] T. Tufarelli, M. S. Kim, and F. Ciccarello, Phys. Rev. A **90**, 012113 (2014).

[43] H. Zheng and H. U. Baranger, Phys. Rev. Lett. **110**, 113601 (2013).

[44] C. Cohen-Tannoudji, J. Dupont-Roc, and G. Grynberg, *Atom-Photon Interactions: Basic Processes and Applications* (Wiley-VCH Verlag GmbH, Weinheim, Germany, 1998).

[45] W. K. Wootters, Phys. Rev. Lett. **80**, 2245 (1998).

[46] H. Nakazato, M. Namiki, and S. Pascazio, Int. J. Mod. Phys. B **10**, 247 (1996).

[47] P. Facchi, *Quantum Time Evolution: Free and Controlled Dynamics*, PhD Thesis, Università di Bari, Italy (2000), http://www.ba.infn.it/∼facchi/lectures/thesis.pdf

[48] J. D. Jackson, *Classical Electrodynamics* (John Wiley & Sons, New York, 1999).

[49] H. Zheng, D. J. Gauthier, and H. U. Baranger, Phys. Rev. Lett. **111**, 090502 (2013).

[50] V. Paulisch, H. J. Kimble, A. Gonzalez-Tudela, *Universal Quantum Computation in Waveguide QED using Decoherence Free Subspaces*, arXiv:1512.04803 (2015).

[51] A. F. van Loo, A. Fedorov, K. Lalumière, B. C. Sanders, A. Blais, and A. Wallraff, Science **342**, 1494 (2013).

[52] Kevin Lalumière, Barry C. Sanders, A. F. van Loo, A. Fedorov, A. Wallraff, and A. Blais, Phys. Rev. A 88, 043806 (2013).

[53] Y.-L. L. Fang and H. U. Baranger, Phys. Rev. A **91**, 053845 (2015).

[54] T. S. Tsoi and C. K. Law, Phys. Rev. A **78**, 063832 (2008).